



EARTHQUAKE ENGINEERING

From
Engineering Seismology
to Performance-Based
Engineering

Edited by

**Yousef Bozorgnia
Vitelmo V. Bertero**



CRC PRESS

EARTHQUAKE ENGINEERING

From Engineering Seismology to Performance-Based Engineering

EARTHQUAKE ENGINEERING

From Engineering Seismology to Performance-Based Engineering

Edited by

Yousef Bozorgnia
Vitelmo V. Bertero



CRC PRESS

Boca Raton London New York Washington, D.C.

CRC Press
Taylor & Francis Group
6000 Broken Sound Parkway NW, Suite 300
Boca Raton, FL 33487-2742

© 2004 by Taylor & Francis Group, LLC
CRC Press is an imprint of Taylor & Francis Group, an Informa business

No claim to original U.S. Government works
Version Date: 20150116

International Standard Book Number-13: 978-0-203-48624-5 (eBook - PDF)

This book contains information obtained from authentic and highly regarded sources. Reasonable efforts have been made to publish reliable data and information, but the author and publisher cannot assume responsibility for the validity of all materials or the consequences of their use. The authors and publishers have attempted to trace the copyright holders of all material reproduced in this publication and apologize to copyright holders if permission to publish in this form has not been obtained. If any copyright material has not been acknowledged please write and let us know so we may rectify in any future reprint.

Except as permitted under U.S. Copyright Law, no part of this book may be reprinted, reproduced, transmitted, or utilized in any form by any electronic, mechanical, or other means, now known or hereafter invented, including photocopying, microfilming, and recording, or in any information storage or retrieval system, without written permission from the publishers.

For permission to photocopy or use material electronically from this work, please access www.copyright.com (<http://www.copyright.com/>) or contact the Copyright Clearance Center, Inc. (CCC), 222 Rosewood Drive, Danvers, MA 01923, 978-750-8400. CCC is a not-for-profit organization that provides licenses and registration for a variety of users. For organizations that have been granted a photocopy license by the CCC, a separate system of payment has been arranged.

Trademark Notice: Product or corporate names may be trademarks or registered trademarks, and are used only for identification and explanation without intent to infringe.

Visit the Taylor & Francis Web site at
<http://www.taylorandfrancis.com>

and the CRC Press Web site at
<http://www.crcpress.com>

Foreword

The International Code Council® (ICC®) is pleased to join CRC Press in co-publishing *Earthquake Engineering: From Engineering Seismology to Performance-Based Engineering*. Since its genesis in the early 1900s, ICC, with its former legacy organizations, has been a leader in the development of comprehensive building codes both domestically and internationally. The International Codes® focus on addressing the latest technology on seismic design applications for the purpose of mitigating damage to buildings and structures.

This publication reflects the most recent research on the subject by internationally renowned experts. It provides the reader with an excellent variety and balance of subjects, including a historical background of earthquake engineering, geotechnical and probabilistic aspects of seismic hazards and analysis, performance-based seismic engineering and innovative strategies, the seismic behavior of various structural materials, and techniques for the design of seismically resistant buildings and structures.

CRC Press and the ICC would also like to recognize the contributions of the National Council of Structural Engineers Associations (NCSEA) for its role in advancing the field of structural engineering and seismic safety. Many of the contributors to this publication are also active in NCSEA activities and represent some of the finest talent ever assembled in the field of earthquake engineering.

We highly recommend this handbook as an excellent reference resource for university professors, undergraduate and graduate students, seismologists, architects and practicing engineers.

Richard Okawa, P.E.
ICC Vice President of International Services

Preface

Modern earthquake engineering (EE) is an integration of multidisciplinary knowledge in several areas of basic sciences and science-based engineering with the ultimate goal of reducing the seismic risks to socioeconomically acceptable levels.

In the U.S., the first comprehensive book covering various aspects of EE was published in 1970, the result of a short course on the subject given in September 1965 at the University of California, Berkeley. There have been recent advances and new developments in EE on a wide range of topics, from geosciences and geotechnical engineering to modern performance-based EE. These advances are usually published in scientific and technical journals and reports or presented at national and international conferences. This book has been written with the intention of presenting advances in scientific knowledge on various EE topics in a single volume.

Although it has not been written in a traditional textbook format, this book can serve as a guide for instructors, graduate students and practicing engineers. We hope it will contribute to the teaching of modern EE and its applications to practice, as well as to the formulation and evolution of research programs.

The 19 chapters in this book can be grouped into the following main parts:

- Historical development of EE and its modern goal (one chapter)
- Geoscience principles needed to define seismic hazards (two chapters)
- Engineering characterizations of ground motion, as well as geotechnical hazards (two chapters)
- Deterministic and probabilistic methods of analysis (two chapters)
- Performance-based EE, its applications and future direction (two chapters)
- Innovative strategies and techniques (three chapters)
- Seismic behavior and earthquake-resistant design of building structures using different structural materials (six chapters)
- Seismic analysis and design of nonstructural elements (one chapter)

The multidisciplinary nature of EE makes it very difficult to cover the details of all the scientific and engineering aspects involved in modern EE in a single volume. Due to space constraints and also to the existence of other well-written books and handbooks, we have not covered some important EE topics in this book. These include an elaborate discussion of linear structural dynamics; architectural considerations; seismic behavior and design of lifelines and industrial facilities; risk management; and social, economical and political planning.

The breadth of EE makes it impossible for one person to authoritatively write about all relevant topics. Therefore, to create a comprehensive book on EE, the contributions of many experts are essential. This book is the result of an enormous amount of time and energy spent by a panel of distinguished contributors whose collective experience exceeds 500 years of teaching, research and practice. The efforts and cooperation of the contributors are greatly appreciated.

Yousef Bozorgnia and Vitelmo V. Bertero

March, 2004

List of Cover Photographs

Front Cover (from top)

Background photo: Buckling-restrained braces in the central dining and office facility building, University of California, Berkeley. Photo by William G. Godden, courtesy of National Information Service for Earthquake Engineering (NISEE), University of California at Berkeley.

First photo: Fault scarp near Beni Rached in the 1980 El Asnam, Algeria, earthquake. Photo by Vitelmo V. Bertero, courtesy of National Information Service for Earthquake Engineering (NISEE), University of California at Berkeley.

Second photo: Bearing failure of foundations for Kawagishi-Cho apartment buildings in the 1964 Niigata, Japan, earthquake. Photo by Joseph Penzien, courtesy of National Information Service for Earthquake Engineering (NISEE), University of California at Berkeley.

Third photo: United Nations Industrial Development Organization (UNIDO) demonstration base-isolated building in Indonesia. Photo courtesy of James M. Kelly.

Fourth photo: Banco de America (right) and Banco Central de Nicaragua (left) after the 1972 Managua, Nicaragua, earthquake. Photo by Karl V. Steinbrugge, courtesy of National Information Service for Earthquake Engineering (NISEE), University of California at Berkeley.

Back Cover (from top)

First photo: Test of a welded steel beam-column connection in 1999 at Lehigh University. Photo courtesy of James M. Ricles.

Second photo: Collapse of unreinforced masonry wall in San Francisco in the 1989 Loma Prieta, California, earthquake. Photo by Yousef Bozorgnia.

Third photo: Collapse of unreinforced masonry walls of a commercial building in Coalinga during the 1983 Coalinga, California, earthquake. Photo by Vitelmo V. Bertero, courtesy of National Information Service for Earthquake Engineering (NISEE), University of California at Berkeley.

Fourth photo: Wooden apartment building with collapsed open-front story in the 1994 Northridge, California, earthquake. Photo by Robert K. Reitherman.

Fifth photo: Dislocation of library bookshelves during the 1987 Whittier Narrows, California, earthquake. Photo by N. Taly, courtesy of Earthquake Engineering Research Institute.

Editors

Yousef Bozorgnia is Associate Director of the Pacific Earthquake Engineering Research Center (PEER), University of California at Berkeley. He received his B.S. degree from Sharif (Arya-Mehr) University of Technology, Iran; M.S. degree from the University of California at Berkeley; and Ph.D. degree in Civil Engineering, Structural Engineering and Structural Mechanics, also from the University of California at Berkeley. He spent two years as a postdoctoral research fellow in the department of Civil Engineering at McMaster University, Canada.

Dr. Bozorgnia has 25 years of experience in research and consulting. His experience encompasses two areas of earthquake engineering: structural earthquake engineering and engineering characterization of strong ground motions. He has been principal engineer and managing engineer in different engineering organizations in northern California. His consulting projects have included linear and nonlinear structural analyses, seismic vulnerability assessment, and seismic retrofit design of various structures using different schemes. The structures he has worked on have included low-rise and high-rise steel buildings, reinforced concrete structures, woodframe buildings, masonry structures, and highway bridges. He has also evaluated and analyzed a wide variety of structural and nonstructural systems for industrial facilities including refineries and power plants. He is a registered professional civil engineer in the State of California.

Dr. Bozorgnia's research experience has included analysis of characteristics of earthquake ground motions as well as seismic performance of structural systems. He has carried out research projects on characteristics of hundreds of near-source horizontal and vertical ground motions recorded worldwide, and their damage potential for existing and new structural systems. He is co-developer of near-source ground motion (attenuation) models that are used worldwide in earthquake hazard analysis. His other research projects have ranged from analysis of inelastic response of regular, irregular, and base-isolated buildings to development of improved damage indices for performance-based evaluation of structures. He has also analyzed recorded earthquake response of numerous instrumented structures, and is the author and co-author of more than 60 publications on various issues in earthquake engineering.

Dr. Bozorgnia was involved in post-earthquake reconnaissance and damage assessment of structural and nonstructural elements and systems after the 1989 Loma Prieta (CA), 1990 Manjil (Iran), 1994 Northridge (CA), 1999 Kocaeli (Turkey), and 2003 Bam (Iran) earthquakes.

In 1995, the Earthquake Engineering Research Institute (EERI) awarded Dr. Bozorgnia the U.S. National Earthquake Hazard Reduction Program (NEHRP) Professional Fellowship. He is a member of various scientific and professional organizations and a Fellow of the American Society of Civil Engineers (ASCE).

Vitelmo V. Bertero is presently Professor Emeritus at the Department of Civil and Environmental Engineering, and Research Engineer at the Earthquake Engineering Research Center at the University of California (UC), Berkeley. In 1947 he received his degree in Civil Engineering from the Facultad de Ciencias Matemáticas, Físico-Químicas y Naturales, Universidad del Litoral, Rosario, Argentina, his native country. In 1955 he received his M.S. degree and, in 1957, his Sc.D. degree in civil engineering from Massachusetts Institute of Technology. In 1958 he joined the Department of Civil Engineering at UC Berkeley, where, from 1988 to 1990, he was the Director of the Earthquake Engineering Research Center, and where for the past 46 years he has been carrying out numerous integrated analytical and experimental studies on seismic behavior of civil engineering facilities.

Dr. Bertero has developed comprehensive methods of seismic design of steel moment frames, steel braced frames, reinforced concrete (RC) frames, RC shear walls, and masonry structures. He conducted many pioneering research studies including: elastic and inelastic seismic structural response due to near-fault directivity pulses in the early 1970s; classic experimental work on cyclic behavior of beam-column steel and RC subassemblages; original experimental work on cyclic versus monotonically deformed behavior of RC moment resisting frames and shear walls; innovative study on the understanding and applications of energy-based methods in earthquake-resistant design and damage evaluation; and the development of conceptual framework and the design-objective matrix for performance-based earthquake engineering.

Professor Bertero has published more than 350 papers and reports on various issues in earthquake engineering and received numerous national and international awards for his teaching and original research efforts. In 1990 he was awarded the Berkeley Citation, UC's highest honor. Among several other awards in the USA, he received the ASCE Nathan Newmark Award (1991); ACI Arthur Anderson Award (1989); AISC T.R. Higgins Lectureship Award (1990); and EERI Housner Medal (1995). In 1990, *Engineering News Record* recognized him as the "Construction Man of the Year." His international awards and honors include: the Jai Krishna Award from the India Society of Earthquake Technology (1974); First International Gold Medal Eduardo Torroja from the CSIC, Spain (1989); appointment as the Extraordinary Chair of Javier Barrios Siera at the National University of Mexico (1986); appointment as Honorary Professor in seven universities in South American countries; Honorary Doctoral degrees including "Doctorado Honoris Causa en Ingeniería" from the University of Los Andes, Mérida, Venezuela (1993); and "CUYO" University, Mendoza, Argentina (1997).

Professor Bertero was elected to the Academy of Science of Argentina (1971); Academy of Engineers of Argentina (1989); and the U.S. National Academy of Engineering as Foreign Associate (1990). He is an Honorary Member of the American Concrete Institute (ACI), Fellow of the American Society of Civil Engineers (ASCE), Honorary Member of the Structural Engineers Association of Northern California, and has been a member of the Earthquake Engineering Research Institute (EERI) since 1969.

In 1971–72 Professor Bertero served as the chief technical advisor to the UNESCO Mission at the International Institute of Seismology and Earthquake Engineering, Tokyo. From 1972 to 1978 he served as a member of the Seismic Design Group on the development of comprehensive Seismic Code Provisions ATC 3-06. In 1977 he organized a workshop at UC Berkeley on Earthquake Resistant Reinforced Concrete Building Construction, sponsored by the National Science Foundation — he also edited the three-volume proceedings.

Dr. Bertero has inspected structural and nonstructural damage in numerous earthquakes, including the 1964 Alaska, 1967 Caracas (Venezuela), 1971 San Fernando (CA), 1972 Managua (Nicaragua), 1976 Guatemala, 1977 Caucete, San Juan (Argentina), 1979 Imperial Valley (CA), 1980 El Asnam (Algeria), 1983 Oga Peninsula (Japan); 1983 Coalinga (CA), 1985 Chile, 1985 Michoacan (Mexico), 1986 San

Salvador, 1987 Whittier Narrows (CA), 1988 Spitak (Armenia), 1989 Loma Prieta (CA), 1990 Luzon (Philippines), 1992 Erzincan (Turkey), 1992 Flores (Indonesia), 1994 Northridge (CA), and 1995 Kobe (Japan) earthquakes.

Professor Bertero has been a consultant on various seismic design projects worldwide. He is presently a member of the Seismic Technical Advisory Group for the City of Berkeley (CA). From 1988 to 1992 he was a member of the Advisory Committee to the United States Congress regarding the National Earthquake Hazards Reduction Program (NEHRP). From 1992 to 2000 he was a Director (representing the United States) of the International Association of Earthquake Engineering (IAEE). Professor Bertero is currently the honorary president of the Latin American Association of Seismic Engineering.

Professor Bertero's contributions to earthquake engineering have also included training, advising and mentoring numerous graduate students, postdoctoral fellows and research associates, many of whom are now well-known experts in earthquake engineering. Eleven of the contributors to this book are his former graduate students and research associates. He recently stated, "Nothing is more rewarding than witnessing the success of former students and research associates."

Contributors

Raul D. Bertero

Departamento de Estabilidad
Universidad de Buenos Aires
Buenos Aires, Argentina

Vitelmo V. Bertero

Department of Civil and
Environmental Engineering
University of California
Berkeley, California

Bruce A. Bolt

Department of Earth and
Planetary Science
University of California
Berkeley, California

Yousef Bozorgnia

Pacific Earthquake Engineering
Research Center (PEER)
University of California
Berkeley, California

Kenneth W. Campbell

EQECAT, Inc.
Beaverton, Oregon

Kelly E. Cobeen

Cobeen & Associates Structural
Engineering
Lafayette, California

Michael C. Constantinou

Department of Civil, Structural
and Environmental
Engineering
University at Buffalo
State University of New York
Buffalo, New York

Gregory L. Fenves

Department of Civil and
Environmental Engineering
University of California
Berkeley, California

Filip C. Filippou

Department of Civil and
Environmental Engineering

University of California
Berkeley, California

Luis E. Garcia

Department of Civil and
Environmental Engineering
Universidad de los Andes
Bogotá, Colombia

Eldon M. Gath

Earth Consultants International
Tustin, California

Yihua Huang

Imbsen & Associates
Sacramento, California

James M. Kelly

Department of Civil and
Environmental Engineering
University of California
Berkeley, California

Richard E. Klingner

Department of Civil Engineering
University of Texas
Austin, Texas

Steven L. Kramer

Department of Civil and
Environmental Engineering
University of Washington
Seattle, Washington

Helmut Krawinkler

Department of Civil and
Environmental Engineering
Stanford University
Stanford, California

James O. Malley

Degenkolb Engineers
San Francisco, California

Eduardo Miranda

Department of Civil and
Environmental Engineering
Stanford University
Stanford, California

Kevin Moore

Certus Consulting, Inc.
Oakland, California

Masayoshi Nakashima

Disaster Prevention Research
Institute
Kyoto University
Kyoto, Japan

Mete A. Sozen

School of Civil Engineering
Purdue University
West Lafayette, Indiana

Jonathan P. Stewart

Department of Civil and
Environmental Engineering
University of California
Los Angeles, California

Chia-Ming Uang

Department of Structural
Engineering
University of California, San Diego
La Jolla, California

Roberto Villaverde

Department of Civil and
Environmental Engineering
University of California
Irvine, California

Akira Wada

Structural Engineering Research
Center
Tokyo Institute of Technology
Yokohama, Japan

Yi-Kwei Wen

Department of Civil and
Environmental Engineering
University of Illinois
Urbana, Illinois

Andrew S. Whittaker

Department of Civil, Structural
and Environmental
Engineering
University at Buffalo
State University of New York
Buffalo, New York

Robert S. Yeats

Earth Consultants International
Corvallis, Oregon

Qi-Song “Kent” Yu

Degenkolb Engineers
Portland, Oregon

Contents

1	The Early Years of Earthquake Engineering and Its Modern Goal	1-1
	<i>Vitelmo V. Bertero and Yousef Bozorgnia</i>	
2	Engineering Seismology	2-1
	<i>Bruce A. Bolt</i>	
3	The Role of Geology in Seismic Hazard Mitigation	3-1
	<i>Robert S. Yeats and Eldon M. Gath</i>	
4	Geotechnical Aspects of Seismic Hazards.....	4-1
	<i>Steven L. Kramer and Jonathan P. Stewart</i>	
5	Engineering Characterization of Ground Motion.....	5-1
	<i>Yousef Bozorgnia and Kenneth W. Campbell</i>	
6	Methods of Analysis for Earthquake-Resistant Structures	6-1
	<i>Filip C. Filippou and Gregory L. Fenves</i>	
7	Probabilistic Aspects of Earthquake Engineering	7-1
	<i>Y.K. Wen</i>	
8	Performance-Based Seismic Engineering: Development and Application of a Comprehensive Conceptual Approach to the Design of Buildings	8-1
	<i>Raul D. Bertero and Vitelmo V. Bertero</i>	
9	Performance-Based Earthquake Engineering	9-1
	<i>Helmut Krawinkler and Eduardo Miranda</i>	
10	Innovative Strategies in Earthquake Engineering	10-1
	<i>Akira Wada, Yihua Huang, and Vitelmo V. Bertero</i>	
11	Seismic Isolation	11-1
	<i>James M. Kelly</i>	
12	Seismic Energy Dissipation Systems for Buildings	12-1
	<i>Andrew Whittaker and Michael Constantinou</i>	
13	Seismic Behavior of Reinforced Concrete Buildings	13-1
	<i>Mete Sozen</i>	
14	Earthquake-Resistant Design of Reinforced Concrete Buildings.....	14-1
	<i>Luis E. Garcia and Mete A. Sozen</i>	
15	Seismic Design of Steel Moment-Resisting Frames.....	15-1
	<i>James Malley, Qi-Song "Kent" Yu, and Kevin Moore</i>	

16	Steel Buckling-Restrained Braced Frames	16-1
	<i>Chia-Ming Uang and Masayoshi Nakashima</i>	
17	Seismic Behavior and Design of Masonry.....	17-1
	<i>Richard E. Klingner</i>	
18	Recent Developments in the Seismic Design and Construction of Woodframe Buildings	18-1
	<i>Kelly E. Cobeen</i>	
19	Seismic Analysis and Design of Nonstructural Elements	19-1
	<i>Roberto Villaverde</i>	

1

The Early Years of Earthquake Engineering and Its Modern Goal

1.1	Introduction.....	1-1
1.2	Birth and Growth of EE in the Early Years	1-1
	Events in the Late 19th Century and the 1906 San Francisco Earthquake and Its Aftermath • 1908 Messina (Italy) and 1923 Kanto (Japan) Earthquakes • 1925 to 1933 • The 1933 Long Beach Earthquake and Its Aftermath • Progress in Formulating Building Codes: 1933 to 1959 • Establishment of the Earthquake Engineering Research Institute (EERI) • Historical Conferences in 1952 and 1956 • Applications of Structural Dynamics to EE, Before 1960 • Establishment of the International Association for Earthquake Engineering, 1960 • Further Readings about the Early Years of EE in the United States	
1.3	The Evolution of EE Since 1960	1-10
	The Evolution of EE's Definition and Goal • The Nature of Earthquake Problems, Disaster and Preparedness • Definition, Assessment and Control of Seismic Risk • Multidisciplinary Nature of EE	
1.4	Recent Events, Developments and Future Challenges of EE	1-12
1.5	Closing Remarks	1-14

Vitelmo V. Bertero

Yousef Bozorgnia

1.1 Introduction

This chapter presents an overview of the early years of what presently is called earthquake engineering (EE), especially in the United States. Major events contributing to the growth of EE until 1960 are briefly discussed. We then trace the evolution of the definition of EE and its goal to the present time. The nature of the earthquake problem, the factors that can create an earthquake disaster and the importance of earthquake preparedness are then briefly discussed. The next section includes a summary list of major events, developments and advances since 1960, as well as a brief discussion of future challenges of EE. The final section offers some closing remarks.

1.2 Birth and Growth of EE in the Early Years

This section covers a brief history of EE until 1960, particularly in the United States. A complete history of EE is beyond the scope of this chapter due to space and scope constraints; hence, only selective events

and people integral to EE's early development are discussed. It is not possible to give even a brief overview of EE in the United States without mentioning critical developments in other countries. Therefore, only some major relevant developments are summarized.

According to Hudson (1992), EE is at once a very old and a very new subject. If EE is considered as just the conscious attempts made to improve the earthquake resistance of man-made structures, then it is an old subject, as testified by a 3000-year history of earthquakes in China. If, on the other hand, it is considered as the results of scientifically based multidisciplinary efforts, then it is a relatively new subject. Throughout this chapter, this modern scientific aspect of EE has been kept in mind and emphasized.

As many authors have indicated (e.g., Housner, 1984; Usami, 1988; Hudson, 1992) it is difficult to establish a precise date that EE, in its modern definition, started. However, different time periods of major events and activities related to earthquake investigations, earthquake-resistant design (EQ-RD), and earthquake preparedness have been identified, and a brief discussion is presented here.

1.2.1 Events in the Late 19th Century, and the 1906 San Francisco Earthquake and Its Aftermath

During the late 19th and early 20th centuries, interest in earthquakes and their effects increased in Japan, Italy and the United States (particularly California) (Freeman, 1932; Housner, 1984; Usami, 1988; Hudson, 1992; Elnashai, 2002). This was mainly a consequence of major earthquakes such as: in Japan, the 1855 Edo (Usami, 1988); 1891 Mino-Awari (Housner, 1984) and 1923 Kanto earthquakes; in the United States, the 1906 in San Francisco, California and in Italy, the 1908 Messina.

According to Hu et al. (1996):

Earthquake engineering started at the end of the 19th century when some European engineers suggested designing structures with a few percent of the weight of the structure as the horizontal load. This idea of seismic design was taken up and developed in Japan at the beginning of the 20th century.

Usami (1988) stated:

In the case of Japan, I personally think that the professional practice of earthquake engineering began after a severely damaging earthquake that struck Tokyo (which was then called Edo) in 1855. In the following year, a pamphlet entitled Methods of Fire Prevention, With Illustrations, outlining specific and practical methods for greatly improving the shear-bearing capacity of wooden houses through triangular cross bracing, was published.

Furthermore, Usami (1988) also indicated:

In 1914, Sano, a Japanese engineer, developed a quasi-dynamic theory, which we now call the seismic coefficient method, for designing earthquake resistant wood, brick, reinforced concrete, and steel structures. Sano's work, which was published in a paper entitled Methods for Designing Earthquake Resistant Houses, marked the beginning of quantitative work in earthquake engineering in Japan.

As Housner (1984), Bolt (1996 and Chapter 2 of this book) and Elnashai (2002) have indicated, in the 19th century a number of English engineers became interested in earthquakes and contributed significantly to earthquake knowledge. They included Robert Mallet (a civil engineer), John Milne (a mining engineer) and James Ewing and Thomas Gray (both mechanical engineers). In fact, Robert Mallet invented the word seismology, which is derived from Greek words meaning shake-knowledge; he also coined the term epicenter (Housner, 1984). According to Housner (1984), "Robert Mallet can be called the primeval earthquake engineer."

On April 18, 1906 a major earthquake (M_w 7.9) struck San Francisco and northern California. More than 430 km of the San Andreas Fault was ruptured during this earthquake, which caused considerable damage in San Francisco (see Figure 1.1) and northern California. As pointed out by Housner (1984),



FIGURE 1.1 The 1906 San Francisco earthquake — damaged San Francisco City Hall, looking north from Larkin and Grove streets toward City Hall (behind Majestic Theatre). Photo from Steinbrugge Collection, National Information Service for Earthquake Engineering of the University of California, Berkeley.

although the earthquake received worldwide attention and the damage was extensive, this did not shock engineers into developing earthquake engineering. According to Geschwind (1996), although engineers learned explicit lessons from the 1906 earthquake, for the most part these lessons did not concern the need for more earthquake-resistant construction. Instead, many engineers referred to the need for greater fire prevention and for the use of reinforced concrete as a building material — both of which were the subjects of vigorous campaigns that had long occupied the attention of engineers. There were, however, some engineers who made suggestions beyond general recommendations about better protection against earthquake-induced fire. The most vocal of them was Charles Derleth, Jr., a professor of structural engineering at the University of California (Geschwind, 1996). Derleth repeatedly emphasized the importance of good materials, high grade workmanship, and intelligent design and gave specific examples (Geschwind, 1996). However, Derleth did not see any practical value for attempting to calculate earthquake-induced stresses, as he stated in his 1907 American Society of Civil Engineers (ASCE) paper (Derleth, 1907): “An attempt to calculate earthquake stress is futile. Such calculations could lead to no practical conclusions of value” (Housner, 1984).

As a consequence of the 1906 San Francisco earthquake, the Seismological Society of America (SSA) was established in October 1906, and the Structural Association of San Francisco in June 1906. Nearly a century later, the SSA is still a very active prominent organization dealing with various earthquake issues. The meetings of the Structural Association of San Francisco were mainly concerned with improving fire protection, and the association faded out of existence in December 1906 (Geschwind, 1996).

Also as a result of the 1906 earthquake, a State Earthquake Investigation Commission was formed. The commission produced two volumes of reports. The first, published in 1908, included detailed suggestions on proper construction of wooden houses and occasional advice on how buildings might be strengthened against earthquake. The second volume, published in 1910, contained a theoretical discussion of the 1906 earthquake, in which H.F. Reid (1910) presented the elastic-rebound theory of earthquakes.

1.2.2 1908 Messina (Italy) and 1923 Kanto (Japan) Earthquakes

On December 28, 1908, a large earthquake (magnitude 7.5) devastated the city of Messina (Italy) with a loss of 83,000—to 120,000 lives. A special commission was formed by the government to investigate the earthquake and to provide recommendations. According to Housner (1984), this earthquake was



FIGURE 1.2 The 1925 Santa Barbara earthquake — damaged Hotel California. Photo from Steinbrugge Collection, National Information Service for Earthquake Engineering of the University of California, Berkeley.

responsible for the birth of practical earthquake design of structures, and the commission's report appears to be the first engineering recommendation for earthquake-resistant structures by means of the equivalent static method. The method, apparently proposed by Prof. Panetti, recommended designing the first story to withstand a horizontal force equal to 1/12 the building weight above, and the second and third stories to be designed to withstand a horizontal force equal to 1/8 of the building weight above. Gradually the equivalent static method was used in earthquake countries around the world and was later adopted by building codes. For example, in the late 1920s, the method was applied by Prof. Martel of the California Institute of Technology (Caltech) in the design of a 12-story steel frame building in Los Angeles (Housner, 1984).

Fifteen years later, on September 1, 1935, the magnitude 8.3 Kanto (Japan) earthquake caused severe damages in Tokyo and Yokohama. This earthquake also contributed significantly to the progress of earthquake knowledge in Japan, including the establishment of the Earthquake Research Institute. The institute was at the Imperial College of Tokyo and was headed by Prof. Kyoji Suyehiro. According to Freeman (1932) and Hudson (1992), from its inception the Earthquake Research Institute was devoted not only to basic scientific work in seismology and geophysics, but also to studies directly relevant to EE. Suyehiro was convinced of the importance of the direct measurement of ground acceleration in epicentral areas and it was his efforts that stimulated the development of the strong motion accelerograph. As early as the 1920s, Dr. Suyehiro clearly outlined the type of accelerographs that would be needed (Hudson, 1963).

1.2.3 1925 to 1933

On June 29, 1925 an earthquake of magnitude 6.2 occurred in Santa Barbara, California. Although the number of deaths was small (12 to 14 persons), the damage was considerable (see Figure 1.2). This earthquake led to considerable increase in interest in earthquakes and earthquake preparedness, and according to Steinbrugge (1970), a comparatively large number of reports were published on this earthquake. As a consequence of the Santa Barbara earthquake, the Santa Barbara City Council on December 17, 1925 passed a new building code with a clause requiring buildings to be designed to withstand horizontal forces produced by either earthquakes or wind (Geschwind, 1996).

The 1925 Santa Barbara earthquake led to numerous important activities related to earthquake investigation and earthquake preparedness. Binder (1952) pointed out that the year 1925, in my opinion, marks the real beginning of earthquake engineering studies and research in the United States.

After the 1925 Santa Barbara earthquake, among the people who greatly contributed to the promotion of earthquake preparedness in California was Bailey Willis, a professor emeritus of geology at Stanford University. His idea of initiating a laboratory to do research on earthquake matters at Stanford was one of his numerous professional contributions (Freeman, 1932; Blume, 1972; Geschwind, 1996). Willis insisted on and successfully raised the funds for a shaking table (Geschwind, 1996), which was built in 1927, with Professor Lydik Jacobsen, of the mechanical engineering department at Stanford, in charge. Blume (1972) summarized the experiments carried out by Jacobsen and his associates on the shaking table. For example, a model of a high-rise building was tested from 1930 to 1931 and later Blume and Jacobsen designed a model of the Alexander building in San Francisco. The model was built by Blume in 1934 and tested up to 1937.

Building periods measurements in the United States were pioneered as early as 1912 by Elmer Hall (1912), an associate professor of physics at the University of California at Berkeley (Blume, 1972). Japanese scientists had previously measured wind-induced building motions but no one had measured motions induced by traffic and other minor disturbances. Hall's instrument was used to measure motion in six buildings in San Francisco. In 1931, Byerly et al. (1931) resumed building period measurements in the United States using the same instrument.

Another important earthquake related scientific activity in the United States was in 1927 when earthquakes were recorded by the southern California regional seismographic network, where seismologist Harry Wood was in charge. Wood and Richter (a Caltech graduate in physics) processed the vast amount of data produced by the seismographs (Geschwind, 1996). In the early 1930s, Richter devised a numerical scale for grading instrumentally recorded earthquakes — the Richter magnitude scale (Richter, 1935).

In 1929, Professor R.R. Martel (of Caltech) and John R. Freeman (an insurance executive with a very strong commitment to earthquake preparedness) attended the 1929 World Engineering Congress in Tokyo. They met prominent engineers and scientists, including Professor K. Suyehiro, head of the Earthquake Research Institute, who, in 1926, invented, constructed and used his vibration analyzer. Later, in 1931 Freeman arranged for Professor Suyehiro to come to the United States to give a series of earthquake lectures (Housner, 1997). Suyehiro gave lectures at the University of California at Berkeley, Stanford University, Caltech, and MIT (Suyehiro, 1932). He also gave informal talks covering some Japanese earthquake research at other locations (Freeman, 1932).

In the United States, Freeman followed up Suyehiro's ideas; these efforts culminated in 1931 in an allocation from the U.S. Congress to the U.S. Coast and Geodetic Survey (USCGS) for development of suitable accelerographs (Hudson, 1963). The USCGS developed several prototype instruments for recording strong ground motion. The first such instruments were deployed in late 1932 in selected buildings in the Los Angeles and San Francisco areas. The first significant recordings were obtained less than a year later when, on March 10, 1933, the Long Beach earthquake (magnitude 6.4) struck the Los Angeles area. According to Housner (1984), "This was a most important step in the development of earthquake engineering. For the first time engineers could see the nature of strong ground shaking."

In the early days, John R. Freeman contributed significantly to the evolution of EE and to promoting earthquake preparedness. In 1925, Freeman became interested in earthquake safety and preparedness and was instrumental in inviting Suyehiro to the United States, paying for his travel and to have his lectures published by the ASCE. As mentioned before, Freeman was also very instrumental in the initiation of a program for strong motion earthquake instrumentation in the United States. He talked to the Secretary of Commerce, who was a graduate civil engineer, and convinced him of the importance of earthquake instrumentation (Housner, 1997). In 1932, Freeman published a book titled *Earthquake Damage and Earthquake Insurance* (Freeman, 1932), about which Hudson (1992) stated, "This monumental work not only includes just about everything known about earthquakes at that time, but it is the nearest thing we have in print to a history of earthquake engineering." Similarly, Housner (1983) stated, "I think that the original accelerograph should have been called the Freeman accelerograph in recognition of the big contribution that he made." Housner (1983) also stated: "I should like to talk today about the founding father of the strong ground motion program in the United States — John R. Freeman."



FIGURE 1.3 The 1933 Long Beach, California, earthquake — damaged Jefferson Junior High School. Photo from Steinbrugge Collection, National Information Service for Earthquake Engineering of the University of California, Berkeley.

In his 1932 book, Freeman pointed out many interesting observations about earthquake damage. One of his observations was “that the present state of the art may leave the underwriter of earthquake insurance carrying an unexpectedly large share of the burden of chance, in percent of damage to sound value, on some of these extremely tall American buildings, not because of collapse, but because of damage to the interior finish.”

1.2.3.1 Establishment of the Structural Engineers Associations in Southern and Northern California

In 1929, the Structural Engineers of Southern California was formed and the Structural Engineers of Northern California was founded a year later. Throughout the early 1930s, Prof. Jacobsen repeatedly talked about his shaking table experiments at association meetings, showing how the buildings models responded to horizontal shaking (Geschwind, 1996).

1.2.3.2 Initiation of the Uniform Building Code

The weakness of construction revealed by the 1925 Santa Barbara earthquake caused much motivation in several communities and among engineers, architects, underwriters, property owners, bankers and others toward creating better building laws (Freeman, 1932). As a consequence, in 1927, with the cooperation of many engineers and architects, the Pacific Coast Building Officials Conference adopted the Uniform Building Code (UBC). The provisions required that the building should be designed for a lateral force applied at each floor and roof level as a constant percentage (7.5 to 10%) of the total dead plus live loads of the building above the plane. Although the 1927 UBC provisions were not adopted by some of the larger California cities (Freeman, 1932), the concept of using a constant coefficient to estimate the lateral force for seismic design continued to appear in the next editions of UBC (see Table 1.1).

1.2.4 The 1933 Long Beach Earthquake and Its Aftermath

This earthquake occurred on March 10, 1933 at 5:54 PM. It had a magnitude 6.2 to 6.3 with the epicenter about 15 miles from downtown Long Beach (Steinbrugge, 1970). Because it struck in a more densely populated region than the 1925 Santa Barbara earthquake, this earthquake caused considerably more damage (Geschwind, 1996). It destroyed many buildings in the area, including school buildings (see e.g., Figure 1.3). As Geschwind, (1996) indicated, in the city of Long Beach, 15 of the 35 schools were completely destroyed, and some schools in the city of Los Angeles were also damaged. If the earthquake

had struck several hours earlier, many children may have been killed. As a result, scientists and engineers moved quickly to disseminate their views about the earthquake and earthquake preparedness. Caltech researchers John Budwala, Harry Wood and R.R. Martel were among them.

Perhaps the most influential report about the Long Beach earthquake was from a committee chaired by Robert Milikan. The Milikan report reviewed the damage and concluded that at some time in the future an earthquake of major intensity will occur in this region, and unless existing evils are corrected by adequate protection against earthquakes, disaster must follow (Geschwind, 1996).

This earthquake was a major turning point in the field of earthquake-resistant design (EQ-RD) and construction in California. As pointed out by Binder and Wheeler (1960), the first mandatory seismic codes used to any extent in the United States were published in 1933 following the Long Beach earthquake. Also, as a consequence of the earthquake, two California State laws were passed: (a) the Field Act, which authorized the State Division of Architecture to approve or review all public school plans and specifications and to furnish general supervision of the construction work; and (b) the Riley Act, which made provisions for EQ-RD and construction for more general applications than the Field Act. The strong motion recordings obtained during the 1933 Long Beach earthquake are among the most significant events in the field of EE not only in California but also around the world. Another major development in EE during this time period was the development of the concept of *response spectra* (see Chapter 5), introduced by Maurice Biot, who received his Ph.D. in 1932 under the supervision of Prof. Martel at Caltech (Biot, 1933, 1934, 1941) and expanded by George Housner, who also received his Ph.D. under Prof. Martel's tutelage (in 1941). It should be noted that the concept of response spectra was not used in a specific way in building codes until 1952 (see Table 1.1).

1.2.5 Progress in Formulating Building Codes: 1933 to 1959

The use of a constant coefficient C in the design base shear for buildings, $V = CW$, was adopted in the appendix of the 1927 UBC and in the local codes until 1943.

In 1937 Los Angeles County sponsored an investigation to be conducted by Caltech in collaboration with Stanford University and U.S. Coast and Geodetic Survey to determine improvements in seismic requirements of the Los Angeles Building Code (LABC) (Binder, 1952). These studies indicated that the design requirements of a constant lateral force coefficient did not provide a uniform degree of earthquake protection throughout the varying heights of all buildings. The report emphasized replacing a constant factor with one based on equivalent acceleration that would take into account some important dynamic considerations (Binder, 1952). Thus, building flexibility associated with number of stories was introduced (see Table 1.1). Some of the findings were adopted into the LABC in January 1943 (see Table 1.1). Interestingly, as a result, the 1946 edition of the UBC was basically the same as the 1943 LABC (Binder and Wheeler, 1960).

In 1947, San Francisco adopted a seismic code, also using a variable coefficient C in the design base shear equation, but with a different definition for C.

In 1948, a joint committee of the San Francisco Section of the ASCE and the Structural Engineers Association of Northern California (SEAONC) began a study of EQ-RD (Binder, 1952). The committee published its recommendations in 1952 under Lateral Forces of Earthquake and Wind. For the first time (20 years after the development of the concept of response spectra, period of vibration T of the building was introduced as a means of determining the base shear coefficient C (Blume et al., 1961).

The next major step in the evolution of earthquake codes in California was taken in 1957 by the Seismology Committee of the Structural Engineers Association of California (SEAOC). According to Binder and Wheeler (1960), the committee members of the Central, Northern and Southern Associations of SEAOC worked for 2 years to develop a uniform code to resolve the differences in several codes used in seismic areas of the United States and California. The committee adopted as one of its objectives the development of a seismic code that would confine its provisions to limiting the extent and type of property damage that endanger health and safety (Binder and Wheeler, 1960). It was also agreed that a commentary on the code known as a *Manual of Practice* should complement it. The foreword of this manual includes

the following statement: “The ‘Recommended Lateral Force Requirements’ are not intended to be applied as a substitute for sound engineering judgment” (Binder and Wheeler, 1960).

To consider the inherent ductility and energy dissipation capacities of different structures, a coefficient K was introduced in the base shear equation $V = KCW$, where K values were specified for four types of building construction. According to Blume et al. (1961): “The introduction of K was a major step forward in code writing to provide in some degree for the real substance of the problem — energy absorption — and for the first time to recognize that equivalent acceleration or base shear coefficient C alone is not necessarily a direct index of earthquake resistance and public safety.”

Major changes in seismic codes and provisions have occurred throughout the history of EE. A summary of the key changes in these provisions before 1960 is provided in Table 1.1.

TABLE 1.1 Major Changes in the United States Seismic Design Code (Before 1960)

Date	Code or Provisions
1927	First seismic design appendix in UBC: $V = CW$ ($C = 0.075$ to 0.10)
1933	Los Angeles City Code: $V = CW$ ($C = 0.08$). First enforced seismic code
1943	Los Angeles City Code: $V = CW$ ($C = 60 / (N+4.5)$), $N > 13$ stories
1952	ASCE-SEAONC: $C = K_1 / T_1$ ($K_1 = 0.015$ to 0.025)
1959	SEAOC: $C = KCW$ ($C = 0.05 / (T^{1/3})$)

1.2.6 Establishment of the Earthquake Engineering Research Institute (EERI)

The origin of the EERI can be traced back to the Advisory Committee on Engineering Seismology (ACES). This Committee was formed in 1947 by a small group of individuals in San Francisco to advise the U.S. government on earthquake issues such as strong motion instrumentation (Blume, 1994). The ACES elected Lydik Jacobsen as the chairman, Col. William Fox vice chairman and John Blume as the permanent secretary. Other members of the ACES included R.R. Martel and George Housner. Out of frustration with lack of accomplishment and funding from the government, ACES members formed a nonprofit organization in 1949 and called it the Earthquake Engineering Research Institute (EERI). Perhaps this was the first time the name earthquake engineering was used, at least officially. In the first meeting of the EERI in San Francisco on April 2, 1949, Jacobsen was elected as the president, Housner vice president, Blume secretary and Frank Ulrich treasurer. Blume served as secretary until 1952, when Ray Clough, then a young professor at Berkeley, assumed the office (Blume, 1994). For many years, until 1973, membership in the EERI was by invitation only (Blume, 1994). Today, EERI members are from all over the world. Since its establishment, EERI has contributed significantly toward accomplishment of the modern goal of EE. Only a few years after its formation, the EERI sponsored two historically important EE conferences, as described in the next section.

1.2.7 Historical Conferences in 1952 and 1956

The Symposium on Earthquake and Blast Effects on Structures was held in 1952 at the University of California at Los Angeles (UCLA). C. Martin Duke, a professor at UCLA, chaired the EERI committee that organized the conference. Referring to the symposium’s title, Housner (1997) explained, “We felt there were not enough people interested in earthquake engineering alone to have a successful conference. So we decided to add the topic of bomb blast on structures, which had been an active research field during the war and for some years afterward.” The symposium was a successful event and “it was clear there was a great deal of interest in earthquake engineering” (Housner, 1997). The symposium’s proceedings, published in 1952, stated “it was the first time anyone had gotten out a proceedings on earthquake engineering” (Housner, 1997).

The other important conference was the World Conference on EE (WCEE) (later called the First WCEE), held in 1956 at Berkeley, California. The conference was sponsored by both the EERI and University of California at Berkeley (UCB). John Rinne, a well-known structural engineer and EERI board member from the San Francisco Bay area, suggested the idea and EERI approved (Housner, 1997). The conference was held on the 50th anniversary of the 1906 San Francisco earthquake and brought together researchers and practicing engineers from around the world. However, the organizers of the conference had great difficulty in identifying individuals (especially engineers) in the seismic regions of the world who should be invited to participate. One possible reason for this difficulty was that the name earthquake engineering had almost no national or international recognition, even though the EERI had been in existence for 4 years (Clough, 1992).

The second WCEE was held in Japan in 1960 and since then World Conferences held every four years have successfully brought together many EE researchers, practitioners and public officials. One can follow the trace of growth, advances and developments of EE by following the milestones of the WCEEs (Hudson, 1988).

1.2.8 Applications of Structural Dynamics to EE, Before 1960

As mentioned before, research on bomb blast effects on structures and structural dynamics analyzing the response of structures to such an excitation (loading), as well as for their practical design, was active during and after the World War II. English language books on structural analysis and design for dynamic loads induced by earthquake ground motions started to be published in 1950s. For example, *Structural Design for Dynamic Loads* by Norris et al. (1959), which grew out of a short course taught at MIT during the summer of 1956, pioneered structural design against blast, earthquake ground motions, moving traffic loads and wind load. Since 1960, with the growing interest in earthquake effects and seismic design, numerous books on structural dynamics with applications to analysis and design for blast, earthquake, wind and other dynamic loads, as well as books on EQ-RD have been published. Finally, starting the late 1960s, books on just EE started to be published. For example, books by Borges and Ravara (1969) and Wiegel (1970) can be mentioned here.

1.2.9 Establishment of the International Association for Earthquake Engineering, 1960

Following Prof. Kiyoshi Muto's initial suggestion to Prof. Housner, the International Association for Earthquake Engineering (IAEE) was recommended to be established in 1960 during the second WCEE in Japan (Housner, 1997). The formation of IAEE was a very important development in EE, especially for the countries that did not have their own national earthquake association. Today, many earthquake countries have national associations and are members of the IAEE. Later, in 1972 the journal *Earthquake Engineering and Structural Dynamics* (EESD) was established as the official journal of the IAEE. The EESD was initiated as an international journal to improve international communication in the rapidly growing field of EE and structural dynamics, and also with the hope that it would provide the much needed medium of communication between research workers and practicing engineers (Clough, 1972).

1.2.10 Further Readings about the Early Years of EE in the United States

Readers interested in the history of EE and its developments in the early years, especially in the United States, are encouraged to read excellent publications on this subject, including those by: Freeman (1932), Geschwind (1996), Housner (1983, 1984), Hudson (1988, 1992), Bolt (1996), Roessel and Yao (2002) Elnashai (2002) and Lee et al. (2003). There is also an excellent compilation of oral histories published by EERI that shed light on the early years of EE and the role of its pioneers (see, e.g., Blume, 1994; Degenkolb, 1994; Rinne, 1996; Housner, 1997; Moore, 1998; Popov, 2002; Allen, 2002, among others).

1.3 The Evolution of EE Since 1960

This section presents the evolution of the definition of EE and its goal; discussion of the nature of earthquake problems and the factors that can create an earthquake disaster; earthquake disasters and the importance of preparedness; definition, assessment and the steps involved in controlling seismic risk; and the multidisciplinary nature of EE.

1.3.1 The Evolution of EE's Definition and Goal

The following individuals, among others, have provided definitions for EE:

Okamoto (1973) — “In earthquake engineering a wide range of knowledge that includes geophysics, geology, seismology, vibration theory, structural dynamics, materials dynamics, structural engineering and construction techniques are necessary. More specifically, earthquake engineering is the application of this knowledge to the single objective of building structures that are safe against earthquakes.” From this definition, it is evident that at least until the early 1970s, the main objective and goal of EE was to design and construct structures that could withstand earthquakes and avoid loss of lives. However, performance and cost of the repairs and rehabilitation of existing structural, nonstructural and lifeline systems in various recent earthquakes worldwide have demanded a revised definition of EE.

Housner (1984) — “Earthquake engineering broadly encompasses all non-technical, as well as technical efforts directed toward minimizing the harmful effects of earthquakes.” It is important to note that *nontechnical* issues are also part of this definition. The harmful effects include life safety issues, as well as social, economical and other consequences.

Hudson (1988) — “The subject of earthquake engineering has rapidly evolved from this state of being an experience-based study of past earthquake effects, to its present position as a science-based engineering discipline with an organized body of knowledge, a research program to add to that knowledge, and a working interaction with the basic sciences of geophysics and seismology on the one hand and with the practicing design and construction of engineering works on the other.”

Clough (1992) — “Earthquake engineering is a scientific discipline dedicated to providing at reasonable cost an acceptable level of seismic safety in the design of buildings, lifeline systems, and other special structures.”

Davidovici (1992) — “The aim of earthquake engineering is to define efficient measures against the possible effects of earthquakes. The first aim is to protect life and limb, but the reduction of economic loss is an issue of ever growing importance.”

Hudson (1992) — “Earthquake engineering embraces a very wide range of activities — social, economic, political, scientific and technical. All these aspects contribute to the overall goal of earthquake engineering — to prevent earthquakes from becoming disasters.” It is noted that an earthquake can become a disaster in various respects, such as: loss of human life, financial disaster, disruption of normal life for an extended period of time, among others.

Bertero (1992) — “Earthquake engineering is the branch of engineering that encompasses the practical efforts to reduce, and ideally to avoid, earthquake hazards.” On the basis of the above definitions and the evolution of EE, we propose the following definition:

Earthquake engineering encompasses multidisciplinary efforts from various branches of science and engineering¹ with the goal of controlling the seismic risks to socio-economically acceptable levels.

According to this definition, depending on their social and economical significances, not only life-safety risk but also other risks including financial and health should be controlled.

¹The *American Heritage Dictionary* defines engineering as the application of scientific and mathematical principles to practical ends such as the design, construction, and operation, of efficient and economical structures, equipment, and systems.

1.3.2 Nature of Earthquake Problems, Disaster and Preparedness

Many researchers have discussed the nature of the earthquake problem and particularly the resultant damages. For example, Press (1984) stated, "Earthquakes are a very special type of natural hazard in the sense that they are very rare, low-probability events, whose consequences, when they do occur, are very large in terms of destruction and suffering." A significant feature of earthquake damage is that most of the human and economic losses are not due to the earthquake mechanisms, but are due to failures of human-made facilities such as buildings and lifelines (dams, bridges, transportation systems, etc.), which were supposedly designed and constructed for the comfort of human beings. This means, in principle and in the long term, human beings have the ability to solve the earthquake problem. Given sufficient resources for research and development (R&D), education, training, practical implementation of the R&D results and formulation and implementation of comprehensive earthquake preparedness programs, it would be within our reach to learn where not to build, where and how to build facilities with failure risks at a socio-economically acceptable level and therefore prevent an earthquake disaster.

An unfortunate combination of the following factors can create an earthquake disaster:

- Severity of the earthquake ground motion (EQGM). This depends on, among other factors, the earthquake magnitude, source-to-site distance, direction of fault rupture propagation, local site conditions and depth to basement rock.
- The size and distribution of the population and economic developments.
- The degree of earthquake preparedness, including comprehensive earthquake risk mitigation programs and their implementation.

Undoubtedly, there has been an impressive increase in earthquake engineering knowledge since 1925, which is manifested in great successes in achieving life safety where earthquakes occur. However, in terms of financial loss, for example, if today we were asked, How effective has this increase in knowledge been in *reducing the seismic risks in our urban areas to socio-economically acceptable levels?* we would have to admit that we have not yet fully achieved that main goal of EE (see, e.g., Bertero, 1992, 1996, 1997). As Scawthorn (2003) stated: economic and insured losses from all sources are increasing.

Earthquake preparedness should be emphasized here. The poorer the preparedness, the greater will be the disaster. To prevent an earthquake from becoming a disaster, it is essential to have a comprehensive earthquake risk reduction program and proper efforts to implement the program.

As Hu et al. (1996) stated: it is important to realize that the level of earthquake protection through engineering means is limited by a city's or nation's economic capacity. A high level of engineering protection requires high economic investment

To summarize: earthquakes are inevitable, but the cause of loss of life, injuries and other social and economical losses, is the interaction of the EQGMs with the built environment, thus, we need to control the built environment to reduce seismic risks in our urban and rural areas to socio-economically acceptable levels — indeed, this should be the main goal of EE.

1.3.3 Definition, Assessment and Control of Seismic Risk

According to the glossary of the EERI Committee on Seismic Risk (1984), seismic risk is "the probability that social or economic consequences of earthquakes will equal or exceed specified values at a site, at various sites or in an area during a specified exposure time."

As discussed by Bertero (1992, 1997, 2002), assessing and controlling seismic risk at any given site requires at least the following:

1. Estimating the seismic activity at the site. This requires identification of all seismic sources.
2. Predicting EQGMs (preferably all six components) that could significantly contribute to the seismic risk.

3. Evaluating whether the EQGMs could induce (besides direct significant vibratory motions to the entire facility system) any of the following potential hazards at the site or the surrounding region: surface fault ruptures, tsunamis, seiches, landslides and floods.
4. Predicting whether the predicted EQGMs could induce ground failure, that is, liquefaction, settlement, subsidence, differential compaction, loss of bearing and shearing strength and lateral spreading.
5. Assessing the performance of the facility system under the direct and indirect effects of the predicted EQGMs and estimating the degree of damage and losses. This includes evaluating the serviceability, operability, life safety, near-collapse and collapse performance levels under different levels of earthquake hazards that the facility could undergo during its expected service life and economic consequences and other socio-economical impacts on the community.
6. Evaluating the possibility of the following incidents: fire, flood, release of hazardous materials, environmental impact and other consequences that could affect the built environment.
7. Conducting a cost–benefit analysis of seismic upgrading and replacing existing hazardous facilities.

From the analysis of the above requirements, the complexities of the problems of assessing and controlling seismic risks become clear.

1.3.4 Multidisciplinary Nature of EE

The modern goal of EE is to control the seismic risks to socio-economically acceptable levels. So how do we achieve this goal? The problem of seismic risk reduction cannot be solved just by acquiring knowledge through research. Research must be accompanied by the necessary technological developments and the implementation of the knowledge in practice. In addition to research, what is needed is a translation of current scientific, engineering and architectural know-how into reliable simplified options, which can address socio-political and economical concerns. This will require a multidisciplinary approach and a comprehensive educational program for owners, future users and all others involved in the implementation of the seismic risk reduction. There is a need for multidisciplinary groups of researchers, practicing professionals, users, owners, government officials, insurance industry representatives, and so forth, to develop and ensure the implementation of reliable and suitable policies and strategies that will help reduce and control seismic risks to socio-economically acceptable levels — the modern goal of earthquake engineering.

Evidently, reducing and controlling seismic risk is a complex problem, requiring the integration of knowledge and the collaboration of experts from many disciplines, including: geoscientists, geotechnical engineers, structural engineers, architects, mechanical engineers, materials engineers, electrical and instrumentation engineers, environmental engineers, chemical engineers, contractors, construction managers, social scientists, economists, statisticians, government officials, and politicians. Hu et al. (1996) stated: “From a disciplinary point of view, earthquake engineering spans seismology, engineering, geology and sociology.” They also provided a flow chart presenting interactions among various activities involved in EE studies. Additionally, facility owners should be heavily involved in the decision-making process, determining costs involved and adopting the performance goals of the facilities.

As Newmark and Rosenblueth (1971) stated, “Earthquake engineering is to the rest of the engineering disciplines what psychiatry is to other branches of medicine: It is a study of pathological cases to gain insight into the mental structure of normal human beings. This aspect of earthquake engineering makes it challenging and fascinating, and gives it an educational value beyond its immediate objectives.”

1.4 Recent Events, Developments and Future Challenges of EE

Since 1960, there have been major events and developments that have drastically influenced EE in the United States. There are also major future challenges ahead. Most of such advances are discussed in

various chapters of this book. Only a short list of events, developments and challenges is presented below. A more comprehensive list can be found in NRC (2003).

- Earthquake events such as the 1964 Alaska, 1971 San Fernando, 1985 Mexico, 1985 Chile, 1989 Loma Prieta and 1994 Northridge (U.S.), 1995 Kobe (Japan), 1999 Kocaeli and Düzce (Turkey), 1999 Chi-Chi (Taiwan), 2001 Bhuj (India) and 2003 Bam (Iran) have influenced EE, revealing some weaknesses of EQ-RD and construction practices and also increasing the data and our knowledge about the dynamic characteristics of EQGM, as well as socio-economical consequences of the earthquakes.
- Advances in computer technology have greatly facilitated structural analysis and structural dynamics for EE applications. In 1941, it took 8 hours for a mechanical analyzer to compute and plot a response spectrum (Biot, 1941). Structural analysis capabilities today are much improved.
- Advances in EQ-RD and EQ-RC.
- Construction of the first large U.S. shaking table at CERL at Champaign, Illinois in 1971. The design and construction of a 20×20 -foot shaking table in 1968 and its operation at the Earthquake Simulation Laboratory in 1972 at UCB.
- Establishment of major EE research centers in the United States and development of significant research programs including EERC at the UCB under the leadership of professors Penzien and Clough, Blume Center at Stanford and NCEER at SUNY Buffalo (sponsored by the NSF). Also, three new earthquake research centers have recently been established: PEER Center headquartered at the University of California at Berkeley, MCEER at SUNY Buffalo, and Mid-America Earthquake (MAE) Center at the University of Illinois, Urbana-Champaign. These three centers are funded by the NSF with matching funds from other sources.
- Establishment of several important experimental facilities to conduct EE research including, among others, at: Cornell University UCB, UCSD, UCD, University at Buffalo (SUNY), University of Michigan, University of Minnesota, University of Nevada at Reno, University of Texas at Austin, University of Washington, Georgia Institute of Technology, Lehigh University, Nist, PCA RPI.
- Establishment of an EERC library and NSF-funded NISEE.
- Establishment of the Applied Technology Council (ATC) in 1971 and its first significant activity, ATC 3-06 "Tentative provisions for the development of seismic regulations for buildings," were a turning point, casting a framework of the next generation of seismic design code.
- Establishment of California Universities for Research in Earthquake Engineering (CUREe) in 1988, and its reorganization to Consortium of Universities for Research in Earthquake Engineering (CUREE) in 2000.
- Reports published as the results of the SAC and Woodframe projects funded by FEMA.
- NRC reports prepared by the NAE's Committee on Earthquake Engineering Research in 1962, 1982 and 1989 formulated research programs that later were supported by the NSF.
- In 2001 the NSF funded the George E. Brown Jr. Network for EE Simulation (NEES). Sixteen experimental facilities at 15 universities around the U.S. were funded by NEES.
- In 2003, at the request and support of the NSF, the NRC published a report titled "Preventing earthquake disasters" that discusses a research agenda for NEES.
- Publication of reports from studies conducted at the above-mentioned research centers. Also, EE-specific journals, including *Earthquake Engineering and Structural Dynamics*, *Earthquake Spectra*, *Soil Dynamics and Earthquake Engineering*, *Journal of Earthquake Engineering*, BSSA, among others, have provided media to disseminate research and development.
- Publication of proceedings of the WCEE and other regional and national EE conferences around the world.
- Publications of books, monographs and reports have greatly enhanced our understanding about earthquakes, performance of facilities, and EQ-RD. These include reports published by ATC, EERC, ERI, FEMA, MAE, MCEER NCEER, PEER, SEAOC, USGS, among others.

- Cooperative research programs among the United States and Yugoslavia, Japan, China and other countries have been fruitful for advancement of EE knowledge and practice.
- Advances in engineering seismology and expanding networks of strong motion instruments. Consequently, real-time and near real-time data collection and dissemination are becoming a reality. Also, the increase in the number of instrumented buildings and bridges has enabled us to better understand the behavior and performance of real structures during earthquakes. Additionally, recent significant advances have been made in geotechnical engineering and engineering geology for seismic hazard reduction.
- Advances in innovative strategies and technologies to control the response of facilities to EQGMs, which can be considered individually or in combination, such as seismic isolation, energy dissipation devices, active and semiactive structural control, etc.
- Studies and publications of socio-economic impacts of earthquakes.
- The main goal of EQ-RD, which has been to protect life safety, is being expanded to become more comprehensive. This can be considered a part of a more general framework of performance-based earthquake engineering (P-BEE). There are challenging and exciting research and developments ahead of P-BEE, which are reviewed in various chapters of this book. Related to this same issue is also the evolution of the definition and goal of EE (see Section 1.3.1).

1.5 Closing Remarks

Advances in EE have been extremely impressive. Great lessons have been, and will be, learned about the nature of earthquakes, characteristics of ground motion, performance of geotechnical, structural, non-structural and lifeline systems during earthquakes, and their social and economical impacts. To reach the ultimate goal of EE — to control the seismic risks at socio-economically acceptable levels — the future challenges are to learn new lessons from future significant earthquake events, through not only quick field inspections but particularly through integrated observational, experimental and analytical studies. The objectives of such studies should be to find out what happened, why it happened, and how to prevent the observed undesirable performance of facilities in future earthquakes. An important expected outcome of such studies should be improvement of existing seismic code and development of new and simple but reliable provisions. Such provisions should be easily adapted and applied effectively, not only for the regions of high seismicity but also in those regions of moderate or low seismicity, as well as in developing countries. The outcome of such integrated studies should also include the social and economical aspects that contributed to the observed performance in the earthquake, and those that resulted as a consequence of the earthquake, particularly in the cases when a disaster was created. To apply this effectively will require massive educational and preparedness programs.

The international EE community is facing a major challenge of improving the knowledge and practice in developing countries with the goal of reducing the seismic risks to socio-economically acceptable levels. Ensuring life safety is the thrust of this goal. Involvement of the international EE community in this urgent matter has been recognized before and discussed in previous World Conferences on EE, and it was the central theme in the 12th WCEE, but unfortunately has not yet materialized. This is a grand challenge for industrialized countries in particular to find a way to help developing countries to achieve the modern goal of EE, especially reduction in loss of lives.

Acknowledgments

Charles James, information manager of the National Information Service for Earthquake Engineering (NISEE) and librarian at the Earthquake Engineering Research Center Library at the University of California at Berkeley, provided numerous documents and earthquake damage photos. His cooperation and contributions are greatly appreciated.

List of Acronyms

- ACES — Advisory Committee on Engineering Seismology
ASCE — American Society of Civil Engineers
ATC — Applied Technology Council
BSSA — Bulletin of Seismological Society of America
CERL — Construction Engineering Research Laboratories
CUREe — California Universities for Research in Earthquake Engineering
CUREE — Consortium of Universities for Research in Earthquake Engineering
EE — Earthquake engineering
EERC — Earthquake Engineering Research Center, at the University of California at Berkeley
EERI — Earthquake Engineering Research Institute
EESD — Earthquake Engineering and Structural Dynamics
EQ — Earthquake
EQGM — Earthquake ground motion
EQ-RC — Earthquake-resistant construction
EQ-RD — Earthquake-resistant design
FEMA — Federal Emergency Management Agency
IAEE — International Association for Earthquake Engineering
LABC — Los Angeles Building Code
MAE — Mid-America Earthquake Center
MCEER — Multidisciplinary Center for Earthquake Engineering Research
NAE — National Academy of Engineering
NAS — National Academy of Sciences
NCEER — National Center for Earthquake Engineering Research
NEES — George E. Brown Jr. Network for Earthquake Engineering Simulation
NIST — National Institute of Standards and Technology
NISEE — National Information Service for Earthquake Engineering
NRC — National Research Council
NSF — National Science Foundation
P-BEE — Performance-based earthquake engineering
PCA — Portland Cement Association
RPI — Rensselaer Polytechnic Institute
SAC — Joint venture consisting of SEAOC, ATC and CUREe to manage and administer a program to reduce earthquake hazards in steel moment frame structures
SEAOC — Structural Engineers Association of California
SSA — Seismological Society of America
UBC — Uniform Building Code
UCB — University of California at Berkeley
UCD — University of California at Davis
UCLA — University of California at Los Angeles
UCSD — University of California at San Diego
USGS — United States Geological Survey
WCEE — World Conference on Earthquake Engineering

References

- Allen, C.R. (2002). Connections: The EERI Oral History Series; C.R. Allen, S. Scott, interviewers, EERI.
Bertero, V.V. (1992). Major issues and future directions in earthquake-resistant design. *Proceedings of the 10th World Conference on Earthquake Engineering*, A. A. Balkema, Rotterdam.

- Bertero, V.V. (1996). State-of-the-art report on design criteria. *Proceedings of the 11th World Conference on Earthquake Engineering*, Paper No. 2005.
- Bertero, V.V. (1997). Performance-based seismic engineering: a critical review of proposed guidelines. *Seismic Design Methodologies for the Next Generation of Codes, Proceedings of the International Workshop*, Bled, Slovenia, A.A. Balkema, Rotterdam and Brookfield, Vermont, 1–32.
- Bertero, V.V. (2002). Innovative approaches to earthquake engineering. Chapter 1, *Innovative Approaches to Earthquake Engineering*, G.Oliveto, WIT Press, Southampton, UK.
- Binder, R.W. and Wheeler, W.T. (1960). Building code provisions for aseismic design. *Proceedings of the Second World Conference on Earthquake Engineering*, Japan, III, 1843–1875.
- Binder, R.W. (1952). Engineering aspects of the 1933 Long Beach earthquake. *Proceedings of Symposium on Earthquake and Blast Effects on Structures*, EERI and University of California, 187–221.
- Biot, M.A. (1933). Theory of elastic systems vibrating under transient impulse with application to earthquake-proof buildings. *Proceedings of the National Academy of Sciences*, 19, 262–268.
- Biot, M.A. (1934). Theory of vibration of buildings during earthquake. *Zeitschr. f. Angew. Math. u. Mech.*, 14, 213–223.
- Biot, M.A. (1941). A mechanical analyzer for the prediction of earthquake stresses. *Bull. Seismological Soc. Am*, 31, 151–171.
- Blume, J.A. (1956). Period determinations and other earthquake studies of a fifteen-story building. *Proceedings of the World Conference on Earthquake Engineering*, Berkeley, California. 11–27.
- Blume, J.A. (1972). Early research in the dynamic aspects of earthquake engineering. *Dedication of earthquake simulator laboratory*, Earthquake Engineering Research Center, University of California, Berkeley.
- Blume, J.A., Newmark, N.M. and Corning, L.H. (1961). *Design of multistory reinforced concrete buildings for earthquake motions*. Portland Cement Association, Chicago.
- Blume, J.A. (1994). Connections: The EERI oral history series; John A. Blume, Stanley Scott, interviewer. *EERI, 1994*.
- Bolt, B.A. (1996). From earthquake acceleration to seismic displacement. *The Fifth Mallet–Milne Lecture*, John Wiley & Sons, Chichester, U.K.
- Borges, J.F. and Ravara, A. (2969). Earthquake Engineering. Seismic Laboratório Nacional de Engenharia Civil, Lisbon, Portugal.
- Byerly, P., Hester, J. and Marshall, K. (1931). The natural periods of vibration of some tall buildings in San Francisco. *Bull. Seismological Soc. Am* 21, 268–276.
- Clough, R.W. (1972). Editorial. *Earthquake Engineering and Structural Dynamics*, 1, 3–4.
- Clough, R.W. (1992). Foreword, *Recent Advances in Earthquake Engineering and Structural Dynamic*, V.E. Davidovici (coord. Ed.), Ouest Editions, Nantes, France.
- Davidovici, V.E. (1992). *Recent Advances in Earthquake Engineering and Structural Dynamic*. Ouest Editions, Nantes, France.
- Degenkolb, H.J. (1994). Connections: The EERI oral history series; Henry J. Degenkolb, Stanley Scott, interviewer. *EERI, 1994*.
- Derleth, Ch. Jr. (1907). Discussion on San Francisco Earthquake. *Transactions of the ASCE*, Vol. LIX, 311–323.
- EERI Committee on Seismic Risk (1984). *Earthquake Spectra*, 1, 33–40.
- Elnashai A.S. (2002). A very brief history of earthquake engineering with emphasis on developments in and from the British Isles. *Chaos, Solitons & Fractals*, 13, 967–972.
- Freeman, J.R. (1932). *Earthquake Damage and Earthquake Insurance*. McGraw-Hill, New York.
- Geschwind, C.-H. (1996). Earthquakes and their interpretation: The campaign for seismic safety in California, 1906–1933. Ph.D. Thesis, Johns Hopkins University.
- Hall, E.E. (1912). Vibration of buildings due to street traffic. *Engineering News*, 68, 198–201.
- Housner, G.W. (1983). Earthquake engineering — some early history. *Proceedings of the Golden Anniversary Workshop on Strong Motion Seismometry*, University of Southern California, 7–16.

- Housner, G.W. (1984). Historical view of earthquake engineering. *Proceedings of the 8th World Conference on Earthquake Engineering*, San Francisco, 1, 25–39.
- Housner, G.W. (1997). Connections: The EERI oral history series; G.W. Housner, S. Scott, interviewers. *EERI, 1997.*
- Hu, Y.-X., Liu, S.-C. and Dong, W. (1996). *Earthquake Engineering*. E & FN Spon, London.
- Hudson, D.E. (1963). The measurement of ground motion of destructive earthquakes. *Bull. Seismological Soc. Am*, 53 419–437.
- Hudson, D.E. (1988). Nine milestones on the road to earthquake safety. *Proceedings of the 9th World Conference on Earthquake Engineering*, II, II-3 to II-11.
- Hudson, D.E. (1992). A history of earthquake engineering. *Proceedings, IDNDR International Symposium on Earthquake Disaster Reduction Technology*, Japan, 3–13.
- Lee, W.H.K., Kanamori, H., Jennings, P.C. and Kisslinger (2003). *International Handbook of Earthquake & Engineering Seismology*, Academic Press, London, U.K.
- Moore, W.W. (1998). Connections: The EERI Oral History Series: W.W. Moore, S. Scott, interviewers. *EERI.*
- National Research Council (2003). *Preventing Earthquake Disasters*. The National Academies Press, Washington, D.C.
- Needhan, J. (1971). *Science and Civilization in China*, Vol.4, Part III, Cambridge University Press, Cambridge.
- Newmark, N.M. and Rosenblueth, E. (1971). *Fundamentals of Earthquake Engineering*. Prentice-Hall, Englewood Cliffs, NJ.
- Norris, C.H., Hansen, R.J., Holley, M.J., Biggs, J.M., Namyot, S. and Minami, J.K. (1959). *Structural Design for Dynamic Loads*. McGraw-Hill, New York.
- Okamoto, S. (1973). *Introduction to Earthquake Engineering*. Wiley, New York.
- Popov, E.P. (2002). Connections: The EERI oral history series; Egor P. Popov, Stanley Scott, interviewer. *EERI, 2002.*
- Press, F. (1984). The role of science and engineering in mitigating natural hazards. *Proceedings of the 8th World Conference on Earthquake Engineering*, San Francisco.
- Reid, H.F. (1910). The mechanics of the earthquake. *The California Earthquake of April 18, 1906. Report of the State Earthquake Investigative Commission*, Vol. II, Carnegie Institutions of Washington.
- Richter, C.F. (1935). An instrumental earthquake scale. *Bull. Seismological Soc. Am*, 25, 1–32.
- Rinne, J.E. (1996). Connections: The EERI oral history series; John E. Rinne, Stanley Scott, interviewer. *EERI, 1996.*
- Roessel, J.M. and Yao, J.T.P. (2002). State of the art of structural engineering. *ASCE Journal of Structural Engineering*, 128, 965–975.
- Scawthorn, C. (2003). Earthquakes: A historical perspective. Chapter 1, *Earthquake Engineering Handbook*, W.E.Chen and C.Scawthorn (editors), CRC Press, Boca Raton, FL.
- Steinbrugge, K.V. (1970). Earthquake damage and structural performance in the United States. Chapter 2, *Earthquake Engineering*, R.Wiegel (coord. Ed.), Prentice-Hall, Englewood Cliffs, NJ.
- Suyehiro, K. (1932). Engineering Seismology Notes on American Lectures. *Proceedings, ASCE*, 58(4).
- Usami, T. (1988). Future prospects for earthquake engineering. *Bull. Seismological Soc. Am*, 78, 2110–2113.
- Wiegel, R.L. (19970). *Earthquake Engineering*. Prentice-Hall, Englewood Cliffs, NJ.

2

Engineering Seismology

2.1	The Goals of Engineering Seismology.....	2-1
2.2	Continental Tectonics and Seismicity	2-3
	Seismogenic Faults • Earthquake Occurrence Statistics	
2.3	Basic Earthquake Properties.....	2-8
	Earthquake Magnitude	
2.4	Earthquake and Ground Motion Prediction	2-15
	Special Strong Motion Characterization • Coherency of Wave Motion • Time-History Duration • Near-Fault Ground Motions • Estimating Time Histories • Available Strong Motion Recordings • Vertical Ground Motions	
2.5	Attenuation Estimation and Uncertainties.....	2-25
	Construction of Attenuation Relations • Rapid Response: ShakeMaps	
2.6	Future Challenges	2-30

Bruce A. Bolt

2.1 The Goals of Engineering Seismology

Seismology has long contributed to engineering. The two founders of seismology, Robert Mallet (1810–1881), a civil engineer, and John Milne (1850–1913), a mining engineer, defined seismology as the scientific study of earthquakes. Both posed, in different words, three key questions for earthquake engineers:

1. What is the mechanical explanation for damage or lack thereof when structures are subjected to seismic strong motion?
2. What are the essential characteristic properties of the seismic wave inputs to the affected structures?
3. What is the seismicity, i.e., a specified region's earthquake source characteristics?

Robert Mallet, after the great Neapolitan earthquake of 1857 in southern Italy, set out to explain the masses of dislocated stone and mortar in terms of mechanical principles. In doing so he established much of the basic vocabulary of seismology such as *seismology*, *hypocenter* and *isoseismal*. The close links between engineering and seismology have continued ever since. In this tradition, it is part of strong motion seismology to explain and predict the large amplitude, long-duration shaking observed in damaging earthquakes. At seismology's scientific beginning, in the first years of the twentieth century, however, the greatest seismological advances occurred in studying waves from distant earthquakes using very sensitive seismographs. Because the wave amplitudes in even a nearby magnitude 5 earthquake would exceed the dynamic range of the then current seismographs, seismologists could accomplish little fundamental work on the more rare large earthquakes of engineering importance.

The situation is dramatically different now. Perhaps the first modern observational advance followed the 1971 San Fernando, California, earthquake (magnitude 6.5). Hundreds of records of the strong motion of the ground became available — notably the peak horizontal ground acceleration of 1.2 g recorded on

the abutment of the Pacoima Dam. These records raised questions on the significance of topographic amplification (see Spudich et al. 1996 for a later case history of this effect). In 1999, an even larger set of recordings was obtained in the Chi-Chi earthquake in Taiwan (magnitude 7.6). This earthquake source had an extraordinary surface fault displacement and over 400 free-field measurements of ground accelerations and ground velocity were made.

This recent availability of instrumental recordings of intense seismic wave motions, especially near their sources in various geological conditions, has been the essential ingredient in providing quantitative answers to engineering questions such as those considered by Mallet and Milne. It is now evident that simple scaling of ground response, based on earthquake magnitude, distance and peak ground acceleration from an epicenter, is often an unrealistic and simplistic representation of strong shaking at a site. Such factors as duration of strong shaking, source dimension and mechanism and wave phasing (time-history evolution) are crucial in seismic analysis and structural design (see Bolt 1996).

The aim of this chapter is to provide some of the latest understanding about earthquakes that is most relevant to engineering design and hazard analysis: what causes their occurrence in space and time, their characteristic wave patterns, their likely damage mechanisms and their essential strong motion parameterization. This chapter also includes an outline of current methodologies for the estimation of strong seismic ground motion and seismic hazard. Additional helpful background on the subject may be found in Chapters 5 and 7.

Soil-related problems have caused major economic loss in past earthquakes. Classic examples of this type of damage are the 1964 earthquakes of Niigata, Japan and Anchorage, Alaska. In Niigata, the maximum ground acceleration was approximately 0.16g, which, considering the amount of damage, was not high. The expansion of the modern city had involved reclamation of land along the Shinano River. In the newly deposited and reclaimed land areas, many buildings tilted or subsided as a result of soil liquefaction. Three thousand eighteen houses were destroyed and 9,750 were moderately or severely damaged in Niigata Prefecture alone, most because of cracking and unequal settlement of the ground. About 15,000 houses in Niigata City were inundated by the collapse of a protective embankment along the Shinano River. Yet the number of deaths was only 26. More modern examples of this aspect of seismological engineering are given in Chapter 4.

Surface fault displacements can cause severe local damage, but compared with damage caused by strong ground shaking, this type of damage is, though striking, rather rare. Yeates et al. (1997) provide a comprehensive review of at-risk seismogenic faults worldwide. Even in very large earthquakes, the area exposed to direct surface fault displacement is much smaller than the area affected by strong ground shaking. A recent dramatic example of damage caused by fault displacement occurred in the 1999 Chi-Chi, Taiwan, earthquake where the low-angle reverse fault ruptured through many built-up areas (Figure 2.1). The total length of the fault rupture was about 80 km, the maximum horizontal fault displacement reached about 9 m and vertical offsets reached 1 to 4 m. Even in this case, the total area damaged by direct fault offsets was only a small percentage of the area damaged by strong ground shaking.

The most significant threat from such fault-induced changes in ground elevations is the damage they can cause to structures such as bridges and dams. In contrast, earthquake-induced landslides and avalanches, although responsible for major destruction, are fortunately localized. A noteworthy example of this kind of damage occurred in the Peru earthquake of May 31, 1970. This earthquake of magnitude 7.7 led to the greatest seismological disaster yet experienced in the Western Hemisphere. An enormous debris avalanche from the north peak of Huascaran Mountain amounting to 50 million or more cubic meters of rock, snow, ice and soil, traveled 15 km from the mountain to the town of Yungay with an estimated speed of 320 km per hour. At least 18,000 people were buried under this avalanche, which covered the towns of Ranrahirca and most of Yungay.

Seismic sea waves, or *tsunamis*, are long water waves generated by sudden ground displacements under oceans. The most common cause is the impulsive displacement along a submerged fault associated with a large earthquake, although large submarine landslides are often the direct cause of major tsunamis. Because of the great earthquakes that occur around the Pacific, this ocean is particularly prone to seismic sea waves. A recent discussion of tsunamis of engineering interest can be found in Hébenstreit (1997).

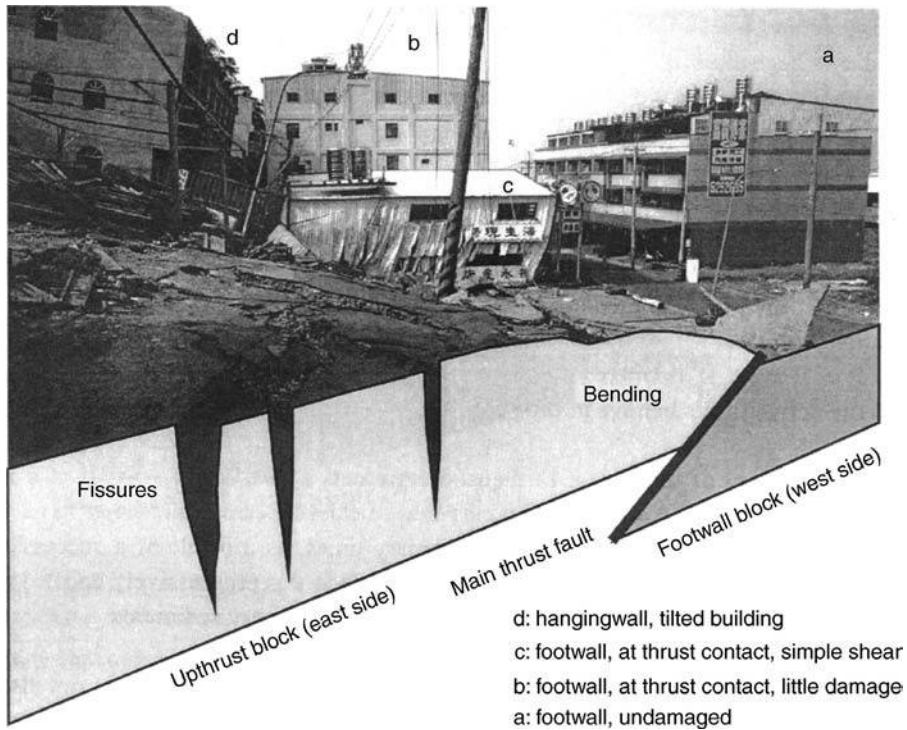


FIGURE 2.1 Damage effects of thrust faulting of the Chelungpu fault in the 1999 Chi-Chi, Taiwan, earthquake at Fengyuan. Damage was usually smaller on the footwall (western) side. (Courtesy National Center for Research on Earthquake Engineering, Taiwan.)

2.2 Continental Tectonics and Seismicity

The geological model of plate tectonics provides the most coherent global explanation of the occurrence of the majority of earthquakes. The basic concept is that the Earth's outermost part (called the *lithosphere*) consists of several large and fairly stable rock slabs called *plates*. The ten largest plates are mapped in Figure 2.2. Each plate extends to a depth of about 80 km and includes the Earth's outermost rigid rocky layer, called the *crust*.

The moving plates of the Earth's surface also provide an explanation of the various mechanisms of seismic sources. Collisions between adjacent lithospheric plates, destruction of slab-like plates as they descend or *subduct* into a dipping zone beneath island arcs and tectonic spreading along mid-oceanic ridges produce significant straining and fracturing of the regional crustal rocks. The earthquakes in these tectonically active boundary regions are called *plate-edge earthquakes*. The very hazardous large earthquakes of Chile, Peru, the eastern Caribbean, Central America, Southern Mexico, California, Southern Alaska, the Aleutians, the Kuriles, Japan, Taiwan, the Philippines, Indonesia, New Zealand and the Alpine-Caucasian-Himalayan belt are of the plate-edge type.

As the mechanics of the lithospheric plates have become better understood, long-term predictions of place and size become possible for plate-edge earthquakes. For example, many plates spread toward the subduction zones at long-term geological rates of 2 to 5 cm (about 1 to 2 inches) per year. Therefore, in active arcs like the Aleutian and Japanese Islands and subduction zones like Chile and western Mexico, the history of large earthquake occurrence flags areas that currently lag in earthquake activity.

Many large earthquakes are produced by slips along faults connecting the ends of offsets in the spreading oceanic ridges and the ends of island arcs or arc-ridge chains (see Figure 2.2). In these regions, plates slide past each other along what are called *transform faults*. Considerable work has been done on

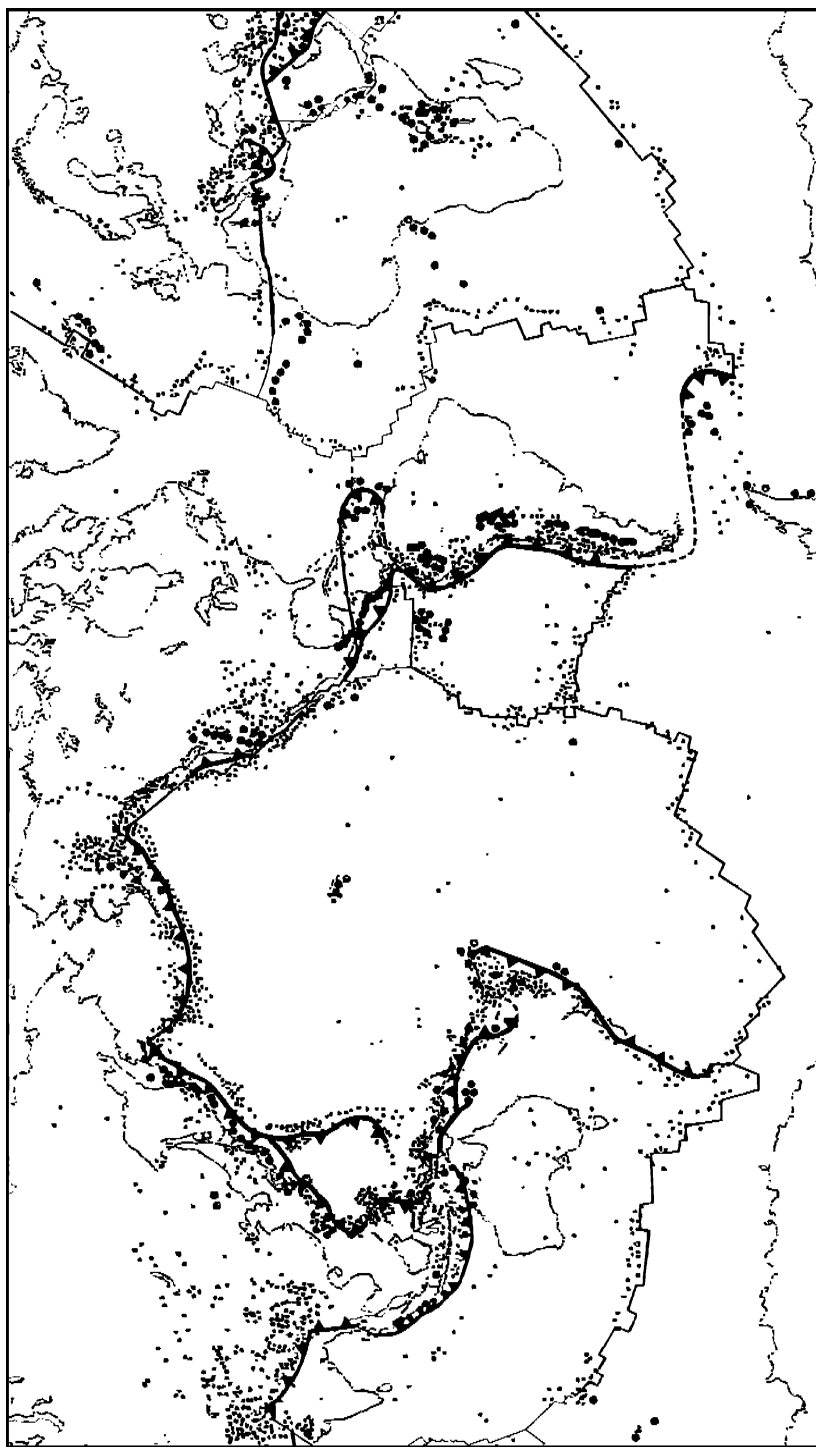


FIGURE 2.2 The major tectonic plate margins (heavy lines) and sample of most active seismic areas (heavy and light dots). Subduction zones marked with triangles (down dip).

the estimation of strong ground motion parameters for the design of critical structures in earthquake-prone countries with either transform faults or ocean-plate subduction tectonics, such as Japan, Alaska, Chile and Mexico. The Himalayas, the Zagros (Iran) and the Alpine regions are examples of mountain ranges formed by *continent-to-continent collisions*. These collision zones are regions of high present-day seismic activity.

Although simple plate-tectonic theory provides a general understanding of earthquakes and volcanoes, it does not explain all seismicity in detail, for within continental regions, away from boundaries, large devastating earthquakes sometimes occur. These *intraplate* earthquakes can be found on nearly every continent (see Yeates et al. 1997). A recent example of such an intraplate earthquake (2001) was the disastrous Bhuj ($M = 7.7$) earthquake in western India in the seismically active Kutch province. In the United States, the most famous intraplate earthquakes occurred in 1811–1812 in the New Madrid area of Missouri, along the Mississippi River and in 1886, the Charleston, South Carolina earthquake. Northern China is the location of a further notable group, including the Tanlu fault, which seems to bear no simple mechanical relation to the present plate edges.

The first seismological task is to locate earthquake centers worldwide (see the Internet Web site <http://www.iris.washington.edu>). During an earthquake, seismic waves radiate from the earthquake source below the ground surface as opposite sides of a slipping fault rebound in opposite directions thus decreasing the strain energy in the rocks. Consequently, the seismic source is spread out through a volume of rock. Nevertheless, it is often convenient to model a simplified earthquake source as a point from which the waves first emanate. This point is called the *earthquake focus*. The point on the ground surface directly above the focus is called the *earthquake epicenter*.

Although many foci are situated at shallow depths, in some regions they are hundreds of kilometers deep; such regions are the *plate subduction zones*. On average, the frequency of the occurrence of earthquakes in these regions declines rapidly below a depth of 200 km, but some foci are as deep as 680 km. Rather arbitrarily, earthquakes with foci from 70 to 300 km deep are called *intermediate focus* and those below this depth are termed *deep focus*. It should be noted that some intermediate and deep-focus earthquakes are located away from the Pacific region, for example, in the Hindu Kush, in Romania, in the Aegean Sea and under Spain.

From earthquake wave readings at different seismographic observatories, the position of the center of an earthquake can be calculated. In this way, a uniform picture of earthquake distribution around the world has been obtained and indeed forms the basis of the plate tectonic model of earthquake dynamics (see Figure 2.2).

In the interior of old continents, particularly in the regions of Pre-Cambrian Shields (e.g., Canada, Brazil, Australia and India), intraplate earthquakes are of small size and occurrence rate. In Europe, however, earthquake activity is quite widespread. And to the south, Turkey, Greece, Yugoslavia, Italy, Spain and Portugal have long endured the ravages of shifting plates, and large numbers of people have died in disasters throughout the years. An earthquake off southwest Iberia on November 1, 1755 produced an immense tsunami, which caused many of the 50,000 to 70,000 deaths in Lisbon.

On average, 10,000 people die each year from earthquakes. A UNESCO study assigns damage losses from earthquakes amounting to \$10 billion from 1926 to 1950. In Central Asia in this interval two towns and 200 villages were destroyed. Since then several towns including Agadir (1960), Skopje (1963), Managua (1972), Gemona (1976), Tangshan (1976), Mexico City (1985), Spitak (1988), Kobe (1995), cities in Turkey and Taiwan (1999), towns in India (2001) and hundreds elsewhere have been severely damaged by ground shaking. The shallow-focus earthquakes (focus depth less than 70 km) wreak the most devastation, and they contribute about three-quarters of the total energy released in earthquakes throughout the world. In California, for example, all of the known earthquakes to date have been shallow focus. In fact, it has been shown that the great majority of earthquakes occurring in central California originate from foci in the upper 10 km of the Earth, and only a few are as deep as 15 km.

Most moderate-to-large shallow earthquakes are followed, in the ensuing hours and even in the next several months, by numerous, usually smaller earthquakes in the same vicinity. These earthquakes are called *aftershocks*, and large earthquakes are sometimes followed by incredible numbers of them. The great Rat Island earthquake, caused by subduction under the Aleutian Islands on February 4, 1965 was,

within the next 24 days, followed by more than 750 aftershocks large enough to be recorded by distant seismographs. Aftershocks are sometimes energetic enough to cause additional damage to already weakened structures. This happened, for example, a week after the Northridge, California earthquake of January 17, 1994. Some weakened structures in the San Fernando Valley sustained additional cracking from aftershocks measuring a magnitude of 5.5. A few earthquakes are preceded by smaller *foreshocks* from the source area, and it has been suggested that these can be used to predict the main shock but attempts along this line have not proven statistically successful.

As Figure 2.2 illustrates, volcanoes and earthquakes often occur together along the margins of plates around the world. Like earthquakes, there are also intraplate volcanic regions, such as the Hawaiian volcanoes in which earthquakes and volcanic activity are physically related. Despite these tectonic connections between volcanoes and earthquakes, there is no evidence that all moderate-to-major shallow earthquakes are not essentially all of the strain release, fault-rebound type. Those moderate-to-large earthquakes that can be reasonably associated with volcanoes are relatively rare and fall into three categories:

1. volcanic steam explosions
2. shallow earthquakes arising from magma movements
3. physically interacting tectonic earthquakes

2.2.1 Seismogenic Faults

The mechanical aspects of geological faults are the key factors in understanding the generation of strong seismic motions. First, the kinematics of the fault slip is important. The *dip* of a fault is the angle that the fault surface makes with a horizontal plane and the *strike* is the direction of the fault line exposed or projected at the ground surface relative to the north. A *strike-slip* fault, sometimes called a transcurrent fault, involves displacements of rock laterally, parallel to the strike. If when we stand on one side of a fault and see that the motion on the other side is from left to right, the fault is a *right-lateral* strike slip. Similarly, we can identify *left-lateral* strike slip. A *dip-slip* fault is one in which the motion is largely parallel to the dip of the fault and thus has vertical components of displacement. A *normal* fault is one in which the rock above the inclined fault surface moves downward relative to the underlying crust. Faults with an almost vertical slip are also included in this category.

A *reverse* fault is one in which the crust above the inclined fault surface moves upward relative to the block below the fault. *Thrust* faults belong to this category but are generally restricted to cases when the dip angle is small. In *blind thrust* faults, the slip surface does not penetrate to the ground surface. In most cases, fault slip is a mixture of strike slip and dip slip and is called *oblique* faulting.

For over a decade it has been known that displacement in fault zones occurs not only by sudden rupture producing an earthquake but also by slow differential slippage of the sides of the fault. The fault is said to be undergoing *tectonic creep*. Slippage rates range from a few millimeters to several centimeters so that over time they may have critical engineering consequences. Sometimes an aseismic slip is observed at the ground surface along or in the vicinity of a ruptured fault that has produced an earlier substantial earthquake. For example, along the San Andreas Fault break in the June 27, 1966 earthquake near Parkfield, California, the offset of the road pavement increased by a few centimeters in the days following the main earthquake. Continued strain of the crustal rock after the initial major offset is probably reduced partly in aftershocks and partly by the nonelastic yielding of the weaker surface rocks and subsidiary slip as they accommodate to the new tectonic stresses in the region.

Fault offset and slip pose high risk for certain types of structures. When such structures including dams and embankments must be laid across active faults, the design usually incorporates joints or flexible sections in the fault zone. Field observations of fault offsets from world-wide earthquakes have been regressed as functions of earthquake magnitude and fault types (e.g., Wells and Coppersmith, 1994). An often-used general log-linear form is

$$\log D = -5.46 + 0.82 M_w \quad (2.1)$$

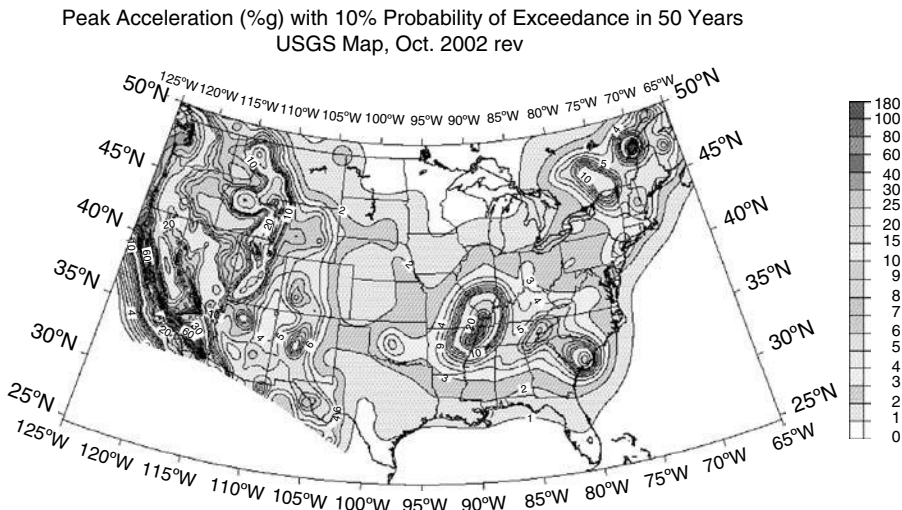


FIGURE 2.3 Recent seismic hazard map of the United States (after Frankel et al., 2002).

where D is the maximum offset (in meters) and M_w is moment magnitude.

A recent wide-ranging overview of the mechanics of active faulting has been given by Jackson (2001) in the Eighth Mallet–Milne Lecture. Although his field examples are drawn largely from the Eastern Mediterranean and the Middle East (including a useful table of source parameters of earthquakes in the region $10\text{--}50^\circ \text{N}$, $16\text{--}70^\circ \text{E}$, determined by seismic wave analysis), his discussion of the geological basis of strong-motion seismology and seismic hazard analysis is of general application. His central conclusion is that continental tectonics (specially applicable to earthquake engineering) is quite different from oceanic tectonics. Tectonic plate boundaries are not the key features of many actively deforming continental regions, and the seismic hazard of some continents is closely linked to the interior active fault systems, such as those that occur in Iran (e.g., the fault rupture in the great 31 August 1968 Dasht-e-Bayz earthquake). Modern global positioning system (GPS) and synthetic aperture radar (SAR) images (the latter first used seismologically to study the 1992 Landers, California, earthquake source) are now providing reliable measures of rates-of-slip and fault dislocation patterns in such regions (see Bolt, 2003).

2.2.2 Earthquake Occurrence Statistics

There are two widely noted features of earthquake occurrence: first, earthquakes tend to occur in clusters. This clustering is both spatial and temporal, and is sometimes referred to as *swarms*, *foreshock activity* and *aftershock activity*. Second, the fault ruptures that generate earthquakes decrease the amount of strain present at the locations along the fault where rupture occurs. This tectonic strain rebuilds gradually over time, eventually achieving a critical level at which another earthquake or sequence of earthquakes, is generated.

When seismicity catalogs are used in hazard analysis to estimate hazard maps (see Figure 2.3) and spectral curves (e.g., Frankel et al. 1996), the most common, although certainly not completely correct, assumption is that earthquakes conform to a Poisson process. This assumption implies that seismicity in any time period is independent of previous seismicity and necessitates some *ad hoc* analysis to remove the dependent events catalogued as clusters (e.g., Electric Power Research Institute 1986).

Several probability models reflect efforts at modeling the first type of behavior called *self-exciting*. Earthquake catalogs are modeled as realizations of triggering, branching, or epidemic-type point processes, and all the referenced models have the feature that the instance of earthquake at point (x, t_1) in space and time increases the likelihood of an earthquake at point (y, t_2) in space and time, where t_1 is less than t_2 . The likelihood of a particular realization may be specified by the conditional rate of the point

process; such models prescribe that the conditional rate of the earthquake process *increases* as more earthquakes occur. The amount the conditional rate increases as a result of one previous earthquake is generally assumed to taper off as both time and epicentral distance from the previous earthquake increase.

The second type of earthquake behavior is called *self-correcting*. In some cases, small events and/or aftershocks are removed from earthquake catalogs under study. According to such models, the conditional rate at a point (y, t_2) in space and time depends on the strain present at point y and time t_2 . As the occurrence of an earthquake at a nearby point x at a previous time t_1 decreases the strain at point y , such an event will generally *decrease* the conditional rate at (y, t_2) .

It would appear that these two classes of models are diametrically opposed: the first prescribes that earthquakes make future nearby earthquakes more likely; the other predicts that earthquakes make future nearby events less likely. Published examples indicate that the first type of model tends to provide a close fit to earthquake catalogs, especially catalogs containing many events, whereas the second type generally fits poorly unless aftershocks are screened out of the catalog. Although the second class still generally provides less than spectacular fit to the data, such models are commonly employed largely because of their agreement with basic seismological strain-release theory.

The dilemma suggests that a combined model, which incorporates both aspects of earthquake behavior, may be an improvement (Schoenberg and Bolt 2000). To account for any short-term clustering behavior of an earthquake sequence, the alternative model proposed here displays *self-exciting* behavior in the short run; that is, an event at (x, t_1) increases the conditional rate at (y, t_2) for t_1 slightly less than t_2 and x near y . In addition, to agree with the strain-release theory, the model exhibits *self-correcting* behavior over the longer term; that is, an event at (x, t_1) decreases the conditional rate at (y, t_2) for t_1 much less than t_2 and x near y .

The simplest self-exciting form (see Ogata 1988) is

$$g(t) = \frac{\kappa}{(t + \phi)^\theta}, \quad (2.2)$$

which corresponds to the long-used modified formula originally due to F. Omori for aftershock frequency. Here $g(t)$ is the trigger density function and κ, ϕ and θ are the parameters to be estimated when linear increase of strain is introduced. The combined probability density $\lambda(t)$ for the combined processes may be written as

$$\lambda(t) = \alpha + \beta t + \int_0^t \left[\frac{\kappa}{(t-s+\phi)^\theta} - \nu \right] dN(s), \quad (2.3)$$

where N is the number of earthquakes, and α and β are constants to be also determined by regression of the seismicity data.

Such a model may be called a short-term exciting, long-term correcting (SELC) model. Detailed seismic hazard examples are given in Schoenberg and Bolt (2000). The last formula can be recommended for improved seismic hazard analysis and mapping.

2.3 Basic Earthquake Properties

When the seismic ground motions in solid rock or soil are not too extreme, the waves involved can be explained in terms of linear elastic theory (i.e., Hooke's law applies). In this most common case, three basic types of elastic waves make up the shaking that is felt and causes damage in an earthquake. These waves are similar in many important ways to the observed waves in air, water and elastic solids, but only two of these waves propagate within a body of solid rock and soil. The faster of these body waves is appropriately called the primary or *P wave*. Its motion is the same as that of a sound wave, in that, as it

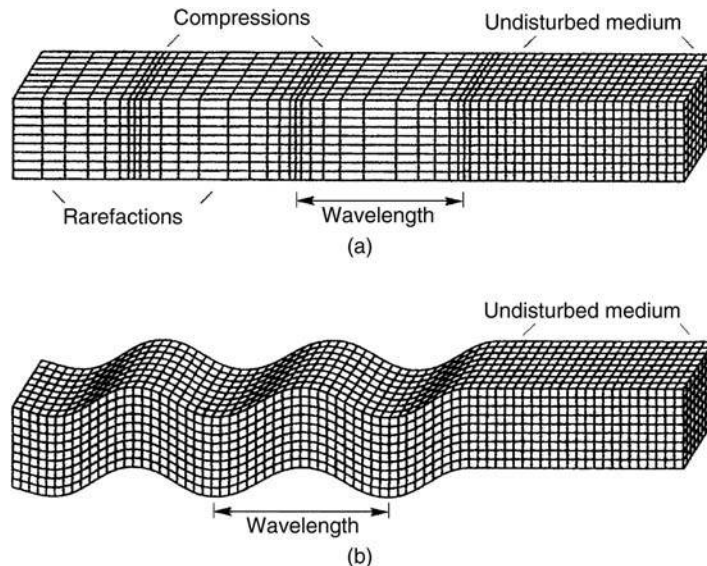


FIGURE 2.4 Deformation produced by body waves (a) P-wave; (b) SV- (vertically polarized) wave (Bolt, B.A., 2003. *Earthquakes*. 5th ed., W.H. Freeman, New York. With permission).

spreads out, it alternately pushes (compresses) and pulls (dilates) the rock (see Figure 2.4). These P waves, just like acoustic waves, are able to travel through both solid rock, such as granite and alluvium, and liquid material, such as volcanic magma or the water of lakes and oceans.

The slower seismic wave through rocks and soil is called the secondary or S wave. As an S wave propagates, it shears the rocks sideways at right angles to the direction of travel. Thus, at the ground surface, S waves can produce both vertical (SV) and horizontal (SH) motions. The S waves cannot propagate in the liquid parts of the Earth, such as lakes, so that, as expected from the theory, their amplitude is significantly reduced in partially liquefied soil. The speed of P and S seismic waves depends on the density and elastic properties of the rocks and soil through which they pass. In earthquakes, P waves are felt first. The effect is similar to a sonic boom that bumps and rattles windows. Some seconds later, S waves arrive with their significant component of side-to-side motion, so that, for upward wave incidence, the ground shaking is both vertical and horizontal. This S wave motion is the most effective in damaging structures. Mathematically, the velocity for P waves is

$$V_p = \sqrt{\frac{k + \frac{4\mu}{3}}{\rho}} \quad (2.4)$$

and for S waves it is

$$V_s = \sqrt{\frac{\mu}{\rho}} \quad (2.5)$$

where k and μ are the bulk modulus and rigidity, respectively, and ρ is density.

The third basic type of earthquake wave is called a *surface wave* because its motion is restricted to near the Earth's surface. Such waves correspond to ocean waves that do not disturb the water at depth. Similarly, as the depth below the ground surface increases, the soil or rock displacements decrease.

Surface waves in earthquakes are of two types (see Figure 2.5). The first is called a *Love wave*. Its motion is the same as that of SH waves that have no vertical displacement; it moves the ground side to side in

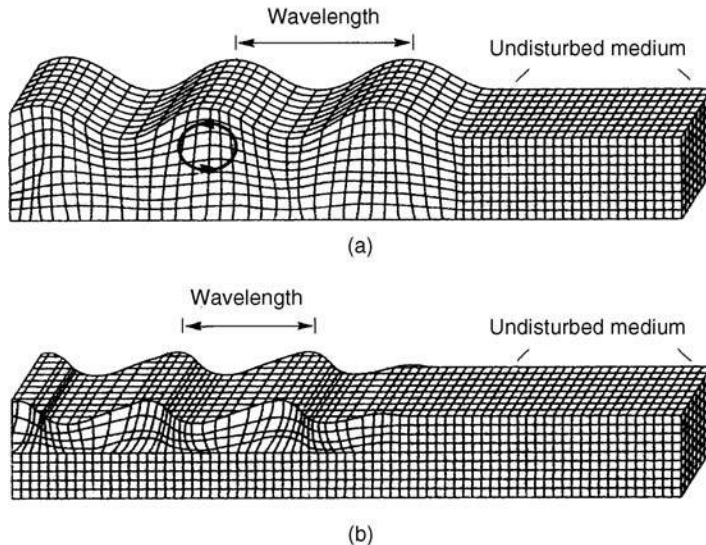


FIGURE 2.5 Deformations produced by surface waves: (a) Rayleigh wave (vertical motion); (b) Love wave (horizontal motion). (Bolt, B.A., 2003. *Earthquakes*. 5th ed., W.H. Freeman, New York. With permission).

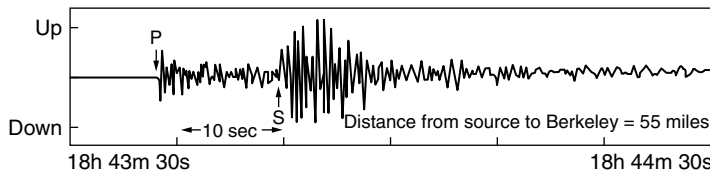


FIGURE 2.6 Seismogram at Berkeley, California, from a magnitude 5.3 earthquake located 90 km away, northeast of Santa Cruz on 27 June 1988. This recording of the vertical component of ground motion clearly shows the separate onsets of the P and S waves. Time increases on the trace from left to right.

a horizontal plane parallel to the Earth's surface, but at right angles to the direction of propagation. The second type of surface wave is called a *Rayleigh wave*. Like ocean waves, the particles of rock displaced by a Rayleigh wave move both vertically and horizontally in a vertical plane oriented in the direction in which the waves are traveling. The orbits are usually in a retrograde sense (see Bullen and Bolt, 1985, Figure 5.4). As shown by the arrows in Figure 2.5, each point in the rock moves in an ellipse as the wave passes.

Surface waves travel more slowly than body waves and Love waves travel faster than Rayleigh waves in the same geological formation. It follows that as the seismic waves radiate outward from the earthquake point source (such as an explosion) into the rocks of the Earth's crust, the different types of waves separate out from one another in a predictable pattern. However, because large earthquake sources are spacially extended faults, overlapping waves often obscure this separation of wave types.

An illustration of the simple theoretical wave pattern at a site 90 km from the fault source is shown in Figure 2.6. Recall that Love waves have no vertical component of ground motion. Thus, in this example, because this seismograph component records only the vertical motion of the ground, the seismogram contains only P waves, vertically polarized S waves and Rayleigh waves. (The horizontally polarized component SH wave can place large demands on a structure.)

As body seismic waves (the P and S waves) move through layers of rock in the crust they are reflected or refracted at the interfaces between rock types. To complicate matters further, whenever either one is

reflected or refracted, some of the energy of one type is converted to waves of the other type. When the elastic moduli differ from one layer to another, the layers act as wave filters that amplify the waves at some frequencies and deamplify them at others. Marked resonance effects occur at certain frequencies. On P and S waves reaching the surface of the ground, most of their energy is reflected back into the crust, so that the surface is affected almost simultaneously by upward- and downward-moving waves. For this reason considerable amplification of shaking typically occurs near the surface — sometimes doubling the amplitude of the upcoming waves. This surface amplification enhances the shaking damage produced at the surface of the Earth. Indeed, in many earthquakes mineworkers below ground report less shaking than do people on the surface.

It should be noted that seismic S waves travel through the rocks and soils of the Earth with a rotational component. Such torsional components of ground motion are thought to have important effects on the response of certain types of structures. Some building codes now take rotational ground motion into consideration.

Seismic waves of all types are progressively damped as they travel because of the nonelastic properties of the rocks and soils (e.g., Nuttli 1974). The attenuation of S waves is greater than that of P waves, but for both types attenuation increases as wave frequency increases. A useful seismological parameter to measure damping is the parameter Q such that the amplitude A at a distance d of a wave frequency f (Hertz) and velocity c is given by

$$A = A_0 e^{-(\pi f d / Qc)} \quad (2.6)$$

For P and S waves in sediments, Q is approximately 500 and 200, respectively.

The above physical description has been verified closely for waves recorded by seismographs at a considerable distance from the wave source (*the far field*), but is not adequate to explain important details of the heavy shaking near the source of an energetic earthquake (*the near field*). As noted above, near a rupturing fault, the strong ground shaking in the associated earthquake consists of mixtures of seismic waves that have not separated distinctly. Although this complication makes identification of P, S and surface waves on strong-motion records obtained near the rupturing fault difficult, there has been recent progress in this skill, based on correlations between actual recordings and theoretical modeling. This advance has made feasible the computation of realistic ground motions at specified sites for engineering design purposes.

Three final points about seismic waves are worth emphasizing here. First, earthquake waves are much affected by soil elastic properties. For example, in weathered surface rocks, in alluvium and water-saturated soil, the sizes of P, S and surface waves either increase or decrease depending on wave frequency as they propagate through the surficial nonhomogenous geological structures. Under extreme conditions of wave amplitude and geotechnical properties, the linear elastic behavior breaks down and nonlinear effects become significant (e.g., Darragh and Shakal 1991).

Second, patterns of incoming seismic waves are modified by the three-dimensional nature of the underground geological structures. Instrumental evidence on this effect came recently from the 1989 Loma Prieta, California earthquake. Strong motion recordings indicated that there were reflections of high-frequency S waves from the base of the Earth's crust at a depth of about 20 km under the southern San Francisco Bay (Somerville and Yoshimura, 1990). Also, in this earthquake, it was likely (Lomax and Bolt 1992) that large differences in the rock structure from one side of the San Andreas Fault to the other produced variations in ground motion by *lateral* refraction of S waves across this deep crustal velocity contrast. The effect produced significant S wave amplitude variation as a function of azimuth from the seismic source, in a period range of about 1 to 2 sec. In addition, there was measurable scattering of shear waves by deep alluvial basins in the southern part of the San Francisco Bay. Overall, the seismic intensity was enhanced in a region between San Francisco and Oakland, about 10 km wide by 15 km long (This assymetrical wave effect is illustrated by computer modeling in Figure 2.8. See also color insert following page 2-30).

Because of special features of engineering importance, discussion of the seismic wave patterns near the fault source is found in Section 2.4. As may be seen in Figure 2.7, time histories of the seismic waves contain pulse-like patterns of behavior that are crucial to the earthquake response of large structures.

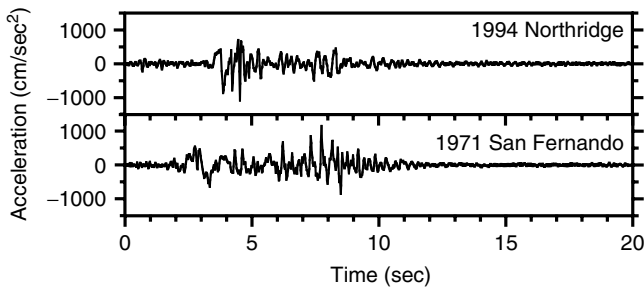


FIGURE 2.7 Comparison of same horizontal component of ground acceleration recorded on the same instrument at Pacoima Dam in the 1994 Northridge earthquake ($M_w = 6.7$) and the 1971 San Fernando earthquake ($M_w = 6.7$).

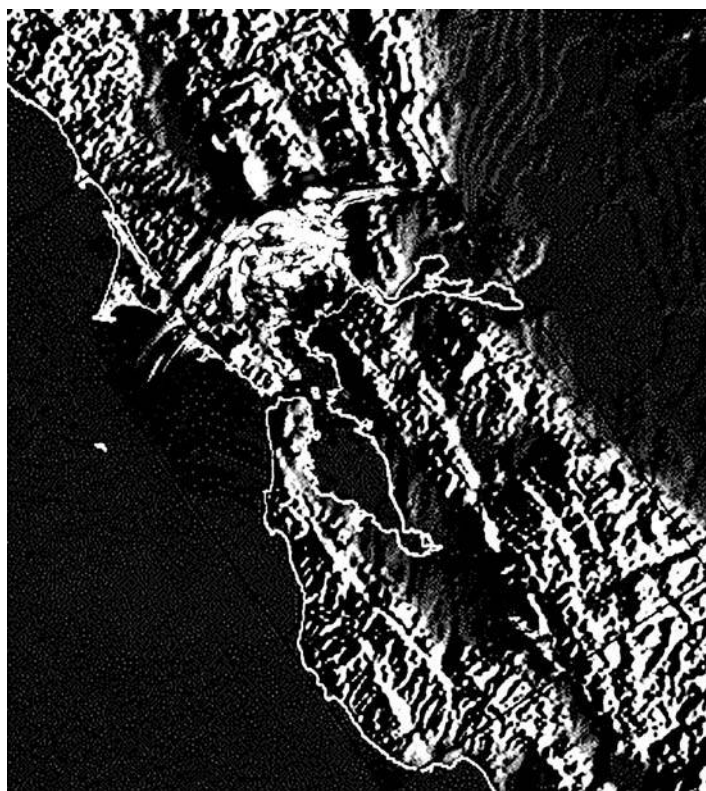


FIGURE 2.8 Computed ground motions generated by constant velocity rupture northward of the Hayward fault (red line). Wave intensities defined by color intensities. See also color insert following page 2-30. (courtesy of D. Dreger).

2.3.1 Earthquake Magnitude

The original yardstick of earthquake *intensity* for the strength of an earthquake is still useful and has in modified form been lately incorporated into the Internet-available ShakeMaps (see Section 2.5.2). Seismic intensity is assessed from field observations of damage to works of humans, of changes to the ground surface and of human reaction to the shaking. Because such earthquake intensity assessments do not depend on instruments, but on the actual reporting of the effects in the meizoseismal zone, intensities can be assigned even to historical earthquakes, and in this way, still form a vital part of modern estimates of seismological risk.

In the United States, the traditional intensity scale is the Modified Mercalli Scale (MMI) of 1931. Essentially similar scales are used in other countries. MMI has 12 levels, I through XII, and its description is widely available (see, e.g., Bolt 2003). An inherent weakness in the MMI and most other scales is the difficulty in inferring wave frequency information of the type critical for engineering resistant design.

The instrumental measure of earthquake size began with a definition by C. Richter, whereby the magnitude of a local earthquake was the logarithm to base ten of the maximum seismic wave amplitude in microns (10^{-4} cm) recorded on a Wood–Anderson seismograph located at a distance of 100 km from the earthquake epicenter, and has been significantly extended. Thus, one unit increase in magnitude implies a *ten-fold increase* in the amplitude of the earthquakes waves. Because the fundamental period of the Wood–Anderson seismograph is about 0.8 sec, it selectively amplifies those seismic waves with periods ranging from 0.5 to 1.5 sec. It follows that since the natural period of many building structures is within this range, the local or Richter magnitude, M_L , remains of value to engineers. Generally, shallow earthquakes have to attain Richter magnitudes of more than 5.5 before significant damage occurs even near the source of the waves.

The definition of the magnitude entails that it has no theoretical upper or lower limits. However, the size of an earthquake is limited at the upper end by the strength of the rocks of the Earth's crust. Since 1935, only a few earthquakes have been recorded on seismographs that have had a magnitude over 8.0 (see, e.g., Table 2.1). At the other extreme, highly sensitive seismographs can record earthquakes with a magnitude of less than –2.

Today, a variety of magnitude scales based on different formulas for epicentral distance and ways of choosing and measuring an appropriate wave amplitude, have emerged:

Surface Wave Magnitude (M_S) is based on measuring the amplitude of surface waves with a period of 20 sec. Surface waves with a period around 20 sec are often dominant on the seismograph records of distant earthquakes (epicentral distances of more than 1000 km).

Body Wave Magnitude (m_b) measures the amplitude of the P wave, which is not affected by the focal depth of the source, whereas deep focus earthquakes have no trains of surface waves.

Moment Magnitude (M_W) scale was devised because of the shortcomings of M_L , m_b , and to a lesser degree M_S in distinguishing between the size of great earthquakes. This scale assigns a magnitude to the earthquake in accordance with its seismic moment (M_0), which is a direct mechanical measure of the size of the earthquake source:

$$M_W = \log M_0 / 1.5 - 10.7 \quad (2.7)$$

where M_0 is in dyn-cm. M_0 can be estimated from the recorded wave spectra.

The M_L scale progressively underestimates the strength of earthquakes produced by large fault ruptures. The saturation point for this scale is about $M_L = 7$. The body wave magnitude (m_b) saturates at about the same value. In contrast, the M_S , which uses the amplitude of waves with wavelengths of about 60 km saturates at about $M_S = 8$. Its inadequacy in measuring the size of great earthquakes can be illustrated by comparing values for the San Francisco earthquake of 1906 and the great Chilean earthquake of 1960. Both earthquakes had an M_S of 8.3. However, the area that ruptured in the San Francisco earthquake was approximately 15 km deep and 400 km long whereas the area that ruptured in the Chilean earthquake was equal to about half of the state of California. Clearly the Chilean earthquake was a much larger event.

The M_W is the only extant magnitude scale that does not suffer from saturation for great earthquakes. The reason is that it is directly based on the forces that work at the fault rupture to produce the earthquake and not the amplitude and limited frequencies of specific types of seismic waves. Hence, as can be expected, when moment magnitudes were assigned to the 1906 San Francisco earthquake and the 1960 Chilean earthquake, the magnitude of the San Francisco earthquake dropped to 7.9, whereas the magnitude of the Chilean earthquake was raised to 9.5. M_S and M_W for some massive earthquakes are compared in Table 2.1.

TABLE 2.1 Magnitudes of Some Massive Earthquakes

Date	Region	M _S	M _W
January 9, 1905	Mongolia	8.25	8.4
January 31, 1906	Ecuador	8.6	8.8
April 18, 1906	San Francisco	8.25	7.9
January 3, 1911	Turkestan	8.4	7.7
December 16, 1920	Kansu, China	8.5	7.8
September 1, 1923	Kanto, Japan	8.2	7.9
March 2, 1933	Sanriku	8.5	8.4
May 24, 1940	Peru	8.0	8.2
April 6, 1943	Chile	7.9	8.2
August 15, 1950	Assam	8.6	8.6
November 4, 1952	Kamchatka	8	9.0
March 9, 1957	Aleutian Islands	8	9.1
November 6, 1958	Kurile Islands	8.7	8.3
May 22, 1960	Chile	8.3	9.5
March 28, 1964	Alaska	8.4	9.2
October 17, 1966	Peru	7.5	8.1
August 11, 1969	Kurile Islands	7.8	8.2
October 3, 1974	Peru	7.6	8.1
July 27, 1976	China	8.0	7.5
August 16, 1976	Mindanao	8.2	8.1
March 3, 1985	Chile	7.8	7.5
September 19, 1985	Mexico	8.1	8.0
September 21, 1999	Taiwan	7.7	7.6
November 2, 2002	Alaska	7.0	7.9

In light of the above discussion, the limits of different scales have been suggested for rating shallow earthquakes of various magnitudes: M_L or m_b for magnitudes between 3 and 7; M_S for magnitudes between 5 and 7.5; and M_W for all magnitudes.

A commonly used formula to estimate earthquake magnitude from fault dimension for world-wide strike-slip cases is

$$M_S = 6.10 + 0.70 \log_{10} L \quad (2.8)$$

where L is observed fault rupture length in kilometers (for a discussion of the problems with data regression in this case, see Bullen and Bolt 1985, pp. 437—438). Because the mechanical continuity of the active fault needed for a hazard estimate is often uncertain, various proposals have been made to limit the value of L by establishing *segmentation* of the fault structure. For example, often continental basin faults consist of *en echelon* off-set sections (e.g., in the East Africa seismic rift zone). Basin-and-range topography (e.g., Nevada and Utah) is often the result of segmental normal faults with subparallel strikes (see Yeates and Allen, 1997).

The geological determination of segments of faults is made from their geometric structure or behavioral discontinuities. One or more of the following criteria are often used: gaps in associated seismicity, *en echelon* fault trace offsets, cross-stratigraphic structures and changes in topography, slip rate, and fault strike. For example, the segmental sequence of the Wastach fault zone in Utah, (USA), has been exhaustively described in this way. These studies led to the concept of the *characteristic earthquake* (Schwartz and Coppersmith 1984). The notion that a particular fault segment repeatedly generates earthquakes of a maximum moment size (and even mechanism) is not predictable by extrapolation from the usual recurrence formula:

$$\log N = a + bM \quad (2.9)$$

Application to deterministic hazard analyses remains debatable because of important known exceptions, notably the Landers, California, earthquake source ($M_W=7.3$) of June 28, 1992. In this case, surface

ruptures occurred on an *en echelon* series of strike-slip faults with a step-over of slip at the ends of the segments. Fault slip continued through three mapped fault divisions not believed to be part of a single through-going fault.

2.4 Earthquake and Ground Motion Prediction

The most important seismological aspect of hazard mitigation is the prediction of the strong ground motion likely at a particular site (see Reiter 1990; Bolt 1996). Nevertheless, the aspects of earthquake prediction that still receive the most publicity are the prediction of the place, size and time of the earthquake. Of course, prediction of the region where earthquakes are likely to occur has long been achieved by seismicity studies using earthquake observatories. In addition, useful probability estimates of long-term hazard can be inferred from geological measurements of the slip rate of faults (see, e.g., Sieh 1978), regional strain changes, and so on.

By contrast, short-term temporal forewarning, in either a deterministic or a probabilistic sense, has proved elusive, although many attempts have been made to find effective clues. For example, in 1975, Chinese officials, using increased seismicity (foreshocks) and animal restlessness, evacuated a wide area before the damaging Haicheng earthquake (see Bolt, 2003). In sharp contrast, no forewarnings were issued before the 1976 Tangshan earthquake disaster. Elsewhere, emphasis has been placed on geodetic changes, such as geodimeter and GPS measurements of deformation of the Californian crust along the San Andreas fault. *Ex post facto* premonitory changes in the ground level have been claimed in a number of seismic zones worldwide, but the theoretical basis remains doubtful.

A much publicized prediction experiment in California depended on the recognition of a 22-year periodicity in moderate magnitude (M_L about 5.5) earthquakes centered on the San Andreas fault near Parkfield (Bakun and McEvilly, 1984). Similar size earthquakes were recorded in 1901, 1922, 1934 and 1966. In addition, available seismograms allowed quantitative comparison of the source mechanisms for the 1922, 1934 and 1966 earthquakes and indicated similarities. There followed the installation of many monitoring instruments to try to detect precursors for a possible 22-yearly repetition. These included changes in the ground water table, radon concentration, seismicity morphology and fault slippage. The prediction of repetition of such a characteristic earthquake in the years 1988 ± 4 , or since, proved unsuccessful. Worldwide, in the last two decades, no large damaging earthquakes have been predicted in any short-term meaningful sense. Realistic prediction of strong ground motion has, in contrast, significantly improved.

2.4.1 Special Strong Motion Characterization

As discussed in Section 2.3 and illustrated by actual accelerograms in Figure 2.7, large earthquakes produce ground motions near the fault source that are not only of large amplitude and period, but have more distinctive pulse-like wave patterns than the motions, say, 15 km away. The study of synthesized motions computed from finite-element or finite-difference models that incorporate the regional geological structure and realistic fault rupture help in understanding these differences. An example of the evolution of the seismic wave field in the case of a realistic if simplified geological model in the San Francisco Bay Area and the right-lateral rupture of the Hayward fault (strike slip) is shown in Figure 2.8. Only the horizontal component of the ground motion is plotted. There are several notable features in the computed horizontal intensity of the surface motion. First, the wave pattern is not symmetric about the fault, a consequence of the different rock properties in the region. Second, much more wave energy propagates in the direction of the fault rupture (south-to-north in this case) than opposite to it, a result of the moving wave source (the fault rupture) continually catching up with the radiated waves along the direction of faulting. This *directivity effect* is discussed in Section 2.4.4. Third, there are distinctive spatial variations of the ground motion with azimuth and site position related to local geology. The relevance of these intensity variations to earthquake engineering and hazard estimation has long been known, but their importance for the nonlinear behavior of soils and structures has only recently become widely appreciated (Heaton et al. 1995; Bolt 1996; Somerville et al. 1997).

Engineering characterization of motions, as illustrated in Figure 2.8, may also be given in terms of response spectra (see Joyner and Boore, 1982; Elghadamsi et al. 1988. This aspect of engineering seismology is addressed at length in Chapter 5).

2.4.2 Coherency of Wave Motion

Structures with multiple supports respond to the varying free-field accelerations applied to the supports. It follows that complete dynamic analysis of such structures requires suitably phased time histories applied at each support or equivalent modal response analysis with complete phase information appropriate to the local tectonic zone. In common practice, the usual engineering response spectrum describes only the amplitude of the acceleration motion and does not define the wave phase behavior incident to bridges and dams. Yet out-of-phase wave motions cause differential ground accelerations and differential rotations along the base of the structure. The concept of incoherency has been introduced into earthquake engineering to deal with these problems.

The appropriate measurement of the likeness of two wave trains has the technical name *coherency* and quantitative measures can be obtained in the time domain through simple cross-correlation in frequency- or time-dependent spectra. In the frequency domain, the complex coherency (see Abrahamson and Bolt 1987) between input points one and two is

$$C_{12}(w) = S_{12}(w)/[S_{11}(w)s_{22}(w)]^{1/2} \quad (2.10)$$

where S is the cross-spectral matrix. General curves have been derived from observations by seismograph arrays and applied to synthesized earthquake ground motions as realistic inputs to structures. Wave coherency, including the lag due to the passage of the waves across the structures, was incorporated, for example, in soil—structure interaction calculations for the 1998 seismic safety evaluation by PG&E of the Diablo Canyon nuclear reactor in California and in response analysis of large bridges for the California Department of Transportation. It has been shown that there is a high degree of transferability of these curves between different geological sites (see Abrahamson 1992). Specifically, a comparison of coherency functions for both vertical and horizontal motions indicated no significant difference in coherency reductions in the range 1 to 10 Hz for separation distances between input points of 400, 800 and 1500 m (Chiu, Amerbekian and Bolt 1995). For 4 Hz horizontal wave motions and a separation of input points of 400 m, a typical coherency reduction factor is 60 percent.

2.4.3 Time-History Duration

Field studies demonstrate that the *duration* of strong ground shaking is often a critical factor in how foundation materials and structures respond (see Novikova and Trifunac, 1994). Soil response in particular depends heavily on the increases in pore water pressure with cyclic input (Seed and Idriss, 1982). Also, nonlinear degradation of damaged structures (such as caused in large aftershocks) can lead to collapse. Recently, Bommer and Martinez-Pereira (1999), who reviewed 30 different definitions of strong ground motion duration, studied the characterization of ground shaking persistence in depth. They classify this general parameter into three generic classes: *bracketed*, *uniform* and *significant durations*. The first types were named by Bolt (1973) and the last was developed by Arias (1970). The first approach stresses the importance of frequency dependence and threshold level. By contrast, *significant duration* estimates are computed from the seismic energy evolution represented by the simple integral of the square of the ground acceleration, velocity, or displacement time histories. A common form is the *Arias Intensity*:

$$I_A = \frac{\pi}{2g} \int_0^\tau a^2(t) dt \quad (2.11)$$

where τ is the record length.

For a particular rock site, the shaking duration is a regression function of earthquake magnitude (or moment) (Bommer and Martinez-Pereira 1999),

$$\log D_E = 0.69 M_W - 3.70 \quad (2.12)$$

where D_E is Effective Duration in seconds as defined by Bommer and Martinez-Pereira. Site conditions are also very important (see Bard and Bouchon 1980), as illustrated by the development of seismic wave resonance in alluvial valleys (e.g., the 10-cycle dispersed seismic wave train recorded in the marginal Lake Texcoco zone of the 1985 Mexico City earthquake at distances of 350 km from the seismic source [see Bolt, 2003, pp. 278–281]. A recent computed model of this effect is shown in Figure 2.13 (Olsen et al. 1995).

2.4.4 Near-Fault Ground Motions

As mentioned earlier, near-fault ground motions often contain significant wave pulses. For strike-slip fault sources they dominate the horizontal motion and may appear as single or double pulses with single- or double-sided amplitudes. The duration (period) of the main pulse may range from 0.5 sec to 5 sec or more for the greatest magnitudes. These properties depend on the type, length and complexity of the fault rupture. There are two causes of these long-period pulses: first, constructive interference of the dynamic shaking due to directivity of the fault rupture; second, movement of the ground associated with the permanent offset of the ground. Their azimuthal dependence in both cases is a consequence of the elastic rebound of the rupturing fault. A descriptive term is the rapid fling of the ground during the fault slip. To keep these two effects separate, the terms *directivity pulse* and *fling step* have been used for the rupture directivity and elastic rebound effects, respectively (see Bolt and Abrahamson 2003). The two generated pulses attenuate differently from one another so that their separate measurements should not be statistically combined in a single sample.

Consider the implications for seismic-resistant design. *Rupture directivity* effects occur when the fault rupture source is toward the site and the slip direction (on the fault plane) is aligned with the rupture direction (Somerville et al. 1997). The horizontal recordings of stations in the 1966 Parkfield, California and the Pacoima station in the 1971 San Fernando, California (Bolt 1975), earthquake (see Figure 2.10) were the first to be discussed in the literature as showing near-fault velocity pulses. These cases, with maximum amplitudes of 78 and 113 cm/sec, respectively, consisted predominantly of horizontally polarized SH wave motion and were of a relatively long period (about 2 to 3 sec).

Additional recordings (compare Figure 2.10) in the near field of large sources have confirmed the pervasive presence of energetic pulses of this type, and they are now included routinely in the synthetic ground motions for seismic design purposes. Most recently, the availability of instrumented measured ground motion close to the sources of the 1994 Northridge earthquake (Heaton et al. 1995), the 1995 Kobe earthquake (Nakamura, 1995), and particularly the 1999 Chi-Chi earthquake (see Figure 2.9) provided important recordings of the velocity pulse under different conditions. Many detailed relevant studies of the Chi-Chi source and ground motions have already been published in a special volume of the *Bulletin of the Seismological Society of America* (Teng et al. 2001).

In the case of a fault rupture toward a site at a more or less constant velocity (almost as large as the S wave velocity), most of the seismic energy from the extended fault rupture arrives in a short time interval resulting in a single large long-period pulse of velocity and displacement, which occurs near the beginning of the record (see Figure 2.10). This wave pulse represents the cumulative effect of most all the seismic radiation from the moving dislocation. Coincidence of the radiation-pattern maximum for tangential motion and the wave focusing due to the rupture propagation direction toward the recording site produces a large displacement pulse normal to the fault strike (see Bullen and Bolt 1985, p. 443).

The directivity of the fault rupture causes spatial variations in ground motion amplitude and duration around faults and produces systematic differences between the strike-normal and strike-parallel components of the horizontal ground motion amplitudes (Somerville et al. 1997). These variations generally grow in size with increasing period. Modifications to empirical strong ground motion attenuation



FIGURE 2.9 Relief map showing ruptured Chelengpu fault trace (red line), epicenter of aftershocks, ground displacement in centimeters and sample horizontal ground accelerations. Star is epicenter, circle is thrust mechanism (after Y.-B. Tsai). See also color insert following page 2-30.

relations have been developed to account for the effects of rupture directivity on strong-motion amplitudes and durations based on an empirical analysis of near-fault recordings (Somerville et al. 1997). The ground motion parameters that have been modified include the average horizontal response spectral acceleration, the duration of the acceleration time history, and the ratio of strike-normal to strike-parallel spectral acceleration.

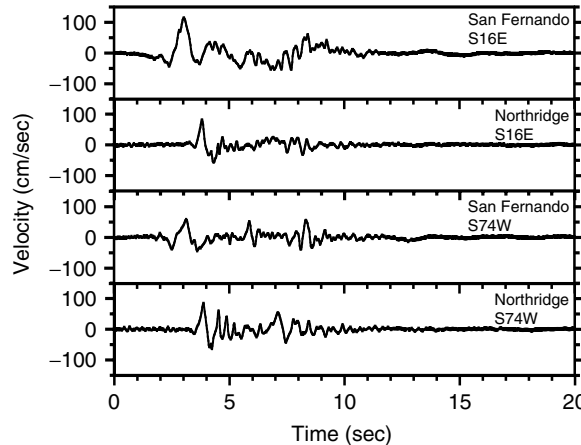


FIGURE 2.10 Ground motion velocity pulses at Pacoima Dam comparing the 1971 San Fernando, California, and 1994 Northridge, California, earthquakes.

Key results are that when rupture propagates toward a site, the response spectral amplitude is larger for periods longer than 0.6 sec. For sites located close to the faults, the strike-normal spectral acceleration is larger than the strike-parallel spectral acceleration at periods longer than 0.6 sec in a manner that depends on magnitude, distance and azimuth.

As in acoustics, the amplitude and frequency of the directivity pulse have a geometrical focusing factor that depends on the angle between the direction of wave propagation from the source and the direction of the source velocity. Instrumental measurements show that such directivity focusing can modify the amplitude velocity pulses by a factor of up to 10, while reducing the duration by a factor of 2. Whether single or multiple, the pulse may vary in the *impetus* nature of its onset and in its half-width period. A clear illustration is the recorded ground velocity of the October 15, 1979 Imperial Valley, California, earthquake generated by a strike-slip fault source (Figure 2.11). In this case, the main rupture front moved toward El Centro and away from Bonds Corner. Similar effects hold for thrust fault sources (see Somerville and Abrahamson, 1995).

Fling-step components occur when the site is located close to a seismogenic fault with significant surface rupture. The fling-step pulse occurs on the ground displacement component parallel to the slip direction. For strike-slip earthquakes, the rupture directivity is observed on the fault normal component and the static displacement fling-step is observed on the fault parallel component. Thus, for strike-slip earthquakes, the rupture directivity pulse and the fling-step pulse will separate themselves onto the two orthogonal horizontal components. For dip-slip earthquakes, the vectorial resolution is more complicated: although the rupture-directivity pulse is strongest on the fault normal component at a location directly up-dip from the hypocenter, a fling-step pulse may also occur on the horizontal component perpendicular to the strike of the fault. Thus, for dip-slip faults, directivity-pulse effects and fling-step effects may occur on the same component.

Prior to the 1999 Turkey and Taiwan earthquakes, nearly all of the observed large long-period pulses in near-fault ground motions were caused by rupture directivity effects. The Lucerne recording from the 1992 Landers, California, earthquake contained a directivity pulse on the fault normal component and a very long period fling-step pulse on the fault parallel component. Also, the ground motion data from the 1999 Izmit, Turkey, and Chi-Chi, Taiwan, earthquakes contain examples of large long-period velocity pulses due to the fling step. As an illustration, taken from Bolt and Abrahamson (2003), a horizontal component of velocity recorded at station TCU068 of the Chi-Chi earthquake is shown in Figure 2.12. These ground motions occur on the hanging wall near the northern end of the fault rupture and have the largest horizontal peak velocities ever recorded (300 cm/s on the north-south component). The velocity pulse from the fling-step effect velocity at TCU068 can be seen to be one-sided. If the fling step

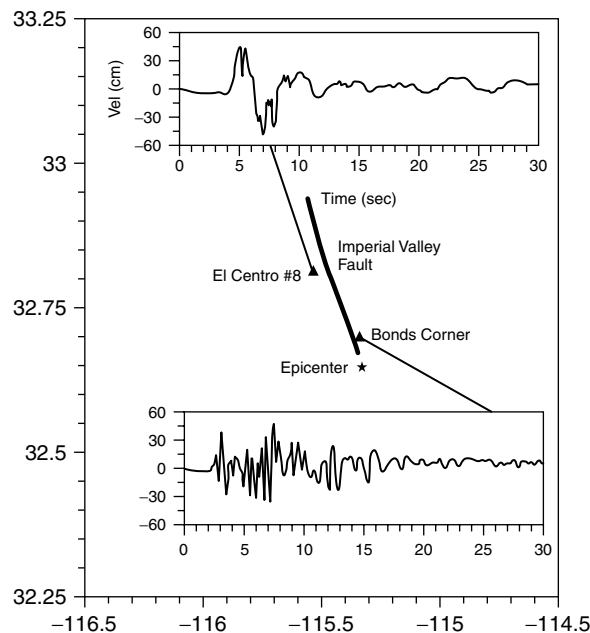


FIGURE 2.11 Velocity time histories (230 Comp) from the 1979 Imperial Valley, California, earthquake at the Bonds Corner and El Centro Differential Array strong ground motion recording sites (after Bolt and Abrahamson, *International Handbook of Earthquake and Engineering Seismology*, 2003).

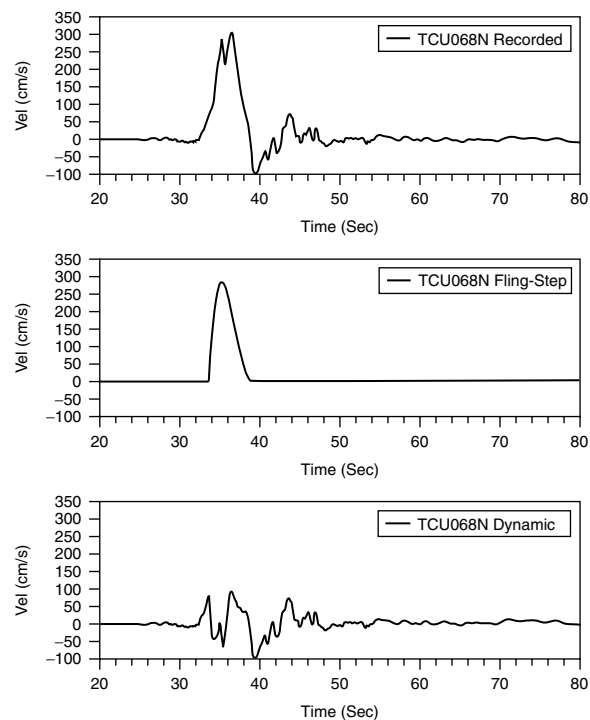


FIGURE 2.12 Velocity time histories for the north-south component of station TCU068 in the 1999 Chi-Chi earthquake (see Figure 2.9) separated into dynamic shaking and fling-step components (after Bolt and Abrahamson, *International Handbook of Earthquake and Engineering Seismology*, 2003).

is separated from dynamic shaking, the peak velocity of the dynamic component of shaking is reduced to about 100 cm/s, a more characteristic value of the amplitude of seismic S waves with this period. Chen et al. (2001) further discuss key records from the Taiwan earthquake.

Robust estimates that predict the peak velocity from fling steps are not available at this time. In the displacement ground motion, the fling step can be parameterized simply by the amplitude of the tectonic deformation and the *rise time* (the time it takes for the fault to slip at a point). A suggested algebraic form for this permanent near-fault strain is

$$v = a \cot^{-1} bx \quad (2.13)$$

where v is the horizontal surface fling displacement parallel to the rebounded fault and x is the perpendicular distance away from the fault.

2.4.5 Estimating Time Histories

At the fault dislocation itself, there is a finite time for slip to take place in the form of an elastic rebound of each side of the fault leading to a decrease of overall crustal strain. The slip can have vertical components, as well as horizontal components, and can vary along the fault. The waves are produced near the moving dislocation front as a result of the release of the strain energy in the slippage. In many ways this model resembles the radio waves being radiated from a finite antenna. At the far field, the theory of radio propagation gives complete solutions for the reception of radio signals through stratified media. However, when the receiver is very near to the extended antenna, the signal becomes mixed because of the finiteness of the source and interference through antenna end effects. In the earthquake source case, the main source parameters in the fault model are as follows: rupture length (L), rupture width (W), fault slippage (offset) (D), rupture velocity (V), rise time (T) and roughness (asperity) distribution density ($\phi(x)$). Rise time estimates remain uncertain, perhaps 2 to 10 sec in large fault ruptures.

The main work in theoretical seismology on source properties today continues to be the determination of those parameters that are essential, whether the selected set is an optimal one, and how best to estimate each parameter from field observations and from analysis of the seismograms made in the near field and the far field.

A number of papers on synthetic seismograms have recently been published that illustrate the theoretical approach and demonstrate how numerical models for seismic waves near the source can be computed realistically (see papers in Archuleta, 1984; Bolt, 1987; O'Connell, 1999). Nevertheless, there are difficulties in the purely synthetic prediction of modeling certain observed complexities and there is a lack of uniqueness in the physical formulations. It is recommended that for engineering purposes, such synthetic motions should be compared when possible with the three observed orthogonal components of acceleration, velocity or displacement at a site.

Numerical modeling can be particularly helpful in predicting the effect of certain special geological structures on hazard at a site. Consider, for example, the response of the Los Angeles alluvial basin to a large earthquake from a slip of the San Andreas Fault (Olsen et al. 1995). A computer simulation was made in 1995 that gives wave motion for a three-dimensional finite-difference model when the source is a magnitude 7.75 earthquake along the 170 km section of the San Andreas Fault between Fort Tejon Pass and San Bernardino. The results are graphed in Figure 2.13. The wave propagation is represented as horizontal particle velocities of the ground parallel to the San Andreas Fault. After 40 sec, ground motion in the basin begins to intensify and 10 sec later the entire basin is responding to large amplitude surface waves. (The waves shown are spectrally limited to frequencies below 0.4 Hz. In reality, the actual ground motions would contain much higher ground frequencies.) The component of motion perpendicular to the strike is 25 percent larger than the parallel component near the fault due to the directivity of the rupture (see Section 2.4.4). This simulation predicted long-period peak ground velocities greater than 1 m/sec in some areas in Los Angeles, even though the main trough of the basin is about 60 km

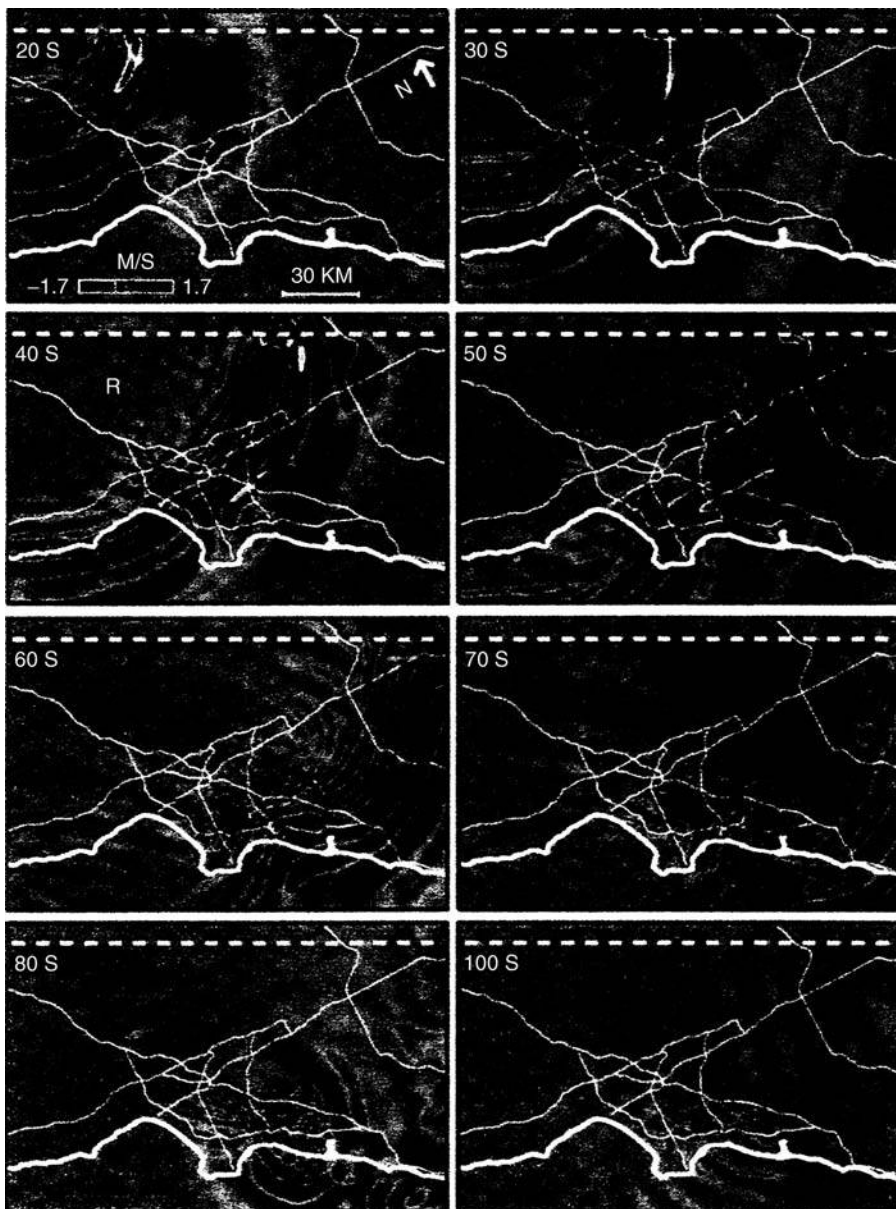


FIGURE 2.13 Snapshots of simulated wave propagation in the Los Angeles area for hypothetical earthquake; the snapshots depict the horizontal particle velocities that represent shaking parallel to the San Andreas fault from 20 sec to 100 sec after the origin time of the rupture. Red depicts large amplitudes of both positive and negative polarity. R depicts an area of local resonance above the deepest part of the San Fernando Valley. (Olsen, K.B. Site amplification in the Los Angeles basin from three-dimensional modeling of ground motion, *Bull. Seism. Soc. Am.*, 90, 577–594, 2003.)

from the fault. Later analysis of the same region can be found in Olsen (2000). He suggests that computed amplitude factors (up to six in deeper parts of the basin) should be used as a guide with caution.

Instead of purely synthetic models, quasi-empirical seismic strong ground motions, based on modified actual recordings of similar earthquakes, are now most commonly used to estimate seismic hazard. Two equivalent representations are considered together. The first is the seismogram or *time history* of the ground motion at the site. The second is the Fourier or *response spectra* for the whole motion at the site.

TABLE 2.2 Examples of Near-Fault Strong-Motion Recordings from Crustal Earthquakes with Large Peak Horizontal Ground Motions

Earthquakes	Magnitude (M_W)	Source Mechanism	Distance (km)*	Acc (g)	Vel (cm/sec)	Disp (cm)
1940 Imperial Valley (El Centro, 270)	7.0	Strike slip	8	0.22	30	24
1971 San Fernando (Pacoima 164)	6.7	Thrust	3	1.23	113	36
1979 Imperial Valley (EC 8, 140)	6.5	Strike slip	8	0.60	54	32
1992 Eritzican (Eritzican, 000)	6.9	Strike Slip	2	0.52	84	27
1989 Loma Prieta (Los Gatos, 000)	6.9	Oblique	5	0.56	95	41
1992 Landers (Lucerne, 260)	7.3	Strike Slip	1	0.73	147	63
1992 Cape Mendocino (Cape Mendocino, 000)	7.1	Thrust	9	1.50	127	41
1994 Northridge (Rinaldi, 228)	6.7	Thrust	3	0.84	166	29
1995 Kobe (Takatori, 000)	6.9	Strike Slip	1	0.61	127	36
1999 Kocaeli (SKR, 090)	7.4	Strike Slip	3	0.41	80	205
1999 Chi-Chi (TCU068, 000)	7.6	Thrust	1	0.38	306	940

* Surface distance from fault source.

These two representations of seismic hazard are connected by appropriate transformations between the time and frequency domains.

In the simplest time-history representation, the major interest has traditionally been in the peak amplitudes of ground acceleration, velocity and displacement as a function of frequency. In recent work related to large and critical structures, however, the pattern of wave motion has been recognized as crucial in earthquake engineering because the nonlinear response of such structures is often dependent on the sequence of arrival of the various types of waves (see Bolt 1996). In other words, damage would be different if the ground motion were run backward rather than in the actual sequence of arrival. In this respect, synthesis of input motions entails that phase spectra should be considered along with the amplitude spectrum. The phasing of the various wave types on the artificial seismograms can be checked by seismological estimation of times of arrival of the P, S, directivity pulse, fling and surface waves. In this way, a realistic envelope of amplitudes in the time histories can be obtained.

In the usual construction method, the initial step is to define, from geological and seismological information, the appropriate earthquake sources for the site of interest. The fault source selection may be deterministic or probabilistic and may be decided on grounds of acceptable risk (Reiter 1990). Next, specification of the propagation path distance as well as the P, S, and surface wave velocities along the path is made. (These speeds allow calculation of the appropriate wave propagation delays between the source and the multisupport points of the structure (see Section 2.4.2) and the angles of approach of the incident seismic waves.)

Computation of realistic motion then proceeds as a series of nonlinear iterations, starting with the most appropriate observed strong-motion record available, called the *seed motion*, to a set of more specific time histories, which incorporate the seismologically defined wave patterns. The seed strong motion accelerograms are chosen to approximate the seismic source type (dip-slip, etc.), and geological specifications for the seismic zone in question. A set of suggested time histories is listed in Table 2.2. Many digitized records of samples can be downloaded using the Virtual Data Center (VDC) Web site of the Consortium of Organizations for Strong-Motion Observational Systems (COSMOS) (see Internet Web site <http://www.cosmos-eq.org>) among others. Applying engineering constraints, such as a selected response amplitude spectrum, controls the frequency content. Such *target spectra* are obtained, for example, from previous engineering analyses, and from earthquake building codes (see, e.g., UBC 1997). The fit between the final iteration and the target spectrum should fall within one standard error. Each predicted time history must fit within a few percent of the specified peak ground acceleration and displacement, as well as any predicted velocity pulse and fling (see Section 2.4.4). To ensure an adequate range of phase patterns, at least three sets of time histories are recommended, starting from different seed earthquakes. When three component sets of input time histories are needed, checks for interset independence (correlation, say, below 5 to 10 percent) should be made by computing cross-correlations.

Engineering experience demonstrates that the structural response grows rapidly with the repetition of pulses of input motion. Increased number of multiple pulses in the velocity time history increases the nonlinear demand on the structure. Illustrations can be found in recordings of the 1994 Northridge and 1989 Loma Prieta, California, earthquakes. Damage in the 1995 Kobe, Japan, earthquake was also perhaps increased by the presence of two consecutive pulses in the ground velocity as recorded near the ruptured fault.

2.4.6 Available Strong Motion Recordings

For engineering seismology use, it is advantageous to record directly either the ground acceleration or the ground displacement. If the natural period of the recording seismometer is very short compared with the predominant period of the ground motion, the recorded signal is directly proportional to the acceleration of the ground. In this case also, sensitivity of the accelerometer is small, which is an advantage in recording strong ground motion. Because instrument design can provide relatively small devices (most recently MEMS silicon chip instruments) that are not sensitive to long-term tilts, drifts of the ground have been the preferred type of recorder rather than displacement meters. In past decades, recording used an analogue signal on paper or films. Such recordings are still obtained by the reliable AR-20s, of which many thousands remain in service around the world. Because large earthquakes are rare events, many strong motion accelerometers do not record continuously, but are triggered by the initial P wave in the earthquake. The result is to lose part of the initial ground motion. Thus cross-correlation of ground motions between neighboring instruments cannot be performed. Analogue records require automatic digitization to allow integration to ground velocity and displacement and conversion to frequency spectra.

These days, instruments record digitally in both the free field of earthquakes (i.e., away from structures) and in structures with solid-state memories and absolute time marking, usually obtained from GPS satellite clocks. The digital signals are usually streams of 12- or 16-bit words. The common 12-bit word uses 72 dB (i.e., $20 \log_{10}^{12}$) dynamic range and is immediately accessible for processing in computers.

Corrections must be carried out, even with digital recordings, to allow for nonlinear response of the accelerometer device. For engineering purposes, fidelity must be ensured in the integration to the now essential ground velocity and displacement. Various procedures have been suggested to establish a zero-acceleration line, such as assuming second-degree polynomial for the base line followed by subtraction. Another method for processing digital seismic wave histories (Iwan and Chen 1994), is to compute the average ordinates of the acceleration velocity over the final segment of the record and equate them to zero. In older standard processing, filters are applied to remove waves with periods greater than about 8 to 10 sec. Above such long periods, users are warned not to assume that the response spectrum from such filtered records or the modified time histories are complete. Recently, it has been established that with special care in the choice of filters and high dynamic range records, displacement ground motions out to DC levels can be obtained. This ability has been checked in the case of the 1999 Chi-Chi, Taiwan, earthquake for strong-motion recordings near the Chelungpu fault against field measurements of the fault offset (see Figure 2.9) and against adjacent GPS measurements.

Digital datasets in various countries and from various earthquake engineering groups often have different formats and processing methods. Important sets have been obtained in the United States by the U.S. Geological Survey (USGS) and the California Strong-Motion Instrumentation Program (CSMIP) of the Division of Mines and Geology (CDMG), in 2002 renamed the California Geological Survey (CGS). Recordings of these organizations and others in the United States are now available on the Consortium of Strong-Motion Observation Systems' (COSMOS) Virtual Data Center (VDC) maintained at the University of California, Santa Barbara. COSMOS has set up uniform standards for processing and provides a number of services for the Web user (see Internet Web site <http://www.cosmos-eq.org>). As of early 2004, the COSMOS VDC contained over 1800 acceleration traces for 393 earthquakes and 2500 stations. The center contains important recordings from the Chi-Chi, Taiwan, earthquake and sets from Turkey, Armenia, Costa Rica, New Zealand and India. The webpage provides checks of data quality and a connection directory to the original sources for large downloads. Another important dataset (ISESD)

became available in 2000 for strong-motion recordings from Europe and the Middle East available at <http://www.ised.cv.ic.ac.uk> (Ambraseys, Smit, Berardi, Rinaldis, Cotton and Berge-Thierry 2000).

2.4.7 Vertical Ground Motions

Joint consideration of the vertical motion of the ground with horizontal components is becoming more usual in earthquake-resistant design of large structures such as concrete arch dams. Striking frequency content differences between vertical and horizontal components of strong ground motions have been described over many years in numerous studies of various earthquakes recorded in different parts of the world. Recent examples can be found in Bard and Bouchon (1980), Bozorgnia and Niazi (1993) and Bozorgnia et al. (1999). These studies consistently find higher frequency content of the vertical ground motions in alluvial basins compared with the horizontal motions. The feature is of practical importance because of the connection between the overall high-frequency content of the vertical strong ground motions and their peak ground accelerations (PGA). Another distinct feature of vertical strong ground motions is their greater incoherency compared with the horizontal wave components at the same sites. Consistent observations of low coherency of vertical ground motions have led to the incorporation of low-coherence empirical functions for vertical components into engineering design practices.

The importance of understanding the mechanism of the generation of vertical strong ground motions has been emphasized by recent analyses (e.g., Shakal et al. 1994; Bozorgnia et al. 1999) of the ratio of vertical-to-horizontal PGA from the acceleration records of the 1994 Northridge, California, earthquake. In this earthquake, most of the sites with such high ratios were deep soil sites, often in alluvial basins. In particular, of the nine sites with a ratio of vertical-to-horizontal PGA of unity and more, only one was located on a rock site.

Many strong-motion recordings in alluvial basins have behavior agreeing with the hypothesis that S-to-P wave conversion and wave scattering at the basin—bedrock interface are an important mechanism for supplying energy to vertical components of strong ground motions. The differences for P and S waves of the combined scattering and inelastic attenuation in sedimentary basins appear to be mainly responsible for the observed frequency content differences of the vertical and horizontal components of ground motions. In one study (Amirbekian and Bolt, 1998), of observations after the 1994 Northridge, California, the main shock provided evidence in agreement with the hypothesis that S-to-P converted waves are the dominant vertical ground motions recorded at such alluvial sites. In addition, the explanation that vertical motions are mainly S-to-P converted waves provides a reason for another feature of vertical ground motions: namely, their low coherence compared with simultaneously arriving horizontal motions.

Further experimental validation is needed concerning both the origin of the energy in vertical strong ground motions and, particularly, about the factors affecting the frequency content of vertical motions. In the meantime, simple amplitude scaling of horizontal motions to represent vertical motions should be avoided. Further discussions on vertical seismic motions can be found in Frankel (1999) and Campbell and Bozorgnia (2003).

2.5 Attenuation Estimation and Uncertainties

As indicated in earlier sections, the prediction of ground motions and seismic hazard curves for engineering purposes involves a number of assumptions and extrapolations (see Reiter, 1990). A major difficulty is ignorance of the actual wave attenuation for the region in question. The importance of attenuation factors in calculation of predicted ground motion at arbitrary distances has generated much work on robust empirical attenuation forms and on appropriate transference of measurements based on geological criteria.

Usually wave attenuation changes significantly from one geological province to another and local regional studies are advisable to calibrate the parameters involved. A discussion is given by Bullen and Bolt (1985) (and, e.g., Ambraseys and Bommer 1991; 1995; Toro et al. 1997; Raoof et al. 1999). Results for North America have been recently summarized (Abrahamson and Shedlock 1997). In the latter paper,

attenuation relations were grouped into three main tectonic categories: shallow crustal earthquakes in active tectonic regions (e.g., California), shallow crustal earthquakes in stable continental regions (e.g., eastern United States), and subduction zone (e.g., the Aleutian Islands) earthquakes. Because peak ground motions from subduction zone earthquakes generally attenuate more slowly than those from shallow crustal earthquakes in tectonically active continental regions, ground motions for the different sources should be estimated separately.

One way to address regionalization of attenuation relations is to estimate a constant scale factor to adjust a global attenuation model to a specific region. (This can reflect differences in the earthquake source or differences in the site geology categories.) This procedure allows measurement over a range of distances to fix the slope of the local attenuation relation while maintaining the magnitude scaling of the global model. Additional parameters can be made region-specific. An example of this approach to regionalizing attenuation relations as more strong-motion data become available is given by McVerry and Zhao (1999).

The description of attenuation estimations that follows is taken substantially from Bolt and Abrahamson (2003). Although horizontal ground motions are dealt with here, some statistics on vertical motions have been published (e.g., Abrahamson and Litehiser 1989). In any case, the statistical samples in the estimation of attenuation relations start by examining random variability and scientific uncertainty in ground motions differently (e.g., Toro et al. 1997). For a given model, *variability* is defined as the randomness in the ground motions that will occur in future earthquakes. It is usually expressed as the standard deviation of the fitted attenuation equation. By contrast, *uncertainty* is defined as the scientific uncertainty in the ground motion model due to limited information; including alternative attenuation results often treats the measure of ignorance. Further, in seismic hazard analyses, the terms *aleatory* and *epistemic* have been introduced to describe variability and uncertainty, respectively (see Chapter 7).

The Northridge, California, earthquake of January 17, 1994 allowed an important comparison between (a) the theoretical seismological expectations and actual seismic wave recordings and (b) behavior of earthquake-resistant structures (see Bolt 1996). This magnitude 6.7 earthquake struck southern California at 4:31 AM local time. The earthquake source rebound occurred on a southerly dipping blind-thrust fault. The rupture began at a focus about 18 km deep under the Northridge area of the San Fernando Valley. The rupture then propagated along a 45° dipping fault to within about 4 km of the surface under the Santa Susannah Mountains. No major surface fault rupture was observed, although the mountainous area sustained extensional surface fracturing at various places with uplifts of tens of centimeters. The causative fault dipped in the opposite sense to an adjacent one that caused the neighboring 1971 San Fernando earthquake.

Like the 1971 San Fernando, California, earthquake, the 1994 shaking tested many types of design such as base isolation and the value of the latest Uniform Building Codes. Peak accelerations, recorded by strong-motion accelerometers in Los Angeles and the San Fernando Valley area, were systematically larger than predicted by average curves obtained from previous California earthquakes. It is notable that the ground motions at the Olive View Hospital (see Figure 2.7) are similar to those obtained at the Pacoima Dam abutment site in the 1971 thrust earthquake. Both recordings show a directivity pulse and are useful *seed* motions for some engineering response studies.

As mentioned in Section 2, although different measures of earthquake magnitude are still used, particularly with historical data, the moment magnitude (M_W) is now usually adopted as a standard measure of size in attenuation statistics. Also, nowadays, some form of closest distance to the rupture is used as the distance parameter rather than epicentral or hypocentral distance (Joyner and Boore, 1988; Ambraseys and Bommer 1995). It is important to use the appropriate distance measure for a given attenuation relation. The most common source, ray path and site parameters are magnitude, distance, style-of-fault, directivity and site classification. Rupture directivity is defined in detail in Section 2.4.4 and is not discussed here. In some studies, additional parameters are used: hanging-wall flag, rupture directivity parameters, focal depth and soil depth classification.

There are also differences in site classification schemes in different regions that make comparison of estimates of ground motions from alternative estimates difficult. Broad site categories such as rock, stiff-

soil, and soft-soil are common, but more quantitative site classifications based on the S-wave velocity, such as the average S-wave speed in the top 30 m (e.g., Boore et al. 1997) are now preferred. Most attenuation relations simply use a site category such as deep soil; however, this general category covers a wide range of soil depths from less than 100 m to several kilometers of sediments. Some attenuation relations (e.g., Campbell 1997) use an additional site parameter to describe the depth of the sediment.

A style-of-faulting algebraic flag is needed in the regression to separate the effects of different source types. For the common shallow crustal earthquakes, seismic ground motions differ systematically when generated by strike-slip, thrust, or normal mechanisms (e.g., Somerville and Abrahamson 1995; Toro et al. 1997; Saikia and Somerville, 1997). Given the same earthquake magnitude, distance to the site and site condition, the ground motions from thrust earthquakes tend to be (about 20–30 percent) larger than the ground motions from strike-slip earthquakes and the ground motions from normal faulting earthquakes tend to be smaller (about 20 percent) than the ground motions from strike-slip earthquakes. For subduction earthquakes, the ground motions systematically differ from those generated by interface or intraslab earthquakes (e.g., Youngs et al. 1997). Again, for the same magnitude, distance and site condition, the ground motions from intra-slab earthquakes tend to be about 40 percent larger than the ground motions from interslab earthquakes.

For thrust faults, high-frequency ground motions on the upthrown block (hanging wall side of a thrust fault) are larger than on the downdropped block (footwall) (e.g., Somerville and Abrahamson 1995). This increase in ground motions on the hanging wall side is in part an artifact of using a rupture distance measure. If a site on the hanging wall and footwall are at the same rupture distance, the site on the hanging wall side is closer to more of the fault than the site on the footwall side.

2.5.1 Construction of Attenuation Relations

Regression analyses require an assumed functional form for the attenuation. Two types of magnitude scaling are used in attenuation relations. In the first case, the shape of the attenuation with distance is independent of magnitude. A typical form of this type of model for rock site conditions is given in Equation 2.14:

$$\ln Y(M, R, F) = c_1 + c_2 M + c_3 M^2 + c_4 \ln(R + c_5) + c_6 F \quad (2.14)$$

where Y is the ground motion parameter (e.g., peak acceleration or response spectral value), M is the magnitude, R is the distance measure and F is a flag for the style-of-faulting (reverse, strike slip, normal). A widely used example of this form was derived by Boore et al. (1997).

Alternatively, the specific curvature of the attenuation equation is magnitude dependent (see Figure 2.14) (see Youngs et al. 1995). The available observational evidence on this point is that at short distances, the spacing between curves of increasing magnitude decreases. This saturation of the ground motion implies that at short distances, moderate magnitude earthquakes produce similar levels of shaking as large magnitude earthquakes. (Durations would differ.) Some attenuation relations use a combination of these two models with constant attenuation shapes for moderate magnitudes (e.g., $M < 6.5$) and saturation for larger magnitudes.

Two appropriate algebraic forms are shown in Equations 2.15 and 2.16: replacing c_5 in Equation 2.14 with a magnitude-dependent term, $f_1(M)$; or replacing the distance slope, c_4 , in Equation 2.14 with a magnitude-dependent slope, $f_2(M)$. For rock ground site conditions, the relations are

$$\ln Y(M, R, F) = c_1 + c_2 M + c_3 M^2 + c_4 \ln[R + f_1(M)] + c_6 F \quad (2.15)$$

and

$$\ln Y(M, R, F) = c_1 + c_2 M + c_3 M^2 + [c_4 + f_2(M)] \ln(R + c_5) + c_6 F \quad (2.16)$$

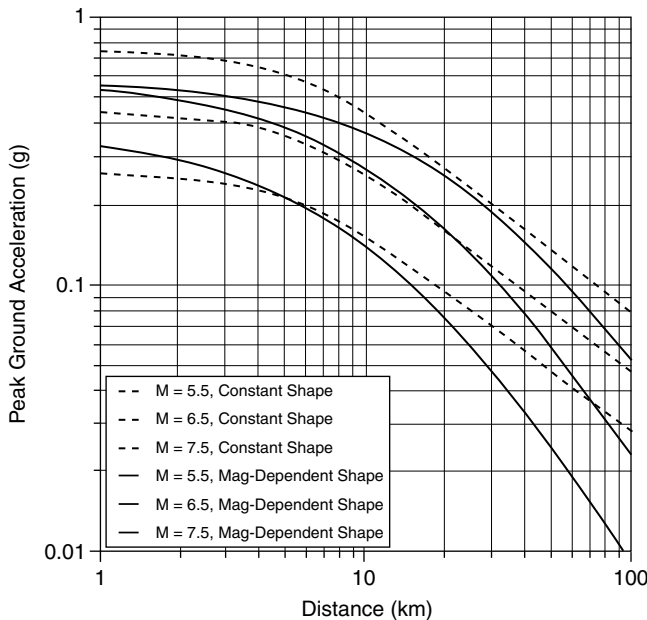


FIGURE 2.14 Comparison of constant and magnitude dependent shapes of attenuation relations.

A commonly assumed function $f_1(M)$ is

$$f_1(M) = c_7 \exp(c_8 M) \quad (2.17)$$

If $c_3 = 0$ (which is common for high frequencies) and $c_8 = -c_2/c_4$, then the ground motion at zero distance is magnitude independent and the model has complete magnitude saturation. If $c_8 > -c_2/c_4$, then the model is oversaturated. In that case, at short distances, the median ground motion is reduced as the magnitude increases. An example of an attenuation relation based on Equation 2.16 is given by Abrahamson and Silva (1997). For the functional form, $f_2(M) = c_9 M$, the model has complete saturation if $c_8 = -c_2/\ln(c_5)$. If $c_8 < -c_2/\ln(c_5)$, then the model is oversaturated.

At distances less than about 50 km, the above two different functional forms of the attenuation relation lead to similar curves, but at large distances, they become different (Figure 2.14). Because most engineering interest has been on attenuation relations for shallow crustal earthquakes in active tectonic regions for distances less than 50 km, these gradual differences have not been studied in detail.

In the Eastern United States, some researchers have suggested incorporating a variation in the distance slope of the attenuation relation to accommodate the increase in ground motions due to supercritical reflections from the base of the crust (e.g., Nutti 1975; Atkinson and Boore 1995; Saikia and Somerville 1997; Campbell 2002). Incorporating a multilinear form of the attenuation relation with different c_4 terms for different distance ranges usually accomplishes this, typically leading to a flattening of the attenuation curve at distances of about 100 km. This is most significant for regions in which the high activity sources are at a large distance from the site.

An important statistical issue in developing attenuation relations is the uneven sampling of the data from different earthquakes. For example, in some cases, an earthquake may have only one or two recordings (e.g., the 1940 El Centro event), whereas some of the recent earthquakes have hundreds of recordings (e.g., the 1999 Chi-Chi earthquake). Should the well-recorded earthquakes overwhelm the poorly recorded earthquakes? Should the poorly recorded earthquakes be given equal weight as the well-recorded earthquakes? The use of statistical weights can reduce this uneven sampling problem. There are two extremes: give equal weight to each data point or give equal weight to each earthquake. The random

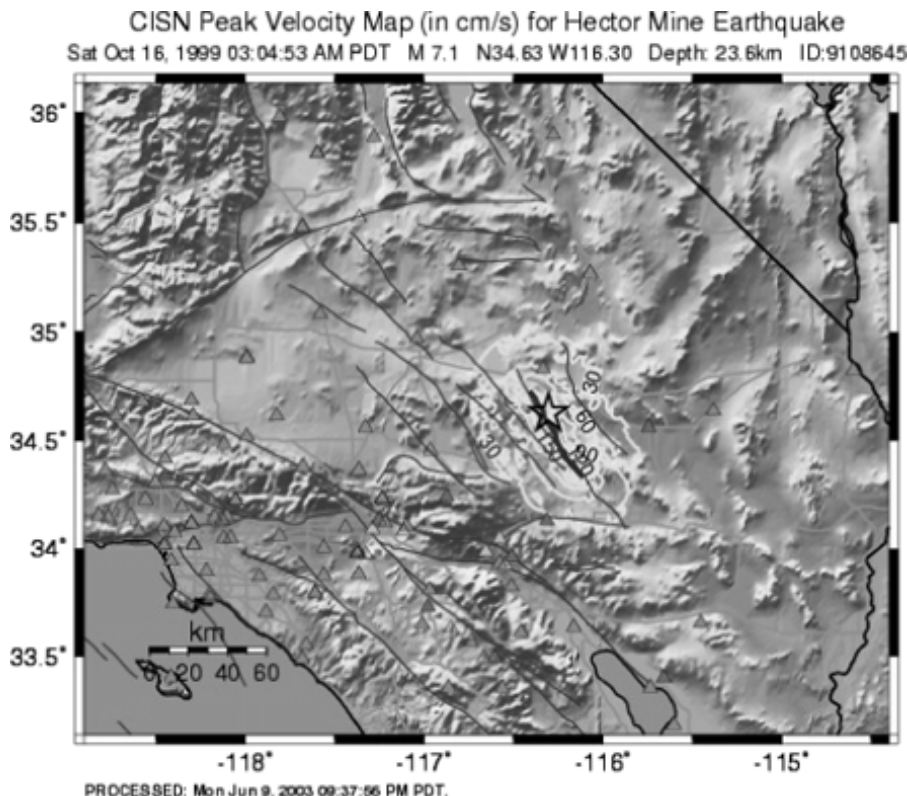


FIGURE 2.15 TriNet peak velocity map. See also color insert following page 2-30.

effects model (Brillinger and Preisler 1984) uses a weighting scheme that varies between equal weight to each earthquake and equal weight to each data point depending on the distribution of the data.

In addition to the median measure of ground motion, the standard deviation of the measured ground motion parameters is also important for either deterministic or probabilistic hazard analyses. Worldwide, it is common to use a constant standard deviation, but recently, several attenuation relations have attributed magnitude or amplitude dependence to the standard deviation. For example, Abrahamson and Silva (1997) allow the standard deviation to vary as a function of the magnitude of the earthquake. The regression result is that the standard deviation is smaller for large magnitude earthquakes. Campbell and Bozorgnia (2003) allow the standard deviation to vary as a function of the amplitude of the ground motion. The result is that the standard deviation is smaller for larger amplitudes of ground motion. Both of these models can have significant effect on the estimation of design ground motions.

Finally, the above discussion referred primarily to ground acceleration and more rarely for displacement (see Gregor and Bolt 1997) as a random variable. Attenuation curves for velocity are also published (see papers in Abrahamson and Shedlock 1997).

2.5.2 Rapid Response: ShakeMaps

An important point in summarizing the present status of assessment of seismic strong-ground motions is that in a number of countries digital strong-motion systems linked to communication centers (telephone, wireless, or satellite) have now been installed. These provide processed observational data within a few minutes after shaking occurs. In California usage, a ShakeMap is a computer-generated representation of ground shaking produced by an earthquake (see Figure 2.15). The computation produces a range of ground-shaking levels at sites throughout the region using relations that depend on distance from the earthquake source, the rock and soil conditions through the region, and on variations in the

propagation of seismic waves due to complexities in the structure of the Earth's crust. One format of the maps contours peak ground velocity and spectral acceleration at 0.3, 1.0 and 3.0 sec and gives the display in graduated color.

Not only peak ground acceleration and velocity maps are computed using instrumental measurements, but by empirical correlations of the various scales, approximate Modified Mercalli Intensity estimates are mapped. These maps make it easier to relate the recorded ground motions to the felt shaking and damage distribution. In a scheme used in the Los Angeles basin, the Instrumental Intensity map is based on a combined regression of recorded peak acceleration and velocity amplitudes (see Wald et al. 1999).

In 2001, such ShakeMaps for rapid response purposes became available publicly on the Internet (www.trinet.org/shake) for significant earthquakes in the Los Angeles region and the Bay Area of California. Similar maps are available in other countries. They represent a major advance not only for emergency response, but also for scientific and engineering purposes. Their evolution and improvement will no doubt be rapid.

2.6 Future Challenges

The seismological problems dealt with in this chapter will no doubt be much extended in subsequent years. First, greater sampling of strong-ground motions at all distances from fault sources of various mechanisms and magnitudes will inevitably become available. An excellent example is the dense recording of the 1999 Chi-Chi, Taiwan, earthquake (see Loh and Liao 2000).

Another interesting recent case contains observations from the major Alaska earthquake of November 3, 2002. This 7.9 magnitude earthquake was caused by a rupture along the Denali fault for 200 km., with right lateral offsets up to 10 m. A number of strong-motion records were obtained; fault offset under the Trans-Alaskan oil pipeline did not cause pipe breakage.

Second, more realistic 3D numerical models will solve the problem of the sequential development of the wave mixtures as the waves pass through different geological structures. Two difficulties may persist: the lack of knowledge of the roughness distribution along the dislocated fault and, in many places, quantitative knowledge of the soil, alluvium and crustal rock variations in the region. For these reasons, probabilistic estimation as a basis of engineering decisions will be necessary.

A recent significant ingredient in general motion measurement is correlation with precisely mapped coseismic ground deformations. Networks of GPS instruments will no doubt help greatly in future understanding of the source problem and the correct adjustment to strong-motion displacement records. A broad collection of standardized strong-motion time histories represented by both amplitude spectra and phase spectra is now being accumulated in virtual libraries for easy access on the Internet. Such records will provide greater confidence in seismologically sound selection of ground motion estimates.

Additional instrumentation to record strong ground motion remains a crucial need in earthquake countries around the world (see <http://www.cosmos-eq.org> for updated information and access to a comprehensive strong-motion recording database). Such basic systems should measure not only free-field surface motions, but also downhole motions to record the wave changes as they emerge at the Earth's surface.

In particular, many contemporary attenuation estimates for ground velocity and displacement will no doubt be improved as more recorded measurements are included, rendering earlier regressions obsolete. The statistical basis for the separation of the probability distributions as functions of the various key parameters will become more robust. To keep abreast of changes, ground motion attenuation model information may be found at <http://www.geohazards.cr.usgs.gov/earthquake.html>. Click on Engineering Seismology, then on Ground Motion Information.

Acknowledgments

Professors Ralph Archuleta and Douglas Dreger provided copies of figures. Dr. Yousef Bozorgnia offered helpful comments. Ms. Claire Johnson skillfully constructed the manuscript. My thanks to all.

Glossary

- accelerometer** — a seismograph for measuring ground acceleration as a function of time.
- active fault** — a fault along which slip has occurred, either in historical or Holocene or Quaternary time, or earthquake foci are located.
- asperities (fault)** — roughness on the fault surface subject to slip.
- blind thrust** — a thrust-fault deep in the crust with no or only indirect surface expression such as a fold structure.
- body-wave magnitude** — magnitude of an earthquake as estimated from the amplitude of body wave.
- digital recording** — a series of discrete numerical digits.
- duration (of strong shaking)** — the time interval between the first and last peaks of strong ground motion above a specified amplitude.
- epicenter** — the point on the Earth's surface directly above the focus (or hypocenter) of an earthquake.
- fault** — a fracture or zone of fractures in rock along which the two sides have been displaced relative to each other parallel to the fracture. The total fault off-set may range from centimeters to kilometers.
- focal depth (of earthquakes)** — the depth of the focus below the surface of the Earth.
- intensity (of earthquakes)** — a measure of ground shaking obtained from the damage done to structures built by humans, changes in the Earth's surface, and felt reports.
- isoseismal** — contour lines drawn to separate one level of seismic intensity from another.
- liquefaction (of soil)** — process of soil and sand behaving like a dense fluid rather than a wet solid mass during an earthquake.
- Love waves** — seismic surface waves with only horizontal shear motion transverse to the direction of propagation.
- magnitude (of earthquakes)** — a measure of earthquake size, determined by taking the common logarithm (base 10) of the largest ground motion recorded during the arrival of a seismic wave type and applying a standard correction for distance to the epicenter.
- moment (of earthquakes)** — a measure of earthquake size related to the leverage of the forces (couples) across the area of the fault slip, equal to the rigidity of the rock times the area of faulting times the amount of slip. Dimensions are dyne-cm (or Newton-meters).
- moment magnitude** — magnitude M_w of an earthquake estimated from the seismic moment.
- plate (tectonic)** — a large, relatively rigid segment of the Earth's lithosphere that moves in relation to other plates over the deeper interior. Plates meet in convergence zones and separate at divergence zones.
- plate tectonics** — a geological model in which the Earth's crust and uppermost mantle (the lithosphere) are divided into a number of more-or-less rigid segments (plates).
- prediction (of earthquakes)** — the forecasting in time, place, and magnitude of an earthquake; the forecasting of strong ground motions.
- P wave** — the primary or fastest wave traveling away from a seismic event through the rock and consisting of a train of compressions and dilatations of the material.
- Rayleigh waves** — seismic surface waves with ground motion only in a vertical plane containing the direction of propagation of the waves.
- risk (seismic)** — the probability of life and property loss from an earthquake hazard within a given time interval and region.
- scarp (fault)** — a cliff or steep slope formed by displacement of the ground surface.
- seismicity** — the occurrence of earthquakes in space and time.
- seismology** — the study of earthquakes, seismic sources, and wave propagation through the Earth.
- strong ground motion** — the shaking of the ground near an earthquake source made up of large amplitude seismic waves of various types.
- S wave** — the secondary seismic wave, traveling more slowly than the P wave and consisting of elastic vibrations transverse to the direction of travel. It cannot propagate in a liquid.

References

- Abrahamson, N.A. (1992). Generation of spatially incoherent strong motion time histories. *Proc., 10th World Conf. Earthq. Engrg.*, pp. 845–850, Madrid, Spain.
- Abrahamson, N.A. and Bolt, B.A. (1987). Array analysis and synthesis mapping of strong ground motion. In, *Strong Motion Synthetics*, B.A. Bolt, Ed., Academic Press, Orlando, FL, pp. 55–90.
- Abrahamson, N.A. and Litchiser, J.J. (1989). Attenuation of vertical peak acceleration. *Bull. Seism. Soc. Am.*, 79, 549–580.
- Abrahamson, N.A. and Shedlock, J.M. (1997). Overview. *Seism. Res. Letters*, 68, 9–23.
- Abrahamson, N.A. and Silva, W. (1997). Empirical response spectral attenuation relations for shallow crustal earthquakes. *Seism. Res. Letters*, 68, 94–127.
- Ambraseys, N.N. and Bommer, J. J. (1991). The attenuation of ground accelerations in Europe. *Earthq. Engrg. Struc. Dyn.*, 20, 1179–1202.
- Ambraseys, N.N. and Bommer, J. J. (1995). Attenuation relations for use in Europe: An Overview. *Proc., 5th Society for Earthq. and Civil Engrg. Dyn. Conf. on European Seismic Design Practice*, pp., 67–74, Chester, England.
- Ambraseys, N.N., Smit, P., Berardi, R., Rinaldis, D., Cotton, F. and Berge-Thierry, C.(2001). Dissemination of European strong-motion data. <http://www.ised.cv.ic.ac.uk>.
- Amirbekian, R.V. and Bolt, B.A. (1998). Spectral comparison of vertical and horizontal seismic strong ground motions in alluvial basins. *Earthq. Spectra*, 14, 573–595.
- Archuleta, R. (1984). A faulting model for the 1969 Imperial Valley earthquake. *J. Geophys. Res.*, 889, 4559–4584.
- Arias (1970). A measure of earthquake intensity. In: *Seismic Design for Nuclear Power Plants*, R. Hansen, Ed., MIT Press, Cambridge, MA, pp. 438–483.
- Atkinson, G. and Boore, D. (1995). Ground motion relations for eastern North America. *Bull. Seism. Soc. Am.*, 85, 17–30.
- Bakun, W. H. and McEvilly, R.V. (1984). The Parkfield, California, earthquake prediction experiments. *J. Geophys. Res.*, 89, 3051–3055.
- Bard, P.Y. and Bouchon, M. (1980). The seismic response of sediment-filled valleys, Part 2: the case incident P and SV waves. *Bull. Seism. Soc. Am.*, 70, 1921–1941.
- Bolt, B.A. (1973). Duration of strong motion. *Proc., 5th World Conf. Earthq. Engrg.*,pp. 1304–1315, Rome, Italy.
- Bolt, B.A. (1975). The San Fernando earthquake, 1971. Magnitudes, aftershocks, and fault dynamics. Chapter 21, *Bulletin 196*, Calif. Div. of Mines and Geology, Sacramento, CA.
- Bolt, B.A. (1987). *Seismic Strong Motion Synthetics*. B.A. Bolt (Ed), 328 pp, Academic Press, Orlando, Florida.
- Bolt, B.A. (1996). From earthquake acceleration to seismic displacement. Fifth Mallet-Milne Lecture, *Soc. Earthq. Civil Engrg. Dyn.*, 50 pp, London.
- Bolt, B.A., (2003). *Earthquakes*. 5th ed., W. H. Freeman, New York.
- Bolt, B.A. and Abrahamson, N. A. (2003). Estimation of strong seismic ground motions. In: *International Handbook of Earthquake and Engineering Seismology*, Part B, IASPEI.
- Bommer, J.J. and Martinez-Pereira, A. (1999). The effective duration of earthquake strong motion. *J. Earthq. Engrg.*, 3, 127–172.
- Boore, D.M., Joyner, W., Fumal, T (1997). Equations for estimating horizontal response spectra and peak acceleration from western North American earthquakes: A summary of recent work. *Seism. Res. Lett.*, 68, 128–153.
- Bozorgnia, Y., Campbell, K.W and Niazi, M. (1999). Vertical ground motion: characteristics, relationship with horizontal component, and building-code implications. *Proc., SMIP99 Sem. on Utilization of Strong-Motion Data*, San Francisco, CA.
- Bozorgnia, Y. and Niazi, M. (1993). Distance scaling of vertical and horizontal response spectra of the Loma Prieta earthquake. *Earthq. Engrg. Struc. Dyn.*, 22, 695–707.

- Brillinger, D.R. and Preisler, H.K. (1984). Further analysis of the Joyner-Boore attenuation data. *Bull. Seism. Soc. Am.*, 75, 61–614.
- Bullen, K. and Bolt, B.A. (1985). *An Introduction to the Theory of Seismology*. 4th ed., Cambridge University Press, Cambridge.
- Campbell, K.W. (1997). Empirical near-source attenuation relationships for horizontal and vertical components of peak ground acceleration, peak ground velocity, and pseudo absolute acceleration response spectra. *Seism. Res. Lett.*, 68, 154–179.
- Campbell, K.W. (2003). Prediction of strong ground motion using the hybrid empirical method: example application to eastern North America. *Bull. Seism. Soc. Am.*, 93, 1012–1033.
- Campbell, K.W. and Bozorgnia, Y. (1994). Near-source attenuation of peak horizontal acceleration from worldwide accelerograms recorded from 1957 to 1993. *Proc., 5th U.S Nat. Conf. Earthq. Engrg.*, 3, pp. 283–292, Chicaco, IL.
- Campbell, K.W. and Bozorgnia, Y. (2003). Updated near-source ground motion (attenuation) relations for the horizontal and vertical components of peak ground acceleration and acceleration response spectra. *Bull. Seism. Soc. Am.*, 93, 314–331.
- Chen, K.-C., Huang, B.-S., Wang, J.-W., Huang, W.-G., Chang, T.-M., Hwang, R.-D., Chiu, H.-C. and Tsai, C.-C. (2001). An observation of rupture pulses of the 20 September 1999 Chi-Chi, Taiwan, earthquake from near-field seismograms. *Bull. Seism. Soc. Am.*, 91, 1247–1254.
- Chiu, H.-C., Amirbekian, R.V. and Bolt, B. A. (1995). Transferability of strong ground motion coherency between the SMART1 and SMART2 arrays. *Bull. Seism. Soc. Am.*, 85, 342–348.
- Darragh, R. B. and Shakal, A. F. (1991). The site response of two rock and soil station pairs to strong and weak ground motions. *Bull. Seism. Soc. Am.*, 81, 1885–1899.
- Electric Power Research Institute (1986). Seismic hazard methodology for the central and eastern United States. EPRI Project P101-22, *Publication NP-4726*.
- Elghadamsi, F.E., Mohraz, B., Lee, C.T. and Moayyad, P. (1988). Time-dependent power spectral density of earthquake ground motion. *Int. J. Soil Dyn. Earthq. Engrg.*, 7, 15–21.
- Frankel, A. (1999). How does the ground shake? *Science*, 183, 2032–2033.
- Frankel, A., Mueller, C., Barnhard, T., Perkins, D., Leyendecker, E., Dickman, N., Hanson, S., and Hopper, M. (1996). National seismic-hazard maps. *U.S. Geol. Surv. Open-File Rept.* 96-532, 1–110.
- Gregor, N.J. and Bolt, B.A. (1997). Peak strong motion attenuation relations for horizontal and vertical ground displacements. *J. Earthq. Engrg.* 1, 275–292.
- Heaton, T.H., Hall, J. F., Wald, D.J. and Halling, M.W. (1995). Response of high-rise and base-isolated buildings to a hypothetical M_w 7.0 blind thrust earthquake. *Science*, 267, 206–211.
- Hebenstreit, G.T. (Ed.), (1997). *Perspectives on Tsunami Hazard Reduction: Observations, Theory, and Planning*, Kluwer, Dordrecht.
- Iwan, W.D. and Chen, X. (1994). A measure of earthquake intensity. In, *Seismic Design for Nuclear Power Plants*, R. Hanson, Ed., pp., 438–487. MIT Press, Cambridge, MA.
- Jackson, J. (2001). Living with earthquakes: Know your faults. *J. Earthq. Engrg.*, 5, 1–123.
- Joyner, W.B. and Boore, D.M. (1982). Prediction of earthquake response spectra. *U.S. Geol. Surv. Open Filed Rpt.* 82–977.
- Joyner, W.B. and Boore, D.M. (1988). Measurement, characteristics and prediction of strong ground motion. *Proc., Specialty Conf. on Earthq. Engrg. and Soil Dyn. II*, 43–pp. 102, ASCE Park City, UT.
- Loh, C.-H. and Liao, W.-I. (2000). *Inter. Workshop Annual Commemoration of Ch-Chi Earthquake*. Nat. Cen. for Res. on Earthq. Engrg., Taipei, Taiwan, R.O.C.
- Lomax, A. and Bolt, B.A. (1992). Broadband waveform modelling of anomalous strong ground motion in the 1989 Loma Prieta earthquake using three-dimensional geological structures. *Geophys. Res. Lett.*, 19:1963–1966.
- McVerry, G.H. and Zhao, J.X. (1999). A response spectrum model for New Zealand including high attenuation in the volcanic zone. Institute of Geological and Nuclear Science, Ltd.
- Nakamura, Y. (1995). Waveform and its analysis of the 1995 Hyogo-ken-Nanbu earthquake. *Report 23C*, Railway Tech. Rec. Inst. Tokyo.

- Novikova, E.I. and Trifunac, M.D. (1994). Duration of strong motion in terms of earthquake magnitude, epicentral distance, site conditions and site geometry *Earthq. Engrg. Struc. Dyn.*, 23, 1023–1043.
- Nuttli, O.W. (1974). Seismic wave attenuation and magnitude relations for East and North America. *J. Geophys. Res.*, 78, 896–885.
- O'Connell, D.R. (1999). Replication of apparent nonlinear seismic response with linear wave propagation model. *Science*, 283, 2045–2050.
- Ogata, Y. (1988). Statistical models for earthquake occurrences and residual analysis for point processes *J. Am. Stat. Assoc.* 82, 9–27.
- Olsen, K.B. (2000). Site amplification in the Los Angeles basin from three-dimensional modeling of ground motion. *Bull. Seism. Soc. Am.*, 90, 577–594.
- Olsen, K.B., Archuleta, R.J. and Matarese, J.R. (1995). Three-dimensional simulation of a magnitude 7.75 earthquake on the San Andreas fault. *Science*, 270, 1628–1632.
- Raooff, M., Herrmann, R.B. and Malagnini, L. (1999). Attenuation and excitation of three-component ground motion in Southern California. *Bull. Seism. Soc. Am.*, 89, 888–902.
- Reiter, L. (1990). *Earthquake Hazard Analysis: Issues and Insights*, Columbia Univ. Press, New York.
- Saikia, C.K. and Somerville, P.G. (1997). Simulated Hard-Rock Motions in Saint Louis, Missouri, from large New Madrid earthquakes. *Bull. Seism. Soc. Am.*, 87, 123–139.
- Schoenberg, F. and Bolt, B.A. (2000). Short-term exciting and long-term correcting models for earthquake catalogs. *Bull. Seism. Soc. Am.*, 90, 849–858.
- Schwartz, D.P. and Coppersmith, K.J. (1984). Fault behavior and characteristic earthquakes: examples from the Wasatch and San Andreas fault zones. *J. Geophys. Res.*, 89(B7), 5681–5698.
- Seed, H.G. and Idriss, I.M. (1982). *Ground Motions and Soil Liquefaction During Earthquakes*, Earthq. Engng. Res. Inst. (EERI), Berkeley, CA.
- Shakal, A., et al. (1994). CSMIP strong motion records from the Northridge, California earthquake of January 17, 1994. *Report No. OSMS 94-07*, California Strong Motion Instrumentation Program, California Division of Mines and Geology, California Department of Conservation, Sacramento, Calif., pp. 57–63.
- Shin, T.C., Kuo, K.W., Lee, W.H.K., Teng, T.L. and Tsai, Y.-B. (2000). A preliminary report on the 1999 Chi-Chi (Taiwan) earthquake. *Seism. Res. Lett.*, 71, 24.
- Sieh, K.E. (1978). Prehistoric large earthquakes produced by slip on the San Andreas fault at Pallett Creek, California. *J. Geophys. Res.*, 83(B8), 3907–3939.
- Somerville, P.G. and Abrahamson, N.A. (1995). Ground motion prediction for thrust earthquakes. *Proc. SMIP95 Seminar*, Cal. Div. of Mines and Geology, San Francisco, CA, 11–23.
- Somerville, P.G., Smith, N.F., Graves, R.W. and Abrahamson, N.A. (1997). Modification of empirical strong ground motion attenuation relations to include the amplitude and duration effects of rupture directivity. *Seism. Res. Lett.*, 68(1), 199–222.
- Somerville, P.G. and Yoshimura, Y. (1990). The influence of critical Moho reflections on strong ground motions recorded in San Francisco and Oakland during the 1989 Loma Prieta earthquake. *Geophys. Res. Lett.*, 17, 1203–1206.
- Spudich, P., Hellweg, M. and Lee, W.H.K. (1996). Directional topographic site response at Tarzana observed in aftershocks of the 1994 Northridge, California, earthquake: Implications for main shock motions. *Bull. Seism. Soc. Am.*, 86 Suppl. 1, Part B, S193–S208.
- Teng, T.-L., Tsai, Y.-B. and Lee, W.H.K. eds. (2001). Dedicated issue on the Chi-Chi, Taiwan, earthquake of 20 September 1999. *Bull. Seism. Soc. Am.*, 91(5), 893–1395.
- Toro, G.R., Abrahamson, N.A. and Schneider, J.F. (1997). Model of strong ground motions from earthquakes in central and eastern North America: best estimates and uncertainties. *Seism. Res. Lett.*, 68, 41–57.
- Uniform Building Code (1997). International Conference of Building Officials, Whittier, CA.
- Wald, D.J., Quitoriano, V., Heaton., T.H., Kanamori, H., Scrivner, C.W. and Worden, C.B. (1999). TriNet 'ShakeMaps': rapid generation of peak ground motion and intensity maps for earthquakes in southern California. *Earthquake Spectra*, 15, 537–555.

- Wells, D.L. and Coppersmith, K. J. (1994). New empirical relationships among magnitude, rupture length, rupture area and surface displacements,. *Bull. Seism. Soc. Am.*, 84, 974–1002.
- Yeates, R.S., Sieh, K. and Allen, C.R. (1997). *The Geology of Earthquakes*, Oxford University Press, New York.
- Youngs, R.R., Abrahamson, N.A. and Sadigh, K. (1995). Magnitude-dependent variance of peak ground acceleration. *Bull. Seism. Soc. Am.*, 85, 1161–1176.
- Youngs, R.R., Chiou, S.-J., Silva, W.J. and Humphrey, J.R. (1997). Strong ground motions attenuation relationships for subduction zone earthquakes. *Seism. Res. Lett.*, 68, 58–73.

3

The Role of Geology in Seismic Hazard Mitigation

Robert S. Yeats

Eldon M. Gath

3.1	Introduction.....	3-1
3.2	Paleoseismology	3-2
3.3	Surface Rupture	3-5
3.4	Blind Thrusts	3-6
3.5	Strong Ground Motion	3-8
3.6	Earthquake-Induced Landslides.....	3-8
3.7	Liquefaction	3-9
3.8	Case Histories	3-10
	Introduction • San Bernardino Valley College: Surface Rupture Hazard • Moorpark Housing Development: Mitigation by Structural Design • Los Angeles Sewer Line: The Problem of Blind Thrusts • Balboa Boulevard Pipeline: Deformation or Liquefaction? • Assessment of Ground Deformation at an Automobile Assembly Facility, Koçaeli, Turkey • Village Reconstruction After the 2002 Nahrin, Afghanistan Earthquake	
3.9	Summary and Conclusions	3-17

What's past is prologue.

William Shakespeare

The Tempest, Act II

3.1 Introduction

The contribution of geology to seismic hazard mitigation is that the past is the key to the future. Where an earthquake has occurred in the past, it is likely to occur again. The primary role of the geologist is to locate paleo-earthquakes using paleoseismology, locate and characterize the faults that generate them and develop a quantitative understanding of the style, magnitude, frequency and recency of earthquakes on those faults as a guide to their future behavior. Geology, therefore, is both locative and predictive. It can be used to forecast the size of the earthquake, the location of the fault rupture, the surface deformation anticipated where the fault does not reach the surface, and the local site amplification factors that will impact strong ground shaking and soil failures. Geology provides the quantitative foundation on which other aspects of seismic hazard mitigation are based.

Early studies of earthquake hazards were conducted following major earthquakes in Marlborough, New Zealand, in 1888; Mino-Owari, Japan, in 1891; Assam, India, in 1897 and San Francisco, California, in 1906. In all of these investigations, geologists played leading roles. The careful fault-rupture descriptions of Alexander McKay of New Zealand, Bunjiro Koto of Japan and G. K. Gilbert of the United States set a standard that has rarely been exceeded (see personal vignettes in Yeats et al., 1997). All of these studies focused on the surface effects of the earthquake, including crustal deformation. Aside from Gilbert, though, these researchers did not consider the implications in future planning and engineering design.

In subsequent decades, geologists continued to play a role, albeit a subordinate one due to two developments. One was the Wood–Anderson seismograph, designed in the 1920s, which resulted in an increasingly important role played by geophysicists. Another was the adoption in California of the first local building codes taking earthquake resistance into consideration, starting after the 1925 Santa Barbara earthquake and accelerating after the Long Beach earthquake of 1933. The public outcry after the Long Beach earthquake led to the adoption of the Field and Riley Acts by the State of California, resulting in an increasingly important role for structural engineers. For the half century that followed the 1906 San Francisco earthquake, geologists working on earthquake-related problems were almost entirely university professors or employees of the U.S. Geological Survey (see historical summaries by Geschwind [2001] and Yeats [2001]).

The development of building codes regulating the quality of building construction was not accompanied by ordinances dealing with the safety of building sites until 1952, when the City of Los Angeles adopted the first grading ordinance in the United States and set up a grading section within the Department of Building and Safety. This move was triggered not by earthquakes but by landslides, which were an increasing problem as the expanding population of Los Angeles moved into the surrounding foothills. By 1963, development projects were required to be supported by both geotechnical engineering and engineering geology reports, and grading operations had to be supervised by both a soils engineer and an engineering geologist. This led to the establishment of geological consulting firms and to the employment of geologists in larger consulting engineering firms. For example, F. Beach Leighton, a professor of geology at Whittier College, established a geological consulting practice in a spare room of his home, then expanded to a large organization with offices throughout southern California.

California now requires geological consultation mainly due to two acts of the legislature: the Alquist–Priolo Earthquake Fault Zoning Act, first adopted in 1972 to regulate construction on or near active faults and the Seismic Hazard Mapping Act of 1990, dealing with land subject to liquefaction and earthquake-induced landsliding. The state agency given principal responsibility for these laws is the California Geological Survey (formerly the Division of Mines and Geology), which, in addition, assists local governments in adopting Seismic Safety Elements as part of their General Plans, based on a law passed in 1971.

California has the most advanced earthquake-protective legislation in the United States, perhaps in the world (Yeats, 2001), but other states have not followed its lead in evaluating the safety of building sites. Oregon, for example, has upgraded its building codes close to California standards, but its land-use laws protecting against geologic hazards are essentially unchanged. As a result, building sites in Oregon, like those in other states in harm's way from earthquakes, fall victim to what has become known as Slosson's Law, advanced by geological consultant and former California State Geologist James Slosson: The quality of professional work will sink to the lowest level that government will accept.

This chapter presents examples from consulting practice in which geology was important, even critical, to seismic hazard mitigation. Most examples are from California, where geological studies are required, but the chapter is written with the objective that a state-of-the-art analysis anywhere in the world will include geological factors, whether or not it is required by state or local law.

For more details about the geological background, refer to McCalpin (1996) and Yeats et al. (1997).

3.2 Paleoseismology

Clients want to know when the next earthquake is likely to strike near the project site, and how much damage the earthquake will do. Short-term prediction is not yet on the horizon and may never be in our

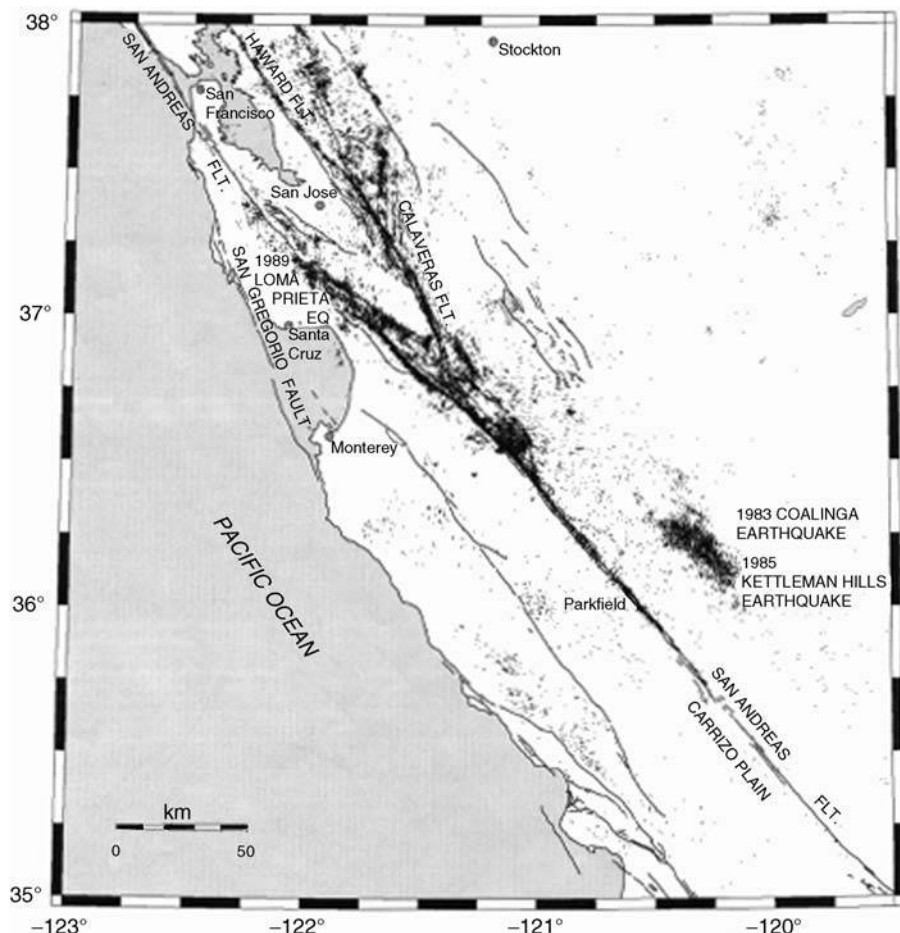


FIGURE 3.1 Seismicity of central California, 1980–1986, to compare the seismicity of that part of the San Andreas fault that ruptured in 1857 (Carrizo Plain, lower right corner), which is not imaged by earthquakes at all, to the seismicity of that part of the fault that ruptures frequently, as at Parkfield, or creeps accompanied by very small earthquakes (between Parkfield and Loma Prieta), which images the fault very well. That part of the fault crossing the San Francisco Peninsula ruptured in 1906, but is not well imaged by earthquakes. From David Oppenheimer, U.S. Geological Survey, reprinted from Yeats (2001) with permission from Oregon State University Press.

lifetimes. So we must rely on *probabilistic* forecasts that give the likelihood of an earthquake striking in a timeframe of interest, commonly the life of the project being evaluated, or *deterministic* forecasts that give the largest earthquake (measured in peak ground accelerations and velocities and response spectra) that is likely to affect the project area. Deterministic forecasts are useful for *critical facilities* such as large dams or nuclear power plants.

It is standard practice to report the instrumental and historical seismicity of the region surrounding a project site as an indication of potential earthquake hazard. Yet this practice gives too short a time sample to be of significant value. Seismographs have been in place for only a century, and modern broadband seismographs have been in place for only a few decades. The historical record for, say, California, is reliable for only about 150 years except for a few population centers along the coast, where it is slightly longer. This time period is too short to identify the most recent earthquake on the Cascadia Subduction Zone, the southern San Andreas fault or earthquakes of $M > 7$ in the Los Angeles metropolitan region (Rubin et al., 1998; Dolan and Rockwell, 2001).

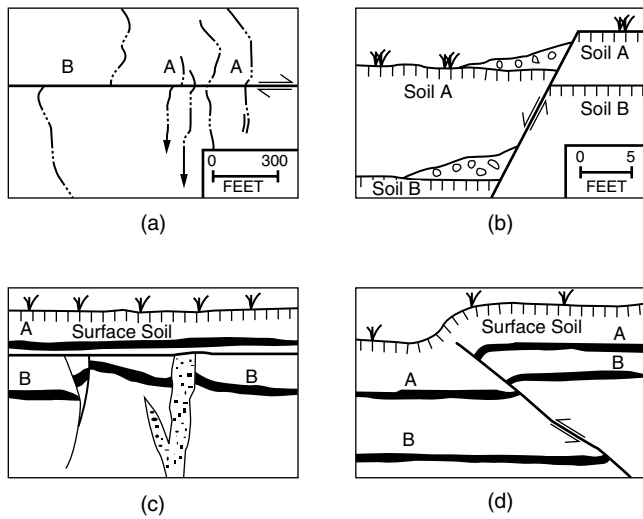


FIGURE 3.2 Geological evidence for paleo-earthquakes. (a) Map of intermittent streams (dot-line pattern) crossing San Andreas fault in Carrizo Plain, California. Streams labeled A show offset by the 1857 Fort Tejon earthquake. Stream B was offset by this earthquake and by earlier ones as well. (From Kerry Sieh, Earth Consultants International.) (b) Trench exposure of a normal fault in which the block overlying the fault (hanging wall) moved relatively down. Grass symbols mark ground surface and vertical lines mark soil horizons. During the most recent earthquake, the soil was covered by debris (colluvial wedge) shed from the fault scarp. Soil B was offset by the same earthquake and also by a prehistoric earthquake that formed a now-buried colluvial wedge. (c) Trench exposure of a fault and a sand dike formed by liquefaction. Age of the earthquake is bracketed by the age of the oldest unfaulted horizon A and the age of the youngest faulted horizon B. (d) Trench exposure of reverse fault, where the hanging wall moves relatively upward, deforming the surface soil into a scarp. Offset of horizon A is the same as that of the surface soil, but offset of horizon B is greater, indicating displacement by an earlier earthquake.

Furthermore, instrumental seismicity, even using state-of-the-art seismographs, is a poor guide to potential hazard except in the most general terms. Most of the 1857 rupture zone and part of the 1906 rupture zone on the San Andreas fault have very low seismicity (Figure 3.1; Yeats, 2001, pp. 200–202). The Cascadia subduction zone off the coast of the Pacific Northwest has the potential for an earthquake of M_w 9, but very few earthquakes have been recorded on the subduction zone, and virtually none north of California. The reason is that earthquakes, large and small, reflect the sudden release of strain, whereas measuring the buildup of strain is more important in addressing concerns about potential earthquakes. If the fault zone in question is strong, there is no reason to assume that an earthquake on that fault will telegraph its punch by small earthquakes, although some earthquakes on faults in China and Greece were preceded by enough foreshocks to alarm the local population (Yeats, 2001, pp. 193–196).

Both historical and instrumental seismicity are useful in characterizing faults that have very short earthquake return times, like the San Andreas fault at Parkfield where the recurrence interval is a few decades. Historical seismicity is useful for faults for which the recurrence interval is significantly shorter than the historical record, such as the Motagua fault in Guatemala, the North Anatolian fault in Turkey and some faults in Iran and China. But for most faults, especially those in the western United States, neither historical nor instrumental seismicity is able to provide information about a complete earthquake cycle. The geologic record, which is thousands or even tens of thousands of years long, is able to span a complete cycle and may span several cycles.

The geologist's duty, then, is to determine the slip rate and the earthquake recurrence interval of faults near the site (line sources of Reiter [1990]). In addition, it may be necessary to determine the recurrence interval for a region comprising several faults (area source), and allow for faults that have not yet been identified (floating earthquake). The slip rate can be determined by the offset of features of known age, with the age determined generally by radiocarbon dating or other techniques, such as optically stimulated

luminescence, which does not require carbon (Noller et al., 2000). The feature may be an offset stream channel across the San Andreas fault (Figure 3.2a), an offset marine platform and beach cliff or an offset horizon in a bulldozer or backhoe trench excavation across a fault (Figures 3.2b–d). Slip rates determined in this way can be compared with rates derived from plate tectonics (which are based on timeframes of hundreds of thousands to millions of years) and with strain accumulation rates (which are based on repeated surveys using the Global Position System, spanning a timeframe of several years). For metropolitan Los Angeles, slip rates have been determined on faults over the long term (millions of years) to the short term (thousands of years to a few years). For several faults, the Southern California Earthquake Center has determined that the short-term rate, which is critical in hazard estimation, differs significantly from the long-term rate.

Urbanization has prevented subsurface excavations across many faults in Los Angeles, although subsurface investigation remains a desirable goal. In the San Francisco Bay Area, the BAPEX (Bay Area Paleoseismic Experiment) project is a focused effort to refine the understanding of short-term slip rates and recurrence intervals. Based on paleoseismic evidence gathered to date, the Bay Area is under a long-term forecast of two chances out of three for an earthquake of magnitude greater than 6.7 in the next 30 years, and one chance out of three for an earthquake of this size on the heavily urbanized northern Hayward fault and the adjacent Rodgers Creek fault (Working Group on California Earthquake Probabilities, 1999).

Individual earthquakes in a trench excavation can be recognized by wedges of colluvial debris shed from a fault scarp during an earthquake (Figure 3.2b), liquefaction features such as sand dikes (Figure 3.2c) and marine shorelines suddenly uplifted in the past few thousand years during an earthquake. A fault strand exposed in a trench can terminate upward against a younger unfaulted sedimentary layer (Figure 3.2c), or layers tilted during an earthquake can be overlain by flat-lying sediments. The age of the earthquake is bracketed by dating the youngest faulted or tilted sediments (layer B, Figure 3.2c) and the oldest unfaulted or flat-lying sediments (layer A, Figure 3.2c). Using these criteria in trench exposures across the San Andreas fault south of Palmdale at Pallett Creek and nearby areas, eight prehistoric earthquakes extending back 1300 years were identified in addition to the rupture during the 1857 Fort Tejon earthquake of M 7.9 (Sieh, 1978; Sieh and LeVay, 1998).

The earthquake recurrence time t is equal to the slip per earthquake s divided by the slip rate on the fault, v :

$$t = s/v$$

Slip per event is determined by field observations after a surface-rupturing earthquake, by observations of displacement in a trench or series of trenches and by offsets of small streams or cultural features across a fault.

If earthquake recurrence were periodic, forecasting the next one would be straightforward. But paleoseismic time histories show that earthquake recurrence is not periodic. And in some cases, most notably along the central San Andreas fault, earthquakes are not characteristic — that is, the same segment of fault may generate earthquakes of different fault displacements, implying different magnitudes, at different times (Grant, 1996).

The large number of earthquakes on the Central Nevada Seismic Zone east of Reno (1903, 1915, 1932, 1934 and four in 1954) does not correlate with the long-term earthquake recurrence interval on this zone's faults (which is many thousands of years for the same fault segment). This inconsistency suggests that earthquakes cluster in time. Coseismic strain release across the Eastern California Shear Zone in the last 60 years has been many times more than that across the nearby San Andreas fault, though the slip rate across the Eastern California Shear Zone is only a small fraction of that across the San Andreas fault.

The magnitude of a paleo-earthquake can be estimated on the basis of the length of the fault source and the maximum displacement during an individual earthquake. Wells and Coppersmith (1994) prepared regression relationships among magnitude, rupture length and displacement for 216 historical earthquakes. Although there are differences between regions, these relationships are used to estimate magnitude from geological data.

One of the earthquakes on the Eastern California Shear Zone, the Landers earthquake of M 7.3 in 1992, provided evidence that an earthquake can jump from fault to fault. Trench excavations across faults

in the Los Angeles Basin show evidence of fault displacements that are too large for the earthquake to have been limited to the fault that was trenched (Rubin et al., 1998). The concern about rupture on multiple faults is that if the earthquake is larger, the area of strong shaking is larger, and the duration of strong shaking is longer.

This leads to the idea that an earthquake rupture might cascade from fault to fault, like buttons ripping off a shirt. To evaluate this possibility, it is necessary to obtain subsurface information on all faults in a region, especially the Los Angeles region where recurrence intervals on most faults are measured in thousands of years and thus subject to rigorous paleoseismic analysis.

3.3 Surface Rupture

Earthquake faults are of three types (Figure 3.2). *Strike-slip faults* are characterized by motion parallel to the Earth's surface, offsetting streams (Figure 3.2a) and cultural features. The best-known example is the San Andreas fault, with surface rupture in the Fort Tejon earthquake of 1857 and the San Francisco earthquake of 1906. *Normal faults* are characterized by the Earth's crust pulling apart, causing one side of the fault, the upper block, called the *hangingwall*, to drop down with respect to the other side (Figure 3.2b). Examples include surface rupture in the Pleasant Valley earthquake of 1915 and the Dixie Valley earthquake of 1954, both in western Nevada. *Reverse faults* are characterized by the Earth's crust being forced together so that the hangingwall rides up over the other block (Figure 3.2d). Examples include surface rupture accompanying the San Fernando (Sylmar) earthquake of 1971 and the Chi-Chi, Taiwan, earthquake of 1999.

The Alquist-Priolo (A-P) Act arose as a consequence of damage from the reverse fault that ruptured across residential suburbs in the San Fernando Valley in the 1971 San Fernando (Sylmar) earthquake. The eastern section of the surface rupture was known to be a fault but was not recognized as active; the western section was not recognized as a fault prior to the earthquake. The Act was precipitated in part by uncontrolled development across the San Andreas fault in the San Francisco Bay Area and in the suburbs of San Bernardino and across the Hayward and Calaveras faults east of San Francisco Bay.

Most young faults in California have been identified and characterized on the basis of the age of their most recent rupture (Jennings, 1994), and some of these faults have been zoned under A-P. To fall under the jurisdiction of A-P, the fault must be demonstrated as active, based on evidence that the fault has undergone surface rupture in the past 11,000 years. (As Clarence Allen of Caltech observed, a fault that has moved recently is likely to move again. Stated a different way, *what has happened, can happen*.) In addition to being active, a fault zoned under A-P must be clearly defined in the field by a geologist (Hart and Bryant, 1997).

A-P zone boundaries are set at 500 ft from most active faults but can be as low as 200 ft for less significant faults. Within an A-P zone, special studies must demonstrate to a high standard that a project within the zone is safe against surface rupture. In practice, the most common investigative technique is to excavate a trench across a proposed building site and map the walls of the trench for the presence of possible active faults (Figure 3.2b-d). Dating the recency of fault activity requires the presence of unfaulted datable sediments. If these sediments are older than 11,000 years, no fault at the site would be zoned under A-P, whether exposed by the trench or not.

The law establishes a setback from a zone of surface faulting based on recommendations by the geologist. By law, this setback is 50 ft, but the setback can be decreased or increased on the recommendation of the project geologist. How wide should the setback be around a fault identified under A-P as active? At most project sites, the published fault location is not detailed enough to make construction decisions. The geologist, through careful analysis of the topography and subsurface evidence from trench excavations and boreholes, must locate and characterize the site-specific hazard of the fault zone, which may consist of a network of separate faults, any of which could damage or destroy a nearby building.

A-P has been criticized for attacking the wrong problem. In the 1971 earthquake, the damage from surface rupture was considerably less than the damage from other causes such as strong shaking or liquefaction. The next three urban earthquakes in California — 1987 Whittier Narrows, 1989 Loma Prieta



FIGURE 3.3 Damage from surface rupture on the Chelungpu reverse fault in Fengyuan City, Taiwan, accompanying the September 21, 1999, Chi-Chi earthquake of M 7.6. Photo taken 5 months after the earthquake. The cleared area on the upthrown side of the fault was formerly covered with buildings that were completely destroyed, with loss of life; the remains of these structures were subsequently removed. Damage to buildings on the downthrown side of the fault (far right) was severe, but the buildings were not totally destroyed. If an Alquist-Priolo setback had been in effect prior to development of this area, losses of life and property would have been greatly reduced. Photo by Robert Yeats, reproduced from Yeats (2001) with permission of Oregon State University Press.

and 1994 Northridge — were not accompanied by surface rupture, yet losses from each of the last two earthquakes were measured in billions of dollars. But the Chi-Chi, Taiwan, earthquake of September 21, 1999 was accompanied by many miles of surface rupture on the Chelungpu reverse fault in developed areas. Nearly complete devastation resulted along the fault rupture with great loss of life, particularly on the upthrown (hangingwall) side of the fault (Figure 3.3). The fault had been mapped prior to the earthquake; if A-P had been in effect prior to development, many lives would have been saved and property losses would have been greatly reduced (Yeats, 2001, pp. 334–335).

Many California cities and counties, through their public safety elements, have adopted a more stringent interpretation to include more faults than those zoned by the state under A-P.

3.4 Blind Thrusts

The Whittier Narrows, Loma Prieta and Northridge earthquakes, together with an earlier earthquake in 1983 that destroyed most of the downtown section of Coalinga, California, were not accompanied by surface rupture. These earthquakes activated reverse faults, but fault rupture stopped several miles beneath the surface. Such faults are called blind thrusts (Figure 3.4). They are not well defined at the surface, so they are not zoned under A-P. The four earthquakes mentioned above struck faults that were not recognized at the time as active; in fact, the Northridge earthquake fault was not known at all. Yet these faults generally have surface expression as sedimentary layers uplifted and folded into anticlines (Figure 3.4). Characterization of the degree of activity of blind thrusts requires the use of petroleum industry well logs and seismic profiles as well as topographic features such as river terraces and marine shorelines that have been upwarped during many past blind-thrust earthquakes (Stein and King, 1984; Anderson, 1990; Stein and Ekström, 1992; Shaw and Shearer, 1999). The Northridge blind thrust came up beneath a surface reverse fault dipping in the opposite direction. The evidence of its presence, discovered later, was the uplift of both blocks of the surface fault (Yeats and Huftile, 1995; Huftile and Yeats, 1996). Analysis of the overlying fold permitted an estimate of the long-term slip rate on the blind thrust (Davis and Namson, 1994; Huftile and Yeats, 1996).

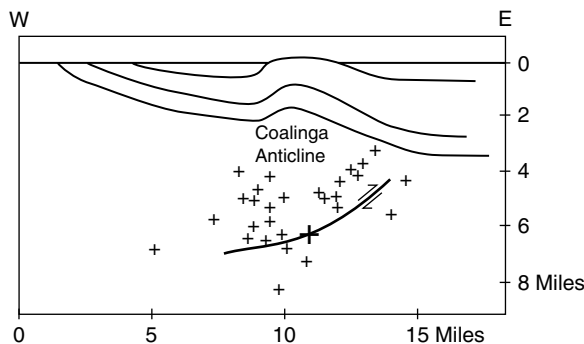


FIGURE 3.4 Cross section of the Coalinga, California, blind-thrust earthquake of May 2, 1983. Large plus symbol marks main shock; smaller plus symbols are aftershocks. Curved line is the fault plane based on modeling of surface deformation and on seismic-reflection profile. Layers above the main shock are bowed upward into an anticline. Based on work by R.S. Stein of the U.S. Geological Survey and G.C.P. King of the Institut de Physique du Globe de Paris.

If the surface evidence of the blind thrust is limited to broad warping of the surface in anticlines, then the main effects (aside from strong shaking) are the change in gradient of railway lines and pipelines. However, anticlinal warping is commonly accompanied by secondary faults, resulting from sedimentary layers slipping along bedding as the layers are folded (*flexural-slip faulting*). Anticlinal warping also stems from the formation of faults or parasitic folds resulting from *bending moment* imposed during folding [Yeats et al., 1981, 1997; Osokin et al., 2000]. Treiman (1995) reported flexural-slip reverse faults that broke the ground surface of building pads graded for a housing development in Santa Clarita, California during the 1994 Northridge earthquake. The Coyote Pass escarpment in East Los Angeles is a steep, localized fold scarp that accompanied uplift of a large anticline to the north (Osokin et al., 2000).

3.5 Strong Ground Motion

Soft surficial sediments tend to amplify seismic waves, resulting in the bowl of jello effect. This was illustrated by comparing the shaking at Fort Mason, west of Fisherman's Wharf in San Francisco, with the shaking elsewhere in the city during the 1906 earthquake. Captain M. L. Walker at Fort Mason felt the 1906 earthquake but then went back to sleep, thinking that it was no more than a mild shaker. Seismograms of aftershocks of the 1989 Loma Prieta earthquake recorded much lower velocities of seismic waves at Fort Mason than in the Marina District farther west, an echo of 1906. Fort Mason is referred to as a rock site, and the Marina District as a soil site.

One of the worst examples is Mexico City, built on soft clay, silt and sand of ancient Lake Texcoco. An earthquake in 1985 on the Pacific Coast, hundreds of miles away from Mexico City caused great damage in Mexico City, because of the large population concentrated there and the amplification of seismic waves by the soft sediments of Lake Texcoco, Mexico City's bowl of jello.

Identification of low-lying areas subject to strong ground motion is facilitated by shear-wave velocity measurements in boreholes, but the geologist can define the limits of such areas by analysis of the depositional setting of sediments underlying the site in question based on topographic maps, aerial photos, cores taken in boreholes and high-resolution, shallow-penetration seismic profiles. Also, the configuration of basins based on wells and deeper-penetration seismic profiles obtained by the petroleum industry is important because sedimentary basins trap earthquake waves and cause them to echo off basin margins, increasing the duration of strong shaking. The Los Angeles basin is an example of a deep sedimentary basin that could trap seismic waves (Olsen et al., 1995).

3.6 Earthquake-Induced Landslides

Large earthquakes generate thousands of landslides. The Northridge earthquake triggered more than 11,000 landslides, mostly in the Santa Susana Mountains and in the hills north of the Santa Clara River (Harp and Jibson, 1996). Some of these are relatively small, but a few have dimensions measured in miles and would be catastrophic if they struck an urban area. The El Salvador earthquake of January 13, 2001 (M_w 7.6) triggered a landslide in the Las Colinas middle-income suburb of San Salvador, more than 60 mi away from the epicenter, killing about 400 people (Lomnitz and Rodríguez, 2001).

Some earthquake-triggered landslides occur offshore and result in tsunamis. The great 1964 Alaska earthquake caused submarine landslides at Seward and Valdez, generating tsunami waves up to 160 ft high that devastated the waterfronts of both towns (Hampton et al., 1993). Location and characterization of tsunamis generated by offshore landslides depend on detailed analysis of offshore topography, requiring multibeam sidescan sonar and bathymetric imagery. This can be very significant in investigating critical facilities along the coast, such as nuclear power plants and liquefied natural gas plants.

Landslides, like active faults, tend to occur in places that have had landslides in the past, commonly in prehistoric times. These ancient landslides can be recognized by the geologist based on aerial photo analysis and field work. The origin can be extremely heavy rainfall instead of an earthquake, but the result to built structures is the same. The geologist can also recognize factors that lead to landslides. For example, cutting into a slope in which bedding dips in the same direction as the slope can trigger downslope movement, a major problem along the central Oregon coast at Newport and on the north side of the Santa Clara River near Ventura, California. Another factor leading to landslides is the presence of weak sediments at the surface, such as wind-blown silt in the Portland Hills in Portland, Oregon, and glacial sediments in beach cliffs near Seattle, Washington. The Las Colinas slide in El Salvador occurred in fine wind-blown ash deposits that due to their low strength, have the potential for slope failure (Lomnitz and Rodríguez, 2001).

Scott Burns, an engineering geologist at Portland State University, uses the three-strike rule. Rule 1 is unstable soil, rule 2 is a steep slope and rule 3 is the landslide trigger, either earthquake shaking or heavy rainfall that saturates the ground. By careful selection of building sites, rules 1 and 2 can be avoided so that neither an earthquake nor heavy rainfall will trigger a landslide on a project site.

3.7 Liquefaction

Liquefaction occurs when the soil beneath the surface actually behaves like a fluid under strong shaking (Obermeier, 1994; S. Obermeier, in McCalpin, 1996, pp. 331–396). The breakup of the Turnagain Arm housing development in a suburb of Anchorage in the 1964 Alaska earthquake was largely due to the liquefaction of a sand layer in the Bootlegger Clay underlying the subdivision. Much of the damage in the Marina District of San Francisco in the 1989 Loma Prieta earthquake was the result of liquefaction of the artificial fill emplaced after the 1906 earthquake. Sediments in the floodplain of the Los Angeles River and Ballona Creek liquefied in the 1994 Northridge earthquake, destroying buildings and snapping sewer and water lines. The most spectacular surface effects of the February 28, 2001 Nisqually, Washington earthquake (Figure 3.5) were caused by liquefaction, including damage to subdivisions in Olympia and to Boeing Field. In several instances, liquefaction during the Nisqually earthquake occurred at the same places as liquefaction due to earthquakes in 1949 and 1965. These liquefaction-prone areas had been identified prior to the earthquake on maps published by the Washington Division of Geology and Earth Resources (Yeats, 2004).

Sediments most susceptible to liquefaction are clean, cohesionless, water-saturated sand generally within 30 ft of the surface, deposited in the Holocene Epoch, over the last 10,000 years. The liquefiable sediments may be overlain by a relatively impermeable layer, a clay cap. If the sediments are found on slopes, even those as low as 1°, the impermeable layer, and structures built on it, can move as a lateral spread, rupturing underground utility lines. Broken underground gas lines in the Marina District ignited in 1989, causing a large fire.



FIGURE 3.5 Sand boils in the Nisqually River delta caused by liquefaction accompanying the February 28, 2001 Nisqually, Washington, earthquake of M 6.8. Photo by Pat Pringle, Washington Division of Geology and Earth Resources.

Although the susceptibility of a sediment layer can be measured by the Standard Penetration Test (SPT), areas likely to contain liquefiable sediments can be identified by the geologist using analysis of air photos, detailed digitized topography, natural exposures and carefully selected boreholes. For example, liquefaction effects of the New Madrid, Missouri earthquakes of 1811–1812 are still visible on air photos taken a century and a half later (S. Obermeier in Yeats et al., 1997, Figure 12-9).

3.8 Case Histories

3.8.1 Introduction

The remainder of this chapter presents several case histories from consulting practice, where geologic analysis played a major role in planning and engineering decisions concerning a development project. The examples do not consider critical facilities such as dams or power plants, where geologic input, including subsurface excavations, has been required by the Federal government for decades. Most examples are from California, where the law requires that geologic factors be considered in the decision-making process. Two examples from outside the United States are studies following earthquakes in which there was severe damage and loss of life.

Outside California, including neighboring states, geologic input is commonly not required by law due to long-established custom. The absence of such input may lead to poor siting decisions, leading to unnecessary damage to built structures. The success of California laws in reducing losses (Yeats, 2001, p. 341) may lead to requirements by insurers for geologic input, even where local and state laws are lacking. As the state of the art in California expands the standard of practice elsewhere, lawsuits following major earthquake damage may lead to a greater consideration of geologic factors in planning and siting decisions.

3.8.2 San Bernardino Valley College: Surface Rupture Hazard

San Bernardino Valley College was constructed in the late 1920s on Bunker Hill to avoid the flooding expected from the Santa Ana River and Lytle Creek, which flank the hill on either side. In the early 1930s, excavations for the foundation of the library revealed a fault, confirming an earlier conclusion of Men-denhall (1905). The college then retained J. P. Buwalda of Caltech, who confirmed that the college campus

was being constructed across the surface trace of the San Jacinto fault, which is capable of generating future surface-rupturing earthquakes (Allen, 1978). Buwalda recommended a 1000-ft setback within which no buildings should be constructed. Although the original four buildings, all impacted by the presence of the fault, were completed without consideration of the presence of faulting, Buwalda's recommendation did guide new construction through the 1940s.

Then, during the 1950s and 1960s, siting of new buildings during an expansion program was done without regard for the location of the San Jacinto fault. During the late 1960s and early 1970s, a consulting firm excavated trenches to screen new building sites for the presence of faults (Allen, 1978; E.M. Gath in Healy, 1998). This resulted in the relocation of the Liberal Arts building away from the San Jacinto fault, but it also revealed that several older buildings were severely compromised by the presence of faults. But no solutions were proposed, and no effort was made to establish the risk that these buildings posed to students and staff.

Studies elsewhere showed that the San Jacinto fault has a slip rate of about a half inch per year, and the absence of fault creep is evidence that this slip is released in large earthquakes. The San Jacinto fault has been the source of more historical earthquakes of $M > 6$ than any other onshore fault in California (Petersen and Wesnousky, 1994), although no surface-rupturing historical earthquake has been documented near the college site. The Working Group on California Earthquake Probabilities (1995) forecast that the San Bernardino Valley segment of the San Jacinto fault has a 40% probability of a large earthquake in the next 30 years, most likely an earthquake of magnitude 6.7 to 7.3, with strike-slip offsets at the surface of at least 6 ft. The fault has been zoned under the A-P Act.

As part of a team engaged in long-term planning for the redevelopment and remodeling of the campus, another geological consultant sought to locate, in detail, the traces of the San Jacinto fault across the campus. The primary objectives were to evaluate the risk to existing facilities and to recommend sites for new buildings away from those faults. Secondary objectives were to evaluate the level and duration of strong ground motion, surface deformation and liquefaction. This information would be incorporated into a risk assessment for proposed new buildings and improved seismic performance of existing buildings.

Data were collected from 16 trenches, including those excavated by the previous consultant. Additional data were acquired from 45 closely spaced cone penetrometer test probes (CPTs), 33 boreholes and two downhole shear-wave velocity profiles for the upper 60 ft of sedimentary section (Figure 3.6).

The fault zone is clearly defined within a 60- to 120-ft zone bounded by two fault strands, with only minor displacement faults between these strands. Geological investigations supported by radiocarbon dating showed that the eastern strand, extending beneath the most heavily built-up part of the campus, has experienced repeated surface rupture in the past 10,000 years. For the western fault strand, the absence of datable sediments limited the determination of the age of most recent rupture to the last 25,000 years, although it was recommended that setbacks be established for that strand as well as the eastern strand. In addition, a previously unrecognized zone of folding (Greek Theatre fold) was found in a zone 280 ft wide between the main fault zone and the eastern margin of Bunker Hill (closely spaced contours in Figure 3.6); this zone was interpreted as the surface expression of a blind thrust fault. Other previously unrecognized faults were mapped based on air photo interpretation and the analysis of CPTs and boreholes.

Modeling indicates that the next earthquake on the San Jacinto fault or the nearby San Andreas fault would be accompanied by ground shaking with peak horizontal accelerations between 0.8 and 1.2g. Another possibility is a near-fault velocity pulse at periods of 3 sec that could exceed 3g. On the positive side, evidence for liquefaction was rare, with a single possible lateral spread dated at about 6000 years ago. The Campus Center, Administration, Library, Life Sciences and Art Buildings straddle the main trace of the San Jacinto fault and will experience large offsets in the next earthquake (Figure 3.6). The Auditorium, North Hall, Physical Sciences and Chemistry Buildings and several additional structures are in areas that have experienced less disruption, principally ground warping, in the recent prehistoric past. A previously unknown secondary fault (Northeast faults, Figure 3.6) may extend under the Technical Building, although its precise location is poorly constrained.

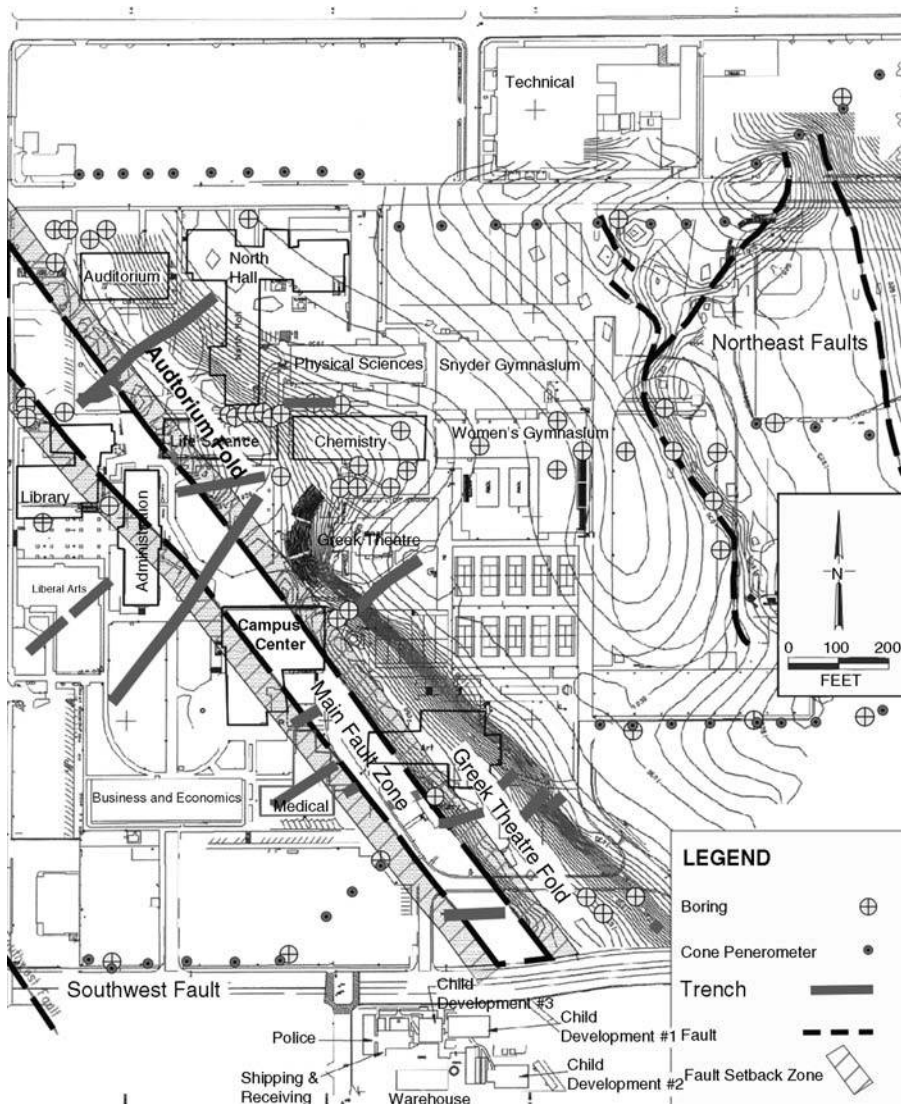


FIGURE 3.6 Map of part of campus of San Bernardino Valley College, crossed by the San Jacinto active fault, locating trenches, borings and cone penetrometer sites, recommended setbacks and location of secondary faults as of the beginning of 1999. Contours are on a stream terrace surface 10,000 years old; contour interval 1 foot. See also color insert following page 2-30. (From Gath et al., in preparation.)

The structural engineering consultant concluded that the hazard to those buildings astride the main fault zone cannot be mitigated except by removal. A minimum setback of 50 ft was accepted by the college to insure against short secondary faults and warps not identified in existing trenches, consistent with the mandate of the California State Architect regarding the construction of school buildings. Ground deformation would be less severe for buildings within the setback zone but not astride the main fault trace. Structural engineers have evaluated these buildings to determine whether they could be strengthened against the expected deformation or if demolition would be the best solution (E. M. Gath in Healy, 1998). The investigation identified large portions of the campus that are free of faults and secondary seismic hazards, where at-risk buildings could be relocated. The only danger to these structures would be strong ground motion, which could be mitigated by structural engineering.

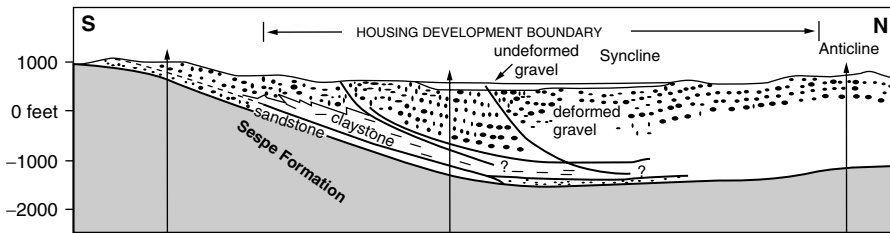


FIGURE 3.7 Diagrammatic cross section through Moorpark housing development. Sespe Formation: bedded sedimentary rocks largely of middle Tertiary age. Overlying strata are Quaternary in age, consisting of a basal marine sandstone, overlying marine claystone, and non-marine gravels. Deformed gravels are probably no younger than 500,000 years. Heavy lines show low-angle thrusts on south limb of syncline. These thrusts were interpreted as shallow, emerging from the claystone layer, rather than continuing downward to seismogenic depths and comprising independent earthquake sources. “Undeformed gravels” are cut by faults and are locally tilted, but displacement on faults nowhere exceeds 6 inches. Deep control provided by oil wells (derrick symbols and vertical lines); shallow control from trenches and borings.

3.8.3 Moorpark Housing Development: Mitigation by Structural Design

Moorpark, in Ventura County, California, is a small town now being transformed into a suburb of Los Angeles, along with the adjacent countryside. Tentative Tract 5054 was proposed as a large housing development north of the Simi active fault, in an area not previously known to be tectonically active. Much to the surprise of the geological consultant, however, trench excavations revealed the presence of gravels that are folded and cut by thrust faults (low-angle reverse faults). These deformation features were so widespread in the tract that the plan reviewer for the City of Moorpark became concerned that the entire development might be compromised.

A second geological consultant was retained to review the geology revealed by trenches and boreholes as well as the geological evolution of the landscape. The consultant concluded that the folding and faulting accompanied the formation of a shallow downfold (syncline) as a result of bending moment as the upper part of the bedrock formation, acting as a beam, was crowded in the concave-upward core of the syncline (cf. Yeats, 1986). The thrust faults do not penetrate downward into older rocks and are thus not independent seismic sources (Figure 3.7).

A second issue was whether the ground-rupture potential of these faults and the tilting potential of the folds would prevent development. The consultant identified two younger sedimentary sequences that were deposited across the folded and faulted gravels after most of the folding and faulting had taken place. These sedimentary layers were the result of sheet floods and sediment transport from Big Mountain and Oak Ridge to the north. The youngest formation, occurring as broad sediment-filled channels that were incised into the older formations, was radiocarbon dated as at least 50,000 years old, a time corresponding to relatively wet climate resulting in regional deposition of sediments throughout this part of California. (Only the youngest sequence is illustrated in Figure 3.7, where it is labeled “undeformed gravel.”)

The youngest channel-fill deposit was exposed in enough trench excavations that it could be observed to postdate nearly all the folding and faulting of the older formations. The deformation features observed in this deposit could be used as a proxy for future faulting and tilting of foundations in the tract. The maximum displacement on any fault in this deposit is 6 in.; in most trenches, it is 1 in. or less. Broad warping across the folds resulted in dips no greater than 7°; in most of the tract, the formation is not tilted at all. The 7° dip could have been the cumulative effect of many earthquakes in the past 50,000 years, possibly secondary effects of earthquakes on the nearby Simi fault to the south. The maximum displacement could also have been the result of several earthquakes, but as a worst case, it could have resulted from a single earthquake.

Using these data, a structural engineer was able to design buildings that would accommodate safely the small amount of tilting and displacement that might occur, recognizing that the total deformation

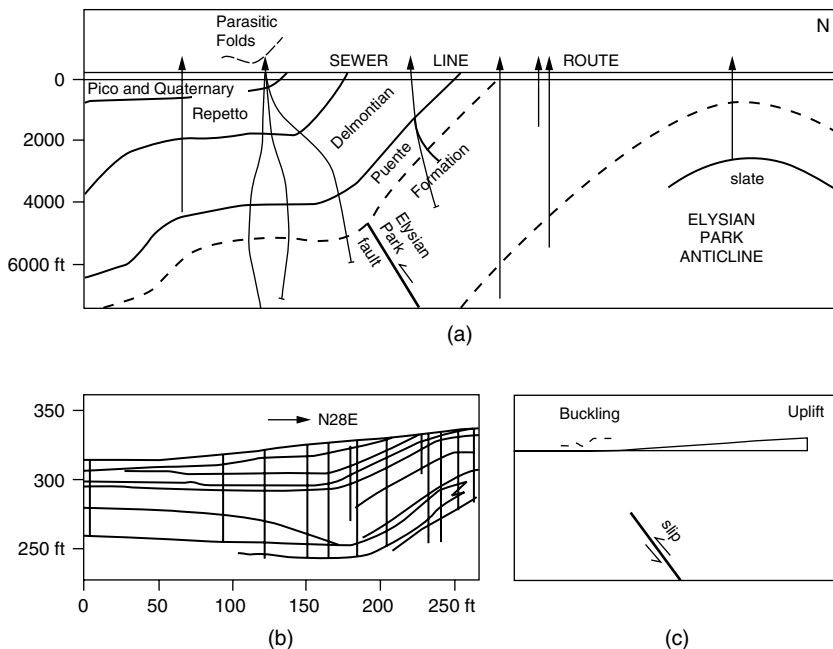


FIGURE 3.8 Diagrammatic cross section along Los Angeles sewer line route following the Los Angeles River. Bedrock formations are based on oil well control (derrick symbol, straight and curved lines). Parasitic folds related to bending moment (Oskin et al., 2000) are found at the boundary between flat-lying strata (left) and the south flank of the Elysian Park anticline (right). Slip on the blind Elysian Park fault would result in an increase in gradient between the crest of the anticline and the flat-lying strata to the left, in addition to buckling of the parasitic folds. (b) Parasitic fold at the Coyote Pass escarpment, with vertical lines showing borehole control, after Oskin et al. (2000). Buckling during an earthquake would be concentrated on parasitic folds like this one. (c) Slip on the blind Elysian Park fault would result in an increase in gradient due to uplift of the crest of the anticline with respect to flat-lying strata, in addition to buckling of parasitic folds.

in the past 50,000 years has been small. This solution is an example of mitigation by structural design, in which geological conditions are taken into account and mitigated against in designing buildings in the project. This is in contrast to the intent of the A-P Act, which is mitigation by avoidance, using setbacks.

3.8.4 Los Angeles Sewer Line: The Problem of Blind Thrusts

The City of Los Angeles has designed a trunk sewer line between the San Fernando Valley and the downtown area, following the Los Angeles River through the narrows between the Santa Monica Mountains and the Elysian Hills. The sewer line right-of-way does not cross any major faults, but it does cross the Elysian Park anticline, which masks at depth the north-dipping Elysian Park blind thrust (Figure 3.8), identified after the 1987 Whittier Narrows earthquake as a source of major earthquakes (Oskin et al., 2000). The Elysian Hills and adjacent Repetto Hills and Monterey Park Hills have been uplifted over hundreds of thousands of years as repeated earthquakes caused displacement on the blind thrust. The fault does not reach the surface, therefore, it is not clearly defined and is thus not subject to regulation under the A-P Act.

The issue was the potential hazard to the sewer line from an earthquake on the Elysian Park blind thrust. Uplift of the Elysian Park anticline would change the gradient of the sewer line and might place it in compression. What would be the effect of a single earthquake?

In addition to boreholes acquired by the City, other boreholes had been drilled nearby to the east on the right-of-way for the proposed Los Angeles Metro Red Line Subway. These boreholes, and a detailed

study of the evolution of the landscape, revealed secondary anticlines at the boundary between the south limb of the Elysian Park anticline and the nearly flat-lying strata of the Las Cienegas structural shelf (Bullard and Lettis, 1993; Osokin et al. 2000; Figure 3.8b). As was the case at Moorpark, these secondary folds, called parasitic folds by Osokin et al. (2000), were formed by compressional crowding in the concave-upward edge of the folded bedrock, acting as a deforming beam. These folds deformed terraces of streams that had cut through the hills as they were uplifted; dating of these deformed terrace deposits allowed the rate of folding to be determined.

Osokin et al. (2000) found that the blind Elysian Park thrust could produce an earthquake of magnitude 6.2 to 6.7, with fault displacements of 3 to 5 ft. At the crest of the anticline, the uplift was calculated to be about 2.5 ft, increasing the gradient of the sewer line on the south limb of the anticline by 0.5°. Shortening of the pipeline would be 1.6 to 2.5 ft. This deformation can be incorporated into the engineering design of the pipeline.

A second problem arose because the shortening is not distributed equally throughout the south limb of the anticline but is concentrated in the parasitic folds low on the south limb of the anticline. The most prominent of these folds is the Coyote Pass escarpment, where the dip of sediments steepens locally to 26° (Figure 3.8b). Osokin et al. (2000) had estimated an earthquake recurrence interval of 500 to 1300 years. The consultant assumed that the bedrock across the Coyote Pass escarpment began to be deformed at the time of the dated stream terrace, 70,000 to 80,000 years, which would mean that the escarpment had been deformed accompanying 60 to 160 earthquakes, with each increasing the dip of the south limb of the escarpment structure by 0.14 to 0.37°. This would be superimposed on the broad increase in gradient across the entire south limb of the Elysian Park anticline (Figure 3.8c). These factors were also incorporated into the engineering design of the pipeline.

3.8.5 Balboa Boulevard Pipeline: Deformation or Liquefaction?

Among the most spectacular television images of the 1994 Northridge earthquake were a blazing fire and gushing water main on Balboa Boulevard north of Rinaldi Street in the San Fernando Valley (Figure 3.9). This was the result of both extensional and compressional surface deformation of gas and water pipelines, as determined by Hecker et al. (1995a, 1995b), Hart et al. (1995), Holzer et al. (1999) and Johnson et al. (1996). What caused the pipeline failure? Could the pipeline be rebuilt along Balboa Boulevard, or would it have to be relocated?

Balboa Boulevard follows the drainage of Bull Canyon and Bee Canyon across the Mission Hills, an active anticline that arose after the drainage had already been established (area of shaded bedrock, Figure 3.9). The pipeline route follows a gentle southward gradient through the Mission Hills, along the old drainage. The southern margin of Mission Hills is formed by the steeply north-dipping Mission Hills reverse fault, which is considered to be an active earthquake source even though it underwent no surface displacement during either the 1971 San Fernando (Sylmar) earthquake or the 1994 Northridge earthquake (Figure 3.9; Tsutsumi and Yeats, 1999).

The pipeline owner wanted to know why the pipeline failed. The theories about the failure included: (1) ground shaking, (2) shaking-induced soil failures and (3) tectonic deformation related to triggered slip on a blind fault. A fourth possible origin, surface rupture of the Mission Hills fault, had already been eliminated on the basis of detailed mapping immediately after the earthquake. In addition to surface mapping, the data set included a set of oil-exploratory wells in and adjacent to Mission Hills, necessary to locate the Mission Hills fault (Tsutsumi and Yeats, 1999, shown in Figure 3.9, top); sixteen CPT boreholes obtained along an alley west of Balboa Boulevard (Holzer et al., 1999; Figure 3.9, bottom); a detailed study of deformed cultural features, including releveling after the earthquake (Johnson et al., 1996) and a Global Positioning System (GPS) re-survey (Hudnut et al., 1996).

If the damage zones were due to strong ground shaking only, the Mission Hills fault could have served as a wave guide for the 1994 seismic waves. The inactive Frew fault, farther south in the subsurface, could have also served this role. However, there is little damage to structures in which ground deformation is not also involved (Johnson et al., 1996), and deformation was greatest in the north-south region around

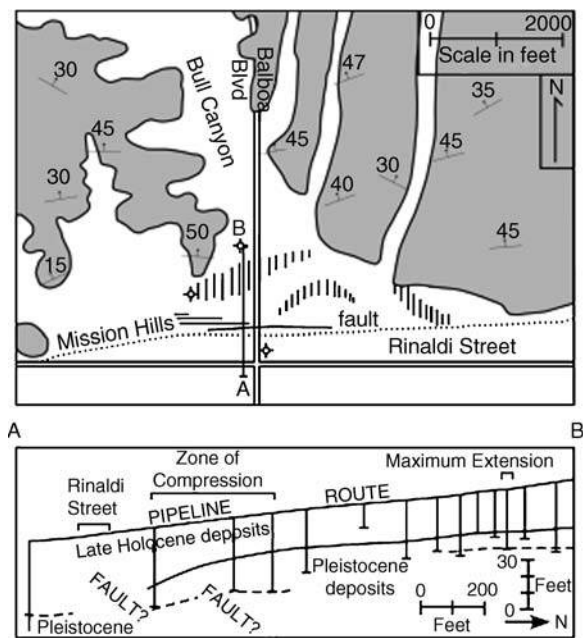


FIGURE 3.9 (Top) Geologic map of Balboa Boulevard, where pipelines ruptured in the 1994 Northridge earthquake. Geology modified from Shields (1977) and Dibblee (1991; 1992). Bedrock is shaded, with arrows in direction of dip of strata. Clear areas covered by late Quaternary alluvial deposits. Open circles with crosses show oil-well control for location of Mission Hills fault. Vertical lines, areas of extension; horizontal lines, areas of compression in 1994 earthquake. A-B locates cross section (bottom) with linear array of CPT and SPT soundings to define shallow geologic units, including boundary between Pleistocene and Holocene alluvial deposits. Modified from Holzer et al. (1999).

Balboa Boulevard rather than being distributed east–west along the surface projection of the Mission Hills fault. These observations were considered evidence that ground shaking without soil deformation was not a likely origin of the pipeline failure.

Holzer et al. (1999) observed that the failure zone along their CPT profile was restricted to the area where the water table was within the liquefiable sediment deposited during the Holocene (that is, during the past 10,000 years); up to 10 ft of Holocene sediments were water saturated. Geotechnical tests of the Holocene sediments showed that they could have been liquefied under the accelerations measured during the earthquake. Farther south, the water table deepened across a ground-water cascade, probably across the Mission Hills fault. Sediments did not liquefy there because the water table was too deep, and the sediments are older there and less subject to cyclic loading accompanying liquefaction. To the north, the sediments are older and more consolidated, and liquefaction also did not occur there. In addition, the compressive ground deformation measured near Rinaldi Street was more than canceled out by the extension farther north, an argument for a lateral spread of the impermeable surface material above the liquefied layer. The direction of compressional deformation was downslope, consistent with a lateral spread.

However, O'Rourke and Palmer (1994) reported that the liquefiable layer was not water saturated at the time of their study, in contrast to Holzer et al. (1996), who stated that the water table had changed very little from the time of their study, July, 1995, and the following March and June, 1996. Moreover, loose sand did not vent to the surface, common in liquefaction and lateral spreading, although Holzer et al. (1999) attributed this to the small thickness of the liquefiable layer.

Johnson et al. (1996) concluded that the localization of damage was due in large part to secondary, triggered movement on faults that did not reach the surface. Their argument was that the faults are zones of weakness, and if the orientation of a fault is close to a plane of high shear stress, it can rupture. The surface deformation caused by the earthquake measured by GPS had a southward-sloping gradient down

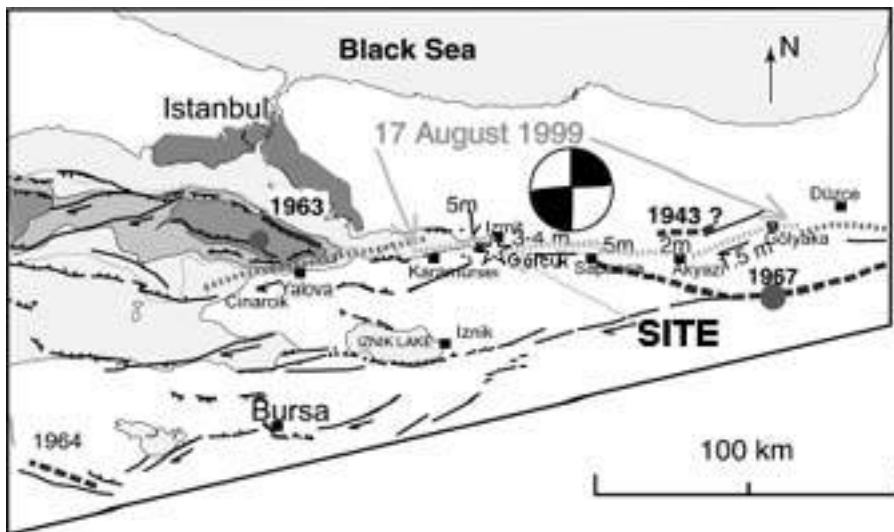


FIGURE 3.10 Map of the Istanbul, Turkey, region showing the 1999 surface rupture on the North Anatolian fault near the automobile assembly plant. Dashed lines in the Marmara Sea locate undersea faults that did not rupture in 1999 but have ruptured in previous cycles, including a large earthquake in 1766. An earthquake in 1894 may have ruptured an offshore fault at the eastern end of the Marmara Sea between Istanbul and the North Anatolian fault. See also color insert following page 2-30.

Balboa Boulevard with an inflection attributed by Johnson et al. (1996) to the Mission Hills fault at depth. It is difficult to explain this perturbation by lateral spreading, which should not have a significant vertical component of deformation. Moreover the linear distribution of zones of high extensional and compressional strain was more compatible with a tectonic rather than a liquefaction or lateral-spread origin.

In summary, studies of the Balboa pipeline failure were not successful in pinpointing the origin of the failure, although two hypotheses of origin could be ruled out. Arguments for and against the other two, soil failure or triggered rupture of the Mission Hills fault, were inconclusive. The Balboa pipeline problem did illustrate the necessity of geological background studies in the siting of pipelines, that is, surface rupture on faults is not the only concern.

3.8.6 Assessment of Ground Deformation at an Automobile Assembly Facility, Koçaeli, Turkey

The 1999 M 7.4 Izmit earthquake in Turkey was the result of a rupture of the North Anatolian fault (Barka et al. 2002; Barka, 1992) within 30 ft of a new automobile assembly plant in Koçaeli. In this area, the predominantly right-lateral strike-slip fault turns 90° to the right, forming an extensional down-dropped block known as the Gölçük Stepover (Figure 3.10). The 10 ft of right-lateral displacement east and west of the assembly plant resulted in 5 ft of east-side-down normal faulting adjacent to the plant. Damage to the plant was extensive due to strong shaking and coseismic warping that sheared off many of the foundation pile supports. The damage set back the completion date for plant construction and led company management to question the long-term viability of a plant located at this site. The question asked by management was: should we abandon the site or repair the damaged structures?

Two trenches were excavated to depths of 15 to 20 ft across the fault (Klinger et al., 2003). Detailed logging of the sediments exposed in the trench walls showed clear evidence of two prior ruptures at the same location as the 1999 rupture. Each rupture event was similar in size to the 5-ft vertical displacement during the 1999 earthquake. That is, the 1999 rupture event was characteristic (see Glossary). Each past rupture event was followed by collapse of the fault scarp and sedimentary burial in the intervening years between earthquakes. Radiocarbon dating of the two buried colluvial wedges (the material accumulated by collapse or erosion of the fault scarp; see Figure 3.2b) allowed correlation of the more recent paleo-

earthquakes to a historically recorded earthquake in AD 1719 (Ambraseys and Finkel, 1991; Ambraseys, 2002). The older event may have taken place at the same time as an earthquake in 1509 that Ambraseys (2001) located in the northeastern Marmara Sea south of Istanbul. Another earthquake in the region in 1894 produced lower intensities at the plant site than the 1719 or 1999 earthquakes (Parsons et al., 2000; Ambraseys, 2002; Barka et al., 2002). No other surface-rupturing events were preserved in the sediment record, indicating that this segment of the North Anatolian fault ruptures only in large characteristic earthquakes, similar to the 1999 event.

Therefore, based on the paleoseismic record, the facility management felt sufficiently confident to authorize repair of the facility rather than relocate it. Since the three earthquakes were separated by 200 to 300 years in time, the seismic design for the plant retrofit was based on rupture from a more distant westerly segment of the North Anatolian fault in Marmara Sea south of Istanbul that has not ruptured in this current seismic cycle (Stein et al., 1997). By analyzing the pattern, timing and magnitude of past earthquakes, it was possible to reassure management that the site could be safely rebuilt, and simultaneously to save significant retrofit costs by using ground motions from a more distant event expected in the near future over the much larger but improbable near-fault motions that would not be expected during the lifetime of the plant.

3.8.7 Village Reconstruction After the 2002 Nahrin, Afghanistan Earthquake

A geological consulting firm was hired by Shelter for Life International, a nongovernmental organization funded by the Office of Foreign Disaster Assistance of the U.S. Department of State, to survey more than 70 villages heavily damaged or destroyed by an earthquake of M 6.1 on March 25, 2002 (Yeats and Madden, 2003). Approximately 1200 lives were lost, principally due to the poor quality of mud-block construction. Site conditions were important in two ways. Houses constructed on bedrock underwent much less damage than those built on the floodplain of the Nahrin River. In addition, villages built on the crests of ridges underlain by loess (wind-blown silt) were much more severely damaged than those built in nearby swales, a condition attributed to the focusing of seismic waves on ridge crests. The consultants recommended that villages be rebuilt away from ridge crests in loess and on bedrock where possible. Where this was not possible, additional reinforcement against lateral forces was recommended.

3.9 Summary and Conclusions

The case histories show how geological factors are important in seismic hazard analysis. Case histories are more common in California, where surface faulting is regulated by the A-P Act. But surface faulting is also a hazard in the Seattle, Washington, metropolitan area; Portland, Bend and Klamath Falls, Oregon; Reno and Las Vegas, Nevada; and Salt Lake City, Provo and Ogden, Utah. None of these urban areas has legislation in place to regulate construction on active faults. Earthquake-induced liquefaction and landsliding are also regulated in California by the Seismic Hazards Mapping Act; the California Geological Survey is preparing liquefaction and landsliding maps for the state's major urban areas. The states of Oregon and Washington are preparing similar maps, but no legislation requires their use in urban planning and in the siting of structures. The Nisqually, Washington earthquake of February 28, 2001, caused extensive liquefaction and lateral spreading in the cities of Olympia and Seattle. These effects were largely limited to areas that had been previously identified on maps prepared by the Washington Division of Geology and Earth Resources as subject to liquefaction.

In states where geological investigations are not required, some jurisdictions oppose them, possibly because what they don't know won't hurt them. Not so long ago, this was not as legally risky as it is today. Geologists in the major urban centers of California have increased the quality of their practice to the point where sites subject to earthquake-related hazards: surface rupture, liquefaction, lateral spreading and landsliding, can be identified in advance without resorting to very costly investigating tools. At present, the state of the art has been developed in the Los Angeles and San Francisco Bay metropolitan areas so that it is now becoming the standard of practice. As the increasing quality of the practice of

engineering geology and geotechnical engineering radiates out from these centers of excellence, a developer might be held negligent if such practices were not followed and a hazard developed. In addition, insurance companies may require that more attention be paid to site conditions, as they are now doing for the earthquake resistance of structures. The result will be communities that are increasingly resistant to the catastrophic threat from earthquakes.

Acknowledgments

We thank Tania Gonzalez, Christopher Madden, Tom Rockwell, Kerry Sieh and Christian Walls of Earth Consultants International and Jon Bray, Doug Honegger, Mark Oborne and Mason Redding of cooperating firms for valuable discussions about the projects used as examples. Kerry Sieh of Earth Consultants International is the source for Figure 3.2a. Illustrations were prepared by Kristi Weber. This is Contribution No. 708 of the Southern California Earthquake Center. The Southern California Earthquake Center is funded by NSF Cooperative Agreement EAR-0106924 and USGS Cooperative Agreement 02HQAG0008.

Glossary

- active fault** — A fault that has had sufficient recent displacement so that, in the opinion of the user of the term, further displacement in the foreseeable future is considered likely.
- active tectonics** — Tectonic movements that are expected to occur or have occurred within a time span of concern to society.
- anticline** — A fold, generally convex upward, whose core contains the stratigraphically older rocks.
- bending-moment fault** — Fault formed due to bending of a flexed layer during folding. Normal faults characterize the convex side, placed in tension, and reverse faults characterize the concave side, placed in compression.
- blind fault** — A fault that does not extend upward to the Earth's surface, and never has. It usually terminates upward in the axial region of an anticline. If its dip is $<45^\circ$, it is a blind thrust.
- characteristic earthquake** — The largest earthquake that is thought to occur repeatedly on a given fault.
- colluvial wedge** — A prism-shaped deposit of fallen and washed material at the base of (and formed by erosion from) a fault scarp or other slope, commonly taken as evidence in outcrop of a scarp-forming event such as an earthquake.
- earthquake segment** — That part of a fault zone that has ruptured during an individual earthquake.
- event horizon** — A bedding plane within a stratigraphic sequence that represents the ground surface at the time of a paleoseismic event.
- fault** — A fracture or a zone of fractures along which displacement has occurred parallel to the fracture.
- fault creep** — Steady or episodic slip on a fault at a rate too slow to produce an earthquake.
- fault scarp** — A slope formed by the offset of the Earth's surface by a fault.
- fault slip rate** — The rate of displacement on a fault averaged over a time period encompassing several earthquakes.
- flexural-slip fault** — A bedding fault formed by layer-parallel slip during flexural-slip folding.
- footwall** — The underlying side of a nonvertical fault surface.
- gouge** — A thin layer of fine-grained highly cataclastic material within a fault zone.
- hangingwall** — The overlying side of a nonvertical fault surface.
- lateral spread** — A displacement of nonliquefiable material on a slope that may be as low as 0.1° , overlying a cohesionless, liquefied layer of large areal extent.
- left-lateral fault** — A strike-slip fault across which a viewer would see the block on the other side move to the left.
- mean recurrence interval** — The mean time between earthquakes of a given magnitude, or within a given magnitude range, on a specific fault or within a specific area.
- normal fault** — A fault in which movement of the hangingwall is downward relative to the footwall.

- paleoseismology** — The investigation of individual earthquakes decades, centuries or millennia after their occurrence.
- primary surface rupture** — Surface rupture that is directly connected to subsurface displacement on a seismic fault.
- reverse fault** — A fault characterized by movement of the hangingwall block upward relative to the footwall.
- right-lateral fault** — A strike-slip fault across which a viewer would see the adjacent block move to the right.
- seismic moment** — The area of a fault rupture multiplied by the average slip over the rupture area multiplied by the shear modulus of the affected rocks.
- seismogenic structure** — One that is capable of producing an earthquake.
- shutter ridge** — A linear hill or scarp sloping in a direction opposite to the overall topographic gradient, formed by strike-slip or oblique-slip offset of irregular topography.
- slickensides** — A polished and smoothly striated surface that results from slip along a fault surface. The striations themselves are slickenlines.
- slip vector** — The magnitude and orientation of dislocation of formerly adjacent features on opposite sides of a fault.
- stepover** — Region where one fault ends, and another *en échelon* fault of the same orientation begins. Described as either right or left depending on whether the bend or step is to the right or left as one progresses along the fault.
- tectonic geomorphology** — The study of landforms that result from tectonic processes.

References

- Allen, J.T., Jr. (1978). History of geological investigations at the San Bernardino Valley College Campus, 1935–1978, in French, J., Ed., *Geologic Guidebook to the Santa Ana River Basin, Southern California*, South Coast Geological Society Field Trip Guidebook, 45–50.
- Ambraseys, N.N. (2001). The earthquake of 1509 in the Sea of Marmara, Turkey, revisited. *Bull. Seism. Soc. Am.*, 91, 1397–1416.
- Ambraseys, N.N. (2002). The seismic activity of the Marmara Sea region over the last 2000 years. *Bull. Seism. Soc. Am.*, 92, 1–18.
- Ambraseys, N.N., and Finkel, C.F. (1991). Long-term seismicity of Istanbul and of the Marmara Sea region. *Terra Nova*, 3, 527–539.
- Anderson, R. (1990). Evolution of the Santa Cruz Mountains by advection of crust past a San Andreas fault bend. *Science*, 249, 397–401.
- Barka, A. (1992). The North Anatolian fault zone. *Annales Tectonicae, supplement to 6*, 164–195.
- Barka, A., Akyüz, H.S., Sunal, G., Çakir, Z., Dikbas, A., Yerli, B., Armijo, R., Meyer, B., de Chabalier, J.B., Rockwell, T., Dolan, J.R., Hartleb, R., Dawson, T., Christofferson, S., Tucker, A., Fumal, T., Langridge, R., Stenner, H., Lettis, W., Bachhuber, J. and Page, W. (2002). The surface rupture and slip distribution of the 17 August 1999 Izmit earthquake (M 7.4), North Anatolian fault. *Bull. Seism. Soc. Am.*, 92, 43–60.
- Bullard, T.F., and Lettis, W.R. (1993). Quaternary fold deformation associated with blind thrust faulting, Los Angeles Basin, California. *J. Geophys. Res.*, 98, 8349–8369.
- Davis, T.L., and Namson, J. (1994). A balanced cross section of the 1994 Northridge earthquake, southern California. *Nature*, 372, 167–169.
- Dibblee, T.W., Jr. (1991). Geologic map of the San Fernando and Van Nuys (north 1/2) quadrangles, Los Angeles County, California. Dibblee Foundation Map DF-33, scale 1:24,000.
- Dibblee, T.W., Jr. (1992). Geologic map of the Oat Mountain and Canoga Park (north 1/2) quadrangles, Los Angeles County, California. Dibblee Foundation Map DF-36, scale 1:24,000.
- Dolan, J.F., and Rockwell, T.K. (2001); Paleoseismologic evidence for a very large ($M_w > 7$), post-A.D. 1660 surface rupture in the eastern San Cayetano fault, Ventura County, California. *Bull. Seism. Soc. Am.*, 91, 1417–1432

- Gath, E.M., Gonzalez, T., Sieh, K., Zekioglu, A. and Fleming, K. (2004); Earthquake risk at San Bernardino Valley College: Hazard mitigation astride the San Jacinto fault in southern California.[in preparation]
- Geschwind, C.-H. (2001). *California Earthquakes: Science, Risk, and the Politics of Hazard Mitigation, 1906-1977*. Baltimore, Johns Hopkins University Press, 337 p.
- Grant, L.B. (1996). Uncharacteristic earthquakes on the San Andreas fault. *Science*, 272, 826–827.
- Hampton, M.A., Lemke, R.W. and Coulter, H.W. (1993). Submarine landslides that had a significant impact on man and his activities: Seward and Valdez, Alaska. *U.S. Geol. Survey Bull.* 2002, 122–134.
- Harp, E.L., and Jibson, R.W. (1996). Landslides triggered by the 1994 Northridge, California, earthquake. *Bull. Seism. Soc. Am.*, 86, S319–S332.
- Hart, E.W., and Bryant, W.A. (1997, with periodic revisions) Fault-rupture hazard zones in California. *California Division of Mines and Geology Special Publication* 42, 38 p.
- Hart, E.W., Treiman, J.A. and Bryant, W.A. (1995). The search for fault rupture after the Northridge earthquake. *California Division of Mines and Geology Special Publication* 116, 89–101.
- Healy, T. (1998). *Ethical Issues and Earthquake Risk Reduction*. EERI Endowment Fund White Paper, Earthquake Engineering Research Institute, 59–61.
- Hecker, S., Ponti, D.J., Garvin, C.D. and Hamilton, J.C. (1995a). Characteristics and origin of ground deformation produced in Granada Hills and Mission Hills during the January 17, 1994 Northridge, California, earthquake. *California Division of Mines and Geology Special Publication* 116, 111–131.
- Hecker, S., Ponti, D.J., Garvin, C.D., Powers, T.J., Fumal, T.E., Hamilton, J.C., Sharp, R.V., Rymer, M.J., Prentice, C.S. and Cinti, F.R. (1995b). Ground deformation in Granada Hills and Mission Hills resulting from the January 17, 1994, Northridge, California, earthquake. *U.S. Geol. Survey Open-File Report* 95-62, 11 p.
- Holzer, T.L., Bennett, M.J., Tinsley, J.C., III, Ponti, D.J. and Sharp, R.V. (1996). Causes of ground failure in alluvium during the Northridge, California, earthquake of January 17, 1994. In 6th U.S.-Japan workshop on earthquake-resistant design of lifeline facilities and countermeasures against soil liquefaction. Tokyo, Japan.
- Holzer, T.L., Bennett, M.J., Tinsley, J.C., III, Ponti, D.J. and Sharp, R.V. (1999). Causes of ground failure in alluvium during the Northridge, California, earthquake of January 17, 1994, in Hamada, M., and O'Rourke, T.D., Eds., U.S.-Japan workshop on earthquake resistant design of lifeline facilities and countermeasures against liquefaction, 6th, Tokyo, 1996, Proc. National Center for Earthquake Engineering Research Technical Report NCEER 96-0012, 345–360.
- Hudnut, K.W., Shen, Z., Murray, M., McClusky, S., King, R., Herring, T., Hager, B., Feng, Y., Fang, P., Donnellan, A. and Bock, Y. (1996). Coseismic displacements of the 1994 Northridge, California, earthquake. *Bull. Seism. Soc. Am.*, 86, S19–S36.
- Huftile, G.J., and Yeats, R.S. (1996). Deformation rates across the Placerita (Northridge $M_w = 6.7$ aftershock zone) and Hopper Canyon segments of the western Transverse Ranges deformation belt. *Bull. Seism. Soc. Am.*, 86, S3–S18.
- Jennings, C.W. (1994). Fault activity map of California and adjacent areas with locations and ages of recent volcanic eruptions, scale 1:750,000. *California Division of Mines and Geology Geologic Data Map No. 6*, with explanatory pamphlet, 92 p.
- Johnson, A.M., Fleming, R.M., Cruikshank, K.M. and Packard, R.F. (1996). Coactive fault of the Northridge earthquake — Granada Hills area, California. *U.S. Geol. Survey Open-File Report* 96-523, 66 p.
- Klinger, Y., Sieh, K., Altunel, E., Akoglu, A., Barka, A., Dawson, T., Gonzalez, T., Meltzner, A., and Rockwell, T. (2003). Paleoseismic evidence of characteristic slip on the western segment of the North Anatolian fault, Turkey. *Bull. Seism. Soc. Am.*, 93, 2317–2332.
- Lomnitz, C., and Rodríguez E., S. (2001). El Salvador 2001: Earthquake disaster and disaster preparedness in a tropical volcanic environment. *Seismological Research Letters*, 72, 346–351.
- McCalpin, J.P. (1996). *Paleoseismology*. San Diego, California, Academic Press, 587 p.
- Mendenhall, W.C. (1905). The hydrology of San Bernardino Valley, California. *U.S. Geol. Survey Water-Supply Paper* 142, 124 p.

- Noller, J.S., Sowers, J.M. and Lettis, W.R., eds. (2000). *Quaternary Geochronology Methods and Applications*: American Geophysical Union Reference Shelf 4, 582 p.
- Obermeier, S. (1994). Using liquefaction features in paleoseismic analysis. *U.S. Geol. Survey Open-File Report 94-663*, chapter A, 58 p.
- Olsen, K.B., Archuleta, R.J. and Matarese, J.R. (1995). Three-dimensional simulation of a magnitude 7.75 earthquake on the San Andreas fault. *Science*, 270, 1628–1632.
- O'Rourke, T.D., and Palmer, M.C. (1994). Earthquake performance of gas transmission pipelines during the Northridge earthquake. *NCEER Bull.* 5(2), 1–5.
- Osokin, M., Sieh, K., Rockwell, T., Miller, G., Guptill, P., Curtis, M., McArdle, S. and Elliot, P. (2000). Active parasitic folds on the Elysian Park anticline: Implications for seismic hazard in central Los Angeles, California. *Geol. Soc. Am. Bull.* 112, 693–707.
- Parsons, T., Toda, S., Stein, R., Barka, A., and Dieterich, J.M. (2000). Heightened odds of large earthquakes near Istanbul: An interaction-based probability calculation. *Science*, 288, 662–665.
- Petersen, M., and Wesnousky, S.G. (1994). Fault slip rates and earthquake histories for active faults in southern California. *Bull. Seism. Soc. Am.*, 84, 1608–1649.
- Reiter, L. (1990). *Earthquake Hazard Analysis—Issues and Insights*. New York, Columbia University Press, 254 p.
- Rubin, C.M., Lindvall, S.C., and Rockwell, T.K. (1998). Evidence for large earthquakes in metropolitan Los Angeles. *Science*, 281, 398–402.
- Shaw, J.H., and Shearer, P.M. (1999). An elusive blind-thrust fault beneath metropolitan Los Angeles. *Science*, 283, 1516–1518.
- Shields, K.E. (1977). Structure of the northwestern margin of the San Fernando Valley, Los Angeles County, California. MS thesis, Ohio University, Athens, 82 p.
- Sieh, K. (1978). Prehistoric large earthquakes produced by slip on the San Andreas fault at Pallett Creek, California. *J. Geophys. Res.* 83, 3907–3939.
- Sieh, K., and LeVay, S. (1998). *The Earth in Turmoil*. New York, W.H. Freeman, 324 p.
- Stein, R.S., Barka, A., and Dieterich, J. (1997). Progressive failure on the North Anatolian fault since 1939 by earthquake stress triggering. *Geophys. J. Int.*, 128, 594–604.
- Stein, R.S., and Ekström, G. (1992). Seismicity and geometry of a 110-km-long blind thrust fault: 2. Synthesis of the 1982–1985 California earthquake sequence. *J. Geophys. Res.* 97, 4865–4883.
- Stein, R.S., and King, G.C.P. (1984). Seismic potential revealed by surface folding: 1983 Coalinga earthquake. *Science*, 224, 869–872.
- Treiman, J.A. (1995). Surface faulting near Santa Clarita. *Calif. Division of Mines and Geology Special Publication 116*, 103–110.
- Tsutsumi, H., and Yeats, R.S. (1999). Tectonic setting of the 1971 Sylmar and 1994 Northridge earthquakes in the San Fernando Valley, California. *Bull. Seism. Soc. Am.*, 89, 1232–1249.
- Wells, D.L., and Coppersmith, K.J. (1994). New empirical relationships among magnitude, rupture length, rupture area, and surface displacement. *Bull. Seism. Soc. Am.*, 84, 974–1002.
- Working Group on California Earthquake Probabilities (1995). Seismic hazards in southern California: probable earthquakes 1994–2024. *Bull. Seism. Soc. Am.*, 85, 379–439.
- Working Group on California Earthquake Probabilities (1999). Earthquake probabilities in the San Francisco Bay Region: 2000–2030 — a summary of findings. U.S. Geol. Survey Circular 1189 and <http://quake.usgs.gov/study/wg99/of99-517/index.html>
- Yeats, R.S. (1986). Active faults related to folding, in *Active Tectonics*: Washington, D.C., National Academy Press, pp. 63–79.
- Yeats, R.S. (2001). *Living with Earthquakes in California — A Survivor's Guide*. Corvallis, Oregon State University Press, 406 p.
- Yeats, R.S. (2004). *Living with Earthquakes in the Pacific Northwest — A Survivor's Guide*. 2nd ed., Revised and Expanded. Corvallis, Oregon State University Press, 390 p.
- Yeats, R.S., Clark, M., Keller, E. and Rockwell, T. (1981). Active fault hazard in southern California: Ground rupture versus seismic shaking. *Geol. Soc. Am. Bull.* 92, 189–196.

- Yeats, R.S., and Huftile, G.J. (1995). The Oak Ridge fault system and the 1994 Northridge earthquake. *Nature*, 373, 418–420.
- Yeats, R.S., and Madden, C. (2003). Damage from the Nahrin, Afghanistan, earthquake of 25 March, 2002. *Seismological Research Letters*, 74, 305–311.
- Yeats, R.S., Sieh, K., and Allen, C.R. (1997). *The Geology of Earthquakes*. New York, Oxford University Press, 568 p.

4

Geotechnical Aspects of Seismic Hazards

Steven L. Kramer

Jonathan P. Stewart

4.1	Introduction	4-1
4.2	Site Characterization.....	4-2
	Site Exploration • Field Tests • Laboratory Tests • Model Tests	
4.3	Dynamic Soil Properties.....	4-6
	Shear Modulus and Damping • Nonlinear Characterization • Dynamic Shear Strength	
4.4	Site Response.....	4-10
	Types of Site Effects • Site Classification • Site Amplification Factors • Site Response Analysis	
4.5	Soil–Foundation–Structure Interaction.....	4-21
	Introduction • Inertial Interaction • Kinematic Interaction • Implementation in Seismic Design Standards	
4.6	Ground Failure.....	4-36
	Liquefaction • Landslides • Retaining Structures	
4.7	Soil Improvement	4-66
	Densification Techniques • Reinforcement Techniques • Grouting and Mixing Techniques • Drainage Techniques	
4.8	Future Challenges	4-69

4.1 Introduction

Observations of damage during numerous historical earthquakes have shown that geotechnical factors can have a strong influence on the performance of man-made and natural structures during earthquakes. The origin of the field of geotechnical earthquake engineering can be traced to the damaging earthquakes in Niigata, Japan and Alaska in 1964. Then, the field experienced significant growth during the rise of the nuclear power industry during the 1960s and 1970s. In recent years, the field has evolved with the rise of the performance-based engineering paradigm for earthquake engineering coupled with the lessons learned from significant earthquakes in California, Japan, Turkey and Taiwan between 1989 and 1999. As a result of this ongoing process, theories and analytical procedures are now available for many of the important problems faced by practicing geotechnical engineers. This chapter provides an overview of these problems and the tools and techniques that are available for their solution.

Geotechnical materials, from soil to rock to waste products, influence the damage earthquakes cause in two primary ways: (1) by modifying the manner in which the ground shakes at a particular site; geotechnical materials may cause amplification or attenuation of seismic waves, and (2) through the process of ground failure in which a mass of soil experiences permanent deformations (e.g., settlement or landslide). Both can cause significant damage to, and even the destruction of, structures and con-

structed facilities, and both must be considered in seismic hazard evaluation and earthquake-resistant design.

Although many important advances have been made, geotechnical earthquake engineering remains a relatively young field. Early procedures for evaluating site response used linear or equivalent linear approximations of soil stress-strain behavior, and early procedures for ground failure analysis used pseudo-static approximations of earthquake loading. Though these types of approximations allowed many important advances in our understanding of soil response, as well as the development of many useful practical methods of analysis, newer procedures that more realistically represent soil behavior continue to be developed and used more commonly in practice. In particular, nonlinear site response analyses that can account for hysteretic energy dissipation, pore-pressure generation and the accumulation of permanent strain are now available. These analyses can provide improved representations of seismic response at sites with soft and weak soils. They can also be used to evaluate ground failure hazards in terms of permanent deformations, rather than the historical metric of a pseudo-statically based factor of safety. The trend toward consideration of nonlinear effects on site response and ground failure will be at the center of future developments in geotechnical earthquake engineering.

This chapter begins with a description of available methods for site characterization (Section 4.2) and evaluation of dynamic soil properties (Section 4.3), factors that are required for evaluating both site response effects and the potential for ground failure. Site response (Section 4.4) and the interaction of soils and structures (Section 4.5) are covered in the next two sections. The potential for ground failure, through such mechanisms as soil liquefaction, landslides and retaining structure instability are covered in Section 4.6. Finally, Section 4.7 provides an overview of methods available for mitigating geotechnical seismic hazards.

4.2 Site Characterization

One of the first, and most important, steps in a geotechnical earthquake engineering hazard evaluation or design program is site characterization. This involves acquisition, synthesis and interpretation of qualitative and quantitative information about the site of interest. The information should include historical and current data on surface and subsurface geometry, soil and rock properties and groundwater conditions. It is an activity whose importance to the hazard evaluation and design process can hardly be overemphasized.

The basic elements of site characterization for geotechnical earthquake engineering purposes are the same as for typical geotechnical engineering problems: review of the available published data, field reconnaissance and subsurface investigation. These activities are described in a number of standard geotechnical engineering textbooks (Holtz and Kovacs, 1981; Terzaghi et al., 1996; Coduto, 1999; Das, 2002); those with particular applicability to geotechnical earthquake engineering problems are described in the following sections.

4.2.1 Site Exploration

Site exploration usually begins with a thorough review of the available information about the site and its surroundings. Geotechnical reports for the site, or for the surrounding structures and facilities, may be available from various government agencies (state or local engineering departments, construction permitting departments, etc.). Geologic maps at different scales may be available and can provide important information on regional and local geology. Other types of maps, such as topographic maps, fault maps, hazard (landslide, liquefaction, etc.) maps and depth-to-bedrock maps, may also be available. Stereo-paired aerial photographs can reveal important aspects of site geomorphology (e.g., existing ground failures), as can low-sun-angle aerial photographs. In densely vegetated areas, the relatively new technique, LIDAR, can be used to see through the vegetation and image the ground surface. All of these sources of information can provide valuable insight into subsurface soil and groundwater conditions, and can help guide the planning of an efficient field reconnaissance and subsurface investigation.

Field reconnaissance, often performed by geologists trained to see and interpret subtle topographic features, can provide useful information on site conditions and past occurrences of ground failure. Observations of scarps, tension cracks, bulges, hummocky terrain, displaced ditches or fences, displaced walls or pavements, cracked foundations and leaning trees or poles can indicate potential problems.

The above-mentioned activities allow the collection of data from which subsurface conditions can be inferred. Such inferences, however, are rarely sufficient for site-specific design or evaluation, and must be confirmed and supplemented by hard data. Subsurface investigations, accomplished by trenching, drilling and sampling and *in situ* testing, can provide the quantitative data that are frequently required as input to hazard evaluation and design. Surface mapping of faults, outcrops, joints, bedding planes, slides and other features should also be performed. Subsurface investigations should be conducted to depths sufficient to define the pertinent engineering properties of all soil and rock units that significantly contribute to site response and potential ground failure. Logging and sampling should take place at sufficient intervals to detect weak zones or seams that could contribute to ground failure.

4.2.2 Field Tests

A number of tests can be performed in the field to measure soil properties under *in situ* conditions. These tests allow the effects of *in situ* stress, thermal, chemical and structural states — which can be destroyed by sampling — to be reflected in the measured properties. Field tests often sample large volumes of soil and do so quite economically. The tests most commonly used in geotechnical earthquake engineering practice can be divided into those that measure low-strain properties and those that measure properties at intermediate to high strains.

Low-strain field tests typically induce seismic waves in the soil and seek to measure the velocities at which these waves propagate. Because the strain amplitudes associated with these waves are quite low, the measured velocity of shear waves (v_s) can be used, along with the soil density, to compute the corresponding low-strain shear modulus.

$$G_{\max} = \rho v_s^2 \quad (4.1)$$

where ρ = soil mass density. Seismic reflection and seismic refraction tests are staples of conventional geophysical exploration, and can provide information on subsurface layer thicknesses and propagation velocities without the need for soil borings. Nevertheless, these techniques are not commonly used in geotechnical earthquake engineering practice because they cannot detect soft layers below stiff layers and because s-wave velocities can be more effectively evaluated using other techniques described below. A relatively new technique that can be used to determine subsurface layer thicknesses and wave propagation velocities, and also requires no borings, is the spectral analysis of surface waves (SASW) test (Heisey et al., 1982; Nazarian and Stokoe, 1983; Stokoe et al., 1994). In this test, two or more vertical receivers are placed on the ground surface in line with a vibration source. The output of both receivers is recorded and transformed into the frequency domain. The phase angles between the recorded responses can be computed for each frequency in the transformation and used to compute an apparent travel time of the surface waves from one receiver to the other. The surface wave phase velocity can be computed as a function of frequency by knowing the distance between the receivers. The variation of phase velocity with frequency (i.e., the dispersion) is a function of the variation of stiffness with depth, and is therefore used for computing the stiffnesses of the underlying soil layers. Because SASW profiling can be conducted from the ground surface (i.e. without borings), can detect low-velocity layers and can be used to considerable depth, it has seen increasing use in earthquake engineering applications.

Other low-strain tests require borings, which may add to the cost of their use if borings already made for other purposes cannot be used. In the down-hole test, a vibration source is placed on the ground surface adjacent to a borehole. A receiver is lowered into the borehole and secured against its sides at the depth of interest. An impulsive load is then applied at the source using explosives or a triggered hammer. The waveform recorded at the receiver is then recorded and the time interval required for the wave to

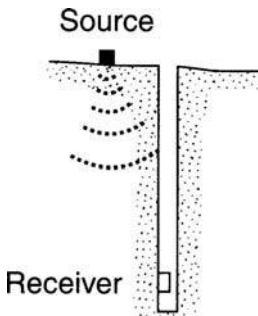


FIGURE 4.1 Source–receiver configurations for downhole test.

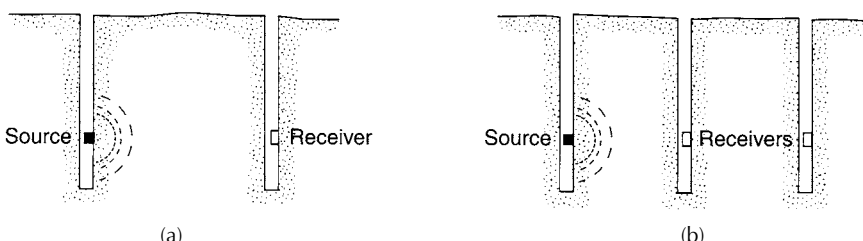


FIGURE 4.2 Configurations for cross-hole seismic test: (a) single receiver, and (b) multiple receivers.

travel from the source to the receiver measured. The average shear wave velocity can easily be computed by knowing the distance between the source and receiver. The down-hole test (Figure 4.1) is repeated at a number of intervals (often 1 m depth intervals) to allow plotting of the average shear wave travel time as a function of receiver depth. The derivative of this curve represents the variation of shear wave velocity with depth. Wave velocities within individual layers can be measured directly by use of the cross-hole seismic test. The cross-hole test (Figure 4.2) makes use of more than one boring; a source is placed in one boring and a receiver is placed at the same depth in each of the other boreholes. An impulsive disturbance is applied at the source and the travel times to each of the receivers is measured. The wave propagation velocity can be computed by knowing the distances between receivers. When more than two boreholes are used, travel times between holes with receivers can be used to compute wave velocities; this approach benefits from the fact that any delays due to receiver–borehole coupling will be nearly equal for both receivers and therefore cancelled in the time delay. A relatively new test for measuring wave propagation velocities is the suspension logger test. In this test, a suspension logger (Figure 4.3) is lowered into a fluid-filled borehole. The suspension logger has a single source and two receivers; the receivers are mounted approximately 1 m apart along the length of the logger. The source produces an impulsive disturbance that travels through the borehole fluid into the surrounding soil. As the disturbance propagates through the soil, it refracts some energy back into the borehole fluid. When that energy reaches the two receivers, the difference between the travel times can be computed. The wave propagation velocity is computed as 1 m divided by the difference in travel times, and applies for the soil domain between the receivers. The suspension logger is particularly valuable for measuring shear wave velocity with a high level of vertical resolution and to obtain velocity measurements at large depths — since both the source and receiver are at the depth of interest within the boring, problems with wave attenuation and dispersion are eliminated.

In the field, development and measurement of large-strain soil behavior is more difficult and few proven techniques are available. An *in situ* borehole torsional test (Henke and Henke, 1991) advances two thin concentric tubes into the soil below the bottom of a boring. Torque is applied to the inner tube and used, along with its measured rotation, to evaluate the stress–strain behavior of the soil. Riemer et al. (2001) have developed a similar device for measuring dynamic properties of cohesive soil deposits. The device performs cyclic torsional shear tests on freestanding specimens beneath the bottom of a cased borehole, with the goal of measuring local strains on soil that has not been signifi-

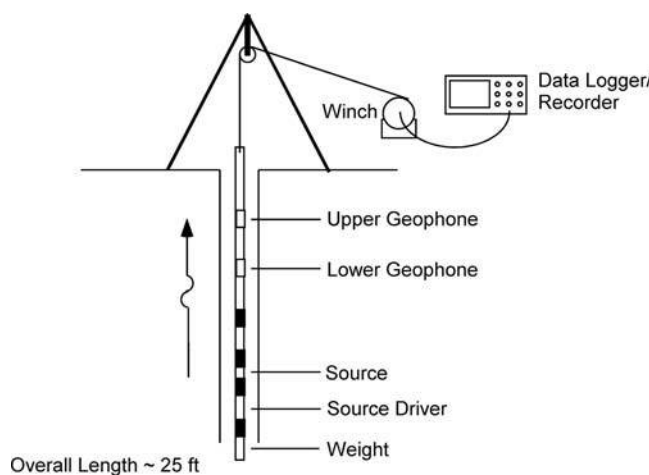


FIGURE 4.3 Schematic illustration of the suspension logger test.

cantly disturbed by the drilling, sampling or unloading and reloading processes associated with conventional laboratory testing. The device is capable of modulus and damping measurements over a range of shear strains from $10^{-3}\%$ to nearly 1%.

4.2.3 Laboratory Tests

In some cases, it is desirable to test soil samples in the laboratory. If conditions are expected to change between the time the samples are obtained and the time at which earthquakes are of concern, laboratory tests offer the potential for creating the changed conditions such that their effect will be reflected in the measured soil properties. For example, a site that is to be filled prior to development will subject subsurface soils to greater effective stresses at the time an earthquake than the current stresses, therefore, laboratory samples of the *in situ* soil could be consolidated to the anticipated future stress levels and then tested under those stress conditions. Laboratory tests can be divided into those that operate at low-strain levels and those that operate at higher strain levels.

In the resonant column test, a cylindrical test specimen is excited harmonically in torsion. Starting with a low torque amplitude and a low loading frequency, a frequency sweep is performed to identify the frequency at which the greatest angular rotation is exhibited — this is the fundamental frequency of the specimen. Knowing the dimensions and polar moments of inertia of both the soil specimen and the loading head, the average (secant) shear modulus can be computed. By repeating the test with successively increased loading amplitudes, the variation of secant shear modulus with strain amplitude can be measured. When the resonant frequency is identified, termination of the harmonic torque will place the test specimen in free vibration; by measuring the resulting amplitude decay, the damping ratio of the test specimen can also be computed. Another laboratory test in which low-strain stiffness can be measured is the bender element test. Bender elements comprise two thin piezoelectric materials bonded together and wired in such a way that one expands and the other contracts when a voltage is applied to them. The opposing deformations cause the element to bend one way under a positive voltage and the other under a negative voltage. Bender elements can be inserted into the top and bottom of a soil specimen (e.g., typically triaxial); application of a sharp voltage pulse to one causes a shear wave that travels through the soil. When that shear wave reaches the other bender element, the deflection of the receiving bender element produces a voltage that can be measured. By measuring the time required for the wave to travel from the source to the receiver, and knowing the distance between each, the shear wave velocity of the specimen can be measured nondestructively.

Other laboratory tests are capable of measuring soil response at moderate to high strain levels. Most of these tests are derived from conventional tests by adding dynamic loading capabilities to the testing apparatus. Cyclic triaxial testing has been used for many years to investigate pore-pressure generation, stiffness degradation and damping characteristics. With local strain measurements (measurements of axial strain over approximately the central third of the triaxial specimen), bedding and end restraint effects can be minimized, allowing low-strain as well as high-strain response to be measured. Cyclic simple shear testing has also been used for the measurement of small- to high-strain response. Resonant column tests have been modified to allow cyclic torsional shear testing to strain levels above those achieved by the conventional resonant column test.

4.2.4 Model Tests

Each of the previously described laboratory tests measures the response of an element of soil consolidated and loaded so that stresses and strains are constant throughout the element. Actual problems, however, involve many elements of soil subjected to different initial, loading and boundary conditions. Model tests, in which a scale model of the site of interest is subjected to dynamic loading, can be used to investigate the response of a soil profile or soil-structure system.

The dynamic behavior of geotechnical models is usually tested using 1g shaking tables or shaking tables mounted on centrifuges. 1g shaking tables can be quite large and thereby allow the testing of large models, which has some advantages with respect to ease of instrumentation and use of realistic materials. However, the strong pressure dependence of soil behavior (particularly their contractive–dilative volume change tendencies) causes difficulties in scaling model behavior to be consistent with field behavior. The geotechnical centrifuge allows the imposition of prototype scale stresses on a small scale model — the vertical stress at the bottom of a 1-foot-high model accelerated to 100g, for example, would be equal to that at the bottom of a 100-feet-thick soil deposit under 1g conditions. While model tests are not sufficiently refined at this point to produce direct evidence of prototype soil behavior, they are very useful for investigating failure modes and mechanisms and for calibration of computational models that can be used to predict field performance.

4.3 Dynamic Soil Properties

Both site response and ground failure are strongly influenced by properties of soil. Site response is primarily influenced by the properties that control wave propagation, particularly stiffness and damping. Ground failure is influenced by those properties, but also by the shear strength of the soil. Of course, both site response and ground failure are part of the same continuous spectrum of nonlinear soil behavior. However, the manner in which methods for their analysis developed (largely influenced by the constraints of available computer systems at the time) has led to a precedent of their being treated separately. Thus, different methods of analysis characterize soil properties differently.

Soils, in contrast to many structural materials, are highly nonlinear even at very low strains. This nonlinearity causes soil stiffness to decrease and damping to increase with increasing shear strain amplitude. The variation of stiffness with strain can be expressed in either of two ways — by shear modulus curves or by nonlinear backbone (stress–strain) curves, which are related to each other as shown in Figure 4.4.

4.3.1 Shear Modulus and Damping

During the early 1970s, the capabilities of available computer systems were such that one-dimensional site response analyses were considered computationally intensive. To save on computer time, the concept of an equivalent linear method of analyses (Section 4.4.4.1) was developed; retaining linearity allowed solution of the governing equations in the frequency domain where computation of the response at high frequencies could be ignored without significant loss of accuracy. The effects of nonlinearity are approximated by performing a series of linear analyses in which the average, or secant, shear modulus and the damping ratio are varied until their values are consistent with the level of strain induced in the soil.

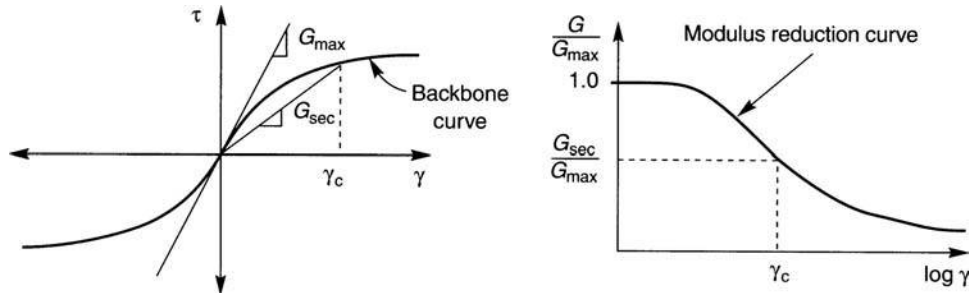


FIGURE 4.4 Relationship between (a) backbone curve and (b) modulus reduction curve.

Laboratory tests have shown that the dynamic stiffness of soils principally depends on soil density, effective confining pressure, soil plasticity and strain amplitude. In the equivalent linear approach, it is common to describe the secant shear modulus as the product of the maximum shear modulus (i.e., the shear modulus at very low strain levels), G_{max} , and a modulus reduction factor, G/G_{max} . The maximum shear modulus is optimally obtained from field measurements of shear wave velocity, but can be estimated from parameters such as penetration resistance when shear wave velocity data are not available, e.g.,

$$G_{max}(\text{psf}) = 20,000 (N_1)_{60}^{1/3} (\sigma'_m)^{1/2} \quad (4.2)$$

$$G_{max}(\text{kPa}) = 1634 q_c^{1/4} (\sigma'_v)^{3/8} \quad (4.3)$$

where $(N_1)_{60}$ is the corrected standard penetration test (SPT) resistance, σ'_m is the mean effective stress in psf, q_c is the CPT tip resistance in kPa and σ_v is the vertical effective stress in kPa (Ohta and Goto, 1976; Seed et al., 1986; Rix and Stokoe, 1991). Additional methods for estimating small strain shear wave velocity based on surface geology (Wills and Silva, 1998) and local measurements of soil properties such as void ratio or shear strength are also available (Fumal and Tunsley, 1985; Dickenson, 1994).

Modulus reduction behavior is usually expressed graphically in terms of modulus reduction curves. Modulus reduction behavior is strongly dependent upon shear strain amplitude and plasticity index (Figure 4.5a); for cohesionless and low-plasticity soils it is also influenced by mean effective stress (Figure 4.6a). The influence of effective confining pressure decreases with increasing plasticity index (PI), and is generally not significant for $PI \geq 30$. Damping is affected by the same factors that affect modulus reduction behavior, but in the opposite sense (factors that cause modulus reduction ratio to decrease cause damping ratio to increase). Commonly used damping curves for soils of different plasticities and for cohesionless soils are shown in Figures 4.5b and 4.6b.

4.3.2 Nonlinear Characterization

Nonlinear site response analyses follow the evolution of nonlinear, inelastic soil behavior in a step-by-step fashion in the time domain and therefore require characterization of the stress-strain behavior of the soil. This is usually accomplished by specification of a backbone curve (to describe the nonlinearity) and a set of unloading-reloading rules (to describe the inelasticity). The simplest form of backbone curve is a hyperbolic curve, which requires the maximum shear modulus, G_{max} , and the shear strength, τ_{max} , i.e.,

$$F_{bb}(\gamma) = \frac{\gamma}{\frac{1}{G_{max}} + \frac{\gamma}{\tau_{max}}} \quad (4.4)$$

where γ is the shear strain. Other functions can be used to describe the backbone curve and, indeed, it is possible to create a backbone curve that is consistent with a particular modulus reduction curve.

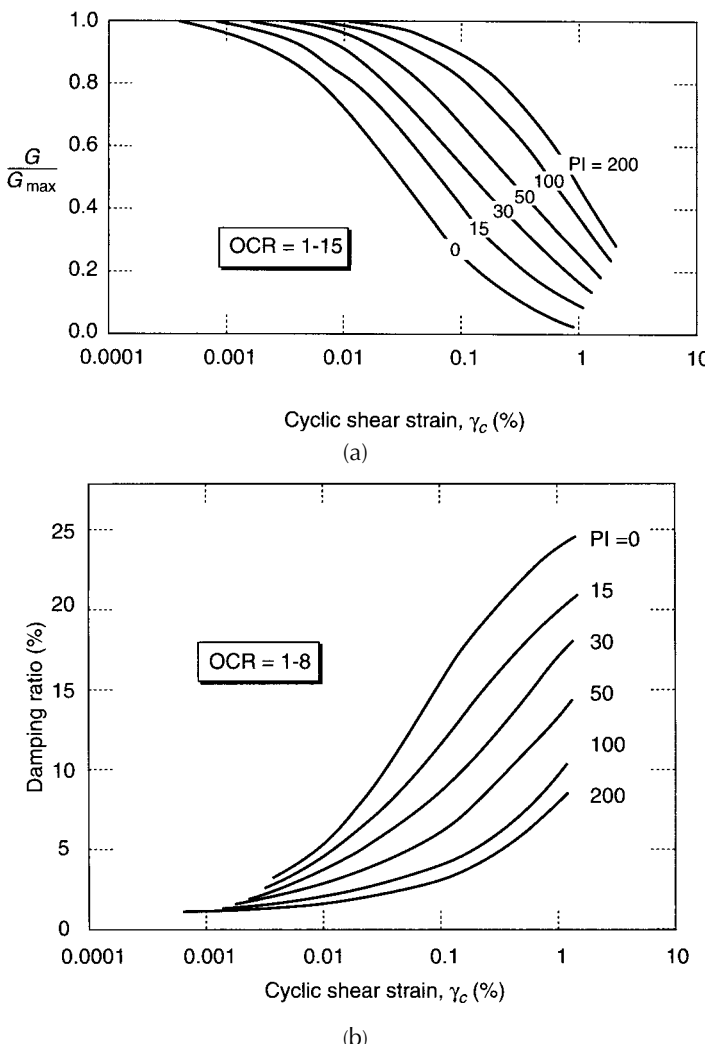


FIGURE 4.5 Vucetic–Dobry model: (a) modulus reduction curves and (b) damping curves. (From Vucetic, M. and Dobry, R. J. *Geotech. Engrg.*, ASCE, 117, 89–107, 1991. With permission.)

Unloading–reloading behavior is generally handled by sets of rules such as those of Masing (1926) or Cundall-Pyke (Pyke, 1979). The nature of these rules controls the shapes of the hysteresis loops and, therefore, the damping behavior of the soil. Hence, damping is taken to be a natural consequence of the nonlinear inelastic behavior of the soil.

For more advanced analytical models, e.g., those with plasticity-based constitutive models, specialized laboratory testing may be required. Most plasticity-based constitutive models have parameters that describe the shape of the yield and plastic potential surfaces, and of the variation of the plastic modulus. The specific tests required to calibrate those models vary from one model to another, but generally include consolidation, triaxial compression and triaxial extension tests; other types of tests may also be required.

4.3.3 Dynamic Shear Strength

The shear strength of dynamically loaded soil is a complex and incompletely understood subject. The strength can be influenced by pore-pressure generation, by rate effects and cyclic degradation. Selection of an appropriate strength for design and analysis should be performed by an experienced geotechnical

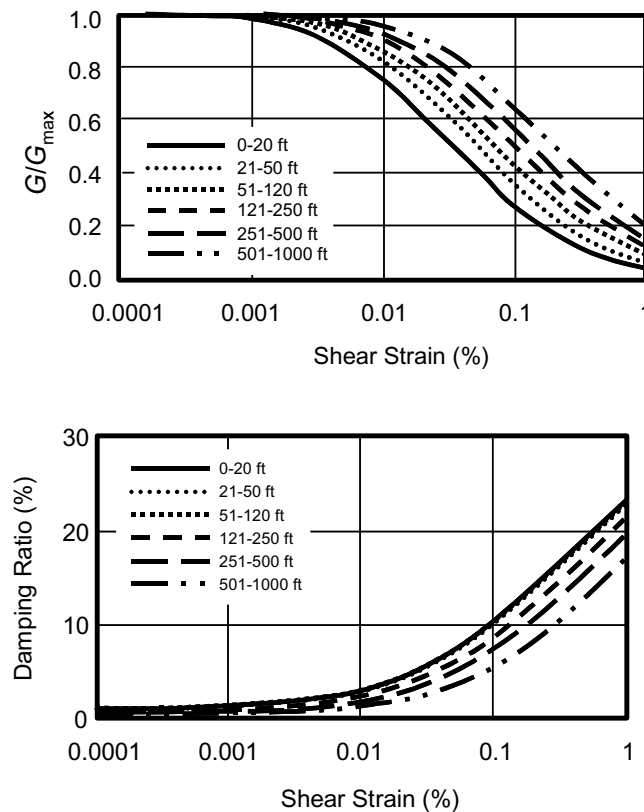


FIGURE 4.6 EPRI model: (a) modulus reduction curves and (b) damping curves.

engineer. Due to space constraints here we do not provide a full discussion of all of the factors that an engineer would need to consider in determining that strength. Guidelines for dynamic strength parameter selection that have recently been adopted for use in California are described by Blake et al. (2002). Some general principles and observations are given in the following paragraphs.

Dry cohesionless soils are perhaps the most straightforward since they do not produce excess porewater pressure or exhibit rate effects. Drained conditions can be assumed and seismic stability analyses performed using effective stress strength parameters. When saturated, cohesionless soils exhibit complex behavior, which is discussed in more detail in Section 4.6.1. Seismic loading of saturated soil will generally occur under undrained conditions (unless the soil is very permeable and very thin), but pore pressures can dissipate rapidly following (and, in some cases, during) earthquake shaking. Both drained and undrained conditions may need to be checked, and the residual strength (Section 4.6.1.5) must be estimated for soils expected to liquefy.

Fine-grained plastic soils may develop excess porewater pressure and also exhibit rate effects and cyclic degradation. Rate effects tend to increase the strength (by 10 to 40% per log cycle of strain rate, with higher values corresponding to more plastic soils) and degradation effects tend to decrease strength. Cyclic testing of many plastic clays has shown that the net effect of rate effects (at about a 1 Hz loading frequency) and cyclic degradation is a postcyclic undrained shear strength that varies from about 80 to 100% of the static (monotonic) undrained shear strength (Andersen et al., 1988; Azzouz et al., 1989; Zergoun and Vaid, 1994; Idriss and Boulanger, 2004); the 0.8–1.0 range being associated with the equivalent number of stress cycles applied by the earthquake (upper end of range for low-magnitude earthquakes, lower end for large-magnitude earthquakes). Care should always be taken to evaluate the possibility of historical shearing (due to previous landslides, bedding plane slip during folding, loading

and unloading, etc.). The available shearing resistance of such soils should be reduced to residual values, which are expressed using effective stress parameters, because soils at residual conditions are not expected to generate pore pressures during earthquakes. Moreover, rate and cyclic degradation effects for such materials can be neglected.

Negative pore pressures are present in unsaturated soils. Limited experimental and centrifuge studies have shown that at saturation levels of 88% and 44%, these negative pore pressures may rise (i.e., become less negative) during rapid cyclic loading (Sachin and Muraleetharan, 1998; Muraleetharan and Wei, 2000). The available information is far from exhaustive, but these studies preliminarily suggest that at the pre-shaking saturation levels considered, the pore pressures can rise to nearly zero, but are unlikely to become positive. Positive pore pressures are more likely to develop in materials with higher degrees of saturation (e.g., >90%), because the relative scarcity of air bubbles within the soil matrix. Based on these considerations, Blake et al. (2002) recommended that drained effective stress strength parameters be used with an assumption of zero pore pressure for seismic stability analyses involving materials with moderate saturation levels (< 90%).

4.4 Site Response

4.4.1 Types of Site Effects

The ground motion attenuation relationships presented in Chapter 5 provide estimates of ground motion intensity measures that apply for a given site condition, which is typically described using broad categories such as rock and soil. Experience from previous earthquakes has repeatedly shown that the intensity of ground shaking, and the intensity of the damage it produces, are strongly influenced by local site conditions. Actual conditions at strong motion recording sites are highly variable with respect to local geotechnical conditions, possible basin effects and surface topography, and hence estimates from attenuation relationships necessarily represent averaged values across the range of possible site conditions. The intent of this section is to describe various means by which information on site conditions can be used to improve the accuracy of ground motion predictions, that is, improve the estimates from attenuation models. This improvement in ground motion prediction generally involves (1) removing potential bias in median ground motion estimates and (2) reducing the uncertainty in ground motion estimates, as measured by the standard error term, σ .

As applied here, the term *site effects* represents local ground response effects, basin effects and the influence of surface topography on ground motion. Local ground response refers to the influence of relatively shallow geologic materials on (nearly) vertically propagating body waves. These effects are ideally modeled using the full soil profile, but for sites with very deep sediments the modeling domain generally does not extend beyond depths of about 100 m. Several examples of recordings where such effects were significant are presented subsequently in Section 4.4.3.

The term *basin effects* refers to the influence of two- or three-dimensional sedimentary basin structures on ground motions, including critical body wave reflections and surface wave generation at basin edges. Ground motions in the Santa Monica area during the 1994 Northridge earthquake provided an excellent example of the basin edge effect (see Figure 4.7). Motions north of the basin edge, which is defined by the westward-striking Santa Monica fault, have significantly smaller amplitudes and durations than those within the basin, as shown in the figure. The large-amplitude and large-duration velocity waveforms south of the fault have been shown by Graves et al. (1998) to be associated with constructive interference of direct waves with basin-edge generated surface waves.

Site effects due to surface topography (i.e., topographic effects) can amplify the ground shaking that would otherwise be expected on level ground along ridges or near the tops of slopes. Surface topography can similarly de-amplify ground shaking in canyons or near the base of slopes. Details about topographic amplification on ridgelines are presented by Geli et al. (1988) and Bard (1995); information on slope crest topographic amplification is presented by Ashford et al. (1997) and Ashford and Sitar (1997).

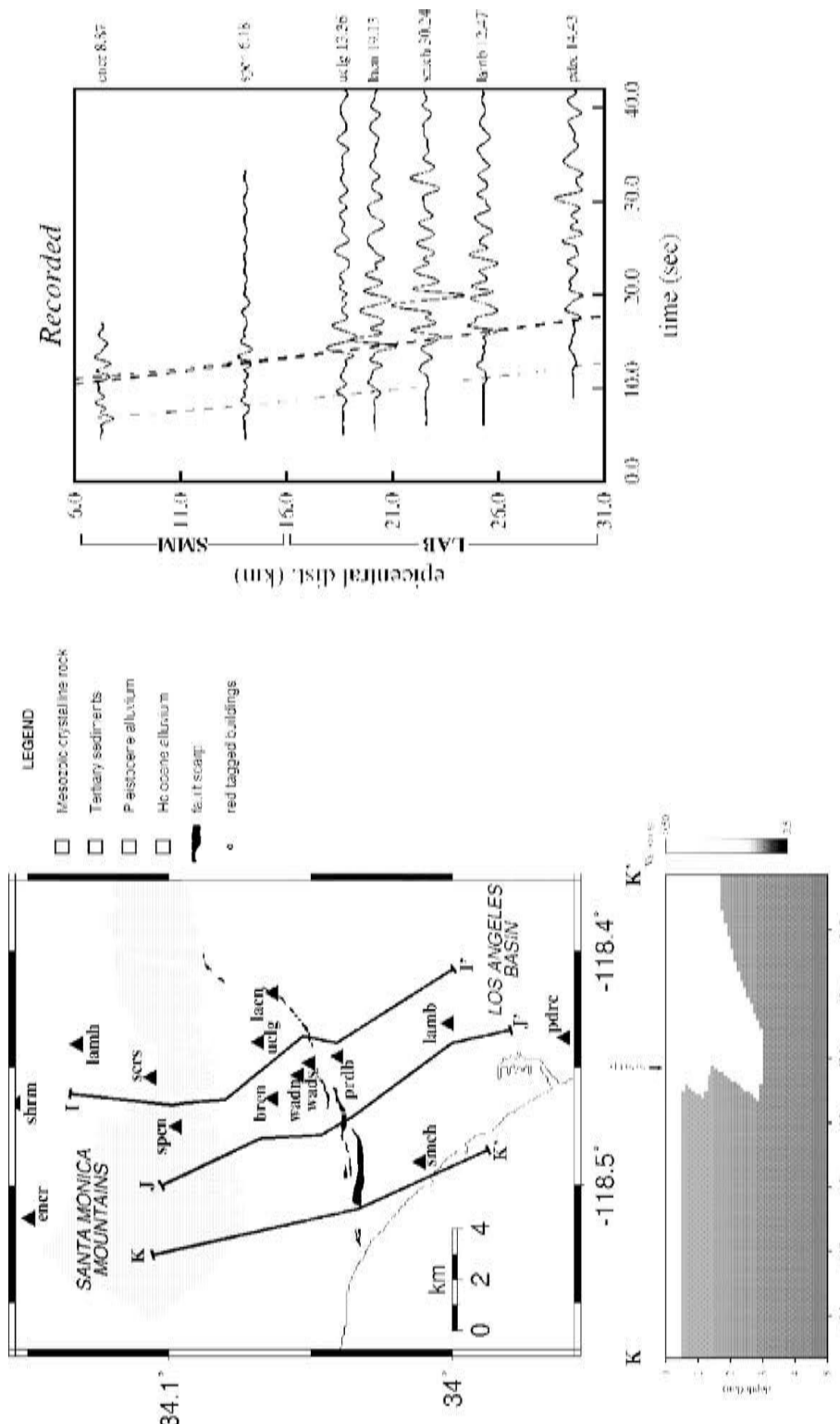


FIGURE 4.7 Basin effects in Santa Monica from the 1994 Northridge earthquake. See text for explanation. (From Graves, R.W. et al. *Bull. Seism. Soc. Am.*, 88, 1224-1242, 1998. With permission.)

TABLE 4.1 Site Categories in NEHRP Provisions for the Design of New Structures

NEHRP Category	Description	Mean Shear Wave Velocity to 30 m
A	Hard Rock	>1500 m/s
B	Firm to hard rock	760–1500 m/s
C	Dense soil, soft rock	360–760 m/s
D	Stiff soil	180–760 m/s
E	Soft clays	<180 m/s
F	Special study soils, e.g., liquefiable soils, sensitive clays, organic soils, soft clays >36 m thick	

Source: Dobry, R., et al., *Earthquake Spectra*, 16, 41–67, 2000. With permission.)

After reviewing various site classification schemes, the following sections describe two basic procedures by which site effects can be accounted for in engineering design: the use of site amplification factors and the use of site-specific ground response analyses. Basin response analysis procedures remain in the calibration stage of development, and are not widely used in practice. Accordingly, these procedures are not discussed. Models for topographic effects are also not discussed. Additional information on both effects can be found in the aforementioned references and Stewart et al. (2001).

4.4.2 Site Classification

Recorded ground motions can show distinct amplitudes at sites with different geologic characteristics. Site categorization schemes that have been used to represent site condition include:

- Averaged shear wave velocity in the upper 30 m, V_{s-30} , (e.g., Borcherdt, 1994; Dobry et al., 2000)
- Surface geology (e.g., Tinsley and Fumal, 1985; Park and Elrick, 1998; Stewart et al., 2003c)
- Geotechnical data, including sediment stiffness, depth and material type (Seed and Idriss, 1982; Rodriguez-Marek et al., 2001)

The V_{s-30} scheme is the most widely used site classification procedure in modern practice. Accordingly, this scheme is discussed in detail below. Information on other schemes is provided in the references.

The V_{s-30} -based schemes are rooted in wave propagation theory, which suggests that ground motion amplitude should depend on the density and shear wave velocity of near-surface media (e.g., Bullen, 1965; Aki and Richards, 1980). Density has relatively little variation with depth, and so shear wave velocity is the logical choice for representing site conditions. Initial efforts at V_s -based representations of site condition utilized average velocity over the depth range corresponding to one-quarter wavelength of 1-Hz ground motions (Joyner et al., 1981). However, the depths associated with this method are often deeper than can economically be reached with boreholes. Accordingly, the V_{s-30} parameter was proposed to overcome this difficulty and has found widespread use in practice. Based on empirical studies by Borcherdt and Glassmoyer (1994), Borcherdt (1994) recommended V_{s-30} as a means of classifying sites for building codes, and similar site categories were selected for the NEHRP seismic design provisions for new buildings (Dobry et al., 2000). The site classification scheme in the NEHRP provisions is presented in Table 4.1.

4.4.3 Site Amplification Factors

Site amplification factors represent for a given ground motion intensity measure (such as spectral acceleration), the ratio of that parameter for a given site category to the value of the parameter for a reference category (usually rock). Accordingly, amplification factors are a convenient tool by which to adjust the moments (median and standard deviation) of attenuation relationships to account for the effects of site condition. However, site condition remains relatively crudely represented with amplification factors, quantified only by site conditions that affect the categorization per the classification scheme.

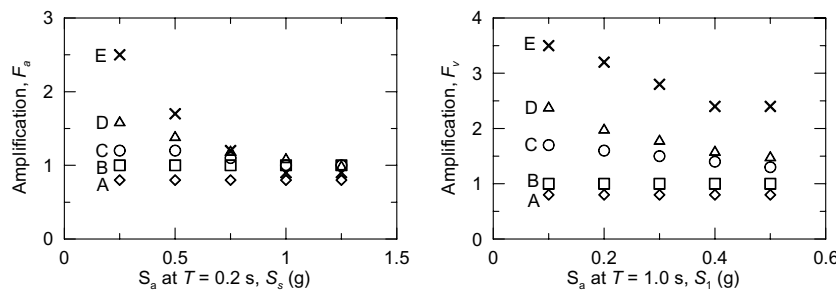


FIGURE 4.8 Site factors F_a and F_v given in NEHRP provisions (BSSC, 2001).

Site amplification factors are generally inferred from strong motion recordings using techniques described by Field and Jacob (1995), or are derived from analyses using engineering models of wave propagation (Dobry et al., 1994; Seed et al., 1994; Silva et al., 1999, 2000). The site amplification factors that appear in modern seismic design codes, such as the 1997 UBC (ICBO, 1997), 2000 NEHRP (BSSC, 2001) and 2000 IBC (ICC, 2000), were originally developed for publication in the 1994 NEHRP Recommended Provisions for Seismic Regulations for New Buildings and Other Structures (BSSC, 1995). The specific factors given in the provisions are F_a , which is defined over a low-period range ($T = 0.1$ to 0.5 sec), and F_v , which is defined over a mid-period range ($T = 0.4$ to 2.0 sec). These NEHRP site factors are shown in Figure 4.8, and were derived using both observational and analysis-based approaches (Dobry et al., 2000).

The observational studies were performed by Borcherdt and Glassmoyer (1994), Borcherdt (1994) and Joyner et al. (1994) using strong motion data recorded in the San Francisco Bay Area during the 1989 Loma Prieta earthquake. The resulting amplification factors (F_a and F_v) apply for relatively weak shaking (peak horizontal acceleration, PHA ≈ 0.1 g). The analytical studies consisted of 1-D equivalent linear and nonlinear ground response analyses by Dobry et al. (1994) and Seed et al. (1994), and were used to extend the F_a and F_v values to rock PHA ≈ 0.4 g or 0.5g. For both the empirical and analytical studies, site factors were defined relative to a competent rock site condition, which in the San Francisco Bay Area corresponds specifically to Franciscan formation bedrock of Cretaceous and Jurassic age.

Since the development of the NEHRP amplification factors, a number of verification studies have been performed to evaluate their validity based on non-Loma Prieta data sets. For example, Borcherdt (2002), Harmsen (1997) and Field (2000) evaluated amplification factors from strong motion data recorded in southern California using approaches in which the amplification is defined relative to firm rock site conditions. Steidl (2000) and Stewart et al. (2003c) evaluated amplification factors from relatively large data sets using an approach in which amplification is evaluated relative to soft rock site conditions that are more typical of the average site condition for rock in attenuation relations.

One important outcome of these studies was that the variation of amplification levels with reference motion amplitude, which had been assessed through theoretical analysis for the NEHRP provisions, was found to be consistent with observation both at small periods (F_a) and at longer periods (F_v) (as shown in Figure 4.9). A second important outcome was the significant variability of amplification factors derived from the various studies. In Figure 4.10, weak motion amplification factors from the above studies are compared to the NEHRP factors for the lowest level of reference motion amplitude (shown at the logarithmic mid-point between V_{s-30} category boundaries). Field, Harmsen and Stewart et al. found variations in amplification with V_{s-30} (i.e., slopes of the curves in Figure 4.9) that are generally similar to NEHRP, whereas the slopes found by Steidl are flatter. The vertical offset between the relations shown in Figure 4.9 is related to the slope of the curves and the V_{s-30} value at which the amplification is unity (which, in turn, is the effective reference site velocity for that site amplification model). Since the slopes of the NEHRP, Field, Harmsen and Stewart et al. curves are generally similar, the difference between these is largely due to different reference site velocities, which increases in the order of Stewart et al. ($V_{s-30} \approx 500$ to 600 m/sec),

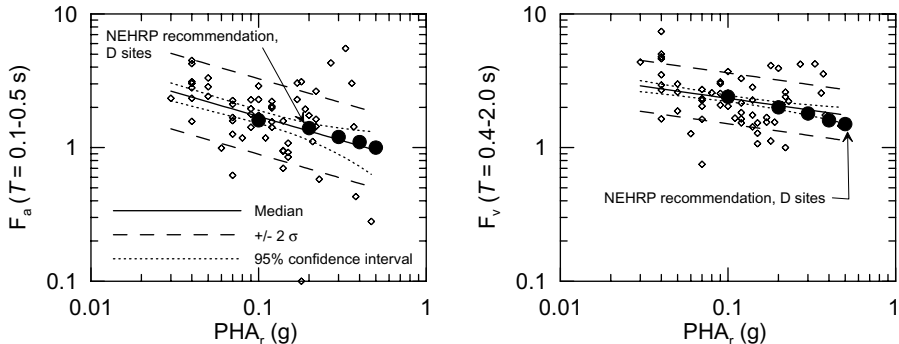


FIGURE 4.9 Averaged spectral amplification versus reference motion peak acceleration (PHA_r) for Northridge earthquake recordings at D sites (Borcherdt, 2002), as compared to NEHRP site factors (BSSC, 2001). Note: Reference motions for NEHRP factors modified from published values according to $\text{PHA}_r = S_s/2.5$ (for F_a) and $\text{PHA}_r = S_1$ (for F_v).

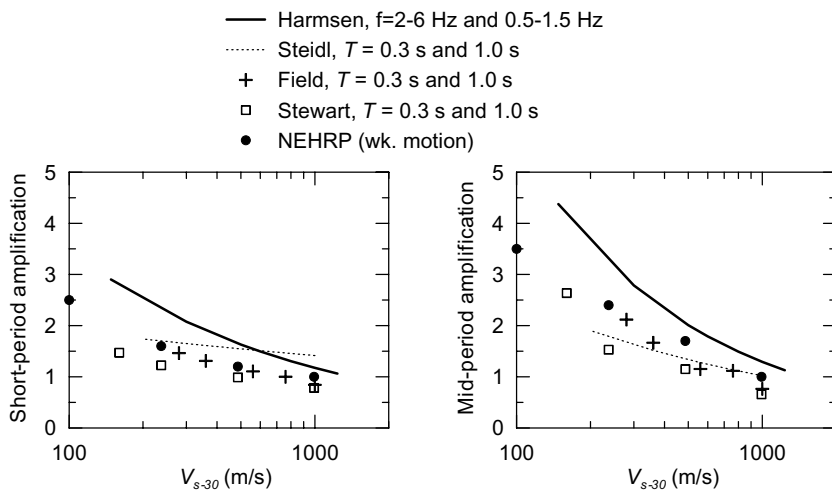


FIGURE 4.10 Averaged median spectral amplification versus V_{s-30} from various investigators (Harmsen, 1997; Field, 2000; Steidl, 2000; Stewart et al., 2003c) compared with NEHRP factors for low-amplitude shaking.

Field ($V_{s-30} = 760$ m/sec), NEHRP (Category B, $V_{s-30} \approx 1000$ m/sec) and Harmsen ($V_{s-30} \approx 1140$ to 1360 m/sec). A comparison to the Steidl results is not possible because the amplification factors do not reach unity over the range of velocities considered.

Since amplification factors are very sensitive to the reference site condition (e.g., as shown by the variability of the results in Figure 4.10), the application of amplification factor models must appropriately consider the site condition corresponding to the reference motion. For most applications, reference motions are evaluated using attenuation relations. When such relations are developed based on rock site recordings in tectonically active regions (e.g., Abrahamson and Silva, 1997; Campbell and Bozorgnia, 2003; Sadigh et al., 1997), available borehole compilations suggest that the reference site condition corresponds to relatively soft rock with $V_{s-30} = 520$ –620 m/sec (Silva et al., 1997; Boore et al., 1997). Of the above amplification factors, only those of Steidl (2000) and Stewart et al. (2003c) are appropriate for use with this reference site condition. The Stewart et al. (2003c) factors are shown in Figure 4.11 for NEHRP categories and are compared to the NEHRP amplification values. The figure shows that the

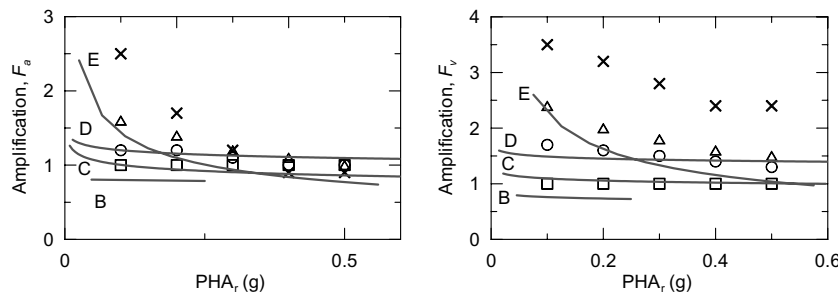


FIGURE 4.11 Spectral amplification factors as a function of NEHRP Categories B-E, as evaluated by Stewart et al. (2003c) (lines). NEHRP factors from Figure 4.8 are shown for comparison (symbols).

NEHRP factors are biased (too large) for the soft rock reference site condition. This bias underscores the need to use compatible reference site conditions when amplification factors are used to modify ground motion predictions from attenuation relationships.

4.4.4 Site Response Analysis

As described in Section 4.4.1, site response processes can include 1-D ground response effects, basin effects and topographic effects. The principal focus of this section is on ground response effects, with discussion on methods of ground response analysis, verification against data of the results of 1-D analyses and guidelines for the application of ground response analyses. Multidimensional site response analyses, which can account for topographic effects and the effects of locally irregular stratigraphy, are also briefly discussed. The multidimensional models have practical limitations on the size of the application domain, which preclude their use for large-scale basin response modeling. Such modeling is typically performed within the context of seismological source-path-site simulations, and is beyond the scope of this chapter. The dynamic soil properties to be used in conjunction with ground response analysis procedures discussed herein were presented in Section 4.3.

4.4.4.1 Equivalent Linear Ground Response Models

Most ground response analysis models solve equations of motion for one-dimensional wave propagation. For 1-D models, the principal characteristic distinguishing various analysis routines is the soil material model, which can be equivalent linear or nonlinear. Equivalent linear modeling is described here, while nonlinear modeling is described in the following section. The relative merits and reliability of equivalent linear and nonlinear methods of analysis are discussed subsequently in Section 4.4.4.3.

Nonlinear behavior of soil can be approximated by an equivalent linear characterization of dynamic properties (Seed and Idriss, 1970). The most widely used computer program for 1-D ground response analysis utilizing this model is currently SHAKE91 (Idriss and Sun, 1991), which is a modified version of the program SHAKE (Schnabel et al., 1972). The program uses an equivalent linear, total stress analysis procedure to compute the response of a 1-D, horizontally layered viscoelastic system subjected to vertically propagating shear waves. The program uses the exact continuum solution to the wave equation adapted for use with transient motions through the Fast Fourier Transform algorithm. A similar solution algorithm is available for 2-D site geometries, which is programmed in FLUSH (Lysmer et al., 1975), while a time-domain 2-D solution algorithm is available in the program QUAD4 (Hudson et al., 1994; Idriss et al., 1973).

The equivalent linear method models the nonlinear variation of soil shear moduli and damping as a function of shear strain. The hysteretic stress-strain behavior of soils under symmetrical cyclic loading is represented by an equivalent modulus, G , corresponding to the secant modulus through the endpoints of the hysteresis loop and equivalent linear damping ratio, β , which is proportional to the energy loss from a single cycle of shear deformation. For a given soil layer, G and β are assumed to be constant with time during the earthquake shaking. An iterative procedure, based on linear dynamic analysis, is per-

formed to find the shear moduli and damping ratios corresponding to the computed shear strains, as follows:

1. Initial estimates of the G and β are made for each layer.
2. The estimated G and β values are used to compute the ground response, including time histories of shear strain for each layer.
3. An effective shear strain is determined for each layer as a fraction of the maximum strain. This fraction is generally calculated as $n = 0.1 \times (m - 1)$, where m = earthquake magnitude (Idriss and Sun, 1992).
4. From this effective shear strain, new equivalent linear values of G and β are evaluated for each layer based on the modulus reduction and damping curves presented previously in Section 4.3.
5. Steps 2 to 4 are repeated until the G and β values used in the calculations are consistent with the calculated effective shear strains.

An alternative solution to the ground response problem with equivalent-linear material characterization has been developed by Silva and co-workers (e.g., Silva and Lee, 1987; Schneider et al., 1993). In this approach, control motions are represented with power spectral density functions instead of individual time histories. The rock power spectrum is propagated through a one-dimensional soil profile using the plane wave propagators of Silva (1976). Random vibration theory (RVT) is used to compute probabilistic estimates of peak time-domain values of shear strain or acceleration from the power spectrum. This procedure, coded into the computer program RASCAL (Silva and Lee, 1987), produces what can be considered as the mean of an extensive set of analyses of different input motions with a single analysis.

4.4.4.2 Nonlinear Ground Response Models

Nonlinear models solve the one-dimensional wave equation by direct numerical integration in the time domain. A variety of material models are used, which range from relatively simple cyclic stress-strain relationships (e.g., Ramberg and Osgood, 1943; Finn et al., 1977; Pyke, 1979; Vucetic, 1990) to advanced constitutive models incorporating yield surfaces, hardening laws and flow rules (e.g., Wang, 1990). A model by Pestana and Nadim (2000) allows the use of a relatively simple hysteretic nonlinear analysis (e.g., Salvati et al., 2001) or a more sophisticated analysis utilizing an advanced constitutive relationship (e.g., Biscontin et al., 2001). Nonlinear methods can be formulated in terms of effective stresses to allow modeling of the generation, redistribution and eventual dissipation of excess pore pressure during and after earthquake shaking, whereas equivalent linear methods can only perform total stress analysis.

Cyclic nonlinear models generally consist of a backbone curve and rules that describe unload-reload behavior, pore-pressure generation and cyclic modulus degradation. Backbone curves can be constructed from modulus reduction curves coupled with the small-strain shear modulus, G_{\max} (i.e., the shear modulus at shear strains of $10^{-4}\%$ or smaller). Unload-reload rules can similarly be formulated to reproduce hysteretic damping values expected from standard curves of damping ratio versus shear strain (see Section 4.3.1). However, these formulations tend to predict damping ratios approaching zero at small strains, which is unrealistic. This is resolved by the introduction of a viscous damping term that applies across all strain levels.

The features that differentiate nonlinear ground response analysis programs are (1) the numerical integration schemes used in the solution of the wave equation and (2) the constitutive models for cyclic stress-strain behavior, cyclic modulus degradation and pore-pressure generation. Probably the most widely used computer program for nonlinear analysis is DESRA-2 (Lee and Finn, 1978) and its successors. The program evaluates the dynamic response of a multiple-degree-of-freedom lumped mass system. Soil model parameters were originally developed only for sands. A number of programs have been created as offspring of DESRA-2, including recent versions D-MOD_2 (Matasovic, personal communication) and DESRA-MUSC (Qiu, 1997). As an example, program D-MOD_2 allows the modeling of clays and sands, uses updated stress-strain and cyclic degradation-pore water pressure generation relationships and allows simulation of seismically induced slip that may occur along weak interfaces.

TABLE 4.2 Verification Studies of 1-D Ground Response Analysis Programs

Earthquake	Soil Condition - Recording Locations	Reference	Codes Investigated
(a) Nearby Rock-Soil Pairs			
1985 Michoacan-Guerrero	Soft clay - Mexico City (2)	Seed et al. [1987]	SHAKE
1989 Loma Prieta	Bay mud - San Francisco Bay Area (11 sites)	Idriss [1990]; Dickenson [1994]	SHAKE; SHAKE, MARDESRA
1989 Loma Prieta	Deep stiff clay - Oakland, Emeryville; Gilroy (4 sites)	Chang [1996]; Darragh and Idriss [1997]	SHAKE, DMOD; SHAKE
1994 Northridge	Deep alluvium - Sylmar, Hollywood, Santa Monica (3 sites)	Chang et al. [1996]	SHAKE, DMOD
(b) Vertical Arrays			
unnamed $m = 6.2, 7.0$ events	Soft silt - Lotung	Chang [1990] and Li et al. [1998]; Beresnev et al. [1995]; Borja et al. [1999]; Elgamal et al. [1995]	SUMDES; DESRA2; SPECTRA; unnamed code
1995 Kobe	Liquefiable sand - Kobe Port Island	Wang et al. [2001]; Elgamal et al. [1996]	SUMDES; unnamed code
1987 Superstition Hills	Liquefiable sand - Wildlife site, CA	Matsovic and Vucetic [1996]	DMOD

Most nonlinear analysis routines, such as the DESRA series, analyze only one horizontal component of ground response. The effects of simultaneous shaking in three directions can be considered with advanced constitutive models, which are implemented into programs such as DYNA1D (Prevost, 1989), SUMDES (Li et al., 1992), SPECTRA (Borja and Wu, 1994) and AMPLE (Pestana and Nadim, 2000). These models incorporate a yield surface that describes the limiting stress conditions for which elastic behavior is observed, hardening laws that describe changes in the size and shape of the yield surface as plastic deformation occurs and flow rules that relate increments of plastic strain to increments of stress. Some of these nonlinear codes (e.g., AMPLE, Pestana and Nadim, 2000) allow specification of an initial (static) shear stress profile for estimation of permanent displacement in gently sloping ground. Such models require a relatively large number of parameters, and the associated parametric uncertainty in the analysis results is generally poorly defined.

Nonlinear multi-dimensional ground response analyses are sometimes performed for critical structures such as earth dams. These approaches are briefly discussed in Section 4.6.2.3.

4.4.4.3 Verification Studies for 1-D Analysis Methods and Differences between Results of Equivalent Linear and Nonlinear Analyses

Many studies have been performed using SHAKE and various nonlinear codes to verify the effectiveness of 1-D wave propagation analysis routines. These routines can be most effectively verified when the input motion is reasonably well known, which is the case when a rock recording is available near a soil recording, or from vertical array data. We focus here on these types of verification studies. However, it is noted that additional verification studies of the equivalent linear technique have been performed using input motions calculated from a seismological simulation technique (EPRI, 1993; Silva et al., 1997).

A number of verification studies have utilized data from pairs of nearby rock and soil recordings. The rock motion is taken as input to ground response analyses, and the computed and recorded soil motions are compared. Several examples of studies of this type are summarized in Table 4.2(a). At the soft soil sites considered in these studies, ground response effects as modeled by SHAKE (Schnabel et al., 1972) and MARDESRA (Mok, 1990, personal communication) were able to predict variations between soil and rock spectra across a broad period range reasonably well (e.g., Dickenson, 1994). Results were mixed for deep stiff soil sites, with relatively good predictions at northern California deep clay sites for $T \leq 1$ sec

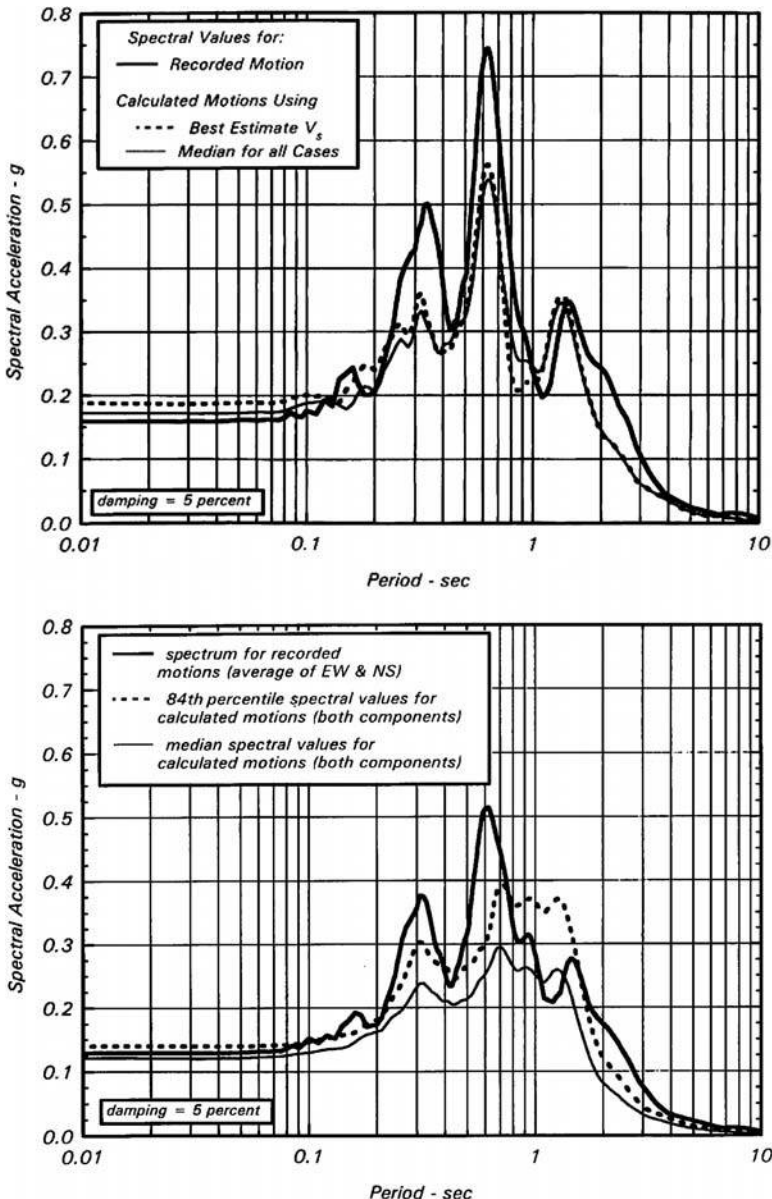


FIGURE 4.12 Comparison of acceleration response spectrum of recorded motion at Treasure Island strong motion site (1989 Loma Prieta earthquake) with calculated spectra from ground response analyses. Calculations in upper frame utilized nearby rock recording (Yerba Buena Island) as control motion; lower frame presents statistical variation in calculated spectra for suite of control motions from rock sites in region surrounding Treasure Island. (From Idriss, I. M., Report to National Institute of Standards and Technology, Gaithersburg, Maryland, 1993. With permission.)

and relatively poor predictions for many Los Angeles area alluvial sites (Chang, 1996). The difference in model accuracy at Bay Area and Los Angeles area sites may be associated with basin effects (particularly at long periods), as the basin geometry at the Bay Area sites is relatively wide and shallow as compared with the Los Angeles area sedimentary basins.

One noteworthy outcome of these studies is that the prediction accuracy for soil spectra is strongly dependent on rock (control) motion characteristics. For example, as shown in Figure 4.12, Idriss (1993) found predicted spectra at the Treasure Island (soil) recording site to provide a good match to the recorded

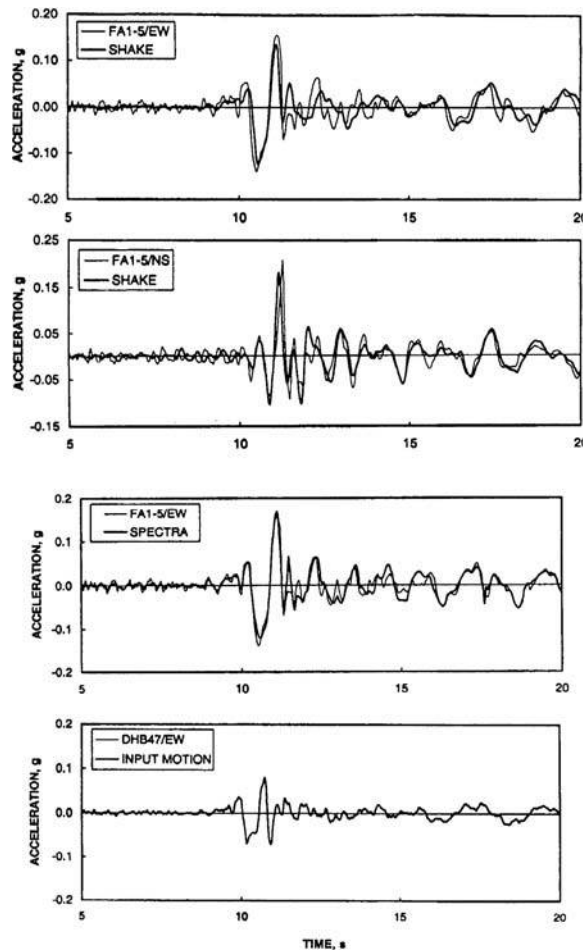


FIGURE 4.13 Comparison of recorded ground surface accelerations and predictions by SHAKE (top two frames) and SPECTRA (third frame from top). Bottom frame shows recording at base of array (47-m depth). (From Borja, R. I. et al., *J. Geotech. Geoenvirons. Eng.*, ASCE, 125, 187–197, 1999. With permission.)

spectrum when the control motion is taken from the nearby Yerba Buena Island (rock) seismograph (top frame of Figure 4.12), but a highly variable match when control motions are taken from other rock stations in the San Francisco–Oakland–Berkeley area (bottom frame). Since rock motion characteristics cannot be known *a priori*, this suggests that significant uncertainty is introduced to ground response analysis results from uncertainty and variability in input motion characteristics.

A more direct verification of one-dimensional ground response analysis procedures is enabled by recordings from vertical arrays. Many such arrays have been installed worldwide, and a few that have recorded strong ground motion (i.e., $\text{PHA} > 0.1\text{g}$) are listed in Table 4.2(b). Data from one of these arrays, the Lotung large-scale seismic test site in Taiwan, have been used to validate several one-dimensional ground response analysis codes including SUMDES (Chang et al., 1990; Li et al., 1998; Wang et al., 2001), DESRA2 (Beresnev et al., 1995), SPECTRA (Borja et al., 1999) and an unnamed research code (Elgamal et al., 1995). Example results from one of these studies are shown in Figure 4.13, which applies for the SPECTRA code. Both the fully nonlinear SPECTRA analysis and the equivalent linear SHAKE analysis provide excellent matches in the time domain to the recorded motions. Other studies have shown improved matches in the time domain for nonlinear codes (e.g., Chang et al., 1990; Wang et al., 2001).

An important outcome of many of the verification studies cited above is that prediction residuals from nonlinear methods were not significantly smaller than those from equivalent linear methods (a notable exception is the Kobe Port Island site, which liquefied). However, the amplitude of shaking at most of these sites was relatively small in comparison to typical design-basis ground motions in seismically active regions such as California.

Studies by EPRI (1993) and Silva et al. (2000) have compared the results of equivalent linear and nonlinear analyses in a nonverification context (i.e., there are no recorded motions against which to compare the results). Silva et al. (2000) used simulated input motions with a wide range of amplitudes in equivalent linear (RASCAL, Silva and Lee, 1987) and nonlinear (DESRA-MUSC, Qiu, 1997) ground response analyses for the calculation of amplification factors. In general, there was good agreement between the two approaches over most of the frequency range 0.1 to 100 Hz. However, for large input motions and soft soil profiles, the nonlinear damping exceeded that for the equivalent linear damping, and the nonlinear amplification factors were below the equivalent linear factors. Which of these sets of amplification factors is more nearly correct (based on comparisons to data) is unknown, and further comparative study of nonlinear and equivalent linear analyses is therefore needed.

4.4.4.4 Application of 1-D Analysis Methods

Ground response analyses require detailed site characterization and significant engineering time and effort. Hence, for their use to be justified in practice, such analyses should improve the accuracy of predicted ground motions or decrease the level of uncertainty in these estimates relative to what would be obtained from more simplified procedures, such as attenuation or attenuation with amplification factors.

Baturay and Stewart (2003) performed ground response analyses for a large number of sites with strong motion recordings to identify the geologic and geotechnical conditions where ground response analyses significantly and consistently improve predictions of ground motion intensity measures (such as spectral acceleration) relative to other models. They also identified the dispersion associated with ground response predictions, so as to enable the results of such analyses to be utilized within probabilistic seismic hazard analyses.

Spectral ordinates from ground response analyses were found to be unbiased at low period ($T \leq \sim 1$ sec), but underestimated at long periods ($T \geq 1$ sec) for deep basin sites. At soft clay sites (e.g., NEHRP Category E or Holocene lacustrine/marine sediments), ground response analyses reduce the dispersion in spectral accelerations at $T < 1$ sec relative to alternative models. This dispersion reduction was not observed for stiff soil sites (NEHRP C or D) or at longer periods. Moreover, ground response analyses provide a more accurate estimate of spectral shape for soft clay sites than for stiff sites, and only for soft clay is spectral shape estimated more accurately than with attenuation relationships. These results suggest that ground response analyses are beneficial for estimating ground motions at soft soil sites relative to attenuation with or without amplification factors. However, ground response analyses are not clearly beneficial for relatively stiff soil or soft rock sites such as NEHRP C-D or Quaternary alluvium/Tertiary.

For ground response analyses to be of use within the context of probabilistic seismic hazard analyses, it is necessary to know whether the median outcome of such analyses is biased and the standard deviation that should be used with the median. As noted previously, median predictions from ground response have not been found to be biased at short periods ($T < 1$ sec), but can underpredict long-period spectral ordinates for sites in basins.

The dispersion in ground response results (σ_g) can be separated into two components — uncertainty about the location of the computed median intensity measure (which can be readily quantified as part of the ground response analyses) and uncertainty due to various modeling errors such as the inaccurate physics of the site response model and unknown features of the input motions (which cannot be readily quantified as part of an individual, site-specific analysis). The second uncertainty parameter, denoted as the net dispersion ($\sigma_{g\text{-}net}$), was quantified by Baturay and Stewart (2003) from the difference between the total category variance from ground response results and the variance of the median ground response prediction using equivalent-linear analyses. As shown in Figure 4.14, for $T < 1$ sec, these $\sigma_{g\text{-}net}$ values

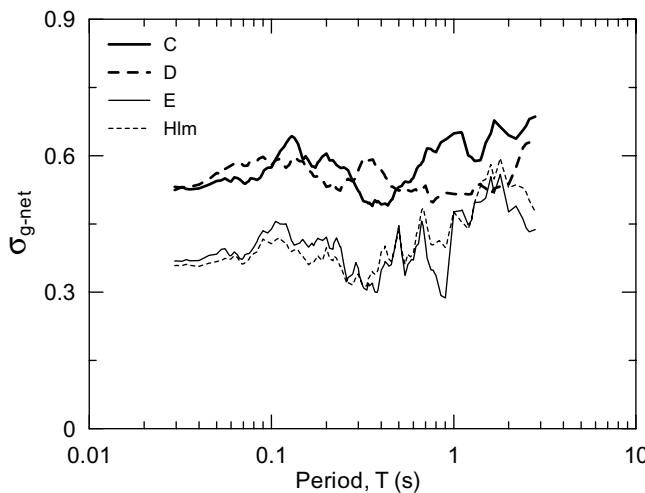


FIGURE 4.14 Variation with period of dispersion in ground response predictions associated with factors other than the ground response model estimation error for NEHRP Categories C-E and Holocene lacustrine/marine sediments (Hlm). (From Baturay, M.B. and Stewart, J.P. *Bull Seism. Soc. Am.*, 93, 2025–2042, 2003. With permission.)

range from about 0.38 for NEHRP Category E to 0.56 for NEHRP Categories C-D for $T < 1$ sec. The overall dispersion for use in PSHA can be calculated from these values and the standard error of the median ($se_{g\text{-out}}$) as follows:

$$(\sigma_g)^2 = (\sigma_{g\text{-net}})^2 + (se_{g\text{-out}})^2 \quad (4.1)$$

The standard error of the median ($se_{g\text{-out}}$) can be readily calculated as part of the ground response calculations, and is related to variable levels of soil nonlinearity induced by a large suite of input motions and variability in computed motions due to parametric uncertainty in soil properties. At longer periods ($T > 1$ sec), total dispersion can be estimated from attenuation or amplification factor models.

Based on the above, ground response analyses can be used to estimate the probability density function (PDF) of response spectral accelerations at a soil site for use in probabilistic seismic hazard analyses. Ground response analyses should be performed using a suite of input motions appropriately scaled to match the target spectrum in an average sense across the frequency range of interest (see Baturay and Stewart, 2003 for details). The number of time histories in the suite should be large enough to provide a stable estimate of both the median and $se_{g\text{-out}}$. The calculated median can be taken as the median of the PDF at small periods (due to the lack of bias in the analysis results), but care should be exercised at long periods for sites in basins, where attenuation relationships are less biased. The standard deviation (σ_g) can be evaluated as described above.

4.5 Soil–Foundation–Structure Interaction

4.5.1 Introduction

The response of a structure to earthquake shaking is affected by interactions between three linked systems: the structure, the foundation and the geologic media underlying and surrounding the foundation. A seismic soil–foundation–structure interaction (SFSI) analysis evaluates the collective response of these systems to a specified free-field ground motion. The term free-field refers to motions not affected by structural vibrations, and represents the condition for which motions are derived with the procedures described in Chapter 5 and Section 4.4.

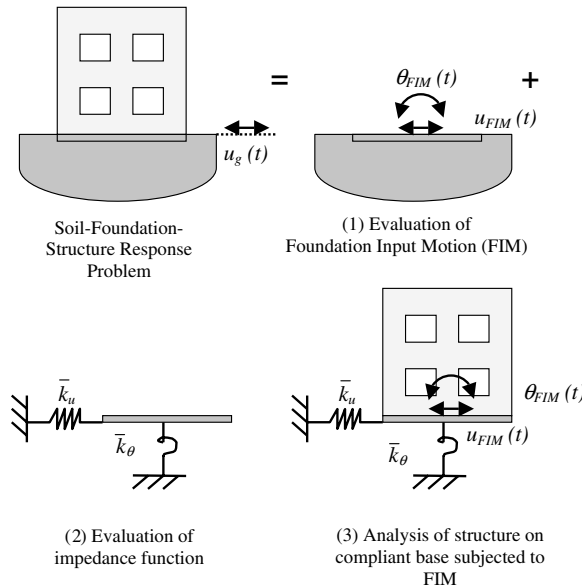


FIGURE 4.15 Substructure approach to analysis of the soil–structure interaction problem.

SFSI effects are absent for the theoretical condition of rigid foundation and soil conditions. Accordingly, SFSI effects reflect the differences between the actual response of the structure and the response for the theoretical, rigid base condition. Visualized within this context, three SFSI effects can be important in engineering design:

- *Foundation stiffness and damping.* Inertia developed in a vibrating structure gives rise to base shear, moment and torsional excitation, and these loads in turn cause displacements and rotations of the foundation relative to the free field. These relative displacements and rotations are only possible because of compliance in the soil–foundation system, which can significantly contribute to the overall structural flexibility in some cases. Moreover, the relative foundation-free field motions give rise to energy dissipation via radiation damping (i.e., damping associated with wave propagation into the ground away from the foundation, which acts as the wave source) and hysteretic soil damping, and this energy dissipation can significantly affect the overall system damping. Since these effects are rooted in the structural inertia, they are referred to as inertial interaction effects.
- *Variations between free-field and foundation-level ground motions.* The differences between foundation and free-field motions result from two processes. The first is known as kinematic interaction, and results from the presence of stiff foundation elements on or in soil, which cause foundation motions to deviate from free-field motion as a result of base-slab averaging and embedment effects. The second process is related to the structure and foundation inertia, and consists of the relative foundation-free field displacements and rotations described above.
- *Foundation deformations.* Flexural, axial and shear deformations of foundation elements occur as a result of loads applied by the superstructure and the supporting soil medium. Such deformations represent the seismic demand for which foundation components should be designed. These deformations can also significantly affect the overall system behavior, especially with respect to damping.

Methods of SFSI analysis that can be used to evaluate the above effects can be categorized as direct and substructure approaches. In a direct analysis, the soil and structure are included within the same model and analyzed in a single step. The soil is often discretized with solid finite elements and the structure with finite beam elements. Because assumptions of superposition are not required, true nonlinear analyses are possible (e.g., Borja et al., 1992 and Weidlinger Assoc., 1978), although the analyses are more typically

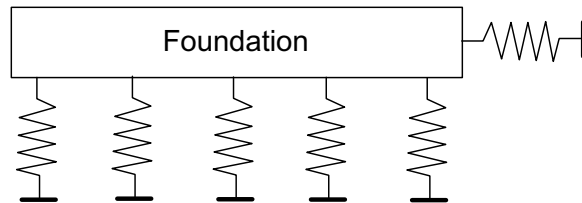


FIGURE 4.16 Uncoupled Winkler spring model.

performed using equivalent linear soil properties (Lysmer et al., 1975, 1981). Direct analyses can solve all three of the SFSI problems described above, although solution of the kinematic interaction problem is beyond the ability of most commercial computer codes as it requires careful specification of input motions that properly account for wave inclination and incoherence effects.

In a substructure analysis, the SFSI problem is broken down into three distinct parts that are combined to formulate the complete solution. The superposition inherent to this approach requires an assumption of linear soil and structure behavior. Referring to Figure 4.15, the three steps in the analysis are as follows:

- *Evaluation of a foundation input motion* (FIM), which is the motion that would occur on the base slab if the structure and foundation have no mass. The deviation of the FIM from the free-field motion is dependent on the stiffness and geometry of the foundation and soil. The variation between these motions is expressed by a transfer function that represents the ratio of foundation and free-field motions in the frequency domain. Since inertial effects are neglected, the transfer function represents the effects of kinematic interaction only.
- *Determination of the impedance function*. The impedance function describes the stiffness and damping characteristics of foundation–soil interaction. It should account for the soil stratigraphy and foundation stiffness and geometry, and is typically computed using equivalent linear soil properties appropriate for the *in situ* dynamic shear strains. Impedance functions can be evaluated for multiple independent foundation elements, or (more commonly) a single 6×6 matrix of impedance functions (for three translational and three rotational degrees of freedom) is used to represent the complete foundation. In the latter case, the foundation is assumed to be rigid, which precludes the use of SFSI analyses for foundation element design.
- *Dynamic analysis* of the structure supported on a compliant base represented by the impedance function and subjected to a base excitation consisting of the FIM.

The remainder of this section focuses on the evaluation of SFSI effects as represented by impedance and transfer functions, which implies the use of substructure methods of analysis. The body of literature on soil–structure interaction is truly enormous, and a complete review of the state-of-knowledge is beyond the scope of this chapter, although key resources are cited at appropriate locations in the text. Rather, the emphasis here is on practical tools for SFSI analysis that have been used in practice. Efforts to calibrate or verify analysis procedures against field performance data are noted where applicable. The final subsection below provides an overview of how SFSI effects are accounted for in several important guideline documents for professional practice. The issue of foundation deformations and seismic design of foundations is briefly reviewed in that subsection.

4.5.2 Inertial Interaction

4.5.2.1 Soil–Foundation–Structure System Behavior

It is common in SFSI analysis to represent the stiffness and damping characteristics of soil–foundation interaction through the use of springs and dashpots attached to the foundation elements. A model that is generally applicable to shallow foundations consists of a series of spring and dashpot elements distributed along the foundation as independent, complex-valued Winkler springs (Figure 4.16) in the vertical

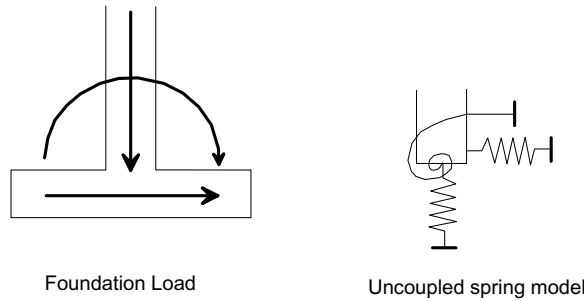


FIGURE 4.17 Uncoupled elasto-plastic spring model for rigid footings.

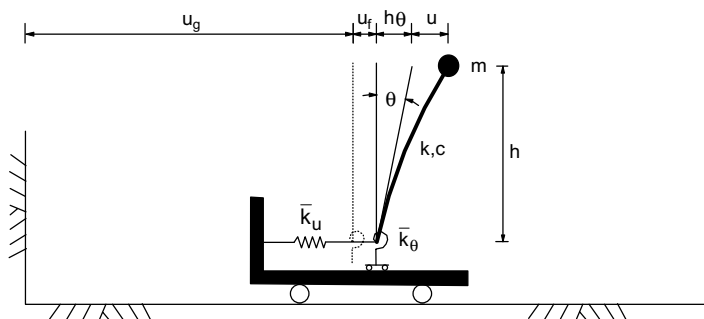


FIGURE 4.18 Simplified oscillator model for analysis of inertial interaction under lateral excitation.

direction, and a single horizontal spring. As described further in Section 4.5.2.2, the complex nature of the spring coefficients implies that the springs include both stiffness and damping components. The model in Figure 4.16 allows for foundation flexure in the vertical direction, but not axial foundation deformations.

A more simplified representation of the soil–foundation interaction problem results from an assumption of foundation rigidity. In this case, the foundation has only six degrees of freedom (three translational, two rocking, one torsional), and the interaction can be represented by complex-valued springs for each direction (Figure 4.17). In general, within the foundation stiffness and damping matrix, coupling terms between the degrees of freedom are nonzero, but these terms are often neglected in practice.

As depicted in Figure 4.15, system response analyses can be performed with the interaction springs attached to the foundation elements using the FIM as the input motion at the foundation level. Such analysis will inherently include the effects of soil–foundation interaction into the calculated response. The effects of inertial SFSI could be assessed by repeating the response analysis without the springs and dashpots (i.e., rigid base) and comparing the results of the two analyses. The SFSI effects are manifested by a lengthening of the building period from the fixed base case (T) to the flexible-base case (\tilde{T}), and by a change in the damping ratio (from ζ to $\tilde{\zeta}$). These effects have been evaluated as closed-form expressions for the simple case of a single degree-of-freedom structure supported by a rigid foundation and excited in one lateral direction (Figure 4.18). In this case, the impedance function is represented by terms for the rocking (\bar{k}_θ) and translation (\bar{k}_u) foundation vibration modes. A vertical foundation degree of freedom also exists (impedance term \bar{k}_v), but does not affect \tilde{T} or $\tilde{\zeta}$.

Veletsos and Meek (1974) found that the flexible-base period of the oscillator in Figure 4.18 subject to horizontal excitation can be evaluated as

$$\frac{\tilde{T}}{T} = \sqrt{1 + \frac{k}{k_u} + \frac{kh^2}{k_\theta}} \quad (4.5)$$

where $T = 2\pi\sqrt{k/m}$ is the fixed-base period of the oscillator in Figure 4.18, k_u and k_θ are the real parts of \bar{k}_u and \bar{k}_θ , respectively, and h is the height of the mass above the base of the oscillator. The quantity \tilde{T}/T in Equation 4.5 is referred to as a period lengthening ratio. The flexible-base damping ratio has contributions from the viscous damping in the structure as well as radiation and hysteretic damping in the foundation. Jennings and Bielak (1973), Bielak (1975, 1976) and Veletsos and Nair (1975) expressed the flexible-base damping $\tilde{\zeta}$ as

$$\tilde{\zeta} = \tilde{\zeta}_0 + \frac{\zeta}{(\tilde{T}/T)^3} \quad (4.6)$$

where $\tilde{\zeta}_0$ is referred to as the foundation damping factor and represents the damping contributions from foundation–soil interaction (with hysteretic and radiation components). A closed-form expression for $\tilde{\zeta}_0$ is presented in Veletsos and Nair (1975).

For the simple case of a circular foundation with radius r on a uniform halfspace with velocity V_s and hysteretic damping ratio β , the relationships between the fixed- and flexible-base oscillator properties depend on h/r and the dimensionless parameters defined below:

$$h/(V_s T) \quad (4.7)$$

$$\gamma_m = \frac{m}{\rho r^2 h \pi} \quad (4.8)$$

These parameters represent the ratio of the soil-to-structure stiffness and structure-to-soil mass, respectively. For conventional building structures, $h/(V_s T) < 0.5$ and $\gamma_m \approx 0.1$ to 0.2 (a representative value of $\gamma_m = 0.15$ is recommended by Veletsos and Meek (1974)).

The variations of \tilde{T}/T and $\tilde{\zeta}_0$ with $h/(V_s T)$ and h/r based on the analytical solution of Veletsos and Nair (1975) are shown in Figure 4.19. The results show that \tilde{T}/T increases with $h/(V_s T)$ and h/r , for $h/r > 1$. Flexible-base damping $\tilde{\zeta}$ can actually increase or decrease relative to ζ depending on \tilde{T}/T and foundation damping factor $\tilde{\zeta}_0$. In Figure 4.19, $\tilde{\zeta}_0$ is seen to increase with $h/(V_s T)$ and decrease with h/r , indicating that lateral movements of the foundation (which dominate at low h/r) dissipate energy into soil more efficiently than foundation rocking (which dominates at high h/r). The contributions to foundation damping from radiation and hysteretic damping are compared in Figure 4.19 (the solid lines represent the sum of the hysteretic and radiation damping, the dashed lines represent radiation damping only); the significance of hysteretic damping is seen to increase with increasing h/r due to the decreased radiation damping effect.

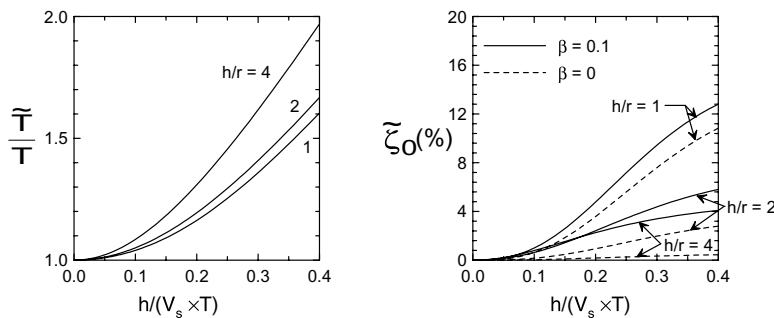


FIGURE 4.19 Period lengthening ratio and foundation damping factor for single degree-of-freedom structure with rigid circular foundation on viscoelastic halfspace ($\nu = 0.4$, $\gamma_m = 0.15$).

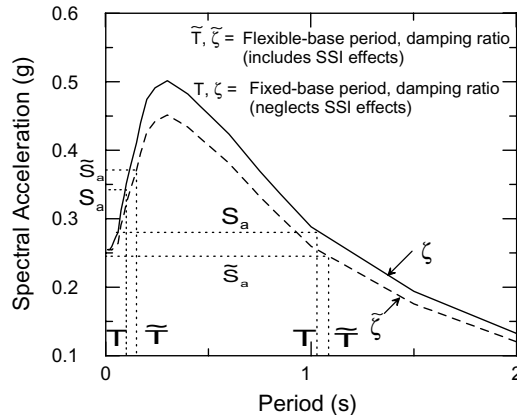


FIGURE 4.20 Schematic showing effects of period lengthening and foundation damping on design spectral accelerations for realistic spectral shape. (From Stewart, J.P. et al., *Earthquake Spectra*, 19, 677–696, 2003b. With permission.)

The above analysis procedure for \tilde{T}/T and $\tilde{\zeta}_0$ has been found to reproduce reasonably accurately SFSI effects on first-mode vibration properties of actual structures, as inferred from system identification analyses of recorded motions (Stewart et al., 1999). These case history studies revealed that the single most important parameter controlling the significance of inertial interaction is $h/(V_s T)$, and that inertial SFSI effects are generally negligible for $h/(V_s T) < 0.1$. This condition occurs for flexible structures such as moment frame buildings located on competent soil. Conversely, inertial SFSI effects tend to be significant for stiff structures such as shear wall or braced frame buildings, particularly when located on soft soil.

The effect of inertial SFSI on the base shear for a building structure is illustrated in Figure 4.20 (note that peak base shear is commonly computed from spectral acceleration at the first mode). The spectral acceleration for a flexible-base structure (\tilde{S}_a) is obtained by entering the spectrum drawn for effective damping ratio $\tilde{\zeta}$ at the corresponding elongated period \tilde{T} . For buildings with periods greater than about 0.5 sec, using \tilde{S}_a in lieu of S_a typically reduces base shear demand, whereas in very stiff structures SFSI can increase the base shear.

4.5.2.2 Analysis of Impedance Functions

4.5.2.2.1 Basic Case

The impedance function for a rigid foundation is represented in Figure 4.18 by \bar{k}_u and \bar{k}_θ , and may also include a coupling spring. Simplified impedance function solutions are available for rigid circular or rectangular foundations located on the ground surface and underlain by a uniform, visco-elastic halfspace. A thorough listing of impedance functions for these and other shapes is provided in Gazetas (1991a, 1991b). To illustrate the formulation of impedance functions and to provide a widely applicable solution, we discuss here in detail the solution for circular foundation shapes. It should be noted that if a distributed spring model such as that shown in Figure 4.16 is used, the stiffness of the distributed springs is calculated by normalizing the complete foundation stiffness by area or moment of inertia, as described further in Section 4.5.4. Accordingly, analysis of the foundation impedance function is always a required step in substructure-based SFSI analyses.

Terms in the impedance function are expressed in the form

$$\bar{k}_j = k_j(a_0, \nu) + i\omega c_j(a_0, \nu) \quad (4.9)$$

where j denotes either deformation mode u or θ , ω is angular frequency (rad/sec), a_0 is a dimensionless frequency defined by $a_0 = \omega r/V_s$, r = foundation radius, V_s = soil shear wave velocity, ν = soil Poisson

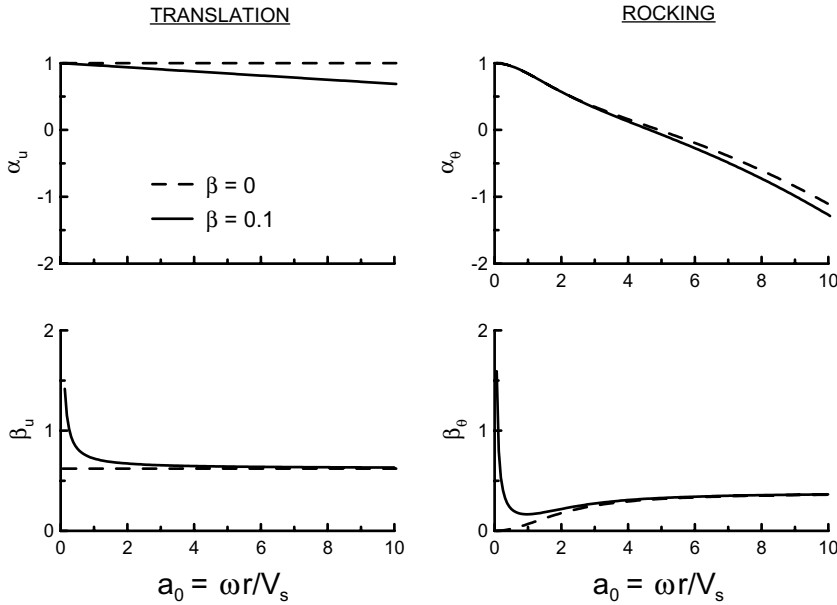


FIGURE 4.21 Foundation stiffness and damping factors for elastic and viscoelastic halfspaces ($\nu = 0.4$). (Adapted from Veletsos, A.S. and Verbic, B., *J. Earthquake Eng. Struct. Dyn.*, 2, 87–102, 1973.)

ratio and $i = \sqrt{-1}$. Foundation radii can be computed separately for translational and rotational deformation modes to match the area (A_f) and moment of inertia (I_f) of the actual foundation (i.e., $r_u = \sqrt{A_f/\pi}$, $r_\theta = \sqrt[4]{4I_f/\pi}$). There are corresponding $(a_0)_u$ and $(a_0)_\theta$ values as well.

The real stiffness and damping of the translational and rotational foundation springs and dashpots are expressed, respectively, by

$$k_u = \alpha_u K_u \quad c_u = \beta_u \frac{K_u r_u}{V_s} \quad (4.10a)$$

$$k_\theta = \alpha_\theta K_\theta \quad c_\theta = \beta_\theta \frac{K_\theta r_\theta}{V_s} \quad (4.10b)$$

where α_u , β_u , α_θ , and β_θ express the frequency dependence of the impedance terms, and K_u and K_θ represent the static stiffnesses of a disk on the surface of a halfspace,

$$K_u = \frac{8}{2-\nu} G r_u \quad K_\theta = \frac{8}{3(1-\nu)} G r_\theta^3 \quad (4.11)$$

where G is the soil dynamic shear modulus. The frequency-dependent values of α_u , β_u , α_θ , and β_θ for a rigid circular foundation on the surface of a visco-elastic halfspace are presented in Figure 4.21 (Veletsos and Wei, 1971; Veletsos and Verbic, 1973).

Validation studies for the above and similar impedance function formulations have been conducted by Lin and Jennings (1984) and Crouse et al. (1990) for small foundations (<3 m plan dimension), and by Luco et al. (1988), Wong et al. (1988) and de Barros and Luco (1995) for larger scale building foundations (up to 25 m plan dimension). These studies have generally found reasonably good agreement between experimental observations and analytical predictions, although the data for damping are especially sparse.

The above solutions for rigid, circular foundations on a halfspace can provide reasonable estimates of foundation impedance in many cases. However, the potentially significant effects of nonuniform soil profiles, embedded foundations, noncircular foundation shapes, flexible foundations and piles or piers beneath the base slab should be accounted for in some cases. The following briefly discusses the effects of these factors on impedance functions.

4.5.2.2.2 Nonuniform Soil Profiles

Gazetas (1991b) provides solutions for the impedance of rigid foundations overlying soil for which the shear stiffness increases with depth according to prescribed functions. For profiles having a gradual increase of stiffness with depth, foundation stiffness can often be reasonably estimated using halfspace impedance function formulations in which soil properties are taken as average values between the surface and a depth of about $0.75r_u$ or $0.75r_\theta$ (Stewart et al., 2003b). The use of equivalent halfspace formulations is less effective for damping, however, particularly at low frequencies (Gazetas, 1991b). At these low frequencies, wave reflections reduce the radiation damping effect. Hence the impedance model overestimates damping at low frequencies. Gazetas (1991b) provides alternative models for this condition.

For the case of a finite soil layer overlying a much stiffer material, the presence of the stiff material increases the static stiffness and changes the frequency dependence of stiffness and damping. The increased static stiffnesses can be estimated as follows (Kausel, 1974),

$$(K_u)_{FL} = K_u \left(1 + \frac{1}{2} \frac{r_u}{d_s} \right) \quad (K_\theta)_{FL} = K_\theta \left(1 + \frac{1}{6} \frac{r_\theta}{d_s} \right) \quad (4.12)$$

where $(K_u)_{FL}$ and $(K_\theta)_{FL}$ are the static horizontal and rocking stiffnesses of the foundation on a finite soil layer, and d_s is the depth of the layer. These corrections are generally appropriate when the surface layer has a shear wave velocity less than half of that for the deeper layer (Stewart et al., 2003b).

The frequency dependence of stiffness terms follows the general trends for a halfspace in Figure 4.21, but has oscillations associated with the natural frequency of the stratum at low levels of soil damping. For hysteretic damping exceeding about 7%, Roessel (1980) found that the oscillations can be neglected. With regard to damping, the key issue is a lack of radiation damping at frequencies less than the fundamental frequency of the finite soil layer. Halfspace damping ratios can be used for frequencies greater than the soil layer frequency, and a transition to zero radiation damping at smaller frequencies can be defined as per Elsabee and Morray (1977).

4.5.2.2.3 Embedded Foundations

The impedance of embedded foundations differs from that of shallow foundations in several important ways. First, the static stiffness of embedded circular foundations is increased according to the factors given below,

$$(K_U)_E = K_U \left(1 + \frac{2}{3} \frac{e}{r_u} \right) \quad (K_\theta)_E = K_\theta \left(1 + 2 \frac{e}{r_\theta} \right) \quad (4.13)$$

where e = embedment depth. The second important difference between embedded and surface foundations is that the embedded foundations have much larger damping due to the greater foundation–soil contact area.

An approximate model for the impedance of embedded foundations consists of the modified static stiffness terms from Equation 4.13 coupled with the dynamic modifiers for a surface foundation in Figure 4.21. This solution provides reasonable estimates of foundation damping for embedment ratios $e/r < 0.5$ (Stewart et al., 1999). For more deeply embedded foundations, alternative formulations should be used such as Bielak (1975) or Apsel and Luco (1987). Caution should also be exercised for embedded foun-

dations with poor quality backfill against basement walls — for such foundations, gapping is likely and impedance functions should probably be formulated using shallow foundation models.

4.5.2.2.4 Foundation Shape

Impedance functions for foundations of arbitrary shape are commonly analyzed as equivalent circular mats, provided that the foundation aspect ratio in plan is less than 4:1 (Roesset, 1980). As described previously, an equivalent radius for translational stiffness is derived by equating the areas of the mats, while an equivalent radius for rocking stiffness is derived by equating the moments of inertia of the mats.

Combining a number of analytical impedance function solutions from the literature for foundations of arbitrary shape, Dobry and Gazetas (1986) found that the use of equivalent circular mats is acceptable for aspect ratios less than 4:1, with the notable exception of dashpot coefficients in the rocking mode. The radiation damping component of rocking dashpot coefficients was found to be underestimated by the equivalent disk assumption at low frequencies. Hence, radiation dashpot coefficients for oblong, noncircular foundations should be calculated using impedance function formulations for rectangular foundations, such as those found in Gazetas (1991a, 1991b).

4.5.2.2.5 Foundation Flexibility

Impedance functions for flexible circular foundation slabs supporting shear walls have been evaluated for a number of wall configurations, including: (1) rigid core walls (Iguchi and Luco, 1982), (2) thin perimeter walls (Liou and Huang, 1994) and (3) rigid concentric interior and perimeter walls (Riggs and Waas, 1985). These studies focused on the effects of foundation flexibility on rocking impedance; the horizontal impedance of flexible and rigid foundations is similar (Liou and Huang, 1994). Foundation flexibility effects on rocking impedance are most significant for a rigid central core with no perimeter walls. For this case, the flexible foundation has significantly less stiffness and damping than the rigid foundation. The reductions are most significant for narrow central cores and large deviations between soil and foundation slab rigidity. Hence, corrections for foundation flexibility effects should be made to rocking impedance terms for structures having central core shear walls in accordance with the analytical results of Iguchi and Luco (1982). Use of the rigid foundation assumption introduces much smaller errors to rocking impedance terms for other wall configurations.

4.5.2.2.6 Pile or Drilled Shaft Foundations

The presence of piles or drilled shafts beneath foundation grade beams or a base mat can significantly affect impedance functions. If the shallow elements (base slab, grade beams) remain in contact with the soil, these elements may significantly contribute to the lateral stiffness and damping of the foundation, whereas the deep foundations will control the lateral response if a gap is present between the base slab and the soil. The rocking impedance is significantly affected by deep foundation elements because of their large axial stiffness relative to the soil. In practice, pile caps are generally assumed to be not in contact with soil due to anticipated soil settlement. This leads to low assessments of stiffness and damping if cap-soil contact is actually present during earthquake shaking.

The vertical and lateral stiffness of deep foundation elements are generally analyzed on a site-specific basis using models in which distributed Winkler springs are attached to beam-column structural elements to represent the pile (e.g., programs APILE and LPILE, Reese et al., 1998, 2000). The damping behavior of single piles and pile groups can be analyzed for small strain conditions using analytical solutions such as those presented by Gazetas (1991b). However, complexities of the nonlinear pile response, including gap formation and pile-to-pile interaction, make the analysis of damping for realistic, large strain conditions a challenging topic that remains an active subject of research.

4.5.3 Kinematic Interaction

As noted in Section 4.5.1, kinematic interaction results from the presence of stiff foundation elements on or in soil, which causes foundation motions to deviate from free-field motions as a result of base-slab averaging and embedment effects. In this section, these phenomena are described and simple models for the analysis of transfer functions for shallow foundations at the ground surface, embedded shallow foundations and pile

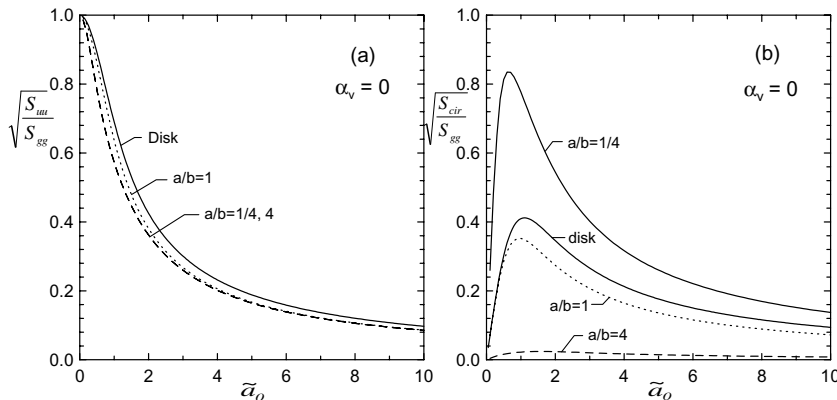


FIGURE 4.22 Amplitude of transfer function between free-field motion and FIM for vertically incident incoherent waves (Veletsos and Prasad, 1989; Veletsos et al., 1997).

foundations are presented. Following the presentation of these formulations for transfer functions, recommendations are provided regarding how transfer functions can be used to modify a free-field response spectrum or time history suite to estimate foundation input motions for use in practice.

4.5.3.1 Shallow Foundations at the Ground Surface

Base-slab averaging results from inclined or incoherent incident wave fields. Motions of surface foundations are modified relative to the free-field when incident waves impinge upon the foundation with an angle to the vertical axis, α_v , or when the incident wave is incoherent. The first case is referred to as the wave passage effect and the second case as the ground motion incoherence effect. In the presence of these wave fields, translational base-slab motions are reduced relative to the free-field, and rotational motions are introduced. The reductions of base-slab translation, and the introduction of torsion and rocking, are all effects that tend to become more significant with increasing frequency. The frequency dependence of these effects is primarily associated with the increased effective size of the foundation relative to the seismic wavelengths at higher frequencies. In addition, ground motions are more incoherent at higher frequencies.

Veletsos and Prasad (1989) and Veletsos et al. (1997) developed useful models for base-slab averaging that combine an analytical representation of the spatial variation of ground motion with rigorous treatment of foundation-soil contact. The models evaluate the response of rigid, massless circular and rectangular foundations on the surface of an elastic halfspace to incoherent SH waves propagating either vertically or at an angle α_v to the vertical. Results are expressed in terms of a transfer function between translational and torsional foundation motions and free-field motion. The translational component of foundation motion is denoted with subscript u and the torsional rotation component with subscript ϕ . Torsional motions at the foundation edge or circumference (denoted S_{cir}) are represented by the product of foundation dimension and rotational angular distortion (e.g., $S_{cir} = b^2 \cdot S_{\phi\phi}$ for rectangular foundations). The transfer function amplitudes computed by Veletsos and his co-workers are presented in Figure 4.22 for circular and rectangular foundations subject to vertically incident incoherent SH waves. Similar curves are available for nonvertically incident coherent waves in the references. These figures are prepared such that the foundation dimension $2a$ is measured parallel to the direction of SH wave polarization, and $2b$ is the perpendicular dimension. The transfer functions for translational and circumferential torsional motions on the base slab are denoted as $\sqrt{S_{uu}/S_{gg}}$ and $\sqrt{S_{cir}/S_{gg}}$, where S_{uu} and S_{gg} denote power spectral density functions of the foundation translation and free-field motion, respectively (note that $\sqrt{S_{xx}/S_{yy}} \approx \bar{u}_{xx}/\bar{u}_{yy}$, where \bar{u}_{ii} is the Fourier amplitude of motion u_{ii}). The transfer functions in Figure

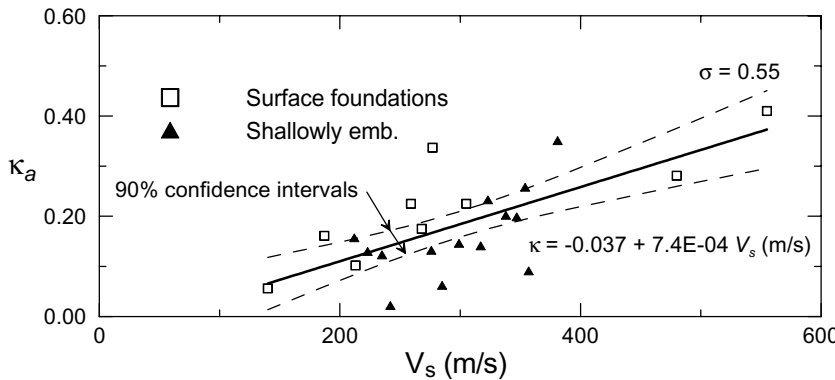


FIGURE 4.23 κ_a versus V_s results of linear regression. (From Kim, S. and Stewart, J.P., *J. Geotech. Geoenvir. Eng.*, ASCE, 129, 323–335, 2003. With permission.)

4.22 are plotted against the dimensionless frequency parameter \tilde{a}_0 , defined as follows for circular and rectangular foundations, respectively,

$$\tilde{a}_0 = a_0 \sqrt{\kappa^2 + \sin^2 \alpha_v} \quad \text{Circular}$$

$$\tilde{a}_0 = \frac{\omega b_e}{V_{s,r}} \sqrt{\kappa^2 + \sin^2 \alpha_v \left(\frac{b}{b_e} \right)^2} \quad \text{Rectangular} \quad (4.14)$$

where $a_0 = \omega r/V_{s,r}$, $V_{s,r}$ denotes a strain-reduced shear wave velocity, $b_e = \sqrt{ab}$, and κ denotes a ground motion incoherence parameter that is quantified below.

Figure 4.22 indicates that the lateral transfer functions for circular and various rectangular geometries are similar to each other for small \tilde{a}_0 . As noted by Veletsos et al. (1997), the near equivalence of the results for different aspect ratios ($a/b = 1/4\text{--}4$) of rectangular foundations suggests that translational transfer functions primarily depend on the foundation area. The torsional transfer function results show a relatively high degree of sensitivity to a/b , with higher torsional motions occurring for lower a/b .

Kim and Stewart (2003) calibrated the above analysis procedure against observed foundation and free-field ground motion variations as quantified by frequency-dependent transmissibility function amplitudes, $|H|$. The above analytical models were fit to $|H|$ for the assumed condition of a rigid base slab and vertically propagating, incoherent incident wave field. The ground motion incoherence parameter, κ , was calibrated from the fitting process. Since the limiting assumptions of the model were not strictly satisfied for actual structures, the results of the identification were denoted apparent κ values (κ_a) that reflect not only incoherence effects, but also possible foundation flexibility and wave inclination effects. Parameter κ_a was found to be correlated to average soil shear wave velocity as shown in Figure 4.23. These values of κ_a can be used with Figure 4.22 (assuming $\alpha_v = 0$) to define site-specific transfer functions given the foundation radius (r) and effective velocity (V_s). In these procedures, effective foundation radius is defined as $r = \sqrt{A_f/\pi}$ and the effective V_s for the site is defined as $r/(\text{travel time for shear wave to travel from depth } r \text{ to ground surface})$. Depth is measured down from the base of the foundation.

Limitations of this approach include: (1) foundations should have large in-plane stiffness, ideally a continuous mat foundation or interconnected footings and grade beams; (2) for nonembedded foundations, the foundation dimension should be less than 60 m unless the foundation elements are unusually stiff; (3) the approach should not be used for embedded foundations with $e/r > 0.5$; (4) the approach should not be used for pile-supported structures in which the cap and soil are not in contact; and (5) the approach should not be used where significant wave inclination effects are likely, such as sites near basin edges.

4.5.3.2 Embedded Shallow Foundations

When subjected to vertically propagating coherent SH waves, embedded foundations experience a reduction in base-slab translational motions relative to the free-field, and rocking motions are introduced. The rocking is caused by incompatible shear strains along the sides of the excavation and the free-field.

Elsabee and Morray (1977) and Day (1978) have developed analytical transfer functions relating base-slab translational and rocking motions to free-field translations for an incident wave field consisting of vertically propagating, coherent SH waves. Base-slab averaging does not occur within this wave field, but foundation translations are reduced relative to the free-field due to ground motion reductions with depth and wave scattering effects. Day (1978) used finite element analyses to evaluate the base motions of a rigid cylindrical foundation embedded in a uniform elastic halfspace ($\beta = 0$, $v = 0.25$) and subjected to vertically incident, coherent SH waves. Elsabee and Morray (1977) performed similar studies but for the case of a visco-elastic soil layer of finite depth over a rigid base ($\beta = 0.05$ and $v = 0.33$). The amplitude of the halfspace and finite soil layer transfer functions is shown together in Figure 4.24 for foundation embedment-to-radius ratio $e/r = 1.0$. The primary difference between the two solutions is oscillations in the finite soil layer case at high frequencies. The following approximate transfer function amplitudes developed by Elsabee and Morray (1977) are also shown in Figure 4.24:

$$\text{translation: } |H_u(\omega)| = \begin{cases} \cos\left(\frac{e}{r}a_0\right) & a_0 \leq 0.7 \cdot \bar{a}_0 \\ 0.453 & a_0 > 0.7 \cdot \bar{a}_0 \end{cases} \quad (4.15)$$

$$\text{rocking: } |H_\theta(\omega)| = \begin{cases} \frac{0.257}{r} \left(1 - \cos\left(\frac{e}{r}a_0\right)\right) & a_0 \leq \bar{a}_0 \\ \frac{0.257}{r} & a_0 > \bar{a}_0 \end{cases} \quad (4.16)$$

where $\bar{a}_0 = \pi/2 \cdot r/e$. Normalized frequency \bar{a}_0 corresponds to the fundamental frequency of the soil from the surface to depth e ($\bar{a}_0 = 2\pi f_1 r/V_s$ where $f_1 = V_s/4e$).

The results in Figure 4.24 can be contrasted with the behavior of a surface foundation, which would have no reduction of translational motions and no rocking motions when subjected to vertically incident coherent shear waves. Transfer function amplitudes in the presence of more realistic incident wave fields can be estimated at each frequency by the product of the transfer function ordinates from the previous section (for base-slab averaging) and those from this section at the corresponding frequency.

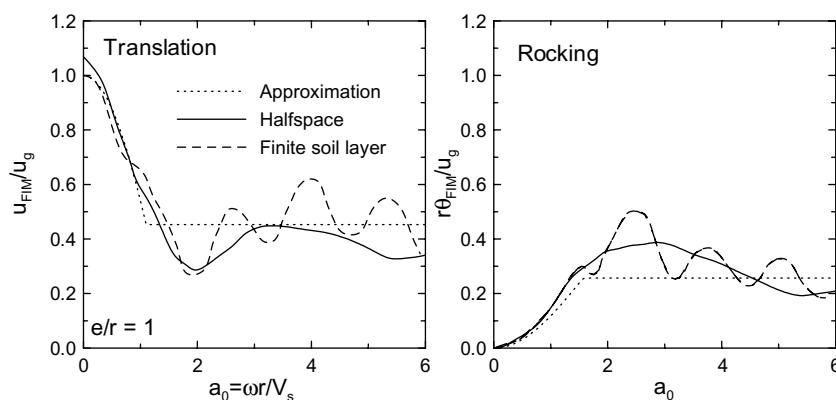


FIGURE 4.24 Transfer function amplitudes for embedded cylinders. (Day, 1978; Elsabee and Morray, 1977).

Elsabee and Morray (1977) found these transfer functions to also be applicable to nonhomogeneous soil profiles, provided V_{sr} is averaged across the embedment depth. Mita and Luco (1989) found that solutions for circular foundations can be extended to square foundations, provided the radius of the equivalent cylinder is the average of the radii necessary to match the area and moment of inertia of the square base.

The analysis procedure described herein has been verified against recorded motions from two relatively deeply embedded structures with circular foundations having $e/r = 0.9$ and 2.9 (Kim, 2001). Embedment effects dominated the kinematic interaction for these deeply embedded foundations; for foundations with $e/r < 0.5$ Kim (2001) found that the embedment and base-slab averaging models should be coupled to accurately simulate observed transfer functions.

4.5.3.3 Pile Foundations

The seismic response of a pile-supported foundation differs from that of a surface foundation due to the increased stiffness of the pile-soil system as compared to soil only, and due to scattering of seismic waves off the piles. Most theoretical studies of kinematic effects associated with pile-soil interaction have been performed for single piles or pile groups with a rigid cap not in contact with the ground. These studies have shortcomings for buildings for which soil settlement away from the pile cap is unlikely, such as friction piles installed in stiff soils. Relatively few studies have investigated kinematic interaction effects for pile-supported foundations with cap-soil contact.

Fan et al. (1991) summarized the results of a series of previous numerical studies on the kinematic response of vertical piles in elastic soil subjected to vertically incident harmonic shear waves and bonded to a massless rigid cap suspended above the ground (references in Fan et al. (1991)). The results were presented as a set of dimensionless graphs that enable evaluation of the effects of relative pile rigidity (E_p/E_s), pile slenderness (pile length/diameter, L/d), soil layering, pile spacing (s/d), pile head fixity and number of piles. These results generally indicate significant effects of E_p/E_s , head fixity and soil layering on the kinematic response of single free-head piles subject to vertically incident shear waves. The effect of L/d was relatively minor. Pile groups subjected to vertically incident shear waves were generally found to have similar horizontal transfer functions to those of single piles. Pile group effects are more pronounced for torsional and rocking vibration modes. Additional results for piles subject to nonvertically incident waves have been presented by Mamoon and Ahmad (1990), and indicate less kinematic interaction (i.e., transfer function ordinates closer to one) at low frequencies.

Verification studies by Kim and Stewart (2003) of the analysis procedure by Fan et al. showed that these procedures are generally not capable of reproducing observed foundation and free-field ground motion variations. The observed variations were better explained by the procedures for shallow foundations presented above. The poor comparison likely resulted from slab-soil contact at many of the building sites considered by Kim and Stewart (2003).

4.5.3.4 Application of Transfer Functions to Calculation of Foundation Motions

The analysis of free-field motions generally results in the specification of a design-basis acceleration response spectrum. Sometimes suites of time histories are specified that are compatible with this spectrum. The question addressed in this section is how this spectrum or time history suite should be modified once the transfer function amplitude for the site has been evaluated using the analysis procedures described above.

When free-field motions are specified as time histories, modified time histories representing the foundation input motion can be evaluated as follows:

1. Calculate the Fourier transforms of the free-field time histories.
2. Multiply the amplitude of the free-field motions by the transfer function amplitude at corresponding frequencies.
3. Use the amplitudes from step 2 along with the phase angles of the free-field motions, and perform reverse Fourier transforms to estimate FIM time histories.
4. If needed, a revised response spectrum that accounts for kinematic interaction effects could be calculated from the FIM time histories.

It should be noted that maintaining the free-field phase angles in step 3 is not strictly correct. However, models for phase adjustment are not available for kinematic interaction effects, and the assumption of consistent phase should not significantly bias the amplitude of estimated FIMs.

When free-field motions are specified only as response spectral ordinates, the evaluation of a modified response spectrum consistent with the FIM is needed. Veletsos and Prasad (1989) evaluated ratios of foundation and free-field response spectral ordinates (at 2% damping) for conditions where the corresponding transfer function ordinates could be readily determined. A comparison indicates that transfer function ordinates provide a reasonable estimate of response spectral ratios for low frequencies (e.g., <5 Hz), but at high frequencies (≥ 10 Hz) transfer function ordinates are significantly smaller than response spectrum ratios. The inconsistency at high frequencies is attributed to the low energy content of free-field excitation and the saturation of spectral ordinates at these frequencies. Response spectral ordinates at these high frequencies can be conservatively estimated using the transfer function ordinates at about 5 Hz. Accordingly, the following procedure is recommended:

1. For frequencies <5 Hz, estimate foundation response spectral ordinates as the product of free-field response spectral ordinates and the transfer function amplitude at the corresponding frequency.
2. For frequencies >5 Hz, estimate foundation response spectral ordinates as the product of free-field response spectral ordinates and the transfer function amplitude at 5 Hz.

It should be noted that the free-field spectrum assumed by Veletsos and Prasad (1989) has a frequency–energy distribution typical of active tectonic regions. Where motions are likely to have much higher frequency contents (i.e., mid-plate tectonic regions), saturation frequencies higher than 5 Hz would likely be appropriate.

4.5.4 Implementation in Seismic Design Standards

4.5.4.1 Inertial and Kinematic Interaction

Formal provisions for soil–structure interaction are included in several important design standards for earthquake engineers: the NEHRP Recommended Provisions for Seismic Regulations for New Buildings and Other Structures (BSSC, 2001) and ATC-40: Seismic Evaluation and Retrofit of Concrete Buildings (ATC, 1996), which forms the basis of the FEMA-273 and 356 guideline documents (FEMA, 1997, 2000).

The NEHRP guidelines for new buildings employ a force-based specification of structural capacity and seismic demand. Seismic demand is represented by a base shear force that is proportional to the product of building mass and first mode spectral acceleration. Inertial interaction effects are accounted for through analysis of a period lengthening ratio and foundation damping factor, which modify the base shear in a manner similar to the schematic illustration in Figure 4.20. However, the NEHRP provisions employ a flat spectral shape at small periods and restrict the flexible-base damping (ζ_f) to values larger than the fixed-base damping (ζ). These restrictions ensure that SFSI can only decrease the base shear demand. Kinematic interaction effects are ignored in the provisions, which is conservative since kinematic interaction effects reduce seismic demand.

It should be noted that the NEHRP SFSI analysis procedures have a significant shortcoming, which is the lack of a link between base shear reduction factors intended to represent structural ductility (i.e., R -values) and SFSI effects. As noted by Crouse (2001), existing R -values may to some extent reflect beneficial effects of SFSI, and modifying base shear for both effects may be unconservative in some cases. Accordingly, there is a research need to revisit R -values, and define values that truly represent only structural ductility effects.

U.S. seismic design practice for existing buildings uses a displacement-based representation of structural capacity (ATC 40, FEMA 273, FEMA 356). The system performance is represented by a lateral force–displacement relationship calculated using a so-called pushover analysis. In a pushover analysis a prescribed vertical distribution of static lateral load is applied to a structure, and the nonlinear deformation response of the structure–foundation–soil system is evaluated based on an appropriate system model. The cumulative lateral load (i.e., base shear) can be plotted against a control point displacement to provide a concise representation of the nonlinear system behavior. This curve is referred to as the

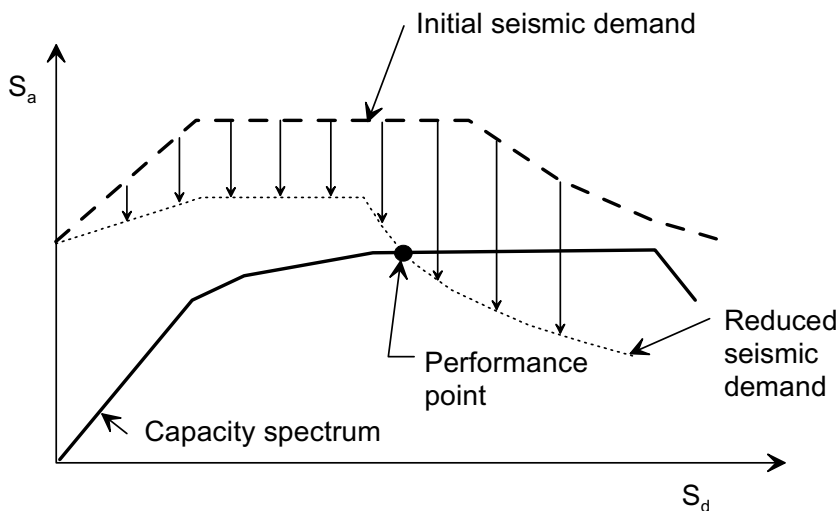


FIGURE 4.25 Use of capacity and demand spectra to define performance point. (Adapted from Comartin, C.D. et al., *Earthquake Spectra*, 16, 241–262, 2000.)

capacity curve. A point on this curve defines a damage state in the building, since the deformation of all of the structural components can be related to the control point displacement.

The expected seismic structural performance is assessed by combining the capacity curve with an acceleration–displacement response spectra (ADRS) as illustrated in Figure 4.25. The ADRS represents the seismic demand, and consists of a plot of elastic spectral acceleration (S_a) versus spectral displacement (S_d). The demand spectrum is reduced, as appropriate, to account for the inelastic deformation of the structure. The ADRS is compared to the capacity spectrum, which is the capacity curve normalized by building mass and corrected for higher mode effects. The capacity and demand spectra meet at the performance point, which represents the expected structural performance given the seismic demand. Additional details on these methods of analysis are provided in Chapter 9.

The effects of SFSI on the above process are two-fold. First, SFSI affects demand spectra through the effective system damping (inertial interaction) and spectral shape (kinematic interaction). These SFSI effects are neglected in current design documents (e.g., ATC-40 and FEMA 273, 356) because demand spectra in these documents represent expected free-field shaking levels and the system damping is taken as 5%, which is generally intended to represent structural damping only. Second, capacity assessment is controlled by nonlinear component models used to evaluate the capacity curve. Among these nonlinear component models are distributed foundation springs (e.g., Figure 4.16) that are described by an elastic-plastic force–displacement relationship evaluated as follows:

1. The foundation stiffness is evaluated using the full dimension of the foundation system for vertical (k_v), rocking (k_θ) and translational (k_u) vibration modes. Procedures for this analysis are presented in Section 4.5.2.2.
2. The lateral spring stiffness is taken as the value from (1), and the foundation is assumed to be rigid laterally.
3. The stiffness intensities of distributed vertical springs are calculated once as k_v divided by the foundation area (A_f) and again as k_θ divided by foundation moment of inertia (I_f). If the difference between the two is small, a representative average is taken. If the difference is large and the footing is vibrating primarily in vertical translation or rocking, the stiffness intensity for the dominant deformation mode is used. The stiffness of a particular vertical spring element is then calculated as the stiffness intensity multiplied by the tributary area for the spring.

4. The spring force is limited to the foundation bearing capacity, which is evaluated using traditional methods. The spring is plastic (i.e., continues to deform at constant force) after yield at the bearing capacity.

4.5.4.2 Design of Foundation Elements

Existing code-based design procedures for shallow foundations in new buildings are based on providing adequate capacity to ensure lack of flexural or shear failure in foundation components (ICBO, 1997; SEAOC Seismology Committee, 2001). These analysis procedures employ simplified soil pressure distributions, and no analyses of foundation element deformations are performed.

Design procedures in ATC-40 for shallow foundations call for direct structural modeling of foundation components with the soil reactions and structural loads placed on the foundation (ATC, 1996). These analyses can employ distributed spring models for foundation–soil interaction as illustrated in Figure 4.16, or for very stiff foundation systems, the foundation may be assumed to be rigid.

The structural design of deep foundation elements generally requires direct structural modeling of pile response to head loads. These models generally model the pile as a beam-column element and the soil with distributed reaction springs. In some cases, additional kinematic loading associated with the free-field soil response may also be accounted for in the analysis (e.g., Nikolaou et al., 2001; Mylonakis, 2001); such effects can be especially important in liquefied soil or soft clays. The analyses produce estimates of axial load, shear and moment distributions, which are used to appropriately detail the structural section to resist those loads.

4.6 Ground Failure

Under low to moderate levels of shaking, free-field soil deposits will experience little or no permanent deformation. When the response to earthquake shaking is very strong, permanent strains may occur within the deposit due to volume change in the soil or due to shear deformations that accrue during increments of shaking where the applied shear stresses exceed the strength of the soil. These permanent strains result in permanent deformations that are often referred to as ground failure. Ground failure can be observed in the form of landslides, flow slides and lateral spreads, and can contribute to the failure of foundations and retaining structures.

4.6.1 Liquefaction

Liquefaction is a term used to describe a range of phenomena in which the strength and stiffness of a soil deposit are reduced due to the generation of porewater pressure. While it is possible for liquefaction to be caused by static loading, it is most commonly induced by earthquakes. Liquefaction occurs most commonly in loose, saturated, clean to silty sands but has also been observed in gravels and nonplastic silts. Ground failures with characteristics similar to liquefaction failures have also been observed in low-plasticity silty clays. Liquefaction can produce damage ranging from small slumps and lateral spreads to massive flow slides with displacements measured in tens of meters. It can cause foundations and retaining structures to settle and tilt, or can tear them apart through large differential displacements.

4.6.1.1 Examples

Liquefaction has occurred in numerous earthquakes, and left its mark in the geologic and historical record. Evidence of past liquefaction (Figure 4.26a), termed paleoliquefaction, has been used to evaluate seismic hazards in areas where instrumental and historical data are sparse. The subject of liquefaction came to the forefront of geotechnical earthquake engineering with the 1964 earthquakes in Niigata, Japan and Alaska. In Niigata, liquefaction caused lateral spreading (Figure 4.26b) and loss of bearing capacity (Figure 4.26c). More recently, strong earthquakes in California, such as Loma Prieta (1989) and Northridge (1994), Japan (1995), Turkey (1999) and Taiwan (1999) have provided additional evidence of the damaging effects of liquefaction (Figure 4.26d).

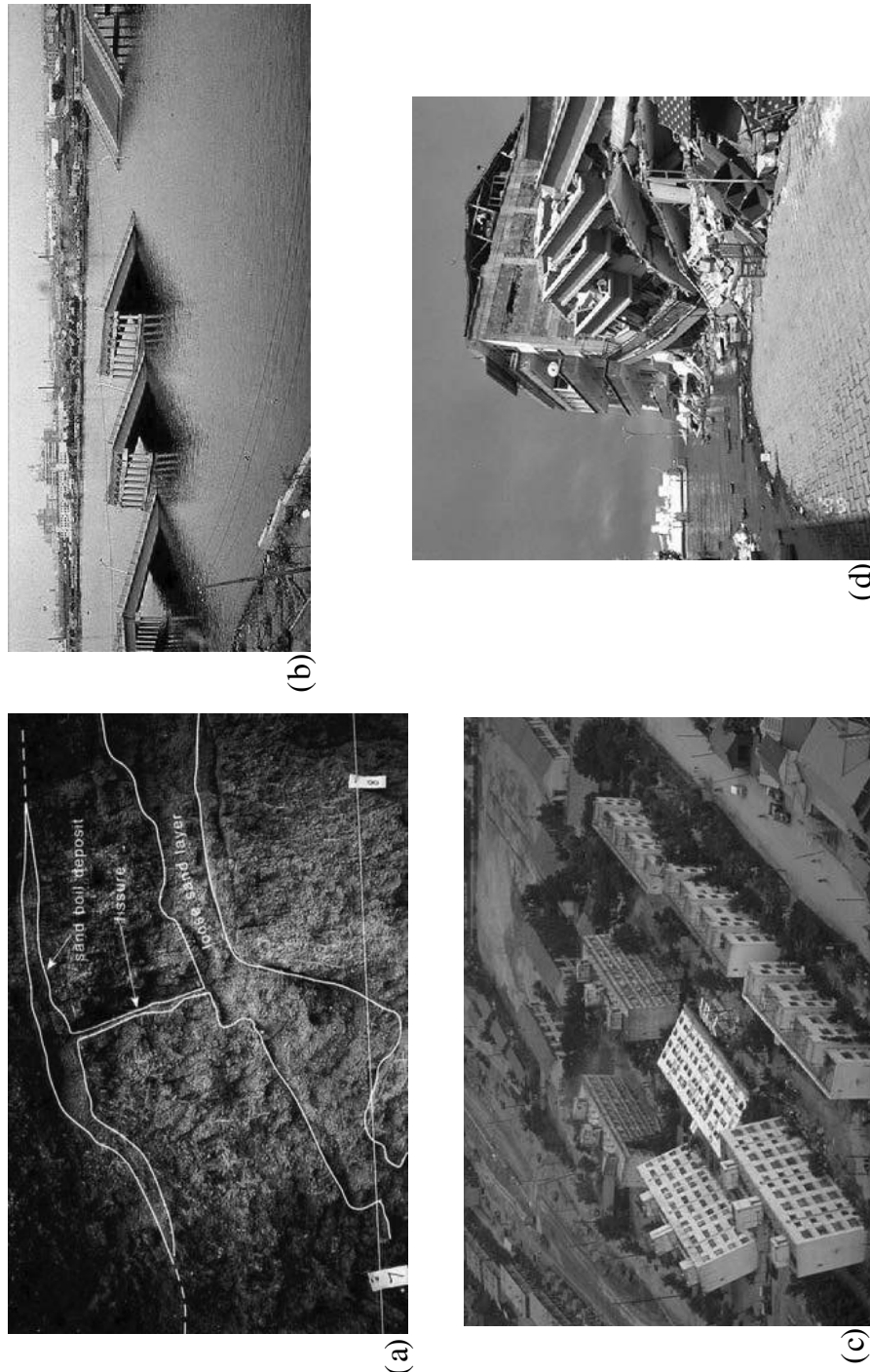


FIGURE 4.26 (a) Paleo-evidence of liquefaction in the form of buried sand boil (photo: U.S. Geological Survey), (b) lateral spreading damage to Showa bridge from 1964 Niigata earthquake (photo: J. Penzien), (c) bearing failure of foundations for Kawagishi-cho apartment buildings in 1964 Niigata earthquake (photo: J. Penzien), (d) subsidence of waterfront area in 1999 Turkey earthquake (photo: K. Elwood).

4.6.1.2 Terminology

The basic mechanisms that produce liquefaction behavior can be divided into two main categories. Flow liquefaction can occur when the shear stresses required to maintain static equilibrium of a soil mass are greater than the shear strength of the soil in its liquefied state. If liquefaction is triggered by earthquake shaking, the inability of the liquefied soil to resist the required static stresses can cause large deformations, or flowslides, to develop. The second mechanism, cyclic mobility, occurs when the initial static stresses are less than the shear strength of the liquefied soil, and occurs more frequently than flow liquefaction. Cyclic mobility leads to incremental deformations that develop during earthquake shaking; the deformations may be small or quite large depending on the characteristics of the soil and the ground shaking. In the field, cyclic mobility can produce lateral spreading beneath even very gentle slopes and in the vicinity of free surfaces such as riverbeds.

4.6.1.3 Susceptibility

Not all soils are susceptible to liquefaction, so the first step in the performance of a liquefaction hazard evaluation is determination of liquefaction susceptibility. Liquefaction susceptibility can be evaluated using historical, geologic, compositional and state criteria.

Because liquefaction has frequently been observed to occur at the same location when site conditions are unchanged (Youd, 1984), evidence of the historical occurrence of liquefaction, either observed or in the form of paleoliquefaction, can be taken as evidence of liquefaction susceptibility. Geologic conditions can also indicate susceptibility to liquefaction; soils deposited in fluvial deposits, and colluvial and aeolian deposits when saturated, are likely to be susceptible to liquefaction. Liquefaction is also observed in alluvial-fan, alluvial-plain, beach, terrace, playa and estuarine deposits, but not as consistently as in those listed previously. Younger soil deposits are generally more susceptible to liquefaction than older deposits. The physical composition of a soil deposit will play a strong role in determining its liquefaction susceptibility (Kramer, 1996). Uniformly graded clean sands composed of rounded particles are inherently most susceptible to liquefaction. Well-graded soils and soils with angular particles are less susceptible. The presence of fines, particularly plastic fines ($PI > 10$), tends to decrease liquefaction susceptibility.

The liquefaction susceptibility of a given soil is also influenced by its state, i.e., its *in situ* effective stress and density conditions. The tendency of a soil to contract, or densify, under cyclic loading conditions has long been known to be influenced by both density and effective stress. Loose soils are much more susceptible to liquefaction than dense soils and, for a given density, soils under high effective confining pressures are more susceptible to liquefaction than soils at a low effective confining pressure. High values of the state parameter (Been and Jeffries, 1985), defined as the difference between the void ratio and the steady state void ratio, indicate increasing contractiveness and, hence, increasing susceptibility to liquefaction; the state parameter can be estimated from CPT resistance (Been et al., 1986, 1987).

Clayey soils can also exhibit strain-softening behavior when subjected to earthquake shaking, which can produce failures that have many of the same characteristics as liquefaction failures. Wang (1979) proposed the following four criteria (which were subsequently adopted by Seed and Idriss, 1982), the satisfaction of all of which would indicate the potential for strain-softening behavior:

1. Clay fraction (finer than 0.005 mm) $\geq 15\%$
2. Liquid limit, $LL \leq 35\%$
3. Natural water content, $w \geq 0.9LL$
4. Liquidity index ≤ 0.75

These criteria have been the subject of considerable discussion among geotechnical engineers. To account for the differences in Chinese and U.S. practice, the U.S. Army Corps of Engineers modified the measured index properties by decreasing the clay fraction by 5%, increasing the liquid limit by 1% and increasing the natural water content by 2% before applying these criteria to a clayey silt in the foundation of Sardis Dam (Finn et al., 1994). Andrews and Martin (2000) recommended that soils with clay contents (using 0.002 mm threshold) $< 10\%$ and a liquid limit of the #40 fraction less than 32% be considered susceptible to strain softening, that soils with more than 10% clay content and $LL \geq 32\%$ be considered nonsuscep-

tible and other soils be sampled and tested for susceptibility. More recently, investigations of ground damage in the 1999 Turkey and Taiwan earthquakes (e.g., Sancio et al., 2003) have found that the first criterion (clay fraction) was ineffective in distinguishing between sites where damage did and did not occur; these results suggest that this criterion could be eliminated without loss of predictive capability.

4.6.1.4 Initiation

If a soil deposit has been determined to be susceptible to liquefaction, the second step in a liquefaction hazard evaluation is consideration of the potential for initiation of liquefaction. This generally involves characterization of the intensity of seismic loading that the soil will be subjected to and characterization of the liquefaction resistance of the soil. By characterizing both loading and resistance in common terms, the two can be compared to determine the liquefaction potential of the soil.

4.6.1.4.1 Approaches

Several approaches to the characterization of loading and resistance have been proposed for the liquefaction problem. Historically, the cyclic stress method has been commonly used for evaluation of liquefaction potential. More recently, energy-based methods have been proposed. Each approach has advantages, and both are described in the following paragraphs.

The most well documented and commonly used procedure for evaluation of liquefaction potential is referred to as the cyclic stress approach. In the cyclic stress approach, both the loading imposed on the soil by the earthquake and the resistance of the soil to liquefaction are characterized in terms of cyclic shear stresses. By characterizing both loading and resistance in common terms, they can be directly compared to quantify the potential for liquefaction. The cyclic stress approach benefits from the fact that cyclic stress amplitudes can be computed relatively easily and accurately, and from the fact that it has been verified as a conservative predictor of liquefaction by field observations. Its drawbacks include its potential conservatism and the fact that liquefaction is not as closely related to shear stress amplitude as it is to other aspects of soil response. The cyclic stress method represents the classic approach to evaluation of liquefaction potential. It has been thoroughly tested and validated as a useful practical approach for evaluation of liquefaction potential and, therefore, its continued use is recommended for at least the near future.

Although the cyclic stress method has seen widespread use in geotechnical engineering practice, it is well established that pore-pressure generation is more closely related to strain amplitude than stress amplitude. As a result, methods based on strain amplitude (e.g., Dobry et al., 1982) would be expected to provide more reliable predictions of liquefaction. However, the difficulty in predicting strain amplitude has kept strain-based approaches from being used in practice. A quantity that reflects both cyclic stress and strain amplitude is dissipated energy. Nemat-Nasser and Shokooh (1979) developed a relatively simple theory that related soil densification (drained conditions) and pore-pressure generation (undrained conditions) to dissipated energy. Others have since attempted to characterize the relationship between excess pore pressure and dissipated energy experimentally. Arias intensity (Arias, 1970) is a ground motion parameter that reflects the total energy absorbed by a population of single-degree-of-freedom oscillators. This relationship to energy makes it attractive as a potential measure of liquefaction loading and resistance. Kayen and Mitchell (1997) developed a procedure by which Arias intensity could be used to evaluate liquefaction potential. Because Arias intensity reflects the amplitude, frequency content and duration of earthquake motion, the use of proxies such as the magnitude scaling factor (MSF) necessary for the cyclic stress approach, is not required. The Arias intensity approach is very promising, with a number of distinct advantages over the cyclic stress method. It should be considered for use in parallel with the cyclic stress method for important projects to provide a check on the results of the cyclic stress method and to allow identification of liquefaction potential under conditions for which the cyclic stress method is not particularly sensitive, such as in the vicinity of strong impedance contrasts that tend to affect shear strain (and Arias intensity) much more than shear stress.

4.6.1.4.2 Characterization of Liquefaction Loading

The level of loading imposed on a potentially liquefiable soil is a function of the ground motion the soil is subjected to. It is important to recognize that the entire ground motion affects the soil; therefore, the amplitude, frequency content and duration of the motion are all potentially important.

Cyclic Stress Approach — For the purposes of liquefaction evaluation using the cyclic stress approach, loading is typically characterized in terms of the cyclic stress ratio, CSR, which is defined as the ratio of the equivalent cyclic shear stress, τ_{cyc} , to the initial vertical effective stress, σ'_{vo} .

$$CSR = \frac{\tau_{cyc}}{\sigma'_{vo}} \quad (4.17)$$

The equivalent cyclic shear stress is generally taken as equal to 65% of the peak cyclic shear stress, a value arrived at by comparing rates of porewater pressure generation caused by transient earthquake shear stress histories with rates caused by uniform harmonic shear stress histories (Seed et al., 1975; Liu et al., 2001). In the widely used simplified method, the peak cyclic shear stress is estimated from the peak ground surface acceleration and a depth reduction factor, r_d , which represents the average rate at which peak shear stress attenuates with depth. In the simplified method, therefore, the cyclic stress ratio is defined as

$$CSR = 0.65 \frac{a_{max}}{g} \frac{\sigma_{vo}}{\sigma'_{vo}} r_d \quad (4.18)$$

where a_{max} is the peak ground surface acceleration that would be expected to occur in the absence of liquefaction, i.e., the value of a_{max} predicted by an attenuation relationship or a total stress ground response analysis in which excess pore pressure generation is not considered (Youd et al., 2001), σ_{vo} and σ'_{vo} are the initial total and effective vertical stresses, and r_d is a depth reduction factor (Figure 4.27) that accounts for the effect of soil compliance on shear stress amplitude. It should be noted that this value of a_{max} may differ from the actual value of a_{max} that would occur at the surface of a liquefiable soil profile. The simplified method is very commonly used in geotechnical engineering practice.

To account for the fact that peak acceleration alone is an insufficient measure of earthquake loading, frequency content and duration effects are accounted for using earthquake magnitude as a proxy in the form of a magnitude scaling factor, MSF. Youd et al. (2001) recommend estimation of the MSF using

$$MSF = \left(\frac{7.5}{M_w} \right)^n \quad (4.19)$$

where n is within the range of 2.56 to 3.3 for $M_w \leq 7.5$, and is equal to 2.56 for $M_w > 7.5$. The magnitude scaling factor can be used to define a magnitude-weighted peak acceleration

$$a_{max,M7.5} = a_{max}/MSF \quad (4.20)$$

from which the cyclic stress ratio for any arbitrary magnitude can be defined as

$$CSR_{M7.5} = 0.65 \frac{a_{max,M7.5}}{g} \frac{\sigma_{vo}}{\sigma'_{vo}} r_d \quad (4.21)$$

Energy Approach — Kayen and Mitchell (1997) noted that Arias intensity is equal to the total energy absorbed by a population of simple oscillators spaced evenly in frequency, and proposed that the lique-

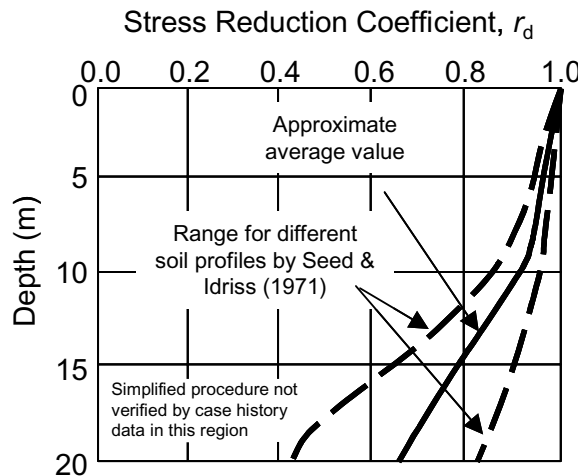


FIGURE 4.27 Variation of depth reduction factor, r_d , for simplified cyclic stress method. (Modified from Youd, T.L. et al. *J. Geotech. Geoenviron. Eng.*, ASCE, 127, 817–833, 2001. With permission.)

fraction potential could be evaluated using Arias intensity. Arias intensity (two-component) can be computed from two orthogonal accelerograms as

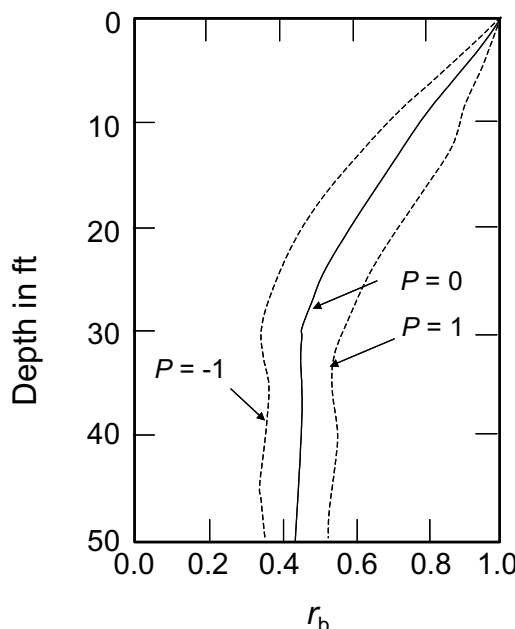


FIGURE 4.28 Variation of depth reduction factor, r_b , for Arias intensity method. Variable P represents number of standard deviations above mean value. (Modified from Kayen, R.E. and Mitchell, J.K. (1997). *J. Geotech. Geoenviron. Eng.*, ASCE, 123, 1162–1174. With permission.)

$$I_h = \frac{\pi}{2g} \left[\int_0^{t_o} a_x^2(t) dt + \int_0^{t_o} a_y^2(t) dt \right] \quad (4.22)$$

where t_o is strong motion duration. Kayen and Mitchell proposed alternative methods for estimation of Arias intensity and its variation with depth within a given soil profile. As with the cyclic stress method, Arias intensities can be computed using site-specific ground response analyses; computed accelerograms at depths of interest can be integrated to obtain Arias intensities. In an analog to the simplified method, Kayen and Mitchell defined an Arias intensity depth reduction factor,

$$r_b = \frac{I_h(z)}{I_h(z=0)} \quad (4.23)$$

which varies with depth as illustrated in Figure 4.28. Kayen and Mitchell also developed attenuation relationships for two-component ground surface Arias intensity as functions of magnitude and source–site distance

$$\text{Rock sites: } \log I_h = M - 4.0 - 2\log r^* + 0.63P \quad (4.24a)$$

$$\text{Alluvium sites: } \log I_h = M - 3.8 - 2 \log r^* + 0.61P \quad (4.24b)$$

$$\text{Soft soil sites: } \log I_h = M - 3.4 - 2 \log r^* \quad (4.24c)$$

where $r^* = \sqrt{r^2 + \Delta^2}$, P = exceedance probability relative to standard deviation about mean ($P = \pm 1$ for $\pm 1\sigma$), r = closest surface distance to fault rupture plane and Δ = earthquake focal depth. Travasarou et al. (2003) present a more sophisticated attenuation relationship for Arias intensity.

The use of Arias intensity as a scalar measure of loading and resistance offers potential advantages relative to the vector measures (peak acceleration and earthquake magnitude) used in the cyclic stress approach.

4.6.1.4.3 Characterization of Liquefaction Resistance

Liquefaction resistance is also typically expressed by means of the same parameters used to characterize earthquake loading. For the cyclic stress approach, liquefaction resistance is expressed in terms of a cyclic stress ratio commonly referred to as the cyclic resistance ratio, CRR. The cyclic resistance ratio is defined as the cyclic stress ratio that just causes initial liquefaction. In the Arias intensity approach, liquefaction resistance is expressed in terms of the level of Arias intensity required to trigger initial liquefaction. In practice, liquefaction resistance is typically determined by correlation to *in situ* penetration resistance. These correlations are based on case histories of sites at which surficial evidence of liquefaction, primarily in the form of sand boils and ground failure, was and was not observed. Both SPT- and CPT-based correlations are available, as discussed in the following sections.

Cyclic Stress Approach — Early procedures for evaluation of liquefaction potential using the cyclic stress approach determined liquefaction resistance from the results of laboratory tests. Subsequent investigations showed that laboratory test results were significantly influenced by a number of factors, such as soil fabric, that could not be reliably replicated in laboratory test specimens. As a result, it is now most common to relate cyclic resistance ratio to corrected standard penetration test resistance, i.e., $(N_1)_{60}$ or corrected CPT tip resistance, q_{c1} . The SPT has the advantage of a long history of use and the ability to recover a physical sample of the soil (which can be used for classification and index testing), but it is generally performed at discrete intervals. The CPT provides a continuous record of penetration resistance that can resolve thin seams and layers that would likely be missed by SPT testing; however, the CPT

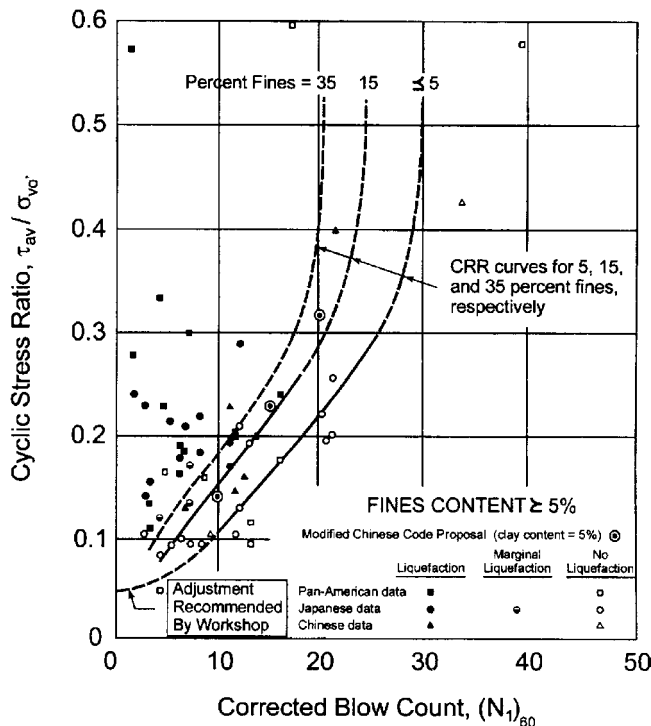


FIGURE 4.29 Variation of CRR with corrected standard penetration resistance, $(N_1)_{60}$. (From Youd, T.L. et al., *J. Geotech. Geoenviron. Eng.*, ASCE, 127, 817–833, 2001. With permission.)

provides no sample so classification must be performed by inference. Ideally, both techniques would be used together to estimate liquefaction resistance for a given project site.

SPT-Based Resistance — Liquefaction resistance is known to increase with increasing soil density, hence, it should increase with *in situ* parameters that also increase with the density. Standard penetration resistance has long been used as an indicator of liquefaction resistance. In recent years, however, the variability of measured SPT resistance has been increasingly recognized and steps have been taken to standardize the equipment and procedures used to perform that test. The use of these standards, and correction of test results to account for deviations from those standards, allow more reliable evaluation of liquefaction hazards. Youd et al. (2001) presented a graphical relationship between CRR and $(N_1)_{60}$ (Figure 4.29) that is a modest update to earlier work by Seed et al. (1985). Note that the CRR has a threshold value of 0.05, which indicates that motions producing $CSR_M \leq 0.05$ would not be expected to cause liquefaction. This graphical relationship was originally developed for magnitude 7.5 earthquakes; when used with CSR_M values developed using the magnitude-weighted peak acceleration, it can be used for any magnitude. The graphical relationship of Figure 4.29 for clean sands (fines content < 5%) can be approximated by the equation

$$CRR = \frac{1}{34-N} + \frac{N}{13.5} + \frac{50}{[10N+45]^2} - \frac{1}{200} \quad (4.25a)$$

where $N = (N_1)_{60}$ and is limited to values below 30. For silty sands, an equivalent clean sand penetration resistance can be computed as

$$(N_1)_{60cs} = \alpha + \beta(N_1)_{60} \quad (4.25b)$$

where

$$\alpha = \begin{cases} 0 & \text{for } FC \leq 5\% \\ \exp[1.76 - (190/FC^2)] & \text{for } 5\% < FC < 35\% \\ 5.0 & \text{for } FC \geq 35\% \end{cases} \quad (4.25c)$$

$$\beta = \begin{cases} 1.0 & \text{for } FC \leq 5\% \\ 0.99 + (FC^{1.5}/1000) & \text{for } 5\% < FC < 35\% \\ 1.2 & \text{for } FC \geq 35\% \end{cases} \quad (4.25d)$$

Under sloping ground conditions and at depths that produce high effective confining pressures, the CRR obtained from Figure 4.29 can be modified by correction factors for initial shear stress and effective confining pressure. The modified CRR can be expressed as

$$CRR_{\sigma,\alpha} = CRR \cdot K_{\sigma} \cdot K_{\alpha} \quad (4.26)$$

where K_{σ} is a confining pressure correction factor (Figure 4.30) and K_{α} is an initial shear stress correction factor (Harder and Boulanger, 1997). Boulanger (2003) presents a promising approach to estimation of K_{σ} as a function of relative density and effective confining pressure. The use of the initial shear stress correction factor, K_{α} , was recently discussed at length by a group of experts who concluded that the Harder and Boulanger (1997) K_{α} curves “should not be used by nonspecialists in geotechnical earthquake engineering or in routine engineering practice” (Youd et al., 2001).

Other investigators (e.g., Liao et al., 1988; Youd and Noble, 1997; Toprak et al., 1999; Seed et al., 2001) have evaluated uncertainty in liquefaction resistance. Seed et al., reviewed liquefaction (and nonliquefaction) case histories with very careful consideration of loading, resistance and model uncertainties, and used a Bayesian updating approach to develop an expression for the probability of liquefaction given various loading and resistance parameters:

$$P_L(N_{1,60}, CSR, M_w, \sigma'_v, FC) = \Phi \left[\frac{\left(N_{1,60}(1+0.004FC) - 13.32 \cdot \ln(CSR) \right)}{2.70} - \frac{\left(-29.53 \cdot \ln(M_w) - 3.70 \cdot \ln(\sigma'_v) + 0.05FC + 44.97 \right)}{2.70} \right] \quad (4.27)$$

where Φ is the standard normal cumulative distribution function. Seed et al. also present procedures by which deterministic liquefaction evaluations can be performed using standard terms such as r_d and K_{σ} ; however, the relationships for those terms are defined differently for use with Seed et al.’s procedure. It is critically important that relationships for different procedures be used consistently — mixing terms from different procedures can lead to erroneous results.

CPT-Based Resistance — CPT tip resistance can also be used to estimate CRR. Early procedures for CPT-based estimation of CRR were based on case histories in which the available SPT data were converted to equivalent CPT data using common empirical correlations. In recent years, however, more case histories with direct CPT measurements have become available.

Robertson and Wride (1998) presented a curve relating CRR to the corrected, normalized CPT tip resistance for clean sands in magnitude 7.5 earthquakes. The clean sand curve can be approximated by

$$CRR_{7.5} = \begin{cases} 0.833 \frac{(q_{c1N})_{cs}}{1000} + 0.05 & \text{for } (q_{c1N})_{cs} < 50 \\ 93 \left[\frac{(q_{c1N})_{cs}}{1000} \right]^3 + 0.08 & \text{for } 50 \leq (q_{c1N})_{cs} < 160 \end{cases} \quad (4.28)$$

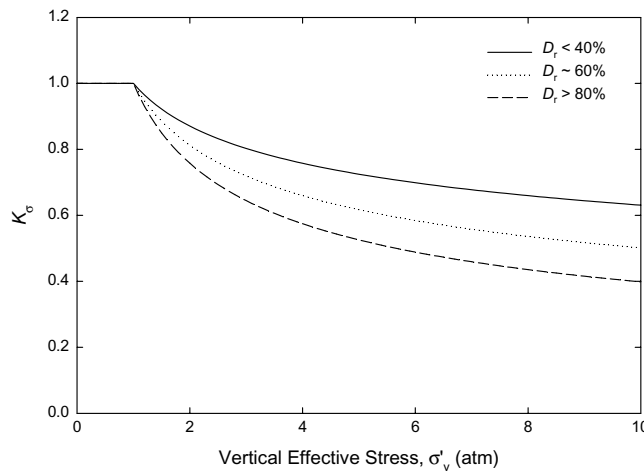


FIGURE 4.30 Variation of overburden correction factor, K_σ , with overburden pressure. (From Harder, L.F. and Boulanger, R.W., *Proceedings, NCEER Workshop on Evaluation of Liquefaction Resistance of Soils*, 167–190, 1997. With permission.)

where $(q_{c1N})_{cs}$ is clean sand CPT tip resistance normalized to approximately 100 kPa (1 atm). The normalized tip resistance can be computed from

$$q_{c1N} = K_c \left(\frac{q_c}{p_a} \right) \left(\frac{p_a}{\sigma'_{vo}} \right)^n \quad (4.29)$$

where

$$K_c = \max [1.0 - 0.403I_c^4 + 5.581I_c^3 - 21.13I_c^2 + 33.75I_c - 17.88]$$

$$I_c = \sqrt{(3.47 - \log Q)^2 + (1.22 + \log F)^2}$$

$$Q = \frac{q_c - \sigma_{vo}}{p_a} \left(\frac{p_a}{\sigma'_{vo}} \right)^n$$

$$F = \frac{f_s}{q_c - \sigma_{vo}} \times 100\%$$

q_c is the measured tip resistance and n is an exponent that varies with soil type. Because the CPT does not provide samples from which soil type can be determined, the selection of n requires classification of the soil through interpretation of CPT results (n values of 0.5 and 1.0 are appropriate for clean sands and clays, respectively; silts and silty sands will have intermediate values).

Toprak et al. (1999) applied a logistic regression technique to a USGS database of liquefaction observations from the 1989 Loma Prieta earthquake, and obtained the relationship

$$\text{Logit } P_L = \ln \left(\frac{P_L}{1-P_L} \right) = 11.6896 - 0.0567 (q_{c1N})_{cs} + 4.0817 \ln(\text{CSR}) \quad (4.30)$$

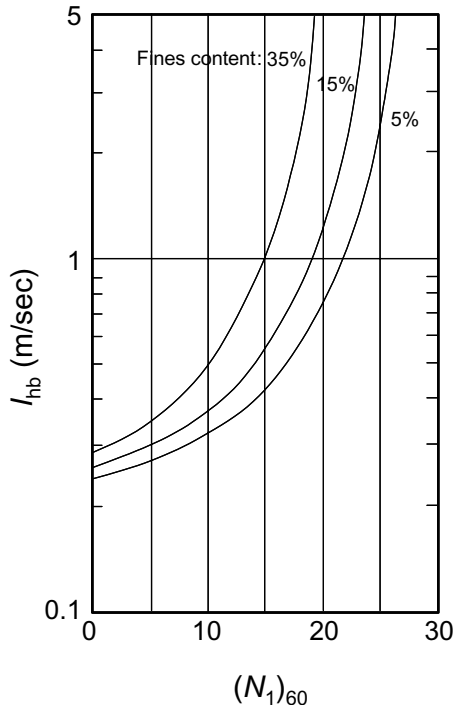


FIGURE 4.31 Variation of Arias intensity required to trigger liquefaction with corrected standard penetration resistance, $(N_1)_{60}$. (Modified from Kayen, R.E. and Mitchell, J.K., *J. Geotech. Geoenviron. Eng.*, ASCE, 123, 1162–1174, 1997. With permission.)

This relationship should only be used with recognition of the limited database from which it was developed.

Now, SPT-based procedures are most commonly used in practice, in part because of the relatively robust database on which they are based and in part because of the familiarity of most practicing geotechnical engineers with the SPT test. The databases for other *in situ* tests, particularly the CPT, are rapidly growing, and as familiarity with these tests and interpretation of their results increase, it is anticipated that their use for liquefaction hazard evaluation will increase.

Arias Intensity Approach — Experimental studies have shown that excess pore pressure increases with increasing energy, and that the energy required to produce initial liquefaction increases with increasing soil density. The relationship between energy and excess pore pressure, however, is scattered and soil specific. As a result, the level of Arias intensity required to produce initial liquefaction is usually obtained by empirical correlation to penetration resistance.

SPT-Based Resistance — Kayen and Mitchell reviewed case histories in which liquefaction had and had not been observed and estimated Arias intensities for each. Using this information and available SPT data, they were able to estimate the level of Arias intensity required to trigger initial liquefaction, I_{hb} , as a function of $(N_1)_{60}$ (Figure 4.31).

Silty sands are typically observed to have a lower SPT resistance than clean sands with the same resistance to liquefaction. Kayen and Mitchell recommend that correction for fines content be accomplished by

$$(N_1)_{60,cs} = (N_1)_{60,ss} + \Delta N_1 \quad (4.31)$$

where $(N_1)_{60,cs}$ = clean sand equivalent SPT resistance, $(N_1)_{60,ss}$ = silty sand SPT resistance and ΔN_1 = correction factor for fines content (FC) given by

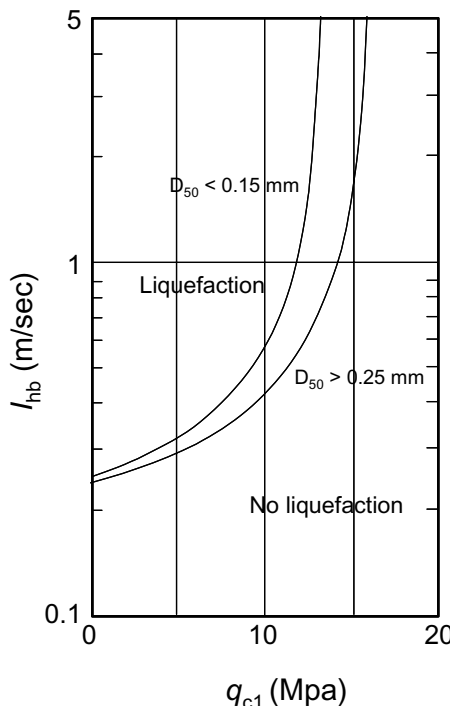


FIGURE 4.32 Variation of Arias intensity required to trigger liquefaction with corrected cone penetration resistance, q_{c1} . (Modified from Kayen, R.E. and Mitchell, J.K., *J. Geotech. Geoenvir. Eng.*, ASCE, 123, 1162–1174, 1997. With permission.)

$$(N_1)_{60,cs} = \begin{cases} 0 & \text{for } FC \leq 5\% \\ \frac{7}{30}(FC - 5) & \text{for } 5\% < FC < 35\% \\ 7 & \text{for } FC \geq 35\% \end{cases} \quad (4.32)$$

CPT-Based Resistance — Kayen and Mitchell also used the available field data and the empirical CPT/SPT relationship of Robertson and Campanella (1985) to develop the relationship between corrected cone tip resistance, q_{c1} , and triggering Arias intensity, I_{hb} , shown in Figure 4.32.

4.6.1.4.4 Evaluation of Liquefaction Potential

The potential for initiation of liquefaction in a particular earthquake is usually expressed in terms of a factor of safety against liquefaction. The factor of safety is defined in the usual way — as a ratio of capacity to demand. In the case of liquefaction, the factor of safety can be expressed as

$$\text{Cyclic Stress Approach: } FS = CRR/CSR \quad (4.33)$$

$$\text{Arias Intensity Approach: } FS = I_{hb}/I_h \quad (4.34)$$

Factor of safety values less than 1 indicate that initial liquefaction is likely. It should be noted that this factor of safety does not distinguish between flow liquefaction and cyclic mobility, and provides no information on postliquefaction behavior. Because it is based on case history data where liquefaction is evidenced by ground surface disruptions such as sand boils, cracks, ground oscillation, etc., it provides an indication of the likelihood of such effects at the site of interest. Probabilistic methods for evaluating triggering of liquefaction (e.g., Seed et al., 2001) quantify the potential for the initiation of liquefaction with a probability of liquefaction (P_L) in lieu of FS.

4.6.1.5 Effects

Liquefaction can affect a wide variety of civil structures and facilities through modification of the ground motion and development of permanent deformations. Liquefaction has caused surficial structures to settle, suffer bearing failure and move laterally. It has produced landslides and failures of retaining structures, and caused light, buried structures to float. The effects of liquefaction depend on the characteristics of the soil and the loading — in some cases, liquefaction occurs relatively early in a ground motion and produces severe effects, but in others liquefaction may not occur until near the end of the record, in which case effects may be relatively modest. The primary effects of liquefaction, and available procedures for estimating their severity, are described in the following paragraphs. It should be noted that analytical techniques for predicting liquefaction effects are generally much less maturely developed than techniques for predicting liquefaction initiation (as described in Section 4.6.1.4).

4.6.1.5.1 Alteration of Ground Motion

Soil deposits will tend to amplify some components of a ground motion and attenuate others. The most strongly amplified components will be those at and near the characteristic site period, which is a function of the stiffness and thickness of the soil deposit. As excess porewater pressures increase in a liquefiable soil, the stiffness of the soil decreases, leading to a lengthening of the characteristic site period during shaking. As this transition takes place, the tendency of the soil deposit to amplify high frequency components of the ground motion will generally decrease. Thus, the development of liquefaction can lead to an overall decrease in acceleration amplitudes (which generally reflect the higher frequency components of a ground motion), and to an increase in velocity and displacement amplitudes. In some cases, the cyclic displacements that occur at the surface of a liquefiable soil deposit are large enough to fracture and disrupt the surface; this phenomenon is referred to as ground oscillation.

4.6.1.5.2 Surface Manifestation of Liquefaction

Liquefaction may or may not result in significant permanent deformations of the ground surface. Ishihara (1985) and Youd and Garris (1995) found through detailed analysis of field case history data that the occurrence of liquefaction in some layer of a deposit is not necessarily associated with damage to structures and disruption of the ground surface. Ishihara states: “Only when the development of liquefaction is sufficiently extensive through the depth of a deposit and shallow enough in proximity to the ground surface do the effects of liquefaction become disastrous, leading to sand boiling and ground fissuring with various types of associated damage to structures and underground installations.”

Ishihara (1985) investigated the conditions under which liquefaction effects are manifest at the ground surface in terms of the thickness of liquefiable strata and overlying nonliquefiable strata. A widely used outcome of these analyses is the boundary curves shown in Figure 4.33. Using a larger data set than that of Ishihara, Youd and Garris (1995) found the boundary curves in Figure 4.33 are accurate for sites not subject to ground oscillation or lateral spread. Criteria for evaluating the potential for lateral spreading are provided in Section 4.6.1.5.5. Sites are likely to be subject to ground oscillation if they have laterally continuous liquefiable strata that enable decoupling of the surface soil layers from the liquefiable strata. In addition, it should be noted that Figure 4.33 applies essentially for sandy soils. Its reliability for fine-grained materials has not been verified, and such verification work remains a research need.

4.6.1.5.3 Settlement

Sands tend to densify when subjected to cyclic loading, a fact taken advantage of when vibratory rollers are used to compact them. Densification due to the vibrations of earthquakes, however, leads to settlement of the ground surface and potential damage to surficial and buried structures. This densification can occur in both unsaturated soils and saturated sands, although they occur much more quickly (almost immediately) in unsaturated soils than in saturated sands (in which they may take a day or more to develop). Ground settlement due to contractive volumetric strains in unsaturated soil is referred to as seismic compression. Tokimatsu and Seed (1987) developed procedures for estimation of seismic compression of sands; the procedures were recently updated by Stewart and Whang (2003) for applications involving compacted soils.

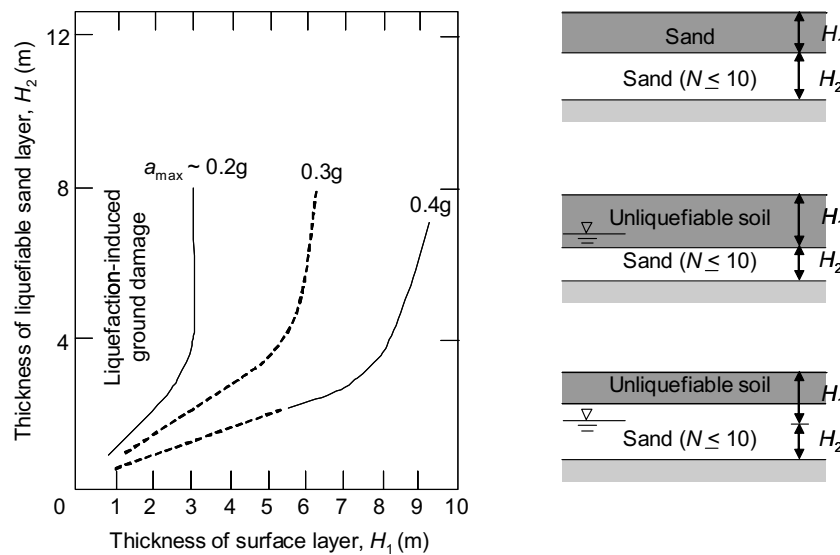


FIGURE 4.33 Empirical relationships for estimating conditions under which surficial evidence of liquefaction can be expected. Surficial evidence can be expected for H_1-H_2 pairs that plot above each of the indicated curves. (From Ishihara, K., *Proceedings, Eleventh International Conference on Soil Mechanics and Foundation Engineering*, 1, 321–376, 1985. With permission.)

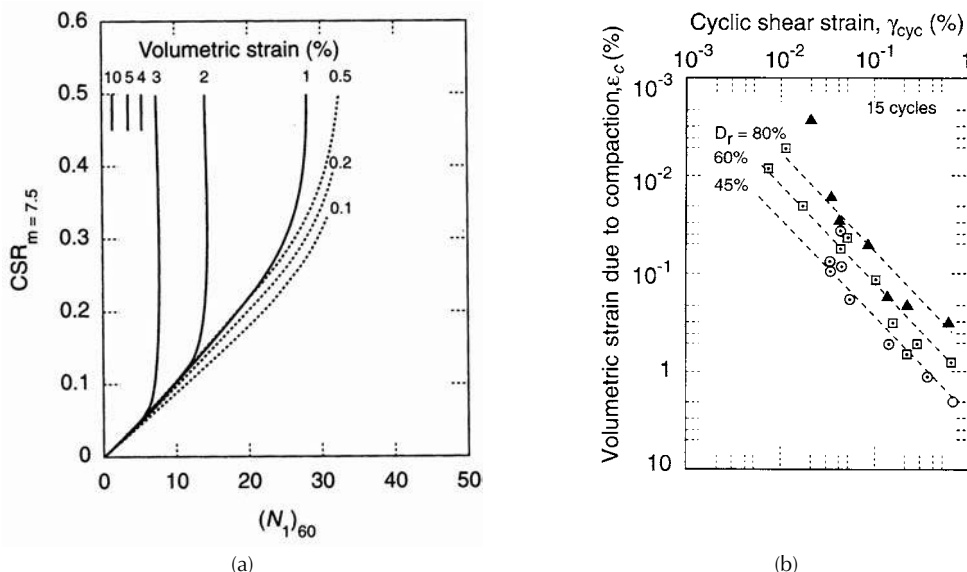


FIGURE 4.34 (a) Estimation of volumetric strain from liquefaction from $CSR_{m=7.5}$ and SPT penetration resistance and (b) volumetric strain from seismic compression as function of shear strain amplitude and relative density. (From Tokimatsu, K. and Seed, H.B., *J. Geotech. Engrg.*, ASCE, 113, 861–878, 1987. With permission).

TABLE 4.3 Magnitude Scaling Factor (MSF)

Values for Volumetric Strain Computation

$$(CSR_{m=7.5} = MSF \times CSR_m)$$

Magnitude, M	5½	6	6¾	7½	8½
MSF	1.50	1.32	1.13	1.0	0.89

The dissipation of excess porewater pressure generated by earthquake shaking leads to settlement of saturated sands. Although settlement of saturated sands occurs more slowly than seismic compression of unsaturated soils, both phenomena are influenced by the same primary factors (i.e., soil density, shaking amplitude, number of cycles of shaking, etc). For example, the chart in Figure 4.34a allows estimation of the volumetric strain following liquefaction from the magnitude-corrected cyclic stress ratio, $CSR_{m=7.5}$ (Table 4.3) and SPT resistance. The chart in Figure 4.34b allows estimation of volumetric strain from seismic compression of dry sand from shear strain amplitude and relative density. Details on the application of these procedures are described in Tokimatsu and Seed (1987). Ishihara and Yoshimine (1992) developed an alternative procedure for estimation of postliquefaction settlement that also allows estimation of volumetric strain based on the FS for liquefaction triggering coupled with SPT blow count, relative density or CPT tip resistance.

4.6.1.5.4 Stability

Liquefaction can lead to a marked reduction in soil strength and, hence, to potential instability. When liquefaction occurs the shear strength of the soil can be reduced to a residual strength that is a function of the density of the soil. Moderately dense soils may dilate upon unidirectional shearing and develop a relatively large residual strength, but the residual strength of loose soils can be quite low. If the residual strength is lower than the shear stress required to maintain static equilibrium, flow liquefaction can occur; the result can be a flow slide, a loss of supporting capacity or other failure. Evaluation of the potential for such instabilities requires estimation of the residual strength of the liquefied soil.

While three primary approaches have been proposed for evaluation of residual strength, each has significant limitations that leave the geotechnical profession unable to estimate residual strength with high accuracy. Given the high sensitivity of residual strength to *in situ* density, the difficulty of determining the *in situ* density of the types of soils that are most susceptible to liquefaction and flow sliding, and the inherent spatial variability of soil density, these difficulties are not unexpected. The uncertainty in residual strength estimates must be recognized, however, and taken into account in evaluation of postearthquake stability.

A laboratory testing-based approach to evaluation of residual strength was proposed by Poulos et al. (1985). This approach involves careful undisturbed sampling, laboratory testing of undisturbed specimens consolidated to confining pressures high enough to ensure contractive behavior and correction of the measured test results for confining pressure effects to obtain an estimate of the strength under *in situ* confining pressures. The procedure is rational, but the user must be aware of the sensitivity of its results to uncertainties in the input parameters, particularly the *in situ* void ratio of the soil and potential void redistribution effects.

Other approaches recognize that the undrained conditions assumed in the laboratory-based approach do not exist in all flow failures in the field. These approaches correlate the residual strengths backcalculated from actual flow failures to *in situ* test parameters, particularly $(N_1)_{60}$. Seed and Harder (1990) analyzed a series of flow slides and found that the residual strength varied with the clean sand corrected SPT resistance, $(N_1)_{60\text{-cs}}$, as shown in Figure 4.35. The clean sand value is given by

$$(N_1)_{60\text{-cs}} = (N_1)_{60} + N_{\text{corr}} \quad (4.35)$$

where N_{corr} is obtained from Table 4.4. As Figure 4.35 shows, there is a wide band of residual strengths for a given $(N_1)_{60\text{-cs}}$ value. A normalized strength approach has also been applied to the residual strength problem. Assuming that the consolidation curve and steady-state line of sand are parallel, the residual strength should be proportional to the major principal effective stress prior to earthquake shaking. Stark and Mesri (1992) proposed that the strength ratio should be proportional to $(N_1)_{60\text{-cs}}$ but Olson and Stark (2002) recently modified this approach to predict strengths using

$$\frac{S_r}{\sigma'_{vo}} = 0.03 + 0.0075(N_1)_{60} \pm 0.03 \quad \text{for } (N_1)_{60} \leq 12 \quad (4.36)$$

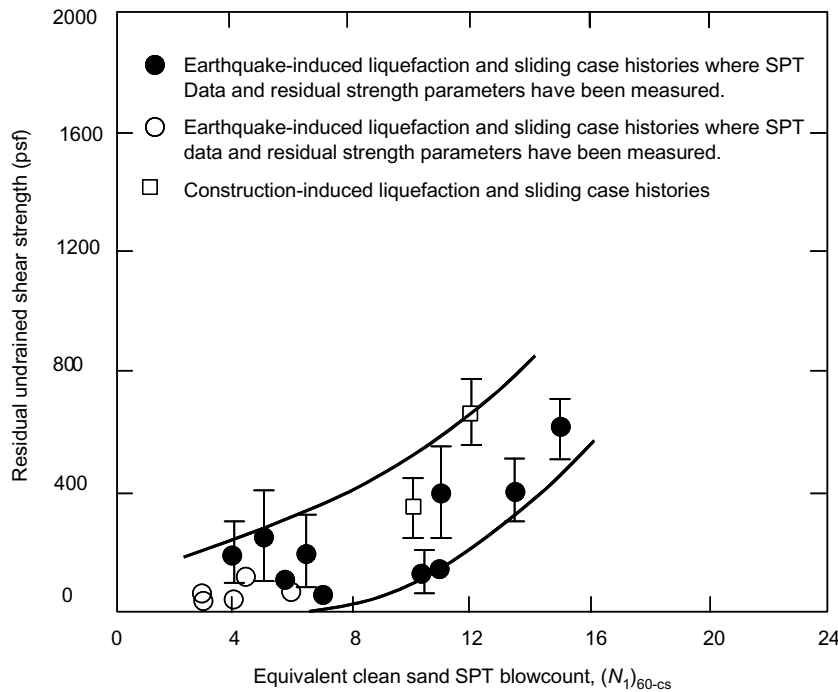


FIGURE 4.35 Estimation of residual strength of liquefied soil from SPT resistance. (From Seed, R.B. and Harder, L.F., *Proceedings, H. Bolton Seed Memorial Symposium*, Vol. 2, 351–376, 1990. With permission.)

TABLE 4.4 Fines Content Correction, in Terms of Increment of SPT Resistance to be Added to $(N_1)_{60}$ for Estimation of Residual Strength Using Procedure of Seed and Harder (1990)

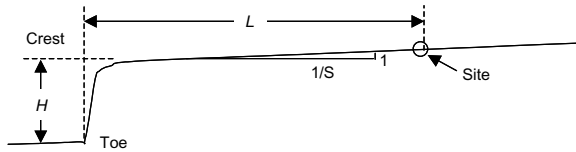
Percent Fines	0	10	25	50	75
ΔN	0	1	2	4	5

$$\frac{S_r}{\sigma'_{vo}} = 0.03 + 0.0143(q_{cl})_{60} \pm 0.03 \quad \text{for } q_{cl} \leq 6.5 \text{ Mpa} \quad (4.37)$$

where the ± 0.03 term is interpreted as approximating one standard deviation about the trendline, which also implies significant uncertainty in residual strength.

4.6.1.5.5 Lateral Spreading

Lateral spreading can produce significant and damaging lateral displacements of the ground surface. The mechanics of the processes by which lateral spreads develop is sufficiently complex that their permanent deformations are generally predicted by empirical means. Youd et al. (2002) modified the work of Bartlett and Youd (1992) to correct errors, add new case histories and adjust the functional form of a predictive equation for lateral spreading displacement. The modifications were made in a step-by-step process with new regression at each step. The modifications resulted in a more robust equation, but the predicted displacements were of approximately the same accuracy (within a factor of plus or minus two) as those of Bartlett and Youd (1992). The final predictive equation developed by Youd et al. (2002) is as follows:



L = Distance from toe of free face to site
 H = Height of free face (crest elev. – toe elev.)
 W = Free-face ratio = $(H/L)(100)$, in percent
 S = Slope of natural ground toward channel, in percent

FIGURE 4.36 Illustration of variables used in Youd et al. (2002) lateral spreading model.

$$\begin{aligned} \log D &= \beta_0 + \beta_{\text{off}} + \beta_1 M + \beta_2 \log R^* + \beta_3 R + \beta_4 \log W + \beta_5 \log S \\ &\quad + \beta_6 \log T_{15} + \beta_7 \log(100 - F_{15}) + \beta_8 \log(D50_{15} + 0.1 \text{ mm}) \end{aligned} \quad (4.38)$$

where T_{15} is the cumulative thickness (in meters) of soil with $(N_1)_{60} < 15$, R is the horizontal distance from the seismic source in kilometers, S is the slope of the ground surface in percent (see Figure 4.36), W is the free-face ratio in percent (see Figure 4.36), F_{15} is the average fines content in the materials contributing to T_{15} in percent, $D50_{15}$ is the mean grain size of the materials contributing to T_{15} in millimeters and

$$R^* = R + 10^{(0.89M-5.64)}$$

The resulting displacement D is in units of meters. The coefficients of either the $\log S$ or $\log W$ term must have a value of zero, i.e., the site must be treated as an infinite slope or a free-face. Likewise, when the coefficient for $\log S$ is zero, β_{off} should also be zero (i.e., the β_{off} term should be used only if there is also a free-face).

TABLE 4.5 Parameters for Youd et al. (2002) Lateral Spreading Model

β_0	β_{off}	β_1	β_2	β_3	β_4	β_5	β_6	β_7	β_8	R^2 (%)
-16.213	-0.500	1.532	-1.406	-0.012	0.592	0.338	0.540	3.413	-0.795	83.6

4.6.2 Landslides

4.6.2.1 Types of Landslides and Conditions under Which They Occur

Landslides, defined for the purpose of this discussion as seismically induced permanent shear deformations within geologic media, represent a significant source of ground failure during earthquakes. These shear deformations need to be distinguished from ground settlements associated with volumetric strains that arise from postliquefaction pore pressure dissipation or seismic compression. Earth slopes strongly shaken during earthquakes can be subject to surface displacements from both shear and volumetric strain accumulation. The subject of this section is related to the shear deformation problem; volumetric strains are covered separately in Section 4.6.1.

Whether induced by earthquakes or other processes, landslides can be subdivided into several generalized categories (Varnes, 1978; Keefer, 1984):

1. Masses of disrupted slide material, such as rock falls or avalanches

2. Relatively coherent slide masses whose displacement is accommodated along well-defined slip surfaces or across relatively broad, distributed shear zones
3. Lateral spreads and flow slides associated with soil strength loss due to pore pressure increase

Examples of these types of landslides are shown in Figure 4.37 . Local geologic, hydrologic and topographic conditions provide the principal means of evaluating which type of landslide mechanism is most likely for a given site. This is a crucial step in engineering analyses of slope stability, because different analysis procedures are appropriate for different landslide mechanisms.

As described by Keefer (1984) and illustrated in Figure 4.37a, disrupted slides and falls occur in areas of high topographic relief (slopes steeper than 35–40°) and tend to involve closely jointed or weakly cemented materials. Rock avalanches are a particularly damaging type of disrupted slide, involving slide masses that originate in steep terrain and disintegrate into streams of rock that travel large distances (on the order of kilometers) at high velocities. A critically important feature of many disrupted rock and soil falls is a significant loss of shear strength upon initiation of slide movement. This loss of shear strength is a characteristic feature of cemented materials, and has important implications for analysis (as discussed further below).

Coherent landslides can occur in rock or soil materials and at slope angles much lower than those for disrupted slides and falls. Coherent slides in rock typically involve slip along basal surfaces weakened by weathering, jointing or prior shearing, or along bedding planes and other discontinuities that dip out of slope (e.g., Figure 4.37b). Keefer (1984) reports that coherent slides in rock masses have occurred on slopes as shallow as 15°. Coherent slides in soil can occur along basal slip surfaces or relatively distributed shear zones. These slides most commonly involve fill embankments (sliding occurring within the embankment materials or in relatively soft foundation soils, e.g., Rogers (1992), Bardet et al. (2002)), but have also been widely documented in natural alluvial soils (Keefer, 1984).

Lateral spreads and flows can occur in soil on very mild slopes or behind a free-face if the soil is geologically young, has a granular texture and the groundwater table occurs at shallow depths. The principal technical issues associated with these types of slides are related to the triggering of liquefaction and the estimation of postliquefaction residual strengths. Both of these issues are addressed in Section 4.6.1. If these postliquefaction strengths exceed static shear stresses, the problem is one of cyclic mobility, which in a slope stability context is analogous to lateral spreads. If the postliquefaction strengths are less than static shear stresses, flow slides will occur that can involve very large displacements, such as shown in Figure 4.37c.

4.6.2.2 Static Analysis Methods

Slope stability analyses involve a comparison of the gravity induced stresses in a slope to the available soil strength and any externally provided resistance (e.g., retaining walls). For slopes in which the shear stresses required to maintain equilibrium under static gravitational loading approach the available shear resistance, the additional dynamic stresses needed to produce instability would be small. Accordingly, the seismic stability of a slope can be closely related to its static stability. For this reason, as well as the close link between many static and seismic stability analysis procedures, static stability analysis procedures are briefly summarized here.

Procedures for the analysis of slope stability under static conditions include limit equilibrium methods and stress-deformation methods. A state-of-the-art review of these methods is presented by Duncan (1996). The following sections discuss critical issues related to the use of limit equilibrium and stress-deformation methods of analysis. Strength parameter selection, perhaps the most important component of any slope stability analysis, is discussed in Section 4.2 and by Blake et al. (2002).

4.6.2.2.1 Limit Equilibrium Methods — Definition and Use of Factor of Safety

Limit equilibrium methods solve for one or more of the three equations of equilibrium: horizontal force, vertical force and moment. The equilibrium calculations are performed for a rigid slide mass over a defined slip surface. An assumption inherent to limit equilibrium methods is rigid-perfectly plastic soil



(a)

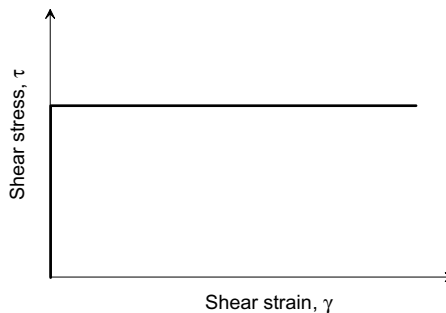


(b)

FIGURE 4.37 (a) Example of disrupted landslide — rockfall in central Taiwan from 1999 Chi Chi Taiwan earthquake (photo: J.P. Bardet). (b) Head scarp of coherent landslide at Junliau Switching Station, Taiwan induced by 1999 Chi Chi earthquake (photo: J.P. Stewart). Slide movements of approximately 1.0 to 1.5 m occurred along a bedding plane in rock. (c) Flow slide at Tapo Canyon Tailings Dam, California, 1994 Northridge earthquake (photo: Y. Moriwaki).



(c)

FIGURE 4.37 (continued)**FIGURE 4.38** Stress-strain curve for rigid-perfectly plastic material, which is the assumed condition in limit equilibrium slope stability analyses.

behavior, which is depicted in Figure 4.38. The results of limit equilibrium analyses are expressed as a factor of safety (FS), which is defined as

$$FS = \frac{\text{Available Shear Strength}}{\text{Equilibrium Shear Stress}} \quad (4.39)$$

The slope is considered to be at the point of failure when the factor of safety equals one, i.e., the available soil shear strength exactly balances the shear stress induced by gravity. A slope has reserve strength when $FS > 1$. Typical minimum FS values for use in slope design are about 1.5 for static long-term stability and 1.25 for static short-term stability.

Generally, the probability of slope failure decreases as the factor of safety increases. However, a unique relationship between probability of failure and FS cannot be established because of the wide variability of uncertainties in input parameters from site-to-site. In most cases, the largest sources of uncertainty in a slope stability analysis are the soil strength and groundwater conditions. Other factors contributing to uncertainty include the imperfect nature of mathematical models for slope stability calculations and the ability of the analyst to find the critical failure surface geometry.

The potential failure surfaces that should be analyzed for slope stability are any geometric configuration on which the slope might reasonably be envisioned to experience failure. The intent of analyses is to consider all such surfaces so that the critical surface having the lowest factor of safety can be identified. Examples of the types of failure surfaces that should be considered are illustrated in Figure 4.39 and are described below:

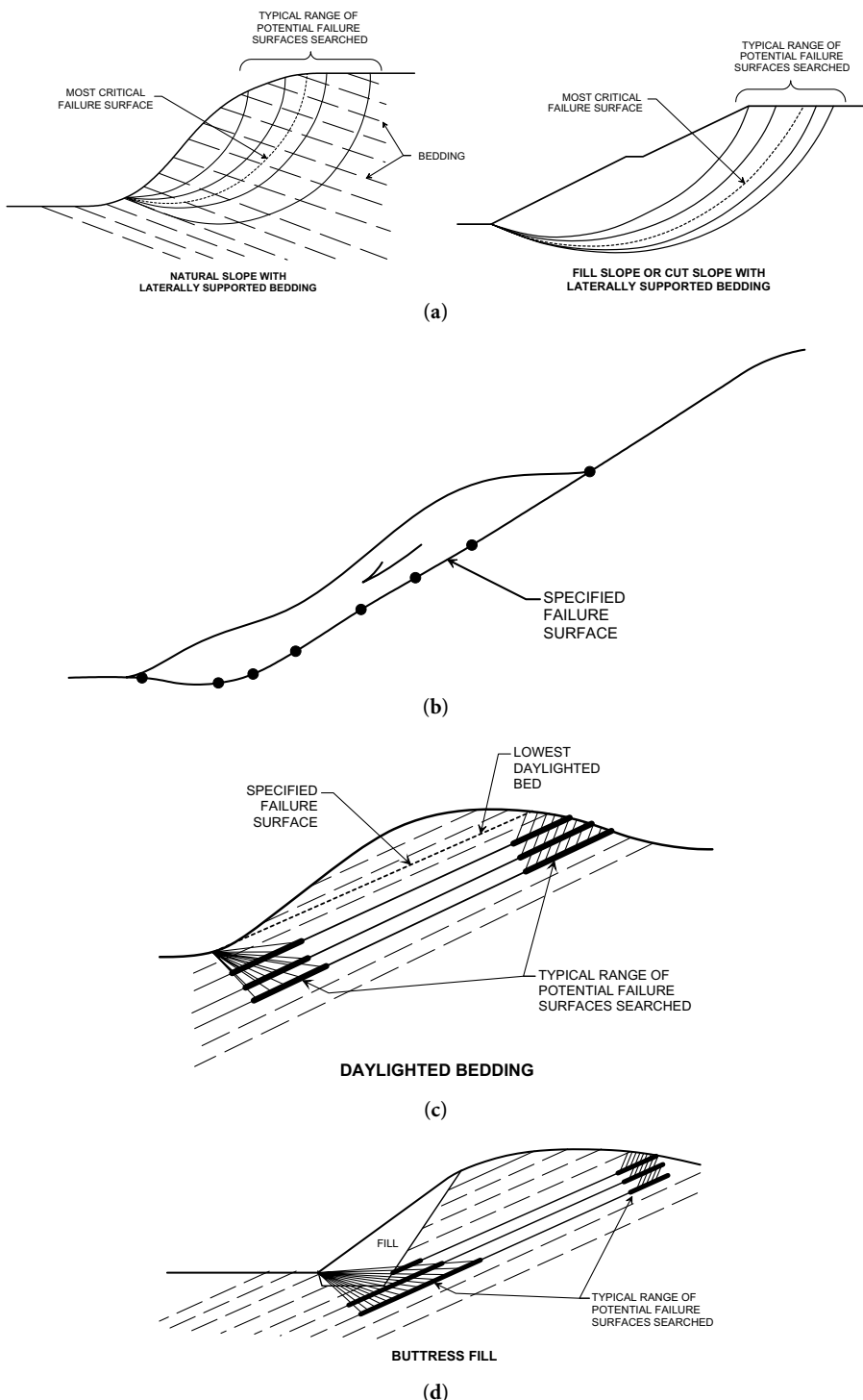


FIGURE 4.39 (a) Examples of use of circular failure surface geometry. (b) Example of use of specified failure surface geometry for existing landslide. (c) Potentially critical failure surfaces for slope with daylighted bedding planes. (d) Example of composite failure surfaces combining along-bedding and cross-bedding failure. (From Blake, T.F. et al. Report published by Southern California Earthquake Center, 2002. With permission.)

- *Circular failure surfaces* (Figure 4.39a): Slopes with laterally supported bedding, fill slopes and embankments
- *Predefined failure surface geometries established from geologic exploration* (Figure 4.39b): Slopes having layers of weak materials or weak interfaces such as bedding planes, existing landslide slip-surfaces, faults or joints
- *Planar failure surfaces* (Figure 4.39c): Most commonly occurs in rock slopes with unsupported bedding planes. The most critical surface in such a slope may be defined by the lowest bedding plane exposed by the slope face, or deeper seated surfaces as indicated in Figure 4.39c.
- *Composite failure surfaces* (Figure 4.39d): Composite failure surfaces that consist of linear slip-surfaces along bedding planes in the upper portions of the slope in combination with slip surfaces across bedding planes and through fill in the lower portions of the slope. This condition occurs when bedding planes form a nondaylighting dip-slope.

In conjunction with any of the above geometries, it may be appropriate to consider the formation of tension cracks near the top of a slope, especially if the slide material possesses cohesion and low factors of safety are used in design.

TABLE 4.6 Characteristics of Commonly Used Methods of Limit Equilibrium Analysis

Method	Date	Equilibrium Conditions Satisfied	Shape of Slip Surface	Assumptions
Friction circle method (Taylor)	1937	Moment and force equilibrium	Circular	Resultant tangent to friction circle
Ordinary method of slices (Fellenius)	1927	Moment Equilibrium of entire mass	Circular	Normal force on base of slice is $W \cos \alpha$ and shear force is $W \sin \alpha$
Method of slices (Fellenius)	1910	Force equilibrium of each slice		No interslice forces
Bishop's modified method	1955	Vertical equilibrium and overall moment equilibrium	Circular	Side forces are horizontal
Janbu's simplified	1968	Force equilibrium	Any shape	Side forces are horizontal
Modified Swedish method (U.S. Army Corps of Engineers method)	1970	Force equilibrium	Any shape	Side force inclinations are equal to the parallel to the slope
Lowe and Karafith's method	1960	Vertical and horizontal force equilibrium	Any shape	Side force inclinations are average of slope surface and slip surface (varies from slice to slice)
Janbu's generalized method	1968	All conditions of equilibrium	Any shape	Assumes heights of side forces above the base vary from slice to slice
Spencer's method	1967	All conditions of equilibrium	Any shape	Inclinations of side forces are the same for every slice; side force inclination is calculated in the process of the solution
Morgenstern and Price's method	1965	All conditions of equilibrium	Any shape	Inclinations of side forces follow a prescribed pattern; side forces can vary from slice to slice
Sarma's method	1973	All conditions of equilibrium	Any shape	Magnitudes of vertical side forces follow prescribed patterns

Source: Blake, T.F. et al., Report published by Southern California Earthquake Center, 2002. With permission.

4.6.2.2.2 Limit Equilibrium Methods — Analysis Procedures

Table 4.6 presents a number of commonly used limit equilibrium methods of slope stability analysis. Relatively simple methods that do not satisfy all conditions of equilibrium were developed before the

use of computers was widespread. More complex methods are most practical for computer application. The various methods of limit equilibrium analysis differ from each other with regard to the equilibrium conditions satisfied and the assumptions made regarding the location and orientation of the internal forces between the assumed slices (which also balance the number of unknowns in the problem with the number of equations).

The methods of Morgenstern and Price, Spencer, Sarma, Taylor and Janbu's generalized procedure of slices satisfy all conditions of equilibrium and involve reasonable assumptions. Bishop's modified method does not satisfy all conditions of equilibrium, but is as accurate as methods that do, provided it is used only for circular surfaces. Duncan (1996) has found all of these methods to provide answers within 5% of each other.

4.6.2.2.3 Stress-Deformation Methods

Stress-deformation methods of slope stability analysis within a finite element (FE) or finite difference (FD) framework allow the stress-strain behavior of soil or rock to be taken into consideration. A state-of-the-art review of several such methods is provided by Duncan (1996). The use of such methods is required for assessments of static slope displacement, and may be desirable for stability calculations if a complex subsurface stratigraphy is encountered.

Advantages of the FE and FD approaches to slope stability analysis over limit equilibrium methods are:

- No prior assumption needs to be made about the shape or location of the failure surface. Failure occurs through the zones within the soil mass where the shear strength is unable to sustain the applied shear stresses.
- Because FE and FD methods do not utilize slices there is no need to make simplifying assumptions about slice side forces. FE and FD methods preserve global equilibrium until failure occurs.
- If realistic soil constitutive models are used with well-defined model input parameters, FE and FD methods can provide insight into deformations at working-stress levels.
- FE and FD methods illustrate progressive failure up to and including overall shear failure. By contouring shear strains, it is possible to identify potential failure surfaces.

Unfortunately, the above benefits can be offset by difficulties in defining parameters for some material constitutive models. Accordingly, selection of an appropriate constitutive model and definition of the model parameters is a critical step in stress-deformation methods of analysis.

For nonlinear analyses using complex constitutive models that attempt to reproduce volumetric changes accurately in undrained or partially drained conditions, the incremental application of gravity can produce different results than would be obtained if gravity is applied all at once or if the depositional process (natural or man-made) is explicitly modeled. However, if a simplified elasto-plastic model is used in FE and FD analyses, the factor of safety appears to be unaffected (Griffiths and Lane, 1999). Therefore, if the primary goal of the FE and FD analyses is to obtain a factor of safety, a simplified Mohr-Coulomb elasto-plastic model can be used with an instantaneous gravity turn-on procedure (Griffiths and Lane, 1999). To determine the factor of safety from FE and FD analyses, the shear strength reduction technique can be used (Matsui and San, 1992). In that procedure, the FS of a soil slope is defined as the number by which the original shear strength parameters must be divided to bring the slope to the point of failure (as indicated by displacements deemed to be excessive based on project requirements). Comparative studies among FE, FD and limit equilibrium methods have shown that similar results can be obtained by each of them (Griffiths, 1980; 1989; Potts et al., 1990; Matsui and San, 1992; Griffiths and Lane, 1999).

FE and FD methods are powerful tools that can provide significant insight into the potential slope performance to an experienced user. A user should be thoroughly familiar with the soil constitutive model and solution algorithm before relying on the results of these types of analyses.

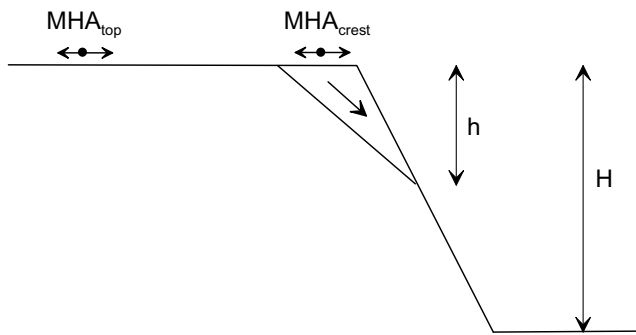


FIGURE 4.40 Schematic illustration of slope geometry considered by Ashford and Sitar (2002) for steep slopes of weakly cemented rock/soil.

4.6.2.3 Seismic Analysis Methods

4.6.2.3.1 Introduction and Overview of Applications for Different Categories of Landslides

An analysis of seismic slope stability begins with an assessment of whether the earthquake is likely to significantly weaken the slope material, for example through soil liquefaction or through the initiation of deformation in a weakly cemented soil or rock mass that subsequently de-aggregates. If the slope material is potentially susceptible to liquefaction, the engineer must first evaluate whether liquefaction is likely to be triggered, using the procedures in Section 4.6.1. If liquefaction is likely, appropriate postliquefaction residual strengths must be accounted for in slope stability analyses. If these strengths are sufficient to maintain static stability (static FS > 1), the problem is classified as cyclic mobility, and is typically analyzed using displacement-based analysis procedures for a coherent slide mass, or for very flat slopes, the lateral spread analysis methods presented in Section 4.6.1. Flow slides occur if the static FS < 1 using postliquefaction strengths (Section 4.6.1.5).

If the problem involves weakly cemented rock and soils, pseudo-static analysis procedures can be used to check whether the shear stress during earthquake shaking approaches the peak (cemented) strength. If this strength is reached, a disrupted slide or fall can occur (Ashford and Sitar, 2002).

Stability analyses for slopes comprising materials whose strength is unlikely to be significantly compromised by the earthquake tend to focus on prediction of the slope deformations that might accumulate during earthquake shaking. These procedures are formulated differently than those for weakly cemented rocks and soils described above. As noted previously, these displacement-based analysis procedures can also be used for cyclic mobility problems in liquefiable soils, although consideration must be given to strength degradation over the duration of earthquake shaking.

The remainder of this section is organized into subsections presenting three different methods of analysis: pseudo-static, displacement-based analysis and stress-deformation approaches. The application of these methods to the different classes of stability failures introduced in Section 4.6.2.1 is synthesized below:

- *Disrupted slides and falls:* Best analyzed using pseudo-static procedures
- *Coherent slides:* Generally analyzed using a displacement-based approach or pseudo-static methods calibrated for a particular realization of slope displacement. Stress-deformation approaches are also possible
- *Lateral spreads and flows:* Beyond the scope of this section. See Section 4.6.1.5 for lateral spreads. If a site is subject to a flow slide condition, further analysis of slope stability is not warranted, the critical issue becomes one of mitigation (Section 4.7).

As with any stability analysis, proper assessment of shear strength for seismic slope stability analyses is crucial. This topic is covered in Section 4.3.3.

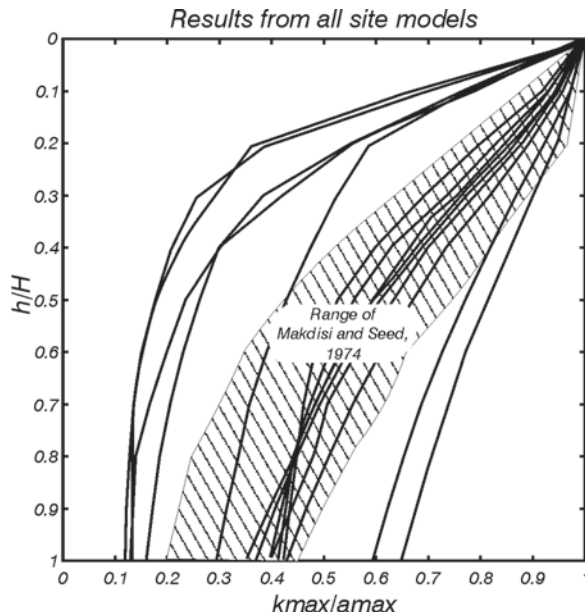


FIGURE 4.41 Seismic coefficient profiles evaluated for steep slopes compared to a range of values from Makdisi and Seed (1978). (From Ashford, S.A. and Sitar, N., *J. Geotech. Geoenviron. Eng.*, ASCE, 128, 119–128, 2002. With permission.)

4.6.2.3.2 Pseudo-Static Methods

Pseudo-static methods of seismic slope stability analysis involve the use of a destabilizing horizontal seismic coefficient (k) within a conventional limit equilibrium slope stability calculation. The seismic coefficient represents the fraction of the weight of the sliding mass that is applied as an equivalent horizontal force acting through the centroid of the slide mass. The factor of safety against shear failure is evaluated with the equivalent horizontal force applied to the slope.

The key step in a pseudo-static analysis is the selection of the seismic coefficient, k . In modern practice, there are two principal applications of pseudo-static methods of analysis: (1) as the primary method of analysis for slopes potentially subject to disrupted slides and falls; and (2) for coherent landslides, as a screen analysis tool intended to distinguish sites with low potential for earthquake-induced landslide development from those sites for which more detailed analyses are warranted.

Application to Disrupted Slides and Falls — Ashford and Sitar (2002) recommend the use of a pseudo-static approach for the analysis of landslide potential in steep, weakly cemented slopes. The slope geometry utilized in the analysis procedure is shown in Figure 4.40. The seismic coefficient is evaluated as follows:

1. Evaluate the maximum horizontal acceleration in the free-field behind the slope crest (MHA_{top}). In this context, free-field refers to motions not influenced by surface topography. If the site condition behind the slope crest is not a standard reference site condition (i.e., rock or soil), ground response analyses or the use of site amplification factors may be appropriate for the estimation of MHA_{top} .
2. Estimate the maximum horizontal acceleration at the slope crest as $MHA_{crest} = 1.5 \times MHA_{top}$. The factor of 1.5 is intended to account for topographic amplification effects.
3. Estimate the slope height H and the distance from the slope crest to the base of slide plane, h .
4. Estimate the maximum seismic coefficient likely to occur within the slope (k_{\max}) using Figure 4.41. Ashford and Sitar indicate that the upper end of the range of $k_{\max}/(MHA_{crest}/g)$ values should be used for steep slopes (around 75°), whereas the average of the Makdisi and Seed range is appropriate for less steep slopes (45°).

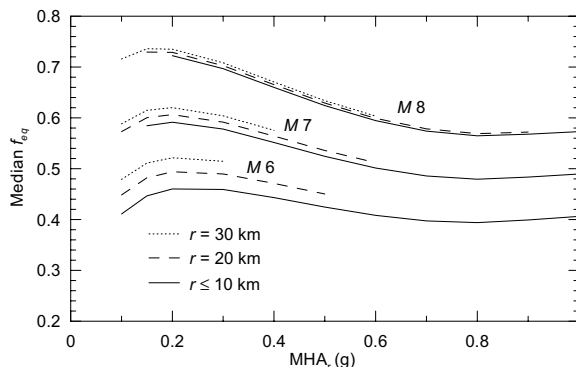


FIGURE 4.42 Relationship between f_{eq} ($= k/MHA_r$) as a function of MHA_r and seismological condition for slope displacement level of 5 cm. (From Stewart, J.P. et al., *Earthquake Spectra*, 19, 697–712, 2003a. With permission.)

TABLE 4.7 Features of Various Screen Analysis Procedures for Seismic Slope Stability

	Seed [1979]	H-G & F [1984] ^a	Bray et al. [1998]	Stewart et al. [2003a]
Application	Dams	Dams	Landfills	Residential, commercial
Limiting Displacement (cm)	100	100	15 to 30	5 to 15
Assumed seismicity	6.5 and 8.25	3.8 to 7.7 (most 6.6)	8	user-selected m and r
Seismic coefficient	0.1 for M = 6.5, 0.15 for M = 8.25	0.5 * MHA _r /g ^b	0.75 * MHA _r /g ^b	$f_{eq} * MHA_r/g$, f_{eq} in Figure 4.42 ^b
Factor of safety	1.15	1.0	1.0	1.0

^a H-G&F = Hynes-Griffin and Franklin [1984]

^b MHA_r = maximum horizontal acceleration for reference site condition, generally taken as firm rock

- The horizontal seismic coefficient is taken as $0.65 \times k_{max}$, and a pseudo-static stability analysis is performed using peak strengths for the slope material. The factor 0.65 is intended to offset other potential sources of conservatism in the analysis procedure, and is not intended to suggest that these slopes, which often comprise brittle materials, have a deformation tolerance (Ashford, 2002, personal communication). Slopes with $FS > 1$ will theoretically be stable, although higher factors of safety will generally be desirable for use in design given uncertainties in strength parameters and the analysis procedure.

Application to Coherent Landslides in Ductile Soil — Pseudo-static methods have been used for many years as a screen procedure to differentiate sites with low potential for earthquake-induced landslide development from those sites for which more detailed analyses are warranted. Most screen procedures used in modern practice are calibrated based on more sophisticated displacement-based analysis procedures, which are described in the next section. Several such screen procedures include the following:

- Seed (1979) procedure for application to earth dams
- Hynes-Griffin and Franklin (1984) procedure for application to earth dams
- Bray et al. (1998) procedure for application to solid-waste landfills
- Stewart et al. (2003a) procedure for application to hillside residential and commercial construction

Important conditions that underlie these screen procedures include the level of displacement considered tolerable for a specific application and the seismological conditions (i.e., magnitude, site–source distance) associated with the ground motions used to calculate displacements. For the above screen procedures,

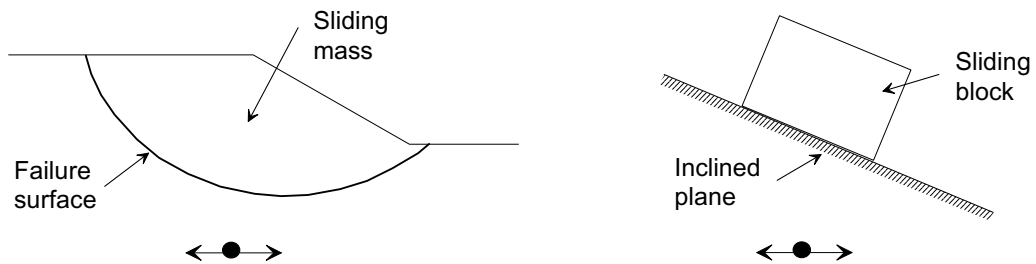


FIGURE 4.43 Analogy between (a) potential seismically induced landslide and (b) rigid block resting on inclined plane.

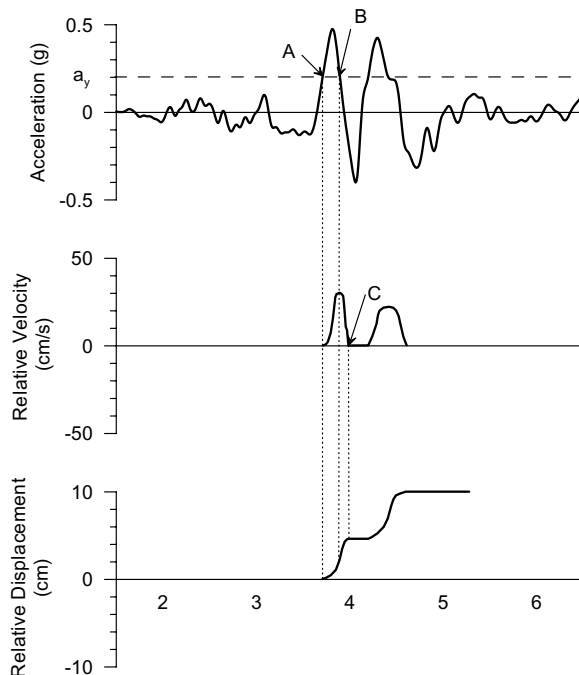


FIGURE 4.44 Development of permanent slope displacement for earthquake ground motion. (From Wilson, R.C. and Keefer, D.K., U.S. Geological Survey Professional Paper 1360, 317–345, 1985. With permission.)

these conditions are listed in Table 4.7 along with the recommended seismic coefficients and their associated minimum factors of safety. The seismic coefficients that have been recommended for residential and commercial construction, shown in Figure 4.42, demonstrate the important effect of magnitude on seismic coefficient for a given tolerable displacement.

Another important consideration associated with screen procedures is the level of conservatism employed in their development. The procedures for dams and landfills were formulated very conservatively, meaning that a large percentage of the sites that fail the screen would be expected to have slope displacements smaller than the threshold values used in the development of the screen if the design ground motion amplitude of MHA_r were to occur at the site. The procedure for residential and com-

mercial construction was developed less conservatively. The differing levels of conservatism account for the fact that f_{eq} values in Figure 4.42 ($u = 5$ cm) for magnitude 6.5 earthquakes approximately match the 0.5 value recommended for dams by Hynes-Griffin and Franklin (1984, $u = 100$ cm).

4.6.2.3.3 Displacement-Based Methods of Analysis

Newmark Integration Procedure for Sliding Rigid Block — A pseudo-static seismic coefficient and its associated factor of safety represent a relatively crude index of seismic slope stability because they do not account for the time-varying nature of the seismic excitation of a slide mass. Newmark (1965) developed an improved indicator of slope stability by recognizing that displacements accrue in a slope as a result of increments of time during which the seismic excitation causes the factor of safety to drop below one. As illustrated in Figure 4.43, Newmark drew an analogy between this situation and that of a rigid block resting on an inclined plane, which will slide down the plane whenever the inertial excitation produces basal stresses that exceed the shear strength at the block-plane interface.

Using Newmark's model, the displacement of a rigid block can be calculated for any base excitation time history if the acceleration that causes the initiation of slip is known. This acceleration is known as the yield acceleration, and is denoted a_y . There is a corresponding seismic coefficient that is referred to as $k_y = a_y/g$, where g = acceleration of gravity. Parameter k_y can be calculated using conventional limit equilibrium stability calculations by introducing static lateral forces of $k \times W$ (where W = weight of the slide mass) through the centroid until the value of k that reduces the factor of safety to one is identified. This value of k is equal to k_y .

As illustrated in Figure 4.44, the calculation of displacement given an accelerogram and a_y involves first integrating across the portion of the accelerogram where the block and the base will have differing velocities. As shown in the figure, the differential velocity begins at the instant of time when acceleration first exceeds a_y (point A in Figure 4.44) and increases throughout the time period during which $a > a_y$. When the acceleration drops below a_y (point B in Figure 4.44), the differential velocity is at a local maximum. Differential velocity will decrease while $a < a_y$ until it goes to zero (point C in Figure 4.44), at which time the block and base will again resume coherent motion until the next occurrence of basal slip. Once the time history of differential velocity has been computed as described above (and as represented in the middle frame of Figure 4.44), the differential displacement is simply calculated by integrating across the differential velocity time history (as shown in the bottom frame of Figure 4.44).

The above procedure is convenient to apply, especially with the availability of modern computer programs that can efficiently perform calculations for many time histories (e.g., Jibson and Jibson, 2003). However, a number of issues can critically affect the outcome of such analyses, and should be borne in mind by the engineer, such as:

- The slide mass above a basal slip plane is not truly rigid, and the dynamic response of the mass could give rise to: (a) amplification or de-amplification of the base motion depending on the velocity structure of the site and the potential for resonance between the input motion and slide mass, and (b) wave reversals within the slide mass depending on the frequency content of incident waves and depth and shear wave velocity structure of the slide mass. These effects will be collectively referred to as vertical ground motion incoherence, and have been investigated by a number of researchers including Kramer and Smith (1997) and Bray and Rathje (1998).
- Calculated displacements are highly sensitive to characteristics of the input motions such as amplitude, duration and frequency content. Moreover, even for a set of time histories for which these characteristics are consistent, calculated displacements can show significant variability due to essentially random phasing of the waveforms. Accordingly, time histories must be carefully selected to match the expected seismic loading for a project site (for example, as evaluated from the results of de-aggregated probabilistic seismic hazard analyses), and a sufficient number of time

histories should be selected to enable both the median displacement and the standard deviation of displacements to be reliably characterized.

- The shear strength parameters used to evaluate yield coefficient k_y must be appropriate for the seismic loading condition. These parameters will typically be different from those used for static stability analyses, as discussed in Section 4.3.3.
- The occurrence of basal slip of a slide mass causes its motions to deviate from those that would be present in the absence of slip. When analysis of the dynamic response of the slide mass is performed independently of the analysis of relative displacement, the analyses are said to be de-coupled. A coupled analysis considers the dynamic response and the basal slip together. Displacements calculated from de-coupled and coupled analyses generally differ (Lin and Whitman, 1983; Gazetas and Uddin, 1994; Kramer and Smith, 1997; Rathje and Bray, 2000).

The implication of the vertical ground motion incoherence effects discussed above is that acceleration time histories selected from a strong motion database should not be used in their as-recorded state for Newmark sliding block analyses if the dynamic response of the slide mass is likely to be significant. The slide mass response is insignificant if the wavelength of the incident waves significantly exceeds the slide depth or, expressed another way, the period of the slide mass (T_s) is much smaller than the mean period of the input motion (T_m , evaluated from Rathje et al., 1998).

Bray and Rathje (1998) recommend that if $T_s/T_m < 0.2$, the slide mass response is insignificant, and the mass can be considered to be rigid. However, for $T_s/T_m > 0.2$, a ground response analysis should be performed that is appropriate for the site geometry to evaluate the horizontal equivalent acceleration time history, HEA(t). HEA/g represents the ratio of the time-dependent horizontal inertial force applied to a slide mass during an earthquake to the weight of the mass. The maximum value of HEA is denoted MHEA, which can be related to the maximum seismic coefficient by $k_{\max} = \text{MHEA}/g$. HEA time histories can generally be evaluated from one- or two-dimensional ground response analyses using computer programs such as SHAKE or QUAD4M (Idriss and Sun, 1992; Hudson et al., 1994). Rathje and Bray (1999) have found that 1-D analyses generally provide a conservative estimate of HEA(t) for deep sliding surfaces within two-dimensional slope geometries and a slightly unconservative estimate for shallow surfaces near slope crests.

The implication of the difference between sliding block displacements evaluated from de-coupled and coupled analyses is that the more conventional, de-coupled analyses can produce biased estimates of slope displacement. Rathje and Bray (2000) found that de-coupled analyses are significantly conservative for $T_s/T_m < 1.0$. For larger period ratios, de-coupled displacements may be conservative or unconservative, the unconservative situation being more likely for $k_y/k_{\max} > 0.4$. As of this writing, there are no widely distributed computer programs available for the analysis of coupled sliding block displacements.

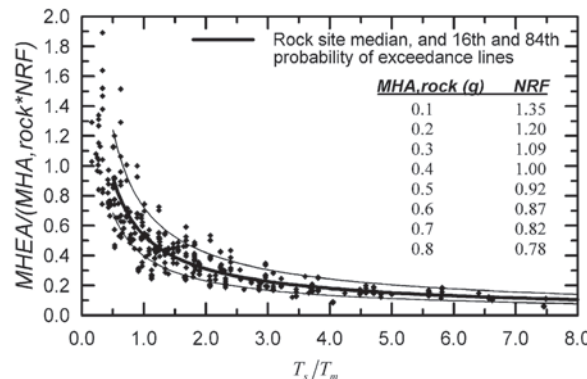
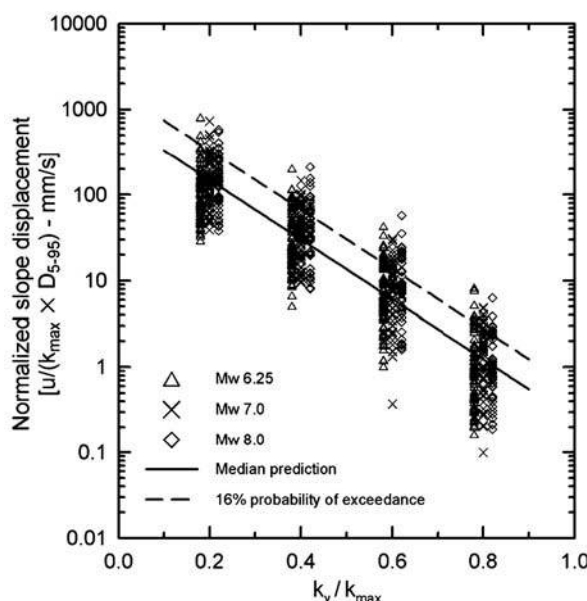
Simplified Procedures for Estimating Newmark Displacements — A number of simplified procedures have been developed that can be used to estimate Newmark sliding block displacements. The investigators listed in Table 4.8 have developed these procedures by performing de-coupled displacement analyses for a range of slope configurations and input motions. As listed in Table 4.8, factors distinguishing these models include the ground motion intensity measures that are correlated to displacement, the inclusion (or noninclusion) of vertical incoherence effects within the slide mass, the slope geometry and the number of earthquake motions used in the analyses.

A good example of these procedures is the method proposed by Bray and Rathje (1998) and Bray et al. (1998). This procedure was originally developed for landfills but has also found recent widespread use for hillside residential and commercial construction (Blake et al., 2002). The procedure has two basic steps: analysis of the seismic demand accounting for vertical incoherence effects, and evaluation of normalized displacement.

Bray and Rathje (1998) and Bray et al. (1998) define the spatially averaged peak acceleration of a slide mass as the maximum horizontal equivalent acceleration (MHEA). MHEA is evaluated as a function of MHA_r from calculations of wave propagation through an equivalent one-dimensional slide mass. As shown in Figure 4.45,

TABLE 4.8 Simplified Procedures for Estimating Newmark Sliding Block Displacements

Reference	Slope Configuration	Vertical Incoherence (Y/N)	Input Motion Intensity Measures	No. of Motions
Franklin and Chang [1977]	Dam (2-D)	N	k_{\max}	354
Makdisi and Seed [1978]	Dam (2-D)	Y	k_{\max}, T_o	4
Yegian et al. [1991]	Dam (2-D)	N	k_{\max}, N_{eq}, T_o	354
Bray and Rathje [1998]	Landfill (1-D)	Y	k_{\max}, D_{5-95}, T_m	309

**FIGURE 4.45** Normalized MHEA for deep-seated slide surface versus normalized fundamental period of slide mass (From Bray, J.D. and Rathje, E.M., *J. Geotech. Geoenviron. Eng.*, ASCE, 124, 242–253, 1998. With permission.)**FIGURE 4.46** Normalized sliding displacement (Modified from Bray, J.D. and Rathje, E.M. (1998). *J. Geotechn. Geoenviron. Eng.*, ASCE, 124, 242–253, 1998. With permission.)

MHEA is normalized by the product of MHA_r and a nonlinear response factor (NRF), which accounts for nonlinear ground response effects as vertically propagating shear waves pass through the slide mass. Parameter MHA_r is used as the normalizing ground motion even for sites where the foundation materials are soil because site condition was not found to significantly affect MHEA (except for deep soft clay sites such as NEHRP E sites, for which site-specific analyses were recommended). The ratio MHEA/(MHA_r × NRF) differs from unity as a result of vertical ground motion incoherence within the slide mass, and is related in Figure 4.45 to the ratio of the small-strain period of the sliding mass (T_s) to the mean period of the input motion (T_m). The ratio MHEA/(MHA_r × NRF) is less than unity for $T_s/T_m > \sim 0.5$, and is variable with an average of about 1.0 for $T_s/T_m < \sim 0.5$.

Bray and Rathje (1998) developed a statistical model that relates slope displacements from a Newmark-type analysis (u) to the amplitude of shaking in the slide mass ($k_{\max} = \text{MHEA}/g$), significant duration of shaking (measured as the time between 5 and 95% normalized Arias intensity, D_{5-95}) and the ratio k_y/k_{\max} . A statistical model was established from regression analysis of 309 Newmark-displacement values calculated from ground motion records from magnitude 6.25 to 8 earthquakes at each of four k_y/k_{\max} ratios. The model and data are shown in Figure 4.46, and indicate a lognormal distribution of normalized displacement $u/(k_{\max} \cdot D_{5-95})$ for a given k_y/k_{\max} ratio. The median of this lognormal distribution is described by

$$\log_{10}\left(\frac{u}{k_{\max} \cdot D_{5-95}}\right) = 1.87 - 3.477 \cdot \frac{k_y}{k_{\max}} \quad (4.40)$$

where u is the median displacement in centimeters and D_{5-95} is in units of seconds. The standard deviation of the normalized displacement is 0.35 in \log_{10} units.

Whether evaluated through formal Newmark integration or the simplified procedure described above, the calculated displacement u should be recognized as an index of slope performance, and does not necessarily correspond to the actual displacement of the slope.

4.6.2.3.4 Stress-Deformation Methods of Analysis

The pseudo-static and displacement-based methods described above are by far the most widely used procedures for seismic slope stability analysis. However, both provide relatively crude indices of slope performance. For some applications, more sophisticated stress-deformation analyses, implemented in dynamic finite element or finite difference computer codes, may be able to provide improved insight.

In modern practice, stress-deformation approaches are most commonly implemented in finite element or finite difference analyses that employ nonlinear inelastic soil models. The nonlinear methods can be formulated in terms of effective stresses to allow modeling of the generation, redistribution and eventual dissipation of excess pore pressure during and after earthquake shaking, e.g., DYNAFLOW (Prevost, 1981), FLAC (Itasca Consulting Group, 1998) and OpenSees (<http://www.openses.berkeley.edu>). Such approaches may be desirable for stability problems involving potentially liquefiable soils, but require relatively sophisticated soil constitutive models. Examples of several such constitutive models include those of Iai (1991), Manzari and Dafalias (1997), Elgamal et al. (1998) and Li (2002). Some of these models require a significant number of parameters, some of which may be poorly constrained by data. Engineers applying such methods must consider the trade-off between model rigor and the effect of uncertainty in model parameters on analysis results.

Other programs employ cyclic stress-strain models formulated in terms of total stresses, which can be a relatively efficient yet effective method of analysis for slide masses not subject to liquefaction (Finn et al., 1986). More approximate methods of stress-deformation analyses have also been developed, including the strain potential approach (Seed et al., 1973) and stiffness reduction approach (Lee, 1974; Serff et al., 1976). An overview of these approaches can be found in Section 10.6.1.4 of Kramer (1996).

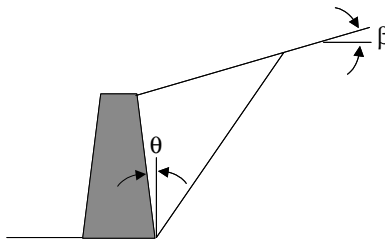


FIGURE 4.47 Schematic illustration of retaining wall.

4.6.3 Retaining Structures

Earth retaining structures can be subjected to lateral loads during earthquake shaking that are substantially increased from those present under long-term static conditions. Damage to various types of retaining structures has been observed in past earthquakes. Free-standing stiff retaining walls maintain equilibrium through a combination of active, passive and sliding forces as the wall tends to translate and rotate under their action. Coulomb earth pressure theory, which assumes that the shear strength of the backfill soil is mobilized on a planar potential failure surface, predicts a static active thrust of

$$P_A = \frac{1}{2} K_A \gamma H^2 \quad (4.41)$$

where

$$K_A = \frac{\cos^2(\phi - \theta)}{\cos^2 \theta \cos(\delta + \theta) \left[1 + \sqrt{\frac{\sin(\delta + \phi) \sin(\phi - \beta)}{\cos(\delta + \theta) \cos(\beta - \theta)}} \right]^2} \quad (4.42)$$

ϕ is the friction angle of the soil, δ is the angle of interface friction between the wall and the soil, and β and θ are as shown in Figure 4.47. The static active thrust is considered to act at a height $H/3$ above the base of the wall.

Okabe (1926) and Mononobe and Matsuo (1929) developed a pseudo-static extension of Coulomb theory to estimate the total thrust acting on a wall under seismic conditions. Assuming pseudo-static accelerations of $a_h = k_h g$ and $a_v = k_v g$ in the horizontal and vertical directions, respectively, the Mononobe-Okabe active thrust is given by

$$P_{AE} = \frac{1}{2} K_{AE} \gamma H^2 (1 - k_v) \quad (4.43)$$

where

$$K_{AE} = \frac{\cos^2(\phi - \theta - \psi)}{\cos \psi \cos^2 \theta \cos(\delta + \theta + \psi) \left[1 + \sqrt{\frac{\sin(\delta + \phi) \sin(\phi - \beta - \psi)}{\cos(\delta + \theta + \psi) \cos(\beta - \theta)}} \right]^2} \quad (4.44)$$

and $\psi = \tan^{-1}[k_h/(1 - k_v)]$ subject to the condition $\phi - \beta \geq \psi$. Experimental results indicate that the dynamic component of the total active thrust, i.e., $\Delta P_{AE} = P_{AE} - P_A$, acts at a height of approximately $0.6H$ above the base of the wall. Procedures for estimation of the permanent displacement of gravity

retaining walls, based on an approach analogous to the Newmark sliding block procedure described in Section 4.6.2.3.3, have been presented by Richards and Elms (1979) and Whitman and Liao (1985).

There are many types of retaining structures other than the conventional stiff walls described above. Ebeling and Morrison (1993) provide a thorough review of the seismic design of retaining structures commonly used in waterfront structures. Ling et al. (1997) describe seismic design procedures for reinforced earth-type retaining structures.

4.7 Soil Improvement

When earthquake hazard investigations indicate significant ground failure potential, improvement of the *in situ* soils may be warranted. Soils have been modified to reduce their compressibility and increase their stiffness and strength in response to static loads for many years. Many of these soil improvement techniques also provide benefits for the case of seismic loading, and the need to mitigate seismic hazards has led to the development of new techniques.

Currently, there are a variety of soil improvement techniques available for mitigation of seismic hazards. The most commonly used can be divided into four main categories: densification techniques, reinforcement techniques, grouting and mixing techniques and drainage techniques. The following subsections provide brief descriptions of these techniques and the conditions under which their use is most appropriate. More detailed information can be found in textbooks such as Van Impe (1989), Hausmann (1990), Bell (1993) and Moseley (1993). Also, organizations such as the Geo-Institute of ASCE and the International Society for Soil Mechanics and Geotechnical Engineering (ISSMGE) have technical committees on soil and ground improvement that organize technical conferences on a regular basis; up-to-date information on a variety of soil improvement techniques can often be found in the proceedings of these conferences, including Rollins (1994), Hryciw (1995), Schaefer et al. (1997) and Johnsen et al. (2003).

4.7.1 Densification Techniques

The method of soil deposition or placement affects soil particle structure, which, in turn, influences the soil behavior. Soils deposited by settling through water, whether naturally or as hydraulic fill, will generally have a loose particle structure. Loose soils are generally weak and compressible, which are undesirable characteristics in almost any case, and are also highly contractive when sheared. The contractive nature of these soils renders them susceptible to liquefaction under seismic loading. As a result, the engineering properties of most soils, but particularly granular soils, can be improved by densification.

Because densification techniques decrease the total volume of the soil, they produce some amount of ground surface settlement. Some techniques minimize settlement by placing additional soil below the ground surface during densification; the volume of added soil is intended to balance the volume change due to densification. They do not eliminate settlement, though, so their use must be evaluated carefully if structures or utilities that could be damaged by settlement are present.

4.7.1.1 Vibratory Techniques

Cohesionless soils, particularly those that are most susceptible to liquefaction, can generally be densified efficiently by vibration. Several vibratory techniques are available and commonly used for mitigation of seismic hazards.

Vibroflotation uses a torpedo-shaped probe (the vibroflot) with rotating weights mounted eccentrically on its central shaft. Electrical or hydraulic power is used to rotate the weights, which provide horizontal vibrations. The vibroflot is lowered by a crane to the bottom of the deposit to be densified (using a combination of vibration and air or water jetting). The vibroflot is then withdrawn while vibrating in a series of 2 to 3 ft increments at an overall rate of about 1 ft/min. The vibrations of the probe produce local liquefaction of the soil around the probe; following pore pressure dissipation, the soil comes to equilibrium in a denser state. The conical depression that usually forms above the probe at the ground surface can be filled with clean sand or gravel. Alternatively, bottom-feed systems can introduce gravel

or crushed stone through the tip of the vibroflot, leaving behind a stone column that provides the benefits of reinforcement and drainage in addition to densification. Vibroflotation is usually performed in a grid-like pattern across a site. The spacing of the individual penetration points depends on the soil type and the power of the vibroflot, but is usually on the order of 6 to 10 ft.

Vibro rod systems use vibratory pile driving hammers to vibrate long probes into the soil in a grid pattern. The probe is pushed into the soil and then pulled out while being vibrated. The Terraprobe system uses 30-in. diameter steel pipe piles; the Vibro-Wing system uses a thin central rod to which radially projecting wings have been attached. Vibro rod systems apply vertical, rather than horizontal, vibrations to the soil so the reduced horizontal radius of influence requires somewhat closer grid spacings than used with vibroflotation.

Dynamic compaction requires no penetration of the ground surface; a heavy weight (6 to 30 t) is raised by a crane to a predetermined height (35 to 100 ft) and dropped. The weight is usually dropped three to eight times in one place before moving to an adjacent grid point. The ground surface is heavily disrupted (with impact craters) and requires surface rolling, but the impact energy produces densification to depths of 30 to 40 ft. Densification follows porewater pressure dissipation that, depending on the permeability of the treated soil, can take from 1 to 2 days (clean sands and gravels) to 1 to 2 weeks (sandy silts) to complete.

Blasting has also been used to densify soils, and may be particularly useful in soils that contain many boulders or other obstructions that could hamper the effectiveness of vibratory probes. Because it produces strong vibrations and considerable noise, it is most commonly used in relatively remote environments.

4.7.1.2 Compaction Grouting

Pumping a low slump grout into loose soils under high pressure, a process known as compaction grouting, can also densify the soil. This process forms an intact bulb or column of grout by displacing the soil around the end of the grout pipe; the soil is densified and subjected to increased confinement due to the pressure imposed on the grout during pumping. The hardened grout also acts as a stiff and strong inclusion within the soil. Grout point spacings of 3 to 15 ft have been used; larger spacings are typically used with larger treatment depths since the higher overburden pressure permits the use of higher grouting pressures.

4.7.1.3 Discussion

Densification techniques can be used in different soils, but vibratory techniques are best suited to relatively clean sands and gravels (fines contents less than 20% and clay contents less than 3%). Blasting is most effective in loose sands with less than 20% silt and less than 5% clay; its effectiveness can be dramatically reduced by larger quantities of fines or seams of fine-grained soils. Dynamic compaction and compaction grouting can be used in cohesive soils, but their seismic applications are usually for the mitigation of liquefaction hazards. Disturbance of the surrounding environment, in terms of noise, vibration and permanent ground deformation, is an important consideration that frequently controls the selection of a soil improvement technique.

4.7.2 Reinforcement Techniques

The overall strength and stiffness of some soil deposits can be increased efficiently by the installation of discrete inclusions that reinforce the soil. The inclusions can consist of structural elements or of geomaterials such as gravel or crushed stone.

4.7.2.1 Stone Columns

Installation of dense columns of gravel or crushed stone, known as stone columns, can provide substantial improvement of a potentially liquefiable soil. The column is generally installed by displacing the native soil by driving a capped casing through which the stone is later installed, or through the use of vibroflotation. The compacted stone is denser and stronger than the native soil; installation of a grid of stone columns can provide significant reinforcement of the native soil. Vibrations during installation tend to densify the native soil, and installation of the stone may also increase the effective lateral stresses in the

surrounding soil. Stone columns may provide additional improvement by acting as drains that inhibit the development of high porewater pressures during earthquakes.

4.7.2.2 Compaction Piles

Loose, granular soils can be improved by the installation of displacement piles, usually prestressed concrete or timber piles, which are left in the soil after driving. The vibration and displacement during driving densify and produce increased lateral stresses in the surrounding soil. The shear, flexural and tensile strength of the piles themselves also provide resistance to soil deformations.

4.7.3 Grouting and Mixing Techniques

Soil properties can often be improved by injecting or mixing cementitious grouts into the soil. Grouts improve the soil by cementing the contacts of the particles and by filling the voids between particles with low-compressibility material. Grouting involves injection of grout materials in such a manner that the structure of most of the soil remains intact; mixing intentionally destroys the structure of the soil by mechanically or hydraulically mixing grout materials with the soil. Grouting and mixing techniques are generally somewhat expensive, but can be accomplished with little vibration or surface deformation and hence can be used in situations where other soil improvement techniques cannot be used.

4.7.3.1 Grouting

Permeation grouting refers to the injection of liquid grout of such low viscosity that it can permeate the voids of the soil without disturbing the soil structure. Both particulate grouts (aqueous suspensions of cement, fly ash, bentonite, microfine cement or a combination thereof) and chemical grouts (silica and lignin gels or phenolic and acrylic resins) can be used. Selection of grout type is strongly influenced by the pore size of the soil; although nearly any type of grout can be used in soils with large voids (e.g., gravels and coarse sands), lower viscosity chemical grouts may be required to achieve permeation in fine sands. The effectiveness of permeation grouting can be strongly reduced by the presence of fines. Grout pipe spacings are typically on the order of 4 to 8 ft; soil improved by permeation grouting can have shear strengths of 50 to 300 psi.

Intrusion grouting is a procedure in which a more viscous (and generally stronger) grout is injected into the soil under pressure to cause controlled fracturing of the soil. Upon initial grouting, fractures develop along planes of weakness, which may be bedding planes or minor principal stress planes. After allowing the initial grout to cure, intrusion grouting is often repeated to fracture the soil along different planes. Eventually, a network of intersecting grout lenses can be formed. While some densification may occur due to displacement by the viscous grout, most of the improvement is thought to result from the increased stiffness and strength of the soil mass from the hardened lenses of grout.

4.7.3.2 Mixing

Soil mixing is a process in which cementitious material is mechanically mixed into the soil using a hollow stem auger and mixing paddle arrangement. Soil mixing rigs may have single augers or groups of two to eight augers. As the augers penetrate into the soil, grout is pumped through their stems and mixed with the soil by the auger flights and mixing paddles. The mixing process continues as the augers are withdrawn from the soil. The mixing process leaves behind a column of strong, mixed soil-cement of dimensions that depend on the specific dimensions of the augers or paddles. By overlapping the columns before the grout cures, walls and cellular structures can be constructed below the ground surface. Soil mixing can be used in nearly any type of inorganic soil; it has been used to improve soils to depths of 70 ft in the United States and 200 ft in Japan.

Jet grouting, despite its name, can actually be thought of as a mixing procedure since it destroys the original structure of the treated soil and replaces the original soil with a soil-cement mixture. In the case of jet grouting, the mixing is accomplished hydraulically. A hollow tube with a horizontally oriented nozzle at its lower end is placed in a previously drilled borehole. The injection nozzle is rotated and grout

pumped through it at high pressure; air and water may also be injected to aid in the mixing process. The resulting jet of grout cuts through the soil, thereby mixing the grout and soil particles and leaving behind a column of strong, mixed soil-cement as the nozzle is raised from the bottom of the boring to the top. The diameter of the jet-grouted column depends on the soil conditions and the manner in which the jet grouting is performed. Diameters of about 3 ft have been obtained in sandy gravels using single-jet (grout only) systems, and diameters of up to 8 ft have been obtained in similar materials using a triple-jet (grout, water and air) system.

4.7.4 Drainage Techniques

Ground failure is frequently associated with the interaction between soil particles and groundwater, even under static loading conditions. Under seismic conditions, the interaction is often even more important. The potential for ground failure, or the level of deformations associated with ground failure, can often be reduced by lowering the groundwater table prior to shaking or by increasing the rate at which excess porewater pressures dissipate during and after earthquake shaking.

The installation of stone columns introduces zones of dense, relatively high-permeability material in which porewater pressures can be expected to remain nearly hydrostatic during shaking. As such, earthquake-induced excess porewater pressures can be rapidly dissipated by the horizontal flow of water into the stone columns. The rate of dissipation depends on the size and spacing of the stone columns, and on the permeability and compressibility of the native soil into which they are installed. Stone columns may therefore achieve a degree of liquefaction hazard mitigation by suppressing the buildup of porewater pressure sufficiently to prevent initial liquefaction from occurring; it is important to recognize, however, that postearthquake settlement may still occur.

4.8 Future Challenges

Geotechnical Earthquake Engineering has seen a number of changes in its short history. While many impressive advances have been made, new techniques and procedures are being developed to address the many challenges that remain.

Characterization of sites and soil behavior will always remain a crucial aspect of seismic design and hazard mitigation. Procedures for more accurate characterization of the three-dimensional geometry and the spatial variability of soil properties are needed as analytical tools and techniques become more powerful. Methods for the detection and characterization of thin seams of low permeability soils or preexisting failure surfaces are needed. Techniques for more accurate characterization of *in situ* soil behavior, including *in situ* material damping and behavior at moderate to large strain levels are also needed.

With respect to ground motions and site response, the development of attenuation models and site factors that apply for consistent reference site conditions, including empirically validated yet physically robust models for basin amplification effects is needed. To provide estimates of ground motions for conditions where recorded data are unavailable, validated seismological simulation procedures are needed. For improving the accuracy with which geotechnical hazards (e.g., slope stability, liquefaction, response of specific classes of buildings, etc.) can be evaluated, identification of the ground motion intensity measures that are most critical for use in specific applications, and subsequent development of attenuation models and site amplification factors for those intensity measures are needed. Finally, there remains a need for development of attenuation models and site factors for tectonic regimes where ground motion recordings are sparse or unavailable, such as the central and eastern United States.

Perhaps the greatest challenges in the area of soil–foundation–structure interaction are related to the incorporation of SFSI models into practice. Unlike most of the other topics discussed in this chapter, SFSI effects are routinely ignored in practice, which stems in large part from engineers' lack of familiarity with the topic. Important technical issues that remain to be addressed include kinematic interaction effects for piles and pile groups, evaluation of foundation damping for nonlinear foundation and soil

conditions and complex foundation configurations and the development of field test inventories that enable robust validation and calibration of theoretical models.

Soil liquefaction remains an important part of geotechnical earthquake engineering practice. The historical emphasis in liquefaction hazard evaluation has been on identifying liquefaction-susceptible soils and their potential for liquefaction under given levels of earthquake shaking. Important recent advances in characterization of liquefaction resistance from SPT and CPT resistance have been made, but there appears to be opportunity for additional advances with improved characterization of the loading associated with earthquake shaking. Future developments in liquefaction are likely to focus principally on the effects of liquefaction, particularly with regard to prediction of the permanent deformations of liquefied soil masses and structures supported on or within them.

In the early days of geotechnical earthquake engineering practice, the stability of landslides and retaining structures was commonly evaluated using simple, pseudo-static techniques, and the use of those techniques persists to a large degree even today. Evaluation of the stability of natural and man-made geotechnical structures, however, is clearly moving toward prediction of permanent deformations. Practical and more advanced procedures for prediction of permanent deformations of these structures are available, but have not been adequately validated against field case-history data. Accordingly, calibration work for these procedures remains an important research need. Because of the difficulty inherent in making *a priori* predictions, characterization of the true uncertainty in permanent deformation predictions (i.e., by comparisons with case-history data) will also be required.

Mitigation of geotechnical seismic hazards will continue to be a significant part of geotechnical earthquake engineering practice, and further advances in the development and application of soil improvement techniques will be needed. Improved procedures for validation of the effectiveness of various soil improvement techniques are needed, as are procedures for better defining the geometric extent of improvement required for different levels of hazard mitigation.

Finally, the continuing emergence of performance-based earthquake engineering (PBEE) poses new challenges to geotechnical earthquake engineers. PBEE will require improved characterization of uncertainties in the parameters on which geotechnical performance predictions are based, and improved understanding of how those uncertainties affect uncertainties in performance. PBEE will require geotechnical earthquake engineers to work more closely with seismologists, other earth scientists and structural engineers; geotechnical earthquake engineers will need to become more familiar with the theories, procedures and tools of those related professions. PBEE will require, for many structures, explicit consideration of all of the factors described in the preceding paragraphs, and will provide a framework for their consideration in evaluation of overall performance. Continuing development of PBEE will aid the geotechnical earthquake engineering profession in meeting many of these future challenges.

List of Symbols

A_f	area of foundation
a, b	halfwidth of foundation in direction normal and perpendicular to horizontal projection of inclined incident wave ray path, respectively
a_{\max}	peak absolute acceleration
a_0	normalized frequency, $= \omega r/V_s$
\tilde{a}_0	dimensionless frequency parameter accounting for incoherence and wave inclination
a_y	yield acceleration
b_e	$\sqrt{a \cdot b}$
CSR	cyclic stress ratio
CRR	cyclic resistance ratio
D_{5-95}	duration parameter (5–95% on Husid plot)
E_p	Young's modulus of pile material
E_s	Young's modulus of soil
e	foundation embedment

F	dimensionless cone penetration test sleeve resistance
FIM	foundation input motion (motion on base slab that accounts for kinematic interaction effects)
FS	factor of safety against shear failure
F_a, F_v	ground motion amplification factors at short- and mid-periods, respectively
G	secant shear modulus
G_{\max}	maximum shear modulus
g	acceleration of gravity
I_c	soil behavior type index
I_f	moment of inertia of foundation
I_h	Arias intensity
K_A	static active earth pressure coefficient
K_{AE}	pseudo-static active earth pressure coefficient
K_a	correction factor to CRR for effects of initial static shear stress
K_c	principal stress ratio
K_σ	correction factor to CRR for effects of initial effective overburden stress
k_θ, K_θ	dynamic and static rotational stiffnesses for foundation on halfspace
k_{\max}	peak value of spatially averaged seismic coefficient within landslide mass
k_u, K_u	dynamic and static translational stiffnesses for foundation on halfspace
k_y	seismic coefficient that reduced the factor of safety for a slope to unity, also known as the yield coefficient
L/d	pile length to diameter ratio
LL	liquid limit
MHA	maximum horizontal acceleration (same as PHA)
MSF	magnitude scaling factor
M_w	moment magnitude
N_{corr}	fines content correction for SPT resistance
$(N_1)_{60}$	corrected standard penetration resistance
s/d	pile spacing to diameter ratio
P_A	static active thrust on retaining wall
P_{AE}	pseudo-static active thrust on retaining wall
PHA	peak horizontal acceleration (same as MHA)
PI	plasticity index
P_L	probability of liquefaction
p_a	atmospheric pressure
Q	dimensionless cone penetration test tip resistance
q_c	cone penetration test tip resistance
q_{cl}	normalized cone penetration test tip resistance
r_u, r_θ	radii that match the area and moment of inertia, respectively, of assumed circular foundation in impedance function formulations to the actual foundation area and moment of inertia
r_b	Arias intensity depth reduction factor
r_d	shear stress depth reduction factor
S_r	undrained residual strength of liquefied soil
\tilde{T}	flexible-base period for fundamental mode of structure
T	generic response spectral period, or in context of soil-structure interaction, the fixed base structural period
T_s	period of landslide mass
T_m	mean period of earthquake ground motion
V_s	shear wave velocity
V_{s-30}	average shear wave velocity in upper 30 m
α_v	inclination angle of incident seismic waves with respect to vertical

α_u, β_u	dimensionless parameters expressing the frequency dependence of foundation translational stiffness and damping
$\alpha_\theta, \beta_\theta$	dimensionless parameters expressing the frequency dependence of foundation rocking stiffness and damping
β	equivalent linear hysteretic damping ratio
γ_m	Ratio of structure-to-soil mass
γ	shear strain
κ	ground motion incoherence parameter
ρ	soil density
σ	standard error term (in natural logarithmic units)
σ'_v	vertical effective stress
σ'_{vo}	initial vertical effective stress
σ'_m	mean effective stress
τ_{max}	maximum shearing resistance
τ_{cyc}	cyclic shear stress
$\zeta, \tilde{\zeta}$	fixed- and flexible-base damping ratios for fundamental mode of structure
ξ_0	Foundation damping factor
ν	Soil Poisson ratio

References

- Abrahamson, N.A. and Silva, W.J. (1997). Empirical response spectral attenuation relations for shallow crustal earthquakes, *Seism. Res. Lett.*, 68, 94–127.
- Aki, K. and Richards, P.G. (1980). *Quantitative Seismology*, Vol. 1, W.H. Freeman, San Francisco, CA.
- Andersen, K., Leven, A. and Hsein, D. (1988). Cyclic soil data for design of gravity structures, *J. Geotech. Eng.*, ASCE, 114 (5), 517–530.
- Andrews, D.C.A. and Martin, G.R. (2000). Criteria for liquefaction of silty soils, *Proceedings, 12th World Conference on Earthquake Engineering*, Auckland, New Zealand.
- Applied Technology Council, ATC (1996). Seismic evaluation and retrofit of concrete buildings, Report No. 96-01, Seismic Safety Commission, State of California, November.
- Apsel, R.J. and Luco, J.E. (1987). Impedance functions for foundations embedded in a layered medium: an integral equation approach, *J. Earthquake Eng. Struct. Dyn.*, 15, 213–231.
- Arias, A. (1970) A measure of earthquake intensity, in *Seismic Design for Nuclear Power Plants*, Hansen, R.J., Ed. MIT Press, Cambridge, MA, 438–483.
- Ashford, S.A. and Sitar, N. (1997). Analysis of topographic amplification of inclined shear waves in a steep coastal bluff, *Bull. Seism. Soc. Am.*, 87, 692–700.
- Ashford, S.A. and Sitar, N. (2002). Simplified method for evaluating seismic stability of steep slopes, *J. Geotech. Geoenvir. Eng.*, ASCE, 128, 119–128.
- Ashford, S.A., Sitar, N., Lysmer, J., and Deng, N. (1997). Topographic effects on the seismic response of steep slopes, *Bull. Seism. Soc. Am.*, 87, 701–709.
- Azzouz, A.S., Malek, A.M. and Baligh, M.M. (1989). Cyclic behavior of clays in undrained simple shear, *J. Geotech. Eng.*, ASCE, 115 (5), 637–757.
- Bard, P-Y. (1995). Effects of surface geology on ground motion: recent results and remaining issues, *Proc. 10th European Conference on Earthquake Engineering*, Duma (Ed.), Rotterdam, 305–323.
- Bardet, J.P., Rathje, E.M., and Stewart, J.P.: principal authors (2002). Chapter 8: Ports. Bhuj, India Earthquake of January 26, 2001 Reconnaissance Report, S.K. Jain, W.R. Lettis, C.V.R. Murtry, and J.P. Bardet, Eds., *Earthquake Spectra*, Supplement A to Vol. 18, 101–130.
- Bartlett, S.F. and Youd, T.L. (1992). Empirical analysis of horizontal ground displacement generated by liquefaction-induced lateral spread, Technical Report NCEER-92-0021, National Center for Earthquake Engineering Research, Buffalo, New York.

- Baturay, M.B. and Stewart, J.P. (2003). Uncertainty and bias in ground motion estimates from ground response analyses, *Bull. Seism. Soc. Am.*, 93, 2025–2042.
- Been, K. and Jeffries, M.G. (1985). A state parameter for sands, *Geotechnique*, 35, 99–112.
- Been, K., Crooks, J.H.A., Becker, D.E., and Jeffries, M.G. (1986). The cone penetration test in sands: Part I, state parameter interpretation, *Geotechnique*, 36, 239–249.
- Been, K., Jefferies, M.G., Crooks, J.H.A., and Rothenburg, L. (1987). The cone penetration test in sands: Part II, general inference of state, *Geotechnique*, 37, 285–300.
- Bell, F.G. (1993). *Engineering Treatment of Soils*, E & F Spon, London, 302 pp.
- Beresnev, I.A., Wen, K.L. and Yeh Y.T. (1995). Seismological evidence for nonlinear elastic ground behavior during large earthquakes, *Soil Dyn. Earthquake Eng.*, 14, 103–114.
- Bielak, J. (1975). Dynamic behavior of structures with embedded foundations, *J. Earthquake Eng. Struct. Dynamics*, 3, 259–274.
- Bielak, J. (1976). Modal analysis for building–soil interaction, *J. Eng. Mech.*, ASCE, 102, 771–786.
- Biscontin, G, Pestana, J.M., Nadim, F., and Anderson, K. (2001). Seismic response of normally consolidated cohesive soils in gently inclined submerged slopes, *Proc. 4th Int. Conf. Recent Advances in Geotech. Eqk. Eng. Soil Dyn.*, Paper 5.32.
- Blake, T.F., Hollingsworth, R.A., and Stewart, J.P., Eds. (2002), *Recommended Procedures for Implementation of DMG Special Publication 117 Guidelines for Analyzing and Mitigating Landslide Hazards in California*, Report published by Southern California Earthquake Center, University of Southern California, available at <http://www.scec.org/resources/catalog/hazardmitigation.html>
- Boore, D.M., Joyner, W.B., and Fumal, T.E. (1997). Equations for estimating horizontal response spectra and peak acceleration from western North American earthquakes: A summary of recent work, *Seism. Res. Lett.*, 68, 128–153.
- Borcherdt, R.D. (1994). Estimates of site-dependent response spectra for design (methodology and justification), *Earthquake Spectra*, 10, 617–653.
- Borcherdt, R.D. (2002). Empirical evidence for acceleration-dependent amplification factors, *Bull. Seism. Soc. Am.*, 92, 761–782.
- Borcherdt, R.D. and Glassmoyer, G. (1994). Influences of local geology on strong and weak ground motions recorded in the San Francisco Bay region and their implications for site-specific building code provisions, The Loma Prieta, California Earthquake of October 17, 1989 — Strong Ground Motion, U.S. Geological Survey Professional Paper 1551-A, A77–A108
- Borja, R.I., Chao, H.Y., Montans, F.J. and Lin, C.H. (1999). Nonlinear ground response at Lotung LSST site, *J. Geotech. Geoenvir. Eng.*, ASCE, 125, 187–197.
- Borja, R.I., Smith, H.A., Wu, W-H., and Amies, A.P. (1992). A methodology for nonlinear soil-structure interaction effects using time-domain analysis techniques, Report No. 101, Blume Earthquake Engineering Center, Stanford University, June.
- Borja, R.I. and Wu, W.H. (1994). Vibration of foundations on incompressible soils with no elastic region, *J. Geotech. Eng.*, ASCE, 120, 1570–1592.
- Boulanger, R.W. (2003). Relating K_a to relative state parameter index, *J. Geotech. Geoenvir. Eng.* ASCE, 129, 770–773.
- Bray, J.D. and Rathje, E.M. (1998). Earthquake-induced displacements of solid-waste landfills, *J. Geotech. Geoenvir. Eng.*, ASCE, 124, 242–253.
- Bray, J.D., Rathje, E.M., Augello, A.J., and Merry, S.M. (1998). Simplified seismic design procedure for geosynthetic-lined, solid-waste landfills, *Geosynth. Int.*, 5, 203–235.
- Building Seismic Safety Council, BSSC (1995). *NEHRP Recommended Provisions for Seismic Regulations for New Buildings*, FEMA, Washington D.C., 1994 ed.
- Building Seismic Safety Council, BSSC (2001). *NEHRP Recommended Provisions for Seismic Regulations for New Buildings*, FEMA, Washington D.C., 2000 ed.
- Bullen, K.E. (1965). *An Introduction to the Theory of Seismology*, Cambridge University Press, Cambridge.

- Campbell, K.W. and Bozorgnia, Y. (2003). Mutually consistent near-source attenuation relations for the horizontal and vertical components of PGA and acceleration response spectra, *Bull. Seism. Soc. Am.*, 93, 314–331.
- Chang, S.W. (1996). Seismic response of deep stiff soil deposits, Ph.D. dissertation, University of California, Berkeley.
- Chang, S.W., Bray, J.D. and Seed, R.B. (1996). Engineering implications of ground motions from the Northridge earthquake, *Bull. Seism. Soc. Am.*, 86, S270–S288.
- Chang, C.-Y., Mok, C.M., Power, M.S., Tang, Y.K., Tang, H.T. and Stepp, J.C. (1990). Equivalent linear versus nonlinear ground response analyses at Lotung seismic experiment site, *Proc. 4th U.S. National Conf. Eqk. Eng.*, Vol. 1.
- Coduto, D.P. (1999). *Geotechnical Engineering: Principles and Practices*, 5th ed., Prentice Hall, Upper Saddle River, NJ, 759 pp.
- Comartin, C.D., Niewiarowski, R.W., Freeman, S.A., and Turner, F.M. (2000). Seismic retrofit and evaluation of concrete buildings: a practical overview of the ATC 40 document, *Earthquake Spectra*, 16, 241–262.
- Crouse, C.B. (2001). Commentary on soil-structure interaction in U.S. seismic provisions, *2nd UJNR Workshop on Soil-Structure Interaction, Proceedings*, Tsukuba, Japan.
- Crouse, C.B., Hushmand, B., Luco, J.E., and Wong, H.L. (1990). Foundation impedance functions: Theory versus Experiment, *J. Geotech. Eng.*, ASCE, 116, 432–449.
- Darragh, R.B. and Idriss, I.M. (1997). A tale of two sites: Gilroy #2 and Treasure Island — Site response using and equivalent linear technique, NEHRP Professional Fellowship Report, EERI, Oakland, CA.
- Das, B.M. (2002). *Principles of Geotechnical Engineering*, Brooks/Cole, Pacific Grove, CA, 589 pp.
- Davies, M.R.C., Ed. (1997). *Ground Improvement Geosystems: Densification and Reinforcement*, Thomas Telford Ltd. 508 pp.
- Day, S.M. (1978). Seismic response of embedded foundations, *Proc. ASCE Convention*, Chicago, IL, October, Preprint No. 3450.
- de Barros, F.C.P. and Luco, J.E. (1995). Identification of foundation impedance functions and soil properties from vibration tests of the Hualien containment model, *J. Soil Dyn. Earthquake Eng.*, 14, 229–248.
- Dickenson, S.E. (1994). The dynamic response of soft and deep cohesive soils during the Loma Prieta earthquake of October 17, 1989, Ph.D. dissertation, University of California, Berkeley.
- Dobry, R., Borcherdt, R.D., Crouse, C.B., Idriss, I.M., Joyner, W.B., Martin, G.R., Power, M.S., Rinne, E.E., and Seed, R.B. (2000). New site coefficients and site classification system used in recent building seismic code provisions, *Earthquake Spectra*, 16, 41–67.
- Dobry, R. and Gazetas, G. (1986). Dynamic response of arbitrarily shaped foundations, *J. Geotech. Eng.*, ASCE, 112, 109–135.
- Dobry, R., Ladd, R.S., Yokel, F.Y., Chung, R.M., and Powell, D. (1982). Prediction of pore water pressure buildup and liquefaction of sands during earthquakes by the cyclic strain method, *NBS Building Science Series 138*. National Bureau of Standards, 150 pp.
- Dobry, R., Martin, G.R., Parra, E. and Bhattacharyya, A. (1994). Development of site-dependent ratios of elastic response spectra (RRS) and site categories for building seismic codes, *Proceedings of the 1992 NCEER/SEAOC/BSSC Workshop on Site Response During Earthquakes and Seismic Code Provisions*, G.R. Martin, Ed., University of Southern California.
- Duncan, J.M. (1996). State of the art: Limit equilibrium and finite element analysis of slopes, *J. Geotech. Eng.*, American Society of Civil Engineers, 122, 577–597.
- Ebeling, R.M. and Morrison, E.E. (1993). The seismic design of waterfront retaining structures, NCEL Report R-939, Naval Civil Engineering Laboratory, Port Hueneme, California, 256 pp.
- Electrical Power Research Institute, EPRI (1993). Guidelines for determining design basis ground motions. Volume 1: Method and guidelines for estimating earthquake ground motion in eastern North America, Report No. EPRI TR-102293, Palo Alto, CA.
- Elgamal, W.-W., Parra, E., Yang, Z., Dobry, R., and Zeghal, M. (1998). Liquefaction constitutive model, *Proceedings, International Workshop on the Physics and Mechanics of Soil Liquefaction*, P.V. Lade and J.A. Yamamuro, Eds., Baltimore, Maryland, Balkema, 269–282.

- Elgamal, A.-W., Zeghal, M., and Parra, E. (1996). Liquefaction of reclaimed island in Kobe, Japan, *J. Geotech. Eng.*, 122, 39–49.
- Elgamal, A.W., Zeghal, M., Tang, H.T., and Stepp, J.C. (1995). Lotung downhole array. I: Evaluation of site dynamic properties, *J. Geotech. Eng.*, ASCE, 121, 350–362.
- Elsabee, F. and Morray, J.P. (1977). Dynamic behavior of embedded foundations, Report. No. R77-33, Department. of Civil Engineering., MIT, Cambridge, MA.
- Fan, K., Gazetas, G., Kaynia, A., Kausel, E., and Ahmad, S. (1991). Kinematic seismic response of single piles and pile groups, *J. Geotech. Eng.*, ASCE, 117, 1860–1879.
- Federal Emergency Management Agency, FEMA (1997). NEHRP guidelines for the seismic rehabilitation of buildings, FEMA 273; FEMA 274; FEMA (Series) 273; FEMA (Series) 274, Federal Emergency Management Agency, Washington, D.C., 2 v.
- Federal Emergency Management Agency, FEMA (2000). Prestandard and commentary for the seismic rehabilitation of buildings, FEMA (Series) 356, Federal Emergency Management Agency, Washington, D.C., 1 v. (various pagings)
- Field, E.H. (2000). A modified ground motion attenuation relationship for southern California that accounts for detailed site classification and a basin depth effect, *Bull. Seism. Soc. Am.*, 90, S209–S221.
- Field, E.H. and Jacob, K.H. (1995). A comparison and test of various site-response estimation techniques, including three that are not reference-site dependent, *Bull. Seism. Soc. Am.*, 85, 1127–1143.
- Field, E.H. et al. (2000). Accounting for site effects in probabilistic seismic hazard analyses of southern California: Overview of the SCEC Phase III report, *Bull. Seism. Soc. Am.*, 90, S1–S31.
- Finn, W.D.L., Ledbetter, R.H., and Wu, G. (1994). Liquefaction in silty soils: Design and analysis, *Ground Failures under Seismic Conditions*, Geotechnical Special Publication 44, ASCE, New York, 51–76.
- Finn, W. D. L., Lee, K. W. and Martin, G. R. (1977). An effective stress model for liquefaction, *J. Geotech. Eng. Div.*, ASCE, 103, 517–553.
- Finn, W.D.L., Yogendrakumar, M. Yoshida, M. and Yoshida, N. (1986). *TARA-3: A Program to Compute the Response of 2-D Embankments and Soil-Structure Interaction Systems to Seismic Loadings*, Department of Civil Engineering, University of British Columbia, Vancouver.
- Franklin, A.G. and Chang, F.K. (1977). *Earthquake Resistance of Earth and Rockfill Dams; Permanent Displacements of Earth Embankments by Newmark Sliding Rigid Block Analysis*, Miscellaneous Paper S-71-17, Department of the Army, Waterways Experiment Station, Vicksburg, MS.
- Fumal, T.E. and Tinsley, J.C. (1985). Mapping shear-wave velocities of near-surface geologic materials, in *Evaluating Earthquake Hazards in the Los Angeles Region*, Ziony, J.I. (Ed.), U.S. Geological Survey, Reston, VA, Prof. Paper 1360, 127–150.
- Gazetas, G. (1991a). Formulas and charts for impedances of surface and embedded foundations, *J. Geotech. Eng.*, 117, 1363–1381.
- Gazetas, G. (1991b). Chapter 15: *Foundation Vibrations, Foundation Engineering Handbook*, H.-Y. Fang, Ed., 2nd ed., Chapman and Hall, New York.
- Gazetas, G. and Uddin, N. (1994). Permanent deformation on preexisting sliding surfaces in dams, *J. Geotech. Eng.*, 120, 2041–2061.
- Geli, L., Bard, P-Y., and Jullien, B. (1988). The effect of topography on earthquake ground motion: a review and new results, *Bull. Seism. Soc. Am.*, 78, 42–63.
- Graves, R. W., A. Pitarka, and P. G. Somerville (1998). Ground motion amplification in the Santa Monica area: effects of shallow basin edge structure, *Bull. Seism. Soc. Am.*, 88, 1224–1242.
- Griffiths, D.V. (1980), Finite element analyses of walls, footings, and slopes, Ph.D. thesis, University of Manchester.
- Griffiths, D.V. (1989). Computation of collapse loads in geomechanics by finite elements, *Ing Arch* 59, 237–244.
- Griffiths, D.V. and Lane, P.A. (1999). Slope stability analysis by finite elements, *Géotechnique*, 49, 387–403.
- Harder, L.F. and Boulanger, R.W. (1997). Application of K_σ and K_α correction factors, *Proceedings, NCEER Workshop on Evaluation of Liquefaction Resistance of Soils*, National Center for Earthquake Engineering Research, State University of New York at Buffalo, 167–190.

- Harmsen, S.C. (1997). Determination of site amplification in the Los Angeles urban area from inversion of strong motion records, *Bull. Seism. Soc. Am.*, 87, 866–887.
- Hausmann, M.R. (1990). *Engineering Principles of Ground Modification*, McGraw-Hill, New York, 632 pp.
- Heisey, J.S., Stokoe, K.H., and Meyer, A.H. (1982). Moduli of pavement systems from spectral analysis of surface waves, *Transportation Research Record* 853, Transportation Research Board Washington, D.C.
- Henke, W. and Henke, R. (1991). In situ torsional cylindrical shear test — laboratory results, *Proceedings, Second International Conference on Recent Advances in Geotechnical Earthquake Engineering and Soil Dynamics*, St. Louis, Missouri, 1, 131–136.
- Holtz, R.D. and Kovacs, W.D. (1981). *An Introduction to Geotechnical Engineering*, Prentice-Hall, Englewood Cliffs, NJ, 733 pp.
- Hryciw, R.D. Ed. (1995). Soil improvement for earthquake hazard mitigation, Geotechnical Special Publication No. 49, New York, ASCE, 145 pp.
- Hudson, M., Idriss, I. M., and Beikae, M. (1994). QUAD4M: a computer program to evaluate the seismic response of soil structures using finite element procedures and incorporating a compliant base, Center for Geotechnical Modeling, Department of Civil and Environmental Engineering, University of California, Davis.
- Hynes-Griffin, M.E. and Franklin, A.G., (1984). Rationalizing the seismic coefficient method, Miscellaneous Paper GL-84-13, Department of the Army, Waterways Experiment Station, Vicksburg, MS.
- Iai, S. (1991). A strain space multiple mechanism model for cyclic behavior of sand and its application, *Earthquake Engineering Research Note No. 43*, Port and Harbor Research Institute, Ministry of Transport, Japan.
- Idriss, I.M. (1990). Response of soft soil sites during earthquakes *Proc. H. Bolton Seed Memorial Symposium*, J.M. Duncan Ed., 2, 273–290.
- Idriss, I.M. (1993). Assessment of site response analysis procedures, Report to National Institute of Standards and Technology, Gaithersburg, MD, Dept. of Civil & Environmental Engineering., University of California, Davis.
- Idriss, I. M.; Lysmer, J.; Hwang, R.; Seed, H. B. (1973). QUAD-4: a computer program for evaluating the seismic response of soil structures by variable damping finite element procedures, Report No. UCB/EERC-73/16, Earthquake Engineering Research Center, University of California, Berkeley, 79 pp.
- Idriss, I.M. and Boulanger, R.W. (2004). Semi-empirical procedures for evaluating liquefaction potential during earthquakes, *Proc. 11th Int. Conf. Soil Dyn. Earthquake Eng. and 3rd Int. Conf. Earthquake Geotech Eng.*, Vol. I, 32–56.
- Idriss, I.M. and Sun, J.I. (1991). User's manual for SHAKE91: A computer program for conducting equivalent linear seismic response analyses of horizontally layered soil deposits, Center for Geotech. Modeling, University of California, Davis.
- Idriss, I.M. and Sun, J.I. (1992). SHAKE91: A computer program for conducting equivalent linear seismic response analyses of horizontally layered soil deposits, Center for Geotech. Modeling, University of California, Davis.
- Iguchi, M. and Luco, J.E. (1982). Vibration of flexible plate on viscoelastic medium, *J. Eng. Mech.*, ASCE, 108, 1103–1120.
- International Code Council, ICC (2000). *International building code 2000*, International Code Council, Falls Chuch, VA, 756 pp.
- International Conference of Building Officials, ICBO (1997). *Uniform building code*, International Conference of Building Officials, Whittier, CA, 3 v.
- Ishihara, K. (1985). Stability of natural deposits during earthquakes, *Proceedings, Eleventh International Conference on Soil Mechanics and Foundation Engineering*, 1, 321–376.
- Ishihara, K. and Yoshimine, M. (1992). Evaluation of settlements in sand deposits following liquefaction during earthquakes, *Soils Foundations*, 32 173–188.
- Itasca Consulting Group (2002). FLAC – Fast Lagrangian Analysis of Continua, Version 4.0, *Itasca Consulting Group, Inc.* Minneapolis, MN.
- Jennings, P.C. and Bielak, J. (1973). Dynamics of building-soil interaction, *Bull. Seism. Soc. Am.*, 63, 9–48.

- Jibson, R.W. and Jibson, M.W. (2003). Java programs for using Newmark's method and simplified decoupled analysis to model slope performance during earthquakes, Version 1.0, Open File Report 03-005, U.S. Geological Survey. CD-ROM publication.
- Johnsen, L.F., Byle, M.J. and Bruce, D.A. Eds. (2003). Grouting and ground treatment, Geotechnical Special Publication No. 120 ASCE, Reston, VA, 508 pp.
- Joyner, W.B. (2000). Strong motion from surface waves in deep sedimentary basins, *Bull. Seism. Soc. Am.*, 90, S95–112.
- Joyner, W., Fumal, T.E., and Glassmoyer, G. (1994). Empirical response spectral ratios for strong motion data from the 1989 Loma Prieta, California, earthquake, *Proceedings of the 1992 NCEER/SEAOC/BSSC Workshop on Site Response During Earthquakes and Seismic Code Provisions*, G.R. Martin, Ed., University of Southern California.
- Joyner, W.B., Warrick, R.E., and Fumal, T.E. (1981). The effect of Quaternary alluvium on strong ground motion in the Coyote Lake, California earthquake of 1979, *Bull. Seism. Soc. Am.*, 71, 1333–1349.
- Kausel, E. (1974). Forced vibrations of circular foundations on layered media, Report. No. R74-11, Department of Civil Engineering., MIT, Cambridge, MA.
- Kayen, R.E. and Mitchell, J.K. (1997). Assessment of liquefaction potential during earthquakes by Arias intensity, *J. Geotech. Geoenvir. Eng.*, ASCE, 123, 1162–1174.
- Keefer, D.K. (1984). Landslides caused by earthquakes, *Geol. Soc. Am. Bull.*, 94, 406–421.
- Kim, S. (2001). Calibration of simple models for seismic soil structure interaction from field performance data, Ph.D. dissertation, University of California, Los Angeles.
- Kim, S. and Stewart, J.P. (2003). Kinematic soil-structure interaction from strong motion recordings, *J. Geotech. Geoenvir. Eng.*, ASCE, 129, 323–335.
- Kramer, S.L. (1996). *Geotechnical Earthquake Engineering*, Prentice Hall, Upper Saddle River, NJ, 653 pp.
- Kramer, S. L. and Smith, M. W. (1997). Modified Newmark model for seismic displacements of compliant slopes, *J. Geotech. Geoenvir. Eng.*, 123, 635–644.
- Lee, K.L. (1974). Seismic permanent deformations of earth dams, Report No. UCLA-ENG-7497, School of Engineering and Applied Science, University of California, Los Angeles.
- Lee, Y. and Anderson, J.G. (2000). A custom southern California ground motion relationship based on analysis of residuals, *Bull. Seism. Soc. Am.*, 90, S170–S187.
- Lee, M. K. W., and Finn, W. D. L. (1978). Dynamic effective stress response analysis of soil deposits with energy transmitting boundary including assessment of liquefaction potential, The University of British Columbia, Faculty of Applied Science.
- Li, X.S. (2002). A sand model with state-dependent dilatancy, *Geotechnique*, 52, 173–186.
- Li, X. S., Shen, C. K., and Wang, Z. L. (1998). Fully coupled inelastic site response analysis for 1986 Lotung earthquake, *J. Geotech. Geoenvir. Eng.*, ASCE, 124, 560–573.
- Li, X. S., Wang, Z. L., and Shen, C. K. (1992). SUMDES: A nonlinear procedure for response analysis of horizontally layered sites subjected to multi-directional earthquake loading, Department of Civil Engineering, University of California, Davis.
- Liao, S.S.C., Veneziano, D., and Whitman, R.V. (1988). Regression models for evaluating liquefaction probability, *J. Geotech. Eng.*, ASCE, 114, 389–411.
- Lin, A.N. and Jennings, P.C. (1984). Effect of embedment on foundation-soil impedances, *J. Eng. Mech.*, ASCE, 110, 1060–1075.
- Lin, J.-S. and Whitman, R. V. (1983). Decoupling approximation to the evaluation of earthquake-induced plastic slip in earth dams, *Earthquake Eng. Struct. Dyn.*, 11, 667–678.
- Ling, J.I., Leschinsky, D. and Perry, E.B. (1997). Seismic design and performance of geosynthetic-reinforced soil structures, *Geotechnique*, 47, 933–952.
- Liou, G.-S. and Huang, P.-H. (1994). Effect of flexibility on impedance functions for circular foundations, *J. Eng. Mech.*, ASCE, 120, 1429–1446.
- Liu, A.H., Stewart, J.P., Abrahamson, N.A., Moriwaki, Y. (2001). Equivalent number of uniform stress cycles for soil liquefaction analysis, *J. Geotech. Geoenvir. Eng.*, ASCE, 127, 1017–1026.

- Luco, J.E., Trifunac, M.D., and Wong, H.L. (1988). Isolation of soil-structure interaction effects by full-scale forced vibration tests, *J. Earthquake Eng. Struct. Dyn.*, 16, 1–21.
- Lysmer, J., Tabatabaei-Raissi, M., Tajirian, F., Vahdani, S., and Ostdan, F. (1981). SASSI: A system for analysis of soil-structure interaction, Report No. UCB/GT-81/02, Geotech. Engineering., University of California, Berkeley, April.
- Lysmer, J., Udaka, T., Tsai, C.-F., and Seed, H.B. (1975). FLUSH — A computer program for approximate 3-D analysis of soil structure interaction problems, Report. No. UCB/EERC-75/30, Earthquake Engineering Research Center, University of California, Berkeley.
- Makdisi, F.I., and Seed, H.B., (1978). Simplified procedure for estimating dam and embankment earthquake-induced deformations, *J. Geotech. Eng.*, ASCE, 104, 849–867.
- Mamoon, S.M. and Ahmad, S. (1990). Seismic response of piles to obliquely incident SH, SV, and P waves, *J. Geotech. Eng.*, ASCE 116, 186–204.
- Manzari, M.T. and Dafalias, Y.F. (1997). A critical state two-surface plasticity model for sands, *Geotechnique*, 49, 252–272.
- Masing, G. (1926). Eigenspannungen und verfestigung beim Messing, *Proceedings, Second International Congress on Applied Mechanics*, Zurich, Switzerland.
- Matasovic, J. and Vučetić, M. (1996). Analysis of seismic records from the Wildlife Liquefaction site, *Proc. 11th World Conf. Earthquake Eng.*, Disc 1, Paper 209.
- Matsui, T. and San, K.-C. (1992). Finite element slope stability analysis by shear strength reduction technique, *Soils Foundations*, Japanese Society of Soil Mechanics and Foundation Engineering, 32, 59–70.
- Mita, A. and Luco, J.E. (1989). Dynamic response of a square foundation embedded in an elastic halfspace, *J. Soil Dyn. Earthquake Eng.*, 8, 54–67.
- Mononobe, N. and Matsuo, H. (1929). On the determination of earth pressures during earthquakes, *Proceedings, World Engineering Congress*, 9.
- Mosely, M.P., Ed. (1993) *Ground Improvement*, Blackie Academic & Professional, London, 218 pp.
- Muraleetharan, K.K. and Wei, C. (2000). Prediction of static and dynamic behavior of unsaturated soil embankments using the theory of mixtures with interfaces (TMI), *Proc. Engineering Mechanics Conference*, New Orleans, CD-ROM proceedings.
- Mylonakis, G. (2001). Simplified model for seismic pile bending at soil layer interfaes, *Soils and Foundations*, 41 (4), 47–58.
- Nazarian, S. and Stokoe, K.H. (1983). Use of spectral analysis of surface waves for determination of moduli and thicknesses of pavement systems, *Transportation Research Record No. 954*.
- Nemat-Nasser, S. and Shokooh, A. (1979). A unified approach to densification and liquefaction of cohesionless sand in cyclic shearing, *Can. Geotech. J.*, 16 649–678.
- Newmark, N.M., (1965). Effects of earthquakes on dams and embankments, *Geotechnique*, 15, 139–160.
- Nicolaou, S., Mylonakis, G., Gazetas, G. and Tazoh, T. (2001). Kinematic pile bending during earthquakes: Analysis and field measurements, *Geotechnique*, 51 (5), 425–440.
- Ohta, Y. and Goto, N. (1976). Estimation of s-wave velocity in terms of characteristic indices of soil, *Butsuri-Tanko*, 29, 34–41.
- Okabe, S. (1926). General theory of earth pressures, *J. Japan Soc. Civil Eng.*, 12(1), 1277–1323.
- Olson, S.M. and Stark, T.D. (2002). Liquefied strength ratio from liquefaction flow failure case histories, *Can. Geotech. J.*, 39, 629–647.
- Park, S. and Elrick, S. (1998). Prediction of shear wave velocities in southern California using surface geology, *Bull. Seism. Soc. Am.*, 88, 677–685.
- Pestana, J.M. and Nadim, F. (2000). Nonlinear site response analysis of submerged slopes, Report No. UCB/GT/2000-04, Department of Civil & Environmental Engineering, University of California, Berkeley.
- Potts, D.M., Dounias, G.T., and Vaughan, P.R. (1990). Finite element analysis of progressive failure of Carsington embankment, *Geotechnique*, 40, 79–102.
- Poulos, S.J., Castro G., and France, J.W. (1985). Liquefaction evaluation procedure, *J. Geotech. Eng.*, ASCE, 111, 772–792.

- Prevost, J.H. (1981). *DYNAFLOW: A Nonlinear Transient Finite Element Analysis Program*, Department of Civil Engineering, Princeton University, Princeton, New Jersey.
- Prevost, J.H. (1989). DYNA1D — A computer program for nonlinear seismic site response analysis: Technical documentation, Report. No. NCEER-89-0025, National Center for Earthquake Engineering Research, Buffalo, N.Y.
- Pyke, R. M. (1979). Nonlinear soil models for irregular cyclic loadings *J. Geotech. Eng. Div.*, ASCE, 105, 715–726.
- Pyke, R., Seed, H.B., and Chan, C.K. (1975). Settlement of sands under multi-directional loading, *J. Geotech. Eng. Div.*, ASCE, 101, 379–398.
- Qiu, P. (1997). Earthquake induced nonlinear ground deformation analyses, Ph.D. dissertation, University of Southern California.
- Ramberg, W. and Osgood, W.R. (1943). Description of stress-strain curves by three parameters, Technical Note 902, National Advisory Committee for Aeronautics, Washington, D.C.
- Rathje, E.M., Abrahamson, N.A., and Bray, J.D. (1998). Simplified frequency content estimates of earthquake ground motions, *J. Geotech. Geoenviron. Eng.*, 124, 150–159.
- Rathje, E.M. and Bray, J.D. (1999). Two dimensional seismic response of solid-waste landfills, *Earthquake Geotechnical Engineering*, Proceedings of the Second International Conference on, A.A. Balkema, Rotterdam, 2, 655–660.
- Rathje, E.M. and Bray, J.D. (2000). Nonlinear coupled seismic sliding analysis of earth structures, *J. Geotech. Geoenviron. Eng.*, 126, 1002–1014.
- Reese, L.C., Wang, S.T., and Arrellaga, J. (1998). APILE Plus: A program for the analysis of the axial capacity of driven piles, Version 3.0, Ensoft, Inc., Austin, TX.
- Reese, L.C., Wang, S.T., Isenhower, W.M., and Arrellaga, J. (2000). LPILE Plus: A program for the analysis of the axial capacity of driven piles, Version 4.0, Ensoft, Inc., Austin, TX.
- Richards, R. and Elms, D. (1979). Seismic behavior of gravity retaining walls. *J. Geotech. Eng. Div.* 105, 449–464.
- Riemer, M. F., Grizzle, C., and Safaqah, O. (2001). Measurement of dynamic properties of clay using the downhole freestanding shear device, *Proc. Fourth International Conference on Recent Advances in Geotechnical Earthquake Engineering and Soil Dynamics* [computer file], University of Missouri-Rolla, Rolla, Missouri, 6 pp., Paper No. 1.38.
- Riggs, H.R. and Waas, G. (1985). Influence of foundation flexibility on soil-structure interaction, *J. Earthquake Eng. Struct. Dyn.*, 13, 597–615.
- Rix, G.J. and Stokoe, K.H. (1991). Correlation of initial tangent modulus and cone penetration resistance, *Calibration Chamber Testing*, International Symposium on Calibration Chamber Testing, A.B. Huang, Ed., Elsevier, New York, 351–362.
- Robertson, P.K. and Campanella, R.G. (1985). Liquefaction potential of sands using the CPT, *J. Geotech. Eng.*, ASCE, 111, 384–403.
- Robertson, P.K. and Wride, C.E. (1998). Evaluating cyclic liquefaction potential using the cone penetration test, *Can. Geotech. J.*, 35, 442–459.
- Rodriguez-Marek, A., Bray, J.D., and Abrahamson, N.A. (2001). An empirical geotechnical seismic site response procedure, *Earthquake Spectra*, 17, 65–87.
- Roesset, J.M. (1980). A review of soil-structure interaction, in *Soil-Structure Interaction: The Status of Current Analysis Methods and Research*, J.J. Johnson, Ed., Report. No. NUREG/CR-1780 and UCRL-53011, U.S. Nuclear Regulatory Com., Washington DC, and Lawrence Livermore Lab., Livermore, CA.
- Rogers, J.D. (1992). Seismic response of highway embankments, *Transportation Research Record*, No. 1343, 52–62.
- Rollins, K.M., Ed. (1994) *In-situ* deep soil improvement, Geotechnical Special Publication No. 45, ASCE, New York, 150 pp.

- Sachin, D. and Muraleetharan, K.K. (1998). Dynamic behavior of unsaturated soil embankments, Geotechnical Special Publication 75, *Geotechnical Earthquake Engineering and Soil Dynamics III*, American Society of Civil Engineers, Reston, Virginia, 2, 890–901.
- Sadigh, K., Chang, C.-Y., Abrahamson, N.A., Chiou, S.J., and Power, M.S. (1993). Specification of long-period ground motions: updated attenuation relationships for rock site conditions and adjustment factors for near-fault effects, *Proc. Seminar on Seismic Isolation, Passive Energy Dissipation, and Active Control*, Applied Technology Council Publication No. 17-1, 1, 59–70.
- Sadigh, K., Chang, C.-Y., Egan, J.A., Makdisi, F., and Youngs, R.R. (1997). Attenuation relations for shallow crustal earthquakes based on California strong motion data, *Seism. Res. Lett.*, 68, 180–189.
- Salvati, L. A., Lok, M.-H., and Pestana, J.M. (2001). Seismic response of deep stiff granular soil deposits, *Proc. 4th Int. Conf. Recent Advances in Geotech. Eqk. Eng. Soil Dyn.*, Paper 3.30.
- Sancio, R.B., Bray, J.D., Stewart, J.P., Youd, T.L., Durgunoğlu, H.T., Önalp, A., Seed, R.B., Christensen, C., Baturay, M.B., and Karadaylar, T. (2003). Correlation between ground failure and soil conditions in Adapazari, Turkey, *Int. J. Soil Dyn. Earthquake Eng.*, 22, 1093–1102.
- Schaefer, V.R., Sharp, K.D., Drumheller, J.C. and Abramson, L.W., Eds. (1997). Ground improvement, ground reinforcement and ground treatment: Developments 1987–1997, Geotechnical Special Publication No. 69, ASCE, Reston, VA, 632 pp.
- Schnabel, P.B., Lysmer, J. and Seed, H.B. (1972). SHAKE: A computer program for earthquake response analysis of horizontally layered sites, Report No. EERC 72/12, Earthquake Engineering Research Center, University of California, Berkeley.
- Schneider, J.F., Silva, W.J., and Stark, C.L. (1993). Ground motion model for the 1989 $m6.9$ Loma Prieta earthquake including effects of source, path, and site, *Earthquake Spectra*, 9, 251–287.
- SEAOC (Structural Engineers Assn. of California) Seismology Committee, Ad Hoc Foundation Committee (2001). USD/LRFD/limit state approach to foundation design, *Proc. 70th Annual Convention, Structural Engineers Association of California*, Structural Engineers Assn. of California, Sacramento, 215–225.
- Seed, H.B., (1979). Considerations in the earthquake-resistant design of earth and rockfill dams, *Geotechnique*, 29, 215–263.
- Seed, R.B., Cetin, K.O., Moss, R.E.S., Kammerer, A.M., Wu, J., Pestana, J.M., and Riemer, M.F. (2001). Recent advances in soil liquefaction engineering and seismic site response evaluation, *Proc. 4th Int. Conf. on Recent Advances in Geotech. Eqk. Eng. Soil Dyn.*, Paper No. SPL-2.
- Seed, R.B., Dickenson, S.E., and Mok, C.M. (1994). Site effects on strong shaking and seismic risk: recent developments and their impact on seismic design codes and practice, *Structures Congress XII: Proceedings of Papers Presented at the Structures Congress '94*, Atlanta, GA, ASCE, New York, 1, 573–578.
- Seed, R.B. and Harder, L.F. (1990). SPT-based analysis of cyclic pore pressure generation and undrained residual strength, *Proceedings, H. Bolton Seed Memorial Symposium*, University of California, Berkeley, 2, J.M. Duncan Ed., 351–376.
- Seed, H.B. and Idriss, I.M. (1970). Soil moduli and damping factors for dynamic response analyses, Report EERC 70-10, Earthquake Engineering Research Center, University of California, Berkeley.
- Seed, H.B. and Idriss, I.M. (1971). Simplified procedure for evaluating soil liquefaction potential, *J. Soil Mech. Found. Div.*, ASCE, 107, 1249–1274.
- Seed, H. B. and Idriss, I. M. (1982) Ground motions and soil liquefaction during earthquakes, Monograph Series, 5, Earthquake Engineering Research Institute.
- Seed, H.B., Idriss, I.M., Makdisi, F., and Banerjee, N. (1975). Representation of Irregular Stress Time Histories by Equivalent Uniform Stress Series in Liquefaction Analyses, EERC 75-29, Earthquake Engineering Research Center, University of California, Berkeley.
- Seed, H.B., Lee, K.L., Idriss, I.M., and Makdisi, F.I. (1973). Analysis of the slides in the San Fernando dams during the earthquake of Feb. 9, 1971, Report No. EERC 73-2, Earthquake Engineering Research Center, University of California, Berkeley, 150 pp.

- Seed, H.B., Romo, M.P., Sun, J.I., Jaime, A., and Lysmer, J. (1987). Relationships between soil conditions and earthquake ground motions in Mexico City in the earthquake of September 19, 1985, Report No. UCB/EERC-87/15, Earthquake Engineering Research Center, University of California, Berkeley.
- Seed, H.B. and Silver, M.L. (1972). Settlement of dry sands during earthquakes, *J. Soil Mech. Found. Div.*, 98, 381–397.
- Seed, H.B., Wong, R.T., Idriss, I.M., and Tokimatsu, K. (1986). Moduli and damping factors for dynamic analyses of cohesionless soils, *J. Geotech. Eng.*, ASCE, 112, 1016–1032.
- Serff, N., Seed, H.B., Makdisi, F.I., and Chang, C.-Y. (1976). Earthquake-induced deformations of earth dams, Report No. EERC 76-4, Earthquake Engineering Research Center, University of California, Berkeley, 140 pp.
- Silva, W.J. (1976). Body waves in a layered anelastic solid, *Bull. Seism. Soc. Am.*, 66, 1539–1554.
- Silva, W.J., Abrahamson, N., Toro, G., and Costantino, C. (1997). Description and validation of the stochastic ground motion model, Report to Brookhaven National Laboratory, Associated Universities, Inc., Upton, NY.
- Silva, W.J., Darragh, R., Gregor, N., Martin, G., Abrahamson, N., and Kircher, C. (2000). Reassessment of site coefficients and near-fault factors for building code provisions, Report to U.S. Geological Survey, National Earthquake Hazards Reduction Program.
- Silva, W.J. and Lee, K. (1987). WES RASCAL code for synthesizing earthquake ground motions, in State of the Art for Assessing Earthquake Hazards in the United States, Report 24, U.S. Army Engineers Waterway Experiment Station, *Misc. Paper S-73-1*.
- Silva, W.J., Li, S., Darragh, R., and Gregor, N. (1999). Surface geology based strong motion amplification factors for the San Francisco Bay and Los Angeles areas, Report to Pacific Earthquake Engineering Research Center.
- Stark, T.D. and Mesri, G. (1992). Undrained shear strength of sands for stability analysis, *J. Geotech. Eng.*, ASCE, 118, 1727–1747.
- Steidl, J.H. (2000). Site response in southern California for probabilistic seismic hazard analysis, *Bull. Seism. Soc. Am.*, 90, S149–S169.
- Stewart, J.P., Blake, T.M., and Hollingsworth, R.A. (2003a). A screen analysis procedure for seismic slope stability, *Earthquake Spectra*, 19, 697–712.
- Stewart, J.P., Chiou, S.-J., Bray, J.D., Somerville, P.G., Graves, R.W., and Abrahamson, N.A. (2001). Ground motion evaluation procedures for performance based design, Report No. PEER-2001/09, Pacific Earthquake Engineering Research Center, University of California, Berkeley, 229 pp.
- Stewart, J.P., Kim, S., Bielak, J., Dobry, R., and Power, M. (2003b). Revisions to soil structure interaction procedures in NEHRP design provisions, *Earthquake Spectra*, 19, 677–696.
- Stewart, J.P., Liu, A.H., and Choi, Y. (2003c). Amplification factors for spectral acceleration in tectonically active regions, *Bull. Seism. Soc. Am.*, 93, 332–352.
- Stewart, J.P., Seed, R.B., and Fenves, G.L. (1999). Seismic soil-structure interaction in buildings. II: Empirical findings, *J. Geotech. Geoenv. Eng.*, ASCE, 125, 38–48.
- Stewart, J.P. and Whang, D.H. (2003). Simplified procedure to estimate ground settlement from seismic compression in compacted soils, *Proc. 7th Pacific Conference on Earthquake Engineering*, Christchurch, New Zealand, February, Paper 46.
- Stokoe, K.H. II, Wright, S.G., Bay, J.A. and Roesset, J.M. (1994). Characterization of geotechnical sites by SASW method, *Geophysical Characterization of Sites*, R.D. Woods, Ed., A.A. Balkema, Rotterdam, 15–25.
- Suzuki, Y., Tokimatsu, K., Koyamada, K., Taya, Y. (1995). Field correlation of soil liquefaction based on CPT data, *Proceedings of the International Symposium on Cone Penetration Testing, CPT'95*, Linkoping, Sweden, 2, 583–588.
- Terzaghi, K., Peck, R.B., and Mesri, G. (1996). *Soil Mechanics in Engineering Practice*, Wiley Interscience, New York, 592 pp.

- Tinsley, J.C. and Fumal, T.E. (1985). Mapping quaternary sedimentary deposits for areal variations in shaking response, in *Evaluating Earthquake Hazards in the Los Angeles Region*, Ziony, J.I. (Ed.), U.S. Geological Survey, Reston, VA, Prof. Paper 1360, 101–126.
- Tokimatsu, K. and Seed, H.B. (1987). Evaluation of settlements in sand due to earthquake shaking, *J. Geotech. Eng.*, ASCE, 113, 861–878.
- Toprak, S., Holzer, T.L., Bennett, M.J., and Tinsley, J.C. (1999). CPT- and SPT-based probabilistic assessment of liquefaction potential, *Proceedings of the Seventh U.S.-Japan Workshop on Earthquake Resistant Design of Lifeline Facilities and Countermeasures Against Soil Liquefaction*, Technical Report MCEER-99-0019, Multidisciplinary Center for Earthquake Engineering Research, University at Buffalo, State University of New York, 69–86.
- Travarasou, T., Bray, J.D., and Abrahamson, N.A. (2003). Empirical attenuation relationship for Arias intensity, *Earthquake Eng. Struct. Dyn.* 32, 1133–1155.
- Van Impe, W. F. (1989). *Soil Improvement Techniques and Their Evolution*, A.A.Balkema, Rotterdam, 125 pp.
- Varnes, D.J. (1978). Slope movement types and processes, in *Landslides — Analysis and Control*, National Academy of Sciences Transportation Research Board Special Report 176, Schuster, R.L. and Krizek, R.J. eds., 12–33.
- Veletsos, A.S. and Meek, J.W. (1974). Dynamic behavior of building-foundation systems, *J. Earthquake Eng. Struct. Dyn.*, 3, 121–138.
- Veletsos, A.S. and Nair V.V. (1975). Seismic interaction of structures on hysteretic foundations, *J. Struct. Eng.*, ASCE 101, 109–129.
- Veletsos, A.S. and Prasad, A.M. (1989). Seismic interaction of structures and soils: Stochastic approach, *J. Struct. Eng.*, ASCE, 115, 935–956.
- Veletsos, A.S., Prasad, A.M., and Wu, W.H. (1997). Transfer functions for rigid rectangular foundations, *J. Earthquake Eng. Struct. Dyn.*, 26, 5–17.
- Veletsos, A.S. and Verbic, B. (1973). Vibration of viscoelastic foundations, *J. Earthquake Eng. Struct. Dyn.*, 2, 87–102.
- Veletsos, A.S. and Wei, Y.T. (1971). Lateral and rocking vibrations of footings, *J. Soil Mech. and Found. Div.*, ASCE, 97, 1227–1248.
- Vucetic, M. (1990). Normalized behavior of clay under irregular cyclic loading, *Can. Geotech. J.*, 27, 29–46.
- Vucetic, M. and Dobry, R. (1991) Effect of soil plasticity on cyclic response, *J. Geotech. Eng.*, ASCE, 117(1), 89–107.
- Wang, W. (1979). Some findings in soil liquefaction, Water Conservancy and Hydroelectric Power Scientific Research Institute, Beijing, China.
- Wang, Z. L. (1990). Bounding surface hypoplasticity model for granular soils and its applications, Ph.D. thesis, University of California, Davis.
- Wang, Z.L., Chang, C.-Y., and Mok, C.M. (2001). Evaluation of site response using downhole array data from a liquefied site, *Proc. 4th Int. Conf. Recent Advances in Geotech. Eqk. Eng. Soil Dyn.*, Paper 4.30.
- Weidlinger Associates (1978). Nonlinear soil-structure interaction, Report No. EPRI NP-945, Electrical Power Research Institute, Palo Alto, CA
- Whitman, R.D. and Liao, S.S.C. (1985). Seismic design of retaining walls Misc. Pper GL-85-1, U.S. Army Engineer Waterways Experiment Station Vicksburg, MS.
- Wills, C.J. and Silva, W. (1998). Shear wave velocity characteristics of geologic units in California, *Earthquake Spectra*, 14 (3), 533–556.
- Wilson, R.C. and Keefer, D.K. (1985) Predicted areal limits of earthquake-induced landsliding, in *Evaluating Earthquake Hazards in the Los Angeles Region*, Ziony, J.I. (Ed.), U.S. Geological Survey, Reston, VA, Prof. Paper 1360, 317–345.
- Wong, H.L., Trifunac, M.D., and Luco, J.E. (1988). A comparison of soil-structure interaction calculations with results of full-scale forced vibration tests, *J. Soil Dyn. Earthquake Eng.*, 7, 22—31.
- Yegian, M.K., Marciano, E.A., and Ghahraman, V.G. (1991). Earthquake-induced permanent deformations: probabilistic approach, *J. Geotech. Eng.*, 117, 35–50.

- Youd, T.L. (1984). Recurrence of liquefaction at the same site, *Proc. 8th World Conf. Earthquake Eng.*, 3, 231–238.
- Youd, T.L. and Garris, C.T. (1995). Liquefaction-induced ground surface disruption, *J. Geotech. Eng.*, 121, 805–809.
- Youd, T.L., Hansen, C.M., and Bartlett, S.F. (2002). Revised multilinear regression equations for prediction of lateral spread displacement, ASCE, *J. Geotech. Geoenviron. Eng.*, 128, 1007–1017.
- Youd, T.L., and Noble, S.K. (1997), Liquefaction criteria based on probabilistic analyses, *NCEER Workshop on Evaluation of Liquefaction Resistance of Soils*, National Center for Earthquake Engineering Research Technical Report NCEER-97-0022, 201–216.
- Youd, T.L. et al. (2001). Liquefaction resistance of soils: Summary report from the 1996 NCEER and 1998 NCEER/NSF workshops on evaluation of liquefaction resistance of soils, *J. Geotech. Geoenviron. Eng.*, ASCE, 127, 817–833.
- Zergouni, M. and Vaid, Y.P. (1994). Effective stress response of clay to undrained cyclic loading, *Canadian Geotech. J.*, 31, 714–727.

5

Engineering Characterization of Ground Motion

5.1	Introduction.....	5-1
5.2	Strong-Motion Recordings..... Historical Perspective • Examples of Acceleration and Velocity Time Series • Processing Strong-Motion Records • Sources of Strong-Motion Records	5-2
5.3	Characteristics of Strong-Motion Spectra..... Introduction • Fourier Spectra • Elastic Response Spectra • Elastic Design Spectra • Arias Intensity and Strong- Motion Duration • Drift Spectrum • Inelastic Response Spectra • Energy Spectra • Damage Spectra • Strong- Motion Spectra: A Summary	5-5
5.4	Ground Motion (Attenuation) Relations	5-27
	Introduction • Model Parameters • Analysis Methods • Ground Motion (Attenuation) Relations Used by USGS • Effects of Near-Fault Directivity • Vertical Ground Motion	
5.5	Ground Motion Representation in the <i>International Building Code</i>	5-57
	Introduction • Maximum Considered Earthquake (MCE) • Design Spectra in the IBC • Site-Specific Ground Motion in IBC	
5.6	Future Challenges	5-61
	Development of the Next Generation of Ground Motion (Attenuation) Relations • Better Understanding and Modeling of Fault Rupture Directivity and Fling • Inclusion of the Directivity Effects in Probabilistic Hazard Analysis • Near Real-Time Spatial Distribution of Damage Potential of Ground Motions • Vertical Design Spectra • Ground-Motion Parameters for Performance-Based Earthquake Engineering • Modeling Cumulative Damage Potential of Earthquake Ground Motions	

Yousef Bozorgnia

Kenneth W. Campbell

5.1 Introduction

“The basic data of earthquake engineering are the recordings of ground accelerations during earthquakes. A knowledge of the ground motion is essential to an understanding of the earthquake behavior of structures” (Housner, 1970a). Recorded ground motion time series contain valuable characteristics and information that are used directly, or indirectly, in seismic analysis and design. Parameters such as peak

ground motion values (acceleration, velocity and displacement), measures of the frequency content of the ground motion, duration of strong shaking and various intensity measures play important roles in seismic evaluation of existing facilities and design of new systems.

This chapter presents *engineering* characteristics of strong ground motion. Seismological aspects of ground motion, which are related to the topics presented in this chapter, are covered in Chapter 2. In Section 5.2, we provide a historical perspective of strong-motion recordings and present numerous examples of ground acceleration and velocity time series, followed by a list of the agencies that provide strong ground motion records. In Section 5.3, we discuss the characteristics and applications of various strong-motion *spectra* and their associated parameters. These include Fourier spectra, elastic response spectra, elastic design spectra, drift spectra, inelastic spectra, inelastic design spectra, energy spectra, damage spectra and other parameters such as Housner Spectrum Intensity and Arias Intensity. Strong-motion spectra have widespread applications in probabilistic and deterministic seismic hazard analysis, seismic analysis and design, quantification of damage potential of ground motion, near real-time post-earthquake response, among many others. Discussions about the recent ground motion relations, or *attenuation relations*, used in the 2002 U.S. National Seismic Hazard Maps are presented in Section 5.4. These maps provide the fundamental data for the latest seismic design requirements in the United States. Also presented in Section 5.4 are recent advances on the engineering characteristics of fault rupture directivity, vertical ground motion and hanging wall and footwall effects. In Section 5.5, the methodology and technical reasons behind the representation of the ground motion in the *International Building Code (IBC)*, which includes recent seismic design provisions in the United States, are elaborated. The chapter is concluded with a discussion about the future challenges on characterizing strong ground motion for engineering applications.

5.2 Strong-Motion Recordings

5.2.1 Historical Perspective

After the 1925 Santa Barbara, California earthquake, a program to study strong ground motion was initiated in the United States. In 1932, strong-motion instruments were deployed at selected sites in California, and the first significant strong motions were recorded during the March 10, 1933 Long Beach, California, earthquake (M_w 6.4). In 1940, the M_w 6.9 Imperial Valley, California, earthquake was recorded in the basement of a concrete building located in El Centro. The site was located about 6 km from ground rupture observed during the earthquake. For many years, the El Centro recording was used throughout the world for seismic analysis and design. In recent years, however, several studies have shown that, compared with more recent near-source recordings, the El Centro record has limited damage potential (e.g., Mahin and Bertero, 1981; Bozorgnia and Bertero, 2002). In 1966, at a site located about 80 m from ground rupture associated with the M_w 6.1 Parkfield earthquake in central California, the first strong-motion recording in excess of 0.5 g (g = acceleration of gravity = 981 cm/sec²) was recorded. There was considerable debate at the time whether or not even higher ground motions were possible.

Near-source recordings in excess of 0.5 g have now become commonplace, and several accelerations exceeding 1 g have been recorded. The largest recording to date (larger than 2 g) is the vertical acceleration obtained during the M_w 6.8 Nahanni earthquake, which occurred in 1985 in a remote area of the Northwest Territories, Canada (Campbell, 2000a). There are now tens of thousands of strong-motion instruments located throughout the world. Several earthquakes have triggered over 50 accelerographs, including the 1971 San Fernando (M_w 6.6), 1984 Morgan Hill (M_w 6.2), 1987 Whittier Narrows (M_w 6.0), 1989 Loma Prieta (M_w 6.9), 1994 Northridge (M_w 6.7), 1995 Hyogo-ken Nanbu (Kobe, M_w 6.9) and 1999 Chi-Chi (M_w 7.6). Dense networks in urban areas form the backbone of recording systems designed to provide a near real-time assessment of ground shaking within minutes after an earthquake to aid in emergency response and post-earthquake applications. For example, in California, TriNet (Wald et al., 1999) and CISN (Lin et al., 2002) automatically generate contour maps (a program called ShakeMap) of basic strong-motion parameters and

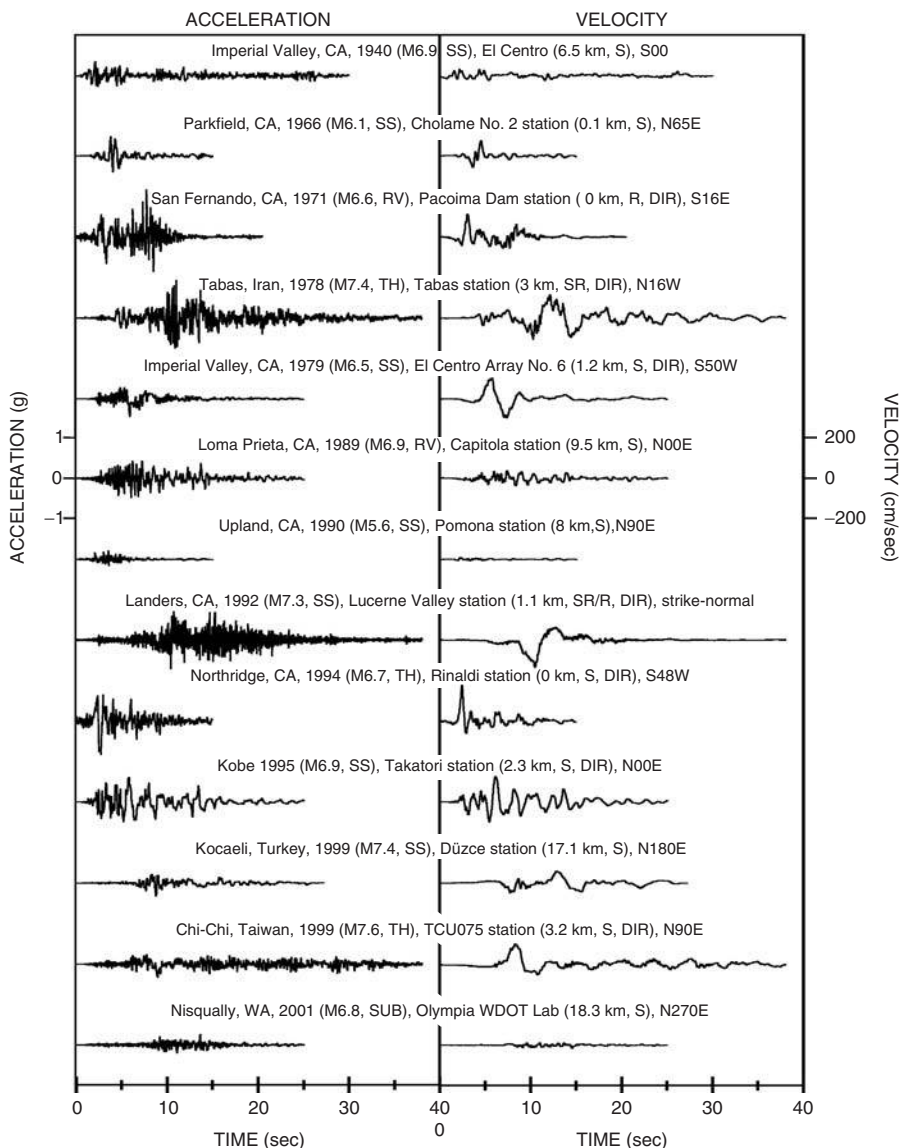


FIGURE 5.1 Selected recorded ground accelerations (plotted at the same scale), and the corresponding ground velocities. SS = strike-slip faulting; RV = reverse faulting; TH = thrust faulting; SUB = subduction intraslab earthquake; S = soil site; R = rock site; SR = soft rock site; DIR = record includes fault rupture directivity effects. Distance measure is from the recording site to surface projection of fault rupture plane (epicentral distance for the Nisqually earthquake).

post them on the Internet in near real-time. Due to their success, similar networks and programs are being developed in different regions of the country as well.

5.2.2 Examples of Acceleration and Velocity Time Series

Ground motions recorded at different sites and in different earthquakes will vary significantly due to several factors, including, but not limited to, earthquake magnitude, faulting mechanism, distance from the recording site to the earthquake source, local site condition, depth of sediments, basin and other wave-focusing effects and source directivity effects. Figure 5.1 presents plots of selected recorded ground

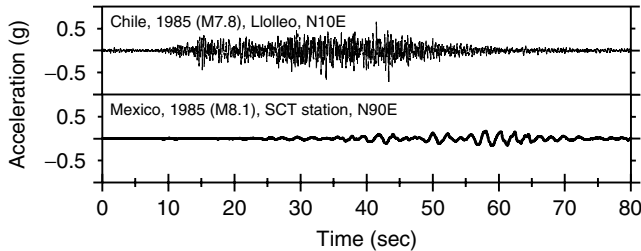


FIGURE 5.2 Ground accelerations recorded during the March 3, 1985 Chile and September 19, 1985 Mexico earthquakes.

accelerations (plotted on the same scale) and the corresponding time variation of the ground velocity. In this figure, the largest peak ground acceleration is 1.17 g for the 1971 San Fernando earthquake recorded at Pacoima Dam and the largest peak ground velocity is 178 cm/sec for the 1994 Northridge earthquake at Rinaldi Receiving Station. Special characteristics of the ground motions affected by fault rupture directivity are discussed in Section 5.4.5. In some instances, a large peak velocity may be associated with a so-called fling step displacement pulse. An example of such a case for the 1999 Chi-Chi, Taiwan earthquake is presented in Chapter 2. Depending on various factors, especially earthquake magnitude and local site response, recorded ground motions can have a long duration. Examples of long duration ground motions with repeated cycles of ground oscillations are shown in Figure 5.2 for the 1985 earthquakes in Chile ($M_w 7.8$) and Mexico ($M_w 8.1$). Generally, long duration strong motions will have high damage potential. Structural members and systems subjected to repeated cycles of strong motions become increasingly vulnerable (e.g., see experimental studies by Bertero et al., 1977). Hence, duration should also be taken into account in the quantification of damage potential of earthquake ground motion.

5.2.3 Processing Strong-Motion Records

The primary strong-motion recording device used throughout a large region of the United States is the SMA-1 analog mechanical-optical system. SMA-1 instruments are rapidly being replaced by digital accelerographs. Digital instruments extend the dynamic range of strong-motion recordings to accelerations as small as 0.001g and to frequencies as high as 50 Hz or greater (Campbell, 2000a). The analog traces of ground motion must be digitized, processed for baseline distortion and instrument response, filtered and integrated to obtain velocity and displacement (see Hudson, 1979; Campbell, 2000a for more details). Ground accelerations recorded by digital instruments also usually need corrections for offset in the acceleration baseline (Boore et al., 2002; USGS, 2002). This correction usually affects only the long period portion of the response spectrum.

Various computer programs can process digitized accelerograms. The United States Geological Survey (USGS) developed *BAP*, strong-motion processing software for personal computers (Converse, 1992), and its mainframe version called *AGRAM*. These programs provide various useful data processing functions. There are also other computer programs that can be used for specific computations using strong-motion records. For example, *SPECEQ* (Nigam and Jennings, 1968; NISEE, 1999) is widely used for the computation of elastic response spectra. Other computer routines are also available through the National Information Service for Earthquake Engineering (NISEE, 1999). Commercially available software packages such as *MATLAB®* (2002) and *Strong Motion Analyst* (SMA) (Kinematics, 2003) can also be employed for data processing and analyzing recorded ground motion.

5.2.4 Sources of Strong-Motion Records

Various federal, state and local agencies, as well as many universities, operate strong-motion networks. For example, in the United States, the USGS National Strong Motion Program (NSMP) has the responsibility of operating and producing strong-motion networks and data at the federal level. In California, the major source of strong-motion data comes from the California Strong Motion Instrumentation Program (CSMIP) of the

TABLE 5.1 Selected Sources of Strong-Motion Recordings and Their Parameters

Source	Web Site and Reference
California Strong Motion Instrumentation Program (CSMIP)	http://www.consrv.ca.gov/cgs/smip/
California Integrated Seismic Network (CISN)	http://docinet3.consrv.ca.gov/csmip/cisn-edc/default.htm
U.S. Geological Survey (USGS)	http://nsmp.wr.usgs.gov/
U.S. Geological Survey (USGS)	CD ROM of digitized strong-motion accelerograms of North and Central American Earthquakes, 1933–1986 (Seekins et al., 1992; http://nsmp.wr.usgs.gov/cdrom.html)
Consortium of Organizations for Strong-Motion Observation Systems (COSMOS) 'TriNet', and 'ShakeMap'	http://db.cosmos-eq.org/
University of Southern California (USC) US National Geophysical Data Center (NGDC/NOAA) Pacific Earthquake Engineering Research (PEER) Center SAC steel project, strong-motion database	http://www.trinett.org/ http://earthquake.usgs.gov/shakemap http://www.usc.edu/dept/civil_eng/Earthquake_eng http://www.ngdc.noaa.gov/seg/hazard/strong.html http://peer.berkeley.edu/smcat/search.html http://nisee.berkeley.edu/data/strong_motion/sacsteel/ground_motions.html
Caltech strong motion database (SMARTS)	Diskettes of selected records (http://www.eerl.caltech.edu/smarts/smarts.html)
Pacific Northwest Seismograph Network (PNSN) European Strong-Motion Database (ESD)	http://www.geophys.washington.edu/SEIS/PNSN/SMO/ http://www.iesd.hi.is/ESD_Local/frameset.htm http://www.k-net.bosai.go.jp/
Japan, Kyoshin Net (K-Net); National Research Institute for Earth Science and Disaster Prevention (NIED) Japan, KiK-Net; National Research Institute for Earth Science and Disaster Prevention (NIED)	http://www.kik.bosai.go.jp/kik/index_en.shtml
Mexico, Guerrero Accelerograph Network	http://www.seismo.unr.edu/ftp/zeng/GUERRERO/guerrero.html http://seiscpc2.ethz.ch/strong_motion/home.jsp http://www.cwb.gov.tw/V4e/index.htm For the 1999 Chi-Chi earthquake, a CD of strong motion records was also produced by Lee et al. (2001) http://angora.deprem.gov.tr/indexen.htm
Turkey, General Directorate of Disaster Affairs	

California Geological Survey (CGS). Strong-motion recordings and a summary of recorded strong-motion parameters can be obtained from a variety of sources, including those listed in Table 5.1.

5.3 Characteristics of Strong-Motion Spectra

5.3.1 Introduction

Various types of ground-motion parameters and spectra can quantify numerous characteristics of strong ground motion. Ground-motion spectra are used in a wide variety of applications, such as seismic hazard analysis, seismic design, ground motion scaling for analysis and design, quantification of damage potential of recorded motions and performance-based earthquake engineering.

Some of the strong-motion parameters and spectra discussed in the following sections are based solely on the recorded free-field ground motion and are, therefore, independent of any structural model and response. Other strong-motion parameters and spectra are based on the *elastic* and *inelastic* response of single-degree-of-freedom (SDF) systems, or other generic models, each excited by the free-field ground motion.

5.3.2 Fourier Spectra

One way to characterize the frequency content of a recorded ground motion is to represent the ground motion in the frequency domain through its Fourier spectrum. The Fourier transform of the ground acceleration time series, $a_g(t)$, is defined as

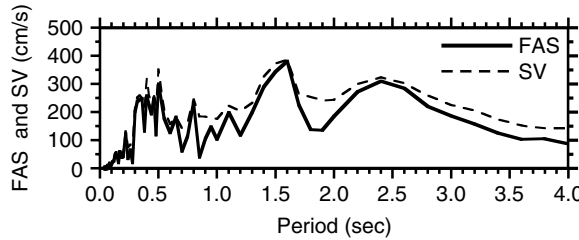


FIGURE 5.3 Fourier amplitude spectrum (FAS) and zero-damped spectral velocity (SV) of the ground acceleration recorded at Sylmar County Hospital (NS component) during the 1994 Northridge, California, earthquake.

$$F(\omega) = \int_0^{T_0} a_g(t) e^{-i\omega t} dt \quad (5.1)$$

where $F(\omega)$ is the Fourier transform of the ground acceleration, ω is circular frequency (rad/sec), T_0 is time duration and $i = (-1)^{1/2}$. Given the Fourier spectrum, $F(\omega)$, the time series $a_g(t)$ can be recovered through the inverse Fourier transform

$$a_g(t) = \frac{1}{2\pi} \int_{-\infty}^{\infty} F(\omega) e^{i\omega t} d\omega \quad (5.2)$$

Equation 5.1 can be rewritten as

$$F(\omega) = \underbrace{\int_0^{T_0} a_g(t) \cos \omega t dt}_{=C(\omega)} - i \underbrace{\int_0^{T_0} a_g(t) \sin \omega t dt}_{=S(\omega)} \quad (5.3)$$

where, it is evident that $F(\omega)$ is a complex-valued function, which can be represented by its amplitude (modulus) and a phase angle. The amplitude of $F(\omega)$, called the Fourier amplitude spectrum, $FAS(\omega)$, and the phase of $F(\omega)$, called the Fourier phase spectrum, $\Phi(\omega)$, are calculated by (e.g., Clough and Penzien, 1993; Hudson, 1979)

$$FAS(\omega) = \sqrt{C^2(\omega) + S^2(\omega)} \quad (5.4a)$$

$$\Phi(\omega) = -\tan^{-1}[S(\omega)/C(\omega)] \quad (5.4b)$$

Given a digitized, or digitally recorded, ground acceleration time series, the computation of the Fourier spectrum is usually performed by a discrete Fourier transform and fast Fourier transform (FFT) technique (Clough and Penzien, 1993; Humar, 1990; Press et al., 1992). Various computer programs can be employed to calculate $FAS(\omega)$, usually shortened to FAS, including BAP (Seekins et al., 1992) and MATLAB (2002). Slightly different definitions of the Fourier transform may be used in different computer programs; thus, care should be taken in interpreting the output results. The FAS of the processed ground accelerations are usually published by the various recording agencies. An example of published FAS is shown in Figure 5.3 for the north-south component of the ground acceleration recorded during the 1994 Northridge earthquake at the Sylmar County Hospital. In this figure, the FAS is plotted versus period ($=2\pi/\omega$). Spectral velocity (SV) is also plotted in this figure for comparison. The definition and characteristics of SV are provided in Section 5.3.3.

Ground motion is either recorded digitally or digitized (sampled) in the time domain. Therefore, there is a limit on the amount of short- and long-period information that can be extracted from it. The shortest

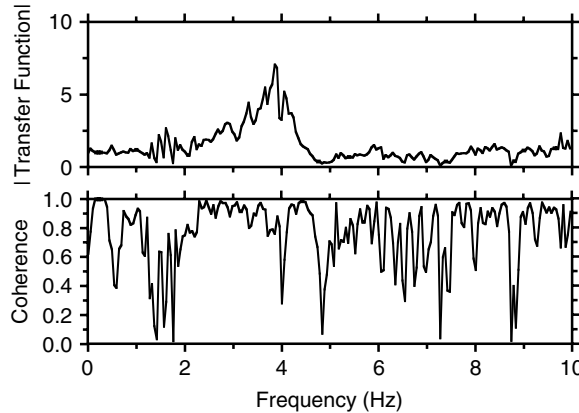


FIGURE 5.4 Example of a transfer function and coherence between the vertical accelerations recorded at the roof and base of a 14-story steel building located in El Segundo, California, during the Northridge, California, earthquake. (Adapted from Bozorgnia et al. (1998). Vertical response of twelve structures recorded during the Northridge earthquake. *Earthquake Spectra*, 14, 411–432.)

period that can be represented by the Fourier spectrum is referred to as the *Nyquist* period, which is two times the time digitization (or sampling) interval of the ground motion (Humar, 1990; Takahashi et al., 1972). For example, if the interval of digitization of an acceleration record is 0.02 sec, the shortest period in the Fourier spectrum of the record is 0.04 sec. In the computation of the FAS using the discrete Fourier transform, the frequency resolution, (that is, the shortest frequency interval at which the FAS can be computed) is inversely proportional to the record length (Humar, 1990). This is a practical limit on the frequency resolution of the Fourier spectrum.

Applications of Fourier spectra are widespread in earthquake engineering and seismology and serve as the fundamental means of examining the frequency content of recorded ground motion or structural response. Also, other functions commonly used in spectral analysis techniques are dependent on Fourier spectra. These functions include the power spectral density function (or autospectrum) as well as the cross-spectrum, coherence function and transfer function between two motions recorded at different locations. Definitions and details of these functions can be found in Bendat and Piersol (1980). Two of these functions are mentioned herein. The Power spectral density (PSD) function can be computed as FAS^2/T_0 . In practice, however, there are different methods to reduce the variance of the computed PSD (e.g., see the signal processing toolbox of MATLAB). The coherence function between two recorded motions, $x(t)$ and $y(t)$, is defined as

$$\gamma_{xy}^2 = \left| S_{xy} \right|^2 / (S_{xx} S_{yy}) \quad (5.5)$$

where $|S_{xy}|$ is the amplitude of the cross-spectrum of $x(t)$ and $y(t)$, and S_{xx} and S_{yy} are their PSD functions. In Equation 5.5, all the terms are functions of frequency. A high value of coherence at a given frequency indicates that the two recorded signals are highly correlated at that frequency. In structural earthquake engineering, coherence, cross-spectra and transfer functions can be used to examine the recorded structural response (e.g., Celebi, 1993). Examples of a transfer function (TF) and coherence function are presented in Figure 5.4 for a pair of vertical motions recorded at the roof and base of a 14-story steel building (Bozorgnia et al., 1998). The TF may be used to identify the natural frequencies of the system and the correlation of the motions at a given frequency can be examined through the coherence function. For example, using Figure 5.4, a frequency of about 3.9 Hz can be identified as the vertical natural frequency of the system, which also corresponds to a high coherence, that is, the roof and base vertical motions are strongly correlated at that frequency. There are also various applications of Fourier spectra

and their related functions in engineering seismology. For example, Abrahamson et al. (1991) used the complex-valued coherency function to study the spatial variation of ground motion (see Chapter 2). Another important application of Fourier spectra in engineering seismology is its use in the so-called stochastic method which is used to estimate ground motion from fundamental seismological parameters in areas where there are an insufficient number of strong-motion recordings (e.g., Campbell, 2003d; Boore, 2003). These stochastic motions are then used to develop attenuation relations for these areas. Fourier spectra are also used in site-response studies, such as those done with one-dimensional, vertically propagating seismic-wave analysis.

5.3.3 Elastic Response Spectra

5.3.3.1 Definitions and Examples

The concept of elastic response spectrum was introduced by Maurice A. Biot (Biot 1933, 1934, 1941; see also Bozorgnia, 2003; and Chapter 1). The technique is now a fundamental method in earthquake engineering (Housner 1941; Housner et al., 1953; Hudson, 1962). The elastic response spectrum represents the maximum response (over time) of a linear elastic SDF system versus its natural period (or frequency) when excited by a ground acceleration time history. The natural period, T (sec), of the SDF system is related to the circular frequency, ω (rad/sec), and cyclic frequency, f (cycles/sec or Hz), through the expression

$$\omega = \sqrt{(k/m)} = 2\pi f = 2\pi/T \quad (5.6)$$

where k and m are the stiffness and mass of the system, respectively. The SDF system can have different values of damping ratio, usually specified as a percentage of the critical damping (e.g., see Chopra, 2001). The response quantity of the SDF system can be one of the following:

S_d = maximum deformation of the SDF system relative to the ground

SV = maximum velocity of the SDF system relative to the ground

SA = maximum absolute (total) acceleration of the SDF system

S_v (or PSV) = pseudo-velocity = ωS_d

S_a (or PSA) = pseudo-acceleration = $\omega^2 S_d$

For response spectra, the absolute values of these quantities are used. The maximum elastic restoring force (or the base shear) in the SDF system is

$$F_e = k S_d = m \omega^2 S_d = m S_a \quad (5.7)$$

The elastic *seismic coefficient*, a term commonly used in earthquake-resistant design, is defined as

$$C_e = F_e/w = S_a/g \quad (5.8)$$

where w is the weight of the system and g is the acceleration of gravity. Because of their physical interpretations and practical applications, S_v and S_a are the preferred choices by earthquake engineers as opposed to SV and SA . Examples of S_a , S_v and S_d response spectra are presented in Figure 5.5 for a 5% damped SDF system subjected to the ground motion recorded at the Rinaldi Receiving Station during the 1994 Northridge earthquake.

Applications of response spectra are extensive in earthquake engineering, including its use in the characterization of ground motion and in the elastic dynamic structural analysis by the modal superposition method (Clough and Penzien, 1993; Chopra, 2001).

It is evident from the definition of the response spectrum as compared with the FAS that the response spectrum, in a sense, combines the characteristics of the ground motion excitation and the response of the structure (Hudson, 1962). It thus brings together under one representation the major parameters of

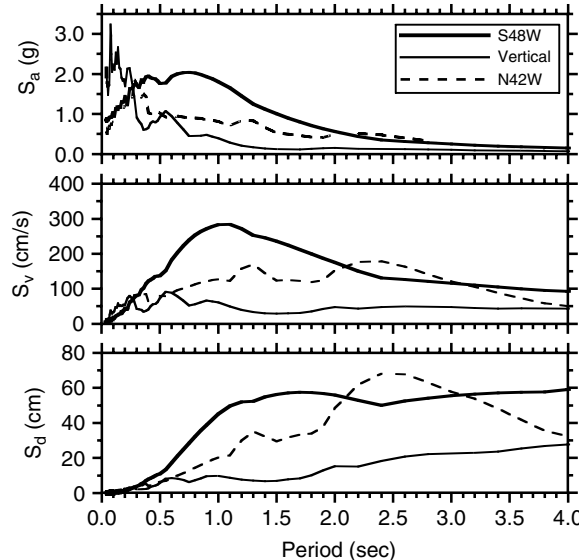


FIGURE 5.5 Elastic pseudo-acceleration (S_a), pseudo-velocity (S_v), and relative displacement (S_d) response spectra for 5% damping for the ground motion recorded at the Rinaldi Receiving Station during the 1994 Northridge, California, earthquake.

interest to the earthquake engineer. It can be shown (Hudson, 1979), as is also evident from Figure 5.3, that the FAS ordinates (of acceleration records) are less than, or equal to, the undamped SV ordinates.

The difference between S_v and SV and between S_a and SA are generally negligible for most of the typical period and damping ranges of engineering interest (Hudson, 1962). For zero damping (an undamped system), $S_a = SA$ but $S_v \neq SV$ (Hudson, 1979). At very long periods (for example, for very flexible structures), the absolute (or total) deformation of the mass will become very small and consequently the relative deformation of the mass with respect to the ground will approach the ground displacement. Therefore, at very long periods, S_d will approach the peak ground displacement; SV will approach the peak ground velocity; and SA will approach zero. However, for the same case (very long periods), S_v and S_a both approach zero. Thus, at long periods, there is a considerable difference between SV and S_v (Hudson, 1979). At very short periods, (for example, very stiff structures), the relative deformation of the mass with respect to the ground will be very small; therefore, the total acceleration of the mass will approach the ground acceleration. Hence, SA and S_a approach the peak ground acceleration (PGA) for all damping ratios.

By definition, elastic response spectra are for *linear elastic systems* and unless they are modified appropriately, they will not include features of inelastic structural response. For the same reason, elastic response spectra do not include the cumulative damage due to the number of inelastic cycles of structural deformations and the cumulative damage due to the foreshocks, the main shock and the aftershocks. A function that does include these cumulative effects is the hysteretic energy spectrum (see Section 5.3.8).

5.3.3.2 Effects of Damping on Response Spectra

The effect of damping on response spectra is to reduce the spectral ordinates; however, the amount of this reduction depends on various factors, including the period of the structure and the frequency content of the ground motion. Because of the basic characteristics of response spectra at very short and very long periods, viscous damping does not have much influence in these period ranges. In the intermediate period range, however, damping has its greatest effect on the response reduction. Figure 5.6 shows response spectra of the Rinaldi Receiving Station (S48W component) record for various damping ratios. Approximate procedures to scale an elastic design spectrum for different damping values are presented in Section 5.3.4.

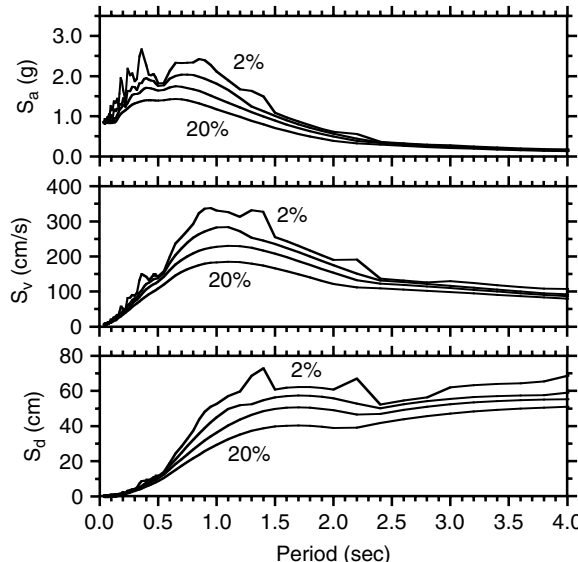


FIGURE 5.6 Elastic pseudo-acceleration (S_a), pseudo-velocity (S_v) and relative displacement (S_d) response spectra for 2, 5, 10 and 20% damping for the ground motion recorded at Rinaldi Receiving Station (S48W component) during the 1994 Northridge, California, earthquake.

5.3.3.3 Scaling of Response Spectra with PGA

As mentioned before, at very short periods, the spectral acceleration approaches the peak ground acceleration (PGA). PGA has been traditionally widely used by earthquake engineers to characterize the severity of ground motion. In practice, however, the importance of PGA alone to quantify the damage potential of the recorded ground motion may have been overemphasized. It should be noted that scaling of the entire amplitude of a ground acceleration time history results in scaling of its elastic response spectrum over the entire period range. However, a single high acceleration spike in a record, resulting in a spurious PGA, is not necessarily associated with high spectral ordinates over the entire period range and, hence, it does not necessarily represent a high damage potential of this ground motion. This is demonstrated in Figure 5.7. In this figure the response spectrum of the recorded motion at Düzce (EW component) during the August 17, 1999 Kocaeli, Turkey, earthquake is plotted. Also shown in this figure is the response spectrum in which time history has been altered by increasing the amplitude of the peak acceleration pulse by a factor of 2. Similarly, the response spectra for the original and the altered records of the El Centro ground motion are also plotted in Figure 5.7(c). It should be noted that in these cases, the entire time history is not scaled but only the amplitude at the peak spike is increased. It is evident from Figure 5.7 that from a practical point of view, an increase in the amplitude of the acceleration pulse of the time history mainly affects the short-period (high frequency) range of the response spectrum.

5.3.3.4 Response Spectra in Near Real-Time

Elastic response spectra of recorded ground motions are usually published by the recording agencies for 0, 2, 5, 10 and 20% damping ratios. Also, following an earthquake in the United States, in near real-time, maps of spatial distributions of elastic spectral accelerations of the recorded ground motions at selected periods are generated by TriNet (Wald et al., 1999) and CISN (Lin, et al., 2002) (see also Chapter 2). Called ShakeMaps, these maps are automatically generated and posted on the Internet for various post-earthquake applications. Although originally these maps were developed for Southern California, ShakeMap has been or is being implemented for many other regions of the United States, including Northern California, Utah and the Pacific Northwest. The current list of available regions and ShakeMaps are accessible on the Internet at <http://earthquake.usgs.gov/shakemap/>

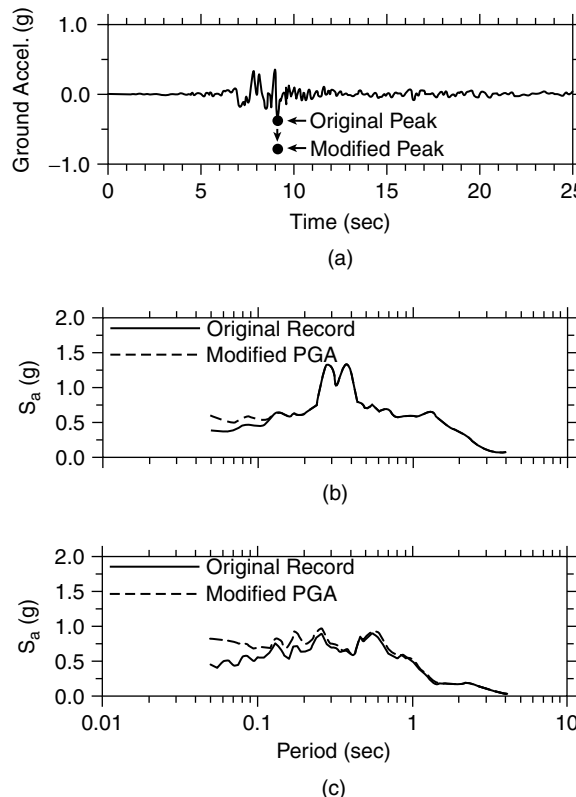


FIGURE 5.7 (a) Ground acceleration recorded at Düzce (EW component) during the August 17, 1999 Kocaeli, Turkey, earthquake; the original and modified peak accelerations are marked. (b) The corresponding pseudo-acceleration response spectra (S_a) for 5% damping. (c) The response spectrum (5% damping) for the El Centro (NS component) recording from the 1940 Imperial Valley earthquake, and the spectrum for the modified record. The El Centro time history (not shown) was modified in the same manner as in the top figure (a).

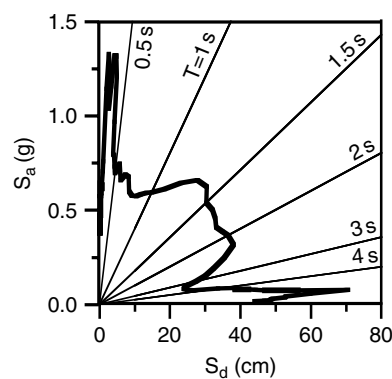


FIGURE 5.8 An acceleration-displacement (AD) diagram, also referred to as an acceleration-displacement response spectrum (ADRS) for 5% damping for the Düzce (EW component) recording of the August 17, 1999 Kocaeli, Turkey, earthquake.

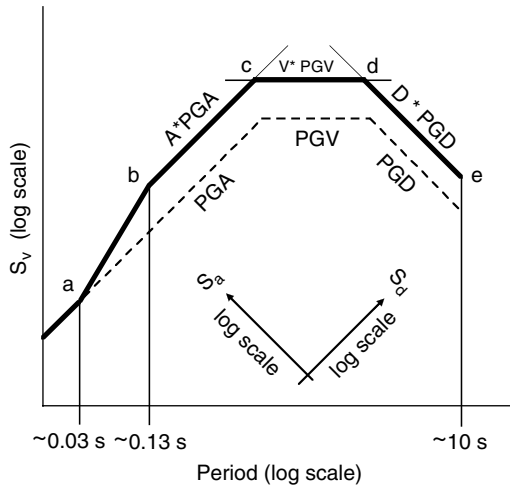


FIGURE 5.9 Elastic horizontal design spectrum according to Newmark and Hall. (Adapted from Chopra and Goel (2001). Direct displacement-based design: use of inelastic vs. elastic design spectra, *Earthquake Spectra*, 17, 47–64.)

5.3.3.5 Different Formats of Response Spectra

The data associated with response spectra can be presented in different formats. The most commonly used format, as mentioned previously and plotted in Figures 5.5 and 5.6, is a plot of the spectral ordinate (acceleration, velocity, or displacement) in linear scale versus natural period or natural frequency (in linear scale). This format is also used in most of the seismic design codes. However, more details of the spectra at shorter periods can be revealed by using a logarithmic scale for the period (Figure 5.7).

Another format for presenting the response spectrum is the acceleration-displacement (AD) diagram, also referred to as the *acceleration-displacement response spectrum* (ADRS). It is a plot of S_a versus S_d with periods represented by lines radiating from the origin. An example of an AD diagram is shown in Figure 5.8. The AD format of the response spectrum has been used by structural engineers for simplified analysis procedures to estimate the deformation demanded by the earthquake ground motion (Freeman, 1995; Chopra and Goel, 1999). The AD format has the visual advantage of being able to overlay the acceleration-displacement demand and the capacity diagrams of a structure on the same plot (see for example, Figure 9.6 in Chapter 9). A disadvantage of the AD diagram is that for long periods the spectral points become close to each other.

The spectra can also be shown in a *tripartite* logarithmic format. In this format, the three response spectra parameters S_a , S_v and S_d are combined such that S_v is on the vertical axis and period is on the horizontal axis, both on a logarithmic scale. S_a can be read off an axis rotated 45° counterclockwise and S_d can be read off an axis rotated 45° clockwise from the vertical axis. Thus, the lines with 45° slopes represent constant S_a lines and the lines with 135° slopes represent constant S_d lines (Figure 5.9). Apparently, this type of paper was first introduced sometime before 1958 by Edward Fisher (Housner, 1997). In recent years, practical applications of the tripartite logarithmic format have been curtailed.

5.3.3.6 Housner Spectrum Intensity

Spectrum intensity (SI) is defined as the area under the pseudo-velocity response spectrum (S_v) over the period range 0.1 to 2.5 sec (Housner, 1952). It is a measure of the intensity of ground shaking for elastic structures. As Housner (1975) states:

The spectrum intensity is a single number that is a good measure of the intensity of ground shaking as regards its effect on the elastic vibrations of structures. It has, however, been observed that it is not necessarily a good measure of the severity of shaking as indicated by the damage. This was demonstrated, for example, by the 1966 Parkfield, California earthquake where the motion close to

the fault had an unprecedently large spectrum intensity but caused very little observed damage. This was attributed to the fact that, although very intense, the strong shaking had a very short duration.

The computed SI at different recording stations can be used to construct a contour map of SI in a geographical area affected by the earthquake (Bozorgnia and Bertero, 2001a). Such a map can be used to examine the spatial distribution of the general intensity of the ground motion that impacts elastic structures.

5.3.4 Elastic Design Spectra

5.3.4.1 Introduction

Whereas a response spectrum is computed for a specific ground motion, for design purposes it is more appropriate to use a design spectrum. A design spectrum is based on a statistical analysis of a collection of numerous spectra of different recorded ground motions in different earthquakes, with possible modifications based on engineering experience. In the history of earthquake engineering, design spectra have been proposed by various engineers. Biot (1941) suggested that: "When we possess a collection of earthquake spectrums at a given location, it is suggested that a simplified envelope should be used as a standard spectrum for the purpose of design in that region." Widely used design spectra were developed by Housner (1970b), Seed et al. (1976), Newmark et al. (1973) and Newmark and Hall (1982). Also, various editions of building codes and seismic design guidelines have recommended design spectra. In Section 5.5, the design spectrum recently recommended in the International Building Code (IBC, 2000) is discussed. In the following sections, two additional examples of design spectra are presented. The first is the design spectrum proposed by Newmark and Hall (1982), which has been used extensively in research and engineering practice, and the second is a design spectrum proposed by FEMA-356 (2000).

5.3.4.2 Newmark-Hall Elastic Design Spectrum

The design spectrum proposed by Newmark and Hall (1982) is schematically plotted in Figure 5.9. This figure is plotted in the format of a tripartite logarithmic plot, the preferred plotting method proposed by these authors for reasons that will become obvious below. The Newmark-Hall procedure to construct an elastic design spectrum is as follows:

1. Estimate peak ground acceleration (PGA), peak ground velocity (PGV) and peak ground displacement (PGD); e.g., using an attenuation relation and relationships between these parameters as discussed below. Draw PGA, PGV and PGD lines on a tripartite logarithmic plot at constant values of S_a , S_v and S_d , respectively (see Figure 5.9).
2. Parallel to the PGA, PGV, and PGD lines, draw another set of lines at values equal to $A \times \text{PGA}$, $V \times \text{PGV}$ and $D \times \text{PGD}$, where A , V and D are dynamic amplification factors for acceleration, velocity and displacement, respectively, as specified next. Values of A , V and D for use in developing a median design spectrum (50% probability of nonexceedance of the spectral ordinates), are given in Equation 5.9 and those proposed for use in developing a median plus one standard deviation spectrum (84.1% probability of nonexceedance) are given in Equation 5.10:

$$A = 3.21 - 0.68 \ln \xi; \quad V = 2.31 - 0.41 \ln \xi; \quad D = 1.82 - 0.27 \ln \xi \quad (5.9)$$

$$A = 4.38 - 1.04 \ln \xi; \quad V = 3.38 - 0.67 \ln \xi; \quad D = 2.73 - 0.45 \ln \xi \quad (5.10)$$

where ξ is the damping ratio in percent (i.e., for 5% damping ratio, $\xi = 5$). Equation 5.10 obviously results in a more conservative design spectrum than Equation 5.9.

3. Approximate periods for corner points a , b and e , are shown in Figure 5.9. Corner points c and d are the crossing points of the $A \times \text{PGA}$, $V \times \text{PGV}$ and $D \times \text{PGD}$ lines. In practice, periods for points c and d fall in ranges of approximately 0.5–0.7 and 3–4 sec, respectively.

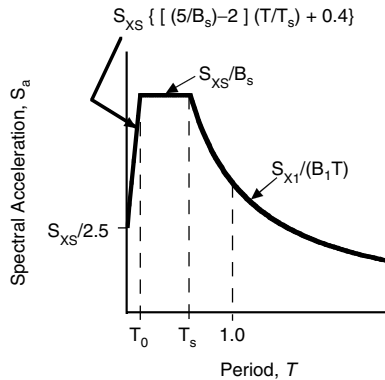


FIGURE 5.10 Elastic horizontal design spectrum recommended by FEMA-356 [2000]. Corner periods are $T_s = (S_{x1} B_s) / (S_{xs} B_1)$ and $T_0 = 0.2 T_s$.

4. For periods shorter than about 0.03 sec, the design spectrum follows the constant PGA line.

As mentioned above, the first step in constructing a Newmark-Hall design spectrum is to estimate PGA, PGV and PGD. In practice, however, it may be difficult to accurately estimate PGD. This is, in part, due to its sensitivity to the filtering parameters used to process the acceleration record during double integration. To simplify the construction of the design spectrum, Newmark and Hall (1982) suggested approximate rules to estimate PGV and PGD for a given value of PGA. Based on an analysis of several strong-motion records, they suggested that the ratio of PGV/PGA may be taken as 48 and 36 inches/sec/ g for competent soil and rock, respectively; and the dimensionless ratio (PGA \times PGD)/PGV² may be taken as 6 (consistent units should be used in this relation to make it unitless).

5.3.4.3 FEMA-356 Elastic Design Spectrum

According to FEMA-356 (2000), a pre-standard document for seismic rehabilitation of buildings, different levels of ground motion are used to achieve different structural performance levels. Two Basic Safety Earthquake (BSE) levels, BSE-1 and BSE-2 are defined, where the BSE-2 level is a more severe level of ground motion than the BSE-1 level. For example, the basic safety objective achieves the dual goals of (a) life safety structural performance for the BSE-1 ground-motion level; and (b) collapse prevention for the BSE-2 ground-motion level.

The procedure to construct the elastic spectra for the BSE-2 and BSE-1 ground motion levels, is as follows:

1. For the BSE-2 ground motion level, the spectral accelerations S_s (at period of 0.2 sec) and S_1 (at period of 1.0 sec) are obtained using the approved contour maps for the Maximum Considered Earthquake (MCE). These maps can be found on the USGS Internet web site at <http://geohazards.cr.usgs.gov/eq/>. The MCE ground motion is based on a combination of deterministic and probabilistic estimates and may be interpreted as a “collapse ground motion” (Leyendecker et al., 2000). The details of the characteristics of the MCE ground motion are presented in Section 5.5.
2. S_s and S_1 for the BSE-2 ground-motion level are adjusted for local site conditions. These adjusted spectral accelerations are denoted S_{xs} and S_{x1} . The procedure to adjust the spectral ordinates for local site conditions is similar to that of the IBC (2000) and is outlined in Section 5.5.2.
3. For the BSE-1 ground motion level, the spectral accelerations S_{xs} and S_{x1} are taken as the smaller of the following:
 - The values of S_s and S_1 taken from approved contour maps of spectral accelerations for 10% probability of exceedance in 50 years, adjusted for local site conditions (see Section 5.5.2).
 - 2/3 of the values of the spectral ordinates determined for the BSE-2 ground motion level (step 2, above).

4. Given spectral accelerations S_{xs} and S_{xi} , the elastic horizontal spectra for the BSE-2 and BSE-1 ground motion levels are constructed according to Figure 5.10. In this figure, B_s and B_i are damping modification factors (or damping coefficients, in FEMA-356 terminology) to modify S_{xs} and S_{xi} , respectively, for damping values other than 5%. The recommended values of B_s and B_i are given in Table 5.2 A more detailed discussion about the damping modification factors is provided in Section 5.3.4.4. In summary, given S_{xs} , S_{xi} , B_s and B_i , one can determine the corner periods T_s and T_0 (see Figure 5.10), and the design spectrum can be constructed as indicated in the figure. For 5% damping, B_s and B_i are unity, and the ratio of the peak of the design spectrum over the zero-period acceleration is 2.5. This amplification factor is consistent with the previous editions of the *Uniform Building Code*, e.g., UBC (1994).

TABLE 5.2 Damping Modification Factors^a

Damping Ratio (%)	Newmark and Hall (1982) ^b			FEMA-356 (2000)	
	Acceleration (A)	Velocity (V)	Displacement (D)	B_s	B_i
2	0.77	0.81	0.85	0.80	0.80
5	1.00	1.00	1.00	1.00	1.00
10	1.29	1.21	1.16	1.30	1.20
20	1.80	1.53	1.37	1.80	1.50
30	2.36	1.80	1.54	2.30	1.70
40	3.02	2.07	1.68	2.70	1.90
50	3.85	2.34	1.81	3.00	2.00

^a See also Naeim and Kircher (2001) for more details.

^b Using Equation 5.9 of this chapter.

5.3.4.4 Modification of Design Spectra for Damping Values

It is common practice to specify a design spectrum for a 5% damping ratio. However, depending on the structural (or fluid) material behavior and the level of ground motion excitation, a design spectrum for other damping values may be needed. For example, a steel liquid storage tank located at a rock site has a damping ratio of 2 to 3% for the horizontal impulsive mode (Whittaker and Jury, 2000). Approximate equivalent viscous damping values for various systems are given, for example, by Newmark and Hall (1982).

An approximate procedure to derive a design spectrum for a damping ratio other than 5% is to divide the 5% damped spectral ordinates by a *damping modification factor*. There are different procedures and damping modification factors, including those by Newmark and Hall (1982), Rosenblueth (1980), Idriss (1993), Abrahamson and Silva (1996), FEMA-356 (2000), among others (see also a summary of selected procedures by McGuire et al., 2001). The Newmark and Hall (1982) and FEMA-356 (2000) procedures are presented below.

Equation 5.9 or 5.10 by Newmark and Hall (1982) can be used to compute the damping modification factors. For example, between points *b* and *c* in Figure 5.9, a 2% damped median design spectral ordinate may be approximately derived by dividing the 5% damped median design spectral ordinate by a factor of $(3.21 - 0.68 \ln 5)/(3.21 - 0.68 \ln 2) = 0.77$. The damping modification factors calculated by this procedure are listed in Table 5.2 (Naeim and Kircher, 2001). These modification factors are for adjusting the dynamic amplification factors *A*, *V* and *D* (see Figure 5.9) of the 5% damped spectrum to derive a spectrum for other damping values.

As mentioned previously, FEMA-356 (2000) also recommends damping modification factors B_s and B_i to scale spectral accelerations at periods of 0.2 and 1.0 sec, respectively (see Figure 5.10). These factors are also listed in Table 5.2. As Naeim and Kircher (2001) have pointed out, for damping ratios less than about 20%, B_s and B_i are almost the same as those recommended by Newmark and Hall (1982) for the

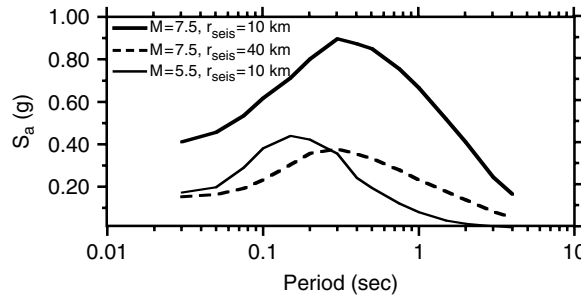


FIGURE 5.11 Pseudo-acceleration (S_a) spectra for the average of the two horizontal components for 5% damping at a stiff soil site and for strike-slip faulting, based on the Campbell and Bozorgnia (2003) ground motion (attenuation) relations. Here r_{seis} is the shortest distance from the site to the seismogenic rupture zone of the fault (see Section 5.4).

acceleration and velocity dynamic amplification factors, respectively. For damping ratios higher than 20%, B_S and B_1 are less than the factors recommended by Newmark and Hall (1982), i.e., the FEMA-356 spectrum becomes more conservative than that proposed by Newmark and Hall. This is due to the decision by code and guideline development groups to choose conservative damping modification factors for design of highly damped systems (Naeim and Kircher, 2001).

It should be noted that the validity of the damping modification factors given in Table 5.2, for response spectra of near-fault ground motions that are dominated by severe long-period pulses has yet to be determined.

5.3.4.5 Scaling a Fixed-Shape Spectrum

In general, the *shape of a smoothed spectrum* is a function of different parameters, including magnitude, source-to-site distance, local site conditions and direction of fault rupture propagation. An example is presented in Figure 5.11. This figure shows horizontal spectral acceleration for 5% damping at a stiff soil site, strike-slip faulting, M_w 5.5 and 7.5 and distances of 10 and 40 km from the seismic source. The spectra are based on statistical analyses of 443 recordings from 36 worldwide shallow earthquakes of magnitude 4.7 to 7.7 (for details, see Campbell and Bozorgnia, 2003). In Figure 5.11, compare, for example, the two spectra for M_w 7.5 and M_w 5.5, both at a distance of 10 km from the source. It is evident that the larger magnitude results in larger spectral ordinates, but more at long periods than at short periods.

In the same figure, compare the spectrum of the M_w 5.5 earthquake at distance of 10 km with that of M_w 7.5 earthquake at a distance of 40 km. These spectra have comparable PGA values (compare the spectra at a very short period). However, the spectrum of the smaller earthquake at smaller distance is richer at short periods than that of the larger earthquake at larger distance.

Therefore, using a fixed spectral shape and scaling it with a single parameter such as PGA to account for the effects of magnitude and other factors, is not conceptually justified. The shape of a design spectrum should take into account the effects of various parameters including magnitude, distance, local site conditions, fault rupture directivity effects, among other factors.

5.3.5 Arias Intensity and Strong-Motion Duration

Arias intensity (I_A) is a ground motion parameter related to the *spectrum* of the energy demanded by a strong-motion record, as defined below. Because I_A is closely related to a widely used definition of strong-motion duration, a discussion of duration is also provided in this section.

The commonly used version of Arias intensity (Arias, 1970) is the sum of total energy per unit weight in a set of undamped elastic SDF systems having frequencies uniformly distributed in the range of zero to infinity, evaluated at the end of the ground motion record. It can be shown (Arias, 1970; Trifunac and Brady, 1975) that the above definition can be translated into the following expression for the Arias Intensity:

$$I_A = (\pi/2g) \int_0^{t_d} [a_g(t)]^2 dt \quad (5.11)$$

where $a_g(t)$ is the ground acceleration, t_d is the total duration of the record and g is the acceleration of gravity.

Influences of source-to-site distance, magnitude and local site condition on I_A have been recently examined. For example, Kayen and Mitchell (1997) examined the correlation of I_A with magnitude and distance for different soil conditions and used the Arias intensity approach to assess the liquefaction potential of soil deposits during earthquakes (see also Chapter 4). Recently, Travasarou et al. (2003) used a larger number of recordings and developed the following attenuation relation for I_A

$$\begin{aligned} \ln(I_A) = & c_1 + c_2(M_w - 6) + c_3 \ln(M_w / 6) + c_4 \ln(r_{rup}^2 + h^2)^{0.5} \\ & + [s_{11} + s_{12}(M_w - 6)] S_C + [s_{21} + s_{22}(M_w - 6)] S_D + f_1 F_N + f_2 F_R \end{aligned} \quad (5.12)$$

where I_A is the average Arias intensity (m/s) of the two horizontal components; M_w is moment magnitude; r_{rup} is the closest distance to the rupture plane (km); h is a fictitious depth term (km) determined by the regression; F_N and F_R are indicator variables for the fault mechanism and are respectively both 0 for strike-slip faults, 1 and 0 for normal faults, and 0 and 1 for reverse or reverse-oblique faults; S_C and S_D are indicator variables for the soil type and are respectively both 0 for site category B, 1 and 0 for site category C, and 0 and 1 for site category D, where B is for competent rock, C is for weathered soft rock and shallow stiff soil, and D is for deep stiff soil. The computed values of the coefficients are as follows: $c_1 = 2.80$, $c_2 = -1.981$, $c_3 = 20.72$, $c_4 = -1.703$, $h = 8.78$, $s_{11} = 0.454$, $s_{12} = 0.101$, $s_{21} = 0.479$, $s_{22} = 0.334$, $f_1 = -0.166$ and $f_2 = 0.512$. The model is applicable for earthquakes with M_w between 4.7 and 7.6. The standard deviation of the random error in the above relationship was found to be a function of the median predicted Arias intensity and soil type. In fact, the error is smaller for soil sites D, larger for soil sites C and the largest for soil sites B.

Travasarou et al. (2003) also found that the average I_A of two horizontal components is insensitive to forward directivity in the near-fault region; however, the Arias intensity in the fault-normal direction was approximately 20% higher and in fault-parallel direction was approximately 20% lower than the average I_A .

Strong-motion duration is an important parameter that may contribute to the performance of structural and geotechnical systems during earthquakes. For example, experimental studies have shown that structural systems and components subjected to cycles of inelastic deformations become more vulnerable due to cumulative damage (e.g., Bertero et al., 1977). This is usually the case if the strong-motion duration is relatively long. Therefore, strong-motion duration may play an important role in assessing the damage potential of earthquake ground motion. The cumulative effects of strong-motion duration are included in hysteretic energy and damage spectra (see Sections 5.3.8 and 5.3.9).

Strong-motion duration can be defined in different ways. A review of various definitions is given by Bommer and Martinez-Pereira (1999). Chapter 2 also provides more discussion about the strong-motion duration. Most commonly used definitions of strong-motion duration are defined below.

Bracketed duration was defined by Bolt (1973) as the elapsed time between the first and last acceleration excursions greater than a given level (e.g., 0.05g).

Significant duration is defined based on the time variation of the integral of the square of the ground acceleration time history. This definition is related to the *Arias intensity*, as defined previously, if t_d in Equation 5.11 is replaced with time t ; and hence, the result of Equation 5.11 will become a function of time. Two common definitions of the significant duration are the time intervals between 5 and 95% and between 5 and 75% of the integral of the square of the ground acceleration (Trifunac and Brady, 1975; Stewart et al., 2001). An example of the evolution of I_A is presented in Figure 5.12 for the 1978 Tabas, Iran, earthquake (M_s 7.4) recorded at Tabas (N16W component). As marked in this figure, the time interval between 5% and 95% of I_A represents a significant duration of the record. An example of the use of significant duration in engineering practice is the evaluation of seismic slope stability (see Section 4.6.2.3.3 in Chapter 4: Displacement-Based Methods of Analysis).

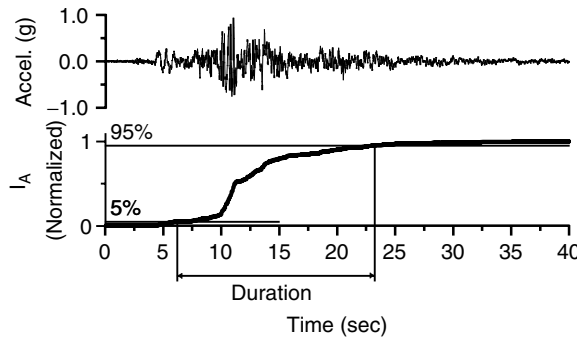


FIGURE 5.12 Ground acceleration of the 1978 Tabas, Iran, earthquake ($M_s = 7.4$) recorded at Tabas (N16W component), and the corresponding evolution of the Arias intensity.

5.3.6 Drift Spectrum

The drift spectrum represents approximately the story drift ratio in multi-story buildings demanded by the ground motion (Iwan, 1997). The formulation is based on the linear elastic response of a uniform continuous cantilevered shear beam model, where interstory drift is computed as the first derivative of the displacement response of the beam model (see also Kim and Collins, 2002). The drift spectrum has been proposed for quantifying the seismic demand on linear elastic systems subjected to near-fault pulse type ground motions. To generate the drift spectrum, ground velocity and displacement time histories are needed as input motions (Iwan, 1997). Hence, accurate processing of the ground motion records, especially for near-fault ground motions, is important for developing a drift spectrum.

The story drift of the shear beam model can be computed at different heights of the model, though it is commonly computed at the base. As an example, Figure 5.13 presents the drift spectrum evaluated at the base of a shear beam model for the Northridge earthquake recorded at Sylmar County Hospital (NS component).

The drift spectrum has the same fundamental limitations as the other linear elastic response parameters, i.e., it does not directly reveal information about inelastic response. Recently, Kim and Collins (2002) have also found that for ground motions that exhibit a permanent ground displacement, the formulation of the drift spectrum predicts residual drift values at the end of the record. This is inconsistent with the linear elastic behavior assumed in developing the model. As a result, Kim and Collins (2002) have proposed improved models for computing drift spectra. However, the improved models do not have the computational simplicity of the original drift spectrum model.

5.3.7 Inelastic Response Spectra

5.3.7.1 Introduction and Definitions

A severe ground motion generally demands large deformations on various structural systems, and inelastic structural response and hysteretic energy dissipation are generally inevitable in typical structures. This fact has been recognized since the early years of earthquake engineering. For example, Biot (1941) realized that a severe ground motion can demand excessively high stresses in an undamped *elastic* structural model; and he concluded:

Observations of the effect of actual earthquakes indicate that for most structures such high stresses are not reached and this points out the importance of the damping or other causes of stress reduction. Considerable hysteresis damping will set in as soon as the yield point in some part of the building is reached.

For a structure to behave elastically during a severe ground shaking, its strength, in general, must be considerably higher than the minimum requirements recommended in building codes. Therefore, in a major earthquake, many types of structures respond inelastically, and in fact, their survival depends on

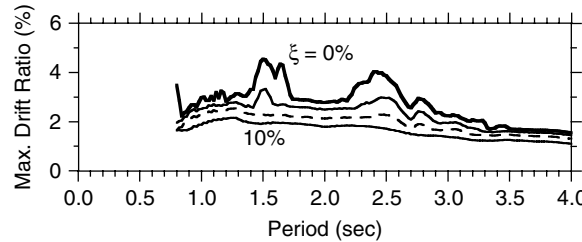


FIGURE 5.13 Drift spectra (elastic) for 0, 2, 5 and 10% damping evaluated at the base of the building model for the Sylmar County Hospital (NS component) recording of the Northridge, California, earthquake.

proper inelastic behavior and hysteretic energy dissipation. Therefore, an *elastic* response spectrum, although a very important concept with widespread applications, has a limited capability to predict structural damage in severe earthquakes. An inelastic response spectrum (IRS) includes some fundamental features of inelastic dynamic behavior.

An IRS represents the maximum response of an inelastic (nonlinear) SDF system versus its initial (elastic) natural period when it is excited by a ground acceleration record. As discussed before, for the computation of an *elastic* response spectrum, only two system parameters must be specified: natural period and damping ratio. For computation of an IRS, in addition to these parameters, the complete force-deformation characteristics of the SDF system must be specified, including its loading, unloading and re-loading behavior. The inelastic force-deformation relationship of the SDF system can be idealized as bilinear, trilinear, stiffness and strength degrading, among others.

One of the traditional parameters used in the IRS as well as in seismic design is the displacement ductility ratio (μ), which is defined as

$$\mu = u_{\max}/u_y \quad (5.13)$$

where u_{\max} and u_y are, respectively, the maximum and yield deformations of the SDF system (the deformations are all relative to the ground). By definition, $\mu \leq 1$ indicates an elastic response and $\mu > 1$ indicates inelastic behavior.

In the process of constructing an inelastic spectrum, the following variables are also commonly used in research and practice. Consider a generic force-deformation relationship as shown in Figure 5.14. In this figure, F_y is the equivalent yield strength; F_s is the design strength according to the seismic provisions and F_e is the elastic strength demand if the system were to remain elastic. The relationships among these forces are as follows (Uang and Bertero, 1991; Uang, 1991; FEMA-369, 2001):

$$F_s = F_e/R \quad (5.14a)$$

$$F_y = F_e/R_d \quad (5.14b)$$

$$\Omega = F_y/F_s \quad (5.14c)$$

where, in terms of building code terminology, R is the response modification coefficient to compute the design strength F_s from the elastic design strength F_e (obtained from an elastic design spectrum; see Equation 5.7 and also Section 5.3.4); R_d is the reduction factor due to the available ductility of the system; and Ω represents the system overstrength factor which relates the design strength (F_s) to the equivalent yield strength of the system (F_y). In seismic design, usually $R > 1.0$; thus, structures are designed for forces smaller than demanded for a completely elastic response (FEMA-369, 2001). Values of R , R_d and Ω are dependent on the basic seismic-force-resisting structural system (SEAOC, 1999; IBC, 2000). For example, according to the International Building Code (IBC, 2000), for special steel moment frames $R = 8$.

5.3.7.2 Different Formats of Inelastic Response Spectra

Inelastic response spectra can be presented in different formats. The most commonly used formats are given below.

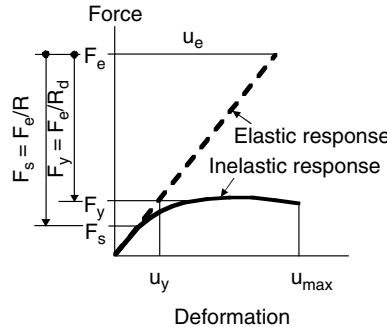


FIGURE 5.14 Elastic and inelastic force-deformation relationships. (Adapted from Uang, C.M. (1991). Establishing R (or R_w) and C_d factors for building seismic provisions. *ASCE Journal of Structural Engineering*, 117, 19–28.)

5.3.7.2.1 Displacement Ductility Spectrum

Given the characteristics of an inelastic SDF system, including its force-deformation relationship with specified yield strength and damping ratio, the IRS can be presented in a plot of the computed (or demanded) displacement ductility (μ) versus the initial elastic period (T). In this format, the yield strength of the SDF system is specified, and the maximum deformation u_{\max} and displacement ductility factor μ demanded by the ground motion, are computed. In practice, the equivalent yield strength can be determined either according to the seismic provisions in a building code, i.e., based on a reduced elastic design spectrum, or using the results of a static nonlinear (pushover) analysis.

An example of IRS is plotted in Figure 5.15. The different inelastic spectra in this figure are for a 5% damping ratio and a bilinear force-deformation relationship (i.e., two different linear force-deformation relationships for $u < u_y$ and $u > u_y$) with a post-yield stiffness equal to 1% of the initial elastic stiffness. For Figure 5.15, the yield strength of the system is specified based on the elastic spectrum recommended in the UBC (1994) for soil type S_2 in seismic zone 4, reduced by the factor R_d (see Figures 5.14 and 5.15(a), and Equation 5.14b). Figure 5.15 shows that using a period-independent reduction factor (R_d), can result in large ductility demands, especially at short periods. IRS for other recently recorded near-source ground motions have also been computed by Bozorgnia and Mahin (1998).

Figure 5.16 presents an example of the effects of multiple events on inelastic spectra. Figure 5.16(a) shows the ground acceleration time histories recorded at Düzce during the August 17, 1999 Kocaeli and November 12, 1999 Düzce earthquakes in Turkey. The time history plot includes 10 seconds of zero ground acceleration added in between the recorded ground motions in the two events. Figure 5.16(b) shows displacement ductility spectra of the first and second ground motions independently, as well as the ductility spectrum for the combined acceleration time histories. The inelastic spectra shown in this figure are for an SDF system with 5% damping and an elastic-perfectly-plastic (EPP) force-displacement relationship with yield strength based on the elastic spectrum of UBC (1997) reduced by $R_d=3.4$. Figure 5.16(b) shows that the displacement ductility spectrum for the combined ground motions is predominated by the November 1999 event and may not necessarily include strong cumulative effects of the first and second events (Bozorgnia and Bertero, 2002). Other parameters such as hysteretic energy include stronger cumulative effects of multiple events (see Section 5.3.8).

5.3.7.2.2 Constant Ductility Spectrum

An IRS can also be presented as a plot of the computed yield strength (F_y) of an SDF system versus its initial elastic period for a given value of ductility (μ). An example of such IRS is plotted in Figure 5.17. To construct such a constant-ductility IRS, first various values of period T and F_y are assumed and the displacement ductility demands are computed. Then, through an interpolation process, the required values of F_y are determined to result in a pre-specified value of displacement ductility ratio. Figure 5.17

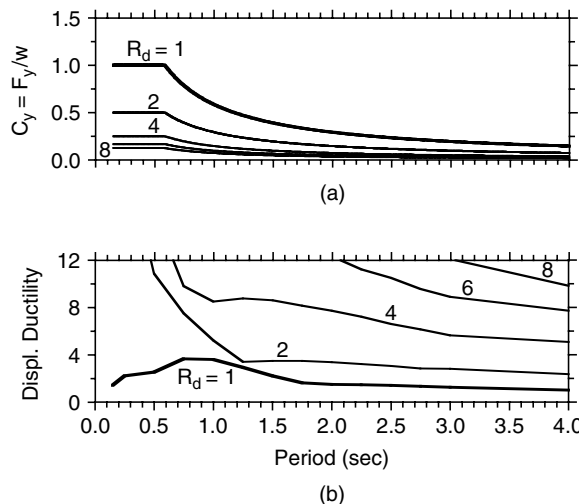


FIGURE 5.15 Given C_y (top figure), the computed inelastic response spectra, in terms of displacement ductility ratios, are plotted (bottom figure). The inelastic response spectra are for the 1994 Northridge, California, earthquake recorded at Rinaldi Receiving Station (S48W component). The SDF system has 5% damping and a bilinear force-deformation relationship.

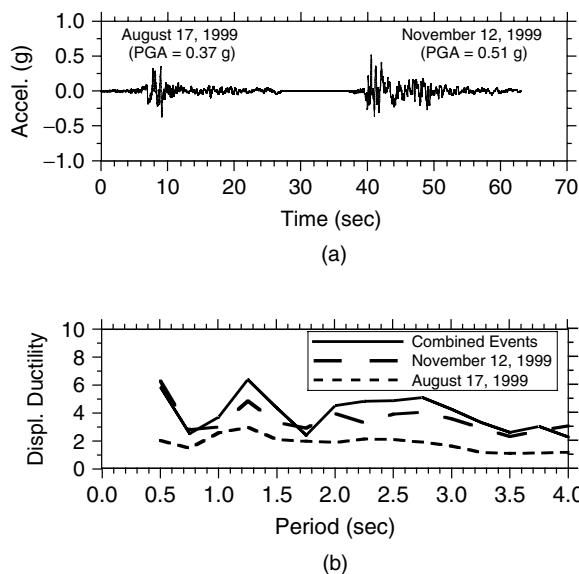


FIGURE 5.16 Ground accelerations (a); and displacement ductility ratio spectra (b); for the Düzce (EW component) recordings of the August 17, 1999 Kocaeli ($M_w = 7.4$) and November 12, 1999 Düzce ($M_w = 7.1$) earthquakes in Turkey.

shows the results of this process for the 1994 Northridge earthquake recorded at Rinaldi Receiving Station. The IRS in this figure are for a 5% damping and a bilinear force-deformation relationship with a post-yield stiffness equal to 1% of the initial elastic stiffness. The curve for $\mu = 1$ corresponds to the elastic response spectrum. It is evident from this figure that for the intermediate period range, if the structural system can provide a moderate ductility, a substantial reduction in the required yield strength (F_y) can be achieved.

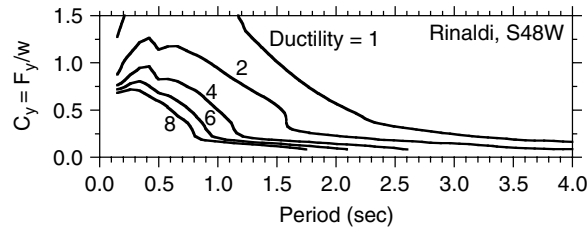


FIGURE 5.17 Constant-ductility inelastic response spectra for the 1994 Northridge, California, earthquake recorded at Rinaldi Receiving Station (S48W component). The SDF system has 5% damping and a bilinear force-deformation relationship.

5.3.7.3 Computer Programs to Construct Inelastic Response Spectra

There are various computer programs with different capabilities to compute inelastic response spectral ordinates. General purpose inelastic dynamic analysis software packages can also be used for this task. Publicly available computer programs for the generation of inelastic response spectra include NONSPEC (Mahin and Lin, 1983); BISPEC (Hachem, 2000); and NSPECTRA (Reinhorn et al., 1999). For example, the results shown in Figures 5.15 and 5.16 were computed using NONSPEC with additional post-processing.

5.3.7.4 Inelastic Design Spectra

Inelastic response spectra are for specific ground motions; however, for general use, smoothed inelastic design spectra may be more applicable. Examples of proposed inelastic design spectra are given below:

5.3.7.4.1 Newmark–Hall Inelastic Design Spectrum

Given the *elastic* design spectrum and assumed (or available) displacement ductility ratio (μ) of an SDF system, an *inelastic* design spectrum is constructed by modifying the elastic design spectrum. The procedure is as follows. The first step is to construct an elastic design spectrum (see Section 5.3.4.2 and Figure 5.9). Consider an elastic-perfectly-plastic (EPP) force-deformation relationship, which is a special case of the bilinear force-deformation relationship with a zero postyield stiffness. The Newmark–Hall procedure to construct an inelastic design spectrum for such a system is summarized in Figure 5.18. In the short period range, the flat portion of the elastic acceleration spectrum is reduced by a factor of $(2\mu - 1)^{0.5}$. This is based on an assumption that the areas under the force-displacement curves for the elastic and inelastic systems are equal (see Figure 5.14). At longer periods, the elastic acceleration design spectrum is reduced by a factor of μ . This is based on an assumption (Newmark and Hall, 1982) that the maximum deformations of the EPP and the elastic systems are approximately the same, i.e., $u_e = u_{max}$ in Figure 5.14. In Figure 5.18, point c' is obtained as the intersection of the flat and decaying portions of the inelastic design spectrum. Thus, given the period and available displacement ductility (μ), and using the inelastic design spectrum (Figure 5.18), the design yield strength (F_y) can be determined.

5.3.7.4.2 Other Inelastic Design Spectra

The process of generating the inelastic design spectrum shown in Figure 5.18 may be further simplified by using a period-independent (constant) reduction factor R_d , instead of using two factors R_{d1} and R_{d2} . This simplified version of constructing an inelastic design spectrum is conceptually similar to the procedure used in various building codes to reduce an elastic design spectrum to determine the strength (base shear) of the system. Other researchers have also proposed to use values for the strength reduction factor R_d as a means to reduce an elastic design spectrum to construct an inelastic design spectrum. For example, Krawinkler and Nassar (1992) proposed the following reduction factor R_d for a bilinear force-deformation relationship:

$$R_d = [c(\mu - 1) + 1]^{1/c} \text{ where } c(T, \alpha) = [T^{\alpha} / (1 + T^{\alpha})] + [b/T] \quad (5.15)$$

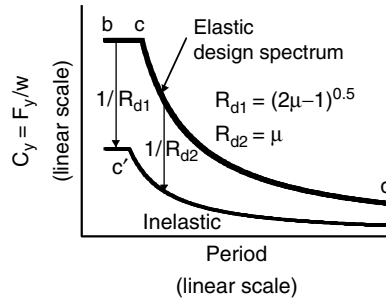


FIGURE 5.18 Inelastic design spectrum according to Newmark and Hall (1982). Points b , c and d correspond to those marked in Figure 5.9. See also Mahin and Bertero (1981).

where T is the natural period and parameters a and b are functions of α (the ratio of post-yield stiffness over initial elastic stiffness). For example, for $\alpha = 0$, the following values are used: $a = 1.0$ and $b = 0.42$. Similarly, for $\alpha = 2\%$, one should use $a = 1.0$ and $b = 0.37$; and for $\alpha = 10\%$, one should use $a = 0.8$ and $b = 0.29$.

Miranda and Bertero (1994) also examined numerous reduction factors previously proposed and concluded that the strength reduction factor is a function of available displacement ductility, period of the system and the site condition. Other recent studies on this subject include that by Vidic et al. (1994). A summary and comparison of some of the recent studies on R_d values have been provided by Chopra and Goel (1999).

5.3.8 Energy Spectra

The *elastic* response spectrum, although an important measure with extensive applications, has limitations in quantifying the damage potential of ground motion. For example, among its other limitations, it does not directly include the effects of inelastic structural response, which are generally associated with damage. Inelastic response spectra, in the form of maximum deformation ductility and inelastic design strength spectra, reveal some fundamental features of inelastic response and structural damage. However, among their other limitations, an IRS does not necessarily reveal information on the cumulative effects of number of cycles of inelastic deformations. The energy spectrum, especially the *hysteretic energy spectrum* defined below, can provide additional important information about the damage potential of the earthquake ground motion related to these cumulative effects.

Seismic input energy to an inelastic SDF system (E_I) is balanced as follows (Uang and Bertero, 1990; Bertero and Uang, 1992)

$$E_I = E_H + E_K + E_S + E_\xi \quad (5.16)$$

where E_H , E_K , E_S and E_ξ are irrecoverable dissipated hysteretic energy, kinetic energy, recoverable elastic strain energy and dissipated viscous damping energy, respectively. The absorbed energy E_A is given by

$$E_A = E_H + E_S = \int F du \quad (5.17)$$

where F is the restoring force and u is the deformation response (relative to the ground) of the mass of the SDF system. Hysteretic energy (E_H) is the amount of energy the structure must dissipate through inelastic nonlinear response. If the structure can dissipate the hysteretic energy demanded by the earthquake, it will survive without collapsing. If the structure remains elastic, i.e., no significant damage is expected, E_H will be zero. In general, a high hysteretic energy demanded by the ground motion is an indication of a high degree of damage. The details of the time history of the inelastic deformation can

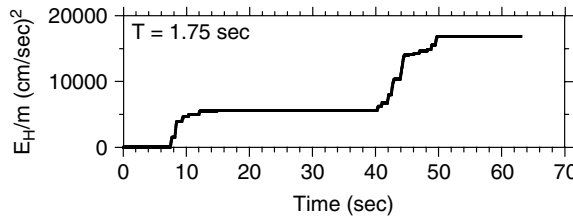


FIGURE 5.19 Time variation of hysteretic energy per unit mass at period $T = 1.75$ sec for the ground accelerations recorded at Düzce (EW component) during the August 17, 1999 Kocaeli ($M_w = 7.4$) and November 12, 1999 Düzce ($M_w = 7.1$) earthquakes in Turkey (see Figure 5.16(a) for the input ground motion).

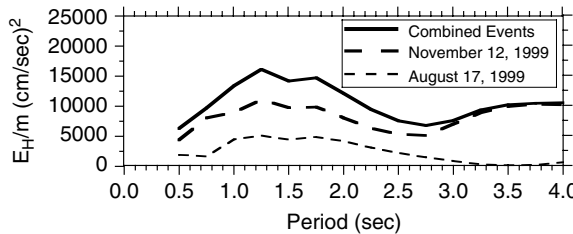


FIGURE 5.20 Hysteretic energy spectra per unit mass for the individual ground motions recorded at Düzce (EW component) during the August 17, 1999 Kocaeli and November 12, 1999 Düzce earthquakes in Turkey, and for the combined ground motion time histories (see Figure 5.16(a) for input time histories).

also play an important role in this process. Hysteretic energy by definition includes the cumulative effects of repeated cycles of inelastic response. Therefore, the cumulative damage effects of strong-motion duration are also included in this parameter.

An example of the time variation of E_H is presented in Figure 5.19 for the ground motions recorded at Düzce during the August and November 1999 earthquakes in Turkey. The characteristics of the inelastic SDF system are the same as those used for Figure 5.16(b). It is evident from Figure 5.19 that E_H includes the cumulative effects of the two events. The hysteretic energy spectrum presents the maximum (over time) of the hysteretic energy for a series of inelastic SDF systems. Figure 5.20 shows E_H spectra per unit mass for the 1999 earthquakes in Turkey recorded at Düzce (see Figure 5.16(a) for the input ground motions). For this figure, the mechanical characteristics of the SDF system are the same as those used for Figure 5.16(b). E_H spectra, such as those shown in Figure 5.20, reveal the cumulative damage potential due to a multiple sequence of ground shakings.

For practical reasons, it is convenient to use a normalized version of E_H . Various versions of normalized E_H have been introduced. For example, Mahin and Bertero (1976, 1981) defined normalized hysteretic energy (NHE) as

$$\text{NHE} = E_H / (F_y u_y) \quad (5.18)$$

where F_y and u_y are the yield strength and deformation of the SDF system, respectively (see Figure 5.14). Equivalent hysteretic velocity V_H (Akiyama, 1985; Uang and Bertero, 1988) has also been defined as

$$V_H = (2 E_H / m)^{1/2} \quad (5.19)$$

where m is the mass of the system. Other recent developments on various forms of energy spectra include the use of energy-based concepts for seismic design and evaluation by Fajfar (1992) and Fajfar and Vidic (1994), the investigation of various normalized energy-based parameters by Bruneau and Wang

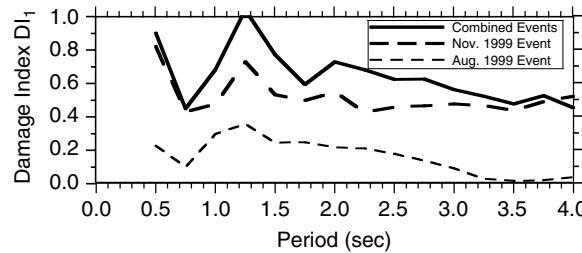


FIGURE 5.21 Damage spectra for the individual ground motions recorded at Düzce (EW component) during the August 17, 1999 Kocaeli and November 12, 1999 Düzce earthquakes in Turkey and for the combined ground motion time histories (see also Figure 5.16(a)).

(1996), the investigation of the use of elastic input energy for seismic hazard analysis by Chapman (1999) and Decanini and Mollaoli (1998), the attenuation of absorbed energy spectra by Chou and Uang (2000) and the presentation of the relationship between elastic input energy spectrum and Fourier amplitude spectrum of the ground acceleration by Ordaz et al. (2003), among others.

5.3.9 Damage Spectra

Structural performance and damage limit states can be quantified by a *damage index* (DI). A well-defined damage index is a normalized quantity that will be zero if the structure remains elastic (i.e., no significant damage is expected) and will be one if there is a potential of failure. Other structural performance states (such as operational, life-safe, near collapse, etc.) correspond to values of DI between zero and one. The *damage spectrum* represents the variation of a damage index over structural period for a series of SDF systems subjected to a ground motion record (Bozorgnia and Bertero 2001a, 2001b, 2003).

A damage spectrum, therefore, can quantify the damage potential of the recorded earthquake ground motion. For example, Bozorgnia and Bertero (2001a, 2001b, 2002, 2003) defined an improved damage spectrum based on a combination of normalized displacement ductility and hysteretic energy spectra for an inelastic SDF system

$$DI_1 = [(1 - \alpha_1) (\mu - \mu_e) / (\mu_{mon} - 1)] + \alpha_1 (E_H/e_{Hmon}) \quad (5.20)$$

where μ ($= u_{max}/u_y$) is displacement ductility ratio; μ_e ($= u_{elastic}/u_y$) is the ratio of the maximum elastic portion of deformation over the yield deformation; μ_{mon} is the displacement ductility capacity of the system under monotonically increasing lateral deformation; E_H is the hysteretic energy demanded by the earthquake ground motion; e_{Hmon} is the hysteretic energy capacity of the system under monotonically increasing lateral deformation; and $0 \leq \alpha_1 \leq 1$ is a constant. Equation 5.20 is an improved version of the DI_{PA} defined by Park and Ang (1985), which is a widely used damage index (for more details see Bozorgnia and Bertero, 2001b). It can be shown that for an elastic-perfectly-plastic SDF system, e_{Hmon} is related to μ_{mon} and, hence, Equation 5.20 is greatly simplified.

If the system remains elastic (so that $\mu_e = \mu \leq 1$ and $E_H = 0$), DI_1 will become zero. On the other hand, under a monotonically increasing lateral deformation, if the maximum displacement demand (u_{max}) reaches the displacement capacity of the structure (u_{mon}), i.e., an indication of failure, DI_1 will be one. Also, it is evident from Equation 5.20 that the normalized displacement ductility and hysteretic energy spectra are special cases of the damage spectrum and that they can be derived by assigning α_1 values of zero and one, respectively (Bozorgnia and Bertero, 2003). Examples of damage spectra are presented in Figure 5.21 for the EW component of the ground motions recorded at Düzce during the 1999 earthquakes in Turkey. The basic characteristics of the inelastic SDF system are the same as those used for Figure 5.16(b), with the following additional parameters: $\mu_{mon}=8$ and $\alpha_1=0.29$ (Bozorgnia and Bertero, 2002). Other characteristics of damage spectra, including the attenuation of damage spectral ordinates

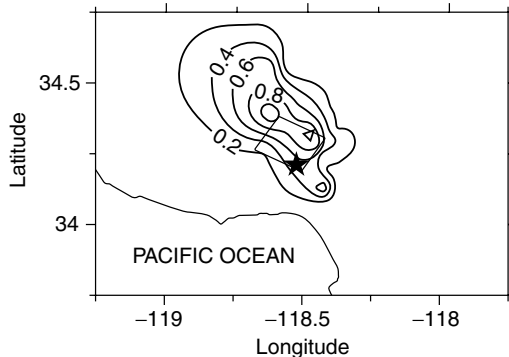


FIGURE 5.22 Distribution of the computed damage spectral ordinate (DI_1) at a 1.0 sec period for the horizontal ground motions recorded in the Northridge, California, earthquake. The epicenter and surface projection of the fault plane are also shown.

with source-to-site distance, have also been examined (see Bozorgnia and Bertero, 2002, 2001b). Following an earthquake, near real-time contour maps of damage spectral ordinates at selected periods can provide useful information on the spatial distribution of damage potential of the recorded ground motions for specified types of structures. Figure 5.22 shows the distribution of the damage spectral ordinate at 1.0 sec period for the horizontal motions recorded during the Northridge earthquake. For this figure, the basic characteristics of the inelastic SDF system are the same as those used in Figure 5.21, except $\mu_{\text{mon}} = 12$, $\alpha_1 = 0.27$, and no near-source factors are used. Utilization of an up-to-date inventory of existing structures together with the damage spectra can be used to identify the expected damage or losses for post-earthquake applications.

The damage spectra presented in a format such as that in Figure 5.21 can be used for seismic performance assessment of existing facilities. For performance-based design of new structures, the value of DI (corresponding to the desired performance) can be specified and the structural strength determined. For such applications, it is desirable to construct strength spectra for constant values of DI (Bozorgnia and Bertero, 2002). Figure 5.23 shows an example of such strength spectra for the El Centro (NS component) recording of the 1940 Imperial Valley earthquake. In this figure, consistent with previous results, a zero value for DI corresponds to an elastic spectrum. Also, as expected, the design strength decreases by increasing the value of DI. In the lower range of DI, a moderate increase in the value of DI (i.e., accepting minor damage) results in a significant reduction in the design strength.

5.3.10 Strong-Motion Spectra: A Summary

A wide variety of strong-motion parameters and spectra were discussed in Section 5.3. To give an overall perspective, it is convenient to classify their characteristics using the following categories:

- Parameters that are measures of free-field ground motion or reveal some basic ground motion characteristics, independent of any structural systems and models. These include peak ground motion values (acceleration, velocity and displacement), strong-motion duration and Fourier spectra of the ground motion. Arias intensity, as related to the integral of the square of the ground acceleration time history, falls in this category; however, it belongs also to the next category, as explained below.
- Spectra and parameters that are related to *elastic* response of SDF and continuous shear beam models. These include elastic response spectra, spectrum intensity, elastic design spectra and drift spectrum. The Arias intensity falls also in this category, because, it is defined as the sum of total energy per unit weight in a set of elastic SDF systems. This category includes important spectra and parameters with extensive applications in earthquake engineering. However, such spectra and

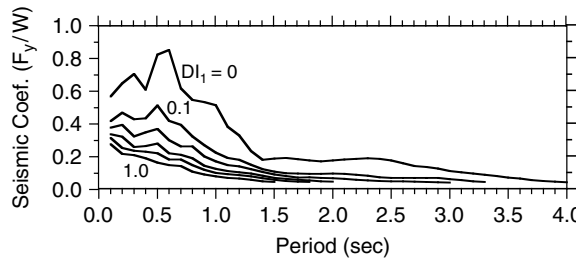


FIGURE 5.23 Strength spectra for constant values of damage index ($DI_1 = 0, 0.1, 0.2, 0.4, 0.6, 1.0$) for an elastic-perfectly-plastic SDF system with 5% damping subjected to the El Centro (NS) recording of the 1940 Imperial Valley, California, earthquake. (From Bozorgnia, Y. and Bertero, V.V., 2002. Improved damage parameters for post-earthquake applications. *Proc. SMIP02 Seminar on Utilization of Strong-Motion Data*, Los Angeles, 61–82.)

parameters do not directly include the effects of amplitude and number of cycles of *inelastic* structural deformations (which are generally associated with damage), unless such effects are approximately and indirectly included.

- *Inelastic* response spectra in the form of maximum displacement ductility and strength spectra (for constant values of ductility) are based on maximum response of inelastic SDF systems. The inelastic spectra reveal some fundamental features of inelastic response and structural damage. However, they do not necessarily include the cumulative effects of number of cycles of inelastic response.
- Energy spectra, especially the *hysteretic energy spectrum*, can provide additional important information about the damage potential of the earthquake ground motion related to the cumulative damage effects. Hysteretic energy spectrum represents the dissipated hysteretic energy (due to yielding) in an *inelastic* SDF system. It includes the cumulative effects of cycles of inelastic response and strong-motion duration. For practical engineering applications, it is more convenient to normalize the demanded hysteretic energy spectra with respect to a measure of energy dissipation capacity of the system.
- Damage spectra represent variation of a damage index for an *inelastic* SDF system versus period. A well-defined damage spectrum will be zero if the response remains elastic and will be one if there is a potential of failure. Other structural performance states (such as operational, life-safe, near collapse, etc.) correspond to values of the damage spectral ordinates between zero and one. This makes the damage spectrum a promising tool for performance-based damage assessment of existing structures and performance-based design of new structures. If in the formulation of damage spectrum, cumulative parameters such as hysteretic energy are included, the damage spectrum would be influenced by the cumulative effects of strong-motion duration.

It is evident that there are some, but not total, overlaps in the information revealed by the various spectra discussed herein. Also, some types of spectra are simpler than others, requiring less input information and simpler computations. Besides their simplicity, however, their reliable applicable ranges must not be overlooked.

5.4 Ground Motion (Attenuation) Relations

5.4.1 Introduction

An essential element in both deterministic and probabilistic seismic hazard analyses is the ability to estimate strong ground motion from a specified set of seismological parameters. This estimation is carried out using a ground motion relation, or what engineers commonly refer to as an attenuation relation. A ground motion relation is a mathematical equation (i.e., a model) that relates a given strong-motion parameter to one or more parameters of the earthquake source, wave propagation path and local site

conditions, collectively referred to as seismological parameters. These parameters are discussed at length below, but first it is useful to examine the mathematical structure and seismological basis of the ground motion relation itself.

The ground motion relation, in its most basic form, can be described by a mathematical equation of the form

$$\ln Y = c_1 + c_2 M - c_3 \ln R - c_4 R + \varepsilon \quad (5.21)$$

where $\ln Y$ is the natural logarithm of the strong-motion parameter of interest, M is earthquake magnitude, R is source-to-site distance or a term involving this distance and ε is a random error term with a mean of zero and a standard deviation of $\sigma_{\ln Y}$. The mathematical form of Equation 5.21 can be traced back to the basic principles of earthquake seismology (Richter, 1958; Lay and Wallace, 1995). The term $c_2 M$ is consistent with the definition of earthquake magnitude as a logarithmic measure of the amplitude of ground motion. The term $-c_3 \ln R$ is consistent with the geometric spreading of the seismic wave front as it propagates away from the earthquake source. The parameter c_3 will vary with distance depending on the seismic wave type, such as whether it is a direct (body) wave or a surface wave and the effect of crustal structure, such as critical reflections off the base of the crust. The term $-c_4 R$ is consistent with the anelastic attenuation of seismic waves caused by material damping and scattering as they propagate through the crust. In practice (e.g., see Section 5.4.4.2), ground motion relations are more complex than implied by Equation 5.21. This additional complexity is needed to account for the effects of near-source behavior, faulting mechanism, local site conditions, source directivity and radiation pattern, the hanging-wall and footwall and tectonic environment. Figure 5.24 shows a typical example of a ground motion relation for peak ground acceleration (PGA).

The discussion in this chapter is limited to those ground motion relations that are used in the most recent (2002) update of the USGS national seismic hazard maps (Frankel et al., 2002). Even though these maps will not find their way into the building codes for several years, the ground motion relations on which they are based will be adopted in engineering practice almost immediately. Because of space limitations, only three of these ground motion relations are provided in equation form (see Section 5.4.4.2). The remainder of the relations are presented in Appendix A to this section that is posted on the accompanying Internet web site of the book (www.crcpress.com/e_products/downloads/download.asp?cat_no=1439). The discussion in this chapter is focused on providing guidance on the use of these relations and a description of how they were applied in the development of the 2002 USGS hazard maps. Other more broadly based compilations are given by Campbell (2003a, 2003b, 2003d).

5.4.2 Model Parameters

5.4.2.1 Ground Motion Parameters

Strong motion parameters typically used in engineering practice can be classified as either time-domain or frequency-domain. PGA and PGV are the most common examples of time-domain parameters. They represent the maximum absolute amplitude of the ground motion measured from a recorded or synthetic time history. PGD is another, albeit, less used peak-domain parameter. The most common frequency-domain parameters are S_a , S_v and S_d response spectral ordinates, which are related to one another through the relationships given in Section 5.3.3.1.

5.4.2.2 Earthquake Magnitude

Earthquake magnitude is used to quantify the size of an earthquake. There are many different scales that are used to define magnitude (see also Chapter 2), but all of the ground motion relations discussed in this chapter use moment magnitude (designated M_w in this chapter but alternatively denoted M by many seismologists). By definition, M_w is related to seismic moment, M_0 , a measure of the seismic energy radiated by an earthquake, by the formula (Kanamori, 1978; Hanks and Kanamori, 1979)

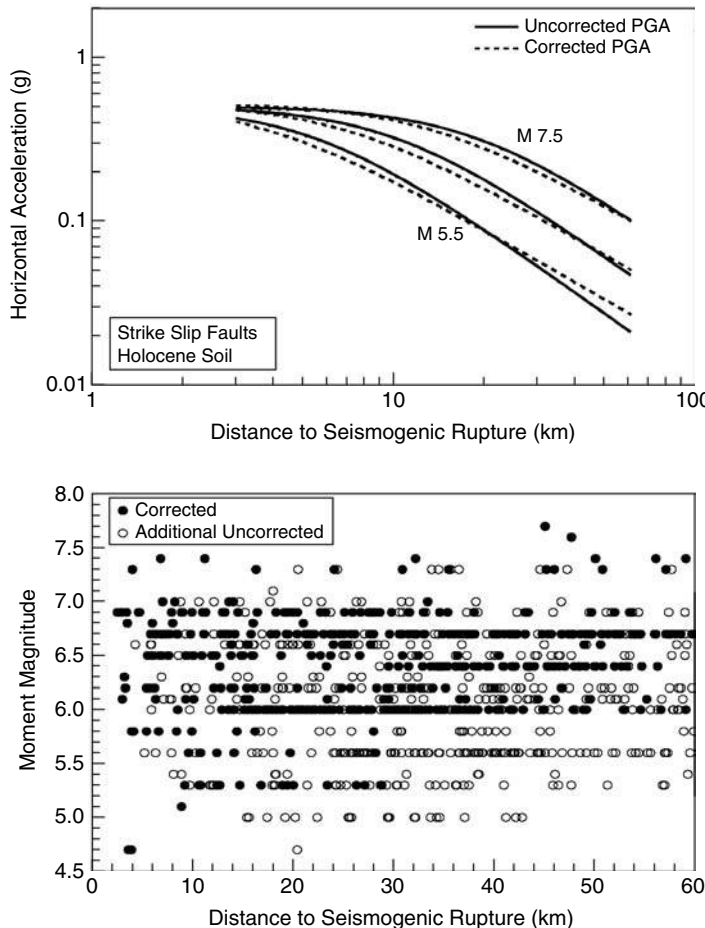


FIGURE 5.24 Example PGA ground motion relation (top) and its associated database (bottom). Uncorrected recordings refer to analog or digital acceleration time histories that have not been processed and, therefore, can only provide estimates of PGA. Corrected recordings refer to acceleration time histories that have been processed to derive velocity and displacement time histories, response spectra, and Fourier amplitude spectra. (From Bozorgnia, Y., Campbell, K.W. and Niazi, M. (1999). Vertical ground motion: characteristics, relationship with horizontal component, and building-code implications. *Proceedings, SMIP99 Seminar on Utilization of Strong-Motion Data*, San Francisco, California, 23–49.)

$$M_w = \frac{2}{3} \log M_0 - 10.7 \quad (5.22)$$

where $M_0 = \mu A_f \bar{D}$ or $2\mu E_s / \Delta\sigma$, μ is the shear modulus of the crust in the source region, A_f is the fault rupture area, \bar{D} is the average displacement over the fault rupture plane, $\Delta\sigma$ is the average static stress drop over the fault rupture plane and E_s is the radiated seismic energy. The definition based on $A_f \bar{D}$ allows M_0 to be derived from geological faulting parameters that are easily observed in the field, at least for large surface-rupturing earthquakes. The definition based on $E_s / \Delta\sigma$ allows M_0 to be derived from instrumental measurements routinely obtained from seismological networks.

5.4.2.3 Source-to-Site Distance

Source-to-site distance is used to characterize the diminution of ground motion in terms of both geometric and anelastic attenuation, as it propagates away from the earthquake source. Distance measures

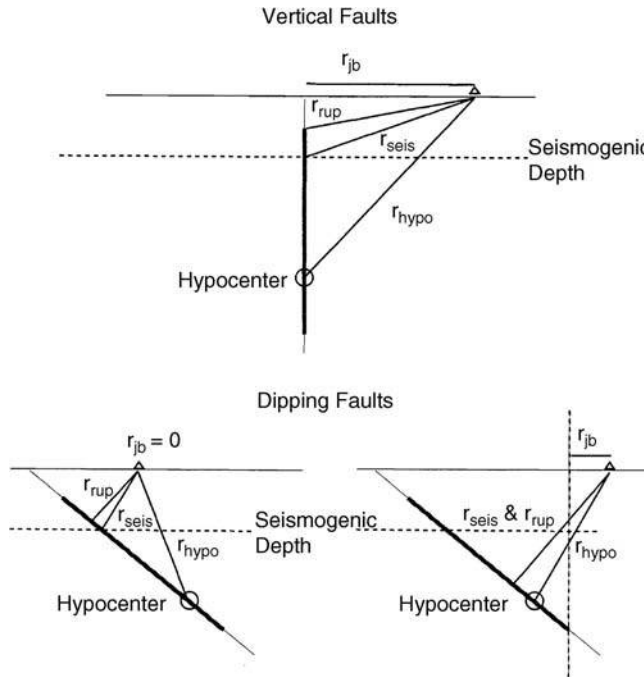


FIGURE 5.25 Relationship between distance measures used in the development of the ground motion relations. (From Abrahamson, N.A. and Shedlock, K.M. (1997). Overview. *Seismological Research Letters*, 68, 9–23.)

can be grouped into two broad classes depending on whether they treat the earthquake as a point source or as a finite source. Point-source distance measures include epicentral distance, r_{epi} , and hypocentral distance, r_{hypo} , where

$$r_{hypo} = \sqrt{r_{epi}^2 + h_{hypo}^2} \quad (5.23)$$

and h_{hypo} is the focal (hypocentral) depth of the earthquake. Generally speaking, r_{epi} and r_{hypo} are poor measures of distance for earthquakes with large rupture areas (i.e., large magnitudes). They are primarily used for characterizing distances from small earthquakes that can be reasonably represented by a point source. Experience has shown that ground motion relations that use point-source measures should not be used to estimate ground motions close to large earthquakes unless some approximate adjustment is made to account for finite-faulting effects.

The three finite-source distance measures used in the ground motion relations presented in this chapter are the closest horizontal distance to the vertical projection of the fault rupture plane, r_{jb} , the closest distance to the fault rupture plane, r_{rup} and the closest distance to the seismogenic part of the fault rupture plane, r_{seis} . The definition of r_{seis} assumes that fault rupture within the near-surface sediments or shallow fault gouge is non-seismogenic and not of engineering interest. These distance measures are schematically defined in Figure 5.25. Although r_{jb} is reasonably easy to estimate for a future (e.g., Design) earthquake, the distance measures r_{rup} and r_{seis} are not so easily determined, particularly when the earthquake is not expected to rupture the entire seismogenic width of the crust. In such cases, it is important to take into account the expected depth to the top of the fault rupture plane. If rupture-specific information is not available, the average depth to the top of the inferred fault rupture plane, d_{rup} , or to the seismogenic part of this plane, d_{seis} , can be calculated from (Campbell, 2000b)

$$d_i = \begin{cases} \frac{1}{2} [H_{top} + H_{bot} - W \sin(\delta)] & d_i \geq H_i \\ H_i & \text{otherwise} \end{cases} \quad (5.24)$$

where the subscript i is equal to rup or seis depending on the distance measure of interest, H_{bot} is the depth to the bottom of the seismogenic part of the crust, H_{top} is the depth to the top of the fault, H_{seis} is the depth to the top of the seismogenic part of the fault, δ is the dip of the fault, and W is the down-dip width of the fault rupture plane. There are many relationships that can be used to calculate W , but one often used in engineering practice is given by Wells and Coppersmith (1994)

$$\log W = -1.01 + 0.32M_W \quad (5.25)$$

where W is measured in kilometers and the standard deviation of $\log W$ is 0.15.

Campbell (1997) recommends restricting the seismogenic depth used to calculate r_{seis} to $H_{seis} \geq 3$ km, even when the fault ruptures above this depth. This recommendation is based on several factors, including: (1) observations of aftershock distributions and background seismicity, (2) slip distributions on fault rupture planes derived from earthquake modeling studies and (3) an independent assessment of the depth of seismogenic faulting by Marone and Scholz (1988).

Many of the ground motion relations discussed in this chapter include near-source distance terms that account for the widely held belief that short-period strong-motion parameters should become less dependent on magnitude, i.e., they should saturate, close to the causative fault. Most engineers and seismologists consider such behavior to be an accepted behavior of near-fault ground motion. The ground motion relation shown in Figure 5.24 exhibits such behavior at short distances.

5.4.2.4 Faulting Mechanism

The faulting mechanism, or style of faulting, of an earthquake characterizes the direction of slip on the fault plane, seismologically defined as the rake (Lay and Wallace, 1995). Rake is a continuous variable representing the angle between the direction of slip on the fault plane and the orientation of the fault on the Earth's surface (its strike). Rake has not been used directly in any ground motion relation. Instead, the faulting mechanism has been classified in terms of two or more faulting categories. These categories are typically defined as strike-slip, reverse and normal. The values of rake that correspond to these categories are 0° for pure left-lateral strike-slip faulting, 180° for pure right-lateral strike-slip faulting, 90° for pure reverse faulting and 270° for pure normal faulting (Lay and Wallace, 1995). Alternatively, some seismologists use a rake of -90° to define pure normal faulting. Thrust faulting is a special case of reverse faulting in which the dip of the rupture plane is shallow, typically less than 45° . A combination of strike-slip and either reverse or normal faulting (oblique faulting) has a rake that falls between those given above. It has been common practice in the past to put strike-slip and normal-faulting events into a single strike-slip category. However, a recent study by Spudich et al. (1999) suggests that normal-faulting events, or for that matter strike-slip events in an extensional tectonic regime, might have lower ground motions than other types of shallow crustal earthquakes. All of the ground motion relations discussed in this chapter predict higher ground motions for reverse and reverse-oblique earthquakes than for strike-slip and normal earthquakes.

A great deal of interest has been generated in blind thrust faults by seismologists and engineers after unusually large ground motions were observed during the 1987 Whittier Narrows, California, the 1988 Saguenay, Canada and the 1994 Northridge, California, earthquakes. Whether similarly high ground motions can be expected from all future blind thrust earthquakes is at present speculative. However, it cannot be ruled out, considering the current limited observational database. The higher ground motions observed during blind thrust earthquakes have been found to correspond to higher-than-average stress

drops. More theoretical and empirical studies will be needed before there is a clear understanding why these three earthquakes produced such high stress drops and how such events might be predicted in the future. The Campbell and Bozorgnia (2003) ground motion relation is the only one discussed in this chapter that includes differences between reverse and thrust events. This relation predicts higher short-period ground motions for thrust events as would be expected if these differences were due to higher stress drops.

5.4.2.5 Local Site Conditions

Local site conditions describe the type of deposits that lie beneath the site. They are usually described in terms of surface or near-surface geology, shear-wave velocity and sediment depth. The latter two descriptions are preferred because they represent physical quantities that can be related directly to the dynamic response of the underlying geological deposits. Traditionally, local site conditions have been classified as soil or rock. Many ground motion relations discussed in this chapter still use this simple classification. However, Boore et al. (1997), Rodriguez-Marek et al. (2001), Campbell and Bozorgnia (2003) and Stewart et al. (2003) have clearly demonstrated the importance of a more refined site classification scheme in the prediction of near-source ground motion. Park and Elrick (1998) and Wills and Silva (1998) have also shown that a more refined geological classification appears to be warranted based on measured shear-wave velocities in various geological units in California.

There are typically two methods for classifying a site in terms of shear-wave velocity, here denoted V_s . The first is the average value of V_s in the top 30 m (100 ft) of the deposit, referred to here as 30-m velocity, V_{30} . The second is the average value of V_s over a depth equal to a quarter-wavelength of a ground-motion parameter of specified period or frequency, referred to here as effective velocity. The 1997 edition of the *Uniform Building Code* (UBC) and the 2000 edition of the *International Building Code* (IBC) use the 30-m velocity as the primary basis for defining National Earthquake Hazard Reduction Program (NEHRP) site categories and their associated site factors that are used to adjust design ground motions for local site effects (Table 5.3; see also Chapter 4). Other properties of the soil profile such as standard penetration resistance, unconfined shear strength and depth of soft soil are also used to define the NEHRP site class, but these properties are not listed in Table 5.3, see also Chapter 4. The California Geological Survey (Wills et al., 2000) modified the NEHRP site classification scheme to incorporate boundary site categories, which they used for the purpose of developing a site conditions map for California (Table 5.3; see also Chapter 4). The 30-m velocity is calculated from the formula

$$V_{30} = \left(\sum_{i=1}^n d_i \right) / \left(\sum_{i=1}^n (d_i / V_{Si}) \right) \quad (5.26)$$

where d_i is the thickness and V_{Si} is the shear-wave velocity of the i th soil layer. Progressively deeper soil layers are used until the summation in the numerator of Equation 5.26 equals 30 m (100 ft). Boore et al. (1997) developed the only ground motion relation discussed in this chapter that uses V_{30} as a site parameter. However, Choi and Stewart (2003) and Stewart et al. (2003) developed nonlinear site factors for NEHRP site categories B through E that can be used with the ground motion relations of Abrahamson and Silva (1997), Sadigh et al. (1997) and Campbell and Bozorgnia (2003). The NEHRP site categories proposed by the California Geological Survey (CGS) were defined by relating measured values of V_{30} to mapped geological units in California. However, the CGS defined overlapping velocity ranges for their site categories that make their use difficult in practice. For site categories E through BC, the CGS defines nominal values of V_{30} (Table 5.3) in the GIS version of the California site-conditions map that avoids the ambiguity in estimating V_{30} knowing the site category. The CGS assigns a nominal 30-m velocity value of 1000 m/sec to NEHRP B, although the writers prefer the nominal value given in Table 5.3, which is listed as 1130 m/sec, the midpoint of the velocity range that defines this category. Because of the overlapping velocity ranges, an ambiguity arises when attempting to assign a particular site to a CGS site category when 30-m velocity is known. Because there is no consensus on how this should be done, a non-overlapping

TABLE 5.3 Definition of NEHRP Site Classes Based on Shear-Wave Velocity

NEHRP Site Class ^a			30-m Velocity, V_{30} (m/sec)		
Code	CGS	Soil Profile Name	Code	Cgs ^b	Nominal ^c
A	A	Hard rock	≥ 1500	≥ 1695	1890
—	AB	A-B boundary		1315–1695	1500
B	B	Rock	760–1500	945–1315	1130
—	BC	B-C boundary	—	660–945	760
C	C	Very dense soil and soft rock	360–760	460–660	560
—	CD	C-D boundary	—	315–460	360
D	D	Stiff soil	180–360	225–315	270
—	DE	D-E boundary	—	165–225	180
E	E	Soft soil	< 180	< 165	150

^a National Earthquake Hazard Reduction Program (NEHRP) site class definitions: Code, as defined in the 1997 *Uniform Building Code* (UBC) and the 2000 *International Building Code* (IBC); CGS, as defined by the California Geological Survey (Wills et al., 2000) and extended by the writers to include A and AB site classes.

^b Approximate ranges of V_{30} proposed by the writers to use in assigning CGS NEHRP site-classes when V_{30} is known.

^c Single best estimate of V_{30} to use for each NEHRP site class when no other information is available.

range of V_{30} values is proposed and listed in Table 5.3. However, because there is no unique way of defining these ranges, the user must apply his or her own judgment in deciding what CGS site category should be used to correspond to a specific value of V_{30} . The values listed in Table 5.3 are meant to be used only as a guide. There is no such ambiguity in the range of 30-m velocity for the code-based NEHRP site categories. However, there is an ambiguity in defining a nominal value for the first and last building-code categories, which are defined by inequalities in V_{30} . In this case, a reasonable estimate of the nominal value of V_{30} based on published sources is provided in Table 5.3. The value for soft soil (E) is that given for intertidal mud by Wills and Silva (1998). The value for hard rock (A) is that reported by Savy et al. (1987) for older sedimentary rock sites in the eastern United States.

Joyner et al. (1981) proposed effective velocity as a site parameter, which is related to the non-resonant amplification produced as a result of the energy conservation of seismic waves that propagate vertically upward through a deposit of gradually changing velocity. This parameter is defined as the average velocity from the surface to a depth corresponding to a quarter-wavelength of a strong-motion parameter of specified period or frequency. Effective velocity can be calculated from Equation 5.26 by summing to a depth corresponding to a quarter-wavelength rather than to 30 m. This depth is given by the equation (Boore, 2003)

$$D_{1/4}(f) = \sum_{i=1}^n d_i \quad (5.27)$$

where $T = 1/f$ is the period of interest. Progressively deeper soil layers are used in the above summation until the equality $\sum_{i=1}^n d_i/V_{Si} = T/4$ is achieved. Effective velocity is used to calculate site amplification factors using the stochastic method (Boore, 2003). This is important because several of the Eastern North America (ENA) ground motion relations discussed in this chapter were developed using this method.

Sediment or basin depth is the depth to the basement-rock horizon beneath the site. Basement rock is a geological term that is used to describe the more resistant, generally crystalline rock that lies beneath layers or irregular deposits of younger, relatively deformed sedimentary rock. This parameter is not generally used in engineering practice and is not included in any of the ground motion relations discussed in this chapter. First proposed empirically over several decades ago, its importance has been recently

recognized by several seismologists. For example, based on empirical and theoretical considerations, Joyner (2000) found that long-period spectral amplifications predicted from the sediment-depth term given in Campbell (1997, 2000b) were similar to those derived from the effects of traveling surface waves generated at the edge of the Los Angeles basin. Lee and Anderson (2000), Field (2000) and Field and the SCEC Phase III Working Group (2000) found that sediment depth could be used to approximately account for the modeled 3-D response of the Los Angeles basin. Rodriguez-Marek et al. (2001) found that the depth to bedrock with $V_s \geq 760$ m/sec was an important parameter in estimating site response from the 1989 Loma Prieta and 1994 Northridge, California, earthquakes. Campbell and Bozorgnia (2003) evaluated sediment depth as a parameter in their ground motion relation and also found it to be important, especially at long periods. However, they chose not to include it in their relation at that time because they found from past experience, e.g., in applications involving the ground motion relation of Campbell (1997, 2000b), that it is often misunderstood and misinterpreted by engineers.

5.4.2.6 Stress Drop

Stress drop, or more correctly dynamic or Brune stress drop (Brune, 1970, 1971), is one of the parameters that controls the high-frequency amplitude of ground motion. It is related to the amount of stress that is relieved at the rupture front during an earthquake. Theoretical studies have shown that higher stress drop results in higher short-period ground motion. None of the ground motion relations discussed in this chapter explicitly include stress drop as a parameter. However, stress drop is one of the parameters that is included in the calculation of ground motion using the stochastic method, which was used to develop several of the ENA ground motion relations discussed in this chapter.

As discussed above, relatively high stress drops are likely to have been the cause of the relatively high ground motions observed during some recent blind thrust earthquakes. On the other hand, low stress drops might have been the cause of the relatively low short-period ground motions observed during the 1999 Chi-Chi (M_w 7.6), Taiwan, earthquake (Tsai and Huang, 2000; Boore, 2001), the 1999 Kocaeli (M_w 7.4), Turkey, earthquake (Anderson, 2000, 2003) and, at least based on preliminary ground motions available at the time this book went to press, the 2002 Denali (M_w 7.9), Alaska, earthquake. The observation of relatively low short-period ground motions during the Chi-Chi earthquake is particularly significant because it is a large thrust earthquake, which had been expected from previous empirical and theoretical studies to have relatively large ground motion. This earthquake did, however, have relatively large ground motion on the hanging wall of the rupture plane and relatively large PGV and long-period S_a as had been expected. The relatively low stress drops implied for the Taiwan, Turkey and Alaska earthquakes could be a result of large total slip on the causative faults (Anderson, 2003) or large surface ruptures (Somerville, 2000). More study will be needed to better understand the phenomena that might have contributed to these low ground motions. If these earthquakes are found to be typical of similar large earthquakes worldwide, the implication is that the current ground motion relations might be overpredicting short-period ground motions from large earthquakes, something that has been suggested from observations of precariously balanced rocks near great earthquakes on the San Andreas fault (Brune, 1999).

5.4.2.7 Hanging-Wall and Footwall Effects

Generally speaking, the hanging wall is that portion of the crust that lies above the rupture plane of a dipping fault and the footwall is that portion of the crust that lies below this plane. Sites located on the hanging wall of a reverse or thrust fault generally exhibit higher-than-average ground motion. The hanging-wall effect is probably caused by a combination of radiation pattern, source directivity, decoupling of the hanging-wall and footwall during rupture propagation and the entrapment of seismic waves within the hanging-wall wedge of the crust (that portion between the rupture plane and the Earth's surface). Theoretical ground-motion modeling has consistently shown that higher ground motion can be expected on the hanging wall of reverse and thrust faults and that lower ground motion can be expected on the footwall of such faults (Anderson, 2003; Brune 2001). This is consistent with the observation of shattered rock on the hanging wall of thrust faults in Southern California and the lack of such shattered

rock and the presence of precariously balanced rocks on the footwall of at least two thrust faults in this same region (Brune, 2001). It is also consistent with observed ground motion from the 1994 Northridge earthquake (Abrahamson and Somerville, 1996) and the 1999 Chi-Chi earthquake (Shin et al., 2000). Two of the ground motion relations discussed in this chapter include a hanging-wall term (Abrahamson and Silva, 1997; Campbell and Bozorgnia, 2003).

5.4.2.8 Tectonic Environment

Tectonic environment refers to the state of stress and the seismological properties of the crust. It has a significant impact on the amplitude and attenuation of strong ground motion. It has traditionally been classified into four basic types for the purpose of estimating strong ground motion: (1) shallow crustal earthquakes in a tectonically active region, (2) shallow crustal earthquakes in a tectonically stable region, (3) intermediate-depth earthquakes (also known as Wadati-Benioff or intraslab earthquakes) within the down-going crustal plate of a subduction zone and (4) earthquakes along the seismogenic interface of the down-going and overriding crustal plates of a subduction zone. The shallow crustal environment can be further subdivided into compressional and extensional regimes. Each of these tectonic environments is represented by at least one of the ground motion relations discussed in this chapter.

A detailed discussion of the different tectonic environments and their global distribution is provided by Moores and Twiss (1995). A shallow crustal environment refers to the seismogenic part of the crust, which generally varies from 10 to 30 km in thickness, depending on the region. A tectonically active environment is one in which large earthquakes are relatively frequent and tectonic deformation is relatively large. It is usually located in the vicinity of tectonic plate margins. Such regions are typically characterized by relatively low stress drops and relatively high anelastic attenuation. A tectonically stable environment is one in which large earthquakes are relatively infrequent and tectonic deformation is relatively small. It is usually located away from plate margins in an intraplate region characterized by very old continental crust. Such regions are typically characterized by relatively high stress drops and relatively low anelastic attenuation. Johnston (1996) presents a series of maps that show the geographic distribution of tectonically active and tectonically stable continental regions worldwide. A compressional regime is one in which the crust is undergoing shortening. It is typically associated with relatively high stress drops. An extensional regime is one in which the crust is undergoing lengthening and is typically associated with relatively low stress drops. Zoback (1992) presents a stress map that shows the geographic distribution of compressional and extensional regimes worldwide.

A subduction zone is a region in which one tectonic plate (usually oceanic crust) thrusts beneath, or is *subducted* by, another tectonic plate (usually continental crust). Subduction interface earthquakes, some of which are the largest in the world, occur along the seismogenic boundary of the subducting and overriding plates. Depending on the age of the subducting plate, this interface occurs to depths ranging anywhere from 20 to 50 km. So-called Wadati-Benioff, or intraslab, earthquakes occur within the subducting plate below the subduction interface zone as it descends into the Earth's mantle.

5.4.3 Analysis Methods

5.4.3.1 Strong Motion Database

In regions where strong-motion recordings are abundant, ground motion relations are developed from statistical regression analysis. This requires a suitable strong-motion database. Engineering estimates of ground motion are intended to provide estimates of ground motion on level ground in the free field, unaffected by any man-made or natural structures, or what engineers refer to as soil-structure interaction effects. This means that these recordings should not be located on or near a large structure, in an area of strong topographic relief, or below the ground surface. All of these situations have been shown to significantly modify free-field ground motion in some situations. Although it is generally agreed upon that non-free-field recordings should be excluded from a strong-motion database, there is no consensus on what constitutes such a recording. Furthermore, because the majority of the available recordings were obtained in or near a man-made structure, it is impossible to restrict the database to truly free-field

recordings without restricting their number to the point where a statistical analysis might not be meaningful. All of the empirical ground motion relations discussed in this chapter have attempted to screen out non-free-field recordings to some degree, albeit using different and sometimes conflicting criteria. A recent study by Stewart (2000) will help in providing a more quantitative basis for identifying such recordings in the future.

Stewart (2000) evaluated the conditions for which recordings obtained at the foundation of a structure can be expected to provide a reasonably unbiased estimate of free-field ground motion with minimal uncertainty. He found that variations between spectral accelerations recorded in the free field and those recorded on a nearby building foundation correlated well with dimensionless parameters that strongly influence kinematic and inertial soil-structure interaction phenomena, such as embedment ratio, dimensionless frequency (the product of wave frequency and foundation radius normalized by soil shear-wave velocity) and structure-to-soil stiffness ratio. Stewart also found that low frequency components of spectral acceleration recorded on shallow foundations provide reasonable estimates of free-field ground motion. However, such was not the case for PGA or, in some cases, even PGV.

Stochastic, theoretical and hybrid empirical (semi-theoretical) analysis methods are typically used to develop a synthetic strong-motion database in areas where there are an insufficient number of strong-motion recordings. These synthetic data are used to develop a ground motion relation in much the same manner that actual data are used. The stochastic method uses a stochastic representation of the ground motion, shaped by simple seismological models of the source spectrum and propagation path and a mathematical representation of the response of an SDF oscillator, to derive a set of synthetic strong-motion parameters for a desired set of magnitudes and distances (Campbell, 2003a, 2003b, 2003d; Boore, 2003). One of the important aspects of the stochastic method is whether a single-corner or a double-corner source spectrum is used (Atkinson and Boore, 1998), because the latter results in relatively low mid-to-long period ground motions compared to the one-corner source spectrum. Of the five ENA ground motion relations discussed in this chapter, three were developed using the stochastic method (Atkinson and Boore, 1995, 1997; Frankel et al., 1996; Toro et al., 1997) and, of these, only the Atkinson and Boore relation was based on the two-corner source spectrum. The theoretical method uses kinematic or dynamic dislocation models of the earthquake rupture process, together with empirical or theoretical Greens functions and seismic ray theory, to develop synthetic strong-motion parameters. Because of its greater complexity, only one of the ENA ground motion relations discussed in this chapter used the theoretical method (in this case the kinematic approach) in its derivation (Somerville et al., 2001). Because it has only recently gained the interest of seismologists, only one of the ENA ground motion relations (Campbell, 2001, 2003c) was developed using the hybrid empirical method. This method uses the stochastic method to adjust empirical ground motion relations developed for one region, in this case Western North America (WNA), to estimate synthetic strong-motion parameters in another region, in this case ENA, where there are a limited number of strong-motion recordings. These adjustments take into account differences in the earthquake source, wave propagation and site-response characteristics between the two regions.

5.4.3.2 Regression Analysis

Whether developed from recorded or synthetic ground motion data, all ground motion relations are derived using a statistical fitting procedure known as regression analysis (e.g., Draper and Smith, 1981). Regression analysis is used to determine the best estimate of the coefficients in the relation (e.g., the coefficients c_1 through c_4 in Equation 5.21) using any number of statistical fitting procedures, such as least squares or maximum likelihood. Three different methods were used to develop the ground motion relations discussed in this chapter: (1) weighted nonlinear least-squares regression; (2) two-step least squares regression and (3) random-effects regression. Each of these methods has its own strengths and weaknesses; however, they all attempt to mitigate the bias introduced by the uneven distribution of recordings with respect to magnitude, distance and other seismological parameters. An advantage of the latter two methods is that they provide a direct estimate of the intra-earthquake and inter-earthquake

components of randomness, although these components can be derived, albeit indirectly, using the first method as well.

5.4.3.3 Predicted Value

Because the predicted value from Equation 5.21 is the logarithm of Y , this prediction represents the mean value of $\ln Y$, or what is referred to statistically as the median (50th-percentile) value of Y . By definition, the median value is exceeded by 50% of the underlying observations. The $100 \times (1 - \alpha)$ -percentile estimate of the mean of n_0 future observations of $\ln Y$ is statistically given by the formula (Draper and Smith, 1981)

$$\ln Y_{1-\alpha} = \ln Y + t_v(\alpha) \sqrt{\frac{\sigma_{\ln Y}^2 + \sigma_{\ln Y}^2}{n_0}} \quad (5.28)$$

where $t_v(\alpha)$ is the Student's t -statistic for an exceedance probability of α and for $v = n - p$ degrees of freedom (this statistic is widely available in statistic books), $\sigma_{\ln Y}$ is the standard error of the mean value of $\ln Y$ (a measure of modeling uncertainty) and $\sigma_{\ln Y}$ is the standard error of regression (a measure of randomness). The standard error of regression is given by

$$\sigma_{\ln Y} = \sqrt{\frac{1}{n-p} \sum_{i=1}^n (\ln Y_i - \bar{\ln Y})^2} \quad (5.29)$$

where n is the number of recordings, p is the number of regression coefficients, $\ln Y_i$ is the i th recorded value, and $\bar{\ln Y}_i$ is the i th predicted value. The $100 \times (1 - \alpha)$ -percentile estimate of a single future observation of $\ln Y$, the most common application of Equation 5.28, is calculated by setting $n_0 = 1$.

It is common engineering practice to calculate the $100 \times (1 - \alpha)$ -percentile estimate of a single future value of $\ln Y_i$ by setting $\sigma_{\ln Y} = 0$ and replacing the t -statistic with the standard normal variable, z . These assumptions reduce Equation 5.28 to its more commonly used form

$$\ln Y_{1-\alpha} = \ln Y + z_\alpha \sigma_{\ln Y} \quad (5.30)$$

where z_α is the standard normal variable for an exceedance probability of α (this variable is widely available in statistics books). Although statistically incorrect, results using Equation 5.30 are not significantly different from those using Equation 5.28 unless the predicted value is derived from an extrapolation of the regression equation or from a regression equation that is based on very few recordings. In the first case, the value of $\sigma_{\ln Y}$ is non-negligible and, in the second case, the z -statistic is inaccurate. When Equation 5.30 is used to predict ground motion, it is engineering practice to account for epistemic uncertainty by using several ground motion (attenuation) relations to predict $\ln Y$. However, even such practice will not necessarily account for all of the epistemic uncertainty inherent in the estimation of ground motion.

5.4.4 Ground Motion (Attenuation) Relations Used by USGS

5.4.4.1 General Description

All ground motion relations have certain limitations. These limitations stem from issues that arise during their development, such as the number and distribution of recordings, the data selection criteria, the selection of a functional form, the theoretical assumptions and the choice of seismological parameters used to define the source, path and site effects. It is dangerous to assume that any engineering model can be extrapolated beyond its data, theoretical assumptions, or geographic region of applicability and still provide a reliable estimate of ground motion. In fact, some of the ground motion relations presented in this and the next section have specific caveats regarding their use, which are noted when known.

However, these caveats are often ignored in seismic hazard analysis for practical reasons. Such is the case in the development of the 1996 and 2002 USGS national seismic hazard maps.

The shallow crustal ground motion relations used in the 2002 USGS hazard maps are segregated into two tectonic regions: WNA and ENA. WNA is further segregated into extensional, compressional and subduction regimes. The division between WNA and ENA has traditionally been taken as 105° W. Longitude. A somewhat more detailed definition of this boundary has been proposed by Frankel et al. (1996, 2000, 2002). Because ENA is tectonically stable, earthquakes in this region are typically associated with higher stress drops and lower anelastic attenuation, resulting in higher ground motion at short periods and large distances.

The USGS used four ground motion relations for compressional regimes in WNA; namely, Abrahamson and Silva (1997), Boore et al. (1997), Sadigh et al. (1997) and Campbell and Bozorgnia (2003). Although not specifically used in the development of the hazard maps, the Sadigh et al. (1993) ground motion relation is presented along with these authors' 1997 relation because it is widely used in engineering practice to predict the vertical component of ground motion for rock sites. For extensional regimes in WNA, the USGS used the above four ground motion relations, each evaluated for strike-slip and normal faulting (see discussion below) along with the Spudich et al. (1999) relation. All of these relations were developed from regression analyses of strong-motion recordings using the empirical method. The USGS used five ground motion relations for ENA; namely, Atkinson and Boore (1995, 1997), Frankel et al. (1996), Toro et al. (1997), Somerville et al. (2001) and Campbell (2001, 2003c). All of these relations were developed from regression analyses of synthetic strong-motion parameters calculated using either the stochastic, theoretical (kinematic), or hybrid empirical method and are, therefore, non-empirical. The Atkinson and Boore relation was updated by D. Boore to represent the NEHRP B-C Boundary site condition.

Great interface earthquakes of M_w 8.3 and 9.0 on the Cascadia Subduction Zone (Cascadia S. Z.) dominate the seismic hazard along the western coasts of Oregon and Washington. The USGS used two ground motion relations for modeling subduction interface events; namely, Youngs et al. (1997) and Sadigh et al. (1997). The Youngs et al. relation was evaluated for interface events and the Sadigh et al. relation for reverse-faulting events (see discussion below). The hypocentral depth was fixed at 20 km when evaluating the Youngs et al. relation. Weights for each relation are defined as a function of distance so that the Youngs et al. And Sadigh et al. relations have equal weight at relatively close distances and the Youngs et al. relation has 100% weight at relatively larger distances. The USGS used a constant distance range of 70 ± 15 km for the M_w 8.3 event and 60 ± 15 km for the M_w 9.0 event, independent of period, to define the distance range over which the weights were linearly varied. However, in reality, this range is period dependent. The maximum magnitude that is allowed in the Sadigh et al. relation is 8.5, so M_w was set to this value for the M_w 9.0 event. The USGS used the Youngs et al. relation and two versions of a new relation developed by Atkinson and Boore (2003), both evaluated for intraslab conditions, for intermediate-depth (Wadati-Benioff) events associated with the Cascadia S. Z. The hypocentral depth used in the Youngs et al. relation and the depth to the top of faulting used to estimate r_{rup} in both relations was fixed at 50 km.

Table 5.4 lists relevant information concerning the ground motion relations that were used in the development of the 2002 USGS hazard maps. This information includes the subregion in which they were applied, the weight assigned to them for the given subregion, whether they predict the vertical component of ground motion (V) in addition to the average horizontal component (H), the range of periods for which they are applicable, the seismological parameters that are included in each, and the range of magnitudes and distances for which they are considered valid. In parentheses, beneath the region designation, is a description of the method that was used to develop each relation. For the WNA relations, the subregion indicates whether they were used for compressional and extensional regimes. The extensional regime includes the Basin and Range province, which generally extends from the eastern front of the Cascade and Sierra Nevada Mountains to the western front of the Rocky and Wasatch Mountains. This regime includes eastern California (including Imperial Valley), eastern Oregon, eastern Washington, southern Idaho, western Utah, Arizona, Nevada and New Mexico (Frankel et al., 2002). For the ENA

relations, the subregion indicates whether they were used for faults and for background seismicity (also known as gridded or smoothed seismicity). Explicitly modeled ENA faults include those responsible for the 1811–1812 New Madrid sequence and the 1876 Charleston earthquake. Background seismicity can have a maximum magnitude as large as M_w 7.5; nevertheless, the USGS did not use the Somerville et al. (2001) relation for such earthquakes, even though the authors of the relation recommend its use for events of $M_w \geq 6$. The model parameters enclosed in parentheses are the alternative symbols used to describe the ground motion relations presented in the Appendix A provided on the accompanying Internet site and in Campbell (2003a, 2003b, 2003d). This alternative notation was used to provide a consistent set of notation among the different ground motion relations.

Among the ENA models, only those of Somerville et al. (2001) and Campbell (2001, 2003c) explicitly include near-source scaling characteristics. The others, because they are based on point-source seismological models, require their distance measures to be modified or capped to give realistic ground-motion estimates at near-source distances. In the development of the USGS hazard maps, the hypocentral distance used by Atkinson and Boore (1995, 1997) and Frankel et al. (1996) was replaced by the closest distance to the surface projection of faulting, r_{jb} , as suggested by Boore (2003). Furthermore, a fictitious depth was used to force the relation to asymptotically approach a limiting amplitude at short distances, similar to those relations that use a finite-fault distance measure. In addition, absolute amplitude caps were applied to both the median estimates and the upper tails of the aleatory distributions of PGA and selected spectral accelerations in ENA (Table 5.5). All of the ground-motion aleatory distributions (the random distribution of ground motion about the median), including those for the WNA and Cascadia S. Z., were truncated at ± 3 standard deviations in the probabilistic seismic hazard analysis. Two fictitious depths, 5 and 10 km, were used to limit near-source ground motions computed from the point-source ground motion relations, depending on whether the source was modeled as background seismicity or finite faulting, respectively. The depth of 5 km used for background seismicity was also used with those ground motion relations that use the fault-distance measures r_{rup} and r_{seis} (Table 5.4).

Table 5.6 lists the faulting categories used in each of the WNA ground motion relations. These categories are defined in terms of the rake and the values of the faulting mechanism (style-of-faulting) parameters used in each relation, according to the alternative notation used in the Appendix A published on the accompanying Internet site and in Campbell (2003a, 2003b, 2003d). The rake is an important parameter because it corresponds to a physically meaningful quantity of the earthquake source — the orientation of slip on the fault — that ultimately determines the focal mechanism of the earthquake. The faulting mechanism parameter is a convenient way of statistically describing the effects of the rake on the predicted ground motion in the regression analysis. Only the WNA ground motion relations include a faulting mechanism parameter. However, some of these relations either do not specify the range of rakes that correspond to a given faulting category or give an incomplete description of these rakes. The values of rake included in Table 5.6 were determined based on discussions with the authors of the relations. The faulting categories given in italics are those used in the development of the 2002 USGS hazard maps. For purposes of developing these maps, all faults were placed into one of three faulting categories, characterized as strike slip, normal, or reverse. Reverse-oblique faulting was placed into the reverse-faulting category. Although Spudich et al. (1999) distinguished between strike slip and normal faulting, they found no significant difference in the two and, as a result, did not include a faulting mechanism parameter in their ground motion relation. The Sadigh et al. (1997) relation was evaluated for reverse faulting when used for estimating ground motions for Cascadia S. Z. interface events. In addition to a faulting mechanism parameter, the Abrahamson and Silva (1997) and Campbell and Bozorgnia (2003) ground motion relations include a hanging-wall term. However, the USGS evaluated the Abrahamson and Silva relation for hanging-wall effects only for reverse faults and for sites located directly over the rupture plane or its horizontal extension, a restriction not imposed by the authors. The USGS did not attempt to apply a more general hanging-wall model, such as that described by Campbell (2003a, 2003b, 2003d), to all of the relations. Nor did they attempt to apply a general source directivity term to any of the ground motion relations, such as that described in Section 5.4.5.3. Such a directivity term is often used in engineering practice.

TABLE 5.4 Ground Motion Relations Used in the 2002 USGS National Seismic Hazard Maps

Ground Motion Relation	Region	Subregion	Weight	Comp	Periods	Model Parameters ^b	Validity
Abrahamson and Silva (1997)	WNA (Empirical)	Compressional	0.250	H, V	PGA, 0.02 – 5.0	$M(M_w), r_{hyp}, F_5 S(S_{Soil}), HW, \bar{PGA}_{rock} (A_{Rock})$	$5.0 \leq M_w \leq 8.0, r_{hyp} \leq 100 \text{ km}$
Boore et al. (1997)	WNA (Empirical)	Extensional	0.200	H	PGA, 0.10 – 2.0	$M(M_w), r_{jp} b_{iss}(c_s), b_{lrs}(c_u), V_S (V_{30})$	$5.5 \leq M_w \leq 7.5, r_{jp} \leq 80 \text{ km}$
Campbell and Bozorgnia (2003)	WNA (Empirical)	Compressional	0.250	H, V	PGA, 0.05 – 4.0	$M_{hyp} r_{hyp}, f_{jp}, F_{AV}, F_{TP}, S_{VS}, S_{SR}, S_{R0}, HW$	$4.7 \leq M_w \leq 8.0, r_{hyp} \leq 100 \text{ km}$
Sadigh et al. (1993, 1997)	WNA (Empirical)	Extensional	0.200	H, V	PGA, 0.07 – 4.0	$M(M_w), r_{hyp} (F), (S_{Soil})$	$4.0 \leq M_w \leq 8.0, r_{hyp} \leq 100 \text{ km}$
Sprudich et al. (1999)	WNA (Empirical)	Compressional	0.250	H, V	PGA, 0.10 – 2.0	$M(M_w), r_{jp} \Gamma (S_{Soil})$	$5.0 \leq M_w \leq 7.7, r_{jp} \leq 100 \text{ km}$
Atkinson and Boore (1995, 1997)	ENA (Stochastic)	Background	0.286	H	PGA, 0.10 – 1.0	$M(M_w), r_{hyp}, (S_{Dep})$	$4.0 \leq M_w \leq 8.2, 10 \leq r_{hyp} \leq 1000 \text{ km}^c$
Campbell (2001, 2003c)	ENA (Hybrid)	Faults	0.250	H	PGA, 0.02 – 4.0	$M_{hyp} r_{hyp}$	$5.0 \leq M_w \leq 8.2, r_{hyp} \leq 1000 \text{ km}$
Frankel et al. (1996)	ENA (Stochastic)	Background	0.286	H	PGA, 0.1 – 2.0	$M(M_w), R(r_{hyp})$	$4.4 \leq M_w \leq 8.2, 10 \leq r_{hyp} \leq 1000 \text{ km}$
Toro et al. (1997)	ENA (Stochastic)	Faults	0.250	H	PGA, 0.03 – 2.0	$M(M_w), r_{jp}$	$4.5 \leq M_w \leq 8.0, 1 \leq r_{jp} \leq 500 \text{ km}$
Somerville et al. (2001)	ENAs (Kinematic)	Background	0.286	H	PGA, 0.04 – 4.0	$M(M_w), r(r_{jp})$	$6.0 \leq M_w \leq 7.5, r_{jp} \leq 500 \text{ km}$
Youngs et al. (1997)	Cascadia S. Z. (Empirical)	Interface	0.5 – 1 ^a	H	PGA, 0.08 – 3.0	$M(M_w), r_{hyp}, H(h_{hyp}), Z_T(z_i), (S_{Soil})$	$5.0 \leq M_w \leq 8.2, 10 \leq r_{hyp} \leq 500 \text{ km}$
Sadigh et al. (1997)	Cascadia S. Z. (Empirical)	Intraslab	0.500	H	PGA, 0.08 – 3.0	$M(M_w), r_{hyp} (F), (S_{Soil})$	$4.0 \leq M_w \leq 8.0, r_{hyp} \leq 100 \text{ km}$
Atkinson and Boore (2003)	Cascadia S. Z. (Empirical)	Intraslab: Global	0.250	H	PGA, 0.04 – 3.0	$M(M_w), D_{fault}(r_{hyp}), h(h_{hyp}), sl(f_3(A_B)), PGA_{rx}, S_C$	$5.5 \leq M_w \leq 8.3, 10 \leq r_{hyp} \leq 300 \text{ km}$
		Intraslab: Cascadia	0.250			S_{DP}, S_E	

^a Weights linearly range between values shown from $r_{hyp} = 55\text{--}85 \text{ km}$ for the $M_w = 8.3$ scenario and from $r_{hyp} = 45\text{--}75 \text{ km}$ for the $M_w = 9.0$ scenario.

^b Parameters in parentheses are alternative notation used in this chapter.

^c Limits increased by D. Boore (personal communication, 2002) for use in the 2002 USGS national seismic hazard maps.

TABLE 5.5 ENA Ground Motion Caps and NEHRP B-C Boundary Adjustment Factors

Period (sec)	Ground Motion Caps (g) ^a		Adjustment Factors
	Median	Upper Tail	
PGA	1.5	3.0	1.52
0.1	3.0	6.0	1.74
0.2	3.0	6.0	1.76
0.3	3.0	6.0	1.72
0.5	3.0	6.0	1.58
1.0	—	—	1.34
2.0	—	—	1.20

^aCaps are applied after applying the adjustment factors.

TABLE 5.6 Faulting Mechanism Categories Used in the WNA and Cascadia Subduction Zone Ground Motion Relations

Ground Motion Relation	Faulting Category ^a	F	F _{RV}	F _{TH}	Rake, λ ^b
Abrahamson and Silva (1997)	<i>Strike slip</i>	0	—	—	0–30°, 150–210°, 330–360°
	<i>Normal</i>	0	—	—	210–330°
	Reverse-oblique	0.5	—	—	30–60°, 120–150°
	<i>Reverse</i>	1.0	—	—	60–120°
	<i>Unknown, random</i>	0.5	—	—	Unknown or random rake
Boore et al. (1997)	<i>Strike slip</i>	c_{1s}	—	—	0–30°, 150–210°, 330–360°
	<i>Normal</i>	c_{1s}	—	—	210–330°
	<i>Reverse</i>	c_{1r}	—	—	30–150°
	<i>Unknown, random</i>	c_{1u}	—	—	Unknown or random rake
Campbell and Bozorgnia (2003)	<i>Strike slip</i>	—	0	0	0–22.5°, 157.5–202.5°, 337.5–360°
	<i>Normal</i>	—	0	0	202.5–337.5°
	Reverse	—	1.0	0	22.5–157.5° ($\delta > 45^\circ$)
	Thrust	—	0	1.0	22.5–157.5° ($\delta \leq 45^\circ$)
	<i>Reverse or Thrust</i>	—	0.5	0.5	Unknown or random dip
	<i>Unknown, random</i>	—	0.25	0.25	Unknown or random rake
Sadigh et al. (1993, 1997) WNA	<i>Strike slip</i>	0	—	—	0–45°, 135–225°, 315–360°
	<i>Normal</i>	0	—	—	225–315°
	<i>Reverse</i>	1.0	—	—	45–135°
	<i>Unknown, random</i>	0.5	—	—	Unknown or random rake
Sadigh et al. (1993, 1997) (Cascadia S. Z. interface)	<i>Strike slip</i>	0	—	—	0–45°, 135–225°, 315–360°
	<i>Normal</i>	0	—	—	225–315°
	<i>Reverse</i>	1.0	—	—	45–135°
	<i>Unknown, random</i>	0.5	—	—	Unknown or random rake
Spudich et al. (1999)	<i>Strike slip</i>	—	—	—	0–45°, 135–225°, 315–360°
	<i>Normal</i>	—	—	—	225–315°

^a Faulting categories used in the 2002 USGS national seismic hazard maps are given in italics.

^b Based on the convention of Lay and Wallace (1995).

Table 5.7 lists the site categories used in each of the ground motion relations. These categories are defined in terms of the values of the specified site parameters, which in turn are approximately related to an average or preferred value of 30-m velocity and a corresponding NEHRP site category. Two sets of NEHRP site categories are given, one originally defined for use in the building codes and one defined by the CGS (Wills et al., 2000), which differ from the former in the specific use of boundary site categories (see Section 5.4.2.5 and Table 5.3). The CGS's NEHRP classification has been extended to include the A and A-B boundary site categories in Table 5.7 for applications outside of California. The site parameters are given in terms of the alternative notation used in the Appendix A published on the accompanying Internet site and in

TABLE 5.7 Site Categories Used in the Ground Motion Relations

Ground Motion Relation	Site Category ^a	Site Parameter						NEHRP Site Class		Adjustment Factors for BC ^c	
		S_{soil}	S_{vrs}	S_{S_R}	S_{FR}	S_{deep}	S_C	S_D	S_E		
Abrahamson and Silva (1997)	Generic rock	0	—	—	—	—	—	—	—	620	C
	Generic soil	1.0	—	—	—	—	—	—	—	310	D
Boore et al. (1997)	30-m velocity	—	—	—	—	—	—	—	—	All	All
Campbell and Bozorgnia (2003)	Firm soil	—	0	0	0	—	—	—	—	298	D
	Very firm soil	—	1.0	0	0	—	—	—	—	368	C
	Soft rock	—	0	1.0	0	—	—	—	—	421	CD
	Firm rock	—	0	0	1.0	—	—	—	—	830	C
	Generic rock	—	0	0.5	0.5	—	—	—	—	620	BC
	Generic soil	—	0.25	0	0	—	—	—	—	310	CGS
Sadigh et al. (1997)	Generic rock	0	—	—	—	—	—	—	—	620	—
	Generic soil	1.0	—	—	—	—	—	—	—	310	—
Spudich et al. (1999)	Generic rock	0	—	—	—	—	—	—	—	310	D
	Generic soil	1.0	—	—	—	—	—	—	—	760	D
Atkinson and Boore (1995, 1997)	Very hard rock	—	—	—	—	0	—	—	—	2800	A
	<i>Firm rock (BC)^d</i>	—	—	—	—	—	—	—	—	760	B
	Deep stiff soil	—	—	—	—	1.0	—	—	—	500	D
	Very hard rock	—	—	—	—	—	—	—	—	2800	A
	<i>Firm rock (BC)</i>	—	—	—	—	—	—	—	—	760	BC
	Very hard rock	—	—	—	—	—	—	—	—	2800	A
	Very hard rock	—	—	—	—	—	—	—	—	2800	A
Campbell (2001, 2003c)	Generic rock	0	—	—	—	—	—	—	—	620	—
Frankel et al. (1996)	Generic soil	1.0	—	—	—	—	—	—	—	310	D
Toro et al. (1997)	Generic rock	0	—	—	—	—	—	—	—	620	C
Somerville et al. (2001)	Generic soil	1.0	—	—	—	—	—	—	—	310	CGS
Youngs et al. (1997)	Generic rock	0	—	—	—	—	—	—	—	620	—
Sadigh et al. (1997)	Generic soil	1.0	—	—	—	—	—	—	—	310	D
Atkinson and Boore (2003)	NEHRP B	—	—	—	—	0	0	—	—	1130	B
	NEHRP BC ^e	—	—	—	—	0.5	0	—	—	760	BC
	NEHRP C	—	—	—	—	1.0	0	—	—	560	C
	NEHRP D	—	—	—	—	0	1.0	—	—	270	D
	NEHRP E	—	—	—	—	0	0	1.0	—	150	E

^a Site categories used in the 2002 USGS national seismic hazard maps to evaluate the ground motion relations for the NEHRP B-C boundary are given in Italics. ^bValue of V_{30} that best represents the given site category in the judgment of the writers. ^cAdditional multiplicative factors used by the USGS to adjust ground motions to the B-C boundary ($V_{30} = 760$ m/sec) in the 2002 USGS national seismic hazard maps: Campbell and Bozorgnia (2003) adjustments are based on the site term of Boore et al. (1997), where the coefficient c_{ϕ} denoted b_v by Boore et al. is the period-dependent regression coefficient given on the accompanying Internet site and in the compilations of Campbell (2003a, 2003b, 2003d); Adjustment factors for very hard rock are from Frankel et al. (1996) and are listed in Table 5.5. ^d Category added by D. Boore (personal communication, 2002) for use in 2002 USGS national seismic hazard maps.

^eRecommended by G. Atkinson (personal communication, 2002) for use in 2002 USGS national seismic hazard maps.

Campbell (2003a, 2003b, 2003d). They can be related to the site parameters originally defined by the authors of the relations using Table 5.4. The relationship between each site category and V_{30} is admittedly crude, but useful, because V_{30} is the only site parameter that corresponds to a physically quantifiable attribute of a profile's site-response characteristics. For those ENA ground motion relations listed in Table 5.7 that predict ground motion on very hard rock ($V_{30} = 2800$ m/sec), the USGS adjusted them to the NEHRP B-C boundary ($V_{30} = 760$ m/sec) using the adjustment factors given in Table 5.5 (Frankel et al. 1996, 2000, 2002).

The specific site categories used by the USGS to evaluate the WNA ground motion relations for the NEHRP B-C Boundary are, in some cases, inconsistent with the estimated values of V_{30} that correspond to these site categories. This apparent bias was introduced either at the suggestion of the authors of the relations or by default (e.g., when there was insufficient evidence to the contrary [Frankel et al. 2002]). At least in one case, the coauthors themselves disagree as to an appropriate value of V_{30} . For example, W. Silva (personal communication, 2002) believes that the average value of V_{30} is around 510 m/sec for sites classified as generic rock in the Abrahamson and Silva (1997) ground motion relation; whereas, N. Abrahamson (personal communication, 2002) believes that this value lies somewhere between 510 and 760 m/sec, the value assumed by the USGS at his suggestion. B. Youngs (personal communication, 2002) believes that the average value of V_{30} for sites classified as generic rock in the Sadigh et al (1993, 1997) ground motion relations is in the upper range that defines NEHRP C, much less than the 760 m/sec value assumed by the USGS at his suggestion. An independent assessment by Choi and Stewart (2003) indicates that the lower V_{30} values originally recommended by W. Silva and B. Youngs appear to be consistent with the generic rock sites used by both the Abrahamson and Silva (1997) and Sadigh et al (1993, 1997) relations. Because of this controversy, unless there is evidence to the contrary, the average value of V_{30} for generic soil and generic rock should be taken as 310 and 620 m/sec, respectively (Table 5.7), consistent with the recommendation of Boore and Joyner (1997). There is a project currently under way by the Pacific Engineering Research Center (PEER) Lifelines Program (<http://peer.berkeley.edu>) that will hopefully resolve the ambiguities noted above. The purpose of that project is to compile a comprehensive strong-motion database and to have several WNA ground-motion experts, including those listed in Table 5.4, develop the next generation of WNA ground motion relations. These new relations will redefine the state-of-the-practice and will no doubt be used in future updates of the USGS hazard maps.

5.4.4.2 Example Relations for WNA, ENA and Cascadia S. Z.

It is not possible to present the equations for all of the ground motion relations used in the 2002 USGS hazard maps discussed in this chapter. Instead, three relations representing the three major tectonic environments in the United States are presented. These are the Campbell and Bozorgnia (2003) relation, representing WNA, the Campbell (2001, 2003c) relation, representing ENA and the Youngs et al. (1997) relation, representing Cascadia S. Z interface and intraslab events. The remaining ground motion relations are given in Appendix A of this chapter on the accompanying Internet site and are discussed extensively in Campbell (2003a, 2003b, 2003d).

The WNA ground motion relation of Campbell and Bozorgnia (2003) is given by the equation

$$\ln Y = c_1 + f_1(M_W) + f_2(M_W, r_{seis}, S) + f_3(F) + f_4(S) + f_5(HW, M_W, r_{seis}) \quad (5.31)$$

where magnitude scaling is given by the function

$$f_1(M_W) = c_2 M_W + c_3 (8.5 - M_W)^2, \quad (5.32)$$

distance scaling and near-source (nonlinear) site response is given by the functions

$$f_2(M_W, r_{seis}, S) = c_4 \ln R, \quad (5.33)$$

$$R = \sqrt{r_{seis}^2 + g(S)^2 \left(\exp[c_5 M_W + c_6 (8.5 - M_W)^2] \right)^2}, \quad (5.34)$$

$$g(S) = c_7 + c_8 (S_{VFS} + S_{SR}) + c_9 S_{FR}, \quad (5.35)$$

the effects of faulting mechanism are given by the function

$$f_3(F) = c_{10} F_{RV} + c_{11} F_{TH}, \quad (5.36)$$

far-source (linear) site response is given by the function

$$f_4(S) = c_{12} S_{VFS} + c_{13} S_{SR} + c_{14} S_{FR}, \quad (5.37)$$

and hanging-wall effects are given by the functions

$$f_5(HW, M_W, r_{seis}) = HW f_3(F) f_{HW}(M_W) f_{HW}(r_{seis}), \quad (5.38)$$

$$HW = \begin{cases} 0 & r_{jb} \geq 5 \text{ km or } \delta > 70^\circ \\ (S_{VFS} + S_{SR} + S_{FR})(5 - r_{jb})/5 & r_{jb} < 5 \text{ km and } \delta \leq 70^\circ \end{cases} \quad (5.39)$$

$$f_{HW}(M_W) = \begin{cases} 0 & M_W < 5.5 \\ M_W - 5.5 & 5.5 \leq M_W \leq 6.5, \\ 1 & M_W > 6.5 \end{cases} \quad (5.40)$$

$$f_{HW}(r_{seis}) = \begin{cases} c_{15} (r_{seis}/8) & r_{seis} < 8 \text{ km} \\ c_{15} & r_{seis} \geq 8 \text{ km} \end{cases}. \quad (5.41)$$

In these equations, Y is either the average horizontal or vertical component of PGA or 5%-damped $S_a(g)$, M_W is moment magnitude, r_{seis} is the closest distance to the seismogenic part of the rupture plane (km) and r_{jb} is the closest distance to the surface projection of the rupture plane (km). The faulting mechanism parameters, F_{RV} and F_{TH} , are defined in Table 5.6 and the site parameters, S_{VFS} , S_{SR} and S_{FR} , are defined in Table 5.7. The hanging-wall parameter, HW , which quantifies the geometric and associated effects related to the hanging wall, evaluates to zero for firm soil site conditions, for $r_{jb} \geq 5$ km, or for a fault dipping greater than 70° . A more detailed definition of these parameters can be found in Section 5.4.2.

The standard deviation of $\ln Y$ is defined as a function of magnitude according to the expression

$$\sigma_{\ln Y} = \begin{cases} c_{16} - 0.07 M_W & M_W < 7.4 \\ c_{16} - 0.518 & M_W \geq 7.4 \end{cases}, \quad (5.42)$$

or as a function of PGA according to the expression

$$\sigma_{\ln Y} = \begin{cases} c_{17} + 0.351 & \text{PGA} \leq 0.07g \\ c_{17} - 0.132 \ln \text{PGA} & 0.07g < \text{PGA} < 0.25g \\ c_{17} + 0.183 & \text{PGA} \geq 0.25g \end{cases} . \quad (5.43)$$

The magnitude-dependent version of the standard deviation was used in the development of the 2002 USGS hazard maps. The authors of the relation, however, prefer the PGA-dependent version. The regression coefficients of this ground motion relation are listed in Table 5.8. The relation is considered to be valid for $4.7 \leq M_W \leq 8.0$ and $r_{seis} \leq 100$ km. Guidance on setting the faulting mechanism and site parameters is given in Tables 5.6 and 5.7. Figure 5.26 compares the spectral accelerations predicted by this relation with those predicted by the other WNA relations listed in Table 5.4.

The ENA ground motion relation of Campbell (2001, 2003c) is given by the equation

$$\ln Y = c_1 + f_1(M_W) + f_2(M_W, r_{rup}) + f_3(r_{rup}) \quad (5.44)$$

where magnitude scaling is given by the function

$$f_1(M_W) = c_2 M_W + c_3 (8.5 - M_W)^2 , \quad (5.45)$$

and distance scaling is given by the functions

$$f_2(M_W, r_{rup}) = c_4 \ln R + (c_5 + c_6 M_W) r_{rup} , \quad (5.46)$$

$$R = \sqrt{r_{rup}^2 + [c_7 \exp(c_8 M_W)]^2} , \quad (5.47)$$

$$f_3(r_{rup}) = \begin{cases} 0 & r_{rup} \leq 70 \text{ km} \\ c_9 (\ln r_{rup} - \ln 70) & 70 < r_{rup} \leq 130 \text{ km} \\ c_9 (\ln r_{rup} - \ln 70) + c_{10} (\ln r_{rup} - \ln 130) & r_{rup} > 130 \text{ km} \end{cases} . \quad (5.48)$$

The standard deviation of $\ln Y$ is defined as a function of magnitude according to the expression

$$\sigma_{\ln Y} = \begin{cases} c_{11} + c_{12} M_W & M_W < 7.16 \\ c_{13} & M_W \geq 7.16 \end{cases} . \quad (5.49)$$

In these equations, Y is the average horizontal component of PGA or 5%-damped S_a (g), r_{rup} is the closest distance to the rupture plane (km), and all of the other parameters are as defined previously. The regression coefficients of this relation are listed in Table 5.9. The relation is considered to be valid for $5.0 \leq M_W \leq 8.2$ and $0 \leq r_{rup} \leq 1000$ km, but the WNA empirical database on which it is based is restricted to earthquakes up to about magnitude 7.5 and distances up to about 100 km. The relation can be realistically extrapolated to larger magnitudes and distances because of its physically based functional form and its seismologically constrained geometric and anelastic attenuation. The relation predicts ground motion for very hard rock typical of glacially scoured cratonic shield areas of ENA (Table 5.7). Figure 5.27 compares the spectral accelerations predicted by this relation with those predicted by the other ENA relations listed in Table 5.4.

The subduction-zone ground motion relation of Youngs et al. (1997) is given by the equation

TABLE 5.8 Coefficients for the WNA Ground Motion Relation

T (s)	c_1	c_2	c_3	c_4	c_5	c_6	c_7	c_8	c_9	Average Horizontal Component	c_{10}	c_{11}	c_{12}	c_{13}	c_{14}	c_{15}	c_{16}	c_{17}
PGA																		
0.05	-4.033	0.812	0.036	-1.061	0.766	0.034	0.941	-0.005	-0.018	0.343	0.351	-0.123	-0.138	-0.289	0.370	0.920	0.219	
0.075	-3.740	0.812	0.036	-1.121	0.724	0.032	0.958	-0.004	-0.028	0.302	0.362	-0.140	-0.158	-0.205	0.370	0.940	0.239	
0.10	-3.076	0.812	0.050	-1.252	0.648	0.040	0.121	-0.005	-0.051	0.243	0.333	-0.150	-0.196	-0.208	0.370	0.952	0.251	
0.15	-2.661	0.812	0.060	-1.308	0.621	0.046	0.166	-0.009	-0.068	0.224	0.313	-0.146	-0.253	-0.258	0.370	0.958	0.257	
0.20	-2.270	0.812	0.041	-1.324	0.613	0.031	0.212	-0.033	-0.081	0.318	0.344	-0.176	-0.267	-0.284	0.370	0.974	0.273	
0.30	-2.999	0.812	0.030	-1.153	0.704	0.026	0.098	-0.014	-0.038	0.296	0.342	-0.148	-0.183	-0.359	0.370	0.981	0.280	
0.40	-3.511	0.812	0.007	-1.080	0.752	0.007	0.059	-0.007	-0.022	0.359	0.385	-0.162	-0.157	-0.585	0.370	0.984	0.283	
0.50	-3.556	0.812	-0.035	-0.964	0.842	-0.036	0.023	-0.002	-0.004	0.406	0.479	-0.122	-0.130	-0.701	0.370	0.990	0.289	
0.75	-3.709	0.812	-0.071	-0.964	0.842	-0.074	0.021	-0.002	-0.002	0.347	0.419	-0.108	-0.124	-0.796	0.331	1.021	0.320	
1.0	-3.867	0.812	-0.101	-0.964	0.842	-0.105	0.019	0	0	0.329	0.338	-0.073	-0.072	-0.858	0.281	1.021	0.320	
1.5	-4.093	0.812	-0.150	-0.964	0.842	-0.155	0.019	0	0	0.217	0.188	-0.079	-0.056	-0.954	0.210	1.021	0.320	
2.0	-4.311	0.812	-0.180	-0.964	0.842	-0.187	0.019	0	0	0.060	0.064	-0.124	-0.116	-0.916	0.160	1.021	0.320	
3.0	-4.817	0.812	-0.193	-0.964	0.842	-0.200	0.019	0	0	-0.079	0.021	-0.154	-0.117	-0.873	0.089	1.021	0.320	
4.0	-5.211	0.812	-0.202	-0.964	0.842	-0.209	0.019	0	0	-0.061	0.057	-0.054	-0.261	-0.889	0.039	1.021	0.320	
Vertical Component																		
0.05	-3.108	0.756	0	-1.287	0.587	0	0.142	0.046	-0.040	0.253	0.173	-0.135	-0.138	-0.256	0.630	0.975	0.274	
0.075	-1.918	0.756	0	-1.517	0.498	0	0.309	0.069	-0.023	0.058	0.100	-0.195	-0.274	-0.219	0.630	1.031	0.330	
0.10	-1.504	0.756	0	-1.551	0.487	0	0.343	0.083	0.000	0.135	0.182	-0.224	-0.303	-0.263	0.630	1.031	0.330	
0.15	-1.672	0.756	0	-1.473	0.513	0	0.282	0.062	0.001	0.168	0.210	-0.198	-0.275	-0.252	0.630	1.031	0.330	
0.20	-2.323	0.756	0	-1.280	0.591	0	0.171	0.045	0.008	0.223	0.238	-0.170	-0.175	-0.270	0.630	1.031	0.330	
0.30	-2.998	0.756	0	-1.131	0.668	0	0.089	0.028	0.004	0.234	0.256	-0.098	-0.041	-0.311	0.571	1.031	0.330	
0.40	-4.536	0.756	-0.015	-0.736	0.007	-0.128	0.736	0.050	0.010	0.004	0.249	0.328	-0.026	0.082	-0.265	0.488	1.031	0.330
0.50	-4.651	0.756	-0.035	-0.812	0.931	-0.043	0.012	0	0	0.299	0.317	-0.017	0.022	-0.257	0.428	1.031	0.330	
0.75	-4.903	0.756	-0.071	-0.812	0.931	-0.087	0.012	0	0	0.243	0.354	-0.020	0.092	-0.293	0.383	1.031	0.330	
1.0	-4.950	0.756	-0.101	-0.812	0.931	-0.124	0.012	0	0	0.295	0.418	0.078	0.091	-0.349	0.299	1.031	0.330	
1.5	-5.073	0.756	-0.150	-0.812	0.931	-0.184	0.012	0	0	0.266	0.315	0.043	0.101	-0.481	0.240	1.031	0.330	
2.0	-5.292	0.756	-0.180	-0.812	0.931	-0.222	0.012	0	0	0.114	0.115	0.033	-0.022	-0.503	0.240	1.031	0.330	
3.0	-5.748	0.756	-0.193	-0.812	0.931	-0.238	0.012	0	0	0.179	0.159	-0.010	-0.047	-0.539	0.240	1.031	0.330	
4.0	-6.042	0.756	-0.202	-0.812	0.931	-0.248	0.012	0	0	0.237	0.134	-0.059	-0.267	-0.606	0.240	1.031	0.330	

Source: Adapted from Campbell, K.W. and Bozorgnia, Y. (2003). Updated near-source ground motion (attenuation) relations for the horizontal and vertical components of PGA and acceleration response spectra. *Bulletin of the Seismological Society of America*, 93, 314–331.

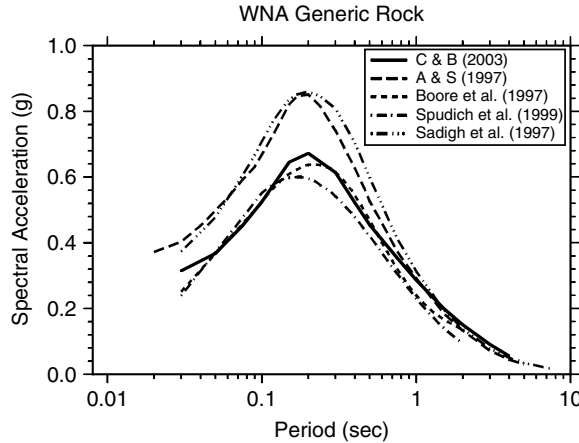


FIGURE 5.26 Comparison of 5%-damped pseudo-acceleration (S_d) response spectra predicted by the WNA ground motion relations listed in Table 5.4. The relations are evaluated for $M_W = 7$, $r_{jb} = r_{rup} = 10$ km, $r_{seis} = 10.4$ km ($d_s = 3$ km), strike-slip faulting, and generic rock site conditions (see Tables 5.6 and 5.7). PGA is plotted at 0.03-sec period. A & S (1997) refers to Abrahamson and Silva (1997) and C & B (2003) refers to Campbell and Bozorgnia (2003).

TABLE 5.9 Coefficients for the ENA Ground Motion Relation

T (s)	c_1	c_2	c_3	c_4	c_5	c_6	c_7	c_8	c_9	c_{10}	c_{11}	c_{12}	c_{13}
0.01	0.0305	0.633	-0.0427	-1.591	-0.00428	0.000483	0.683	0.416	1.140	-0.873	1.030	-0.0860	0.414
0.02	1.3535	0.630	-0.0404	-1.787	-0.00388	0.000497	1.020	0.363	0.851	-0.715	1.030	-0.0860	0.414
0.03	1.1860	0.622	-0.0362	-1.691	-0.00367	0.000501	0.922	0.376	0.759	-0.922	1.030	-0.0860	0.414
0.05	0.3736	0.616	-0.0353	-1.469	-0.00378	0.000500	0.630	0.423	0.771	-1.239	1.042	-0.0838	0.443
0.075	-0.0395	0.615	-0.0353	-1.383	-0.00421	0.000486	0.491	0.463	0.955	-1.349	1.052	-0.0838	0.453
0.10	-0.1475	0.613	-0.0353	-1.369	-0.00454	0.000460	0.484	0.467	1.096	-1.284	1.059	-0.0838	0.460
0.15	-0.1901	0.616	-0.0478	-1.368	-0.00473	0.000393	0.461	0.478	1.239	-1.079	1.068	-0.0838	0.469
0.20	-0.4328	0.617	-0.0586	-1.320	-0.00460	0.000337	0.399	0.493	1.250	-0.928	1.077	-0.0838	0.478
0.30	-0.6906	0.609	-0.0786	-1.280	-0.00414	0.000263	0.349	0.502	1.241	-0.753	1.081	-0.0838	0.482
0.50	-0.5907	0.534	-0.1379	-1.216	-0.00341	0.000194	0.318	0.503	1.166	-0.606	1.098	-0.0824	0.508
0.75	-0.5429	0.480	-0.1806	-1.184	-0.00288	0.000160	0.304	0.504	1.110	-0.526	1.105	-0.0806	0.528
1.0	-0.6104	0.451	-0.2090	-1.158	-0.00255	0.000141	0.299	0.503	1.067	-0.482	1.110	-0.0793	0.543
1.5	-0.9666	0.441	-0.2405	-1.135	-0.00213	0.000119	0.304	0.500	1.029	-0.438	1.099	-0.0771	0.547
2.0	-1.4306	0.459	-0.2552	-1.124	-0.00187	0.000103	0.310	0.499	1.015	-0.417	1.093	-0.0758	0.551
3.0	-2.2331	0.492	-0.2646	-1.121	-0.00154	0.000084	0.310	0.499	1.014	-0.393	1.090	-0.0737	0.562
4.0	-2.7975	0.507	-0.2738	-1.119	-0.00135	0.000074	0.294	0.506	1.018	-0.386	1.092	-0.0722	0.575

Source: Adapted from Campbell, K.W. (2001). Development of semi-empirical attenuation relationships for CEUS. U.S. Geological Survey, Award 01HQGR0011, final report; and from Campbell, K.W. (2003). Prediction of strong ground motion using the hybrid empirical method and its use in the development of ground motion (attenuation) relations in eastern North America. *Bulletin of the Seismological Society of America*, 93, 1012–1033.

$$\ln Y = c_1 + f_1(M_W) + f_2(M_W, r_{rup}, h_{hypo}) + f_3(z_T) \quad (5.50)$$

where magnitude scaling is given by the function

$$f_1(M_W) = c_2 M_W + c_3 (10 - M_W)^3, \quad (5.51)$$

distance and depth scaling are given by the functions

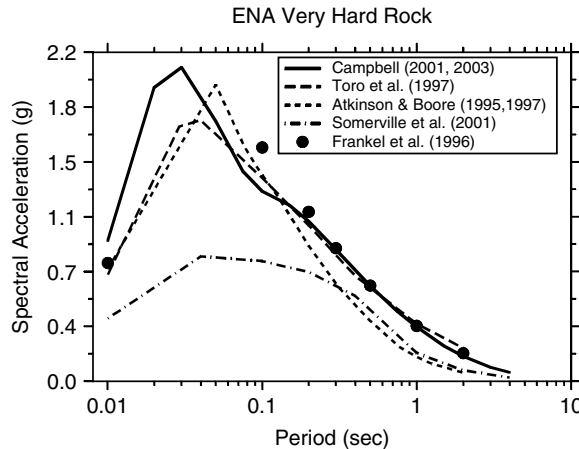


FIGURE 5.27 Comparison of 5%-damped pseudo-acceleration (S_a) response spectra predicted by the ENA ground motion relations listed in Table 5.4. The relations are evaluated for $M_W = 7$, $r_{jb} = r_{rup} = 10$ km, $r_{hypo} = 14.1$ km ($h_{hypo} = 10$ km), and very hard rock site conditions (see Tables 5.6 and 5.7). PGA is plotted at 0.01 sec period. The values of PGA and spectral acceleration predicted by the Frankel et al. (1996) relation are divided by the factors given in Table 5.5 to adjust them from firm rock to very hard rock site conditions. The Frankel et al. relation is plotted as single spectral ordinates to emphasize the lack of spectral ordinates below 0.1 sec.

$$f_2(M_W, r_{rup}, h_{hypo}) = c_4 \ln R + c_5 h_{hypo}, \quad (5.52)$$

$$R = r_{rup} + c_6 \exp(c_7 M_W), \quad (5.53)$$

and the type of event (interface or intraslab) is given by the function

$$f_3(z_T) = c_8 z_T. \quad (5.54)$$

The standard deviation is given as a function of magnitude according to the expression

$$\sigma_{\ln Y} = \begin{cases} c_9 + c_{10} M_W & M_W \leq 8.0 \\ c_{11} & M_W > 8.0 \end{cases}. \quad (5.55)$$

In these equations, Y is the average horizontal component of PGA or 5%-damped S_a (g), h_{hypo} is focal depth (km), $z_T = 0$ for subduction interface events and 1 for subduction intraslab (intermediate-depth or Wadati-Benioff) events, and all of the other parameters are as defined previously. The regression coefficients of this relation are listed in Table 5.10. The authors of the relation do not explicitly state the range of magnitudes and distances for which they considered the relation to be valid, but the database is constrained to $5.0 \leq M_W \leq 8.2$ and $10 \leq r_{rup} \leq 500$ km. Nonetheless, the relation is used to evaluate ground motions for a $M_W = 9.0$ earthquake on the Cascadia S. Z. in the 2002 USGS hazard maps. Figure 5.28 compares the spectral accelerations predicted by this relation with those predicted by the other subduction-zone relations listed in Table 5.4.

5.4.5 Effects of Near-Fault Directivity

5.4.5.1 Introduction

Under certain conditions, ground motions recorded at stations located near faults can exhibit two special characteristics: (a) fault rupture directivity or directivity pulse; and (b) a fling step (see Chapter 2). The fault rupture directivity can be either forward or backward. Forward rupture directivity occurs when the

TABLE 5.10 Coefficients for the Subduction-Zone Ground Motion Relation

$T(s)$	c_1	c_2	c_3	c_4	c_5	c_6	c_7	c_8	c_9	c_{10}	c_{11}
Generic rock											
PGA	0.2418	1.414	0	-2.552	0.00617	1.7818	0.554	0.3846	1.45	-0.1	0.650
0.075	1.5168	1.414	0	-2.707	0.00617	1.7818	0.554	0.3846	1.45	-0.1	0.650
0.1	1.4298	1.414	-0.0011	-2.655	0.00617	1.7818	0.554	0.3846	1.45	-0.1	0.650
0.2	0.9638	1.414	-0.0027	-2.528	0.00617	1.7818	0.554	0.3846	1.45	-0.1	0.650
0.3	0.4878	1.414	-0.0036	-2.454	0.00617	1.7818	0.554	0.3846	1.45	-0.1	0.650
0.4	0.1268	1.414	-0.0043	-2.401	0.00617	1.7818	0.554	0.3846	1.45	-0.1	0.650
0.5	-0.1582	1.414	-0.0048	-2.360	0.00617	1.7818	0.554	0.3846	1.45	-0.1	0.650
0.75	-0.9072	1.414	-0.0057	-2.286	0.00617	1.7818	0.554	0.3846	1.45	-0.1	0.650
1.0	-1.4942	1.414	-0.0064	-2.234	0.00617	1.7818	0.554	0.3846	1.45	-0.1	0.650
1.5	-2.3922	1.414	-0.0073	-2.160	0.00617	1.7818	0.554	0.3846	1.50	-0.1	0.700
2.0	-3.0862	1.414	-0.0080	-2.107	0.00617	1.7818	0.554	0.3846	1.55	-0.1	0.750
3.0	-4.2692	1.414	-0.0089	-2.033	0.00617	1.7818	0.554	0.3846	1.65	-0.1	0.850
Generic soil											
PGA	-0.6687	1.438	0	-2.329	0.00648	1.097	0.617	0.3648	1.45	-0.1	0.650
0.075	1.7313	1.438	-0.0019	-2.697	0.00648	1.097	0.617	0.3648	1.45	-0.1	0.650
0.1	1.8473	1.438	-0.0019	-2.697	0.00648	1.097	0.617	0.3648	1.45	-0.1	0.650
0.2	0.8803	1.438	-0.0019	-2.464	0.00648	1.097	0.617	0.3648	1.45	-0.1	0.650
0.3	0.1243	1.438	-0.0020	-2.327	0.00648	1.097	0.617	0.3648	1.45	-0.1	0.650
0.4	-0.5247	1.438	-0.0020	-2.230	0.00648	1.097	0.617	0.3648	1.45	-0.1	0.650
0.5	-1.1067	1.438	-0.0035	-2.140	0.00648	1.097	0.617	0.3648	1.45	-0.1	0.650
0.75	-2.3727	1.438	-0.0048	-1.952	0.00648	1.097	0.617	0.3648	1.45	-0.1	0.650
1.0	-3.5387	1.438	-0.0066	-1.785	0.00648	1.097	0.617	0.3648	1.45	-0.1	0.650
1.5	-5.7697	1.438	-0.0114	-1.470	0.00648	1.097	0.617	0.3648	1.50	-0.1	0.700
2.0	-7.1017	1.438	-0.0164	-1.290	0.00648	1.097	0.617	0.3648	1.55	-0.1	0.750
3.0	-7.3407	1.438	-0.0221	-1.347	0.00648	1.097	0.617	0.3648	1.65	-0.1	0.850
4.0	-8.2867	1.438	-0.0235	-1.272	0.00648	1.097	0.617	0.3648	1.65	-0.1	0.850

Source: Adapted from Youngs, R.R., Chiou, S.J., Silva, W.J. and Humphrey, J.R. (1997). Strong ground motion attenuation relationships for subduction zone earthquakes. *Seismological Research Letters*, 68, 58–73.

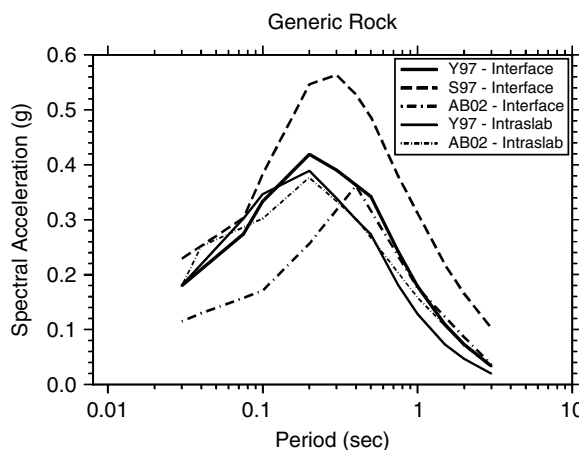


FIGURE 5.28 Comparison of 5%-damped pseudo-acceleration (S_a) response spectra predicted by the *subduction-zone ground motion relations* listed in Table 5.4. The relations are evaluated for $M_W = 8.5$, $r_{rup} = 50$ km, and $h_{hypo} = 15$ km for interface events ($z_T = 0$) and $M_W = 7$, $r_{rup} = 50$ km, and $h_{hypo} = 50$ km for intralab events ($z_T = 1$) for generic rock site conditions (see Tables 5.6 and 5.7). PGA is plotted at 0.03 sec period. Y97 refers to Youngs et al. (1997), S97 refers to Sadigh et al. (1997), evaluated for a reverse faulting mechanism, and AB02 refers to Atkinson and Boore (2003).

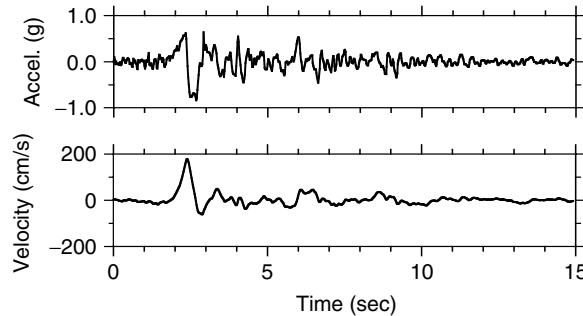


FIGURE 5.29 Recorded ground acceleration, and the computed velocity, from the 1994 Northridge, California, earthquake, Rinaldi Receiving Station (S48W component).

rupture front propagates toward the site and the direction of slip on the fault is aligned with the site (Somerville et al. 1997). Backward directivity occurs when rupture propagates away from the site. Forward directivity will cause a large long-period pulse on the strike-normal component of ground motion. The fling step occurs on the ground displacement component parallel to the fault slip direction and is associated with a permanent displacement of the ground (see Chapter 2).

Near-fault directivity pulses have been observed in numerous earthquakes, most notably the 1971 San Fernando, 1978 Tabas, 1992 Landers, 1994 Northridge, 1995 Kobe, 1999 Kocaeli and 1999 Chi-Chi events. The structural damage potential of such near-fault long-period pulses was first revealed by Bertero et al. (1978) and subsequently confirmed by recorded motions in other earthquakes (e.g., Anderson and Bertero, 1987; Hall et al. 1995; Bozorgnia and Mahin, 1998; Alavi and Krawinkler, 2001). Figure 5.29 shows an example of a strong near-fault pulse recorded in the 1994 Northridge earthquake at Rinaldi Receiving Station (CIT-SMART, 1996). It is evident from this figure that the pulse is associated with a very large ground velocity.

A seismological overview of source directivity and radiation pattern is given in Section 5.4.5.2 (see Chapter 2 for more details). In subsequent sections, the proposed modification of ground motion relations to include fault rupture directivity effects is presented and a brief discussion about engineering implications of near-fault records is provided.

5.4.5.2 Seismological Overview of Source Directivity and Radiation Pattern

Radiation pattern is the geographic asymmetry of the ground motion caused by the fault-rupture process. It is closely related to faulting mechanism. The radiation pattern can be perturbed by source directivity, which causes an increase or decrease in the ground motion as a result of the propagation of the rupture, analogous to the Doppler effect in sound. Ground-motion amplitudes in the forward direction of rupture propagation are increased while those in the backward direction are decreased as a result of source directivity. This effect is particularly important during unilateral faulting. The general concept of radiation pattern and source directivity is shown schematically in Figure 5.30. Source directivity has its largest positive effect on the long-period horizontal ground-motion component that is oriented perpendicular or normal to the rupture plane (the fault-normal or strike-normal component). A schematic showing the radiation pattern for a vertical strike-slip fault and its effect on the fault-normal and fault-parallel components of near-fault ground displacement is shown in Figure 5.31.

Source directivity is a well-known seismological property (Lay and Wallace, 1995) and has been observed or proposed as a factor in controlling the azimuthal dependence of strong ground motion during several past earthquakes (see discussions by Campbell, 2003a, 2003b, 2003d).

5.4.5.3 Modification of Ground Motion Relations for Source Directivity

Source directivity was not used directly in the development of the ground motion relations presented in Section 5.4.4. However, Somerville et al. (1997) and Abrahamson (2000) have developed a simple empir-

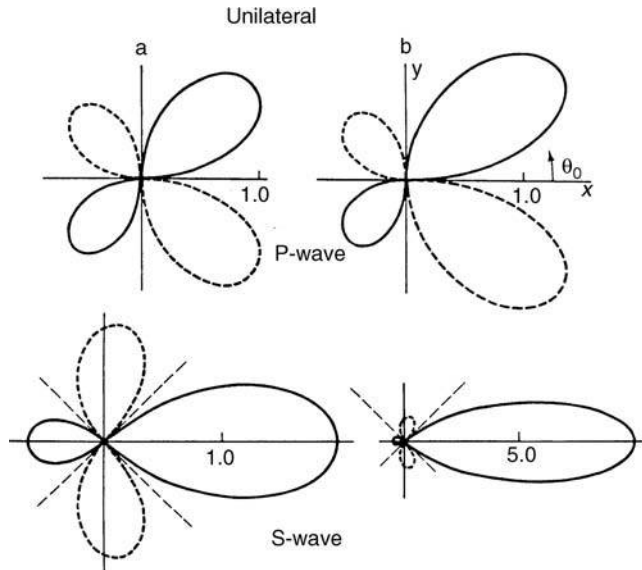


FIGURE 5.30 Radiation pattern showing the variability of compressional and horizontal shear-wave amplitude for a fault rupture propagating from left to right. The diagrams on the left are for a rupture propagation velocity of 0.5 times the shear-wave velocity of the crust and those on the right are for a rupture propagation velocity of 0.9 times the shear-wave velocity of the crust. The amplitude of the lobes represents the relative amplitude of ground motion. The larger lobes are an indication of rupture directivity. Rupture directivity increases with increasing rupture velocity (From Lay, T. and Wallace, T.C. (1995). *Modern Global Seismology*. Academic Press, San Diego. With permission.)

ically based engineering model that can be used to estimate the effects of source directivity and radiation pattern on the prediction of the fault-normal and fault-parallel components of spectral acceleration. Somerville et al. (1997) also provide a list of near-source time histories that contain significant directivity and other near-source effects that can be used in engineering practice.

It should be noted that Somerville (2000) suggests that the simple empirical models proposed by Somerville et al. (1997) and Abrahamson (2000) might be too simplistic. He has found that the near-fault directivity effects observed in recent earthquakes, including the 1999 Chi-Chi and 1999 Kocaeli events, appear to manifest themselves as narrow-band pulses, whose period increases with increasing magnitude. This increase in period with magnitude can actually lead to lower values of spectral acceleration at mid periods ($T \approx 1$ sec) for events of $M_W > 7\frac{1}{4}$. This observation is inconsistent with the assumption of monotonically increasing spectral amplitudes with magnitude that is the basis for the simple engineering model. However, the directivity pulse model needs more development before it can be used in engineering practice. Until then, the simple engineering model of Somerville et al. (1997) and Abrahamson (2000) presented below can be used to estimate rupture directivity effects.

Somerville et al. (1997) found that rupture directivity effects cause spatial variations in the radiation pattern, as well as differences between the fault-normal and fault-parallel components of horizontal ground motion. These effects are significant at periods of 0.6 sec and greater and generally increase in size with increasing period. Abrahamson (2000) found that there were several aspects of the spatial component of the Somerville et al. (1997) rupture directivity model that needed to be modified to make it more generally applicable for engineering practice, such as in probabilistic seismic hazard analysis (PSHA).

The proposed model for incorporating source directivity effects is given by

$$\ln Y_{Dir} = \ln Y + f_1(DR, \xi)T(r_{rup})T(M_W) + f_2(r_{rup}, M_W, \xi) \quad (5.56)$$

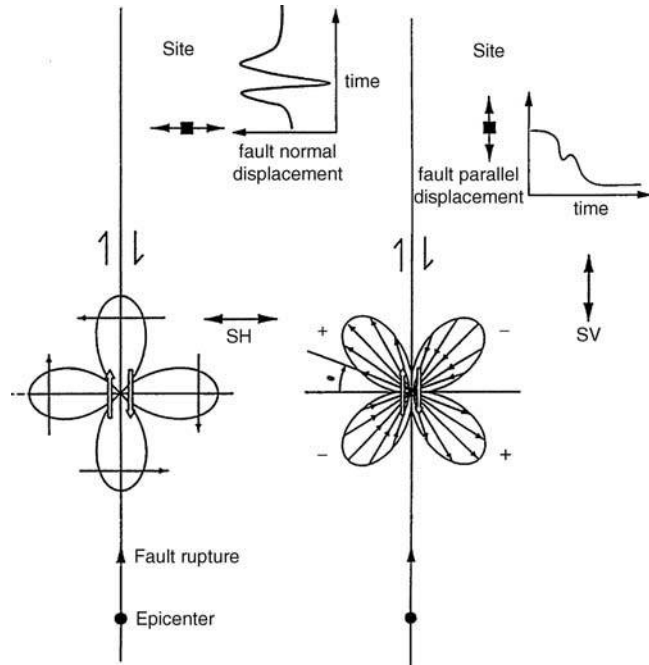


FIGURE 5.31 Radiation pattern for a vertical strike-slip fault showing its effect on the fault-normal and fault-parallel components of near-fault ground displacement. (From Somerville, P.G., Smith, N.F., Graves, R.W. and Abrahamson, N.A. (1997). Modification of empirical strong ground motion attenuation relations to include the amplitude and duration effects of rupture directivity. *Seismological Research Letters*, 68, 199–222.)

where Y is the average horizontal component of PGA or spectral acceleration with average directivity effects and Y_{Dir} is the value of Y with these effects explicitly taken into account, and where, for strike-slip faulting,

$$f_1(DR, \xi) = \begin{cases} c_1 + 1.88c_2(s/L)\cos(\theta) & \text{for } s/L \leq 0.4 \\ c_1 + 0.75c_2\cos(\theta) & \text{for } s/L > 0.4 \end{cases} \quad (5.57)$$

For dip-slip faulting,

$$f_1(DR, \xi) = c_1 + c_2(d/W)\cos\phi \quad (5.58)$$

and where

$$f_2(r_{rup}, M_W, \xi) = \begin{cases} \frac{1}{2}(\cos 2\xi)[c_3 + c_4 \ln(r_{rup} + 1) + c_5(M_W - 6)] & \text{for fault-normal} \\ -\frac{1}{2}(\cos 2\xi)[c_3 + c_4 \ln(r_{rup} + 1) + c_5(M_W - 6)] & \text{for fault-parallel} \\ 0 & \text{for } \xi \geq 45^\circ \end{cases} \quad (5.59)$$

$$T(r_{rup}) = \begin{cases} 1 & \text{for } r_{rup} \leq 30 \text{ km} \\ 1 - (r_{rup} - 30)/30 & \text{for } 30 < r_{rup} < 60 \text{ km} \\ 0 & \text{for } r_{rup} \geq 60 \text{ km} \end{cases} \quad (5.60)$$

$$T(M_W) = \begin{cases} 1 & \text{for } M_W \geq 6.5 \\ 1 - (6.5 - M_W)/0.5 & \text{for } 6.0 < M_W < 6.5 \\ 0 & \text{for } M_W \leq 6.0 \end{cases} \quad (5.61)$$

The standard deviation of the predicted strong-motion parameter when directivity effects are taken into account is calculated from the expression.

$$\sigma_{\ln Y, Dir} = \sigma_{\ln Y} - 0.05 c_2 / 1.333 \quad (5.62)$$

where $\sigma_{\ln Y, Dir}$ is the standard deviation of $\ln Y_{Dir}$ and $\sigma_{\ln Y}$ is the standard deviation of $\ln Y$.

In these equations, r_{rup} is the closest distance to the fault rupture plane (km); the length and width ratios, $DR = s/L$ and d/W , are defined as the fraction of fault rupture length, L , and fault rupture width, W , that ruptures toward the site for strike-slip faults and dip-slip faults, respectively, and $\xi = \theta$ and ϕ are the azimuth and zenith angles between the fault rupture plane and the ray path to the site for strike-slip and dip-slip faults, respectively. These parameters are defined schematically in Figure 5.32.

The regression coefficients for the Somerville et al. (1997) and Abrahamson (2000) rupture directivity model are listed in Table 5.11. Note that in this table the values of c_1 and c_2 depend on the faulting

TABLE 5.11 Coefficients for the Source Directivity Model

$T(s)$	Strike Slip		Dip Slip		c_3	c_4	c_5
	c_1	c_2	c_1	c_2			
0.6	0	0	0	0	0.027	-0.0069	0
0.7	—	—	—	—	0.050	-0.0127	0
0.75	-0.084	0.185	-0.045	0.008	0.061	-0.0155	0
0.8	—	—	—	—	0.070	-0.0178	0
0.9	—	—	—	—	0.088	-0.0220	0
1.0	-0.192	0.423	-0.104	0.178	0.104	-0.0255	0
1.5	-0.344	0.759	-0.186	0.318	0.164	-0.0490	0.034
2.0	-0.452	0.998	-0.245	0.418	0.207	-0.0613	0.059
2.5	—	—	—	—	0.280	-0.0816	0.078
3.0	-0.605	1.333	-0.327	0.559	0.353	-0.1007	0.093
3.5	—	—	—	—	0.415	-0.1172	0.106
4.0	-0.713	1.571	-0.386	0.659	0.456	-0.1282	0.118
4.5	—	—	—	—	0.462	-0.1307	0.128
5.0	-0.797	1.757	-0.431	0.737	0.450	-0.1269	0.137
6.0	—	—	—	—	0.424	-0.1223	0.152

Source: Adapted from Somerville, P.G., Smith, N.F., Graves, R.W. and Abrahamson, N.A. (1997). Modification of empirical strong ground motion attenuation relations to include the amplitude and duration effects of rupture directivity. *Seismological Research Letters*, 68, 199–222; and from Abrahamson, N.A. (2000). Effects of rupture directivity on probabilistic seismic hazard analysis. *Proceedings, 6th International Conference on Seismic Zonation*, Palm Springs, California, 6 p.

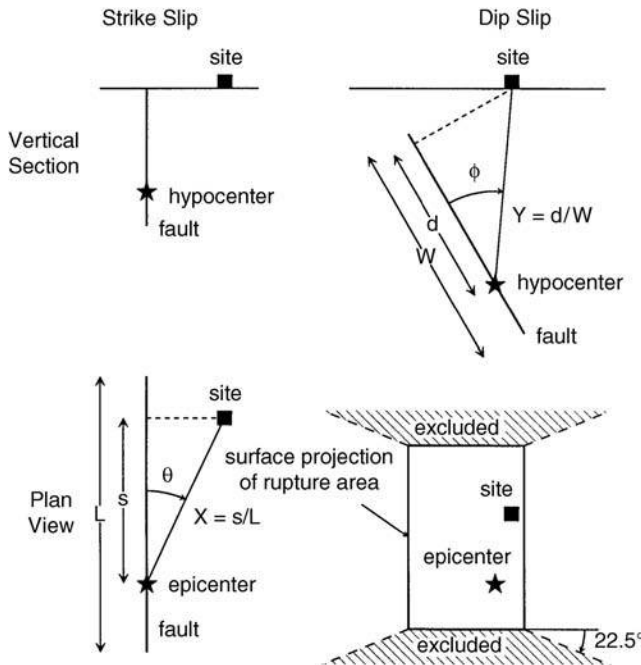


FIGURE 5.32 Definition of fault-rupture directivity parameters used in the engineering model of source directivity effects. (From Somerville, P.G., Smith, N.F., Graves, R.W., and Abrahamson, N.A. (1997). Modification of empirical strong ground motion attenuation relations to include the amplitude and duration effects of rupture directivity. *Seismological Research Letters*, 68, 199–222.)

mechanism, where dip slip is a generic term for reverse, thrust and normal faulting. According to this model, maximum spatial directivity effects for strike-slip faulting occur when $(s/L)\cos\theta=0.4$, $M_w \geq 6.5$, and $r_{rup} \leq 30$ km and can result in an increase of up to 68% in the average horizontal component of 5-sec spectral acceleration. Minimum spatial directivity effects occur at this same period when $r_{rup} \leq 30$, $M_w \leq 6$, or $r_{rup} \geq 60$ km and can result in a 55% reduction in spectral acceleration. Maximum and minimum spatial directivity effects are smaller for dip-slip faulting for the same magnitudes, distances, and period, or about +36% when $(d/W)\cos(\phi)=1$ and -35% when $(d/W)\cos(\phi)=0$. Maximum fault-normal and fault-parallel effects occur at large magnitudes and long periods when $\theta=\phi=0$. At 5 seconds, these effects can result in an increase of up to 39% in the fault-normal component of spectral acceleration and a decrease of up to 28% in the fault-parallel component of spectral acceleration when $M_w = 7.5$ and $r_{rup} = 0$ km. Because the spatial and fault-normal directivity effects are multiplicative, the total maximum positive directivity effects at 5 seconds can approach a factor of 2.3 for strike-slip faulting and a factor of 1.9 for dip-slip faulting.

5.4.5.4 Engineering Implications of Near-Fault Ground Motions

Fault rupture directivity pulses have important practical implications for the seismic design and analysis of civil engineering facilities. These near-fault pulses can cause very large inelastic deformation demands on a structure. For example, Figure 5.15(b) shows large displacement ductility demands over a relatively wide period range for the near-fault ground motion recorded at the Rinaldi Receiving Station from the Northridge earthquake. The effects of near-fault pulses on structures have been discussed by numerous investigators, including Bertero et al. (1978, 1999); Mahin and Bertero (1981); Anderson and Bertero (1987, 2002); Challa and Hall (1994); Iwan (1994, 1997); Hall et al. (1995); Bozorgnia and Mahin (1998); Malhotra (1999); Alavi and Krawinkler (2001); among others.

Pre-1997 editions of the *Uniform Building Code* (e.g., UBC, 1994) did not have provisions covering near-source effects for fixed-base structures. In fact, fixed-base structures located in the same seismic

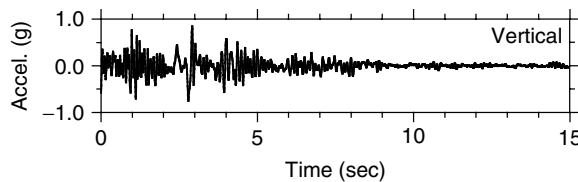


FIGURE 5.33 Vertical ground acceleration recorded in the 1994 Northridge, California, earthquake at Rinaldi Receiving Station.

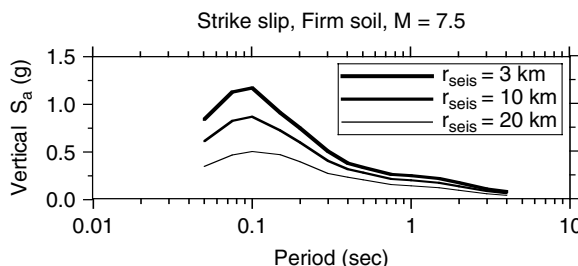


FIGURE 5.34 Median vertical acceleration response spectra for 5% damping and distances from seismogenic faulting of 3, 10, and 20 km. (Adapted from Campbell, K.W. and Bozorgnia, Y. (2003). Updated near-source ground motion (attenuation) relations for the horizontal and vertical components of PGA and acceleration response spectra. *Bulletin of the Seismological Society of America*, 93, 314–331.)

zone, with the same site category, were assigned the same elastic design spectrum, regardless of their proximity to active faults. If one wanted to take these effects into account, the only alternative was to develop a site-specific design spectrum. In the 1997 edition of the UBC, near-source factors were introduced in the main body of the code to increase the design base shear (or strength) of structures located within 15 km of active faults. The near-source elastic design spectra in the 1997 UBC are generally compatible with the average of the two horizontal components; however, this code does not specifically address the larger ground motion expected for the strike-normal component (Somerville, 1998).

A recent U.S. seismic code, the *International Building Code* (IBC, 2000), does not explicitly have near-source factors, because the artificial truncation of ground motion in a seismic zone is not a feature of this code, and the design spectral ordinates attain high values in the vicinity of seismic sources that are judged capable of generating large earthquakes (UBC-IBC Structural, 2000; see also Section 5.5). However, the 1996 USGS hazard maps, which are the basis for the seismic provisions in the 2000 IBC, as well as the 2002 USGS hazard maps do not specifically include directivity effects (Frankel et al. 2002). Therefore, these effects are only accounted for in an average sense through somewhat higher near-fault ground motions and standard deviations at longer periods represented by the ground motion relations used in the probabilistic seismic hazard analysis.

5.4.6 Vertical Ground Motion

Characteristics of the vertical component of ground motion are significantly different than those of the horizontal component. This is clearly evident in the recorded ground acceleration time histories. Compare, for example, the vertical ground acceleration recorded at Rinaldi Receiving Station during the Northridge earthquake (Figure 5.33) with that of the horizontal component recorded at this same station (Figure 5.29). It is evident from this comparison that the vertical component is richer in high frequency content than the horizontal component. This results in high vertical response spectral ordinates at short periods (Figure 5.5). Other examples of vertical response spectra are plotted in Figure 5.34. This figure presents the median vertical response spectra for an earthquake of M_w 7.5 at distances of 3, 10 and 20

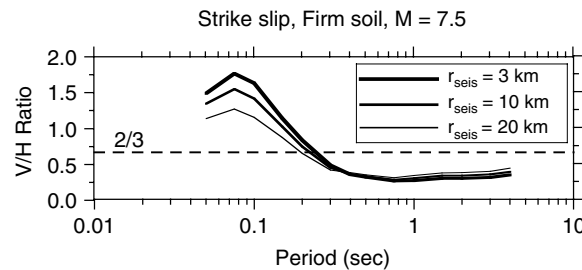


FIGURE 5.35 Vertical-to-horizontal (V/H) spectral ratio for 5% damping and distances from seismogenic faulting of 3, 10 and 20 km. (Adapted from Campbell, K.W. and Bozorgnia, Y. (2003). Updated near-source ground motion (attenuation) relations for the horizontal and vertical components of PGA and acceleration response spectra. *Bulletin of the Seismological Society of America*, 93, 314–331.)

km from the seismogenic part of the causative fault for a firm soil site, approximately equivalent to NEHRP soil category D (Campbell and Bozorgnia, 2003). As this figure shows, vertical spectral acceleration can be high at short periods, especially at sites close to the fault. Other empirical models have shown similar behavior for soil sites.

High vertical spectral acceleration at short periods can affect structural systems and components that have short *vertical* natural periods. In fact, vertical structural periods are generally short, as have been measured, identified, or computed by a number of investigators. For example, based on the recorded structural response of twelve instrumented structures, Bozorgnia et al. (1995a, 1998) identified a range of 0.075 to 0.26 sec for vertical natural periods of several structural systems and components. Another example is the study by Collier and Elnashai (2001), who analyzed a four-story reinforced concrete frame building of typical 1960s European construction and computed a vertical fundamental period of about 0.07 sec.

In recent years, analyses of hundreds of vertical ground motions recorded worldwide have identified distinct characteristics for the vertical component and its relationship to horizontal components (e.g., Niazi and Bozorgnia, 1989, 1991, 1992; Bozorgnia et al., 1995b, 1996, 1999; Watabe et al. 1990; Silva, 1997; Amirkhanian and Bolt, 1998; Darragh et al. 1999; Ambraseys and Douglas, 2000; Beresnev et al. 2002; Bozorgnia and Campbell, 2004).

The vertical-to-horizontal (V/H) spectral ratio is a strong function of natural period, source-to-site distance, and local site conditions. Bozorgnia et al. (1999) showed that the behavior of the V/H spectral ratio with distance is different for firm soil (NEHRP soil category D) than for stiffer soil and rock sites. For firm soil sites close to active faults, V/H spectral ratios can easily exceed unity, approaching a factor of 1.8 or greater at short periods. Some examples of V/H spectral ratios predicted from the ground motion relations of Campbell and Bozorgnia (2003) for distances of 3, 10 and 20 km are plotted in Figure 5.35. It is evident from this figure that a period-independent ratio of 2/3 is a grossly unconservative approximation of the V/H spectral ratio at short periods, and is a relatively conservative approximation at long periods (see also Bozorgnia et al. 1999, and Bozorgnia and Campbell, 2004 for more details). Therefore, using the period-independent ratio of 2/3 to derive a vertical spectrum from a horizontal spectrum, as suggested in some engineering guidelines (e.g., Section 1.6.1.5.2 of FEMA-356, 2000) is not justified, especially at firm soil sites located near active faults.

Investigators (e.g., Silva, 1997; Amirkhanian and Bolt, 1998) have offered seismological explanations for the observed dependence of the V/H spectral ratio on distance and local site conditions. For example, Amirkhanian and Bolt (1998) concluded that the high-amplitude and high-frequency vertical accelerations that are observed on near-source accelerograms are most likely generated by the conversion of shear-waves to compressional waves within the transition zone between the underlying bedrock and the overlying softer sedimentary layers. Recently, based on analysis of five significant earthquakes in California, Beresnev et al. (2002) found that SV-waves dominate vertical motions at periods longer than about 0.1 sec; and at shorter periods, P-waves may become a significant contributor to the vertical motions.

5.5 Ground Motion Representation in the International Building Code

5.5.1 Introduction

Compared to previous editions of the *Uniform Building Code* (UBC, 1994, 1997), the *International Building Code* (IBC, 2000) includes major revisions in the characterization of ground motion for seismic design in the United States. It is intended to serve as a single code for the entire country, which comprises very different seismic regions. The challenge is to define a design earthquake that results in a uniform seismic safety margin for these different seismic provinces.

The main steps involved in developing the seismic design spectra in the IBC (2000), FEMA-368 (2001) and SEI/ASCE 7-02 (ASCE, 2002) are as follows:

- Given the site location, spectral accelerations at 0.2 sec and 1.0 sec are obtained from a set of published contour maps. These maps represent the maximum considered earthquake (MCE) ground motion (see Section 5.5.2). The MCE spectral accelerations are adjusted for local site effects (see Section 5.5.2).
- The MCE ground motion may be interpreted as a “collapse ground motion” (Leyendecker et al. 2000). For seismic *design*, the soil-adjusted MCE spectral ordinates are multiplied by a factor of 2/3 (see Section 5.5.3).
- The seismic design spectrum is constructed given the design spectral ordinates at 0.2 and 1.0 sec (see Section 5.5.3).

In the following sections, the main concepts behind the MCE ground motion are summarized, followed by the details of the steps in constructing the design spectrum.

5.5.2 Maximum Considered Earthquake (MCE)

“The most severe earthquake effects considered” in the IBC is what is referred to as the maximum considered earthquake, or MCE. This acronym is different than, and should not be confused with, a similar one traditionally used to represent the maximum capable earthquake or the maximum credible earthquake used in some previous publications and regulations. The MCE ground motion is quantified by the MCE maps published as part of the IBC. These maps are based on a combination of the results of probabilistic and deterministic estimates of ground motion. The background and concepts behind the MCE and the design spectrum in the IBC are discussed next.

5.5.2.1 Probabilistic Seismic Hazard Maps of the United States

The USGS has carried out comprehensive probabilistic seismic hazard analyses of the entire United States (see Frankel et al. 1996, 2000, 2002 for more details). There are hazard maps for different spectral ordinates and for different mean return periods. The return periods include 475 years (corresponding to 10% probability of exceedance in 50 years; abbreviated as 10% in 50 years) and 2475 years (corresponding to 2% probability of exceedance in 50 years, or 2% in 50 years). The latest USGS hazard maps, which were the 2002 edition at the time this chapter was written, can be found at the USGS Internet web site <http://geohazards.cr.usgs.gov/eq/>. These maps are updated approximately every three years.

The USGS hazard maps have quantitatively revealed important differences between the ground motion characteristics in different regions of the United States. For example, they have shown that the difference between the ground motions for 10% in 50 years and 2% in 50 years in the western United States is typically less than the difference between these two ground motion levels in the central and eastern United States (Leyendecker et al., 2000). Figure 5.36 presents an example of such a difference. For a site in San Francisco, California, the ratio of spectral accelerations for 2% in 50 years over that of 10% in 50 years is around 1.5; whereas, the ratio is greater than 4.4 at Charleston, South Carolina. The significance of this observation, as related to the definition of the design spectrum in the IBC, is elaborated in the following discussion about the structural seismic safety margin.

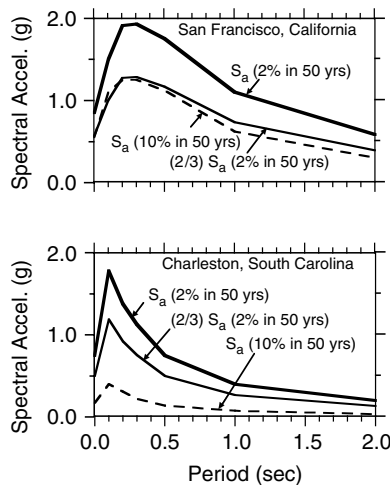


FIGURE 5.36 Uniform hazard response spectra for 2% and 10% probability of exceedance in 50 years for San Francisco, California, and Charleston, South Carolina. For comparison, two thirds of the 2% in 50 years spectra are also plotted. (Adapted from Leyendecker, E.V., Hunt, R.J., Frankel, A.D. and Rukstales, K.S. (2000). Development of maximum considered earthquake ground motion maps. *Earthquake Spectra*, 16, 21–40.)

5.5.2.2 Structural Seismic Safety Margin

The Seismic Design Procedures Group (SDPG), a committee of engineers and earth scientists, examined the safety margin against collapse of conventionally designed structures. The SDPG concluded that “the collective opinion of the SDPG was that the seismic margin contained in the 1997 NEHRP Provisions provides, as a minimum, a margin of about 1.5 times the design earthquake ground motion. In other words, if a structure is subjected to a ground motion 1.5 times the design level, the structure should have a low likelihood of collapse. The SDPG recognized that quantification of this margin is dependent on the type of structure, detailing requirements, etc., but the 1.5 factor was considered a conservative judgment appropriate for structures designed in accordance with the 1997 NEHRP Provisions.” (Leyendecker et al. 2000).

Considering a desire to prevent collapse if a relatively rare but high level of ground motion associated with a 2% in 50 year probability were to occur, and taking into account the approximate minimum seismic margin of 1.5 against collapse, the IBC generally defines design ground motion as 1/1.5 (=2/3) times the 2% in 50 year ground motion. There are, however, important exceptions to this rule, especially near active faults in coastal California, as explained below. Referring to Figure 5.36, it is evident that for a site in San Francisco, 2/3 times the uniform hazard spectrum for 2% in 50 years is generally comparable to the traditional design spectrum for 10% in 50 years. However, for Charleston, 2/3 times the spectrum for 2% in 50 years is higher than that for 10% in 50 years (Leyendecker et al., 2000). Therefore, the IBC design philosophy accounts, to some extent, for the possibility of a rare but catastrophic earthquake in the eastern United States.

5.5.2.3 Ground Motions in Coastal California

In coastal California, the 2% in 50 year ground motion is generally conservative compared with a spectrum defined as 1.5 times the design ground motion recommended in the recent editions of the UBC. The 1.5 factor is the approximate seismic margin used by the SDPG to bring the design ground motion to the MCE level. Considering this comparison, as well as the observed performance of structures in coastal California in recent earthquakes, the SDPG defined the MCE as the 2% in 50 year ground motion only until it reaches 1.5 times the basic ground motion corresponding to Seismic Zone 4 in the UBC. The limits on the probabilistically defined ground motion value are sometimes referred to as plateaus (Leyendecker et al. 2000). Specifically, these plateaus are quantified by two spectral accelerations:

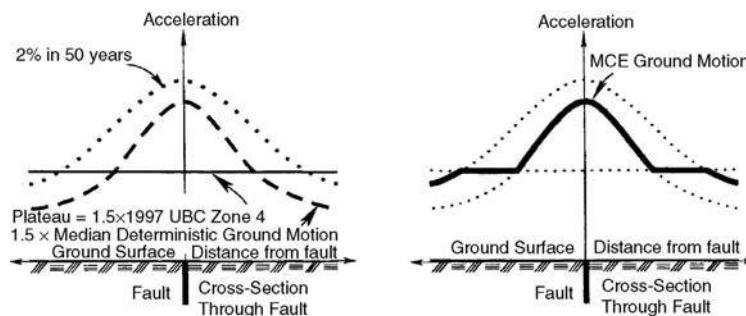


FIGURE 5.37 Procedure to integrate probabilistic and deterministic ground motions to obtain the *Maximum Considered Earthquake* (MCE) ground motion. (From Leyendecker, E.V., Hunt, R.J., Frankel, A.D., and Rukstales, K.S. (2000). Development of maximum considered earthquake ground motion maps. *Earthquake Spectra*, 16, 21–40.)

1.5g for a spectral acceleration at 0.2 sec and 0.6g for a spectral acceleration at 1.0 sec. These values include the 1.5 scale factor.

Above the plateau, the ground motion is specified according to 1.5 times the median deterministic ground motions derived from the ground motion relations that were used to develop the probabilistic values. However, the deterministic values are not used unless they are *less than* the probabilistic values. The procedure to integrate the probabilistic and deterministic values to obtain the MCE ground motion is illustrated in Figure 5.37. Besides being the seismic margin, the scale factor of 1.5 also is an approximate factor to scale up the median ground-motion value to the median plus one standard deviation value, or 84th percentile. For example, in the ground motion relation developed by Campbell and Bozorgnia (2003), the median plus one standard deviation value of the horizontal spectral acceleration at 1.0 sec can be obtained by multiplying the median spectral acceleration by a factor of 1.65 when $\text{PGA} \geq 0.25 \text{ g}$.

Close to active faults, defining the design earthquake ground motion based on the median deterministic value is also consistent with the concept of the Near-Source Factors introduced in the 1997 UBC (Kircher, 1999). In the 1997 UBC the introduction of Near-Source Factors became necessary in view of the artificial truncation of peak ground acceleration at 0.4 g in Seismic Zone 4. In the IBC, these factors are not found because the design ground motions can attain high values in the vicinity of the active faults (UBC-IBC Structural, 2000). It should be noted, however, that the current MCE maps do not include fault rupture directivity effects (Frankel et al. 2002); so in the fault-normal direction these near-fault deterministic ground motions would even be higher if these effects were taken into account (see Section 5.4.5).

5.5.2.4 MCE Maps

The MCE ground motion, as defined above, is quantified by two sets of contour maps of elastic spectral accelerations. Given the site location, the spectral accelerations at short structural period (0.2 sec), S_s , and at 1.0-sec period, S_1 , are obtained from these MCE maps. The maps are printed in the IBC and can also be found at the USGS Internet web site <http://geohazards.cr.usgs.gov/eq/>. The spectral accelerations are for a 5% damping ratio. The period of 0.2 sec was chosen to represent S_s because in the central and eastern United States the spectral acceleration at 0.2 sec is larger than that at 0.3 sec and better quantifies the larger short-period frequency content in this region. In the western United States, there is little difference between the spectral accelerations at 0.2 and 0.3 sec (e.g., Figure 5.36).

5.5.2.5 Adjustment for Local Site Conditions

The reference site condition for the MCE maps is firm rock with a nominal average shear-wave velocity of 760 m/sec in the top 30 m of the site profile (Frankel et al. 1996, 2000, 2002). This corresponds to the boundary of NEHRP site categories B and C as defined in the IBC. For other site conditions, the MCE ground motions are adjusted by using the site coefficients F_a and F_v specified in IBC Tables 1615.1.2(1) and 1615.1.2(2), respectively (for FEMA-368, use FEMA Tables 4.1.2.4a and 4.1.2.4b, respectively; for

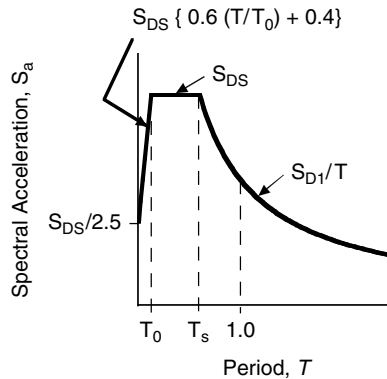


FIGURE 5.38 Elastic design spectrum in the IBC (2000) and FEMA-368 (2001) for 5% damping. Corner periods are $T_s = S_{D1}/S_{DS}$ and $T_0 = 0.2 T_s$.

SEI/ASCE 7-02, use ASCE Tables 9.4.1.2.4a and 9.4.1.2.4b, respectively). The details of the site categories are discussed in Chapter 4 (see also Table 5.3). Given the site coefficients F_a and F_v , the site-adjusted spectral ordinates S_{MS} (at 0.2-sec period) and S_{M1} (at 1.0-sec period) are defined as

$$S_{MS} = F_a S_S \quad (5.63)$$

$$S_{M1} = F_v S_1 \quad (5.64)$$

These site-adjusted values are used to construct the design spectra, as explained below.

5.5.3 Design Spectra in the IBC

The MCE ground motion may be interpreted as a “collapse ground motion” (Leyendecker et al. 2000). Thus, the actual ground motion used in seismic design is lower than this level. In the IBC, the design ground motion is quantified by two spectral accelerations: S_{DS} , the design spectral acceleration at 0.2 sec, and S_{D1} , the design spectral acceleration at 1.0 sec. These elastic design spectral accelerations are defined as

$$S_{DS} = (2/3) S_{MS} \quad (5.65)$$

$$S_{D1} = (2/3) S_{M1} \quad (5.66)$$

Given the design spectral accelerations, S_{DS} and S_{D1} , the 5% damped general elastic design spectrum is constructed according to Figure 5.38.

It should be noted that, by comparing the design spectrum in Figure 5.38 to that given in FEMA-356 (2000) as shown in Figure 5.10, the IBC design spectrum can be derived from the FEMA-356 spectrum by assigning a 5% damping ratio (i.e., $B_s = B_1 = 1.0$) and setting $S_{XS} = S_{DS}$ and $S_{X1} = S_{D1}$.

5.5.4 Site-Specific Ground Motion in the IBC

The IBC allows for the development of MCE response spectrum using site-specific methods in lieu of one developed using the general procedure described in Section 5.5.3 of this chapter. Such a study must account for the regional seismicity and geology; the expected recurrence rates and maximum magnitudes of events on known faults and source zones; the locations of the site with respect to these faults and source zones; near-source effects, if any; and the characteristics of the subsurface site conditions. In general, the MCE ground motion is defined as the 2% in 50 year site-specific ground motion. However, if either the 2% in 50 year 0.2-sec or 1.0-sec spectral acceleration exceeds the deterministic limits given in Figure 5.39, the MCE ground motion is taken as the lesser of the probabilistic MCE ground motion or 1.5 times the deterministic site-specific median ground motion resulting from a characteristic earth-

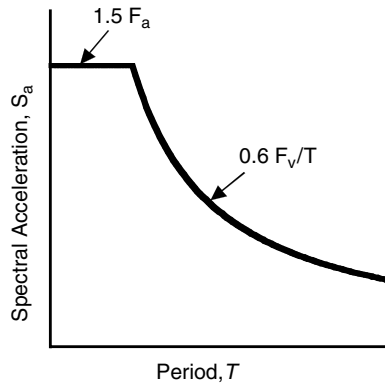


FIGURE 5.39 Deterministic limit on the site-specific MCE response spectrum.

quake on any known active fault in the region, but shall not be taken as less than the deterministic limit given in Figure 5.39. The site-specific design spectrum is the larger of $2/3$ of the site-specific MCE spectrum or 80% of the general design spectrum described in Section 5.5.3 of this chapter.

5.6 Future Challenges

As indicated in this chapter, in recent years there have been significant advances in the engineering characterization of strong ground motion. There are, however, numerous exciting challenges confronting earth scientists and earthquake engineers concerning the characterization of ground motion for engineering applications. These challenges include, but are certainly not limited to, the following:

5.6.1 Development of the Next Generation of Ground Motion (Attenuation) Relations

The next generation of ground motion relations will need to be applicable to a wider range of magnitudes and distances than existing relations so it will not be necessary to extrapolate them beyond their range of applicability as is currently done in engineering practice. These future relations will also need to incorporate finer distinctions in site categories (e.g., Hard rock, soft rock, very stiff soil, stiff soil and soft soil; instead of simply soil and rock) or directly use the average shear-wave velocity in the top 30 m of the site profile as defined in recent building codes to better account for site effects. Additionally, future ground motion relations will need to systematically include near-fault directivity effects, hanging wall and footwall effects, sediment depth and other parameters that are used in one or more of the currently available ground motion relations. There are ongoing research efforts to systematically develop such next generation ground motion relations that are expected to take a major step towards obtaining these goals.

5.6.2 Better Understanding and Modeling of Fault Rupture Directivity and Fling

Currently used wide-band modifications of ground motion relations to develop elastic response spectra need to be enhanced to include the observed narrow-band characteristics of near-fault pulses. The observed period of such pulses increases with magnitude. Such a characteristic needs to be reliably modeled and included in the engineering prediction of ground motion. Also, there is a need to reliably quantify and simplify the effects of fault rupture directivity and fling for the design of civil engineering facilities.

5.6.3 Inclusion of the Directivity Effects in Probabilistic Hazard Analysis

In the United States, the 1996 and 2002 national seismic hazard maps that provide the fundamental data for seismic design, do not include fault rupture directivity effects. The hazard analysis for sites located near active faults should incorporate such effects, once the wide-band versus narrow-band issues regarding near-fault pulses are resolved. Inclusion of such effects can have important consequences on the seismic design of civil engineering systems.

5.6.4 Near Real-Time Spatial Distribution of Damage Potential of Ground Motions

Currently, after an earthquake, maps of various traditional ground-motion parameters, including elastic spectral ordinates, are automatically generated in near real-time and posted on the Internet. For rapid performance-based damage assessment of structures, the currently mapped parameters need to be supplemented with other damage-related parameters, for example, strong-motion duration and damage indices. For practical near real-time post-earthquake damage and loss assessments, it would also be desirable to combine the mapped spatial distributions of these ground-motion and damage parameters with an inventory of the existing structural and lifeline facilities.

5.6.5 Vertical Design Spectra

In recent years the understanding of the near-source characteristics of vertical ground motion has greatly advanced. These characteristics will need to be reliably simplified and translated into simple rules for developing vertical design spectra.

5.6.6 Ground-Motion Parameters for Performance-Based Earthquake Engineering

There is a need to identify and predict improved and more reliable ground-motion parameters for performance-based earthquake engineering. Such parameters should be comprehensive enough to include the effects of various important seismological parameters such as magnitude, source-to-site-distance, faulting mechanism and other characteristics. This will require an even greater degree of interaction among earth scientists and engineers than has been achieved in the past.

5.6.7 Modeling Cumulative Damage Potential of Earthquake Ground Motions

Cumulative damage potential of ground motions in foreshocks, the main shock, aftershocks and multiple events needs to be modeled and reliably simplified for practical applications.

Acknowledgments

We would like to recognize the constructive comments of Prof. V.V. Bertero, Prof. C.M. Uang, Prof. J.P. Stewart, Dr. M. Hachem and T. Travarasrou, which are greatly appreciated. We would also like to recognize all of the researchers and practicing engineers and seismologists, past and present, without whose work this chapter would not have been possible.

Glossary

Anelastic attenuation — The diminution of ground motion with distance from the source due to material damping and scattering of waves from inhomogeneities in the crust.

Attenuation relation — An equation or tabulation used to estimate a strong-motion parameter from one or more seismological parameters; also known as a ground motion relation.

Basement rock — The more resistant, generally crystalline rock that lies beneath layers or irregular deposits of younger, relatively deformed sedimentary rock.

Critical reflection — The incidence angle below which the ground-motion ray is completely reflected off a layer of higher wave velocity.

Damage spectrum — A plot of variation of a damage index for an inelastic single-degree-of-freedom (SDF) system versus undamped natural period or frequency, when excited by a specified ground motion time history.

Epicenter — The point on the Earth's surface directly above the hypocenter.

Faulting mechanism — The type or style of faulting defined by the direction of slip on the fault rupture plane; usually referred to by such terms as strike slip, reverse, thrust, normal or oblique.

Focus — See hypocenter.

Footwall — That portion of the crust that lies below the fault or fault rupture plane.

Frequency — The reciprocal of period – that is, the number of cycles of oscillation per unit of time (e.g., One second). Usually measured in terms of hertz (1 Hz = 1 cycle per second).

Geometric attenuation — The diminution of ground motion with distance from the source as the area of the wave front expands.

Ground motion — The vibration of the ground in the time or frequency domain measured by a seismometer that records acceleration, velocity or displacement, or an estimate of this vibration or a ground-motion parameter that characterizes this vibration.

Ground motion relation — Same as attenuation relation.

Hanging wall — That portion of the crust that lies above the fault or fault rupture plane.

Hypocenter — The point within the Earth where the earthquake rupture begins (see also focus).

Hysteretic energy spectrum — A plot of the maximum hysteretic energy (due to yielding) in an inelastic SDF system versus undamped natural period or frequency, subjected to a specified ground motion time history at its base.

Inelastic response spectrum — A plot of the maximum response of an inelastic SDF system versus undamped natural period or frequency, subjected to a specified ground motion time history at its base.

Local site conditions — A qualitative or quantitative description of the material properties of the soil and sedimentary rock layers above basement rock.

Magnitude — An instrumental or seismological measure of an earthquake's size proportional to the logarithm of the amplitude or energy of ground motion.

Maximum Considered Earthquake (MCE) — The most severe earthquake effects considered in the *International Building Code* (IBC) and other recent U.S. codes and standards.

Natural frequency — The reciprocal of natural period.

Natural period — The period of an oscillator or structure during free (i.e., unforced) vibration.

Period — The duration of time (e.g., number of seconds) required to complete one oscillation.

Radiation pattern — A geometric description of the amplitude of ground motion and the sense of initial motion at the source which for shear waves has a low-order symmetry that can be used to infer the faulting mechanism.

Rake angle — The angle between the direction of slip on the fault rupture plane and the fault strike.

Response spectrum (elastic) — A plot of the maximum response of a viscously damped linear elastic SDF system versus undamped natural period or frequency, when subjected to a specified ground motion time history at its base.

Seismogenic — That part of the Earth's crust that is capable of generating ground motion at periods of engineering interest, usually 10 sec or less.

Seismological parameter — A parameter used to characterize a seismological property of the earthquake source, the propagation medium, or the response of the materials beneath the site.

Shear-wave velocity — The speed at which shear waves travel through a material; shear waves are waves whose amplitude is perpendicular to the direction of propagation and are the most potentially damaging to man-made structures.

Source directivity — The azimuthal perturbation of the radiation pattern due to rupture propagation on the fault in which the amplitude increases in the direction of rupture and decreases in the opposite direction.

Stress drop — The amount of stress released at the rupture front during an earthquake.

Strike — The orientation of a fault on the Earth's surface, usually measured clockwise from north.

Strong ground motion — Ground motion having the potential to cause measurable damage to a structure's architectural or structural components; usually associated with a PGA of 0.05g or greater.

Strong-motion parameter — A parameter characterizing the amplitude of strong ground motion in the time domain (time-domain parameter) or the frequency domain (frequency-domain parameter).

Time history — A data set, usually composed of one vertical and two orthogonal horizontal components, describing a strong-motion parameter (such as ground acceleration) as a function of time.

Tectonic environment — The type of tectonic deformation that occurs in a region; usually described by such terms as active, stable, compressional, extensional or subduction.

List of Symbols

Ground Motion Parameters

PGA	Peak ground acceleration (g)
PGV	Peak ground velocity (cm/sec)
PGD	Peak ground displacement (cm)
SA	Maximum absolute (total) acceleration of SDF system
SV	Maximum velocity of SDF system relative to the ground
S_d	Maximum deformation of an elastic SDF system relative to the ground
S_v	PSV = Pseudo-velocity = ωS_d
S_a	PSA = Pseudo-acceleration = $\omega^2 S_d$
Y	Peak ground motion (generic)
Y_{Dir}	Peak ground motion (generic) including rupture directivity effects
$\sigma_{\ln Y}$	Standard deviation of $\ln Y$
$\sigma_{\ln Y, Dir}$	Standard deviation of $\ln Y_{Dir}$ (i.e., when directivity effects are included)

Magnitude Parameters

m_{Lg}	Lg-wave magnitude used in eastern United States (equivalent to m_N in Canada)
M	Earthquake magnitude (generic)
M_s	Surface-wave magnitude
M_w	Moment magnitude (equivalent to M)

Distance Parameters

r_{epi}	Epicentral distance (km)
r_{hypo}	Hypocentral distance (km)
r_{jb}	Closest distance to the surface projection of the rupture plane (km)
r_{rup}	Closest distance to the rupture plane (km)
r_{seis}	Closest distance to the seismogenic part of the rupture plane (km)
R	Distance to the earthquake source (generic)

Depth Parameters

d_{rup}	Average depth to top of the rupture plane (km)
d_{seis}	Average depth to top of the seismogenic part of the rupture plane (km)
h_{hypo}	Hypocentral depth (also focal depth) (km)
H_{bot}	Depth to the bottom of the seismogenic part of the fault (km)
H_{top}	Depth to the top of the fault (km)
H_{seis}	Depth to the top of the seismogenic part of the fault (km)

Faulting Mechanism Parameters

F	Indicator variable for the type or style of faulting
F_{RV}	Indicator variable for reverse faulting ($\delta > 45^\circ$) in Campbell and Bozorgnia model
F_{TH}	Indicator variable for thrust faulting ($\delta \leq 45^\circ$) in Campbell and Bozorgnia model
W	Down-dip width of the fault rupture plane (km)
λ	Rake (direction of slip vector on the fault plane): 0°, pure left-lateral faulting 90°, pure reverse faulting 180°, pure right-lateral faulting 270° or -90°, pure normal faulting

Site Parameters

S_C	Indicator variable for very dense soil and soft rock in building code site class
S_D	Indicator variable for stiff soil in building code site class
S_E	Indicator variable for soft soil in building code site class
S_{VFS}	Indicator variable for very firm soil in Campbell and Bozorgnia site class
S_{SR}	Indicator variable for soft rock in Campbell and Bozorgnia site class
S_{FR}	Indicator variable for firm rock in Campbell and Bozorgnia site class
S_{Deep}	Indicator variable for deep stiff soil in eastern North America
S_{Soil}	Indicator variable for generic soil in western North America
V_{30}	Average value of V_S in the top 30 m (100 ft) of a site profile
V_S	Shear-wave velocity (generic)

Hanging-Wall Parameters

HW	Indicator variable for a site located on the hanging wall of the rupture plane
------	--

Source Directivity Parameters

d	Effective rupture width for estimating directivity effects for dip-slip faults
DR	Fraction of fault rupture length (s/L) or width (d/W) rupturing towards a site
L	Length of the fault rupture plane
s	Effective rupture length for estimating directivity effects for strike-slip faults
ϕ	Zenith angle between fault rupture plane and ray path to a site for dip-slip faults
θ	Azimuth angle between rupture plane and ray path to a site for strike-slip faults

Generic Inelastic Systems and Seismic Code Parameters

F_e	Maximum restoring force if the system were to remain elastic
F_y	Equivalent yield strength
u_{max}	Maximum deformation of the inelastic SDF system
u_y	Yield deformation of the inelastic SDF system

μ	Displacement ductility ratio = u_{\max}/u_y
R	Response modification coefficient
S_S	Mapped MCE spectral acceleration (5% damping) at a period of 0.2 sec
S_1	Mapped MCE spectral acceleration (5% damping) at a period of 1.0 sec
S_{MS}	MCE spectral acceleration (5% damping) at a period of 0.2 sec, adjusted for site effects
S_{M1}	MCE spectral acceleration (5% damping) at a period of 1.0 sec, adjusted for site effects
S_{DS}	Design spectral acceleration (5% damping) at a period of 0.2 sec
S_{D1}	Design spectral acceleration (5% damping) at a period of 1.0 sec

Miscellaneous Parameters

f	Seismic wave or oscillator frequency ($1/T$, Hz)
g	fraction of gravity (980.6550 cm/sec ²)
T	Wave or oscillator period ($1/f$, sec)
z_T	Indicator variable for subduction interface and intraslab events
δ	Angle of the fault plane with respect to the Earth's surface (dip angle)

References

- Abrahamson, N.A. (2000). Effects of rupture directivity on probabilistic seismic hazard analysis. *Proceedings, 6th International Conference on Seismic Zonation*, Palm Springs, California, 6 p.
- Abrahamson, N.A. and Somerville, P.G. (1996). Effects of the hanging wall and footwall on ground motions recorded during the Northridge earthquake, *Bulletin of the Seismological Society of America*, 86, S93–S99.
- Abrahamson, N.A. and Silva, W.J. (1996). Empirical ground motion models. *Report submitted to Brookhaven National Laboratory*.
- Abrahamson, N.A. and Silva, W.J. (1997). Empirical response spectral attenuation relations for shallow crustal earthquakes. *Seismological Research Letters*, 68, 94–127.
- Abrahamson, N.A., Schneider, J.F. and Stepp, J.C. (1991). Empirical spatial coherency functions for applications to soil-structure interaction analysis. *Earthquake Spectra*, 7, 1–27.
- Akiyama, H. (1985). *Earthquake-Resistant Limit-State Design of Buildings*. University of Tokyo Press, Tokyo.
- Alavi, B. and Krawinkler, H. (2001). Effects of near-fault ground motions on frame structures. *Report No. 138*, The John A. Blume Earthquake Engineering Center, Stanford University.
- Ambraseys, N. and Douglas, J. (2000). Reappraisal of the effect of vertical ground motions on response. *Report ESEE 00-4*, Imperial College of Science, Technology and Medicine, London.
- American Society of Civil Engineers (2002). Minimum design loads for buildings and other structures. *SEI/ASCE 7-02*, Reston, Virginia.
- Amirbekian, R.V. and Bolt, B.A. (1998). Spectral comparison of vertical and horizontal seismic strong ground motions in alluvial basins. *Earthquake Spectra*, 14, 573–595.
- Anderson, J.C. and Bertero, V.V. (1987). Uncertainties in establishing design earthquakes. *ASCE Journal of Structural Engineering*, 113, 1709–1724.
- Anderson, J.C. and Bertero, V.V. (2003). Performance improvement of tall steel buildings subjected to pulse-type ground motions. *Proceedings, 7th U.S. National Conference on Earthquake Engineering*, Boston.
- Anderson, J.G. (2000). Expected shape of regressions for ground motion parameters on rock. *Bulletin of the Seismological Society of America*, 90, S43–S52.
- Anderson, J.G. (2003). Strong motion seismology. In *International Handbook of Earthquake and Engineering Seismology*, Part B, Ed. W.H.K. Lee, H. Kanamori, P.C. Jennings and C. Kisslinger, Academic Press, London.
- Arias, A. (1970). A measure of earthquake intensity. In *Seismic Design for Nuclear Power Plants*, Ed. R.J. Hansen, MIT Press, Cambridge, Massachusetts.

- Atkinson, G.M. and Boore, D.M. (1995). New ground motion relations for eastern North America. *Bulletin of the Seismological Society of America*, 85, 17–30.
- Atkinson, G.M. and Boore, D.M. (1997). Some comparisons between recent ground motion relations. *Seismological Research Letters*, 68, 24–40.
- Atkinson, G.M. and Boore, D.M. (1998). Evaluation of models for earthquake source spectra in eastern North America. *Bulletin of the Seismological Society of America*, 88, 917–934.
- Atkinson, G.M. and Boore, D.M. (2003). Empirical ground-motion relations for subduction zone earthquakes and their application to Cascadia and other regions. *Bulletin of the Seismological Society of America*, 93, 1703–1729.
- Bendat, J.S. and Piersol, A.G. (1980). *Engineering Applications of Correlation and Spectral Analysis*. John Wiley & Sons, New York.
- Beresnev, I.A., Nightengale, A.M. and Silva, W.J. (2002). Properties of vertical ground motions. *Bulletin of the Seismological Society of America*, 92, 3152–3164.
- Bertero, V.V. and Uang, C.M. (1992). Issues and future directions in the use of an energy approach for seismic-resistant design of structures, In *Nonlinear Seismic Analysis and Design of Reinforced Concrete Buildings*, Ed. P. Fajfar and H. Krawinkler, 3–22.
- Bertero, V.V., Anderson, J.C. and Sasani, M. (1999). Impulse earthquake ground motions: A historical and critical review. *Proceedings, ASCE 1999 Structures Congress*, New Orleans, 91–94.
- Bertero, V.V., Mahin, S.A. and Herrera, R.A. (1978). Aseismic design implications of near-fault San Fernando earthquake records. *Earthquake Engineering and Structural Dynamics*, 6, 31–42.
- Bertero, V.V., Popov, E.P., Wang, T.Y. and Vallenás, J. (1977). Seismic design implications of hysteretic behavior of reinforced concrete structural walls, *Proceedings, 6th World Conference on Earthquake Engineering*, Vol. II, India, 1898–1904.
- Biot, M.A. (1933). Theory of elastic systems vibrating under transient impulse with an application to earthquake-proof buildings. *Proceedings, National Academy of Sciences*, 19, 262–268.
- Biot, M.A. (1934). Theory of vibration of buildings during earthquake. *Zeitschrift für angewandte Mathematik und Mechanik*, 14, 213–223.
- Biot, M.A. (1941). A mechanical analyzer for the prediction of earthquake stresses. *Bulletin of the Seismological Society of America*, 31, 151–171.
- Bolt, B.A. (1973). Duration of strong ground motion. *Proceedings, 5th World Conference on Earthquake Engineering*, Rome, 1304–1313.
- Bommer, J.J. and Martinez-Pereira, A. (1999). The effective duration of earthquake strong motion. *Journal of Earthquake Engineering*, 3, 127–172.
- Boore, D.M. (2001). Comparisons of ground motions from the 1999 Chi-Chi Earthquake with empirical predictions largely based on data from California. *Bulletin of the Seismological Society of America*, 91, 1212–1217.
- Boore, D.M. (2003). Prediction of ground motion using the stochastic method. *Pure and Applied Geophysics*, 160, 635–676.
- Boore, D.M. and Joyner, W.B. (1997). Site amplification for generic rock sites. *Bulletin of the Seismological Society of America*, 87, 327–341.
- Boore, D.M., Joyner, W.B. and Fumal, T.E. (1997). Equations for estimating horizontal response spectra and peak acceleration from western North American earthquakes: A summary of recent work. *Seismological Research Letters*, 68, 128–153.
- Boore, D.M., Stephens, C.D. and Joyner, W.B. (2002). Comments on baseline correction of digital strong-motion data: Examples from the 1999 Hector Mine, California, earthquake. *Bulletin of Seismological Society of America*, 92, 1543–1560.
- Bozorgnia, Y. (2003). An introduction to the classic paper: A mechanical analyzer for the prediction of earthquake stresses, by Maurice Biot. *Seismological Research Letters*, 74, 312.
- Bozorgnia, Y. and Bertero, V.V. (2001a). Evaluation of damage potential of recorded earthquake ground motion. *Seismological Research Letters*, 72, 233.

- Bozorgnia, Y. and Bertero, V.V. (2001b). Improved shaking and damage parameters for post-earthquake applications. *Proceedings, SMIP01 Seminar on Utilization of Strong-Motion Data*, Los Angeles, 1–22.
- Bozorgnia, Y. and Bertero, V.V. (2002). Improved damage parameters for post-earthquake applications. *Proc. SMIP02 Seminar on Utilization of Strong-Motion Data*, Los Angeles, 61–82.
- Bozorgnia, Y. and Bertero, V.V. (2003). Damage spectra: Characteristics and applications to seismic risk reduction. *ASCE Journal of Structural Engineering*, 129.
- Bozorgnia, Y. and Campbell, K.W. (2004). The vertical-to-horizontal response spectral ratio and tentative procedures for developing simplified V/H and vertical design spectra. *Journal of Earthquake Engineering*, 8, 175–207.
- Bozorgnia, Y. and Mahin, S.A. (1998). Ductility and strength demands of near-fault ground motions of the Northridge earthquake. *Proceedings, 6th U.S. National Conference on Earthquake Engineering*, Seattle, Washington.
- Bozorgnia, Y., Campbell, K.W. and Niazi, M. (1999). Vertical ground motion: Characteristics, relationship with horizontal component, and building-code implications. *Proceedings, SMIP99 Seminar on Utilization of Strong-Motion Data*, San Francisco, 23–49.
- Bozorgnia, Y., Mahin, S.A. and Brady, A.G. (1995a). Vertical responses of twelve instrumented structures recorded during the Northridge earthquake. *Report*, Earthquake Engineering Research Institute (ERI), Oakland, California, 275 p.
- Bozorgnia, Y., Niazi, M. and Campbell, K.W. (1995b). Characteristics of free-field vertical ground motion during the Northridge earthquake. *Earthquake Spectra*, 11, 515–525.
- Bozorgnia, Y., Mahin, S.A. and Brady, A.G. (1998). Vertical response of twelve structures recorded during the Northridge earthquake. *Earthquake Spectra*, 14, 411–432.
- Bozorgnia, Y., Niazi, M. and Campbell, K.W. (1996). Relationship between vertical and horizontal ground motion for the Northridge earthquake. *Proceedings, 11th World Conference on Earthquake Engineering*, Acapulco, Mexico.
- Brune, J. (1970). Tectonic stress and the spectra of seismic shear waves. *Journal of Geophysical Research*, 75, 4997–5009.
- Brune, J. (1971). Correction: Tectonic stress and the spectra of seismic shear waves. *Journal of Geophysical Research*, 76, 5002.
- Brune, J.N. (1999). Precarious rocks along the Mojave section of the San Andreas fault, California: Constraints on ground motion from great earthquakes. *Seismological Research Letters*, 70, 29–33.
- Brune, J.N. (2001). Shattered rock and precarious rock evidence for strong asymmetry in ground motions during thrust faulting. *Bulletin of the Seismological Society of America*, 91, 441–447.
- Bruneau, M. and Wang, N. (1996). Normalized energy-based methods to predict the seismic ductile response of SDOF structures. *Engineering Structures*, 18, 13–28.
- Campbell, K.W. (1997). Empirical near-source attenuation relationships for horizontal and vertical components of peak ground acceleration, peak ground velocity, and pseudo-absolute acceleration response spectra. *Seismological Research Letters*, 68, 154–179.
- Campbell, K.W. (2000a). Engineering seismology. In *Encyclopedia of Physical Science and Technology*, 3rd ed., Academic Press, San Diego.
- Campbell, K.W. (2000b). Erratum: Empirical near-source attenuation relationships for horizontal and vertical components of peak ground acceleration, peak ground velocity, and pseudo-absolute acceleration response spectra. *Seismological Research Letters*, 71, 353–355.
- Campbell, K.W. (2001). Development of semi-empirical attenuation relationships for CEUS. *Report to the U.S. Geological Survey, Award 01HQGR0011*, final report.
- Campbell, K.W. (2003a). Strong motion attenuation relations. In *International Handbook of Earthquake and Engineering Seismology*, Part B, Ed. W.H.K. Lee, H. Kanamori, P.C. Jennings and C. Kisslinger, Academic Press, London.
- Campbell, K.W. (2003b). A contemporary guide to strong motion attenuation relations. In *International Handbook of Earthquake and Engineering Seismology*, Handbook CD, Eds. W.H.K. Lee, H. Kanamori, P.C. Jennings and C. Kisslinger, Academic Press, London.

- Campbell, K.W. (2003c). Prediction of strong ground motion using the hybrid empirical method and its use in the development of ground motion (attenuation) relations in eastern North America, *Bulletin of the Seismological Society of America*, 93, 1012–1033.
- Campbell, K.W. (2003d). Engineering models of strong ground motion. In *Earthquake Engineering Handbook*, Ed. W.F. Chen and C. Scawthorn, CRC Press, Boca Raton, Florida.
- Campbell, K.W. and Bozorgnia, Y. (2003). Updated near-source ground motion (attenuation) relations for the horizontal and vertical components of peak ground acceleration and acceleration response spectra. *Bulletin of the Seismological Society of America*, 93, 314–331.
- Celebi, M. (1993). Seismic response of eccentrically braced tall building. *ASCE Journal of Structural Engineering*, 119, 1188–1205.
- Challa, V.R.M. and Hall, J.F. (1994). Earthquake collapse analysis of steel frames. *Earthquake Engineering and Structural Dynamics*, 23, 1199–1218.
- Chapman, M.C. (1999). On the use of elastic input energy for seismic hazard analysis. *Earthquake Spectra*, 15, 607–635.
- Choi, Y. and Stewart, J.P. (2003). Nonlinear site amplification as a function of 30 M shear wave velocity. *Earthquake Spectra*, in press.
- Chopra, A.K. (2001). *Dynamics of Structures: Theory and Applications to Earthquake Engineering*. 2nd ed., Prentice Hall, Upper Saddle River, New Jersey.
- Chopra, A.K. and Goel, R.K. (1999). Capacity-demand-diagram method based on inelastic design spectrum. *Earthquake Spectra*, 15, 637–656.
- Chopra, A.K. and Goel, R.K. (2001) Direct displacement-based design: Use of inelastic vs. Elastic design spectra. *Earthquake Spectra*, 17, 47–64.
- Chou, C.C. and Uang, C. M. (2000). Establishing absorbed energy spectra — an attenuation approach. *Engineering and Structural Dynamics*, 29, 1441–1455.
- CIT-SMARTS (1996). Caltech strong motion accelerogram record transfer system. Report and computer disks, Earthquake Engineering Research Laboratory, California Institute of Technology, <http://www.eerl.caltech.edu/smarts/smarts.html>.
- Clough, R.W. and Penzien, J. (1993). *Dynamics of Structures*. 2nd ed., McGraw-Hill, New York.
- Collier, C.J. and Elnashai, A.S. (2001). A procedure for combining vertical and horizontal seismic action effects. *Journal of Earthquake Engineering*, 5, 521–539.
- Converse, A.M. (1992). BAP, basic strong-motion accelerogram processing software. *U.S. Geological Survey Open-File Report* 92-296A.
- Darragh, R., Silva, W.J. and Gregor, N. (1999). Bay Bridge downhole array analyses. *Report submitted to Earth Mechanics, Inc.*, Fountain Valley, California.
- Decanini, L.D. and Mollaioli, F. (1998). Formulation of elastic earthquake input energy spectra. *Earthquake Engineering and Structural Dynamics*, 27, 1503–1522.
- Draper, N.R. and Smith, H. (1981). *Applied Regression Analysis*. 2nd ed., John Wiley & Sons, New York.
- Fajfar, P. (1992). Equivalent ductility factors, taking into account low-cycle fatigue. *Earthquake Engineering and Structural Dynamics*, 21, 837–848.
- Fajfar, P. and Vidic, T. (1994). Consistent inelastic design spectra: Hysteretic and input energy. *Earthquake Engineering and Structural Dynamics*, 23, 523–537.
- Federal Emergency Management Agency (2000). Prestandard and commentary for the seismic rehabilitation of buildings. *FEMA-356*, Washington, D.C.
- Federal Emergency Management Agency (2001). 2000 Edition NEHRP recommended provisions for seismic regulations for new buildings and other structures, Part 1, Provisions. *FEMA-368*, Washington, D.C.
- Federal Emergency Management Agency (2001). 2000 Edition NEHRP recommended provisions for seismic regulations for new buildings and other structures, Part 2, Commentary. *FEMA-369*, Washington, D.C.

- Field, E.H. (2000). A modified ground-motion attenuation relationship for Southern California that accounts for detailed site classification and a basin-depth effect. *Bulletin of the Seismological Society of America*, 90, S209–S221.
- Field, E.H. and the SCEC Phase III Working Group (2000). Accounting for site effects in probabilistic seismic hazard analyses of Southern California: Overview of the SCEC Phase III report. *Bulletin of the Seismological Society of America*, 90, S1–S31.
- Frankel, A., Mueller, C., Barnhard, T., Perkins, D., Leyendecker, E., Dickman, N., Hanson, S. And Hopper, M. (1996). National seismic hazard maps: Documentation June 1996, U.S. Geological Survey Open-File Rept. 96-532.
- Frankel, A.D., Mueller, C.S., Barnhard, T.P., Leyendecker, E.V., Wesson, R.L., Harmsen, S.C., Klein, F.W., Perkins, D.M., Dickman, N.C., Hanson, S.L. and Hopper, M.G. (2000). USGS national seismic hazard maps. *Earthquake Spectra*, 16, 1–19.
- Frankel, A.D., Petersen, M.D., Mueller, C.S., Haller, K.M., Wheeler, R.L., Leyendecker, E.V., Wesson, R.L., Harmsen, S.C., Cramer, C.H., Perkins, D.M. and Rukstales, K.S. (2002). Documentation for the 2002 update of the national seismic hazard maps. U.S. Geological Survey Open-File Rept. 02-420.
- Freeman, S.A. (1995). A review of practical approximate inelastic seismic design procedures for new and existing buildings. *Proceedings, 64th Annual Convention of the Structural Engineers Association of California*, Indian Wells, California, 311–331.
- Hachem, M.M. (2000). Bispec. [Http://www.ce.berkeley.edu/~hachem/bispec/index.html](http://www.ce.berkeley.edu/~hachem/bispec/index.html)
- Hall, J.F., Heaton, T.H., Halling, M.W. and Wald, D.J. (1995). Near-source ground motion and its effects on flexible buildings. *Earthquake Spectra*, 11, 569–605.
- Hanks, T.C. and Kanamori, H. (1979). A moment-magnitude scale, *Journal of Geophysical Research*, 84, 2348–2350.
- Housner, G.W. (1941). Calculating the response of an oscillator to arbitrary ground motion. *Bulletin of the Seismological Society of America*, 31, 143–149.
- Housner, G.W. (1952). Spectrum intensities of strong-motion earthquakes. *Proceedings, Symposium on Earthquake and Blast Effects on Structures*, Eds. C.M. Duke and M. Feigen, Los Angeles, 21–36.
- Housner, G.W. (1970a). Strong ground motion. In *Earthquake Engineering*, Ed. R.L.Wiegel, Prentice-Hall, Upper Saddle River, New Jersey.
- Housner, G.W. (1970b). Design spectrum. In *Earthquake Engineering*, Ed. R.L. Wiegel, Prentice-Hall, Upper Saddle River, New Jersey.
- Housner, G.W. (1975). Measures of severity of earthquake ground shaking. *Proceedings, U.S. National Conference on Earthquake Engineering*, Ann Arbor, Michigan, 25–33.
- Housner, G.W. (1997). Connections: The EERI oral history. Stanley Scott, Interviewer, Earthquake Engineering Research Institute (EERI), Oakland, California.
- Housner, G.W., Martel, R.R. and Alford, J.L. (1953). Spectrum analysis of strong-motion earthquakes. *Bulletin of the Seismological Society of America*, 43, 49–71.
- Hudson, D.E. (1962). Some problems in the application of spectrum techniques to strong-motion earthquake analysis. *Bulletin of Seismological Society of America*, 52, 417–430.
- Hudson, D.E. (1979). *Reading and Interpreting Strong Motion Accelerograms*. Monograph, Earthquake Engineering Research Institute, Berkeley, California.
- Humar, J.L. (1990). *Dynamics of Structures*. Prentice-Hall, Upper Saddle River, New Jersey.
- IBC (2000). *International Building Code*, International Code Council, Falls Church, Virginia.
- Idriss, I.M. (1993). Procedures for selecting earthquake ground motions at rock sites. *NIST GCR 93-625*, National Institute of Standards and Technology.
- Iwan, W.D. (1994). Near-field considerations in specification of seismic design motions for structures. *Proceedings, 10th European Conference on Earthquake Engineering*, 1, 257–267.
- Iwan, W.D. (1997). Drift spectrum: Measure of demand for earthquake ground motions. *ASCE Journal of Structural Engineering*, 123, 397–404.
- Johnston, A.C. (1996). Seismic moment assessment of earthquakes in stable continental regions, I. Instrumental seismicity. *Geophysical Journal International*, 124, 381–414.

- Joyner, W.B. (2000). Strong motion from surface waves in deep sedimentary basins. *Bulletin of the Seismological Society of America*, 90, S95–S112.
- Joyner, W.B., Warrick, R.E. and Fumal, T.E. (1981). The effect of Quaternary alluvium on strong ground motion in the Coyote Lake, California, earthquake of 1979. *Bulletin of the Seismological Society of America*, 71, 1333–1349.
- Kanamori, H. (1978). Quantification of earthquakes, *Nature*, 271, 411–414.
- Kayen, R.E. and Mitchell, J.K. (1997). Assessment of liquefaction potential during earthquakes by Arias intensity. *ASCE Journal of Geotechnical And Geoenvironmental Engineering*, 123, 1162–1174.
- Kim, J., and Collins, K.R. (2002). Closer look at the drift demand spectrum. *ASCE Journal of Structural Engineering*, 123, 942–945.
- Kinemetrics (2003). Strong Motion Analyst (SMA), software package, Kinematics, Inc., Pasadena, California.
- Kircher, C.A. (1999). United States building code approach to variations in regional seismicity. 1999 Annual Meeting of the New Zealand Society of Earthquake Engineering, Rotorua, New Zealand.
- Krawinkler, H. and Nassar, A.A. (1992). Seismic design based on ductility and cumulative damage demands and capacities. In *Nonlinear Seismic Analysis and Design of Reinforced Concrete Buildings*, Eds. Fajfar and Krawinkler, Elsevier Applied Science, New York.
- Lay, T. and Wallace, T.C. (1995). *Modern Global Seismology*. Academic Press, San Diego.
- Lee, W.H.K., Shin, T.C., Kuo, K.W., Chen, K.C. and Wu, C.F. (2001). Data files from CWB free-field strong-motion data from the 21 September Chi-Chi, Taiwan, earthquake. *Bulletin of Seismological Society of America*, 91, 1390.
- Lee, Y. and Anderson, J.G. (2000). Potential for improving ground-motion relations in southern California by incorporating various site parameters. *Bulletin of the Seismological Society of America*, 90, S170–S186.
- Leyendecker, E.V., Hunt, R.J., Frankel, A.D., and Rukstales, K.S. (2000). Development of maximum considered ground motion maps. *Earthquake Spectra*, 16, 21–40.
- Lin, K.W., Shakal, A., Huang, M., Stephens, C. and Savage, W. (2002). Dissemination of strong-motion data via Internet quick report and Internet data report at the CISN engineering data center. *Proceedings, SMIP02 Seminar on Utilization of Strong-Motion Data*, Los Angeles, 115–126.
- Mahin, S.A. and Bertero, V.V. (1976). Problems in establishing and predicting ductility in aseismic design. *Proceedings, International Symposium on Earthquake Structural Engineering*, St. Louis, Missouri, 613–628.
- Mahin, S.A. and Bertero, V.V. (1981). An evaluation of inelastic seismic design spectra. *ASCE Journal of Structural Division*, 107, 1777–1795.
- Mahin, S.A. and Lin, J. (1983). Construction of inelastic response spectra for single-degree-of-freedom systems. UCB/EERC-83/17, Earthquake Engineering Research Center, University of California, Berkeley.
- Malhotra, P.K. (1999). Response of buildings to near-field pulse-like ground motions. *Earthquake Engineering and Structural Dynamics*, 28, 1309–1326.
- Marone, C. and Scholz, C.H. (1988). The depth of seismic faulting and the upper transition from stable to unstable slip regimes. *Geophysical Research Letters*, 15, 621–624.
- MATLAB (2002). Product of The Mathworks, Inc., Natick, Massachusetts.
- McGuire, R.K., Silva, W.J. and Costantino, C.J. (2001). Technical basis for revision of regulatory guidance on design ground motions: hazard- and risk-consistent ground motion spectra guidelines. NUREG/CR-6728, U.S. Nuclear Regulatory Commission, Washington, DC.
- Miranda, E. and Bertero, V.V. (1994). Evaluation of strength reduction factors for earthquake-resistant design. *Earthquake Spectra*, 10, 357–379.
- Moores, E.M. and Twiss, R.J. (1995). *Tectonics*. W.H. Freeman and Company, New York.
- Naeim, F. and Kircher, C.A. (2001). On the damping adjustment factors for earthquake response spectra. *The Structural Design of Tall Buildings*, 10, 361–369.

- Newmark, N.M. and Hall, W.J. (1982). *Earthquake Spectra and Design*. Monograph, Earthquake Engineering Research Institute, Berkeley, California.
- Newmark, N.M., Blume, J.A. and Kapur, K.K. (1973). Seismic design spectra for nuclear power plants. *ASCE Journal of Power Division*, 99, 287–303.
- Niazi, M. and Bozorgnia, Y. (1989). Behavior of vertical ground motion parameters in the near-field. *Seismological Research Letters*, 60, 4.
- Niazi, M. and Bozorgnia, Y. (1991). Behavior of near-source peak vertical and horizontal ground motions over SMART-1 array, Taiwan. *Bulletin of the Seismological Society of America*, 81, 715–732.
- Niazi, M. and Bozorgnia, Y. (1992). Behavior of near-source vertical and horizontal response spectra at SMART-1 array, Taiwan. *Earthquake Engineering and Structural Dynamics*, 21, 37–50.
- Nigam, N.C. and Jennings, P.C. (1968). Digital calculation of response spectra from strong-motion earthquake records. Earthquake Engineering Research Laboratory, California Institute of Technology, Pasadena.
- NISEE (1999). *National Information Service for Earthquake Engineering Software Library*, University of California, Berkeley.
- Ordaz, M., Huerta, B. and Reinoso, E. (2003). Exact computation of input-energy spectra from Fourier amplitude spectra. *Earthquake Engineering and Structural Dynamics*, 32, 597–605.
- Park, S. and Elrick, S. (1998). Predictions of shear-wave velocities in Southern California using surface geology. *Bulletin of the Seismological Society of America*, 88, 677–685.
- Park, Y.J. and Ang, A.H.S. (1985). Mechanistic seismic damage model for reinforced concrete. *ASCE Journal of Structural Engineering*, 111, 722–739.
- Press, W.H., Teukolsky, S.A., Vetterling, W.T., and Flannery, B.P. (1992). *Numerical Recipes in C, the Art of Scientific Computing*. 2nd ed., Cambridge University Press, Cambridge, United Kingdom.
- Reinhorn, A.M., Barron, R., Valles, R.E. and Sivaselvan, M.V. (1999). NSPECTRA: Nonlinear analysis program for inelastic spectra with degradation and deterioration of structural systems. Department of Civil, Structural, and Environmental Engineering, State University of New York at Buffalo, <http://civil.eng.buffalo.edu/nspectra/>
- Richter, C.F. (1958). *Elementary Seismology*. W.H. Freeman and Company, San Francisco.
- Rodriguez-Marek, A., Bray, J.D. and Abrahamson, N.A. (2001). An empirical geotechnical seismic site response procedure. *Earthquake Spectra*, 17, 65–87.
- Rosenblueth, E. (1980). Characteristics of earthquakes. In *Design of Earthquake Resistant Structures*, Ed. E. Rosenblueth, John Wiley & Sons, New York.
- Sadigh, K., Chang, C.Y., Abrahamson, N.A., Chiou, S.J. and Power, M.S. (1993). Specification of long-period ground motions: Updated attenuation relationships for rock site conditions and adjustment factors for near-fault effects. *Proceedings, ATC-17-1 Seminar on Seismic Isolation, Passive Energy Dissipation, and Active Control*, San Francisco, 1, 11–23.
- Sadigh, K., Chang, C.Y., Egan, J.A., Makdisi, F. and Youngs, R.R. (1997). Attenuation relationships for shallow crustal earthquakes based on California strong motion data. *Seismological Research Letters*, 68, 180–189.
- Savy, J.B., Bernreuter, D.L. and Chen, J.C. (1987). A methodology to correct for effect of the local site characteristics in seismic hazard analyses In *Ground Motion and Engineering Seismology*, Ed. A.S. Cakmak, Elsevier, Amsterdam, 243–255.
- SEAOC (1999). *Recommended Lateral Force Requirements and Commentary*, 7th ed., Seismology Committee, Structural Engineers Association of California.
- Seed, H.B., Ugas, C. and Lysmer, J. (1976). Site-dependent spectra for earthquake-resistant design. *Bulletin of the Seismological Society of America*, 66, 221–243.
- Seekins, L.C., Brady, A.G., Carpenter, C. and Brown, N. (1992). Digitized strong-motion accelerograms of North and Central American Earthquakes 1933–1986. CD-ROM, U.S. Geological Survey *Digital Data Series (DDS)* #7.
- Shin, T.C., Kuo, K.W., Lee, W.H.K., Teng, T.L. and Tsai, Y.B. (2000). A preliminary report on the 1999 Chi-Chi (Taiwan) earthquake. *Seismological Research Letters*, 71, 24–30.

- Silva, W. (1997). Characteristics of vertical strong ground motions for applications to engineering design. NCEER-97-0010, National Center for Earthquake Engineering Research, Buffalo, New York.
- Somerville, P. (1998). Development of an improved representation of near-fault ground motions. *Proceedings, SMIP98 Seminar on Utilization of Strong-Motion Data*, Oakland, California, 1–20.
- Somerville, P. (2000). New developments in seismic hazard estimation. *Proceedings, 6th International Conference on Seismic Zonation*, Palm Springs, California, 25 p.
- Somerville, P., Collins, N., Abrahamson, N., Graves, R. And Saikia, C. (2001). Ground motion attenuation relations for the central and eastern United States. *U.S. Geological Survey, Award 99HQGR0098*, final report.
- Somerville, P.G., Smith, N.F., Graves, R.W. and Abrahamson, N.A. (1997). Modification of empirical strong ground motion attenuation relations to include the amplitude and duration effects of rupture directivity. *Seismological Research Letters*, 68, 199–222.
- Spudich, P., Joyner, W.B., Lindh, A.G., Boore, D.M., Margaris, B.M. and Fletcher, J.B. (1999). SEA99: A revised ground motion prediction relation for use in extensional tectonic regimes. *Bulletin of the Seismological Society of America*, 89, 1156–1170.
- Stewart, J.P. (2000). Variations between foundation-level and free-field earthquake ground motions. *Earthquake Spectra*, 16, 511–532.
- Stewart, J.P., Chiou, S. J., Bray, J.D., Graves, R.W., Somerville, P.G. and Abrahamson, N.A. (2001). Ground motion evaluation procedures for performance-based design. PEER 2001/09, Pacific Earthquake Engineering Research Center, University of California, Berkeley.
- Stewart, J.P., Liu, A.H. and Choi, Y. (2003). Amplification factors for spectral acceleration in tectonically active regions. *Bulletin of Seismological Society of America*, 93, 332–352.
- Takahashi, Y., Rabins, M.J. and Auslander, D.M. (1972). *Control and Dynamic Systems*. Addison-Wesley Publishing Co., Reading, Massachusetts.
- Toro, G.R., Abrahamson, N.A. and Schneider, J.F. (1997). Model of strong ground motions from earthquakes in central and eastern North America: Best estimates and uncertainties. *Seismological Research Letters*, 68, 41–57.
- Travarasou, T., Bray, J.D. and Abrahamson, N.A. (2003). Empirical attenuation relationship for Arias intensity. *Earthquake Engineering and Structural Dynamics*, 32, 1133–1155.
- Trifunac, M.D. and Brady, A.G. (1975). A study on the duration of strong earthquake ground motion. *Bulletin of Seismological Society of America*, 65, 581–626.
- Tsai, Y.B. and Huang, M.W. (2000). Strong ground motion characteristics of the Chi-Chi, Taiwan earthquake of September 21, 1999. *Earthquake Engineering and Engineering Seismology*, 2, 1–21.
- Uang, C.M. (1991). Establishing R (or R_w) and C_d factors for building seismic provisions. *ASCE Journal of Structural Engineering*, 117, 19–28.
- Uang, C.M. and Bertero, V.V. (1988). Implications of recorded earthquake ground motions on seismic design of building structures. UCB/EERC-88/13, Earthquake Engineering Research Center, University of California, Berkeley.
- Uang, C.M. and Bertero, V.V. (1991). UBC seismic serviceability regulations: Critical review. *ASCE Journal of Structural Engineering*, 117, 2055–2068.
- Uang, C.M. and Bertero, V.V. (1990). Evaluation of seismic energy in structures. *Earthquake Engineering and Structural Dynamics*, 19, 77–90.
- UBC (1994). *Uniform Building Code* 1994 ed., Vol. 2, International Conference of Building Officials, Whittier, California.
- UBC (1997). *Uniform Building Code*. 1997 ed., Vol. 2, International Conference of Building Officials, Whittier, California.
- UBC-IBC Structural (2000). *UBC-IBC Structural Comparison and Cross Reference (1997-2000)*. International Conference of Building Officials, Whittier, California.
- United States Geological Survey (2002). Notes on the processing of digitally recorded data. [Http://nsmp.wr.usgs.gov/processing.html#notes](http://nsmp.wr.usgs.gov/processing.html#notes)

- Vidic, T., Fajfar, P. and Fischinger, M. (1994). Consistent inelastic design spectra: Strength and displacement. *Earthquake Engineering and Structural Dynamics*, 23, 507–521.
- Wald, D.J., Quitoriano, V., Heaton, T.H., Kanamori, H., Scrivner, C.W. and Worden, C.B. (1999). TriNet “shakemaps”: Rapid generation of peak ground motion and intensity maps for earthquakes in southern California. *Earthquake Spectra*, 15, 537–555.
- Watabe, M., Tohido, M., Chiba, O. and Fukuzawa, R. (1990). Peak accelerations and response spectra of vertical strong motions from near-field records in USA. *Proceedings, 8th Japan Earthquake Engineering Symposium*, 1, 301–306.
- Wells, D.L. and Coppersmith, K.J. (1994). New empirical relationships among magnitude, rupture length, rupture width, rupture area, and surface displacement. *Bulletin of the Seismological Society of America*, 84, 974–1002.
- Whittaker, D. and Jury, R.D. (2000). Seismic design loads for storage tanks. *Proceedings, 12th World Conference on Earthquake Engineering*, Paper No. 2376, Auckland, New Zealand.
- Wills, C.J. and Silva, W. (1998). Shear-wave velocity characteristics of geologic units in California. *Earthquake Spectra*, 14, 533–556.
- Wills, C.J., Petersen, M., Bryant, W.A., Reichle, M., Saucedo, G.J., Tan, S., Taylor, G. and Treiman, J. (2000). A site-conditions map for California based on geology and shear-wave velocity. *Bulletin of the Seismological Society of America*, 90, S187–S208.
- Youngs, R.R., Chiou, S.J., Silva, W.J. and Humphrey, J.R. (1997). Strong ground motion attenuation relationships for subduction zone earthquakes. *Seismological Research Letters*, 68, 58–73.
- Zoback, M.L. (1992). First- and second-order patterns of stress in the lithosphere: The world stress map project. *Journal of Geophysical Research*, 97, 11,703–11,728.

6

Methods of Analysis for Earthquake- Resistant Structures

6.1	Introduction.....	6-2
	Structural Analysis Procedures • Models of Structures	
	Loads and Boundary Conditions • Notation	
6.2	Equilibrium	6-6
	Node Equilibrium • Equilibrium of Basic System of Element	
	Forces • Lower Bound Theorem of Plastic Analysis	
6.3	Geometric Compatibility.....	6-11
	Displacement–Deformation Relationship under Large	
	Displacements • Linear Approximation of	
	Displacement–Deformation Relation • Compatibility	
	Relationship for Elements with Moment Releases	
6.4	Equilibrium in Deformed Configuration	6-16
6.5	Principle of Virtual Work	6-18
	Virtual Work Principles for the Structure • Virtual Work	
	Principles for an Element • Upper Bound Theorem of Plastic	
	Analysis • Example of Plastic Analysis	
6.6	Force–Deformation Relationships.....	6-23
	Section Response • Material Models	
6.7	Frame Elements	6-28
	Basic Relationships • Concentrated Plasticity Elements •	
	Distributed Inelasticity Elements	
6.8	Solution of Equilibrium Equations.....	6-36
	Newton–Raphson Iteration • Load Incrementation • Load	
	Factor Control during Incrementation • Load Factor	
	Control during Iteration • Structure State	
	Determination • State Determination of Elements with	
	Force Formulation • Nonlinear Solution of Section State	
	Determination	
6.9	Nonlinear Geometry and P-Δ Geometric Stiffness.....	6-43
	Resisting Forces and Element Tangent Stiffness Matrix •	
	Geometric Stiffness Matrix • P-Δ Geometric Stiffness	
6.10	Examples of Nonlinear Static Analysis	6-47
6.11	Dynamic Analysis.....	6-52
	Free Vibration • Modal Analysis for Linear Response •	
	Earthquake Excitation • Numerical Integration of	
	Equations of Motion for Linear Response • Numerical	
	Integration of Equations of Motion for Nonlinear Response	
6.12	Applications of Linear and Nonlinear Dynamic	
	Analysis.....	6-57
6.13	Conclusions.....	6-61
6.14	Future Challenges	6-62

Filip C. Filippou

Gregory L. Fenves

6.1 Introduction

This chapter presents structural analysis methods for designing earthquake-resistant structures. The focus is on structural models consisting of frame elements for modeling beam, column and brace members, which is the common type of modeling for buildings and bridges in current earthquake engineering practice. Structural analysis software often used in engineering design incorporates one or more of the methods of analysis presented in this chapter. The chapter discusses sources of nonlinear material and geometric behavior. It covers plastic analysis methods for collapse load and plastic deformation determination under the assumption of elastic-perfectly plastic material response. It briefly describes nonlinear hysteretic material models and uses these to derive the hysteretic response of sections under the interaction of biaxial moment and axial force. This chapter further discusses concentrated inelasticity frame elements, and compares two approaches for the derivation of the force-deformation relation of distributed inelasticity frame elements. The effect of nonlinear geometry is presented in the general form of the corotational formulation for frame elements under large displacements. Consistent approximations are introduced to arrive at simplified nonlinear geometry methods that suffice in many design situations, in particular, the so-called $P\Delta$ geometric stiffness. The chapter concludes with a discussion of linear and nonlinear dynamic response under ground excitation. The key features of the analysis methods in this chapter are illustrated with examples of static and dynamic nonlinear response of components and structures. The chapter concludes with a few important observations and a discussion of future challenges for improving structural analysis procedures for earthquake-resistant design.

6.1.1 Structural Analysis Procedures

The analysis of a structural system to determine the deformations and forces induced by applied loads or ground excitation is an essential step in the design of a structure to resist earthquakes. A structural analysis procedure requires: (i) a model of the structure, (ii) a representation of the earthquake ground motion or the effects of the ground motion and (iii) a method of analysis for forming and solving the governing equations. There is a range of methods from a plastic analysis to a sophisticated nonlinear, dynamic analysis of a detailed structural model that can be used, depending on the purpose of the analysis in the design process. This chapter presents structural analysis procedures for earthquake-resistant design. The focus is on methods for structural models consisting of frame elements for modeling beam, column and brace members, which is the common type of modeling for buildings and bridges. Structural walls are often modeled with beam elements at the centerline and rigid joint offsets, even though this does not properly account for the uplift effect that may be important for this type of lateral load resisting system.

An important decision in a structural analysis is to assume whether the relationship between forces and displacements is linear or nonlinear. Linear analysis for static and dynamic loads has been used in structural design for decades. Nonlinear analysis methods are widely used, because emerging performance-based guidelines require representation of nonlinear behavior. There are two major sources of nonlinear behavior. The first is a nonlinear relationship between force and deformation resulting from material behavior such as ductile yielding, stiffness and strength degradation or brittle fracture. The second type of nonlinear behavior is caused by the inclusion of large displacements in the compatibility and equilibrium relationships. This chapter presents the nonlinear methods of analysis for both types of behavior. Linear methods are a special case.

An earthquake analysis generally includes gravity loads and a representation of the ground motion at the site of the structure. Earthquake ground motion induces the mass in a structure to accelerate, and the resulting response history can be computed by dynamic analysis methods. In many design procedures it is common to perform a dynamic analysis with a response spectrum representation of the ground motion expected at the site (Chopra, 2001). For response history analysis, several analyses with different ground motion histories of the earthquake hazard are generally required. (See Chapter 5 for more information about the definition of earthquake ground motion in a structural analysis.)

TABLE 6.1 Structural Analysis Procedures for Earthquake-Resistant Design

Category	Analysis Procedure	Force–Deformation Relationship	Displacements	Earthquake Load	Analysis Method
Equilibrium Linear	Plastic Analysis Procedure	Rigid-plastic	Small	Equivalent lateral load	Equilibrium analysis
	Linear Static Procedure	Linear	Small	Equivalent lateral load	Linear static analysis
	Linear Dynamic Procedure I	Linear	Small	Response spectrum	Response spectrum analysis
Nonlinear	Linear Dynamic Procedure II	Linear	Small	Ground motion history	Linear response history analysis
	Nonlinear Static Procedure	Nonlinear	Small or large	Equivalent lateral load	Nonlinear static analysis
	Nonlinear Dynamic Procedure	Nonlinear	Small or large	Ground motion history	Nonlinear response history analysis

For many design procedures, however, it is common to use equivalent static loads that represent the effects of the earthquake on the structure. Traditional design procedures use a static linear analysis with a response modification coefficient to represent the effects of ductile, nonlinear behavior. In contrast, newer design procedures utilize a nonlinear static (pushover) analysis to determine the force–displacement relationship for the structure, and the inelastic deformation of its members.

After a structural model and earthquake loading are defined, an analysis method is needed to compute the response. The governing equations are formed using equilibrium, compatibility and force–deformation relationships for the elements and the structure, and are expressed in terms of unknown displacements (or degrees of freedom, referred to as DOFs in this chapter). To elucidate the theory and provide a compact mathematical representation, the fundamental relationships are expressed using matrix algebra. Since the governing equations may have a large number of degrees of freedom, they must be solved numerically using a computer-based analysis method. Nearly all structural analyses for earthquake-resistant design are performed using software that incorporates one or more of the analysis methods presented in this chapter. Modern software generally includes graphical features for visualizing the forces and deformations computed from an analysis. Before using any new structural analysis software, the engineer should conduct an independent verification to ensure that the software provides correct solutions.

The structural analysis procedures used in earthquake-resistant design are summarized in Table 6.1. Recent guidelines for seismic rehabilitation of buildings pioneered the requirements for dynamic and nonlinear analysis procedures, particularly FEMA 356 (FEMA, 2000a) and the predecessor FEMA 273 (FEMA, 1997). The ATC-40 guidelines for reinforced concrete buildings (ATC, 1996b) emphasize the use of a nonlinear static (pushover) analysis procedure to define the displacement capacity for buildings. The classification of analysis procedures in Table 6.1 is generally applicable to design regulations for new buildings, such as in the 2000 NEHRP recommended provisions (FEMA, 2001) and recent guidelines for steel moment frame buildings (FEMA, 2000b, c) and for bridges (ATC, 1996a). These provisions and guidelines are required for the selection of the analysis procedure depending on the seismic design category, performance level, structural characteristics (e.g., regularity or complexity), response characteristics (e.g., the fundamental vibration period and participation of higher vibration modes), amount of data available for developing a model and confidence limits (in a statistical sense) for performance evaluation. Design provisions for structures with seismic isolation systems and supplemental energy dissipation generally require a dynamic analysis procedure.

The analysis procedures in Table 6.1 are in order of increasingly rigorous representation of structural behavior, but also increasing requirements for modeling and complexity of the analysis. As described in Section 6.2, plastic analysis only requires the equilibrium relationships, and is useful for capacity design procedures (Paulay and Priestley, 1992). For a given load distribution and flexural strength of members, plastic analysis gives the collapse load and the location of plastic hinges in members. The linear static procedure has been a traditional structural analysis method for earthquake-resistant design (UBC, 1997),

but it does not represent the nonlinear behavior or the dynamic response of a structure caused by an earthquake ground motion. The simplest dynamic analysis method is based on a linear model of the structure, which permits use of vibration properties (frequencies and mode shapes) and simplification of the solution with a modal representation of the dynamic response. An estimate of the maximum structural response can be obtained with response spectrum analysis, or the maximum can be computed by response history analysis with specific earthquake ground motion records. Linear dynamic analysis methods are covered in depth by Chopra (2001).

Increasingly, engineers are using, and design guidelines are requiring, nonlinear analysis in the design process, because a severe earthquake ground motion is expected to deform a structure into the inelastic range. Nonlinear analysis methods can provide the relationship between a lateral load representing the effect of the earthquake ground motion and the displacements of the structure and deformations of the members. The results are often presented as a pushover or capacity curve for the structure. More detailed response history of a structure (sometimes called the seismic demand) can be computed by nonlinear dynamic analysis methods, particularly the cyclic response, degradation and damage measures for the members.

For the earthquake analysis of many types of structures it is reasonable to assume that the foundation and soil are rigid compared to the structure itself and that the supports of the structure move in phase during an earthquake ground motion. Soil–structure interaction, as described in Chapter 4, modifies the input motion to a structure because of wave propagation and energy dissipation in the soil, however, this phenomenon is not discussed in this chapter. For two-dimensional analysis the ground motion is specified in the horizontal and vertical directions; the two horizontal and the vertical ground motion components are specified for three-dimensional analysis. The assumption of uniform ground motion may not be valid for long-span bridges because of wave passage effects, differential site response and incoherence of the ground motion.

6.1.2 Models of Structures

A structural analysis is performed on a model of the structure — not on the real structure — so the analysis can be no more accurate than the assumptions in the model. The model must represent the distribution and possible time variation of stiffness, strength, deformation capacity and mass of the structure with accuracy sufficient for the purpose of the analysis in the design process.

All structures are three dimensional, but it is important to decide whether to use a three-dimensional model or simpler two-dimensional models. The analysis methods are the same whether the model is two-dimensional or three-dimensional. Generally, two-dimensional models are acceptable for buildings with regular configuration and minimal torsion; otherwise, a three-dimensional model is necessary with a representation of the floor diaphragms as rigid or flexible components. Analysis of bridges is generally based on three-dimensional models, although nonlinear analysis is typically used for two-dimensional models of bridge piers (ATC, 1996a, Priestley et al., 1996).

A structural model of a frame consists of an assembly of frame elements connected at nodal points (or nodes) in a global coordinate system, as illustrated in Figure 6.1. The geometry of the structural model is described by the position of the nodes in a global coordinate system, denoted by X, Y and Z. In the graphic representations of the structural model, nodes have a small black square (see Figure 6.1).

Two nodes define a frame element, which may be either straight or curved. This chapter is limited to straight elements because a curved element can always be approximated by several straight elements at the expense of increased modeling effort and computational cost. The element geometry is established in a local coordinate system x, y, z (see Figure 6.1). As will be shown later in this chapter, the force–deformation relationship for the element is obtained from the integration of functions of x along the element axis between the nodes. These functions represent the section forces (such as shear, bending and axial forces), the corresponding section deformations and the relationship between section forces and deformations.

The element response can be completely described by the relation between the force vector \mathbf{p} and the displacement vector \mathbf{u} . For three-dimensional (3d) elements, the force vector has 12 components: at each

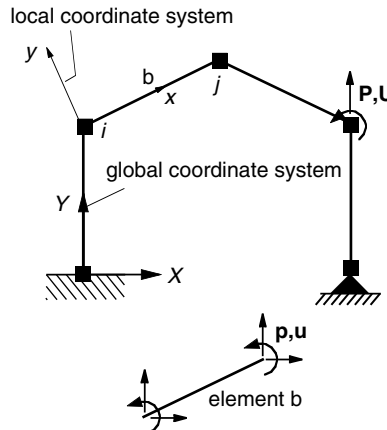


FIGURE 6.1 Local and global reference systems and notation.

node there are three forces in the local x, y, z coordinate system and three moments about the axes of the local coordinate system. In the two-dimensional (2d) case there are two forces and one moment at each node, providing six components of the force vector. The displacement vector is defined in an analogous manner and includes translations in the direction of the local axes and rotations about the local axes at each node.

Before concluding this section on structural modeling with frame elements, it is worth noting that for many structural systems the joints connecting members may be substantial in size and have modes of deformation that affect the system behavior. In such cases the model needs to account for at least the finite size of the joint region. The topic of joint deformation is more advanced than the scope of this chapter but models for joints can be included in the analysis methods presented herein.

Finite element methods with continuum elements (Bathe, 1995) can provide a more refined distribution of stress and strain in solid, plate and shell models of structural components such as walls, diaphragms and joints, but with the exception of walls, this level of refinement is generally not warranted for earthquake-resistant design. This chapter does not discuss the details of finite element methods for continuum elements, although most of the solution methods are applicable for models that include continuum finite elements as well as frame elements.

6.1.3 Loads and Boundary Conditions

Loads are specified forces applied to elements or nodes. Gravity loads may be applied to elements or considered as nodal loads depending on the gravity load path. The vector of nodal loads for a structure is denoted by \mathbf{P} , with six components of force at each node for 3d problems and three components for 2d problems. In contrast with nodal loads, element loads are included in the element force–deformation relationship as distributed loads $\mathbf{w}(x)$ defined in the local coordinate system for the element.

Each node undergoes translations and rotations that can be combined into a displacement vector of three translations and three rotations at each node in the 3d case. The displacements of all nodes are collected into a single displacement vector \mathbf{U} for the entire model in which each component is a degree of freedom. We separate the set of all global DOFs into two subsets: the DOFs with unknown displacement values and the DOFs with specified displacement value. Each DOF in the model must be included in one of the two sets. The unknown displacements are called the free DOFs and are denoted by \mathbf{U}_f . The second set of displacements corresponds to the restrained DOFs and is denoted by \mathbf{U}_d . The restrained DOFs are generally assigned a value of zero to indicate a fixed displacement, but nonzero support displacement problems can be considered. The selection of restrained displacements at the supports is an important step in the structural modeling, and the supports of a model are commonly identified with the symbols shown in Figure 6.2 for typical 2d cases. The arrows in Figure 6.2 indicate the restrained DOFs, and thus the corresponding support reactions of each support type.

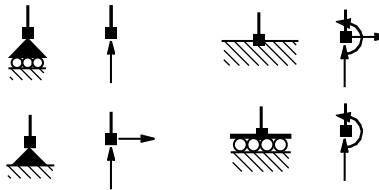


FIGURE 6.2 Typical support symbols for the 2d case.

TABLE 6.2 Notation for Structural Analysis

Quantity	Symbol
(a) Symbols for Structural (Global) System	
Global coordinate system for structure	X,Y,Z
Displacements of structure at DOFs	U
Applied loads to structure DOFs	P
Resisting forces for structure at DOFs	P _r
Structure equilibrium matrix for DOFs	B
Structure compatibility matrix for DOFs	A
Structural stiffness, mass and damping matrices	K, M, C
(b) Symbols for Elements	
Local coordinate system for element	x,y,z
Basic element deformations	v
Element nodal displacements in local coordinate system and global coordinate system	ū, u
Basic element forces	q
Element nodal forces in local and global coordinate system	Ȑp, p ^{el}
Basic element flexibility and stiffness matrices	f, k

Since the displacements are partitioned into two sets, so is the nodal force vector, \mathbf{P} . The nodal forces at the free DOFs of the model are specified as nodal loads, and are denoted by \mathbf{P}_f . For earthquake analysis this would normally include only the gravity loads with all other nodal loads equal to zero. The forces at the restrained DOFs are the support reactions and are denoted by \mathbf{P}_d . These can be evaluated once the equations for the free DOFs are solved.

6.1.4 Notation

A consistent notation assists in elucidating the fundamental structural analysis concepts. In general, uppercase symbols are matrices or vectors representing the structural system (Table 6.2a), whereas lowercase symbols represent quantities associated with individual elements (Table 6.2b). Vectors and matrices are written in boldface.

6.2 Equilibrium

All structural analysis methods in Table 6.1 require satisfaction of equilibrium. This section presents the fundamental equilibrium relationships for nodes and elements in the model.

6.2.1 Node Equilibrium

With imaginary cuts around each node we separate nn nodal-free bodies and ne element-free bodies, as shown in Figure 6.3, in which nn is the number of nodes and ne is the number of elements in the model. Three force equilibrium equations and three moment equilibrium equations must be satisfied for each

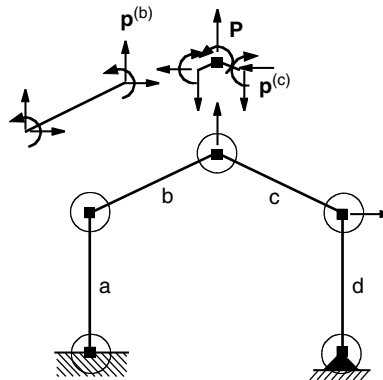


FIGURE 6.3 Node and element free body equilibrium.

node-free body for the 3d case and two force equilibrium and one moment equilibrium equations for a node in the 2d case. Using the 2d case for simplicity and examining the nodal equilibrium equations, it is apparent that the equilibrium equations involve the summation of element forces at a node when all element forces are expressed in the global coordinate system. An element is identified with a superscript in parentheses and the correspondence between element DOF and global DOF can be supplied by an array, known as an *id*-array with the number of entries equal to the number of element DOFs. With the relationship between element and global DOF for each element, the force vector for an element *el* can be mapped to the contribution of the element force vector to the global resisting force vector, represented symbolically as $\mathbf{p}^{(el)} \rightarrow \mathbf{P}_{r,id}^{(el)}$, in which $\mathbf{P}_{r,id}^{(el)}$ has nonzero terms corresponding to the forces in the element, as represented by the *id*-array. Using this relationship the nodal equations of static equilibrium are written as:

$$\mathbf{P} - \mathbf{P}_r = \mathbf{0} \quad \text{or} \quad \begin{pmatrix} \mathbf{P}_f \\ \mathbf{P}_d \end{pmatrix} - \mathbf{P}_r = \mathbf{0} \quad \text{with} \quad \mathbf{P}_r = \sum_{el} \mathbf{P}_{r,id}^{(el)} = \mathbf{A}_{el} \mathbf{p}^{(el)} \quad (6.1)$$

Equation 6.1 states that the applied forces \mathbf{P} consisting of forces at free DOFs \mathbf{P}_f and forces at restrained DOFs \mathbf{P}_d are in equilibrium with the resisting forces \mathbf{P}_r , which are the sum of the element contributions $\mathbf{p}^{(el)}$. The mapping of element DOFs to global DOFs followed by summation of the element contributions, as denoted by the symbol \mathbf{A}_{el} , indicates assembly of all element contributions, which is known as the direct assembly procedure.

Equation 6.1 assumes that the loading is applied so slowly that the resulting accelerations at the free DOFs can be neglected. If this is not the case, the equations of static equilibrium are extended using Newton's second law stating that

$$\mathbf{P} - \mathbf{P}_r = \mathbf{M} \ddot{\mathbf{U}}^t \quad (6.2)$$

in which $\ddot{\mathbf{U}}^t$ is the acceleration with respect to a fixed frame of reference. Equation 6.2 is also known as the equation of motion for a structural model. It is worthwhile to state explicitly the dependence of the resisting forces on the displacement and displacement rate (velocity) vector.

$$\mathbf{P}_r = \hat{\mathbf{P}}_r(\mathbf{U}, \dot{\mathbf{U}})$$

which allows for velocity-dependent resistance (viscous damping).

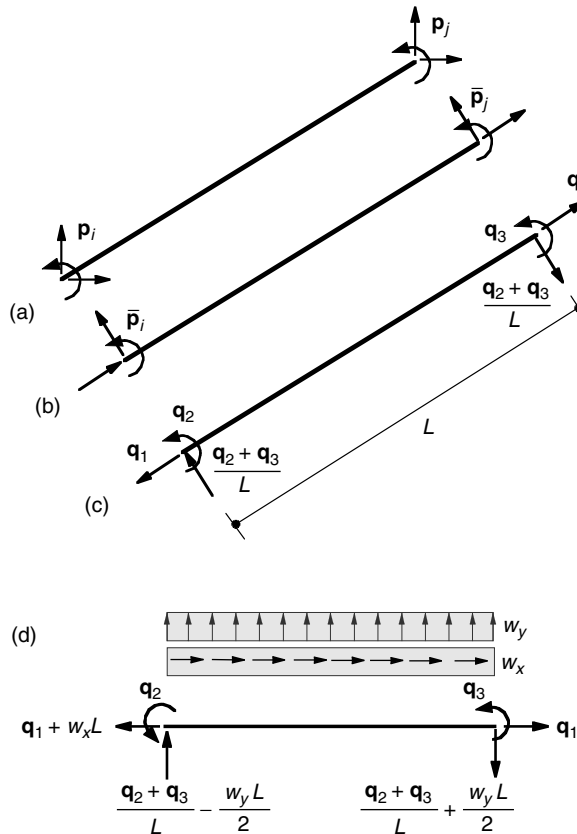


FIGURE 6.4 Element forces in global, local and basic reference systems.

6.2.2 Equilibrium of Basic System of Element Forces

Turning attention to the free body for a 3d frame element, there are 12 unknown forces, with six at the imaginary cuts at each end of the element but only six independent equilibrium equations. Figures 6.4a and b show the end forces in the global and local coordinate systems for a 2d frame element, with the quantities in the local system denoted by a bar. A rotation matrix can be used to transform vectors between the two coordinate systems.

Because the element forces need to satisfy the equilibrium equations they are not independent. We select a subset of element forces and express the remainder in terms of the subset to assure that the equilibrium of the free body is satisfied. The independent element forces are called the basic forces, \mathbf{q} . In the 2d case there are three basic forces, and in this chapter we select the axial force and the two end moments, as shown in Figure 6.4c. The three equilibrium equations for the element-free body are used to express the remaining element forces in terms of the basic forces.

The equilibrium equations can be satisfied in the undeformed configuration, if the displacements are small relative to the dimensions of the structure. However, if the displacements are large, the equilibrium needs to be satisfied in the deformed configuration. The latter leads to nonlinear geometric effects, which are presented after the geometric compatibility relationships are defined for large displacements. Equilibrium of an element-free body in the undeformed configuration is shown in Figure 6.4c and stated as follows:

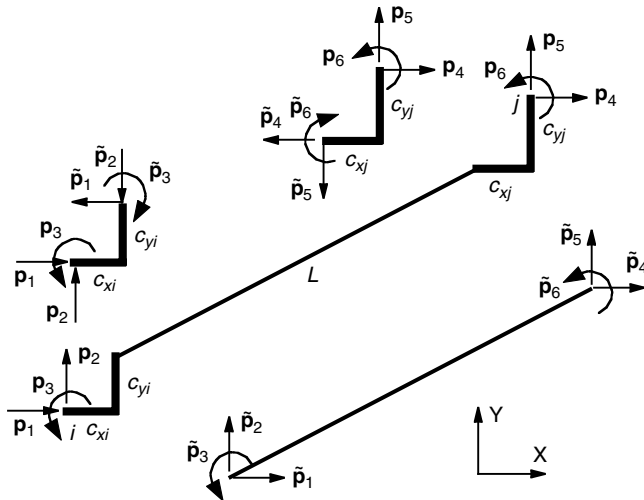


FIGURE 6.5 Force transformation (equilibrium) for rigid-end offsets.

$$\bar{p}_1 = -q_1$$

$$\bar{p}_2 = \frac{q_2 + q_3}{L}$$

$$\bar{p}_3 = q_2$$

$$\bar{p}_4 = q_1$$

$$\bar{p}_5 = -\frac{q_2 + q_3}{L}$$

$$\bar{p}_6 = q_3$$

or, $\bar{p} = \begin{pmatrix} \bar{p}_1 \\ \bar{p}_2 \\ \bar{p}_3 \\ \bar{p}_4 \\ \bar{p}_5 \\ \bar{p}_6 \end{pmatrix} = \begin{bmatrix} -1 & 0 & 0 \\ 0 & \frac{1}{L} & \frac{1}{L} \\ 0 & 1 & 0 \\ 1 & 0 & 0 \\ 0 & -\frac{1}{L} & -\frac{1}{L} \\ 0 & 0 & 1 \end{bmatrix} \begin{pmatrix} q_1 \\ q_2 \\ q_3 \end{pmatrix} = b q$

If element loads are included, 6.3 is modified to include the effect of the element loads,

$$\bar{p} = b q + \bar{p}_w$$

where \bar{p}_w is the vector of element forces due to the loads on the element. Figure 6.4d shows these forces for the case of uniform transverse and longitudinal distributed loads. The matrix b represents the equilibrium transformation matrix from the basic system to the complete system of element forces in local coordinates. We noted earlier that the transformation of the element end forces from the local to the global coordinate system involves a rotation transformation of the end forces at each end, expressed by $p = b_r \bar{p}$. Combining 6.3 with the rotation to the global coordinate system gives the element forces in the global system expressed in terms of the basic forces and element loads:

$$p = b_r b q + b_r \bar{p}_w \quad (6.4)$$

The statement of element equilibrium can be extended to other cases, such as for rigid-end offsets to represent finite joint size. The element forces at the ends of the deformable portion of the element are denoted by \tilde{p} , and the equilibrium of the rigid-end offsets is shown in Figure 6.5. The equilibrium relationship is $p = b_r \tilde{p}$,

and noting that $\tilde{\mathbf{p}} = \mathbf{b}_r \mathbf{b} \mathbf{q} + \mathbf{b}_r \bar{\mathbf{p}}_w$, the element forces become $\mathbf{p} = \mathbf{b}_j \mathbf{b}_r \mathbf{b} \mathbf{q} + \mathbf{b}_j \mathbf{b}_r \bar{\mathbf{p}}_w$. In a compact notation the element equilibrium in the undeformed configuration can be stated as

$$\mathbf{p} = \mathbf{b}_g \mathbf{q} + \mathbf{p}_w \quad \text{with } \mathbf{b}_g = \mathbf{b}_j \mathbf{b}_r \mathbf{b} \quad \text{and } \mathbf{p}_w = \mathbf{b}_j \mathbf{b}_r \bar{\mathbf{p}}_w \quad (6.5)$$

in which the equilibrium matrix \mathbf{b}_g transforms the basic forces to the element end forces in global coordinates and \mathbf{p}_w accounts for the effect of element loading. The equilibrium matrix \mathbf{b}_g is made up of at least the product $\mathbf{b}_r \mathbf{b}$. The transformation of the dependent element forces $\bar{\mathbf{p}}_w$ in 6.4 to the global coordinate system includes at least the rotation matrix \mathbf{b}_r . After substituting 6.5 into the assembly operation in 6.1, the global resisting force vector is

$$\mathbf{P}_r = \mathbf{A}_{el} \mathbf{p}^{(el)} = \mathbf{A}_{el} \left(\mathbf{b}_g^{(el)} \mathbf{q}^{(el)} + \mathbf{p}_w^{(el)} \right) \quad (6.6)$$

For convenience of later discussion in this chapter, the basic forces of all elements are collected into a single vector \mathbf{Q} . After noting that the assembly operation in 6.6 only affects the rows of \mathbf{p} and thus only the rows of \mathbf{b}_g and \mathbf{p}_w , 6.6 can be written in the compact form,

$$\mathbf{P}_r = \mathbf{B} \mathbf{Q} + \mathbf{P}_w \quad (6.7)$$

The structure equilibrium matrix \mathbf{B} results from the assembly of the rows of \mathbf{b}_g while the columns are collected from each element. Partitioning 6.7 into free and restrained DOFs, as indicated in 6.1, the equilibrium of the structure is represented by

$$\begin{pmatrix} \mathbf{P}_f \\ \mathbf{P}_d \end{pmatrix} = \begin{pmatrix} \mathbf{B}_f \\ \mathbf{B}_d \end{pmatrix} \mathbf{Q} + \mathbf{P}_w \quad (6.8)$$

Equation 6.8 is very significant in structural analysis because it must be satisfied for any frame structure, made of linear or nonlinear material, under the limitation that equilibrium is satisfied in the undeformed configuration. The number of equilibrium equations in the free partition, nf , is the number of rows in \mathbf{B}_f , and the number of columns is the number of unknown basic forces, nq . For a statically determinate structure, nf and nq are equal, and \mathbf{B}_f is square and invertible, if the structure has a stable equilibrium configuration. Hence, for a statically determinate structure, given the applied forces at the free DOFs, \mathbf{P}_f , we can solve the first partition in 6.8 for the unknown basic forces \mathbf{Q} . If the support reactions are desired, the second partition in 6.8 can be evaluated for \mathbf{P}_d .

For a statically indeterminate structure the number of unknown basic element forces, nq , is greater than the number of equilibrium equations, nf , at the free DOFs. Thus, the size of the \mathbf{B}_f matrix gives the degree of static indeterminacy NOS = $nq - nf$. In statistically indeterminate structures, the equilibrium equations must be satisfied, but they are not sufficient to give a unique solution.

6.2.3 Lower Bound Theorem of Plastic Analysis

Since structures designed to resist earthquakes are rarely statically determinate, the most significant application of the structural equilibrium equations in 6.8 is for plastic analysis (Livesley, 1975). Assuming perfectly plastic material response requires that the basic element forces satisfy the plastic condition $|\mathbf{Q}| \leq \mathbf{Q}_p$, where \mathbf{Q}_p are the plastic capacities of the elements. The applied forces at the free DOFs in 6.8 are written as the product of a load factor λ and a reference force vector \mathbf{P}_{ref} that gives the distribution of the applied loads, such as the equivalent lateral earthquake loads. The lower bound theorem of plastic analysis states that the collapse load factor λ_c is the largest load factor that satisfies the equilibrium equations in 6.8 and the plastic condition. We can write this as follows:

$$\lambda_c = \max \lambda \quad \text{for} \quad \lambda P_{\text{ref}} = B_f Q \quad \text{and} \quad |Q| \leq Q_p \quad (6.9)$$

Considering that the plastic capacity may be different under positive basic forces than under negative ones, and collecting the unknowns of the problem λ and Q into a single vector, the equations in 6.9 are written in the compact form of a linear programming problem:

$$\lambda_c = \max \begin{bmatrix} 1 & 0 \end{bmatrix} \begin{pmatrix} \lambda \\ Q \end{pmatrix} \quad \text{for} \quad \begin{bmatrix} P_{\text{ref}} & -B_f \end{bmatrix} \begin{pmatrix} \lambda \\ Q \end{pmatrix} = 0 \quad \text{and} \quad \begin{bmatrix} 0 & I \\ 0 & -I \end{bmatrix} \begin{pmatrix} \lambda \\ Q \end{pmatrix} \leq \begin{pmatrix} Q_p^+ \\ Q_p^- \end{pmatrix} \quad (6.10)$$

Q_p^+ is the plastic capacity for a positive basic force and Q_p^- is the capacity for a negative basic force, respectively (both in absolute value), and I is the $nq \times nq$ identity matrix. The linear programming problem in 6.10 can be readily solved using the simplex method with widely available mathematical software packages such as Matlab® or Mathcad®.

The solution of the linear programming problem in 6.10 yields a unique collapse load factor λ_c according to the lower bound theorem of plastic analysis. Even though the collapse load factor is unique, the basic forces at collapse Q_c are unique only if a complete collapse mechanism forms. This requires that NOS+1 basic forces reach the plastic capacity (in other words, that NOS+1 plastic hinges form), where NOS is the degree of static indeterminacy. This requirement derives from the equilibrium equations in 6.10, i.e., from the requirement that

$$\begin{bmatrix} P_{\text{ref}} & -B_f \end{bmatrix} \begin{pmatrix} \lambda_c \\ Q_c \end{pmatrix} = 0 \quad (6.11)$$

There are $nq+1$ unknowns and nf available equations of equilibrium in 6.11. Because $\text{NOS} = nq - nf$, there are NOS+1 more unknowns than available equations of equilibrium. With the value at NOS+1 basic forces equal to the corresponding plastic capacity at collapse, there are as many unknowns in 6.11 as the number of equilibrium equations. A partial mechanism forms if fewer than NOS+1 basic forces reach the plastic capacity. In this case, there exists an infinite number of combinations of the remaining basic forces that satisfy the equilibrium equations in 6.11. A unique solution can only be obtained with an additional assumption about the force-deformation behavior of the elements before reaching the plastic capacity, which we will pursue later in this chapter.

6.3 Geometric Compatibility

The statement of geometric compatibility is analogous to the process of establishing the equilibrium equations of the structural model. Each node can undergo three translations and three rotations in the 3d case; for the 2d case each node undergoes two translations and one rotation. The displacements of all nodes in the model are collected in the displacement vector \mathbf{U} . From the compatibility between elements and nodes, the displacements at the end of an element are equal to the corresponding DOF displacements at the nodes (see Figure 6.6). This correspondence between global and element DOFs is provided again by the *id*-array of each element, and the compatibility can be written symbolically as

$$\mathbf{u}^{(el)} = \mathbf{U}_{id} \quad (6.12)$$

Equation (6.12) indicates that an extraction from the global displacement vector \mathbf{U} of only the degrees of freedom corresponding to the entries in the *id*-array of the element *el* takes place. The length of the vectors in 6.12 is, consequently, equal to the number of element DOFs.

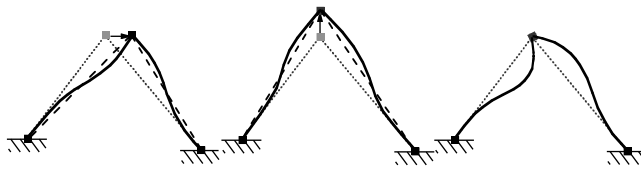


FIGURE 6.6 Compatibility between nodal and element end displacements.

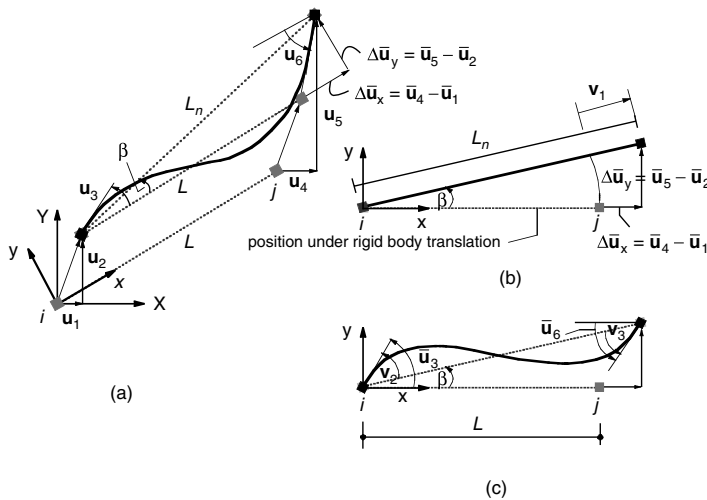


FIGURE 6.7 Deformed configuration of two-node one-dimensional element under large displacements.

As described in Section 6.1.3, the displacement vector for the structure is partitioned into free DOFs \mathbf{U}_f , which are unknown at the start of the analysis, and the displacements at the restrained DOFs \mathbf{U}_d , which are specified.

6.3.1 Displacement–Deformation Relationship under Large Displacements

Figure 6.7 shows a two-node frame element in the undeformed and deformed configuration under given end displacements. Since the rigid-body displacement of the element does not generate element deformations, Figure 6.7 shows three stages for representing the relationship between displacement and deformation. Figure 6.7a provides the overview of the entire process and identifies the rigid-body translation of the element. The relative displacements $\Delta\bar{u}_x$ and $\Delta\bar{u}_y$ in the local reference system are convenient for describing the relative position of node j with respect to node i . This relative translation results in an extension v_1 of the element in Figure 6.7b. As long as the ends follow the rigid-body rotation of the element axes through the angle β , no other deformation arises in Figure 6.7b, as illustrated by the rotation of the black squares representing the end nodes. Since the end rotations are independent DOFs, each end is subjected to an additional rotation past angle β and the element can deform, as shown in Figure 6.7c. The rotation of the end tangent to the deformed shape relative to the chord line for the element results from flexural deformation. There are two rotations caused by the flexural deformations, v_2 and v_3 , in Figure 6.7c, one at each element end. Counterclockwise rotations measured from the chord to the tangent are positive, consistent with the sign convention for the end moments.

With the definition of element deformations, v , it is now possible to derive the relationship between the element deformations and the end displacements, \bar{u} , in the local coordinate system. Using Figures 6.7b and 6.7c, the element deformations for the general case of large displacements and moderate deformations can be given as

$$\begin{aligned} v_1 &= \frac{1}{2L} (L_n^2 - L^2) \\ v_2 &= \bar{u}_3 - \beta \\ v_3 &= \bar{u}_6 - \beta \end{aligned} \quad (6.13)$$

$$\text{with } L_n = \sqrt{(L + \Delta \bar{u}_x)^2 + (\Delta \bar{u}_y)^2} \quad (6.14)$$

$$\beta = \arctan \frac{\Delta \bar{u}_y}{L + \Delta \bar{u}_x}$$

In 6.13 we have used the definition of the Lagrange strain for the length change of the element. In a typical structural analysis for earthquake engineering, the engineering strain is a sufficient approximation, so the extension is $v_1 = L_n - L$. The arctan function when expanded by a Taylor series about the point $\Delta \bar{u}_x = 0, \Delta \bar{u}_y = 0$ gives for the chord rotation:

$$\beta = \frac{\Delta \bar{u}_y}{L} \left[1 - \frac{\Delta \bar{u}_x}{L} + \dots \right]$$

Similarly, expansion of the first equation in 6.13 gives the change in length of the element:

$$v_1 = \Delta \bar{u}_x + \frac{1}{2} \frac{\Delta \bar{u}_x^2}{L} + \frac{1}{2} \frac{\Delta \bar{u}_y^2}{L}$$

Factoring L out on the right-hand side of the above expression gives

$$v_1 = L \left[\frac{\Delta \bar{u}_x}{L} + \frac{1}{2} \left(\frac{\Delta \bar{u}_x}{L} \right)^2 + \frac{1}{2} \left(\frac{\Delta \bar{u}_y}{L} \right)^2 \right] \quad (6.15)$$

In earthquake engineering applications the axial strain $\Delta \bar{u}_x / L$ has values of order 10^{-3} to 10^{-2} . In this case the first quadratic term on the right-hand side of 6.15 is of order 10^{-6} to 10^{-4} and can be neglected.

The relative transverse displacement (commonly called the drift), $\Delta \bar{u}_y / L$, is of order 10^{-2} to 10^{-1} , so that the second quadratic term in 6.15 can be of the same order as the linear term. In such situations the element deformation should be approximated with

$$v_1 = L \left[\frac{\Delta \bar{u}_x}{L} + \frac{1}{2} \left(\frac{\Delta \bar{u}_y}{L} \right)^2 \right] \quad (6.16)$$

The relation between the displacement components in the global and the local coordinate systems uses the rotation transformation for the translation components, whereas the rotations in the plane are not affected. The rotation angle for the transformation of the translation components corresponds to the angle of the undeformed element x -axis relative to the global X -axis (note that the positive element x -axis points from node i to node j). The translation components at each element end are transformed independently. The transformation of the end displacements is expressed symbolically by $\bar{u} = a_r u$.

6.3.2 Linear Approximation of Displacement–Deformation Relation

In the cases where the relative transverse displacement of the element, $\frac{\Delta \bar{u}_y}{L}$, is of order 10^{-2} or less, the quadratic term in 6.16 can be neglected and a linear compatibility relation remains $v_1 = \Delta \bar{u}_x$. In the expression for the angle β the term $\frac{\Delta \bar{u}_x}{L}$ is very small relative to unity and can be neglected in any case. With these approximations, the compatibility relations between element deformations and end displacements in the local coordinate system become linear:

$$\begin{aligned} v_1 &= \Delta \bar{u}_x = \bar{u}_4 - \bar{u}_1 \\ v_2 &= \bar{u}_3 - \frac{\Delta \bar{u}_y}{L} = \bar{u}_3 - \frac{\bar{u}_5 - \bar{u}_2}{L} \quad \text{or} \quad \mathbf{v} = \begin{pmatrix} v_1 \\ v_2 \\ v_3 \end{pmatrix} = \begin{bmatrix} -1 & 0 & 0 & 1 & 0 & 0 \\ 0 & \frac{1}{L} & 1 & 0 & -\frac{1}{L} & 0 \\ 0 & \frac{1}{L} & 0 & 0 & -\frac{1}{L} & 1 \end{bmatrix} \begin{pmatrix} \bar{u}_1 \\ \bar{u}_2 \\ \bar{u}_3 \\ \bar{u}_4 \\ \bar{u}_5 \\ \bar{u}_6 \end{pmatrix} = \mathbf{a} \bar{\mathbf{u}} \quad (6.17) \\ v_3 &= \bar{u}_6 - \frac{\Delta \bar{u}_y}{L} = \bar{u}_6 - \frac{\bar{u}_5 - \bar{u}_2}{L} \end{aligned}$$

Comparing 6.17 with 6.3, we note that the compatibility matrix \mathbf{a} is the transpose of the equilibrium matrix \mathbf{b} . The same relation holds for matrices \mathbf{a}_r and \mathbf{b}_r . If the element has rigid-end offsets, the compatibility matrix \mathbf{a}_j between the displacements at the ends of the deformable portion of the element and those at the ends of the complete element is similarly the transpose of the equilibrium matrix \mathbf{b}_j . The generality of this observation will be proven in the following section.

After combining the compatibility relationships, the element deformations can be expressed in terms of the element end displacements in the global coordinate system:

$$\mathbf{v} = \mathbf{a} \bar{\mathbf{u}} = \mathbf{a} \mathbf{a}_r \mathbf{a}_j \mathbf{u} = \mathbf{a}_g \mathbf{u} \quad (6.18)$$

The compatibility transformation matrix \mathbf{a}_g is the transpose of the equilibrium matrix \mathbf{b}_g in 6.5. With 6.12 the basic element deformations can now be expressed in terms of the global displacement vector components that correspond to the element as $\mathbf{v} = \mathbf{a}_g \mathbf{u} = \mathbf{a}_g \mathbf{U}_{id}$.

It is worthwhile to collect the element deformations into a single vector \mathbf{V} for the structural model. In this process the element compatibility matrices can be combined with the aid of the *id*-array to give the structural compatibility matrix \mathbf{A} . After this combination, the compatibility between the element deformations and the free and restrained DOFs at the nodes assumes the following form:

$$\mathbf{V} = \mathbf{A} \mathbf{U} = \begin{bmatrix} \mathbf{A}_f & \mathbf{A}_d \end{bmatrix} \begin{pmatrix} \mathbf{U}_f \\ \mathbf{U}_d \end{pmatrix} \quad (6.19)$$

From the process of forming the structural compatibility matrix \mathbf{A} , we observe that it is the transpose of the equilibrium matrix \mathbf{B} in 6.7 and 6.8. The same is obviously true for submatrices \mathbf{A}_f and \mathbf{B}_f and \mathbf{A}_d and \mathbf{B}_d , respectively. In practice, only one of these matrices need be established and the other is obtained as its transpose. In the following we assume that the compatibility matrix \mathbf{A} is assembled and the equilibrium matrix is obtained by transposition. Thus, we alternate our reference to the equilibrium matrix as \mathbf{B} or \mathbf{A}^T , as circumstances require.

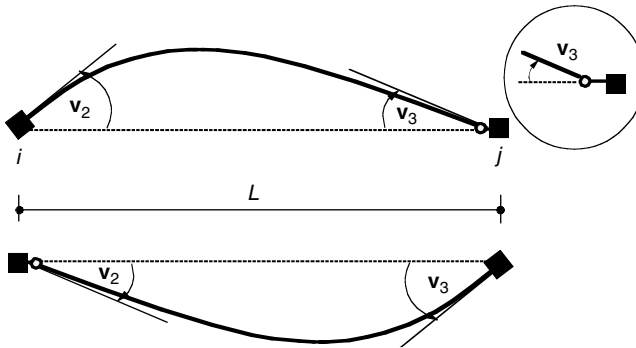


FIGURE 6.8 Flexural deformations for element with moment release.

6.3.3 Compatibility Relationship for Elements with Moment Releases

It is worth looking in more detail into the case of a frame element with a moment release at one end because of later consideration of plastic hinges. A moment release at one end is achieved by introducing a hinge at the end. Referring to Figure 6.8 the element deformations \mathbf{v} are measured from the chord to the tangent at the element side of a hinge at one end or the other. If an end moment is released to zero, the rotations at the ends are no longer independent, and we will show later that for a prismatic, linear elastic beam the deformation at a moment release is one half the value of the deformation at the opposite end, but of opposite sign. The total deformations $\tilde{\mathbf{v}}$ at the element ends are measured from the chord to the tangent at the node side of the hinge. These are the sum of the element deformations \mathbf{v} and the hinge deformations \mathbf{v}_h . The following relationships for a moment release at end i or end j can be established from Figure 6.8:

$$\begin{pmatrix} \mathbf{v}_2 \\ \mathbf{v}_3 \end{pmatrix} = \begin{pmatrix} 1 & 0 \\ -\frac{1}{2} & 0 \end{pmatrix} \begin{pmatrix} \tilde{\mathbf{v}}_2 \\ \tilde{\mathbf{v}}_3 \end{pmatrix} \text{ for hinge at end } j \quad \begin{pmatrix} \mathbf{v}_2 \\ \mathbf{v}_3 \end{pmatrix} = \begin{pmatrix} 0 & -\frac{1}{2} \\ 0 & 1 \end{pmatrix} \begin{pmatrix} \tilde{\mathbf{v}}_2 \\ \tilde{\mathbf{v}}_3 \end{pmatrix} \text{ for hinge at end } i$$

For convenience, the geometric relationships for the two cases can be combined into a single relation by introducing a binary variable as moment release code for each end. Variable mr assumes the value 0 when the end is continuous, and the value 1 when a release is present at the corresponding end. With this variable we can write the above transformation relations in a compact form,

$$\begin{pmatrix} \mathbf{v}_2 \\ \mathbf{v}_3 \end{pmatrix} = \begin{pmatrix} 1-mr_i & -\frac{1}{2}(1-mr_j)mr_i \\ -\frac{1}{2}(1-mr_i)mr_j & 1-mr_j \end{pmatrix} \begin{pmatrix} \tilde{\mathbf{v}}_2 \\ \tilde{\mathbf{v}}_3 \end{pmatrix}$$

which now holds also for the case without moment releases, a moment release at either end and moment releases at both ends. After combining the flexural deformations with axial deformation, which is unaffected by the moment releases, the basic compatibility relationship is

$$\mathbf{v} = \mathbf{a}_h \tilde{\mathbf{v}} \quad \text{with} \quad \mathbf{a}_h = \begin{bmatrix} 1 & 0 & 0 \\ 0 & 1-mr_i & -\frac{1}{2}(1-mr_j)mr_i \\ 0 & -\frac{1}{2}(1-mr_i)mr_j & 1-mr_j \end{bmatrix} \quad (6.20)$$

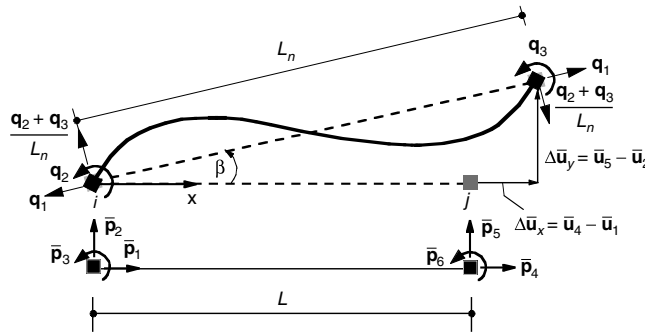


FIGURE 6.9 Equilibrium of frame element in deformed configuration.

A precise definition of the hinge rotation will be useful when plastic hinges are considered. The hinge rotations \mathbf{v}_h are the difference between the deformations $\tilde{\mathbf{v}}$ and the element deformations \mathbf{v} . Consequently, hinge rotations are measured from the tangent at the element side of the hinge to the tangent at the node side. We can, therefore, write the hinge rotation as

$$\mathbf{v}_h = \tilde{\mathbf{v}} - \mathbf{v} = (\mathbf{I} - \mathbf{a}_h)\tilde{\mathbf{v}}$$

where \mathbf{I} is the identity matrix, and the total end deformations $\tilde{\mathbf{v}}$ are given by 6.18. In conclusion, the geometric compatibility relationship $\mathbf{v} = \mathbf{a}_h \mathbf{a}_g \mathbf{u}$ covers all cases of frame elements with or without end moment releases. This result will be used in the subsequent discussion of plastic hinge rotations and in the development of the force-deformation relationship of elasto-plastic elements.

6.4 Equilibrium in Deformed Configuration

With the definition of the element compatibility relationship under large displacements we can now establish the equilibrium relationship for an element in the deformed configuration. Assuming that the basic forces act on the deformed element, \mathbf{q}_1 acts always along the deformed element chord and it changes orientation as the element deforms. This approach is known as corotational formulation (Crisfield, 1990, 1991), but other names such as member-bound reference system or physical coordinates have also been used (Argyris, et al., 1979, Elias, 1986).

The element end forces in the reference frame of the deformed element can be expressed in terms of the basic forces by satisfying the equilibrium equations of the element-free body in the deformed configuration, as illustrated in Figure 6.9. These equations are identical to those in Figure 6.4c except for the fact that the deformed element length L_n is used in place of L . Subsequently, all forces are transformed from the member-bound coordinate system to the local coordinate system by a rotation through angle β , defined as the angle between the chord of the deformed element and the undeformed position (Figure 6.9). The equilibrium equations are

$$\bar{\mathbf{p}} = \begin{pmatrix} \bar{\mathbf{p}}_1 \\ \bar{\mathbf{p}}_2 \\ \bar{\mathbf{p}}_3 \\ \bar{\mathbf{p}}_4 \\ \bar{\mathbf{p}}_5 \\ \bar{\mathbf{p}}_6 \end{pmatrix} = \begin{bmatrix} -\frac{(L + \Delta\bar{\mathbf{u}}_x)}{L_n} & -\frac{\Delta\bar{\mathbf{u}}_y}{L_n^2} & -\frac{\Delta\bar{\mathbf{u}}_y}{L_n^2} \\ -\frac{\Delta\bar{\mathbf{u}}_y}{L_n} & \frac{L + \Delta\bar{\mathbf{u}}_x}{L_n^2} & \frac{L + \Delta\bar{\mathbf{u}}_x}{L_n^2} \\ 0 & 1 & 0 \\ \frac{L + \Delta\bar{\mathbf{u}}_x}{L_n} & \frac{\Delta\bar{\mathbf{u}}_y}{L_n^2} & \frac{\Delta\bar{\mathbf{u}}_y}{L_n^2} \\ \frac{\Delta\bar{\mathbf{u}}_y}{L_n} & -\frac{L + \Delta\bar{\mathbf{u}}_x}{L_n^2} & -\frac{L + \Delta\bar{\mathbf{u}}_x}{L_n^2} \\ 0 & 0 & 1 \end{bmatrix} \begin{pmatrix} \mathbf{q}_1 \\ \mathbf{q}_2 \\ \mathbf{q}_3 \end{pmatrix} = \mathbf{b}_u \mathbf{q} \quad (6.21)$$

This relationship is equivalent to 6.3 except that equilibrium is now satisfied in the deformed configuration. The subscript of the equilibrium matrix \mathbf{b}_u is a reminder that the equilibrium depends on the end displacements. For applications in earthquake engineering analysis, it is reasonable to approximate the equilibrium matrix in 6.21 by expanding the terms of \mathbf{b}_u in a Taylor series and including only terms that have a consistent order of magnitude. The expansion of the terms in the equilibrium matrix is

$$\begin{aligned}\frac{(L + \Delta\bar{u}_x)}{L_n} &\approx 1 - \left(\frac{\Delta\bar{u}_y}{L} \right)^2 \\ \frac{\Delta\bar{u}_y}{L_n} &\approx \frac{\Delta\bar{u}_y}{L} \left[1 - \frac{\Delta\bar{u}_x}{L} - \frac{1}{2} \left(\frac{\Delta\bar{u}_y}{L} \right)^2 \right] \\ \frac{(L + \Delta\bar{u}_x)}{L_n^2} &\approx \frac{1}{L} \left[1 - \frac{\Delta\bar{u}_x}{L} - \left(\frac{\Delta\bar{u}_y}{L} \right)^2 \right] \\ \frac{\Delta\bar{u}_y}{L_n^2} &\approx \frac{\Delta\bar{u}_y}{L^2} \left[1 - 2 \frac{\Delta\bar{u}_x}{L} - \left(\frac{\Delta\bar{u}_y}{L} \right)^2 \right]\end{aligned}$$

Recalling the order of magnitude of the terms $\frac{\Delta\bar{u}_x}{L}$ and $\frac{\Delta\bar{u}_y}{L}$ in comparison with unity, we conclude that we can neglect the factors in square brackets and the quadratic term in the first expression. With these approximations the equilibrium relations in 6.21 simplify to

$$\bar{\mathbf{p}} = \begin{pmatrix} \bar{\mathbf{p}}_1 \\ \bar{\mathbf{p}}_2 \\ \bar{\mathbf{p}}_3 \\ \bar{\mathbf{p}}_4 \\ \bar{\mathbf{p}}_5 \\ \bar{\mathbf{p}}_6 \end{pmatrix} = \begin{pmatrix} -1 & -\frac{\Delta\bar{u}_y}{L^2} & -\frac{\Delta\bar{u}_y}{L^2} \\ -\frac{\Delta\bar{u}_y}{L} & \frac{1}{L} & \frac{1}{L} \\ 0 & 1 & 0 \\ 1 & \frac{\Delta\bar{u}_y}{L^2} & \frac{\Delta\bar{u}_y}{L^2} \\ \frac{\Delta\bar{u}_y}{L} & -\frac{1}{L} & -\frac{1}{L} \\ 0 & 0 & 1 \end{pmatrix} \begin{pmatrix} \mathbf{q}_1 \\ \mathbf{q}_2 \\ \mathbf{q}_3 \end{pmatrix} = \mathbf{b}_u \mathbf{q} \quad (6.22)$$

The relationship in 6.22 is a consistent representation of the effect of large displacements on the equilibrium of a frame element. For many models undergoing moderate deformations, it is reasonable to further simplify

6.22 by neglecting the contribution of the shear force $\frac{\mathbf{q}_2 + \mathbf{q}_3}{L}$ to the axial force, because of the small

magnitude of shear relative to the axial force, and because the transverse deformation, $\frac{\Delta\bar{u}_y}{L}$, does not exceed 0.1 in most cases (about 10% drift of the element). With this approximation 6.22 simplifies further to

$$\bar{\mathbf{p}} = \begin{pmatrix} \bar{\mathbf{p}}_1 \\ \bar{\mathbf{p}}_2 \\ \bar{\mathbf{p}}_3 \\ \bar{\mathbf{p}}_4 \\ \bar{\mathbf{p}}_5 \\ \bar{\mathbf{p}}_6 \end{pmatrix} = \begin{pmatrix} -1 & 0 & 0 \\ -\frac{\Delta\bar{u}_y}{L} & \frac{1}{L} & \frac{1}{L} \\ 0 & 1 & 0 \\ 1 & 0 & 0 \\ \frac{\Delta\bar{u}_y}{L} & -\frac{1}{L} & -\frac{1}{L} \\ 0 & 0 & 1 \end{pmatrix} \begin{pmatrix} \mathbf{q}_1 \\ \mathbf{q}_2 \\ \mathbf{q}_3 \end{pmatrix} = \mathbf{b}_{p\Delta} \mathbf{q} \quad (6.23)$$

The approximate equilibrium equation in 6.23 is often used in the so-called P- Δ analysis of structures.

The transformation of the end forces $\bar{\mathbf{P}}$ from the local to the global coordinate system and any further equilibrium transformations addressed earlier are not affected by the equilibrium transformation of the basic system in Figure 6.9. Thus, the general case of element equilibrium can be expressed as

$$\mathbf{P} = \mathbf{b}_j \mathbf{b}_r \mathbf{b}_u \mathbf{q}$$

By selecting the transformation matrix \mathbf{b}_u depending on the needs of the analysis, one can accommodate large displacements with \mathbf{b}_u from 6.21, P- Δ geometry with $\mathbf{b}_u = \mathbf{b}_{P\Delta}$ from 6.23 and linear geometry under small displacements with $\mathbf{b}_u = \mathbf{b}$ from 6.5.

6.5 Principle of Virtual Work

The virtual work principles are convenient representations of the equations of equilibrium and the conditions of geometric compatibility. With virtual work we can express the equilibrium and compatibility equations, which are vectorial, by a scalar work equation. These principles are derived by starting from either the equilibrium or compatibility equations of an element, converting these into integral form by multiplication with a virtual field, performing integration by parts that introduces the boundary terms and then summing up all element contributions. In the following we only state the final result of the derivation.

6.5.1 Virtual Work Principles for the Structure

The principle of virtual displacements is equivalent to the satisfaction of the equations of equilibrium in the structure. It states that the work done by a set of virtual displacements on the external forces (external work) is equal to the work done by the compatible virtual deformations on the element forces (internal work), if the external forces are in equilibrium with the element forces, and vice versa. In the absence of element loads the principle of virtual displacements is

$$\delta \mathbf{U}^T \mathbf{P} = \delta \mathbf{V}^T \mathbf{Q} \quad (6.24)$$

where the virtual displacements $\delta \mathbf{U}$ and deformations $\delta \mathbf{V}$ satisfy the compatibility requirement as $\delta \mathbf{V} = \mathbf{A} \delta \mathbf{U}$ in 6.19. Substituting this condition for the virtual displacements in 6.24 gives

$$\delta \mathbf{U}^T \mathbf{P} = \delta \mathbf{V}^T \mathbf{Q} = \delta \mathbf{U}^T \mathbf{A}^T \mathbf{Q} \rightarrow \delta \mathbf{U}^T (\mathbf{P} - \mathbf{A}^T \mathbf{Q}) = 0 \quad (6.25)$$

If 6.25 holds for arbitrary virtual displacements $\delta \mathbf{U}$, then $\mathbf{P} - \mathbf{A}^T \mathbf{Q} = 0$ and the converse is also true. Therefore the principle gives the equilibrium equations, $\mathbf{P} - \mathbf{A}^T \mathbf{Q} = 0$ in 6.7, demonstrating that the equilibrium matrix is equal to the transpose of the compatibility matrix, $\mathbf{B} = \mathbf{A}^T$.

The principle of virtual forces is equivalent to the satisfaction of the conditions of geometric compatibility. It states that, if the deformations are compatible with the displacements, then the complementary work of a set of virtual external forces on the displacements is equal to the work of the virtual internal forces that are in equilibrium with the external forces on the deformations. The reverse is also true. In compact form the principle of virtual forces is

$$\delta \mathbf{P}^T \mathbf{U} = \delta \mathbf{Q}^T \mathbf{V} \quad (6.26)$$

Substituting the equilibrium requirement for the virtual forces $\delta \mathbf{P} = \mathbf{B} \delta \mathbf{Q}$, into 6.26 gives

$$\delta P^T U = \delta Q^T V \rightarrow \delta Q^T B^T U = \delta Q^T V \rightarrow \delta Q^T (B^T U - V) = 0$$

which provides the geometric compatibility requirement in 6.19 along with the condition that $B^T = A$.

6.5.2 Virtual Work Principles for an Element

We now turn our attention to an individual frame element, see for example, Figures 6.4 and 6.7. The external work is done by the end forces on the corresponding displacements, whereas the internal work is done by the basic forces on the corresponding deformations. Without further derivation, we state this requirement as

$$\delta u^T p = \delta v^T q \quad (6.27)$$

The condition of geometric compatibility of the virtual displacements is $\delta v = a_g^T \delta u$, which upon substitution into 6.27 gives

$$\delta u^T p = \delta v^T q = \delta u^T a_g^T q \rightarrow \delta u^T (p - a_g^T q) = 0 \rightarrow p - a_g^T q = 0 \quad (6.28)$$

Comparing 6.28 with the element equilibrium equations in 6.5 shows that $b_g = a_g^T$.

We can generalize this fact by stating that if a set of displacements transforms from one system to another according to the relationship $v = a_g u$, then the forces corresponding to these displacements transform according to the contragradient relationship $p = a_g^T q$. Similarly, if a set of forces transforms from one system to another according to $p = b_g q$, then the corresponding displacements transform according to $v = b_g^T u$. Consequently, we only need to establish either the force or displacement transformation relationship from one coordinate system to another using the equilibrium or compatibility conditions, respectively.

Returning now to the virtual work statement for a single element, we can derive the internal work from the integral of the stress product with the corresponding virtual strains over the element volume V :

$$\delta v^T q = \int_V \delta \epsilon^T \sigma dV \quad (6.29)$$

where ϵ is a vector containing the components of the strain tensor and σ is a vector with the corresponding components of the stress tensor arranged in the same order. In many applications of nonlinear structural analysis, we limit ourselves to the internal work of the axial stress σ_x and shear stress τ on the axial strain ϵ_x and shear strain γ , respectively. In this case 6.29 reduces to

$$\delta v^T q = \int_V (\delta \epsilon_x \sigma_x + \delta \gamma \tau) dV \quad (6.30)$$

From the principle of complementary virtual work for the element we obtain the corresponding compatibility relationship for the element:

$$\delta q^T v = \int_V (\delta \sigma_x \epsilon_x + \delta \tau \gamma) dV$$

These virtual work statements will be used in the next section for deriving the force-deformation relationships for linear and nonlinear elements.

6.5.3 Upper Bound Theorem of Plastic Analysis

We return to the problem of plastic analysis and complement the earlier development in Section 6.2.3 with the determination of the plastic collapse load factor by the upper bound theorem of plastic analysis. To state the latter it is necessary to formulate the external and internal plastic work past the point of maximum load. The assumption of perfect plasticity leads to the conclusion that only plastic deformation increments arise in the elements once a collapse mechanism has formed. The plastic deformation increments must satisfy the conditions of geometric compatibility for the free DOFs, which is written in a form similar to 6.19:

$$\Delta V_p = A_f \Delta U_f \quad (6.31)$$

The external plastic work increment is $\lambda P_{ref}^T \Delta U_f$. The internal work consists of the product of the plastic capacities of the elements and the plastic deformation increments. Because the plastic capacities have been defined as absolute values in 6.9, the plastic deformation increments are defined as $\Delta V_p^+ = \Delta V_p$ if $\Delta V_p \geq 0$, otherwise it is zero; $\Delta V_p^- = -\Delta V_p$ if $\Delta V_p \leq 0$, otherwise it is zero. With this definition the internal plastic work increment becomes $Q_p^+ \Delta V_p^+ + Q_p^- \Delta V_p^-$ and 6.31 changes to $\Delta V_p^+ - \Delta V_p^- = A_f \Delta U_f$, noting moreover that $\Delta V_p^+ \geq 0$ and $\Delta V_p^- \geq 0$.

The upper bound theorem of plastic analysis states that the collapse load factor λ_c is the smallest load factor satisfying the condition of incremental plastic work and geometric compatibility. This is stated in a compact form as

$$\begin{aligned} \lambda_c = \min \lambda \quad & \text{for } \lambda P_{ref}^T \Delta U_f = (Q_p^+)^T \Delta V_p^+ + (Q_p^-)^T \Delta V_p^- \\ \Delta V_p^+ - \Delta V_p^- = A_f \Delta U_f \quad & \text{and } \Delta V_p^+ \geq 0, \Delta V_p^- \geq 0 \end{aligned} \quad (6.32)$$

Equation 6.32 can be written in the standard form of linear programming by constraining $P_{ref}^T \Delta U_f = 1$ and noting that the unknowns of the problem are now ΔU_f , ΔV_p^+ and ΔV_p^- (Livesley, 1975). With these considerations, 6.32 is written in a compact form by collecting the unknowns in a single vector:

$$\lambda_c = \min \begin{bmatrix} 0 & Q_p^+ & Q_p^- \end{bmatrix} \begin{pmatrix} \Delta U_f \\ \Delta V_p^+ \\ \Delta V_p^- \end{pmatrix} \quad \text{for} \quad \begin{bmatrix} P_{ref}^T & 0 & 0 \\ -A_f & I & -I \end{bmatrix} \begin{pmatrix} \Delta U_f \\ \Delta V_p^+ \\ \Delta V_p^- \end{pmatrix} = \begin{pmatrix} 1 \\ 0 \\ 0 \end{pmatrix} \quad (6.33)$$

$$\text{with } \Delta V_p^+ \geq 0, \Delta V_p^- \geq 0$$

Comparing 6.33 with 6.10 and recalling that $A_f = B_f^T$, we conclude that the upper bound theorem of plastic analysis in 6.33 is the dual problem of linear programming to the lower bound theorem in 6.10, so that the solution of one satisfies the other. Consequently, the collapse load factor from either 6.10 or 6.33 is the unique solution of the plastic analysis problem. It is also interesting to observe from 6.31 that the columns of the compatibility matrix represent the independent collapse mechanisms of the structural model. The dependent collapse mechanisms can be obtained by linear combination of these columns.

6.5.4 Example of Plastic Analysis

The two-story frame in Figure 6.10a (Horne and Morris, 1982) illustrates the concepts of plastic analysis. With the assumption that axial deformations are negligibly small, there are ten free DOFs, as shown in Figure 6.10b. The plastic moment capacities of the columns and girders are enclosed in a circle in Figure 6.10a and the reference loading is also shown.

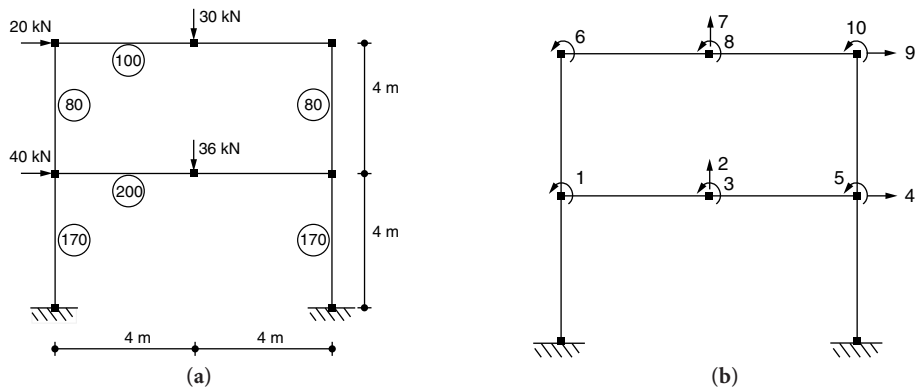


FIGURE 6.10 (a) Two-story frame. (b) Free global DOFs without axial deformations.

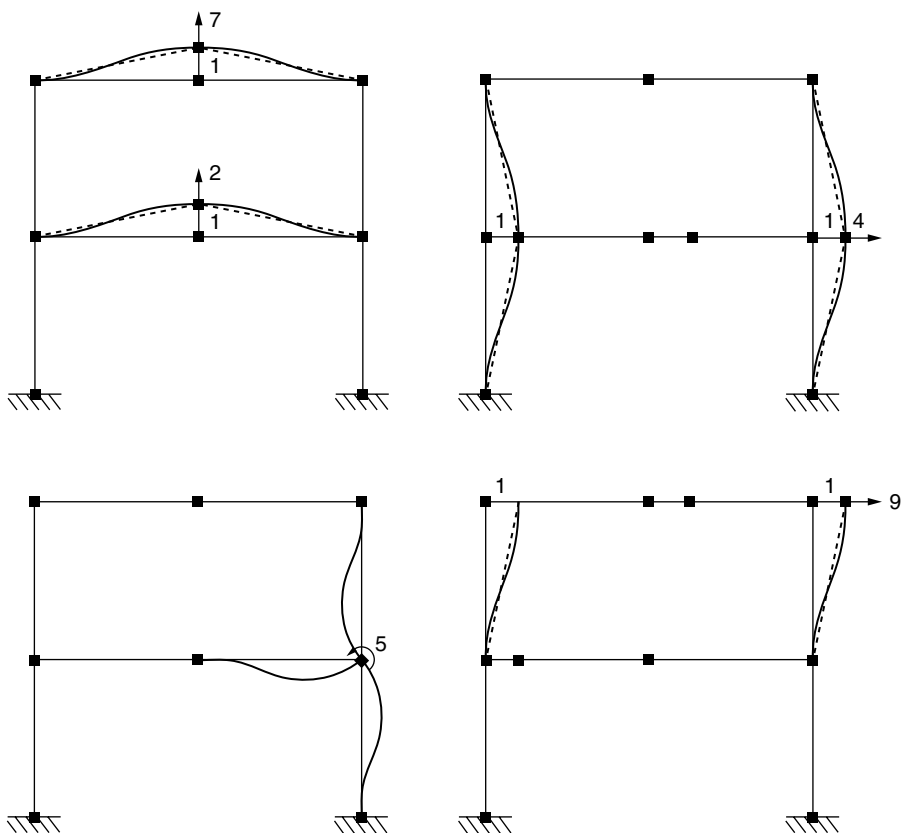


FIGURE 6.11 Typical deformed shapes for global DOFs of two-story frame.

The first step consists in setting up the compatibility matrix A_f relating the element deformations to the DOFs of the model. The model has eight elements with two deformations each, since axial deformations are neglected. Thus, the compatibility matrix has 16 rows and 10 columns. The deformed shapes for the vertical and horizontal translation DOFs and for one rotation DOF are shown in Figure 6.11.

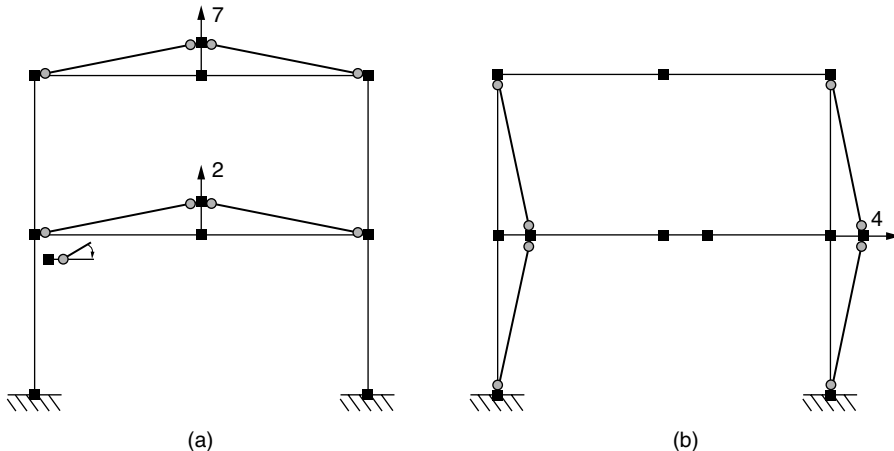


FIGURE 6.12 A few independent collapse mechanisms.

Denoting the story height by h and the girder span by $2l$, the compatibility matrix is

$$\mathbf{A}_f = \begin{bmatrix} 0 & 0 & 0 & 1/h & 0 & 0 & 0 & 0 & 0 & 0 \\ 1 & 0 & 0 & 1/h & 0 & 0 & 0 & 0 & 0 & 0 \\ 1 & -1/l & 0 & 0 & 0 & 0 & 0 & 0 & 0 & 0 \\ 0 & -1/l & 1 & 0 & 0 & 0 & 0 & 0 & 0 & 0 \\ 0 & 1/l & 1 & 0 & 0 & 0 & 0 & 0 & 0 & 0 \\ 0 & 1/l & 0 & 0 & 1 & 0 & 0 & 0 & 0 & 0 \\ 0 & 0 & 0 & 1/h & 1 & 0 & 0 & 0 & 0 & 0 \\ 0 & 0 & 0 & 1/h & 0 & 0 & 0 & 0 & 0 & 0 \\ 1 & 0 & 0 & -1/h & 0 & 0 & 0 & 0 & 1/h & 0 \\ 0 & 0 & 0 & -1/h & 0 & 1 & 0 & 0 & 1/h & 0 \\ 0 & 0 & 0 & 0 & 0 & 1 & -1/l & 0 & 0 & 0 \\ 0 & 0 & 0 & 0 & 0 & 0 & -1/l & 1 & 0 & 0 \\ 0 & 0 & 0 & 0 & 0 & 0 & 1/l & 1 & 0 & 0 \\ 0 & 0 & 0 & -1/h & 0 & 0 & 0 & 0 & 1/h & 1 \\ 0 & 0 & 0 & -1/h & 1 & 0 & 0 & 0 & 1/h & 0 \end{bmatrix}$$

The columns of the compatibility matrix represent the independent collapse mechanisms of the frame. Columns 1, 3, 5, 6, 8, 10 represent the joint mechanisms, columns 2 and 7 the beam mechanisms and columns 4 and 9 the story mechanisms. Figure 6.12 shows the beam mechanisms and the lower story mechanism in which a gray circle indicates a plastic hinge. Plastic rotations are measured from the tangent at the element side of the hinge to the tangent at the node side. Consequently, the lower girder rotation at the left end in Figure 6.12a is negative. The similarity of the shape for the mechanism with the corresponding deformed shape in Figure 6.11 is evident.

The equilibrium equations of the problem are $\lambda P_{\text{ref}} = \mathbf{B}_f \mathbf{Q} = \mathbf{A}_f^T \mathbf{Q}$. We can elect to solve either the lower bound problem in 6.10 or the upper bound problem in 6.33. With either approach the collapse load of the frame is $\lambda_c = 2.50$. Only six plastic hinges form at collapse, as shown in Figure 6.13b, indicating a partial collapse mechanism since NOS = 6. Consequently, there are more unknown \mathbf{Q} values than the available equations of equilibrium in 6.11, and the moment distribution in Figure 6.13a is not unique. In this regard, the double hinge at midspan of the upper girder counts as one.

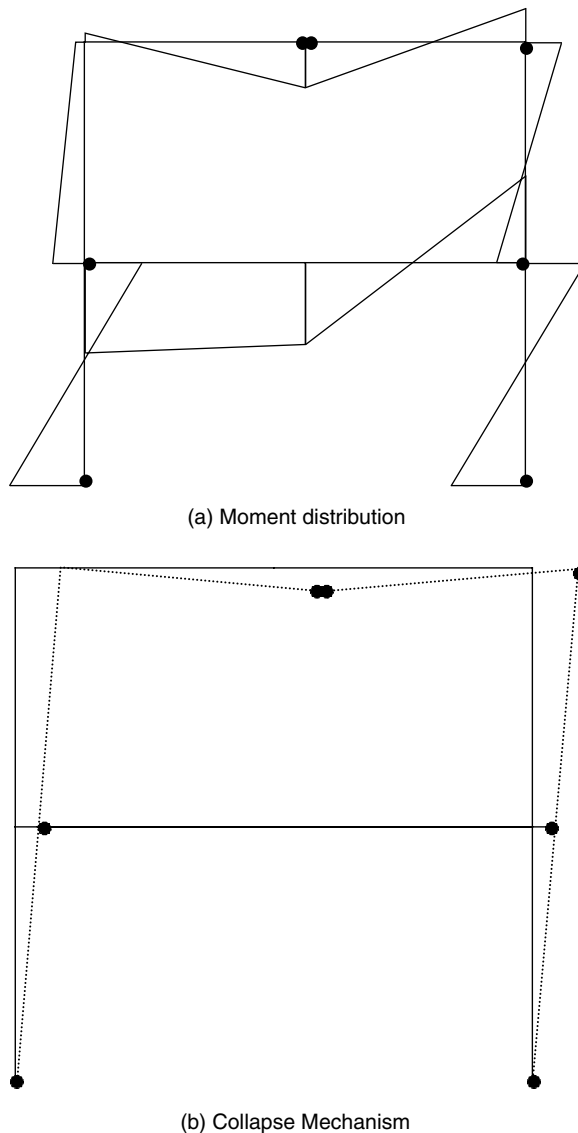


FIGURE 6.13 Moment distribution and mechanism at incipient collapse.

6.6 Force–Deformation Relationships

The previous sections have developed the equilibrium and compatibility relationships for a frame element, which only depend on the element geometry and not on the constituent materials of the element. It is now necessary to relate the element basic forces to the corresponding deformations. To do so in a systematic manner we start with the consideration of the section response and show how it is established by integration of material response. Subsequently, we briefly describe a few material models used in the examples of this chapter.

6.6.1 Section Response

We return to the virtual work statement for an element in 6.30 and rewrite the integral over the element volume as integration over the section at a location x followed by integration over the element length:

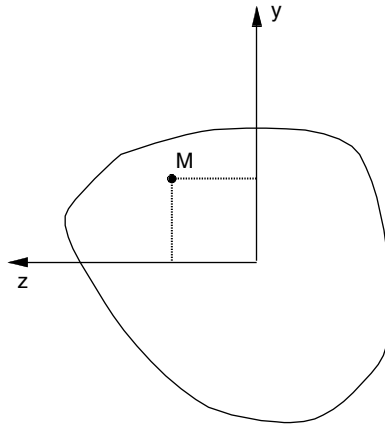


FIGURE 6.14 Cross section with coordinate axes.

$$\delta v^T q = \int_L \left[\int_A (\delta \epsilon_x \sigma_x + \delta \gamma \tau) dA \right] dx \quad (6.34)$$

The strain and stress are functions of the position x along the element axis and the position within the cross section specified in local coordinates y and z . The axial strain at point M in Figure 6.14 can be written as the product of two functions,

$$\epsilon_x(x, y, z) = a_s(y, z) e(x) \quad (6.35)$$

where $e(x)$ are the section deformations and $a_s(y, z)$ represents the strain distribution at section x . When shear deformations are small, Bernoulli's assumption of plane sections remaining plane proves an excellent approximation. In this case the strain distribution at section x is

$$a_s(y, z) = [1 \quad -y \quad z] \quad (6.36)$$

and the section deformation vector, $e(x)$, consists of the axial strain at the coordinate origin ϵ_a , the curvature about the z -axis κ_z and the curvature about the y -axis κ_y . Figure 6.14 shows an arbitrary section. The sign convention in 6.36 follows the right-hand rule for rotation and the definition of tensile strain as positive. The integration of the virtual work expression over the cross-section area A becomes

$$\int_A \delta \epsilon \sigma dA = \delta e^T(x) \int_A a_s^T(y, z) \sigma dA = \delta e^T(x) \int_A \begin{pmatrix} 1 \\ -y \\ z \end{pmatrix} \sigma dA = \delta e^T(x) s(x)$$

and the virtual work for the element in 6.34 can be written as

$$\delta v^T q = \int_L \delta e^T(x) s(x) dx \quad (6.37)$$

The work terms corresponding to the section deformations $e(x)$ are the section forces $s(x)$ defined according to

$$s(x) = \int_A \begin{pmatrix} 1 \\ -y \\ z \end{pmatrix} \sigma dA = \begin{pmatrix} N(x) \\ M_z(x) \\ M_y(x) \end{pmatrix} \quad (6.38)$$

The right-hand side of 6.38 is the standard definition for the axial force and bending moments about the z - and y -axes, respectively.

We define the section stiffness matrix $\mathbf{k}_s(x)$ as the partial derivative of the section forces $\mathbf{s}(x)$ with respect to section deformations $\mathbf{e}(x)$. With this definition and the rules of differentiation, the section stiffness is

$$\mathbf{k}_s(x) = \frac{\partial \mathbf{s}(x)}{\partial \mathbf{e}(x)} = \int_A \begin{pmatrix} 1 \\ -y \\ z \end{pmatrix} \frac{\partial \sigma}{\partial \epsilon} \frac{\partial \epsilon}{\partial e(x)} dA = \int_A \begin{pmatrix} 1 \\ -y \\ z \end{pmatrix} \frac{\partial \sigma}{\partial \epsilon} [1 \quad -y \quad z] dA = \int_A \frac{\partial \sigma}{\partial \epsilon} \begin{bmatrix} 1 & -y & -yz \\ -y & y^2 & z \\ z & z & z^2 \end{bmatrix} dA \quad (6.39)$$

Equation 6.39 uses 6.35 for the derivative of the axial strain with respect to $e(x)$. The partial derivative of stress with respect to strain is the tangent modulus, E_t , of the material stress-strain relationship.

For the special case of linear elastic material with modulus E , 6.39 gives the standard definition for the section stiffness under axial and flexural behavior,

$$\mathbf{k}_s(x) = E \int_A \begin{bmatrix} 1 & -y & z \\ -y & y^2 & -yz \\ z & -yz & z^2 \end{bmatrix} dA = E \begin{bmatrix} A & Q_z & Q_y \\ Q_z & I_z & I_{yz} \\ Q_y & I_{yz} & I_y \end{bmatrix} \quad (6.40)$$

in which Q denotes the first moment and I the second moment of area, respectively. For linear elastic material the section force-deformation relationship becomes

$$\mathbf{s}(x) = \mathbf{k}_s(x) \mathbf{e}(x) \quad (6.41)$$

It is possible to select the origin at the centroidal axis of the section and the orientation of the $y-z$ axes along the principal axes, which renders the off-diagonal terms of the section stiffness in 6.40 equal to zero. Although the centroidal axis is a useful reference point for a homogeneous section with linear elastic material, it is meaningless for the general case of a section with nonlinear materials.

In the general case of a nonlinear stress-strain relationship it is not possible to evaluate the integrals in 6.38 and 6.39 in closed form. Therefore, numerical integration is needed, which gives the value of an integral as a summation,

$$\int_A g(y, z) dA \approx \sum_{i=1}^{nIP} w_i g(y_i, z_i) \quad (6.42)$$

in which $g(y, z)$ is the function to be integrated, nIP is the number of integration points and w_i is the weight at integration point i . Different integration rules can be used in 6.42, but discontinuities associated with the stress distribution in 6.38 and the tangent modulus in 6.39, particularly under cyclic load reversals, favor low order integration schemes such as midpoint, trapezoidal or Simpson's rule. The accuracy of integration is improved with a larger number of integration points. The midpoint rule is the most common integration scheme in the application of nonlinear analysis in earthquake engineering and gives rise to the name layer model for y -integration or fiber model for $y-z$ integration. It is worth noting that the midpoint rule exactly integrates linear polynomials. Consequently, the quadratic stiffness terms in 6.39 are not accurately represented even for the linear elastic case. For the typical number of integration points the error is, however, very small.

We conclude this section by summarizing that the cross-section response can be obtained by integration of the stress-strain response of the materials. A kinematic assumption about the strain distribution is

typically the starting point. In the general case of including all components of the strain tensor $\boldsymbol{\epsilon}(x, y, z)$ we write

$$\begin{aligned} \text{section kinematics or compatibility} \quad & \boldsymbol{\epsilon}(x, y, z) = \mathbf{a}_s(y, z)\boldsymbol{\epsilon}(x) \\ \text{section equilibrium} \quad & \mathbf{s}(x) = \int_A \mathbf{a}_s^T(y, z)\boldsymbol{\sigma} dA \\ \text{section stiffness} \quad & \mathbf{k}_s(x) = \int_A \mathbf{a}_s^T(y, z) \frac{\partial \boldsymbol{\sigma}}{\partial \boldsymbol{\epsilon}} \mathbf{a}_s(y, z) dA \end{aligned} \quad (6.43)$$

Definitions for section deformations and corresponding forces need to be generalized accordingly. $\partial \boldsymbol{\sigma} / \partial \boldsymbol{\epsilon}$ is, in general, a 6×6 matrix representing the tangent material stiffness. The examples of this chapter are limited to uniaxial material response.

Before completing the discussion of force-deformation relationships, we mention that the section response can be directly defined in terms of explicit or implicit section force-deformation relations. Such an approach is based on the extension of plasticity theory to section force resultants and deformations (McGuire et al., 2000). While this approach is an excellent choice for homogeneous sections of metallic material, it is doubtful whether it constitutes a robust alternative to the integration of material response for sections composed of several materials. This is particularly the case under complex interactions of the constituent materials that may lead to softening response, as is the case for reinforced concrete sections.

6.6.2 Material Models

A key ingredient for establishing the section response with 6.43 is the constitutive model of the material. Under the assumptions in the preceding section, uniaxial material models suffice for many applications in earthquake engineering analysis. Thus, relatively complex uniaxial material relations can be deployed without difficulty. However, the high computational cost of integrating a complex material response, usually limits the selection to a few relatively simple hysteretic models.

For applications in performance-based earthquake engineering it is important to distinguish between path-dependent and path-independent material models. In a path-independent model the current stress is a function of current strain only. Thus, the material follows the same path whether it is loading or unloading. In static pushover analysis of structures this may be sufficient, if one can assume that limited unloading, if any, will take place. This is often the case. In cyclic static or dynamic analysis a path-dependent material model is required. In this the current stress depends on the current strain and several other variables, such as the strain history and internal variables, that describe the state of material damage. The more complex the path of loading-unloading of a material model, the higher the number of internal variables required in its description with a consequent increase in computational cost.

For the purposes of this chapter we limit ourselves to a brief description of three relatively simple material models which are used in the examples of this chapter: a bilinear elasto-plastic model with kinematic and isotropic hardening and a more involved version that includes the Bauschinger effect. Both models are suitable for describing the hysteretic behavior of steel. Finally, we briefly describe a simple hysteretic model for concrete.

Figure 6.15 shows a bilinear elasto-plastic model with kinematic and isotropic hardening. The isotropic hardening depends on the amount of plastic strain in the opposite stress direction, which is why it is only evident under compressive stress. The bilinear model is a good representation of the behavior of metals and is often used in earthquake analysis when the Bauschinger effect is not important for the simulations. It is computationally advantageous for its simplicity. When the Bauschinger effect is important, the stress-strain relation of Menegotto-Pinto in Figure 6.16 gives a very good representation of the material response (Menegotto and Pinto, 1973). It is particularly important for the computational economy of analysis of frame structures that the model expresses stress directly as function of strain. The

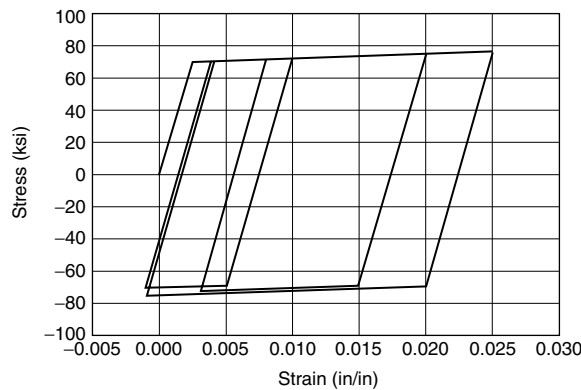


FIGURE 6.15 Hysteretic bilinear stress-strain relationship.

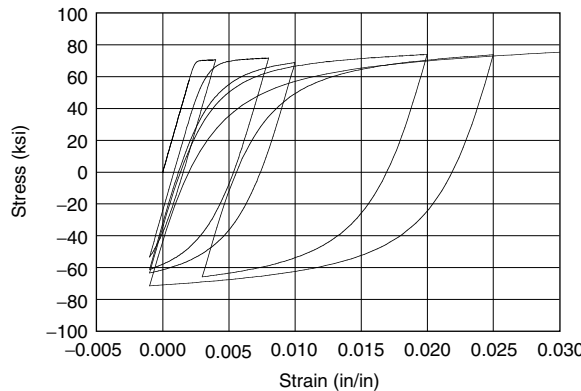


FIGURE 6.16 Hysteretic steel stress-strain relation by Menegotto-Pinto.

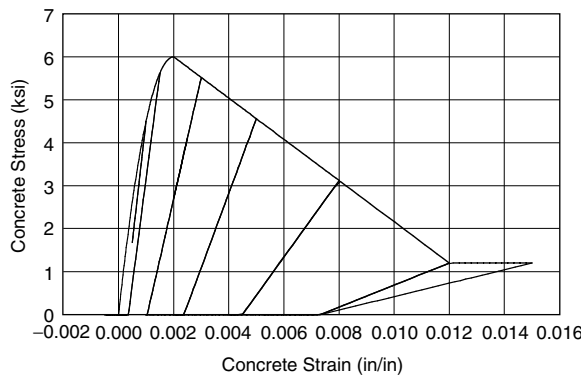


FIGURE 6.17 Hysteretic concrete stress-strain relation.

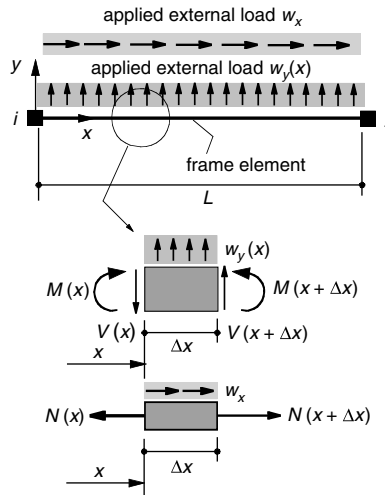


FIGURE 6.18 Equilibrium in undeformed configuration of frame element.

limitation of the model lies in its inability to reach the point of last unloading upon reloading in the same stress direction. This is evident in Figure 6.16. Details of the model implementation and parameter selection can be found elsewhere (Filippou et al., 1983).

Figure 6.17 shows a simple hysteretic model for concrete. The monotonic behavior in compression is represented by a parabolic ascending curve followed by a linear descending curve to a residual stress of between 10 and 20% of the compression strength. The slope of the descending curve can be adjusted to represent the effect of concrete confinement provided by transverse reinforcement (Scott et al., 1982). The unloading-reloading path is also linear with decreasing modulus that follows the observations of an extensive experimental study (Karsan and Jirsa, 1969). Several unloading-reloading cycles are shown in Figure 6.17. The model in Figure 6.17 does not account for the tensile strength of concrete and the effect of tension softening. On the other hand it is computationally very simple. More sophisticated models of concrete response under tensile stress are available at the expense of computational complexity (CEB, 1996). Their use is important when the precracked and preyield response of reinforced concrete structures is of particular interest.

6.7 Frame Elements

After having established equilibrium, compatibility and section force-deformation relationships, we now develop nonlinear frame elements with a range of applicability in structural analysis procedures for earthquake engineering. We discuss the advantages and limitations of each approach in the formulation of the frame elements. Emphasis is placed on a rigorous derivation of the element response and on the presentation of the element state determination process, which consists in computing the basic forces and the stiffness matrix that correspond to given element deformations.

6.7.1 Basic Relationships

The differential equations of equilibrium for a frame element in the undeformed configuration can be written, with reference to Figure 6.18, for axial and moment equilibrium, as

$$\begin{aligned} \frac{\partial N}{\partial x} + w_x(x) &= 0 \\ \frac{\partial^2 M}{\partial x^2} - w_y(x) &= 0 \end{aligned} \quad (6.44)$$

in which w_x and w_y are the axial and transverse components of the distributed element load, respectively. An important characteristic of frame elements is that, under linear geometry, the differential

equations in 6.44 can be solved independently of the displacements and of the material response. In the absence of element loading the homogeneous solution of the differential equations in 6.44 gives a constant axial force and a linear bending moment distribution. We use the basic forces \mathbf{q} as boundary values of the problem to obtain the statement of equilibrium:

$$\mathbf{s}(x) = \begin{pmatrix} N(x) \\ M(x) \end{pmatrix} = \begin{pmatrix} \mathbf{q}_1 \\ \mathbf{q}_2 \left(\frac{x}{L} - 1 \right) + \mathbf{q}_3 \frac{x}{L} \end{pmatrix} = \begin{bmatrix} 1 & 0 & 0 \\ 0 & \left(\frac{x}{L} - 1 \right) & \frac{x}{L} \end{bmatrix} \begin{pmatrix} \mathbf{q}_1 \\ \mathbf{q}_2 \\ \mathbf{q}_3 \end{pmatrix} = \mathbf{b}(x)\mathbf{q} \quad (6.45)$$

The matrix $\mathbf{b}(x)$ represents the force-interpolation functions and can be regarded also as an equilibrium transformation matrix between section forces $\mathbf{s}(x)$ and basic forces \mathbf{q} . In the presence of element loads, the internal forces represent the particular solution of the differential equations in 6.44, which only need to satisfy homogeneous boundary conditions. For uniform element loads the axial force is a linear function and the bending moment is a quadratic function. Denoting the particular solution by $\mathbf{s}_w(x)$, the equilibrium equations are

$$\mathbf{s}(x) = \mathbf{b}(x)\mathbf{q} + \mathbf{s}_w(x) \quad (6.46)$$

After setting up the equilibrium relations the geometric compatibility of the frame element can be established with the principle of virtual forces. The complementary virtual work is analogous to the virtual work principle in 6.37

$$\delta\mathbf{q}^T \mathbf{v} = \int_L \delta\mathbf{s}^T(x) \mathbf{e}(x) dx \quad (6.47)$$

Using 6.46 for the equilibrium relation of the virtual force system, $\delta\mathbf{s}(x) = \mathbf{b}(x)\delta\mathbf{q}$, and after substitution into 6.47 gives the compatibility statement as

$$\mathbf{v} = \int_L \mathbf{b}^T(x) \mathbf{e}(x) dx \quad (6.48)$$

the individual basic deformation quantities in 6.48 can be evaluated with the force-interpolation functions $\mathbf{b}(x)$ from 6.45:

$$\begin{aligned} v_1 &= \int_0^L \epsilon_a(x) dx \\ v_2 &= \int_0^L \left(\frac{x}{L} - 1 \right) \kappa(x) dx \\ v_3 &= \int_0^L \frac{x}{L} \kappa(x) dx \end{aligned} \quad (6.49)$$

It is important to emphasize that the compatibility relationships in 6.46, 6.48 and 6.49 hold true for any material response as long as the transverse displacements are sufficiently small that virtual force equilibrium can be satisfied in the undeformed configuration.

For the special case of linear elastic material response, the section relationship in 6.41 can be inverted to give the section deformations in terms of the section forces. We can generalize it by adding nonmechanical initial deformations $\mathbf{e}_0(x)$, such as caused by temperature and shrinkage strains

$$\mathbf{e}(x) = [\mathbf{k}_s(x)]^{-1} \mathbf{s}(x) + \mathbf{e}_0(x) = \mathbf{f}_s(x) \mathbf{s}(x) + \mathbf{e}_0(x) \quad (6.50)$$

with $\mathbf{f}_s(x)$ the section flexibility matrix. Substituting 6.50 into 6.48 and using 6.46 gives

$$\begin{aligned} \mathbf{v} &= \int_L^L \mathbf{b}^T(x) \{ \mathbf{f}_s(x) [\mathbf{b}(x)\mathbf{q} + \mathbf{s}_w(x)] + \mathbf{e}_0(x) \} dx \\ \mathbf{v} &= \left[\int_L^L \mathbf{b}^T(x) \mathbf{f}_s(x) \mathbf{b}(x) dx \right] \mathbf{q} + \int_L^L \mathbf{b}^T(x) \mathbf{f}_s(x) \mathbf{s}_w(x) dx + \int_L^L \mathbf{b}^T(x) \mathbf{e}_0(x) dx = \mathbf{f} \mathbf{q} + \mathbf{v}_w + \mathbf{v}_0 \end{aligned} \quad (6.51)$$

in which \mathbf{f} is the element flexibility matrix, \mathbf{v}_w are the deformations due to element loads and \mathbf{v}_0 the deformations due to nonmechanical effects. In the general case of a tapered frame element with variable cross section, substitution of the force-interpolation functions from 6.45 gives

$$\mathbf{f} = L \int_0^1 \begin{bmatrix} \frac{1}{EA(\xi)} & 0 & 0 \\ 0 & \frac{(1-\xi)(1-\xi)}{EI(\xi)} & -\frac{(1-\xi)\xi}{EI(\xi)} \\ 0 & -\frac{(1-\xi)\xi}{EI(\xi)} & \frac{\xi\xi}{EI(\xi)} \end{bmatrix} d\xi \quad (6.52)$$

with $\xi = x/L$. For general functions $EA(\xi)$ and $EI(\xi)$, 6.52 needs to be integrated numerically. Among the various schemes, Gauss or Gauss–Lobatto integration is preferred for the smallest number of function evaluations for a given accuracy level. Details of these integration schemes can be found in textbooks on finite element analysis (Bathe, 1995). In the specific case of a uniform prismatic frame element, 6.52 simplifies to

$$\mathbf{f} = \begin{bmatrix} \frac{L}{EA} & 0 & 0 \\ 0 & \frac{L}{3EI} & -\frac{L}{6EI} \\ 0 & -\frac{L}{6EI} & \frac{L}{3EI} \end{bmatrix} \quad (6.53)$$

For the case of linear elastic material, the deformation–force relation in 6.51 is inverted to give the force–deformation relation in the following form:

$$\mathbf{q} = \mathbf{f}^{-1} (\mathbf{v} - \mathbf{v}_w - \mathbf{v}_0) = \mathbf{k} \mathbf{v} + \mathbf{q}_w + \mathbf{q}_0$$

where \mathbf{k} is the basic stiffness matrix as the inverse of the flexibility matrix, and \mathbf{q}_w and \mathbf{q}_0 are the fixed-end forces under the element loads and the nonmechanical deformations, respectively. With $\mathbf{k} = \mathbf{f}^{-1}$ and \mathbf{f} from 6.53, the basic stiffness matrix of a prismatic frame element is

$$\mathbf{k} = \mathbf{f}^{-1} = \begin{bmatrix} \frac{EA}{L} & 0 & 0 \\ 0 & \frac{4EI}{L} & \frac{2EI}{L} \\ 0 & \frac{2EI}{L} & \frac{4EI}{L} \end{bmatrix} \quad (6.54)$$

The use of moment releases at the ends of a frame element was presented in Section 6.3.3. For the case that the element has a moment release at end j and thus $\mathbf{q}_3 = 0$, 6.53 shows that $\mathbf{v}_3 = -\frac{1}{2}\mathbf{v}_2$, as already used in the compatibility relation of a prismatic, linear elastic frame element with a moment release in 6.20. For the frame element with a moment release at one or both ends, the compatibility relation in 6.20 and the contragradient property of force and displacement transformations give

$$\tilde{\mathbf{q}} = \mathbf{a}_h^T \mathbf{q} = \mathbf{a}_h^T (\mathbf{k}\mathbf{v} + \mathbf{q}_w + \mathbf{q}_0) = \mathbf{a}_h^T \mathbf{k} \mathbf{a}_h \tilde{\mathbf{v}} + \mathbf{a}_h^T (\mathbf{q}_w + \mathbf{q}_0) = \tilde{\mathbf{k}} \tilde{\mathbf{v}} + \tilde{\mathbf{q}}_w + \tilde{\mathbf{q}}_0$$

For the case that there is a moment release at end j , with the stiffness matrix \mathbf{k} from 6.54 this gives

$$\mathbf{a}_h = \begin{bmatrix} 1 & 0 & 0 \\ 0 & 1 & 0 \\ 0 & -\frac{1}{2} & 0 \end{bmatrix} \quad \tilde{\mathbf{k}} = \mathbf{a}_h^T \mathbf{k} \mathbf{a}_h = \begin{bmatrix} \frac{EA}{L} & 0 & 0 \\ 0 & \frac{3EI}{L} & 0 \\ 0 & 0 & 0 \end{bmatrix}$$

6.7.2 Concentrated Plasticity Elements

6.7.2.1 Truss or Brace Element

The simplest nonlinear element is the prismatic truss or brace element. In this case there is only one basic force \mathbf{q}_1 , which is equal to the normal force in the truss element $s_1 = N$. The normal force is equal to the axial stress multiplied by the cross-sectional area A . The axial stress is related to the axial strain by the material constitutive relation. Finally, the axial strain is related to the element deformation \mathbf{v}_1 by $\epsilon = \mathbf{v}_1/L$. Thus, the element state determination is as follows: given \mathbf{v}_1 , determine ϵ ; use the material constitutive relation to get the corresponding axial stress σ ; finally, compute the basic force with $\mathbf{q}_1 = s_1 = \sigma A$. The tangent stiffness matrix of the element can be readily obtained by the chain rule of differentiation

$$\mathbf{k}_t = \frac{\partial \mathbf{q}_1}{\partial \mathbf{v}_1} = A \frac{\partial \sigma}{\partial \epsilon} \frac{\partial \epsilon}{\partial \mathbf{v}_1} = \frac{E_t A}{L}$$

where E_t is the tangent modulus of the material.

6.7.2.2 Elastic Perfectly Plastic Beam

The next element of interest is a frame element with concentrated flexural hinges at the ends, where moments are assumed to be largest under the combination of gravity and lateral forces due to earthquake excitation. Although this is correct for columns, it is often an approximation for girders, where the combination of gravity and lateral forces, particularly in higher building floors, may lead to the formation of a plastic hinge away from the member ends. In such case, it is advisable to subdivide the member into two or more frame elements. The limitation that plastic hinges can only take place at specific locations

along the span is sufficiently accurate, particularly if one allows for plastic hinges to form at the outer quarter span points using three frame elements for the member.

The simplest way of accounting for the interaction between axial force and bending moment in the potential plastic hinge locations at the column ends is to use the axial forces from an elastic analysis under gravity loading to determine the plastic flexural capacity of the hinges. The girders are subjected to a small axial force so that the variation of this force during the analysis can be neglected. If significant overturning moments develop in the structure during the nonlinear pushover analysis under lateral forces, the axial force in the columns changes appreciably during the analysis and more sophisticated modeling of the axial force-bending moment interaction at the column plastic hinges is required.

The state determination of the frame element can be undertaken with an event-to-event strategy: given the element deformations \mathbf{v} , estimate the basic forces by using as tangent stiffness the elastic stiffness of the element \mathbf{k}_e , i.e., $\mathbf{k}_{t1} = \mathbf{k}_e$ and $\mathbf{q} = \mathbf{k}_{t1}\mathbf{v}$. The end moments are compared with the corresponding plastic capacities \mathbf{q}_p . If these are not exceeded, then the basic force estimate is correct and the tangent stiffness is equal to the elastic stiffness. If the end moments exceed the corresponding plastic capacity, then the ratios $\mathbf{q}_2/\mathbf{q}_{p2}$ and $\mathbf{q}_3/\mathbf{q}_{p3}$ express the amount of overshoot. The first event factor η_1 is the inverse of the larger ratio:

$$\eta_1 = \min\left(\frac{\mathbf{q}_{p2}}{\mathbf{q}_2}, \frac{\mathbf{q}_{p3}}{\mathbf{q}_3}\right)$$

The initial deformations are scaled with this ratio, known as an event factor, the moment release code is set to unity for the end with the event factor, and a new tangent stiffness matrix \mathbf{k}_{t2} is formed. The new estimate of the basic forces is

$$\mathbf{q} = \mathbf{k}_{t1}\eta_1\mathbf{v} + \mathbf{k}_{t2}(1 - \eta_1)\mathbf{v}$$

If another hinge has not formed, then the basic force estimate is correct and the tangent stiffness of the element is \mathbf{k}_{t2} . If a second hinge forms, then the last deformation increment is scaled by the new event factor η_2 , the tangent stiffness is updated (which turns out to be zero in the presence of two hinges) and the end forces become

$$\mathbf{q} = \mathbf{k}_{t1}\eta_1\mathbf{v} + \mathbf{k}_{t2}(1 - \eta_1)\eta_2\mathbf{v}$$

With this procedure a maximum of two iterations is required for convergence under monotonic loading. Even under cyclic loading the number of iterations does not exceed two, because the plastic hinges at the ends can be either open or closed. It is important to note, however, that cyclic loading requires that the process be conducted with deformation increments instead of total deformations and that the state of the hinges, the basic forces and the tangent stiffness matrix be saved from one iteration of the global equilibrium equations to the next.

6.7.2.3 Two-Component Parallel Model

The frame element with concentrated plastic hinges at the ends is straightforward in its implementation, but is also limited to elastic-perfectly plastic behavior. Thus, it can be a useful addition to the plastic analysis of Section 6.2.3 by providing the complete force-displacement relation of the structural model up to incipient collapse. For a more realistic representation of material behavior the inclusion of strain hardening is important. In such case the simple elasto-plastic frame element needs to be combined in parallel with a linear elastic frame element to form the two-component model (Clough et al., 1965).

The two-component model consists of an elasto-plastic element in parallel with a linear elastic element. The latter represents the strain hardening response of the frame member. The fact that the elements are in parallel implies that

$$\mathbf{v} = \mathbf{v}_e = \mathbf{v}_p \quad \mathbf{q} = \mathbf{q}_e + \mathbf{q}_p \quad \mathbf{k} = \mathbf{k}_e + \mathbf{k}_p \quad (6.55)$$

where subscripts e and p denote the elastic component and the elasto-plastic component, respectively. The state determination process of the element is straightforward, because of the first relation in 6.55: given \mathbf{v} the deformations of each component are known. For the elastic component the basic forces are $\mathbf{q}_e = \mathbf{k}_e \mathbf{v}_e$ and for the elasto-plastic component the state determination process of the preceding section determines the end forces. The same is true for the stiffness. Once the end forces and tangent stiffness of the elasto-plastic element are determined, then the last two equations in 6.55 yield the resisting forces and the stiffness of the entire element. This simplicity of the state determination process is characteristic of elements with an assumption about the deformation distribution.

The main difficulty with the two-component model is the calibration of the element parameters. Under uniform curvature the section stiffness of the linear elastic component can be set equal to the strain hardening section stiffness of the frame member. The initial stiffness of the elasto-plastic component can then be determined to make up the difference between the initial stiffness of the frame member and the strain hardening stiffness. Unfortunately, the case of uniform curvature is of little use in earthquake engineering analysis. Rather the calibration of the model parameters takes place under antisymmetric curvature with the point of inflection at member midspan. Another limitation of the two-component model is its inability to handle different plastic moment capacities under positive and negative curvature. For these reasons the two-component model has been superceded in earthquake engineering analysis by the one-component model (Giberson, 1967). It is worth discussing in some detail the formulation of this element, because it is characteristic of a class of elements that are based on an assumption about the internal force distribution. These elements play an important role in modern earthquake engineering analysis, because they represent exactly the force distribution in the member and result in a robust numerical implementation.

6.7.2.4 One-Component Series Model

The one-component model consists of a linear elastic element connected in series with a rigid-plastic linear hardening spring at each end. The conditions governing the response of the element are

$$\mathbf{q} = \mathbf{q}_e = \mathbf{q}_p \quad \mathbf{v} = \mathbf{v}_e + \mathbf{v}_p \quad \mathbf{f} = \mathbf{f}_e + \mathbf{f}_p \quad (6.56)$$

It is convenient to establish these relations with a substructure approach to the statically determinate structure. Limiting attention to the flexural contribution, the force-interpolation functions for the basic forces \mathbf{q}_2 and \mathbf{q}_3 are

$$\mathbf{b} = \begin{bmatrix} 1 & 1 & 0 & 0 \\ 0 & 0 & 1 & 1 \end{bmatrix}$$

and the composite flexibility matrix of the subelements is

$$\mathbf{f}_c = \begin{bmatrix} \mathbf{f}_i & 0 & 0 & 0 \\ 0 & \frac{L}{3EI} & -\frac{L}{6EI} & 0 \\ 0 & -\frac{L}{6EI} & \frac{L}{3EI} & 0 \\ 0 & 0 & 0 & \mathbf{f}_j \end{bmatrix}$$

where \mathbf{f}_i and \mathbf{f}_j are the spring flexibilities at ends i and j , respectively. From the product $\mathbf{b}^T \mathbf{f}_c \mathbf{b}$ we obtain the last relation in 6.56 with \mathbf{f}_e given by the flexural terms in 6.53 and \mathbf{f}_p by the following expression

$$\mathbf{f}_p = \begin{bmatrix} \mathbf{f}_i & 0 \\ 0 & \mathbf{f}_j \end{bmatrix}$$

The flexibility coefficients f_i and f_j are zero for a moment less than the flexural plastic capacity and then assume a value equal to the inverse of the strain hardening stiffness. Because the two end springs are independent, their properties can also be specified independently. Moreover, it is possible to specify a different plastic capacity and a different strain hardening stiffness under a positive than under a negative curvature. This makes the one-component model more versatile than the two-component model. Another advantage of this model is its ability to account for the effect of element loads by the inclusion of v_w from 6.51 so that $v = fq + v_w$ with f from 6.56. The calibration of the model parameters takes place under antisymmetric curvature with the point of inflection at member midspan. This may not be a reasonable approximation for the case of a different plastic capacity under a positive than under a negative curvature.

It is important to discuss the process of element state determination for the one-component model, because it is characteristic of the class of elements that are based on an assumption about the internal force distribution. Because the element is implemented in a standard computer program that is based on the direct stiffness method of analysis, it is expected to return the resisting forces and current stiffness matrix for given element deformations v . In order to highlight the fact that these deformations are given we denote them with the symbol \hat{v} . From the middle equation in 6.56 we have

$$\hat{v} - v = 0 \quad \text{where} \quad v = v_e + v_p$$

Because the deformations of the elastic and plastic components of the one-component model are functions of the basic forces q we formally write that

$$\hat{v} - v(q) = 0 \tag{6.57}$$

and note that we are dealing with a nonlinear system of equations, because of the rigid-plastic linear hardening component. The solution of the nonlinear system can be obtained with the Newton–Raphson algorithm, as will be discussed in more detail in the following section. We defer, therefore, the discussion of the state determination process of this class of elements until then. We note at this stage, however, that 6.57 implies an iterative process of state determination at the element level. An alternative approach that bypasses the element iteration is also possible.

6.7.3 Distributed Inelasticity Elements

The limitation of concentrated plasticity elements is that inelastic deformations take place at predetermined locations at the ends of the element. While this may be a reasonable assumption in lower floors of moment-resisting frames, it does not account for the possibility of inelastic deformations taking place within the element in the upper floors of the building model. Another, in many respects more serious limitation, is the fact that concentrated plasticity elements require calibration of their parameters against the response of an actual or ideal frame element under idealized loading conditions. This is necessary, because the response of concentrated plasticity elements derives from the moment–rotation relation of their components. In an actual frame element the end moment–rotation relation results from the integration of the section response. This can be achieved directly with elements of distributed inelasticity. In this case there are two approaches: the force formulation or the displacement formulation.

In the force formulation we make use of the fact that the internal forces $s(x)$ at a distance x from end i of a two-node frame element are given as the product of the force-interpolation functions $b(x)$ and the basic forces q according to 6.45. In the presence of element loads we need to modify this relation according to 6.46. It is important to note that these relations hold for any material response, as long as the equilibrium can be satisfied in the undeformed configuration. The element deformations can then be established by the principle of virtual forces from 6.48. This implies that the section deformations $e(x)$ can be obtained from the section forces $s(x)$. In reality, this relation is not available, but its inverse is. Thus, $e(x)$ needs to be established from the solution of the nonlinear system of equations

$$\mathbf{b}(x)\mathbf{q} + \mathbf{s}_w(x) - \mathbf{s}(\mathbf{e}(x)) = 0$$

For the solution of the nonlinear system of equations in 6.57 we also need to establish the change of the element deformations with \mathbf{q} . This change is reflected by the derivative of the expression in 6.48 with respect to \mathbf{q} . We obtain

$$\frac{\partial \mathbf{v}}{\partial \mathbf{q}} = \frac{\partial}{\partial \mathbf{q}} \int_L \mathbf{b}^T(x) \mathbf{e}(x) dx = \int_L \mathbf{b}^T(x) \frac{\partial \mathbf{e}(x)}{\partial \mathbf{s}(x)} \frac{\partial \mathbf{s}(x)}{\partial \mathbf{q}} dx = \int_L \mathbf{b}^T(x) \mathbf{f}_s(x) \mathbf{b}(x) dx \quad (6.58)$$

where $\mathbf{f}_s(x)$ is the section flexibility, which can be obtained as the inverse of the section stiffness matrix in 6.39. The derivative of the section forces with respect to \mathbf{q} is obtained from 6.46. We call the expression in 6.58 the tangent flexibility matrix \mathbf{f}_t of the element.

In the displacement formulation we assume that the axial and transverse displacements at distance x from the end node i are supplied by the product of suitable displacement interpolation functions $\mathbf{a}(x)$ with the element deformations \mathbf{v} . For a two-dimensional element we write

$$\mathbf{u}(x) = \mathbf{a}(x)\mathbf{v} = \begin{bmatrix} \mathbf{a}_1(x) & 0 & 0 \\ 0 & \mathbf{a}_2(x) & \mathbf{a}_3(x) \end{bmatrix} \begin{pmatrix} \mathbf{v}_1 \\ \mathbf{v}_2 \\ \mathbf{v}_3 \end{pmatrix}$$

The displacement interpolation functions correspond to the solution of the differential equation for a linear elastic, prismatic frame element. It is important to note that these functions thus only approximate the response of a frame element with distributed inelasticity. This has important ramifications under large inelastic deformations, as a later example will demonstrate. The section deformations at x can be obtained by application of the small deformation theory of beam kinematics: the axial strain ϵ_a at the reference axis is the first derivative of the axial displacement, and the curvature is the second derivative of the transverse displacement. We write formally

$$\mathbf{e}(x) = \begin{bmatrix} \frac{\partial}{\partial x} & 0 \\ 0 & \frac{\partial^2}{\partial x^2} \end{bmatrix} \begin{pmatrix} \mathbf{u}_1(x) \\ \mathbf{u}_2(x) \end{pmatrix} = \begin{bmatrix} \frac{\partial}{\partial x} & 0 \\ 0 & \frac{\partial^2}{\partial x^2} \end{bmatrix} \begin{bmatrix} \mathbf{a}_1(x) & 0 & 0 \\ 0 & \mathbf{a}_2(x) & \mathbf{a}_3(x) \end{bmatrix} \begin{pmatrix} \mathbf{v}_1 \\ \mathbf{v}_2 \\ \mathbf{v}_3 \end{pmatrix} = \mathbf{a}_e(x)\mathbf{v} \quad (6.59)$$

The element forces \mathbf{q} are established from the principle of virtual displacements in 6.37 using the variation of 6.59 for the virtual displacement field. We obtain

$$\mathbf{q} = \int_L \mathbf{a}_e^T(x) \mathbf{s}(x) dx \quad (6.60)$$

The section forces $\mathbf{s}(x)$ in 6.60 are directly obtained from the section constitutive relation for given section deformations $\mathbf{e}(x)$. The latter, in turn, are directly obtained from the given element deformations \mathbf{v} by 6.59. Thus, the path from the given element deformations \mathbf{v} to the corresponding forces \mathbf{q} is straightforward in the displacement formulation, which explains its appeal. This should not distract from the serious drawback of the method, which lies in the approximate nature of the displacement interpolation functions.

The change of element forces \mathbf{q} with deformation is also required. This is obtained from the derivative of 6.60 with respect to \mathbf{v} , which yields

$$\frac{\partial \mathbf{q}}{\partial \mathbf{v}} = \frac{\partial}{\partial \mathbf{v}} \int_L \mathbf{a}_e^T(x) \mathbf{s}(x) dx = \int_L \mathbf{a}_e^T(x) \frac{\partial \mathbf{s}(x)}{\partial \mathbf{e}(x)} \frac{\partial \mathbf{e}(x)}{\partial \mathbf{v}} dx = \int_L \mathbf{a}_e^T(x) \mathbf{k}_s(x) \mathbf{a}_e(x) dx \quad (6.61)$$

where $\mathbf{k}_s(x)$ is the section stiffness matrix from 6.39, and the derivative of the section deformations with respect to \mathbf{v} is obtained from 6.59. The expression in 6.61 is the tangent stiffness matrix \mathbf{k}_t of the element.

The expressions in 6.48, 6.58, 6.60 and 6.61 for the state determination of the distributed inelasticity elements involve integrals over the element length. The evaluation of these integrals is accomplished numerically. In analogy with 6.42 the integrals are evaluated as

$$\int_L g(x) dx \approx \sum_{l=1}^{nIP} w_l g(x_l)$$

The most suitable numerical integration methods use the Gauss or the Gauss–Lobatto rule which optimize accuracy of smooth integrands for a given number of integration points (Bathe, 1995). The Gauss–Lobatto rule is particularly suitable when it is important to include the ends of the element in the evaluation. This is indeed the case in earthquake engineering applications, where the largest inelastic deformations quite often take place at the element ends. Four integration points suffice for the integrals in 6.48, 6.58, 6.60 and 6.61 as long as we are not interested in the effect of the midspan section. In the latter case, which is important in girders under significant gravity loads, five integration points are recommended. However, the inclusion of the effect of gravity loads can only be accommodated with the force formulation. By contrast, in the displacement formulation, the section forces in 6.60 are derived from the section deformations and do not include the effect of loads on the elements, such as due to gravity. The latter are included as external virtual work contribution by modification of 6.60 according to

$$\mathbf{q} + \int_L \mathbf{a}^T(x) \mathbf{w}(x) dx = \int_L \mathbf{a}_e^T(x) \mathbf{s}(x) dx \quad (6.62)$$

We conclude from 6.62 that the initial or fixed-end forces of the displacement formulation are not different from those of a linear elastic, prismatic frame element. Moreover, in this case the element loads only affect the element forces and do not affect the internal force distribution. This is another serious limitation of the displacement formulation.

6.8 Solution of Equilibrium Equations

The equilibrium equations in 6.1 constitute the starting point for linear or nonlinear structural analysis methods. We focus our attention on the free DOFs of the model and write for the applied and resisting forces the system of equations:

$$\mathbf{P}_f - \mathbf{P}_{rf} = 0 \quad (6.63)$$

The subscript f is dropped for brevity of notation, and the reactions at the restrained DOFs can be evaluated after the equations for the free DOFs are solved. In the general case the resisting forces are implicit functions of the displacements \mathbf{U} at the DOFs of the structural model and 6.63 becomes a set of nonlinear equations in the unknown displacements \mathbf{U}

$$\mathbf{P} - \mathbf{P}_r(\mathbf{U}) = 0 \quad (6.64)$$

where we assume that the applied forces \mathbf{P} do not depend on the displacements \mathbf{U} . Equation 6.64 applies to static analysis. For dynamic analysis it will be generalized with the inclusion of inertia effects in a later section.

6.8.1 Newton–Raphson Iteration

To develop a solution algorithm for the nonlinear system of equations in 6.64, the resisting forces are expanded in a Taylor series about an initial displacement vector \mathbf{U}_0 :

$$\mathbf{P}_r(\mathbf{U}) = \mathbf{P}_r(\mathbf{U}_0) + \frac{\partial \mathbf{P}_r}{\partial \mathbf{U}} \Big|_0 (\mathbf{U} - \mathbf{U}_0) + \frac{1}{2} \frac{\partial^2 \mathbf{P}_r}{\partial \mathbf{U}^2} \Big|_0 (\mathbf{U} - \mathbf{U}_0)^2 + \dots \quad (6.65)$$

Truncating the Taylor series after the linear term and substituting the expression of the resisting forces from 6.65 in 6.64 we obtain a linear system of equations for the unknown displacements \mathbf{U} . Denoting the displacement increment by $\Delta \mathbf{U} = \mathbf{U} - \mathbf{U}_0$, the linearized equilibrium relationship from 6.65 is

$$\mathbf{P} - \mathbf{P}_r(\mathbf{U}_0) = \frac{\partial \mathbf{P}_r}{\partial \mathbf{U}} \Big|_0 \Delta \mathbf{U} = \mathbf{K}_{t0} \Delta \mathbf{U} \quad (6.67)$$

Equation 6.67 includes the tangent stiffness matrix, \mathbf{K}_t , for the free DOFs of the structural model as the derivative of the global resisting force vector with respect to the displacements. This derivative is evaluated at \mathbf{U}_0 in 6.67. The term (l, m) of the stiffness matrix represents the partial derivative of the resisting force at DOF l with respect to the displacement at DOF m . The tangent stiffness matrix is obtained by direct assembly of the tangent stiffness matrices of the elements in the structural model after the latter have been transformed to the global coordinate system, as will be discussed later in this section.

The solution of 6.67 yields the displacement increment $\Delta \mathbf{U}$. An improved estimate of the solution to the system of equilibrium equations in 6.64 can be obtained with $\mathbf{U}_1 = \mathbf{U}_0 + \Delta \mathbf{U}$. The repetition of this process will converge to the solution of the nonlinear set of equilibrium equations in 6.64 under certain conditions. This iterative procedure is known as Newton–Raphson algorithm. An important characteristic of the Newton–Raphson iteration is that the process converges with a quadratic rate to the solution. This can be observed by a slight modification of 6.65:

$$\begin{aligned} \mathbf{P}_r(\mathbf{U}) &= \mathbf{P}_r(\mathbf{U}_0) + \frac{\partial \mathbf{P}_r}{\partial \mathbf{U}} \Big|_0 (\mathbf{U} - \mathbf{U}_1 + \mathbf{U}_1 - \mathbf{U}_0) + \frac{1}{2} \frac{\partial^2 \mathbf{P}_r}{\partial \mathbf{U}^2} \Big|_{\xi} (\mathbf{U} - \mathbf{U}_0)^2 \\ \mathbf{P}_r(\mathbf{U}) &= \mathbf{P}_r(\mathbf{U}_0) + \frac{\partial \mathbf{P}_r}{\partial \mathbf{U}} \Big|_0 (\mathbf{U}_1 - \mathbf{U}_0) + \frac{\partial \mathbf{P}_r}{\partial \mathbf{U}} \Big|_0 (\mathbf{U} - \mathbf{U}_1) + \frac{1}{2} \frac{\partial^2 \mathbf{P}_r}{\partial \mathbf{U}^2} \Big|_{\xi} (\mathbf{U} - \mathbf{U}_0)^2 \\ 0 &= \frac{\partial \mathbf{P}_r}{\partial \mathbf{U}} \Big|_0 (\mathbf{U} - \mathbf{U}_1) + \frac{1}{2} \frac{\partial^2 \mathbf{P}_r}{\partial \mathbf{U}^2} \Big|_{\xi} (\mathbf{U} - \mathbf{U}_0)^2 \end{aligned}$$

where the last equation results from the use of 6.67 for the first two terms of the second equation. By taking absolute values of the last expression we arrive at the desired result $|\mathbf{U} - \mathbf{U}_1| \leq c |\mathbf{U} - \mathbf{U}_0|^2$, where c is a constant. This means that the error between the solution and iterate is less than the square of the error for the previous iterate. This characteristic is used in simulation studies to ascertain that the stiffness matrix is indeed tangent to the structural response, because the latter fact can have important ramifications for the convergence of the Newton–Raphson algorithm. The constant c depends on the second derivative of the resisting force, or the change in the tangent stiffness. Large changes in stiffness result

in large constants and slower convergence. As will be covered in the following, the convergence can be improved by a load incrementation strategy.

The Newton–Raphson algorithm proceeds in the following steps:

1. At the start of iteration j , compute the resisting forces $\mathbf{P}_{rj-1} = \mathbf{P}_r(\mathbf{U}_{j-1})$ and the tangent stiffness \mathbf{K}_{uj-1} for the displacements at the end of the previous iteration \mathbf{U}_{j-1} .
2. Solve the linearized system of equations $\mathbf{P}_{uj} = \mathbf{P} - \mathbf{P}_{rj-1} = \mathbf{K}_{uj-1}\Delta\mathbf{U}_j$ for $\Delta\mathbf{U}_j$.
3. Update the displacement vector $\mathbf{U}_j = \mathbf{U}_{j-1} + \Delta\mathbf{U}_j$, advance the iteration index and return to step 1 repeating steps 1 to 3 until convergence. The convergence criterion will be discussed later in this section.

The convergence of the algorithm depends on the initial displacement to start the iteration, the characteristics of the tangent stiffness matrix \mathbf{K}_t and the convergence criterion. It is important that the initial guess be close to the actual solution.

6.8.2 Load Incrementation

To improve the convergence of the Newton–Raphson algorithm for nonlinear structural analysis, it is necessary to incorporate a procedure for incrementing the load to limit the changes in the structural state for each load increment. Instead of applying the load in one step, the solution is divided into several steps, and it proceeds with load factor increments whose magnitude can be adjusted depending on the state of the structure. Within each load step the Newton–Raphson iteration process can be used to solve the equilibrium equations.

We assume that the applied loads are grouped in load patterns with independent histories. The simplest case is a single applied force pattern \mathbf{P}_{ref} , and this case has some important applications in the nonlinear static analysis of structures under equivalent lateral earthquake loads. The notation for the load incrementation procedure uses a superscript in parentheses to denote the load step number with index k while a subscript denotes the iteration number in each load step with index j . The applied force vector at load step k can, therefore, be written as

$$\mathbf{P}^{(k)} = \lambda^{(k)} \mathbf{P}_{ref}$$

where the load factor $\lambda^{(k)}$ results from a series of increments,

$$\lambda^{(k)} = \lambda^{(k-1)} + \Delta\lambda^{(k)}$$

so that the applied force vector at load step k can also be written as

$$\mathbf{P}^{(k)} = \mathbf{P}^{(k-1)} + \Delta\lambda^{(k)} \mathbf{P}_{ref}$$

The equilibrium equations at load step k become

$$\mathbf{P}^{(k)} - \mathbf{P}_r^{(k)} = \mathbf{P}^{(k-1)} + \Delta\lambda^{(k)} \mathbf{P}_{ref} - \mathbf{P}_r^{(k)}$$

and the starting displacement vector for satisfying the above equilibrium equations is $\mathbf{U}_0^{(k)} = \mathbf{U}^{(k-1)}$, that is the state at the end of the previous load step. If the load factor increment is held constant during the equilibrium iterations, then the iteration process consists of the three steps presented earlier with the unbalanced force given by $\mathbf{P}_{uj}^{(k)} = \mathbf{P}^{(k-1)} + \Delta\lambda^{(k)} \mathbf{P}_{ref} - \mathbf{P}_{rj-1}^{(k)}$. Only the resisting force vector is updated during the equilibrium iterations.

6.8.3 Load Factor Control during Incrementation

The load factor increment can be changed in the Newton–Raphson algorithm so that large increments are applied when the structure stiffness does not change much, and the increments are reduced when

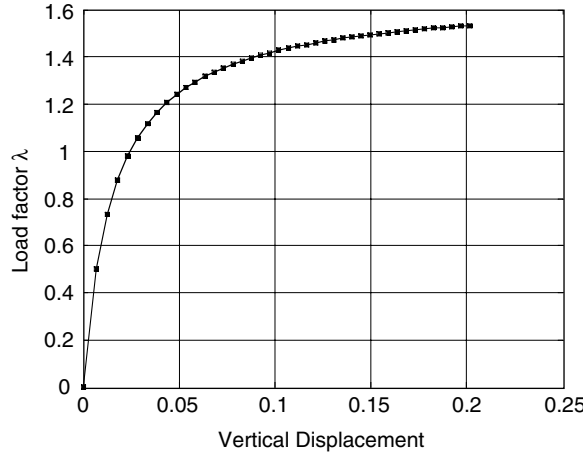


FIGURE 6.19 Load-displacement response with load factor control during incrementation.

the stiffness changes. An excellent parameter for this purpose is the current stiffness parameter (Bergan, 1978). This parameter is the scalar product of the reference force vector and the corresponding displacements caused by the forces. Denoting the displacements under the reference force vector with \mathbf{U}_t , the stiffness parameter is defined as

$$S_p = \mathbf{P}_{\text{ref}}^T \mathbf{U}_t = \mathbf{P}_{\text{ref}}^T \mathbf{K}_t^{-1} \mathbf{P}_{\text{ref}}$$

The initial value of the parameter $S_p^{(0)}$ is computed with the initial tangent stiffness matrix. The following expression gives the change in the load factor for load step k (Bergan, 1978),

$$\Delta\lambda^{(k)} = \Delta\lambda^{(0)} \left| \frac{S_p^{(0)}}{S_p^{(k-1)}} \right|^{\gamma} \quad (6.68)$$

where $S_p^{(k-1)}$ is the stiffness parameter at the end of the previous load step $k-1$, $\Delta\lambda^{(0)}$ is the load factor increment for the first load step with $k=1$, commonly selected to be about 30% of the collapse load factor, and γ is a constant between 0.5 and 1.2, with 1.0 being a commonly used value. Figure 6.19 shows the load-displacement response of a structural model with an exponent value of $\gamma=1$. The model is a truss structure with nonlinear material response. It is clear from the figure that with load factor adjustment during incrementation it is possible to approach the maximum strength of the model even though the tangent stiffness becomes nearly singular.

6.8.4 Load Factor Control during Iteration

Load incrementation allows the Newton-Raphson algorithm to approach the maximum strength, but it cannot compute the postpeak response. For tracing the postpeak response, the incrementation procedure needs to be further modified so as to control the load during the equilibrium iterations. In this case the applied force vector is updated during the equilibrium iterations of a load step. With a subscript denoting the iteration number, the unbalanced force is

$$\mathbf{P}_{uj}^{(k)} = \mathbf{P}_j^{(k)} - \mathbf{P}_{ij-1}^{(k)} = \mathbf{P}_{j-1}^{(k)} + \Delta\lambda_j^{(k)} \mathbf{P}_{\text{ref}} - \mathbf{P}_{ij-1}^{(k)} \quad (6.69)$$

During the first iteration, $j=1$, the first term on the right-hand side of 6.69 is equal to the force vector at the end of the previous load step, $\mathbf{P}_0^{(k)} = \mathbf{P}^{(k-1)}$. Since all superscripts in 6.69 refer to load step k , these are not included in the following equations for brevity of notation. Using the Newton-Raphson algorithm, the following system of linear equations of equilibrium is solved at each iteration:

$$\mathbf{P}_{uj} = \mathbf{K}_{tj-1} \Delta \mathbf{U}_j \quad (6.70)$$

Substituting 6.69 into 6.70 gives

$$\mathbf{P}_{j-1} + \Delta \lambda_j \mathbf{P}_{ref} - \mathbf{P}_{rj-1} = \mathbf{K}_{tj-1} \Delta \mathbf{U}_j = \mathbf{K}_{tj-1} (\Delta \mathbf{U}_{rj-1} + \Delta \lambda_j \mathbf{U}_{rj-1}) \quad (6.71)$$

so that

$$\mathbf{P}_{j-1} - \mathbf{P}_{rj-1} = \mathbf{K}_{tj-1} \Delta \mathbf{U}_{rj-1}$$

$$\mathbf{P}_{ref} = \mathbf{K}_{tj-1} \mathbf{U}_{rj-1}$$

With the decomposition of displacement increments into two terms on the right-hand side of 6.71, a separate condition can be introduced to determine the load factor increment during iteration j . Several schemes have been proposed for the purpose and there is extensive literature on the subject (Clarke and Hancock, 1990, Crisfield, 1991). The schemes that prove particularly useful for the nonlinear static (pushover) analysis of structures with equivalent lateral earthquake loads involve load control during iterations under constant displacement at a single selected degree of freedom (sometimes referred to as the control node). In this case, we impose a condition on degree of freedom n , such that $\Delta U_{nj} = \Delta \lambda_j U_{tnj-1} + \Delta U_{rnj-1} = 0$, to determine the load factor increment $\Delta \lambda_j$. An alternative is to use the condition of constant external work to determine the load factor, which leads to the condition that $\Delta W_j = \Delta \mathbf{U}_j^T \Delta \lambda_j \mathbf{P}_{ref} = 0$. After substituting $\Delta \mathbf{U}_j$ from 6.71, the load factor is given by

$$\Delta \lambda_j = -\frac{\Delta \mathbf{U}_{rj-1}^T \mathbf{P}_{ref}}{\mathbf{U}_{tj-1}^T \mathbf{P}_{ref}}$$

With load control during equilibrium iterations the steps of the Newton-Raphson algorithm for a single load step are:

1. Start with the structure state determination for the displacements at the end of the previous iteration $j-1$ in load step k and determine the tangent stiffness matrix \mathbf{K}_{tj-1} and resisting force vector \mathbf{P}_{rj-1} . The applied force vector \mathbf{P}_{j-1} is also known since $\mathbf{P}_{j-1} = \lambda_{j-1} \mathbf{P}_{ref}$.
2. Compute the displacements \mathbf{U}_{rj-1} under the reference force vector and the residual displacement increments $\Delta \mathbf{U}_{rj-1}$ with the equations following 6.71. Since this step involves the solution of a system of equations under different force vectors, the tangent stiffness need only be factored once followed by separate back substitutions for each system of equations.
3. Determine the load factor increment $\Delta \lambda_j$ and the resulting displacement increments $\Delta \mathbf{U}_j$:

$$\Delta \mathbf{U}_j = \Delta \lambda_j \mathbf{U}_{tj-1} + \Delta \mathbf{U}_{rj-1}$$

4. Update the displacements and the load factor:

$$\mathbf{U}_j = \mathbf{U}_{j-1} + \Delta \mathbf{U}_j$$

$$\lambda_j = \lambda_{j-1} + \Delta \lambda_j$$

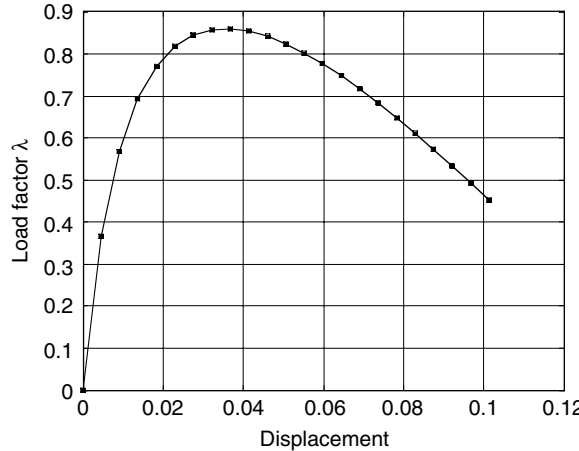


FIGURE 6.20 Load–displacement response with load factor control during iteration.

Update the iteration index and repeat steps 1 through 4 until convergence. Convergence is measured by the ratio of the relative work increment ΔW_j in iteration j to the initial work increment at iteration $j=1$ where

$$\Delta W_j = \Delta \mathbf{U}_j^T (\mathbf{P}_{j-1} + \Delta \lambda_j \mathbf{P}_{\text{ref}} - \mathbf{P}_{r,j-1})$$

Figure 6.20 shows the load–displacement response of the same truss structure as in Figure 6.19, for the case that the truss elements have a softening modulus equal to 10% of the initial modulus. The figure shows how the load control algorithm permits the tracing of the postpeak response.

6.8.5 Structure State Determination

A key step in the Newton–Raphson algorithm is the structure state determination, which involves the determination of the resisting force vector and structure stiffness matrix for given structural displacements and their increments. The tangent stiffness matrix of the structure is obtained by the partial derivative of the resisting forces with respect to the displacements at the global DOFs. Applying the chain rule of differentiation to 6.1 gives

$$\mathbf{K}_t = \frac{\partial \mathbf{P}_r}{\partial \mathbf{U}} = \frac{\partial}{\partial \mathbf{U}} \sum_{el} \mathbf{P}_{r,id}^{(el)} = \mathbf{A}_{el} \frac{\partial \mathbf{p}^{(el)}}{\partial \mathbf{u}^{(el)}} \frac{\partial \mathbf{u}^{(el)}}{\partial \mathbf{U}} \quad (6.72)$$

The assembly operation on the right-hand side involves row indexing and summation of the element contributions. Each row of the element resisting forces will produce as many columns as the number of element DOFs in vector \mathbf{u} in the operation $\mathbf{A}_{el} \frac{\partial \mathbf{p}^{(el)}}{\partial \mathbf{u}^{(el)}}$. With 6.12 these columns will be postmultiplied by a matrix with a single nonzero term of unity in each row. This unit value is located at the column that corresponds to the global DOF number to which the element DOF in the corresponding row maps.

Postmultiplication by this matrix amounts to mapping the column numbers of $\frac{\partial \mathbf{p}^{(el)}}{\partial \mathbf{u}^{(el)}}$ to the column numbers corresponding to the global DOF numbers for the DOFs of this element. From 6.72 we conclude

that the global tangent stiffness matrix \mathbf{K}_t of the structure can be obtained by direct assembly (row indexing and summation) of the element stiffness coefficients in the global coordinate system, as long as the columns of the element stiffness matrix are mapped to the global DOF numbers corresponding to the element DOFs of the particular element. This is written in compact form as

$$\mathbf{K}_t = \sum_{el} \mathbf{A}_{el} \mathbf{k}_t^{(el)} \quad (6.73)$$

The assembly of the resisting force vector \mathbf{P}_r follows 6.1.

The partial derivative of the element forces with respect to the element displacements in the global reference system represents the element tangent stiffness matrix in the global coordinate system. The tangent stiffness matrix of the element can be obtained from 6.5 by the chain rule of differentiation,

$$\mathbf{k}_t^{(el)} = \frac{\partial \mathbf{p}}{\partial \mathbf{u}} = \frac{\partial}{\partial \mathbf{u}} (\mathbf{a}_g^T \mathbf{q}) = \mathbf{a}_g^T \frac{\partial \mathbf{q}}{\partial \mathbf{v}} \frac{\partial \mathbf{v}}{\partial \mathbf{u}} = \mathbf{a}_g^T \mathbf{k}_t \mathbf{a}_g \quad (6.74)$$

where \mathbf{k}_t is the tangent stiffness of the basic element. Linear geometry is assumed in 6.74 so that the transformation matrix \mathbf{a}_g does not depend on the displacements \mathbf{u} , and 6.18 can be used for the derivative of the element deformations with respect to \mathbf{u} .

6.8.6 State Determination of Elements with Force Formulation

The Newton–Raphson algorithm can be used for the solution of the system of nonlinear equations in 6.57. We present it here because the state determination of this class of elements is not well known in the literature. For iteration j

$$\hat{\mathbf{v}} - \mathbf{v}_{j-1} - \left. \frac{\partial \mathbf{v}}{\partial \mathbf{q}} \right|_{j-1} \Delta \mathbf{q}_j = 0$$

Noting that the element stiffness is the inverse of the flexibility matrix, we can obtain the increment of the element forces $\Delta \mathbf{q}_j$ according to

$$\Delta \mathbf{q}_j = \mathbf{k}_{t,j-1} (\hat{\mathbf{v}} - \mathbf{v}_{j-1})$$

and update the element forces to $\mathbf{q}_j = \mathbf{q}_{j-1} + \Delta \mathbf{q}_j$. We solve for the section deformations and increments at the integration points from

$$\mathbf{b}(x) \mathbf{q}_j + \mathbf{s}_{w_j}(x) - \left(\mathbf{s}_{j-1}(x) + \left. \frac{\partial \mathbf{s}}{\partial \mathbf{e}} \right|_{j-1} \Delta \mathbf{e}_j(x) \right) = 0$$

noting that the derivative of the section forces with respect to section deformations is the last section stiffness matrix $\mathbf{k}_{s,j-1}(x)$. After determining $\Delta \mathbf{e}_j(x)$, we update the section deformations to $\mathbf{e}_j(x) = \mathbf{e}_{j-1}(x) + \Delta \mathbf{e}_j(x)$. Finally, we determine the current element deformations from the principle of virtual forces

$$\mathbf{v}_j = \int_L \mathbf{b}^T(x) \mathbf{e}_j(x) dx$$

and return to the beginning of the algorithm with a new deformation residual $\hat{\mathbf{v}} - \mathbf{v}_j$.

The above process implies an iterative element state determination for each iteration of the solution of the global equilibrium equations (Ciampi and Carlesimo, 1986, Taucer et al., 1991). An alternative scheme has also been used with success whereby the element state determination consists of a single iteration that works in tandem with the global equilibrium equations (Neuenhofer and Filippou, 1997). In either case by setting $j=1$ in the element state determination algorithm we conclude that we need to store the element forces \mathbf{q}_{j-1} and the section deformations $\mathbf{e}_{j-1}(x)$ from a global iteration to the next.

6.8.7 Nonlinear Solution of Section State Determination

The section state determination forms part of the algorithm of the state determination of elements with distributed inelasticity, but is also important in its own right in the determination of moment–curvature and interaction diagrams of sections. Therefore, we briefly describe the process of section state determination for a couple of cases. In the simplest case the section deformations \mathbf{e} are given. Using the assumption of section kinematics we determine the strain at the integration points of the cross section $\boldsymbol{\varepsilon}_i$ according to the first equation in 6.43 and use the material constitutive relation to obtain the corresponding stress and material stiffness. We then determine the section forces \mathbf{s} and the section stiffness \mathbf{k}_s by numerical evaluation of the integrals in 6.43. This is the process used at every integration point of the distributed inelasticity elements during state determination. The same process can be used to obtain the interaction diagram of a cross section, in which case the section deformations \mathbf{e} are set so as to describe the limit state of the section.

In the determination of the moment–curvature diagram the problem is slightly different. In this case the curvatures are specified along with the axial force acting on the cross section. The corresponding axial strain is determined from the single available equilibrium equation, the axial force equilibrium. We write symbolically

$$\hat{N} - N(\boldsymbol{\varepsilon}_a, \kappa) = 0$$

where the symbol over the axial force N denotes the given value. Because this is a scalar equation, different solution methods can be used. We show here the application of the Newton–Raphson solution. For this we write for the step of load incrementation

$$\hat{N} - \left(N_0 + \frac{\partial N}{\partial \boldsymbol{\varepsilon}_a} \Delta \boldsymbol{\varepsilon}_a + \frac{\partial N}{\partial \kappa} \Delta \kappa \right) = 0$$

where N_0 denotes the axial force value of the last load step. We note also that the derivatives of the axial force with respect to the section deformations correspond to terms (1,1) and (1,2) of the section stiffness matrix \mathbf{k}_s . Because the curvature increment is specified, we solve the above equation for the initial increment of the axial strain $\Delta \boldsymbol{\varepsilon}_a$ according to

$$\frac{\partial N}{\partial \boldsymbol{\varepsilon}_a} \Delta \boldsymbol{\varepsilon}_a = \hat{N} - \left(N_0 + \frac{\partial N}{\partial \kappa} \Delta \kappa \right)$$

During subsequent iteration corrections the curvature increment is set equal to zero.

6.9 Nonlinear Geometry and P-Δ Geometric Stiffness

The element tangent stiffness matrix in Section 6.8.5 was derived on the assumption of linear geometry, in which case the element equilibrium equations are satisfied in the undeformed configuration and the

compatibility relation between element deformations and end displacements in the global reference system does not depend on the displacements. In the general case of nonlinear geometry, the element equilibrium equations need to be satisfied in the deformed configuration according to Section 6.4, and the compatibility relation between element deformations and end displacements in the global reference system becomes nonlinear on account of large displacements. For applications in earthquake engineering, approximations of the nonlinear equilibrium and compatibility relations are possible, as will be discussed in the following.

6.9.1 Resisting Forces and Element Tangent Stiffness Matrix

As discussed in Section 6.4, the equilibrium in the deformed configuration is expressed in the local coordinate system. Thus, the resisting forces $\bar{\mathbf{p}}$ for given end displacements $\bar{\mathbf{u}}$ in the local coordinate system are given by either 6.21, 6.22 or 6.23 depending on the desired accuracy in the geometrically nonlinear analysis. The compatibility transformation $\bar{\mathbf{u}} = \mathbf{a}_r \mathbf{u}$ is used to transform the end displacements from the global to the local coordinate system. After obtaining the element end forces $\bar{\mathbf{p}}$ in the local coordinate system from either 6.21, 6.22 or 6.23, the rotation transformation $\mathbf{p} = \mathbf{a}_r^T \bar{\mathbf{p}}$ transforms the element resisting forces to the global coordinate system.

For the element stiffness matrix, we proceed in an analogous manner:

$$\frac{\partial \mathbf{p}}{\partial \mathbf{u}} = \frac{\partial}{\partial \mathbf{u}} (\mathbf{a}_r^T \bar{\mathbf{p}}) = \mathbf{a}_r^T \frac{\partial \bar{\mathbf{p}}}{\partial \bar{\mathbf{u}}} \frac{\partial \bar{\mathbf{u}}}{\partial \mathbf{u}} = \mathbf{a}_r^T \bar{\mathbf{k}} \mathbf{a}_r \quad (6.75)$$

There is nothing special in this transformation process relative to linear geometry. However, the tangent element stiffness matrix $\bar{\mathbf{k}}$ in the local reference system requires additional consideration for geometrically nonlinear analysis. Using the resisting forces in 6.21, the chain rule of differentiation for the element stiffness matrix $\bar{\mathbf{k}}$ in the local reference system gives

$$\bar{\mathbf{k}} = \frac{\partial \bar{\mathbf{p}}}{\partial \bar{\mathbf{u}}} = \frac{\partial}{\partial \bar{\mathbf{u}}} (\mathbf{b}_u \mathbf{q}) = \frac{\partial \mathbf{b}_u}{\partial \bar{\mathbf{u}}} \mathbf{q} + \mathbf{b}_u \frac{\partial \mathbf{q}}{\partial \mathbf{v}} \frac{\partial \mathbf{v}}{\partial \bar{\mathbf{u}}} \quad (6.76)$$

The element stiffness matrix in the local coordinate system in 6.76 is composed of two contributions: the geometric stiffness $\bar{\mathbf{k}}_g$ arising from the change of the equilibrium matrix with end displacements $\bar{\mathbf{u}}$, and the material stiffness $\bar{\mathbf{k}}_m$, which represents the transformation of the tangent basic stiffness $\mathbf{k}_t = \frac{\partial \mathbf{q}}{\partial \mathbf{v}}$ to the local coordinate system.

Using the deformation-large displacement relations in 6.13 and 6.14, the derivative of \mathbf{v} relative to $\bar{\mathbf{u}}$ is as follows:

$$\begin{aligned} \frac{\partial \mathbf{v}_1}{\partial \bar{\mathbf{u}}} &= \frac{L_n}{L} \frac{\partial L_n}{\partial \bar{\mathbf{u}}} = \frac{L_n}{L} \frac{1}{L_n} \left(-\left(L + \Delta \bar{\mathbf{u}}_x \right) \quad -\Delta \bar{\mathbf{u}}_y \quad 0 \quad L + \Delta \bar{\mathbf{u}}_x \quad \Delta \bar{\mathbf{u}}_y \quad 0 \right) \\ \frac{\partial \mathbf{v}_2}{\partial \bar{\mathbf{u}}} &= \left(0 \quad 0 \quad 1 \quad 0 \quad 0 \quad 0 \right) - \frac{1}{L_n} \left(\frac{\Delta \bar{\mathbf{u}}_y}{L_n} \quad -\frac{L + \Delta \bar{\mathbf{u}}_x}{L_n} \quad 0 \quad -\frac{\Delta \bar{\mathbf{u}}_y}{L_n} \quad \frac{L + \Delta \bar{\mathbf{u}}_x}{L_n} \quad 0 \right) \\ \frac{\partial \mathbf{v}_3}{\partial \bar{\mathbf{u}}} &= \left(0 \quad 0 \quad 0 \quad 0 \quad 0 \quad 1 \right) - \frac{1}{L_n} \left(\frac{\Delta \bar{\mathbf{u}}_y}{L_n} \quad -\frac{L + \Delta \bar{\mathbf{u}}_x}{L_n} \quad 0 \quad -\frac{\Delta \bar{\mathbf{u}}_y}{L_n} \quad \frac{L + \Delta \bar{\mathbf{u}}_x}{L_n} \quad 0 \right) \end{aligned}$$

By comparison of the above expressions with 6.21, it is clear that contragradient holds, so that

$$\frac{\partial \mathbf{v}}{\partial \bar{\mathbf{u}}} = \mathbf{a}_u = \mathbf{b}_u^T$$

when the difference between L_n and L in $\partial\mathbf{v}_1/\partial\bar{\mathbf{u}}$ is neglected. Thus, 6.76 becomes

$$\bar{\mathbf{k}} = \bar{\mathbf{k}}_g + \bar{\mathbf{k}}_m = \frac{\partial \mathbf{b}_u}{\partial \bar{\mathbf{u}}} \mathbf{q} + \mathbf{b}_u \mathbf{k}_t \mathbf{b}_u^T = \frac{\partial \mathbf{a}_u^T}{\partial \bar{\mathbf{u}}} \mathbf{q} + \mathbf{a}_u^T \mathbf{k}_t \mathbf{a}_u \quad \text{with } \mathbf{k}_t = \frac{\partial \mathbf{q}}{\partial \mathbf{v}} \quad (6.77)$$

The form of 6.77 reinforces the earlier statement that the material stiffness is equal to the tangent basic stiffness transformed to the local coordinate system. Combining 6.77 with 6.75 gives the element stiffness matrix in the global coordinate system including the geometric and material stiffness contributions:

$$\mathbf{k}^{el} = \mathbf{a}_r^T \left(\frac{\partial \mathbf{a}_u^T}{\partial \bar{\mathbf{u}}} \mathbf{q} + \mathbf{a}_u^T \mathbf{k}_t \mathbf{a}_u \right) \mathbf{a}_r = \mathbf{a}_r^T \bar{\mathbf{k}}_g \mathbf{a}_r + \mathbf{a}_r^T \mathbf{a}_u^T \mathbf{k}_t \mathbf{a}_u \mathbf{a}_r \quad (6.78)$$

It is important to emphasize that 6.78 holds for all element types, as long as the element force-deformation relation is defined in the basic system. Of equal importance is the fact that by separating the geometric transformations from the actual element formulation in 6.78 different geometric theories can be implemented for the same element by selecting the form of the compatibility matrix \mathbf{a}_u . Under linear geometry matrix \mathbf{a}_u simplifies to 6.17 and is displacement independent. Thus, the geometric stiffness is zero and the element stiffness matrix reduces to 6.74 with $\mathbf{a}_g = \mathbf{a}\mathbf{a}_r$, as defined in 6.18 without rigid end offsets.

6.9.2 Geometric Stiffness Matrix

There remains the task of determining the geometric stiffness $\bar{\mathbf{k}}_g$ in 6.77 and 6.78 by taking the derivative $\partial \mathbf{b}_u / \partial \bar{\mathbf{u}}$. This operation is performed column by column noting that the derivative of the first column multiplies the axial force \mathbf{q}_1 and supplies the contribution $\bar{\mathbf{k}}_{g1}$ to the geometric stiffness matrix, whereas the derivatives of the second and third columns multiply the end moments \mathbf{q}_2 and \mathbf{q}_3 , respectively. These can be combined to give the contribution $\bar{\mathbf{k}}_{g23}$ to the geometric stiffness matrix. From the derivative of the first column of \mathbf{b}_u the $\bar{\mathbf{k}}_{g1}$ contribution is

$$\bar{\mathbf{k}}_{g1} = \frac{\mathbf{q}_1}{L_n} \begin{bmatrix} s^2 & -cs & 0 & -s^2 & cs & 0 \\ -cs & c^2 & 0 & cs & -c^2 & 0 \\ 0 & 0 & 0 & 0 & 0 & 0 \\ -s^2 & cs & 0 & s^2 & -cs & 0 \\ cs & -c^2 & 0 & -cs & c^2 & 0 \\ 0 & 0 & 0 & 0 & 0 & 0 \end{bmatrix} \quad (6.79)$$

in which

$$c = \frac{L + \Delta\bar{\mathbf{u}}_x}{L_n} \quad \text{and} \quad s = \frac{\Delta\bar{\mathbf{u}}_y}{L_n}$$

From the second and third columns of \mathbf{b}_u we obtain

$$\bar{\mathbf{k}}_{g23} = \frac{\mathbf{q}_2 + \mathbf{q}_3}{L_n} \frac{1}{L_n} \begin{bmatrix} -2sc & c^2 - s^2 & 0 & 2sc & -c^2 + s^2 & 0 \\ c^2 - s^2 & 2cs & 0 & -c^2 + s^2 & -2cs & 0 \\ 0 & 0 & 0 & 0 & 0 & 0 \\ 2sc & -c^2 + s^2 & 0 & -2sc & c^2 - s^2 & 0 \\ -c^2 + s^2 & -2cs & 0 & c^2 - s^2 & 2cs & 0 \\ 0 & 0 & 0 & 0 & 0 & 0 \end{bmatrix} \quad (6.80)$$

In the scalar factor for the matrix in 6.80, the deformed element length is used in the denominator because the first term represents the shear force in the deformed element configuration. With this identification a comparison of the two matrices in 6.79 and 6.80 is possible. In slender compression elements the shear force is often significantly less than the axial force, so that the contribution \bar{k}_{g23} is in such cases significantly smaller than \bar{k}_{gl} and can often be neglected.

6.9.3 P- Δ Geometric Stiffness

We introduce now an approximation of nonlinear geometry that is often used in structural analysis for earthquake-resistant design. It is known by the name $P-\Delta$ analysis, but this name is confusing for the following reason: when referring to a single member it is convenient to distinguish between the effect of axial force on the free body equilibrium of the entire member, the so-called $P-\Delta$ effect and the effect of the axial force on the internal forces in the deformed configuration, the so-called $P-\delta$ effect. Such distinction is, however, not relevant when the member is subdivided into several elements. In such case, even an element that only accounts for the $P-\Delta$ effect can approximate the effect of the axial force on the internal forces of the member. The greater the number of elements used to model a compression member the more accurate the approximation of the internal forces.

To avoid confusion, we refer to the approximation of the exact geometric transformation by the name $P-\Delta$ truss geometric stiffness. In this case we assume that the equilibrium matrix is given by $b_{p\Delta}$ in 6.23 and the resulting geometric stiffness matrix is

$$\bar{k}_g = \bar{k}_{p\Delta} = \left(\frac{\partial}{\partial \bar{u}} b_{p\Delta} \right) q = \frac{q_1}{L} \begin{bmatrix} 0 & 0 & 0 & 0 & 0 & 0 \\ 0 & 1 & 0 & 0 & -1 & 0 \\ 0 & 0 & 0 & 0 & 0 & 0 \\ 0 & 0 & 0 & 0 & 0 & 0 \\ 0 & -1 & 0 & 0 & 1 & 0 \\ 0 & 0 & 0 & 0 & 0 & 0 \end{bmatrix} \quad (6.81)$$

Equations 6.81 and 6.79 are similar, leading to the observation that the former can be obtained from the latter by setting $c \approx 1$, $s \approx 0$ and $L_n \approx L$. A difficulty arises, however, in using a consistent deformation-displacement relation for $\partial v / \partial \bar{u}$. We do not pursue this subject further here and note that commonly a_u is set equal to the linear compatibility matrix a in 6.77. With these assumptions, the element stiffness in the global coordinate system is

$$k^{el} = a_r^T \bar{k}_{p\Delta} a_r + a_g^T k_t a_g \quad (6.82)$$

Although simple, the element stiffness matrix in 6.82 deviates quickly from the tangent stiffness to the element-force deformation relation, thus resulting in poor convergence behavior even under moderate displacements.

The geometrically nonlinear behavior with the exact transformation in 6.77 and the matrices in 6.79 and 6.80, or, with the approximate geometrically nonlinear behavior in 6.82 can be improved as necessary by subdividing the compressed member into smaller elements. In such case, the deformations of the actual member relative to the chord of the elements can be made as small as necessary, so that even a very simple basic force-deformation relation can yield excellent results. Thus, the trade-off is between a smaller number of elements with more accurate force-deformation relation and a large number of very simple elements. The decision as to which approach to follow depends on the element library of the computer software used for the structural analysis. The power of the corotational approach lies in its ability to represent accurately nonlinear geometry under large displacements with simple basic force-deformation relations. We will illustrate this in the examples of the following section.

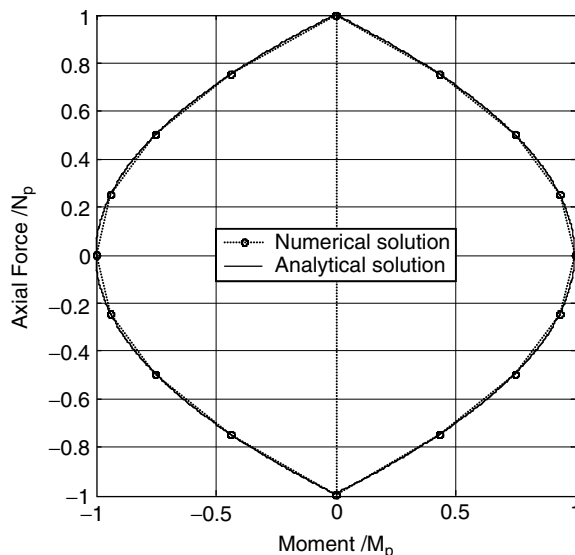


FIGURE 6.21 Axial force-bending moment interaction diagram of rectangular section with elastic-perfectly plastic material; analytical and numerical solution with eight midpoint evaluations.

6.10 Examples of Nonlinear Static Analysis

The examples in this section provide a brief overview of the type of problems that are encountered in structural analysis for earthquake engineering.

The response of sections made of one or several materials is of interest in the assessment of local response. Furthermore, it is an important ingredient in the determination of hysteretic element response. The selection of the number of integration points for sufficient accuracy is of particular interest. Figure 6.21 shows the axial force-bending moment interaction diagram of a rectangular section with bilinear elastic-perfectly plastic material. Because the results are normalized with respect to the plastic axial and flexural capacity, N_p and M_p , respectively, the dimensions and material properties are not relevant. Figure 6.21 shows clearly that the numerical solution with eight (8) midpoint evaluations for the integrals of 6.43 gives excellent accuracy. The same is true for the monotonic moment-curvature relation of the same section under three different axial load levels of 0, 30 and 60% of the plastic axial capacity N_p in Figure 6.22. In this example the closed-form solution is available and the comparison shows that a few midpoint evaluations suffice for the accurate representation of the section response. The section stiffness in 6.43 involves quadratic terms of the coordinates and is, therefore, more sensitive to the number of integration points. Usually 10 to 15 midpoint evaluations suffice for the purpose. Under biaxial loading 25 (5×5) to 64 (8×8) fibers yield excellent accuracy. For wide flange sections three layers in each flange and four layers in the web are recommended. In a reinforced concrete section the hysteretic response is dominated by the behavior of reinforcing steel. Thus, it is important to represent the area and distribution of reinforcement relatively well and then use 16 (4×4) or 25 (5×5) fibers for the concrete. A larger number of fibers may be necessary for distinguishing between cover concrete and core concrete confined by transverse reinforcement.

Figure 6.23 shows a three-story steel frame under the action of vertical and horizontal forces. The material is assumed to be elastic-perfectly plastic. The vertical and horizontal forces are collected into the same reference force vector, so that both are incremented in the following nonlinear static pushover analyses. In typical analyses the vertical forces due to gravity are kept constant, while the lateral forces are incremented to collapse. Figure 6.24 shows the relation between load factor and top story horizontal

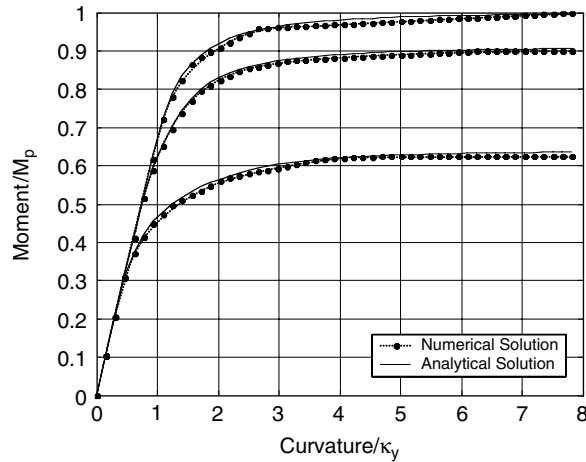


FIGURE 6.22 Moment–curvature relation for rectangular section with elastic-perfectly plastic material; analytical and numerical solution with eight midpoint evaluations under axial force of 0%, 30% and 60% of N_p .

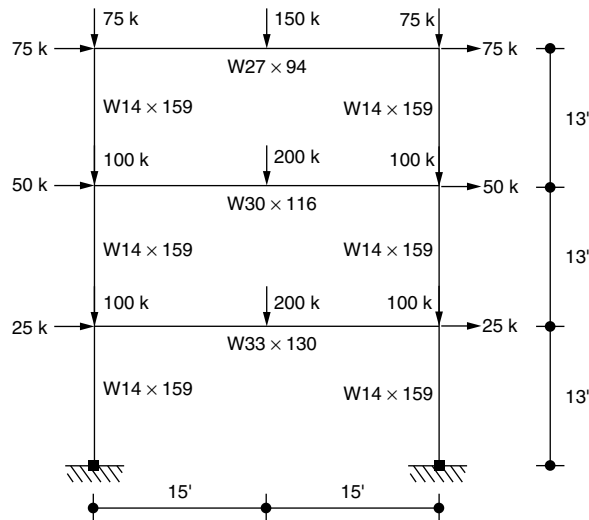
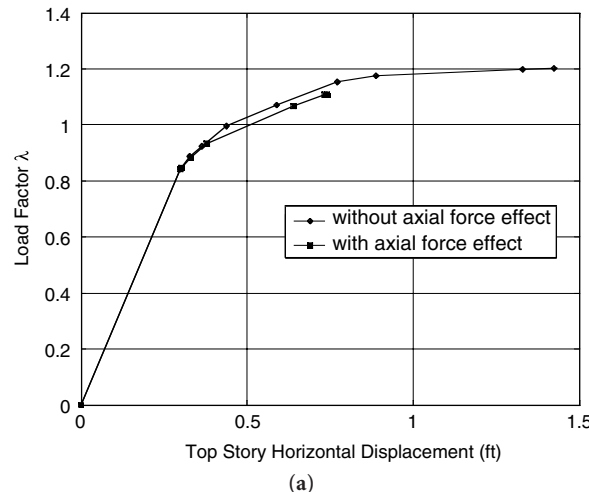


FIGURE 6.23 Geometry, member sizes and reference loading for three-story, one-bay steel frame.

displacement. The results are obtained with the elastic-perfectly plastic element of Section 6.7.2.2. Figure 6.24 shows the load-displacement response for two cases:

- In the first case the plastic flexural capacity does not account for the effect of the axial force
- In the second case a linear elastic analysis under the application of the vertical forces yields the axial forces in the columns. These are used to reduce the plastic flexural capacity of the members according to the LRFD specification. This approach does not account for the change in axial force in the columns on account of the overturning moments due to the lateral forces. Nonetheless, it gives a relatively accurate estimate of the collapse load factor of the frame, as will be shown later. It is interesting to observe that while the collapse load factor is not very different between the two cases, a collapse mechanism forms at a significantly smaller horizontal displacement in the case in which the effect of the axial force on the plastic flexural capacity is accounted for. The cause for this is apparent from Figures 6.24b and c, which show the collapse mechanism for the two



(a)

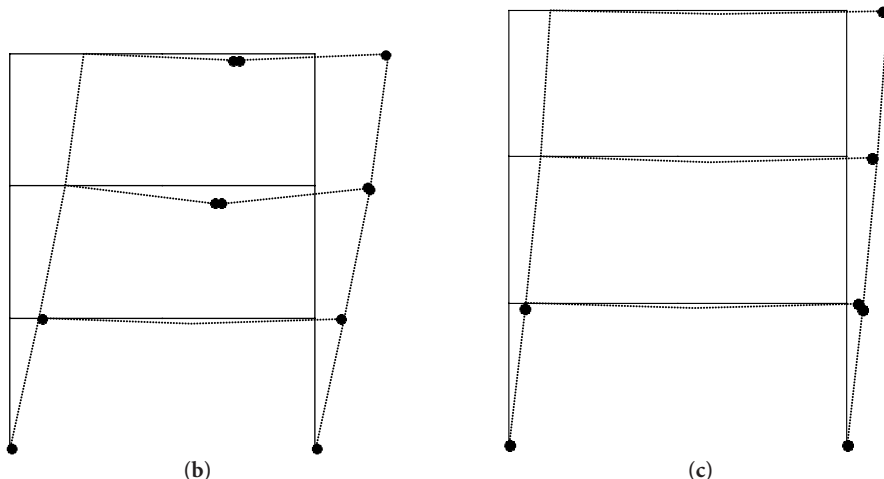
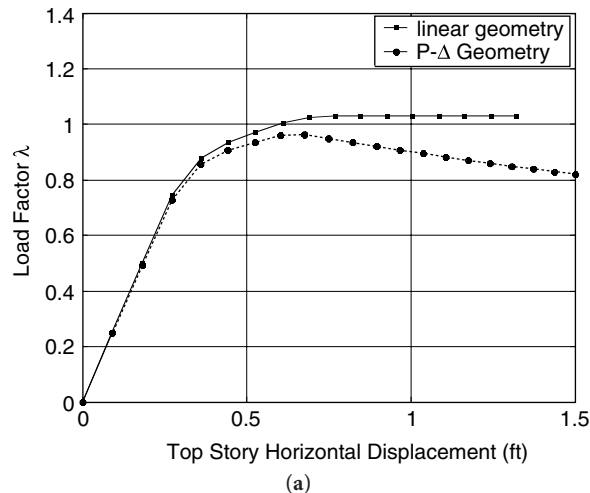


FIGURE 6.24 (a) Load factor–top story displacement relation for three-story, one-bay steel frame with and without effect of axial force on plastic moment capacity (elastic-perfectly plastic frame element). (b) Collapse mechanism of steel frame without effect of axial force on plastic moment capacity (magnification factor = 5). (c) Collapse mechanism of steel frame with effect of axial force on plastic moment capacity (magnification factor = 5).

cases. In the first case an almost complete collapse mechanism forms with nine plastic hinges, as shown in Figure 6.24b. In the second case a partial first story collapse mechanism forms, as shown in Figure 6.24c. Clearly, the difference in collapse mechanism of the two cases significantly affects the plastic rotations of the first-story columns for a given horizontal displacement.

Figure 6.25 shows the load factor–top story displacement response of the same frame for the case that a distributed inelasticity element with layer section is used. In this example the force formulation of Section 6.7.3 is used with five control sections. Each section is discretized into 20 layers, 5 in each flange and 10 in the web. Figure 6.25 shows the results of two analyses: in the first case the geometry is linear, while in the second the P-Δ geometric stiffness of Section 6.9.3 is included in the element formulation.

The comparison of the response in Figure 6.25 with that in Figure 6.24a, shows that the axial force variation on account of the overturning moments results in a reduction of the collapse load factor. With a layer discretization of the cross section this effect is automatically accounted for. From the response in Figure 6.25 we conclude that the effect of the P-Δ geometric stiffness becomes noticeable for values of



(a)

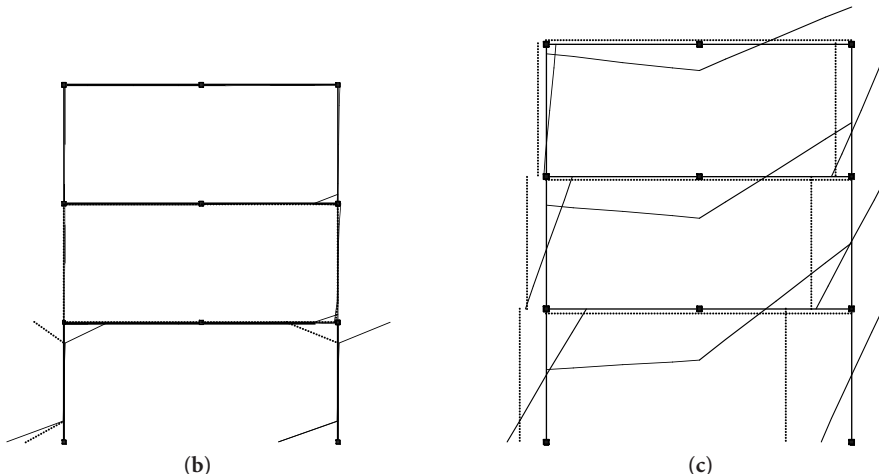
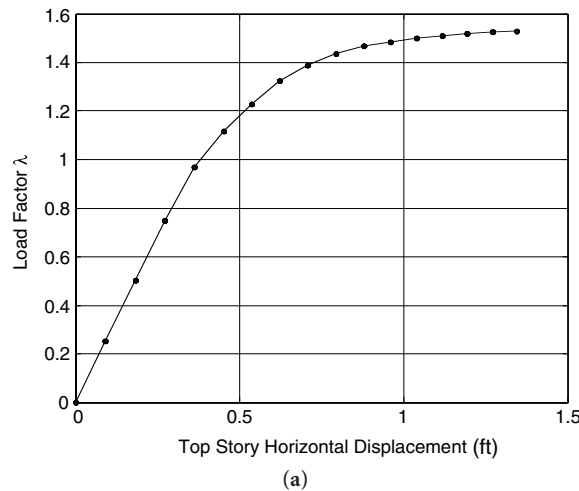
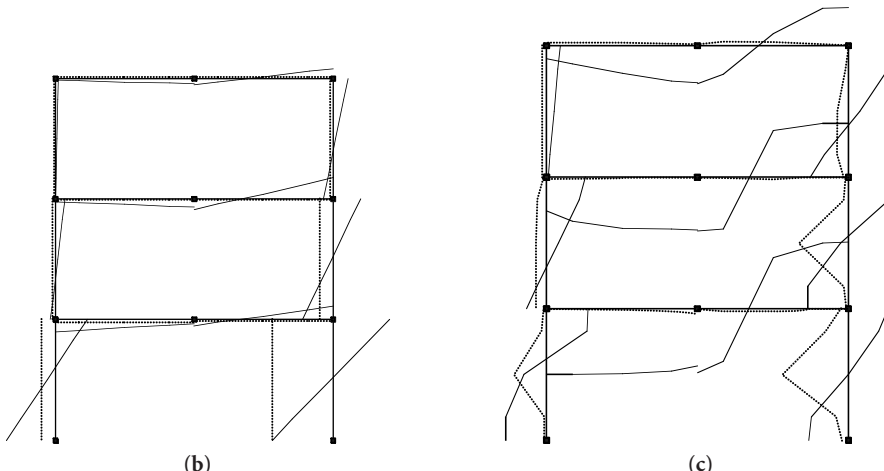


FIGURE 6.25 (a) Load factor–top story displacement relation for three-story steel frame; distributed inelasticity element with force formulation and five control sections; layer section with 20 layers. (b) Curvature (solid line) and axial strain (dashed line) distribution for three-story steel frame at maximum displacement; distributed inelasticity element with force formulation. (c) Moment (solid line) and axial force (dashed line) distribution for three-story steel frame at maximum displacement; distributed inelasticity element with force formulation.

the top story horizontal displacement larger than 0.35 ft, which amounts to an average story drift of 1%. Clearly, it is essential to include this effect in the pushover analysis of frame structures. Finally, Figure 6.25 shows that the load control measures that were discussed in Sections 6.8.3 and 6.8.4 permit the tracing of the load-displacement response past the point of peak strength. This is true for the case of softening response and for the case of linear geometry where the load factor remains practically constant after attaining the maximum value. Figures 6.25b and c show the distributions of section deformations and section forces, respectively, at maximum displacement under linear geometry. In the force formulation the distribution of section forces is always exact, as reflected by the constant axial force and linear bending moment distributions in Figure 6.25c. The section deformations in Figure 6.25b show that large inelastic strains take place at the top and bottom end sections of the first-story columns. The accuracy of the inelastic strain estimate depends on the integration weight of the end sections in the element response. In this respect four or five integration points yield results of comparable accuracy to proposals of plastic hinge length estimation. Figure 6.25b shows that an element with inelastic zones of finite length



(a)



(b)

(c)

FIGURE 6.26 (a) Load factor–top story displacement relation for three-story steel frame under linear geometry; distributed inelasticity element with displacement formulation and five integration points; layer section with 20 layers. (b) Curvature (solid line) and axial strain (dashed line) distribution for three-story steel frame at maximum displacement; distributed inelasticity element with displacement formulation. (c) Moment (solid line) and axial force (dashed line) distribution for three-story steel frame at maximum displacement; distributed inelasticity element with displacement formulation.

at the ends and an elastic core is an excellent compromise between concentrated and distributed inelasticity elements for modeling the inelastic response of columns. The distributed inelasticity elements are particularly suitable for the representation of the inelastic response of girders with significant influence of gravity loads.

Figure 6.26a to c shows the response of the same frame under linear geometry with elements based on the displacement formulation. With only one element per member, this model overestimates the collapse load factor by almost 50%, as shown in Figure 6.26a. The cause of this discrepancy is apparent in Figures 6.26b and c, which show the distribution of section deformations and section forces at maximum displacement, respectively. In the basic displacement formulation a constant axial strain and linear curvature distribution is assumed, as shown in Figure 6.26b. The corresponding axial force and bending moment at each section need to satisfy the material response, while equilibrium is not satisfied in a strict sense, but only for the element. This results in the rather unusual axial force and bending moment distributions of Figure 6.26c. To improve the accuracy of the results members with yielding

should be subdivided into several smaller elements, thus increasing significantly the computational cost. Alternatively, higher order elements with internal nodes can be used permitting higher order polynomials for the displacement interpolation functions. Neither approach, however, is completely successful, particularly under cyclic loading conditions, and the force formulation is preferable for inelastic frame elements with distributed inelasticity.

6.11 Dynamic Analysis

The equations of motion at the structural DOFs according to 6.2 are

$$\mathbf{P}(t) - \mathbf{P}_r(\mathbf{U}, \dot{\mathbf{U}}) = \mathbf{M} \ddot{\mathbf{U}}^t \quad (6.83)$$

where a dot denotes differentiation with respect to time and we have explicitly noted the variation of applied forces $\mathbf{P}(t)$ with time. \mathbf{M} is the mass matrix of the structure, $\ddot{\mathbf{U}}^t$ is the total acceleration in a fixed reference frame, and the resisting forces \mathbf{P}_r in general depend on the displacement and velocity at the global DOFs. If the resisting forces are simply linear functions of velocity and displacement, we can simplify 6.83 to the following

$$\mathbf{P}(t) - \mathbf{C} \dot{\mathbf{U}} - \mathbf{K} \mathbf{U} = \mathbf{M} \ddot{\mathbf{U}}^t \quad (6.84)$$

where \mathbf{C} is the viscous damping matrix for the free DOFs of the model.

6.11.1 Free Vibration

Setting the forcing function $\mathbf{P}(t)$ equal to zero in 6.84 and assuming that the viscous damping is zero and that the fixed reference frame is the base of the structure, hence $\ddot{\mathbf{U}}^t = \ddot{\mathbf{U}}$, give the free vibration problem:

$$\mathbf{M} \ddot{\mathbf{U}} + \mathbf{K} \mathbf{U} = \mathbf{0} \quad (6.85)$$

The solution of 6.85 can be expressed in terms of the vibration mode shapes Φ and natural vibration frequencies ω , as defined by the eigenvalue problem:

$$\mathbf{K}\Phi = \omega^2 \mathbf{M}\Phi$$

The number of pairs of ω_i, Φ_i that satisfies the eigenvalue problem is equal to the number of free DOFs, although in practice much fewer modes are necessary to represent the dynamic response under earthquake excitation. The eigenfrequencies can be collected in a diagonal matrix and the eigenmodes in a matrix of the form

$$\Omega = \begin{bmatrix} \omega_1 & 0 & 0 \\ 0 & \ddots & 0 \\ 0 & 0 & \omega_n \end{bmatrix} \quad \Phi = [\Phi_1 \quad \dots \quad \Phi_n]$$

These satisfy the equation

$$\mathbf{K}\Phi = \mathbf{M}\Phi\Omega^2 \quad (6.86)$$

The key characteristic of the mode shapes is that they are orthogonal with respect to the mass and stiffness matrices. Premultiplying both sides of 6.86 by Φ^T gives the following relationship:

$$\Phi^T K \Phi = \Phi^T M \Phi \Omega^2 \quad (6.87)$$

both sides of which are diagonal matrices because of orthogonality (Chopra, 2001). Since the modes can be scaled arbitrarily we select a scaling such that $\Phi^T M \Phi = I$, where I is the identity matrix. This is known as orthonormality property of the vibration modes. With this scaling of the eigenmodes we obtain from 6.87 that

$$\Omega^2 = \Phi^T K \Phi \quad (6.88)$$

6.11.2 Modal Analysis for Linear Response

Returning to the solution of the free vibration problem in 6.85 with initial conditions on the displacement, U_0 , and velocity, \dot{U}_0 , the displacement vector can be represented as summation of contributions of the vibration modes:

$$U = \Phi Y \quad (6.89)$$

in which $Y=Y(t)$ are called the generalized coordinates. Usually much fewer generalized coordinates are needed compared with the number of free DOFs. After substituting 6.89 into 6.85 and premultiplying the equation by Φ^T we obtain

$$\Phi^T M \Phi \ddot{Y} + \Phi^T K \Phi Y = 0$$

which on account of 6.88 and the orthogonality of the mode shapes gives

$$\ddot{Y} + \Omega^2 Y = 0 \quad (6.90)$$

6.90 are uncoupled second order initial value problems with the following solution for mode k :

$$Y_k(t) = Y_{0k} \cos \omega_k t + \frac{\dot{Y}_{0k}}{\omega_k} \sin \omega_k t$$

Using 6.89 the initial values for the generalized coordinates can be expressed in terms of the initial conditions by premultiplying both sides of the equation with $\Phi^T M$:

$$\begin{aligned} \Phi^T M U_0 &= \Phi^T M \Phi Y_0 = Y_0 \Rightarrow Y_0 = \Phi^T M U_0 \\ \Phi^T M \dot{U}_0 &= \Phi^T M \Phi \dot{Y}_0 = \dot{Y}_0 \Rightarrow \dot{Y}_0 = \Phi^T M \dot{U}_0 \end{aligned}$$

For the more interesting forced vibration case with damping in 6.84 we obtain

$$\Phi^T M \Phi \ddot{Y} + \Phi^T C \Phi \dot{Y} + \Phi^T K \Phi Y = \Phi^T P(t)$$

which on account of the orthogonality properties of the vibration modes gives

$$\ddot{Y} + [\Phi^T C \Phi] \dot{Y} + \Omega^2 Y = \Phi^T P(t) \quad (6.91)$$

For a general damping matrix all modes are coupled through the damping terms in 6.91. However, since damping is generally assumed, it is reasonable to use the so-called Rayleigh damping and express the

damping matrix in terms of the mass and stiffness matrix: $\mathbf{C} = \alpha_0 \mathbf{M} + \alpha_1 \mathbf{K}$. Since the mode shapes are orthogonal to \mathbf{M} , and \mathbf{K} , they are also orthogonal to this specific form of the damping matrix. Substitution of Rayleigh damping into (6.91) gives

$$\ddot{\mathbf{Y}} + (\alpha_0 \mathbf{I} + \alpha_1 \Omega^2) \dot{\mathbf{Y}} + \Omega^2 \mathbf{Y} = \Phi^T \mathbf{P}(t) \quad (6.92)$$

The Rayleigh damping coefficients α_0 and α_1 are selected to match the desired damping ratio for two modes, oftentimes the two lowest, but not always. Calling these modes k and m we can write

$$\begin{aligned} \alpha_0 + \alpha_1 \omega_k^2 &= 2\zeta_k \omega_k \\ \alpha_0 + \alpha_1 \omega_m^2 &= 2\zeta_m \omega_m \end{aligned} \quad (6.93)$$

With given damping ratios ζ_k and ζ_m we can solve the two equations in 6.93 for α_0 and α_1 (Chopra, 2001). The damping ratio for another mode is given by

$$\zeta_n = \frac{1}{2} \left(\frac{\alpha_0}{\omega_n} + \alpha_1 \omega_n \right)$$

6.11.3 Earthquake Excitation

In the case of earthquake excitation the support DOFs are assumed to move together through a specified ground acceleration history, $\ddot{\mathbf{U}}_g(t)$, in the global coordinate system, which generally has two components for 2d problems (a horizontal and a vertical acceleration) and three components for 3d problems (two horizontal accelerations and one vertical acceleration). The key step is to define the acceleration with respect to the fixed reference frame as the sum of the acceleration of the support DOFs and the additional acceleration of the free DOFs relative to the supports, expressed as follows:

$$\ddot{\mathbf{U}}^t = \ddot{\mathbf{U}} + \mathbf{R} \ddot{\mathbf{U}}_g(t) \quad (6.94)$$

The number of columns in \mathbf{R} is equal to the number of specified support acceleration components. For each component, the column of \mathbf{R} corresponds to the displacements of the free DOFs due to a unit displacement of the corresponding support. If all supports move as a rigid body, then \mathbf{R} represents the rigid-body displacement of the entire structure. For linear systems, this procedure can be generalized to include different motions at the supports, in which case \mathbf{R} represents the displacements of the free DOFs due to unit displacement of each support and is obtained by solving the static support displacement problem (Clough and Penzien, 1993).

Under the assumption of no applied nodal loads, the substitution of 6.94 into 6.83 or 6.84 gives the equations of motion due to earthquake excitation for the nonlinear and linear models, respectively:

$$\begin{aligned} \mathbf{M} \ddot{\mathbf{U}} + \mathbf{P}_r(\mathbf{U}, \dot{\mathbf{U}}) &= -\mathbf{M} \mathbf{R} \ddot{\mathbf{U}}_g(t) \\ \mathbf{M} \ddot{\mathbf{U}} + \mathbf{C} \dot{\mathbf{U}} + \mathbf{K} \mathbf{U} &= -\mathbf{M} \mathbf{R} \ddot{\mathbf{U}}_g(t) \end{aligned} \quad (6.95)$$

6.11.4 Numerical Integration of Equations of Motion for Linear Response

Because of the difficulty of solving the linear differential equation for arbitrary variation of forcing functions as a function of time (earthquake excitation is a particularly complex case in point), it is necessary to use a numerical method to solve 6.95. In the case of linear elastic response of the structural

system we use modal analysis and thus integrate numerically m single DOF differential equations of the form

$$\ddot{Y}_k + (\alpha_0 + \alpha_1 \omega_k^2) \dot{Y}_k + \omega_k^2 Y_k = P_k(t)$$

where $P_k(t) = -(\Phi^T M R) \ddot{U}_g(t)$. In general, the number of modes should be selected based on the frequency content and spatial participation of the modes as indicated by the participating mass (Chopra, 2001).

In the numerical solution of differential equations the acceleration, velocity and displacement at time $t + \Delta t$ are defined in terms of the acceleration, velocity and displacement at time t . To keep the notation short we use subscript $i+1$ for time $t + \Delta t$ and subscript i for time t , respectively. Because the equations are the same whether we are dealing with a single DOF or a multi-DOF system we use the latter in the following presentation for generality.

Newmark introduced one of the most widely used methods of numerical integration in earthquake engineering (Newmark, 1959). It uses the following relations between displacement, velocity and acceleration at time steps i and $i+1$:

$$\begin{aligned} \dot{U}_{i+1} &= \dot{U}_i + (1-\gamma)\Delta t \ddot{U}_i + \gamma \Delta t \ddot{U}_{i+1} \\ U_{i+1} &= U_i + \Delta t \dot{U}_i + \left(\frac{1}{2} - \beta \right) \Delta t^2 \ddot{U}_i + \beta \Delta t^2 \ddot{U}_{i+1} \end{aligned} \quad (6.96)$$

where subscript f for the free DOFs has been dropped for convenience. With the second equation in 6.96, \ddot{U}_{i+1} can be expressed in terms of the displacement at time step $i + 1$ and the response at the previous time step:

$$\ddot{U}_{i+1} = \frac{1}{\beta \Delta t^2} (U_{i+1} - U_i) - \frac{1}{\beta \Delta t} \dot{U}_i - \left(\frac{1}{2\beta} - 1 \right) \ddot{U}_i \quad (6.97)$$

Substituting 6.97 into the first equation in 6.96 gives the velocity, \dot{U}_{i+1} :

$$\begin{aligned} \dot{U}_{i+1} &= \dot{U}_i + (1-\gamma)\Delta t \ddot{U}_i + \frac{\gamma}{\beta \Delta t} (U_{i+1} - U_i) - \frac{\gamma}{\beta} \dot{U}_i - \left(\frac{1}{2\beta} - 1 \right) \gamma \Delta t \ddot{U}_i \\ &= \frac{\gamma}{\beta \Delta t} (U_{i+1} - U_i) + \left(1 - \frac{\gamma}{\beta} \right) \dot{U}_i + \left(1 - \frac{\gamma}{2\beta} \right) \Delta t \ddot{U}_i \end{aligned} \quad (6.98)$$

We introduce now the following constants for a given time step Δt :

$$C_0 = \frac{1}{\beta \Delta t^2} \quad C_1 = \frac{1}{\beta \Delta t} \quad C_2 = \frac{\gamma}{\beta \Delta t} \quad C_3 = \left(\frac{1}{2\beta} - 1 \right) \quad C_4 = \left(\frac{\gamma}{\beta} - 1 \right) \quad C_5 = \left(\frac{\gamma}{2\beta} - 1 \right) \Delta t$$

and rewrite 6.97 and 6.98 in a more compact form:

$$\ddot{U}_{i+1} = C_0 (U_{i+1} - U_i) - C_1 \dot{U}_i - C_3 \ddot{U}_i \quad (6.99)$$

$$\dot{U}_{i+1} = C_2 (U_{i+1} - U_i) - C_4 \dot{U}_i - C_5 \ddot{U}_i \quad (6.100)$$

We use 6.97 and 6.98 in two ways: first we substitute the velocity and acceleration in the equations of motion 6.84 at time $t + \Delta t$, i.e.,

$$\mathbf{P}_{i+1} - \mathbf{C}\dot{\mathbf{U}}_{i+1} - \mathbf{K}\mathbf{U}_{i+1} = \mathbf{M}\ddot{\mathbf{U}}_{i+1} \quad (6.101)$$

and obtain a system of equations for the unknown displacement at time $t + \Delta t$:

$$\mathbf{P}_{i+1} - \mathbf{C} [C_2(\mathbf{U}_{i+1} - \mathbf{U}_i) - C_4\dot{\mathbf{U}}_i - C_5\ddot{\mathbf{U}}_i] - \mathbf{K}\mathbf{U}_{i+1} = \mathbf{M}[C_0(\mathbf{U}_{i+1} - \mathbf{U}_i) - C_1\dot{\mathbf{U}}_i - C_3\ddot{\mathbf{U}}_i]$$

After collecting terms for the unknown displacement at time $t + \Delta t$ we get

$$(C_0\mathbf{M} + C_2\mathbf{C} + \mathbf{K})\mathbf{U}_{i+1} = \mathbf{P}_{i+1} + \mathbf{U}_i(C_0\mathbf{M} + C_2\mathbf{C}) + (C_1\dot{\mathbf{U}}_i + C_3\ddot{\mathbf{U}}_i)\mathbf{M} + (C_4\dot{\mathbf{U}}_i + C_5\ddot{\mathbf{U}}_i)\mathbf{C}$$

or, in short, a system of linear equations:

$$\mathbf{K}_{\text{eff}}\mathbf{U}_{i+1} = \mathbf{P}_{\text{eff}} \quad (6.102)$$

Solving for the displacements at time $t + \Delta t$ from 6.102, 6.97 and 6.98 gives the velocities and accelerations at the free DOFs at time $t + \Delta t$, thus advancing the solution of the equation of motion by one time increment. Repeating this process for the necessary number of time steps gives the solution as a function of time.

Because a solution of simultaneous equations is required in 6.102, Newmark's numerical solution belongs to the class of implicit methods. The numerical stability and accuracy of such methods are discussed elsewhere (Hughes, 2000).

6.11.5 Numerical Integration of Equations of Motion for Nonlinear Response

Newmark's time integration algorithm can now be used to solve the equations of motion for a general nonlinear model of a structure. In this case 6.101 is written as follows for time $t + \Delta t$

$$\mathbf{P}_{i+1} - \mathbf{P}_r(\dot{\mathbf{U}}_{i+1}, \mathbf{U}_{i+1}) = \mathbf{M}\ddot{\mathbf{U}}_{i+1}$$

Assuming that the resisting forces are linearly dependent on the velocity, the equations of motion become

$$\mathbf{P}_{i+1} - \mathbf{C}\dot{\mathbf{U}}_{i+1} - \mathbf{P}_r(\mathbf{U}_{i+1}) = \mathbf{M}\ddot{\mathbf{U}}_{i+1} \quad (6.103)$$

Since 6.103 is a nonlinear system of equations, the Newton–Raphson algorithm is needed to solve it. In analogy with the static case, it is necessary to obtain the derivative of 6.103 with respect to the unknown displacements at time $t + \Delta t$. The velocities and accelerations are expressed in terms of these displacements using the result from Newmark's method. Thus, the chain rule of differentiation on 6.103 gives the effective stiffness matrix at time step $i+1$:

$$\begin{aligned} \mathbf{K}_{\text{eff}} &= \frac{\partial}{\partial \mathbf{U}_{i+1}} [\mathbf{M}\ddot{\mathbf{U}}_{i+1} + \mathbf{C}\dot{\mathbf{U}}_{i+1} + \mathbf{P}_r(\mathbf{U}_{i+1})] - \frac{\partial}{\partial \mathbf{U}_{i+1}} \mathbf{P}_{i+1} \\ \mathbf{K}_{\text{eff}} &= \frac{\partial}{\partial \ddot{\mathbf{U}}_{i+1}} (\mathbf{M}\ddot{\mathbf{U}}_{i+1}) \frac{\partial \ddot{\mathbf{U}}_{i+1}}{\partial \mathbf{U}_{i+1}} + \frac{\partial}{\partial \dot{\mathbf{U}}_{i+1}} (\mathbf{C}\dot{\mathbf{U}}_{i+1}) \frac{\partial \dot{\mathbf{U}}_{i+1}}{\partial \mathbf{U}_{i+1}} + \frac{\partial \mathbf{P}_r(\mathbf{U}_{i+1})}{\partial \mathbf{U}_{i+1}} \end{aligned} \quad (6.104)$$

where we note that the applied forces \mathbf{P}_{i+1} do not depend on the displacements \mathbf{U}_{i+1} . After substituting 6.99 and 6.100 in 6.104, we conclude that the effective stiffness is similar to the linear case except for the fact that the tangent stiffness matrix is used,

$$\mathbf{K}_{\text{eff}} = C_0 \mathbf{M} + C_2 \mathbf{C} + \mathbf{K}_{t_{i+1}}$$

where $\mathbf{K}_{t_{i+1}} = \frac{\partial \mathbf{P}_r(\mathbf{U}_{i+1})}{\partial \mathbf{U}_{i+1}}$ in accordance with the tangent stiffness definition in 6.72. The force unbalance vector of the equation in 6.103 is also needed. It expresses the amount of equilibrium error under inclusion of the mass and damping terms. It is given by

$$\mathbf{P}_u = \mathbf{P}_{i+1} - \mathbf{P}_r(\mathbf{U}_{i+1}) - \mathbf{M}\dot{\mathbf{U}}_{i+1} - \mathbf{C}\ddot{\mathbf{U}}_{i+1} \quad (6.105)$$

Substituting the expressions in 6.99 and 6.100 for the acceleration and velocity at time $t + \Delta t$ in a slightly modified form in 6.105 gives the unbalanced force vector as

$$\mathbf{P}_u = \mathbf{P}_{i+1} - \mathbf{P}_r(\mathbf{U}_{i+1}) - \mathbf{M}(C_0 \Delta \mathbf{U}_{i+1} - C_1 \dot{\mathbf{U}}_i - C_3 \ddot{\mathbf{U}}_i) - \mathbf{C}(C_2 \Delta \mathbf{U}_{i+1} - C_4 \dot{\mathbf{U}}_i - C_5 \ddot{\mathbf{U}}_i) \quad (6.106)$$

where $\Delta \mathbf{U}_{i+1} = \mathbf{U}_{i+1} - \mathbf{U}_i$. Note that during Newton–Raphson iterations \mathbf{U}_{i+1} is updated during each iteration, while \mathbf{U}_i , of course, remains constant and equal to the displacement values at the previously converged time step. With this in mind we collect terms in 6.106 as follows

$$\mathbf{P}_u = \mathbf{P}_{i+1} + \mathbf{M}(C_1 \dot{\mathbf{U}}_i + C_3 \ddot{\mathbf{U}}_i) + \mathbf{C}(C_4 \dot{\mathbf{U}}_i + C_5 \ddot{\mathbf{U}}_i) - \mathbf{P}_r(\mathbf{U}_{i+1}) - C_0 \mathbf{M} \Delta \mathbf{U}_{i+1} - C_2 \mathbf{C} \Delta \mathbf{U}_{i+1} \quad (6.107)$$

The first half of the right-hand side in 6.107, i.e., $\mathbf{P}_{i+1} + \mathbf{M}(C_1 \dot{\mathbf{U}}_i + C_3 \ddot{\mathbf{U}}_i) + \mathbf{C}(C_4 \dot{\mathbf{U}}_i + C_5 \ddot{\mathbf{U}}_i)$ does not change during a time step and can be considered the effective applied force. The second half, namely $-\mathbf{P}_r(\mathbf{U}_{i+1}) - C_0 \mathbf{M} \Delta \mathbf{U}_{i+1} - C_2 \mathbf{C} \Delta \mathbf{U}_{i+1}$ needs to be updated with every new estimate of the displacements \mathbf{U}_{i+1} during equilibrium iterations and can be regarded as the effective resisting force vector.

6.12 Applications of Linear and Nonlinear Dynamic Analysis

As an example of the structural analysis methods presented in this chapter, this section presents the nonlinear dynamic analysis of a 20-story moment-resisting steel frame building. The example building, designed for the seismic hazard in Los Angeles, has been used in the SAC studies to assess the performance of steel moment-resisting frame buildings (Gupta and Krawinkler, 1999). The building has 20 stories above ground level and two basement levels. The total height above the ground is 265 ft and the story height is 13 ft except for the ground level story of 18 ft height. The North-South frames consist of five bays with perimeter box columns of 15×15 with various thicknesses and interior columns with wide flange sections varying from $W24 \times 335$ to $W24 \times 84$. The beams consist of various wide flange section members ranging between $W30 \times 108$ and $W21 \times 50$.

The structural model of the NS frame, shown in Figure 6.27, consists of two-node frame elements connected at nodes representing the joints. Centerline dimensions are used and the joints are assumed to be rigid. The base of the columns is hinged and the perimeter basement columns are constrained in the horizontal direction at the ground level to represent the embedment of the basement, although a more refined model could include soil–foundation–structure interaction effects. The frame elements represent distributed inelasticity with five control sections. Each element has section properties with a discretization of typically 60 layers (fibers), although as described in Section 6.10 a smaller number can

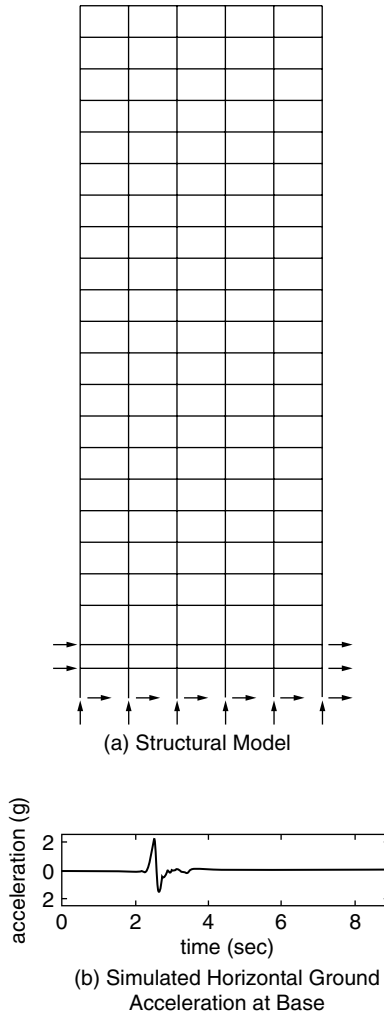


FIGURE 6.27 Model for 20-story moment-resisting frame (Gupta and Krawinkler, 1999) and ground motion for simulations.

suffice. The material model for the steel is a bilinear plasticity model with 2% strain hardening ratio. The structural model has 585 free DOFs for the translational and rotational components at the nodes.

The mass of the building is represented by lumped masses at the nodes of the model. The gravity resisting frames in the building are not included in the model, but they contribute substantial P- Δ effects to the moment-resisting frame. To account for the destabilizing effect of the gravity loads on the gravity resisting frames, the loads are collected to an additional column member that is attached to the moment-resisting frame by truss members. This is commonly known as leaning column approach. The geometric compatibility transformation for the beams and columns, including the leaning column, uses the P- Δ transformation presented in Section 6.9.3.

The lower vibration mode shapes and periods, using the stiffness matrix of the building under linear elastic behavior, are shown in Figure 6.28. For dynamic analysis, Rayleigh damping is assumed based on a damping ratio of 0.02 in the first two vibration modes.

The horizontal ground motion record used in this example analysis is obtained from the simulation of a fault rupture and resulting wave propagation in a $10\text{ km} \times 10\text{ km}$ region (Bao et al., 1996). The location of the station is in the forward rupture directivity region and is about 1 km from the surface

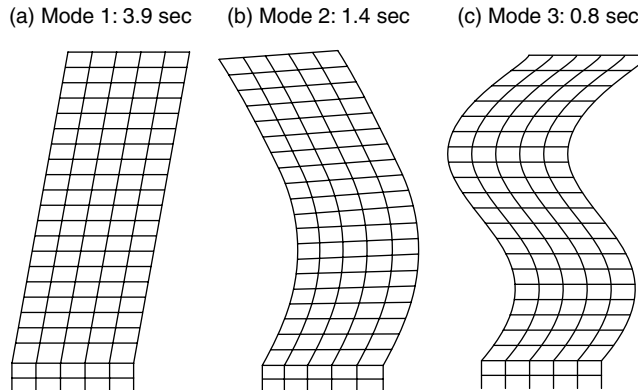


FIGURE 6.28 Lower three vibration modes and periods of 20-story building.

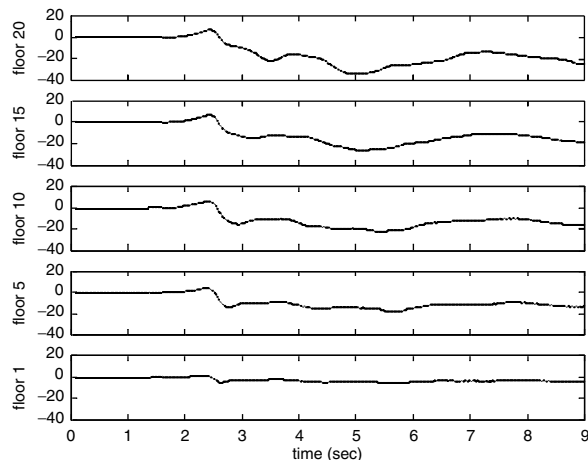


FIGURE 6.29 Displacement history (in inches) at five floor levels in 20-story building due to horizontal ground acceleration.

projection of the fault. The simulated ground motion has a pulse with large peak ground acceleration of 2 g. Although such large peak ground accelerations have not been recorded to date under this condition, the simulated record has the large pulse that is characteristic of near-source ground motion and it may be considered a very severe case for the expected ground motion. The purpose of using the large simulated record is to investigate the inelastic behavior of the frame in an extreme event. The ground motion acceleration record is shown in Figure 6.27b, and it is applied as horizontal free-field acceleration at the base of the model. For the nonlinear dynamic analysis, the Newmark time integration method is used with 1800 time steps of $\Delta t = 0.005$ sec. The equilibrium equations at each time step are solved using the Newton–Raphson algorithm, and typically three or four iterations were required for convergence. On a desktop computer the analysis took three to five minutes, demonstrating the computational efficiency of the nonlinear dynamic analysis methods.

The history of displacement at five floors is shown in Figure 6.29. The propagation of the ground motion pulse over the height of the building can be clearly seen. The maximum horizontal roof displacement of 38 in. results in residual deformation at the end of the 9-sec response history. The envelopes of maximum horizontal floor displacement and drift are shown in Figure 6.30. The largest story drift occurs in the first floor, with a drift ratio of 0.026, and the upper floors.

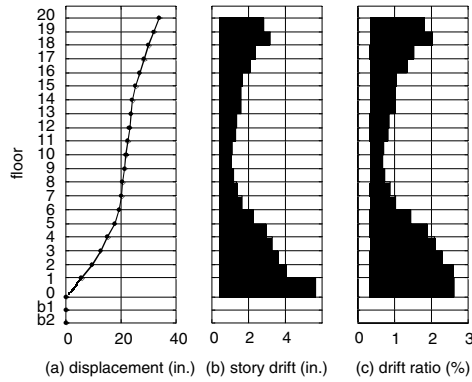


FIGURE 6.30 Envelope of maximum floor displacement and story drift for 20-story building due to horizontal ground motion.

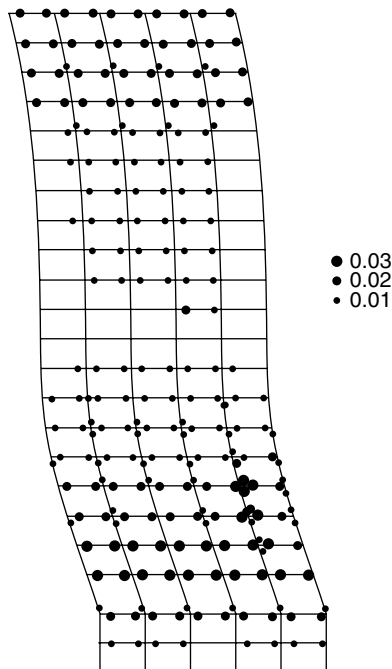


FIGURE 6.31 Maximum plastic hinge rotations in 20-story building due to horizontal ground motion. Deformed shape is the residual deformation after the earthquake (magnified by 20).

The location and maximum values of the plastic hinge rotations in the beams and columns are shown in Figure 6.31. Most of the hinges form at the end of the beams, with the largest rotation, reaching 0.030 rad, in floors 3 to 5, and somewhat smaller plastic hinging in the upper four floors. Plastic hinges form at the bases of the tall columns at the ground level, as would be expected in a sway mechanism, but limited column hinging of approximately 0.01 rad occurs at perimeter and interior columns also in floors 3 to 5. In addition there is limited plastic hinging in upper floor columns (16 to 18). The deformed shape in Figure 6.31 shows the residual displacements of the frame after the earthquake ends, with the shape magnified by a scale factor of 20 for plotting.

The modeling and computation for this example were done with OpenSees — Open System for Earthquake Engineering Simulation (<http://opensees.berkeley.edu>). OpenSees is an open-source software

framework for simulation of structural and geotechnical systems. The software design includes all the models, element formulations and solution methods presented in this chapter, in addition to more advanced features. Section 6.14 provides additional information about OpenSees.

6.13 Conclusions

The objective of this chapter has been to present the methods of structural analysis in a manner that unifies static and dynamic analysis for linear and nonlinear models. The emphasis has been on providing a consistent approach for satisfying the equations of equilibrium, compatibility and force-deformation. The methods presented in this chapter encompass the major structural analysis procedures used in earthquake-resistant design, and they recognize the increasing importance of nonlinear analysis procedures. The presentation has been limited to frame elements, although the methods can be extended to include joints, walls, diaphragms and foundation components.

Plastic analysis methods are very useful in the capacity design of structures but are limited to elastic-perfectly plastic behavior. Concentrated plasticity beam models are computationally simple and are capable of accounting for the effects of axial force-shear-bending moment interaction. These models, however, require calibration under idealized assumptions about either the force or the deformation distribution within the member. Furthermore, they require that the location of inelastic deformations be specified *a priori* and, typically, do not include the effect of distributed element loading. Distributed inelasticity frame elements do not suffer from the limitations of calibration and *a priori* specification of the location of inelastic deformation, but are computationally more demanding. In the displacement formulation the assumed displacement interpolation functions are not a satisfactory approximation of the deformation distribution in the member, unless the latter is subdivided into several elements. Adaptive mesh refinement methods have been proposed for the purpose. The force formulation offers the advantage that the force-interpolation functions are exact under the assumption of linear geometry. Consequently, a single element with several integration points (control sections) suffices for the representation of the inelastic behavior of the member. Moreover, the force formulation accounts directly for the effect of distributed element loads in girders, which can cause inelastic deformations to arise within the member span, instead of the member ends. Four integration points are recommended for the typical case without element loads, while five integration points should be used in the presence of element loading. By integrating the material response over the control sections with the so-called layer or fiber section models, it is possible to directly account for the interaction of axial force and bending moment. Simple uniaxial normal stress-strain models suffice for the purpose. Studies show that a few layers or fibers suffice to yield an excellent representation of the hysteretic response of the section. Under uniaxial bending eight to ten layers are usually sufficient for rectangular sections. For wide flange sections three layers in each flange and four layers in the web are recommended. Under biaxial loading 25 (5×5) to 64 (8×8) fibers yield excellent accuracy. In a reinforced concrete section the hysteretic response is dominated by the behavior of reinforcing steel. Thus, it is important to represent the area and distribution of reinforcement relatively well and then use 16 (4×4) or 25 (5×5) fibers for the concrete. A larger number of fibers may be necessary for distinguishing between cover concrete and core concrete confined by transverse reinforcement.

Under nonlinear geometry the most significant contribution arises from the rigid-body displacements of the frame element. It is possible to isolate this effect with the corotational formulation, in which the element response is defined in the basic system without rigid-body modes. The end forces of the basic system are then transformed exactly to the local coordinate system of the undeformed element. In this case the tangent stiffness matrix of the element is made up of two contributions: the transformation of the material stiffness from the basic to the local system and the geometric stiffness matrix. Consistent approximation of the displacement terms in the equilibrium equations and in the deformation-displacement relations leads to approximate theories of nonlinear geometry, such as the P- Δ geometric stiffness. The advantage of the presented approach is that one element type can accommodate several nonlinear geometric transformations. The effect of nonlinear geometry should be included in the nonlinear static

(pushover) analysis of buildings for average relative story drifts in excess of 1%. When the relative story drift varies considerably over the height of the structure, it is important to include the effect of nonlinear geometry when the maximum inter-story drift exceeds 2%.

The strength softening response of structural systems under nonlinear material and geometry can be traced with load control strategies. Among these the load control strategy under constant displacement at a particular degree of freedom proves very useful in the nonlinear static (pushover) analysis of buildings, when the horizontal translation at a floor is representative of the response of the entire building, or, a single soft story collapse mechanism forms. In more complex cases the load control strategy under constant external work is an excellent alternative.

Most structural analysis is performed using computer software that implements one or more of the analysis methods described in this chapter. When using computer software for analysis, the engineer must confirm that the assumptions and limitations of the models are appropriate for the structural analysis problem under consideration.

6.14 Future Challenges

Nonlinear structural analysis is becoming more important in earthquake-resistant design, particularly with the development of performance-based earthquake engineering, which requires more detailed information about the displacements, drifts and inelastic deformation of a structure than traditional design procedures. Nevertheless, many challenges remain in the field of structural analysis to meet the goal of providing predictive simulations of the performance of a structure under earthquake excitation. The challenges encompass the needs for research in analysis and simulation, improved technology for structural analysis software and education of students and design professionals in structural analysis advances.

The Pacific Earthquake Engineering Research Center has undertaken the development of the Open System for Earthquake Engineering Simulation (OpenSees) to address these challenges. The OpenSees software is called a framework because it is an integrated set of software components used to build simulation applications for structural and geotechnical engineering problems. OpenSees is not a “code,” by the usual definition of a program, to solve a specific class of problems. Rather it involves a set of classes and objects that represent models, perform computations for solving the governing equations and provide access to databases for the processing of results. At its most fundamental level, OpenSees can be viewed as a set of objects that are accessed through a defined application program interface (API). The framework was designed using object-oriented principles, and is implemented in C++, a widely used object-oriented programming language. The development of OpenSees is open-source, meaning that all versions of the program, documentation, examples, are available on the website (<http://opensees.berkeley.edu>) for researchers, professionals and students interested in using and contributing to the software.

PEER’s OpenSees research and development addresses three major future challenges. The first challenge is to improve the models of structural behavior of components, and particularly the representation of damage under cyclic loading. Although the computational methods for analysis have become more sophisticated in the past decade, the models used in many nonlinear analyses consist of very simple elements. Simple nonlinear models, such as the lumped plasticity models described in Section 6.7.2, provide an indication of the nonlinear behavior of a structure, but they do not include several important aspects of behavior that can have an appreciable effect on performance. For example, the interaction between flexure and shear, particularly in reinforced concrete members, is poorly understood and current models only approximately attempt to capture this phenomenon, if it is included at all. Beyond the component models, system models of structures are generally very approximate. Quite often these models are two dimensional with the approximation of three-dimensional effects. In particular, models for slabs and diaphragms are rarely used in earthquake analysis, and structural walls are represented with beam-column elements. The simple system models can only provide an approximate assessment of the failure sequence, particularly for structures with components of limited ductility and brittle behavior, which

then requires significant judgment and interpretation on the part of the engineer about the performance of the system. Another important system aspect rarely considered in an analysis is the interaction between the structure, foundation components and soil during an earthquake. In many cases, soil–foundation–structure interaction can affect the response and it should be included in the model and analysis of the system. As with all models, there are great challenges in validating the models using experimental and field-observation data and characterizing the sensitivity of the modeled response in terms of the uncertainty in identifying the parameters of the models. Each of these issues has been a subject of research in PEER and new models and approaches, particularly for soil–structure–foundation interaction, have been incorporated into OpenSees.

A second major area of challenge is the observation that the improvements in structural analysis methods and software have not kept pace with the rapid improvement in computing over the past decade. It is common for an engineer to perform a nonlinear analysis of a structure on a desktop computer today. However, it is often with software that uses simple models because the rate of innovation in the software has not been as rapid as the hardware technology that produced the high-performance computer on the desktop. There are tremendous opportunities with new technology for major improvements in structural analysis for earthquake engineering. Considering hardware, there will be increasing computational power on not only individual computers, but also on networks of computers connected together in a design office or remote computational centers that will allow for parallel computation transparent to the user. This computational power will allow routine analysis of complete three-dimensional models. Perhaps even more important are the challenges that must be met to develop the analysis software of the future. New advances in software engineering of modularity and open standards hold promise in the earthquake engineering field for advances in software development to support analysis and design applications. In addition to modeling and computational aspects, modular and open software can provide improved facilities for the visualization of structural behavior, linkages to databases for experimental data and validation studies and design databases. Software can provide support for engineers to collaborate, not only on analysis, but also on integrating the analysis with the design process. The OpenSees framework addresses these shortcomings by providing well-defined interfaces to software components for modeling and analysis, and also software tools for equation solvers, visualization, databases and distributed network communication.

The third challenge is educating future and current earthquake engineers in modern methods of structural analysis and application to earthquake-resistant design, and also implementation in modern computational environments, such as OpenSees. This chapter has presented the fundamentals of analysis in a way that can be integrated into undergraduate and graduate curricula, serve as a framework for future advances and provide the necessary background for engineers to use nonlinear analysis methods with confidence. It is hoped that the consistent exposition of the fundamentals and examples of structural analysis applications is a step toward the goal of improving the education of engineers on this important subject.

References

- Argyris, J. H., Hilpert, O., Malejannakis, G. A. and Scharpf, D. W. (1979). On the Geometrical Stiffness of a Beam in Space: a Consistent Virtual Work Approach. *Computer Methods in Applied Mechanics and Engineering*, 20, 105–131.
- ATC. (1996a). Improved Seismic Design Criteria for California Bridges: Provisional Recommendations. ATC-32, Applied Technology Council.
- ATC. (1996b). Seismic Evaluation and Retrofit of Concrete Buildings. ATC-40, Applied Technology Council.
- Bao, H., Bielak, J., Ghattas, O., O'Hallaron, D. R., Kallivokas, L. F., Shewchuk, J. R. and Xu, J. (1996). Earthquake Ground Motion Modeling on Parallel Computers. *Supercomputing '96*, Pittsburgh, Pennsylvania.
- Bathe, K.-J. (1995). *Finite Element Procedures*, Prentice Hall, New York.

- Bergan, P. G. (1978). Solution Techniques for Nonlinear Finite Element Problems. *International Journal of Numerical Methods and Engineering*, 12, 1677–1696.
- CEB, C. E.-I. d. B. (1996). RC elements under cyclic loading. 230, CEB, Comité Euro-International du Béton.
- Chopra, A. K. (2001). *Dynamics of Structures: Theory and Applications to Earthquake Engineering*, 2nd. ed., Prentice Hall, New York, N.Y.
- Ciampi, V. and Carlesimo, L. (1986). A Nonlinear Beam Element for Seismic Analysis of Structures. *8th European Conference on Earthquake Engineering*, Lisbon, 6.3/73–6.3/80.
- Clarke, M. J. and Hancock, G. J. (1990). A study of incremental-iterative strategies for non-linear analyses. *International. Journal of Numerical Methods and Engineering*, 29, 1365–1391.
- Clough, R. W., Benuska, K. L. and Wilson, E. L. (1965). Inelastic Earthquake Response of Tall Buildings. *Third World Conference on Earthquake Engineering*, Wellington, New Zealand.
- Clough, R. W. and Penzien, J. (1993). *Dynamics of Structures*, 2nd ed., Prentice Hall, New York.
- Crisfield, M. A. (1990). A consistent co-rotational formulation for non-linear, three dimensional, beam elements. *Computer Methods in Applied Mechanics and Engineering*, 81, 131–150.
- Crisfield, M. A. (1991). *Non-Linear Finite Element Analysis of Solids and Structures*, John Wiley & Sons, West Sussex.
- Elias, Z. M. (1986). *Theory and Methods of Structural Analysis*, John Wiley & Sons, New York.
- FEMA (1997). NEHRP Guidelines for the Seismic Rehabilitation of Buildings. FEMA 273, Federal Emergency Management Agency, Washington, D.C.
- FEMA (2000a). Prestandard and Commentary for the Seismic Rehabilitation of Buildings. FEMA 356, Federal Emergency Management Agency, Washington, D.C.
- FEMA (2000b). Recommended Seismic Design Criteria for New Steel Moment-Frame Buildings. FEMA 350, Federal Emergency Management Agency, Washington, D.C.
- FEMA (2000c). Recommended Seismic Evaluation and Upgrade Criteria for Existing Welded Steel Moment-Frame Buildings. FEMA 351, Federal Emergency Management Agency, Washington, D.C.
- FEMA (2001). NEHRP Recommended Provisions for Seismic Regulations for New Buildings and Other Structures, 2000 Edition: Part 1-Provisions (FEMA 368), Part 2-Commentary (FEMA 369). Federal Emergency Management Agency, Washington, D.C.
- Filippou, F. C., Popov, E. P. and Bertero, V. V. (1983). Effects of Bond Deterioration on Hysteretic Behavior of Reinforced Concrete Joints. UCB/EERC-83/19, Earthquake Engineering Research Center, University of California, Berkeley.
- Giberson, M. F. (1967). The Response of Nonlinear Multistory Structures Subjected to Earthquake Excitation, Ph.D. Dissertation, California Institute of Technology, Pasadena.
- Gupta, A. and Krawinkler, H. (1999). Seismic demands for performance evaluation of steel moment resisting frame structures. Report No. 132, John A. Blume Earthquake Engineering Center, Stanford University.
- Horne, M. R. and Morris, L. J. (1982). *Plastic Design of Low-Rise Frames*, MIT Press, Cambridge, MA.
- Hughes, T. J. R. (2000). *The Finite Element Method: Linear Static and Dynamic Finite Element Analysis*, Dover, New York.
- Karsan, I. D. and Jirsa, J. O. (1969). Behavior of concrete under compressive loadings. *Journal of the Structural Division*, ASCE, 95, 2543–2563.
- Livesley, R.K. (1975). Matrix Methods of Structural Analysis, 2nd. ed., Pergamon Press, Oxford, U.K.
- McGuire, W., Gallagher, R. H. and Ziemian, R. D. (2000). *Matrix Structural Analysis*, John Wiley & Sons, New York.
- Menegotto, M. and Pinto, P. E. (1973). Method of Analysis for Cyclically Loaded Reinforced Concrete Plane Frames Including Changes in Geometry and Non-Elastic Behavior of Elements under Combined Normal Force and Bending. *IABSE Symposium on Resistance and Ultimate Deformability of Structures Acted on by Well Defined Repeated Loads*, Lisbon, 15–22.
- Neuenhofer, A. and Filippou, F. C. (1997). Evaluation of nonlinear frame finite element models. *Journal of Structural Engineering*, ASCE, 123, 958–966.

- Newmark, N. M. (1959). A method of computation for structural dynamics. *Journal of Engineering Mechanics Division, ASCE*, 85(EM3), 69–74.
- Paulay, T. and Priestley, M. J. N. (1992). *Seismic Design of Reinforced Concrete and Masonry Buildings*, Wiley Interscience, New York.
- Priestley, M. J. N., Seible, F. and Calvi, M. (1996). *Seismic Design and Retrofit of Bridges*, Wiley Interscience, New York.
- Scott, B. D., Park, R. and Priestley, M. J. N. (1982). Stress-strain behavior of concrete confined by overlapping hoops at low and high strain rates. *ACI Structural Journal*, 79, 13–27.
- Taucer, F. F., Spacone, E. and Filippou, F. C. (1991). A Fiber Beam-Column Element for Seismic Analysis of Reinforced Concrete Structures. *UCB/EERC-91/17*, Earthquake Engineering Research Center, University of California, Berkeley.
- UBC (1997). Uniform Building Code, International Council of Building Code Officials.

Glossary

- basic element forces** — set of independent element forces in equilibrium equations of element free body
- concentrated or lumped inelasticity** — inelastic deformations may arise at specific locations along the element axis, typically at the element ends
- corotational formulation** — element force–deformation relation is set up in a reference system that moves with the element as it deforms
- distributed inelasticity** — inelastic deformations may arise anywhere along element axis
- element deformations** — relative element end displacements excluding rigid body modes
- layer or fiber section** — integration of material response over the cross section in one or two dimensions by midpoint rule
- load factor control** — relations for load factor adjustment during load incrementation and/or equilibrium iterations
- local coordinate system** — orthogonal Cartesian coordinate system with x-axis coinciding with the line connecting the end nodes of the element
- modal analysis** — decomposition of linear dynamic response in eigenvector contributions
- nonlinear geometry** — large displacement compatibility relations and equilibrium in the deformed configuration
- nonlinear response** — nonlinear relation between displacements at global degrees of freedom and corresponding resisting forces
- P-Δ geometric stiffness** — small displacement compatibility relations and equilibrium in the deformed configuration for axial force effect only
- push-over analysis** — step-by-step nonlinear analysis to collapse under constant gravity loads and a reference lateral force vector with gradually increasing load factor
- section deformations** — deformation measures of infinitesimal slice of frame element
- section forces** — resultant forces at section of frame element
- structural model** — collection of points (structural nodes) in space interconnected by structural elements

7

Probabilistic Aspects of Earthquake Engineering

7.1	Introduction	7-1
7.2	Characterization of Uncertainty	7-2
	Classical Methods • Bayesian Method	
7.3	Uncertainty in Demand and Probabilistic Treatments	7-6
	Source • Path and Site • Ground Excitation and Structural Response • Simulation and Monte Carlo Methods	
7.4	Uncertainty in Capacity and Probabilistic Treatments ..	7-18
	Material Characteristics • Uncertainty in Member Capacity • Uncertainty in System Capacity	
7.5	Reliability of Structural Systems	7-24
	FORM and SORM • Demand Versus Capacity Formulation in FEMA/SAC Procedure • Method of Simulation	
7.6	Probabilistic Codes and Standards.....	7-29
	LRFD Based on FORM • FEMA/SAC Procedure • Target Reliability • Reliability and Redundancy	
7.7	Future Challenges	7-39
	Impact of Demand Spatial Correlation • Quantification of Epistemic Uncertainty • Conversion from Structural Response to Physical Damage and Loss • Risk Communication Issues	

Yi-Kwei Wen

7.1 Introduction

Among the loadings on structures that engineers have to consider for performance evaluation and design, seismic deformation is the most challenging, due to the large uncertainty associated with the forces and structural responses that it produces. The earthquake occurrence time, its magnitude, rupture surface features, seismic wave attenuation and amplification, and finally the dynamic response behavior of the structure and the structural capacity to withstand damage and collapse cannot be predicted with certainty. Methods of probability and statistics are required to include these uncertainties and their effects on the structural performance evaluation and design.

Until recently, probabilistic treatment of seismic loads was limited to the selection of design parameters of earthquake ground motion on the basis of return period such as peak or spectral acceleration. These ground motion parameters were then multiplied by a series of factors to arrive at the design seismic loads. The uncertainty was treated implicitly by allowing conservatism in the design forces on the basis of professional judgment and experience and was calibrated such that the resultant designs did not deviate significantly from acceptable practice. As a result, the reliability of such design to withstand damage and collapse was unknown and undefined.

The major losses suffered during recent earthquakes such as the 1994 Northridge, 1995 Kobe, 1999 Turkey and 1999 Chi-Chi earthquakes, however, have prompted the reevaluation of the entire design

process and more concentration on the uncertainty issue. As a result, considerable research has been undertaken and significant progress has been made in uncertainty modeling and applications to performance evaluation and design. This chapter summarizes some of these important research developments.

First, characterization of uncertainties as aleatory (inherent variability) and epistemic (modeling errors) and their probabilistic treatment by classical and Bayesian methods are introduced. The uncertainties in earthquake engineering problems are then described in terms of demand on and capacity of the system. *Demand* includes the uncertainty propagation from seismic source to path, site, ground motions, excitation intensity measures, structural responses and system limit states. *Capacity* includes uncertainty in material properties, member and system capacity to withstand various limit states including incipient collapse are briefly described. The reliability analysis of probability of prescribed limit states under seismic loads over a given period by the first-order reliability method (FORM), the recently proposed FEMA/SAC procedure and smart simulation then follow. Applications of the reliability analysis to probabilistic codes and standards are described. The important and unresolved issues of target reliability and reliability and redundancy are discussed. Finally, future challenges in the treatment of uncertainty in earthquake engineering are discussed.

7.2 Characterization of Uncertainty

To understand the impact of uncertainty in earthquake engineering, it is instructive to first characterize uncertainty. Uncertainty can be described in terms of those originating from inherent randomness and modeling errors. The former is commonly referred to as aleatory (*alea*, Latin for dice) and the latter as epistemic (related to our knowledge), e.g., whether one gets a head or tail in flipping a real coin once is aleatory, whereas the probability of getting a head exactly 50% of the time is epistemic. Aleatory uncertainty is irreducible because of either the nature of the problem or our inability to reduce the uncertainty such as in the physics associated with the extreme sensitivity of the final outcomes of the coin flipping to the initial conditions in tossing. The epistemic uncertainty in principle can be reduced as our knowledge improves such as by repeating the tossing a number of times, which leads to less uncertainty regarding the probability of getting a head. In earthquake engineering, for example, the earthquake's occurrence time, magnitude and distance of the next severe earthquake are inherently random, which is aleatory. Whether a certain probability distribution and distribution parameters (mean and coefficient of variation), or an attenuation equation, we used are correct based on a small number of observations of past events is part of the modeling errors, which is epistemic. The same is true of structural capacity. Similarly, the variability in steel yielding strength, member stiffness, damping ratio and ductility capacity are aleatory; and the errors in the structural analysis models used in describing these parameters are epistemic. As our knowledge about seismic events and structures improves with observations, analyses and experiments, better models with smaller uncertainties can be developed. In earthquake engineering, the emphasis so far has been placed on aleatory uncertainty; nevertheless, epistemic uncertainty and its impacts on performance evaluation and design are receiving serious attention recently. Hereafter, for simplicity, aleatory uncertainty will be referred to as "randomness" and epistemic uncertainty as "uncertainty."

Treatment of both randomness and uncertainty can be handled by either a classical or a Bayesian statistical method. The treatment of the randomness is generally modeled by a random variable if it is time invariant. For example, in many situations we assume structural capacity to be approximately time invariant and therefore can be modeled by a random variable. The random variable is then characterized by its moments (mean, standard deviation, skewness, etc.) and probability distribution on the basis of data or engineering judgment and experience. If randomness, such as the earthquake's time of occurrence, is time variant, it can be treated by a random process, such as Poisson point process, renewal point process and Markov process. The ground motion time history for the site of a given earthquake can be treated as a continuous Gaussian process. The parameters of these processes are estimated on the basis of data or engineering judgment and experience. Given the model and parameters, these random variable and random process models allow one to evaluate the probability of an event of interest to the engineer

such as that of a prescribed structural limit state being exceeded over a given period of time, which in turn allows the engineer to make rational design or retrofit decisions. The uncertainty in the models, however, also affects the engineer's decision since a change in the model parameter values or a change in the model itself would definitely change the probability of structural limit state.

7.2.1 Classical Methods

In the classical method, uncertainty is generally treated by the method of confidence interval. For example, a small number of observations results in uncertainty associated with the mean occurrence rate of a Poisson process. Similarly, a small number of tests contribute to the uncertainty in the mean yield strength of a structural steel. The classical method states that the mean value calculated from the samples is also a random variable with a standard deviation that decreases proportionally to the square root of the sample size. One can put limits on this parameter, which depends on the confidence level associated with those limits and the sample size. Alternatively, one can work with a random variable, which is the difference between the (unknown) true mean and sample mean and depends on the sample size, and thereby account for the epistemic uncertainty. In structural reliability analysis, one can account for the uncertainty on the basis of judgment and experience by allowing excitation and resistance model parameters to be random variables and as a result the probability of limit state calculated will also be uncertain and can be described by a confidence interval.

Consider an example of a structure with a random capacity X modeled by a normal distribution with mean μ_x and standard deviation σ_x under a deterministic demand d . The limit-state probability accounting for the randomness only (with known μ_x and σ_x) is given by

$$P(X < d) = \Phi\left(\frac{d - \mu_x}{\sigma_x}\right) \quad (7.1)$$

in which Φ is cumulative distribution function of a standard normal variate. Now assume that σ_x is known, but μ_x is uncertain and modeled by a normal random variable with mean \bar{X} and standard deviation S_x . Therefore, the limit-state probability given in Equation 7.1 is also a random quantity with a probability distribution. One can show (Ang and Tang, 1984) that the mean and q percentile values of P are given by

$$E[P] = \int_{-\infty}^{\infty} \Phi\left\{\frac{d - \mu_x}{\sigma_x}\right\} f_{\mu_x}(\mu) d\mu = \Phi\left\{\frac{d - \bar{X}}{\sqrt{\sigma_x^2 + S_x^2}}\right\} \quad (7.2)$$

$$P_q = \Phi\left\{\frac{(d - \bar{X}) + S_x \Phi^{-1}(q)}{\sigma_x}\right\} \quad (7.3)$$

Note that the uncertainty measure S_x appears in both equations. Comparing Equations 7.1 and 7.2, one can see that the net effect of additional uncertainty in μ_x is that the total uncertainty increases and as a result the limit-state probability increases. From Equation 7.3 one can calculate the confidence interval for the limit-state probability to account for the epistemic uncertainty. Table 7.1 shows the dependence of confidence intervals on the epistemic uncertainty parameter S_x . One concludes from Table 7.1 and Equation 7.3 that the 50 percentile value of the limit-state probability of 0.023 is equivalent to $\mu_x = \bar{X}$, since $\Phi^{-1}(0.5) = 0$ and Equation 7.3 reduces to Equation 7.1, i.e., the case in which only randomness is considered. Note that the mean value estimate of the limit-state probability is always higher than the median since the uncertainty in μ_x has been considered in the integral for the mean estimate. When the uncertainty in the mean capacity is half the capacity randomness, one can use the 85% value of 0.069 to indicate that we are uncertain about the true limit-state probability but 85% confident that it is less

TABLE 7.1 Mean and Percentile Value of Limit-state Probability as Function of S_x/σ_x ($d = 1$, $\bar{x} = 2$, and $\sigma_x = 0.5$)

Percentile, q (%)	$S_x/\sigma_x = 0.5$	$S_x/\sigma_x = 1.0$
5	0.0029	0.00013
15	0.0058	0.0012
25	0.0097	0.0037
50	0.023	0.023
Mean	0.037	0.078
75	0.048	0.093
85	0.069	0.168
95	0.119	0.361

than 0.069. Alternatively, one can use the 15% to 85% interval of 0.0058 to 0.069 to indicate that due to the uncertainty, we are 70% confident that the true limit-state probability will lie somewhere within the above interval. The interval increases to 0.0012 to 0.168 when the uncertainty is equal to the randomness ($S_x = \sigma_x$). Such wide intervals clearly indicate the importance of the effects of parameter uncertainty and modeling errors on the reliability performance evaluation. Classical methods, other than those due to sample size, generally do not offer a rigorous procedure to construct the model for uncertainty such as those based on judgment and experience and combination with randomness. Often, the nature of the problem and engineering convenience dictate the approach used as shown in the above example.

Another convenient method — treatment of the uncertainty as a multiplying factor applied to the randomness — is as follows (Ang and Tang, 1984):

$$X = N \tilde{X} \quad (7.4)$$

in which \tilde{X} is the randomness and N is the correction factor to account for the uncertainty, which is also a random variable. μ_N is mean (bias) and δ_N is coefficient of variation (uncertainty) of N . The mean of X is then approximated by

$$\mu_X \approx \mu_N \mu_{\tilde{X}} \quad (7.5)$$

and the coefficient of variation X by

$$\delta_X \approx \sqrt{\delta_N^2 + \delta_{\tilde{X}}^2} \quad (7.6)$$

in which both randomness and uncertainty are considered and combined. Note that the above method can be extended to the situation where \tilde{X} is a function of a set of random variables $\tilde{X} = g(Y_1, Y_2, \dots, Y_n)$. Using a first-order Taylor series approximation for g , one obtains

$$\mu_X \approx \mu_N \mu_g \quad (7.7)$$

in which

$$\mu_g \approx g(\mu_{Y_1}, \mu_{Y_2}, \dots, \mu_{Y_n}) \quad (7.8)$$

and

$$\delta_X \approx \sqrt{\delta_N^2 + \delta_g^2} \quad (7.9)$$

in which

$$\delta_g \approx \frac{1}{\mu_g} \sum_i \sum_j \frac{\partial g}{\partial Y_i} \left|_{\mu_Y} \right. \frac{\partial g}{\partial Y_j} \left|_{\mu_Y} \right. \rho_{ij} \sigma_{Y_i} \sigma_{Y_j} \quad (7.10)$$

The partial derivatives are evaluated at the mean values of Y_i , μ_y , and ρ_{ij} denotes the correlation coefficient between Y_i and Y_j . $\rho_{ii} = 1$, when $i = j$, and $\rho_{ij} = 0$ if Y_i and Y_j are statistically independent.

7.2.2 Bayesian Method

In the Bayesian method, the judgment- and experience-based information and the statistical information collected from sampling and observations are treated separately first and combined later. This allows one to construct an initial (prior) distribution for the parameters of the models as random variables based on the current state of knowledge including judgment and experience. The sample observations in various forms such as real numerical data, upper or lower bound can be incorporated into the prior model to arrive at the final combined (posterior) distribution or a model that is consistent with the sample observations and judgment or experience. Consider a random variable X with density function $f_X(x)$ and uncertain parameter θ described by a prior distribution $f'(\theta)$. Given sample observation of X , $\epsilon : \{X_1, X_2, \dots, X_n\}$, the sample likelihood function is given by

$$L(\theta) = P(\epsilon | \theta) = \prod_{i=1}^n f_X(x_i | \theta) \quad (7.11)$$

in which $f_X(x_i | \theta)$ is the probability (density function) of realization of the sample value X_i given the distribution parameter θ . From the Bayesian theorem, the posterior distribution of θ consistent with the sample observations is then

$$f''(\theta) = k L(\theta) f'(\theta) \quad (7.12)$$

where

$$k = \left[\int_{-\infty}^{\infty} L(\theta) f'(\theta) d\theta \right]^{-1} \quad (7.13)$$

is the normalizing constant.

Equations 7.12 and 7.13 are a formal procedure for updating the uncertainty. The uncertainty (coefficient of variation) in the posterior distribution is always less than that in the prior distribution or the sample likelihood function. The performance can be evaluated on the basis of random variable X after the Bayesian updating with a density function

$$f_X(x) = \int_{-\infty}^{\infty} f_X(x | \theta) f''(\theta) d\theta \quad (7.14)$$

in which the uncertainty in the parameter is considered using the posterior distribution. The Bayesian method is therefore a more flexible and rigorous approach in treating and combining randomness and uncertainties. The mathematics, however, is more involved, and in many situations mathematically convenient (conjugate) distribution models are required for closed form solutions. In spite of the flexibility and rigor of the Bayesian method, it has only now begun to receive attention in earthquake engineering.

An example of the Bayesian method on the coin-tossing problem is as follows. One can model the coin tossing as a repeated trial or a Bernoulli sequence (model) with a probability of getting a head in each trial (parameter) to be uncertain and unknown. If there is absolutely no information regarding the probability of this coin landing with a head on top, one can assume it to be a random variable uniformly distributed between 0 and 1 (prior distribution). If one observes r heads (sampling observations) after n tosses, then from the Bayesian posterior distribution (Equation 7.12) the probability of getting a head in any trial is

$$\frac{r+1}{n+1}$$

(see, e.g., Ang and Tang, 1975). For example, if only one toss is performed and a head is observed, the resultant probability is 0.667, not 1.0 as would be the case in accordance with the classical relative frequency estimate. This is the best assessment of the probability under the circumstance. This result approaches the classical relative frequency definition of probability r/n when n becomes very large — as it should be since the prior model does not contain any specific information. The results would be different if the prior distribution is more informative (e.g., assuming on the basis of observation of the shape of the coin that the prior probability is uniformly distributed between 0.4 and 0.7) and the sample size is not very large. Therefore, the Bayesian method would be a valuable method of treating and combining randomness with uncertainty when there is a strong judgment/experience basis and relatively small number of sample observations. Such situations occur quite often in earthquake engineering.

7.3 Uncertainty in Demand and Probabilistic Treatments

In structural performance evaluation, it is convenient to describe the system performance in terms of demand and capacity. The demand can be the force (shear, bending moment, axial forces, overturning moment) or the response (displacement, velocity, acceleration, drift, ductility, energy dissipation) in the system caused by ground excitation. The capacity of the system is the maximum force or response that the system can withstand without member or system failure. The member or system failure can be described by various limit states of interest to engineers. For example, commonly used limit states expressed in terms of response demand are drift limits corresponding to various performance requirements from immediate occupancy (IO) to collapse prevention (CP). In theory, the capacity and demand depend on the excitation and the structural property. Consider the performance of a structural system for a given period of time. The demand as described above, such as system global drift, is clearly a quantity that fluctuates in time and highly uncertain depending on the seismic excitation during the period. The capacity is primarily a property of the system, which depends on the type of excitation. It is a common practice to use the maximum response or force over a given time period (annual or per 50 years) as the demand variable. For example, a 10% probability of exceedance in 50 years is commonly used as the probability threshold for selecting the design earthquake. The uncertainty in the demand can be traced back to the chain of events that causes the response or force as shown in Figure 7.1. They are briefly described as follows with emphasis laid on the uncertainty modeling and treatment. Details can be found in the previous chapters and the extensive literature on these subjects.

7.3.1 Source

Over a period of time, the threat of seismic excitation to a given system at a given site can be due to events at different times and of different magnitudes, distances, focal depths and rupture surface geometries and features. The randomness and uncertainty of these major source parameters are briefly discussed in the following.

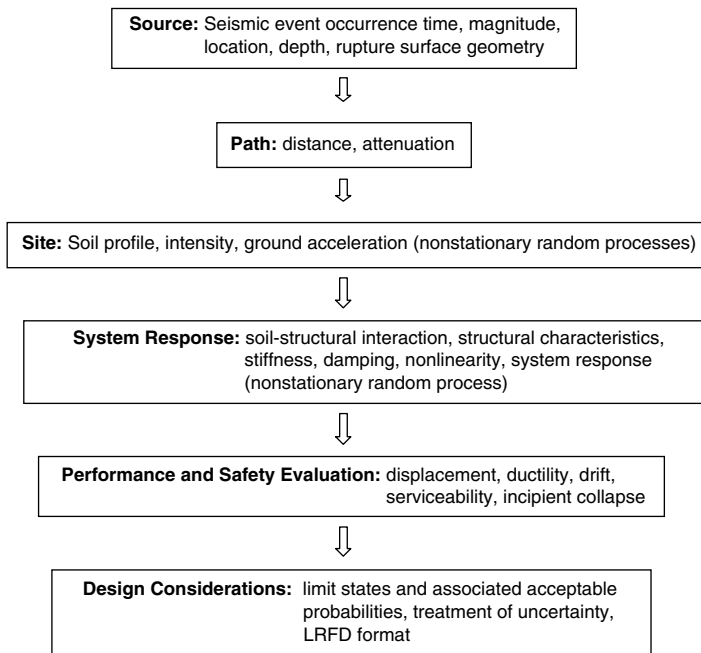


FIGURE 7.1 Probabilistic performance evaluation and design for earthquakes.

7.3.1.1 Occurrence Time

The random occurrence in time can be modeled by random processes, such as from the simple Bernoulli sequence, its limiting form, and Poisson process, to more involved renewal and Markov processes. These models allow one to calculate the probability of the number of occurrences over a given period. The Bernoulli and Poisson processes are time independent or models with no memory so that the probability of number of occurrences depends only on the time interval considered and is independent of the calendar time and past history. The only parameter included in the model is the annual probability of occurrence, p , for the Bernoulli sequence, or mean occurrence rate, ν , for the Poisson process. In spite of the rather restrictive assumption, these two models from which we derive the concept of return period are quite robust and have been widely used. Often, the return period has been used without checking the validity of the time-independence assumption associated with the underlying models. According to the Poisson model, the number of occurrences, N , over an interval $(0, t)$ is given by

$$P_t(N=r) = \frac{(\nu t)^r}{r!} e^{-\nu t} \quad (7.15)$$

The mean waiting time between two consecutive occurrences is $1/\nu$, which is the return period. If a Bernoulli sequence is used, the return period is $1/p$. When ν is calculated based on a short record, the uncertainty could be significant. The Bayesian method outlined in Equations 7.11 to 7.14 can be used to incorporate the effect of such uncertainty. If n_0 earthquakes were recorded in the last t_0 years, the Bayesian prediction is (e.g., Ang and Tang, 1975)

$$P_t(N=r) = \frac{(r+n_0)!}{r!n_0!} \frac{(t/t_0)^r}{(1+t/t_0)^{r+n_0+1}} \quad (7.16)$$

The difference could be significant when n_0 is small. For example, in the case $n_0 = 2$, $t_0 = 10$, $t = 1$, the probabilities of occurrence of at least one event ($N \geq 1$) in a given year according to Equations 7.15 and 7.16 are 0.181 and 0.249, respectively. In general, the Poisson model works well for a large number of sources. Individually, their occurrences may show time dependence but collectively the occurrences over time tend to become less dependent and can be approximated by a Poisson process. When dealing with individual and in particular large-scale events such as characteristic earthquakes along well-defined faults with good records of the past occurrences, the renewal and Markov processes are often used to incorporate the time dependence. For example, a renewal process has been used in the probabilistic prediction of large events in the western United States(Working Group on California Earthquake Probabilities, 1995) in which the random time intervals between occurrences are assumed to be a lognormal random variable. The probability of the number of occurrences of a renewal process for a given period would depend on past history, and the mathematics is more involved. Often the interest is on the next occurrence within t years from now knowing the last event occurred t_0 years before. Counting the time from the last event, the probability is given by

$$P(T < t_0 + t | T > t_0) = P(t_0 < T < t_0 + t) / P(T > t_0) \quad (7.17)$$

in which T is the interoccurrence time, that is, a lognormal random variable. The above probability can be calculated easily when the mean and standard deviations of T are known since the two parameters required in the lognormal probability calculation in Equation 7.17 can be determined from these two moments. Note that the probability depends on the time interval $(0, t)$ and records of the past occurrence given by t_0 . The Poisson model would yield

$$P(T < t) = P_t(N \geq 1) = 1 - e^{-vt} \quad (7.18)$$

because the independence assumption implies that past history has no bearing on future occurrences. The difference between the two models could be significant. For example, consider the characteristic event of the 1964 Alaska earthquake. Assume an average recurrence time of 700 years and a coefficient of variation of 60%. According to Equation 7.17 using a lognormal distribution for T with $t_0 = 39$ and $t = 50$, the probability of a repeat of the event between 2003 and 2053 is 0.00028, and according to Equation 7.18 with $v = 1/700$ and $t = 50$, the probability is 0.069.

7.3.1.2 Epicenter Location

The exact location of a future earthquake epicenter is unknown. Random spatial distribution models can be used for this purpose. In the past, line and areal source models were used in which the epicenter was assumed to follow certain distribution on the line or within a well-defined region. Such distributions can be obtained from occurrence statistics collected from the records of past earthquakes. For example, in the context of a Poisson occurrence model, one can express the mean occurrence rate of future events per unit area as function of the location $v(x,y)$ for an areal source and $v(l)$ as function along the line source. One can then evaluate the probability of occurrence of various events within the area or along the line. The occurrence rate of events in a given region, the random magnitude and spatial distribution of epicenter given the occurrence in time can be used to model the temporal and spatial randomness of future events as will be shown in Section 7.3.3.

7.3.1.3 Magnitude

The magnitude variability is generally described by the Gutenberg–Richter equation, which expresses the logarithmic frequency as a linear equation of magnitude for a certain range of the magnitude

$$\text{Log}N = a - b M \quad \text{for } m_L < M < m_U \quad (7.19)$$

The implication is that the variability of magnitude given the occurrence of an earthquake can be modeled by a truncated exponential probability density of the following form:

$$f_M(m) = Cb e^{-b(m-m_L)} \quad \text{for } m_L < M < m_U \quad (7.20)$$

The randomness in magnitude is therefore captured by the above distribution. Depending on the range, the variability in magnitude described by the above distribution in terms of coefficient of variation is large and close to 1. When data are limited the uncertainty in parameters a , b , m_U , and m_L could also be important.

7.3.1.4 Rupture Surface

There are many other random parameters of the source such as the size and geometry of the rupture surface, stress drop and slip variation within the surface that could also be important factors for consideration. The effects of the randomness of these parameters are, to a certain extent, absorbed in the attenuation equation and seldom explicitly considered in seismic risk analysis. The exception is in simulation of individual large events. For example, random field models have been developed for the slip variation within the rupture surface and used in simulation of ground motions (e.g., Somerville et al., 1997; Wen and Wu, 2001).

7.3.2 Path and Site

As the seismic waves propagate from the source through the rock and soil to the ground surface at the site, they are attenuated or amplified and many factors contribute to the uncertainty in the attenuation and amplification processes. The effects of many other random parameters associated with the source are also included in the attenuation model. As a result, the randomness in the attenuation model is usually very large as can be seen from the large scatter of attenuation of various ground motion intensity measures such as spectral ground acceleration and velocity based on observations during earlier earthquakes. As shown in previous chapters, the forms of the attenuation equations are usually the result of the modification of the wave propagation theory by observational results. The most important independent variables in the attenuation equations are the magnitude (M), distance (R) and site soil classification (S). In view of the large uncertainty, the attenuation equation $A(M, R, S)$ generally describes the central value, and the scatter is modeled by a random variable. When the intensity measures are plotted on a logarithmic graph, generally the scatter approximately follows a normal distribution. Therefore, given M , R and S , the intensity measure, e.g., spectral acceleration S_a , at the site is approximately a lognormal random variable with expected (mean) value, $E(\log S_a)$, described by the attenuation equation; i.e.,

$$E[\log S_a(M, R, S)] = A(M, R, S) \quad (7.21)$$

The scatter is given by $\sigma_{\log S_a}$, in which σ denotes standard deviation. σ , in general, is also a function of M and S (e.g. Boore and Joyner, 1994) but as an approximation it is usually regarded as a constant. Therefore, in such a formulation, all the randomness in wave propagation from the source to the site and some randomness associated with the source are captured by $\sigma_{\log S_a}$. Note that the mean and standard deviations in these equations are expressed in terms of $\log S_a$ and not S_a . After proper conversion, the mean and coefficient of variation of S_a are

$$E(S_a) = \exp[2.3A + 0.5(2.3\sigma)^2] \quad (7.22)$$

$$\delta_{S_a} = \sqrt{e^{(2.3\sigma)^2} - 1} \quad (7.23)$$

in which A and σ are the attenuation equation prediction and scatter in log scale, respectively. For example, a scatter of $\sigma_{\log S_a} = 0.3$ — a value commonly seen in attenuation equations — actually means a coefficient of variation of 78% in S_a . The probability that S_a exceeds a given limit of a_0 is therefore given by

$$P(S_a > a_0 \mid M, R, S) = 1 - \Phi \left[\frac{\ln a_0 - 2.3A(M, R, S)}{2.3\sigma} \right] \quad (7.24)$$

Note that the above equation describes the randomness in attenuation alone when M , R and S are known. M , R and S are also random variables, which would influence the demand on the structural system. The uncertainty in attenuation equation (modeling errors) is evident from the various forms of attenuation equations for the same region, which give different results. Again, generally such uncertainty is not considered explicitly.

7.3.3 Ground Excitation and Structural Response

The demand on the structure over a given time period in the future is the ground motions and structural responses that they produce. They are unpredictable and random functions of time. In theory, they can be modeled by a continuous random process whose parameters depend on the source, path, site and structural characteristics. Given the occurrence of an earthquake, the ground excitation in future is therefore a continuous random process of time that depends on magnitude m , distance r and site condition, i.e., $a(t \mid m, r, s)$. The structural response in turn is also a random process that depends on the excitation and the structural characteristics and the excitation parameters. Although such random process models have been developed on the basis of the random process theory and method of random vibration (Wen, 1989, 1990) for excitation and structural responses the nonstationarity in the excitation and quite often nonlinear and inelastic dynamic responses of the system render the theoretical treatment for real structural systems difficult.

7.3.3.1 Excitation Intensity Measures

In performance evaluation, the structural response demands are often described in terms of the maximum responses such as maximum global displacement, interstory drift or energy dissipation over the duration of the excitation. These demand variables are random and the annual maximum or maximum value over 50 years is customarily used. The uncertainty in these demand variables can be traced back to those in the structural characteristics as well as source, path and site parameters. The propagation of uncertainty along the chain of events that leads to the demand variable shown in Figure 7.1 is a complicated process involving random variables and random processes and linear and nonlinear input–output relationship. To simplify the problem, engineers have been trying to find some key ground excitation intensity measures that correlate well with the structural demand variable. The peak ground acceleration, velocity and displacement have been traditionally used for this purpose. These measures generally show poor correlation with the structural response since the structural characteristics are not considered.

Using extensive regression analyses of steel structural systems of different designs and configurations under excitation of recorded ground motions, Luco and Cornell (2002) examined a number of intensity measures that reflect the structural characteristics such as fundamental period and damping ratio. The results showed that the spectral acceleration or displacement at the structure's fundamental period corresponding to a damping ratio of 5% generally accurately predicts the structural response. To incorporate effects of higher modes and inelastic response, intensity measures consisting of the combined first and second mode spectral accelerations or displacement and first mode elastic and inelastic spectral accelerations were examined. They give even better results as indicated by the smaller scatter in the regression relationship compared with using only the fundamental period elastic response. This is achieved, however, at the expense of a more complicated form of the intensity measure. One advantage of using spectral response variable is that these quantities can be directly related to M , R and S via the attenuation equation and additional dependence of structural response on M and R is small and can be

ignored in the approximation (Shome et al., 1998). To consider the effect of biaxial excitation, Wang and Wen (2000) proposed a bidirectional spectral displacement defined as the maximum of the vector sum of the displacements in two principal directions at the two fundamental periods of the structure in the two principal directions. It can be used to better correlate with the biaxial structural response measure such as biaxial drift ratio, which is defined in the same way.

7.3.3.2 Seismic Hazard Analysis

The uncertainty in the seismic excitation can therefore be approximately described in terms of a random variable of the above intensity measure such as the maximum spectral acceleration over a given period of 1 year or 50 years. The probability of exceedance of such a random variable is generally referred to as the seismic hazard curve. For example, if spectral acceleration S_a is used, the probability of exceedance in t (e.g., 50) years is given by

$$P_t(S_a > a) = H_t(a) \quad (7.25)$$

$H_t(a)$ is the hazard curve, which can be constructed from the probabilistic models of the source, path and site using available regional seismicity information. For example, consider a region in which there is a well-defined fault of characteristic earthquakes of known magnitude. The probabilistic distribution of the interoccurrence time and date of last occurrence are also known. There is also an areal source of smaller events whose occurrences can be modeled by a Poisson process with an occurrence rate that is a function of the location, $v(x, y)$; and whose magnitude can be modeled by an exponential distribution on the basis of a Gutenberg–Richter equation. In addition, there is also a line source along which the occurrence rate $v(s)$ and magnitude distribution of future events are known. The attenuation equations for events from these sources have also been established. Assuming the events from these three sources are statistically independent, the seismic hazard over the next t years can be evaluated as follows:

$$P_t(S_a > a) = 1 - [P_C(S_a < a | C)P(C)][P_A(S_a < a)][P_L(S_a < a)] \quad (7.26)$$

in which C denotes the occurrence of characteristic events modeled by Equation 7.17; the conditional probability of spectral acceleration given that the occurrence of the event can be estimated from the attenuation equation model as given in Equations 7.22–7.24. A and L refer to the areal and line sources. The last two terms in Equation 7.26 are obtained by considering the contribution from all future events within the areal and line sources and the occurrence as a Poisson process as follows:

$$P_A(S_a < a) = e^{-t \int \int \int_{xym} v(x, y) P(S_a > a | m, r, s) f_{MA}(m) dx dy dm} \quad (7.27)$$

$$P_L(S_a < a) = e^{-t \int \int_{sm} v(s) P(S_a > a | m, r, s) f_{ML}(m) ds dm} \quad (7.28)$$

in which Equations 7.20 and 7.24 are used and subscripts MA and ML refer to magnitude of events in the areal and line sources. The above procedure allows one to evaluate the spectral acceleration of different periods corresponding to a given probability of exceedance. The resulting response spectra are called uniform-hazard spectra (UHRS). The commonly used probability of exceedance is 50%, 10% and 2% in 50 years as used in the USGS National Earthquake Hazard Mapping Project (Frankel et al., 1996). The UHRS therefore is an efficient way of describing the seismic hazard and ground motion demand on the structure since the response of a linear structure corresponding to the above probability of exceedance can be easily predicted using the well-known modal superposition method.

For nonlinear systems, the UHRS cannot be used directly since modal superposition method can no longer be applied. Efforts were made in the past to extend the concept of UHRS to nonlinear inelastic systems. Researchers (Nassar and Krawinkler, 1992; Miranda and Bertero, 1994; Collins et al., 1996) have

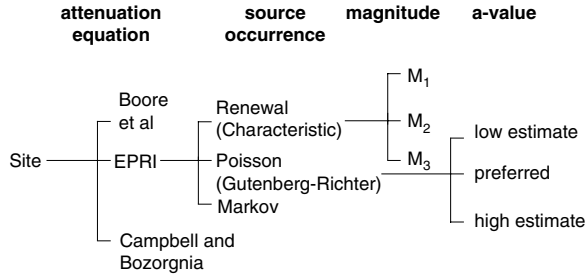


FIGURE 7.2 Logic tree in seismic hazard analysis.

established uniform-hazard inelastic response spectra (UHIRS) on the basis of investigation of a large number of single-degree-of-freedom (SDOF) systems. Empirical rules have been developed so that the UHIRS can be constructed from the linear UHRS. The spectra give the ductility ratio of an SDOF system of given period and yield strength corresponding to a given probability of exceedance. The UHIRS therefore describes the demand on an SDOF inelastic system. Most real structural systems cannot be adequately described by an SDOF system since the effect of higher modes cannot be included; hence the application of UHIRS is limited.

7.3.3.3 Modeling of Epistemic Uncertainty by Logic Tree

When dealing with uncertainty in the selection of magnitude, recurrence model, attenuation equation, etc. in seismic hazard analysis, a logic tree with branches for different models or values is frequently used, each with assigned likelihood based on judgment or experience (e.g., Frankel et al., 1996; Frankel, 1997). It is therefore a method for treating the epistemic uncertainty. At each branch of the tree, further characteristics and uncertainty can be assigned in accordance with the expert's opinion (e.g., SSHAC, 1995). For example, referring to Figure 7.2, going from the site to the source, possible attenuation equations are first identified. The occurrence model is either a memory-less Poisson process according to the Gutenberg–Richter equation, a renewal process for characteristic events with a specified recurrence time distribution or a Markov process with memory specified by a transition matrix. At each branch, candidate models or equations are assigned with a relative likelihood reflecting the judgment or experience of the experts. For example, for a characteristic event, the possible choices of magnitude are M_1 , M_2 or M_3 with given relative likelihood.

In the seismic hazard analysis this relative likelihood of the magnitude is then converted into discrete probability mass function and incorporated into the risk analysis. For example, because of the modeling uncertainty, the result of the seismic hazard analysis as given in Equation 7.26 becomes a random variable. A common practice is to determine the expected (mean) value of the seismic risk by integration (or summation) over all possible combinations of these values weighted by their likelihood (or probability mass). A simpler and more convenient way is to approximate the mean risk estimate by using the mean value at each branch where possible (such as the a and b values in the Gutenberg–Richter equation or the magnitude of a characteristic earthquake) and reduce the number of possible combinations and hence the required numerical effort. A more general approach is to consider the likelihood of each branch and evaluate the risk corresponding to a percentile value (or confidence level) as illustrated by the example in Section 7.2.1. It can be done easily by a Monte Carlo (MC) method as will be shown later. The implications of using the mean value versus the percentile value will be illustrated in an example in the following sections.

7.3.3.4 Probabilistic Structural Response Demand Analysis

To establish the probabilistic relationship between the ground motion intensity measure and the response of MDOF nonlinear systems, one can use the method of random vibration with the ground motion modeled as a random process. Alternatively, one can use a regression analysis of nonlinear time-history responses under recorded ground motions. Because of the inherent nonstationary nature of the random

excitations in earthquakes and the analytical difficulty in modeling complex nonlinear member response behaviors such as brittle fracture in random vibration, the time-history and regression analysis are more practical. To cover a wide range of excitation and structural response in the inelastic range, such ground motions are frequency scaled. Although the frequency content and duration of ground motions due to events of different magnitudes and distances are different and scaling may violate the basic physics of ground motions, results based on extensive investigations (Shome et al., 1998) show that when intensity measure such as spectral acceleration is used in the scaling, the errors are small. The regression analyses therefore allow one to establish the functional relationship between the intensity measure and the structural demand variables such as global (roof) and local (interstory) drifts and energy dissipation (cumulative damage). In the following, the relationship between maximum interstory drift and spectral acceleration is used as an example. The method can be applied to other structural demands under a different intensity measure such as spectral displacement or bidirectional spectral displacement (Wang and Wen, 2000b).

On the basis of extensive regression analyses of response of steel structures, Cornell et al. (2002) proposed that the maximum interstory drift can be expressed as a simple power function of the spectral acceleration:

$$D = a(S_a)^b \quad (7.29)$$

Such a relationship is necessarily approximate and there are large scatters around the regression line, which will be incorporated in the performance analysis as shown in the following. The regression prediction is therefore the estimate of the mean demand conditional on a given value of the excitation intensity measure, $E(D|S_a = a)$. The scatter expressed in terms of the coefficient of variation, $\beta_{D|S_a=a}$, also depends on the intensity but as an approximation, it is often regarded as constant. Therefore, given the excitation intensity the structural response demand can be described by a random variable of a given distribution. The lognormal distribution generally gives a good fit, which can be used to describe the randomness in structural demand variable due to ground motion record-to-record variation even though these ground motions have the same S_a . The probability of the structural demand exceeding in t years can therefore be evaluated by the total probability theorem to incorporate the contribution from all values of S_a .

$$P_t(D > d) = \int_0^{\infty} P(D > d | S_a = a) H'_t(a) da \quad (7.30)$$

in which

$$P(D > d | S_a = a) = 1 - \Phi\left(\frac{\ln d - \lambda}{\beta_{D|S_a=a}}\right)$$

$$\lambda = \ln[a(S_a)^b] - 0.5\beta_{D|S_a=a}^2 = \ln \tilde{D}, \quad \tilde{D} = \text{median value of } D$$

$H'_t(a)$ = derivative of seismic hazard curve

Note that the calculation shown in the above general analytical procedure could be quite involved and has to be carried out numerically. In code procedures and for a fast and approximate evaluation, closed form solution is desirable. Cornell et al. (2002) have shown that if the result of the seismic hazard analysis given above can be approximately described by a power law

$$H_t(a) = k_0 a^{-k} \quad (7.31)$$

in which k specifies the hazard decay and k_0 is the scale factor, the above lognormal distribution assumption for the demand excitation is valid. Equation 7.30 can be evaluated in a closed form

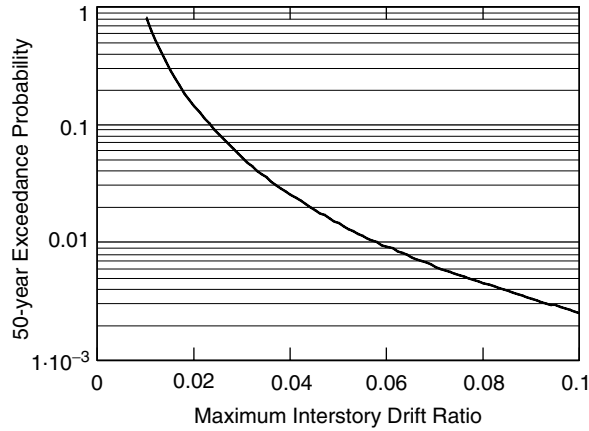


FIGURE 7.3 Fifty-year maximum interstory drift ratio demand curve.

$$P_t(D > d) = H_t(a^d) \exp \left[-\frac{1}{2} \frac{k^2}{b^2} \beta_{D|S_a=a}^2 \right] \quad (7.32)$$

in which a^d is the spectral acceleration level corresponding to the demand d according to Equation 7.29. Equation 7.30 or in more concise form Equation 7.32 therefore describes a probabilistic structural response demand curve in which all the important randomness in excitation and structural response is considered. The first term is the demand curve without consideration of the randomness in the response-excitation relationship. The exponent function is the correction for this randomness. Note that the correction factor involves the structural (b) and hazard (k) parameters. Note that Equation 7.31 is intended for approximating the tail distribution and is no longer valid when the spectral acceleration is very small. The method is demonstrated by a simple numerical example as follows.

Consider a three-story steel structural building with a fundamental period of 1 sec at a location where the 50-year seismic hazard and maximum interstory drift ratio as function of the spectral acceleration can be described by

$$H_{50}(a) = 0.0068 a^{-3} \quad (7.33)$$

$$D = 0.06 a^{1.2} \quad (7.34)$$

The hazard is such that the spectral acceleration at 1 sec is 0.4g corresponding to an exceedance probability of 10% in 50 years and 0.7g corresponding to 2% in 50 years — typical values for a site in the Los Angeles area. The building response is such that the maximum interstory drift ratio is 2% at a spectral acceleration of 0.4g and 4% at 0.7g — reasonable values for such a steel building. Assuming the randomness in the drift ratio-spectral acceleration regression analysis $\beta_{D|S_a} = 0.3$, the 50-year probabilistic maximum interstory drift demand curve according to Equation 7.32 is then

$$P_{50}(D > d) = 0.0068 \left[\left(\frac{d}{0.06} \right)^{\frac{1}{1.2}} \right]^{-3} \exp \left[0.5 \left(\frac{3}{1.2} \right)^2 0.3^2 \right] \quad (7.35)$$

The correction factor to account for the randomness in the demand as given in the exponential function is 1.33 and the 50-year demand curve (shown in Figure 7.3) is simplified to $0.009904(d/0.06)^{-2.5}$.

As demonstrated in previous sections, uncertainties either statistical in nature (such as sampling errors) or empirical in nature (based on judgment) could be important and have not been accounted for in the above formulation. These include uncertainties in the structural response analysis methods, choice of

probability distributions and parameters and assumptions and approximations used in the source, path and site parameters. Treatment and impact of these uncertainties are covered in detail in Sections 7.5.2 and 7.5.3 on probabilistic performance evaluation.

7.3.4 Simulation and Monte Carlo Methods

The above formulation relies on accurate prediction of structural response by the excitation intensity measure. This may not be true for all structural systems under all possible future excitations. For example, the higher mode effects, near-source effects and many detailed structural response behaviors cannot be predicted satisfactorily with any simple intensity measure since in reality the structure response is a function of the whole ground excitation time history. Any scalar intensity measure would fall short in accurately predicting the detailed structural response behavior. An entirely different approach to the evaluation of the probabilistic structural demand that uses the full ground motion time history is the MC method.

7.3.4.1 Monte Carlo Method

Referring to Figure 7.1, instead of using analytical method to tract the propagation of uncertainty as shown in the previous sections, one can imitate nature by generating random variables or random processes required in the chain of events according to the underlying models. It allows one to simulate the future ground excitations at the site and perform time-history analyses of the structure to evaluate the response demand. In other words, one simulates the whole process from the source to structural response on a computer and repeats the process several times. The probabilistic description of the structural demand is therefore given by statistical analysis of the structural responses from the large samples of simulation results. The MC method has been widely used in many disciplines and by many researchers in earthquake engineering. For example, Collins et al. (1996) and Wu and Wen (2000) used available seismicity information in the region surrounding the Los Angeles and Santa Barbara areas for simulation of a large number of ground motions.

The advantages of the MC method are clearly conceptually straightforward and can be applied to systems that are complex and show nonlinear response behavior. However, the MC method bypasses the need for identifying and justifying an intermediate intensity measure. All the propagation of uncertainty including the epistemic uncertainty is captured automatically in the process. For this purpose, the different source models and attenuation equations can be mixed in the simulation according to the logic tree by selecting the model or equation with frequency depending on its assigned likelihood (or probability). The main disadvantage is the considerable numerical effort required, in particular the large number of ground motions and structural response time histories that need to be performed for an accurate estimate of the very low probability level of structural demand. To express the sampling error in terms of the coefficient of variation of the estimated demand exceedance probability, δ_{P_f} , within a given limit, δ_0 , the sample size required is

$$N = 1/p_f \delta_0^2 \quad (7.36)$$

For example, if P_f is 10^{-3} and the desired accuracy is $\delta_0 = 20\%$, the required sample size N is 25,000. For problems of some complexity that each sample run may require significant computation time, the computation problem therefore can easily get out of hand. This problem is especially serious if nonlinear and inelastic structural response behaviors including brittle member failure are to be considered in the structural systems. Another difficulty is the fact that a truly physically based model for simulation of ground excitation should be based on wave propagation models, e.g., the broadband simulation method (Saikia and Somerville, 1997), that would significantly add to the numerical effort. The simulation method is therefore appropriate for systems in which a detailed description of the structural demand is needed and such considerable numerical effort can be justified.

7.3.4.2 Variance Reduction Techniques

The numerical effort in the MC method can be lessened by a smart simulation scheme. There have been earnest efforts of research in this area in the past decade and many numerical schemes have been developed by which the convergence of the MC method can be improved sometimes dramatically. Examples are various variance reduction techniques such as the importance sampling and adaptive sampling methods. A summary of some of the recent developments, for example, can be found in Schueller and Spanos (2001). In the importance sampling method, random variable realizations (sampling) are artificially concentrated at a certain region that is most productive, i.e., one that causes structural limit states to occur. In the adaptive sampling method, simulation is conducted in stages where samplings in later stages are concentrated in more productive regions. Depending on the results of previous stages therefore is much more efficient. The problems associated with these methods include prior knowledge of the system behavior is needed in pinpointing the most productive sampling region that may not be available or reliable enough to prevent gross errors of sampling at the wrong location, or additional extensive analytical or numerical efforts are required that make the method unattractive in practical applications. For these reasons, these methods have not been widely used in probabilistic modeling in earthquake engineering.

7.3.4.3 Method of Deaggregation

An extreme form of the importance sampling that has been used in earthquake engineering is the “deaggregation” concept where only ground motions due to the earthquake of given M and R that contribute most to the “event” under consideration are simulated. The event is generally the spectral acceleration corresponding to a given exceedance probability. Referring to Equations 7.26–7.28, one can see that the probability of a given spectral acceleration exceeding 2% or 10% in 50 years is a result of integration or aggregation of contribution from sources of different M and R, and with different attenuation A. If we deaggregate the integral and identify the combination of M, R and A that contributes the most to the integral, we can use the ground motion time histories of such an event to “represent” the seismic environment for performance evaluation. It is clear that ground motions produced by such method are only a very approximate representation of all possible ground motions that contribute to the event of interest. The approximation could be poor if there is no clearly dominant event. Also, the deaggregation result is dependent on the event of interest and the process has to be repeated each time one considers a spectral acceleration of different period and exceedance probability.

7.3.4.4 SAC Ground Motion Procedure

In a recent SAC/FEMA effort (Somerville et al., 1997), the selection of the ground excitations to match the spectral acceleration with a given probability of exceedance was extended for all periods. The procedure began with the UHRS corresponding to a given probability of exceedance such as 50%, 10% and 2% in 50 years. Recorded and simulated ground motions based on a broadband procedure (Saikia and Somerville, 1997) were then selected and scaled to obtain suites of ten ground motions whose median response spectra match the 5% damping UHRS approximately over a wide range of period and a given probability level. This was done for Los Angeles, Seattle and Boston. Since the selected ground motions were from events of different magnitudes and distances, even with properly chosen scaling factors, the scatter of the response spectra of the ground motion suite compared with the UHRS in terms of coefficient of variation was generally of the order of 30%. Such ground motion suites represent the excitation demand corresponding to a given probability of exceedance. They can be used for evaluation of demand on nonlinear and inelastic systems.

The median value of the structural response under the suite of ten ground motions can be used as the response demand on the structure corresponding to a probability of exceedance of 50%, 10% or 2% in 50 years. Note that unlike the seismic hazard analysis described in Equations 7.26–7.28 where regional seismicity is used, the ground motions selected in this procedure may come from a seismicity environment that is totally different from that of the site. Therefore strictly speaking, the ground motions generated

in this procedure may not represent any possible future events in this region. However, since after the scaling, their response spectra match those obtained using regional seismicity and spectral acceleration is a good predictor of structural response in terms of accuracy and efficiency (Luco and Cornell, 2002), there are good reasons to believe that these ground motions would produce structural response similar to those future ground motions at the site would produce. The SAC ground motions have been used extensively in the SAC Steel Project in performance evaluation and recommendation of reliability based design procedures.

7.3.4.5 Uniform-Hazard Ground Motions

A smart simulation procedure for generating uniform-hazard ground motions (UHGM) similar to the SAC/FEMA procedure was recently proposed by Wen and Wu (2001) for mid-America cities. Although moderate- to large-scale events occurred in the past in mid-America including three between 1812 and 1813 in New Madrid, TN, records that can be of engineering interest are scarce and therefore simulation is the only method of producing ground motion time histories for performance evaluation and design.

The procedure consists of three stages. The first stage is the same as the MC method and was used in Collins et al. (1996). Future events were generated in three cities (Memphis, TN, St. Louis, MO and Carbondale, IL) on the basis of available regional seismicity information, latest attenuation and random-vibration-based ground motion models for the region. The point source model by Atkinson and Boore (1995) was used for noncharacteristic events and the finite-fault model by Beresnev and Atkinson (1998) was used for characteristic events in the New Madrid seismic zone. A Poisson process is assumed for all events. The effect of site soil condition was modeled using the quarter-wavelength model of Boore and Joyner (1991). A large number of events and ground motions equivalent to 90,000 years of records were generated. The second stage involves processing the simulated ground motions to construct the UHRS for each city for both soil and rock sites corresponding to exceedance probabilities of 10% and 2% in 50 years. This essentially achieves the same goal as the seismic hazard analysis using an entirely different approach. The results of the UHRS compared well with those of the USGS National Earthquake Hazard Mapping project. The third stage involves selection of UHGM from a pool of large simulated ground motions such that the response spectra of the selected ground motions match UHRS for all period range in a least square sense.

These ground motions represent the future ground excitation corresponding to probabilities of exceedance 10% and 2% in 50 years. They are generated by events of different magnitudes and distances with different attenuations. Conceptually, the procedure is similar to the deaggregation method except that the matching is done for all periods and there are 10 contributing events of various magnitudes and distances. The matching is similar to that in SAC/FEMA ground motion procedure except that the selected events are possible future events in the region. Figure 7.4 shows the contributing events for the three cities for different hazard levels. Note that at the 10/50 level, future contributing events are mostly close and small or distant and large. At the 2/50 level, almost all are characteristic events from the New Madrid seismic zone.

It has been shown in Wen and Wu (2001) that the median value of the response spectra of the UHGM almost match the target UHRS (within 10% for a wide period range), and the median inelastic response spectra using the ten UHGM also almost match those based on 90,000 years of simulated ground motion records. This indicates that the median value of the structural response to the ten UHGM is an accurate estimate of the structural response demand for both linear and nonlinear systems. Figure 7.5 shows a structural response (column drift ratio %) demand curve for a two-story steel moment frame at Carbondale, IL before and after retrofit using the UHGM. A lognormal assumption is used for the demand curve. Using this curve, one can assess the performance of the building in the next 50 years in terms of the column drift ratio exceedance probability. At the 2% probability level, the drift ratio is 5% without retrofit and 2% after retrofit. One therefore achieves the same goal of determining the probabilistic demand curve such as that shown in Figure 7.3 based on Equation 7.26, but using an entirely different approach.

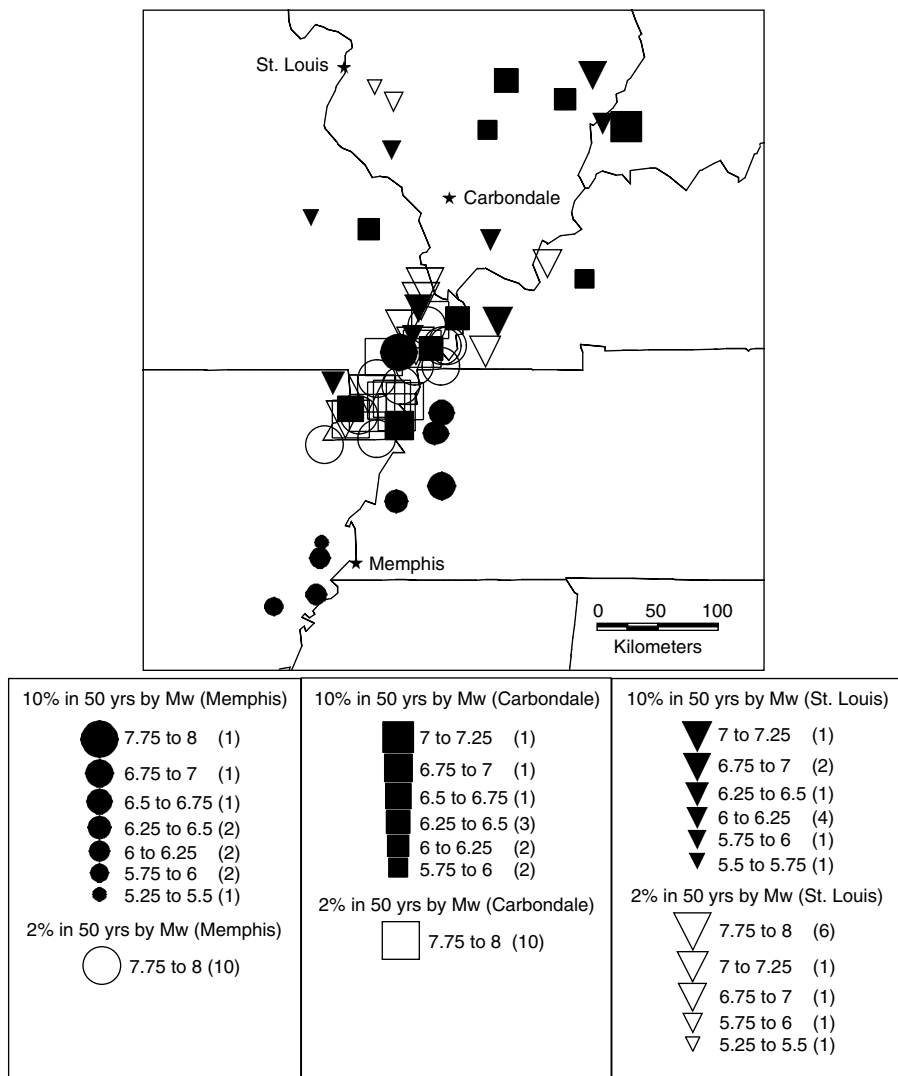


FIGURE 7.4 Epicenters and magnitudes of events contributing to uniform hazard ground motions for Memphis, Carbondale and St. Louis (number of events in the magnitude range is shown in the parentheses) (Wen and Wu, *Earthquake Spectra*, 7, 359–384, 2001.).

7.4 Uncertainty in Capacity and Probabilistic Treatments

Structural capacity, as defined in Section 7.3, is the maximum force, displacement, velocity or acceleration that a member or a system can withstand without failure, or more specifically, without reaching a prescribed limit state. The capacity is therefore dependent on material characteristics, member dimensions, system configuration, limit state under consideration, and methods and models used in describing the capacity. As in the case of demand, (aleatory) randomness and (epistemic) uncertainty are important elements in the evaluation of capacity and need to be carefully considered. In the following the capacity uncertainty and probabilistic treatments of the construction materials structural members and finally structural systems are described. Since capacity is always related to the limit state under consideration, some limit states frequently used in performance evaluation will also be discussed. Again there is a vast literature on this subject; emphasis here is on the uncertainty treatment.

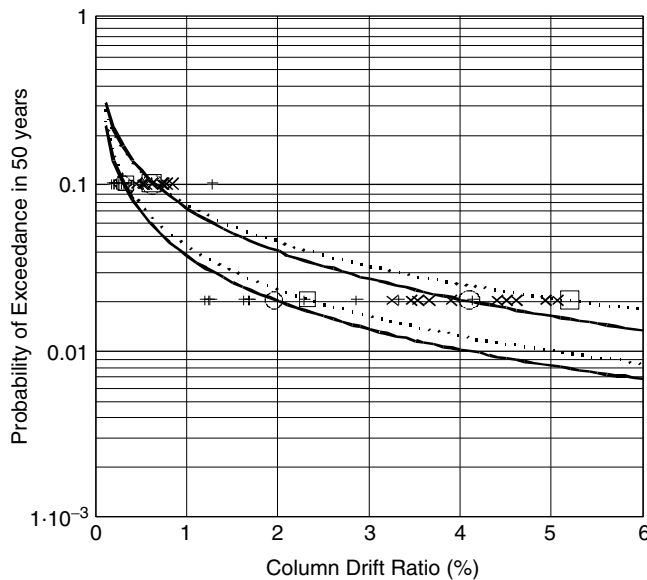


FIGURE 7.5 Probabilistic column drift ratio demand curve of a two-story steel moment frame building at Carbon-dale, IL before and after retrofit with shear walls (data points before retrofit [\times], after retrofit [+], median value (o) and median including structural capacity uncertainty [*]; dashed and solid lines indicate performance curves with and without consideration of capacity uncertainty) (Wen and Wu, *Earthquake Spectra*, 7, 359–384, 2001.).

7.4.1 Material Characteristics

The member and system capacity directly depend on the material strength, which is inherently random. The randomness can be modeled by random variable based on test data. The first two moments, i.e., the mean and standard deviation (or coefficient of variation) are commonly used to describe the central value and the variability. Normal or lognormal distribution is commonly used for convenience. The actual strength of the material of a given member may differ significantly from the nominal values used in member capacity calculation. Therefore, the correspondence between the nominal value and the actual value needs to be established to estimate the real member capacity. The strength variability depends on the material, manufacturing process and sometimes the testing protocol. In general, the variability in masonry and timber construction material is larger than those in reinforced concrete and steel. Material property variability and test data up to 1980 can be found in the report by Ellingwood et al. (1980). For example, the coefficient of variation of strength of timber varies in the range of 10% to 30% depending on species and in flexure or compression; and that of masonry walls varies from 10% to 26% depending on configuration and in compression or flexure. The coefficient of variation of compressive and tensile strength of concrete is approximately 18% and that of the yielding strength of steel reinforcement and steel member elements is approximately 10% or less. Characteristics of construction material such as concrete and structural steel evolve with time. Strength statistics of newer material such as high-strength steel and concrete may be found in more recent literature. For example, statistics on yield and ultimate strength of structural steel under various environmental conditions can be found in the recent FEMA/SAC report (FEMA, 2000).

7.4.2 Uncertainty in Member Capacity

7.4.2.1 Member Capacity under Monotonic Load

The inherent randomness in the material property applies to the structural members made of these construction materials such as steel, concrete, masonry and wood. In addition, there is randomness in the dimensions of the members and also the capacity refers to a particular limit state such as shear,

bending or buckling failure under monotonic or cyclic loading condition. The randomness in terms of the bias (mean capacity or nominal capacity) and coefficient of variation of steel, reinforced concrete, masonry and glulam structural members (beams, columns, and walls) of various configurations and for various limit states can be found in Ellingwood et al. (1980). In most cases the bias factor is between 1.0 and 1.2 and the coefficient of variation is less than 20%. Normal or lognormal distribution has been used to model the capacity randomness. The difference between the two models is small when the coefficient of variation is small.

7.4.2.2 Member Capacity under Cyclic Load-Damage Index

For seismic loading, one is interested in the member capacity under cyclic loading since members in a structural system generally undergo stress reversals of various amplitudes and the member may reach a limit state under the combined action of large deflection and cumulative damage. To account for both effects, various damage indices have been proposed. Park and Ang (1985) developed the most widely used index on the basis of test results of 403 reinforced concrete members. The index is a linear function of maximum displacement δ_m , total hysteretic energy dissipation normalized by member ultimate displacement under monotonic loading δ_u , and yield force Q_y .

$$D = \frac{\delta_m}{\delta_u} + \frac{\beta}{Q_y \delta_u} \int dE \quad (7.37)$$

Different values of the index correspond to different limit states such as 0.4 for serious damage and 1 for complete damage (collapse). Test data show that the damage index capacity of reinforced concrete member can be modeled by a lognormal random variable with a mean value equal to 1.0 and a coefficient of variation of 0.53. This indicates that the randomness in the reinforced concrete member capacity is quite large. The index has been used in damage evaluation of buildings and other structures, e.g., Park et al. (1985).

7.4.2.3 Rotation Capacity of Steel Connection Members

An important structural member in steel buildings is the connections between beams and columns. After the large number of brittle fracture failures found in many buildings due to the 1994 Northridge earthquake, the capacity of connections against rotation demand under cyclic loading during earthquake excitations has attracted much attention among the structural professionals. In the FEMA/SAC project (SAC Steel Project, 2000), a comprehensive testing program of a large number (120) of welded and bolted connections of various configurations has been carried out according to pre-Northridge practice and for post-Northridge design in which many improvements were incorporated. Test results of hundreds of experiments conducted prior to 1994 were also analyzed. The connection rotation capacities for pre- and post-Northridge connections were obtained. The capacity is defined in accordance with two limit states: the rotation limit when plastic deformation occurs, q_p , and the rotation limit, q_g , corresponding to severe damage that the gravity load carrying capacity of the member is compromised. Test data generally show the dependence on the depth of the beam or the depth of the connection element of these capacities and large scatter. The mean values and standard deviations as linear functions of the depth of the beams were established from regression analyses of test results. Depending on the specific connection type and the depth of the beam, the rotation capacity and variability in terms of these two statistics show large variation. For example, the capacity of the post-Northridge welded-flange-bolted-Web connections has the following means and standard deviations:

$$\mu_{\theta_p} = 0.021 - 0.0003d_b \quad (7.38)$$

$$\sigma_{\theta_p} = 0.012 - 0.0004d_b$$

and

$$\mu_{\theta_g} = 0.050 - 0.0006d_b \quad (39)$$

$$\sigma_{\theta_g} = 0.011 + 0.0004d_b$$

For such a connection with a beam depth of 24 inches, $\mu_{\theta_p} = 0.0138$ and standard deviation $\sigma_{\theta_p} = 0.0024$ (or a coefficient of variation $\delta_{\theta_p} = 17.4\%$) and $\mu_{\theta_g} = 0.0256$ and standard deviation $\sigma_{\theta_g} = 0.00206$ ($\delta_{\theta_g} = 8\%$). The variability is moderate. For a free-flange and welded-Web connection with a beam depth of 36 inches, the regression results give $\mu_{\theta_p} = 0.0238$ and $\sigma_{\theta_p} = 0.0032$ ($\delta_{\theta_p} = 134\%$), and $\mu_{\theta_g} = 0.0364$ and $\sigma_{\theta_g} = 0.0604$ ($\delta_{\theta_g} = 166\%$). The variability is very large. Such a large variation in coefficient of variation for different connections could be partly due to the small number of samples used in the regression analysis. Distribution models were not recommended for the capacity. In view of the small sample size and large coefficient of variation, selection of the distribution model should be done with care. Note that with a distribution model, say a normal distribution, one can predict the probability of limit state of plastic deformation or loss of gravity load carrying capacity of the connection member when the rotation demand θ_d is known,

$$P(\text{plastic deformation}) = P(\theta_p < \theta_d) = \Phi\left(\frac{\theta_d - \mu_{\theta_p}}{\sigma_{\theta_p}}\right) \quad (7.40)$$

$$P(\text{loss of gravity load carry capacity}) = P(\theta_g < \theta_d) = \Phi\left(\frac{\theta_d - \mu_{\theta_g}}{\sigma_{\theta_g}}\right) \quad (7.41)$$

Given the demand, the probability of capacity exceeding is also generally referred to as the fragility function. Since under earthquake excitations the demand is also a random variable, the limit-state probability can be evaluated on the basis of a reliability analysis shown in the next section.

7.4.2.4 Bayesian Models of Member Capacity

When calculating member capacity to withstand a prescribed limit state, mathematical models based on mechanics are used. In all mathematical models, there are errors associated with the assumptions and approximations that need to be calibrated against experimental results or field observations. Rigorous tracking of the uncertainty in the mathematical model on the basis of prior knowledge of the mechanical behavior of the components and calibration of the model against experimental data can be done using the Bayesian statistical method as briefly mentioned in Section 7.2.2. Such models have been recently developed for structural members by researchers (e.g., Gardoni et al., 2002; Sasani et al., 2002). The basic concept behind this method can be illustrated by a simple example as follows. Consider a structural member model that predicts the member capacity, y , against a prescribed limit state by the following equation:

$$y = g(\mathbf{q}; \mathbf{x}) + \epsilon \quad (7.42)$$

in which $\mathbf{q} = q_1, q_2, \dots, q_k$ denotes the set of parameters for the mathematical model; $\mathbf{x} = x_1, x_2, \dots, x_n$ represents the sample values of y from experimental or field observations and ϵ is a random variable representing the unknown errors in the model assumed to follow a normal distribution. Within the context of such formulation, given the parameters \mathbf{q} , y is a normal random variable. Calibration of the model parameters in view of observational evidence is formulated by regarding the model parameters as random variables governed by distributions based on prior knowledge (such as mechanics principles,

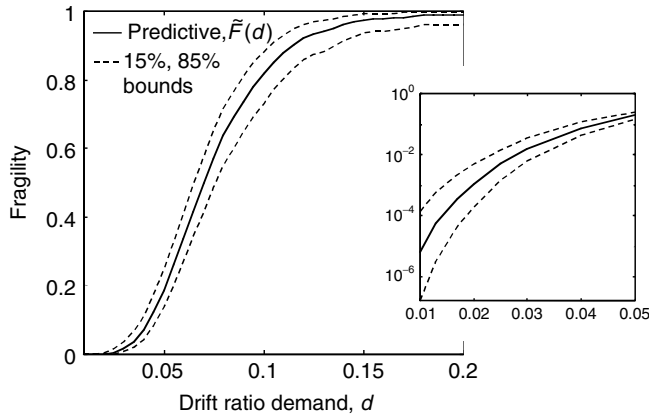


FIGURE 7.6 Conditional probabilistic of failure (fragility) of RC column against drift demand (d) shown in linear scale and log scale for $d < 0.05$ in small figure (Gardoni et al., *J. Eng. Mech.*, ASCE, 128, 1024–1038, 2002.).

structural analysis methods and engineering judgment or experience). According to Equation 7.12, the parameters are calibrated (or updated in Bayesian terminology) in view of sample evidence of y as follows:

$$f''(\mathbf{q}) = k L(\mathbf{q}) f'(\mathbf{q}) \quad (43)$$

in which $f'(\mathbf{q})$ is the prior distribution of the model parameters; $L(\mathbf{q})$ is the sample likelihood function or the conditional probability of observing x given \mathbf{q} and k is the normalizing constant. Note that the epistemic uncertainty such as those associated with knowledge and modeling errors including those due to small sampling (small n) is included in the formulation. In general, for small n and sharp $f'(\mathbf{q})$, i.e., strong knowledge-based information and weak observational information, the prior distribution dominates. On the other hand, if $f'(\mathbf{q})$ is flat or diffuse and n is large, $L(\mathbf{q})$ dominates. The overall uncertainty in the posterior distribution $f''(\mathbf{q})$ is less than $f'(\mathbf{q})$ or $L(\mathbf{q})$. One of the advantages of the Bayesian method is that even incomplete data of x such as those in the form of upper or lower bound due to certainty in the data collecting process or experimental procedure can be incorporated into $L(\mathbf{q})$ without difficulty. The method has been applied for evaluation of the capacity of circular reinforced concrete bridge columns and shear walls to withstand deformation and shear demand due to cyclic loads. The advantage of this model compared with deterministic models was also shown (Gardoni et al., 2002). Figure 7.6 shows the result of the probabilistic prediction of the capacity of RC column against drift ratio demand, i.e., the conditional probability of failure of the column given that it reaches a drift ratio (or fragility curve).

7.4.3 Uncertainty in System Capacity

The description of uncertainty in system capacity is more involved since a structural system consists of many components and the system behavior is complex under dynamic excitation, especially when the system goes into nonlinear range. Therefore, the system capacity can be more conveniently described in terms of the system limit states of interest.

7.4.3.1 System Capacity to Withstand Damage

Commonly used system limit states are those corresponding to different damage states and performance levels. For example in SEAOC Vision 2000 (1995), the five performance (damage) levels were fully operational (negligible), operational (light), life safety (moderate), near collapse (severe) and collapse (complete), and each level is related to a structural response level indicated by a transient and a permanent drift limit. In the FEMA/SAC project for steel buildings, the performance and damage levels were reduced to a more manageable two: IO and CP. The system capacity is described in terms of interstory drift angles.

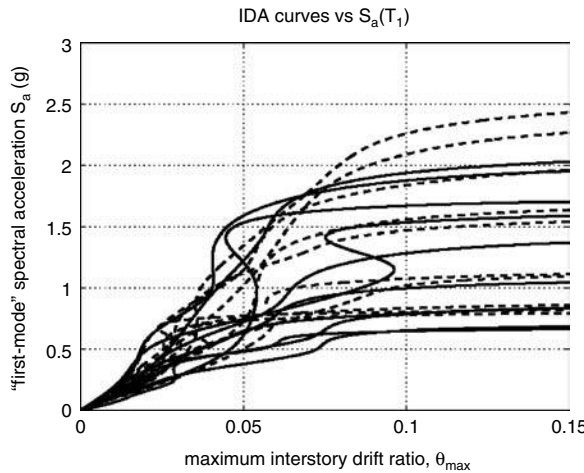


FIGURE 7.7 Results of incremental dynamic analysis of nine-story steel moment-resisting frame with fracturing connection under SAC ground motions (Vamvatsikos and Cornell, *J. Earthquake Eng. Struct. Dyn.*, 31, 491–514, 2002.).

The uncertainty in the system capacity, therefore, can be described in terms of the drift capacity for different performance levels, such as the median drift capacity and its coefficient of variation. The commonly accepted distribution for the capacity is the lognormal distribution for its convenience in reliability analysis and reliability-based design as will be seen in the next section. Structures of different construction materials, configurations and designs would have different drift thresholds. Determination of drift capacities for different performance levels is largely a process of combination of analysis and judgment or experience. The determination of system CP capacity is discussed further in the following.

7.4.3.2 System Capacity to withstand Collapse-Incremental Dynamic Analysis

Of all the limit states and the corresponding system capacities, the most difficult to determine is system collapse. The reason is that the structural dynamics about to collapse is extremely complex and is largely an unsolved problem due to nonlinear member and system response behaviors. The large record-to-record variation of ground motions and structural response behaviors further complicate the matter. The collapse of structures under random excitations is a difficult mathematical problem of stochastic stability. Solutions can be obtained only for simple idealized systems under excitations of simple stochastic processes such as white noise. In the past engineers have used an inelastic static pushover analysis to estimate this capacity. The analysis provides an insight into the structural response behavior at large displacement but considers only the first mode static response, which is different from dynamic response. As a result, such an analysis generally overpredicts the response and underestimates the capacity. Improvements can be made by considering higher modes via modal pushover analysis as shown by Chopra and Goel (2002). Vamvatsikos and Cornell (2002) extended the concept of pushover analysis to dynamic response in the form of incremental dynamic analysis (IDA). The system capacity to withstand collapse is evaluated by dynamic response analyses of the system under a suite of ground motion time histories such as the SAC ground motions. Each time history is scaled according to the spectral acceleration such that the structural response goes from linear elastic to nonlinear inelastic range and finally becomes unstable, i.e., a large increase in response with a small increase in the spectral acceleration. The displacement at the transition point is defined as the system displacement capacity to withstand collapse. Due to the large record-to-record variation of the ground motions and extremely complex structural nonlinear behavior, it is not always easy to pinpoint the transition point. Engineering judgments are often necessary and there are large scatters for different excitations with the same spectral acceleration. Figure 7.7 shows an example of the interstory drift using IDA of a nine-story steel frame under SAC ground motions. The uncertainty in capacity to withstand collapse can be described in terms of the mean and standard deviations of the interstory drift capacity under multiple recorded ground motions from IDA. The

coefficient of variation of this displacement capacity is generally of the order of 30%. Such a process has been used in the FEMA/SAC procedure.

7.5 Reliability of Structural Systems

Because of the large uncertainties in demand and capacity, the performance of the structural systems can be described meaningfully only when these uncertainties are explicitly taken into consideration. In other words, evaluation of the performance needs to be described in terms of reliability of the structural system to withstand various limit states over a given period of time. Since earthquake occurrence, ground excitations and structural responses are random functions of time, reliability is therefore a problem of a vector random process of time passing from a prescribed safe domain to an unsafe domain defined by the limit state. A rigorous mathematical solution of the so-called first passage problem is generally difficult. In reliability analysis, the problem of first passage of random process is often replaced by a more tractable formulation in which a structural performance function corresponding to a given limit state is constructed in terms of a set of random variables representing the uncertainty in the problems. The reliability problem is then solved using the first two moments of the random variable and a first-order or second-order approximation of the performance function commonly referred to as the first order reliability method (FORM) or the second-order reliability method (SORM). In earthquake engineering, a simpler formulation of the problem is used in terms of two variables (demand and capacity) for a given limit state. Alternatively, depending on the problem, a simulation method may be more suitable for evaluating the reliability. These methods and the advantages and disadvantages of their application to earthquake engineering are briefly described in the following.

7.5.1 FORM and SORM

Given a limit state, the performance of a structure can be described by a performance function, $g(\mathbf{X})$, of all the excitation and structural property variables, or basic random variables \mathbf{X} : X_1, X_2, \dots, X_n . The reliability problem is then formulated as follows:

$$\begin{aligned} < 0 &\text{ safe domain (no failure)} \\ g(X_1, X_2, \dots, X_n) &> 0 \text{ unsafe domain (failure)} \\ &= 0 \text{ limit state boundary or surface} \end{aligned} \quad (7.44)$$

Knowing the probability distribution of the basic random variables, one can evaluate the probability of limit state by integration of the joint density function over the unsafe domain. When the number of basic random variables is large and when the performance function $g(\mathbf{X})$ is nonlinear, the integration is generally difficult. The FORM/SORM method essentially replaces $g(\mathbf{X})$ by its first-order or second-order Taylor series expansion at a point \mathbf{X}_0 where the contribution to the failure probability is the maximum (or the most likely failure point). The reliability problem can then be solved in closed form in terms of the first two moments of the basic random variables.

The accuracy of the method is generally very good, especially when the limit-state probability is small. Other advantages of the FORM/SORM is that at the most likely failure point, \mathbf{X}_0 , the linearized performance function can be used as a performance or safety checking equation that can be easily cast into a load resistance factor design (LRFD) format familiar to engineers. \mathbf{X}_0 is therefore called the “design point.” Also, sensitivity analysis of reliability to change in any design variables can be easily carried out using the results of the FORM/SORM analysis. Often, structural system limit states cannot be expressed by single performance function. Under such a circumstance, one needs to perform a system reliability analysis involving unions and intersections of multiple failure modes each of which is described by a performance function ($g_k(\mathbf{X})$; $k = 1$ to n). Software such as CALREL (Liu et al., 1989) can be used for

such an analysis. The FORM/SORM is a robust, well-developed methodology that has been successfully used in formulation of reliability-based design in several codes and standards such as AISC (2001) and ASCE-7 (2002). For earthquake engineering problems, when the structure becomes highly nonlinear and especially when brittle member failures occur, the construction of the performance functions for structural members and systems may be difficult. Recent development of FORM/SORM and application to structural reliability analysis can be found in Der-Kiureghian et al. (2002).

7.5.2 Demand Versus Capacity Formulation in FEMA/SAC Procedure

The reliability problem is considerably simplified if the limit state can be stated in terms of the demand exceeding the capacity. Although this may be an oversimplification in that the capacity and demand may not be always easily defined for certain limit states such as system collapse, simplicity nevertheless offers some advantages in earthquake engineering applications, especially in code procedure formulation. This method is used in the reliability-based, performance-oriented design procedure proposed in the SAC/FEMA Steel Project (Cornell et al., 2002), which is described in the following.

Considering the limit state described in terms of only two random variables, R (capacity) and S (demand), the performance function in Equation 7.44 is now simplified to $g(\mathbf{X}) = R - S$, which is a linear function. The probability of limit state over a given period of time, t , is then given by the probability integral

$$P_t = P_t(R < S) = \int_0^{\infty} P_t(R \leq S | S = s) f_S(s) ds \quad (7.45)$$

Simple closed form solutions of the integration can be obtained when R and S can be modeled by normal or lognormal random variables

$$P_t = 1 - \Phi(\theta) \quad (7.46)$$

$$\theta = \frac{\mu_R - \mu_S}{\sqrt{\sigma_{R}^2 + \sigma_S^2}}, \text{ when both } R \text{ and } S \text{ are normal}$$

$$= \frac{\lambda_R - \lambda_S}{\sqrt{\beta_{R}^2 + \beta_S^2}}, \text{ when both } R \text{ and } S \text{ are lognormal}$$

in which,

$$\beta_x = \sqrt{\ln(1+\delta_x^2)}, \text{ and } \lambda = \ln \mu_x - 0.5 \beta_x^2 = \ln \tilde{x} \quad \tilde{x} = \text{median value of } X.$$

This is not the case when the demand described by Equation 7.32 is not a simple normal or lognormal variable. The closed form solution, however, can still be obtained when the capacity variable R can be modeled by a lognormal random variable and the seismic hazard can be described by a power function given in Equation 7.31.

7.5.2.1 Limit-State Probability Considering Randomness Only

Assume that the capacity randomness can be modeled with a lognormal variate with a median value \tilde{C} and dispersion coefficient β_{CR} . Referring to Equation 7.32, it can be shown that the limit-state probability is given by

$$P_t = H_t(a^{\tilde{C}}) \exp\left[\frac{1}{2} \frac{k^2}{b^2} (\beta_{D|S_a=a}^2 + \beta_{CR}^2)\right] \quad (7.47)$$

Note that the limit-state probability consists of the product of the probability of the spectral acceleration exceeding the median structural capacity and a correction factor that depends on the randomness in the demand and the capacity, as well as the hazard characteristics (k) and demand–capacity relationship (b). The limit-state probability given in Equation 7.47 therefore accounts for all randomness in the problem.

Continuing with the example in Section 7.3.3, and assuming that the median drift ratio capacity of this three-story building to withstand incipient collapse is 0.05 with a dispersion parameter $\beta_{CR} = 0.35$, the 50-year incipient collapse probability of the building is given by

$$\begin{aligned} P_{50} &= H_{50}(a^C) \exp\left[\frac{1}{2} \frac{3^2}{1.2^2} (0.30^2 + 0.35^2)\right] = H_{50}(0.86) e^{0.664} = 0.0107 \times 1.94 \\ &= 0.0208 \end{aligned} \quad (7.48)$$

which corresponds to an annual probability of 0.42×10^{-3} , or a return period of 2380 years.

7.5.2.2 Impact of Uncertainty

Referring to the simple example on the impact of (epistemic) uncertainty on the limit-state probability described in Section 7.2.1 (Equations 7.1 to 7.3), one can see that when the uncertainty is considered the limit-state probability becomes a random variable and needs to be treated as one. Depending on the application, for example, one may want to evaluate the mean value of the limit-state probability of performing a risk or benefit analysis or evaluate the percentile value for a confidence interval estimate. The uncertainty can be conveniently grouped into those in the hazard analysis, excitation–demand relationship and structural capacity estimate. For example, the parameters k_0 and k in the seismic hazard model (Equation 7.31), a and b in the regression equation for structural response (Equation 7.29) and the parameters in structural capacity models (Equations 7.38 to 7.41) may have uncertainty due to modeling (e.g., incorrect functional form) or sampling (small number of test results) errors. For simplicity and tractability in analysis, the uncertainties in the seismic hazard, structural demand and structural capacity models are assumed to be lognormal variables with median values given by the model predictions and dispersion parameters β_{HU} , β_{DU} and β_{CU} . The subscripts H, D and C denote hazard, demand and capacity respectively and U denotes uncertainty. Similarly, the dispersion parameters of the randomness in the demand and capacity are denoted by β_{DR} and β_{CR} , respectively. Incorporating the uncertainty defined above into Equation 7.47, one can obtain the mean estimate of the limit-state probability as follows:

$$E[P_t] = E[H(a^C)] \exp\left[\frac{1}{2} \frac{k^2}{b^2} (\beta_{DR}^2 + \beta_{DU}^2 + \beta_{CR}^2 = \beta_{CU}^2)\right] \quad (7.49)$$

in which

$$E[H(a^C)] = H(a^C) \exp\left[\frac{1}{2} \beta_{HU}\right] \quad (7.50)$$

In other words, effects of randomness and uncertainty are now combined. Note that the expected limit-state probability is equal to the product of mean estimate of the hazard exceeding the median structural capacity and a correction factor that increases exponentially with the total uncertainty in the demand and capacity, and depends on the hazard and regression analysis parameters (k and b). The seismic hazard given in the USGS National Earthquake Hazard Maps is that of the mean hazard (Frankel et al., 1996) with regard to modeling uncertainty; Equation 7.49 is therefore compatible with the USGS hazard maps. Also note that the combination of uncertainty and randomness given by the second term of Equation 7.49 is of the same form as in the simple uncertainty analysis of Equations 7.4 to 7.6.

To estimate the percentile values for a confidence interval estimate, in principle all uncertainty dispersions need to be considered as shown in Section 7.2.1 when one extends the analysis to more than one uncertain parameter. In the FEMA/SAC procedure, it is assumed that the uncertainty in seismic hazard has been incorporated through the mean hazard curve in Equation 7.50. The confidence interval estimate is then obtained as a function of the demand and capacity uncertainty using the mean hazard curve. The limit-state probability corresponding to a percentile level q (probability that the value of q is not exceeded) is given by

$$P_{q,t} = \tilde{P}_t \exp[K_q \beta_L] \quad (7.51)$$

in which

$$\tilde{P}_t = E[H(a^C)] \exp\left[\frac{1}{2} \frac{k^2}{b^2} (\beta_{DU}^2 + \beta_{CU}^2)\right] \quad (7.52)$$

$$\beta_L = \sqrt{\frac{k^2}{b^2} (\beta_{DU}^2 + \beta_{CU}^2)} \quad (7.53)$$

$$K_q = \Phi^{-1}(q) \quad (7.54)$$

\tilde{P}_t is the median (50%) value of P_t . Note that similar to the simple example in Section 7.2.1, the median estimate is the same as that considering only the randomness in the demand and capacity. The q percentile limit-state probability is equal to the product of \tilde{P}_t and a factor that depends on the uncertainty dispersion parameters and the percentile value. K_q is the standard normal variate value corresponding to this percentile value.

Continue with the example given in Equation 7.48 and also consider the uncertainty. One assumes the following:

1. $\beta_{HU} = 0.30$ in the hazard analysis (Equation 7.31)
2. $\beta_{DU} = 0.25$ describes the errors in the demand regression analysis as a function of the spectral acceleration (Equation 7.29)
3. $\beta_{CU} = 0.28$ indicates the uncertainty in the estimate of capacity to withstand collapse calculated using the IDA procedure in Section 7.4.3.

The impact of different uncertainties on the incipient collapse probability can be illustrated as follows. The median incipient collapse probability of this steel building when considering only randomness is 0.0208 (Equation 7.48). According to Equations 7.50 and 7.52, when the seismic hazard analysis uncertainty is included in the form of mean hazard, this median value increases to

$$\tilde{P}_{50} = H_{50}(0.86) \exp\left[\frac{1}{2} \times 0.3\right] e^{0.664} = 0.0241 \quad (7.55)$$

The mean estimate of the 50-year incipient collapse probability considering all uncertainties according to Equation 7.49 is

$$\begin{aligned} E[P_{50}] &= H_{50}(0.86) \exp\left[\frac{1}{2} \times 0.3\right] \exp\left[\frac{1}{2} \frac{3^2}{1.2^2} (0.30^2 + 0.25^2 + 0.35^2 + 0.28^2)\right] \\ &= 0.0107 \times 1.161 \times 3.01 = 0.0374. \end{aligned} \quad (7.56)$$

It is seen that as in the simple example in Section 7.2, the mean estimate is always higher than the median, reflecting the additional effect of uncertainties on demand and capacity. Finally, when these uncertainties are accounted for in the form of a confidence level, the probability is dependent on the confidence level. For example, the incipient collapse probability will not exceed the following value with 85% confidence (Equation 7.51)

$$P_{85\%, 50} = 0.0241 \exp[1.03 \times \sqrt{\frac{3^2}{1.2^2} (0.25^2 + 0.28^2)}] = 0.0616 \quad (7.57)$$

The above performance evaluation procedure has been applied to pre- and post-Northridge steel moment frame buildings (Fouch, 2000; Yun et al., 2002; Lee and Fouch, 2002). For example, buildings designed in accordance with the 1997 NEHRP provisions and constructed with SAC prequalified connections have a confidence level of 90% of meeting the requirement of probability of incipient collapse being less than 0.02 in 50 years.

7.5.3 Method of Simulation

7.5.3.1 Randomization of Capacity

The simulation method can be applied to reliability evaluation when the structural capacity uncertainty is considered. In a direct MC method, one need only randomize the capacity of the structure in accordance with the randomness and uncertainty models as mentioned above in the time-history analysis of the structure. The limit-state probability can then be calculated from the response statistics of the repeated time-history analyses — it is conceptually simple. The difficulty is obvious that the randomization needs to be done for each element, which may be difficult. Also, as in the structural demand analysis, computational effort may be maximum.

7.5.3.2 Uncertainty Correction Factors

To incorporate the effect of capacity uncertainty into the smart simulation procedure and avoid the difficulty of detailed modeling at the component level as mentioned above, one can use a hybrid procedure. The structure is first regarded as deterministic and the smart simulation is performed at a given hazard level, e.g., 50%, 10% or 2% in 50 years to obtain the probabilistic structural demand curve, e.g., the median response to the set of UHGM corresponding to a hazard level as shown in Figure 7.5. At a given hazard level, the effect of the uncertainty can then be incorporated by multiplying the median estimate by a correction factor similar to that given in Equation 7.49. As shown in Figure 7.5, at a given hazard level such as 10% in 50 years or 2% in 50 years, the demand described by the median response to the UHGM corresponds to the probability of exceedance considering only the randomness and uncertainty (if included in the simulation in Section 7) in the excitation. To account for the randomness and uncertainty in the capacity and demand, the limit-state probability is multiplied by a correction factor (Wen and Fouch, 1997)

$$C_F = 1 + \frac{1}{2} S^2 \delta_T^2 \quad (7.58)$$

in which S is the sensitivity coefficient to the change in structural capacity depending on the seismic hazard and the median structural capacity and δ_T is the coefficient of variation of the total randomness and uncertainty in the demand and capacity,

$$\delta_T \approx \sqrt{\delta_{RC}^2 + \delta_{UC}^2 + \delta_{RD}^2 + \delta_{UD}^2} \quad (7.59)$$

in which RC, UC, RD and UD denote randomness and uncertainty in capacity and demand. Alternatively, if the limit-state probability is kept the same, the median value can be multiplied by a correction factor C_D to reflect the effect of total uncertainty as follows:

$$C_D = 1 + \frac{1}{2} S \delta_{T_r}^2 \quad (7.60)$$

The seismic hazard, e.g., in terms of 50-year probability of exceedance of the spectral acceleration, can be generally modeled by a lognormal distribution. If the hazard curve is not available, it can be determined directly from the UHGM. The median values of the spectral acceleration of the UHGM at 10% and 2% in 50 years allow one to determine the two lognormal distribution parameters λ and ζ . The sensitivity coefficient S is then given by

$$S = \frac{\ln a_c - \lambda}{\zeta^2} \quad (7.61)$$

in which a_c is the median capacity of the system expressed in terms of spectral acceleration S_a . Note that when the hazard dispersion measure ζ is large, S is small, indicating that the uncertainty in hazard dominates and the result is not sensitive to the structural capacity uncertainty.

For example, in Figure 7.5, the lognormal fit of 50-year spectral acceleration (for $T = 0.15$ sec after retrofit) hazard for Carbondale, IL gives scale parameter $\lambda = -6.85$ and dispersion parameter $\zeta = 2.07$ (Wen and Wu, 2001). Using Equation 7.60, the sensitivity coefficient S at 10/50 and 2/50 hazard levels is calculated to be 0.618 and 1.0, respectively. Assuming a total uncertainty of $\delta_T = 50\%$ for the structural drift capacity to withstand all limit states, the correction factor, c_f , and C_D are respectively 1.05 and 1.07 at 10/50 hazard level 1.13 and 1.13 at 2/50 hazard level. It is seen that the effects of the demand and capacity total uncertainty are small since they are overshadowed by the large uncertainty in the seismic excitation (large value of the dispersion parameter ζ) in the eastern United States. The median values can then be modified by the correction factors and fitted by a lognormal (dashed) curve as the risk curve of column drift capacity exceeded as shown in Figure 7.5.

7.6 Probabilistic Codes and Standards

Although the uncertainty in seismic loadings has been well recognized by the profession, the incorporation of uncertainty in most building code procedures has been limited to the selection of a design earthquake on the basis of probability, such as 10% in 50 years or a return period of 475 years. This design earthquake is then used in conjunction with a series of factors reflecting the influence of structural period, soil condition, structural inelastic behavior, importance of the structure, etc. These factors are determined on the basis of analysis, judgment and experience and often calibrated in such a way that the resultant designs do not significantly deviate from the acceptable practice at the time. Therefore, despite the simplicity and ease of use of the existing design procedures, a significant shortcoming is that the reliability of the final design is undefined and difficult to quantify.

The major losses caused during recent earthquakes brought into light the reliability of present-day buildings to withstand future earthquakes and as a result the performance-based design (PBD) concept began to receive serious attention from structural engineers. In SEAOC (1995), PBD is described by a performance matrix for various response (drift) limits that the structure has to satisfy during earthquakes of different probabilities of exceedance, i.e., 50% in 30 years (frequent), 50% in 50 years (occasional), 10% in 50 years (rare) and 10% in 100 years (very rare). The addition of more levels of design earthquakes is equivalent to putting more constraints on the structural performance. The selection of these additional design earthquakes and corresponding performance limits, however, needs to be carefully done to ensure internal consistency. Also, since the probability is prescribed on the seismic hazard uncertainties in the

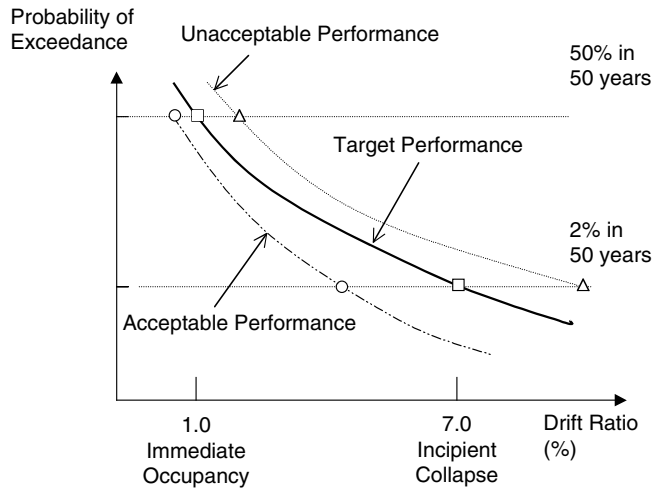


FIGURE 7.8 Bi-level acceptance criteria in terms of 50-year limit state probability in log scale.

structural capacity and demand has not been considered, the reliability of the structure to withstand specific limit state is still unknown.

In a reliability-based design, the limit-state reliability analysis is reversed. In other words, the problem lies in the determination of the required structural capacity for given target reliabilities to withstand a set of structural limit states. Such design procedures have been recently developed that represent a large step forward in accounting for uncertainty in demand and capacity in codes and standards. They are described in the following.

In addition, there are a few open questions related to reliability-based design. One is the age-old question of how safe is safe enough or how one should set the target probabilistic performance curve. Such a curve expressed in terms of exceedance probability in 50 years is shown in Figure 7.8 according to Wen and Foutch (1997) where the building performance is checked at 50% and 2% levels. It can be used to judge the acceptability of performance of existing buildings or new designs depending on whether the performance meets the target. Another is the strongly debated reliability or redundancy factor recently introduced in building codes after the failure of some building structures in recent earthquakes. These two issues are also briefly addressed in the following.

7.6.1 LRFD Based on FORM

If the building response is largely static or can be satisfactorily described by an equivalent static procedure, the uncertainty in loading and resistance can be described by a set of random variables. The limit state can be described in terms of these basic random variables and the reliability analysis can be carried out in a straightforward manner using the well-known and well tested FORM (see Section 7.5.1). In FORM the reliability-based design is formulated at the most likely failure point (or design point) of the basic random variables, which satisfies the limit state function. This method has been used as the basis for reliability-based design and cast in a LRFD format familiar to design engineers,

$$\sum_{i=1}^j \phi_i R_i \geq \sum_{i=1}^k \gamma_i L_i \quad (7.62)$$

in which R_i and L_i are nominal resistances and loads, generally close to the mean values of the resistances and loads; and ϕ_i and γ_i are respectively the resistance and load factors depending on the target reliability and amount of uncertainty in each random variable. These factors are given by:

$$\eta_i = \frac{\mu_i}{X_{ni}} (1 + \alpha_i \beta \delta_i) \quad (7.63)$$

in which η_i is the load or resistance factor; μ_i and X_{ni} are respectively the mean and nominal values; α_i is the sensitivity coefficient, which is positive for load variables and negative for resistance variables; δ_i is the coefficient of variation of the variable X_i ; and β is the target safety index given by

$$\beta = \Phi^{-1}(1 - P_f) \quad (7.64)$$

in which Φ^{-1} is the inverse standard normal cumulative distribution and P_f is the target limit-state probability. The above LRFD design format explicitly accounts for the uncertainty in load and resistance. Note that γ_i is greater than 1 and ϕ_i is less than 1 and also that higher reliability (larger β) and larger uncertainty in the random variables (δ_i) lead to larger γ_i and smaller ϕ_i and consequently larger required design resistance. This has been used in most recent code procedures, e.g., for buildings (ASCE-7, 1999; AISC, 2001) based on Ellingwood et al. (1982) and Galambos et al. (1982), offshore structures (API, 1990) and bridges in the United States (AASHTO, 1994; Kulicki et al., 1995) and Canada (CAN/CSA, 2000).

The reliability checking in these procedures, however, has been done mostly at the member rather than at the system levels. For most buildings under earthquake loads, the responses are dynamic and nonlinear and may have different hysteretic and degrading behaviors including those caused by brittle fractures at the joints, so the problem is much more involved. Although it is possible to combine the FORM and a finite element analysis to solve this problem (e.g., Der-Kiureghian, 1996), it is generally difficult to express the limit states of interest directly in terms of the basic load and resistance random variables, and consequently the modeling and computational problems become much more involved.

7.6.2 FEMA/SAC Procedure

In view of the damages suffered in recent earthquakes, in the SAC/FEMA Joint Venture for Steel Buildings, a reliability-based and performance-oriented design has been developed where all randomness and uncertainty in the load and resistance are explicitly considered and accounted for (FEMA 350, 2000). The critical issues related to such a statistical and reliability framework were reviewed in Wen and Foutch (1997). The theoretical basis for the development of the design procedure can be found in Cornell et al. (2002). The final design format still retains the basic LRFD flavor with additional quantitative treatment of the effect of uncertainty. The results are adopted in the AISC Seismic Provisions (Malley, 2002) and most likely will serve as a prototype for wider adoption in other codes and standards. The probability basis of this design procedure is briefly described in the following.

In the SAC/FEMA procedure, performance is checked at two levels —IO and CP — with associated target probability of 50% and 2% in 50 years respectively. Figure 7.8 shows the performance checking of such a procedure. Assuming the probabilistic performance curves can be described by a distribution such as the lognormal, the two points on the curves allow one to describe and check the performance for a wide range of response. If the probability curve is higher than the target, stiffening, strengthening or other mitigation measures are needed. Given the target probabilistic performance curve, the design involves obtaining a solution to the inverse problem of finding the required structural capacity to meet the requirement. The simple closed form solution of the reliability analysis given in Section 7.5.2 allows one to solve the inverse problem. Referring to Equation 7.49 that gives the mean probability of a limit state over a time period, a reliability-based design involves determination of the required structural median capacity, C , to satisfy a prescribed target mean limit-state probability, $E(P_t) = P_0$. This inverse problem can be solved as follows (Cornell et al., 2002):

$$\left\{ \exp \left[\frac{1}{2} \frac{k}{b} (\beta_{CR}^2 + \beta_{CU}^2) \right] \right\} C \geq \left\{ \exp \left[\frac{1}{2} \frac{k}{b} (\beta_{DR}^2 + \beta_{DU}^2) \right] \right\} \tilde{D}^{P_0} \quad (7.65)$$

Note that this is not a rearrangement of Equation 7.49; therefore it takes a slightly different form. It can be rewritten as

$$\phi \tilde{C} \geq \gamma \tilde{D}^{P_0} \quad (7.66)$$

ϕ is the capacity (resistance) factor and γ is the demand (load) factor. \tilde{D}^{P_0} is the median demand corresponding to $S_a^{P_0}$ — a spectral acceleration of exceedance probability of P_0 . From Equation 7.29, one obtains

$$\tilde{D}^{P_0} = a (S_a^{P_0})^b \quad (7.67)$$

in which $S_a^{P_0}$ is solved from Equation 7.31. Note that from Equation 7.64, smaller P_0 (higher reliability) gives larger \tilde{D}^{P_0} and from Equation 7.66 larger randomness and uncertainty in the demand and capacity give larger γ and smaller ϕ leading to larger design capacity \tilde{C} .

Continuing with the example in the previous section of the three-story steel building, if the target 50-year incipient collapse (defined according to an IDA) probability is 2% what should be the median drift capacity to withstand collapse? Note that since the target probability is lower than the current value of 0.0374 (Equation 7.56), the structural drift capacity to withstand incipient collapse needs to be enhanced. From Equations 7.65 and 7.66 the demand and capacity factors are calculated to be

$$\gamma = \exp \left[\frac{1}{2} \frac{3}{1.2} (0.30^2 + 0.25^2) \right] = 1.21 \quad (7.68)$$

$$\phi = \exp \left[-\frac{1}{2} \frac{3}{1.2} (0.35^2 + 0.28^2) \right] = 0.778 \quad (7.69)$$

and the median drift capacity corresponding to 2% in 50 years spectral acceleration exceedance probability is

$$\tilde{D}^{2\%} = a (S_a^{2\%})^b = 0.06 (0.698)^{1.2} = 0.039 \quad (7.70)$$

Therefore, according to Equation 7.66 the required design median drift capacity to withstand incipient collapse is

$$\tilde{C} = \frac{1.21}{0.778} \times 0.039 = 0.0606 \quad (7.71)$$

Compared with the current median capacity of 0.05, an increase of 21% is required. The above design satisfies the target *mean* limit-state probability considering all the randomness and uncertainty. Alternatively, one can also use a confidence level approach to set the design requirements as follows.

If a design criterion is that there must be a confidence level of at least q that the actual (but uncertain) limit-state probability is less than the allowable value of P_0 , the formulation given in Equations 7.51 to 7.54 can be rearranged in terms of the factored capacity and demand ratio as follows:

$$\lambda_{con} = \gamma \tilde{D}^{P_0} / \phi \tilde{C} \quad (7.72)$$

in which $\gamma, \phi, \tilde{D}^{P_0}$ and \tilde{C} are defined in Equations 7.65 to 7.67, and λ_{con} is the ratio of demand and capacity depending on the confidence level given by

$$\lambda_{con} = \exp\left[-K_x \beta_{UT} + \frac{1}{2} \frac{k}{b} \beta_{UT}^2\right] \quad (7.73)$$

$$K_x = \Phi^{-1}(q), q = \text{confidence level} \quad (7.74)$$

$$\beta_{UT} = \sqrt{\beta_{cu}^2 + \beta_{du}^2}, \text{ total uncertainty in capacity and demand.} \quad (7.75)$$

For example, continuing with the example, if the target $P_0 = 2\%$ in 50 years and a confidence level of $q = 85\%$ is desired. From Equations 7.73 to 7.75, one obtains

$$K_x = \Phi^{-1}(0.85) = 1.04$$

$$\beta_{UT} = \sqrt{0.25^2 + 0.28^2} = 0.375$$

$$\lambda_{con} = \exp\left[-1.04 \times 0.375 + \frac{1}{2} \frac{3}{1.2} 0.375^2\right] = 0.807 \quad (7.76)$$

The required design median drift capacity is then determined from Equation 7.72 as

$$\tilde{C} = \frac{1.21 \times 0.039}{0.807 \times 0.778} = 0.075 \quad (7.77)$$

Compared with the current design of 0.05, an increase of 50% is needed to satisfy this design criterion.

7.6.3 Target Reliability

A critical element in a reliability-based design procedure is the selection of the structural performance levels and the associated acceptable (target) reliability. Another related question, which has not been explicitly addressed in current codes, is the target reliability to withstand different hazards. For example, when both wind and earthquake are important, should uniform reliability be required for design to withstand each hazard? Determination of the target reliability levels for various limit states for one or more hazard requires broader social-economical considerations. The selection of the design hazard levels and the corresponding structural performance requirements have largely been based on professional experience and judgment. While collective professional wisdom may be the only recourse at present, it could lead to unsafe or wasteful designs.

One good example of the problem of reliance on only probability in design decision is the use of maximum considered earthquake (MCE), normally defined as 2% in 50-year event, as the design earthquake. Due to the flatness of the tail of seismic hazard curve in certain locations in eastern United States, the spectral acceleration at this low probability level could almost equal or even exceed some in the most seismic region in the western United States. For example, the 1997 NEHRP hazard map shows that in central San Francisco the MCE expressed in terms of the spectral acceleration is 1.5g at 0.2 sec and 0.75g at 1 sec while in Memphis it is 1.25g at 0.2 sec and 0.4g at 1 sec. It is difficult to justify such large design ground motion (even after some reduction) when the projected per capita annual cost due to earthquakes in Memphis is only \$15 compared with \$200 in San Francisco (Searer and Freeman, 2002b; FEMA, 2001). In other words such a procedure could produce overly conservative and wasteful designs. A more rationale

procedure is to arrive at the target reliability by considering the long-term risk–benefit trade-off such as balancing between initial cost and costs due to damages by future earthquakes.

7.6.3.1 Target Reliability Implied in Current Practice

One commonly used approach to the determination of target reliability levels is comparison of risks of consequence of structural limit states with other societal risks, such as accidents, deaths and industrial hazards. Alternatively, one can compare the notional (calculated) probability of limit states with those implied in current designs and adjust accordingly. This approach has been used, for example, by Ellingwood et al. (1982) in calibrating the target reliability of structural members against practice acceptable at the time in developing the AISC LRFD design recommendations, which have been adopted in ASCE-7 (1999). The need for a more rationale approach to determine target reliability and acceptable risk has recently received serious attention from researchers and engineers (e.g., Ellingwood, 1999). One such approach is to strike a balance between the initial cost and potential huge losses incurred during the structure's lifetime caused by the hazards. Since the life-cycle cost (LCC) depends on the occurrence of limit states and hence the demand and system capacity, it is also highly uncertain and hence needs to be properly treated. An optimal design decision under uncertainty can be reached by minimization of the expected LCC. Recent progress made in application of this approach to seismic design is briefly described in the following.

7.6.3.2 Target Reliability according to Minimum Life-cycle Cost Design Criteria

The design procedure based on optimization considering cost and benefit is generally referred to as level IV reliability-based design. For example, Rosenblueth (1976) made strong and convincing arguments to shift from a semiprobabilistic, second moment or full distribution design format to one based on optimization since it is the only rationale procedure that ensures long-term benefit to society. A rationale approach is based on consideration of costs incurred during the structure's lifetime including construction, maintenance and damage costs, cost of loss of revenue, cost of injury and death and discounting of cost over time (e.g. Ang and Leon, 1997; Wen and Kang, 2001a, b). Since limit states that cause serious consequences and huge costs normally have very small probabilities of occurrence, the design problem is to balance the initial cost of the structure and the expected cost of the consequence of failure.

Central issues in this approach include proper consideration of the uncertainty in demands and capacity and accurately accounting for various costs to arrive at the optimal solution. Following Wen and Kang (2001a, b), over a time period (t) that may be the design life of a new structure or the remaining lifetime of a retrofitted structure, the expected total cost due to all hazards can be expressed as a function of t and the design variable vector X ,

$$E[C(t, X)] = C_0(X) + E \left[\sum_{i=1}^{N(t)} \sum_{j=1}^k C_j e^{-\lambda t_i} P_{ij}(X, t_i) \right] + \int_0^t C_m(X) e^{-\lambda \tau} d\tau \quad (7.78)$$

in which $E[\cdot]$ is the expected value; C_0 is the construction cost for new or retrofitted facility; X is design variable vector, e.g., design loads and resistance; i is severe loading occurrence number including joint occurrence of different hazards such as live, wind and seismic loads; t_i is the loading occurrence time, a random variable; $N(t)$ is the total number of severe loading occurrences in t , a random variable; C_j is cost in terms of present dollar value of consequence of j th limit state at $t = t_i$ including costs of damage, repair, loss of service, and deaths and injuries; $e^{-\lambda t} =$ cost discount factor over time t , λ is discount rate per year; P_{ij} is probability of j th limit states exceeding given the i th occurrence of one or multiple hazards; k is total number of limit states; and C_m is operation and maintenance costs per year. Implicit in the formulation is the assumption that the structure will be restored to its original strength after each hazard occurrence. The design decision problem therefore lies in the determination of X such that $E[C(t, X)]$ is minimized.

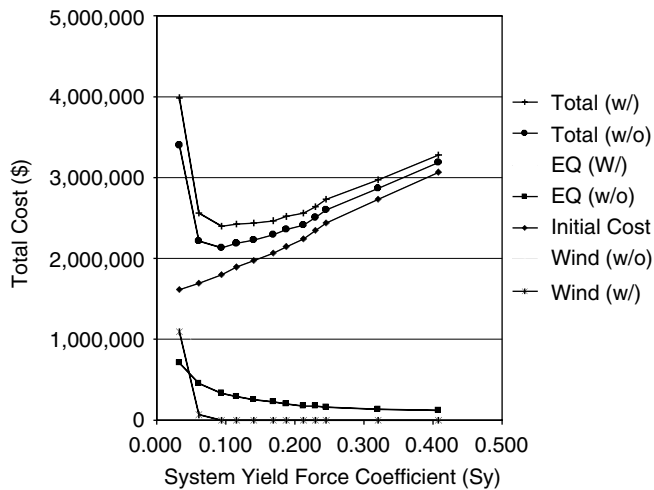


FIGURE 7.9 Life-cycle costs of a nine-story office building as function of system yield force coefficient at Seattle (life = 50 year, discount rate = 5%, w/ and w/o indicate with and without consideration of costs due to deaths and injuries). (Kang and Wen, Structural Research Series No. 629, University of Illinois at Urbana-Champaign, 2000.)

The method was applied to the designs of 3×5 bay, nine-story special moment resisting frame steel office buildings in Los Angeles, CA, Seattle, Washington and Charleston, SC. The building is designed for a wide range of base shear and meets the drift and other requirements of NHERP 97. The system strength is measured by a system yield force coefficient (system yield force determined from a static pushover analysis using DRAIN2D-X divided by the system weight). Five limit states in terms of story-drift are used on the basis of the performance levels of FEMA 273 (1997). The empirical seismic hazard procedure of FEMA 273 is used to calculate the ground excitation demand for a given probability level. The probability of drift ratio was determined from the uniform-hazard response spectra and a method of equivalent nonlinear SDOF system for the building following Collins et al. (1996). The drift ratio is then multiplied by a correction factor (see Section 7.5.3) to incorporate building capacity uncertainty and then converted to damage factor according to FEMA-227 1992).

The maintenance cost is not considered in this study. Initial costs are estimated from Building Construction Cost Data (1996). The nonstructural items were not considered in the initial cost estimation since they are not functions of the design intensity. The damage cost, loss of contents, relocation cost, economic loss (dollar/ft²), cost of injury (\$1000/person for minor and \$10,000/person for serious injuries) and cost of human fatality (\$1,740,000/person) are estimated on the basis of FEMA-227. All costs are given in terms of the value of U.S. dollars in 1992. A constant annual discount rate λ of 0.05 is assumed. Figure 7.9 shows an example of various life cycle (50-year) costs as functions of the structural strength measured by a system yield coefficient S_y (system yield force divided by weight) in Seattle. Note that the expected cost due to earthquake clearly dominates except for very small S_y at which the structure becomes more vulnerable to wind load. The optimal design strength is determined by minimizing the total LCC. At this optimal strength, the increase in initial cost is balanced by the decrease in overall expected failure cost.

Comparison of the optimal strength with seismic loads based on LCC with current design according to NHERP 1997 in the first two rows of Table 7.2 indicates that current design requirements could be enhanced, or in other words, the target reliability index could be set higher, to ensure long-term benefit at all three locations. Comparison of the last three rows of the table shows that the design is often dominated by the hazard that has high intensity and large uncertainty, causing serious consequences (earthquake at Los Angeles and Seattle and hurricane winds at Charleston). The design, however, is not controlled by the dominant hazard as is recommended in most current codes, since the lesser hazard still contributes to the LCC, e.g., earthquake at Charleston and winds at Seattle. The sensitivity of the optimal

TABLE 7.2 Comparison of Design System Strength (Lateral System Yield Force Divided by Weight) Under Winds, Earthquakes and both Hazards (Wen and Kang, 2001)

Hazard (design basis)	Location		
	Los Angeles	Seattle	Charleston
Earthquake (NEHRP 1997)	0.140	0.100	0.075
Earthquake (LCC)	0.198	0.109	0.097
Wind (LCC)	0.073	0.073	0.121
Earthquake and wind (LCC)	0.198	0.115	0.146

NEHRP = National Earthquake Hazard Reduction Program, LCC = Life-Cycle Cost

design to important design parameters such as structural life, discount rate and death and injury cost was investigated. The optimal design was found to be highly dependent on failure consequence and moderately sensitive to the structural life span and discount rate assumptions. It may be sensitive to death and injury cost assumptions, dependent on location and hazard risk characteristics and percentage contribution of such costs to the overall LCC. The question of uniform reliability to withstand different hazards was also examined. The implied reliabilities of the optimal design to wind and earthquake are vastly different indicating that, contrary to common belief, uniform reliability to withstand different hazards is not feasible and should not be recommended.

The results show that the minimum expected LCC approach properly takes into consideration the uncertainty in structural demand and capacity and the broader social-economical issues. It is a promising method for selecting appropriate target reliability for design.

7.6.4 Reliability and Redundancy

Reliability and redundancy have become a serious concern among engineers and researchers after the poor performance of some building structures in recent earthquakes such as the collapse of a parking garage during Northridge earthquake. However, there is a general lack of thorough understanding of redundancy under seismic excitations among engineers that could lead one to question design recommendations for redundancy. The most commonly accepted notion of redundancy is that related to the structural configuration; namely, if the load is distributed among a large number of load-bearing components, it is less likely that all components will fail at the same time compared to a system having only a few components. For example, the reliability/redundancy factor, ρ , in the 1997 Uniform Building Code (ICBO, 1997) is primarily a function of the structural configuration, which can lead to an increase of up to 50% in the design base shear. Engineers have expressed concerns with the new provisions (e.g., Whittaker and Hart, 1999) because the current procedure can promote less desirable designs and impose a penalty on what engineers would generally consider a good, reliable design. A proposal has also been made to remove this provision from the current code until better understanding of reliability and redundancy develops (Searer and Freeman, 2002a).

The reason for this controversy is that many important factors affecting structural performance have not been considered in the ρ factor. Studies of simple parallel systems with random capacity under random static loads by De et al. (1989) and Gollwitzer and Rackwitz (1990) showed that systems with a large number of members have significant redundancy (much higher reliability) only if there is moderate member ductility capacity, low strength correlation among the members and small ratio of load variability compared to those of the member resistance. The reasons include: ductile members continue to carry load after yielding; members with low strength correlation are less likely to fail at the same time; and when the load has large variability it is more likely to have large overload that will cause system failure regardless of the configuration. Bertero and Bertero (1999) have reached similar conclusions in their study of reliability of structural frames under earthquake excitation with both capacity and demand treated as random variables. The implication of these findings in design for seismic loads is that any

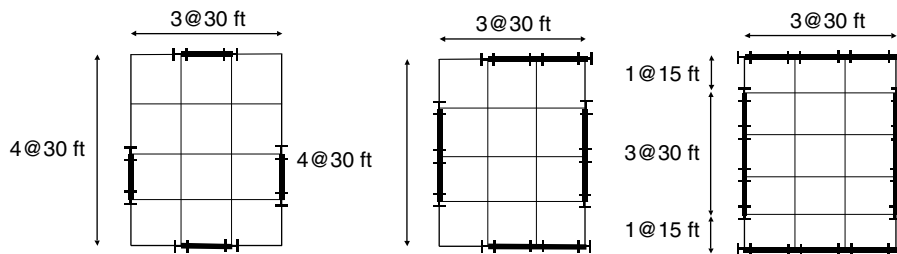


FIGURE 7.10 Plane of three-story, 1 × 1 bay, and 2 × 2 bay, and 3 × 3 bay moment frame systems with equal total lateral resistances.

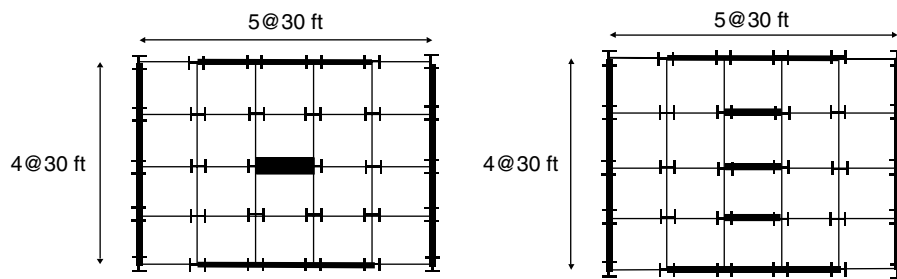


FIGURE 7.11 Plane of five-story one-way dual systems with equal total lateral resistances.

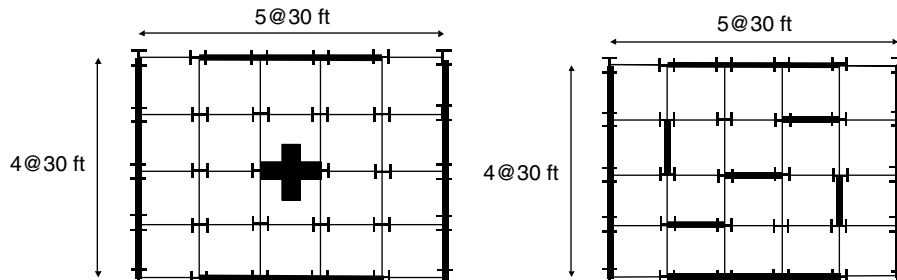


FIGURE 7.12 Plane of five-story two-way dual systems with equal total lateral resistances.

extra reliability and redundancy due to structural configuration should be viewed with utmost care in view of the unfavorable factors: (1) the seismic load uncertainty is known to be generally much larger than that of the member resistance, (2) the member resistance correlation is generally high and (3) many structural components may have very low ductility capacity such as the steel connections in pre-Northridge structures.

For structural systems under dynamic earthquake excitations, the nonlinear response behavior and load redistribution after member failures become considerably more complex than those in a simple parallel system. In view of the large uncertainties in demand and capacity, performance and redundancies of structures under seismic load can be measured meaningfully only in terms of the reliability of the system in which nonlinear structural behaviors are properly considered. In Wen and Song (2002, 2003), redundancies of moment-resisting frames and dual systems (Figures 7.10 to 7.12) were investigated. The structures are assumed to be located in Los Angeles. The systems are designed in accordance with NEHRP 1997 (BSSC, 1997) and the total lateral resistances of systems of different configurations are kept the same, so they have the same fundamental period, stiffness and yield strength. The purpose is to isolate

TABLE 7.3 Comparison of Strength Requirements on the Basis of Uniform-Risk Factor Method and UBC/NEHRP ρ Factor Method (Wen and Song, 2003)

System		1/R _R	ρ
Three-story SMRF system of different number of bays, ductile connections, torsional motions	1 × 1 bay	1.06	1.25
	2 × 2 bay	1.00	1.25
	3 × 3 bay	1.00	1.24
Three-story SMRF system of different number of bays, brittle connections, torsional motions	1 × 1 bay	1.58	1.25
	2 × 2 bay	1.56	1.25
	3 × 3 bay	1.45	1.24
Three-story SMRF system of different number of bays, ductile connections, no torsional motions	4 × 4 bay	1.00	1.24
	6 × 6 bay	1.00	1.00
Five-story, one-way dual system of different number of shear walls	1	1.20	1.50
	2	1.17	1.02
	3	1.03	1.00
Five-story, one-way dual system of different ductility capacity of shear walls	5.4	1.14	1.00
	6.4	1.03	1.00
	7.4	1.00	1.00

the possible important redundancy contributing factors such as system configuration, member ductility capacity (ratio of the displacement at the ultimate strength to that at the system yielding), 3D structural motions and uncertainties in the demand versus capacity. The SAC ground motions (Somerville et al., 1997) are used as excitation. three-dimensional, nonlinear structural models are developed and structural response and reliability analyses are carried out. A uniform-risk redundancy factor, R_R , is also developed as an additional multiplier to the response modification factor, R , in current codes, for design such that systems of different redundancies can meet uniform probabilistic performance requirement.

The results showed that uncertainties in demand and capacity, member ductility capacity and system 3D motions are as important as system configuration. Comparison of response of moment frame systems having ductile connection with those having brittle connections indicates that when torsional motions are ignored, the system configuration has very little effect. When torsional motions are considered, the effect of structural configuration is more important and produces larger differences in response. Under such circumstances, the configuration redundancy is more important for a system with ductile connections. Comparison of response statistics of dual systems indicates that the effects of the number of shear walls, shear wall strength uncertainty and strength correlation are small. This may be attributed primarily to the dominance of the uncertainty in the seismic excitation. Load redistribution and the contribution of the secondary moment frames after the shear wall capacity has been exceeded may further lessen these effects.

The required design forces according to the ρ factor for the dual and SMRF systems are compared with those according to the performance-based uniform-risk redundancy factor (R_R) method in Table 7.3. The performance requirements include probabilities of incipient collapse should be less than 2% in 50 years for the overall (moment frame or dual) system (value used in SAC Steel Project) and 10% in 50 years for the shear walls of the dual system (approximately target life safety level in current codes). The first two rows compare the redundancy factors for three-story SMRF systems of one to three bays and torsional motions. R_R requires little or no increase in the design force if connections are ductile since all three buildings satisfy the performance requirements. If connections are brittle, it requires an increase from 58% for the 1 × 1 bay system to 45% for the 3 × 3 bay system. The ρ factor, on the other hand, requires an increase of 25% for all systems regardless of the number of bays and member ductility capacity. The third row compares the two three-story SMRF systems with ductile connections and no torsional motions. The difference in the number of bays, 4 × 4 against 6 × 6, hence size of columns and beams, causes no notable differences in structural response and both systems satisfy the reliability requirement. Therefore, no increase in design force is required according to R_R . The factor ρ , however, has to be

increased by 24% for a system with a small number of bays. The fourth row compares five-story one-way dual systems with different numbers of shear walls. The three-shear wall system satisfies the performance requirements and no increase in design force is required according to both methods. For the one-shear wall system, ρ needs to be increased by 50% in strength compared with only a 20% increase according to R_R . The last row compares five-story one-way dual systems of different shear wall ductility capacities. The ductility capacity is not considered in ρ whereas R_R needs to be increased by 14% when the ductility capacity is reduced from 7.4 to 5.4.

The uniform-risk redundancy factor approach that considers the uncertainty in the demand and capacity, the ductility capacity of the structural members and 3D motions gives design forces that satisfy the probabilistic performance requirements. ρ in current codes, on the other hand, overestimates the effect of system configuration, fails to consider the effects of system ductility capacity and 3D motions and gives inconsistent results.

7.7 Future Challenges

The summary of probabilistic aspects of earthquake engineering given in this chapter indicates that considerable progresses have been made in the development of methodologies for accounting for uncertainties in demand and capacity, reliability analysis and code formulation. For successful implementation of the methodologies to reduction of loss due to earthquakes by developing more effective code procedures for new structures and retrofit methods for existing structures, additional challenges lie ahead. In addition to the target reliability and redundancy issues, a few additional challenges are described in the following.

7.7.1 Impact of Demand Spatial Correlation

For spatially extended systems such as long bridges, transportation networks, building stock and facilities of a community, the spatial correlation of the seismic excitation becomes important. Approaches based on intensity measures such as spectral acceleration can fail to determine the impact of spatial correlation. An independent assumption of the intensity measures at different locations may significantly underestimate the uncertainty of the demand on the system. An event-based or scenario-type approach based on an earthquake of given magnitude and distance seems most appropriate. A worst-case scenario commonly used in the past, however, does not give a true picture of the seismic demand. It provides little information on long-term planning based on cost versus benefit since its probability is extremely small, and it may be the moderate and more frequent events (e.g., the 1989 Loma Prieta and 1994 Northridge earthquakes) that cause the maximum damages or losses. Simulation of all possible future events and system responses would be computationally impractical. A smart simulation of selecting a limited number of representative events based on the UHGM concept as shown in Section 7.3.4 seems a feasible and promising approach. The average uniform-hazard response spectra of different sites of the area may be used in the screening process because they are a good measure of demand on systems of a wide range of frequency. The small number of uniform-hazard events after the screening (e.g., Figure 7.4) would represent well the future seismic hazard to a particular area. The median responses of the system calculated on the basis of these events corresponding to different hazard levels can then be used to describe the probabilistic demand on the system as shown in Figure 7.5.

7.7.2 Quantification of Epistemic Uncertainty

So far, in uncertainty analysis in earthquake engineering, emphasis has been laid on aleatory uncertainty. The magnitude and impact of epistemic uncertainty have been shown to be a large and even dominating factor. As mentioned above, epistemic uncertainties in source, path and site have been considered in SSHAC (1997). The USGS hazard-mapping project considered the epistemic uncertainty using logic tree but used only the mean value in the national hazard maps. A complete analysis that considers the additional scatter of the hazard due to the epistemic uncertainty and its risk implications

in decision making needs to be explored. In addition, epistemic uncertainties due to discrepancies in different ground motions and structural models and response analysis software have been found to be large; in particular when inelastic, 3D, and torsional and large responses are considered. These uncertainties will have a significant impact on demand and capacity estimates. Efforts initiated in SAC/FEMA in quantifying these uncertainties in steel buildings need to be continued and extended to all types of systems.

7.7.3 Conversion from Structural Response to Physical Damage and Loss

Uncertainty in conversion from structural response to physical damage and loss has been known to be as important as that from the seismic excitation to structural response that has been the subject of this chapter. Many issues involved in this conversion process such as estimation of losses due to economic disruption, business downtime and indirect loss may be beyond an engineer's expertise and require a broader interpretation of the economic aspects of the problem and "soft" or empirical methods such as Delphi consensus approach by a group of people from different areas of expertise. The estimation of the uncertainty in these conversion processes should be emphasized to account for the effect of all uncertainties in the final design decision process on the basis of long-term economic consideration, for example in the code provisions.

7.7.4 Risk Communication Issues

To successfully implement the mitigation measures with proper consideration to uncertainty, communication of probabilistic aspects of earthquake engineering is as important as the technical issues addressed in this chapter. What is the most effective way of communicating risks to stakeholders such as engineers, building owners, occupants, building regulators, insurers, etc.? Should such communication be accurately based on numbers such as probability of 10% in 50 years, which may not be easy for nonspecialists to grasp? Would a scenario-type or graphic description be more appropriate? The major concern in the last approach is a possible distortion of the true risk picture. Probability information such as annual or 50-year exceedance probability and confidence levels still needs to be properly incorporated in a user-friendly way. Different users have different concerns and as a result communication needs to be carried out in different languages. For example, an engineer would understand and use average annual loss in decision making based on LCC whereas an insurer would like to have an estimate of the probable maximum annual loss (PML) corresponding to a small probability according to the specific definition of the PML, etc. The ability to properly communicate the probabilistic aspects of earthquake engineering problems to nonspecialists therefore needs to be emphasized and cannot be overlooked.

Acknowledgments

Communication with B. R. Ellingwood, D. Veneziano, C. A. Cornell and A. Der-Kiureghian is greatly appreciated.

Glossary

Aleatory uncertainty (or randomness) — inherent variability that is irreducible by additional knowledge, information, or data.

Confidence level — a statistical term describing the probability that uncertainty quantity is within a given limit.

Epistemic uncertainty (or uncertainty) — modeling errors that can be reduced with additional knowledge, information, or data.

Fragility function — conditional probability of limit state given the excitation or displacement demand.

- Incremental Dynamic Analysis (IDA)** — dynamic analysis of structural against collapse with incremental increase of ground excitation intensity.
- Performance function** — an algebraic expression of random variables indicating that a limit state occurs when the function is less than zero.
- Randomness** — inherent variability of a physical phenomenon.
- Standard normal variate** — a random variable with a standard normal distribution with zero mean and unit standard deviation.
- Uniform-hazard response spectrum (UHRS)** — response spectrum corresponding to a prescribed probability of exceedance such as 10% in 50 years.
- Uniform-hazard ground motions (UHGM)** — ground motions whose response spectra match the uniform-hazard response spectra.

List of Symbols

<i>a</i>	scale constant in power law drift/spectral acceleration relationship
<i>b</i>	power in drift/spectral acceleration relationship
β	dispersion parameter in a lognormal distribution = $\sqrt{\ln(1+\delta^2)}$
β	reliability (or safety) index
<i>C</i>	structural member or system capacity for a prescribed limit state
\tilde{C}	median (50 percentile) value of <i>C</i>
<i>d</i>	deterministic demand
<i>D</i>	displacement demand variable, e.g., interstory drift ratio, global drift ratio
<i>d</i>	a specified demand threshold
\tilde{D}	median value of <i>D</i>
δ	coefficient of variation
$f_X(x)$	probability density function of random variable X
$f'(\theta)$	prior distribution of parameter
$f''(\theta)$	posterior distribution of parameter
Φ	cumulative distribution of a standard normal variate
Φ^{-1}	inverse function of
ϕ	resistance (or capacity) factor in LRFD design
$g(X)$	performance function of basic random variables X: X_1, X_2, \dots, X_n corresponding to a given limit state
γ	load or demand factor in LRFD design
$H_t(a)$	seismic hazard function; probability of spectral acceleration exceeding "a" in "t" years
<i>k</i>	power constant in seismic hazard power law equation
k_0	scale constant in seismic hazard power law equation
K_q	confidence level coefficient
$L(\theta)$	sample likelihood function of parameter θ
λ	scale parameter in a lognormal distribution = $\ln \mu - 0.5\beta^2$
λ	discount rate
<i>M</i>	earthquake magnitude
μ	mean value
ν	mean occurrence rate of a Poisson process
P_q	<i>q</i> percentile value of P
<i>R</i>	epicentral distance
ρ	correlation coefficient
ρ	reliability/redundancy factor in uniform building code
σ	standard deviation
P_t	probability of exceedance in t years
q	percentile value; confidence level

S	soil classification
S	sensitivity coefficient due to capacity uncertainty
S_a	spectral acceleration
S_x	sample estimate of the standard deviation
t	duration of t years
T	total aleatory and epistemic uncertainty
\bar{X}	sample estimate of the mean value

References

- American Association of State Highway and Transportation Officials (AASHTO), LRFD Design Specifications, 1st ed., 1994.
- American Institution of Steel Construction (AISC), Manual of Steel Construction, Load and Resistance Factor Design, 3rd ed., 2001.
- American Petroleum Institute (API), Recommended Practice for Planning and Construction of Fixed Platform-Load and Resistance Factor Design, 1st ed., (API RP2A-LRFD), 1990.
- American Society of Civil Engineers (ASCE), Minimum Design Loads for Buildings and Other Structures, ASCE-7-98, 1999.
- American Society of Civil Engineers, Minimum Design Loads for Buildings and Other Structures, ASCE-7-2001, 2002.
- Ang, A.H.-S. and Leon, D., Development of target reliability for design and upgrading of structures, *Struct. Saf.*, 19, 91–104, 1997.
- Ang, A.H. and Tang, W.H., *Probability Concepts in Engineering Planning and Design*, Vol. I, John Wiley & Sons, New York, 1975.
- Ang, A.H. and Tang, W.H., *Probability Concepts in Engineering Planning and Design*, Vol. II, John Wiley & Sons, New York, 1984.
- Atkinson, G.M. and Boore, D.M., Ground-motion relations for eastern North America, *Bull. Seismol. Soc. Am.*, 85, 17–30, 1995.
- Beresnev, I.A. and Atkinson, G.M., FINSIM—a FORTRAN program for simulating stochastic acceleration time histories from finite faults, *Seismol. Res. Lett.*, 69, 27–32, 1998.
- Bertero, R.D. and Bertero, V.V., Redundancy in earthquake-resistant design *J. Struct. Eng.*, 125, 81–88, 1999.
- Boore, D.M. and Joyner, W.B., Estimation of ground motion at deep-soil sites in eastern North America, *Bull. Seismol. Soc. Am.*, 81, 2167–2185, 1991.
- Boore, D.M. and Joyner, W.B., Prediction of ground motion in North America, ATC-35-1, 6-1–6-41, 1994.
- Boore, D.M., Joyner, W.B. and Fumal, T.E., Estimation of Response Spectra and Peak Accelerations from Western North American Earthquakes: An Interim Report, Open File Report 93-509, U.S. Geological Survey, 1993.
- Boore, D.M., Joyner, W.B. and Fumal, T.E., Equation for estimating horizontal response spectra and peak accelerations from western North American earthquakes: A summary of recent work. *Seismol. Res. Lett.*, 68, 128–153, 1997.
- Building Construction Cost Data (BCCD) 54th Annual ed., 1996.
- Building Seismic Safety Council, Washington, D.C. (BSSC), NEHRP Recommended provisions for seismic regulations for new buildings, Part 1- Provisions, 1994, 1997.
- Campbell, K.W. and Bozorgnia, Y., Updated near-source ground motion (attenuation) relation for horizontal and vertical components of GPA and acceleration response spectra, *Bull. Seismol. Soc. Am.*, 93, 2003.
- Canadian Standards Association (CSA), Canadian Highway Bridge Design Code, CAN/CSA-S6-00, 2000.
- Chopra, A.K. and Goel, R.K., Evaluation of nonlinear static pushover to estimate seismic deformation, *J. Struct. Eng.*, ASCE, 126, 2000.
- Chopra, A.K. and Goel, R.K. A modal pushover analysis procedure for estimation of seismic demands for buildings. *J. Earthquake Eng. Struct. Dyn.*, 31(3), 561–582. 2002.

- Collins, K.R., Wen, Y.K. and Foutch, D.A., Dual-level design: A reliability-based methodology, *Earthquake Eng. Struct. Dyn.*, 25, 1433–1467, 1996.
- Cornell, C.A., Jalayer, F., Hamburger, R.O. and Foutch, D.A., Probabilistic basis for 2000 SAC Federal Emergency Management Agency steel moment frame guidelines, *J. Struct. Eng.*, ASCE, 128, 526–533, 2002.
- De, R.S., Karamchandani, A. and Cornell, C.A., Study of redundancy in near-ideal parallel structural systems, ICOSSAR '89, *Struct. Saf. Reliab.*, 975–982, 1989.
- Der-Kiureghian, A., Structural reliability methods for seismic safety assessment: A review, *Eng. Struct.*, 18, 412–424, 1996.
- Der-Kiureghian, A., Conte, J., Haukaas, T., Jacquet, S. and Zhang, Y., Computational framework for reliability assessment/4061999.z peer.berkeley.edu/yr4_research/ta2/lc07.html, (PEER website research summary), 2002.
- Ellingwood, B.R., Probability-based structural design: Prospects for acceptable risk bases, keynote lecture, *Proc. 8th Int. Conf. Applications of Statistics and Probability*, Sydney, Australia, pp. 11–18, 1999.
- Ellingwood, B.R., Galambos, T.V., MacGregor, J.G. and Cornell, C.A., Development of a probability based load criteria for American National Institute A58, NBS Special Publication 577, 1982a.
- Ellingwood, B.R., Galambos, T.V., MacGregor, J.G. and Cornell, C.A., Probability-based load criteria: Load factors and load combinations, *J. Struct. Div.*, ASCE, 108, 978–997, 1982b.
- Ellingwood, B.R. (1999). Probability-based structural design: Prospects for acceptable risk bases, keynote lecture. *Proc. 8th Int. Conf. Applications of Statistics and Probability*, Sydney, Australia, Balkema 2000, Vol. I, 11–88.
- Federal Emergency Management Agency (FEMA), FEMA-227 & FEMA-228, a benefit–cost model for the seismic rehabilitation of buildings, Vols. 1 & 2, 1992.
- Federal Emergency Management Agency (FEMA), FEMA-273, HEHRP guidelines for the seismic rehabilitation of buildings, 1997.
- Federal Emergency Management Agency (FEMA), Recommended seismic design criteria for new steel moment-frame buildings, *FEMA 350*, 2000.
- Federal Emergency Management Association (2001), Ranking of U.S. Metropolitan Areas with Future Estimated Earthquake Losses, FEMA, Washington, D.C.
- Foutch, D.A., State-of-the-art Report on Performance Prediction and Evaluation of Moment-resisting Frame Structures, Report No. FEMA-355F, Federal Emergency Management Agency, Washington, D.C., 2000.
- Frankel, A., Simplified approach to incorporating uncertainty in the ground motion computation and mapping process, ATC-35-2, 8-1 to 8-38, 1997.
- Frankel, A., Mueller, C., Barnhard, T., Perkins, D., Leyendecker, E.V., Dickman, N., Hanson, S. and Hopper, M., National Seismic-hazard Maps: Documentation, USGS Open-File Report 96-532, 1996.
- Galambos, T.V.B., Ellingwood, R.J., MacGregor, G. and Cornell, C.A., Probability-based load criteria: assessment of current design practice, *J. Struct. Div.*, ASCE, 108, 959–977, 1982.
- Gardoni, P., Der-Kiureghian, A. and Mosalam, M., Probabilistic capacity models and fragility estimates for RC columns based on experimental observations, *J. Eng. Mech.*, ASCE, 128, 1024–1038, 2002.
- Gollwitzer, S. and Rackwitz, R., On the reliability of Daniels systems, *Struct. Saf.*, 7, 229–243, 1990.
- Harmsen, S., Perkins, D. and Frankel, A., Deaggregation of probabilistic ground motions in the central and eastern United States, *Bull. Seismol. Soc. Am.*, 89, 1–13, 1999.
- International Conference of Building Officials, Whittier, CA (ICBO), Uniform building code, 1997.
- Kang, Y-J. and Wen, Y.K., Minimum lifecycle cost structural design against natural hazards, Structural Research Series No. 629, University of Illinois at Urbana-Champaign, 2000.
- Kulicki, J.M., Mertz, D.R. and Wassef, W.G., Load and resistance factor design for highway bridges, FHWA HI-95-0017, Federal Highway Administration, Washington, D.C., 1995.
- Lee, K. and Foutch, D.A., The performance evaluation of pre-Northridge steel frame buildings with brittle connections, *J. Struct. Eng.*, ASCE, 128, 547–555, 2002.

- Liu, P.-L., Lin, H.-Z and Der-Kiureghian, A., CAREL USER MANUAL, Report No. UCB/SEMM 89/18, University of California, Berkeley, CA, 1989.
- Luco, N. and Cornell, C.A., Structure-specific scalar intensity measures for near source and ordinary earthquake ground motions, *Earthquake Spectra*, 2002, submitted.
- Malley, J.O., Update on US seismic design requirements for steel structures, *Proc. 7th US National Conference on Earthquake Engineering*, Boston, MA July 21–25, 2002.
- Miranda, E. and Bertero, V.V., Evaluation of strength reduction factors for earthquake-resistant design, *Earthquake Spectra*, 10, 357–379, 1994.
- Nassar, A.A. and Krawinkler, H., *Seismic design based on ductility and cumulative damage demands and capacities, Nonlinear Seismic Analysis and Design of Reinforced Concrete Buildings*, Fajfar, P. and Krawinkler, H., Eds., Elsevier, Amsterdam, 1992.
- Park, Y.J. and Ang, A.H.-S., Mechanistic seismic damage for reinforced concrete, *J. Struct. Eng.*, ASCE, 111, 722–739, 1985.
- Park, Y.J., Ang, A.H.-S. and Wen, Y.K., Seismic damage analysis of reinforced concrete buildings, *J. Struct. Eng.*, ASCE, 111, 740–757, 1985.
- Rosenblueth, E., Toward optimal design through building codes, *J. Struct. Div.*, ASCE, 102, 591–607, 1976.
- SAC Steel Project, Seismic Design Criteria for Steel Moment-Frame Structures, SAC CD01-0, 2000.
- Saikia, C.K. and Somerville, P.G., Simulated hard-rock motions in Saint Louis, Missouri, from large New Madrid earthquakes ($Mw \geq 6.5$), *Bull. Seismol. Soc. Am.*, 87, 123–139, 1997.
- Sasani, M., Der-Kiureghian, A. and Bertero, V.V., Seismic fragility of short period reinforced concrete structural walls under near-source ground motions, *Struct. Saf.*, 24, 123–138, 2002.
- Schueller, G. and Spanos, P., Eds., *Proc. Int. Conf. Monte-Carlo Simulation*, Monte-Carlo, June 18–21, 2000.
- Searer, G.R. and Freeman, S.A., Impact of the reliability/redundancy factor on design, *Proc. 7th US National Conference on Earthquake Engineering*, Boston, MA, 2002a.
- Searer, G.R. and Freeman, S.A., Unintended consequences of code modification, *Proc. 7th US National Conference on Earthquake Engineering*, Boston, MA, 2002b.
- Senior Seismic Hazard Analysis Committee (SSHAC), Probabilistic seismic hazard analysis: A consensus methodology, 1995.
- Senior Seismic Hazard Analysis Committee (SSHAC) Recommendations for probabilistic seismic hazard analysis: Guidelines on uncertainty and use experts. U.S. Nuclear Regulatory Commission (NRC), NUREG/CR-6372, Washington D.C., 1997.
- Shome, N., Cornell, A.C., Bazzurro, P. and Carballo, J.E., Earthquakes, records, and nonlinear responses, *Earthquake Spectra*, 14, 469–500, 1998.
- Somerville, P.G., Irikura, K., Graves, R., Sawada, S., Wald, D., Abrahamson, N., Iwasaki, Y., Kagawa, T., Smith, N. and Kowada, A., Characterizing crustal earthquake slip models for the prediction of strong ground motion, *Seismol. Res. Lett.*, 70, 59–80, 1999.
- Somerville, P.G., Smith, N., Punyamurthula, S. and Sun, J. Development of Ground Motion Time Histories for Phase 2 of the FEMA/SAC Steel Project, Report No. SAC/BD-97/04, SAC Joint Venture, Sacramento, CA, 1997.
- Structural Engineering Association of California (SEAOC), Vision 2000, Performance-based seismic engineering of buildings, 1995.
- Vamvatsikos, D. and Cornell, C.A., Incremental dynamic analysis, *J. Earthquake Eng. Struct. Dyn.*, 31, 491–514, 2002.
- Wang, C.-H. and Wen, Y.K., Evaluation of pre-Northridge low-rise steel buildings—Part I, modeling, *J. Struct. Eng.*, ASCE, 126, 1151–1160, 2001a.
- Wang, C.-H. and Wen, Y.K., Evaluation of pre-Northridge low-rise steel buildings—Part II, reliability, *J. Struct. Eng.*, ASCE, 126, 1161–1169, 2000b.
- Wen, Y.K., Methods of random vibration for inelastic structures, *Appl. Mech. Rev.*, ASME, 42, 39–52, 1989.
- Wen, Y.K., *Structural Load Modeling and Combination for Performance and Safety Evaluation*, Vol. 31, Elsevier, Amsterdam, 1990.

- Wen, Y.K. and Foutch, D.A., Proposed Statistical and Reliability Framework for Comparing and Evaluating Predictive Models for Evaluation and Design and Critical Issues in Developing Such Framework, Report No. SAC/BD-97/03, SAC Joint Venture, Sacramento, Ca, 1997.
- Wen, Y.K. and Kang, Y.J., Minimum building life-cycle cost design criteria. I: Methodology, *J. Struct. Eng.*, ASCE, 127, 330–337, 2001a.
- Wen, Y.K. and Kang, Y.J., Minimum building life-cycle cost design criteria. II: Applications, *J. Struct. Eng.*, ASCE, 127, 338–346, 2001b.
- Wen, Y.K. and Song, S.H., Redundancy in performance-based design, *Proc. 7th US National Conference on Earthquake Engineering*, Boston, MA, 2002.
- Wen, Y.K. and Song, S.H., Structural reliability/redundancy under earthquakes, *J. Struct. Eng.*, ASCE, 129, 56–67, 2003.
- Wen, Y.K. and Wu, C.L., Uniform hazard ground motions for mid-America cities, *Earthquake Spectra*, 7, 359–384, 2001.
- Whittaker, A. and Hart, G., Seismic response modification factors, *J. Struct. Eng.*, ASCE, 125, 438–443, 1999.
- Working Group on California Earthquake Probabilities, Seismic hazards in southern California; probable earthquakes, 1994 to 2024, *Bull. Seismol. Soc. Am.*, 85, 379–439, 1995.
- Wu, C.-L. and Wen, Y.K., Earthquake ground motion simulation and reliability implications, Structural Research Series No. 630, University of Illinois at Urbana-Champaign, 2000.
- Yun, S.-Y., Hamburger, R.O., Cornell, C.A. and Foutch, D.A., Seismic performance evaluation for steel moment frames, *J. Struct. Eng.*, ASCE, 128, 534–545, 2002.

8

Performance-Based Seismic Engineering: Development and Application of a Comprehensive Conceptual Approach to the Design of Buildings

8.1	Introduction.....	8-2
	Introductory Remarks • Main Objectives of this Chapter	
8.2	Main Requirements for a Reliable P-BSD	8-4
	Performance-Based Seismic Design Objectives (P-BSDO) • The Need for Multilevel Seismic Design Criteria • The Need for a Probabilistic Design Approach • The Need for Design Spectra for Buildings (n-Degree-of-Freedom-Systems) • The Need for a Preliminary Design Procedure that Considers a Cumulative Damage Index • The Need to Control Deformations and Ductility (Minimum Strength) • The Need for a Conceptual Comprehensive Design Approach for P-BSD	
8.3	Comprehensive Conceptual Approach (CCA) for the P-BSD of Buildings.....	8-8
	Statement of Problem • Establishment of Design EQGMs • Numerical Preliminary Design Procedure	
8.4	Application of the Proposed CCA to the Preliminary Numerical Design of a Ten-Story Building	8-32
	Problem Statement • Establishment of Design EQGMs • Preliminary Analysis • Preliminary Sizing and Detailing	
8.5	Analysis of the Preliminary Design.....	8-48
	Introductory Remarks • Linear Elastic Dynamic Analysis • Nonlinear Analysis: “Push-Over” Analysis • Nonlinear Analysis of an Equivalent SDOF System • Nonlinear Analysis: Time-History Dynamic Analysis • Evaluation of the Performance of the Final Design for the Remaining P-BDO • Limitations of the Nonlinear Analyses That Have Been Conducted	

Raul D. Bertero

Vitelmo V. Bertero

8.6	Summary, Conclusions, Recommendations and Future Trends.....	8-71
	Summary • Conclusions • Recommendations • Future Trends in the Development of Improved CCA for P-BSD and Its Implementation into Simple But Reliable Building Seismic Code • Final Observations	

8.1 Introduction

8.1.1 Introductory Remarks

From analyses of the effects of significant earthquakes (since the early 1980s) we have concluded that the seismic risks in urban areas are increasing and are far from socio-economically acceptable levels. There is an urgent need to reverse this situation and it is believed that one of the most effective ways of doing this is through: (1) the development of more reliable seismic standards and code provisions than those currently available and (2) their stringent implementation for the complete engineering of new engineering facilities and also for the seismic vulnerability assessment of the existing facilities and the upgrading of those considered hazardous. A comprehensive approach for such development and implementation must consider all the aspects involved in the complete engineering of the facilities (see Bertero [1992, 1997a, 1997b, 2000a, 2000b] and Bertero and Bertero [2002]). Thus, the approach should not only consider design aspects but also must deal with the proper detailing and construction of numerical designs, and then with monitoring of the occupancy (function) and the maintenance of the whole facility.

A promising approach toward the above development has been proposed by the SEAOC Vision 2000 Committee in 1995 in its report entitled “Performance-Based Seismic Engineering of Buildings” and which will be denominated as the “performance-based seismic engineering” (P-BSE), although it is also called “performance-based earthquake engineering” (P-BEQE or P-BEE).

The above report presents a conceptual framework for P-BSE, as well as the different methodologies that have been proposed for the application of such framework to the design, construction, occupancy and maintenance, with particular emphasis on the design that has been denominated as “performance-based seismic design” (P-BSD) or “performance-based earthquake resistance design” (P-BEQ-RD) of new buildings. Recognizing that any facility (construction) is subject to excitations due to the potential sources of seismic hazards, and to other types of actions that can be acting, before, during and after the seismic excitations, it has been proposed (Bertero, 1997a; Bertero and Bertero, 2002) to change P-BSE and P-BSD with “performance-based engineering” (P-BE) and performance-based design (P-BD), when the seismic excitations are important. Reasons, importance and examples for the critical combination of all the possible excitations that can act simultaneously with seismic ones are given in Bertero (1997a).

Detailed discussions of what is understood for P-BSE (or P-BEE), P-BSD (or P-BEQ-RD) and guidelines for conducting them have been given in the SEAOC (1995) report, the documents ATC-40 (1996), FEMA-273 and 274 (1997) and in the Prestandards FEMA 356 (2000). Critical reviews of P-BSE have been offered by Bertero (1997a, 2002a). Definitions of P-BE, P-BSE and P-BSD have been presented and discussed by Bertero and Bertero (2002). Krawinkler and Miranda, in Chapter 9 present detailed discussions on P-BEE and its evolution; their chapter also provides a rigorous approach to performance assessment and P-BD. Recently the *Journal of Earthquake Engineering and Structural Dynamics*, Volume 31, No. 3, March 2002, was devoted to P-BEE: eleven contributions address a variety of issues that are summarized by Prof. Paulay in the preface of the volume. From a review of the present literature on P-BSE, and particularly on P-BSD, it can be stated that as concepts they have been well received by the researchers, academicians and professionals working in the field of earthquake engineering. However, the implementation of such concepts in practice has been questioned.

Bertero (2002b) in a paper entitled *Present and Future Perspectives Regarding the Use of P-BSD in USA*, pointed out that the number of structures which have been designed using P-BSD criteria depends on the kind of analysis that is conducted when the pertinent literature is reviewed:

1. If the analysis consists of just a superficial review of the title and abstract of the papers that have been published since 1997, the conclusion is that in a large number of important buildings, structures have been designed using design criteria based on P-BSD.
2. On the other hand, if the review is conducted through a thorough analysis of the seismic hazard data, design criteria and analysis, and design procedures that have been used, this review reveals that there are actually very few buildings that have been designed according to the conceptual framework of P-BSE and the conceptual approach and procedures that are required to conduct P-BSD.

With respect to the future perspectives of P-BE or even of P-BSD in the United States and their implementation in practice, they will continue to be limited to special buildings until the following developments take place:

1. *First*, simple but reliable approaches and numerical procedures for the practical application of P-BSD are developed.
2. *Second*, simple but reliable guidelines, norms, standards and/or seismic provisions for the practical applications of the P-BSD that are developed and implemented in the next generation of standards and building codes which then should be strictly enforced.

Although some simple approaches and procedures have been formulated and are considered for their implementation in the next generation of standards and codes, their reliability is questionable. Most of the methodologies that have been proposed for the practical application of the P-BSD, guided perhaps by the mere design of offering simplicity, have sacrificed some important concepts.

Experience shows that once an approach and the corresponding procedures are introduced in a standard and code, it is very difficult and time demanding to make any changes. It is believed that before any of the so-called simplified approaches for P-BSD and their corresponding methodologies are implemented in a building code, they should be thoroughly calibrated. The question then is, calibrate against what? There is no doubt that it would be ideal to calibrate them using the most sophisticated and reliable approach and procedure for P-BSE and P-BSD that can be developed. However, as pointed out in several publications and in Chapter 9, the reliable quantification of the different design objectives involved in P-BSD will require programs of research, technological developments and education, which will take years to conduct. According to the present status of the action plan that is followed at present in the United States, it will take more than 15 years to develop and approve robust guidelines for P-BSD. The authors believe that the reduction of the present seismic risks in our built environment demand earlier actions.

Documents published by SEAOC (1995, 1996, 1999), ATC-40 (1996), FEMA-273, 274 (1997), FEMA-356 (2000), FEMA-350 (2000) have given guidelines regarding how to apply the concept of P-BSD to new and existing constructions. Furthermore, FEMA-302, 303 (1997) and FEMA-368 (2001) cover the 'NEHRP Recommended Provisions for Seismic Regulations for Buildings and other Structures' and recent codes such as ICC (2000 and 2001) and NFPA 5000 (2003) contain provisions that permit use of the P-BSD concept.

The above publications have contributed significantly toward a better understanding of what P-BSE and particularly P-BSD are, and already some of the guidelines and particularly the recent IBC (ICC, 2000) have provided specific quantification of the different performance-based seismic design objectives (P-BSDO), and provisions for the application of P-BSD concept. However, they do not require or even recommend what the authors consider should be a reliable step-by-step procedure (or methodology) that covers all the aspects involved in the P-BSE conceptual framework proposed by SEAOC (1995), which is illustrated in Figure 10.1 of Chapter 10.

As discussed in Chapters 7 and 9, significant advances have been made through the development of basic procedures for reliability performance procedures, upon the extensive studies done during the SAC project (Cornell et al., 2002) and at present in the PEER project (Cornell and Krawinkler, 2000); still it is not clear how all these advances can be implemented into a robust reliable procedure for P-BSD in a short time, and therefore, into the implementation in a simple but reliable practical code for P-BSD.

Since the late 1980s the authors have been conducting studies regarding how to improve the seismic code provisions to reduce the seismic risks, which resulted in the development of what they have denominated as a comprehensive conceptual approach (CCA) for the P-BSD of buildings (Bertero, 2002; Bertero and Bertero, 1992, 2002; Bertero, 1992, 1997a, 1997b, 2002a, 2000b). Furthermore, they have formulated a three-step approach for its implementation in a simple but reliable P-BSE building code. In doing so, the authors recognize that the CCA should consider conceptually the most reliable procedures that can be developed according to the present state of the art of seismic engineering, but that they should be simple. However, as the authors point out (Bertero and Bertero, 2002), “With the amount of specific software, spreadsheets, and mathematical packages available today, simplicity should be redefined. A numerical procedure is not simpler because an equation has fewer terms or some important parameter is ignored. A numerical procedure is simpler when it is easily understood and when the designer can go from the performance objectives to the design values in an explicit and transparent way.”

8.1.2 Main Objectives of this Chapter

The main objectives of this chapter are to:

1. summarize the main requirements for a reliable P-BSD;
2. briefly describe what is understood for a conceptual P-BSE seismic code and what should be covered;
3. summarize a three-step approach that could be implemented for the final formulation of simple but reliable seismic code regulations;
4. briefly discuss a proposed CCA approach and numerical design procedures for the P-BSD of buildings;
5. present a detailed discussion on the application of the proposed CCA to the design of a ten-story R.C. building and
6. offer a brief summary, some conclusions, recommendations, future trends and final observations.

Because all the above objectives, with the exception of number 5 above, have been discussed in detail in previous publications, the emphasis of the discussions presented here will be on a detailed discussion on the application of the proposed CCA.

8.2 Main Requirements for a Reliable P-BSD

8.2.1 Performance-Based Seismic Design Objectives (P-BSDO)

The conceptual framework for P-BSE developed by SEAOC (1995) encompasses the full range of seismic engineering issues to be addressed in the design of structures for predictable and controlled seismic performance within established levels of risk, and is illustrated in the flowchart of Figure 8.1. As can be seen the first step is the selection of P-BSDOs or performance design objectives (PDOs or just POs). These POs are selected and expressed in terms of expected levels of damage resulting from expected levels of earthquake ground motions (EQGM)(SEAOC, 1995). As discussed in detail in this original document and in Bertero and Bertero (2002), and in Chapter 9 the client makes this selection in consultation with the design professional based on the client's expectations, the seismic hazard exposure, economic analysis and acceptable risk. POs will range from code minimum requirements (usually based on: serviceability requirements under frequent but minor EQGMs; fully operational under occasional but moderate EQGMs; life safety under rare but major EQGMs; and to avoid collapse under the very rare but maximum credible EQGMs) to fully operational under the very rare but maximum considered EQGM. As illustrated in Figure 9.4, a PO is a coupling of expected performance levels with levels of seismic ground motions. A performance level represents a distinct band in the spectrum of damage to the structural and non-structural components and contents, and also considers the consequences of the damage to the occupants and functions of the facility. Four discrete performance levels are identified in the SEAOC (1995) report

(and thus in Figure 9.4). This report gives tables that define the various components of the building. The seismic hazard at a given site is represented as a set of earthquake ground motions and associated hazards with specified probabilities of occurrence. For example, the term “rare earthquake” refers to a set of potential earthquake ground motions that can produce a defined level of damage with a specific mean annual frequency (for example, 475 year return period for standard buildings). The set of earthquake ground motions will vary for different seismic regions and from site to site within a region because of variations in site conditions (topography and soil profile).

Performance objectives (POs) typically include multiple goals for the performance of the constructed building; for example, that it is fully operational in the 43-year event, it offers life safety in the 475-year event and it will not collapse in the 970-year event. The selection of POs sets the acceptability criteria for the design. Design criteria are the rules and guidelines that must be met to ensure that the three major objectives of the design (i.e., performance of function, safety, economy) are satisfied. The performance levels are keyed to limiting values of measurable structural response parameters, such as drift and ductility (monotonic and cumulative), structural damage indexes (DM), interstory drift indexes (IDI) and rate of deformations such as floor velocity, acceleration and even the jerk (in case of frequent minor earthquake ground motions). When the performance levels are selected, the associated limiting values become the acceptability criteria to be checked in later stages of the design. Note that once the limit value of the parameter has been selected for a particular earthquake hazard level, to completely define the design criteria it is necessary to define the acceptable conditional probability of going beyond that limit state (failure probability).

In Bertero and Bertero (2002) it is shown that the POs in Figure 9.4 are the discrete representations of a continuous performance objective curve in the “performance space.” On the vertical axis, the performance space shows the probability of exceedance of a particular performance objective over the life-cycle of the facility (e.g., 50 years). This probability accounts for both the likelihood of earthquake ground motion occurrences (according to its recurrence interval) as well as the acceptable probability of failure when these earthquake ground motions do occur. On the horizontal axis, the performance space shows a measure of structural response (e.g., the IDI).

8.2.2 The Need for Multilevel Seismic Design Criteria

During the 1971 San Fernando earthquake (moment magnitude $M_w = 6.7$), the Olive View Medical Center in Sylmar (California), inaugurated just a few months before, was almost completely destroyed. The hospital was redesigned in 1976 and rebuilt using RC and steel shear walls around the perimeter. During the 1994 Northridge earthquake (moment magnitude $M_w = 6.7$) the new facility resisted floor accelerations of 2.8 g without any significant structural damage. However, the hospital had to evacuate all its patients to other facilities for several days because of breakage of both sprinkler and chilled water lines (EERI, 1995). This example shows very clearly that design for a life safety performance objective for rare earthquake ground motions does not necessarily imply that the facility will be operational after frequent earthquake ground motions.

As shown in Bertero and Bertero (2002), the above situation can be represented in the performance space drawing the performance curves of two typical designs. Design A, which has been done on the basis of the life safety performance objective, does not satisfy the operational and fully operational performance objectives. On the other hand, Design B, which considered from the beginning fully operational and life safety performance objectives, is inside the acceptable design zone.

Furthermore, in the above reference it is also shown that, for example, using a strength design spectra for firm soil at San Francisco if a serviceability limit state is required for a 72 year return period (as suggested for some projects located in California sites with high seismic risks) or even for 43 or 20 years of return period then the serviceability limit state will control the design and innovative design approaches should be used to economically satisfy the performance objectives.

From the above examples it becomes very clear that at least two performance levels should be considered (even for the preliminary design) so that appropriate design decisions could be made to satisfy the

performance objectives. It is also pointed out that at present the serviceability (or fully operational) and life safety levels are the performance levels that should be selected for design since they are the ones for which there exist data and experience. Another advantage is that the serviceability as well as the fully operational limit states can be satisfied by using the very well-known techniques of elastic analysis. Subsequently, response in the nonlinear range (i.e., the life safety limit state) can be estimated using plastic analysis. Thus, the two different stages of behavior (linear and nonlinear) can be controlled using well-established procedures.

8.2.3 The Need for a Probabilistic Design Approach

As discussed in Bertero and Bertero (2002) and in Chapters 7 and 9 (particularly Section 9.3), a probabilistic foundation for the development of a probabilistic design/assessment approach to P-BSE has been proposed (Cornell and Krawinkler, 2000). The proposed strategy can be expressed symbolically by Equation 9.2 of Chapter 9. As discussed below, due to the dominant uncertainties in the demand, it is possible to develop particularly simplified reliable assessments and probabilistic designs using the traditional Load and Resistance Factor Design (LRFD) format (Galambos et al., 1982). Thus, an LRFD format that can be used for strength-, deformation- or damage-based design was developed and explained in detail in Bertero and Bertero (2002).

As a matter of fact, since a COV of about 0.20 could be expected for the capacities and a COV of about 0.80 for the earthquake demand, a simple probabilistic approach could be used for design. This simple approach is based on the fact that due to the dominant uncertainties in the demand it is possible to consider in the design all the random variables as deterministic (and equal to the mean value) except the earthquake demand. Therefore, the design equation for the mean capacity of each parameter X , C_x (where X is any design target parameter such as yield strength C_y , IDI, DM, etc.) could be reduced to a load factor design using (R. Bertero, 1997):

$$\bar{C}_x \geq \bar{D}_x (1 + \beta \text{COV}_{Dx}) = \bar{D}_x + \beta \sigma_{Dx} \quad (8.1)$$

where, \bar{D}_x is the mean demand for the design parameter X , $\sigma_{Dx} = \sqrt{\text{COV}_{Dx}}$ is the standard deviation of the demand for the design parameter X and β is a parameter used to measure the target failure probability, P_f , so that

$$P_f = \Phi(-\beta) \quad (8.2)$$

where $\Phi()$ is cumulative standard normal distribution. For example, for $P_f = 0.20$, $\beta = 0.84$. Note that normal distribution functions are implicit in using Equations 8.1 and 8.2. If necessary, other distribution functions could be adopted following the same approach but using equivalent normal variables obtained with the Rosenblatt transformation (Ang and Tang, 1984).

Therefore, if a conditional failure probability of 0.20 is specified for one PO and a COV of 0.80 is assumed for the earthquake demand parameter under study, the mean value (not the nominal or specified value) of the capacity parameter should be larger than $(1 + \beta \text{COV}_{Dx}) = 1 + 0.84 \times 0.80$ times the mean demand. If a nominal value of the capacity is used, the demand amplification factor should be reduced according to the ratio between mean and nominal capacity. Note that $\beta = 0.84$ ($P_f = 0.20$) is very close to the rule for designing with mean plus one-sigma spectra. However, no reduction factor is necessary with respect to the mean value of the capacity, and the standard deviation, σ_{Dx} , must include all the demand uncertainties (such as earthquake magnitude, type of fault, focus, directional effects, topography, soil profile and structural response).

When a multilevel design criteria is adopted it is important to consider the expected levels of earthquake ground motions, the levels of other types of seismic hazards and other possible types of excitations (such as those due to gravity [including snow], wind, temperature, etc.). Furthermore, it is necessary to have

a reliable estimation of all the possible critical combinations among these different excitations at each of the different levels of severity that are considered. The same performance-based approach used for the earthquake excitations (forces) could be used for each source of excitation. However, since the experience with other excitations using the current code approach seems to be satisfactory, it is reasonable to continue using it. For forces such as those produced by wind and snow the “design load level” is typically defined on the basis of a mean recurrence interval of 50 years, and safety index, σ_{Dx} (i.e., $P_f = 1.35 \cdot 10^{-3}$) is the target conditional probability of exceeding the local ultimate strength given the occurrence of that design load level. In addition, a set of load and force combinations and their factors were recommended for use by the individual material specification writers (Galambos et al., 1982).

The problem is to define the load combination factors used with each earthquake performance objective defined previously. The load combinations are needed for strength-based design and displacement-based and damage-based design. This is because gravity loads can affect the IDI and plastic hinge rotations because of the P- Δ effect and the formation of collapse mechanisms with plastic hinges in the central regions of beams. The gravity load factors can be easily selected if we apply the Turkstra's rule to modeling the load combination (Nowak and Collins, 2000). The rule is based on the observation that when one excitation component reaches an extreme value (in this case the earthquake excitations), the other excitation components are often acting at their instantaneous or arbitrary-point-in-time (APT) values. Since the mean values of APT loads are the same for all the earthquake levels, and if it is considered that their coefficients of variation (COVs) are much smaller than the COV of the earthquake demand, the load combination for each performance objective i could be defined with an LFRD format as

$$(1 + \beta_i COV_{EQ_i}) \overline{EQ} + \frac{\overline{D_{apt}}}{\overline{D_n}} D_n + \frac{\overline{L_{apt}}}{\overline{L_n}} L_n + \frac{\overline{S_{apt}}}{\overline{S_n}} S_n \quad (8.3)$$

Statistical data on loads (Galambos et al., 1982) have shown for dead load, $\overline{D_{apt}} = 1.05 D_n$, and for live load, $\overline{L_{apt}} = 0.24 L_n$. The temporal characteristics of snow forces vary widely with local climatology. From a study of snow and earthquake excitation combinations by Ellingwood and Rosowsky (1996), $\overline{S_{apt}} = 0.20 S_n$, could be used. Therefore, adding $\pm 0.15 D_n$ to the dead load to consider the simultaneous action of the vertical EQGM component, the following excitation factors could be used for frequent, occasional, rare and very rare EQGMs:

$$(1 + \beta_i COV_{EQ_i}) \overline{EQ}_i + 1.20 D_n + 0.24 L_n + 0.20 S_n \quad (8.4a)$$

$$- (1 + \beta_i COV_{EQ_i}) \overline{EQ}_i + 0.90 D_n \quad (8.4b)$$

Where β_i is the target safety index for the performance objective i , and EQ_i and COV_{EQ_i} are the mean value and the coefficient of variation of the corresponding EQGM level. Formulas (8.4) are valid for strength, displacement or damage-based design. Note that in the design, besides the EQ load combinations (8.4a and 8.4b), others (i.e., the load combinations involving dead, live, snow and wind loads) should also be considered.

8.2.4 The Need for Design Spectra for Buildings (n-Degree-of-Freedom-Systems)

This need is discussed in detail in Bertero and Bertero (2002), where it is stated that since the performance levels are keyed to limiting values of local structural response parameters, such as local structural damage indexes (DM), story drift indexes (IDI) and floor accelerations, design spectra of such parameters should be available for the preliminary design. It is obvious that several assumptions must be made to build these spectra for buildings, but in any case these spectra and the knowledge of these assumptions will provide a better design guide than the present SDOF spectra.

Note that if the building is modeled using deflected shapes (discrete model with lumped mass at each floor or continuous model with distributed mass) rather than the SDOFs based on just one lumped mass

system, it is possible to explicitly consider the distribution of local IDI and damage along the building. It is particularly important to consider the amplification of IDI and local damage in one of the stories as the structure response goes deeper in the nonlinear range (i.e., as the displacement global ductility increases). How all this can be done, besides the authors' publication, is illustrated in Sections 8.3 and 8.4.

8.2.5 The Need for a Preliminary Design Procedure That Considers a Cumulative Damage Index

This need and how it is considered in the CCA are discussed in Bertero and Bertero (2002), where its importance is clearly demonstrated, as well as in Sections 8.3 (particularly 8.3.3.1.7) and 8.5 (particularly 8.5.5).

8.2.6 The Need to Control Deformations and Ductility (Minimum Strength)

We have discussed and demonstrated earlier (Bertero and Bertero, 2002), that it is necessary to control the displacement and the maximum global ductility (i.e., minimum strength of building) for controlling damage. The main reason, particularly applicable to buildings, is that the concentration of deformations in the critical story (and therefore the local structural and nonstructural damage) is larger as the structure response goes deeper in the nonlinear range (i.e., when larger global ductility's are used in the design).

8.2.7 The Need for a Conceptual Comprehensive Design Approach for P-BSD

The authors' 2002 paper— after discussing and showing the drawbacks of the simplified procedures for P-BSD that have been offered based on deformation rather than strength, and some that are based on the use of energy concepts — defines and describes what they understand for a “conceptual comprehensive approach (CCA)” to P-BSD. Such an approach is based on the use of a numeric procedure based on a probabilistic multi-level seismic design criteria that from the beginning explicitly considers the performance objectives in terms of deformation, strength, energy dissipation (toughness) and damage for structural and nonstructural components and contents. A conceptual comprehensive P-BSD procedure has been developed and is discussed in the next section. Its application to a specific building is discussed in Sections 8.4 and 8.5.

8.3 Comprehensive Conceptual Approach for the P-BSD of Buildings

8.3.1 Statement of Problem

Recognizing that for reliable application of performance-based seismic engineering (P-B SE), in practice, the code regulations must remain simple and in accordance with the education in earthquake engineering of the practitioners, the following three-step approach could be implemented for the final formulation of the simple seismic code regulations.

8.3.1.1 First Step

Based on the state-of-the-art in earthquake engineering, a “conceptual performance-based code” should be developed, covering all aspects that a seismic code should regulate. Given the different groups of aspects and problems involved in earthquake-resistant design (EQ-RD) and earthquake-resistant construction (EQ-RC), as pointed out in Section 8.1 and in more detail by Bertero (1992) and Bertero and Bertero (1992,1993) it is envisioned that the conceptual seismic code will consist of regulations that can be grouped as follows:

1. Guidelines for assessing seismic activity and sources of potential seismic hazards (damage); restrictions for land use and guidelines for the selection of building sites and corresponding site restrictions and procedures for site suitability analysis.

2. For a selected site and function of a building, conceptual establishment of the EQ-RD criteria, design EQGMs, building performance goals and design methodology.
3. Conceptual overall design of the entire building system, covering restrictions and guidelines regarding selection of building configuration or form (size and shape), foundation, structural layout, structural system, structural materials and nonstructural components (potential unintentional structural components) and their materials.
4. Conceptual performance-based preliminary numerical design of the whole facility system, which requires prediction of the mechanical behavior of such a system and involves: proper modeling of the entire system; estimation of the demand on the structure and its contents (structural and stress analysis) at the different levels of design EQGMs; preliminary sizing and detailing through estimation of the capacities to be supplied to the structure for satisfying the target performance.
5. Reliable analysis of the performance of the preliminarily designed facility when subjected to the expected critical EQGMs at each of the limit states contemplated in the design criteria; and of existing facilities to assess their vulnerability.
6. Final design (detailing).
7. Monitoring of field construction, function (use) and maintenance (alterations, repair and upgrading) of the constructed structure.
8. Conceptual methodology for the upgrading of hazardous facilities (involving assessment of seismic vulnerability).

8.3.1.2 Second Step

In this step, the conceptual code regulations developed in the first step will be applied to the seismic vulnerability assessment of existing buildings and to the design of new buildings with different regular and irregular configurations, structural layouts and structural systems, which preferably have been designed and constructed according to current or modern seismic codes, and whose responses to EQGMs have been either recorded or predicted; and to the upgrading of different types of existing hazardous facilities which preferably have been recently upgraded.

8.3.1.3 Third Step

From the analysis of the results obtained in the second step, a simplified conceptual performance-based code that can be applied properly by the practitioners should be developed. It should clearly state all restrictions in siting and in selection of configuration (or form), foundation systems and structural systems for which such simplified code regulations could be used. For complex buildings, a peer review process should be required in which the conceptual code to be developed in the first step could be used.

Among the different groups of aspects or problems that the conceptual comprehensive performance-based code should regulate, as listed above (*first step*), the following groups must be considered to formulate a conceptual methodology and the corresponding code provisions for the EQ-RD of a building facility:

1. (a) Conceptual establishment of the design criteria according to the desired function (occupancy) and selected performance levels of the building; (b) according to the selected site, conceptual establishment of the design EQGMs, as well as any other source of potential hazard that needs to be considered in the design and (c) formulation of the design methodology.
2. Conceptual overall design (conception) of the entire building system.
3. Conceptual preliminary numerical design of the whole facility system.
4. Reliable analysis of the performance of the preliminary designed building when subjected to the established critical EQGMs.
5. Final design (detailing).

For convenience, in this chapter, the entire above groups with the exception of group 2 (that is not numerical), will be considered under the umbrella of conceptual performance-based methodology for EQ-RD. Therefore, the conceptual methodology for EQ-RD consists of two main parts: the conceptual

overall design (conception) of the facility system and the conceptual methodology for numerical EQ-RD. Although these two main parts are discussed separately below, they are actually intimately interrelated.

8.3.1.4 Conceptual Overall Design

An attempt was made by Bertero (1982) to clarify the conceptual overall design and to explain why it is believed that more attention must be given to it. Conceptual overall design is the avoidance or minimization of problems created by effects of seismic excitations, using understanding of behavior rather than numerical computations.

Conceptual overall design of the facility system involves the choice of overall shape and size of the building, the selection of the structural layout, the structural system, the structural material, type of nonstructural components (particularly those that could become unintentional structural components) and the foundation system. Both the architect and the engineer have to understand how design decisions regarding building layout may have serious seismic effects on the performance structure. The inertial forces depend on the mass (amount and distribution), the damping and the structural characteristics (stiffness, yielding strength, maximum strength and energy absorption and energy dissipation capacities). Arnold (1979) reported that 65% to 80% of buildings designed within the last 15 years were of irregular form. In 2001, Arnold in his Chapter 6 of the Naeim (2001) *The Seismic Design Handbook* stated “it is safe to say that over half of the buildings that have been designed in the last few decades do not conform to the simple uniform building configuration upon which the code is based.” Although there is no universal ideal building configuration, certain basic principles of EQ-RD can be used as guidelines for selecting adequate building and structural configuration (Bertero, 1979, 1982; Arnold, 1979, 1989, 2001; Dowrick, 1987)

8.3.1.5 Comprehensive Conceptual Performance-Based Methodology for Numerical EQ-RD

As discussed previously a comprehensive conceptual P-BSD methodology for the numerical design has been developed. The main objective of the rest of this chapter is to present an application of such methodology using a traditional structural system as illustrated in Figure 8.15. The comprehensive numerical EQ-RD is divided into three main phases: (a) establishment of the design EQGMs; (b) numerical preliminary design procedure and (c) the final design. To arrive at the desired final design, it is necessary to start with a preliminary numerical design procedure, whose main objectives are (1) that the procedure is transparent, i.e., based on fundamental principles of structural dynamics considering the real mechanical behavior of the entire building system, and (2) it leads to a preliminary design that is as close as possible to the desired final design. After evaluation of the suitability of the site selected for the construction of the building according to the established potential seismic and other hazards, the design procedure must start with the specification of desired performance objectives for the entire structural system according to the desired function of the entire building system (structural and non-structural components) and then provide a direct, rational path by which the structure may be designed to attain these goals. The numerical preliminary design (*phase b*) consists of three main groups of steps, as illustrated in Figure 8.1: (i) Preliminary analysis, (ii) preliminary sizing and detailing and (iii) acceptability checks of the preliminary design.

8.3.2 Establishment of Design EQGMs

The first phase of the comprehensive numerical EQ-RD (*phase a*) is the establishment of the design EQGMs. The establishment of design EQGMs covers: (1) acquisition and (2) processing of the data needed for establishing reliable design EQGMs.

8.3.2.1 Acquisition of Data

The data and the problems involved in acquiring design EQGMs can be summarized as follows:

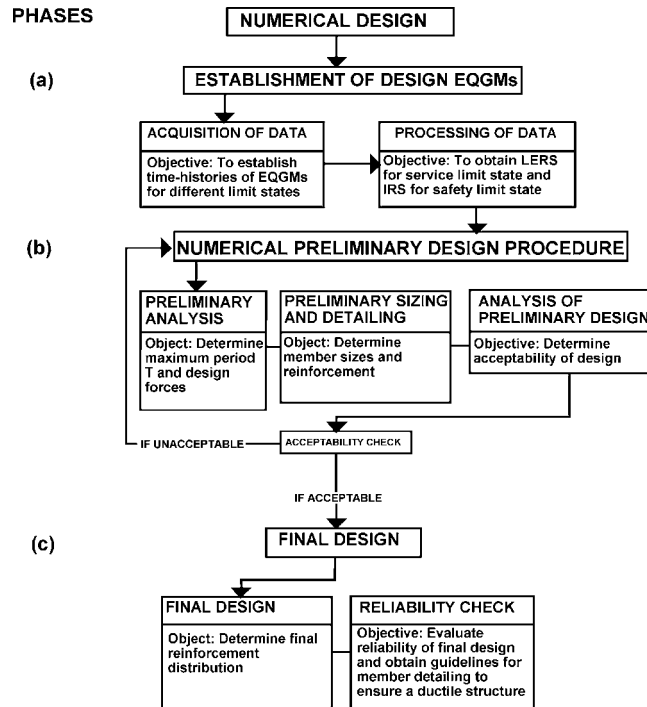


FIGURE 8.1 Steps of the numerical design.

Given: Site of building (soil profile and topography).

Required: Return periods for different levels of possible EQGMs at the site and their damage potential to the entire building system and EQGM time-histories for all the four different performance levels that have to be considered according to the selected P-BDO matrix. It is discussed in Bertero and Bertero (2002) that for preliminary design it is desirable to select at least two of the four performance levels. According to the present available data and experience it is shown in Bertero and Bertero (2002) that selecting the service and safety performance levels is in general the best option.

Solution: Conduct a reliable analysis of the site to assess its suitability for the construction of the desired building. This will be required to identify all the sources of EQGMs that could affect the building; define the seismic activity at the site due to all possible earthquake sources in the form of time histories and recurrence periods (T_R) of EQGMs; select T_R for at least two sets of EQGMs corresponding to the limit states (the service and the safety performance levels).

Ideally, acquisition of data should be based on EQGM records obtained at the site. If there are not enough of such records, the data can be obtained either from EQGMs recorded at sites with similar soil profile and topography, or by using numerical synthesis (Stewart et al., 2001 and Chapters 4 and 5) to generate several probable EQGM time histories.

8.3.2.2 Processing of Data

In this step, the available data about probable future EQGMs at the site are processed to facilitate reliable selection of the *design EQs*. Conceptually, a design earthquake should be the *critical EQGM* for the limit state under consideration, i.e., the EQGM that drives the structure to its critical (maximum) response for the performance level under study. The application of this simple concept in practice has serious difficulties. It has been shown that the reliability of the design earthquakes recommended by current seismic codes is highly questionable. According to recent studies (Bertero, 1991, 1992; Bertero and Bertero, 1993; Bertero and Bertero, 1992; Bertero and Teran-Gilmore, 1993; Bertero and Uang, 1992; Fajfar and Krawinkler, 1997), the problems involved in this step, and their solutions, can be summarized as follows:

Given: Time histories of probable EQGMs at the site for service and safety limit states.

Required: To consider effects on structural and nonstructural components, contents and human sensitivity

- For serviceability limit state: at least the smoothed linear elastic design response spectra (SLEDRS) for strength, C_s , displacement, S_d , pseudovelocity, S_v , total acceleration, total S_a and even jerk for different damping coefficient or ratio (ξ).
- For safety limit state: the SLEDRS and smooth inelastic design response spectra (SIDRS) (for different values of the displacement ductility ratio, μ , and ξ) for C_s , S_d , S_v , total S_a and for the parameters needed for evaluation of the cumulative damage caused for cyclic load reversals [input energy (E_I), energy dissipation (E_D) considering hysteretic damping energy ($E_{H\xi}$), hysteretic plastic deformation energy ($E_{H\mu}$), cumulative ductility ratio (μ_a), number of yielding reversals (NYR), number of equivalent Yielding cycles at maximum μ (NEYC $_{\mu_{max}}$) and damage spectra].

Solution: Computation of the linear elastic response spectra (LERS) and the inelastic response spectra (IRS) (for different values of μ and ξ) for C_s , S_d , S_v , total S_a for each possible EQGM that can be originated at the site from the earthquake sources. From statistical studies of LERS and IRS find SLEDRS and SIDRS, respectively. In smoothing the LERS and IRS, close consideration should be given to the standard deviation, σ , as well as to the uncertainties in the estimation of the dynamic characteristics of future EQGMs (particularly regarding the estimation of the predominant soil period, T_g , according to the site conditions) and the estimation of the fundamental period of the structure. To obtain the critical EQGMs safety level, where some damage is tolerated (i.e., $\mu > 1$), it is necessary to compute for each EQGM the following spectra: E_I , $E_{H\xi}$, $E_{H\mu}$, μ_a , NYR and NEYC $_{\mu_{max}}$ and hysteretic behavior time history. Selection of critical EQGMs can be simplified using proposed damage indices such as modified Park and Ang (1985), Mehanany and Deierlein (2001), Bozorgnia and Bertero (2002) and by the introduction of the factor γ , as discussed in Bertero and Bertero (1992), Bertero and Teran-Gilmore (1993), Fajfar and Krawinkler (1997) and Fajfar (1992).

8.3.3 Numerical Preliminary Design Procedure

This second phase of the proposed conceptual methodology (*phase b*) is devoted to the preliminary design (sizing and detailing of the members and their connections and supports) of the entire building system against the critical combinations of the established design earthquakes with other excitations that can act on the building according to its location and site. As illustrated in Figure 8.1, to arrive at the desired final design it is necessary to start with a preliminary design procedure. The main objective of this phase is to obtain a design that is as close as possible to the desired final design. As illustrated in Figure 8.1, the preliminary design procedure consists of three main steps: (1) preliminary analysis; (2) preliminary sizing and detailing and (3) analysis of preliminary design. Although in Figure 8.1 these steps have been drawn as independent steps, it is important to realize that because seismic demand on a structure depends strongly on the stiffness and strength supply to such structure, the three steps are not independent, and an iterative process is needed.

8.3.3.1 Preliminary Analysis (Part I)

The preliminary analysis can be formulated as follows (Figure 8.2):

Given: Function of building and desired performance design objectives; general configuration, structural layout, structural system, structural materials and nonstructural components and contents (which should have been selected using the guidelines developed for conceptual overall seismic design (Bertero, 1979, 1980, 1992); gravity, wind, snow and other possible loads or excitations; and displacement, strength and dissipated hysteretic energy due to μ and ξ (i.e., $E_{H\mu}$ and $E_{H\xi}$) design spectra for different damping and ductility for frequent minor and rare major EQGMs.

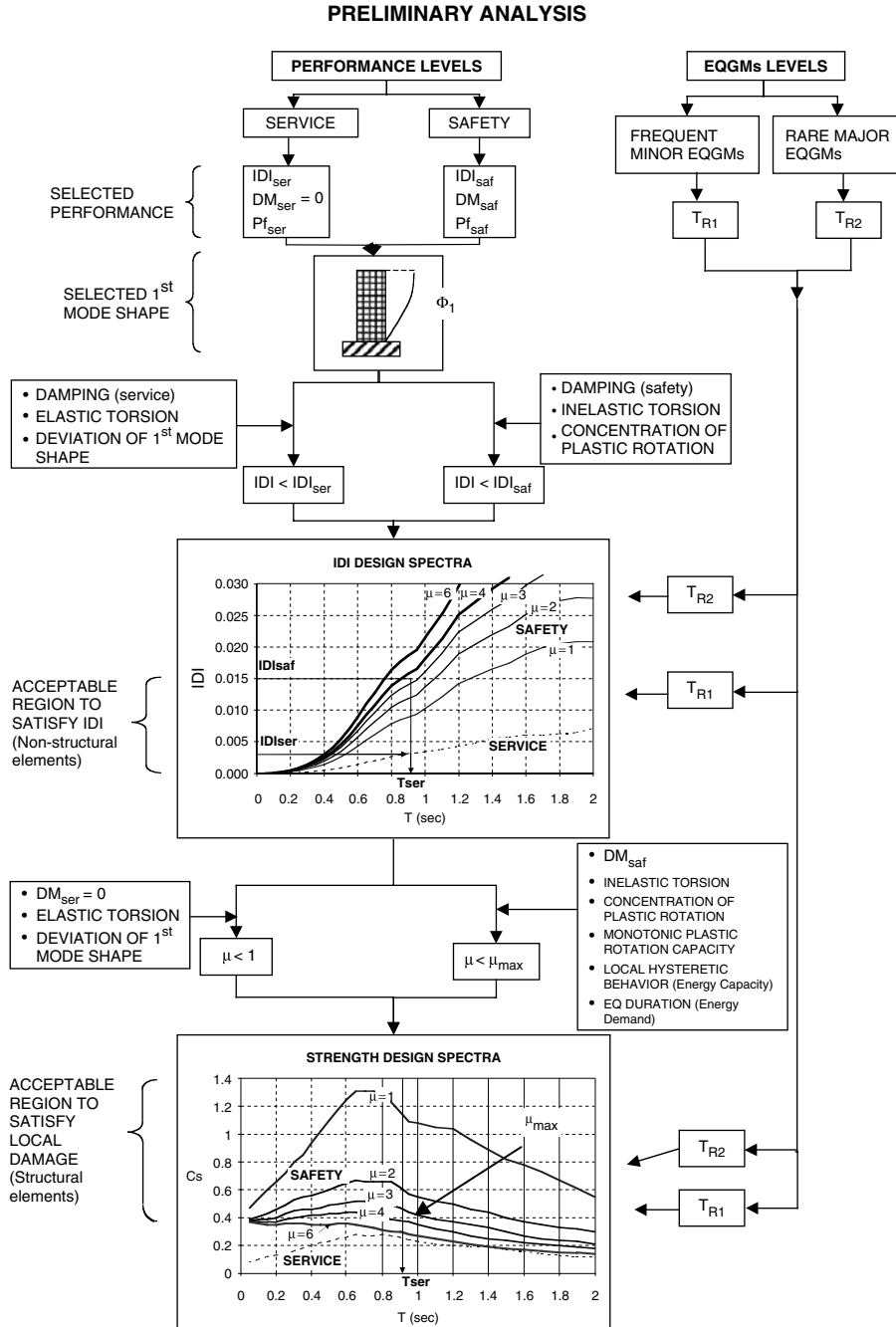


FIGURE 8.2 Flowchart of preliminary analysis.

Required: Establishment of design criteria (according to the acceptable damage levels involved in the desired performance levels when subjected to the corresponding EQGM levels and the levels of other significant excitations), i.e., to establish the minimum lateral stiffness (or maximum period T), minimum strength and minimum toughness of the building that are capable of controlling the design seismic forces, the critical load combinations and the elastic and inelastic

deformations, particularly those that could cause discomfort to the occupants and damage to the nonstructural and structural components.

Solution: To use a comprehensive approach that takes into account from the beginning that the building structure is a MDOF and there can be important torsional effects even under service EQGMs (i.e., in the linear elastic response) and that for the inelastic deformations under the EQGMs corresponding to the safety PL these effects can be different; and that it is also necessary to consider the desired damage index (control of damage) taking into account the second-order effects and the effects of the cumulative damage (or cumulative ductility) due to the inelastic hysteretic behavior of the critical regions of members and of their joints, and the plastic deformations and the corresponding ductility ratio, μ , that can be used, as well as the expected overstrength. A short discussion of the main aspects of the preliminary analysis follows.

8.3.3.1.1 Performance Design Objectives.

To decide about the performance design objectives, the designer should discuss with the client the severity of the expected potential sources of seismic hazards and their corresponding frequency (return period) as well as the number of discrete PLs that should be considered. According to the adopted definition of P-BSD, the following minimum performance levels should be considered initially: (a) Serviceability, (b) fully operational, (c) operational, (d) life safety and (e) near collapse. As discussed in Appendix A of the SEAOC Vision 2000 Committee Report (1995), after the owner expresses the desired return or recurrence period of each of the limit states associated with these PLs, compromise should be reached on such selection depending on the severity of the expected EQGMs at such recurrence periods and the cost of designing for such levels and the probable losses during the life of the structure. Once an agreement has been reached on the PLs and their respective recurrence period, the designer has to establish the corresponding minimum performance design objectives.

The designer should explain to the owner that the following are the minimum design objectives (SEAOC Vision 2000 Committee Report), as well as the initial cost of construction that will demand such design and the probable cost of losses if the limit states associated with the selected performance levels are reached (note that the owner might elect to associate the desired PL with more severe EQGMs than those corresponding to the minimum levels).

- Resist minor EQGMs, which can occur frequently, without damage (service or fully operational limit state).
- Resist moderate EQGMs, which can occur occasionally with controlled structural and nonstructural damage (amount of damage depends on function of facility) (operational limit state)
- Resist expected major EQGMs, which can occur rarely, with controlled damage that cannot endanger the life safety of its occupants or those of adjacent facilities (life safety limit state).
- Resist extreme EQGMs, which can occur very rarely but are probable, with damage up to impending collapse but without collapsing and endangering the lives of its occupants or inducing damage to surrounding facilities (impending collapse limit state).

Already in the SEAOC Vision 2000 Committee Report (1995) it has been noted that for preliminary design, although it would be ideal to carry out the numerical preliminary EQ-SD considering the four or five discrete PLs involved in the P-BDO matrices that have been proposed, in most of the cases, this would not be necessary; according to the data available regarding the seismic hazards levels (SHLs) only a few of the objectives will dominate (control) the design. Furthermore, this report recommended that the preliminary P-BSD be conducted considering at least two of the DO — usually those corresponding to the following PLs: (serviceability and life safety), or (fully operational or operational and life safety or impending collapse). The ideal possible combination of all possible ones is the one requiring just linear elastic analysis and design procedures, i.e., serviceability or fully operational and the other requiring the use of nonlinear analysis and design procedures (particularly just plastic procedures), that is, life safety or impending collapse. The authors have previously recommended that at present it is convenient to use the serviceability and life safety because these are the two DOs for which there are more reliable data and experience.

TABLE 8.1 Performance Design Objectives

Recurrence Interval (years)	EQGM Level			
	Structural Damage		Non-structural Damage	
	Local Damage	Failure Prob.	IDI	Failure Prob.
Serviceability	10	0.00	16%	0.003
Life Safety	500	0.80	16%	0.015

As will be discussed in more detail in Section 8.4 for the application of the proposed CCA to the ten-story building having an RC-SMRF structural system, after an analysis of the requirements for the serviceability and fully operational PLs and the available data for the corresponding hazards to these two PLs it was decided that the serviceability DO will control the elastic demand response. Furthermore, it was also decided that in view of the uncertainties regarding the data on the EQGMs available for these two PLs, it will be desirable to use a probabilistic approach similar to the present conventional LRFD approach rather than to use allowable stress design as required by ACI Codes before the 1998 edition when dealing with service loads. In Section 8.4.3.1, it is shown the equivalence between Serviceability using allowable stresses and First Yielding using LRFD. In view of the high uncertainties in the data available of the recorded EQGMs considered as the ones corresponding to the $T_R = 10$ years (adopted for the serviceability PL), it was also decided not to use the load factor recommended in recent codes but the ones probabilistically obtained as shown in Section 8.2.3. which when applied to service DOs involving EQGM excitations can be written as

$$(1 + \beta_{ser} COV_{EQ_{ser}}) \overline{EQ_{ser}} + 1.20D_n + 0.24L_n + 0.20S_n \quad (8.5a)$$

$$- (1 + \beta_{ser} COV_{EQ_{ser}}) \overline{EQ_{ser}} + .090D_n \quad (8.5b)$$

The designer must select the probability of unacceptable performance of the building (i.e., β_i) for each possible combination of performance level and the corresponding earthquake hazard level selected for design. Table 8.I summarizes the selected limit state design criteria for two levels of earthquake hazard for a particular building. In this case 16% has been selected, since for this probability of unacceptable performance the earthquake design demand corresponds to the mean plus one-sigma spectra as it has been done in practice. Note that $\Phi(-\beta) = 0.16 \rightarrow \beta = 1.0$ and therefore in Equation 8.5a,b, the first term is $(1 + 1.0 COV_{EQ_{ser}}) \overline{EQ_{ser}} = \overline{EQ_{ser}} + \sigma_{EQ_{ser}} = \overline{EQ_{ser}}$, i.e., the mean plus one sigma spectra. Analogous equations can be written for life safety PL, i.e., under mean plus one-sigma EQGM service spectra.

A small target $IDI_{ser} = 0.003$ was selected for serviceability (i.e., under mean plus one-sigma EQGM service spectra) because sensitive partitions (early first cracking) were selected for architectural reasons. Note that since independent requirements have been selected for structural and nonstructural components, the ratio $IDI_{saf}/IDI_{ser} = 0.015/0.003 = 5$ does not imply that the structure reaches a ductility ratio of 5. This happens because if the nonstructural components control the design for service, most of the structure does not reach first yielding at $IDI_{ser} = 0.003$ but does so at larger values.

8.3.3.1.2 Analysis of Gravity, Wind and Other Possible Loads or Excitations

On the basis of structural geometry and building function, gravity, wind and other probable excitations are computed, and the reactive masses to be lumped at each floor level are estimated.

8.3.3.1.3 Analysis of Critical Load Combinations

Serviceability Limit State — For serviceability (i.e., the load combination that in a period of 10 years has a probability of 16% of producing the first yielding), the following load combinations were selected:

$$D_n + L_n \quad D_n + 0.4L_n \pm 1.0W_n \quad 1.05D_n + 0.24L_n \pm 1.0EQ_{ser} \quad (8.6)$$

where D_n is the nominal dead load, L_n is the nominal live load (reduced considering the tributary area), W_n is the nominal wind load and EQ_{ser} is the mean plus one-sigma spectra seismic demand for service estimated as described in Sections 8.3.2.2. and 8.3.3.1.1.

Life Safety Limit State — For life safety (i.e., the load combination that in a period of 500 years has a probability of 16% of producing a level of local damage index $DM = 0.8$ [precollapse] of the structure) the following load combinations were selected:

$$\begin{array}{lll} 1.4 D_n & 1.2 D_n + 1.6 L_n \\ 0.9 D_n - 1.3 W_n & 1.2 D_n + 0.5 L_n + 1.3 W_n & 1.05 D_n + 0.24 L_n \pm 1.0 EQ_{saf} \end{array} \quad (8.7)$$

where D_n is the nominal dead load, L_n is the nominal live load (reduced considering the tributary area), W_n is the nominal wind load and EQ_{saf} is the mean plus one-sigma spectra seismic demand for safety estimated as described in Sections 8.3.2.2. and 8.3.3.1.1.

8.3.3.1.4 Estimation of Damping Ratios.

Energy dissipation not associated with damage is typically accounted for using a viscous damping model. Based on structural materials and structural system, the first mode damping ratio for serviceability and life safety limit state, ξ_{ser} and ξ_{saf} , is estimated. The trend of having less damping as the height of the building increases due to the smaller effects of the radiation damping at the foundations relative to the dissipation of energy at the building itself, the effect of the interaction of the structure with nonstructural elements as well as the fact that these effects can be considerably different for small and large EQGMs, should be considered for evaluation of damping.

8.3.3.1.5 Selection of First Mode Shape.

For preliminary design, the torsion effects will be introduced by amplifying the assumed translational response of the building. Therefore, considering only translational modes, a good estimation of the response of tall buildings can be obtained using the first mode for displacements and the first three modes for story shears (Cruz and Chopra, 1986). For preliminary analysis, only the first mode shape Φ_1 can be selected. Φ_1 can be selected taking into account that

$$\begin{cases} \Phi_{1i} = \frac{z_i}{H} & \text{for linear first mode} \\ \Phi_{1i} \equiv 1 - \cos\left(\frac{\pi z_i}{2 H}\right) & \text{for uniform flexural beam} \end{cases} \quad \Phi_{1i} = \sin\left(\frac{\pi z_i}{2 H}\right) \quad \text{for uniform shear bear} \quad (8.8)$$

where, z_i is the height of the i floor; and H is the total height of the building. Using the mass matrix of the structure, M , obtained from the lumped masses as mentioned in Section 8.3.3.1.2, the parameters of an equivalent SDOF system (generalized-mass, M_1 , and earthquake-excitation factor, Γ_1) can be computed as

$$\Gamma_1 = \Phi_1^T M r \quad M_1 = \Phi_1^T M \Phi_1 \quad (8.9)$$

where, $r^T = [1 \quad \dots \quad 1]$.

8.3.3.1.6 Estimation of Maximum Building Period to Satisfy Serviceability

Assuming that the LEDRS for displacement, $S_d(T, \xi_{ser})$, was obtained following the guidelines of Section 8.3.2, and considering just the first mode elastic response, the following equation has been developed (Bertero and Bertero, 1992; Bertero, 2002) to obtain an upper limit of the design period for the first mode of the structure

$$IDI_{\max} = \frac{\Gamma_1}{M_1} \left(\frac{\Delta\Phi_{li}}{h_i} \right)_{\max} \beta_0 \beta_1 S_d(T_1, \xi_{ser}) \leq IDI_{ser} \Rightarrow T_{1ser} \quad (8.10)$$

where, β_0 is the IDI increase due to deviation of assumed first mode shape; β_1 is the IDI increase due to elastic torsion; $(\Delta\Phi_{li}/h_i)_{\max}$ is the maximum IDI of the first mode shape Φ_1 and h_i is the story height of the i story.

The output of this step is the maximum period of the building, T_{1ser} , to satisfy the required maximum IDI_{ser} for service limit state. For example, from Figure 8.3(a) considering $IDI_{ser} = 0.003$ (Table 8.1.) a maximum period of $T_{1ser} = 0.90$ sec is obtained.

8.3.3.1.7 Estimation of Maximum Building Period and Maximum Global Ductility to Satisfy Life Safety

Assuming that the IDRS for displacement, $S_d(T, \xi_{ser}, \mu)$, was obtained following the guidelines of Section 8.3.2.2., and considering just the first mode elastic response the following equation has been developed (Bertero and Bertero, 1992; Bertero, 2002) to obtain the expected IDI of the building

$$IDI_{\max} = \frac{\Gamma_1}{M_1} \left(\frac{\Delta\Phi_{li}}{h_i} \right)_{\max} \beta_2 \beta_3 S_d(T_1, \xi_{saf}, \mu) \leq IDI_{saf} \quad (8.11)$$

where, β_2 is the IDI increase due to concentration of plastic rotations in one story; β_3 is the IDI increase due to inelastic torsion; μ is the global displacement ductility ratio of the equivalent SDOF system. The importance of increasing the IDI due to the concentration of plastic rotation has been discussed in 8.2.4. and in more detail in Bertero (2002).

As shown in Bertero and Bertero (2002), the maximum local damage, DM_L , can be estimated using

$$DM_L = \left(\frac{IDI - \frac{IDI}{\mu}}{IDI_{umon} - \frac{IDI}{\mu}} + b\gamma^2\mu \frac{IDI}{IDI_{umon}} \right) \beta_2 \beta_3 = \left(\frac{IDI - \frac{IDI}{\mu}}{\theta_{umon} - \frac{IDI}{\mu}} + b\gamma^2\mu \frac{IDI}{\theta_{umon}} \right) \beta_2 \beta_3 \quad (8.12)$$

where, θ_{umon} is the ultimate plastic hinge rotation under monotonic increasing deformation for the critical region, IDI_{umon} is the ultimate IDI under monotonic increasing deformation, IDI is the maximum IDI during the response to the EQGM corresponding to the life safety PL, μ is the maximum global displacement ductility ratio of the equivalent SDOF system during the EQGM, b is a parameter controlling strength deterioration as a function of the amount of dissipated energy by plastic deformation and the parameter γ as defined by Fajfar (1992). Recently Bozorgnia and Bertero (2002) have proposed some modification to Equation 8.12.

θ_{umon} and b depend on the designer decision about kind of connections, detailing, level of axial load and shear at critical hinges and aspect ratio of members. For example, for RC structures the designer could increase the amount of ties at critical plastic hinges (increasing θ_{umon}) to increase the maximum acceptable ductility, or decrease the maximum acceptable ductility for steel structures where welding or local buckling leads to failure under a few inelastic cycles (large b). The spectra corresponding to Equations 8.10 to 8.12 are shown in Figure 8.3. Considering the maximum period required to satisfy IDI_{ser} and the maximum IDI and local damage to satisfy life safety, the acceptable design zone are the rectangles shown in Figures 8.3(a) and (b). If the designer selects the period and ductility inside this zone, serviceability and safety limit state are satisfied. In general, from an economical point of view, it is better to select the period and global ductility from the upper right zone of the rectangle in the graphs of Figure 8.3 (for example, $T = 0.90$ sec and $\mu \geq 3.50$ could be selected in this case).

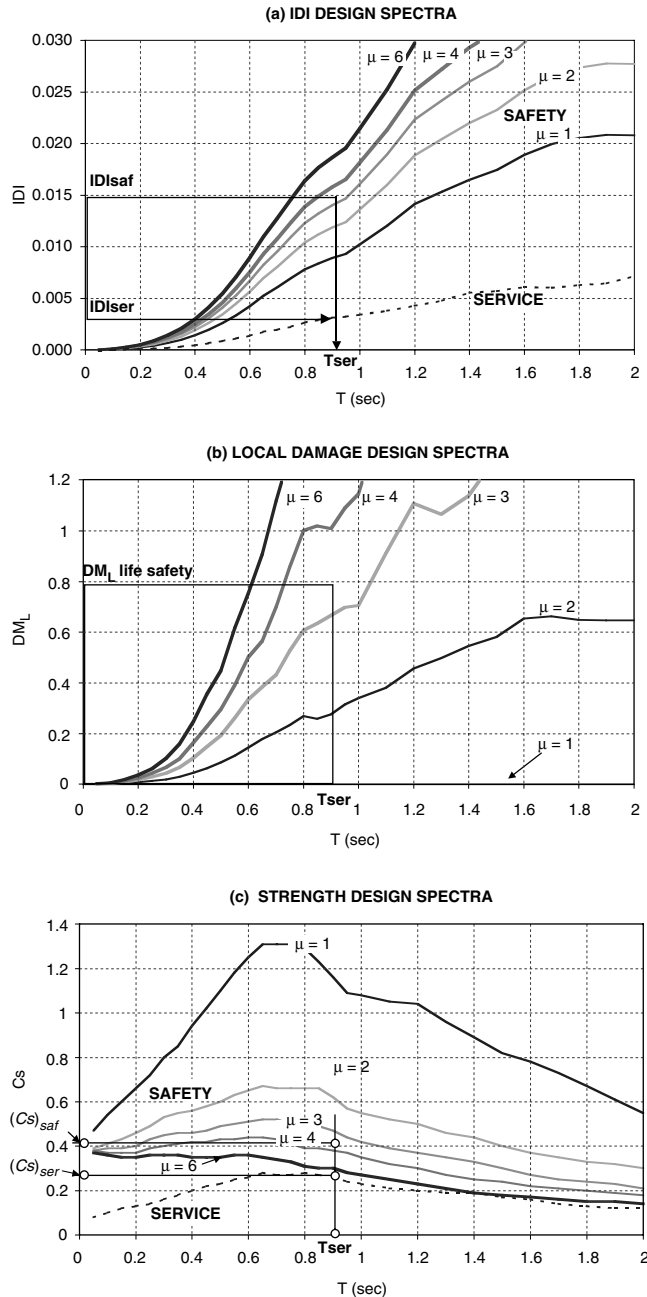


FIGURE 8.3 (a) IDI; (b) local damage; and (c) strength design spectra.

8.3.3.1.8 Estimation of Minimum Equivalent SDOF Strength To Satisfy Serviceability and Life Safety. Once the period T and the global ductility μ are selected as shown in Section 8.3.3.1.7, $S_a(T, \xi_{ser}) = C_s(T, \xi_{ser}, \mu \leq 1)$ define a lower bound on the equivalent SDOF strength to satisfy serviceability ($DM_{ser} = 0$, i.e., elastic behavior) and $C_s(T, \xi_{saf}, \mu)$ define a lower bound on the equivalent SDOF strength to satisfy life safety ($DM_L \leq DM_{saf}$) as shown in Figure 8.3.(c). Note that Equation 8.12 sets the relationship between the maximum local damage (DM_L) of the real MDOF system and the global ductility μ of the equivalent SDOF.

8.3.3.2 Preliminary Sizing and Detailing

The preliminary sizing and detailing step can be stated as follows:

Given: Gravity, wind, snow and other possible loads or excitations; minimum stiffness and strength of an equivalent SDOF system required to satisfy the selected seismic performance; critical load combinations and mechanical characteristics of the structural and nonstructural materials.

Required: Preliminary sizing and detailing of both the structural elements (beam and column sizes and their flexural reinforcements [in the case of moment-resisting space frames]), and the unintentional structural (sometimes called nonstructural) components, which can affect the seismic response of the building.

Solution: (a) To select a first period, T_1 , inside the acceptable zone defined in the preliminary analysis. (b) Using T_1 and the selected first mode shape, to obtain a preliminary sizing for stiffness. (c) Based on these preliminary member sizes, to select a minimum equivalent SDOF strength (or a maximum equivalent SDOF global ductility) inside the acceptable zone defined in the preliminary analysis. (d) Considering MDOF and torsional effects, as well as the expected overstrength, to obtain the seismic design loads for service and safety limit states. (e) Based on application of linear optimization theory, design beams and columns in each story to minimize volume of flexural reinforcement (in the case of RC), using practical requirements and service forces and their moments as constraints so the preliminary design simultaneously considers demands for serviceability and safety.

In the following sections we present the equations developed for doing the preliminary sizing for stiffness and strength, and for obtaining the seismic design loads for service and safety limit state considering MDOF and torsion effects, as well as overstrength. Note that obtention of design forces, estimation of overstrength and attainment of elastic moments to be used as constraints of the optimization design are part of the preliminary analysis rather than of the design step. However, since they are intermediate steps between preliminary sizing for stiffness and preliminary sizing and detailing for strength, they are included in the preliminary design of sizes and reinforcement for the sake of simple presentation. A flowchart for preliminary sizing and detailing is shown in Figure 8.4.

8.3.3.2.1 Preliminary Sizing for Stiffness

Story Stiffness to Satisfy Target Period and First Mode Shape. — It can be proved (Bertero, 2002) using the equilibrium of elastic and inertia forces at each story of the shear beam mathematical model of a building with lumped story masses, m_i (shown in Figure 8.5) that a building with target period T_1 ($\omega_1 = 2\pi/T_1$), and first mode shape Φ_1 is obtained if the story stiffness, k_i , is selected so that

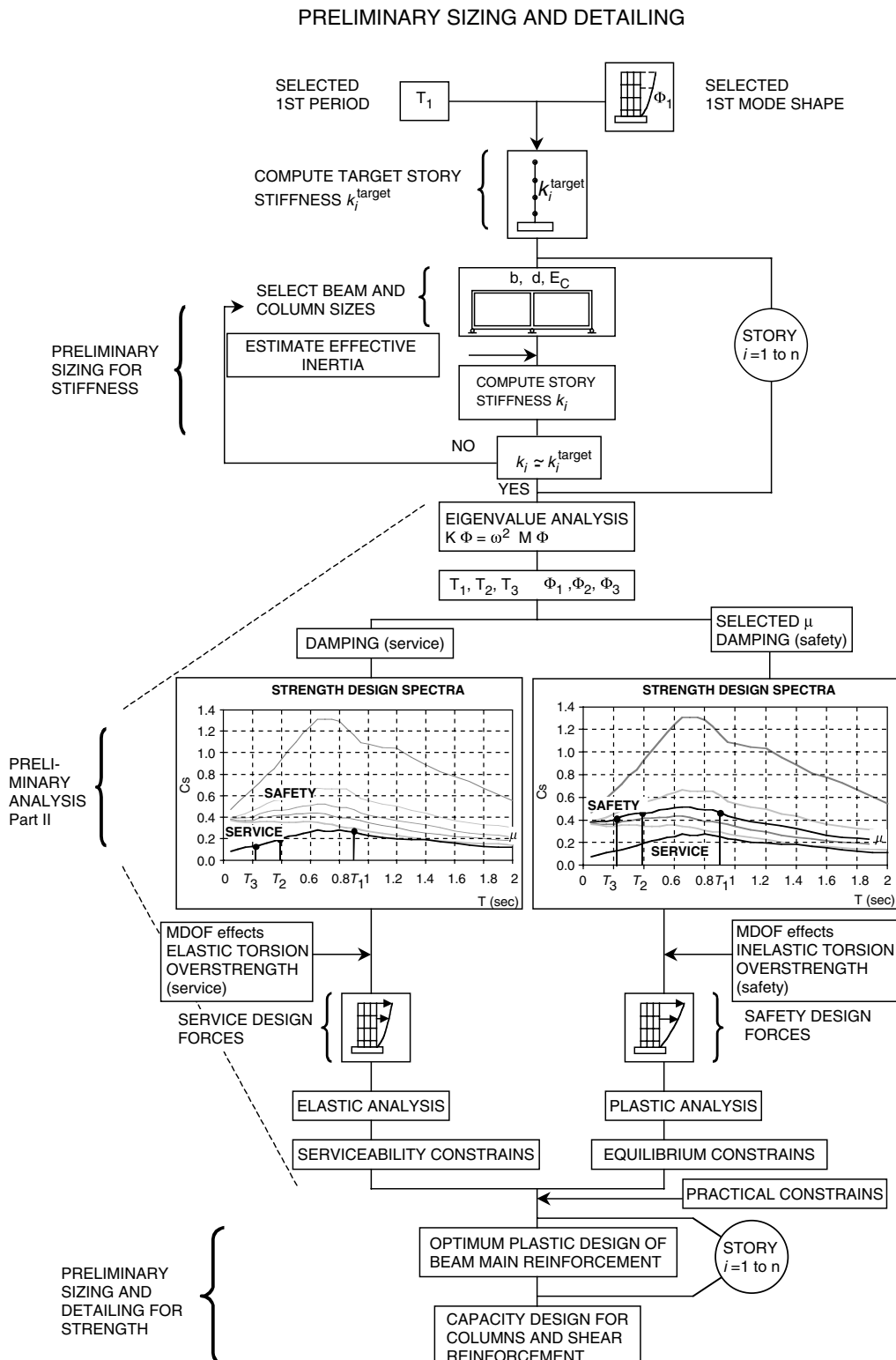
$$k_n = \omega_1^2 m_n \frac{\Phi_{I_n}}{\Phi_{I_n} - \Phi_{I_{n-1}}} , \quad k_i = \omega_1^2 m_i \frac{\Phi_{I_i}}{\Phi_{I_i} - \Phi_{I_{i-1}}} + k_{i+1} \frac{\Phi_{I_{i+1}} - \Phi_{I_i}}{\Phi_{I_i} - \Phi_{I_{i-1}}} \text{ for } i = n-1 \dots (8.13)$$

Selection of Member Sizes to Satisfy Stiffness Requirements — For moment-resisting frames, the preliminary sizes of columns and beams can be obtained considering inflection point at mid-height of the columns and neglecting axial and shear deformations, so that the story stiffness can be written as (Figure 8.6)

$$k_i = \frac{12}{(1+\Psi_i)} \sum_{j=1}^{N_c} \left(\frac{E_c I_{cj}}{L_c^3} \right)_i \quad (8.14)$$

where Ψ_i is the stiffness ratio between columns and beams of story i computed as

$$\Psi_i = \frac{\sum_{j=1}^{N_c} (E_c I_{cj} h)_i}{\frac{1}{2} \sum_{j=1}^{N_b} \left[\left(\frac{E_b I_{bj}}{L_j} \right)_i + \left(\frac{E_b I_{bj}}{L_j} \right)_{i-1} \right]} \quad (8.15)$$

**FIGURE 8.4** Flowchart of preliminary sizing and detailing.

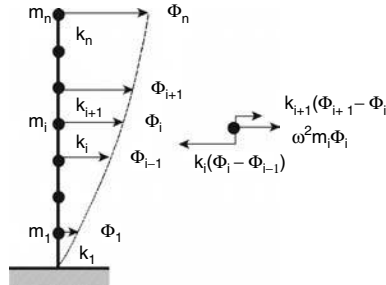


FIGURE 8.5 Mathematical model of the building.

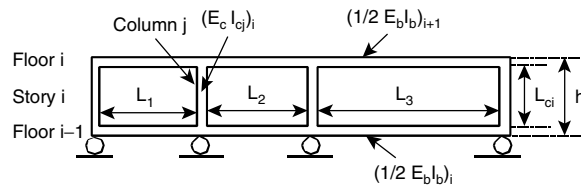


FIGURE 8.6 Substructure to estimate story stiffness for moment resisting frames.

where, N_c is the number of columns in the frame; N_b is the number of beams in the frame; I_c is the effective moment of inertia of columns; I_b is the effective moment of inertia of beams; L_c is the clear height of columns; h is the height of the story; L is the clear span of beams; E_c, E_b is the modulus of elasticity of columns and beams.

If for each story i , it is $L_1 \equiv L_2 \equiv \dots \equiv L_{N_b}$, $I_{c1} \equiv I_{c2} \equiv \dots \equiv I_{cN_c}$, $I_{b1} \equiv I_{b2} \equiv \dots \equiv I_{bN_b}$ (i.e., the spans, the column stiffness and the beam stiffness at a story i are approximately equal) and $E_b = E_c$ (i.e., same concrete is used for beams and columns at story i), then Equations 8.14 and 8.15 can be written as

$$k_i = \frac{N_c}{1 + \Psi_i} \left(\frac{12 E_c I_c}{L_c^3} \right)_i, \quad \Psi_i = \left(\frac{N_c I_c L h}{N_b I_b L^2} \right)_i \quad (8.16)$$

Note that if the assumption of fixed base is done, inflection point at the first story is higher than midheight of the column. Therefore, a first story height h_1 smaller than the real one should be selected to compute the stiffness k_1 of the first story using Equations 8.14 to 8.16

From a given structural layout (h, L, N_c, N_b) $_i$ and structural material (E_c) $_i$, the designer can select column and beam sizes of each story to approximately satisfy the target story stiffness computed from Equations 8.13. To start the process, the designer can use beams and column sizes from gravity design forces, architectural constraints, statistical data from similar buildings and his/her own experience. Using the equations of this section and a spreadsheet program, the preliminary sizing can be quickly done interactively by trial and error. It should be noted that a large uncertainty exists on effective moment of inertia of RC members, especially at this stage of the design, since the effective moment of inertia is particularly sensitive to the amount of the reinforcement (unknown until the design for strength is done).

Problems in the design for stiffness of RC buildings

- **Effective Stiffness of an RC Member.** The main problem is that the effective stiffness of an RC member is a function of the geometrical sizes of the member. The effective stiffness of an RC member at a particular time depends on the sizes, steel amount and detailing, present deformation

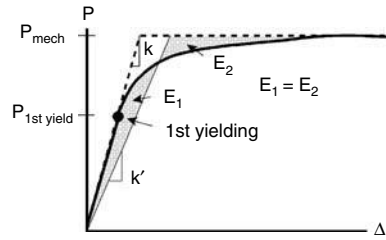


FIGURE 8.7 Stiffness of an equivalent SDOF system.

state, level of axial load and shear along the member, and on the history of load, temperature and shrinkage strains of that member. Even the stiffness of the structure as a whole depends on the amount of rotation that occurs at the end of the members connected at joints and supports (due to slipping of rebars at the joints), interaction with nonstructural elements and soil-structure interaction (SSI) at the foundations.

The uncertainties in the effective stiffness must be considered in the design. Possible approaches are discussed in Bertero and Bertero (1992) and Bertero (2002). In general, $I_{b\text{ eff}} = 0.5 I_{bgross}$ for beams (assumed reinforcement ratio $\rho \approx 0.01$) and $I_{c\text{ eff}} = I_{cgross}$ for columns (assumed to remain under compression during the response) can be used as mean values, where I_{bgross} and I_{cgross} are the gross stiffness of beams and columns. For safety and other damage control limit states, these effective values can be used to obtain the initial elastic stiffness. The complex nonlinear behavior of the members is simplified using a bilinear model that tries to fit the real moment-curvature diagram. The initial linear elastic stiffness is represented by the effective values defined above. After the yielding of the main reinforcement, the deformation hardening is approximated by a line from the yielding point to the point corresponding to the ultimate moment and curvature of the element.

On the other hand, the nonlinear behavior of the structure is considered in the SDOF model used to obtain displacement, strength and damage spectra for preliminary design as described below.

- **Equivalent SDOF System Stiffness.** In the process of using a SDOF system to start the structural design, an equivalent SDOF system has to be defined to represent the elastic and inelastic behavior of the MDOF structure. If the structure has a behavior like that represented in Figure 8.7 (i.e., a gradual formation of plastic hinges and a large difference between first yielding strength and ultimate strength), how the equivalent SDOF model is defined affects the values of the periods that should be considered for serviceability and safety limit state. For example, if a bi-linear model is defined using the equal energy concept, the period $T_{1\text{ser}}$ could be computed using the stiffness at first yielding k for serviceability, while for safety, a larger period $T_{1\text{saf}}$ could be used from the equivalent stiffness k' .
- **Overstiffness.** This is any unintentional stiffness present in the building and not explicitly considered in the equations used to estimate the stiffness of the structure, for example, due to nonstructural components. The overstiffness could be considered in the design process affecting the period T_1 computed from the equations of this Section 8.3.3.2.1. by a reduction factor that could be different for service and safety limit state and whose value should be obtained from the evaluation of statistical data of measured similar buildings.

8.3.3.3 Preliminary Analysis (Part II). Seismic Design Forces

Once member sizes are selected, the story stiffness, k_i , can be estimated (Section 8.3.3.2.1) and the structure stiffness matrix K can be computed. Since K and M have now been estimated, the periods, T_i , modal shapes, ϕ_i , and modal parameters M_i and Γ_i can be obtained. In general, only the first three modes ($i = 1, 2, 3$) need to be considered (Cruz and Chopra, 1986).

8.3.3.3.1 Serviceability Seismic Design Forces

The total base shear can be estimated from the elastic response spectra and the modal parameters as (Clough and Penzien, 1992)

$$V = W \sqrt{\sum_{i=1}^3 \left[\frac{\Gamma_i^2}{M_i} \frac{S_a(T_i, \xi_{ser})}{Mg} \right]^2} \quad (8.17)$$

where W is the total weight and M is the total mass of the building.

The base shear in each structural plane j can be computed taking torsion into account as

$$V_j = \frac{k_j}{K} \beta_{lj} V \quad (8.18)$$

where, k_j/K is the relative stiffness of the frame j with respect to the total stiffness in the considered direction, β_{lj} is the factor to take into account elastic torsion for the j plane of stiffness.

However, because the final designed and constructed structure has a first yielding base shear higher than the level for which it was designed, the design base shear for serviceability can be reduced considering such overstrength, OVS_{ser} , as

$$V_{ser} = \frac{V_{1st\ yield}}{1 + OVS_{ser}} = \frac{V_{1st\ yield}}{\Omega_{ser}} \quad (8.19)$$

Some guidelines for selecting Ω_{ser} are discussed in Bertero (2002). Note that V_{ser} is actually the factored service demanded shear and consequently in computing the necessary shear capacity to the structural elements this capacity should be based on the yielding strength and not on the allowable stresses, strains, forces and deformations, i.e., the real mechanical behavior on which the service PL has been and should physically be defined.

The serviceability design shear for each story k of the building can be computed as

$$S_{ser_k} = \sqrt{\sum_{i=1}^3 \left[\sum_{f=k}^n m_f \Phi_{if} \frac{\Gamma_i}{M_i} S_a(T_i, \xi_{ser}) \right]^2} \frac{1}{\Omega_{ser}} \quad (8.20)$$

where, m_f is the reactive mass lumped at floor f .

The service design shear, S_{jk} , in the k story of the frame (structural plane) j can be computed taking torsion into account as

$$S_{jk} = \frac{k_j}{K} \beta_{lj} S_{ser_k} \quad (8.21)$$

Finally, the service design forces, F_{jk} , at each floor k of frame (structural plane) j can be computed using

$$F_{jk} = S_{jk} - S_{j(k+1)} \quad (8.22)$$

8.3.3.3.2 Life safety seismic design forces

Assuming the simultaneous formation of all the plastic hinges that transform the structure into a mechanism, the demanded base shear for safety can be estimated from the SIDRS and the assumed modal parameters as

$$V_{mech} = W \sqrt{\sum_{i=1}^3 \left[\frac{\Gamma_i^2}{M_i} \frac{C_s(T_i, \xi_{saf}, \mu)}{M} \right]^2} \quad (8.23)$$

However, because the final designed and constructed structure has a strength higher than the strength for which it was designed, the demanded design shear base can be reduced considering such overstrength, OVS_{saf} , as

$$V_{saf} = \frac{V_{mech}}{I + OVS_{saf}} = \frac{V_{mech}}{\Omega_{saf}} \quad (8.24)$$

Some guidelines for selecting Ω_{saf} are discussed in Bertero (2002) and Miranda (1991). The safety design shear for each story k can be computed as

$$S_{saf_k} = \sqrt{\sum_{i=1}^3 \left[\sum_{f=k}^n m_f \Phi_{if} \frac{\Gamma_i}{M_i} g C_s(T_i, \xi_{saf}, \mu) \right]^2} \frac{1}{\Omega_{saf}} \quad (8.25)$$

Inelastic torsion effects are included with a coefficient β_4 , which was developed using rigid-plastic analysis Bertero (1995). The base shear, V_j , in each frame (structural plane) j can be computed so that $\sum V_j = \beta_4 V_{saf}$. Note that, because service constraints regarding strength are independently satisfied, considerable freedom exists for selecting V_j for each plane of strength. The safety design shear, S_{jk} , in the k story of the frame (structural plane) j can be computed taking torsion into account as

$$S_{jk} = \frac{V_j}{\sum V_j} \beta_4 S_{saf_k} \quad (8.26)$$

Finally, the safety design forces, F_{jk} , in each floor k of frame (structural plane) j can be computed using

$$F_{jk} = S_{jk} - S_{j(k+1)} \quad (8.27)$$

8.3.3.4 Preliminary Sizing and Detailing for Strength

Once service and safety seismic forces are obtained, the sizing and detailing for strength can be carried out. Although a conventional design can be recommended, the simultaneous design for service and safety limit state using plastic design is recommended because it is directly related to the capacity design philosophy implicit in code recommendations (Paulay and Priestley, 1992) and minimizes the required volume of flexural reinforcement.

The plastic design consists of a story-wise weak girder-strong column limit design using an optimization procedure. Linear programming techniques are employed to find the beam design moments that minimize an objective function proportional to the required volume of flexural reinforcement. The beam design moments must satisfy equilibrium constraints derived from the kinematic theorem of simple plastic theory (Neal, 1977). Additional constraints are imposed to include serviceability requirements and practical design considerations. The merit function combined with the equilibrium, serviceability and practical constraints comprise a standard linear programming problem. The procedure for preliminary sizing and detailing for strength is summarized as follows.

8.3.3.4.1 Plastic Design Bending Moments for Beams

Consider the floor i of a generic frame with r bays such as that in Figure 8.8. Assume that a design with the same positive bending moment M_i^+ and the same negative bending moment M_i^- in all bays of the i story is required. From the theory of plastic analysis, the following inequalities for the independent beam

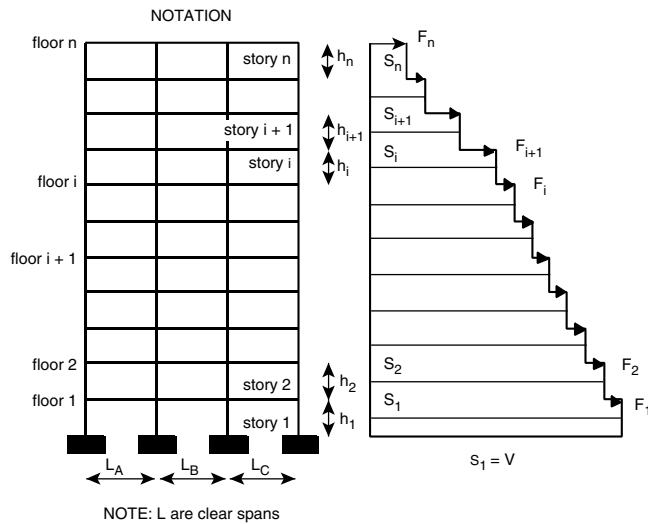


FIGURE 8.8 Generic frame considered for plastic design.

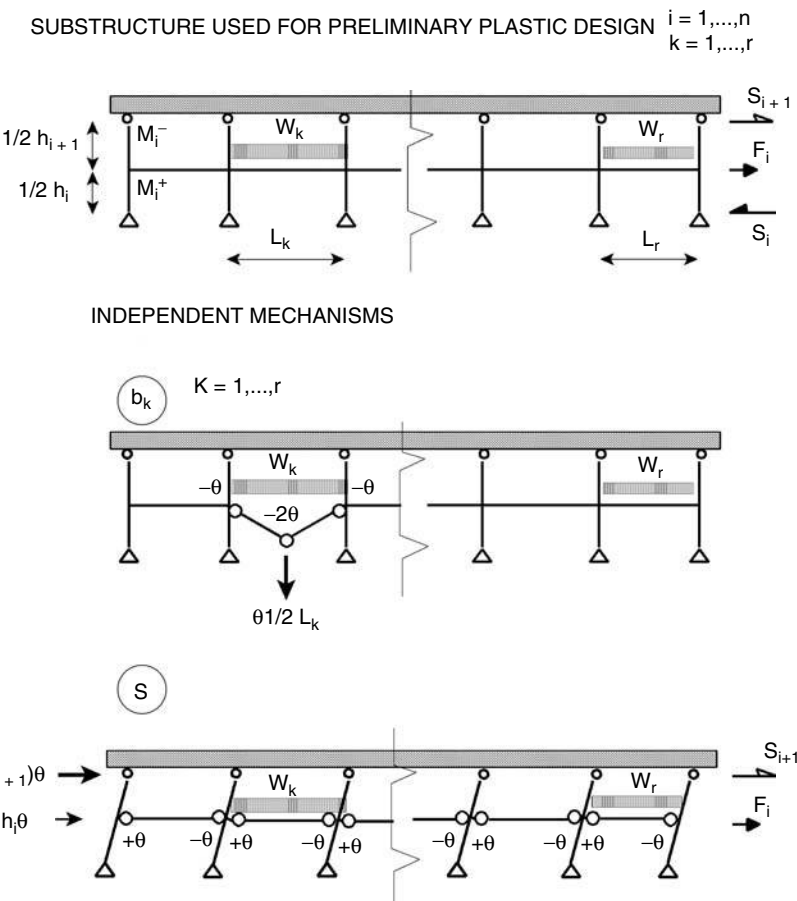


FIGURE 8.9 Substructure used for preliminary plastic design and independent mechanisms.

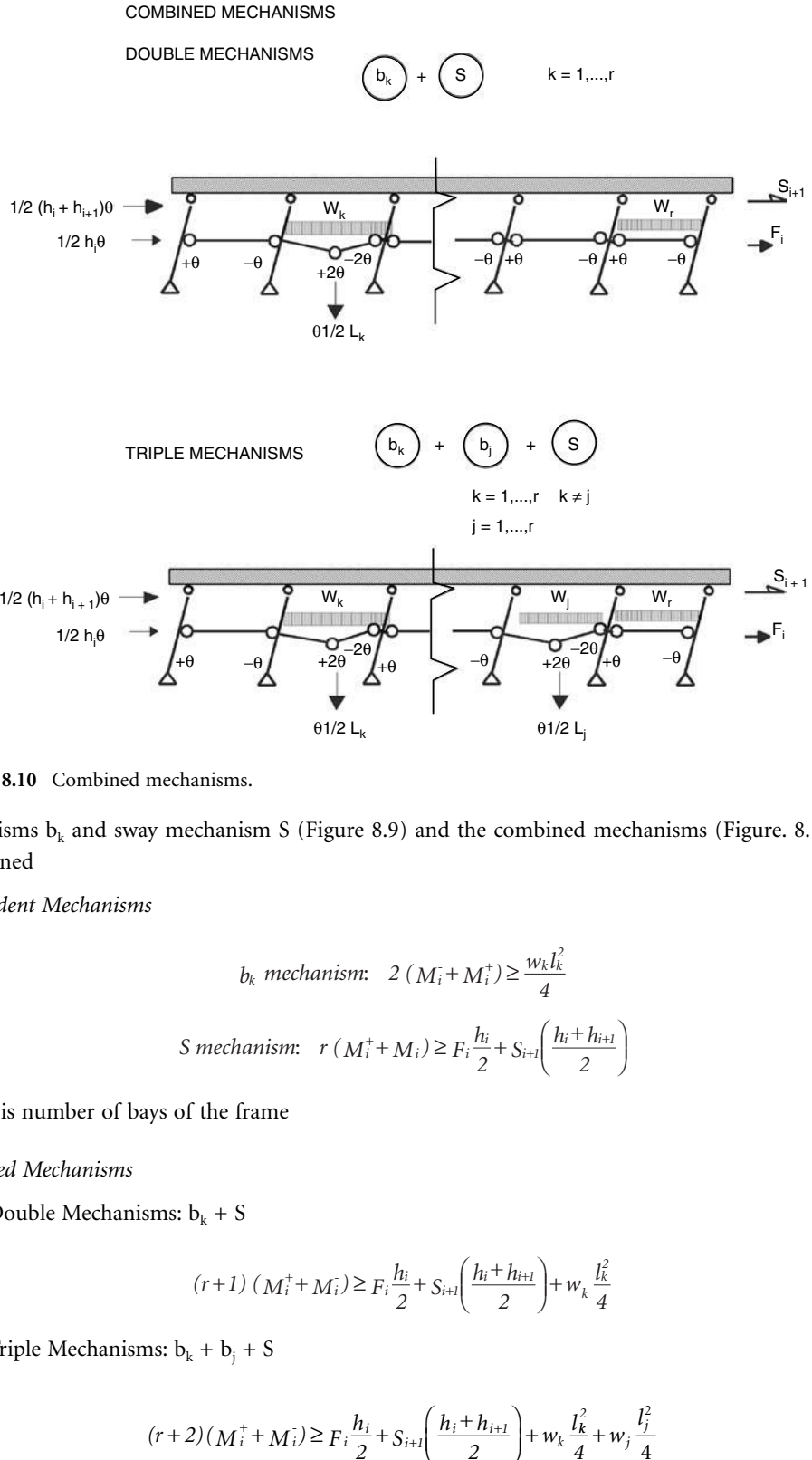


FIGURE 8.10 Combined mechanisms.

mechanisms b_k and sway mechanism S (Figure 8.9) and the combined mechanisms (Figure. 8.10) can be obtained

Independent Mechanisms

$$b_k \text{ mechanism: } 2(M_i^- + M_i^+) \geq \frac{w_k l_k^2}{4} \quad (8.28)$$

$$S \text{ mechanism: } r(M_i^+ + M_i^-) \geq F_i \frac{h_i}{2} + S_{i+1} \left(\frac{h_i + h_{i+1}}{2} \right)$$

where r is number of bays of the frame

Combined Mechanisms

- (a) Double Mechanisms: $b_k + S$

$$(r+1)(M_i^+ + M_i^-) \geq F_i \frac{h_i}{2} + S_{i+1} \left(\frac{h_i + h_{i+1}}{2} \right) + w_k \frac{l_k^2}{4} \quad (8.29)$$

- (b) Triple Mechanisms: $b_k + b_j + S$

$$(r+2)(M_i^+ + M_i^-) \geq F_i \frac{h_i}{2} + S_{i+1} \left(\frac{h_i + h_{i+1}}{2} \right) + w_k \frac{l_k^2}{4} + w_j \frac{l_j^2}{4} \quad (8.30)$$

(c) (j+1) combined mechanisms: $b_1 + \dots + b_j + S$

$$(r+j) (M_i^+ + M_i^-) \geq F_i \frac{h_i}{2} + S_{i+1} \left(\frac{h_i + h_{i+1}}{2} \right) + \sum_{k=1}^j w_k \frac{l_k^2}{4} \quad (8.31)$$

Theoretically, all possible combinations should be considered. However, noting that for the same number of combined mechanisms the left side of the inequality does not change. The design bending moments are obtained when the external work is maximized (i.e., when the right side of the inequality is maximized). It follows that only the spans with the largest values of $w_j l_j^2$ need to be combined.

If $w_j l_j^2$ are sorted so that $w_1 l_1^2 \geq \dots \geq w_j l_j^2 \geq \dots \geq w_r l_r^2$, only the following r+2 equations need to be considered

$$\begin{aligned} M_i^+ + M_i^- &\geq \frac{1}{2} w_1 \frac{l_1^2}{4} \\ M_i^+ + M_i^- &\geq \frac{1}{r} \left(F_i \frac{h_i}{2} + S_{i+1} \left(\frac{h_i + h_{i+1}}{2} \right) \right) \\ M_i^+ + M_i^- &\geq \frac{1}{r+j} \left(\sum_{k=1}^j w_k \frac{l_k^2}{4} + F_i \frac{h_i}{2} + S_{i+1} \left(\frac{h_i + h_{i+1}}{2} \right) \right) \quad j = 1, \dots, r \end{aligned} \quad (8.32)$$

8.3.3.4.2 Optimization problem for designing of beam reinforcement

For construction requirements, it is assumed that constant top and bottom steel is provided for beams of each story of a particular frame. It is assumed that the volume of flexural reinforcement is minimized when $(M_i^+ + M_i^-)$ is minimized (Zagajeski and Bertero, 1977). M_i^+ and M_i^- are the absolute values of the positive and negative design bending moments for all the beams of the floor i in the frame considered. For preliminary design of the corresponding positive and negative beam reinforcement, the following optimization problem can be stated.

Find:

$$M_i^+ \text{ and } M_i^- \quad i = 1, \dots, n \quad n = \text{number of stories}$$

which, considering the constraints imposed by the equilibrium equations, serviceability requirements and practical considerations, minimize $M_i^- + M_i^+$.

The following are the constraints imposed by

(a) Equilibrium Equations:

$$M_i^+ + M_i^- \geq \sum a_{0k} w_k + a_{1i} F_i + a_{2i} S_{i+1} \quad (8.33)$$

where, w_k is the gravity load for beam k; F_i is the lateral load at floor i; S_{i+1} is the shear at story $i+1$; a_{0k} , a_{1i} , a_{2i} are the constants depending on geometrical parameters of story i, span k and the equilibrium equation considered [Equation 8.32].

(b) Serviceability Constraints. The following serviceability requirements are introduced.

To control the response at the real service PL using the demanded yielding strength based on the LRFD format

$$M_i^+ \geq M_{isr}^- \quad \text{and} \quad |M_i^-| \geq |M_{isr}^-| \quad (8.34)$$

where, M_i^+ and M_i^- are the maximum absolute values of the demanded positive and negative elastic bending moment in the beams of the i story under the factored serviceability earthquake forces.

To satisfy the minimum and maximum steel ratio

$$\frac{\sqrt{f_c}}{4f_y} \text{ [in MPa]} \leq \rho^+, \quad \rho^- \leq 0.025 \text{ or } 0.75\rho_b \text{ whichever is smaller} \quad (8.35)$$

where ρ^+ is the bottom and ρ^- is the top reinforcement ratio of beams.

- (c) Practical Constraints. The following practical constraint is introduced to achieve a convenient distribution of top and bottom reinforcement

$$0.75 M_i^- \leq M_i^+ \leq M_i^- \quad (8.36)$$

8.3.3.4.3 Design of Main Reinforcement for Beams

Using M_i^+ and M_i^- obtained in the optimization problem as explained above, the required steel in beams is computed.

8.3.3.4.4 Design Shear in Beams

The design shear in the beams is obtained considering equilibrium and the flexural overstrength as

$$V_i = w_i \frac{L}{2} + \Omega_b \frac{M_i^+ + M_i^-}{L} \quad (8.37)$$

where, w_i is the factored gravity load of the beam at the i story, and $\Omega_b = 1.25$ is the estimated overstrength in the beams.

8.3.3.4.5 Design Moments for Columns

The bending moment in the columns can be computed using equilibrium and the hypothesis of an inflection point at the middle of the columns from the designed beams bending moments (Figure 8.11). For example, the bending moment in an exterior column of the story i can be computed as

$$M_{ei}^T = M_{ei}^B = \frac{L_{ci}}{h_i} \left[M_i^- + \frac{h_c}{2L_A} (M_i^+ + M_i^-) + \frac{h_c}{4} W_A L_A \right] - M_{e(i+1)}^B \quad (8.38)$$

where superscripts T and B stand for column top and bottom, respectively.

For designing, this bending moment is increased by a factor $\Omega_b = 1.25$ taking into account the overstrength in the beams and a factor $\Omega = 1.9$ that considers bi-axial effects (i.e., moments due to the effects of the two EQGMs components) and not midspan inflection point in the columns, so that $M_{ides} = \Omega_b \Omega M_i$ (Paulay and Priestley, 1992).

8.3.3.4.6 Design Axial Load for Columns

The maximum and minimum axial loads in the columns can be computed using equilibrium. For example, the following equation is obtained for the maximum and minimum axial load in an external column of the story i , where the sum involves all floors above the level considered (Figure 8.12)

$$P_i = \sum_{k=i}^n w_k \frac{L_A}{2} \pm \sum_{k=i}^n \Omega_b \frac{M_k^+ + M_k^-}{L_A} \quad (8.39)$$

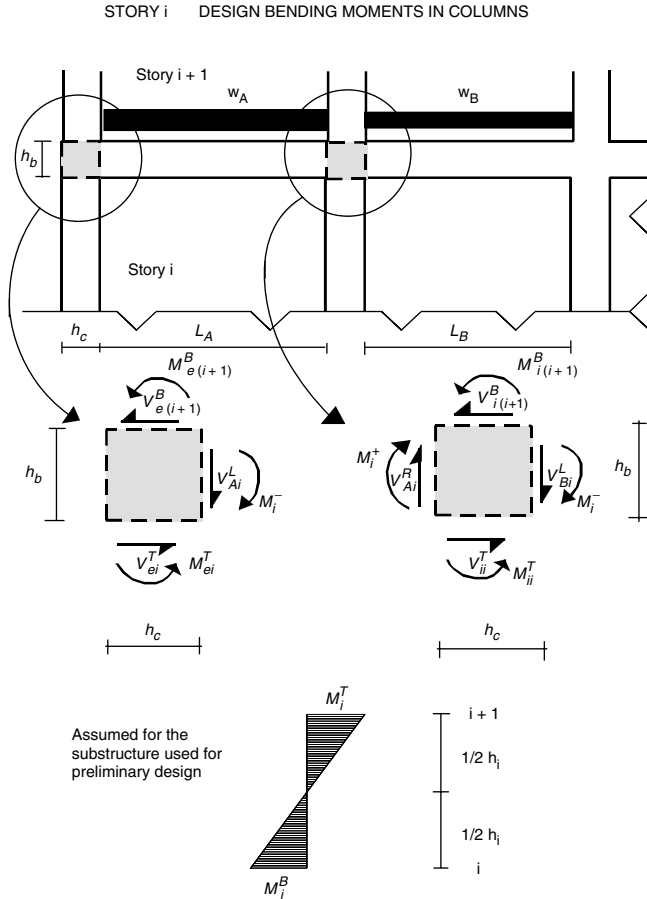


FIGURE 8.11 Design bending moments for columns of a generic story *i*.

8.3.3.4.7 Design of Main Reinforcement in Columns

Using the axial loads and bending moments computed above, the steel in the columns is selected using P-M interaction equations. The steel ratio is limited to $0.01 \leq \rho \leq 0.06$.

8.3.3.4.8 Design Shear in Columns

The shear in the columns can be computed using the bending moments obtained from equilibrium in the columns, $M_i^T = M_i^B$, of the story *i* as (Figure 8.6)

$$V_i = \Omega_b 2M_i^T / L_{ci} \quad (8.40)$$

An approximated value for the shear in the columns (without considering the size of the joint in the equilibrium equations) can also be obtained directly from the ultimate bending moments in the beams considering equilibrium in Figure 8.13

$$\begin{aligned} \text{Story } n: \quad V_n &= \Omega_b \frac{M_n + M_n^+}{h_n/2} \\ \text{Story } i: \quad V_i &= \Omega_b \frac{M_i + M_i^+}{h_i/2} - V_{i+1} \frac{h_{i+1}}{h_i} \end{aligned} \quad (8.41)$$

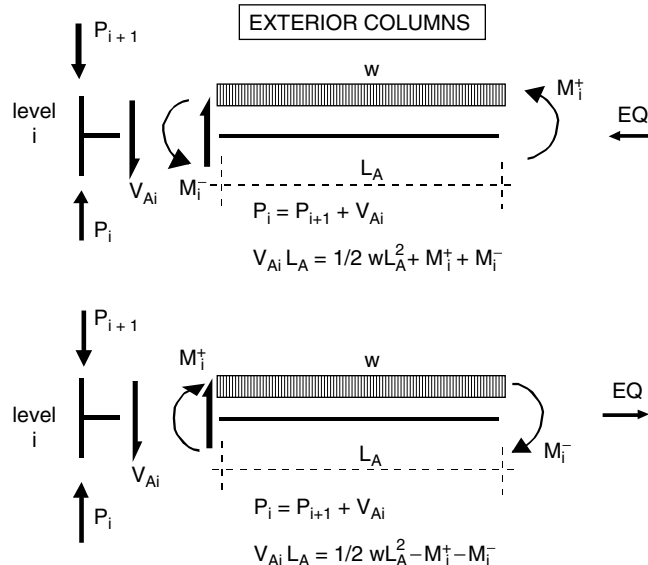


FIGURE 8.12 Equilibrium equations for determining axial forces in external columns.

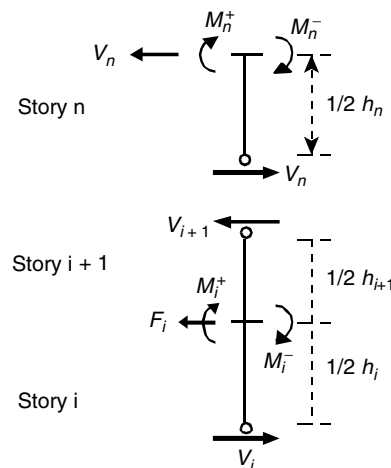


FIGURE 8.13 Approximated shear forces in columns (without considering the size of the joints).

8.3.3.4.9 Problems in the Design for Strength of RC Buildings

First Yielding and Ultimate Design Bending Moment — Since the beam reinforcement design is done simultaneously for first yielding (i.e., factored service demand) and ultimate strength using nominal yielding stress for the steel without a reduction factor, the relationships among the nominal yielding moment used for designing, M_{yn} , the real first yielding moment, M_{1sty} , the real ultimate bending moment, M_u as well as the plastic hinge bending moment at the time of maximum response, M_{ph} , should be clarified.

For Grade 60 steel with nominal yielding stress, $f_{yn} = 420$ MPa, Mirza and MacGregor (1979) report a $f_y = 490$ MPa and a $f_u = 764$ MPa as mean yielding and ultimate stress, respectively. If we assume $j_{1sty} \approx j_u \approx j_{yn}$ as lever arm for first yielding, ultimate and nominal yielding bending moment, the following relationships can be written

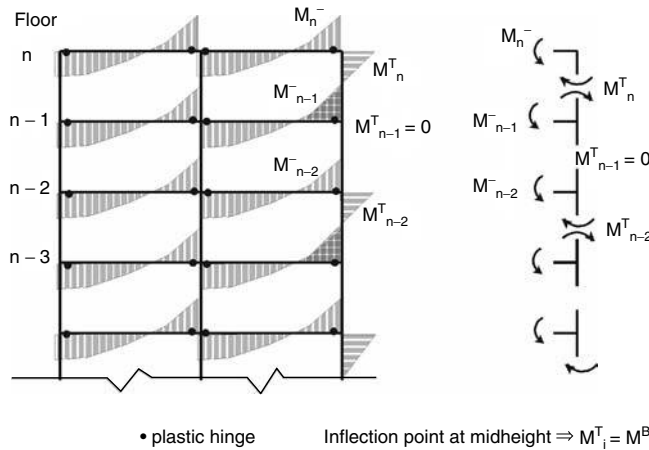


FIGURE 8.14 Zig-zag pattern of design bending moments and shear for columns.

$$\frac{M_{1sty}}{M_{yn}} = \frac{f_y (j_{1sty} d)}{f_{yn} (j_{yn} d)} \approx \frac{490}{420} = 1.17 \quad (8.42)$$

$$\frac{M_u}{M_{yn}} = \frac{f_u (j_u d)}{f_{yn} (j_{yn} d)} \approx \frac{764}{420} = 1.82$$

Assuming that the M_u value is reached under monotonic load for a plastic rotation $\Theta_p \approx 0.06$, and that from the IDI limitations, a maximum $\Theta_p \approx 0.015$ is expected for the structure, the maximum bending moment expected at the critical plastic hinge during the response will be approximately $(0.015/0.06)(M_u - M_{1sty}) + M_{1sty} \approx 1.33M_{yn}$. So that, at time of maximum response $M_{ph}/M_{yn} \leq 1.33$ and $M_{ph}/M_{1sty} \leq (1.33/1.17) \approx 1.14$ are expected at plastic hinges. The same nominal equation can be used to compute the steel required to satisfy first yielding and ultimate limit state if different overstrength factors that consider the ratio M_{ph}/M_{1sty} are used for first yielding and ultimate limit state.

Zig-Zag Pattern of Design Bending Moments and Shears for Columns — The required flexural and shear steel for columns follow a zig-zag pattern (Figure 8.14) as a consequence of using, for preliminary design, a one-story substructure with assumed inflection points at the middle of the columns.

Consider for example, a case in which the designed beam reinforcement for the upper stories, n , $n-1$ and $n-2$ are equal so that $M_n^+ = M_{n-1}^+ = M_{n-2}^+$ and $M_n^- = M_{n-1}^- = M_{n-2}^-$. Assume that using Equation 8.38 the bending moment for the column at story n , M_n^T , is computed. Assume that the geometrical parameters and the gravity loads of Equation 8.38 are the same for stories n , $n-1$ and $n-2$. It is clear that, using Equation 8.38 again, the bending moment for the columns at stories $n-1$ and $n-2$ are, respectively, $M_{n-1}^T = 0$ and $M_{n-2}^T = M_n^T$, where the zig-zag pattern in the columns is easily recognized.

The design bending moment at the column top in the upper story, M_n^T , should be used for design since from equilibrium its value is independent of the position of the inflection point at the column (i.e., $M_{designn} = M_n^T$). From the story $n-1$ to story 2, the design values can be smoothed using a moving average involving several stories. The moving average of three stories has been used in this case, i.e., the design moment for story i was computed as $M_{designi} = (M_{i-1} + M_i + M_{i+1})/3$ for $i = 2, 3, \dots, n-1$. At first story, an inflection point at $\alpha h_1 > 1/2h_1$ from the base should be selected when fixed supports are used. Therefore, the bending moment at the base in this case can be computed as $M_{desig1} = \frac{\alpha}{1-\alpha}(M_1 + M_2 + M_3)/3$.

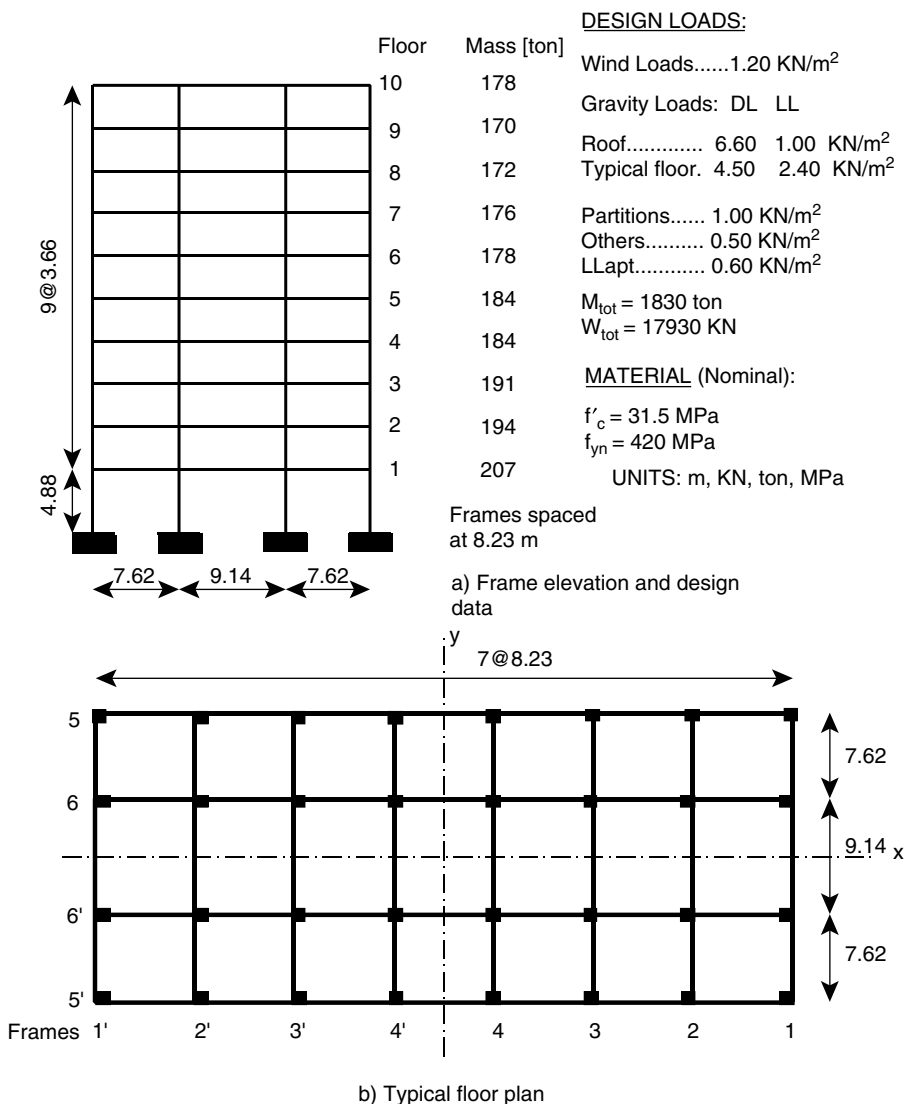


FIGURE 8.15 General configuration and structural lay-out.

8.4 Application of the Proposed CCA to the Preliminary Numerical Design of a Ten-Story Building

8.4.1 Problem Statement

Given:

1. Function of building (ten-story office building)
2. Site location (San Juan, Argentina)
3. Site condition (deep alluvium, mean value of the ground period $T_g = 0.60$ sec [standard deviation of the ground period $\sigma_{T_g} = 0.20$ sec], characteristic damping ratio $\xi_g = 0.45$)
4. General configuration and structural layout (Figure 8.15)

Required: An efficient (optimum) P-BSD of the building.

Solution: The steps for the solution of this problem follow.

Although the ideal would be to start the preliminary design using a 3D approach considering at least the three translational components of the design EQGMs, in general, the preliminary design is done independently for each of the main directions of the building. The results of the two independent analyses should be combined for the design of columns and joints. In Clough and Penzien (1993) it is shown that for statistically combining the two maximum responses produced by the two horizontal components of excitation it is possible to combine the maximum response in each direction with 30% of the maximum response in the other direction. Herein, for the sake of brevity, only the preliminary design for EQGMs forces perpendicular to the largest side of the building is shown.

8.4.2 Establishment of Design EQGMs

According to the steps shown in Figure 8.1, the first step of the preliminary design phase is the establishment of the design EQGMs. Given the site of the building and the site condition and using the procedure described briefly in Section 8.3.2 and in more detail in Bertero and Bertero (1992) and Bertero (2002) for acquiring and processing data, the following spectra needed for preliminary design were obtained:

- The (mean + σ) smoothed linear elastic design response spectra (SLEDRS) for S_a and S_d computed using $\xi_{ser} = 0.03$ for EQGMs with return period $T_R = 10$ years (Figure 8.16).
- The (mean + σ) SLEDRS and SIDRS (for different values of μ) for C_s and S_d computed using $\xi_{sap} = 0.05$, as well as for the parameter γ for evaluation of the cumulative damage caused for cyclic load reversals for EQGMs with return period $T_R = 500$ years (Figure 8.16).

According to the flowchart of Figure 8.1, the following step is the preliminary design procedure. This step can be divided into preliminary analysis, preliminary sizing and detailing and analysis of preliminary design. It must be noted, however, that they are not independent and, in fact, a part of the preliminary analysis process is done between the preliminary sizing for stiffness and the preliminary sizing and detailing for strength as described in Section 8.3.3.

8.4.3 Preliminary Analysis

8.4.3.1 Selection of Performance Design Objectives

8.4.3.1.1 EQGM Levels

Considering the site seismicity, the following two EQGM levels are defined.

1. Frequent minor EQGM $T_R = 10$ years.
2. Rare major EQGM $T_R = 500$ years.

8.4.3.1.2 Performance Levels (PLs)

Considering the building function and type of nonstructural elements and components, the following two PLs are defined.

1. **Serviceability.** The limit of IDI is selected considering that wood-frame gypsum panels will be used for partitions. For these nonstructural elements, tests reported by Oliva (1990) show that gluing the gypsum sheathing to the wood frame, an $IDI_{ser} = 0.003$ can be obtained without visible damage. Since no structural damage is required, a local damage index $DM_{Lser} = 0$ is specified. Note that in RC structures due to cracking, some damage can be unavoidable. This small damage is neglected here and $DM_L = 0$ is considered until first significant yielding of steel. In view of the small IDI and cracking a $\xi = 3\%$ has been assumed for the Service PL.
2. **Life Safety.** To avoid the complete collapse of the panels and other nonstructural elements (ceiling, electrical features, etc) which can jeopardize the life of the occupants, the tolerable IDI for safety is selected as $IDI_{saf} = 0.015$. For life safety, a local damage index $DM_{Lsaf} = 0.8$ is selected as maximum local structural damage.

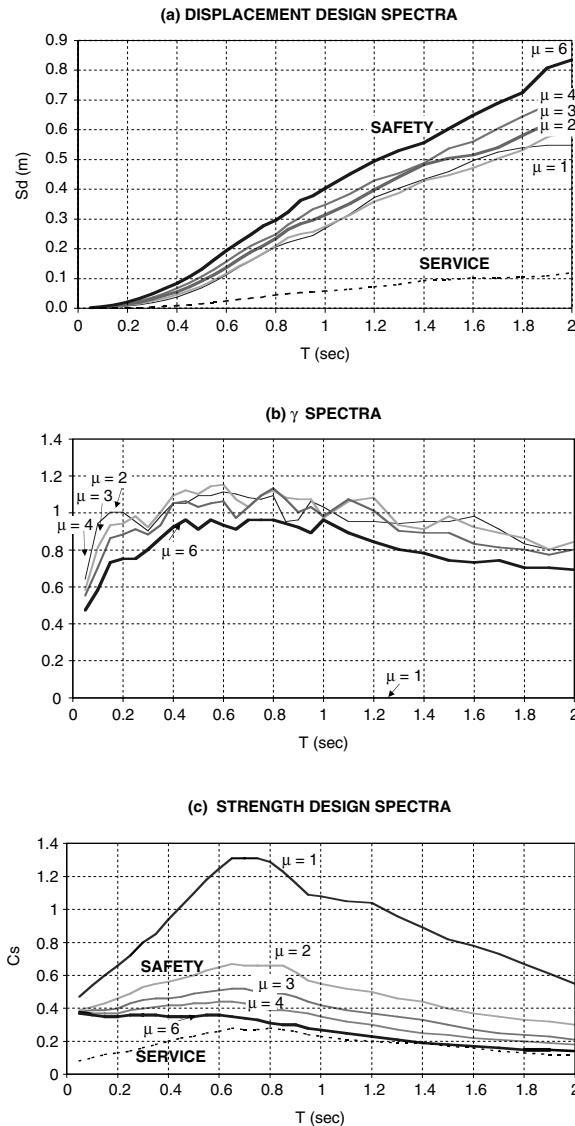


FIGURE 8.16 Mean + sigma smooth design spectra of: (a) displacement; (b) γ , and; (c) strength for service PL $\xi_{ser} = 0.03$; for safety PL $\xi_{saf} = 0.05$.

8.4.3.1.3 Performance Goals

Considering the high seismicity of the site and the function of the building, a probability of 16% that the building does not satisfy serviceability limit state for EQGMs with $T_R = 10$ years, and a probability of 16% that the building does not satisfy life safety limit state for EQGMs with $T_R = 500$ years are selected as performance goals. Note that 16% probability implies using mean + σ design spectra.

8.4.3.1.4 Equivalence between Serviceability Using Allowable Stresses and First Yielding Using LRFD Format

Note that the definition of a PL involves the return period of the EQGMs, the expected damage and the probability that this expected damage be surpassed. In the example, it was selected $T_R = 10$ years for serviceability EQGMs and a probability $p_f = 0.16$ than the critical sections get first yielding. When serviceability is defined using mean values of actions, first yielding is not reached, but a smaller value of

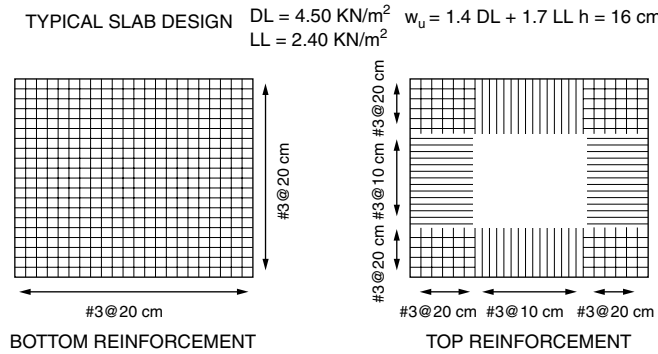


FIGURE 8.17 Design of a typical building slab.

stresses results in the critical sections. Considering a $COV_{EQ} = 0.80$ (coefficient of variation for EQGMs), an amplification factor $(1+\beta COV_{EQ}) = (1+1.00 \cdot 0.8) = 1.8$ is obtained for the earthquake action when using the definition of serviceability with $p_f = 0.16$ with respect to the definition with mean values. Therefore, since the behavior is linear until first yielding, the stresses corresponding to the mean of EQGMs are $1/1.8 = 0.56$ of the yielding stress when earthquake loads completely control the design. If earthquake load and gravity loads are equally important in the design, a ratio $2/(1.8 + 1.0) = 0.71$ is obtained. Therefore, the definition of serviceability with a 16% probability than the critical sections get first yielding (using mean + sigma spectra) is almost the same as that of the definition of serviceability with allowable stresses and mean values for the actions.

8.4.3.2 Geometrical Data and Material Properties

8.4.3.2.1 Geometrical Parameters

Building sizes: L = 57.6 m D = 24.4 m Building height: H = 37.82 m

Radius of gyration of mass (assuming the mass uniformly distributed on the floor):

$$r_g^2 = (L^2 + D^2)/12, \quad r_g = 18.06 \text{ m}$$

Distance (x, y) between each frame and the center of stiffness:

Frame (1),	x ₁ = 28.81 m	y ₁ = 0 m	Frame (4),	x ₄ = 4.12 m	y ₄ = 0 m
Frame (2),	x ₂ = 20.58 m	y ₂ = 0 m	Frame (5),	x ₅ = 0 m	y ₅ = 12.19 m
Frame (3),	x ₃ = 12.35 m	y ₃ = 0 m	Frame (6),	x ₆ = 0 m	y ₆ = 4.57 m

Coordinates x, y of frames (1') to (6') are obtained from symmetry as x_{i'} = -x_i and y_{i'} = -y_i.

8.4.3.2.2 Material Properties

For all stories the following nominal properties are specified:

Concrete, $f'_c = 31.5 \text{ MPa}$

Steel, $f_{yn} = 420 \text{ MPa}$

8.4.3.3 Gravity Loads

The design of the slabs must be carried out in this step. Figure 8.17 shows the design of a typical slab for this building considering strength and stiffness (maximum deflection). Note that a careful design of the slab is important because: (a) it is necessary to design the slab as thin as structurally possible to avoid

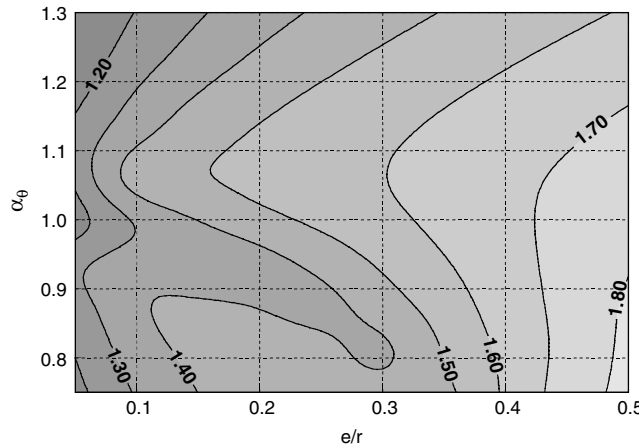


FIGURE 8.18 Maximum displacement ratio between two and one DOFS (hyperbolic spectrum, rectangular plant $L = 2 D$).

unnecessary mass and (b) the slab steel must be considered in the estimation of the flexural beam capacities for shear verification and design of columns and joints.

On the basis of structural geometry and building function, gravity, wind and other probable excitations, and according to previous experience and judgment about seismic requirements, a first guess of beam and column sizes is made. Using these preliminary sizes for slabs, beams and columns as well as those of the nonstructural elements together with the reactive masses to be lumped at each floor level, the mass matrix of the structure M is obtained. The estimated weights are summarized in Figure 8.15.

8.4.3.4 Selection of First Mode Shape and Estimation of Modal Parameters

Since the structure is a moment-resisting space frame, and the design will be done reducing the size of beams from the first floor to the roof, a linear shape for the first mode of vibration was selected. The total mass and first mode parameters are

$$\text{Total mass, } M = 1830 \text{ ton} \quad \text{First mode shape, } \Phi_{1i} = \frac{z_i}{H}$$

$$\text{Damping ratios, } \xi_{ser} = 0.03 \quad \xi_{saf} = 0.05$$

$$\text{First mode parameters, } \Gamma_1 = 1010 \text{ ton} \quad M_1 = 699 \text{ ton (From Equation 8.9)}$$

$$\frac{\Gamma_1}{M_1} = 1.44 \quad \frac{\Gamma_1^2}{M_1 M} = 0.80$$

8.4.3.5 Estimation of Maximum Building Period, T_{1ser} , to Satisfy Serviceability

As indicated by Equation 8.10 (in Section 8.3.3.1.6) it is necessary to make the following estimations:

- Estimation of IDI Increase Due to Deviation of Assumed First Mode Shape β_0 — Since beam and column sizes will be designed based on the target linear first mode, a small value of β_0 is expected. For this building, $\beta_0 = 1.05$ was selected.
- Estimation of IDI Increase Due to Elastic Torsion, β_1 — As discussed in detail in Bertero and Bertero (1992) and Bertero (2002), β_1 can be obtained as a function of α_θ , the relative eccentricity, e/r_g and the aspect ratio of the plant, L/D . In general, an estimation of the relative stiffness of frames is needed to estimate α_θ and the center of stiffness (needed to compute the eccentricity).
- Estimation of rotation–translation stiffness ratio, α_θ — The ratio

$$\alpha_\theta = T_y / T_\theta = \sqrt{K_\theta / (K_y r_g^2)},$$

where T_y and T_θ are the uncoupled translational and rotational periods of vibration, was estimated as follows. Using Equation 8.16 the stiffness in each direction at a particular story for each frame i can be computed as

$$k_{xi} = \frac{N_{cx}}{(1 + \psi_x)} k_{0x} \quad k_{yi} = \frac{N_{cy}}{(1 + \psi_y)} k_{0y} \quad (8.43)$$

where N_c is the number of columns in the frame ($N_{cx} = 8, N_{cy} = 4$); ψ is the column/beam stiffness ratio (assumed $\psi_x = \psi_y$) and k_0 is the column stiffness (assumed $k_{0x} = k_{0y}$). ψ and k_0 are assumed equal for all frames.

The structural stiffness in each direction at a particular story can be written using symmetry as

$$K_x = 2 \sum_{i=5}^6 k_{xi} \quad K_y = 2 \sum_{i=1}^4 k_{yi} \quad K_\theta = 2 \left[\sum_{i=1}^4 (x_i)^2 k_{yi} + \sum_{i=5}^6 (y_i)^2 k_{xi} \right] \quad (8.44)$$

Using Equation 8.43 and defining k_b = the unknown stiffness of each frame along y direction, $k_{xi} = 2 k_{yi} = 2 k_b$ is obtained. Replacing in Equation 8.44 results

$$K_x = 8 k_b \quad K_y = 8 k_b \quad K_\theta = 1.21 r_g^2 8 k_b \quad \alpha_\theta = \sqrt{\frac{K_\theta}{K_y r_g^2}} = 1.1 \quad (8.45)$$

- Estimation of Eccentricity — Because of symmetry, the computed static eccentricities for each story of the building are

$$e_{sx} = 0 \text{ m} \quad e_{sy} = 0 \text{ m}$$

The accidental eccentricity at each story is estimated as,

$$e_{ax} = 0.05 L = 2.88 \text{ m} \quad e_{ay} = 0.05 D = 1.22 \text{ m}$$

The total eccentricities are

$$e_x = e_{sx} + e_{ax} = 2.88 \text{ m} \quad e_y = e_{sy} + e_{ay} = 1.22 \text{ m}$$

- Estimation of β_1 — With $\alpha_\theta = 1.1, e_x/r_g = 0.16$ and $L/D = 2.36$, using Figure 8.18 (from Bertero (2002)) $\beta_1 = 1.50$ is obtained.
- Estimation of Maximum Period to Satisfy Serviceability, $T_{1\text{ser}}$ — Using Equation 8.10 with,

$$\Gamma_1/M_1 = 1.44; \beta_0 = 1.05; \beta_1 = 1.50; (\Delta\Phi_{li}/h_i)_{\max} = 1/H,$$

(constant) for each story; and $IDI_{\text{ser}} = 0.003$, from Figure 8.3 (a) the maximum uncoupled translational period (i.e. the period of the structure without eccentricity) to satisfy serviceability is $T_{1\text{ser}} = 0.90 \text{ sec}$.

8.4.3.6 Estimation of Maximum Building Period and Ductility to Satisfy Safety

As indicated by Equations 8.11 and 8.12 in Section 8.3.3.1.7, to obtain the maximum IDI_{\max} and local damage index DM_L and then the maximum period and ductility to satisfy life safety, it is necessary to make the following estimations.

- Estimation of IDI Increase Due to Concentration of Plastic Rotations in One Story, β_2 . Since optimum plastic design of beam reinforcement will be done using a design force distribution

obtained from modal analysis, a uniform distribution of plastic rotations is expected. This happens because designing in this way, no particular weakness is expected in the capacity with respect to the seismic demand. However, less IDI is anticipated at the lower stories, since more strength is intentionally provided there to have smaller plastic rotations at the column bases of the first story (where plastic rotation capacity can be smaller due to compression axial loads). Therefore, a small value $\beta_2 = 1.2$ was selected.

- Estimation of IDI Increase Due to Inelastic Torsion, β_3 . Assuming that all frames have the same strength, the torsion lever arms (Bertero, 1995) are

$$j_x = \frac{\sum_{i=1}^4 |x_i|}{0.5 \times 4} = 32.92 \text{ m} \quad j_y = \frac{\sum_{i=5}^6 |y_i|}{0.5 \times 2} = 16.76 \text{ m} \quad (8.46)$$

If the accidental eccentricity for elastic and inelastic behavior is equal (in general they will be different), it is $x_R = e_s$, $y_R = e_y$ and using $\alpha = 0.30$, where α is the coefficient for combining the two horizontal components of the earthquake excitation taking the “30 percent rule” used in building design (a discussion on the value of α can be seen in Clough and Penzien, 1992)

$$\begin{aligned} \alpha x_R + y_R &= 2.08 \text{ m} < 0.5 j_x (1 - \alpha) = 11.52 \text{ m} \\ \alpha y_R + x_R &= 3.25 \text{ m} < 0.5 j_y (1 - \alpha) = 5.87 \text{ m} \end{aligned} \quad (8.47)$$

Therefore, a translation mechanism is expected and $\beta_3 = 1.0$ is selected.

Using Equations 8.11 and 8.12 with,

$$\Gamma_1/M_1 = 1.44; \quad \beta_2 = 1.2; \quad \beta_3 = 1.0; \quad (\Delta\Phi_{hi}/h_i)_{\max} = 1/H,$$

(constant) for each story; $IDI_{\text{saf}} = 0.015$; and for this particular structure, considering that appropriate amount of reinforcing steel will be provided to resist the shear at joints and plastic hinges as well as proper detailing of the reinforcement will be done, the following values were selected for local damage:

$$\theta_{\text{saf}} \approx IDI_{\text{saf}} = 0.015; \quad \theta_{\text{umon}} = 0.04; \quad \beta_2 = 1.2; \quad DM_{\text{Lsaf}} = 0.8; \quad \text{and } b = 0.20.$$

Considering the maximum period required to satisfy IDI_{ser} and the maximum IDI_{saf} and local damage to satisfy life safety, the acceptable design zones are the rectangles shown in Figures 8.3(a) and (b). From economical considerations, $T = 0.90$ sec and $\mu = 3.50$ are selected for this building.

At this stage, $S_a(T, \xi_{\text{ser}})$ and $C_s(T, \xi_{\text{saf}}, \mu_{\max})$ define the lower bound on the equivalent SDOF strength to satisfy serviceability (elastic behavior) and life safety as shown in Figure 8.3 (c).

8.4.4 Preliminary Sizing and Detailing

8.4.4.1 General Design Constraints

To obtain economical formwork the following design constraints are considered for beam and column sizes:

- Beam and column will have standard sizes changing in 10 cm increments.
- Beam width or beam depth will remain constant for at least three consecutive stories.
- Where possible, it is preferred to vary beam width than to vary beam depth (for architectural reasons).
- Column sizes will remain constant for at least four consecutive stories.

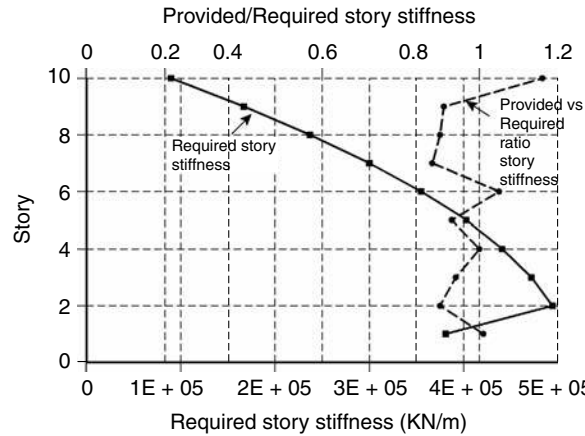


FIGURE 8.19 Required and provided story stiffness.

To minimize the waste of steel due to bar cut-offs and splices, and to speed up the construction process and minimize human error at site, the following design constraint is considered for reinforcement:

- Top and bottom steel will remain constant along the beams of each frame at each story.

8.4.4.2 Preliminary Sizing for Stiffness

Selecting a building with target period $T_1 = 0.90$ sec and linear first mode shape Φ_1 , the required story stiffness, k_i , are computed using Equation 8.13. Beam and column sizes are selected so that the story stiffness is approximately satisfied by Equation 8.16, where for this building (considering as beam length, L_b , the average of the three beam lengths), $N_c = 4$; $N_b = 3$; $E_c = 26,500 \text{ MN/m}^2$; $h_i = 4.88 \text{ m}$, $h_i = 3.66 \text{ m}$ ($i = 2, \dots, 10$); $L_b = (7.62+9.14+7.62)/3 = 8.12 \text{ m}$; $h_{ci} = h_i - d_i$, $L_i = L_b - a_i$; $I_{ci} = (a_i)^4/12$, $I_{bi} = 0.5 b_i(d_i)^3/12$; a_i = size of square column at story i ; b_i = beam width at story i and d_i = beam depth at story i . Note that any method or computer program available could be used to obtain the required story stiffness. In this chapter, the simplified Equation 8.16 was used (in spite of beam lengths not being equal) to show more clearly the different influence of the main design variables.

Due to the assumption of fixed base, inflection point at first story is higher than midheight of the column. Assuming an inflection point at $0.65 h_i$, $h_{eff} = 2(1-0.65)h_i$ is introduced in Equation 8.16 as first story height to select beam and column sizes. If $h_{eff} = h_i$ had been selected for designing, the resulting beam and column sizes at first story would have been larger than needed (to compensate the higher effective first story). As a consequence, the analysis of the preliminary design would have shown a nonuniform pattern of IDI, with smaller IDIs at lower stories. Smaller IDIs at lower stories would have been obtained because, when the offset of the inflection point at first story was not considered, a stiffer-designed first story than was really needed would have been obtained. Using a spreadsheet along with Equations 8.13 and 8.16, beam and column sizes are interactively selected for each story until the stiffness computed from both equations is close enough. Figure 8.19 shows required and provided story stiffness. The decrease in the required first story stiffness is due to the fact that the first story is 33% higher than the others. Because of the construction requirements described in Section 8.4.4.1., the ratio between required and provided story stiffness oscillates between 0.90 and 1.15. The preliminary columns and beam sizes selected to satisfy stiffness are shown in Figure 8.20.

8.4.4.3 Calculation of First Three Modal Parameters

Using the preliminary sizes and stiffness obtained in Section 8.4.4.2 the stiffness matrix K is computed. Using K and the mass matrix M , the eigenvalue problem $K\Phi = \omega^2 M\Phi$ is solved and the following first three modal parameters are obtained

40×80		40×80		40×80	
40×90	90×90	40×90	90×90	40×90	90×90
40×100	90×90	40×100	90×90	40×100	90×90
50×100	90×90	50×100	90×90	50×100	90×90
50×110	90×90	50×110	90×90	50×110	90×90
50×110	100×100	50×110	100×100	50×110	100×100
60×110	100×100	60×110	100×100	60×110	100×100
60×110	100×100	60×110	100×100	60×110	100×100
60×110	100×100	60×110	100×100	60×110	100×100
60×100	100×100	60×100	100×100	60×100	100×100
100×100		100×100		100×100	

FIGURE 8.20 Preliminary sizing for beams and columns (cm).

$$\begin{aligned}
 T_1 &= 0.92 \text{ sec} & \Gamma_1/M_1 &= 1.43 & \Gamma_1^2/(M_1 M) &= 0.79 \\
 T_2 &= 0.38 \text{ sec} & \Gamma_2/M_2 &= 0.64 & \Gamma_2^2/(M_2 M) &= 0.12 \\
 T_3 &= 0.23 \text{ sec} & \Gamma_3/M_3 &= 0.32 & \Gamma_3^2/(M_3 M) &= 0.04
 \end{aligned} \tag{8.48}$$

The first three mode shapes are shown in Figure 8.21. Note that the target linear first mode is obtained and a slightly more flexible structure than required has been designed because the provided story stiffness is on average slightly smaller than required (Figure 8.19). However, since the computed period is only 2% larger than required, and large uncertainties exist in the value of RC member stiffness, the design is considered satisfactory.

8.4.4.4 Serviceability Seismic Design Forces

8.4.4.4.1 Total Base Shear

From Figure 8.16, the following pseudo-accelerations are obtained for the first three modes of the structure, $S_a(T_1) = 0.24 \text{ g}$, $S_a(T_2) = 0.18 \text{ g}$ and $S_a(T_3) = 0.13 \text{ g}$. The total base shear, $V = 0.19 \text{ W}$, is obtained from the elastic design spectra and the modal parameters using Equation 8.17.

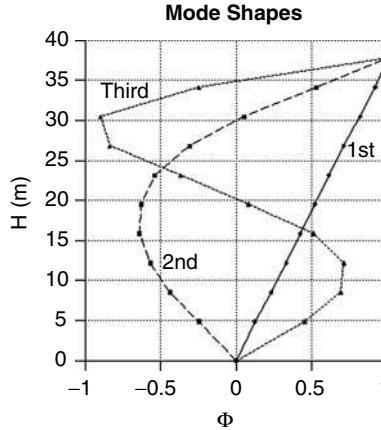


FIGURE 8.21 First three modes.

8.4.4.4.2 Design Base Shear for Each Structural Plane

The base shear in each structural plane j can be computed taking torsion into account using Equation 8.18. Designing for serviceability ($V_j = V_{1st\ yield}$) and considering the service overstrength, Ω_{ser} , the design base shear can be computed using Equation 8.19.

For the critical frame (external frame) the following values were selected: $k_{xj}/K_x = 1/8$; $\beta_{1j} = \beta_1 = 1.50$; and $\Omega_{ser} = 1.10$. $\Omega_{ser} = 1.17/1.05 \approx 1.10$ was selected assuming $M_{1st\ yield}/M_{yn} \approx 1.17$ (Section 8.3.3.4.9) affected by a factor (1/1.05) to account for the stress that increases due to any deviation during the elastic response of the computed modal shapes. Replacing in Equation 8.19, the design base shear for serviceability for external frames is $V_{ser_i} = \frac{1}{8} 1.5 \frac{0.19W}{1.10} = \frac{1}{8} 0.26W$. Therefore, the expected first yielding shear

for external frames is $V_{1st\ yield_i} = \Omega_{ser} V_{ser_i} = 1.10 \frac{1}{8} 0.26W = \frac{1}{8} 0.29W$. Note that the design and first yielding base shear of central frames would be 33% ($1/1.5 = 0.67$) smaller because no amplification due to elastic torsion is required for them. It can be shown (Bertero 2002) that if the eccentricity is considered, the center of torsion has smaller maximum displacement during the EQGM response than when only translation (i.e., no eccentricity) is assumed. As a result, the more interior frames have no amplification due to torsion.

8.4.4.4.3 Design Story Forces and Shears for Each Frame

The serviceability design shear for each story k is computed using Equation 8.20. The service design shear, S_{jk} , in the k story of the frame (structural plane) j is computed taking torsion into account using Equation 8.21. Finally, the service design forces, F_{jk} , in each story k of frame (structural plane) j are computed using Equation 8.22. Figure 8.22 shows the distribution of service earthquake forces obtained for the external frames using these equations.

8.4.4.5 Life Safety Seismic Design Forces

8.4.4.5.1 Total Base Shear

From Figure 8.16 and using $\mu = 3.5$, the following strength seismic coefficients are obtained for the first three modes of the structure, $C_s(T_1) = 0.42$, $C_s(T_2) = 0.42$ and $C_s(T_3) = 0.40$. The total base shear, $V_{mech} = 0.34 W$, is obtained from the design spectra and the modal parameters using Equation 8.23.

8.4.4.5.2 Design Base Shear for Each Structural Plane

Inelastic torsion effects are included with a coefficient β_4 , which amplify design forces when a torsion collapse mechanism is expected for the structure. The base shear, V_j , in each frame (structural plane) j must be selected so that $\sum V_j = \beta_4 V_{mech}$, therefore the following identity can be written

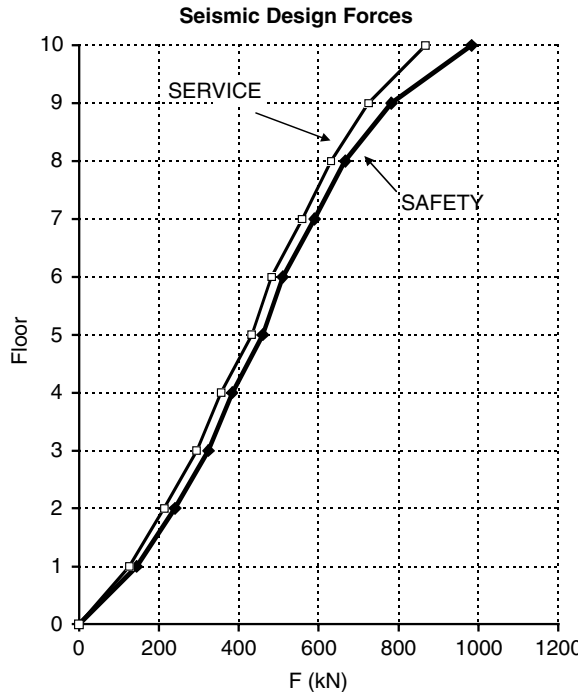


FIGURE 8.22 Distribution of design service and safety earthquake loads for external frames.

$$V_j = \frac{V_j}{\sum V_j} \beta_4 V_{mech} \quad (8.49)$$

The design base shear of each frame j , V_{safj} , can be reduced considering overstrength at collapse, Ω_{saf} , using

$$V_{safj} = \frac{V_j}{\sum V_j} \beta_4 \frac{V_{mech}}{\Omega_{saf}} \quad (8.50)$$

Note that, because service constraints regarding strength are independently satisfied, considerable freedom exists for selecting V_j for each plane of strength. In this case, the strength of each frame was selected so that they reach almost simultaneous yielding during the elastic torsion response, i.e., external frames were designed with more strength.

Therefore, in this case

$$V_4 = 0.7 V_1, V_3 = 0.8 V_1, V_2 = 0.9 V_1$$

were selected, so that

$$V_1 / \sum V_j = 1 / [2(1 + 0.9 + 0.8 + 0.7)] = 1/6.8$$

results for external frames ($j = 1$) for using in Equation 8.50.

$\Omega_{saf} = 1.40$ and $\beta_4 = 1.0$ were also selected for using in Equation 8.50. $\Omega_{saf} = 1.40$ was selected assuming that at the time of maximum response, the capacities at the plastic hinges are $M_{ph}/M_{yn} \approx 1.33$

(Section 8.3.3.4.9) and that about 5% more steel than required is selected because of the discrete variation in number and diameters of bars ($1.33 \times 1.05 = 1.40$). $\beta_4 = 1.0$ was selected because a translation collapse mechanism is expected for the structure. Since a total base shear, $V_{\text{mech}} = 0.34 W$ was obtained above,

replacing in Equation 8.50, the design base shear for safety $V_{\text{saf}_1} = \frac{1}{6.8} 1.0 \frac{0.34W}{1.40} = \frac{1}{8} 0.29W$ is obtained for external frames. Therefore, the expected mechanism base shear for the external frames is

$V_{\text{mech}_1} = \Omega_{\text{saf}} V_{\text{saf}_1} = 1.40 \frac{1}{8} 0.29W = \frac{1}{8} 0.40W$. Note that the design and mechanism base shear of central frames would be 30% smaller because almost simultaneous yielding during the elastic torsion response was intended from the selected strength distribution ($V_4 = 0.7 V_1$).

8.4.4.5.3 Design Story Forces and Shears for Each Frame

The safety design shear for each story k can be computed using Equation 8.25. The safety design shear, S_{jk} , in the k story of the frame (structural plane) j is computed taking torsion into account using Equation 8.26. Finally, the safety design forces, F_{jk} , in each story k of frame (structural plane) j are computed using Equation 8.27. Figure 8.22 shows the distribution of safety earthquake design forces obtained for external frames using these equations. Note the deviation of the straight line due to second and third mode effects. The service and safety design forces are close because of the torsional amplification at service and the larger overstrength at safety.

8.4.4.6 Preliminary Sizing and Detailing for Strength

8.4.4.6.1 Summary

The simultaneous design for service and safety limit state can be carried out using an electronic spreadsheet. Once the preliminary sizing of the member has been conducted to satisfy the required stiffness and the service and safety design forces for each frame have been obtained, elastic analysis of the preliminary sized frames is done using the service design forces. At this stage, preliminary analysis is finished and the preliminary design for strength is carried out using an electronic spreadsheet. First, the following data are introduced into the spreadsheet:

- (a) Story heights, beam spans and concrete strengths at each story.
- (b) Live loads, dead loads and safety earthquake design shear and forces at each story.
- (c) Size of beams and columns at each story obtained from the preliminary design for stiffness.
- (d) The maximum positive and minimum negative bending moment in each story obtained from the elastic analysis.

Using these data, the spreadsheet is used to obtain the preliminary design for strength as follows:

- (e) The positive and negative design bending moment for beams at each story are obtained solving a linear optimization problem using the linear programming capacity of the spreadsheet. Service bending moments and practical requirements are introduced as constraints.
- (f) Main reinforcement is selected for the beams using the optimum design bending moment obtained in (e).
- (g) From equilibrium, shear forces in beams and columns and axial forces and bending moments in columns are computed.
- (h) Preliminary reinforcement is selected for the columns.

The process is repeated until the sizes and steel ratio of the elements are considered satisfactory for the designer (e.g., the requirements defined in Section 8.4.4.1 are achieved).

8.4.4.6.2 Preliminary Design of Main Beam Reinforcement

In the following equations, M_i^+ and M_i^- are the absolute values of the positive and negative design bending moments for all the beams of the floor i in the frame considered. For preliminary design of the corre-

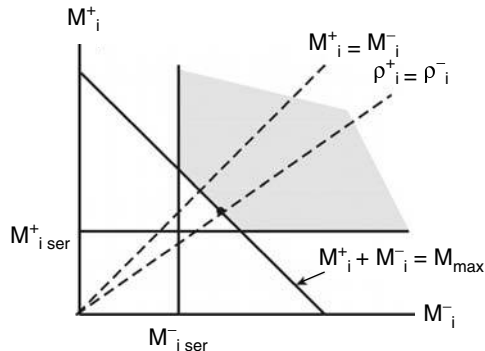


FIGURE 8.23 Optimization problem to design beam reinforcement.

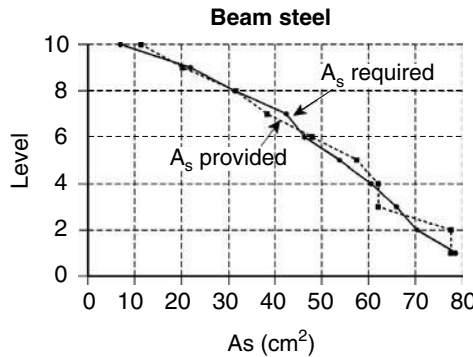


FIGURE 8.24 Required and provided beam reinforcement.

sponding positive and negative beam reinforcement, the optimization problem presented in Section 8.3.3.4.2 needs to be solved.

Since only two variables, M_i^+ and M_i^- , form the optimization problem; it can be easily solved as follows. Because all equilibrium equations (Equation 8.33) are lines parallel to the parametrical line representing the objective function to minimize (Figure 8.23), only the equilibrium constraint with maximum value on the right side needs to be considered. Since safety forces are larger than serviceability forces, a permissible region as indicated in Figure 8.23 is obtained. Note that any selection of design moments on the line $M_i^+ + M_i^- = M_{\max}$ minimizes the objective function of this problem. To simplify the construction process, equal top and bottom reinforcement is selected (unless serviceability control the design) so that calling M_{\max} = maximum value of $(M_i^+ + M_i^-)$ in the equilibrium constraints, the optimum top and bottom steel ratio at story i, $\rho_i^+ = \rho_i^- = \rho_i$, can be computed as

$$\rho_i = \frac{1}{2} \left[\frac{M_{\max}}{b d (d-d') f_y} - \rho_i^{sl} \right] \quad (8.51)$$

$$\rho_i \geq \rho_{\min}, \quad \rho_i \geq \frac{M_{i \text{ ser}}^+}{b d (d-d') f_y}, \quad \rho_i \geq \frac{M_{i \text{ ser}}^-}{b d (d-d') f_y} - \rho_i^{sl}$$

where, $\rho_i^{sl} = A_{si}^{sl} / (bd)$, A_{si}^{sl} is the slab reinforcement inside the effective flange contributing to beam negative moment capacity at story i, and $(d-d')$ is the distance between centroids of the top and bottom flexural reinforcement used as internal lever arm as recommended by Paulay and Priestley (1992).

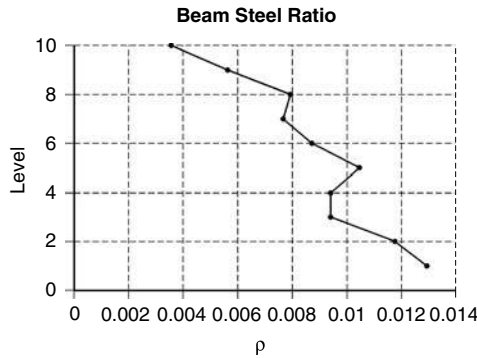


FIGURE 8.25 Provided beam steel ratio.

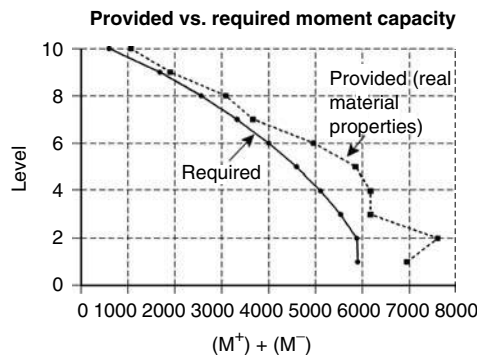


FIGURE 8.26 Required and provided beam moment capacity.

The discrete variation in number and diameter of bars explains the difference between required and provided amount of steel shown in Figure 8.24. This difference remains below 10% except at the roof level where a larger difference is obtained due to minimum steel ratio requirements. The provided beam steel ratio decreases along the height of the building as shown in Figure 8.25. Note that to obtain a straight line first mode shape the story stiffness must decrease along the height of the building as shown in Figure 8.19 and to obtain a uniform pattern of plastic hinge rotation the beam moment capacity must be as shown in Figure 8.26. Since k_i is related with the cube of the beam depth, d_i , (Equation 8.16) but M_i is only proportional to d_i (Equation 8.51), the depth of the beam must decrease slowly to satisfy stiffness than to satisfy strength requirements. To compensate, the steel ratio must also decrease along the height of the frame (Figure 8.25). As expected (Section 8.3.3.4.9) when real material properties are used to compute the first yielding moment, a ratio $M_{1,sty}/M_{1,yn} \approx 1.20$ is obtained from analysis of results shown in Figure 8.26.

Note that because of the assumption of fixed base, inflection point at first story is higher than midheight of the column. As was done for preliminary sizing for stiffness (Section 8.4.4.2) $h_{1,eff} = 2(1-0.65)h_1$ is introduced in the computation of the coefficients of Equation 8.32 as first-story height (inflection point at 0.65 h_1 is assumed). If this correction is not done, the analysis of the preliminary design shows a nonuniform pattern of plastic hinge rotations, with smaller θ_p at lower stories since the assumption of the inflection point at mid-height first story would produce a design with a stronger first story beam than it would be really required. Since $h_{1,eff}$ was used, Figure 8.26 shows that the required bending moment at first level is similar to that of the second level in spite of the fact that the first story is 33% higher than the second.

8.4.4.6.3 Design Shear for Beams

The design shear in beams is obtained using Equation 8.37. The design was done so that $V/(bd) \leq 15.7\sqrt{f_c}$ in KN/m² [$V/(bd) \leq 6\sqrt{f_c}$ in psi] to avoid sliding shear problems. Figure 8.27 shows

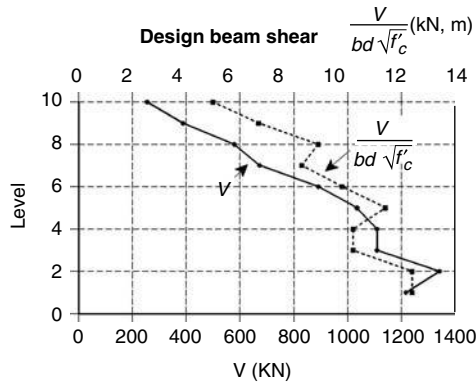


FIGURE 8.27 Shear and normalized shear stress for beams.

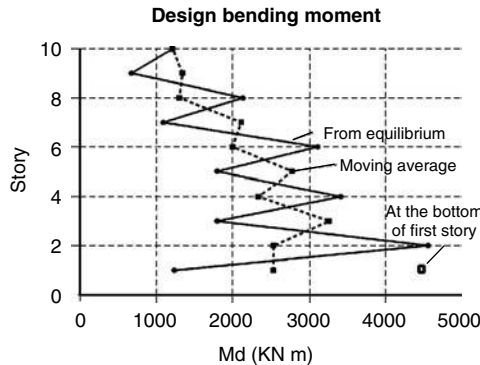


FIGURE 8.28 Design bending moment for exterior column.

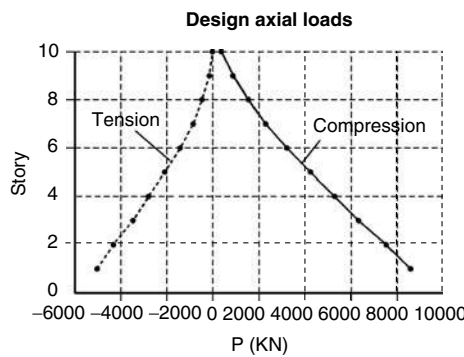


FIGURE 8.29 Design axial load for exterior column.

the shear, V , and the normalized shear stresses $V/(bd\sqrt{f'_c})$ for beams of external frame. Since beam sizes decrease slower than shear for the same reasons mentioned above, the normalized shear stresses decrease along the height of the building as shown in Figure 8.27 and the bottom stories will be critical with respect to shear requirements. Therefore, to avoid sliding shear economically in the case of tall buildings, it could be convenient to increase the beam concrete strength from the top to the bottom of the building.

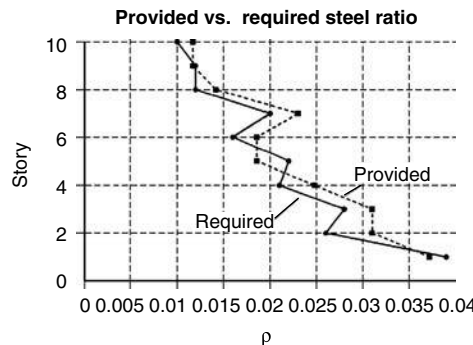


FIGURE 8.30 Provided and required steel ratio for exterior column.

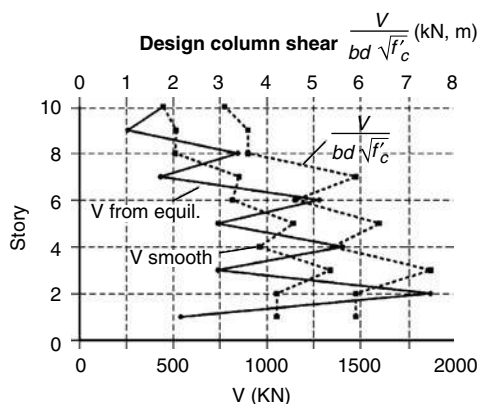


FIGURE 8.31 Shear and normalized shear stress for exterior columns.

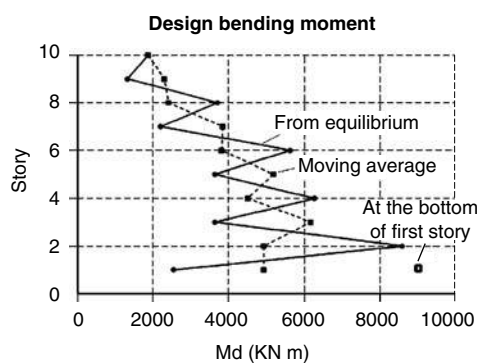


FIGURE 8.32 Design bending moment for interior column.

8.4.4.6.4 Design Moments for Columns

The bending moment in columns can be computed using equilibrium and the hypothesis of an inflection point at the middle of the columns from the designed beam bending moments (Equation 8.38). Figures 8.28 and 8.32 show the design bending moments for exterior and interior columns, respectively. The zig-zag pattern obtained using Equation 8.38 as well as the three-story moving average used for designing

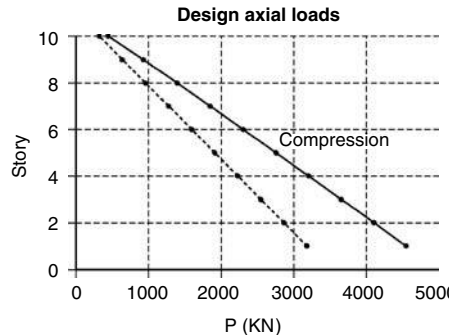


FIGURE 8.33 Design axial load for interior column.

can be seen. Since first story inflection point was assumed at $0.65 h_i$, the bending moment at the base must be amplified using a factor $0.65/(1-0.65) = 1.85$ as shown in Figures 8.28 and 8.32.

8.4.4.6.5 Design Axial Load for Columns

From equilibrium the maximum and minimum axial loads in the columns were computed using Equation 8.39. Figures 8.29 and 8.33 show the design axial loads for exterior columns and interior columns, respectively. Note that high tension loads are expected for exterior columns.

8.4.4.6.6 Design Shear for Columns

The shear in columns can be computed using the design bending moments $M_i^T = M_i^B = M_i$ obtained from equilibrium in the columns of story i using Equation 8.40. Figures 8.31 and 8.35 show the design shear for exterior and interior columns, respectively. Because of the zig-zag pattern of the design column shears, a three-story moving average was used for their sizing. Exterior columns have larger axial loads and smaller bending moments than interior columns. As a consequence, exterior and interior columns tend to have the same sizes, such as in this particular building. Since shear forces are related to bending moments, interior columns tend to be critical with respect to the shear stresses as shown by the values of $V/\left(bd\sqrt{f'_c}\right)$.

8.4.4.6.7 Preliminary Design of Main Reinforcement in Columns

Using the axial loads and smooth bending moments computed above, the steel in the columns is selected from an interaction diagram. The steel ratio is limited to $0.01 \leq \rho \leq 0.06$. Figures 8.30 and 8.34 show the required and designed steel ratio, ρ , for exterior and interior columns, respectively. The discrete variation in number and diameter of bars explains the difference between required and provided amount of steel. Figure 8.36 shows the preliminary design of main reinforcement for beams and columns.

8.5 Analysis of the Preliminary Design

8.5.1 Introductory Remarks

The following analyses were carried out to evaluate the preliminary design:

- (a) Linear Elastic Dynamic Analysis
 - 3D linear elastic response spectrum analysis using the factored serviceability response spectra (i.e., mean + σ SLEDRS, Figure 8.16).
 - 3D linear elastic time-history analysis for critical EQGM with $PGA_{service} = 0.08$ g.
- (b) Nonlinear Static Analysis
 - 2D nonlinear “push-over” tests for the lateral force pattern obtained from the safety spectral modal analysis (Figure 8.22).

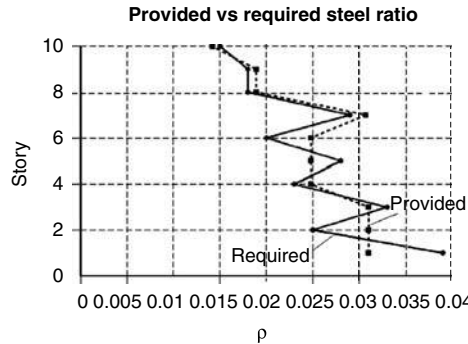


FIGURE 8.34 Provided and required steel ratio for interior column.

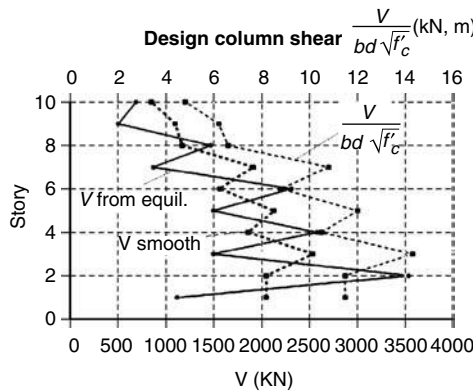


FIGURE 8.35 Shear and normalized shear stress for interior columns.

(c) Nonlinear Dynamic Analysis

2D nonlinear time-history analysis for the critical EQGM with $PGA_{safety} = 0.40$ g.

8.5.2 Linear Elastic Dynamic Analysis

8.5.2.1 3D Linear Elastic Response Spectrum Analysis

8.5.2.1.1 Main Objectives of the Analysis are

- (a) To check the behavior of the structure under factored service EQGMs (i.e. mean $+\sigma$ SLEDRS using the two horizontal components of the EQGMs); to check IDI in order to control nonstructural damage and to obtain the PGA that produces first yielding on the structure.
- (b) To detect any weakness in the structure using the distribution of stress-ratios along the building.
- (c) To estimate the nonlinear behavior of the structure from the distribution of stress-ratio throughout the building.

8.5.2.1.2 Period and Mode Shapes

From the 3D analysis the periods of Table 8.2 were obtained for: (a) $e_{acc} = 0$ in all stories and (b) $e_x acc = 0.05 L$ in all stories. Because of symmetry with $e_{acc} = 0$ the first three modes are uncoupled. The first mode is translation along x; the second mode is translation along y and the third mode is rotation around the center of stiffness. With $e_{acc} = 0.05L$, the second mode is translation along x; the first and the third mode are translations along y coupled with rotations. The center of rotation for the first mode is

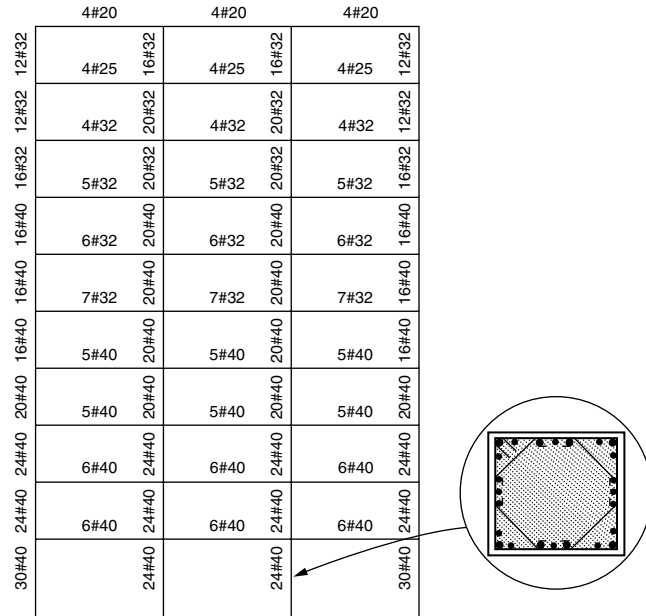


FIGURE 8.36 Preliminary design of main reinforcement for beams and columns (mm).

TABLE 8.2 Period of the Building With and Without Accidental Eccentricity

Mode	Period $e_{acc} = 0$	Period $e_{acc} = .05L$
1	0.93	0.96
2	0.93	0.93
3	0.79	0.77
4	0.36	0.37
5	0.36	0.36
6	0.31	0.30
7	0.19	0.20
8	0.19	0.19
9	0.17	0.16

outside of the building plan in opposite direction to the vector going from the center of stiffness to the center of mass. The center of rotation for the third mode is inside the building plan near the center of mass. Note that for a structure like this, with or without small static eccentricities, the accidental eccentricity has considerable effect on the mode shapes and therefore on the seismic response (however, the periods T_i are not so much affected). As required for the preliminary design, a straight line was obtained for the first mode of the frames when the 2D behavior is considered.

8.5.2.1.3 Lateral Displacements

Figures 8.37 and 8.38 show the envelope of the lateral displacement of the interior and exterior frames with and without consideration of e_{acc} . When e_{acc} is considered, the displacements of the interior frame decrease by 6% while the displacements of the exterior frame increase by 38%. These results were expected from the theoretical analysis of the elastic torsional effects on a two DOFs (Figure 8.18 and Section 8.4.3.5) and in fact 1.50 was the amplification factor due to torsion used for designing of the exterior frame.

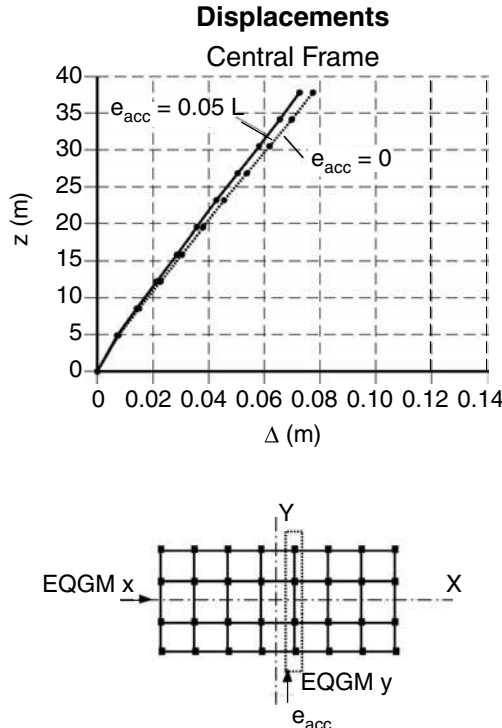


FIGURE 8.37 3D linear elastic response spectrum analysis of central frame (Y displacements).

8.5.2.1.4 Base Shear

The maximum base shears with and without e_{acc} are summarized in Table 8.3. The effect of accidental torsion is to reduce the base shear acting in the main EQGM direction ($y = 100\%$ EQGM) and introduce a torque over the structure. Note that when e_{acc} is considered, the demand on the external frames is increased even though the total base shear is reduced because of the simultaneous torsional effects. The total base shear decreases because the displacement of the center of mass is smaller in the first mode when the accidental torsion is considered than when it is not. The total base shear for the case with $e_{acc} = 0$ is practically equal to the estimated for designing ($V = 0.19 W$).

8.5.2.1.5 IDI ($e_{acc} = 0.05L$)

Figure 8.39 shows the IDI envelope obtained with and without e_{acc} . The target maximum IDI for service PL of 0.003 is slightly surpassed at 8th and particularly at 9th floor levels which correspond to the 7th and 8th stories. Therefore, the design is considered satisfactory for controlling the nonstructural damage under service PL since the stiffness of most of the beams was underestimated. During the seismic response, several beams are not close to the yielding point as it was considered to estimate I_{eff} for beams.

For the maximum displacement at external frames ($\Delta_{roof} = 0.107 \text{ m}$), a straight line displacement shape produces an $IDI_{uniform} = 0.107/37.82 = 0.00283$. The maximum IDI obtained during the 3D response spectrum analysis was 0.00306, i.e., 8% larger than $IDI_{uniform}$; very close to the factor $\beta_0 = 1.05$ used to increase the IDI due to deviation of the assumed first mode shape in the preliminary design.

8.5.2.1.6 Stress Ratio ($e_{acc} = 0.05L$)

The stress ratio λ for the demanded positive and negative bending moments in beams is defined as

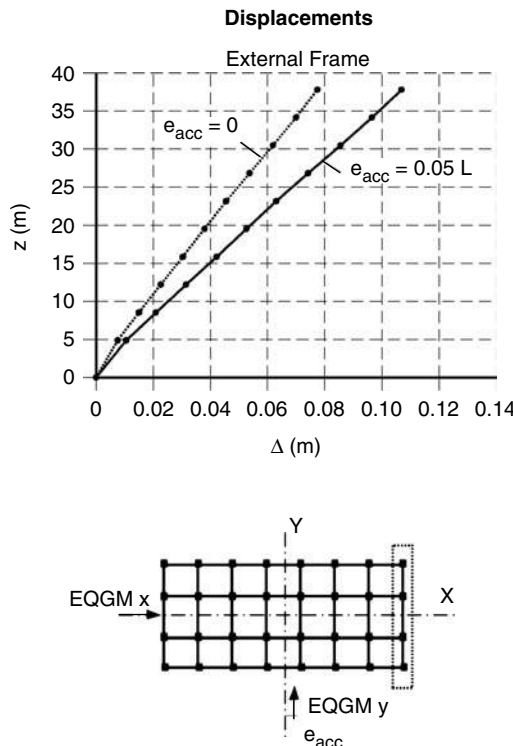


FIGURE 8.38 3D linear elastic response spectrum analysis external frame (Y displacements).

TABLE 8.3 Maximum Base Shear with and without e_{acc} (Serviceability)

Direction	Base Shear $e_{acc} = 0$	Base Shear $e_{acc} = 0.05L$
V_x	0.057 W	0.057 W
V_y	0.191 W	0.167 W

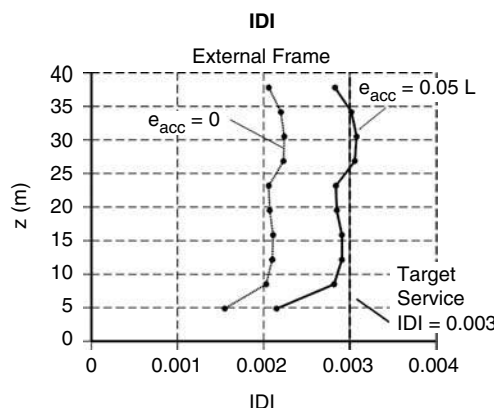


FIGURE 8.39 3D linear elastic response spectrum analysis of external frame IDI.

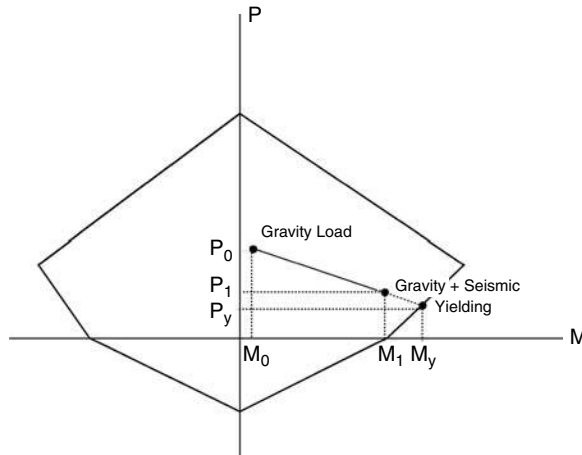


FIGURE 8.40 Determination of stress-ratio for columns.

$$\lambda^+ = \frac{M_i^+ - M_o^+}{M_y^+ - M_o^+} \quad \lambda^- = \frac{M_i^- - M_o^-}{M_y^- - M_o^-} \quad (8.52)$$

where M_0 is the maximum bending moment in the beam for gravity loads, M_i is the maximum bending moment in the beam for the combination of gravity loads and seismic actions and M_y is the yielding moment for the beam.

The same formula can be used for columns. However, an interaction diagram, as shown for a case with bending moment in only one direction in Figure 8.40, has to be used. For columns under biaxial bending moments (as in the building considered here) the 3D interaction diagram for columns must be considered. Figure 8.41 shows the maximum value of the stress-ratio for beams and columns in each story of an internal frame. The stress ratio is proportional to the diameter of the dots plotted at the ends of each member. From analysis of these stress ratios, the following conclusions can be obtained:

1. Since $\lambda_{\max} = 0.95$ was obtained at the roof beam of the central frame, first yielding can be expected in that beam for EQGMs with $\text{PGA} > (0.08/0.95)g = 0.084g$.
2. Since the strength of each frame was selected to reach almost simultaneous yielding during the elastic torsion response ($V_4 = 0.7 V_1$, $V_3 = 0.8 V_1$, $V_2 = 0.9 V_1$), almost similar values are obtained for the stress-ratio in all frames.
3. Since an amplification factor $\beta_1 = 1.5$ was selected due to elastic torsion and a real amplification factor 1.38 was obtained (Figure 8.38), $\lambda_{\max} = 1.38/1.5 = 0.92$ (very close to the obtained value $\lambda_{\max} = 0.95$) was expected where serviceability limit state controls the design.
4. The strong column-weak beam design concept is reflected in the smaller λ obtained for columns. Note that the bottom of the first story columns has the larger stress-ratio, this is because in the preliminary numerical design the inflection point at the first story columns was assumed at $0.65 h_1$, and therefore the bending moment at the base was amplified using a factor $0.65/(1 - 0.65) = 1.85$. However, the obtained first-story inflection point was around $0.75 h_1$, i.e., with a bending moment amplification factor of $0.75/(1 - 0.75) = 3.0$. Therefore, if $\lambda \approx 0.4$ is expected for columns (as is indicated in Figure 8.41), a stress-ratio $\lambda \approx 0.4 \times 3.0/1.85 = 0.65$, close to the obtained value, results at the bottom of the first-story columns.

8.5.2.2 3D Time-History Analysis

8.5.2.2.1 Main Objectives of the Analysis

- (a) To check the behavior of the structure under a service EQGM; to check IDI to control nonstructural damage.

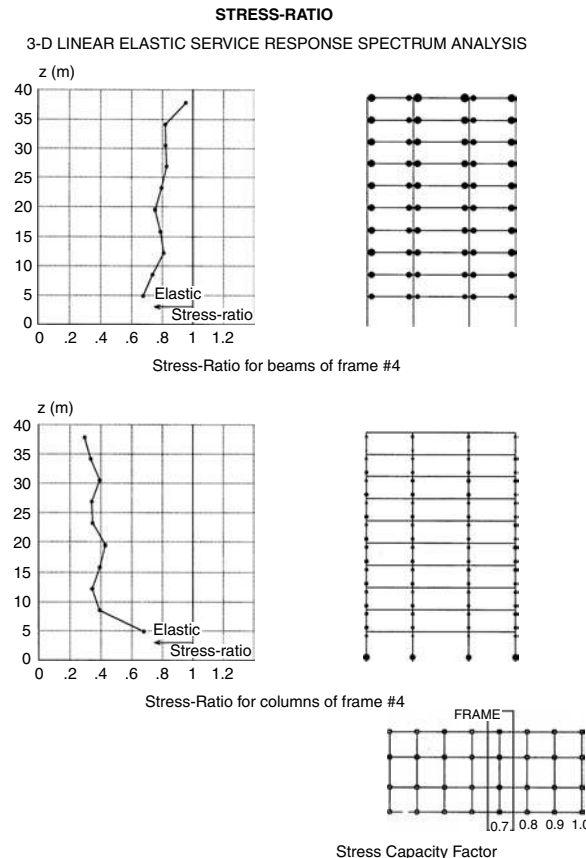


FIGURE 8.41 Stress-ratio for columns and beams.

- (b) To check the LERS modal superposition analysis.
- (c) To use as a reference for the nonlinear time-history analysis. Note that for evaluation of nonlinear behavior it is necessary to run nonlinear time-history analysis. A linear time-history analysis is useful for evaluating the differences between linear and nonlinear behavior. This comparison can be difficult if only LERS modal superposition analysis is done.

8.5.2.2.2 Base Shear and Equivalent Earthquake Forces ($e_{acc} = 0.05 L$)

Figure 8.42(a) shows that the LERS of the selected factored service EQGMs follows the shape of the SLEDRS (mean+sigma) and therefore close results to that obtained in the elastic response spectrum analysis are expected. Note that ideally, SLEDRS should be based on EQGM records obtained at the site. However, since there were not enough of such records, seven probable EQGM time histories were generated by using numerical synthesis. The EQGM with larger demand at the fundamental period of the building was selected as the service time history for these analyses.

Figure 8.42(b) shows a comparison of the design service earthquake forces and the time-history-equivalent earthquake forces for external frames computed from the story shear envelope ($F_i = S_{i+1} - S_i$). Very close agreement exists in the value and distribution of the design and obtained earthquake forces.

8.5.2.2.3 Lateral displacements and IDI ($e_{acc} = 0.05 L$)

Figure 8.42(c) shows the envelope of IDI for the external frame. The target maximum IDI (0.003) is not surpassed. The shape of IDI is quite uniform and very close to that obtained in the SLEDRS analysis.

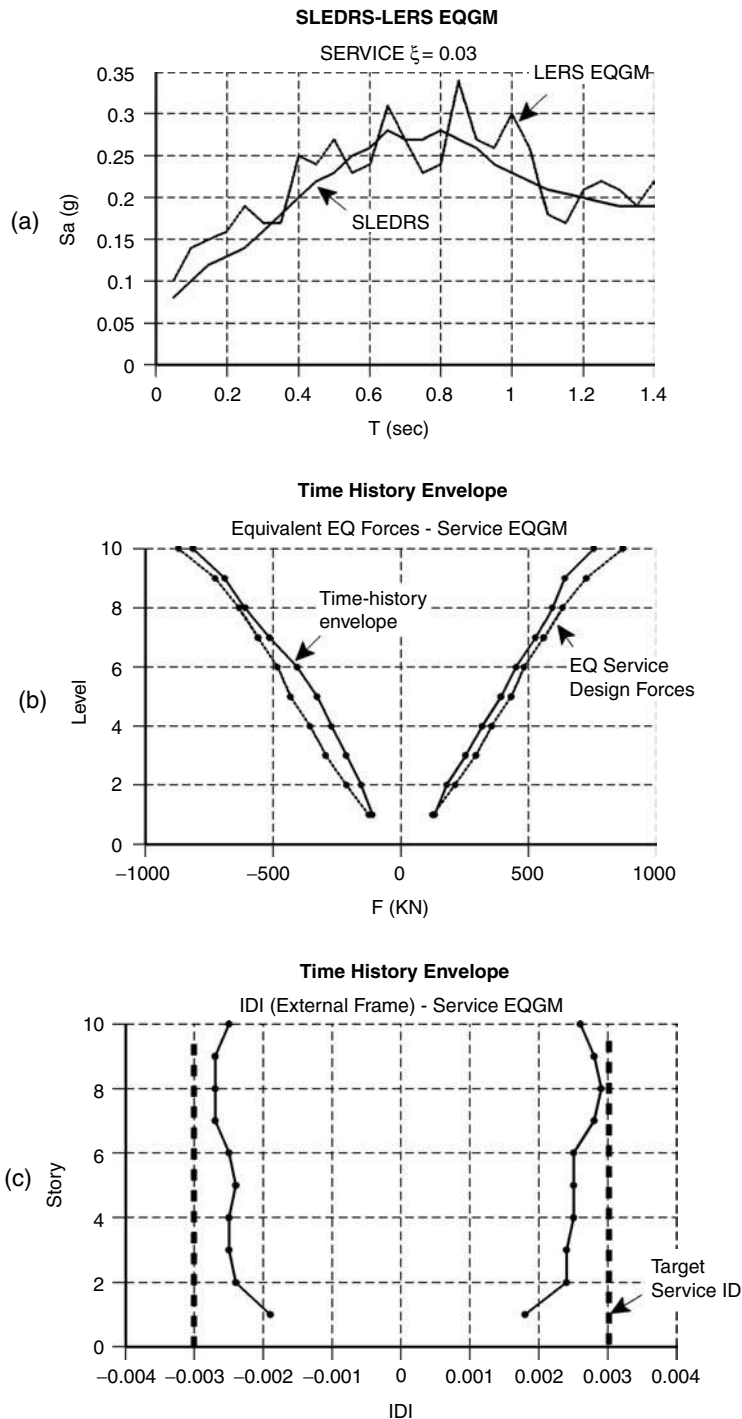


FIGURE 8.42 (a) SLEDRS and LERS of the factored service EQGM used for time-history analysis. (b) Design and time-history envelope of the service equivalent earthquake forces. (c) Envelope of maximum IDI for time-history analysis under service EQGM.

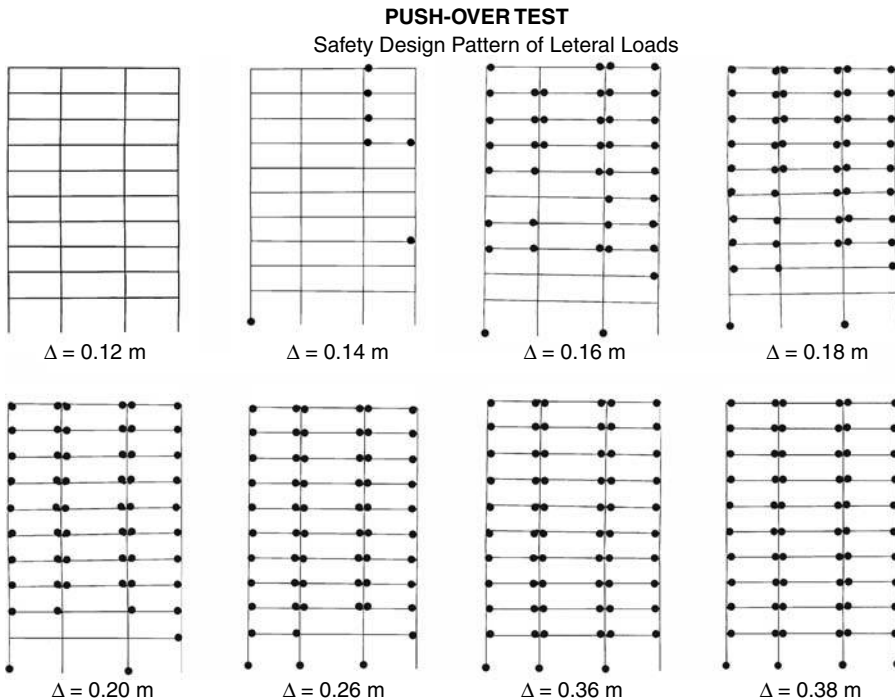


FIGURE 8.43 Sequence of plastic hinge formation for push-over analysis of external frame.

8.5.3 Nonlinear Analysis: “Push-Over” Analysis

8.5.3.1 Main Objectives of the Analysis

- (a) To obtain the maximum shear strength of the structure, V_{mech} , and the mechanism of collapse.
- (b) To evaluate if the structure can achieve the collapse mechanism without exhausting the plastic rotation capacity of the members.
- (c) To obtain the monotonic displacement and global ductility capacity of the structure.
- (d) To estimate the concentration of damage and IDI that can be expected during the nonlinear seismic response.

8.5.3.2 Ultimate Base Shear and Collapse Mechanism

Figure 8.43 shows the sequence of plastic hinge formation. A complete mechanism is obtained for a roof displacement $\Delta_{\text{roof}} = 0.38 \text{ m}$. No partial mechanism is obtained, so that the design is satisfactory in this aspect. The effect of designing a stronger first-story beam to reduce the plastic hinge rotation demand at column base can be noted in the sequence of plastic hinge formation. To obtain a stronger first story beam an inflection point lower than expected was used at first story in the plastic optimum design of beam steel reinforcement (Section 8.4.4.6). Plastic hinge formation at first story beams is not complete until $\Delta_{\text{roof}} = 0.36 \text{ m}$, and the last plastic hinge is obtained at the exterior column base under compression. Note the correlation between the floors where beam steel provided, A_s , is slightly smaller than required A_s (levels 3, 7 and 9) and the plastic hinges formed at $\Delta_{\text{roof}} = 0.14 \text{ m}$. Figure 8.44 shows that $V_{\text{mech}} = 7200 \text{ KN}/17950 \text{ KN} = 0.40 \text{ W}$ is obtained considering $P - \Delta$ effects. The $P - \Delta$ effects tend to counteract the effects of the deformation-hardening so that practically an elasto-perfectly plastic behavior is obtained for the global response. The structure was designed for $V_{\text{saf}} = 0.29 \text{ W}$ and an overstrength $\Omega_{\text{saf}} = 1.4$ was considered so that $V_{\text{mech}} = 0.40 \text{ W}$ was expected, i.e., very close to the obtained value.

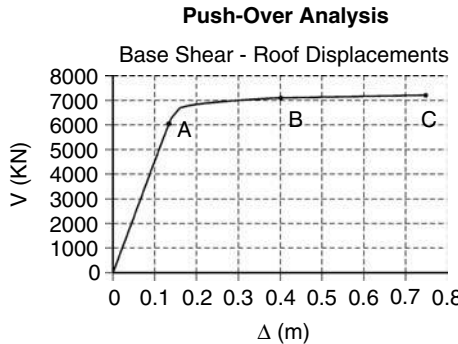


FIGURE 8.44 Base shear-roof displacement for push-over analysis of the external frame.

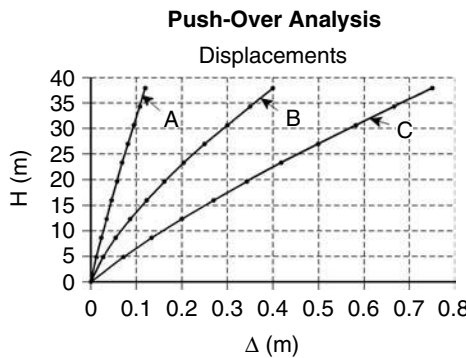


FIGURE 8.45 Displacements for push-over analysis.

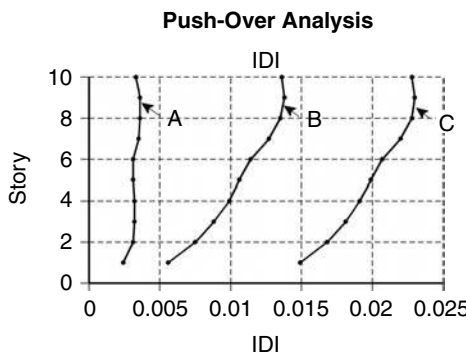


FIGURE 8.46 IDI for push-over analysis.

8.5.3.3 Displacements and IDI

Figures 8.45 and 8.46 show the displacements and IDI, respectively, at (A) first yielding ($\Delta_{roof} = 0.13$ m); (B) $\Delta_{roof} = 0.40$ m and (C) $\Delta_{roof} = 0.75$ m. As the plastic hinge formation progresses, the IDI shape changes, tending to increase at the upper stories, i.e., with lower values at bottom stories as was required to protect first-story columns. However, the concentration of an IDI is still small enough to be considered satisfactory. For example, while for $\Delta_{roof} = 0.75$ m a straight line displacement shape produces a

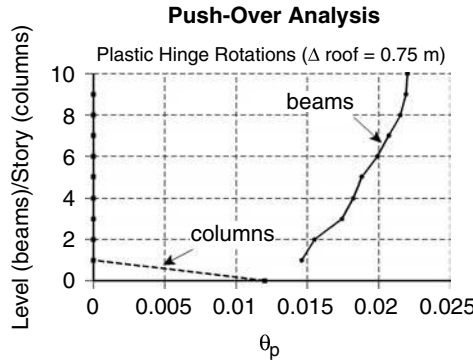


FIGURE 8.47 Plastic hinge rotations for push-over analysis.

$IDI_{\text{uniform}} = 0.75/37.82 = 0.0198$, the maximum IDI obtained during the push-over analysis for that roof displacement was 0.0230, i.e., only 16% larger than IDI_{uniform} .

8.5.3.4 Plastic Hinge Rotation

Figure 8.47 shows the distribution of the maximum plastic hinge rotations of columns and beams in each story and floor respectively for $\Delta_{\text{roof}} = 0.75 \text{ m}$, which corresponds to a global ductility ratio about $\mu = 5$. From comparison of the results presented in Figures 8.46 and 8.47, it becomes clear that for this building a very good approximation to the beam maximum θ_p values can be obtained using the IDIs. A quite uniform distribution of plastic hinge rotations is obtained along the frame (i.e. a maximum to mean θ_p ratio equal to 1.16, Figure 8.47). As shown in Figure 8.44, when the roof reaches a $\Delta = 0.75 \text{ m}$ (i.e., for a ductility ratio $\mu = 5$), the θ_p according to Figure 8.47 indicates that at the base of the external column (which is under a compression axial load of $P = 9120 \text{ KN}$) the maximum plastic hinge rotation is $\theta_p = 0.012$ and that the beams at stories 9 and 10 undergo a maximum plastic hinge rotation of $\theta_p = 0.022$. Note that the plastic hinge rotation at the base of the external column is approximately equal to the plastic hinge rotation at first level beam (Figure 8.47). The smaller maximum plastic hinge rotation at the columns with respect to the beams reflects the fact that the plastic hinges are formed at first level at larger displacements than at the highest levels (Figure 8.43). Using the required ACI confinement (ACI, 1995) (e.g., 2 #5 hoops at 10 cm for columns), the plastic hinge capacity is about 0.05 for beams and 0.032 for columns under the compression load mentioned above. The plastic hinge capacity of beams and first story column under compression is exhausted for $\Delta_{\text{roof}} \approx 1.40 \text{ m}$ ($\mu_{\text{u mon}} \approx 9$).

8.5.4. Nonlinear Analysis of an Equivalent SDOF System

8.5.4.1 Equivalent SDOF System for Nonlinear Analysis

The global behavior of an MDOF system can be analyzed using an equivalent SDOF system as follows. Assume the building responds basically in the first mode shape ϕ (normalized with unitary value at the roof), so that the displacements of the building floors can be computed by $u = \phi u$, where u = roof displacement. The linear elastic response of this generalized SDOF system is given by the following differential equation (Clough and Penzien, 1992)

$$\ddot{u} + 2\xi\omega\dot{u} + \omega^2u = -\frac{L^*}{m^*}\ddot{u}_g; \quad m^* = \Phi^T M \Phi \quad L^* = \Phi^T M 1 \quad (8.53)$$

The yielding base shear, V_y^* , of an equivalent elasto-perfectly plastic SDOFS with the same period, T_1 , ($T_1 = 2\pi/\omega$) and same yielding displacement, u_y , than the first mode period and roof displacement of the real MDOFS, can be computed as

$$V_y^* = k^* u_y = m^* \omega^2 u_y \quad (8.54)$$

Then the yielding base shear coefficient is

$$C_y^* = \frac{V_y^*}{m^* g} = \frac{\omega^2 u_y}{g} \quad (8.55)$$

From Equations 8.53 to 8.55, the global nonlinear response of the building can be estimated from the response of an equivalent SDOFS to EQGMs with ground accelerations amplified by (L^*/m^*) . The equivalent SDOFS has period T = first fundamental period of the building, and yielding base shear coefficient given by Equation 8.55. The displacement time history obtained from this equivalent SDOFS is an estimation of the displacement of the building roof. Note that with these definitions, the energy of the SDOFS is equivalent to the energy of the MDOFS since a variation of the deformation energy, δU , in the MDOFS and in the equivalent SDOFS is obtained from a variation in δu as follows

$$\delta U = \delta u^T R(t) = \delta u \Phi^T R(t) = \delta u V^*(t); \Rightarrow V^*(t) = \Phi^T R(t) \quad (8.56)$$

where $R(t)$ are the resisting force at each floor. Since at yielding $R_y = K \phi u_y$, then

$$V_y^* = \Phi^T R_y = \Phi^T K \Phi u_y = k^* u_y = m^* \omega^2 u_y \quad (8.57)$$

A global damage index for the equivalent SDOFS can be computed as

$$DM = \frac{\mu - 1}{\mu_{u mon} - 1} + b \frac{E_H^*}{V_y^* u_y \mu_{u mon}} = \frac{\mu - 1}{\mu_{u mon} - 1} + b \frac{E_H^* / m^*}{C_y^* g u_y \mu_{u mon}} \quad (8.58)$$

Since Equation 8.58 does not satisfy the requirement that in case the seismic response consists of just a monotonically increasing deformation the DM index should be equal to 1.0; the following modification introduced by Bozorgnia and Bertero (2002) which was recently proposed could be used with advantage

$$DM = (1 - \alpha_1) \frac{u_{max} - u_y}{u_{u mon} - u_y} + \alpha_1 \frac{E_{H max}}{E_{Humon}} \quad (8.59)$$

8.5.4.1.1 Main Objectives of the Analysis

1. To select the critical EQGM for the time-history dynamic analysis of the complete structure. Time-history analyses for the EQGMs used for preliminary design are conducted for the equivalent SDOFS. The damage index, DM, is computed in each case and the EQGM producing the larger DM will be selected to study the building behavior
2. To evaluate the global behavior of the structure under critical EQGMs using data from a push-over analysis.

8.5.4.1.2 Estimation of Maximum Earthquake Response Using Data from Push-Over Analysis

The data obtained from the push-over analysis, complemented with an analysis of an SDOF system, can be used to estimate the maximum earthquake response (Figure 8.48). In this case, an equivalent SDOFS representing the real structure (period $T = 0.92$ sec, $u_y = 0.16$ m [Figure 8.49], $C_y^* = 0.76$ [Equation 8.55], $L^*/m^* = 1.43$ and ultimate monotonic ductility ratio $\mu_{u mon} = 9$ [from push-over analysis]) was used. Several time-history analyses were conducted for this equivalent SDOFS subjected to each one of the design EQGMs (PGA was scaled using L^*/m^*). For the critical EQGM (Figure 8.48) the results obtained

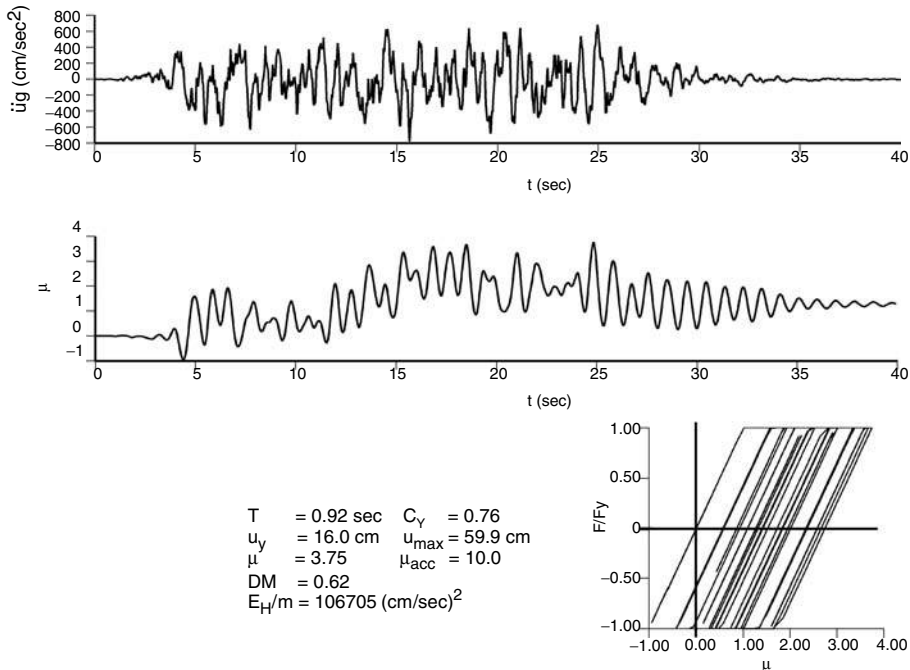


FIGURE 8.48 Equivalent SDOFS response for critical EQGM.

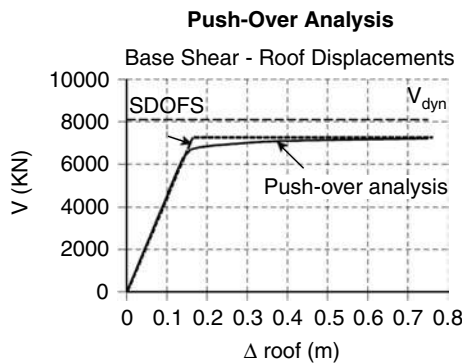
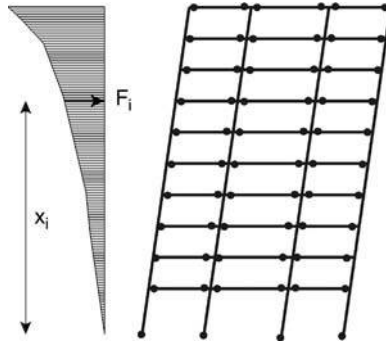


FIGURE 8.49 Dynamic base shear capacity, push-over analysis and equivalent SDOFS.

were: maximum roof displacement $u_{max} = 59.9 \text{ cm}$; maximum ductility ratio $\mu = 3.75$; accumulative ductility $\mu_{acc} = 10.0$ and global damage index $DM = 0.62$. The comparison among these values and the values selected for the design shows an acceptable concordance (Table 8.4).

8.5.4.1.3 Estimation of Ultimate Base-Shear from Plastic Analysis

A good estimation of the capacity of the structure can be obtained using the simple tools of plastic analysis. For example, for a moment-resisting space frame building with constant moment capacity M_i^+ and M_i^- for all the beams (N_b) in each story i of a particular frame, the load factor, λ_{mech} , that transforms the structure into the ideal complete mechanism of Figure 8.50 can be computed using the virtual work theorem as

**FIGURE 8.50** Estimation of V_{mech} using plastic analysis.**TABLE 8.4** Nonlinear Analysis of an Equivalent SDOF System

	u_{\max} [m]	μ_{\max}	DM
Design	$0.015H/\beta_2 = 0.47$	3.5	$0.8/\beta_2 = 0.67$
Equivalent SDOF Analysis	0.59	3.75	0.62

$$\lambda_{\text{mech}} \sum_{i=1}^n F_i x_i = \sum_{\text{all frames}} \left[\sum_{i=1}^n (M_i^+ + M_i^-) N_b + \sum_{k=1}^{N_c} M_k^c \right] \quad V_{\text{mech}} = \lambda_{\text{mech}} \sum_{i=1}^n F_i \quad (8.60)$$

where F_i is the force from the lateral load pattern corresponding to the i story, N_c is the number of columns of the frame and M_k^c is the moment capacity of the column k at the base considering the axial load in the column. Defining x_F = coordinate of the lateral forces resultant, i.e.,

$$x_F = \left(\sum_{i=1}^n F_i x_i \right) / \sum_{i=1}^n F_i \quad (8.61)$$

Equation 8.60 can be written as

$$V_{\text{mech}} = \frac{1}{x_F} \sum_{\text{all frames}} \left[\sum_{i=1}^n (M_i^+ + M_i^-) N_b + \sum_{k=1}^{N_c} M_k^c \right] \quad (8.62)$$

Equation 8.62 shows that V_{mech} depends on the pattern of lateral loads. For example, if the resultant of the inertia forces acts at a lower position during the seismic response as a mechanism of the structure than that assumed for the push-over analysis, a higher V_{mech} can be obtained in the time-history analysis. Using Equation 8.62, $V_{\text{mech}} = 0.40$ W was obtained for the structure analyzed, which is equal to the capacity computed using the push-over analysis.

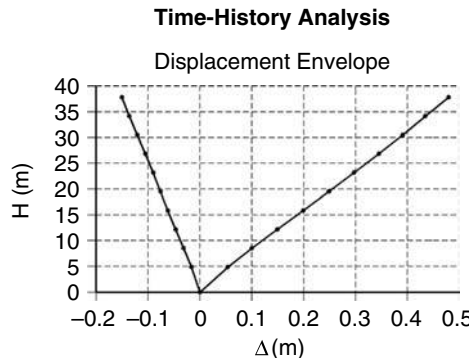


FIGURE 8.51 Displacement envelopes for time-history analysis.

8.5.5 Nonlinear Analysis: Time-History Dynamic Analysis

8.5.5.1 Main Objectives of the Analysis

- (a) To obtain the maximum IDI under safety EQGMs to verify whether nonstructural damage remains below the design level, $IDI_{saf} = 0.015$.
- (b) To obtain maximum shear forces at beam and columns to verify the level of shear stresses assumed for designing.
- (c) To obtain the maximum plastic hinge rotation, accumulative rotation and E_H demand at critical regions and compare them to available expected capacity. Using a damage criterion, to estimate the maximum local structural damage for safety-level EQGM.
- (d) To obtain the resistance-deformation time histories at critical regions and compare available data from experiments. To evaluate the local damage and the reliability of the model to reflect the expected behavior at critical regions.

8.5.5.2 Maximum Dynamic Base Shear

As indicated in Figure 8.49, the maximum dynamic base shear $V_{u\ dyn}$ obtained from the time-history analysis is 8100 kN. Therefore, expressing this $V_{u\ dyn}$ in function of the weight, W , of the reactive mass (17950 kN), it can be written as $V_{u\ dyn} = (8100\text{ kN}/17950\text{ kN})W = 0.45 W$. This value is 13% larger than the maximum base shear obtained from the push-over analysis.

8.5.5.3 Envelopes of Displacement and IDI

Figures 8.51 and 8.52 show the envelopes of displacements and IDI for the structure. A nonsymmetrical pattern of maximum displacements and IDI is obtained. This bias behavior is in agreement with that observed in the time-history displacement of the equivalent SDOF system (Figure 8.48). The distribution of maximum IDI is close to the ideal uniform pattern having a maximum value $IDI_{max} = 0.014$ at story 9, very close to the design limit $IDI_{saf} = 0.015$. For the maximum roof displacement, $\Delta_{roof} = 0.48\text{ m}$, a straight line displacement shape would produce an $IDI_{uniform} = 0.48/37.82 = 0.0127$. So that, the IDI_{max} was only 10% larger than $IDI_{uniform}$. This value is quite close to the factor $\beta_2 = 1.2$ used to consider IDI concentration for preliminary design.

8.5.5.4 Maximum and Accumulative Plastic Hinge Rotation

Figures 8.53 and 8.54 show the maximum plastic hinge rotation, θ_{pmax} , and the accumulative plastic hinge rotation θ_{pac} for beams and columns in each story. Note that, meanwhile, θ_{pmax} is just the maximum value reached by the plastic rotation at a particular hinge respects the original position before the EQGM response, θ_{pac} considers the plastic hinge rotation from the previous yielding reversal of the opposite sign. Although θ_{pmax} is associated to the maximum structural displacement, it is not the real

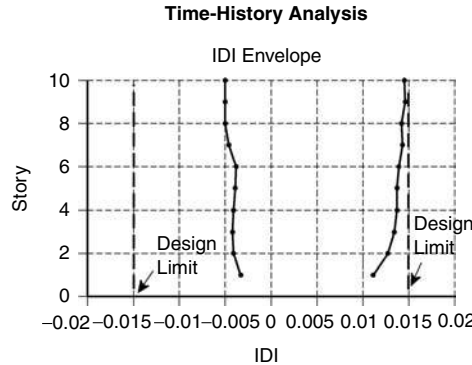


FIGURE 8.52 IDI envelopes for time-history analysis.

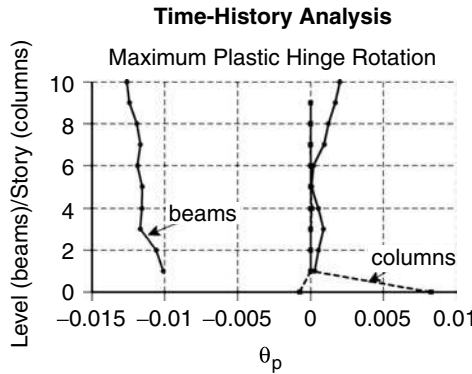


FIGURE 8.53 Maximum plastic hinge rotations for time-history analysis.

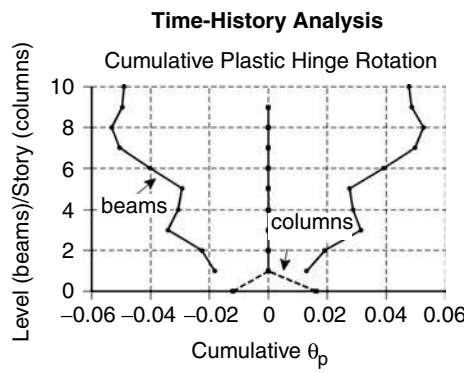


FIGURE 8.54 Cumulative plastic hinge rotation for time-history analysis.

maximum plastic rotation because is measured with respect to the original position and not with respect to the previous yielding reversal of the opposite sign. This limitation of the computer program that was used should be reviewed. Figures 8.55 and 8.56 show the complete distribution of θ_{pmax} and θ_{pac} for external frames. Note that a different pattern is obtained for θ_{pmax} and θ_{pac} . θ_{pmax} follows the nonsymmetrical pattern of IDI, while a symmetrical pattern is obtained for θ_{pac} . Local weaknesses seem to have more local effect on θ_{pac} than on θ_{pmax} (compare third-floor θ_{pac} [Figure 8.54] with provided vs.

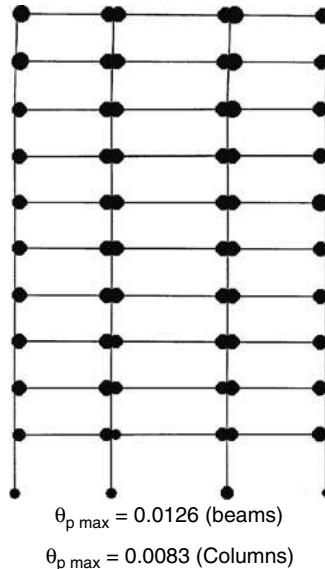


FIGURE 8.55 Time-history analysis: maximum plastic hinge rotations.

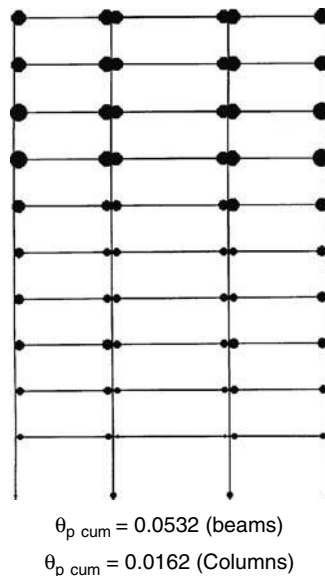


FIGURE 8.56 Time-history analysis: cumulative plastic hinge rotations.

required beam reinforcement in Figure 8.24). Comparison of Figures 8.55 and 8.56 suggests that plastic yielding reversals of the upper five stories without exceeding the maximum plastic hinge rotations could be an explanation for the different pattern obtained for $\theta_{p\max}$ and $\theta_{p\text{acc}}$.

Figure 8.57 shows that a more uniform distribution of plastic hinge rotations is obtained in this case for time-history analysis than for push-over analysis. Figure 8.57 and the larger $V_{u\text{dyn}}$ obtained suggest that a pattern of inertia forces with a lower position of their resultant than that assumed in the design could have happened during the seismic response.

Column plastic hinge rotations are obtained only where the columns join the base at first story. $\theta_{p\max} = 0.0083$, $\theta_{p\text{acc}} = 0.0162$ and a maximum compression $P = -9186$ KN are obtained for the exterior column of the exterior frame.

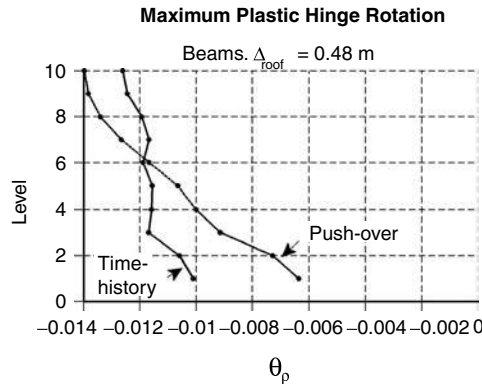


FIGURE 8.57 Comparison of maximum plastic hinge rotation from time-history and push-over analysis (equal Δ_{roof}).

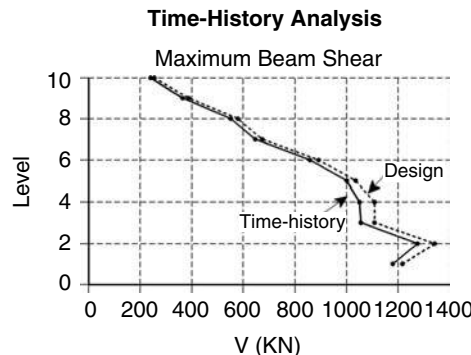


FIGURE 8.58 Time-history and design beam shear.

8.5.5.5 Maximum Shear Forces at Beams and Columns

For beams, a very good correlation was obtained between the design shear forces and the maximum values resulting from the time-history analysis (Figure 8.58). The moving average and the mid-height inflection point used for columns were also satisfactory except for first and second story as shown in Figure 8.59. Shear forces were largely underestimated for first-story exterior columns because they are estimated from equilibrium using beam moment capacities. However, since the main reinforcement is controlled for a load combination resulting in tension axial load for exterior column, and plastic hinges are formed at first-story column bases, the exterior column under compression can take a larger bending moment and therefore a larger shear than assumed for its design. To correct this problem, the first-story shear should be estimated from the moment capacity of the column under compression and the expected position of the inflection point at first story. For the rest of the stories, a moving average can be used to smooth the zigzag pattern of shear forces obtained from equilibrium.

8.5.5.6 Maximum Column Axial Loads

Figure 8.60 shows the comparison between the envelope of column axial loads obtained from the time-history analysis and the design axial loads. Time-history and push-over axial loads are very close suggesting that at time of maximum response, all beams have bending moments $M_{ph,i} \approx \Omega_b M_{yn,i}$.

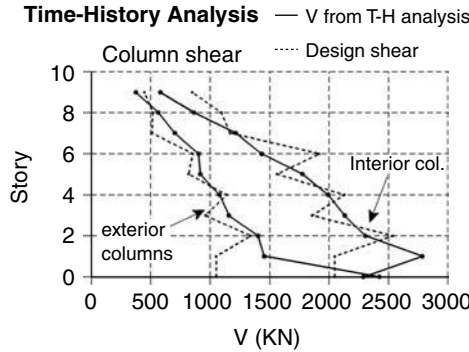


FIGURE 8.59 Time-history and design column shear.

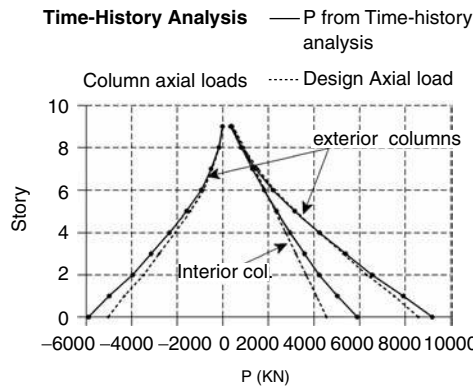


FIGURE 8.60 Time-history and design column axial loads.

8.5.5.7 Local Damage Index, DM_L

The output of the time-history analysis using DRAIN 2DX (Allahabadi and Powell, 1988) can be used directly to compute the local damage index at plastic hinges as follows. DRAIN 2DX produces as output the maximum positive and negative plastic hinge rotation, $\Delta\theta$ and θ_p^- , and the positive and negative accumulative plastic hinge rotation, θ_{pacc}^+ and θ_{pacc}^- . The accumulative plastic hinge rotations are defined as $\theta_{pacc}^+ = \sum \Delta\theta_p^+$ and $\theta_{pacc}^- = \sum \Delta\theta_p^-$, where $\Delta\theta_p^+$ or $\Delta\theta_p^-$ considers the plastic hinge rotation from the previous yielding reversal of opposite sign. Therefore, the positive and negative hysteretical energy for each plastic hinge can be computed as $E_H^+ = M_y^+ \sum \Delta\theta_p^+ = M_y^+ \theta_{pacc}^+$ and $E_H^- = M_y^- \sum \Delta\theta_p^- = M_y^- \theta_{pacc}^-$, where M_y^+ and M_y^- are the positive and negative yielding bending moment, respectively. The total hysteretical energy can be computed as $E_H = E_H^+ + E_H^-$. From the modified Park–Ang damage index (Park and Ang, 1985)

$$DM_L = \frac{\theta_p}{\theta_{pmon}} + b \frac{E_H}{M_y \theta_{pmon}} \quad (8.63)$$

Replacing E_H in Equation 8.63 with its value and assuming $M_y^+ = M_y^- = M_y$ results in

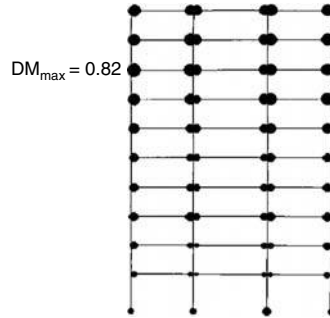


FIGURE 8.61 Damage index obtained from time-history analysis.

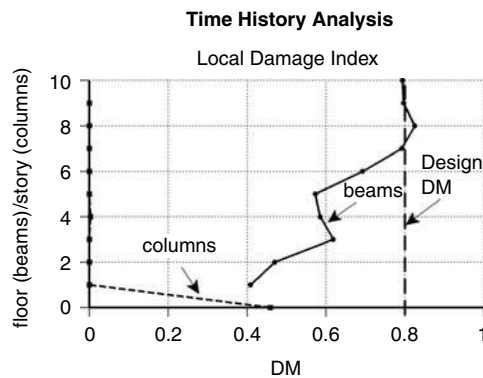


FIGURE 8.62 Maximum damage index at each level from time-history analysis.

$$DM_L = \frac{\theta_p}{\theta_{pumon}} + b \frac{\theta_{pacc}^+ + \theta_{pacc}^-}{\theta_{pumon}} \quad (8.64)$$

where θ_p is the maximum of θ_p^+ and θ_p^- , θ_{pumon} is the monotonic plastic hinge rotation capacity of the section (assumed to be the same for positive and negative rotation) and b is a model parameter. Since there was a lack of confidence in the workmanship, conservatively, $\theta_{pumon} = 0.04$ for beams, $\theta_{pumon} = 0.03$ for columns at the base under compression and b = 0.20 were used to compute damage index for this building using Equation 8.64. Equations similar to Equation 8.59 as suggested by Bozorgnia and Bertero (2002) could also be used.

The local DM_L index obtained for beams and columns are shown in Figures 8.61 and 8.62. A maximum local damage index, $DM_L = 0.82$, is obtained for the exterior beam at floor nine where the maximum accumulative plastic hinge rotation occurs. Since the maximum local damage is close to the target local damage index of $DM_L = 0.80$ and no important concentration of damage is detected and a smaller damage index is obtained for columns ($DM_L = 0.47$), the behavior of the preliminary design can be considered satisfactory for the safety PL.

8.5.5.8 Resistance-Deformation Time-Histories at Critical Regions

Since the maximum damage index was obtained for the exterior plastic hinge at the first beam of the ninth floor, the local seismic demand at that joint was selected to compare its resistance-deformation behavior against test results. Since DRAIN 2DX gives time-history of bending moment and plastic rotations, the total rotation of the end of beams can be obtained adding the elastic rotation as follows

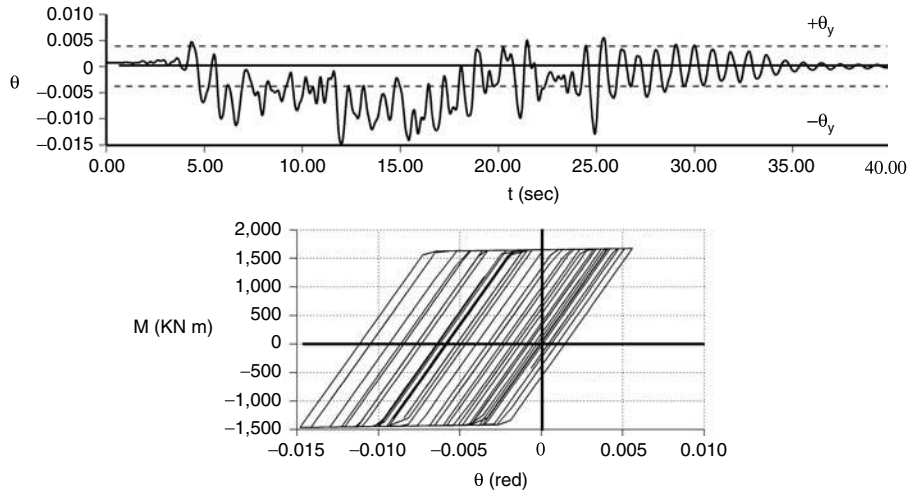


FIGURE 8.63 Moment vs rotation of the end of the beam located at the eighth level and left span.

$$\theta = \theta_p + \theta_e = \theta_p + \frac{L}{6E I_{eff}} [2 \ -1] \begin{Bmatrix} M_i \\ M_j \end{Bmatrix} \quad (8.65)$$

Figure 8.63 shows the time history of the rotations, θ , and the moment-rotation ($M - \theta$) of the end of the beam located at the eighth level (ninth floor) and left span where maximum damage is expected (Figure 8.61). Figure 8.64 shows test result obtained for a half-scale T-beam (Ma et al., 1976). Clearly the model used cannot reproduce the "pinching" in the moment-curvature diagram ($M - \theta$) caused by the Bauschinger effect, shear deformations and particularly fixed-end rotations caused by the slippage of the main reinforcement, which cannot be considered by the bilinear beam-column element that has been used in the analytical model. The normalized hysteretic energy demand computed from Figure 8.63 is smaller than the capacity obtained from Figure 8.64. Note that the maximum plastic rotation and maximum cyclic plastic rotation for the test of Figure 8.64 were 0.038 and 0.068, respectively (Ma et al., 1976).

8.5.6. Evaluation of the Performance of the Final Design for the Remaining P-BDO

From the example presented in this chapter, it is very clear that at least two performance levels should be considered from the preliminary design so that appropriate design decisions could be made to have a final design that will satisfy all the required performance objectives of the P-BDO matrix. Therefore, the problem is to define which two performance levels should be considered. At present, the serviceability or the fully operational and the life safety levels are the performance levels that should be selected for preliminary design since they are the ones for which data and experience exist. Another advantage is that the design for serviceability or fully operational levels with proper consideration of the serviceability level are the limit states that can be conducted and analyzed by using the very well-known techniques of elastic design and analysis. Subsequently, response in the nonlinear range (i.e., the life safety limit state) can be estimated using plastic analysis. Thus, the two different stages of behavior (linear and nonlinear) can be controlled using already well-established procedures.

After the preliminary design has been completed and the final detailing and adjustments have been done, it is necessary to evaluate the performance of the final design for all POs, including the POs that have not been used for the preliminary design. When serviceability (considering the probable require-

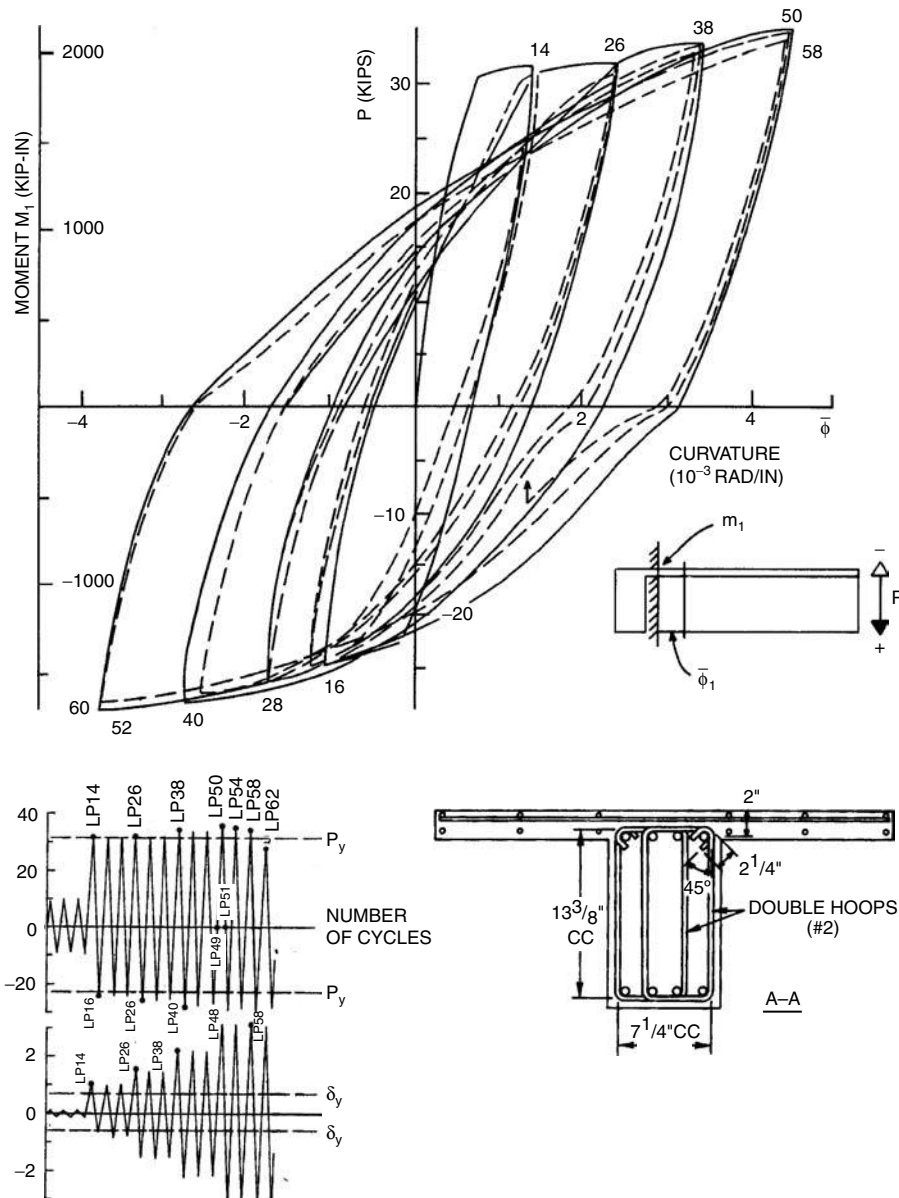


FIGURE 8.64 Test results for a half scale T-beam (Ma et al., 1976).

ments for the fully operational PO) and life safety PO are selected for preliminary design (as in the example of this chapter), the intermediate PO (i.e., the operational PO) is satisfied if the final design satisfies serviceability, fully operational and life safety POs. However, in the cases that the intensity of the hazards corresponding to the operational PO is significantly more severe than that corresponding to the fully operational PO, i.e., close to the life safety PO, it will be necessary to evaluate the performance of the final design for the operational PO.

Furthermore, it will be still necessary to assure that the building will not collapse under the maximum credible earthquake. Therefore, besides the analysis for serviceability and life safety, the performance of the final design should be evaluated controlling the structural damage so that for the maximum considered EQGM the building does not collapse.

8.5.7 Limitations of the Nonlinear Analyses That Have Been Conducted

8.5.7.1 2D Idealization

The real 3D structure was replaced by a 2D model. The following limitations result:

- (a) The torsional behavior is missing.
- (b) It is not possible to consider bi-axial EQGMs (e.g., 100% in one direction and 30% in the other; or the recorded components).

To go beyond this limitation, it is necessary to use a complete 3D nonlinear model.

As discussed in more detail in Chapter 6, several programs are now under development and testing and it is expected to be ready in the near future. For example, the Pacific Earthquake Engineering Research Center (PEER) has embarked on a multiyear effort to develop the open system for earthquake engineering simulation (*OpenSees*). One of the best features of OpenSees is its suitability to support a multidisciplinary approach to P-BSD simulation problems. The software is an “open source,” meaning that all parts of the code are available for users to see, check, track changes and make contributions. The website at <http://opensees.berkeley.edu> provides a download center, supports a revision control system, a method for submitting contributions and a bulletin board for communication.

8.5.7.2 Model of Beams

The beams are modeled using a linear and an elastic–plastic element combined in parallel. The limitations of this model are:

- (a) Lumped plasticity is used.
- (b) The model has to have equal flexural stiffness for positive and negative bending moments.
- (c) Stiffness-degradation behavior is not considered.
- (d) Shear stiffness is constant along the analysis.

It is believed that the best solution for improving the model is the use of fiber elements (Spacone et al., 1996). Fiber elements have been introduced in DRAIN 2DX in 1993 (Prakash, 1993), and they have been implemented also in the OpenSees (2001).

8.5.7.3 Model of Columns

The model of columns, like that of beams, is the combination in parallel of a linear and an elastic–plastic element. An interaction diagram composed of three straight lines is used to model the effects of the axial loads on the bending moment capacity.

The following limitations can be mentioned:

- (a) The axial stiffness is constant along the analysis. This constraint of the model is particularly critical where extensive tension is expected on the exterior columns, which decreases their stiffness significantly. Also, the axial deformation of columns can produce significative changes on the pattern of bending moments on the whole frame.
- (b) At yielding, the flexural stiffness is changed but the axial stiffness remains constant.
- (c) Lumped plasticity is considered.
- (d) Shear stiffness is constant throughout the analysis.

As with beams, but particularly in columns because of the change in stiffness with the axial load, it is believed that the best solution for improvement of the model is the use of fiber elements (Spacone et al., 1996). This is discussed in more detail in Chapter 6.

8.5.7.4 Model of Joints

Joint flexibility can be modeled considering a reduced size of the joint. However, the definition of this reduced size is a difficult problem, and the obtained joint flexibility is independent of the deformation

level, which is not rational. Although rigid joints were used in this work, a better model of the joints can be obtained using the element connection available in DRAIN 2DX (Allahabadi and Powell, 1988).

8.6 Summary, Conclusions, Recommendations and Future Trends

8.6.1 Summary

The need for EQ-RD and EQ-RC approaches that will result in civil engineering facilities that perform more predictably under EQGMs than the approaches that are currently used is identified and justified by reviewing the performance of facilities during the earthquakes of the last two decades, particularly the 1989 Loma Prieta and the 1994 Northridge earthquakes in the United States, Kobe in Japan, Turkey, Taiwan, Colombia and India earthquakes. The number of people made homeless and the amount of economic losses due to physical damage to nonengineered houses and engineered facilities and particularly due to functional and indirect damages has increased to socially and economically unacceptable levels. This is not surprising in view of the insistence of seismic codes on EQ-RD approaches based on just the life safety performance level.

Although the understanding of the basic problems created by earthquakes and of the behavior of structures subjected to EQGMs has improved significantly, and this improvement has been reflected in the formulation of improved code requirements for the design and particularly the detailing of structural member, current seismic code design approaches fall short of realizing the goals and objectives of the worldwide-accepted philosophy of EQ-RD. Present seismic codes are not transparent, i.e., their regulations do not present in a visible way the basic concepts that govern the earthquake performance of civil engineering facilities. Arising from the above need, a comprehensive conceptual framework for seismic engineering called P-BSE has been developed. This framework regulates all the engineering aspects that seismic engineering should cover, particularly those related to performance-based seismic design (P-BSD), i.e., the conceptual overall P-BSD, preliminary numerical design, acceptability analysis, final design and detailing, quality assurance during construction and monitoring of occupancy and maintenance.

In this chapter, a conceptual comprehensive preliminary design approach that satisfies the requirements for P-BSD is applied to a ten-story RC building design. This approach, which considers a probabilistic design methodology, is transparent, i.e., based on well-established fundamental principles of structural dynamics, mechanical behavior of real buildings and comprehensive design and in compliance with the worldwide-accepted philosophy for seismic design. The design procedure starts with the specification of desired performance objectives for the entire structural system, given the hazard environment in which it is to be constructed, and then provides a direct rational path by which the structure may be designed to attain these goals.

Its main advantages are: (1) it leads to a transparent numerical design procedure that considers and checks the selected or desired performance objectives; (2) in spite of the great uncertainties in the quantification of some of the concepts involved in its codification, such quantifications can be improved as new more reliable data become available without changing the philosophy and particularly the format of this codified methodology; (3) such formulation can be used as a basis for improving the education of architects and engineers, as well as for the establishment of the prioritization and program of the focused research needed to improve seismic design, and thus to attain the so much-needed reduction of the current seismic risks in our urban areas to social and economical acceptable levels.

8.6.2 Conclusions

Because this chapter focuses in the application of the CCA, it is convenient to summarize the conclusions in two groups: (1) Those related to the development of a reliable P-BSD approach; and (2) those related to the applications.

8.6.2.1 Conclusions Regarding the Development of a Reliable P-BSD

It has been shown in detail in Bertero, R. and Bertero, V. (2002) that to satisfy the objectives of a reliable P-BSD it is necessary:

- **To start with a multilevel seismic design criteria.** At least two performance levels should be considered (even for the preliminary design) so that appropriate design decisions can be made to satisfy all the performance objectives.
- **To consider a probabilistic design approach.** The ideal approach would be to develop a reliability-based, performance-oriented methodology for design and evaluation, which will permit the designer to calculate the confidence that the building will satisfy the POs. Since a COV of about 0.20 could be expected for the capacities and a COV of about 0.80 for the earthquake ground motions demand, a simple probabilistic approach (using load factors) could be used for design.
- **To consider local structural and nonstructural damage.** It does not make sense to consider a global damage as an average of low and high levels of damage in different regions of a building since a region with low demand cannot avoid the consequences of the damage in more demanded segments of the structure. It is necessary to control the local damage that can jeopardize the life of the building occupants. Therefore, design spectra for buildings that take into account the local concentration of damage is needed. Elastic and inelastic IDI spectra, as well as local damage spectra for buildings, can be developed from the basic equations of the earthquake modal response of n degree of freedom systems.
- **To account for cumulative damage.** It has been shown that for a long duration-periodic earthquake ground motion, the cumulative effect can be more far reaching than the damage due to the maximum IDI only, and could even be responsible for a portion of the local damage of the severe pulse type of ground motions for specific values of a structural period. Also, the cumulative damage due to the main shock could be increased significantly by the effects of the aftershocks.
- **To control displacements and ductility (minimum strength) to limit damage.** It has been shown that the global ductility (i.e., for a given stiffness, the strength of the building) has a very important effect on the level of local damage. Increasing the ductility increases the damage of SDOF system, and the concentration of local damage in a building as the structure response goes deeper into the nonlinear range.
- **To ensure that any simplified numerical preliminary P-BSD procedure should be conceptually sound.** It is shown that some approaches that have been proposed fail in satisfying the requirement of a reliable P-BSD. In particular, it has been concluded that, conceptually, if the prediction of the actual inelastic responses (strength and deformations) is replaced by predicting such responses through a linear elastic analysis considering an equivalent damping coefficient obtained by equating $E_{H\mu}$ to $E_{H\zeta_e}$, this analysis cannot lead to a reliable estimation of the actual responses (strength and deformations) since only one of the main response parameters (strength or deformation) could be fitted.

8.6.2.2 Conclusions Regarding the Application of the Developed CCA

From the application of the CCA approach developed in this chapter, the following conclusions can be summarized.

- **Establishment of design EQGMs.** Ideally, acquisition of needed data should be based on EQGM records obtained at the site. If there are not enough of such records, the data can be obtained either from EQGMs recorded at sites with similar soil profile and topography, or by using numerical synthesis to generate several probable EQGM time histories. Conceptually, a design EQ should be the *critical EQGM* for the limit state under consideration, i.e., the EQGM that drives the structure to its critical (maximum) response for the performance level under study. The application of this simple concept in practice meets with serious difficulties. It has been shown that the reliability of the design EQs recommended by current seismic codes is highly questionable.
- **Performance design objectives.** To decide about the performance design objectives, the designer should discuss with the client the severity of the expected potential sources of seismic hazards and their corresponding frequency (return period), as well as the number of discrete PLs that should

be considered. According to the adopted definition of P-BSD, the following minimum performance levels should be considered initially:

- (a) Serviceability
- (b) Fully Operational
- (c) Operational
- (d) Life Safety
- (e) Near Collapse

In most of the cases, it would not be necessary to consider all of them for preliminary design because only few of the objectives will dominate (control) the design. The ideal possible combination of all possible ones are the one requiring just linear elastic analysis and design procedures, i.e. Serviceability or Fully Operation; and the other requiring the use of non linear analysis and design procedures (particularly simplified linear elastic-perfectly plastic procedures), i.e. Life Safety or Impending Collapse. At present is convenient to use the Serviceability and Life Safety because these are the two DOs for which there are more reliable data and experience.

- **Equivalence between Serviceability using allowable stresses and First Significant Yielding using LRFD format.** Note that the definition of a PL involves not only the return period of the EQGMs and the expected damage but also de probability that this expected damage be surpassed. In the example, it was selected $T_R = 10$ years for serviceability EQGMs and a probability $p_f = 0.16$ than the critical sections get first yielding. When serviceability is defined using just mean values of actions, first yielding is not reached, but a smaller value of stresses results in the critical sections. The definition of serviceability with 16% of probability of the critical sections get first yielding under mean plus sigma spectra is almost the same as the usual definition of serviceability considering allowable stresses for the critical sections under mean values spectra.
- **Problems in the design for stiffness of RC buildings.** The uncertainties in the stiffness of an RC structure must be considered in the design. These uncertainties arise because the effective stiffness of an RC member is not only a function of the geometrical size of the member. The effective stiffness of an RC member at a particular time depends not only on the size, steel amount and detailing, present deformation state, level of the moments, and axial and shear forces, but also on the history of the forces as well as deformations induced by changes in the environment (temperature and humidity) of that member. Even the stiffness of the structure as a whole depends on the amount of rotation that occurs at the end of the members connected at joints or supports (due to slipping of rebars at the joints), interaction with nonstructural elements and soil-structure interaction at the foundations. Thus, there is a need to consider not just one model with the expected initial linear elastic mechanical characteristics of the members, but also another model that considers the degradation of such initial stiffness due to the possible previous time histories of significant excitations that the structural members have already been submitted to when the different levels of EQGMs occur.
- **Overstiffness.** This is any unintentional stiffness present in the building or not explicitly considered in the equations used to estimate the stiffness of the structure, for example, due to nonstructural components. The overstiffness could be considered in the design process affecting the period T_1 by a reduction factor that could be different for service and safety limit state and whose value should be obtained from the evaluation of statistical data of measured responses of similar buildings.
- **Problems in design for strength: Zig-Zag pattern of design bending moments and shears for columns.** The required flexural and shear steel for columns follows a zig-zag pattern as a consequence of using for preliminary design a one-story substructure with assumed inflection points at the middle of the columns. The design bending moment at the column top in the upper story, M_n^T , should be used for design since, from equilibrium, its value is independent of the position of the inflection point at the column. From the story $n - 1$ to story 1, the design values can be smoothed using a moving average involving several stories.
- **Torsional effects.** For a structure with or without small static eccentricities, the consideration of the accidental eccentricity has considerable effect on the mode shapes and therefore on the seismic response (however, the periods T_i are not so much affected). An amplification factor due to elastic

torsion $\beta_1 = 1.38$ was obtained in the 3D linear elastic response spectrum analysis. Since the strength of each frame was selected to reach almost simultaneous yielding during the elastic torsion response ($V_4 = 0.7 V_1$, $V_3 = 0.8 V_1$, $V_2 = 0.9 V_1$), almost similar values are obtained for the stress-ratio in all frames.

- The strong column-weak beam design concept is reflected in the smaller stress-ratio λ obtained for columns. The bottom of the first-story columns has the larger stress ratio because the difference between the assumed in the preliminary design and the real position of the inflection point at the first-story columns. In general, a reasonable uniform stress ratio is obtained along the building. This means that a large concentration of damage during the inelastic response is not expected.
- Maximum θ_p . For the building designed in this example a very good approximation to the beam maximum θ_p values can be obtained using the IDIs. The smaller maximum plastic hinge rotation at the columns with respect to the beams reflects the fact that the plastic hinges are formed at first story at larger displacements than in the beams at the top stories.
- Maximum shear forces at beams and columns. For beams, a very good correlation was obtained between the design shear forces and the maximum values resulting from the time-history analysis. The moving average and the mid-height inflection point used for columns was also satisfactory except for the first and second story. Shear forces were largely underestimated for first-story exterior columns because they are estimated from equilibrium using beam moment capacities. However, since the main reinforcement is controlled for a load combination resulting in tension axial load for exterior column, and plastic hinges are formed at first-story column bases, the exterior column under compression can take a larger bending moment and therefore a larger shear than assumed for its design. To correct this problem, the first-story shear should be estimated from the moment capacity of the column under compression and the expected position of the inflection point at first story. For the rest of the stories, a moving average can be used to smooth the zig-zag pattern of shear forces obtained from equilibrium.
- Limitations of the nonlinear analysis that have been conducted. The real 3D structure was replaced by a 2D model and therefore the following limitations result: the torsional and the biaxial EQGMs effects were not considered. To go beyond this limitation, it is necessary to use a complete 3D nonlinear model. On the other hand, the model of beams and columns was the combination in parallel of a linear and an elastic-plastic element. The main limitation is that the axial stiffness is constant along the analysis. This constraint of the model is particularly critical where extensive tension is expected on the exterior columns, which decreases their stiffness significantly. Significant improvement in the modeling can be obtained by proper use of fiber elements.

8.6.3 Recommendations

8.6.3.1 Recommendations For Improving the Proposed P-BSD Approach That Have Been Applied

In particular, it is urgent to improve the available information regarding the following areas.

- To improve the establishment of all the different types of direct and indirect earthquake hazards, giving particular consideration to the fact that the earthquake hazards are not just consequences of a single event (i.e., a single EQGM history corresponding to the main shock) but consequences of multievents (foreshocks, main shock and aftershocks).
- To quantify the requirements for all performance levels. There is a need for an extensive and coordinated research program to improve the probabilistic definition of structural and nonstructural damage indexes. Particularly there is a need for reliable data (and therefore studies) regarding the interacting effects of floor acceleration and IDI on nonstructural components and utility lines (water, electricity, natural gas) damage, as well as the level of the content damage associated with floor velocities and accelerations.

- To develop more reliable structural damage indexes that can accurately reproduce the effects of all types of excitations that can act simultaneously and all possible load-deformation paths and damage mechanisms that do take into consideration the possible effects of previous ground motions as well as those due to possible aftershocks and future earthquakes.
- To develop more reliable amplification factors for taking into account the concentration of damage in some building stories.
- To develop a preliminary design that considers from the beginning a 3D approach considering at least the three translational components of the design EQGMs.

8.6.3.2 Recommendations for Developing Simple But Reliable P-BSE Building Code Provisions

Recognizing that for reliable application of performance-based seismic engineering (P-B SE) in practice the code regulations must remain simple and in accordance with the education in earthquake engineering of the practitioners, the following three-step approach could be implemented for the final formulation of the simple seismic code regulations.

8.6.3.2.1 First Step

Based on the state of the art in earthquake engineering, a “conceptual performance-based code” should be developed, covering all aspects that a seismic code should regulate. Given the different groups of aspects and problems involved in earthquake-resistant design (EQ-RD) and earthquake-resistant construction (EQ-RC) (Bertero, 1992; Bertero and Bertero, 1993; Bertero and Bertero, 1992), it is envisioned that the conceptual P-BSE building code will consist of regulations that can be grouped as follows.

1. Guidelines for assessing seismic activity and sources of potential seismic hazards; restrictions for land use and guidelines for the selection of building sites and corresponding site restrictions and procedures for site suitability analysis.
2. For a selected site and function of a building, conceptual establishment of the EQ-RD criteria, design earthquake ground motions (design EQGMs), building performance goals and design methodology.
3. Conceptual overall design of the entire building system, covering restrictions and guidelines regarding: selection of building configuration or form (size and shape), foundation, structural layout, structural system, structural materials and nonstructural components (potential unintentional structural components) and their materials. This should include not only the conventional or traditional systems and materials but also the innovative systems as discussed in Chapters 10–12.
4. Conceptual performance-based preliminary numerical design of the whole facility system, which requires prediction of the mechanical behavior of such a system and involves: proper modeling of the entire system; estimation of the demand on the structure and its contents (structural and stress analysis) at the different levels of design EQGMs; preliminary sizing and detailing through estimation of the capacities to be supplied to the structure to satisfy the target performance.
5. Reliable analysis of the performance of: the preliminarily designed facility when subjected to the expected critical EQGMs at each limit state contemplated in the design criteria and of existing facilities to assess their vulnerability.
6. Final design (detailing).
7. Monitoring of field construction, function (use) and maintenance (alterations, repair and upgrading) of the constructed structure.
8. Conceptual methodology for the upgrading of hazardous facilities (involve assessment of seismic vulnerability).

8.6.3.2.2 Second Step

In this step, the conceptual code regulations developed in the first step will be applied to the seismic vulnerability assessment of existing buildings and to the design of new buildings with different regular and irregular configurations, structural layouts and structural systems, which preferably have been designed and constructed according to current or modern seismic codes, and whose responses to EQGMs

have been either recorded or predicted; and to the upgrading of different types of existing hazardous facilities which preferably have been recently upgraded.

8.6.3.2.3 Third Step

From analysis of the results obtained in the second step, a simplified conceptual performance-based code that can be applied properly by the practitioners should be developed. It should state clearly all restrictions in siting and in selection of configuration (or form), foundation systems and structural systems for which such simplified code regulations could be used. For complex buildings, a peer review process is required in which the conceptual code to be developed in the first step could be used. On the other side of construction practice, it is very important to devote special efforts to the solution of (substandard) low-cost housing, particularly the problem of illegal types of construction. Simplified prescriptive design codes and manuals based mostly on clear drawings reflecting the correct and incorrect construction and details that consider the local practice should be produced.

8.6.4 Future Trends in the Development of Improved CCA for P-BSD and Its Implementation into Simple But Reliable Building Seismic Code

As indicated in the introduction, this chapter has several objectives; however, the main objectives were: (i) the CCA to P-BSE and P-BSD; (ii) a simplified probabilistic numerical procedure based on the present state of the art in the technical aspects of earthquake engineering and its application to the P-BSD of a conventional RC SMRF, which can be used to calibrate simplified P-BSD procedures that can be proposed for implementation in the next generation of standards and building seismic codes and (iii) a step-by-step approach that could be used to implement P-BSE in a simple but reliable building seismic code. It has to be clearly pointed out that all these presentations have been done with the ultimate goal of mitigating the current seismic risks in our urban areas.

As pointed out in Chapter 1, in the discussion of the much needed mitigation of the seismic risks, this mitigation requires consideration of the technical aspects of earthquake engineering and the political and socioeconomic aspects of earthquake engineering, which are connected with the problem of minimizing the sum of the investment and probable (or possible) losses. General criteria to minimize this sum are discussed in Chapters 7 and 9, as well as in other publications such as Hu et al. (1996), and in Chapters 2, 21 and 30–34 of Chen and Scawthorn (2003). Thus, in discussing the future trends regarding how to deal with the problems involved in these two different aspects of earthquake engineering, and how to improve the existing or proposed solutions, it has been decided that according to the main objectives of this chapter, it will be convenient to discuss them separately, although it is recognized that they are interrelated.

8.6.4.1 Future Trends for Improving the Solution of the Technical Problems Involved in the CCA and in the Probabilistic Numerical Procedure that Have Been Proposed

Most of the improvements have been covered in the recommendations pointed out in Sections 8.6.3.1 and 8.6.3.2. Recommendations regarding research for a rigorous approach to performance assessment and P-BSD are offered in Chapter 9. Future challenges regarding robust probabilistic procedures are discussed in Chapter 7.

Herein the authors would emphasize the importance of some technical problems that have not been considered in the application of the simplified probabilistic numerical procedure used. They can be grouped as (1)Problems caused by the direct effects of the surface fault rupture and EQGMs and (2) problems caused by indirect effects of the surface fault rupture and EQGMs.

8.6.4.1.1 Problems Caused by the Direct Effects of the Surface Fault Rupture and EQGMs.

Earthquake hazards include direct effects, such as ground fault ruptures, ground shaking, soil liquefaction, lateral spreading, landsliding and differential settlement. Each of these effects can result in facility damage, and therefore can affect the performance level achieved by the facility. The extent to which these hazards may affect facility performance is dependent on the distance of the actual zone of fault rupture from the

site, direction of fault rupture propagation, the geological makeup of the region and the unique geotechnical conditions of the individual site. The effects of all these hazards should be considered and specifically investigated as part of the entire performance-based engineering (P-BE) process. However, only the effects of the vibratory nature of the EQGMs are considered in the design of buildings: thus, there is a need to also consider the hazards due to the possible different types of soil failures.

Furthermore, even considering only the vibratory effect of the EQGMs on the structure, there are the following needs for selecting the proper time histories that can occur and that will be used in the statistical and probabilistic studies that are needed to define the smoothed design spectra that will be used for each hazard level considered in the P-BSDO matrix that was selected:

- For the hazard levels (HLs) corresponding to the PLs that accept damage it is necessary to consider that the occurrence of the significant EQGMs involved in such HLs is not a consequence of a single event, but also of multi-events (foreshocks, main shock and aftershocks);
- In the selection of the EQGM time histories, conceptually it is not correct to consider those that have been recorded at the free-field site, where the building will be constructed (or at similar sites), as it is usually done at present. The EQGMs that the foundation of the building will experience are those that result from the soil–structure interaction (SSI) or soil–foundation–superstructure–interaction (SFSI). The effects of these interactions are discussed in Chapter 4.
- Furthermore, in a building-crowded environment, it is conceptually incorrect to assume (as it is usually done) that the building to be designed will be subjected to EQGMs as if it were completely isolated from the vibratory effects of the adjacent buildings. It is necessary to consider the changes in the time history of the free field EQGMs, due to the dynamic characteristics of the building to be designed, and due to the characteristics of the already existing adjacent buildings or of those that could be constructed in the future.
- There are also several other problems in the built environment of our urban area, which can be caused by the adjacency of buildings. Arnold (1996, 2001) has discussed these problems of which one of the most important is the lateral collapse of a tall building as well as the failure of the external nonstructural components (cladding and window glasses).
- Other problems related to the use of the EQGMs are: (i) how many components recorded are considered in the design procedure, i.e., why the vertical component is not used? and (ii) how the effects of the components of the EQGMs should be combined with the effects of the other actions (loads and deformations) that can act on the building during its service life. There are several questions regarding the last problem, such as: Are the LRFD format and formulas that have been proposed in the Bertero and Bertero (2002) paper the most reliable that can be used? Should the designer consider only the excitations (actions or loads) pointed out in the proposed formulas or consider the probable effects (actions) due to secondary or indirect effects of an earthquake (such as fire, flood, tsunami, health [disease]) and those disasters that can be caused by humans such as to provide security against blast, impact and other threats as are presently discussed worldwide, particularly in the United States?
- Prediction of the performance of the nonstructural components, equipment, utility lines and contents. As it was pointed out in Bertero and Bertero (2002) there is a need for new and better nonstructural damage indexes that consider the interacting effects of floor acceleration and IDI on nonstructural components and utility lines (water, electricity, natural gas) damage, as well as the level of the content damage associated with floor velocities and accelerations. Detailed discussions can be found in Chapters 9 and 19.

8.6.4.1.2 Problems Caused by Indirect Effects of the Surface Fault Rupture and EQGMs

Earthquake hazards also include indirect effects such as fire, flood, tsunami, health (disease). The problems associated with the secondary or indirect effects of earthquakes have been discussed in the Earthquake Engineering Handbook edited by Chen and Scawthorn (2003), where some solutions are also offered.

8.6.4.2 Future Challenges Toward the Implementation of Simple but Reliable Seismic Code

Finally, regarding the future challenges for the development of improved CCA for P-BSD and its implementation into simple but reliable seismic code there is also an urgent need for:

- Applying the proposed CCA for P-BSD to the design of other types of conventional structural systems as well as to innovative systems discussed in Chapter 10.
- A massive education program on P-BSE.

8.6.5 Final Observations

From an analysis of the previous conclusions, recommendations and future trends it would appear that for conducting all the research that is needed and for the development of all the associated technologies that will be required to develop a robust probabilistic numerical procedure for P-BSD will demand a very long time. Thus, it could be concluded that the development of a simple but reliable P-BSE or just P-BSD standards and building codes is a “pipedream.” The authors believe there is an urgent need for a change in present code approach and that the gain of knowledge that has been achieved in the studies already conducted on performance assessment and design, particularly in projects such as SAC (Cornell et al., 2002) and PEER (Cornell and Krawinkler, 2000), there is sufficient information to attempt to apply the proposed CCA and the simplified probabilistic numerical procedure in the three-step approach that has been suggested for the formulation of a simple but reliable P-BSD building code. This proposed approach covers in a rational and transparent way all the aspects that need to be considered for resulting in designed buildings with predictable performance. The main advantage of the proposed CCA is that, notwithstanding the great uncertainties in some of the concepts involved in its codification, the numerical quantification of these concepts can be improved without changing the format of this codified methodology as new more reliable data are acquired.

List of Symbols

a_{0k} , a_{1p} , a_{2i}	constants depending on geometrical parameters of story i and span k
A_{si}^t	slab reinforcement inside the effective flange contributing to beam negative moment capacity at story i
b	damage model parameter
b_i	beam width
COV_{EQ}	coefficient of variation of the earthquake demand
C_s	strength spectra
C_y^*	yielding base shear coefficient
d	distance between top of beam and center of bottom steel
d_i	beam depth at story i
D	shorter side of building plant
\overline{D}_{apt}	mean value of instantaneous or arbitrary-point-in-time dead load
$d-d'$	distance between centroids of the top and bottom flexural reinforcement used as internal lever arm
DM	damage index
DM_L	local damage index
DM_{saf}	maximum allowable local damage index for life safety performance level
DM_{ser}	maximum allowable local damage index for serviceability performance level
D_n	nominal dead load
e	eccentricity
e_{ax} , e_{ay}	accidental eccentricity at each story
E_b	modulus of elasticity of beams
E_c	modulus of elasticity of columns

E_D	energy dissipation
E_H	hysteretic energy
E_H^+, E_H^-	positive and negative hysteretical energy for each plastic hinge
$E_{H\mu}$	hysteretic plastic deformation energy
$E_{H\xi}$	hysteretic damping energy
E_I	input energy
\overline{EQ}	mean earthquake demand
EQ_{saf}	mean plus one-sigma spectra seismic demand for safety
EQ_{ser}	mean plus one-sigma spectra seismic demand for service
e_{sx}, e_{sy}	static eccentricities for each story of the building
e_x, e_y	total eccentricity at each story
F_i	lateral load at floor i
F_{jk}	design forces at each floor k of frame (structural plane) j
f_u	mean ultimate stress
f_y	mean yielding stress
f_{yn}	nominal yielding stress
f'_c	specified concrete strength
g	acceleration of gravity
h	height of the story
H	total height of the building
$h_{1\ eff}$	effective first story height used to consider that at first story usually inflection point is higher than midheight of the column
h_i	height of the i story
$I_b\ eff$	effective moment of inertia of beams
$I_b\ gross$	gross moment of inertia of beams
I_b	effective moment of inertia of beams
$I_c\ eff$	effective moment of inertia of columns
$I_c\ gross$	gross moment of inertia of columns
I_c	effective moment of inertia of columns
IDI	maximum IDI during the EQGM
IDI_{ser}	maximum allowable IDI for service performance level
IDI_{unon}	ultimate IDI under monotonic increasing deformation
j_{1sty}	lever arm for first yielding bending moment
j_x, j_y	torsion lever arms
j_{yn}	lever arm for nominal yielding bending moment
j_u	lever arm for ultimate bending moment
K	structure stiffness matrix
k	stiffness at first yielding
k'	equivalent stiffness for life safety limit state
k_0	column stiffness
k_b	unknown stiffness of each frame
k_i	story stiffness
k_j/K	relative stiffness of the frame j with respect to the total stiffness in the considered direction
k_x, k_y, k_θ	structural stiffness in each direction at a particular story
k_{xi}, k_{yi}	stiffness in each direction at a particular story for each frame i
L	longer side of building plant
L_i	clear span of beams at story i
$\overline{L_{apt}}$	mean value of instantaneous or arbitrary-point-in-time live load
L_c	clear height of columns
l_k	span length of bay k
L_n	nominal live load (reduced considering the tributary area)
M	mass matrix of the structure

M	total mass of the building
M_0	maximum bending moment in the beam for gravity loads
M_1	maximum bending moment in the beam for the combination of gravity loads and seismic actions
M_1	generalized-mass
M_{1sty}	real first yielding moment
M_{ei}^B	bottom bending moment in an exterior column of the story i
M_{ei}^T	top bending moment in an exterior column of the story i
m_f	reactive mass lumped at floor f
M_i^-	design negative bending moment of a beam at i floor
M_i	modal mass of i mode
m_i	lumped story masses
M_i^+	design positive bending moment of a beam at i floor
M_{iser}^+, M_{iser}^-	maximum absolute value of the demanded positive and negative elastic bending moment in the beams of the i story under serviceability earthquake forces
M_k^c	moment capacity of the column k at the base considering the axial load in the column
M_{max}	maximum value of $(M_i^+ + M_i^-)$ in the equilibrium constraints
M_{ph}	plastic hinge bending moment at the time of maximum response
M_u	real ultimate bending moment
M_w	seismic moment magnitude
M_y	yielding moment for the beam
M_y^+, M_y^-	positive and negative yielding bending moment
M_{yn}	nominal yielding moment used for designing
n	number of stories
N_b	number of beams in the frame
N_c	number of columns in the frame
$NEYC_{\mu max}$	number of equivalent yielding cycles at maximum μ
NYR	number of yielding reversals
OVS_{saf}	overstrength at life safety
OVS_{ser}	overstrength at serviceability
PGA_{safety}	peak ground acceleration for life safety EQGMs
$PGA_{service}$	peak ground acceleration for serviceability EQGMs
P_i	column axial load at story i
r	number of bays of a generic frame
r^T	$[1 \dots 1]$
$R(t)$	resisting force at each floor
r_g	radius of gyration of mass
S_a	total acceleration
\overline{S}_{apt}	mean value of instantaneous or arbitrary-point-in-time snow load
S_d	spectral displacement
$S_d(T, \xi_{ser})$	LEDRS for displacement
$S_d(T, \xi_{ser}, \mu)$	IDRS for displacement
S_{i+1}	shear at story $i+1$
S_{jk}	design shear in the k story of the frame (structural plane) j
S_{saf_k}	safety design shear for each story k
S_{ser_k}	serviceability design shear for each story k of the building
S_n	nominal snow load
S_v	pseudovelocity
T_1	first mode period
T_{1saf}	maximum period of the building in order to satisfy life safety limit state
T_{1ser}	maximum period of the building in order to satisfy service limit state

T_g	predominant soil period
T_i	period of i mode
T_R	EQGM return period
T_y	uncoupled translational period of vibration
T	uncoupled rotational period of vibration
\mathbf{u}	displacements of the building floors
u	roof displacement
u_{max}	maximum roof displacement
u_y	yielding displacement
V	total base shear
$V_{1st\ yield}$	first yielding base shear
V_i	column shear at story i
V_j	base shear in each structural plane j
V_{mech}	expected mechanism base shear
V_{saf}	design base shear for life safety
V_{saf_j}	life safety design base shear of each frame j
V_{ser}	design base shear for serviceability
$V_{u\ dyn}$	maximum dynamic base shear
V_y^*	yielding base shear of an equivalent elasto-perfectly plastic SDOFS
W	total weight of the building
w_i	factored gravity load of the beam at the i story
w_k	gravity load for beam k
W_n	nominal wind load
x, y	horizontal and vertical distances between each frame and the center of stiffness
x_F	coordinate of the resultant of lateral forces
z_i	elevation of the i floor
α_θ	T_y/T_θ
β	safety index
β_i	safety index for performance design objective i
β_h	IDI increase due to deviation of assumed first mode shape
β_{ser}	safety index for serviceability
β_1	IDI increase due to elastic torsion
β_{lj}	factor to take into account elastic torsion for the j plane of stiffness
β_2	IDI increase due to concentration of plastic rotations in one story
β_3	IDI increase due to inelastic torsion
β_4	increase of design base shear due to inelastic torsion
$(\Delta\Phi_{li}/h_i)_{max}$	maximum IDI of the first mode shape Φ_l
Δ_{roof}	displacement at building roof
δu	variation of roof displacement
δU	variation of the deformation energy
$\Phi(\cdot)$	normal normalized probability distribution function
Φ_l	first mode shape
Φ_{li}	displacement at i story for first mode
μ	displacement ductility ratio
μ_a	cumulative ductility ratio
μ_{acc}	accumulative ductility
$\mu_{u\ mon}$	ultimate monotonic ductility ratio
Φ_i	i mode shape
Φ	assumed first mode shape
Γ_i	earthquake-excitation factor of i mode
γ	parameter to consider low-cycle fatigue

λ	stress ratio
λ_{mech}	load factor that transforms the structure into a complete mechanism
θ_p	plastic rotation
θ_p^+ , θ_p^-	maximum of θ_p^+ and θ_p^-
θ_p^+, θ_p^-	maximum positive and negative plastic hinge rotation
$\theta_{pacc} \equiv \theta_{p cum}$	accumulative plastic hinge rotation
$\theta_{pacc}^+, \theta_{pacc}^-$	positive and negative accumulative plastic hinge rotation
θ_{pmax}	maximum plastic hinge rotation
θ_{pmon}	monotonic plastic hinge rotation capacity of the section
θ_{umon}	ultimate plastic hinge rotation under monotonic increasing deformation for the critical section
ρ	reinforcement ratio
ρ^+	bottom reinforcement ratio of beams
ρ^-	top reinforcement ratio of beams
ρ_i	optimum top and bottom steel ratio at story i
ρ_i^{sl}	$A_{si}^{sl}/(bd)$
σ_{Tg}	standard deviation of the ground period
Ω	factor that considers bi-axial effects and not mid-span inflection point in the columns
Ω_b	estimated overstrength in beams
ω_1	first mode frequency
ξ	damping ratio
ξ_g	characteristic damping ratio used to simulate EQGMs
ξ_{saf}	first mode damping ratio for life safety performance level
ξ_{ser}	first mode damping ratio for serviceability performance level
ψ	column/beam stiffness ratio
i	stiffness ratio between columns and beams of story i
Ω	overstrength
Ω_{saf}	$1 + OVS_{saf}$
Ω_{ser}	$1 + OVS_{ser}$

Glossary

CCA	Comprehensive conceptual approach
COV	Coefficient of variation
EQGM	Earthquake ground motion
EQ-RC	Earthquake-resistant construction
EQ-RD	Earthquake-resistant design
HL	Hazard Level
IDI	Interstory drift index
IRS	Inelastic response spectra
LERS	Linear elastic response spectra
MDOF	Multidegree of freedom system
OPENSEES	Open System for Earthquake Engineering Simulation
P-BSE	Performance-based seismic engineering
P-BDO	Performance-based design objectives
P-BSD	Performance-based seismic design
PEER	Pacific Earthquake Engineering Research Center
PGA	Peak ground acceleration
PL	Performance Level
RC	Reinforced concrete
SDOF	Single-degree-of-freedom-system

SFST	Soil–foundation–structure interaction
SIDRS	Smooth inelastic design response spectra
SLEDRS	Smoothed linear elastic design response spectra
SSI	Soil–structure interaction

References

- ACI 318-95 (1995). Building code requirements for reinforced concrete. American Concrete Institute, Detroit, Michigan.
- Allahabadi, R. and Powell, G.H. (1988). DRAIN 2DX user guide. Report UCB/EERC-88/06, University of California at Berkeley, California.
- Ang, A. and Tang, W. (1984). *Probability Concepts in Engineering Planning and Design*, Vol. II, John Wiley & Sons, New York.
- Arnold, C. (1979). Configuration and seismic design: A general review. *Proc. 2nd U.S. National Conference on Earthquake Engineering*, Stanford, California, August 22–24, 1979, pp. 22–30.
- Arnold, C. (1989, 2001). Architectural considerations. in *The Seismic Design Handbook*, Naeim, F., Eds., pp. 210–237 (1st ed., 1989); pp. 275–326 (2nd ed., 2001).
- ATC-40 (1996). Seismic evaluation and retrofit of concrete buildings. Report ATC-40, Applied Technology Council, Redwood City, California.
- Bertero, R.D. (1995). Inelastic torsion for preliminary seismic design. *Journal of Structural Engineering*, ASCE, 121, 1183–1189.
- Bertero, R.D. (1997). Acceptability checks for performance-based design. Proceedings of the EERC-CUREe Symposium in Honor of Vitelmo V. Bertero. January 31– February 1, 1997. Berkeley, California, USA.
- Bertero, R.D. (2002). Diseño sismorresistente basado en la performance. Doctoral thesis, Facultad de Ingeniería. Universidad de Buenos Aires, Argentina (in Spanish).
- Bertero, V.V. (1979). Seismic performance of reinforced concrete structures. *Anales de la Academia Nacional de Ciencias Exactas, Físicas y Naturales*, 31, 75–144, Buenos Aires, Argentina.
- Bertero, V.V. (1980). Lessons learned from structures damaged in recent earthquakes. *Proc. 7th World Conference on Earthquake Engineering*, Santiago, Chile, Vol. 4, pp. 257–264.
- Bertero, V.V. (1982). State of the art in the seismic resistant construction of structures. *Proc. 3rd International Microzonation Conference*, University of Washington, Seattle, Washington, Vol.II, pp. 767–808.
- Bertero, V.V. (1991). Structural engineering aspects of seismic zonation. *Fourth International Conference on Seismic Zonation*, Standford University, Standford, California, Vol. 1, pp. 261–321.
- Bertero, V.V. (1992). Major issues and future directions in earthquake-resistant design. Keynote Address, Proceedings, of the 10th World Conference on Earthquake Engineering (10WCEE), Post-Conference Volume, Madrid, Spain, July 19–24, 1992.
- Bertero, V.V. (1997a). Performance-based seismic engineering: a critical review of proposed guidelines. In *Seismic Design Methodologies for the Next Generation of Codes*, Fajfar P. and Krawinkler H., eds., A.A. Balkema, Rotterdam, pp. 1–32.
- Bertero, V.V. (1997b). State-of-the-art report on the use of innovative strategies and techniques to reduce seismic risk. Earthquake Engineering Research Center, University of California, Berkeley.
- Bertero, V.V. (2002a). Innovative approaches to earthquake engineering. *Innovative Approaches to Earthquake Engineering*, G. Oliveto, Eds., WIT Press, Southampton, UK.
- Bertero, V.V. (2002b). Present and future perspectives regarding the use of PBSD design in the USA. *Proc. VII-SNIS*, Cuernavaca, Mexico. (CD-ROM, in Spanish), pp 1–26.
- Bertero, R.D. and Bertero, V.V. (1992). Tall reinforced concrete buildings: conceptual earthquake resistant design methodology. Report No. UCB/EERC-92/16, Earthquake Engineering Research Center, University of California at Berkeley, California, 243 pages.

- Bertero, R.D. and Bertero, V.V. (2002). Performance-based seismic engineering: The need for a reliable conceptual comprehensive approach. *Earthquake Engineering & Structural Dynamics*, 31, 627–652.
- Bertero, V.V. and Bertero, R.D. (1993). Tall reinforced concrete buildings: Conceptual earthquake-resistant design methodology. Paper presented at the VIII Seminario Latinoamericano de Ingeniería Sismorresistente, Mérida, Venezuela, 64 pp.
- Bertero, V.V. and Terán-Gilmore, A. (1993). Use of energy concepts in earthquake-resistant analysis and design: Issues and future directions. *Proc. VIII Seminario Latinoamericano de Ingeniería Sismorresistente*, pp. 1–39, Mérida, Venezuela, July 5–9, 1993.
- Bertero, V.V. and Uang, C.M. (1992). Issues and future directions in the use of an energy approach for seismic-resistant design of structures. *Nonlinear Seismic Analysis and Design of Reinforced Concrete Buildings*, Fajfar, P. and Krawinkler, H., Eds., Elsevier, London. pp. 3–22.
- Bozorgnia, Y. and Bertero, V.V. (2002). Near real-time post-earthquake damage assessment based on reliable damage indices and damage spectra. *Proc. 7th U.S. National Conference on Earthquake Engineering*, Boston, MA, July 2002.
- Chen, W-F and Scawthorn, C. (2003). *Earthquake Engineering Handbook*, CRC Press, Boca Raton, FL.
- Clough, R. and Penzien, J. (1993). *Dynamics of Structures*, 2nd ed. McGraw-Hill, New York.
- Collins, K. and Stojadinovic, B. (2000). Limit states for performance-based design. *Proc. 12 WCEE*. Auckland, New Zealand.
- Cornell, A. and Krawinkler, H. (2000). Progress and challenges in seismic performance assessment. PEER Center News Vol. 3 No. (2).
- Cornell, A., Jalayer, F., Hamburger, R. and Foutch, D. (2002). Probabilistic basis for 2000 SAC federal emergency management agency steel moment frame guidelines, *Journal of Structural Division*, ASCE, Vol. 128, No. 4, April 2002, pp. 526–533
- Cruz, E.F. and Chopra, A.K. (1986). Simplified procedures for earthquake analysis of buildings. *Journal of Structural Division*, ASCE, 112.
- Dowrick, O.J. (1987). *Earthquake Resistant Design For Engineers And Architects*, 1st edn. (1977) John Wiley & Sons, Ltd., New York.
- EERI (1995). Northridge earthquake of January 17, 1994: Reconnaissance report. *Earthquake Spectra*, Vol. 11, supplement C, Earthquake Engineering Research Institute, Oakland, CA, 521 pages.
- Ellingwood, B. and Rosowsky, D. (1996). Combining snow and earthquake loads for limit states design. *Journal of Structural Engineering*, ASCE, 122, 1364–1368.
- Fajfar, P. (1992). Equivalent ductility factors, taking into account low-cycle fatigue. *Earthquake Engineering & Structural Dynamics*, 21, 837–848.
- Fajfar, P. and Krawinkler, H. (1997). Seismic design methodologies for the next generation of codes. *Proc. International Workshop*, Bled, Slovenia, 24–27 June 1997.
- FEMA-273 and 274 (1997). NEHRP guidelines for the seismic rehabilitation of buildings. Federal Emergency Management Agency, Washington, D.C.
- FEMA-302 (1997), NEHRP Recommended Provisions (National Earthquake Hazards Reduction Program) for Seismic Regulations for New Buildings and Other Structures: 1997 ed., Part 1. Federal Emergency Management Agency, Washington D.C.
- FEMA-303 (1997), NEHRP Recommended Provisions (National Earthquake Hazards Reduction Program) for Seismic Regulations for New Buildings and Other Structures: 1997 edition, Part 2. Federal Emergency Management Agency, Washington D.C.
- FEMA-350 (2000). Recommended Seismic Design Criteria for New Steel Moment Frame Buildings. Federal Emergency Management Agency, Washington D.C.
- FEMA-356 (2000). Prestandard and commentary for the seismic rehabilitation of buildings. Federal Emergency Management Agency, Washington D.C.
- FEMA-368 (2001). NEHRP recommended provisions for seismic regulations for new buildings and other structures. Federal Emergency Management Agency, Washington, D.C.
- Galambos, T., Ellingwood, B., MacGregor, J. and Cornell, A. (1982). Probability based load criteria: Assessment of current design practice. *Journal of the Structural Division*, ASCE. 108.

- Hu, Y.-X., Liu, S.-C. and Dong, W. (1996). *Earthquake Engineering*, E & FN Spon, London, UK.
- ICC (2000). 2000 International Building Code, International Code Council. 5203 Leesburg Pike, Suite 600. Falls Church, VA 22041. USA.
- Ma, S.M., Bertero, V.V. and Popov, E.P. (1976). Experimental and analytical studies on the hysteretic behavior of reinforced concrete rectangular and T-beams. Report UCB/EERC-76/02, University of California at Berkeley, California.
- Mehanny, S. and Deierlein, G. (2001). Seismic damage and collapse assessment of composite moment frames. *Journal of Structural Engineering*, ASCE, 127, 1045–1053.
- Miranda, E. (1991). Seismic evaluation and upgrading of existing buildings. Ph.D. Dissertation, University of California Berkeley, California.
- Mirza, S.A. and MacGregor, J.G. (1979). Variability of mechanical properties of reinforcing bars. *Journal of the Structural Division*, ASCE, 105.
- Naeim, F. (2001). *The Seismic Design Handbook*, 2nd ed., Kluwer Academic Publishers, Boston.
- Neal, B.G. (1977). *The Plastic Methods Of Structural Analysis*, Chapman & Hall, London.
- NFPA (2003). 2003 NFPA 5000 Building Construction and Safety Code, National Fire Protection Association, Quincy, Massachusetts, USA.
- Nowak, A. and Collins, K. (2000). *Reliability of Structures*, McGraw-Hill, New York.
- Oliva, M. (1990). Racking behavior of wood-framed gypsum panels under dynamic load. Report No UCB/EERC-85/06, University of California at Berkeley, April 1990.
- OpenSees (2001). Open system for earthquake engineering simulation. *Peer Center News*, 4, University of California. Pacific Earthquake Engineering Research Center.
- Park, Y.J. and Ang, A.H.S. (1985). Mechanistic seismic damage model for reinforced concrete. *Journal of the Structural Division*, ASCE, 111.
- Paulay, T. and Priestley M.J.N. (1992). *Seismic Design of Reinforced Concrete and Masonry Buildings*, John Wiley & Sons, New York.
- Prakash, V. (1993). Drain-2DX base program user guide version 1.10. University of California, Berkeley, November 1993.
- SEAOC Vision 2000 Committee (1995), Performance-based seismic engineering, Report prepared by Structural Engineers Association of California, Sacramento, California.
- SEAOC (1996). Recommended Lateral Force Requirements & Commentary (SEAOC Blue Book). Report prepared by Structural Engineers Association of California, Sacramento, California.
- SEAOC (1999). 1999 Recommended Lateral Force Requirements & Commentary (Blue Book). Report prepared by Structural Engineers Association of California, Sacramento, California.
- Spacone, E., Filippou, F.C. and Taucher, F. (1996). Fiber beam-column model for nonlinear analysis of r/c frames: I. Formulation. *Earthquake Engineering and Structural Dynamics*, 25,, pp.711–725.
- Stewart, J.P., Chiou, S., Bray, J.D., Graves, R.W., Somerville, P.G. and Abrahamson, N.A. (2001). Ground motion evaluation procedures for performance-based design. PEER Report 2001/09, Pacific Earthquake Engineering Research Center, College of Engineering, University of California, Berkeley, September 2001.
- Unified Building Code (1997). International Conference of Building Officials, Whittier, California.
- Zagajeski, S.W. and Bertero V.V. (1977). Computer-aided optimum seismic design of ductile reinforced concrete moment-resisting frames. Workshop on Earthquake Resistant Reinforced Concrete Building Construction, University of California at Berkeley, July 11–15, 1977.

9

Performance-Based Earthquake Engineering

9.1	A Perspective of Performance-Based Earthquake Engineering	9-1
9.2	Evolution of PBEE Design and Performance Criteria in Seismic Codes • Recent Developments in Performance-Based Guidelines • Prediction of Seismic Demands by Means of a Pushover Analysis	9-3
9.3	A Rigorous Approach to Performance Assessment..... Components of Performance Assessment Approach • Intensity Measures, (IMs) • Engineering Demand Parameters (EDPs) • Probability of Global Collapse • Loss Estimation in PBEE • Downtime and Business Losses	9-19
9.4	Performance-Based Design..... Example of Design for Global Stiffness • Design for Maximum Floor Acceleration • Design for Collapse Safety	9-49
9.5	A Glance Toward the Future	9-53

9.1 A Perspective of Performance-Based Earthquake Engineering

Performance-based earthquake engineering (PBEE) implies design, evaluation, construction, monitoring the function and maintenance of engineered facilities whose performance under common and extreme loads responds to the diverse needs and objectives of owners–users and society. It is based on the premise that performance can be predicted and evaluated with quantifiable confidence to make, together with the client, intelligent and informed trade-offs based on life-cycle considerations rather than construction costs alone.

PBEE is a desirable concept whose implementation has a long way to go. There are legal and professional barriers, but there are also many questions whether PBEE will be able to deliver its promises. It promises engineered structures whose performance can be quantified and conformed to the owner's desires. If rigorously held to this promise, PBEE will be a losing cause. We all know that we cannot predict all important seismic demands and capacities with perfect confidence, even in a probabilistic format. There are, nevertheless, compelling reasons to advocate PBEE as a critical area for research and implementation. The objective of seismic engineering should be to design and build better and more economical facilities. Both terms are relative to the status quo. Significant improvements beyond the status quo will not be achieved without a new and idealistic target to shoot for. We need to set this target high and strive to come close to its accomplishment. We may never fully reach it, but will make significant progress if we have a well-defined target. PBEE is the best target available, and we need to focus on it.

Earthquake engineering practice is undergoing drastic changes triggered by a variety of reasons. Improved knowledge about earthquake occurrences and ground motion and structural response char-

acteristics is certainly one of them. The realization from recent earthquakes in the United States and Japan that monetary damage can surpass expectations by a large amount is another one. Perhaps, the most important is the realization that present code design procedures cannot be rationalized sufficiently by first principles to satisfy (a) the designer's desire for a logical explanation of the rules of the game, (b) the owner's desire for sound judgment on the costs and benefits of earthquake protection and (c) society's needs for informed decision making in the face of random (and often highly uncertain) seismic demands as well as uncertain seismic capacities of existing and even new man-made construction.

By now it is widely acknowledged that seismic design explicitly should consider multiple performance objectives. There is a minimum level of protection demanded by society to safeguard adequately against various types of collapse or falling hazards that endanger human lives. But society has responsibilities in addition to life safety, including continuing operation of critical facilities, protection against the discharge of hazardous materials and protection against excessive damage that may have far-reaching consequences for society on a local, regional, national or international level. Moreover, educated owners want options for maximizing the return on their investment or for providing life safety protection to the inhabitants of their facilities beyond the minimum required by society. These options differ between developers and, for instance, corporate owners whose livelihood may depend on the resumption of operation soon after an earthquake.

PBEE implies, for example, accepting damage in seismic events, if that proves the most economic solution. This requires, however, that structural engineers be able to predict these damages and their likelihood so as to make informed decisions. Implementation of such a design decision process necessitates a shift away from the dependence on empirical and experience-based conventions, and toward a design and assessment process more firmly rooted in the realistic prediction of structural behavior under a realistic description of the spectrum of loading environments that the structure will experience in the future. This implies a shift toward a more scientifically oriented design and evaluation approach with emphasis on more accurate characterization and predictions, often based on a higher level of technology than has been used in the past.

This higher level of technology needs to be developed through research. Among others this research should lead to:

- The development of methodologies on which future seismic design codes and practices can be based. Such methodologies need to incorporate new developments in demand and capacity descriptions and loss estimation strategies that are based on probabilistic concepts. The application of these methodologies should result in a performance that can be quantified and should provide consistent seismic protection for existing and new structures.
- The development of more reliable analytical procedures that permit performance evaluation of a wide variety of soil–foundation–structure systems and their components, of nonstructural systems and of building contents, at all levels of performance, ranging from cosmetic structural or non-structural damage to structural deterioration leading to collapse, with due consideration given to the uncertainties inherent in the assessment of seismic demands and capacities.

Performance-based design and assessment by itself will not accomplish improved or more predictable structural performance. Design provides only a set of drawings and instructions to the builder. The quality of the built product will depend on the clarity of the documentation and its communication, and the capability and willingness of the builder to implement the instructions. Thus, performance-based design must be followed by performance-based construction, in which construction engineering services and quality control play key roles.

A rigorous implementation of PBEE may well necessitate radical changes in engineering or construction practices and redirection of research and development (R&D). Architects, engineers and contractors will have to work together rather than take on adversary positions, and academic researchers will have to interact, much more than in the past, with architecture/engineering/construction (AEC) practitioners

who will lead the implementation process. Society will set the performance objectives, and AEC researchers and practitioners will have to find ways to fulfill them. This will be the challenge of PBEE.

9.2 Evolution of PBEE

Most of the concepts that are presently being implemented in the context of PBEE are not new. In various forms they have been explored, tried and partially implemented in past design/evaluation guidelines and standards of various countries and industries (e.g., the nuclear industry). In concept, all past seismic codes are partially performance based, as they attempt to tie design criteria to a performance level, usually that of collapse prevention. The emerging need to consider different criteria associated with various levels of performance has led to a recent emphasis on, and important developments in, PBEE. There is increasing agreement that future seismic codes will have to be performance based, but there are widely divergent viewpoints on the meaning of performance-based design and its methods of implementation. In concept, performance-based design provides the opportunity for society and owners to choose performance goals, and it obliges the designer to formulate and implement a design process that fulfills the stated goals.

This chapter cannot address all of the issues associated with PBEE and its evolution. The reader is referred to recent professional development efforts on this topic (e.g., SEAOC, 1995; FEMA 273, 1996; FEMA 274, 1996; ATC-40, 1996), to papers presented in the 11WCEE Special Theme Session on Seismic Design Criteria (e.g., Bertero, 1996a and 1996b; Cornell, 1996; Hamburger, 1996; Krawinkler, 1996; Moehle, 1996; Otani, 1996), to many of the papers compiled in (Fajfar and Krawinkler, 1997) and to recent summary papers on performance-based design (e.g., Ghobarah, 2001; Fardis, 2002; Hadjian, 2002). Some of the salient features and milestones of past seismic codes and professional developments that have led to the present state of practice in PBEE are summarized below.

9.2.1 Design and Performance Criteria in Seismic Codes

In concept, all seismic codes of the last several decades are performance based, as they attempt to fulfill specific performance goals through prescriptive measures. What has changed with time is the degree to which the prescriptive measures have become first-principle based rather than empirical. Advancements in knowledge in all important aspects of earthquake engineering and by societal demands for accountability for decisions that affect life safety and economy have been driven by the rate of change from empirical rules to first-principle concepts.

9.2.1.1 Early SEAOC Blue Book and UBC Editions

The Seismology Committee of the Structural Engineers Association of California (SEAOC) has been the originator of seismic provisions in the United States (and many other countries) for much of the last 40 years. Since 1959 this committee has published several editions of the *Recommended Lateral Force Requirements and Commentary*, which is informally known as the SEAOC Blue Book. The Blue Book itself has no legal standing, but has been adopted, with only minor modifications, by the International Conference of Building Officials, which published the Uniform Building Code (UBC) until 1997.

Already the first SEAOC Blue Book edition (SEAOC, 1959) expressed the design intent in terms of desired performance, stating that the objective of the lateral force requirements is to produce structures that should be able to resist

- A minor level of earthquake ground motion without damage
- A moderate level of ground motion without structural damage but possibly experience some nonstructural damage
- A major level of ground motion having an intensity equal to the strongest, either experienced or forecast for the building site, without collapse, but possibly with some structural as well as nonstructural damage.

These generic performance goals are contained even in the most recent edition of the SEAOC Blue Book (SEAOC, 1999). Until the early 1970s, generally accepted knowledge was insufficient to provide rigorous quantitative criteria that could back up these desired performance goals. Thus, design criteria were empirical and were based on coefficients that were supposed to account for specific phenomena, and which increased in number as more of the ground motion and response phenomena became known and empirically quantifiable. A well-known example of this empirical approach is the base shear equation (SEAOC, 1980)

$$V = ZIKCSW \quad (9.1)$$

in which

V = design base shear

Z = coefficient related to the seismicity of the region

K = a quality coefficient for the structural system

C = a period-dependent coefficient

S = coefficient for site-structure resonance

W = the seismically effective weight

The use of this design base shear (at the allowable stress design level), together with an elastic drift criterion and prescriptive rules for design detailing, was intended to provide adequate collapse safety as well as damage control. The intent was appropriate, but the quantitative implementation probably resulted in designs with variable margins of safety against collapse (Osteraas and Krawinkler, 1990). Most of these coefficients were based on good engineering judgment but lacked reliance on first principles and disregarded the great uncertainties associated with ground motion intensity and frequency content. Moreover, designs were based on purely elastic concepts without much explicit regard to inelastic behavior and deformation capacity. In most aspects designs were force based, with the primary objective of providing adequate strength to all elements that are part of the lateral load resisting system. Collapse protection was implicitly accomplished by adhering to the following guidelines, which are still the cornerstones of sound seismic design today:

1. Ductility must be provided, through careful detailing, at all locations at which the structure may experience inelastic behavior
2. Components that are important parts of the load path, but cannot be provided with adequate ductility, must be protected from excessive force and deformation demands by adhering to capacity design criteria (e.g., the strong column-weak beam concept, which is intended to protect gravity load resisting columns from excessive combinations of axial forces and bending moments)

Today there are many engineers who believe that a combination of these two guidelines, together with the provision of specified minimum amounts of elastic strength and stiffness, provides adequate protection against excessive damage and collapse.

9.2.1.2 ATC-3-06

During the mid-1970s the U.S. National Science Foundation and the National Bureau of Standards funded a study of great impact. These organizations realized that research knowledge had moved far ahead of engineering implementation and that it was time to translate recent research developments into concepts that could be used in engineering design. The outcome of this study was the ATC-3-06 (1978) document, which has changed the way seismic design was viewed and practiced by engineers. Most of the empirical coefficients used in past design practice were replaced in these tentative provisions by concepts, equations and coefficients that are based on physical principles and in part on the explicit consideration of uncertainties.

Perhaps the most relevant changes had to do with the description of the seismic input. Principles of seismic hazard analysis developed during the '60s (Cornell, 1968) were implemented to develop contour

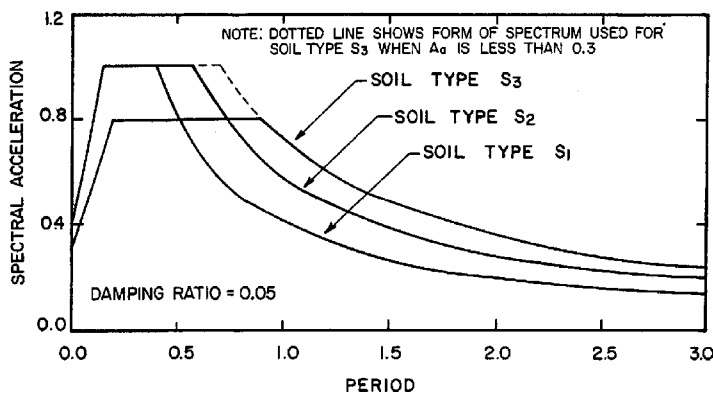


FIGURE 9.1 Examples of ground motion spectra for soil types S_1 to S_3 (ATC-3-06, 1978).

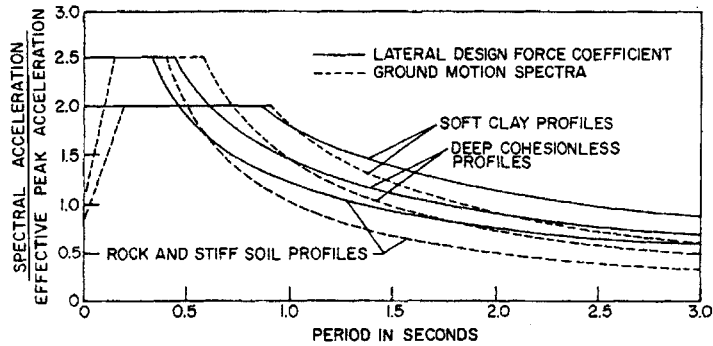


FIGURE 9.2 Comparison of ground motion spectra with design force coefficients (ATC-3-06, 1978).

maps for effective peak acceleration (EPA) and peak velocity (EPV) for a 10/50 hazard (475 years return period), utilizing seismic risk maps published by Algermissen and Perkins (1976). The EPA and EPV values, together with soil profile coefficients were then used to derive ground motion spectra of the type shown in Figure 9.1. These spectra provided a rational (and semiprobabilistic) basis for assessing the seismic input to structures. On the structure side, it was decided that a force-based design based on a single lateral design force coefficient was going to remain as the predominant method of design, with the modal analysis procedure offering an alternative to the determination of seismic load effects. A period-dependent basic (single mode) lateral force coefficient was proposed, which resembled that of the ground motion spectrum, but contained a $T^{-2/3}$ branch in the constant velocity region of the ground motion spectrum. The argument for the exponent $-2/3$, which raises the long period force demand compared to the response spectrum demand, was the potential for significant higher mode effects and the need to provide a more conservative design for long period (usually tall) structures. A comparison of ground motion spectral values and design coefficients is provided in Figure 9.2 (using a response modification factor of 1.0).

The concept of a response modification factor, denoted as R-factor, was introduced to permit elastic force design for a system that is expected to respond inelastically in the design earthquake (corresponding to the 10/50 hazard). The introduction of the R-factor was a necessity in the context of commonly available knowledge in the 1970s, but it caused two problems that are still with us today. First, the R-factor was assumed to be period independent, and its value was tuned for each structural system to be approximately equal to $8/(1.5K)$, with K being the purely empirical and judgmental value already used for about 20 years (see Equation 9.1). Similar R-factors are employed in many of today's seismic codes —

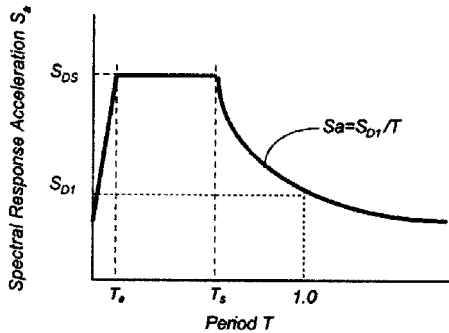


FIGURE 9.3 Design response spectrum. (FEMA 368 (2001). NEHRP recommended provisions for seismic regulations for new buildings and other structures — 2000 ed. U.S. Federal Emergency Management Agency.)

the values may have been refined somewhat but they are still assumed to be period independent. The second problem is that the R-factor is employed to derive seismic design forces for strength design at the component level, which is based on elastic behavior and pays no regard to redistribution due to inelastic behavior. Thus, it does not permit an explicit consideration of the overstrength a structure may have due to gravity load effects, discrete member sizes, redundancy and many other sources. The need to rectify R-factor inconsistencies is a main argument for the implementation of performance-based design.

Despite these inconsistencies, there is no doubt that the ATC-3-06 tentative provisions were a huge step forward in seismic design. They permitted explicit consideration of seismic hazards, assisted greatly in moving from an allowable stress design approach to a component-based strength design approach and provided guidelines for estimating displacement (story drift) demands through the tabulation of deflection amplification factors C_d . These factors, albeit empirical in nature, permitted the estimation of story drifts in the design earthquake from the story drifts computed under the elastic design forces. These estimated drifts could be compared to allowable story drifts that were provided for three seismic hazard exposure groups, which in turn were related to four seismic performance categories. Each building was assigned to a seismic hazard exposure group depending on its importance to post-earthquake recovery and on the number of occupants. Thus, the foundation for performance-based earthquake engineering has been laid.

9.2.1.3 NEHRP 2000 and ASCE 7-02

Most codes presently employed in the United States use the seismic loading criteria recommended in NEHRP 2000 (FEMA 368, 2001) and adopted by ASCE 7-02 (2002) together with specific seismic design criteria spelled out in material specifications (e.g., AISC, 2002, and Chapter 21 of ACI 318-02, 2002). The NEHRP 2000 criteria do not differ greatly from the ATC-3-06 criteria in concept, but have been much improved in detail. Advantage is taken of more elaborate hazard mapping (USGS Seismic Hazard Mapping Project, <http://geohazards.cr.usgs.gov/eq>), and of the concept of a maximum considered earthquake that produces spectral accelerations corresponding to a 2/50 hazard (2475 year return period) but need not exceed 1.5 times the spectral accelerations of the characteristic earthquake. The so obtained short period (usually 0.2 sec) and 1.0 sec spectral accelerations, S_s and S_1 , are then multiplied with site class dependent site coefficients, F_a and F_v (values of F_a and F_v are shown in Table 9.1), and are then multiplied by 2/3 to provide design spectral accelerations S_{D_s} and S_{D_1} that become the anchor points for the design response spectrum shown in Figure 9.3 (see also Chapter 5).

On the structural design side (given the design spectrum), there still exists the empirical and period-independent response modification coefficient R , which is now specified in an extensive table that contains 68 different structural systems. The same extensive table contains overstrength factors (which are relevant when determining the maximum force for component design) and deflection amplification factors. The amplified story drifts have to be limited to maximum permissible values, which enforces displacement control at the design earthquake level. The drift limits, which depend on the seismic use group are shown in Table 9.2. The terms seismic use group and seismic design category have replaced the terms seismic

TABLE 9.1 Values of Site Coefficients F_a and F_v for Adjustment of Spectra

Values of F_v as a Function of Site Class and Mapped 1 Second Period Maximum Considered Earthquake Spectral Acceleration at 1 Second Periods

Site Class	Mapped Maximum Considered Earthquake Spectral Response Acceleration at Short Periods				
	$S_S \leq 0.25$	$S_S = 0.50$	$S_S = 0.75$	$S_S = 1.00$	$S_S \geq 1.25$
A	0.8	0.8	0.8	0.8	0.8
B	1.0	1.0	1.0	1.0	1.0
C	1.2	1.2	1.1	1.0	1.0
D	1.6	1.4	1.2	1.1	1.0
E	2.5	1.7	1.2	0.9	0.9

Coefficient F_v for 1-sec Period

Values of F_v as a Function of Site Class and Mapped 1 Second Period Maximum Considered Earthquake Spectral Acceleration at 1 Second Periods

Site Class	Mapped Maximum Considered Earthquake Spectral Response Acceleration at 1 Second Periods				
	$S_S \leq 0.1$	$S_S = 0.2$	$S_S = 0.3$	$S_S = 0.4$	$S_S \geq 0.5$
A	0.8	0.8	0.8	0.8	0.8
B	1.0	1.0	1.0	1.0	1.0
C	1.7	1.6	1.5	1.4	1.3
D	2.4	2.0	1.8	1.6	1.5
E	3.5	3.2	2.8	2.4	2.4
F	<i>a</i>	<i>a</i>	<i>a</i>	<i>a</i>	<i>a</i>

Source: From (FEMA 368 (2001). NEHRP recommended provisions for seismic regulations for new buildings and other structures — 2000 ed. U.S. Federal Emergency Management Agency.)

TABLE 9.2 Values of Allowable Story Drifts Under Design Earthquake

Structure	Seismic Use Group		
	I	II	III
Structures, other than masonry <i>shear wall</i> or masonry <i>wall frame</i> structures, four stories or less in height with interior walls, partitions, ceilings, and exterior wall systems that have been designed to accommodate the story drifts	0.025 h_{sx}^b	0.020 h_{sx}	0.015 h_{sx}
Masonry cantilever <i>shear wall structures</i> ^c	0.010 h_{sx}	0.010 h_{sx}	0.010 h_{sx}
Other masonry <i>shear wall structures</i>	0.007 h_{sx}	0.007 h_{sx}	0.007 h_{sx}
Masonry <i>wall frame structures</i>	0.013 h_{sx}	0.013 h_{sx}	0.010 h_{sx}
All other structures	0.020 h_{sx}	0.015 h_{sx}	0.010 h_{sx}

Source: From (FEMA 368 (2001). NEHRP recommended provisions for seismic regulations for new buildings and other structures — 2000 ed. U.S. Federal Emergency Management Agency.)

hazard exposure group and seismic performance category of ATC-3-06. As in ATC-3-06, there is a flavor of performance-based design in this approach, but there are no explicit performance objectives except for force and drift limits under the design earthquake.

9.2.1.4 Eurocode

The Eurocode 8 (EN1998-1, 2002) has been the product of much research, discussions and negotiations between all of the European Union nations. It has similarities mostly with the recent U.S. code documents,

but also distinct differences. It states two explicit performance objectives: (a) to protect life under a rare seismic action, by preventing collapse of the structure or parts thereof and maintaining structural integrity and residual load capacity, and (b) to reduce property loss due to a frequent event, by limiting structural and nonstructural damage. The no-local-collapse performance objective is achieved by dimensioning and detailing structural elements for a combination of strength and ductility that provides a safety factor between 1.5 and 2 against a substantial loss of gravity load capacity and lateral load resistance (Fardis, 2002). The damage limitation performance objective is achieved by limiting overall deformations (lateral displacements) of the system to levels acceptable for the integrity of all its parts (including nonstructural ones). The Eurocode specifies spectral shapes, but does not specify hazard levels for the two performance objectives, because the choice of the level of safety and serviceability is left to the discretion of the member nations. The recommendation is to use a 10/50 hazard (475 years return period) for collapse prevention and a 10/10 hazard (95 years return period) for damage limitation. In the design process for strength and ductility, the Eurocode employs a behavior factor q , which is similar to the R-factor used in the United States, however, it explicitly incorporates the overstrength by incorporating the ratio of structure strength at mechanism to structure strength at first plastic hinge formation. Otherwise, presently employed U.S. codes and the Eurocode have comparable basic provisions.

9.2.1.5 Assessment of Modern Codes in the Context of PBEE

Modern codes flirt with the notion of performance, but they seem to skirt the tough issues of commitment to performance objectives and to quantification of limits on engineering parameters that can be related to specific performance objectives. They seem to emphasize structural performance, giving only occasional consideration to the performance of nonstructural and content systems. The implicit expectation appears to be that the code conforming strength and detailing requirements will take care of collapse and life safety issues under very strong earthquakes, and that code specified strength requirements and drift limits will take care of damage control under less severe earthquakes.

9.2.2 Recent Developments in Performance-Based Guidelines

The recent developments in performance-based guidelines were triggered by the necessity to develop assessment criteria for existing structures. Such structures consist of nonconforming elements whose strength and deformation capacities could not be evaluated within the scope of recent code requirements. Thus, safety assessment of such structures necessitated the commitment to various hazard levels and performance objectives. Once this Pandora's box was opened, other considerations of great importance, such as damage control, or immediate occupancy, or continued operation after an earthquake, became of much concern. Thus, in the United States various efforts were initiated during the early 1990s, more or less in parallel, which faced up to the many challenges of performance-based seismic design. The most widely known ones are Vision 2000 (SEAOC, 1995), FEMA 273 and FEMA 274 (1996) and ATC-40 (1996). There appear to be few conceptual differences in the basic framework proposed in these development efforts. The notation and terminology may differ, but not the substance. In general, various performance levels are defined, and performance objectives, which are expressions of the desired performance level for a given level of earthquake ground motion, are specified. And the objective of the iterative design/assessment approach is to develop and tune structural systems such that the performance objectives are fulfilled. The following brief discussion extracts a few salient features from the three aforementioned development efforts.

9.2.2.1 Vision 2000

This effort, which was initiated and supported by the Structural Engineers Association of California, started in 1992 and is still in progress. Its first product of significant impact is the Vision 2000 report cited as SEAOC (1995), which is intended to be applicable to the rehabilitation of existing buildings as well as to the design of new ones. As stated in that report, the goal of Vision 2000 is "...to develop the framework for procedures that yield structures of predictable seismic performance. This framework will

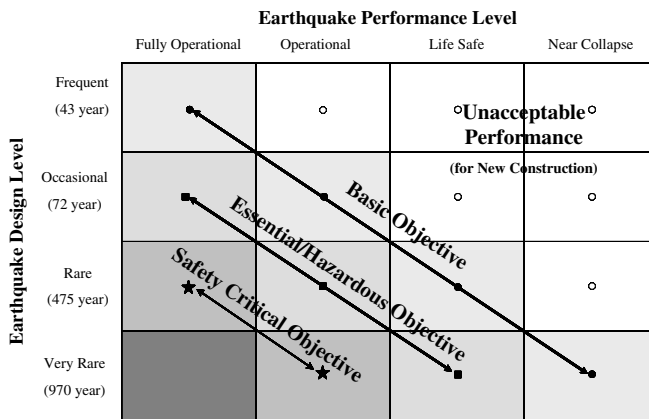


FIGURE 9.4 Performance objectives for buildings, recommended in SEAOC (1995).

explicitly address life-safety, damageability, and functionality issues....” Since the framework was geared toward design, which requires discrete performance criteria, the very important decision up front was made to focus on discrete performance levels and discrete hazard levels. This decision is not a given, because performance could be based on a continuum of a performance measure (e.g., dollar losses) and a continuous hazard curve, see Section 9.3.5.

The performance objectives for buildings of varying importance, in terms of performance levels defined by Vision 2000 and of recommended hazard levels (earthquake design levels) are illustrated in Figure 9.4. Other documents (FEMA 273, 1996; ATC-40, 1996) define performance levels somewhat differently, but in concept use a very similar framework. The importance of the building is tied in with the notions of “basic,” “essential” (such as hospitals and police stations), “hazardous” (containing hazardous materials, but of confined impact), and “safety critical” (such as buildings containing explosives and radioactive materials).

For each performance level the Vision 2000 document contains extensive tables with general damage (condition) descriptions for various structural components and systems, architectural elements, mechanical/electrical/plumbing (MEP) system components and building contents. The descriptions are mostly qualitative, and the challenge is to tie these descriptions to engineering demand parameters that can be predicted in the design and assessment process. The tables do include, however, quantitative limits on permissible transient and permanent story drifts at the various performance levels.

One of the many strong points of the Vision 2000 document is that it proposes a comprehensive design/assessment/build process that incorporates important aspects of:

- Selection of a suitable site
- Selection of suitable structural materials and systems
- Configuration and continuity of load path
- Quality of detailing
- Strength and stiffness
- Consideration of nonstructural and content systems
- Quality and consistency of design
- Quality of design review
- Quality of construction
- Quality of inspection

Each of these aspects and various approaches to implementation of performance-based design are discussed in SEAOC (1995). The document contains a wealth of good information and is valuable reading material for understanding the complexities of PBEE.

TABLE 9.3 Modeling Parameters and Acceptance Criteria for Nonlinear Procedures, Steel Beams in Flexure

Component/ Action	Modeling Parameters			Acceptance Criteria				
	Plastic Rotation Angle, Radians		Residual Strength Ratio	Plastic Rotation Angle, Radians				
	a	b		IO	Primary	Secondary		
Beams—flexure								
a. $\frac{b_f}{2t_f} \leq \frac{52}{\sqrt{F_{ye}}}$ and $\frac{h}{t_w} \leq \frac{418}{\sqrt{F_{ye}}}$	$9\theta_y$	$11\theta_y$	0.6	$1\theta_y$	$6\theta_y$	$8\theta_y$	$9\theta_y$	$11\theta_y$
b. $\frac{b_f}{2t_f} \geq \frac{65}{\sqrt{F_{ye}}}$ or $\frac{h}{t_w} \geq \frac{640}{\sqrt{F_{ye}}}$	$4\theta_y$	$6\theta_y$	0.2	$0.25\theta_y$	$2\theta_y$	$3\theta_y$	$3\theta_y$	$4\theta_y$
c. Other	Linear interpolation between the values on lines a and b for both flange slenderness (first term) and web slenderness (second term) shall be performed, and the lowest resulting value shall be used							

Source: From FEMA 356, U.S. Federal Emergency Management Agency, 2000

9.2.2.2 FEMA 273/356

In parallel with the Vision 2000 effort, the U.S. Federal Emergency Management Agency (FEMA) funded a large project to develop national guidelines for the seismic rehabilitation of buildings. This project resulted in the FEMA 273 (1996) and FEMA 274 (1996) reports, which later were reevaluated and modified, and then published as an ASCE Standard (FEMA 356, 2000). The performance-based framework is similar to that of Vision 2000, i.e., it associates discrete performance levels with discrete hazard levels, but it uses somewhat different hazard levels (50/50, 20/50, 10/50 and 2/50) and defines the performance levels as operational, immediate occupancy (IO), life safety (LS) and collapse prevention (CP). The use of different definitions indicates that the profession is not yet in agreement on performance levels of interest to owners, users and society.

The referenced reports address structural and nonstructural performance levels and provide many quantitative rules. In regard to structural performance, the reports are very specific and provide extensive and prescriptive acceptance criteria for most of the important components of structural systems made of steel, reinforced concrete, wood and masonry. The acceptance criteria are at the component level, and address deformation-controlled behavior (modes in which a component exhibits ductility) and force-controlled behavior (modes that represent nonductile behavior, such as shear in reinforced concrete beams). For deformation-controlled behavior, the reports provide extensive tables of modeling parameters and acceptable deformation values at the IO, LS and CP performance levels. A typical table is reproduced in Table 9.3. The table shows modeling parameters for nonlinear analysis and acceptance criteria for primary and secondary components, with the latter being components that do not significantly contribute to resisting earthquake effects. The modeling parameters a, b and c are illustrated in Figure 9.5. The figure shows that the user is permitted to take advantage of residual strength in analytical modeling, if the appropriate table contains a nonzero value for the parameter c.

The FEMA 273/356 reports made a major contribution to PBEE by providing detailed guidelines for analysis procedures that can be employed to predict the force and deformation demands for performance assessment. Recognizing that nonlinear time history analysis, which is believed to be the most reliable

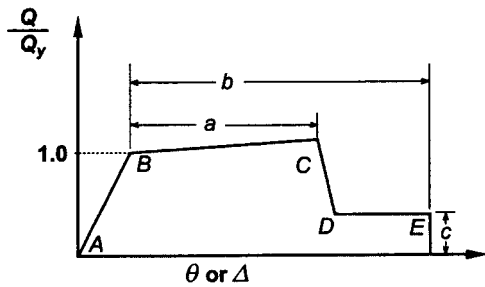


FIGURE 9.5 General force-deformation behavior of structural components. (FEMA 356 (2000). Prestandard and commentary for the seismic rehabilitation of buildings. U.S. Federal Emergency Management Agency.)

prediction method (provided a realistic structural model and proper ground motion recordings are used), will not be employed in the near future for more than a few special cases, much emphasis is placed on simplified analysis procedures, including linear static and linear dynamic procedures, and the nonlinear static (pushover) procedure. In particular, the latter one has received much attention and use in the recent past. It will be briefly discussed in Section 9.2.3. The first step in the pushover analysis is the construction of an equivalent SDOF system that is used to predict the target displacement of the MDOF structure. The target displacement is defined as a reference displacement (usually the roof displacement) the MDOF structure is expected to experience in the design earthquake. In the FEMA 273/356 reports, the primary procedure for the estimation of the target displacement is the application of a series of modification factors to the elastic spectral displacement at the first mode period. These modification factors are intended to account for MDOF effects, differences between elastic and inelastic displacements, P- Δ effects and the effect of different hysteresis shapes on the target displacement. The procedure for estimating the target displacement is the major difference between the nonlinear static procedure proposed in the FEMA 273/356 documents and the ATC-40 document.

9.2.2.3 ATC-40

In parallel with the FEMA-sponsored rehabilitation guidelines, the State of California commissioned the development of seismic evaluation and retrofit guidelines for existing reinforced concrete structures. This project resulted in the ATC-40 document (ATC-40, 1996). The PBEE framework is again similar to that of Vision 2000. Like any other PBEE approach, implementation strongly depends on the ability to predict seismic demands, such as story drifts and plastic hinge rotation demands. As mentioned in the preceding paragraph, the pushover analysis has become the method of choice for many structural engineers. In the ATC-40 document the prediction of the target displacement is based on the capacity spectrum method, rather than on the modification factors discussed in the preceding paragraph. In the capacity spectrum method, the global pushover curve (base shear versus roof displacement relationship) is converted into an equivalent SDOF capacity curve, whose intersection with a modified response spectrum is called the performance point. The displacement associated with the performance point is used as the estimate of the target displacement. The modified response spectrum is obtained from the original 5% damped design spectrum by applying specific rules that replace the effects of hysteresis energy dissipation of the inelastic system by equivalent damping. An illustration of the capacity spectrum approach is provided in Figure 9.6.

This approach intuitively is very attractive because it permits a simple graphical representation of both the capacity curve of the equivalent SDOF system and the ground motion demand represented by the modified response spectrum. It has, however, two flaws that have been known since equivalent linearization has become a popular research topic in the '60s and early '70s. One flaw is that the secant stiffness from the origin to the maximum displacement (as represented by the performance point) is a poor representation of the stiffness of the equivalent linear system, and the other is that the ATC-40 rules for equivalent damping appear to provide inconsistent modifications to the response spectra. Chopra and Goel (1999) have shown that the capacity spectrum method, as implemented in ATC-40, gives results

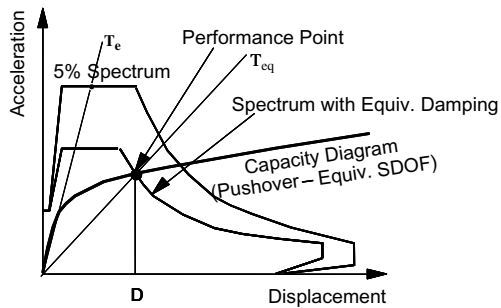


FIGURE 9.6 Illustration of capacity spectrum method.

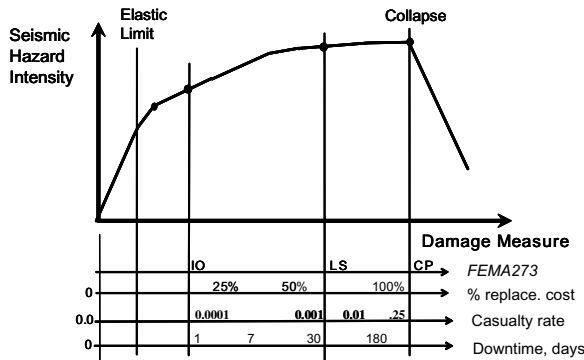


FIGURE 9.7 Conceptual relationship between seismic hazard intensity and structural performance (Courtesy W. Holmes, G. Deierlein).

for target displacements that differ greatly from those provided by others, and in some cases does not converge to a solution. In a recent study reported by Iwan (2002) both of these flaws appear to have been rectified and rules have been proposed that permit a much more consistent target displacement prediction by means of a modified capacity spectrum method.

9.2.2.4 Assessment of Recent Developments in Performance-Based Guidelines

The guidelines summarized in this section, and similar ones developed in other countries, appear to focus on discrete performance levels and discrete hazard levels associated with desired performance. A conceptual relationship between seismic hazard intensity and structural performance is provided in Figure 9.7. Different documents use different limit states (performance levels), which indicates that the profession has not yet agreed on the importance and definition of the performance levels that should become the focus of design and performance assessment. The performance levels are mostly descriptive and address states ranging from fully operational to collapse. Fully operational may be associated with no damage, which implies behavior in the elastic (or nearly elastic) range and a serviceable facility. Conventionally, this limit state is often referred to as serviceability. Other performance levels, such as those defined in the FEMA 273 document, can be located by judgment on the performance curve shown in Figure 9.7.

All guidelines discussed here have in common the description of earthquake intensity in terms of discrete hazard levels associated with satisfactory performance at the various performance levels defined in the guidelines. Thus, the time (return period) dependence of the earthquake intensity is quantified through a probabilistic hazard analysis, but the performance assessment is purely deterministic, using mean but approximate uniform hazard spectra and nominal values for strength, stiffness and deformation

capacities of structural components. Uncertainties in modeling the properties of structural components, and in assigning acceptable values of properties to the various performance levels, are not considered. Thus, given the acceleration spectrum for a specified hazard, all engineering computations and acceptance criteria are deterministic. This does not permit a reliability-based assessment of seismic performance. One can argue that our present state of knowledge on ground motion representation, response prediction and performance acceptance criteria does not justify a fully probabilistic approach for performance assessment, neither for discrete performance levels nor for the continuous performance metrics discussed in the following paragraph. But this argument should not prevent us from striving toward the goal of a comprehensive reliability-based performance assessment. The literature on this subject is growing (e.g., Hadjian, 2002; Wen, 2001, Chapter 7 of this book), and the material presented in Section 9.3 addresses a specific approach to reliability-based seismic performance assessment. Work done as part of the SAC steel frame investigation has also contributed much to the development of basic procedures for reliability-based seismic performance assessment (Cornell et al., 2002; Yun et al., 2002).

Figure 9.7 also shows that there are alternatives to the choice of discrete performance levels and discrete hazard levels for establishing performance objectives. Performance can be expressed in terms of continuous variables, such as percent replacement costs, length of downtime and casualty rate. Specific values of these variables could be associated with specific performance levels, as illustrated in the lower part of Figure 9.7, but the great advantage of these continuous variables is that they can be probabilistically evaluated and do not require the commitment to a predefined performance level. The evaluation of these variables, called decision variables, is discussed in Section 9.3.

It must be said that the focus of this chapter is on system performance due to ground shaking hazards, but other earthquake-generated hazards deserve equal consideration in performance assessment. Vision 2000 (SEAOC 1995) specifically refers to liquefaction, landslides, settlement and fault rupture as hazards that should be considered. These and other related hazards are outside the scope of this chapter.

9.2.3 Prediction of Seismic Demands by Means of a Pushover Analysis

The evaluation of engineering demand parameters (EDPs) on which performance assessment can be based is central to performance assessment. In the context of presently employed procedures, which are the subject of this section, examples of EDPs of interest are maximum story drifts, plastic hinge rotations and member forces. Their evaluation implies availability of a quantitative description of the seismic input. As discussed earlier, the seismic input is usually described in terms of acceleration response spectra that represent the ground motion intensity at the site for specific hazard levels (see Figures 9.1 and 9.3). Thus, the challenge is to use these spectra, together with a mathematical model of the structure, to predict seismic demands with sufficient accuracy. Short of nonlinear dynamic time history analysis (which requires availability of ground motion records that represent the hazard at the site), presently employed procedures have to rely on simplified analysis procedures. The procedure that has found much application in the recent past is the nonlinear static analysis procedure, colloquially called the pushover analysis.

In the pushover analysis, the structure is idealized by an assembly of component models capable of representing the nonlinear monotonic load-deformation characteristics as illustrated in Figure 9.5. An invariant (or sometimes an adaptive) lateral load pattern is applied to the structure and the structure is monotonically pushed under this load pattern (in the presence of constant gravity loads) to large inelastic deformations until a target value is reached at a reference point, usually the center of mass at the roof level. A simple illustration of a pushover is provided in Figure 9.8. The objective is to push the structure to the displacement expected under the design earthquake, called the target displacement, and to evaluate drift demands and component deformation and force demands at this stage. These demands are then compared to acceptable values to assess performance.

The issue of estimating the target displacement has been a matter of much debate over the last few years. In general, an equivalent SDOF system is established (Krawinkler and Seneviratna, 1998; Fajfar, 2002), and either a capacity spectrum approach (ATC-40) or a modification factor approach (FEMA 273/356) is utilized to predict the target displacement. For the latter, relationships between displacements

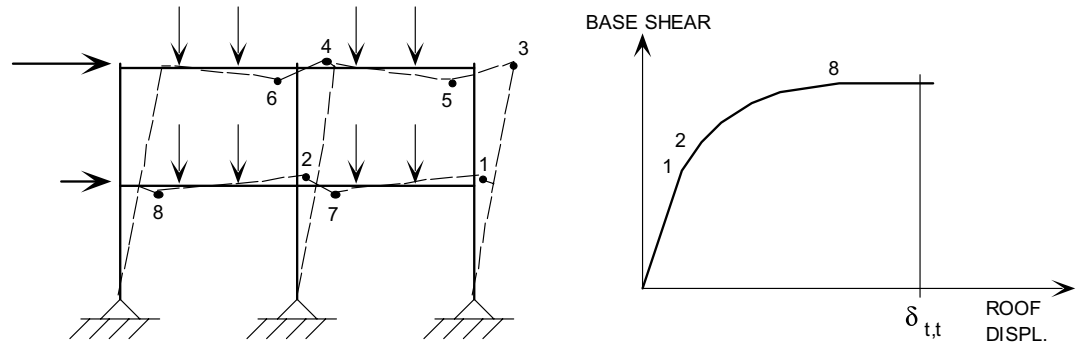


FIGURE 9.8 Illustration of a pushover analysis. (Seneviratna, G.D.P.K. and Krawinkler, H. (1997). Evaluation of inelastic MDOF effects for seismic design. John A. Blume Earthquake Engineering Center Report No. 120, Department of Civil Engineering, Stanford University.)

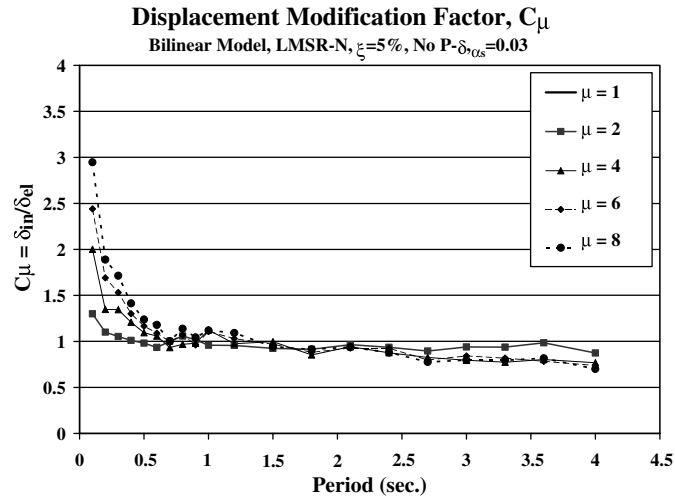


FIGURE 9.9 Ratio of displacements of inelastic to elastic bilinear SDOF systems, for various ductility ratios.

of inelastic and elastic SDOF systems, such as those shown in Figure 9.9, can be utilized to derive modification factors. The effects of different hysteresis behavior (e.g., peak oriented and pinching, see Figure 9.10, rather than bilinear) can be assessed from graphs such as those shown in Figure 9.11. As Figure 9.11 indicates, the effects of pinching the hysteresis loop, compared to a bilinear loop, are small for the maximum SDOF displacement, except for short period systems and constant strength reduction factors ($R = F_{el}/F_{y,in} = 4.0$). As a word of caution, these effects become larger (i.e., the ratio of maximum displacements of pinched system to bilinear system becomes clearly larger or smaller than 1.0) for many MDOF systems, particularly once P-Δ effects are included.

Both the ATC-40 capacity spectrum approach and the FEMA 273/356 modification factor approach for estimating target displacements are in need of improvement. This applies in particular to the P-Δ modification factor for the latter, and applies in general for the former. The recent work summarized in Iwan (2002) accomplishes much of this for the capacity spectrum approach. An obvious alternative to both approaches is the direct use of inelastic constant ductility spectra, as proposed by Fajfar (1999) and Chopra and Goel (1999), although the latter approach in some cases can lead to small but systematic underestimations of inelastic deformations (Miranda 2001). This method is illustrated in Figure 9.12. It consists of representing the MDOF system by an equivalent SDOF system with zero strain hardening,

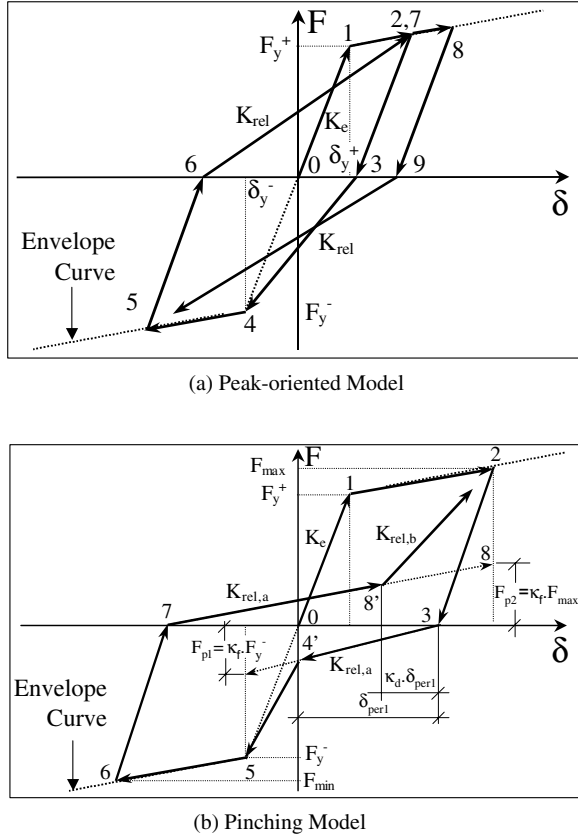


FIGURE 9.10 General load–deformation behavior of peak-oriented and pinching hysteretic models. (Medina, R.A. (2002). Seismic demands of nondeteriorating frame structures and their dependence on ground motions. Ph.D. Dissertation, Dept. of Civil Engineering, Stanford University. With permission.)

and intersecting this bilinear diagram with the appropriate inelastic spectrum that matches the ductility demand obtained at the intersection. This matching may require iteration, which is a small price to pay for accuracy. Constant ductility spectra can be obtained for the hysteretic behavior and the strain hardening that best represent the MDOF structure. More recently, Ruiz-Garcia and Miranda (2003) proposed simplified expressions to estimate ratios of inelastic to elastic displacements that are a function of relative strength, which not only avoid iteration but also the small systematic underestimations when using ratios of inelastic to elastic displacements for constant ductility ratios.

It is noted that much of the discussion in recent years has focused on the estimation of the target displacement, rather than on the estimation of component force and deformation demands obtained from the pushover analysis. The latter is of more importance than the former, simply because the results of a pushover analysis can be misleading unless they are interpreted with great care. It must be emphasized that the pushover analysis is approximate in nature and is based on static loading. As such it cannot represent dynamic phenomena with a large degree of accuracy. It may not detect some important deformation modes that can occur in a structure subjected to severe earthquakes, and it may exaggerate others. Inelastic dynamic response may differ significantly from predictions based on invariant or adaptive static load patterns, particularly if higher mode effects become important. The influence of higher modes, which is neglected in the standard pushover analysis, varies for different response parameters, with the location within the structure, and with the frequency content of the ground motion. In particular, the

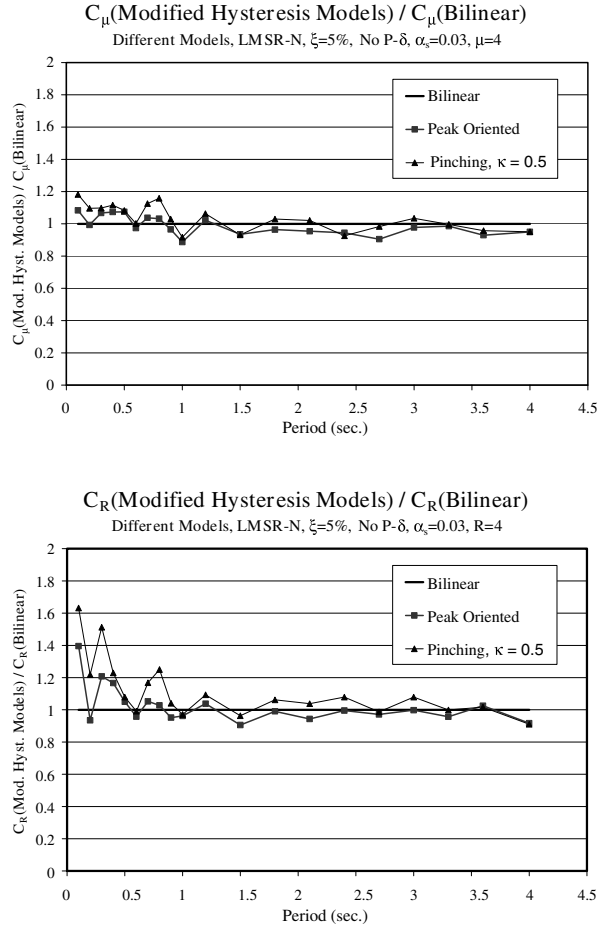


FIGURE 9.11 Ratio of displacements of peak-oriented and pinching systems to bilinear system, (a) for constant ductility ratio $\mu = 4.0$, (b) for constant R-factor $R = 4.0$.

estimation of story and component forces and overturning moments can be strongly affected by higher modes even for buildings of moderate height.

An example of the effects of higher modes on story drifts is illustrated in Figure 9.13, which shows the median ratio of maximum story drift, $\theta_{s,max}$ to maximum roof drift, $\theta_{r,max}$ for a family of generic frame structures, predicted from nonlinear time history analysis using a set of 40 ground motions. Results for various strength levels are presented, characterized in this figure by the ratio $[S_a(T1)/g]\gamma$ (with $\gamma = V_y/W$), which is equal to the response modification factor R for systems without overstrength. The frame structures are designed to have a close to straight line first mode deflected shape, and therefore the ratio $\theta_{s,max}/\theta_{r,max}$ is representative of higher mode effects. These effects clearly increase with the number of stories N (or the period, since $T = 0.1N$ is used), and therefore the pushover analysis procedures with invariant load patterns is expected to provide less accurate story drift predictions as the number of stories increases. (It is noted that the ratio $\theta_{s,max}/\theta_{r,max}$ is not highly sensitive to the structure strength, represented by $[S_a(T1)/g]\gamma$. This observation, which applies only to structures without strength irregularities, also has been made in a study that used code designed multi-bay steel frame structures (Gupta and Krawinkler, 1999).

It must be emphasized that the pushover analysis potentially provides very misleading results for force quantities such as story shear forces and overturning moments. This is illustrated in Figures 9.14 and 9.15 for structures whose lateral load resisting system can be represented by a single shear wall (Senev-

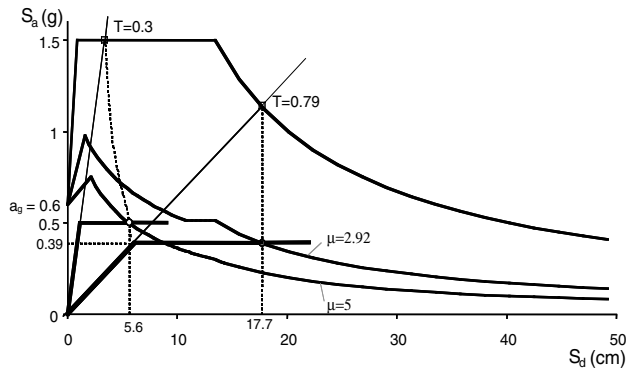


FIGURE 9.12 Two examples of direct use of inelastic spectra for estimating target displacement. (Fajfar, P., *Earthquake Eng. Struct. Dyn.*, 28, 979–993, 1999. With permission.)

MAX-STORY DRIFT/MAX. ROOF DRIFT-T₁=0.1N
Median values, $\xi = 0.05$, Peak-oriented model, B H, K_I, S_I, LMSR-N

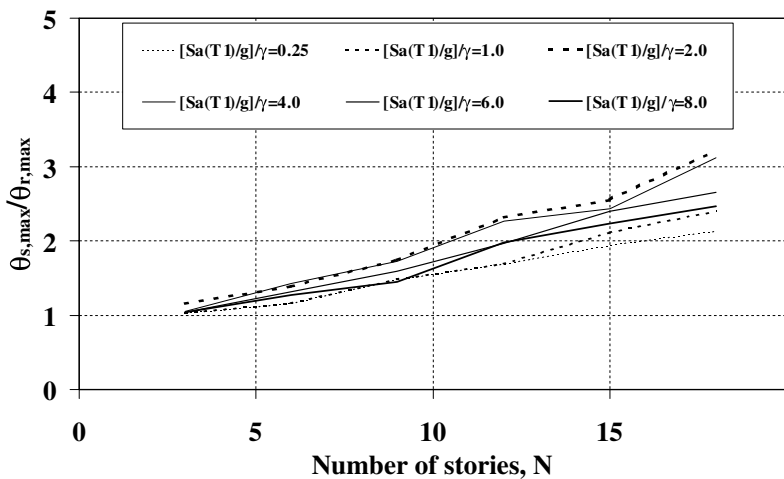


FIGURE 9.13 Median ratio of maximum story drift angle to maximum roof drift angle. (Medina, R.A. (2002). Seismic demands of nondeteriorating frame structures and their dependence on ground motions. Ph.D. Dissertation, Dept. of Civil Engineering, Stanford University. With permission.)

iratna and Krawinkler, 1997). In these wall structures it is assumed that the bending strength of the wall is constant over the height, and the shear strength is so large that the behavior of the wall is controlled by bending. It is also assumed that no strain hardening exists once a plastic hinge has formed in the wall. A pushover analysis will predict hinging at the base of the wall for all rational load patterns. Since a mechanism exists once this single plastic hinge has formed, the wall will rotate around its base, and the lateral loads can no longer be increased. Thus, a pushover analysis will not permit propagation of plastic hinging to other stories and will predict a base shear demand that corresponds to the sum of lateral loads needed to create the plastic hinge at the base.

Nonlinear dynamic time history analysis gives very different results. For taller wall structures higher mode effects significantly amplify the story shear forces that can be generated in the wall once a plastic hinge has formed at the base. This is illustrated in Figure 9.14, which shows mean values of base shear amplification, defined as the maximum base shear from dynamic analysis over pushover base shear causing plastic hinging at the base. The amplification depends on the period (number of stories) of the

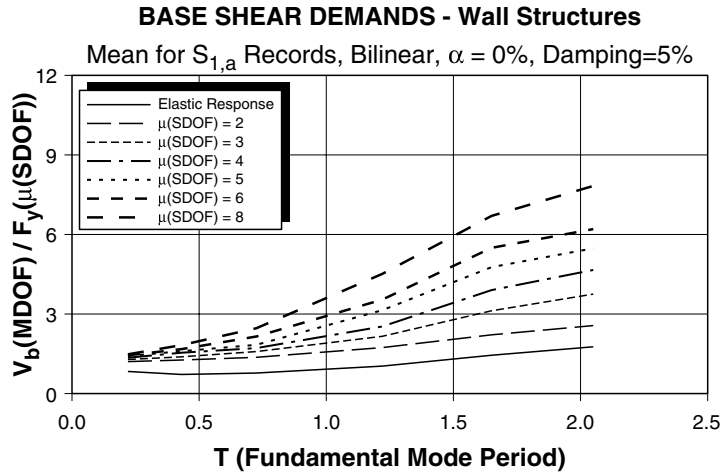


FIGURE 9.14 Amplification of base shear demand for wall structures. (Seneviratna, G.D.P.K. and Krawinkler, H. (1997). Evaluation of inelastic MDOF effects for seismic design. John A. Blume Earthquake Engineering Center Report No. 120, Department of Civil Engineering, Stanford University. With permission.)

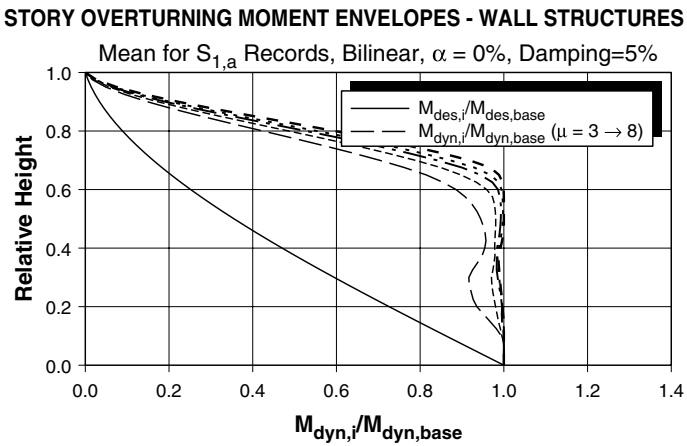


FIGURE 9.15 Story overturning moments for a wall structure with $T = 2.05$ sec. (Seneviratna, G.D.P.K. and Krawinkler, H. (1997). Evaluation of inelastic MDOF effects for seismic design. John A. Blume Earthquake Engineering Center Report No. 120, Department of Civil Engineering, Stanford University. With permission.)

wall structure and on the wall bending strength (represented by $\mu(\text{SDOF})$). The diagram shows that the amplification of base shear demands may be as high as 4 for tall wall structures whose bending strength is within code design expectations ($\mu(\text{SDOF}) \leq 4$). This amplification implies that the base shear demand may be much higher than the base shear obtained from the lateral loads that cause flexural hinging at the base of the structure. Thus, wall shear failure may occur even though the pushover analysis indicates flexural hinging at the base.

Nonlinear dynamic time history analysis also shows that flexural hinging in tall structures is not necessarily limited to the first story — as a pushover analysis would predict. It may propagate into other stories to an extent that depends on the period and flexural strength of the structure. This is illustrated in the story overturning moment envelopes presented in Figure 9.15 for a wall structure with a period of 2.05 sec. The moment envelope obtained from dynamic analyses is very different from that obtained

from a code-type load pattern (solid line). Thus, if such a code load pattern is used in the pushover analysis, a misleading picture of the story overturning moment demand is obtained.

These comments are intended as an expression of caution to the indiscriminate use of the pushover analysis as an all-encompassing panacea for predicting seismic demands. The pushover analysis is a useful but not infallible tool for assessing inelastic deformation demands and for exposing design weaknesses. A thoughtfully performed pushover analysis will provide much insight into structural behavior that controls performance during severe earthquakes. For structures that vibrate primarily in the fundamental mode, such an analysis will very likely provide good estimates of global as well as local inelastic demands. It will also help to expose design weaknesses that may remain hidden in an elastic analysis, such as story mechanisms, excessive deformation demands, strength irregularities and overloads on potentially brittle elements such as columns and connections. If implemented with caution and good judgment, and with due consideration given to its many limitations, the pushover analysis is a great improvement over elastic evaluation procedures. This applies particularly to the seismic evaluation of existing structures whose element behavior cannot be evaluated in the context of presently employed global system quality factors such as the R-factor used in the present U.S. seismic codes.

Many attempts have been made to improve the predictive capabilities of the pushover analysis, particularly by employing adaptive load patterns and accounting for higher mode effects through modal pushovers and subsequent modal combinations of deformations and forces. The reader is referred to the following publications for important contributions (Gupta and Kunnath, 2000; Mwafi and Elnashai, 2001; Fajfar, 2002; Chopra and Goel, 2002; Aydinoglu, 2003), which point toward considerable improvement of the presently employed pushover methods.

9.3 A Rigorous Approach to Performance Assessment

At the end of Section 9.2.2 an assessment was made of the state of practice in performance-based guidelines. These guidelines are based on discrete hazard and performance levels and a deterministic assessment of structural response. Although these existing guidelines provide a significant improvement over current code procedures in which the primary (and often only) explicit concern is prevention of collapse, they have a number of shortcomings: (a) they do not quantify the performance for a continuum of seismic hazard; (b) they cannot distinguish between different degrees of damage within discrete performance levels; (c) they do not provide a quantitative basis for owners and investors to compare the benefits of one performance level with another; (d) they do not offer a framework in which seismic risks can be compared, evaluated and combined with other types of risks that owners and investors face. Furthermore, verification of adequate performance is done at the component level rather than at the system level, and therefore, a certain performance level is not satisfied if a single component fails the performance criteria. Lastly, performance assessment is deterministic (except for the specification of a uniform hazard spectrum) and does not permit explicit consideration of the many sources of uncertainty (aleatory and epistemic) that should be considered in a reliability-based performance assessment.

As a major step toward an integrated probabilistic design/assessment approach to PBEE, the Pacific Earthquake Engineering Research (PEER) Center has focused for several years on the development of procedures, knowledge and tools for a comprehensive seismic performance assessment of buildings and bridges. This section focuses on the general performance assessment methodology developed by PEER researchers for buildings. The approach is aimed at improving decision making about seismic risk by choosing performance goals, and the trade-offs they entail. In the approach, decision variables are identified whose quantification, together with an assessment of important uncertainties, will make it feasible to characterize and manage economic and societal risks associated with direct losses, downtime and collapse and life safety.

As stated at the beginning of this chapter, a comprehensive approach to PBEE is an idealistic target. By now, this target has moved closer to reality. There is still a long way to go, but the recent PEER research has laid the groundwork, established a framework and provided basic tools that make PBEE realizable and an

9-20 Earthquake Engineering: From Engineering Seismology to Performance-Based Engineering

attractive alternative to conventional analysis and design. In particular, significant progress has been made in establishing performance metrics and developing procedures for a rigorous performance assessment that combine seismological, engineering, financial (e.g., dollar losses) and societal (e.g., life safety) considerations. This section tries to summarize the approach developed by PEER researchers for this purpose.

One concern needs to be expressed, and one notion needs to be dispelled, up front. The concern is that the proposed approach relies heavily on the availability of seismological, engineering and financial data (e.g., construction costs and economic conditions after an earthquake). Much of the needed data are of questionable reliability now. This is not a drawback of the approach, but points out an urgent need for data acquisition and modeling. The notion to be dispelled is that the future will consist of only complex probabilistic approaches in structural design. This should be an option at the discretion of the engineer or owner, but should not be necessary for routine designs.

The main objectives of the PBEE development effort are to:

- Facilitate decision making on cost-effective risk management of the built environment in areas of high seismicity
- Facilitate the implementation of performance-based design and evaluation by the engineering profession
- Provide a foundation on which code-writing bodies can base the development of performance-based provisions

The last should result in relatively simple but more transparent and risk-consistent provisions than are contained in present codes and standards.

9.3.1 Components of Performance Assessment Approach

This section is concerned with performance assessment of buildings. The assumption is that all relevant building systems, i.e., the soil–foundation–structure system as well as the nonstructural and content systems, are given. The components of the performance assessment approach (Cornell and Krawinkler, 2000; Krawinkler, 2002; Deierlein et al., 2003), which are illustrated in Table 9.4, are summarized here and are elaborated on in subsequent sections.

TABLE 9.4 Schematics of Performance Assessment Approach

Performance Targets	Decision Variables DV	Damage Measures DM	Engineering Demands EDP	Seismic Hazard IM
• Collapse & Life safety $P_f < y$	• Collapse • Number of casualties	• Fragilities for failure states	• Engrg. analysis (story drift, floor acc.)	• Hazard analysis • Ground motions
• Losses $< x$	• \$ losses	–Structural	–Soil–foundation	
• Downtime $< z$	• Length of downtime	–Nonstructural –Content	–structure system	
$\lambda(DV)$	$G(DV/DM)$	$G(DM/EDP)$	$G(EDP/IM)$	$\lambda(IM)$

By definition, PBEE is based on achieving desired performance targets. They are of concern to society as a whole or to specific groups or individual owners. Performance targets are of the type expressed in the first column of Table 9.4. Of specific interest in the PEER effort are life safety, dollar losses and downtime (or loss of function). It is postulated that a performance target can be expressed in terms of a quantifiable entity and, for instance, its annual probability of exceedance. For instance, $\lambda_s(y)$, the mean annual frequency¹ (MAF) of the loss exceeding y dollars, could be the basis for a performance target. The quantifiable entities, on which performance assessment is based, are referred to as decision variables (DVs). In the assessment methodology the key issue is to identify and quantify decision variables of

¹The MAF is approximately equal to the annual probability for the small values of interest here.

primary interest to the decision makers, with due consideration given to all important uncertainties. Examples of DVs of primary interest are the existence of collapse, the number of casualties, dollar losses and the length of downtime, see the second column of Table 9.4.

To compute DVs and their uncertainties, other variables that define the seismic hazard, the demands imposed on the building systems by the hazard and the state of damage have to be defined and evaluated. The seismic hazard (last column of Table 9.4) is quantified in terms of a vector of intensity measures (IMs), which should comprehensively define the seismic input to the structure. This vector could have a single component, such as spectral acceleration at the first mode period of the structure, $S_a(T_1)$, or could have several components as discussed later. If a single component is used, such as $S_a(T_1)$, the hazard is usually defined in terms of a hazard curve. The outcome of hazard analysis, which forms the input to demand evaluation, is usually expressed in terms of an MAF of IMs, i.e., $\lambda(IM)$, as shown at the bottom of the last column of Table 9.4.

Given the ground motion hazard, a vector of engineering demand parameters (second to the last column of Table 9.4) needs to be computed, which defines the response of the building in terms of parameters that can be related to DVs. The EDP vector should include all parameters of relevance for damage and losses to the soil–foundation–structure system as well as the nonstructural and content systems. Interstory drift is an example of a relevant EDP. Relationships between EDPs and IMs are typically obtained through inelastic simulations, which should incorporate, to the extent feasible, the complete structural, geotechnical, SFSI (soil–foundation–structure interaction) and nonstructural systems. The outcome of this process, which may be referred to as probabilistic seismic demand analysis, can be expressed as $G(EDP|IM)$, as shown at the bottom of the second to the last column of Table 9.4, or more specifically as $G[EDP \geq y | IM = x]$, which is the probability that the EDP exceeds a specified value y , given (i.e., conditional) that the IM (e.g., the spectral acceleration at the first mode period of the structure, $S_a(T_1)$) is equal to a particular value x .

To close the loop, EDPs have to be related to the DVs of interest. In most cases an intermittent variable, called a damage measure (DM), has to be inserted between the EDP and the DV (see the middle column of Table 9.4) simply to facilitate the computation of DVs from EDPs. A DM describes the damage and consequences of damage to a structure or to a component of the structural, nonstructural or content system, and the term $G(DM|EDP)$ can be viewed as a fragility function for a specific damage (failure) state (probability of being in or exceeding a specific damage state, given a value of EDP). The DMs include, for example, descriptions of necessary repairs to structural or nonstructural components. If the fragility functions for all relevant damage states of all relevant components are known, the DVs of interest can be evaluated either directly or by means of cost functions that relate the damage states to repair and replacement costs. The result of this last operation is $G(DV|DM)$, the conditional probability that DV exceeds a specified value, given a particular value of DM.

These steps, which form the basis of performance assessment, can be expressed in the following equation for a desired realization of the DV, such as the MAF of the DV, $\lambda(DV)$, in accordance with the total probability theorem:

$$\lambda(DV) = \iiint G(DV|DM) dG(DM|EDP) dG(EDP|IM) d\lambda(IM) \quad (9.2)$$

This equation, which is often referred to as the framework equation for performance assessment, suggests a generic structure for coordinating, combining and assessing the many considerations implicit in performance-based seismic assessment. Inspection of Equation 9.2 reveals that it “de-constructs” the assessment problem into the four basic elements of hazard analysis, demand prediction, modeling of damage states and failure or loss estimation, by introducing the three intermediate variables, IM, EDP and DM. Then it recouples the elements via integration over all levels of the selected intermediate variables. This integration implies that, in principle, one must assess the conditional probabilities $G(EDP|IM)$, $G(DM|EDP)$ and $G(DV|DM)$ parametrically over a suitable range of DM, EDP and IM levels.

In the written form, the assumption is that appropriate intermittent variables (EDPs and DMs) are chosen such that the conditioning information need not be carried forward (e.g., given EDP, the DMs and DVs) are conditionally independent of IM; otherwise IM should appear after the EDP in the first factor. So, for example, the EDPs should be selected so that the DMs (and DVs) do not also vary with intensity, once the EDP is specified. Similarly one should choose the intensity measures (IM) so that, once it is given, the dynamic response (EDP) is also not further influenced by magnitude or distance (which have already been integrated into the determination of $\lambda(\text{IM})$). This condition can make selection of records a challenge (Cornell and Krawinkler, 2000).

Equation 9.2 may take various forms, depending on the purpose and the decision variable of interest. Examples of variations to this equation are presented in Section 9.3.5.

The following sections address a few of the important issues involved in the steps summarized here, and point out some of the challenges that have to be confronted to permit a consistent implementation of the framework equation.

9.3.2 Intensity Measures (IMs)

Intensity measures are quantities that describe the magnitude (M) and distance (R) dependences (other parameters such as fault mechanism also could be considered) of ground motion characteristics that significantly affect the upstream variables of the performance assessment approach. In the context of Equation 9.2, this implies evaluation of the MAF of IMs through seismic hazard analysis. Of course, simplicity favors scalar measures, and in particular, measures for which hazard analysis results are available. For example, choosing PGA for the IM may be initially appealing, but it implies that the distribution $G(\text{EDP}|\text{IM})$ may have a very large variability, which means that it will require a large sample of records and nonlinear analyses to estimate $G(\text{EDP}|\text{IM})$ with sufficient confidence. A well-selected spectral ordinate (e.g., S_a at the fundamental period T_1) is an improvement over PGA and has been the popular choice in the recent past. It is a matter of debate whether $S_a(T_1)$ is indeed the best choice (best implies a balance between simplicity and accuracy).

$S_a(T_1)$ does not account for the frequency content at $T \neq T_1$, which dominates higher mode effects ($T < T_1$), and period elongation effects for inelastic systems ($T > T_1$). Again, this may lead to $G(\text{EDP}|\text{IM})$ distributions with a very broad variability. This is illustrated in Figure 9.16, which shows incremental dynamic analyses (IDAs, see Section 9.3.3), together with statistical values (Median, 16th and 84th percentile), for the maximum story drift of a nine-story frame structure subjected to 40 ground motions that are scaled so that the S_a at the fundamental period ($T_1 = 0.9$ sec) is the same. Scaling records to a common S_a at T_1 (which is implied by using $S_a(T_1)$ as the IM) results in a median spectrum that resembles a typical spectrum for ordinary (no near-fault characteristics) ground motions, but results in large variability in spectral ordinates at periods even very close to T_1 (see Figure 9.17; $T_1 = 0.5$ sec for the case shown).

Figures 9.16 and 9.17 provide ammunition to search for better IMs. Better implies that the variability should be reduced to permit the use of a smaller number of records (efficiency), and that all significant dependences on magnitude and distance should be represented in the hazard analysis for the improved IM (sufficiency). This is indeed a challenge, particularly if near-fault ground motions start to dominate the hazard at long return period hazards. Several efforts are in progress to find improved IMs, ranging from the use of inelastic displacement spectral values, to combinations of spectral values at modal periods, to the use of vectors that incorporate near-fault parameters such as an equivalent pulse period.

An example of the effect of different IMs on the dispersion of the same EDP is presented in Figure 9.18 (Cordova et al., 2000). The plots represent IDA results for a multi-story frame subjected to eight near-fault ground motions that have a well-defined pulse period T_p . Each point plotted in Figure 9.18a corresponds to the maximum interstory drift ratio (EDP) from a nonlinear time history analysis under a record scaled to a given IM, using $S_a(T_1)$ as IM. The scatter in EDP for this specific IM is very large, particularly for large IM values at which period elongation due to softening dominates the response. Data plotted in Figure 9.18b are for the same structure, but using an IM calculated as a weighted average between $S_a(T_1)$ and $S_a(1.8T_1)$ — with the idea of capturing some of the softening response in the IM.

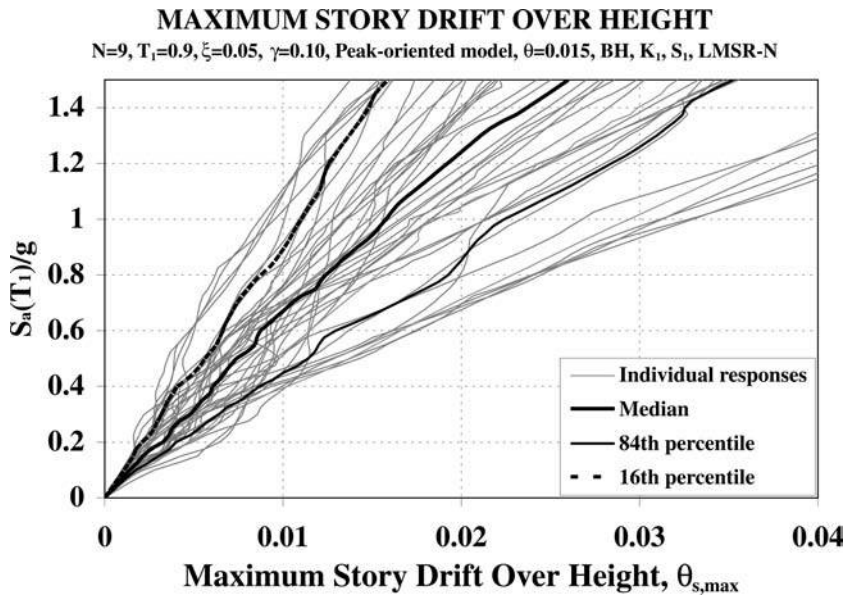


FIGURE 9.16 Record-to-record variability reflected in IDA curves for a nine-story frame structure with $T_1 = 0.9$ sec. (Medina, R.A. (2002). Seismic demands of nondeteriorating frame structures and their dependence on ground motions. Ph.D. Dissertation, Dept. of Civil Engineering, Stanford University. With permission.)

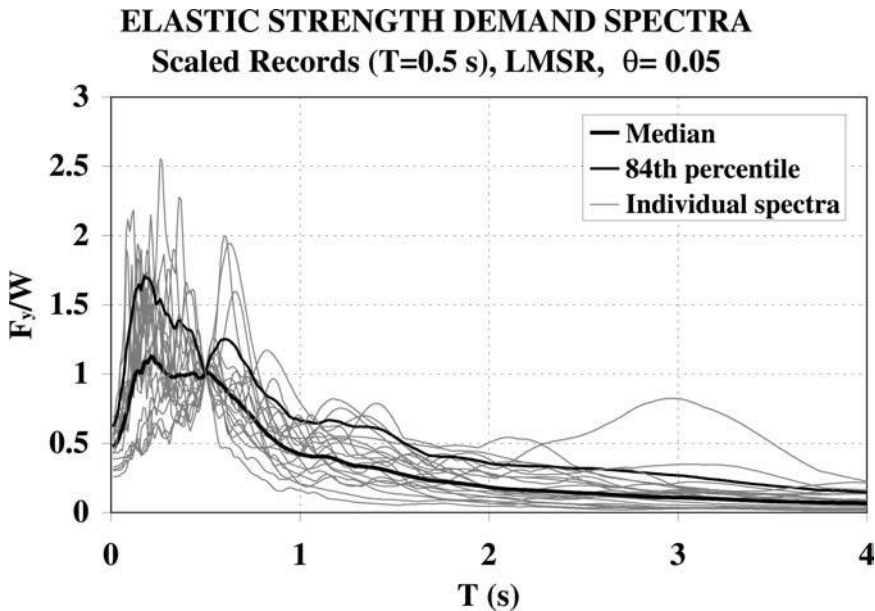


FIGURE 9.17 Set of ground motion spectra scaled to common S_a at $T = 0.5$ sec. (Medina, R.A. (2002). Seismic demands of nondeteriorating frame structures and their dependence on ground motions. Ph.D. Dissertation, Dept. of Civil Engineering, Stanford University. With permission.)

As shown in the figure, the alternative IM significantly reduces the overall scatter at larger intensities under which the structure has softened, but this reduction is at the expense of increased scatter at lower intensities under which the response is elastic. Although alternatives of the type shown in Figure 9.18b show promise, at present there is no consensus on any scalar IM that is significantly better than $S_a(T_1)$.

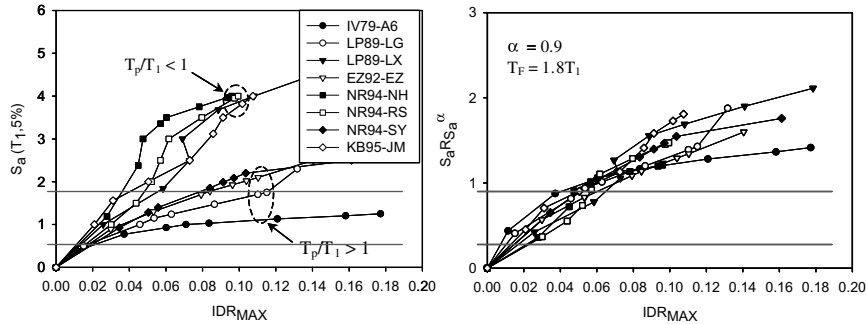


FIGURE 9.18 IDAs with two different intensity measures; (a) IM = $S_a(T_1)$, (b) IM = $S_a R_{sa}^\alpha$. (Cordova, P.P., et al., Proc. 2nd U.S.-Japan Workshop on Performance-Based Earthquake Engineering for Reinforced Concrete Building Structures, 2000. With permission.)

9.3.3 Engineering Demand Parameters (EDPs)

Engineering demand parameters are the product of response prediction, most appropriately from an inelastic dynamic analysis that considers the soil–foundation–structure system resting on top of bedrock. The task of formulating complete system models, which should incorporate modeling uncertainties and should account for all important uncertainties inherent in geotechnical and structural material, component and system properties, will remain a challenge for years to come.

Relevant EDPs depend on the performance target and the type of system of interest. They include story drifts, component inelastic deformations, floor accelerations and velocities, but also cumulative damage terms such as hysteretic energy dissipation. Once identified, they can be computed from different procedures such as by, the now widely employed, incremental dynamic analysis (IDA) procedure (Vamvatsikos and Cornell, 2002). In this procedure, the soil–foundation–structure system is subjected to a ground motion whose intensity is incremented after each inelastic dynamic analysis. The result is a curve that shows the EDP plotted against the IM used to control the increment of the ground motion. IDAs can be carried out for a sufficiently large number of ground motions to perform statistical evaluation of the results. This implies that for a given value of IM, the median value and a measure of dispersion (e.g., 84th percentile) of the response EDP values are computed, with results as shown in the right part of Figure 9.19. These values are computed by assuming a lognormal distribution for EDP/IM, as illustrated in the figure. This provides the information on $dG(\text{EDP}|IM)$ of Equation 9.2.

For use in Equation 9.2, $dG(\text{EDP}|IM)$ must be evaluated for the full range of IM that significantly contributes to the final value of DV. The IDA, however, has a limited range of applicability because the ground motion frequency characteristics change with magnitude and distance, particularly for long return period hazards that may be dominated by near-fault ground motions. Thus, caution must be exercised in defining the range of applicability of an IDA and the associated values of $dG(\text{EDP}|IM)$.

Presuming that the IDA curves and their statistics are valid for the full range of interest, the information in Figure 9.19 can be used to develop a hazard curve for the EDP, using the equation

$$\lambda_{\text{EDP}}(y) = \int P[\text{EDP} \geq y | IM = x] | d\lambda_{\text{IM}}(x)| \quad (9.3)$$

where

- $\lambda_{\text{EDP}}(y)$ = mean annual frequency of EDP exceeding the value y
- $P[\text{EDP} \geq y | IM = x]$ = probability of EDP exceeding y given that IM equals x
- $\lambda_{\text{IM}}(x)$ = mean annual frequency of IM exceeding x (ground motion hazard).

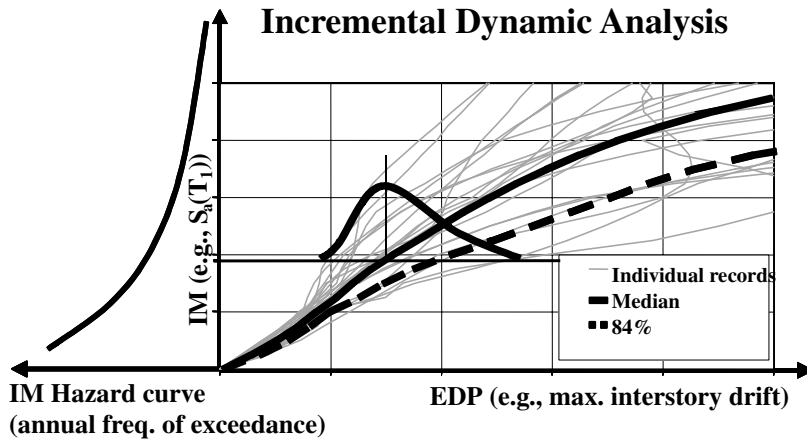


FIGURE 9.19 Incremental dynamic analyses and their use in probabilistic seismic demand analysis.

The EDP hazard curve can be obtained, for a given IM hazard curve, from numerical integration of results of the type shown in Figure 9.19, or through a formulation described by Luco and Cornell (1998), which results in the following expression for the mean annual frequency of EDP exceeding a value y :

$$\lambda_{EDP}(y) = P[EDP \geq y] = k_o \left[(y/a)^{1/b} \right]^{-k} \exp \left[-\frac{1}{2} \frac{k^2}{b^2} \sigma_{\ln EDP|IM}^2 \right] \quad (9.4)$$

This closed-form solution provides good results provided that the following conditions are satisfied:

1. The IM hazard can be described by the widely used equation

$$\lambda_{IM}(x) = P[IM \geq x] = k_o x^{-k} \quad (9.5)$$

2. The following relationship can be locally fit (around the return period of primary interest) to the median EDP–IM data:

$$\hat{EDP} = a(IM)^b \quad (9.6)$$

3. The dispersion of EDP is close to constant for all relevant levels of IM. This condition is often not satisfied as it is observed that the dispersion often increases with the level of inelastic response.

Typical examples of EDP hazard curves, obtained either from numerical integration or from Equation 9.4 are shown in Figure 9.20. The hazard curves are for the roof drift and the maximum story drift of a nine-story frame with a period of 1.8 sec and 10% base shear strength ($\gamma = 0.1$). In this case, the closed-form solutions provide reasonable estimates of the drift hazards obtained from numerical integration.

It is emphasized that the range of applicability of EDP hazard curves extends only over the mean annual frequencies for which the ground motions and analytical models used in the analysis are representative. In regions of strong seismicity, and for return periods exceeding about 500 years ($\lambda = 0.002$), the ordinary ground motions used in the IDAs on which the hazard curve shown in Figure 9.20 is based, are likely unrepresentative because of the increasing importance of near-fault effects. Furthermore, the fact that the EDP predictions for this example are based on nondeteriorating hysteresis models renders the hazard curve questionable for drift values at which deterioration starts to affect the behavior. The issue of deterioration in strength and stiffness is addressed in the next section in the context of collapse safety.

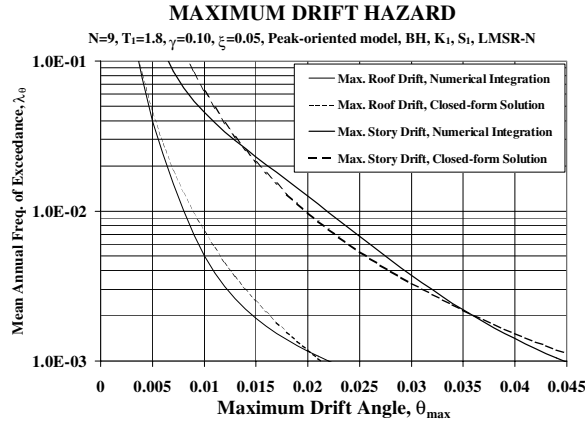


FIGURE 9.20 Examples of hazard curves for engineering demand parameters; nine-story frame structure with $T_1 = 1.8$ sec. (Medina, R.A., Ph.D. Dissertation, Stanford University, 2002. With permission.)

9.3.4 Probability of Global Collapse

Considering the need for a comprehensive performance assessment, which has to include the limit state of collapse, developing component hysteresis models that incorporate all-important phenomena that contribute to demand predictions as the structure approaches collapse becomes a necessity. In earthquake engineering, collapse implies that the structural system, or any part thereof, is incapable of maintaining gravity load carrying capacity in the presence of seismic effects. Local collapse may occur, for instance, if a vertical load carrying component fails in compression, or if shear transfer is lost between horizontal and vertical components (e.g., shear failure between a flat slab and a column). Global (or at least story) collapse will occur if local collapses propagate (progressive collapse) or if an individual story displaces sufficiently so that the second-order P- Δ effects fully offset the first-order story shear resistance and instability occurs (incremental collapse).

In either case, replication of collapse necessitates modeling of deterioration characteristics of structural components. A relatively simple deterioration model is discussed in this section, and is then used to assess collapse behavior. For additional reading on important work on deterioration models the reader is referred to the following publications: (Kunnath et al., 1990, 1997; Sivaselvan and Reinhorn, 2000; Song and Pincheira, 2000).

The deterioration model summarized here attempts to model all-important modes of deterioration that are observed in experimental studies (Ibarra et al., 2002). An example of a monotonic load–displacement response and a superimposed cyclic response of identical plywood shear wall panels is illustrated in Figure 9.21. The monotonic test result shows that the strength is capped and that strength capping is followed by a negative tangent stiffness (which often degrades gradually, a phenomenon that is ignored in the deterioration model discussed here). The cyclic hysteresis response indicates that the strength in large cycles deteriorates with the number and amplitude of cycles, even if the displacement associated with the strength cap has not been reached. It also indicates that strength deterioration occurs in the post capping range, and that the unloading stiffness may also deteriorate. Furthermore, it is observed that the reloading stiffness may deteriorate at an accelerated rate if the hysteresis response is of a pinched nature (as in this example).

Based on these observations, the hysteresis model should incorporate a backbone curve that represents the monotonic response, and deterioration rules that permit modeling of all important deterioration modes and that should be applicable to various basic hysteresis models such as bilinear, peak oriented and pinched models. Thus, as a minimum, the backbone curve has to be trilinear to include strength capping and post cap strength deterioration. The strength cap F_c is associated with the cap deformation, δ_c , and is followed by a post capping tangent stiffness $K_c = \alpha_c K_e$, which is either zero or negative. The

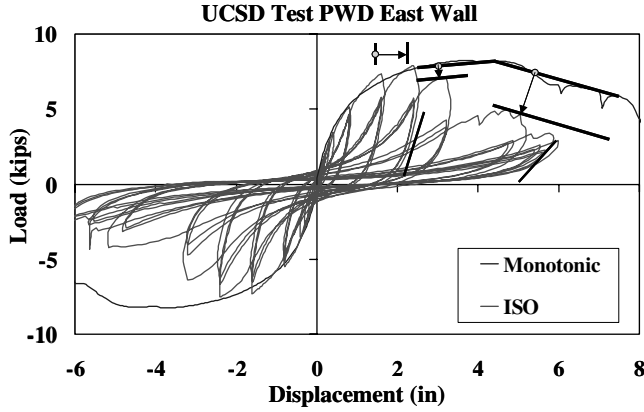


FIGURE 9.21 Experimental results from plywood shear wall tests; modes of deterioration (ISO = loading protocol of International Standards Organization).

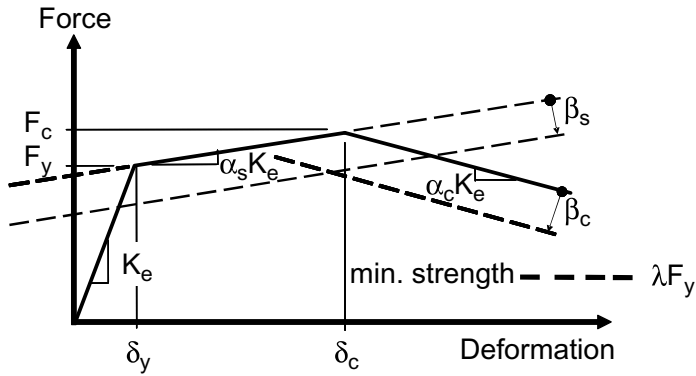


FIGURE 9.22 Backbone curve and its movement with deterioration.

branches of the backbone curve are shown in Figure 9.22. As seen, the ratio δ_c/δ_y may be viewed as the ductility capacity, but deformations larger than δ_c can also be tolerated.

The strain hardening and post capping branches may remain stationary or may deteriorate (i.e., translate toward the origin) in accordance with a relatively simple energy-based deterioration model (Rahnama and Krawinkler, 1993) defined by a deterioration parameter of the type

$$\beta_i = \left(\frac{E_i}{E_t - \sum_{j=1}^i E_j} \right)^c \quad (9.7)$$

in which

β_i is the parameter defining the deterioration in excursion i

E_i is the hysteretic energy dissipated in excursion i

E_t is the hysteretic energy dissipation capacity, expressed as a multiple of $F_y\delta_y$, i.e., $= \gamma F_y\delta_y$

$\sum E_j$ is the hysteretic energy dissipated in all previous excursions

c is the exponent defining the rate of deterioration

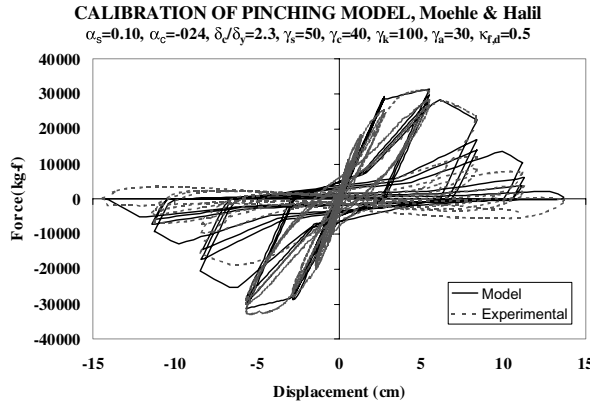


FIGURE 9.23 Comparison between experimental results and analytical predictions for a deteriorating system.

This deterioration parameter can be applied to one or all of the aforementioned deterioration modes. In addition to these deterioration modes, a residual strength of λF_y can be assigned to the model. When such a residual strength is specified, the backbone curve is supplemented by a horizontal line with ordinate λF_y , and the strength will not drop below this value.

Thus, the deterioration model has two parameters defining the capping phenomenon (δ_c (or F_c) and α_c), up to four deterioration parameters ($\gamma_s, \gamma_c, \gamma_k, \gamma_a$), which define the energy dissipation capacity in various deterioration modes, and a residual strength parameter λ (presuming that the exponent in Equation 9.7 is equal to 1.0, which is the only case considered so far).

This model was tested on force–deformation data obtained from experiments on steel, reinforced concrete and wood components. Adequate simulations were obtained by tuning the model parameters to the experimental data. An example comparison of an experimental force–deformation response with its matched deterioration model is shown in Figure 9.23. The test data are from two experiments on an RC column subjected to an axial force and lateral loading (Moehle et al., 2002). An essentially monotonic lateral load test was used to establish the backbone curve, and a cyclic lateral load test was used to determine the deterioration parameters.

The deteriorating hysteresis model summarized here is relatively simple but sufficiently versatile to model all basic deterioration modes in components of different material. The model has been used to perform studies on SDOF systems and generic MDOF structures. Selected results of the SDOF study, which provide insight into the effects of deteriorating component characteristics on the collapse safety of structural systems, are summarized next.

Examples illustrating the effects of cyclic deterioration on the time history response of an SDOF system are shown in Figure 9.24. The backbone curve parameters are indicated in the figure, and γ values of 100 and 25, respectively, are used for the four modes of deterioration. The NR94hol ground motion recorded in the 94 Northridge earthquake is used as input. The small γ value (25 as compared with 100) leads to pronounced cyclic deterioration, which is reflected in the decrease in strength and stiffness evident in Figure 9.24b, which in turn increases the maximum displacement by about 50% compared to the case with slow cyclic deterioration, but does not yet lead to collapse.

Basic response data can be obtained by subjecting SDOF systems to a set of records, and for each record increasing the parameter $(S_a/g)/\eta$ in small increments ($\eta = F_y/W$). In this manner, $(S_a/g)/\eta$ –EDP graphs of the type shown in Figure 9.25a can be generated. As this figure shows, the individual curves tend to approach a zero slope as the parameter $(S_a/g)/\eta$ is increased. A zero slope implies that collapse has occurred because the intensity, defined by $(S_a/g)/\eta$, can no longer be increased. The figure also clearly shows the large dispersion of the results, which is caused by differences in the frequency content of the ground motions. For given $(S_a/g)/\eta$ values, the data can be evaluated statistically, resulting in the indicated

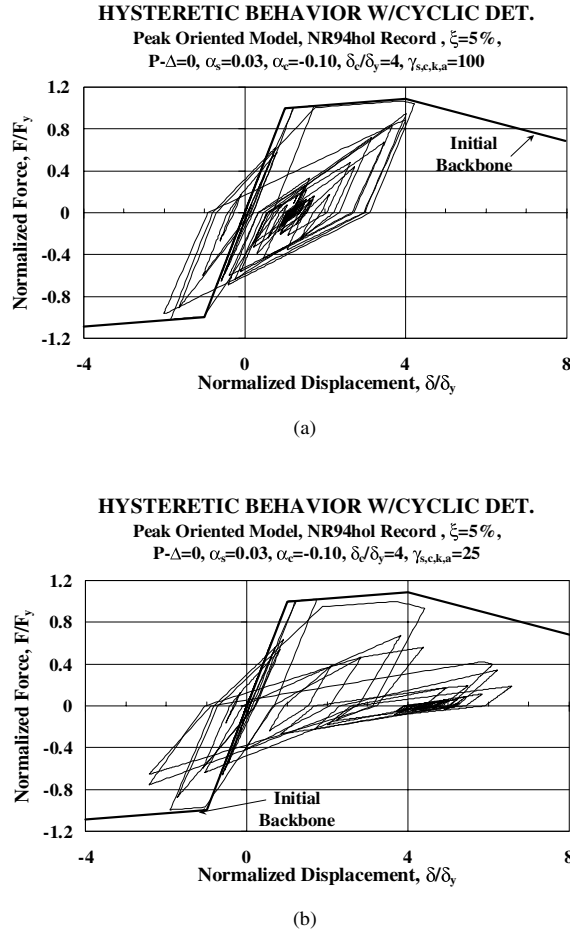


FIGURE 9.24 Effect of cyclic deterioration in time history analysis (a) $\gamma_{s,c,k,a} = 100$, (b) $\gamma_{s,c,k,a} = 25$. (Ibarra L. et al., Proc. 12th European Conference on Earthquake Engineering, London, 2002. With permission.)

median and 84th percentile curves for the selected demand parameter. Curves of this type can be produced for different system parameters, which permits an evaluation of the effects of deterioration. As an example, Figure 9.25b presents four median IDA curves, using SDOF systems with a period of 0.5 sec and the system parameters indicated in the figure. The uppermost curve is for infinitely ductile systems ($\delta_c/\delta_y = \infty$), in which case collapse will never be observed (unless $P-\Delta$ is very large). The other three curves are for systems with finite δ_c/δ_y values. These median curves start to deviate from those of infinitely ductile systems at displacements less than that corresponding to the selected δ_c/δ_y ratios (because of cyclic deterioration), and terminate when 50% of the records have led to the collapse of the SDOF system.

Thus, the last point on these curves represents the median $(S_a/g)/\eta$ value at which the SDOF system collapses. For brevity, it will be denoted from here on as the median collapse capacity. It is a property of the selected structural system and the selected ground motion set. For an SDOF system of given strength (η), it represents the median S_a value leading to collapse, and for a given S_a value (hazard level), it represents the median strength leading to collapse. In the latter context, $(S_a/g)/\eta$ represents the response modification factor (R-factor) without overstrength, and therefore, the median $(S_a/g)/\eta$ value at collapse is equivalent to the median R-factor causing collapse. In the following discussion the median $(S_a/g)/\eta$ value at collapse is used to assess the sensitivity of the collapse capacity to the period and deterioration properties of the structural system.

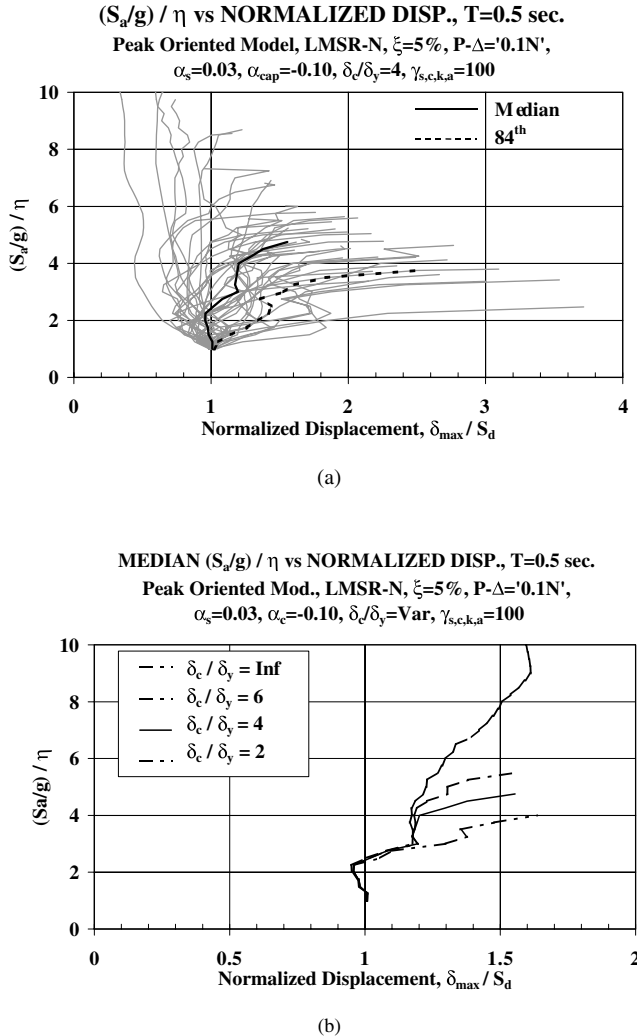


FIGURE 9.25 $(S_a/g)/\eta$ -EDP graphs, (a) for a specific system and individual records, (b) median results for four different systems. (Ibarra L. et al., Proc. 12th European Conference on Earthquake Engineering, London, 2002. With permission.)

An example of the dependence of collapse values of $(S_a/g)/\eta$ on the system period is presented in Figure 9.26, showing data points for individual records as well as median and 16th percentile values. The data are for a system that from here on will be referred to as the base case. It is defined by a δ_c/δ_y value of 4.0, a cyclic deterioration parameter of $\gamma_{s,c,k,a} = 100$ and a post capping slope of $\alpha_c = -0.1$. The results are obtained by performing collapse analysis for SDOF systems whose period is varied in closely spaced intervals. It can be observed that the statistical values for the collapse capacity vary only slightly with period, except in the short period range ($T < 0.6$ sec) in which they decrease considerably. This is also the range in which many past studies have shown that even for nondeteriorating systems the R-factor for constant ductility demands decreases rapidly with a decrease in period.

Figure 9.27 presents curves for median values of $(S_a/g)/\eta$ at collapse versus T , for systems with $\delta_c/\delta_y = 6$, 4 and 2 (all other parameters same as in the base case). If a flat post capping slope ($\alpha_c = -0.1$) exists, it permits a significant increase in $(S_a/g)/\eta$ after δ_c is reached but before the relatively large collapse displacement is attained. Thus, the effect of δ_c/δ_y on collapse values of $(S_a/g)/\eta$ is not very large unless a steep post capping slope exists, in which case collapse occurs soon after δ_c has been reached (see the curve for $\delta_c/\delta_y = 2$ and $\alpha_c = -0.3$ versus $\alpha_c = -0.1$).

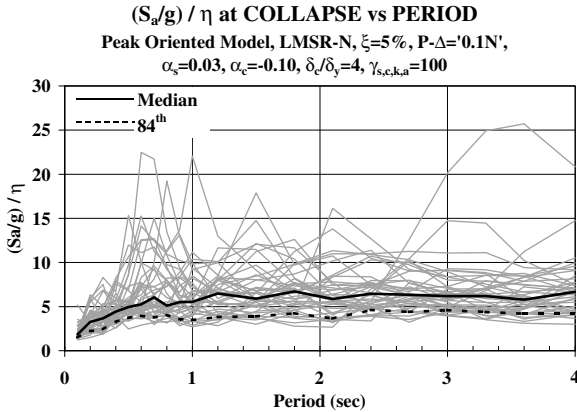


FIGURE 9.26 Variation of collapse capacity with period; base case structural system. (Ibarra, L., Medina, R. and Krawinkler, H. (2002). Collapse assessment of deteriorating SDOF systems. *Proc. 12th European Conference on Earthquake Engineering*, London, Paper Reference 665. With permission.)

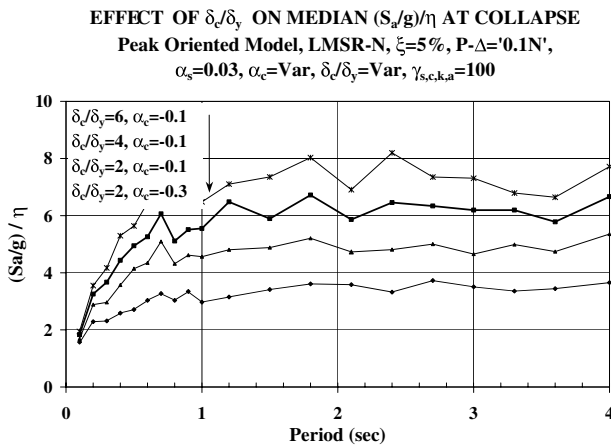


FIGURE 9.27 Effect of δ_c/δ_y ratio on median collapse capacity. (Ibarra, L., Medina, R. and Krawinkler, H. (2002). Collapse assessment of deteriorating SDOF systems. *Proc. 12th European Conference on Earthquake Engineering*, London, Paper Reference 665. With permission.)

The effect of various γ values ($\gamma = \infty$ implies no cyclic deterioration) on the collapse capacity of the base case system ($\gamma_{s,c,k,a} = 100$) is illustrated in Figure 9.28. For SDOF systems, the effect decreases with an increase in period, simply because long period systems undergo a smaller number of inelastic cycles. These observations are consistent with results obtained by Song and Pincheira (2000). The results are for Californian ground motions in earthquakes of magnitude between 6.5 and 6.9, which mostly have a relatively short strong motion duration. Ground motions from very large magnitude earthquakes (and ground motions amplified in soft soil media, e.g., Mexico City) may have much longer strong motion duration, and the cyclic deterioration effects may grow correspondingly.

Figure 9.29 shows $(S_a/g)/\eta$ — period curves for representative systems for a range of combined deterioration parameters. This plot emphasizes the importance of ductility characteristics in the collapse capacity. The parameters that define the backbone curve (δ_c/δ_y and α_c) and the hysteretic energy dissipation capacity (γ) have a significant influence on the collapse capacity of the system. So does the $P-\Delta$ effect, unless the system period is short.

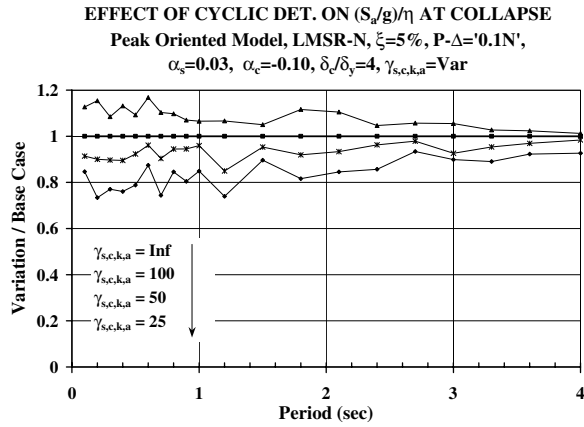


FIGURE 9.28 Effect of variation in cyclic deterioration on collapse capacity of base case. (Ibarra, L., Medina, R. and Krawinkler, H. (2002). Collapse assessment of deteriorating SDOF systems. *Proc. 12th European Conference on Earthquake Engineering*, London, Paper Reference 665. With permission.)

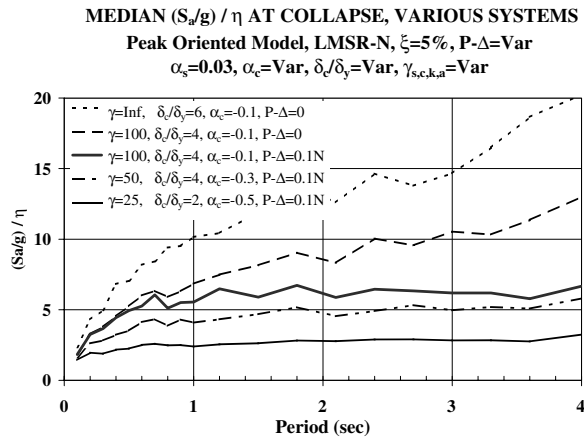


FIGURE 9.29 Effect of combinations of deterioration parameters on median collapse capacity. (Ibarra, L., Medina, R. and Krawinkler, H. (2002). Collapse assessment of deteriorating SDOF systems. *Proc. 12th European Conference on Earthquake Engineering*, London, Paper Reference 665. With permission.)

9.3.4.1 Collapse Fragility Curves

Data of the type shown in Figure 9.25 can be utilized to develop fragility curves, which describe the probability of failure (in this case failure implies collapse), given the value of $(S_a/g)/\eta$. Such fragility curves are obtained from the CDF of the last point of each of the curves shown in Figure 9.25a (the collapse point). Typical results of fragility curves are shown in Figure 9.30 for SDOF systems with $T = 0.5$ sec and various deterioration parameters. This figure demonstrates the large sensitivity of the probability of collapse to the hysteretic properties.

If the collapse fragility curve for a given system has been determined, probabilistic collapse assessment can be carried out according to the following equation:

$$\lambda_f = \int F_{C_{IM}}(x) |d\lambda_{IM}(x)| \quad (9.8)$$

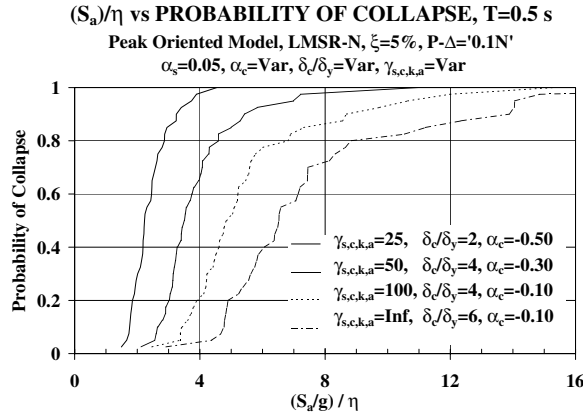


FIGURE 9.30 Collapse fragility curves for systems with various deterioration properties; T = 0.5 sec. (Ibarra, L., Medina, R. and Krawinkler, H. (2002). Collapse assessment of deteriorating SDOF systems. *Proc. 12th European Conference on Earthquake Engineering*, London, Paper Reference 665. With permission.)

where

λ_f = mean annual frequency of collapse

$F_{CIM}(x)$ = probability of IM capacity (i.e., S_a capacity for a given η value) exceeding x

$\lambda_{IM}(x)$ = mean annual frequency of IM exceeding x (ground motion hazard)

Thus, given the IM hazard curve and fragility curves of the type shown in Figure 9.30, it is a matter of numerical integration to compute the mean annual frequency of collapse.

9.3.5 Loss Estimation in PBEE

9.3.5.1 Economic Loss Estimates as Measures of Seismic Performance

The aim of PEER's loss estimation efforts is to describe the seismic performance of structures quantitatively by continuous variables rather than discrete and sometimes subjective performance levels. The loss estimation methodology described in this section provides a continuous and quantitative measure of seismic performance in terms of economic losses for individual buildings. There are various measures of economic loss that can be used. A particularly useful one is the expected annual loss, which corresponds to the economic loss that, on average, occurs every year in the building, $E[L_{Bldg}]$. Owners, lending institutions, insurers and other stakeholders can then quantitatively compare, for example, annual revenues with annual losses, they can compare annual earthquake insurance premiums to annual expected losses, etc. Furthermore, if presented with different design alternatives, and if the cost of each of these alternatives is known, then a cost-benefit analysis can be performed for the building. Therefore, it is clear that quantitative measures of economic losses provide stakeholders with an improved level of information regarding seismic performance that can become the basis for more rational decision making as part of risk management strategies.

In the case of new buildings, owners and investors may be faced with the difficulty of having to decide the level of economic loss that they are willing to accept, which in turn can lead them to decide whether or not to make the investment in the building, or whether to increase the level of investment to improve its seismic performance and decrease the level of losses. In the case of existing buildings, owners or risk managers will have to decide among different alternatives such as: (a) to sell, (b) to demolish and rebuild, (c) to face the losses and repair or replace after earthquake damage occurs, (d) to transfer part of the possible losses through earthquake insurance, (e) to upgrade to decrease the level of loss or (f) any combination of these alternatives. Lending institutions need to decide whether to provide financial resources to the owner or investor. Similarly, insurers may be interested to know the potential economic

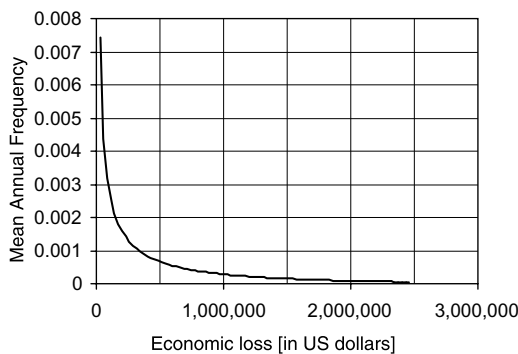


FIGURE 9.31 Example of a loss curve that provides the probability of exceedance of different dollar losses.

losses they may face if a portion of the risk is transferred to them in order to decide the premium that they should charge for accepting the risk. The expected annual loss provides quantitative information to assist stakeholders in making these risk management decisions, hence the expected annual loss for a building, $E[L_{Bldg}]$, is a viable expression of the decision variable economic loss.

The expected annual loss is not the only alternative for a quantitative expression of economic loss. Another feasible expression is the mean annual frequency of exceedance of a given dollar loss. The mean return period of a given dollar loss corresponds to the inverse of the mean annual frequency of exceedance. For small values of mean annual frequency that are of interest in earthquake engineering, the annual probability of exceedance is approximately equal to the mean annual frequency of exceedance. A loss curve can be obtained by plotting dollar losses against their corresponding annual probability of exceedance or against their mean return period. An example is shown in Figure 9.31. This curve has been computed for a seven-story building located in California. It can be seen that small losses such as \$200,000 have an annual probability of exceedance of approximately 0.00182, which corresponds to a return period of 550 years, while the annual probability of losing more than two million dollars in the structure is only approximately 1.5×10^{-4} .

Other measures of economic losses that are useful to stakeholders are the probable maximum loss (PML) and the probability of ruin. A PML can be generally defined as an economic loss that has a small probability of being exceeded. PMLs are commonly used by insurers, reinsurers and lending (mortgage) institutions to define their reserves and their risk transfer policies. Since the term small probability is ambiguous there are many possible ways of defining a PML (ASTM, 1999; SEAONC, 1999; EERI, 2000). Some commonly used definitions are: (i) the expected value of the loss associated with an event with a given return period (e.g. 475 years); (ii) the loss associated with a 90% probability of nonexceedance (or any other probability level) associated with an event with a given return period (e.g. 475 years); (iii) the loss associated with a given return period (e.g., 1000 years). In the first two definitions, defining the seismic event by its return period is equivalent to defining the probability of exceedance of the event over a certain period of time. For example, a 475-year event approximately corresponds to an event whose ground motion intensity has a 10% probability of being exceeded in 50 years. The third definition simply corresponds to defining the PML as one of the points on the loss curve.

Estimating the probability of ruin involves computing the probability that the income, reserves and borrowing capabilities of the stakeholder will not be enough to cover the losses estimated to occur over a period of time (EERI, 2000). The selection of the expression of economic loss to be used as measure of seismic performance will depend among other factors on the alternatives available to manage the risk and on the type of stakeholder. For example, the best suited expression of loss likely will be different for a small business owner than for a large corporate owner or for a local government. Similarly, it likely will be different for the owner who is interested in transferring a large portion of the risk through earthquake insurance than for the insurer or reinsurer absorbing the risk.

9.3.5.2 Building Specific Loss Estimation Methodology

In the proposed approach it is assumed that the total loss resulting from the repair and replacement of all damaged components in the building (either a structural or nonstructural or content component) is equal to the sum of the losses resulting from the repair or replacement of each damaged component. Hence the loss in the building, L_{Bldg} , is treated as a random variable that is computed as

$$L_{Bldg} = \sum_{j=1}^n L_j = L_{j=1} + L_{j=2} + L_{j=3} + \dots + L_{j=n} \quad (9.9)$$

where L_j is a random variable that represents loss in the j th component and n is the total number of components in the building. Equation 9.9 is a simplification, however it reproduces the fact that losses to be paid by owners and other stakeholders result from the sum of repair and replacement costs from individual subcontractors and that these costs usually originate from unitary costs.

Losses to individual components can be computed using PEER's framework equation (Equation 9.2), which assumes that all four random variables (IM, EDP, DM and DV) are continuous random variables. However, economic losses in individual building components are often associated with discrete repair actions, which are discretely triggered at certain levels of damage. For example, the replacement of an individual glass panel represents a discrete repair action because one either replaces the glass panel or not, but one cannot incrementally (continuously) replace the window panel. Similarly, the need to replace the glass panel is triggered when a breakage occurs and the glass needs to be replaced whether the glass panel is slightly broken or completely broken. In the proposed approach, economic losses in individual components are computed from the need to apply discrete repair and replacement actions that are triggered at discrete damage states. In the example just described the discrete damage states would be: (1) distortion and damage to the gaskets caused by relative motion between the glass panel and the window frame, (2) breakage of the glass panel and (3) damage to the window frame. The corresponding repair and replacement actions are: (1) repair and replacement of the gaskets, (2) replacement of the glass panel and (3) replacement of the window frame, respectively. The economic losses for each component are assumed to correspond to the cost of each of the repair and replacement actions required in each damage state. Furthermore, it is assumed that each building component can be damaged only by one type of EDP, in other words, that each component is sensitive to only one type of EDP (e.g., interstory drift or floor acceleration).

To deal with discrete damage states in each component, Equation 9.2 needs to be modified. In particular, the mean annual probability of exceeding a loss level l in the j th component (either a structural or nonstructural or content component) considering a finite number of damage states in the component is given by

$$P[L_j > l] = \sum_{i=1}^m \int_0^\infty \int_0^\infty P[L_j > l | DM = dm_i] P(DM = dm_i | EDP_j = edp) \left| \frac{dP(EDP_j > edp | IM = im)}{dIM} \right| \frac{dv(IM)}{dIM} \quad (9.10)$$

where m is the number of damage states in the j th component, $P[L_j > l | DM = dm_i]$ is the probability of exceedance of a loss level l in the j th component conditioned on knowing that the component is in the i th damage state, $P(DM = dm_i | EDP_j = edp)$ is the probability that the j th component will be in the damage state i given that the component has been subjected to an EDP equal to edp , $P(EDP_j > edp | IM = im)$ is the probability that the EDP affecting the j th component will exceed a certain value edp given that the ground motion intensity measure IM is equal to im , and $\left| \frac{dP(EDP_j > edp | IM = im)}{dIM} \right|$ is the slope of the seismic hazard curve corresponding to the intensity measure IM.

The occurrence of economic losses in most cases will be associated with a much wider range of ground motion intensities than those associated with the collapse limit state, therefore, assuming that the seismic

hazard curve can be described by Equation 9.5 over the whole range on IM of interest, in general, will not be valid, so the integrals in Equation 9.10 are usually solved numerically.

In Equation 9.10 the probability that the j th component will be in damage state i given that component has been subjected to an EDP equal to edp is computed as

$$P(DM_j = dm_i | EDP_j = edp) = P(DM_j > dm_i | EDP_j = edp) - P(DM_j > dm_{i+1} | EDP_j = edp) \quad (9.11)$$

where $P(DM_j > dm_i | EDP_j = edp)$ is the probability of exceeding damage state i in the j th component given that it has been subjected to an EDP equal to edp and $P(DM_j > dm_{i+1} | EDP_j = edp)$ is the probability of exceeding damage state $i+1$ in the j th component given that it has been subjected to an EDP equal to edp. The functions $P(DM_j > dm_i | EDP_j = edp)$ and $P(DM_j > dm_{i+1} | EDP_j = edp)$ correspond to the fragility curves for the i th and $(i+1)$ th damage states of the j th component as a function of EDP, which describe the vulnerability or damageability of the j th component with increasing levels of EDP.

The expected annual loss in the j th component can be computed by replacing $P[L_j > l | DM = dm_i]$ in Equation 9.10 by the expected value of the loss in the j th component given that it is in the i th damage state, $E[L_j | DM = dm_i]$, as follows:

$$E[L_j] = \sum_{i=1}^m \int_0^\infty \int E[L_j | DM = dm_i] P(DM = dm_i | EDP_j = edp) dP(EDP_j > edp | IM = im) \left| \frac{dv(IM)}{dIM} \right| dIM \quad (9.12)$$

From the properties of expectation we know that the expected value of the sum of random variables is equal to the sum of the expected value of each random variable (Benjamin and Cornell, 1970). Hence, the expected annual loss for the whole building resulting from direct physical damage is then computed as the sum of the expected losses in each individual component in the building, that is

$$E[L_{Bldg.}] = \sum_{j=1}^n E[L_j] = E[L_{j=1}] + E[L_{j=2}] + E[L_{j=3}] + \dots + E[L_{j=n}] \quad (9.13)$$

where n is the total number of components in the building.

Although the summation and integrals in Equations 9.12 and 9.13 can be solved in any order, certain sequences provide intermediate results that offer valuable information to the structural engineer, owner(s) and other parties interested in the seismic performance of the building.

For example, the expected value of loss in the j th component, given that it has been subjected to an engineering demand parameter of intensity equal to edp, can be computed as

$$E[L_j | EDP_j = edp] = \sum_{i=1}^m E[L_j | DM = dm_i] P(DM = dm_i | EDP_j = edp) \quad (9.14)$$

where $P(DM = dm_i | EDP_j = edp)$ is given by Equation 9.11. Then the variation (increase) of dollar loss in the j th component with changes (increase) in EDP can then be obtained by plotting EDP_j versus $E[L_j | EDP_j = edp]$. Similarly, the variation of dollar loss from drift-sensitive structural and non-structural components in the k th story of the building can be obtained by plotting EDP_k (drift in story k) versus $\sum E[L_j | EDP_j = edp]$ where p is the number of drift-sensitive components in the k th story of the building.

Another intermediate result that is of interest, particularly for components that contribute significantly to the total loss, is the expected value of the dollar loss in the j th component, given that the building has been subjected to a ground motion with intensity level im, which can be computed as

$$E[L_j | IM = im] = \int_0^\infty E[L_j | EDP_j = edp] dP(EDP_j > edp | IM = im) \quad (9.15)$$

The expected value of dollar loss in the building as a function of the level of ground motion intensity is computed as

$$E[L_{Bldg}|IM=im] = \sum_{j=1}^n E[L_j|IM=im] \quad (9.16)$$

A plot of IM versus $E[L_{Bldg}|IM=im]$ provides information on how the expected value of the loss in the building increases as the ground motion intensity increases. Once this variation is known, the expected annual loss in the building is calculated by integrating the expected value of the loss conditioned to the ground motion intensity over all possible ground motion intensities as follows:

$$E[L_{Bldg}] = \int_0^\infty E[L_{Bldg}|IM=im] dv(IM) \quad (9.17)$$

where $dv(IM)$ can be written as

$$dv(IM) = \left| \frac{dv(IM)}{dIM} \right| dIM \quad (9.18)$$

Substituting 9.18 into 9.17 we obtain

$$E[L_{Bldg}] = \int_0^\infty E[L_{Bldg}|IM=im] \left| \frac{dv(IM)}{dIM} \right| dIM \quad (9.19)$$

As mentioned before, more sophisticated stakeholders such as large corporate owners, mortgage institutions, insurers, reinsurers or other financial institutions, may be interested in estimating the losses that have small probabilities of exceedance or a whole loss curve that describes the mean annual frequency of exceedance of different losses in the building (Figure 9.31). In particular, the mean annual frequency of exceedance of a certain dollar loss l in the building can be computed as

$$P[L_{Bldg} > l] = \int_0^\infty P[L_{Bldg} > l | IM = im] \left| \frac{dv(IM)}{dIM} \right| dIM \quad (9.20)$$

where $P[L_{Bldg} > l | IM = im]$ is the probability of exceeding a certain dollar loss l in the building conditioned to a ground motion intensity measure level im . Based on the central limit theorem, the probability distribution of the sum of random variables will approach the normal distribution if the number of random variables in the sum is large and if their sum is not dominated by a few individual elements. In almost all buildings these conditions are satisfied, so $P[L_{Bldg} > l | IM = im]$ can be estimated by assuming it is normally distributed with its mean given by Equation 9.16 and its variance given by

$$\sigma^2[L_{Bldg} | IM = im] = \sum_{j=1}^n \sigma^2[L_j | IM = im] + 2 \sum_{j=1}^n \sum_{i=i+1}^n \rho_{i,j} \sigma[L_i | IM = im] \sigma[L_j | IM = im] \quad (9.21)$$

where $\sigma^2[L_j | IM = im]$ is the variance of the loss in the j th component conditioned to a ground motion intensity measure level im , $\rho_{i,j}$ is the correlation coefficient between the loss in the i th and j th components, and $\sigma[L_i | IM = im]$ and $\sigma[L_j | IM = im]$ are the standard deviations of the loss in the i th and j th components conditioned to an intensity measure level im , respectively.

There are other loss estimation methodologies that have proposed the estimation of economic losses by adding the losses in individual components. For example, Scholl and Evernden (1979) and Kustu et al. (1982, 1984) developed procedures for estimating economic losses in high-rise buildings and in urban areas. More recently, Porter et al. (2001) developed an assembly-based vulnerability assessment that also relies on the estimation of damage to individual components. In these approaches, loss estimation is based on Monte Carlo simulation. Hence a very large number of simulations is required. In the proposed approach the number of nonlinear response history analyses is much smaller since only the first two moments of the loss are required.

9.3.5.3 Illustration of Loss Estimation for Structural Components

Damage to practically all-structural elements is the result of structural deformations. One of the best parameters to characterize structural deformations during earthquakes is the interstory drift ratio. Hence, for estimating losses resulting from damage to structural components, a good choice of the relevant engineering demand parameter is the interstory drift ratio. Although the estimation of the probability of collapse may require only the estimation of the probability of exceedance of the maximum interstory drift ratio in the building, regardless of the location where this maximum occurs, in the case of loss estimation it is necessary to compute the probability of exceedance of a wide range of interstory drift ratios at every story in the building.

To estimate the damage in structural elements, a relationship between relevant EDPs and different levels of damage, referred to here as damage measures is required. A probabilistic mapping between a structural response parameter and the level of damage in a particular component may be referred to as a fragility function. In this context, fragility functions associate a relevant EDP with the probability of exceeding a certain level of damage. The best source of information for the development of fragility functions is experimental research in which damage levels (states) are documented as a function of the EDP that has the largest influence on the extent of damage (here the interstory drift ratio is used as EDP).

Some of the concepts of loss estimation method described in the previous section are illustrated here, using as an example the losses resulting from structural damage to the interior slab-to-column connections of a flat plate floor system of a seven-story reinforced concrete building representative of older construction in the United States. Four damage states associated with different repair actions are considered. The first damage state, referred to here as damage measure dm_1 , corresponds to initial cracking of sufficient intensity to be noticed, primarily in the top surface of the slab. Since this level of cracking does not represent a significant level of structural damage, the only action required is the patching and painting of the cracks. The second damage state, dm_2 , corresponds to significant cracking in the slab that requires epoxy injection. The third damage state, dm_3 , corresponds to a punching shear failure that produces a sudden drop in the lateral resistance of the connection. The necessary repair action consists in partial demolition and removal of damaged and loose concrete around the column with subsequent pouring of new concrete. The fourth damage state is associated with the loss of vertical load carrying capacity of the slab column connection, which can lead to a local or global collapse of the building.

Figure 9.32a shows an example of a fragility function of an interior slab-to-column connection corresponding to the first damage state. This fragility curve was developed using the results of 74 specimens tested in 15 experimental research projects (Aslani and Miranda, 2003). In this figure the abscissa represents the interstory drift ratio (IDR) at which the first damage state was reported, and the ordinate represents the cumulative probability distribution computed from the sorted data. Hence, the ordinate in a fragility function represents the conditional probability of experiencing or exceeding a damage state conditioned on a given level of EDP. Each dot in this figure represents a different specimen. The first damage state occurs at relatively small levels of deformation corresponding to interstory drift ratios ranging from about 0.2% to 0.8%. A lognormal distribution fit to the data is also shown in the figure. It can be seen that the probability of experiencing or exceeding this damage state can be estimated relatively well using a lognormal distribution.

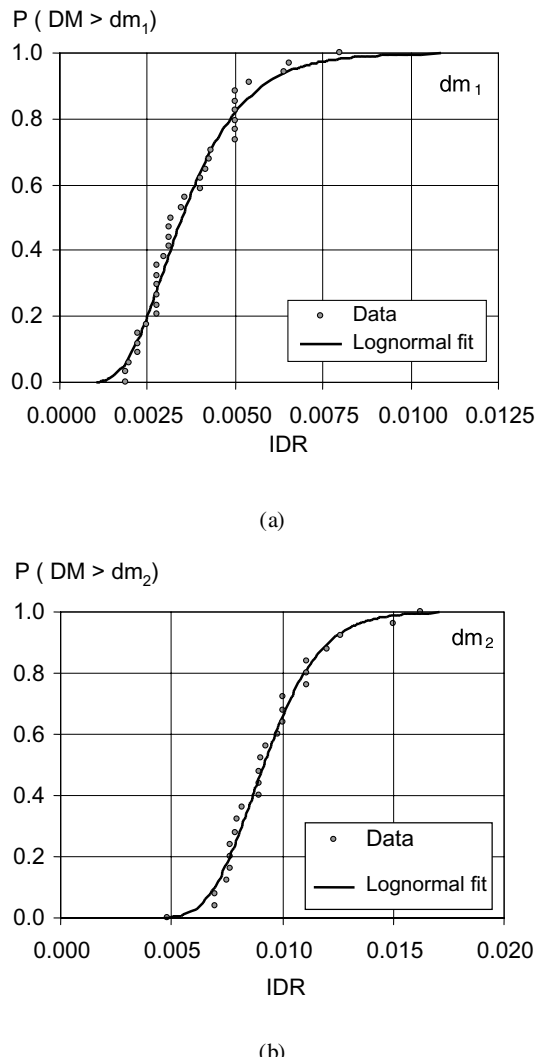


FIGURE 9.32 Fragility functions for damage measures dm_1 and dm_2 in interior reinforced concrete slab-to-column connections of flat plates.

Figure 9.32b shows the fragility curve for the second damage state (significant cracking) that is observed at interstory drift ratios ranging from 0.5% to 1.6%. Again, it can be seen that a lognormal fit leads to relatively good estimations of the probability of experiencing or exceeding the second damage state.

A fragility function associated with the third damage state (punching shear failure) is presented in Figure 9.33. It can be seen that a considerable scatter exists when the prediction of a punching failure is based only on the level of interstory drift ratio. For example, punching shear failures in some specimens are reported at interstory drift ratios as low as 0.6% whereas in other cases punching shear failure occurs at interstory drift ratios as high as 6.3%.

To improve the estimation of this damage state, advantage was taken of recent observations on the influence of gravity loads on the performance of slab-to-column connections (Moehle et al., 1988; Pan and Moehle, 1988; Robertson and Durrani, 1992, Hueste et al., 1999). According to these observations the drift at which a punching shear failure is observed in slab-to-column connections without shear reinforcement decreases significantly as the level of gravity load increases. Figure 9.34 shows the interstory drift at which a punching shear failure was observed in 74 slab–column specimens as a function of the

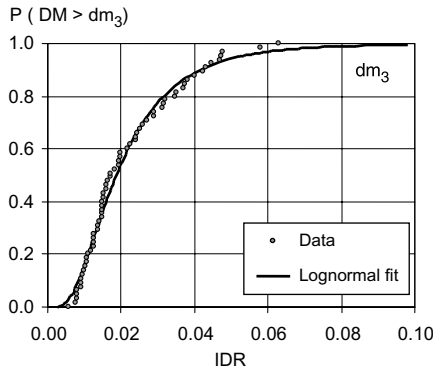


FIGURE 9.33 Fragility function for damage measure dm_3 in interior reinforced concrete slab–column connections of flat plates.

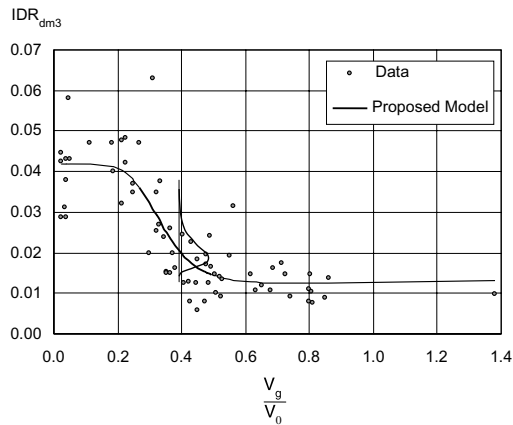


FIGURE 9.34 Interstory drift ratio at which punching shear failure was observed as a function of the gravity shear force ratio.

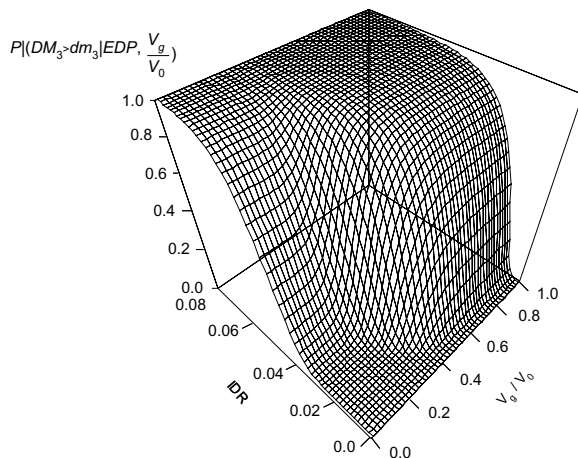


FIGURE 9.35 Probability of experiencing or exceeding a punching shear failure in an interior slab-to-column connection as a function of interstory drift ratio and gravity shear force ratio.

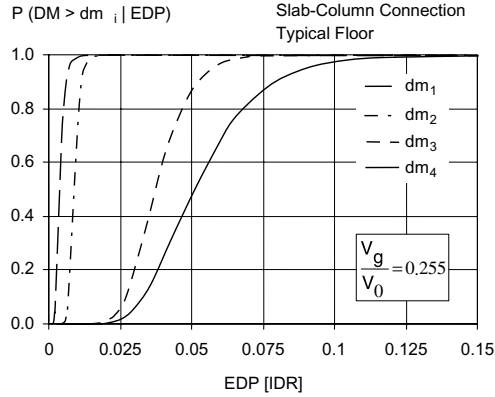


FIGURE 9.36 Fragility functions for four damage measures of slab-to-column connections representative of a flat plate in an existing seven-story reinforced concrete building.

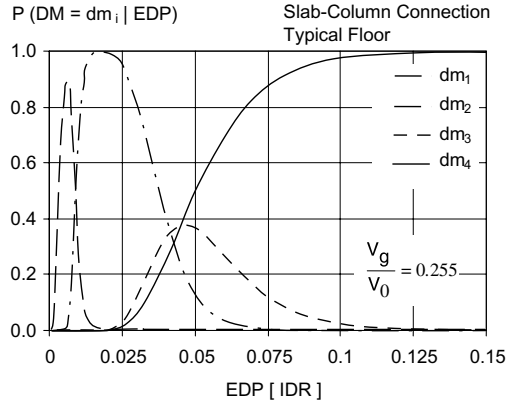


FIGURE 9.37 Probabilities of being in various damage states for an interior slab-to-column connection.

gravity shear force ratio, which is defined as the gravity shear force at the critical section, V_g , normalized by the nominal shear capacity at the same section, V_0 . The model proposed by Aslani and Miranda (2003) to describe the central tendency of the interstory drift ratio at which punching shear failure is expected as a function of the gravity shear force ratio is also shown in the figure. Hence, a significant reduction in scatter can be obtained if the probability of experiencing a punching shear failure is computed not only as a function of the level of imposed peak interstory drift ratio but also as a function of the gravity shear force ratio. As shown in Figure 9.35 this results in a fragility surface rather than a single fragility curve. From this figure it can be seen that the probability of experiencing a punching shear failure increases as the interstory drift ratio and the gravity load ratio increase.

Figure 9.36 shows the fragility functions corresponding to the four damage states for slab-to-column connections with a gravity shear force ratio representative of that in typical floors of the example seven-story reinforced concrete building, whereas Figure 9.37 shows the probability of being in each of the four damage states computed with Equation 9.11 and with the fragility functions shown in Figure 9.36.

Information of the type shown in Figure 9.37 permits the estimation of physical damage to structural elements. However, additional information is needed to estimate the economic losses associated with this physical damage that may occur in individual slab–column connections. In particular, functions describing the repair costs associated with each of the damage states are needed. Examples of loss functions corresponding to the first three damage states in the slab-to-column connections are shown in Figure 9.38. In this figure, the losses are normalized by the mean cost of constructing a new slab–column

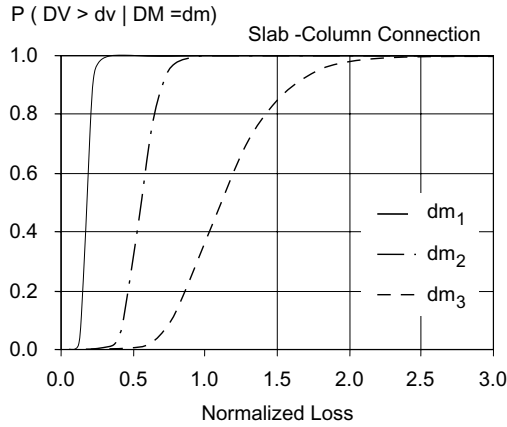


FIGURE 9.38 Probabilities of exceeding a normalized loss in slab-to-column connections conditioned on being in a certain damage state.

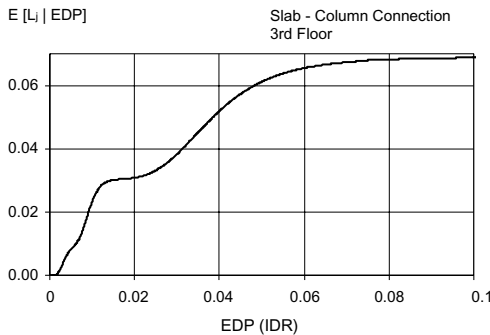


FIGURE 9.39 Variation of expected normalized building loss due to damage in slab-to-column connections as the interstory drift ratio increases.

connection. From this figure it can be seen that the cost associated with repairing a punching shear failure has a relatively high probability of costing more than building a new slab–column connection. This is the result of temporary shoring, demolition and complicated local concrete pours that are required as opposed to construction operations that are required when these elements are being built in a new building.

The variation of the expected value of the normalized building loss due to damage in slab-to-column connection in the third story of the building with changes in EDP (interstory drift), computed by combining the results from Figures 9.37 and 9.38 and using Equation 9.14, is shown in Figure 9.39. An important increase in mean loss is observed with changes in interstory drifts from 0.005 to approximately 0.012, which is produced by significant cracking around the column at these levels of deformation (damage states dm_1 and dm_2).

Figure 9.40 shows the increase in the expected loss in the building produced by damage to slab–column connections as the ground motion intensity increases, which is computed from Equations 9.15 and 9.16. The losses are normalized by the replacement cost of the building and the spectral displacement at the fundamental period of the building ($T_1 = 1.5$ sec) is used as the ground motion intensity measure. The losses corresponding to mean plus or minus one standard deviation are also shown in the figure. It can be seen that considerable uncertainty exists in the estimation of dollar losses for a given ground motion intensity. For example, an elastic spectral displacement of 20 cm damage to slab–column connections

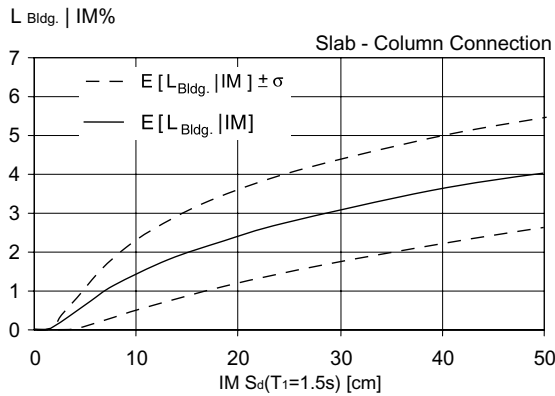


FIGURE 9.40 Variation of normalized losses in the building due to damage to slab-to-column connections as a function of the ground motion intensity.

could result in losses of 1.2% of the cost of the building, but for the same ground motion intensity they could also be three times this value.

9.3.5.4 Illustration of Loss Estimation for Nonstructural Components

In most buildings, damage to nonstructural components is the biggest contributor to direct economic losses resulting from earthquakes. Their large contribution to economic losses stems primarily from two reasons. The first is that nonstructural components (architectural, mechanical, etc.) represent a large percentage of the total construction cost of buildings. For example, in the case of commercial buildings, nonstructural components typically account for 65 to 85% of the total cost of the building. Hence, there is far more investment at risk in these components than in structural components. The second reason is that damage to many types of building nonstructural components is usually triggered at levels of deformation much smaller than those required to initiate structural damage.

Some of the loss estimation concepts described earlier are illustrated here by considering losses due to damage to interior partitions in a seven-story reinforced concrete building. Figure 9.41 shows the fragility curves associated with three damage states for drywall partitions made of gypsum board and metal frames. The first damage state corresponds to cracking of the partition caused by tensile stresses in the gypsum board. The repair action for this damage state consists of pasting, taping, repasting and sanding over all cracks and subsequent repainting of all the partition. The second damage state corresponds to extensive cracking and crushing of the gypsum board. The repair action for the second damage state consists of removing the damaged gypsum boards, replacing them with new boards and subsequently pasting, taping, repasting, sanding over the joints of two gypsum boards and then repainting the partitions. Dots in Figure 9.41 correspond to the results of racking tests conducted in partitions subjected to different levels of interstory drift ratio.

The continuous lines in Figure 9.41 represent fragility functions that have been developed using the results from experimental research and assuming a lognormal distribution. It can be seen that the first damage state can occur at very small levels of deformation. In experimental studies the first damage state was reported in 10% of the specimens at interstory drifts smaller than 0.1% and in approximately 80% of the specimens at interstory drift ratios smaller than 0.5%. These results have very important practical implications since this means that if damage to partitions is to be avoided lateral drifts need to be controlled to very small values, which in many cases will require considerable lateral stiffness in the structure.

The third damage state corresponds to severe damage occurring not only in the gypsum boards but also in the framing. Although some experimental results exist for this damage state for partitions with wood frames, practically no experimental data exist for drywall partitions with metal frames. Hence this

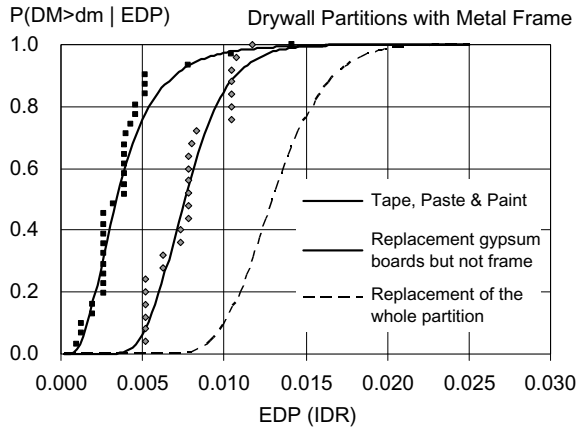


FIGURE 9.41 Fragility functions for three damage states of drywall partitions with metal frames.

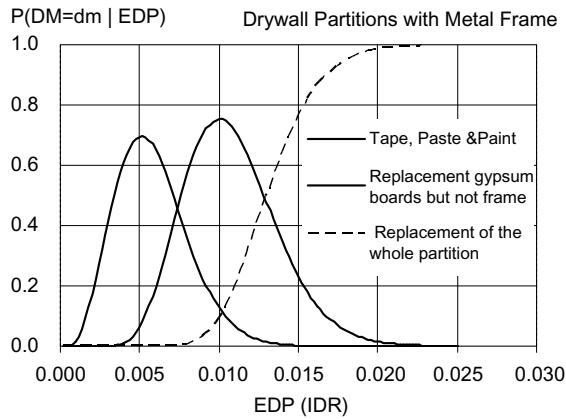


FIGURE 9.42 Probabilities of being in one of the three defined damage states in drywall partitions with metal frames.

third fragility function is shown in Figure 9.41 with a dotted line to indicate that it is not based on experimental results.

Figure 9.42 shows the probability of being in each of these three damage states computed with Equation 9.11 and with the three fragility functions shown in Figure 9.41. It can be seen that according to the available racking tests, drywall partitions that are subjected to interstory drift ratios of 1% have a high probability (approximately 85%) of experiencing considerable damage to the gypsum boards. Similarly, drywall partitions that are subjected to interstory drift ratios of 2% will most likely have to be replaced.

Loss functions for the three previously described damage states in drywall partitions are shown in Figure 9.43. Losses are normalized by the mean cost of installing a new partition. It can be seen that repair costs associated with the first damage state (minor cracking) vary between 20% and 50% of the mean cost of installing a new partition. Repair actions associated with the second damage state, which consist of removing damaged gypsum boards, replacing them with new ones with subsequent pasting, and taping and repainting of the partition can cost anywhere from 40% to 130% of the cost of installing a new partition. Completely removing damage partitions and replacing them with new ones have costs that vary from 70% to 190% of the mean cost of installing a new partition. In most cases the costs associated with the third damage state are larger than the average cost of installing a new partition because

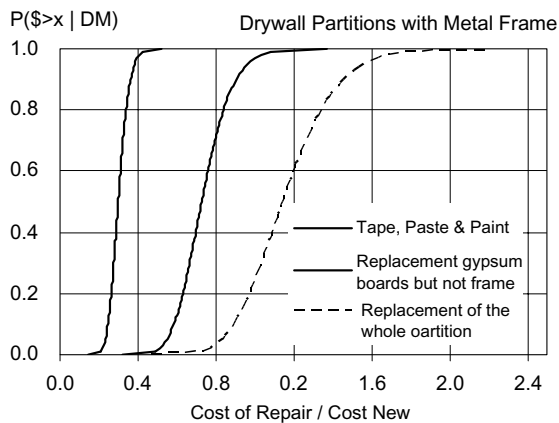


FIGURE 9.43 Loss functions for three damage states in drywall partitions with metal frames.

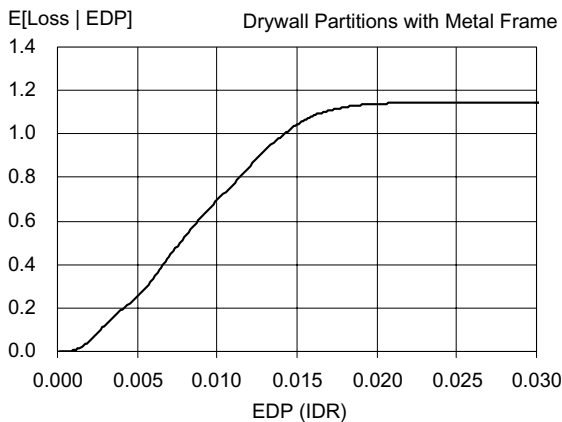


FIGURE 9.44 Variation of expected loss in partition walls as the interstory drift ratio increases.

of the need to first remove the damaged partitions and because of smaller productivity rates in repairs than in new construction.

As mentioned previously, although expected annual losses or loss curves for the building can be computed from Equations 9.19 and 9.20, selected intermediate results also provide valuable information. An example of intermediate results is illustrated in Figure 9.44, which shows the expected value of the loss in interior drywall partitions as a function of the peak interstory drift ratio. It can be seen that mean losses in the order of 70% of the mean cost of installing new partitions is produced at interstory drift ratios of 0.01, and that mean losses approximately equal to the mean cost of installing new partitions are produced at interstory drift ratios of approximately 0.015. Intermediate results such as those shown in Figure 9.44 can be combined with the information on the probability of exceedance of a given interstory drift ratio conditioned on the ground motion intensity, using Equation 9.15, to obtain the variation of the loss in one or more components as a function of the level of ground motion intensity. An example of the variation of normalized losses for the interior partitions installed in the third story of a seven-story reinforced concrete building as a function of the ground motion intensity is shown in Figure 9.45. The ground motion intensity measure is again represented by the linear elastic spectral displacement at the fundamental period of vibration of the structure. It can be seen that the combination of the uncertainty in structural response (EDP) for a given ground motion intensity measure, the uncertainty in

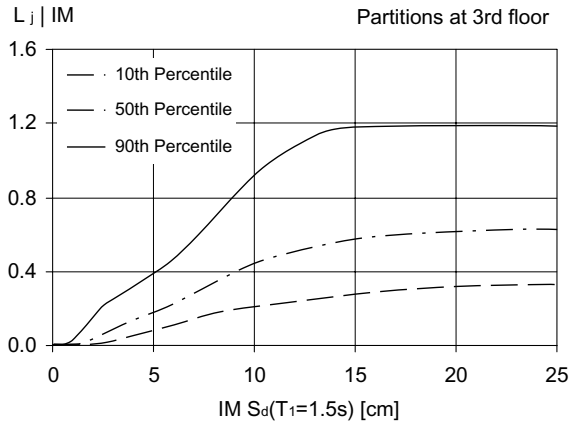


FIGURE 9.45 Variation of normalized losses in interior partition walls in the third story as a function of the level of ground motion intensity.

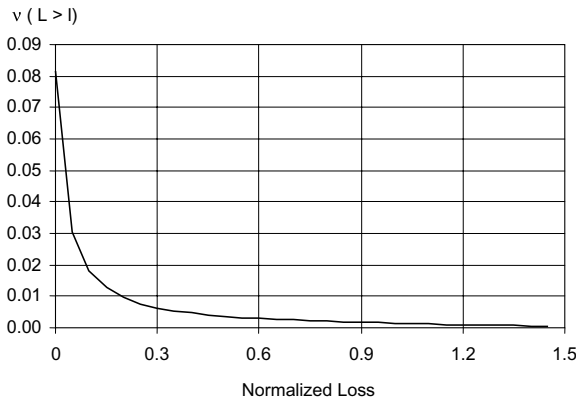


FIGURE 9.46 Normalized loss curve computed for a seven-story reinforced concrete building.

damage for a given structural response and the uncertainty in dollar loss for a given damage state, result in a very large uncertainty in the estimation of economic losses to individual components. For example for a spectral displacement of 10 cm the economic loss in the partitions in the third floor of the structure could vary from less than 20% of the cost of the partitions to practically the total cost of the partitions.

Once losses for individual components have been computed as a function of the intensity measure, the probability of exceeding a certain dollar loss can be computed using Equation 9.20. Figure 9.46 presents a rough estimate of the loss curve computed for the seven-story reinforced concrete building. In this figure the losses are normalized by the total cost of the building. It can be, because for this building, losses corresponding to 10% of the cost of the building have a mean annual frequency of occurrence of approximately 0.02, which means that this level of losses would occur on average every 50 years. Similarly, the probability of experiencing a loss of 50% of the total cost of the structure is approximately 0.003, which is equivalent to saying that the return period of a loss of 50% of the building is approximately 330 years. If the owner judges the probabilities of facing these losses to be too high, he could decide to upgrade the structure to reduce potential losses or decide to transfer the risk by means of earthquake insurance.

9.3.5.5 Concluding Remarks

Measuring seismic performance through economic losses offers significant improvements over currently employed methods that are based on discrete performance levels. In particular, economic losses provide

a continuous and quantitative measure of seismic performance, which can provide the basis for more rational decision making by owners, insurers, lending institutions and other project stakeholders as part of their risk management strategies. The proposed methodology permits the generation of various measures of economic losses that may be appropriate for different purposes or stakeholders. For some stakeholders the expected annual loss may provide sufficient information to base their decisions on whereas other more sophisticated owners may prefer estimates of the probable maximum loss or loss curves. Although the estimation of losses as the sum of losses to individual components is a promising approach, it is recognized that fragility functions have been developed only for a small number of components. A large amount of work is needed in this area before this procedure can be fully implemented. Similarly, while correlation between various response parameters can be obtained from nonlinear response history analyses, information on correlation between losses in different components is very limited. Nevertheless, at present this approach appears to be the most promising one as it provides a framework in which uncertainties in the various parts of the process can be clearly identified and their effect propagated and evaluated.

9.3.6 Downtime and Business Losses

The issue of downtime is perhaps the most important one, and probably the least understood and quantifiable one, in the context of seismic risk management for individual, institutional and corporate owners. The loss of direct income due to downtime, which may be represented by a loss of rent or loss of revenue producing activity (e.g., services or manufacturing) or other business interruptions, and the loss of indirect income, which may be represented by the inability to provide chain-based support services or the inability to fulfill a mission (e.g., teaching and research at a university), often outweighs by far the costs of repairing structural or nonstructural components.

Porter et al. (2001) have made attempts to quantify repair time, which is not necessarily synonymous with downtime. In this work, damage states are combined with repair-duration probability distributions to estimate assembly repair durations. Repair durations are used together with Gantt charts to estimate overall system repair duration.

The basic difficulties in quantifying length of downtime are on account of great uncertainties associated with the availability of labor, materials and capital following a major seismic event, and difficulties relating quantifiable damage and the needs for repair with loss of function and the need for complete, partial or no closure of a facility. Looking ahead, quantification of downtime should be a very fruitful research area for years to come.

Even if downtime could be quantified with confidence, the associated losses will be highly uncertain and strongly case and scenario specific. Estimation of downtime losses is and will remain perhaps the biggest challenge of seismic performance assessment and risk management. Some of the basic issues are identified and discussed in a report that was the outcome of a FEMA project on the benefits of a disaster resistant university (Comerio, 2000). The following paragraphs are paraphrased from this report.

The referenced FEMA study was concerned with assessing the effects of three earthquake scenarios on the campus of the University of California at Berkeley. The three scenarios correspond to return periods of 72, 475 and 975 years (50/50, 10/50, 5/50 hazards), and are referred to as the occasional, rare and very rare earthquake, respectively. The following assessment was made in Comerio (2000) of the earthquake effects associated with downtime or loss of function:

In the immediate aftermath of seismic activity, the principal economic outputs of the university — the educational services provided to students and the research products produced by faculty, staff, and students — are disrupted for a considerable period. Students who would have matriculated are denied the opportunity to graduate, or at the very least, the completion of their education is delayed along with their entrance into the labor market. Scientific research, which would have been completed is lost, or at least delayed. Public service, which would have been provided by faculty and staff, is not undertaken.

The disruption to the educational process has a multiplier effect upon the local economy, as the capital flow provided by the university is eliminated, or at least muted, for some time. In the longer run, the disruption of the routine caused by a major earthquake could lead to a permanent contraction of scholarly research at the university. Activities currently undertaken could move to other universities and other regions, permanently reducing the output of this university. Worse still, some of these productive activities might be eliminated altogether as the physical conditions facilitating scholarly and scientific collaboration are destroyed.

Finally, the role of the university in attracting productive talent to the region and in increasing the supply of human capital and trained graduates in California could be affected as a result of a major earthquake. This could have, perhaps, the most serious consequences for economic welfare in the state.

Specific assessments were made of the short- and long-term impacts of losses on research, the local economy and on human capital. In regard to the aggregate loss in research output, the following results are quoted.

Under the Occasional scenario, it is estimated that \$25.4 million in research output is disrupted (out of some \$355 million per year, which is produced). Under the Rare scenario, the research disruption is estimated to be \$87 million, while under the Very Rare scenario it is estimated to be \$121.8 million.

In regard to losses to the local economy, Comerio (2000) estimates that the university typically contributes \$1.23 billion to the Bay Area economy each year and produces more than 20,000 jobs. The report states that

... the aggregate losses to the local economy are quite large indeed, annually peaking at \$15.4 million, \$147.9 million, and \$860.8 million in reduced gross sales under the three scenarios. In the event of a Very Rare earthquake, the only economic scenario in which a year-long campus closure was considered, the first year losses in three counties include approximately 8,900 jobs, \$680 million in personal income, and \$861 million in sales. For completeness, we also estimated the net stimulus provided by the rebuilding of campus facilities. Although the losses would be offset in the larger economy by the increase in construction jobs generated, it is important to note that the losses and gains reside in very different sectors of the economy.

Regarding loss to human capital, it is stated in Comerio (2000) that

We can only speculate about some of the other economic effects of these earthquake scenarios on the larger economy of the region and the state... The University plays a powerful role in augmenting human capital in the state by attracting talented young men and women from other states — indeed, from throughout the world — who then settle in the state... The loss of the University, its research facilities, and its educational facilities, threaten the capacity to import talented human capital from elsewhere... Overall, the economic analysis suggests that when a university is located in a large metropolitan area with a complex and dynamic economy, the impact from an institutional closure is not entirely represented by the immediate loss of jobs and local sales. Much more important is the university's contribution of highly trained professional workers to the regional economy. If the University of California, Berkeley were forced to close, the interruption of that supply of professionals would have a dramatic impact on the region.

We agree with the assessment made in the last sentence. It demonstrates the importance of intangibles in economic impact assessment, and it also demonstrates that seismic performance assessment, as part of risk management, is a multi-disciplinary process that must incorporate socio-economic considerations as much as engineering and seismology considerations.

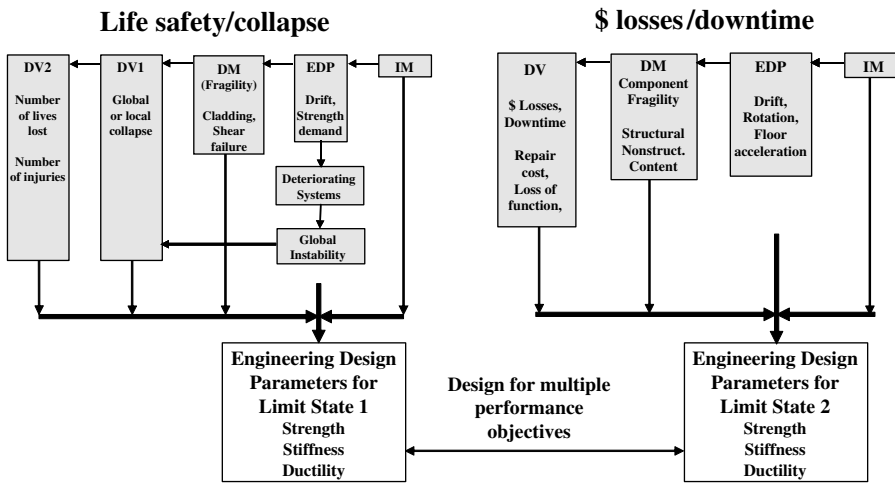


FIGURE 9.47 Performance assessment versus performance-based design.

9.4 Performance-Based Design

Section 9.3 has focused on performance assessment. Assessment implies that the structural, nonstructural and content systems are given (they have been designed already), and that for the given systems DVs (decision variables) are determined whose values should fulfill specified performance targets. For life safety and collapse performance, the process of determining DVs is illustrated in the upper portion of the left half of Figure 9.47, with the information flowing from right to left, as indicated by the light horizontal arrow lines and as summarized here: IMs are determined from hazard analysis; relevant EDPs are predicted from structural analysis for given IMs (and ground motion records); local collapse fragility curves (e.g., for panels of cladding that may drop due to fracture of cladding-to-frame connections, or for floor slabs that may drop because of shear failure at column-to-slab connections — see the curve for dm_4 in Figure 9.36) and global collapse fragility curves of the type shown in Figure 9.30 are used to predict local and global collapse probabilities; and as a last (and not yet fully resolved) step, predictions are made of the number of lives lost and the number of injuries. Similarly, for performance associated with losses and downtime, the process of determining DVs is illustrated in the upper portion of the right half of Figure 9.47, again with the information flowing from right to left.

Design is different from performance assessment, simply by virtue of the fact that the building and its components and systems first have to be created. One can view design as an iterative assessment process that starts with a judgmental conceptual design for which performance assessment is carried out and the design is improved (tuned) in successive iterations until the performance targets are met. This design process is an option, but not a very attractive one. A poor initial conceptual design may be tuned to an extent that it fulfills the performance targets, but it most likely will never become a good design (it is unlikely that a violin with a bad body can ever be tuned to sound like a Stradivarius). Good designs are based on concepts that incorporate performance targets up front in the conceptual design process, so that subsequent performance assessment becomes more of a verification process of an efficient design rather than a design improvement process that may require radical changes of the initial design concept.

We must confess that ways to explicitly design for the continuous DV that control performance and are computed from Equation 9.2 do not exist at this time (and likely will never exist). Thus, it will be necessary to base conceptual design on discrete limit states associated with discrete hazard levels — similar to the way it is practiced in most of the performance-based guidelines summarized in Section 9.2.2. In the conceptual design phase, engineers are used (and likely will be so for many years to come)

to select and rough-proportion structural systems for strength, stiffness (drift limitations), ductility and perhaps energy dissipation and floor accelerations. The art of engineering, which should be practiced in this phase, is to use global information for important limit states to come up with a structural system that fulfills specified performance objectives in the most effective manner. This implies exploration of alternatives, which may be utilizing different structural materials and systems or more advanced technologies such as base isolation or internal energy dissipation devices.

The challenge is to provide the designers (structural, architectural, mechanical) with a small set of most relevant criteria on important EDPs on which good conceptual design can be based. In concept, this means reversing the information flow discussed before for performance assessment, and working toward quantification of relevant EDPs, given that desired performance can be expressed in terms of tolerable DV values at discrete performance levels. This reversal of information flow is indicated in Figure 9.47 with vertical arrow lines that flow into two horizontal arrow lines and merge at the EDP level, which then contains limit values of relevant EDPs (strength, stiffness, ductility, floor acceleration, etc.) that drive design decisions. Which of the EDPs become primary design targets, depends on the building use, as in a hospital with much life-critical equipment (usually acceleration sensitive) the focus will be on different EDPs than in a hotel where performance objectives are driven by a trade-off between losses and income. It is hoped that the collapse and loss estimation studies that are presently being performed, will provide quantitative data for relevant EDPs, given acceptable losses or a tolerable number of casualties at hazard levels that have the largest impact on losses or downtime and life safety or collapse performance.

Given EDP limits and associated IM hazards for various performance levels, such as the two illustrated in Figure 9.47, conceptual design for multiple performance objectives can be performed. Different performance levels and goals will require different design criteria to be applied to different design parameters. In general, performance should be concerned with structural and nonstructural systems as well as building contents, and with various levels of behavior, ranging from cosmetic damage to partial or complete collapse. There is no single design parameter that will control all performance goals at all performance levels. For instance, structural damage threshold likely is controlled by element strength capacities, but strength demands are greatly affected by element deformations that make up the structure stiffness, which in turn controls the inertia forces generated in the structure. Nonstructural damage is controlled mostly by interstory drift limitations, which demand large stiffness. Content damage, on the other hand, is often proportional to floor accelerations, which can be limited by reducing the stiffness and strength of the structure. At the other extreme, life safety and collapse prevention are controlled by the inelastic deformation and energy dissipation capacities of ductile elements and the strength capacity of brittle ones.

This discussion indicates that different performance objectives may impose conflicting demands on strength and stiffness, and that seismic design is likely to become an iterative process in which different performance criteria may lead to a trade-off between strength and stiffness requirements, but in which no compromises can be made on issues of life safety and collapse prevention. This iterative process can be accomplished in two phases; a conceptual design phase in which one or more effective structural systems are configured and rough sized, and a performance assessment phase in which performance of the structural, nonstructural and content systems is evaluated as discussed in the previous sections, and final design decisions and modifications are made.

Two challenges need to be addressed in the context of performance-based conceptual design. One is to develop data on EDP limits associated with specific levels of performance. This implies exploitation of DM–DV relationships and back-figuring of EDPs that provide adequate performance (acceptable values of DVs). Once such EDP limits have been established, together with IMs that represent discrete hazard levels for which the EDP limits apply, the challenge is to devise structural systems that efficiently accommodate these EDP limits. Following are three examples of design aids that can be utilized for this purpose. All examples are concerned with frame structures, for which much statistical information on EDPs has been developed (Medina, 2002).

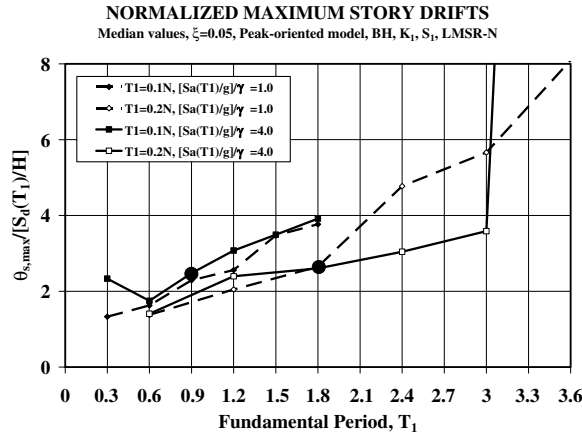


FIGURE 9.48 Median values of normalized maximum story drift for frame structures with $T_1 = 0.1N$ and $T_1 = 0.2N$ (Medina, R.A., Ph.D. Dissertation, Stanford University, 2002. With permission.)

9.4.1 Example of Design for Global Stiffness

A ten-story structure (each story is 3.6-m high) is to be designed in a highly seismic region. A performance criterion could be that the maximum story drift angle at the 2/50 hazard level should not exceed 0.03. The 2/50 earthquake hazard is described by an acceleration spectrum defined by 1.0 g/T in the vicinity of the first mode period. An estimate is needed of the largest acceptable first mode period, T, from which global stiffness criteria can be derived.

A relationship between maximum story drift and T can be obtained from either Figure 9.48 or the following equation

$$\theta_{s,ST,\max} = \alpha_{MDOF} \times \alpha_{INEL} \times \alpha_{P\Delta} \times \alpha_{ST} \left(\frac{S_d}{H} \right) \quad (9.22)$$

In this equation, which is proposed in Gupta and Krawinkler (2000) for steel moment frame structures, the α terms account, in sequence, for transformation from the SDOF spectral displacement S_d to the roof displacement of the MDOF system, for inelasticity effects on the MDOF roof displacement, for P-D effects and for transformation from MDOF roof drift angle to maximum story drift angle. For a mid-rise steel building, these values are estimated as follows (Gupta and Krawinkler, 2000): $\alpha_{MDOF} = 1.1PF_1 = 1.1 \times 1.4$, $\alpha_{INEL} = 0.75$, $\alpha_{P\Delta} = 1.1$ and $\alpha_{ST} = 2.0$ (PF_1 is the first mode participation factor). With these values the maximum story drift, $\theta_{s,\max}$, is estimated as

$$\theta_{s,\max} = 1.54 \times 0.75 \times 1.1 \times 2 \left(\frac{S_d}{H} \right) = 2.5 \left[\left(\frac{T}{2\pi} \right)^2 \left(\frac{9.81}{T} \right) \left(\frac{1}{10 \times 3.6} \right) \right] = 0.0175 T \quad (9.23)$$

and the performance requirement $\theta_{s,\max} \leq 0.0175T \leq 0.03$ leads to the constraint that the first mode period should not exceed 1.7 sec. This provides guidance for the minimum required global stiffness.

The coefficient 2.5 in Equation 9.23 was confirmed, approximately, in an unrelated study in which the ratio $\theta_{s,\max}/[S_d/H]$ was obtained for various frame structures from statistical response evaluation using forty different ground motions (Medina, 2002). Median values of $\theta_{s,\max}/[S_d/H]$ for frames with various number of stories and with $T_1 = 0.1N$ and $0.2N$ are shown in Figure 9.48 for essentially elastic systems, i.e., for $[S_a(T_1)/g]/\gamma = 1.0$, and for inelastic systems $([S_a(T_1)/g]/\gamma = 4.0)$. The median values for nine-story inelastic frames with $T_1 = 0.1N$ and $0.2N$ are indicated with large solid dots. For both periods the median $\theta_{s,\max}/[S_d/H]$ is on the order of 2.5, lending credibility to the estimate provided by Equation 9.23.

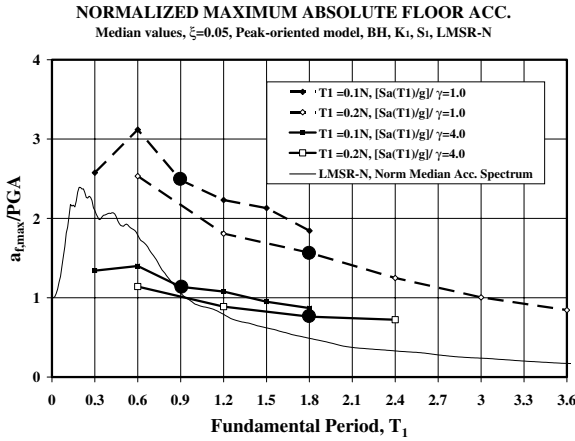


FIGURE 9.49 Median values of normalized maximum floor acceleration for frame structures with $T_1 = 0.1N$ and $T_1 = 0.2N$. (Medina, R.A., Ph.D. Dissertation, Stanford University, 2002. With permission.)

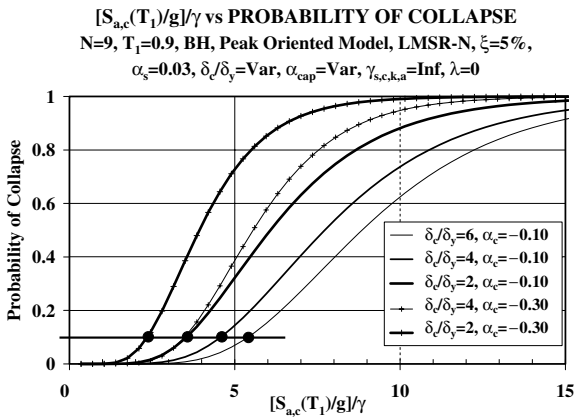


FIGURE 9.50 Collapse fragility curves for nine-story frames with $T_1 = 0.9$ sec; beams with various deterioration properties.

9.4.2 Design for Maximum Floor Acceleration

For protection of contents, maximum floor accelerations become an important EDP. Median data on maximum floor accelerations for the same frames for which Figure 9.48 applies are shown in Figure 9.49. For a nine-story frame structure, the beneficial effect of increasing the flexibility (period) of the frame ($T_1 = 0.2N = 1.8$ sec versus $0.1N = 0.9$ sec) or increasing the extent of inelastic response ($[S_a(T_1)/g]/\gamma = 4.0$ versus 1.0) can be judged from the circled points. The figure also shows that spectral acceleration (as represented by the presented median spectrum) is not a good measure of maximum floor acceleration. Graphs of this type provide information that can be used for floor acceleration control and to assist in the judgment on selecting either a conventional structural system or a system in which floor accelerations are controlled by either passive (base isolation or internal damping) or active control mechanisms. For a more complete discussion on intensity measures that can be used to predict floor acceleration demands the reader is referred to Taghavi and Miranda (2003).

9.4.3 Design for Collapse Safety

Providing collapse safety implies adherence to capacity design concepts, and it also implies design for ductility. The latter is implicitly considered in present design approaches with the judgmental response modification (R) factor or behavior (q) factor. These factors are tied to component detailing (ductility) requirements, and in the design process they are used to reduce the strength design level to a fraction of the value associated with the spectral acceleration at the first mode period. The implicit assumption is that there is a well-established correlation between these factors and the ductility capacity of the structural system. Reality is that this correlation is mostly judgmental and is awaiting quantification.

Data of the type presented in Figure 9.50 should help to achieve such a quantification. The figure shows collapse fragility curves for a nine-story frame structure whose beams have different ductility and deterioration characteristics (it is assumed that the strong column–weak girder concept is adhered to and plastic hinging occurs only at beam ends). The presented results are for components without cyclic deterioration ($\gamma_{s,c,k,a} = \infty$) and with various δ_c/δ_y ratios and α_c values, using the definitions shown in Figure 9.22). For instance, if for a very rare seismic hazard (e.g., 2/50 hazard) a probability of collapse of 0.1 can be tolerated, then the intersections of the horizontal line at $P_c = 0.1$ with the fragility curves provide information on the $[S_a(T_1)/g]/\gamma$ values that should be used for strength design of systems whose components have the indicated ductility and deterioration characteristics (since $[S_a(T_1)/g]/\gamma$, with $\gamma = V_y/W$, is equivalent to the behavior factor q, or the R-factor for systems without any overstrength).

This discussion points out several issues that require careful consideration in performance-based design, PBD. It is postulated that PBD should consist of conceptualizing one or more efficient structural systems to be followed by rigorous performance assessment. The conceptualizing of efficient systems could be based on EDP limits for specific hazard levels and could take advantage of design aids of the type illustrated in Figures 9.48 to 9.50.

9.5 A Glance Toward the Future

Few things are clear about performance-based earthquake engineering except that it will change the way structures will be designed and evaluated, and that much research and development is needed before it can be implemented in a consistent fashion. On the research front there are still many challenges to be addressed, including (but not limited to) the following:

- Develop a consensus on the best way of representing the seismic hazard at the site, by using either “conventional” IMs (e.g., spectral acceleration at the fundamental period), or improved and more complex IMs (capable of better representing the M and R dependences of ground motions, including near-fault effects), or circumventing IMs altogether and describing seismic hazard by seismic source models and ground motion simulations.
- Develop consistent procedures to propagate ground motions from a well-defined site reference location (e.g., bedrock below site) through the site soil medium and into the structure, considering all important effects of soil–foundation–structure interaction.
- Improve analytical models for an efficient and comprehensive prediction of EDPs, DMs and DVs, particularly in the presence of complex structural deterioration modes, such as those created by the interaction of large axial forces, shear forces and bending moments in reinforced concrete columns and walls.
- Develop a consistent process for identifying and quantifying damage states and associated repair costs for important structural, nonstructural and content components and systems.
- Develop processes that will permit a consistent evaluation of length of downtime and associated consequences to owners and society.
- Develop comprehensive procedures for identifying, quantifying and propagating all important uncertainties that will significantly affect the decision variables(s) on which performance assessment is based.

- Establish criteria and formats for comprehensive databases needed for many aspects of the PBEE evaluation process (e.g., for ground motions, experimental data, fragility curves, cost functions, etc.). We have to realize that performance prediction can only be as good (or bad) as is permitted by the data on which it is based. At present, a number of such databases exist, but most of them are extremely thin on data. Filling the databases will be a monumental effort that will require the cooperation of all segments of earthquake engineering, construction and financial communities.

But research in itself will not bring about wide acceptance of PBEE. Without extensive educational efforts, PBEE will not become a feasible alternative to presently employed procedures. In the United States, large legal obstacles also need to be overcome. On one hand it will be necessary to protect designers and builders from excessive exposure to legal actions, and on the other it will be necessary to protect owners and society from inadequate design and construction. Excessive complexity is another obstacle that needs to be overcome. An overriding consideration is that the PBEE methodology should be based on transparent physical concepts that must not make the design process overly complex.

Lastly, PBEE has an uncertain future unless it becomes an attractive process for all stakeholders. In addition to AEC practitioners, stakeholders include, among others, planners, building officials, facility managers, owners, lenders, insurers, reinsurers, insurance commissioners, catastrophe modelers, utility owners and operators and emergency response managers. Identification and involvement of all stakeholder groups in all phases of research, development and implementation of PBEE are critical.

Acknowledgments

The concepts summarized in Sections 9.3 to 9.5 have been the result of extensive studies performed at several universities associated with the PEER Center. This national research center is directed by Professor Jack Moehle, and the research activities are coordinated by the center's associate director Professor Greg Deierlein. The fruitful collaboration with these individuals and many other colleagues at the PEER affiliated universities, and the financial support provided by the PEER Center are much appreciated. Special thanks go to our colleague Professor Allin Cornell, who always has been a most helpful, productive and inspiring source of wisdom in the many stimulating discussions that took place over the years at Stanford's Blume Earthquake Engineering Center. Last but certainly not least, many thanks go to the Ph.D. students and recent Ph.D. graduates who have done most of the work presented in this chapter. These individuals include Dr. Ricardo Medina, Dr. Luis Ibarra-Olivas, Farzin Zareian, Hesameddin Aslani and Shahram Taghavi.

Glossary

ATC — Applied Technology Council

C_d-factor — deflection amplification factor

DM — Damage Measure, a variable used to quantify damage

downtime — the time span after an earthquake in which a facility is incapable, fully or partially, to fulfill its function

DV — decision variable, a variable used to make decisions on acceptable risk

EDP — engineering demand parameter

EPA — effective peak acceleration

expected annual loss — the economic loss that, on average, occurs every year

FEMA — Federal Emergency Management Agency

fragility function — a function expressing the probability of being in or exceeding a specific damage state

IDA — incremental dynamic analysis, a nonlinear analysis in which the ground motion intensity is incrementally increased

IM — intensity measure, a variable used to quantify the intensity of the ground motion

LMSR — large magnitude short distance set of ground motions

- MAF** — mean annual frequency
MDOF system — multi-degree of freedom system
NEHRP — National Earthquake Hazard Reduction Program
PBD — performance-based design
PBEE — performance-based earthquake engineering
performance level — a level of desired and quantifiable performance
performance objective — expression of a desired performance level for a given level of earthquake ground motion
PML — probable maximum loss
pushover analysis — nonlinear static analysis in which the lateral loads (displacements) are incremented
R-factor — response modification factor
SEAOC — Structural Engineers Association of California
SDOF system — single-degree of freedom system
target displacement — the predicted lateral displacement at which component force and deformation demands are evaluated in a pushover analysis

List of Symbols

$E[L_{Bldg}]$	expected annual loss in a building
F_y	yield strength of an SDOF system
H	height of structure
k_0	coefficient of IM hazard curve
k	exponent of IM hazard curve
K_e	elastic stiffness
K_s	strain hardening stiffness
K_c	post capping stiffness
N	number of stories
PF_1	first mode participation factor
$S_a(T_1)$	spectral acceleration at first mode period
$[S_a(T_1)/g]/\gamma$	relative intensity
S_d	spectral displacement
T, T_1	fundamental period of a structure
T_p	pulse period contained in near-fault ground motion
V_y	yield base shear
W	seismically effective weight of structure
α_c	ratio of post capping stiffness to elastic stiffness
α_s	ratio of post-elastic stiffness to elastic stiffness
β_i	parameter defining deterioration in excursion i
δ_y	yield displacement
δ_c	displacement at maximum strength
η	yield coefficient for SDOF system = F_y/W
γ	base shear coefficient for MDOF structure = V_y/W
$\gamma_s, \gamma_c, \gamma_k, \gamma_a$	deterioration parameters
λ	ratio of residual strength to yield strength
$\lambda_{IM}(x)$	mean annual frequency of the variable IM exceeding a value x
μ	ductility ratio
θ	stability coefficient
$\theta_{s,max}$	maximum story drift
ξ	damping ratio

References

- ACI 318-02 (2002). Building code requirements for structural concrete. American Concrete Institute.
- AISC (2002). Seismic provisions for structural steel buildings. American Institute of Steel Construction.
- Algermissen, S.T. and Perkins, D.M. (1976). A probabilistic estimate of maximum acceleration in rock in the contiguous United States. U.S. Geological Survey Open File Report 76-416.
- ASTM (1999). Standard guide for the estimation of building damageability in earthquakes. ASTM-E2026-99, American Society for Testing and Materials, West Conshohocken, PA.
- Aslani, H. and Miranda, E. (2003). Fragility assessment of reinforced concrete interior slab-column connections. Submitted to *Journal of Structural Engineering*, ASCE.
- ASCE 7-02 (2002). Minimum design loads for buildings and other structures. ASCE Standard.
- ATC-3-06 (1978). Tentative provisions for the development of seismic regulations for buildings. Applied Technology Council, California.
- ATC-40 (1996). Seismic evaluation and retrofit of existing concrete buildings. Applied Technology Council, Redwood City, CA.
- Aydinoglu, M.N. (2003). An incremental response spectrum analysis procedure based on inelastic spectral displacements for multi-mode seismic performance evaluation. *Bulletin of Earthquake Engineering, EAEE*, 1, 1-28.
- Benjamin, J.R., and Cornell, C.A. (1970). Probability, Statistics, and Decision for Civil Engineers. McGraw-Hill, New York.
- Bertero, V.V. (1996a). The need for multi-level seismic design criteria. *Proc. 11th World Conference on Earthquake Engineering*, Acapulco, Mexico.
- Bertero V. (1996b). State of the art report on: design criteria. *Proc. 11th World Conference on Earthquake Engineering*, Acapulco, Mexico.
- Bertero V.V. (1997). Performance-based seismic engineering: A critical review of proposed guidelines. *Seismic Design Methodologies for the Next Generation of Codes*, Fajfar and Krawinkler, Eds., AA Balkema, Rotterdam, pp. 1-31.
- Chopra, A.K. and Goel, R.K. (1999). Capacity-demand-diagram methods based on inelastic design spectrum. *Earthquake Spectra*, 15, 637-656.
- Chopra, A.K. and Goel, R.K. (2002). A modal pushover analysis procedure for estimating seismic demands for buildings. *Earthquake. Engineering and Structural Dynamics*, 31, 561-582.
- Comerio, M.C. (2000). The economic benefits of a disaster resistant university: earthquake loss estimation for UC Berkeley. Report WP-2000-02, Institute of Urban and Regional Development, U.C. Berkeley.
- Cordova P.P., Deierlein G.G., Mehanny S.F. and Cornell C.A. (2000). Development of a two parameter seismic intensity measure and probabilistic assessment procedure. Proc, 2nd U.S.-Japan Workshop on Performance-Based Earthquake Engineering for Reinforced Concrete Building Structures, pp. 187-206. PEER Report 2000-10.
- Cornell, C.A. (1968). Engineering seismic risk analysis. *Bulletin of Seismological Society of America*, 58, 1583-1606.
- Cornell, C.A. (1996). Calculating building seismic performance reliability; a basis for multi-level design norms. *Proc. 11th World Conference on Earthquake Engineering*, Acapulco, Mexico.
- Cornell, A. and Krawinkler, H. (2000). Progress and challenges in seismic performance assessment. PEER News, April 2000.
- Cornell, C.A., Jalayer, F., Hamburger, R.O. and Foutch, D.A. (2002). Probabilistic basis for the 2000 SAC Federal Emergency Management Agency steel moment frame guidelines. *ASCE Journal of Structural Engineering* 128, 526-533.
- Deierlein, G.G., Krawinkler, H. and Cornell, C.A. (2003). A framework for performance-based earthquake engineering. *Proc. 2003 Pacific Conference on Earthquake Engineering*, Christchurch, New Zealand.
- EN1998-1 (2002). Eurocode 8: Design of structures for earthquake resistance. Part 1: General rules, seismic actions and rules for buildings. Doc CEN/TC250/SC8/N306, European Committee for Standardization.

- EERI (2000). Financial Management of Earthquake Risk. Publication EF2000-04, Earthquake Engineering Research Institute, Oakland, California, 113 pp.
- Fardis, M.N. (2002). Code developments in earthquake engineering. *Proc. 12th European Conference on Earthquake Engineering*, Elsevier, Amsterdam, paper 845.
- Fajfar, P. and Krawinkler, H., Eds. (1997). *Seismic Design Methodologies for the Next Generation of Codes*. AA Balkema, Rotterdam.
- Fajfar, P. (1998). Trends in seismic design and performance evaluation approaches. *Proc. 11th European Conference on Earthquake Engineering*. AA Balkema, Rotterdam, pp. 237–249.
- Fajfar, P. (1999). Capacity spectrum method based on inelastic demand spectra. *Earthquake Engineering and Structural Dynamics*, 28, 979–993.
- Fajfar, P. (2000). A nonlinear analysis method for performance-based seismic design. *Earthquake Spectra*, 16, 573–592.
- Fajfar, P. (2002). Structural Analysis in Earthquake Engineering — a breakthrough of simplified nonlinear methods. *Proc. 12th European Conference on Earthquake Engineering*, London, Paper Reference 843.
- FEMA 273 (1996). NEHRP guidelines for the seismic rehabilitation of buildings — ballot version. U.S. Federal Emergency Management Agency.
- FEMA 274 (1996). NEHRP commentary on the guidelines for the seismic rehabilitation of buildings — ballot version. U.S. Federal Emergency Management Agency.
- FEMA 356 (2000). Prestandard and commentary for the seismic rehabilitation of buildings. U.S. Federal Emergency Management Agency.
- FEMA 368 (2001). NEHRP recommended provisions for seismic regulations for new buildings and other structures — 2000 edition. U.S. Federal Emergency Management Agency.
- Ghobarah, A. (2001). Performance based design in earthquake engineering: state of development. *Engineering Structures*, 23, 878–884.
- Gupta, A. and Krawinkler, H. (1999). Seismic demands for performance evaluation of steel moment resisting frame structures. John A. Blume Earthquake Engineering Center Report No. 132, Department of Civil Engineering, Stanford University.
- Gupta, A. and Krawinkler, H. (2000). Estimation of seismic drift demands for frame structures, *International Journal for Earthquake Engineering and Structural Dynamics*, 29, 1287–1305.
- Gupta, B. and Kunzath, S.K. (2000). Adaptive spectra-based pushover procedure for seismic evaluation of structures. *Earthquake Spectra* 16, 367–391.
- Hadjian, A.H. (2002). A general framework for risk-consistent seismic design. *Earthquake Engineering and Structural Dynamics*, 31, 601–626.
- Hamburger, R.O. (1996). Implementing performance based seismic design in structural engineering practice. *Proc. 11th World Conference on Earthquake Engineering*, Acapulco, Mexico.
- Hueste, M.D. and Wight, J.K. (1999). Nonlinear punching shear failure model for interior slab-column connections. *Journal of Structural Engineering*, 125, 997–1008.
- Ibarra, L., Medina, R. and Krawinkler, H. (2002). Collapse assessment of deteriorating SDOF systems. *Proc. 12th European Conference on Earthquake Engineering*, London, Paper Reference 665.
- Iwan, W. D. (2002). The use of equivalent linearization in performance based engineering. *Proc. International Conference on Advances and New Challenges in Earthquake Engineering Research* (ICAN-CEER), Harbin, China.
- Krawinkler, H. (1996). A few basic concepts for performance based seismic design. *Proc. 11th World Conference on Earthquake Engineering*, Acapulco, Mexico.
- Krawinkler, H. (1997). Research issues in performance based seismic engineering. *Seismic Design Methodologies for the Next Generation of Codes*, Fajfar, P. and Krawinkler, H., Eds, Balkema, Rotterdam, pp. 47–58.
- Krawinkler, H. and Seneviratna, P. (1998). Pros and cons of a pushover analysis for seismic performance evaluation, *Journal of Engineering Structures*, 20, 452–464.

- Krawinkler, H. (2002). A general approach to seismic performance assessment, Proceedings, International Conference on Advances and New Challenges in Earthquake Engineering Research, ICANCEER 2002, Hong Kong, August 19-20.
- Krawinkler, H., Medina, R. and Alavi, B. (2003). Seismic drift and ductility demands and their dependence on ground motions. *Journal of Engineering Structures*, 25, 637–653.
- Kunnath, S.K., Reinhorn, A.M. and Park, Y.J. (1990). Analytical modeling of inelastic seismic response of R/C structures. *Journal of Structural Engineering*, ASCE, 116, 996–1017.
- Kunnath, S.K., Mander, J.B. and Lee, F. (1997). Parameter identification for degrading and pinched hysteretic structural concrete systems. *Engineering Structures*, 19, 224–232.
- Kustu, O., Miller, D.D. and Brokken, S.T. (1982). Development of damage functions for high-rise building components. Report No. JAB-10145-2, URS/John A. Blume & Associates, San Francisco.
- Kustu, O. and Miller, D.D. (1984). A rational methodology for predicting earthquake losses in urban areas. *Proc. Eighth World Conference on Earthquake Engineering*, EERI, Vol. I, 385–392.
- Luco, N. and Cornell, C. A. (1998). Effects of random connection fractures on the demands and reliability for a 3-story pre-Northridge SMRF structure. *Proc. 6th US National Conference on Earthquake Engineering*, Seattle, Washington.
- Mwafi A.M. and Elnashai A.S. (2001). Static pushover versus dynamic collapse analysis of RC buildings. *Engineering Structures*, 23, 407–424.
- Medina, R.A. (2002). Seismic demands of nondeteriorating frame structures and their dependence on ground motions. Ph.D. Dissertation, Dept. of Civil Engineering, Stanford University.
- Miranda, E. (2001). Estimation of inelastic deformation demands of SDOF Systems, *Journal of Structural Engineering*, ASCE, 127, 1005–1012.
- Miranda, E. and Aslani, H. (2002). Probabilistic estimation of building response for loss estimation. *Proc. ICANCEER 2002*.
- Moehle, J.P., Kreger, M.E. and Leon, R. (1988). Background to recommendations for design of reinforced concrete slab-column connections. *ACI Structural Journal*, 85, 636–644.
- Moehle, J.P. (1996). Displacement based seismic design criteria. *Proc. 11th World Conference on Earthquake Engineering*, Acapulco, Mexico.
- Moehle, J., Elwood, K., Sezen, H. and Lynn, A. (2002). Gravity load collapse of reinforced concrete frames during earthquakes. Uzumeri Symposium, ACI.
- Osteraas, J.D. and Krawinkler, H. (1990). Strength and ductility considerations in seismic design. John A. Blume Earthquake Engineering Center Report No. 90, Department of Civil Engineering, Stanford University.
- Otani, S. (1996). Recent developments in seismic design criteria in Japan. *Proc. 11th World Conference on Earthquake Engineering*, Acapulco, Mexico.
- Pan A.D. and Moehle J.P. (1988). Reinforced concrete flat plates under lateral loading: an experimental study including biaxial effects. Report UCB/EERC-88/16, Earthquake Engineering Research Center, University of California at Berkeley.
- Poland C.D. and Derrick B.H. (1997). Opportunities and pitfalls of performance based seismic engineering. *Seismic Design Methodologies for the Next Generation of Codes*, Fajfar, P. and Krawinkler, H., Editors, AA Balkema, Rotterdam, pp. 69–78.
- Porter, K.A., Kiremidjian, A.S. and LeGrue, J.S. (2001). Assembly-based vulnerability of buildings and its use in performance evaluation. *Earthquake Spectra*, 17, 291–312.
- Priestley MJN. (1997). Displacement-based seismic assessment of reinforced concrete buildings. *Journal of Earthquake Engineering*, ASCE, 1, 157–192.
- Rahnama, M. and Krawinkler, H. (1993). Effects of soft soils and hysteresis model on seismic demands. John A. Blume Earthquake Engineering Center Report No. 108, Department of Civil Engineering, Stanford University.
- Robertson, I.N. and Durrani, A.J. (1992). Gravity load effect on seismic behavior of interior slab-column connections. *ACI Structural Journal*, 89, 37–45.

- Ruiz-Garcia, J. and Miranda, E. (2003) Inelastic Displacement Ratio for Evaluation of Existing Structures, *Earthquake Engineering and Structural Dynamics*, 32, 1237–1258.
- Scholl, R.E. and Evernden, J.F. (1979). Seismic damage assessment for high-rise buildings. Annual technical report URS/John A. Blume & Associates, San Francisco, CA.
- SEAOC (1959). Recommended lateral force requirements and commentary. Seismology Committee, Structural Engineers Association of California, First Edition.
- SEAOC (1980). Recommended lateral force requirements and commentary. Seismology Committee, Structural Engineers Association of California, Fourth Edition Revised.
- SEAOC (1995). Vision 2000 — Performance based seismic engineering of buildings. Structural Engineers Association of California, Sacramento, California, USA.
- SEAOC (1999). Recommended lateral force requirements and commentary. Seismology Committee, Structural Engineers Association of California, Seventh Edition.
- Seneviratna, G.D.P.K. and Krawinkler, H. (1997). Evaluation of inelastic MDOF effects for seismic design. John A. Blume Earthquake Engineering Center Report No. 120, Department of Civil Engineering, Stanford University.
- Sivaselvan, M.V. and Reinhorn, A.M. (2000). Hysteretic models for deteriorating inelastic structures. *Journal of Engineering Mechanics*, 126, 633–640.
- Song, J-K. and Pincheira, J.A. (2000). Spectral displacement demands of stiffness- and strength-degrading systems. *Earthquake Spectra*, EERI, 16, 817–851.
- Taghavi, S. and Miranda, E., (2003) Probabilistic study of peak floor acceleration demands in linear structures, *Proc. 9th International Conference on Application of Statistics and Probability in Civil Engineering*, July 6-9, San Francisco, CA.
- Vamvatsikos, D. and Cornell, C.A. (2002). Incremental dynamic analysis. *Earthquake Engineering and Structural Dynamics* 31, 491–514.
- Wen, Y.K. (2001). Reliability and performance-based design. *Structural Safety*, 23, 407–428.
- Yun, S.Y., Hamburger, R.O., Cornell, C.A. and Foutch, D.A. (2002). Seismic performance evaluation of steel moment frames. *ASCE Journal of Structural Engineering*, 128, 526–533.

10

Innovative Strategies in Earthquake Engineering

Akira Wada

Yihua Huang

Vitelmo V. Bertero

10.1	Introduction	10-1
10.2	Introductory Remarks Regarding Importance of Developing and Implementing Innovative Strategies in Earthquake Engineering.....	10-2
	Main Objectives • Approaches and Methodologies for Performance-Based Seismic Design (P-BSD) • What Are the Innovative Approaches?	
10.3	Use of Innovative Strategies and Techniques in Japan	10-13
	Overview of Seismic Design Trends in Japan • Comparison of the U.S. and Japanese Seismic Design Criteria for SMRF • Deformation of Buildings • Applications of EDS • Concept of DCS • Mechanism of Unbonded Braces • Applications of EDS in Tall Buildings in Japan	
10.4	Summary, Conclusions and Future Challenges.....	10-27

10.1 Introduction

This chapter, which may also be considered an introduction to Chapters 11 and 12, is divided into two main sections:

1. Introductory remarks regarding the importance of developing and implementing innovative strategies in earthquake engineering.
2. Use of innovative strategies and techniques in Japan.

The main purposes of the above two sections are (1) to introduce “innovative strategies,” the reasons for their need and the main promising strategies and techniques that have been proposed and used and (2) to discuss in detail the development and applications of one group of strategies and techniques in Japan.

Detailed discussions of developments and applications of seismic isolation strategies are presented in Chapter 11 and those of energy dissipation strategies and devices are presented in Chapter 12. Thus, Section 10.3 discusses the development and use of energy dissipation strategies in Japan that have been based on the concept of “damage-controlled structures” (DCS) with particular attention on the use of the technique or mechanism of “unbonded braces.”

10.2 Introductory Remarks Regarding Importance of Developing and Implementing Innovative Strategies in Earthquake Engineering

10.2.1 Main Objectives

The main objectives of this section are to:

- Make some comments about
 1. the role and importance of earthquake engineering in controlling the seismic risks in our urban and rural areas
 2. possible reasons for observed increase in seismic risks
 3. the development of a conceptual framework for performance-based seismic engineering (P-BSE)
- Discuss briefly the approaches and methodologies for P-BSD with particular emphasis on
 1. the drawbacks of the existing conventional U.S. design code approaches
 2. the P-BSD approach by Wada et al. (1992) and Connor and Wada (1992)
 3. the P-BSE approach based on the use of energy concept
 4. the derivation of energy equations
 5. the advantages of using energy concepts in P-BSE of structures
 6. how the energy-based concept can be used in P-BSE
 7. innovative approaches for response and damage control (or protective systems)
- Discuss what innovative approaches are and:
 1. to offer a classification and definitions of different systems that have been proposed and used
 2. to mention recent advances in design and construction of innovative structural systems

10.2.1.1 Role and Importance of Earthquake Engineering in Controlling Seismic Risks

Chapter 1 suggests that “earthquake engineering” can be defined as the branch of engineering that encompasses all technical and nontechnical efforts to reduce the seismic risk in urban and rural areas to levels that are socially and economically acceptable to the community in such areas. It is also pointed out that we are far from reducing the seismic risks in our built environment to socio-economically acceptable levels. Earthquakes are inevitable, but earthquake disasters can be controlled. The fault ruptures from which significant earthquakes originate do not directly kill people or even the rupture by itself does not result in great economic losses. The cause of most of the injuries and economic losses is the interaction of the earthquake ground motions (EQGMs) with the built environment. What is needed is the reduction of seismic risks by controlling the built environment and this should be the ultimate goal of earthquake engineering.

10.2.1.2 Observed Increase in Seismic Risks

In some areas of the world, even though seismicity remains constant, the disaster potential of an earthquake, and therefore the seismic risk, increases. A clear example is an increase in economic losses in California as a result of recent seismic events. For example, compare what occurred during the 1989 Loma Prieta earthquake with what happened as a consequence of the great 1906 San Francisco earthquake, as well as what occurred in the 1994 Northridge earthquake when compared with what happened as a consequence of the 1971 San Fernando earthquake. Although the field inspections of the aftermath of the above earthquakes in California have clearly demonstrated that most of the facilities that have been designed and constructed according to the latest building code provisions were able to provide life protection, the economic losses due to the damage to structural and nonstructural components, building contents, utility lines, cost of repair or rehabilitation or both, and loss due to downtime and business interruptions were considerably higher than expected. Similar conclusions have been reached from analysis of what happened in recent earthquakes in Japan (1995 Kobe), Turkey (1999 Kocaeli and Düzce) and Taiwan (1999 Chi-Chi).

Despite the relatively mild level of ground shaking produced, the 1989 M6.9 Loma Prieta earthquake caused more than \$8 billion in direct damage, with several bridges and viaducts suffering serious destruction (partial or total collapses). Although no loss of life occurred in modern buildings, the economic loss was judged by both the structural engineering professionals and public policy makers, as being too large for this moderate event. A need was identified for new building, bridge and viaduct design and construction procedures, which could better meet society's requirement that property and business interruption losses in moderate earthquakes should be controlled to acceptable levels. The need to expand the scope of procedures used to evaluate and rehabilitate existing buildings, bridges and viaducts as well as other civil engineering facilities was also identified.

10.2.1.3 Development of Conceptual Framework for P-BSE

In view of the above needs, the Structural Engineers Association of California (SEAOC), which has been actively engaged in the development of the seismic design and construction provisions in the U.S. building codes, particularly in the Uniform Building Code, recognized the need for the development of a new performance-based methodology for the seismic design and construction of buildings. Thus, in 1992, the SEAOC board of directors established the Vision 2000 Committee, to develop a framework for a next generation of performance-based seismic code. However, not much progress was made till 1994.

On January 17, 1994, the M6.7 Northridge earthquake occurred, resulting in losses estimated at approximately \$20 to 30 billion; losses more severe than those resulting from the Loma Prieta earthquake. Engineers and public policy makers again determined that it is unacceptable to experience this magnitude of loss in these relatively frequent and moderate events. Faced with a need to repair and reconstruct many hundreds of buildings, the California Office of Emergency Services contracted SEAOC to develop recommendations for performance-based design and construction procedures that can be used in practice in the near future. In 1 year the Vision 2000 Committee developed interim performance-based engineering recommendations (SEAOC, 1995).

As is discussed in details in Chapters 8 and 9, the SEAOC (1995) recommendations contain a conceptual framework for P-BSE. Recognizing that the most pressing problems at that time were the need to develop reliable methodologies for the assessment of seismic vulnerability of existing buildings and for the repair, rehabilitation or upgrading of those judged to be hazardous, FEMA supported a project to develop "Guidelines for Seismic Rehabilitation of Buildings," which resulted in the publication of such guidelines in 1997 (FEMA-273 and 274, 1997) and in the recent Prestandard FEMA-356 (2000).

10.2.2 Approaches and Methodologies for Performance-Based Seismic Design (P-BSD)

This section discusses briefly:

1. P-BSD approach considered in the conceptual framework for P-BSE recommended by SEAOC (1995) and drawbacks of the existing conventional U.S. design approach.
2. The P-BSD approach by Wada et al. (1992) and Connor and Wada (1992).
3. P-BSE approach based on the use of energy concept with particular emphasis on derivation of energy equations, advantages of using energy concepts in P-BSE of structures, how the energy-based concept can be used in P-BSE and innovative approaches for response and damage control (or protective systems).

10.2.2.1 P-BSD Approach Considered in the Conceptual Framework for P-BSE Recommended by SEAOC (1995) and Drawbacks of Existing Conventional U.S. Design Approach

As discussed in Chapter 8, the P-BSE framework, illustrated in Figure 10.1, encompasses the full range of engineering activities necessary to create structures with predictable seismic performance. Performance-based seismic engineering begins with the selection of performance objectives and the identification of the potential seismic hazards to be able to establish the design earthquakes, and whether the

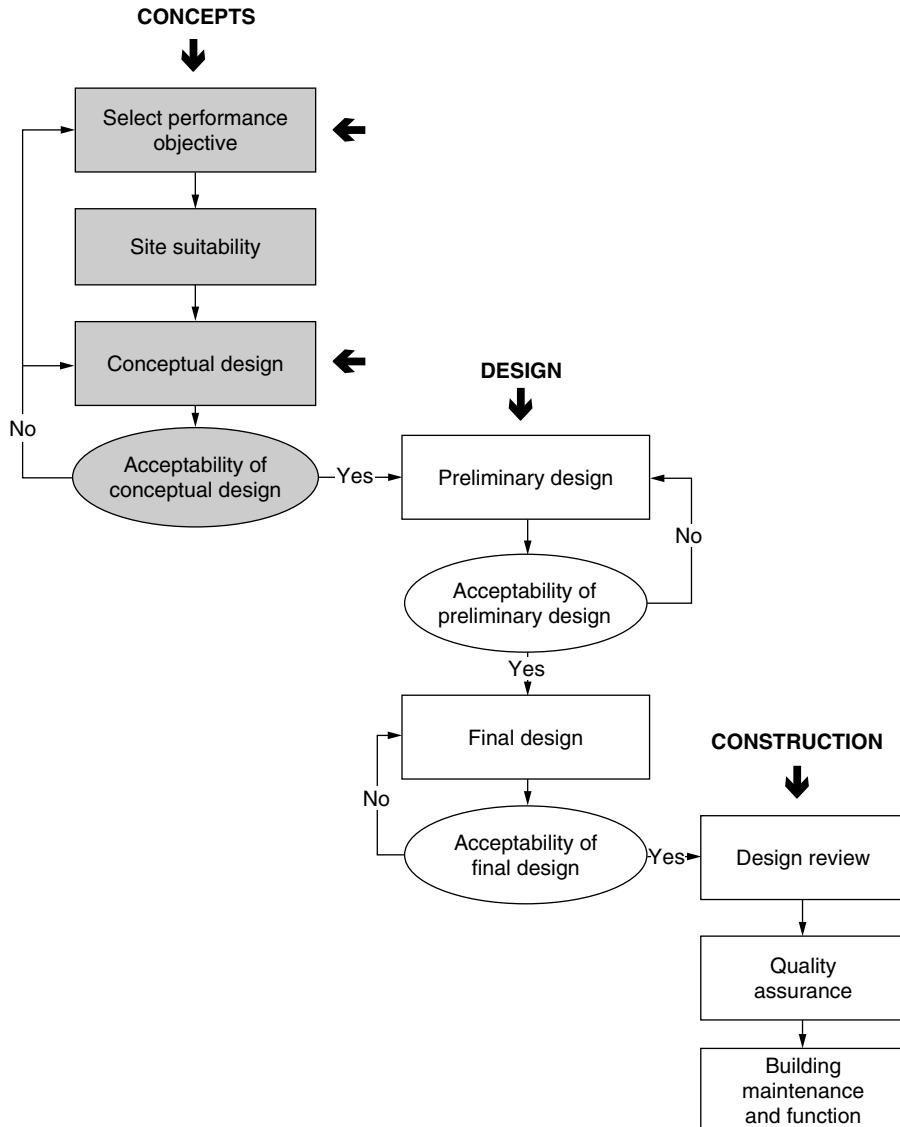


FIGURE 10.1 Conceptual framework for P-BSE. (Adapted from SEAOC Vision 2000 Committee (1995). Performance-based seismic engineering of buildings. Report, Structural Engineers Association of California, Sacramento, CA.)

site selected is suitable for earthquake-resistant construction. This framework then includes the design phase, which includes the conceptual, preliminary and final numerical design and the design acceptability checks and reviews. Finally, the framework concludes with quality assurance during construction and monitoring of building maintenance and its occupancy (or function) after construction. From this framework it is clear that the structural design phase consists of a sequence of three steps and that before starting such steps, it is necessary to select a proper approach that will accomplish the selected specific design performance objectives (performance design criteria). Thus, the designer must have a good overall grasp of all the main aspects of the earthquake problems and of the philosophies, approaches and methodologies available in practice to successfully conduct the total design process.

Critical reviews of the available design philosophies and approaches are summarized in Chapter 8 and in Bertero (1992a, 1992b, 1997a, 1997b), and are discussed in detail in SEAOC Vision 2000 Committee

Report (1995) and also in Oliveto (2002, Chapter 1). From these reviews it becomes clear that to improve the actual performance, and particularly damage control of the real constructed facilities, there is a need to change the existing U.S. seismic design code approach, which is based on the design for the strength capacity demanded by the specified base shear, which in turn depends on the design spectral acceleration. Herein this approach is referred to as “the traditional or conventional design approach.”

Analyses of elastic response spectra of the EQGMs recorded during significant earthquakes have clearly shown that it is not economically feasible to design and construct standard occupancy buildings that will remain elastic under expected severe EQGMs. Thus, to obtain safe and also socially and economically acceptable constructions when they are subjected to severe EQGMs, it is desirable to reduce the demanded elastic strength and, hence, allowing the structure to undergo controllable inelastic (plastic) deformations. For the structure to develop such controllable plastic deformations it is necessary to provide the traditional structures with sufficient *toughness* (energy dissipation capacity through yielding) to avoid an early semibrittle failure. Such toughness in practice is usually represented by the so called “global ductility ratio, μ ,” which is used as one part of the so called “response modification factor, R ,” to reduce the linear design (strength) spectra to determine the required base shear strength (see also Section 10.3.2, Table 10.1).

While there is no doubt that it is desirable to provide the structure with the maximum ductility ratio that is economically feasible, it has to be recognized that physical ductility by yielding of current conventional structural materials leads to damage during a severe EQGM. The larger is the ductility the higher is the damage. Thus, while it is desirable, and should also be recommended to provide the structure with the maximum ductility ratio that is economically feasible, this high ductility ratio should not be misused to excessively reduce the required yielding strength. In other words, it is necessary to control the demanded global ductility by providing sufficient global yielding strength capacity such that the structure is provided with the needed toughness to attain not only a safe building but also to avoid costly damage. Figure 10.2 illustrates the significant damage that is developed when structure and structural components are subjected to large ductility demands.

Because of the above-mentioned drawbacks of the conventional code approach, significant efforts have been devoted to find more reliable approaches and methodologies to control structural seismic performance. In this chapter only the following general approaches that have been recommended in Japan and United States are briefly introduced.

10.2.2.2 Performance-Based Seismic Design Approach Proposed by Wada et al. (1992) and Connor and Wada (1992)

In 1992, Wada et al. discussed the innovative approach of damage-tolerant structures (DTS), or damage-control structures (DCS), which is theoretically based on the performance-based design methodology proposed by Connor and Wada (1992), Connor and Klink (1996) and lately by Connor (2003). This concept and its technology, which has been extensively applied in high-rise buildings in Japan (over 60 m (197 ft)) and started to be applied in design and construction of new buildings in the United States, are discussed in this chapter (Section 10.3) as well as in Chapters 12 and 16.

10.2.2.3 Performance-Based Seismic Design Approach Based on the Use of Energy Concepts

Rather than the traditional or conventional methodology of using the displacement ductility μ_d to establish an inelastic design spectrum to determine the minimum yielding strength for the seismic design of the structure, an alternative was proposed by Housner (1956) to use an energy approach. Although estimates have been made of input energy to single-degree-of-freedom (SDOF) systems (Berg and Tbomaides, 1960), and even of multi-degrees-of-freedom (MDOF) systems, such as steel structures designed in the 1960s for some of the existing recorded EQGMs (Anderson and Bertero, 1969), it is only recently that this approach has gained extensive attention (Akiyama, 1985). This design method is based on the premise that the *energy demand* during an earthquake can be predicted and the *energy supply* of a structural element and of structural system can be established. In a satisfactory design, the energy supply is larger than energy demand.

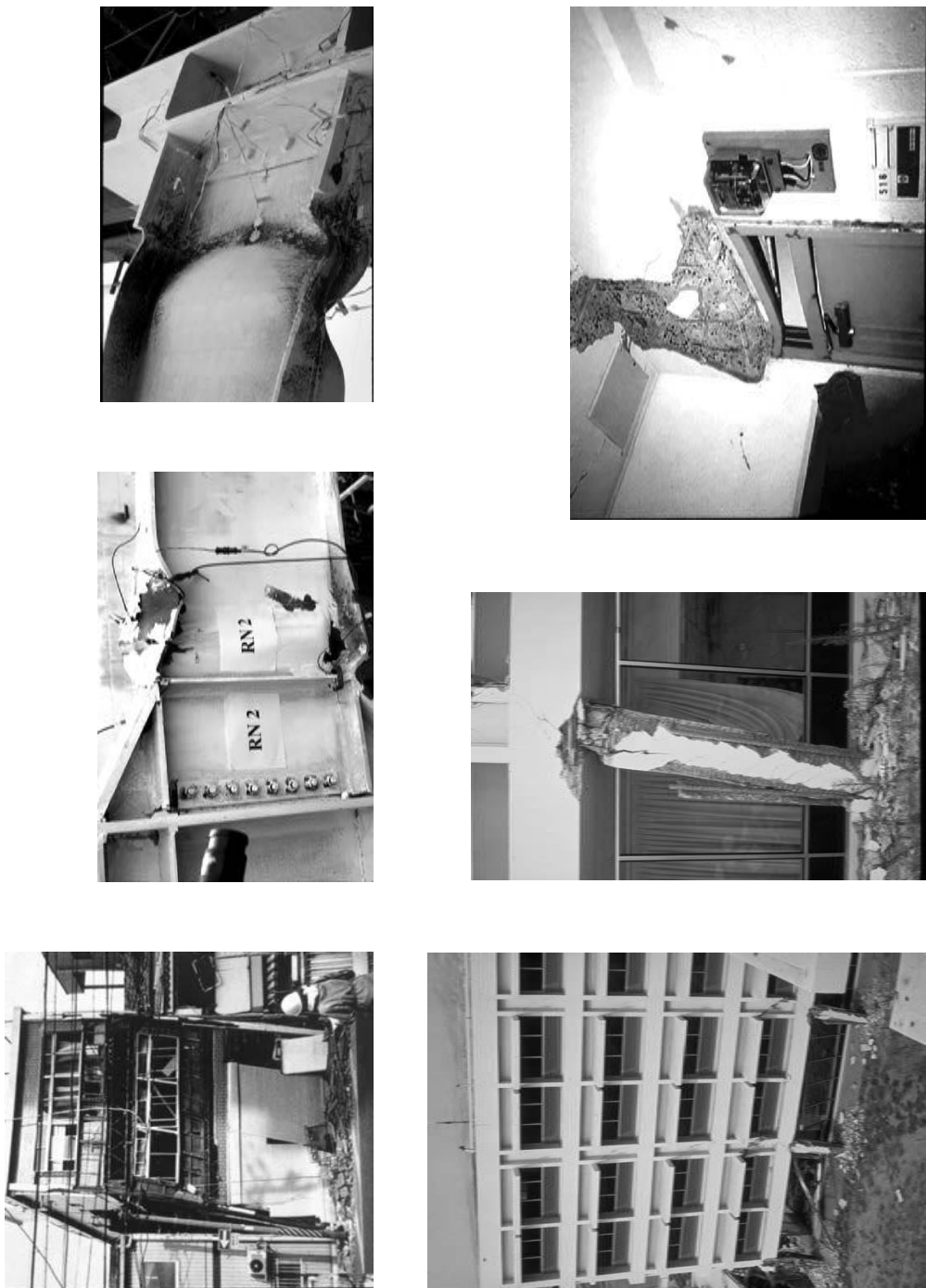


FIGURE 10.2 Photos illustrating significant damage to structures and structural components when they have to develop large ductilities.

As discussed by Bertero (1992a), to develop reliable design methods based on energy approach, it is necessary to derive the energy equations. Although real structures are usually MDOFS, to facilitate the analysis and understanding of the physical meaning of the energy approach, it is convenient to first derive the energy equations for SDOFS and then for MDOFS.

10.2.2.4 Energy Equations

Uang and Bertero (1988) give detailed discussion of the derivation of two basic energy equations (absolute and relative) starting directly from the equilibrium equation of an inelastic viscously damped SDOFS subjected to an EQGM.

The “absolute” energy equation is

$$E_I = E_K + E_S + E_{H\xi} + E_{H\mu} \quad (10.1)$$

where,

E_I = “absolute” input energy

E_K = “absolute” kinetic energy

E_S = elastic strain energy

$E_{H\xi}$ = hysteretic dissipated energy due to viscous damping

$E_{H\mu}$ = hysteretic dissipated energy due to yielding or friction or both

E_I is defined “absolute” input energy because it depends on the absolute ground acceleration. Physically, it represents the inertia force applied to the structure. This force, which is equal to the restoring force plus damping force, is the same as the total force applied to the structure foundation. Therefore, E_I represents the work done by the total base shear at the foundation on the foundation displacement.

The “relative” energy equation is

$$E'_I = E'_K + E'_S + E_{H\xi} + E_{H\mu} \quad (10.2)$$

where,

E'_I = “relative” input energy

E'_K = “Relative” kinetic energy

E'_I is defined as the “relative” input energy because it represents the work done by the static equivalent external force (which is the product of the mass and ground acceleration) on equivalent fixed-base system, that is, it neglects the effect of the rigid body translation of the structure.

10.2.2.4.1 Input Energy to MDOFS

The E_I for an N -story building (N levels above the foundation) can be calculated as follows (Uang and Bertero, 1988)

$$E_I = \int \left(\sum_{i=1}^N m_i (a_t)_i \right) du_g \quad (10.3)$$

where m_i is the lumped mass associated with the i th floor, $(a_t)_i$ is the total acceleration at the i th floor and u_g is the ground displacement. In other words, E_I is the summation of the work done by the total inertia force ($m (a_t)_i$) at each floor through the ground displacement, u_g . Analysis of results obtained from experiments conducted on medium rise steel dual systems indicates that the E_I to a multistory building can be estimated with sufficient practical accuracy by calculating the E_I of SDOF systems using the fundamental period of the multistory structure.

10.2.2.5 Advantages of Using Energy Concepts in Seismic Design of Structures

Equation 10.1 can be rewritten as

$$E_I = E_E + E_D \quad (10.4a)$$

$$E_I = E_K + E_S + E_{H\xi} + E_{H\mu} \quad (10.4b)$$

where $E_E = (E_K + E_S)$ can be considered as the stored elastic energy and $E_D = (E_{H\xi} + E_{H\mu})$ the dissipated energy. Comparing this equation with the basic design equation,

$$\text{Demands} \leq \text{Supplies}$$

it becomes clear that E_I represents the demands and the summation of $E_E + E_D$ represents the supplies. Equation 10.4b points out to the designer that to obtain an efficient design, the first step is to have a good estimate of E_I for the critical EQGM. The designer must then analyze if it is possible to balance this demand with just the elastic behavior of the structure to be designed or will it be convenient to attempt to dissipate as much as possible some of the E_I , i.e., using E_D . As revealed by Equation 10.4b there are three ways of increasing E_D : (1) by increasing the linear viscous damping, $E_{H\xi}$, (2) by increasing the hysteretic energy $E_{H\mu}$ or (3) a combination of increasing $E_{H\xi}$ and $E_{H\mu}$.

Presently it is a common practice to just try to increase the $E_{H\mu}$ as much as possible through inelastic (plastic) behavior of the structure, which implies damage of the structural members. Only since the 1980s has it been recognized that it is possible to increase significantly $E_{H\mu}$ and control the damage throughout the structure through the use of *energy dissipation devices*. Furthermore, as discussed by Bertero (1992b) (in a discussion of the use of an energy equation for rational selection of seismic upgrading strategies for existing hazardous structures) increasing E_D by increasing $E_{H\xi}$ rather than $E_{H\mu}$, has the great advantage that it can control the behavior of the structure under both safety and service levels of EQGMs.

If technically or economically (or both) it is not possible to balance the required E_I either through E_E alone or $E_E + E_D$, the designer has the option of attempting to control (decrease) the E_I to the structure. This can be done by base isolation techniques. A combination of controlling (decreasing) the E_I by base isolation techniques and increasing E_D by the use of energy dissipation devices is a promising innovative strategy not only for achieving efficient earthquake resistant design and earthquake resistant construction of new facilities, but also for the seismic upgrading of existing hazardous structures (Bertero and Whitaker, 1989).

10.2.2.6 How Can the Energy Concepts Be Used in Performance-Based Seismic Design (P-BSD)?

An answer to this question has been offered by Bertero (1992a, 1997a, 1997b, 2002) and is discussed in Chapter 8. Herein only a brief discussion about the answer to this question is presented.

A conceptual methodology for the comprehensive seismic design approach was developed and applied for design of buildings several years ago (Bertero, 1992b; Bertero and Bertero, 1992). This methodology has been slightly modified for performance-based seismic design (P-BSD) according to the recommended design objective matrix (see Figure 9.4 in Chapter 9) and the framework for performance-based seismic engineering (P-BSE) illustrated in Figure 10.1. The conceptual methodology was developed in accordance with the comprehensive design approach and the worldwide-accepted seismic design philosophy and is based on the use of energy concepts and fundamental principles of structural dynamics. It takes into account from the beginning of the earthquake-resistant design procedure, the simultaneous demands (including torsional effects) for strength, deformation and rate of deformation and their combined effects on the E_I and on the required and supplied energy capacities (as presented in Equation 10.4) of the entire facility system. The iterative procedure involved in the comprehensive design approach proposed for P-BSE is illustrated in Figure 10.1, and its detailed discussions are given in Appendix B of the Vision 2000 report (SEAOC, 1995), and in Chapter 8. As indicated in Figure 10.1, the P-BSD is conducted in three steps starting with the conceptual design, as defined next.

- Definition of conceptual earthquake-resistant design of buildings: Conceptual overall earthquake-resistant design is the avoidance or minimization of problems that can be created by the critical combination of the seismic effects with other probable excitations (loading conditions), using a physical understanding of the mechanical (dynamic) behavior of the entire facility, rather than numerical computations (Bertero, 1979, 1982, 1995, 1997a, 2002; Bertero and Bertero, 1992; SEAOC, 1995). Conceptual overall design of the facility involves not only the

choice of overall configuration and size of the facility but also the selection of the structural layout, structural system, structural material, type of nonstructural components (particularly those that could become unintentional structural components), equipment, utility lines and the foundation system.

- In the case of buildings, both the architect and the engineer have to understand how design decisions regarding building layout, and amount and distribution of the mass, may have serious seismic effects on the structure. The inertial forces depend on the mass (amount and distribution), the damping and the structural characteristics (stiffness, yielding strength, maximum strength, energy absorption and energy dissipation capacities). Although there is no universal ideal building and structural configuration, certain basic principles of earthquake-resistant design can be used as guidelines to select adequate building and structural configurations, as well as efficient structural foundation types and systems, nonstructural components, utility lines and their respective materials. A list and brief discussions of the guidelines for the conceptual earthquake-resistant design of the entire building systems are given in Chapter 8. Herein only the following item is mentioned.
- Selection of the proper actual system and approach to be used in the preliminary P-BSD and the final sizing and detailing of the structural members should be based on (or at least considered), the application of energy concepts through the use of the energy balance equation, according to Equation 10.4a and Equation 10.4b. The flow chart presented in Figure 10.3 can facilitate the review discussion on how the above energy equations can be implemented.
- As pointed out previously, the past performance of structures has shown that proper application of the traditional approach based on just the use of the conventional or traditional U.S. code design criteria could result in building construction that provides “Life-Safety” against severe EQGMs. However, in general, it would be difficult to control the damage to socially and economically acceptable levels. The main reason for this difficulty is that the current code design criteria are based on reducing the elastic base shear strength demanded by the EQGM. This reduction in strength can be achieved by requiring that a significant amount of E_I is dissipated through $E_{H\mu}$ (i.e., through yielding or plastic deformation) that could take place at certain critical regions of the structure, which therefore would suffer permanent damage. The key issues with this approach are *first*, reliable selection of where the critical regions are located and *second*, to dimension and detail these critical regions so that they can dissipate sufficient $E_{H\mu}$ so that the facility can be designed for inertial forces significantly lower than those required for attaining solely elastic response. When analyzing the advantages and disadvantages of this approach, it has to be kept in mind to control the $E_{H\mu}$ that would be developed in each critical region where the inelastic deformations would occur. Ductility through yielding of materials is usually associated with damage; the larger the physical ductility, the greater will be the damage.
- Even though the application of the capacity design philosophy (Park and Paulay, 1975; Paulay and Priestley, 1992) can significantly help to control the location of the critical regions, there are still some difficulties with its application in highly redundant, and particularly irregular, structures, and in the prediction of real hysteretic behavior at critical regions (Bertero and Bertero, 1992). As illustrated in Figure 10.3, in the case of a moment-resistant frame structure, the critical regions are usually located in the beam near or adjacent to the beam–column joints. Because of the large variation in the real mechanical characteristics of the structural materials with respect to the nominal values specified in the codes, it is very difficult to locate the critical regions and also to determine the length of these regions and to carry out their proper detailing. Furthermore, even if the critical regions are properly detailed in the drawings, some of the details are very difficult to carry out reliably in the field. Thus, it is not surprising to observe, in experiments, that the hysteretic behavior of the critical regions start to degrade prematurely and that this phenomenon increases significantly with the repetition of reversal cycles of inelastic deformations. This degradation is very difficult to predict because of its high sensitivity to the quality control of the materials and their real detailing, i.e., workmanship in the field. Therefore, it is very difficult to control the

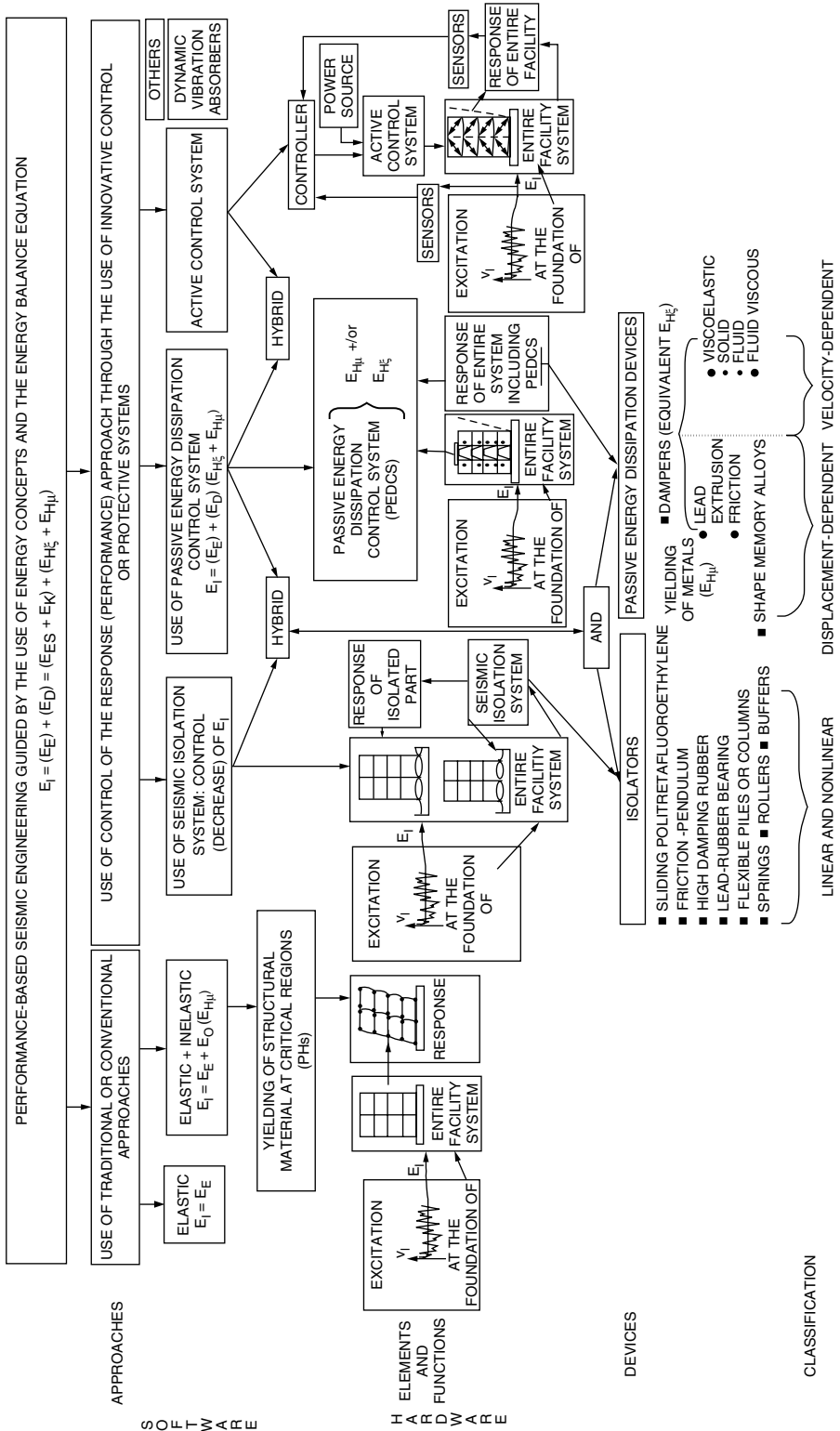


FIGURE 10.3 Flow chart of the conventional and innovative approaches, strategies and techniques for P-BSD. (From Bertero, V.V., 1997, *Seismic Design Methodologies for the Next Generation of Codes*, Fajjar and Krawinkler, Eds., Balkema, Rotterdam and Brookfield, Vermont. With permission.)

real performance (damage) for the entire facility. Furthermore, to achieve significant $E_{H\mu}$ in the critical regions of a structure usually requires large interstory drift. These large interstory drifts result in substantial damage to nonstructural elements (such as infill walls, partitions, lintels and ceilings) as well as to the equipment and contents and the utility lines of the facility.

- Protection of nonstructural components, equipment and building contents. As it has been discussed in several publications (Bertero, 1980, 1992a, 1996, 2002; Gillengerten, 2001; Johnson, 2003; Mayes, 1996, Mayes and Naeim, 2001), and also discussed in Chapters 8, 9, 11, 12 and 19, one of the most difficult issues to address from a conventional building-design point of view is reducing damage to nonstructural components, equipment, utility lines and building contents. This is very often ignored and when addressed can be very expensive to incorporate in conventional design. There are two primary response parameters that cause nonstructural damage. The first is related to the relative drift between floors (usually referred to as interstory drift) and the second is the floor accelerations. Together, these two parameters cause damage to the building contents, architectural facades, partitions, piping and duct work, ceilings, building equipment and elevators. There are two different design philosophies debated within the structural engineering profession that deal with minimizing nonstructural damage. One argues that stiff buildings reduce interstory drift, but their opponents state that they produce high-floor accelerations. The other school of thought argues that flexible buildings are the solution, because they attract less force and tend to reduce floor accelerations. Although this is true, their opponents state that flexible buildings have much higher interstory drifts, and this accentuates damage to components that are sensitive to drift. Clearly what is needed is a design concept that will result in a reduction of both interstory drift and floor accelerations, i.e., new reliable innovative approaches that will result in control of the desired seismic response.

10.2.2.7 Innovative Approaches for Response Control (or Protective Systems)

Historical reviews of the attempts to control the seismic response and damage of buildings, particularly their collapse, show that several such attempts were made in very early civilization (Nedham, 1971). However, in the United States most of the innovative approaches and methodologies, based on the scientific principles of earthquake engineering to control the seismic response of real buildings, have been proposed since the 1980s; few of them have been successfully applied in other countries earlier (since 1970s).

10.2.3 What Are the Innovative Approaches?

As discussed in Oliveto (2002, Chapters 1 and 2), innovative approaches to the problems of seismic engineering are based on the addition of special mechanical or structural devices to what has been called in the United States “conventional structural system” and in Japan called “primary structural system.” The main objective of these approaches is to improve the control of the seismic response (floor acceleration, deformations, drift and plastic deformation). This can be achieved either by controlling the E_I to a significant part of these facilities or by minimizing (or even eliminating) its damaging effects by controlling E_D (particularly $E_{H\mu}$) demand on the traditional primary structural members or by both of these. By controlling these types of energy demand and energy supplies, it is possible to control the interstory drift indices and to lower the accelerations, and thus control the damage to the primary structural members as well as reduce the damage to the nonstructural components, equipment, utility lines and contents of these facilities. This control (reduction) of the damage to the entire facility system is the main reason why these innovative approaches are usually also called protective approaches and the system and the devices used are usually called protective systems and devices.

The above strategy or concept of controlling the dynamic response (structural vibrations) by adding mechanical or structural devices is not new; it has been applied in many other branches of engineering. As has been pointed out in the pertinent literature (Hanson et al., 1993), some of these applications include shock absorbers for vehicles, equipment vibration isolators, pipe restraints and snubbers, shock

isolation devices to mitigate blast effects and mass damping systems to control wind-induced vibration in buildings. However, relatively few of these devices have been applied specifically to control (reduce) the seismic responses. Only in recent years have there been some significant advances in the refinement of available mechanical and structural device hardware and in the development of new ones for application to the earthquake-resistant design and earthquake-resistant construction of new civil engineering facilities and for seismic upgrading of existing systems, particularly bridges, viaducts and buildings.

10.2.3.1 Classification and Definition of Innovative Control (or Protective) Systems for Seismic Effects

10.2.3.1.1 Classification

As indicated in Figure 10.3, the different innovative systems that are available for control of the seismic response of civil engineering facilities can be grouped under the following classification: seismic isolation, passive energy dissipation, active and hybrid control systems and others. This classification is practically the same as has been adopted by ATC-17-1 (1993) and later by FEMA-273 and -274 (1997) and FEMA-356 (2000).

10.2.3.1.2 Definitions

ATC-17-1 (1993) has adopted the following system definitions:

- Seismic isolation systems decouple building and bridge structures from the damaging components of EQGMs. Such systems require that the structure be supported on discrete isolators, which detune the structural system and add substantial damping, examples include elastomeric, friction and sliding devices.
- Passive energy dissipation control systems “add damping” to structures in such a way that they significantly reduce response (and damage) due to EQGMs. Examples include viscoelastic (solid and fluid) dampers, fluid viscous dampers, metallic-yielding and friction devices and lead extrusion systems. All these devices are installed within the structural framing system. A preferred term for “add damping” is “add energy dissipation devices.”
- Active control systems provide seismic protection by imposing forces on a structure that counterbalance the earthquake-induced forces. Inherently more complicated than seismic isolation or energy dissipation systems (EDS), they include computer-controlled actuators that activate bracing or tuned-mass dampers located within the structure.
- Hybrid control systems are usually a combination of active and passive systems. Reduced power demands and improved reliability are the main system features. Passive systems include a combination of seismic isolators or EDS or both.

Although the above definitions are used commonly in the United States, Bertero (1997a, 1997b, 2002) in the discussion of the use of seismic isolation systems and passive energy dissipation devices has suggested some changes, which were guided by the use of energy concepts.

10.2.3.2 Recent Advances in the Design and Construction of Innovative Structural Systems

Recent advances in the design and construction of building structural systems using the innovative strategy and technology of seismic isolation are discussed in Chapter 11. The advances and applications of the strategy and technology of passive energy dissipation devices in the United States are discussed in Chapter 12 and in recent publications by Hanson and Soong (2001), Soong and Dargush (1997) and Constantinou et al. (1998). Chapter 12 also discusses some applications in Japan. As mentioned previously, the present chapter is mainly devoted to discussing the development and use of innovative strategies and techniques of EDS in Japan. These systems are based on the concept of DTS or DCS, which is theoretically based on the performance-based design methodology proposed by Connor and Wada (1992) and its applications using various energy dissipation devices with particular emphasis on the use of

“unbonded braces” or “buckling-restrained braced frames (BRBFs).” This very promising energy dissipation technique is also discussed in Chapters 12 and 16.

10.3 Use of Innovative Strategies and Techniques in Japan

10.3.1 Overview of Seismic Design Trends in Japan

Japanese seismic design standards define two levels (level 1 and 2) of EQGMs and allowable damage for each of these levels. For level 1, small and moderate EQGMs, only minor damage such as cracks in walls and beams are allowed, while human life and the building functions and structure are protected. For level 2, a severe rare EQGM, a building structure may be damaged provided that human life is protected. The current seismic design and research in Japan are based on these requirements. However, since the buildings have recently increased in their sizes, and also because of the need to accommodate expensive computer and communication equipment, as well as the functionality of such equipment, the above conventional design requirements need to be modified. The lessons learned from the Northridge and Hyogoken-Nanbu earthquakes emphasize the need to recognize that the damage to the structural and nonstructural systems designed according to the previous philosophy may result in great human life and economic losses. It is obvious that too large plastic deformation in structural and nonstructural systems of a building should not be allowed for severe EQGMs. Furthermore, construction activities requiring the production of cement and steel raise new concerns about environmental problems, such as ruining rain forests and increasing CO₂. The severity of these problems could be reduced by lengthening the building’s service life. Thus, it became clear that a new design approach was needed such that buildings, especially large important buildings, remain functional not only after moderate EQGMs but even after a severe event. A promising approach appears to be in the use of the concept of “damage-tolerant” structural system, which is described next.

The concept of a “damage-tolerant” structure was proposed in Japan before the Northridge and the Kobe earthquakes (Wada et al., 1992). Damage tolerant means that the acceptable damage due to an earthquake occurs in specific structural components (such as braces, shear walls or supplemental energy dissipating devices) that are added to what is called “primary structural system.” These damaged components are called the “sacrificing members” and function somewhat like a fuse to protect the primary structure from severe damage. After the 1994 Northridge and 1995 Hyogoken-Nanbu earthquakes, “damage-tolerant” or DCS have received increasing attention by researchers and structural engineers especially in the United States and Japan. Therefore, it is not surprising that the investigation of the seismic behavior of DCS and its applications in the design and construction of buildings located in regions of high seismicity have widely increased worldwide (see Chapter 16) (Bertero, 1996, 1997a, 1997b; Housner et al., 1997; Huang, 1995; Huang et al., 1994; Soong and Constantinou, 1994; Soong and Dargush, 1997; Wada et al., 1992, 1997, 1998; Wada and Huang, 1995).

On the cover of the *Engineering News-Record* (Reina and Normile, 1997), the word “sacrificial” was used together with a conceptual picture of a DCS and a short article. The article explains that the energy absorption that occurred from the axial yielding of the damping braces (they call sacrificial braces) that were used in the steel structural system will become the “sacrificed” braces through which high-rise building structure will survive even a severe EQGM. As is discussed later in this chapter, in special moment-resisting frames (SMRFs) the welded flange of the beam-ends become sacrificed. Figure 10.4 shows a sketch of a typical beam–column connection in the United States before the Northridge earthquake. Little energy dissipation can be expected from the plastic deformation of these types of beam ends during a severe EQGM (Bertero, 1980) (as was clearly demonstrated during the Northridge [Engelhardt, 1995, Carper, 1998, Krawinkler, 1994] and the Hyogoken-Nanbu earthquakes [Steel Committee of Kinki Brach, 1995]) because the plastic deformation of the beam ends is equivalent to the method of mounting elasto-plastic energy dissipating devices in series with an elastic frame (Figure 10.5), leading

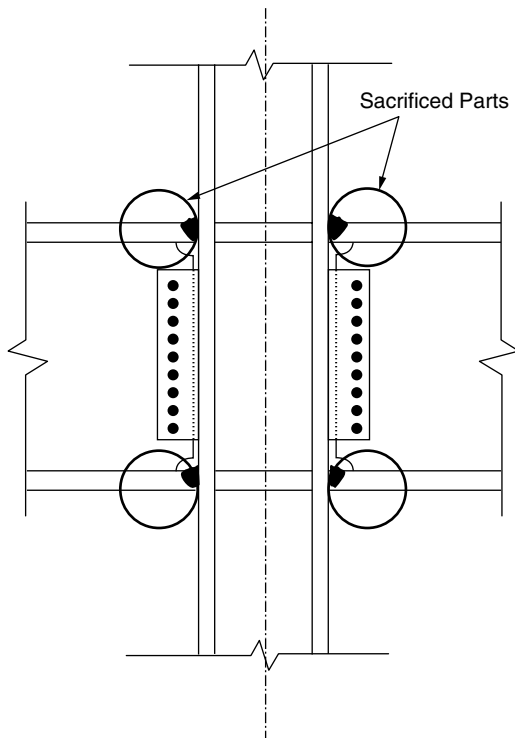


FIGURE 10.4 Typical beam–column connection in the United States before Northridge earthquake.

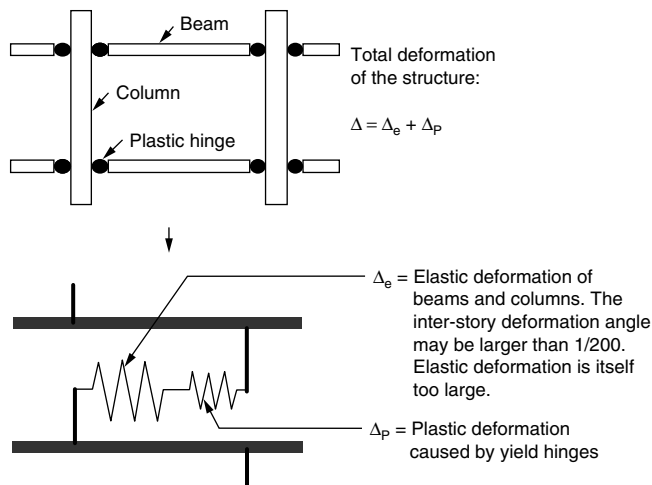


FIGURE 10.5 Strong column–weak beam model.

to large deformation of the whole frame after it becomes plastic mechanism, which demands significant energy dissipation that the welded connections of the flanges cannot supply.

10.3.2 Comparison of U.S. and Japanese Seismic Design Criteria for SMRF

Both the United States and Japan have similar procedures for the design of SMRF structural systems. These procedures are based on consideration of a minimum required strength and maximum acceptable

TABLE 10.1 Comparison of US–Japanese Seismic Design for MRSF Structure

Japan	USA
Building height ≤ 60 m	Base shear
Base shear	$V = \frac{C_V I}{R T} W$ for any earthquake
$V \geq 0.2 R_t Z W$	for moderate earthquake
$V \geq 1.0 R_t Z D_s W$	for severe earthquake
$D_s = 0.25$ for SMRF	
Design PGA:	
$A_g = 0.08g \sim 0.1g$	for moderate earthquake
$A_g = 0.4g \sim 0.5g$	for severe earthquake
Deformation Criteria:	Maximum inelastic response displacement:
$\Delta_s \leq \frac{1}{200} h_s$	for moderate earthquake
Δ_M is not limited for severe earthquake	
Building height > 60 m	$\Delta_M \leq \frac{1}{50} h_s (T > 0.7 \text{ sec})$
Time history analysis have to be done.	
Design PGV:	Design level deformation Δ_s for MRSF
$V_g = 25\text{cm/s}$ ($A_g = 0.25g$) for moderate earthquake	$\Delta_s = \frac{1}{0.7R} \Delta_M = \frac{1}{298} h_s$
$V_g = 50\text{cm/s}$ ($A_g = 0.50g$) for severe earthquake	
Deformation Criteria:	
$\Delta_s \leq \frac{1}{200} h_s$	for moderate earthquake
$\Delta_M \leq \frac{1}{100} h_s$	for severe earthquake

deformation. The required strength is defined by the base shear and the required maximum deformation is defined by the maximum acceptable inter story drift. However, there are differences in the quantifications of these requirements. Table 10.1 lists some typical specifications.

In Japanese seismic design specification, the interstory drift Δ_s (for T greater than or equal to 0.7 sec) is limited to be less than $h_s/200$. In the U.S. seismic specification, however, the interstory drift Δ_s is limited less than $h_s/298$ (for T greater than 0.7 sec), which is why the depth of structural members of the United States is usually designed to be larger than those of Japan. Some detailed discussions of the above specifications are given in the following sections.

10.3.2.1 Seismic Design Criteria for SMRF in Japan

Japanese seismic design methods for building structures are different depending on whether the building height is beyond or under 60 m (197 ft).

For the buildings whose height is less than 60 m (197 ft), elastic design is required using base shear coefficient of 0.2, which is associated with small to moderate EQGM. Interstory drift angle must be less than 0.5%. The maximum acceleration of the ground motion is considered to be 80 to 100 cm/sec². For severe EQGMs whose maximum ground motion acceleration is 400 to 500 cm/sec², five times larger base shear coefficient (i.e., 1.0) should be used for the ultimate state design. This demanded shear force could be reduced depending on the deformation capacity of structure. For the most ductile steel SMRF, the specified D_s factor is 0.25. For reinforced concrete wall structures, which have less ductile capacity, the D_s factor is 0.55. However, there is no specified deformation limit for the ultimate state design in case of a severe EQGM.

Since the initial elastic stiffness of moment resisting steel frame is small, the cross-sectional dimension of most the SMRF structures is controlled by the specified $\Delta_s = 0.5\%h_s$ under the base shear coefficient of 0.2. Because severe EQGMs are considered to have peak ground acceleration A_g equal to five times those specified for the small EQGM, the maximum interstory drift angle under the severe EQGM is assumed to be 1/40. Furthermore, as the plastic deformation starts to develop, resulting in a decrease in stiffness, the interstory drift angle could reach 1/30. This was confirmed by observations of the damaged steel SMRF after the Hyogoken-Nanbu earthquake in 1995.

Time history response analysis is required for the seismic design of tall buildings more than 60 m (197 ft) high. For the small and moderate EQGMs, the maximum velocity of ground motion is considered as 25 cm/sec or the associated maximum acceleration is approximately 250 cm/sec². The interstory drift angle must be controlled to values under 0.5%. For a severe EQGM, the maximum velocity of ground motion is considered as 50 cm/sec or associated maximum acceleration is 500 cm/sec²; the interstory drift angle is required to be less than 1.0%. The main differences in seismic designs between over 60 m (197 ft) high rise buildings and under 60 m (197 ft) low-rise buildings are (1) the magnitude of the maximum acceleration of small and moderate EQGMs used for tall buildings is about 2.5 times larger than low-rise buildings and (2) while there is deformation limit to the tall building for severe EQGMs there is no limit for the low-rise buildings. From these requirements it is evident that in Japan there are more stringent requirements for high-rise buildings than those for low-rise buildings.

10.3.2.2 Seismic Design Criteria for SMRF in the United States

A design method to adjust the required structural strength according to the plastic deformation capacities (ductility capacity) of the structure was first developed in the United States. R factor value has been specified in the U.S. codes since 1988 (ICBO, 1988); 10 years after it had been introduced by the ATC 3-06 report (1978). Factor R is equivalent thinking to the inverse of the Japanese D_s value. Elastic response level is calculated based on the local area factor and structural period. The shear force used for elastic design is obtained from the elastic response force, which is divided by the factor R . For the ductile moment resisting steel frames, UBC 97 (ICBO, 1997) recommends $R = 8.5$; for less ductile reinforced concrete bearing wall structural system, $R = 4.5$ should be used.

The U.S. seismic codes limit the maximum acceptable inelastic response displacement Δ_M , which is not specified in Japan. According to the elastic design procedure in the U.S. code, the design yielding strength is obtained by reducing the required elastic forces by a factor of R , and the maximum elastic demand displacement Δ_s , should be multiplied by a factor $0.7R$ to obtain the maximum inelastic interstory drift Δ_M , i.e., $\Delta_M = 0.7R\Delta_s$. As the U.S. code specifies the maximum acceptable $\Delta_M = (2.5\%)h_s$ for structures having $T < 0.7$ sec and $\Delta_M \leq (2\%)h_s$ for $T \geq 0.7$ sec and to obtain the maximum acceptable or limit in the value of the elastic design level response displacement Δ_s (i.e., the story drift under the design EQGM) the above Δ_M value should be multiplied by a factor of $1/(0.7R)$.

From the above discussions it becomes clear that while in Japan the same deformation limit 1/200, associated with base shear factor of 0.2, is required for all types of structures, in the United States, the deformation limit depends on the inelastic deformation capacity of the structure. Thus, for ductile structures in the United States, the seismic design shear force used in the specified linear elastic design procedure can be reduced.

10.3.2.3 United States–Japan Comparison on the Design of Steel SMRFs

As discussed previously, in Japan, for the building with height less than 60 m (197 ft), the deformation limit requirement is only specified for small and moderate EQGMs. The design base shear for Japanese buildings is larger than that specified in the United States. Therefore, in Japan it is reasonable to design and build all the frames in a structure as SMRF, i.e., all with rigid connections.

In the United States, the code specifies a deformation limit for the design against severe EQGMs and requires that the linear elastic design procedure be based on the reduced values of the base shear forces that will be required by the linear elastic response for the design EQGM. The reduction factor is $1/R$ for shear forces. The deformation is computed according to Table 10.1.

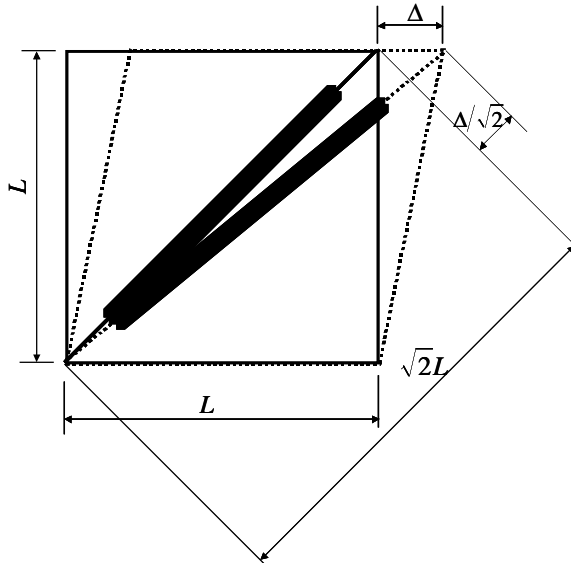


FIGURE 10.6 Axial deformations of brace and shear deformation of frame.

As the required design base shear force is smaller than that in Japan, it is very common to design just few frames to resist the lateral forces induced by the EQGMs and all other frames are designed to resist the gravity loads. Since the base shear force is small, the other frame members do not need to resist the horizontal forces, and thus, the beams are connected to the columns only through web. However, because of the small acceptable lateral deformations, the designer needs to select beams and columns with very large and stiff cross sections for SMRFs. On this basis of the current Japanese knowledge, the SMRFs in the United States can be called passive controlled seismic frames in which the welded connected flanges of the beams at their ends are considered as the energy dissipating devices or “sacrifice members.”

Such kind of steel SMRFs suffered severe damages during the 1994 Northridge earthquake. Therefore, after 1994, in the United States the use of base isolation and energy dissipation devices (particularly unbonded braces) became attractive compared with continuing to use few SMRFs with large-size beams and columns. It is believed that the use of these devices permits a very rational and both technically and economically efficient seismic design, especially in the United States, where the strict requirement limiting the lateral deformation can be met and adequate lateral resistance capacity can be obtained. Because in the above innovative strategies it is not necessary to use very heavy large-size beams and columns demanded by few SMRFs, it is possible to reduce the total amount of steel required for the entire frame structure.

10.3.3 Deformation of Buildings

For a building to be functional, it must have not only structural components (beams, columns and walls), but also partitions, windows, doors, utility lines and equipment. The latter components are called nonstructural members. These nonstructural components are easily severely damaged when the interstory deformation of the building is very large (Oliveto, 2002).

Let us consider the lateral deformation of a frame consisting of a beam and column with a brace placed at 45° , as shown in Figure 10.6. Compared to the lateral shear deformation $\pm\Delta$ occurring in the frame, the expansion and contraction of the brace becomes $\Delta/\sqrt{2}$. Because the brace length is $\sqrt{2}$ times the column length L , the axial strain in the brace becomes 1/2 of the shear deformation angle of the frame. Taking into account the fact that the joints at the brace ends are of high stiffness and that they will remain

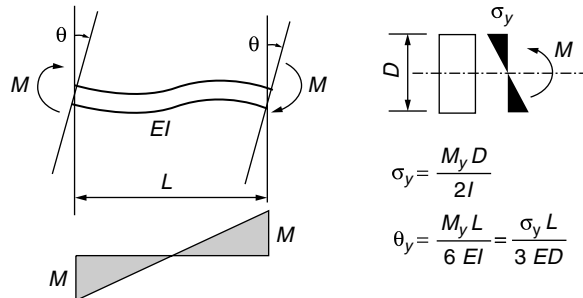


FIGURE 10.7 Deformation angle at beam ends of a rigid frame.

elastic and assuming that the yield strain of the steel brace is 0.1%, it is found that when the brace yields, the story deformation angle is as small as 1/500.

For a steel plate shear wall, according to Von Mises's plastic theory, the yield shear stress of steel is $1/\sqrt{3}$ times the yield normal stress. The shear elastic modulus is $1/2.6$ times Young's modulus. The shear yield strain is then about 1.5 ($=2.6/1.732$) times the axial yield strain. It means that the story deformation angle becomes about 1/667 when the steel plate shear wall begins to yield and it becomes plastic at almost the same level as the small story deformation angle for the brace. It is possible to make the story deformation angle at the beginning of plastic deformation smaller for the brace and steel plate wall by using ultra-low yield steel whose yield strength is between 100 and 200 MPa.

Let us consider the yield deformation angle of a rigid joint frame comprising columns and beams, which receive an asymmetric bending moment (Figure 10.7). The total lateral deformation of a frame structure results from the effects of the following five components: bending deformation and shear deformation of columns, bending deformation and shear deformation of beams, and shear deformation of the panel zone in beam–column joint. In a regular building frame structure, the column section is usually larger than the beam section, and the column height is usually shorter than the beam span. Therefore, the column deformation is much smaller than the beam deformation. The beam bending deformation contributes approximately 50% of the total deformation of the whole frame structure. For the steel structure frame, discussion is focused on the rotational distortion occurring at the beam-ends. Let the span and the depth of the beam be L and D , respectively. Then, the deformation angle θ_y at beam-ends, when the stress of the flange reaches the yield point σ_y becomes $(\sigma_y/3E)(L/D)$ (see Figure 10.7).

$$\theta_y = \frac{M_y L}{6EI} \quad (10.5)$$

$$\sigma_y = \frac{M_y D}{2I} \quad (10.6)$$

$$\theta_y = \frac{\sigma_y L}{3ED} \quad (10.7)$$

The span L of the frame is predetermined and Young's modulus E is a constant of preselected material. Therefore, the deformation at the yield point of the frame can be increased by using steel having a high yield point σ_y and members having a smaller depth D than conventional ones. In other words, the elastic deformation capacity of a frame can be increased using a slender flexible frame manufactured by high-strength steels. As a result, the yield deformation of the moment-resistant frame can be easily determined by selecting the materials and the depth of the structural members. On the contrary, the yield deformation of the controlling members such as braces or shear walls is determined from the overall configuration

of the frame and the yielding strength of the selected material. Thus, the amount of plastic deformation cannot be increased by only adjusting the plate thickness and detailed configuration.

When the plastic deformation of the controlling or energy dissipating members are used in combination with the moment-resisting frame, neglecting problems such as brace buckling, shear failure of shear wall, etc., the following difficulties still occurred. Plastic deformations occur first in each of the controlling members (or regions of these members) rather than in the moment resisting frames, so stiffness and strength deterioration of the controlling members (braces or walls) occurs, while the strength of the frames continues to increase. Therefore, it is difficult to have a reliable estimation of the total response and strength of the structural systems.

The technology of DCS is theoretically founded on motion-based design and is consistent with the concept of performance-based design (Connor, 2003; Connor et al., 1997; Connor and Klink, 1996; Connor and Wada, 1992). This technology is not limited in the design of building structures, even in the design of industrial facilities at present, there is a trend to find better design variables to meet various design requirements. In many cases, the design requirements have to be changed during the long service period of the structure. The most important strategy of designing a structure is to simplify as much as possible the design requirements and design variables. The design strategy of DCS is based on a simple concept. The function of the building structure has two clear design requirements. One is to resist vertical gravity load, another is to resist the effects of EQGMs. In the design process, the whole building structure can be divided into two individual design variables (structural systems). One is the primary structure such as beams and columns, which are designed to resist only the vertical service load; the other is the controlling or energy dissipating system, which is designed to resist the lateral forces resulting from the effects of EQGMs.

10.3.4 Applications of EDS

Building structures must be designed to be able to withstand extremely large deformations that can occur randomly over the service life of the building. The earthquake disasters mentioned previously highlight the need to design and build strong and resilient buildings be able to withstand the effects of severe EQGMs with controlled damage to levels that will allow the function of the building to be restored as soon as possible after such severe EQGMs. Thus, in earthquake-resistant design of building structures, although the priority should be given to protection of human lives against severe rare EQGMs, it is also necessary to control the degree of structural and nonstructural damage to avoid long interruption of the function of the building, because this can result in significant economic loss. This problem has been considered very seriously by many people not only in the United States and Japan but also in other countries.

As discussed previously, the conventional seismic design of SMRF structures is based on the assumption that under severe EQGMs the regions at the ends of the beams can develop sufficiently large plastic deformation to dissipate a significant portion of the earthquake input energy. Thus, this conventional approach for SMRFs, which has been denominated as the “strong-column weak-beam” design, has so far been accepted and applied worldwide by structural engineers. Figure 10.5 shows the concept behind strong column-weak beam SMRF structures. Such structures can be treated as a system of two springs that are connected in series. The total deformation of such structure after the beam-end regions yield is the summation of the elastic deformation Δ_e and the plastic deformation of the plastic hinges Δ_p . Obviously, the plastic hinges at the beam-ends increase the total deformation of the entire structure and reduce the lateral stiffness of the whole building structure. In the United States, the maximum total deformation is limited by the requirement that the total shear or interstory deformation angle should not exceed the values of 0.020 or 0.025, depending on the structural period.

After the Northridge and Hyogoken-Nanbu earthquakes, it was observed that many steel SMRF structures were damaged, although they had been considered the ideal structural system to resist the effects of EQGMs. The main damage has been the brittle fracture at the welded region between the beam-ends and columns (Carper, 1998; Engelhardt and Sabol, 1995; Investigation Committee of Building's Damage, 1995; Krawinkler, 1994; Nakagomi, 1997; Nakagomi and Oka, 1996). Therefore, the practice of

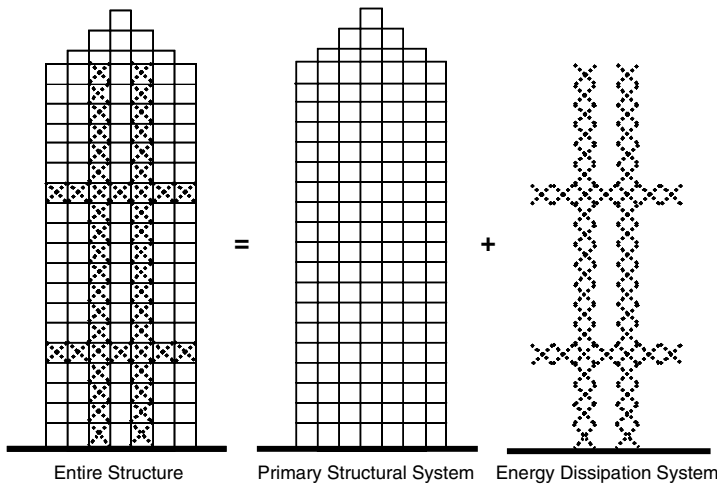


FIGURE 10.8 Concept of damage-controlled structures (DCS).

relying on the primary SMRF structure to absorb and dissipate a significant portion of the input energy of EQGM eventually results in severe damage to these primary structures. Similarly, from an economical point of view, in the case of reinforced concrete SMRF structures, the conventional practice has been just to rely on the plastic deformation at beam-ends to dissipate a large amount of the energy input from the earthquake excitation.

10.3.5 Concept of DCS

As pointed out previously, the basic concept of DCS (Wada et al., 1992, 1997) can be described as follows. The integrated entire building structural system is the combination of two different structures, as shown in Figure 10.8: One is the primary structure composed of beams and columns, which aims to resist the vertical service load. The primary structure is designed to behave elastically and to retain its building service functions even during a severe EQGM. The second is the energy dissipating or damage-controlling system that aims to control the effects of the lateral forces and deformations resulting from the EQGM. Thus, the damage induced by the EQGM is controlled by this energy dissipation system, which is easily checked and repaired or replaced after a severe EQGM.

Figure 10.9 illustrates the structural modeling of a DCS. The damage is controlled within the brace-type energy dissipation system. The primary structural frame and the damage controlling system can be considered a system of two springs connected in parallel. The total deformation of the entire structure Δ is equal to the frame deformation Δ_f and also equal to the deformation Δ_d of the energy dissipating system. The advantage of this structural system is to have a more reliable energy dissipation system with an increased energy dissipation capacity, stiffness and strength of the primary structure without increasing the total deformation of the entire structure.

Figure 10.10 compares the conventional strong column–weak beam structures and the DCS structures with an energy dissipation system (Onishi et al., 1997). For small and moderate EQGMs, the conventional structures are designed to remain elastic. This means that the natural structural damping is the only mechanism that dissipates part of the input energy of these small and moderate EQGMs. Thus, if the natural structural damping is overestimated during the design stage, the primary structure will be subjected to large deformation and force or yield even under small and moderate EQGMs. However, in the case of a DCS the presence of the stiff energy dissipation component will initially restrict the deformations of the primary structure and then as the stiff component will yield under small lateral deformations, it will dissipate a part of the EQGM input energy and it will continue controlling the deformation of the primary structural system.

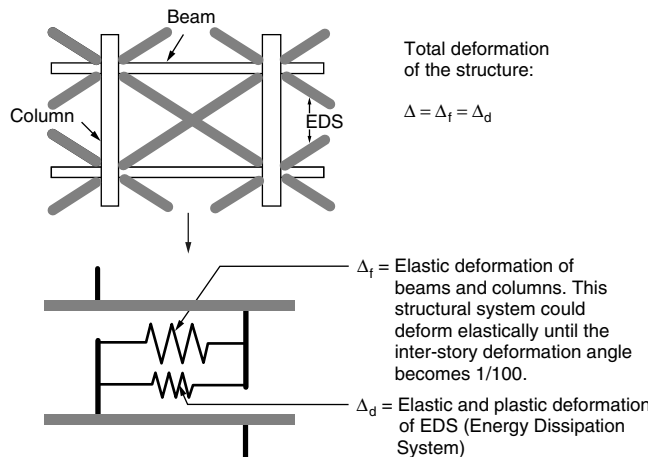


FIGURE 10.9 Structure with energy dissipating system.

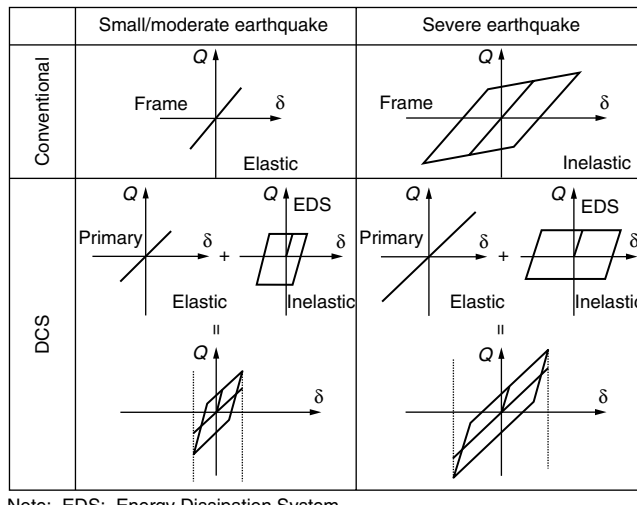


FIGURE 10.10 Comparison between conventional and DCS structural models.

Under severe EQGMs, the conventional SMRF structure relies on its own yielding capacity to dissipate the input energy, and therefore, will sustain large plastic deformations, which means a large amount of damage. The larger the demanded plastic deformations (physical ductility) the larger will be the damage of the entire SMRF system. On the other hand, if a DCS system is used, it will be possible to control the response of its primary structural system such that it remains elastic, because the energy dissipation component or system will increase the stiffness, strength and particularly the energy dissipation capacities of the entire structural system.

The advantage of the DCS is not only in protecting the primary structure from damage during a severe EQGM, but also in reducing the construction cost when compared with that of conventional SMRF. According to the report of Nikkei Architecture, “steel buildings designed as DCS the total weight of the steel can be reduced by 20%” (Nikkei, 1997). Furthermore, as it has been previously pointed out, perhaps a more important advantage of DCS is that after a severe EQGM if its energy dissipation components have been damaged, they can be quickly removed and replaced.

10.3.6 Mechanism of Unbonded Braces

The unbonded brace is a special type of energy dissipation device that was developed by Nippon Steel in Japan, 1987. The unbonded brace is an ideal steel member that is used as the steel core plate bar constrained against buckling by a concrete filled steel tube.

A type of special bond-breaking material, which is called the unbond material, is used between the concrete and core steel plate to reduce the friction action between the steel core plate and the concrete. Thus, the exterior steel tube and concrete are not subjected to the effects of the axial member force that has to be resisted by the unbonded brace. Because of this type of fabrication, the unbonded brace can have an extremely stable hysteretic behavior under both tensile and compressive forces. The stiffness and strength of a building can be adjusted to any desired value by the optimum selection of the cross-section area and strength of core steel plate.

It has been confirmed from many test results (Iwata, 1995; Iwata et al., 1995; Wada, 1988) that the unbonded brace exhibits stable hysteresis if the buckling strength (P_{cr}) of just the steel tube is higher than the product of a safety factor f_s and the yield strength (P_y) of the core steel plate.

$$P_{cr} = \frac{\pi^2 EI}{L_k^2} > f_s P_y \quad (10.8)$$

where P_y is the yield strength of the core steel plate and f_s is the safety factor (1.5 is recommended). I is the geometrical moment of inertia of the steel tube, and L_k is the unbraced length of the unbonded brace. It should be noted that the actual buckling restrained capacity of an unbonded brace depends only on the bending stiffness of the exterior steel tube and the concrete, i.e., it has nothing to do with the material strength and cross section of the core steel plate.

Figure 10.11 shows the test setup for conducting loading cycles on a steel frame only and another steel frame with unbonded brace. The frames were made of high-strength steel. The results shown in Figure 10.12 permit comparison of the hysteretic behavior of such kind of steel frames, i.e., with and without unbonded braces. Figure 10.12a shows the force-displacement hysteretic loops for the steel frame alone (MRF1). The steel frame itself yields and, because it dissipates little energy as a consequence of plastic deformations that were suffered by the frame itself, thus causes damage to the frame. Figure 10.12b shows that the steel frame with unbonded brace (MRF2) through its large hysteretic loops can dissipate a great deal of energy. The steel frame MRF1 was designed with the same strength capacity as the MRF2 plus brace. As almost all the plastic strain energy is dissipated by the unbonded brace, the response of the steel frame remains almost in its elastic range. Thus, the steel frame is not damaged.

The unbonded brace has many good features when it is properly used as a type of energy dissipation device. Some typical advantages of use of the unbonded brace are summarized as follows:

- Simple modeling of its behavior for its structural analysis
- Easy handling of its erection and assembling it to the construction of the structural system
- Stable hysteretic behavior without buckling
- Design flexibility in the selection of stiffness and strength of the entire structural system of a building

There are, however, areas that need to be further studied regarding the performance and damage of the unbonded brace system, including:

- Lack of recentering capacity and amount of permanent deformation
- Checking the damaged braces and criteria for their replacement
- Effects of three components of ground motion
- Study of reliability of connection of the braces with the frame

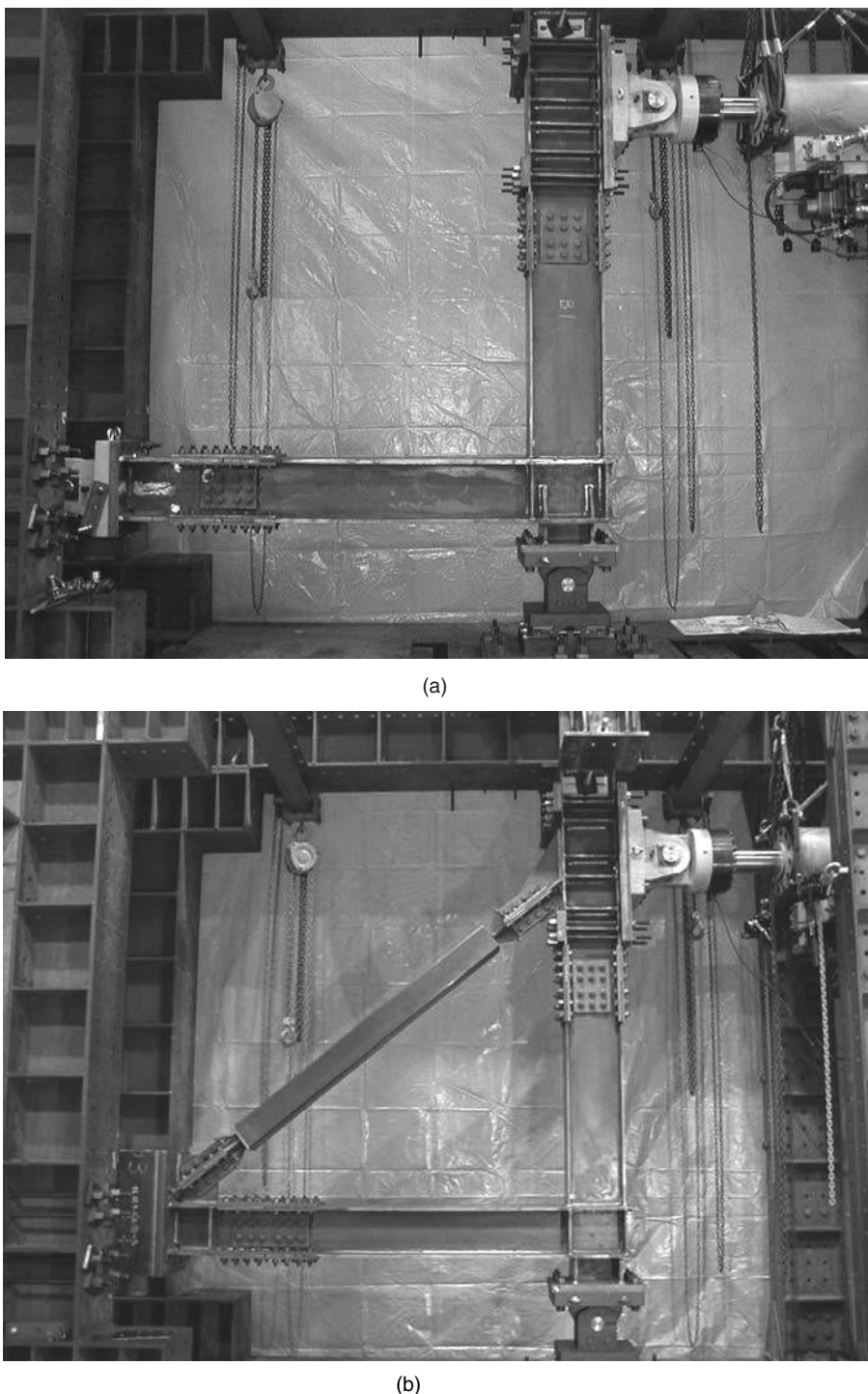


FIGURE 10.11 Test set up for cyclic loading of steel frame without and with unbonded brace. (a) Steel frame only; (b) steel frame with unbonded brace.

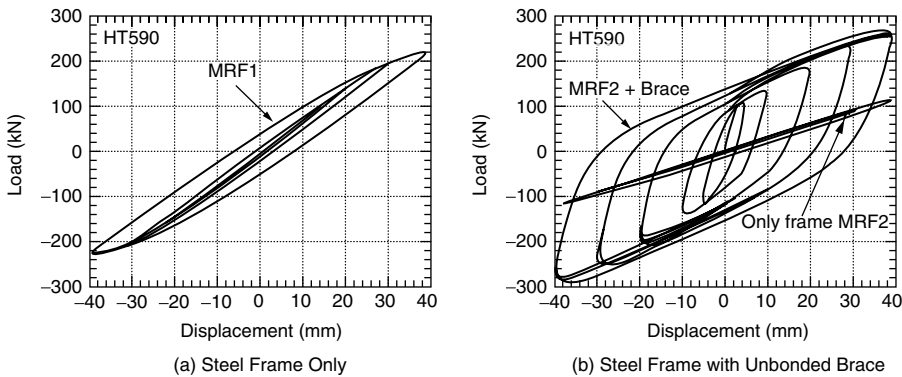


FIGURE 10.12 Hysteretic behavior of steel frames without and with unbonded brace. (a) Steel frame only; (b) steel frame with unbonded brace.



FIGURE 10.13 Central Government Building (courtesy of Kume Sekkei).

10.3.7 Applications of EDS in Tall Buildings in Japan

Since the Hyogoken-Nanbu earthquake, many building projects that were designed based on the concept of DCS has been reviewed by the Japanese Building Center. Table 10.2 provides a list of such typical projects that were designed and constructed between 1995 and 1998. Since 1999, approximately 70% of the high-rise buildings with heights more than 60 m were designed based on this concept of DCS.

10.3.7.1 Central Government Building

The Central Government Building (Figure 10.13) located in Chiyoda-ku, Tokyo, is a typical DCS combining hysteretic energy dissipation of steel shear walls and viscous fluid damper. This building was designed by the Architecture Department of the Ministry of Construction and Kume Sekkei Co., Ltd. The total height is 144.5 m (474.1 ft), including a 55 m antenna tower on the roof. The superstructure above the ground level is a moment-resisting steel frame installed with various EDS, while the underground structure is a steel reinforced concrete frame with reinforced concrete shear walls. The columns

TABLE 10.2 Tall Steel Buildings Designed Based on the Same Concept of DCS between 1995 and 1998

Month, Year	Project Name	Location	Usage	Height (m)	Structure Type	Dampers	Ductility Ratio of Primary Frame
June 1995	International Congress	Osaka	Congress	104	S_F	HD_B	0.95
July 1995	Todai Hospital	Tokyo	Hospital	82	S_F	VD_S	0.93
July 1995	Tohoku dai Hospital	Sendai	Hospital	80	S_F	VD_S	0.97
Aug. 1995	Central Government	Tokyo	Office	100	S_F	HD_S + VD_S	0.78
Oct. 1995	Harumi 1 Chome	Tokyo	Office, shop	175	S_F	HD_B	0.88
Feb. 1996	Toranomon 2 Chome	Tokyo	Office, shop	94	S_F	VD_S	0.94
Mar. 1996	Sankyo	Tokyo	Office	61	S_F	HD_B	0.88
Apr. 1996	Shiba 3 Chome	Tokyo	Office	152	S_F	HD_B	0.97
June 1996	Art Hotel	Sapporo	Hotel	96	S_F	HD_BD	0.85
Aug. 1996	Kanto Post Office	Saitama	Office	130	S_F	VD_S	0.87
Oct. 1996	Nakano Urban	Tokyo	Office, shop	96	S_F	VD_S	0.68
July 1997	DoCoMo Tokyo	Tokyo	Communication, etc.	240	S_F	VD_S	0.79
Oct. 1997	Minato Future	Yokohama	Hotel, shop, office	99	S_F	HD_BD	0.98
Nov. 1997	Nishiguchi Shintoshin	Yamagata	Office, hotel, etc.	110	S_F	HD_B	1.00
Feb. 1998	DoCoMo Nagano	Nagano	Communication	75	S_F	VD_S	0.89
Apr. 1998	East Osaka City	East Osaka	Office	120	S_F	HD_S	1.00
May 1998	Kouraku Mori	Tokyo	Office, Shop	82	S_F	HD_B	1.00
July 1998	Harumi 1 Chome	Tokyo	Office, shop, etc.	88	RC_F	HD_B	1.00
Nov. 1998	Adago 2 Chome	Tokyo	Office, shop	187	S_F	VD_B	0.71
Nov. 1998	Gunnyama Station	Fukushima	Shop, school, etc.	128	S_F	HD_B + VD_S	0.98

a



FIGURE 10.14 Art Hotel in Sapporo (with HD). (Courtesy of Kumagai Corporation.)

and beams of the primary structure used SN490B steel (maximum strength is 490 MPa or 71 ksi). The primary structure is designed to behave elastically even under a severe EQGM whose maximum ground velocity is 50 cm/sec (corresponding to A_g of 500 cm/sec²). Most of the earthquake energy is absorbed and dissipated by the energy dissipating system. The hysteretic dampers (HDs) are steel walls made of extra-low yield point steel (yield point is 100 MPa or 14.5 ksi). The yield shear force level of HDs at the first floor location is assumed to be 5% of the total building weight. The distribution of yield shear force throughout the height of the building is assumed to be proportional to the distribution of yield shear force of the primary structure. On the other hand, the viscous dampers (VD) consist of two movable steel plates hung from the upper beam and three fixed steel plates stood on the bottom beam. The space between the movable steel plates and the fixed steel plates is filled with viscous liquid like silicone oil.

10.3.7.2 Art Hotel in Sapporo

The Art Hotel in Sapporo (Figure 10.14), designed and constructed by Kumagai Corporation, is another damage-controlled building. This building is 96 m (315 ft) high and has 26 stories above the ground. The primary structure is a moment-resisting steel frame that is designed to support only the vertical service load. Two thousands of slit steel dissipation (SSD) whose shape, shown in Figure 10.15, made of mild strength steel (SN490B) with a yielding strength of 325 MPa or 47.14 ksi were installed in the building. During an earthquake shaking the SSD are subjected to shear deformations through the top and bottom bolts and consequently each slender bar experiences bending deformation and starts yielding quickly at the end parts of the bar, even under small shear deformation, because the cross section of each bar is very small. Since the yielding parts of this kind of energy dissipation are easily concentrated on the small end parts of the slender bars, the slits should be manufactured very carefully to avoid excessive local strain concentration. Because one piece of SSD is so light that someone could hold it in one hand, the biggest advantage is that the damaged SSD can be very easily replaced after a severe earthquake.

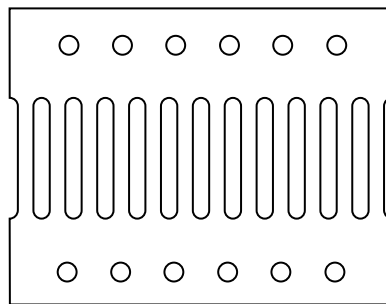


FIGURE 10.15 Details of the steel slit damper (SSD).



FIGURE 10.16 DoCoMo Tokyo Building (with viscous damper) (courtesy of NTT facilities).

10.3.7.3 DoCoMo Tokyo Building

The building shown in Figure 10.16 is located in metropolitan Tokyo. The structural design was made by NTT Power and Building Facilities, Inc. This building has two parts. The lower 27 stories are mainly used for offices, and on the upper 23 stories is the antenna that is used for mobile communication. There are also three stories under ground. The total height of the building is 240 m. The structural system of the upper 23 stories (the antenna system) consists of a steel frame and steel brace structure. The structure of the lower 27 stories is steel frame with 76 viscous damping shear walls in both X and Y directions. The supplemental viscous damping wall system has the same energy dissipation capacity as that of a natural structural damping ratio of 5% in both directions. The viscous damping wall is a high-quality, highly stable damping system that has been used in more than 10 tall building projects since it was first used in a seismic building in 1988. Because of the use of an additional viscous damping wall, the primary steel structure is designed to remain elastic even under a level-2 strong EQGM with a maximum velocity of 50 cm/sec.

10.4 Summary, Conclusions and Future Challenges

After introductory remarks about the need to use innovative strategies, technologies and materials in earthquake engineering, this chapter was devoted to discussing the current trend in Japan for the seismic

design of SMRF structures, that is, to base it on the concept of a DCS instead of just the conventional strong column–weak beam SMRF system. The basic concept for such a design is to consider the integrated building as a combination of two different structural systems: the elastic primary structure that is designed primarily to resist elastically the vertical service loads, and the energy-dissipation structural system or component to resist the effects of lateral EQGMs. The damage caused by the earthquake is controlled by the energy dissipation system. The primary structure remains elastic even during an extremely large EQGM. In this chapter, the concept and philosophy of the DCS were reviewed. Results obtained from some static cyclic loading tests of models of the main part of a steel SMRF and a damage-controlled steel frame were presented. The results clearly show the advantages of the DCS over the conventional SMRF. Selected actual building projects designed on this concept were also discussed, as well as their advantages and disadvantages.

In Japan at the present time, the concept of DCS is being applied only to high-rise buildings over 60 m (197 ft) in height. It has still not yet spread to lower-rise buildings (under 60 m [197 ft]). This is mainly because of a rule that the steel structure must be designed within the elastic region for the base shear coefficient of 0.2 associated with a moderate earthquake. Because this rule has been accepted for more than 50 years — since the end of the World War II — it is not simple to change it. As mentioned in this chapter, the brace and shear wall begins to yield when the interstory deformation angle is about 1/500. Since the primary structure can be kept in its elastic range until the interstory deformation reaches 1/200, it is reasonable to allow the braces or shear walls or both to yield. In 2004, the earthquake-resistant design method for buildings based on energy balance, which was proposed by Professor Hiroshi Akiyama (Akiyama, 1985, 2002), will be included in the National Building Design Law of Japan. According to this building design law, the plastic deformation energy dissipation will be allowed for the seismic members even for a small and moderate earthquake level. Thus, 2004 will be the year when Japanese seismic design methodology drastically changes. At last, the application of the concept of damage controlled seismic design has already begun to spread to the substructure of bridges in both Japan and the United States. It is expected to widely used by the seismic-sensitive countries worldwide.

Glossary

Absolute input energy—This represents the work done by the total base shear at the foundation on the foundation displacement.

Damage tolerant structure—The acceptable damage due to an earthquake that occurs in specific structural components (such as braces, shear walls or supplemental energy dissipating devices) that are added to what is called “primary structural system.” These damaged components are called the “sacrifice members” and function somewhat like a fuse to protect the primary structure from severe damage.

Energy dissipating devices—Special devices, elements or members installed in structures to provide energy dissipation.

Hysteretic energy due to yielding—Energy dissipated during the earthquake as a result of yielding of structural members.

Level 1 (Ground Motion)—Small and moderate EQGMs, only minor damages such as cracks in walls and beams are allowed, while human life and the building functions and structure are protected.

Level 2 (Ground Motion)—A severe rare EQGM, a building structure is allowed to be damaged provided that human life is protected.

Primary structure—The main structure consisting of beams and columns. The primary structure in damage tolerant structure mainly supports vertical dead load.

Relative input energy—This represents the work done by the static equivalent external force (which is the product of the mass and ground acceleration) on equivalent fixed-base system, that is, it neglects the effect of the rigid body translation of the structure.

Special Moment-Resisting Frame—A frame structure consisting of beams and columns, which are connected rigidly. The bending moment can be transferred by the connecting joints.

List of Symbols

A_g	maximum ground acceleration
a_{ti}	total acceleration at the i -th floor
C_V	seismic coefficient varies with soil type and location
D	depth of a beam section
DCS	damage controlled structure
DTS	damage tolerant structure
D_s	a value representing damping characteristics and ductility of building structure, for example, $D_s = 0.25$ for most ductile steel moment resisting frame; $D_s = 0.55$ for most brittle concrete wall structure.
E	Young's ratio of steel
E_D	dissipated energy
E_E	stored elastic energy
E_I	absolute input energy
E_K	absolute kinetic energy
E_S	elastic strain energy
$E_{H\xi}$	hysteretic dissipated energy due to viscous damping
$E_{H\mu}$	hysteretic dissipated energy due to yielding and friction
EDS	energy dissipation system
ENR	<i>Engineering News-record</i>
EQGM	earthquake ground motion
h_s	inter-story height
HD	hysteretic damper
HDB	brace-type hysteretic damper
HDBD	bending-type hysteretic damper like slit and honeycomb damper
HDS	shear wall type hysteretic damper
I	important factor of the building
I	second moment inertia of a beam section
L	span length of a typical beam
M	beam end bending moment
MDOF	multi-degree-of-freedom system
m_i	mass at floor i
P-BSD	performance-based seismic design
P-BSE	performance-based seismic engineering
PGA	peak ground acceleration
PGV	peak ground velocity
R	response modification factor
RCF	reinforced concrete frame
R_t	a value representing vibration characteristics according to the fundamental period of the building and ground condition, for example, for moderate ground condition, $R_t = 1.0$ when T_1 is less than 0.6 sec and $R_t = 0.96/T$ when T is larger than 1.2 sec. When $0.6 \leq T \geq 1.2$, R_t is a continuous curve connecting $R_t = 1.0$ and $R_t = 0.96/T$.
SDOF	single-degree-of-freedom system
SEAOC	Structural Engineers Association of California
SF	steel frame structure
SSD	slit steel dissipation damper
SMRF	special moment-resisting frame
T	fundamental period of the building
V	base shear
VD	viscous damper

VDB	brace type viscous damper
VDS	shear wall type viscous damper
VED	visco-elastic damper
V_g	maximum ground velocity
W	weight of the total building structure
Z	zoning factor between 0.7 and 1.0
μ	ductility ratio
σ_y	yield stress of steel
Δ_M	story deformation under severe earthquake
Δ_S	story deformation under moderate earthquake
θ_y	beam end rotation angle at starting to flange yield

References

- Akiyama H. (1985). *Earthquake-Resistant Limit State Design for Buildings*. University of Tokyo Press, Tokyo.
- Akiyama, H. (2002). *Earthquake-Resistant Design Method for Buildings Based on Energy Balance*. Gihodo Press, Tokyo (in Japanese).
- Anderson, J.J. and Bertero, V.V. (1969). Seismic behavior of multistory frames designed by different philosophies, Report UCB/EERC-69/11. Earthquake Engineering Research Center, University of California, Berkeley.
- ATC-3-06 (1978) Provisions for the development of seismic regulations for building. Applied Technology Council, Palo Alto, CA.
- ATC-17-1 (1993). *Proc. Seminar on Seismic Isolation, Passive Energy Dissipation, and Active Control*. Applied Technology Council, Redwood City, CA.
- Berg, G.V. and Thomaides, S.S. (1960). Energy consumption by structures in strong-motion earthquakes. *Proc. 2nd World Conference On Earthquake Engineering*, Vol. II, pp. 681–697.
- Bertero, V.V. (1979). Seismic performance of reinforced concrete structures. *Anales de la Academia Nacional de Ciencias Exactas, Fisicas y Naturales de Buenos Aires*, Argentina, 31, pp. 75–144.
- Bertero, V.V. (1980). Lessons learned from structures damaged in recent earthquakes. *Proc. 7th World Conference on Earthquake Engineering, Istanbul*, Turkey, Vol. 4, pp. 257–264.
- Bertero, V.V. (1982). State-of-the-art in the seismic resistant construction of structures. *Proc. Third International Earthquake Microzonation Conference*, University of Washington, Seattle, Vol. II, 767–808.
- Bertero, V.V. (1992a). Major issues and future directions in earthquake-resistant design, Report UCB/EERC-92/13. Earthquake Engineering Research Center, University of California, Berkeley.
- Bertero, V.V. (1992b). Seismic upgrading of existing structures. *Proc. Tenth World Conference on Earthquake Engineering*, Vol. 9. Balkema, Rotterdam, pp. 5101–5106.
- Bertero, V.V. (1995). Seismic upgrading of existing buildings. *Proc. Simposio Internacional de Ingeniería Civil, a los 10 Años de los Sismos de 1985*, Sociedad Mexicana de Ingeniería, Sísmica, AC Mexico, D.F., Mexico.
- Bertero, V.V. (1996). Overview of seismic risk reduction in urban areas: role, importance, and reliability of current U.S. seismic codes, performance-based seismic engineering. *Proc. PRC-USA Bilateral Workshop on Seismic Codes*, pp. 10–48.
- Bertero, V.V. (1997a). State-of-the-art report on the use of innovative strategies and techniques to reduce seismic risk. Earthquake Engineering Research Center, University of California, Berkeley.
- Bertero, V.V. (1997b). Performance-based seismic engineering: A critical review of proposed guidelines. In: *Seismic Design Methodologies for the Next Generation of Codes* (Fajfar and Krawinkler, Eds.), Balkema, Rotterdam and Brookfield, Vermont, pp. 1–32.
- Bertero, V.V. (2002). Innovative approaches to earthquake engineering. *Innovative Approaches to Earthquake Engineering* (Oliveto, G., Ed.), WIT Press, Southampton, UK (Chapter 1).

- Bertero, R.D. and Bertero, V.V. (1992). Tall reinforced concrete buildings: Conceptual earthquake-resistant design methodology, Report UCB/EERC-92/16, Earthquake Engineering Research Center, University of California, Berkeley.
- Bertero, R.D., Bertero, V.V. and Teran-Gilmore, A. (1996). Performance-based earthquake-resistant design based on comprehensive design philosophy and energy concepts. *Proc. Eleventh World Conference on Earthquake Engineering*, Pergamon, Elsevier Science Ltd., Paper No. 611, London, U.K.
- Bertero, V.V. and Whittaker, A.S. (1989). Seismic upgrading of existing buildings. *Proc. 5as Jornadas Chilenas de Sismología e Ingeniería Antisísmica*, Vol. 1, pp. 27–46, Santiago, Chile.
- Carper, K.L. (1998). Lessons learned from the 1994 Northridge earthquake: Performance of steel moment frames. *Journal of Performance of Constructed Facilities*, 12(4), 171.
- Connor, J.J. (2003). *Introduction to Structural Motion Control*. Prentice-Hall, Upper Saddle River, NJ.
- Connor, J.J. and Klink, B.S.A. (1996). *Introduction to Motion Based Design*. Computational Mechanics Publications, Southampton, U.K., and Boston.
- Connor, J.J. and Wada, A. (1992). Performance based design methodology for structures. International Workshop on Recent Development in Base-Isolation Techniques for Buildings, Tokyo, pp. 57–70.
- Connor, J.J., Wada, A., Iwata, M. and Huang, Y.H. (1997). Damage-controlled structures. I: Preliminary design methodology for seismically active regions. *Journal of Structural Engineering*, ASCE, 123(4), 423–431.
- Constantinou, M.C., Soong, T.T. and Dargush, G.F. (1998). Passive energy dissipation systems for structural design and retrofit. Monograph Series, Multidisciplinary Center for Earthquake Engineering Research, Buffalo, NY, 1299pp.
- Engelhardt, M.D. and Sabol, T.A. (1995). Lessons learned from the Northridge earthquake: Steel moment frame performance. *Proc. Symposium on a New Direction in Seismic Design*, Tokyo, pp. 1–14.
- FEMA-273 and 274 (1997). NEHRP Guidelines for the Seismic Rehabilitation of Buildings. Federal Emergency Management Agency, Washington, DC.
- FEMA-356 (2000). Prestandard and Commentary for the Seismic Rehabilitation of Buildings. Federal Emergency Management Agency, Washington, DC.
- Gillengerten, J.D. (2001). Design of nonstructural systems and components. In: *The Seismic Design Handbook*, 2nd ed. (Naeim, F., Ed.), Kluwer, Boston.
- Hanson, R.D., Aikens, I., Nims, D.K., Richter, P.J. and Bachman, R. (1993). State-of-the-art and state-of-the-practice in seismic energy dissipation. Report, ATC 17-1. *Proc. ATC-17-1 Seminar on Seismic Isolation, Passive Energy Dissipation, and Active Control*, Applied Technology Council, Redwood City, California, Vol. 2, pp. 449–471.
- Hanson, R.D. and Soong, T.T. (2001). Seismic design with supplemental energy dissipation devices. Monograph, MNO-8. Earthquake Engineering Research Institute, Oakland, CA.
- Housner, G.W. (1956). Limit design of structures to resist earthquakes. *Proc. World Conference on Earthquake Engineering*, Berkeley, California, pp. 5.1–5.13.
- Housner, G.W., Bergman, L.A., Caughey, T.K., Chassiakos, A.G., Claus, R.O., Masri, S.F., Skelton, R.E., Soong, T.T., Spencer, B.F. and Yao, J.T.P. (1997). Structural control: Past, present and future. *Journal of Engineering Mechanics*, ASCE, 123(9), 897–971.
- Huang, Y.H. (1995). Damage controlled seismic design for tall steel buildings, Doctoral Dissertation, Tokyo Institute of Technology, Tokyo, Japan.
- Huang, Y.H., Wada, A. and Iwata, M. (1994). Damage tolerant structures with hysteretic dampers. *Journal of Structural Engineering*, 40B, 221–234.
- International Conference of Building Officials (1988). Uniform Building Code, Vol. 2.
- Investigation Committee of Building's Damage, AIJ. (1995). An interim report of Hyogoken-Nanbu earthquake of 1995 (in Japanese).
- Iwata, M. (1995). Applications of various structural steels to seismic design. *Proc. Symposium on a New Direction in Seismic Design*, Tokyo, pp. 171–194.
- Iwata, M., Huang, Y.H., Kawai, H. and Wada, A. (1995). Study on the damage tolerant structures. *Journal of Technology and Design*, Architectural Institute of Japan, 1, 82–88.

- Johnson, G.S. (2003). Equipment and systems. *Earthquake Engineering Handbook* (Chen and Scawthorn, Eds.), CRC Press, Boca Raton, FL, Ch 20.
- Krawinkler, H. (1994). Preliminary observations and thoughts on building damage in the January 17, 1994 Northridge earthquake. Flash of the Investigation on the Disaster of Northridge Earthquake in 1994, AIJ, Tokyo, pp. 73–82.
- Mayes, R.L. (1996). Seismic isolation retrofit of buildings and bridges. *Proc. International Conference on Retrofitting of Structures*, Columbia University, New York, pp. 230–247.
- Mayes, R.L. and Naeim, F. (2001). Design of structures with seismic isolation. In: *The Seismic Design Handbook*, 2nd ed. (Naeim, F., Ed.), Kluwer, Boston.
- Nakagomi, T. (1997). Failure characteristics of steels. The Trend and Review of Structural Design for External Dynamic Load, AIJ, Tokyo, pp. 298–303 (in Japanese).
- Nakagomi, T. and Oka, M. (1996). Experimental study on effect of the strain velocities on mechanical properties of beam-to-column welded connections (Part I and II). Summaries of Technical Papers of Annual Meeting Architectural Institute of Japan. Vol. C-1, pp. 637–640 (in Japanese).
- Needham, J. (1971). *Science and Civilization in China*, Vol. 4, Part 3. Cambridge University Press, London, UK.
- Nikkei Architecture (1997). Art Hotel Sapporo, two thousand hysteretic dampers reduce 20% steel weight. No. 588, pp. 202–205 (in Japanese).
- Oliveto, G. (2002). *Innovative Approaches to Earthquake Engineering*. WIT Press, Southampton, U.K.
- Onishi, Y., Hayashi, K., Huang, Y.H., Iwata, M. and Wada, A. (1997). Cyclic behaviors of welded beam-column connections used in the damage tolerant structures. *Journal of Structure and Construction Engineering*, AIJ, 501, 143–150.
- Park, R. and Paulay, T. (1975). *Reinforced Concrete Structures*. John Wiley & Sons, New York.
- Paulay, T. and Priestley, M.J.N. (1992). *Seismic Design of Reinforced Concrete and Masonry Buildings*. Wiley, New York.
- Reina, P. and Normile, D. (1997). Fully braced for seismic survival, Cover story seismic design. *Engineering News Record*, July, 34–36.
- SEAOC Vision 2000 Committee (1995). Performance-based seismic engineering of buildings. Report, Structural Engineers Association of California, Sacramento, CA.
- Soong, T.T. and Constantinou, M.C. (1994). *Passive and Active Structural Vibration Control in Civil Engineering*. Springer-Verlag, New York.
- Soong, T.T. and Dargush, G.F. (1997). *Passive Energy Dissipation Systems in Structural Engineering*. John Wiley & Sons, New York.
- Steel Committee of Kinki Branch (1995). Investigation Report on the Damage of Steel Building Structures During 1995 Hyogo-ken Nanbu Earthquake. AIJ (in Japanese)
- Uang, C.-M., Bertero, V.V. (1988). Use of energy as a design criterion in earthquake-resistant design. Report UCB/EERC-88/18. Earthquake Engineering Research Center, University of California, Berkeley.
- Wada, A. et al. (1988). Study on the buckling-restrained unbonded braces by use of concrete filled steel tube. *Journal of Structural Engineering*, 34B, 249–258 (in Japanese).
- Wada, A., Connor, J.J., Kawai, H., Iwata, M. and Watanabe, A. (1992). Damage tolerant structures. Fifth US-Japan Workshop on the Improvement of Building Structural Design and Construction Practices, pp. 1–12.
- Wada, A. and Huang, Y.H. (1995). Preliminary seismic design of damage tolerant tall building structures. *Proc. Symposium on A New Direction in Seismic Design*, Tokyo, pp. 77–93.
- Wada, A., Huang, Y.H. and Nakamura, H. (1998). Dynamic analysis of three dimensional elastic frames incorporating passive energy dissipation systems. *Proc. Second Japan-UK Workshop on Implications of Recent Earthquakes on Seismic Risk*, Tokyo Institute of Technology, Tokyo, pp. 317–328.
- Wada, A., Iwata, M. and Huang, Y.H. (1997). Seismic design trend of tall steel buildings after the Kobe earthquake. *Passive Energy Dissipation and Control of Vibrations of Structures*, Taormina, Italy, pp. 251–269.

11

Seismic Isolation

11.1	Historical Development of Seismic Isolation	11-1
11.2	Theoretical Basis of Seismic Isolation	11-7
11.3	Seismic Isolation Hardware.....	11-10
	Elastomeric-Based Systems • Low-Damping Natural and Synthetic Rubber Bearings • Lead-Plug Bearings • High- Damping Natural Rubber (HDNR) Systems • Other Elastomeric Isolators • Isolation Systems Based on Sliding • Electricité-de-France System • EERC Combined System • The TASS System • Friction Pendulum System • Spring- Type Systems • GERB System • Sleeved-Pile Isolation System	
11.4	Earthquake Regulations for Seismically Isolated Structures	11-17
11.5	Response of Base-Isolated Buildings to Earthquakes... Response of Buildings to the 1994 Northridge Earthquake • Response of Base-Isolated Buildings in Kobe Earthquake	11-20
11.6	Future Challenges for Seismic Isolation	11-27

James M. Kelly

11.1 Historical Development of Seismic Isolation

Many mechanisms, invented over the past century to protect buildings from damaging earthquakes, use some type of support that uncouples them from the ground. Several ideas were proposed to allow a building to slide, for example, using rollers, layers of sand or similar materials. Some examples of buildings built on rollers include a building in Sevastopol, Crimea, and a five-story school in Mexico City, Mexico. However, one building in China has a sand layer between the foundation and the building, specifically designed to allow the building to slide in the event of an earthquake.

These buildings are early examples of innovative earthquake-resistant designs referred to as *base isolation* or *seismic isolation*. Now, widely accepted in earthquake-prone regions of the world for protecting structures from strong ground motion, recent examples of base-isolated construction include structures in Armenia, Chile, China, Indonesia, Italy, Japan, New Zealand, the United States and Uzbekistan.

The concept of base isolation is quite simple. The isolation system reduces the effect of the horizontal components of the ground acceleration by interposing structural elements with low horizontal stiffness between the structure and the foundation. This gives the structure a fundamental frequency that is much lower than both its fixed-base frequency and the predominant frequencies of the ground motion. The first dynamic mode of the isolated structure involves deformation only in the isolation system, the structure above being, for all intents and purposes, rigid. The higher modes producing deformation in the structure are orthogonal to the first mode and, consequently, to the ground motion. These higher modes do not participate in the motion, so that if there is high energy in the ground motion at these higher frequencies, this energy cannot be transmitted into the structure. The isolation system does not absorb the earthquake energy, but deflects it through the dynamics of the system. Although a certain

11-2 Earthquake Engineering: From Engineering Seismology to Performance-Based Engineering

level of damping is beneficial to suppress any possible resonance at the isolation frequency, the concept of isolation does not depend on damping. In fact, excessive damping can reduce the effectiveness of the isolation system by acting as a conduit for energy to be induced in the higher modes of the isolated structure.

Most recent examples of isolated buildings use multilayered laminated rubber bearings with steel reinforcing layers as the load-carrying component of the system. Because of the reinforcing steel plates, these bearings are very stiff in the vertical direction but are soft in the horizontal direction, thereby producing the isolation effect. These bearings are easy to manufacture, have no moving parts, are unaffected by time, and resist environmental degradation.

Many isolation systems, particularly those used in New Zealand and Japan, combine natural rubber bearings with low internal damping and some form of mechanical damper. These include hydraulic dampers, steel bars, steel coils, or lead plugs within the bearing itself. There are several drawbacks to using dampers for isolating structures: every type of damper — except the internal lead plug — requires mechanical connectors and routine maintenance, the yielding of metallic dampers introduces a nonlinearity into the response that complicates the analysis of the dynamic response of the isolated building, and dampers reduce the degree of isolation by causing response in higher modes.

In the United States the most commonly used isolation system is the lead-plug rubber bearing. These bearings are multilayered, laminated elastomeric bearings with lead plugs inserted into one or more circular holes. The lead plugs are used to incorporate damping into the isolation system. Although some isolation systems are composed of only lead-plug rubber bearings, in general they are used in combination with multilayered elastomeric bearings (which do not have lead plugs).

Another method of incorporating damping into an isolation system is to include damping in the elastomer itself. Buildings in the United States, Italy, Japan, China and Indonesia have been isolated using these high-damping natural rubber bearings. The simplicity of this approach is such that its use can be expected to spread rapidly.

The first base-isolated building to be built in the United States used this type of isolator. Located in the city of Rancho Cucamonga about 97 km east of downtown Los Angeles, the Foothill Communities Law and Justice Center (FCLJC), shown in Figure 11.1, is a legal services center for the County of San Bernardino. In addition to being the first base-isolated building in the United States, it was also the first building in the world to use isolation bearings made from high-damping natural rubber. The FCLJC, designed with rubber isolators at the request of the County of San Bernardino, is only 20 km from the San Andreas fault, which runs through the county. Because this fault is capable of generating very large earthquakes on its southern branch, the county has had for many years one of the most thorough earthquake preparedness programs in the United States.

The second most common type of isolation system uses sliding elements. This approach assumes that a low level of friction will limit the transfer of shear across the isolation interface — the lower the coefficient friction, the lesser the shear transmitted. The earliest and simplest of all the proposed systems, it is not without its drawbacks. To provide adequate resistance to wind load and avoid unnecessary movement under small earthquakes or other disturbances, a fairly high value of frictional coefficient is needed. Many frictional surfaces have sliding characteristics sensitive to pressure and to the relative velocity of slip; because the slip process is intrinsically nonlinear, a proper dynamic analysis must also be nonlinear. Furthermore, any sudden change in the stiffness of the overall structure when slipping or sticking occurs has the effect of generating high-frequency vibrations in the structure — vibrations at frequencies that might not be present in the ground motion. The system responds by transforming low-frequency energy in the ground motion into high-frequency energy in the structure.

Another problem with using sliders — and only sliders — in an isolation system is that there is no effective restoring force, thus, the code requirements for the displacement are extremely large. Because this displacement can be in any horizontal direction, the diameter of the bearing plates and the support system must be very large. In addition, the superstructure components bearing on the isolators must be designed for large moments caused by these large displacements.



FIGURE 11.1 Foothills Community Law and Justice Center, Rancho Cucamonga, California: the first base-isolated building in the United States.

There are several ways to introduce a restoring force capability. For example, Kelly (1982) proposed combining sliders and elastomeric bearings, thereby taking advantage of the best features of both types of isolator. Using sliders produces a system with a long period: the rubber bearings control the displacement by providing a centering action, they control torsion, and, if the displacements exceed the design level, they produce a stiffening action. This slider-elastomer combination was used in the seismic rehabilitation of the Mackay School of Mines completed in 1992 at the University of Nevada at Reno (Way and Howard, 1990) and for the Martin Luther King, Jr./Drew Hospital (Watts, California), which uses high-damping rubber isolators and lead-bronze sliders.

Another strategy to produce a restoring force capability in a sliding isolator is to curve the sliding surface. The friction pendulum system (FPS) is a sliding isolation system where the weight of the structure is carried on spherical sliding surfaces that slide relative to each other when the ground motion exceeds a threshold level. The recentering action is generated by raising the building when sliding occurs on the spherical surface. Developed in 1986 (Zayas et al., 1987), this system was first used to retrofit a four-story apartment building in San Francisco badly damaged in the 1989 Loma Prieta, California, earthquake. The retrofit involved installing a steel moment-resisting frame at ground level that supports the upper three floors of a wood-framed structure. Isolators were placed under the columns of the steel frame.

The FPS was also used to seismically retrofit the U.S. Court of Appeals building (Figure 11.2) in San Francisco (Amin and Mokha, 1995). Built in 1905, this five-story, $32,516 \text{ m}^2$ building survived the 1906 San Francisco earthquake. The original structure is a steel gravity frame with unreinforced granite and brick masonry walls. The FPS isolators are installed under the existing steel columns with new concrete for each column and a new rigid diaphragm system above the isolation level. There are now many isolated buildings, both new and retrofit that use the FPS. Recent examples of new construction include the Hayward, California, City Hall and the San Francisco Airport International Terminal building.

Japan is at the forefront of applying isolation method for earthquake-resistant design, with the completion of the first large base-isolated building in 1986. All base isolation projects in Japan are approved by a standing committee of the Ministry of Construction. Many of the completed buildings have experienced earthquakes, and in some cases it has been possible to compare their response with adjacent conventionally designed structures. In every case the response of the isolated building has been highly



FIGURE 11.2 The U.S. Court of Appeals Building in San Francisco, California: retrofitted by friction pendulum isolators.

favorable, particularly for ground motions with high levels of acceleration. Natural rubber bearings with mechanical dampers or lead-plug rubber bearings is the system most commonly used in the past; however, use of high-damping natural rubber isolators is increasing.

The isolation method continues to increase in Japan, especially in the aftermath of the 1995 Kobe earthquake. The superior performance of the West Japan Postal Computer Center has led to a rapid increase in the number of applications for permits for base-isolated buildings, especially for apartment buildings and condominiums.

To date, most base isolation applications have focused on large structures with sensitive or expensive contents, but there is an increasing interest in the application of this technology to public housing, schools and hospitals in developing countries. The challenge in such applications is to develop low-cost isolation systems that can be used in conjunction with local construction methods, such as masonry block and lightly reinforced concrete frames. A number of base-isolated demonstration projects have been completed, are currently under construction, or are in the planning phase. In most cases, an identical structure of fixed-base construction was built adjacent to the isolated building to compare their behavior during earthquakes. There are completed demonstration projects in Italy, Chile, China, Indonesia and Armenia (Taniwangsa, 2002). The demonstration building in Indonesia (Figure 11.3) was funded by the United Nations Industrial Development Organization.

Although isolation techniques have been used for new construction of recently completed buildings, the 1989 Loma Prieta and 1994 Northridge earthquakes in California stimulated much interest in applying these techniques for the retrofit of historic structures. A basic dilemma exists in restoring historic buildings vulnerable to strong ground shaking or damaged in the past by earthquakes. The conservation architect, concerned primarily with preserving a building's historical and cultural value by maintaining its original aesthetic, is adamant for minimum intervention and the conservation of the original structural forms and materials. Safety of the structure is a secondary consideration.

In contrast, the structural engineer is equally adamant to strengthen the structure to a level that will protect life safety and minimize future damage to the repaired structure. Because structural engineers are more familiar with modern structural forms — such as reinforced concrete — than with the masonry



FIGURE 11.3 UNIDO demonstration base-isolated building in Indonesia.

structural forms of most historic buildings, they look to these modern systems to produce the strength required to resist earthquake attack and, equally important, to satisfy code requirements or regulations. But such retrofit strategies often require massive intervention of the original fabric. This conflict must be resolved in a way that satisfies both the restoration architect's need for minimum intervention and for retrofit techniques that are reversible at a later date if necessary, in addition to providing adequate seismic protection that addresses the structural engineer's concern for life safety and code compliance.

Because the structural systems of historic buildings tend to be stiff but brittle, their dynamic behavior tends to amplify the high-frequency components of earthquake shaking, making them vulnerable to those harmonics of the ground motion. An isolation system protects the building from the most dangerous frequencies by producing a low-frequency response. In addition, the seismic isolation alternative reduces the seismic loading on the structure, thereby lowering the earthquake demand. Using isolation to repair and retrofit historical buildings satisfies both the conservation architect's demand to repair structures using original construction methods and materials and the engineer's demand to mitigate hazard from future earthquakes. Furthermore, the process is reversible and the isolation system replaceable. Thus, if a superior form of isolation system is developed in 10 or 100 years, it may replace the current system. Seismic isolation is the only technique currently available that provides seismic protection for historic buildings with minimal intervention.

The first seismic isolation retrofit of a monumental historic building was the restoration in 1989 of the City and County Building in Salt Lake City (Allen and Bailey, 1988) (Figure 11.4). The building is an architectural style called Richardsonian Romanesque and was built in 1894. It is around 160,000 ft with five floors and a 240 ft central tower. The building is unreinforced masonry and was recognized for many years as very inadequate in seismic strength particularly in view of its proximity to the Wasatch fault. Several different rehabilitation schemes were studied for the building. All conventional approaches were found to be very destructive of fabric of the building and in 1984 the idea of using seismic isolation as a less destructive alternative was proposed. A base isolation scheme was developed by Forell/Elsesser



FIGURE 11.4 City and County Building, Salt Lake City, Utah: the first historic building retrofitted by base isolation.

Engineers of San Francisco, under the direction of E. W. Allen and Associates of Salt Lake City, the engineers of record. The implementation of the retrofit scheme was completed in 1989.

Following the successful completion of this project many other seismic isolation retrofits of large historic public buildings have been carried out. These include the United States Court of Appeals Building in San Francisco, Oakland City Hall, San Francisco City Hall and Los Angeles City Hall. Other recently completed projects are the 1906 Hearst Memorial Mining Building on the Berkeley campus of the University of California (Figure 11.5) and the new Asian Art Museum in San Francisco, which is the

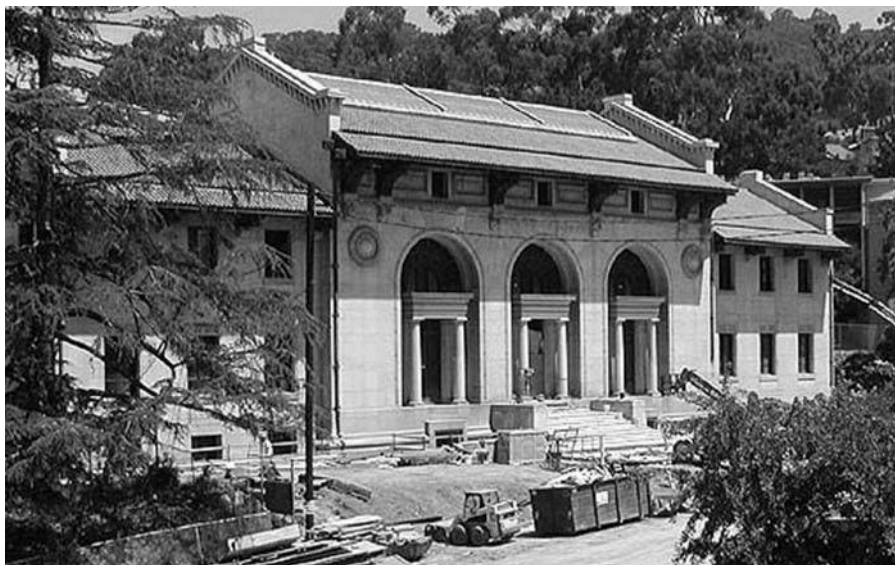


FIGURE 11.5 Hearst Memorial Mining Building on the University of California, Berkeley Campus. An example of base isolation retrofit.

retrofitted former Main Library. The replacement for this building, the new Main Library, is also a base-isolated building.

Increasing acceptance of base isolation throughout the world will lead to many more applications of this technology. The initial scepticism so prevalent when isolation systems were initially proposed is no longer evident. Many of the completed base-isolated buildings have experienced earthquakes and their performance has been as predicted. With the exception of the USC Medical Center in the 1994 Northridge earthquake and the West Japan Postal Center in the 1995 Kobe earthquake, these earthquakes have been either nearby and small or have been moderate and distant, so that the accelerations experienced by isolated structures have not been large. As more isolated buildings are built in earthquake-prone regions of the world, we can anticipate learning more about the behavior of such structures, and it will be possible to reduce the degree of conservatism currently employed in the design of these structures.

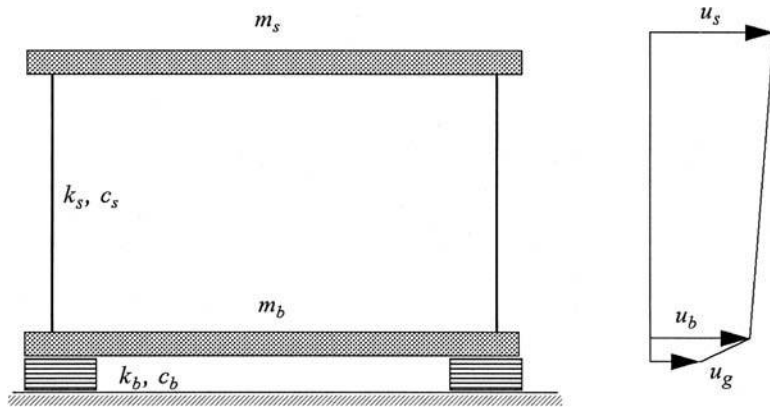


FIGURE 11.6 Parameters of two-degree-of-freedom isolation system model.

11.2 Theoretical Basis of Seismic Isolation

Insight into the behavior of an isolated building can be obtained by using a simple 2-DOF model in which a mass, m_s , representing the superstructure of a building is carried on a linear structural system on a base mass, m_b , which in turn is supported on an isolation system. All the structural elements are assumed to be linearly elastic with linear viscous damping. Because most isolation systems are intrinsically nonlinear, this analysis will be only approximate for such systems; the effective stiffness and damping will have to be estimated by some equivalent linearization process. The parameters of the model are shown in Figure 11.6.

A very detailed analysis of the response of this model to ground motion input is given by Kelly (1990). The important results are summarized here. The main results are expressed in terms of relative displacements, v_s, v_b derived from the absolute displacements, u_s, u_b, u_g , by $v_s = u_s - u_b$ and $v_b = u_b - u_g$.

The fixed-base structural frequency, $\omega_s = \sqrt{k_s/m_s}$, and the isolation frequency (the frequency if the superstructure were rigid), $\omega_b = \sqrt{k_b/(m_s + m_b)}$, are assumed to be very widely separated. Parameter $\epsilon = \omega_b^2/\omega_s^2$ characterizes this separation between the two frequencies and varies between 10^{-1} and 10^{-2} . A mass ratio $\gamma = m_s/(m_s + m_b)$, is also required and is always less than 1.

The damping factors for the structure and isolation system, β_s and β_b , respectively, where $\beta_s = c_s/(2m_s\omega_s)$ and $\beta_b = c_b/(2\omega_b(m_s + m_b))$, are of the same order of magnitude as ϵ . The frequencies of the combined system, denoted by ω_b^* (the shifted isolation frequency) and ω_s^* (modified structural frequency), are given by

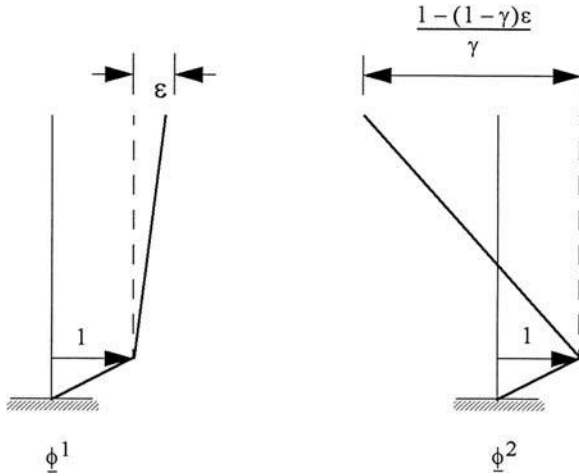


FIGURE 11.7 Mode shapes of two-degree-of-freedom isolation system model.

$$\omega_1^2 = \omega_b^{*2} = \omega_b^2 \left(1 - \gamma \omega_b^2 / \omega_s^2\right)$$

and

$$\omega_2^2 = \omega_s^{*2} = \frac{\omega_s^2}{1 - \gamma} \left(1 + \gamma \omega_b^2 / \omega_s^2\right).$$

In many cases it may be sufficiently accurate to take approximations for the first terms $\omega_b^* = \omega_b$ and $\omega_s^* = \omega_s / (1 - \gamma)^{1/2}$. The isolation frequency is affected only slightly by flexibility in the structure — of order ϵ — while the structural frequency is significantly increased by the presence of the base mass, i.e., the separation between the isolation frequency and the fixed-base structural frequency is increased by combining the two elements.

The mode shapes, $\underline{\phi}_b^i$, ($i = 1, 2$), with $\underline{\phi}_b^1 = 1$, are $\underline{\phi}_b^1 = (1, \epsilon)^T$ and $\underline{\phi}_b^2 = \left(1, -\frac{1-(1-\gamma)}{\gamma} \epsilon\right)^T$. As shown

in Figure 11.7, the structure is nearly rigid in $\underline{\phi}_b^1$, whereas $\underline{\phi}_b^2$ involves deformation in both the structure and the isolation system, with the displacement of the top of the structure of the same order as the base displacement, but opposite in direction.

The frequency of the first mode can be thought of as the modification (due to the flexibility of the superstructure) of the frequency of the isolated model when the structure is rigid, and because the structure is stiff as compared to the isolation system, the modification is small. The second mode is very close to a motion where the two masses, m_s , m_b , are vibrating completely free in space about the center of mass of the combined system. The frequency of this vibration is given by $\omega_s (1 - \gamma)^{-1/2}$ and is modified by the second term $\gamma \omega_b^2 / \omega_s^2$, which comes from the stiffness of the isolation system. The practical significance of this result is that high accelerations in the second mode of an isolated structure do not need to be accompanied by a large base shear. The participation factors, L_1 and L_2 , for the two modes, retaining only terms to order ϵ , are $L_1 = 1 - \gamma \epsilon$ and $L_2 = \gamma \epsilon$.

The effective mass in the first mode is, to the same order,

$$M_1^{eff} = (m_b + m_s) [1 - \gamma(1 - \gamma)\epsilon^2]$$

or to the order ϵ , $M_1^{eff} = (m_b + m_s)$. The same computations for M_2^{eff} give

$$M_2^{eff} = (m_b + m_s) \gamma (1 - \gamma) \epsilon^2 = 0.$$

Together with the shift in the frequencies, these results reveal why the seismic isolation system is effective. The participation factor, L_2 , for the second mode, involving structural deformation, is very small, of order ϵ if the original frequencies, ω_b , ω_s , are well separated. When the frequency of the second mode shifts to a higher value than the original fixed-base frequency, this shift will take the isolated structure out of the range of strong earthquake motion if the earthquake input has large spectral accelerations at the original structural frequency. Moreover, since the participation factor for the second mode is very small, this mode is almost orthogonal to the earthquake input. Therefore, even if the earthquake does have energy at the second mode frequency, it will not be transmitted into the structure. A seismic isolation system works not by absorbing energy; it deflects energy through this property of orthogonality. Energy absorption is, of course, an important part of the behavior of an isolation system. This simple model describes energy dissipation by linear viscous damping; it is also assumed that the uncoupled equations still hold. Now the question is how to select modal damping factors β_b^* and β_s^* .

A natural rubber isolation system, e.g., provides a degree of damping in the range of 10 to 20% of critical damping, with the structure having significantly less, of the order of 2%. Generally, conventional structural analysis assumes that the damping in a structure will be 5% of critical damping, presupposing that some degree of structural and nonstructural damage will occur when a conventional structure experiences strong ground motion. A base isolation system reduces the forces experienced by the structure to such a level that no damage will occur to the structure or to nonstructural elements, such as partitions, and thus a lower value for the structural damping is appropriate.

Neglecting the off-diagonal terms, the damping factors are given by

$$\beta_b^* = \beta_b \left(1 - \frac{3}{2} \gamma \epsilon \right)$$

and

$$\beta_s^* = (\beta_s + \gamma \beta_b \epsilon^{1/2}) (1 - \gamma)^{-1/2}$$

therefore, structural damping is increased by the damping in the bearings to the order of $\epsilon^{3/2}$. The product of β_b and $\epsilon^{1/2}$ may be a significant addition and could be important if β_s is very small, thus demonstrating that damping in the isolators can contribute damping to the structural mode.

We can estimate the response of the system to specific earthquake inputs as follows. If the ground motion, \ddot{u}_g , is specified by a spectrum, $S_d(\omega, \beta)$, the displacement response spectrum for the ground motion at frequency ω and damping factor β , and retaining only the first-order terms in ϵ , we get

$$|v_s|_{max} = \epsilon S_d(\omega_b, \beta_b)$$

and

$$|v_b|_{max} = S_d(\omega_b, \beta_b).$$

Then the design base shear coefficient, C_s , defined by

$$C_s = k_s v_s / m_s = \omega_s^2 v_s$$

becomes

$$C_s = S_a(\omega_b, \beta_b) \left(1 + \frac{\epsilon}{1 - \gamma} \right)^{1/2}.$$

Note that the second term is negligible, indicating that for small ϵ and typical design spectrum, the isolation system can be designed, at least in the initial phase, for a relative base displacement of $S_d(\omega_b, \beta_b)$ and the building for a base shear coefficient of $S_a(\omega_b, \beta_b)$. The reduction in base shear as compared with a fixed-base structure, where $C_s = S_a(\omega_s, \beta_s)$, is given by

$$\frac{S_a(\omega_b, \beta_b)}{S_a(\omega_s, \beta_s)}$$

which for a constant velocity spectrum is ω_b/ω_s , or roughly of the order $\epsilon^{1/2}$; this underestimates the reduction in base shear because in general β_b will be larger than β_s .

11.3 Seismic Isolation Hardware

By now a mature technology, base isolation is used in many countries, and there are a number of acceptable isolation systems, whose mechanisms and characteristics are well understood. Nevertheless, the concept is irresistible to inventors, and many new and different systems or isolators are proposed and patented each year. Many of these new systems have been proven impractical and some might actually be lethal, but the number continues to increase year by year.

Most systems used today incorporate either elastomeric bearings, with the elastomer being either natural rubber or neoprene, or sliding bearings, with the sliding surface being Teflon and stainless steel (although other sliding surfaces have also been used). Systems that combine elastomeric bearings and sliding bearings have also been proposed and implemented.

11.3.1 Elastomeric-Based Systems

Natural rubber bearings were first used in 1969 for the earthquake protection of buildings in a three-story school in Skopje, Macedonia. The system was developed in Switzerland by a Swiss structural engineer K. Stadaucher (Staudacher et al., 1970; Staudacher, 1970), with the construction of the school funded by the Swiss Union as a gift to the people of Skopje after the devastating earthquake of 1967. The bearings, large rubber blocks without steel reinforcing plates (as is common today), compress by about 25% under the weight of the building. The bearings have a vertical stiffness only a few times the horizontal stiffness, and the rubber is relatively undamped. This system was tested on the shake table at the Earthquake Engineering Research Center (EERC) in 1982 (Staudacher, 1982). Characteristic of isolation systems of this kind, the horizontal motion is strongly coupled to a rocking motion, so that purely horizontal ground motion induces vertical accelerations in the rocking mode. The system also includes foam-glass blocks on either side of a rubber bearing, which are intended to act as fuses to prevent movement in the building under wind, internal foot traffic or low seismic input. The system is still in place and is monitored from time to time.

Since the construction of this building, many other buildings have been built on natural rubber bearings with internal steel reinforcing plates that reduce the lateral bulging of the bearings and increase the vertical stiffness. These internal steel plates, referred to as shims, provide a vertical stiffness that is several hundred times the horizontal stiffness. These multilayered elastomer bearings have been used for years to provide vibration isolation for apartment blocks, hospitals and concert halls built over subway lines or mainline railroads. Derham et al. (1975) suggested that this approach could be used to protect buildings from earthquake ground motion, and an intensive experimental and theoretical research

program was begun at EERC to develop this concept. Laminated elastomeric bearings can be differentiated into low-damping or high-damping types.

11.3.2 Low-Damping Natural and Synthetic Rubber Bearings

Low-damping natural rubber bearings (LDRB) and synthetic rubber bearings have been widely used in Japan in conjunction with supplementary damping devices, such as viscous dampers, steel bars, lead bars, frictional devices etc. The elastomer used in Japan is natural rubber, while France has used neoprene in several projects. The isolators typically have two thick steel end plates and many thin steel shims. The rubber is vulcanized and bonded to the steel in a single operation under heat and pressure in a mold. The steel shims prevent bulging of the rubber and provide a high vertical stiffness, but have no effect on the horizontal stiffness, which is controlled by the low shear modulus of the elastomer. The material behavior in shear is quite linear up to shear strains above 100%, with the critical damping in the range of 2 to 3%. The material is not subject to creep, and the long-term stability of the modulus is good.

Isolators can be manufactured with no damping and exactly linear shear behavior. Such bearings were made for an isolation system proposed for nuclear power plant application by the CEGB in the United Kingdom. These bearings, intended for use in conjunction with a viscous damper developed by the German corporation GERB (Kelly and Quiroz, 1992), were tested at EERC, and the tests confirmed that the bearings were completely linear to 150% shear strain and completely without damping. The intent of the design was to provide an isolation system that corresponded exactly to the linear viscous dynamic model. Although the rubber bearings conformed to the model, the test showed that the response of the damper was not that of a linear viscous element.

The advantages of using low-damping elastomeric laminated bearings are: they are easy to manufacture; the compounding and bonding to steel are well understood; they are easy to model; and their mechanical response is unaffected by loading rate, temperature, history or aging. The single disadvantage is that a supplementary damping system is generally needed. These supplementary systems require elaborate connections and, in the case of metallic dampers, are prone to low-cycle fatigue.

Many applications of such a system have been used in Japan. The energy dissipation elements consist of a variety of steel-yielding devices, i.e., tapered rods, coiled yielding springs, lead bars and frictional elements. A variant of this approach, the lead-plug bearing developed in New Zealand in the 1970s, is now the isolation system most frequently used in the United States.

11.3.3 Lead-Plug Bearings

The lead-plug bearing (LRB) was invented in New Zealand in 1975 (Robinson and Tucker, 1977, 1983) and has been extensively used in New Zealand, Japan and the United States. Lead-plug bearings are laminated rubber bearings similar to LDRBs, but contain holes into which one or more lead plugs are inserted. A cut-away model of an LRB is shown in Figure 11.8. The steel plates in the bearing force the lead plug to deform in shear. The lead in the bearing deforms plastically at a flow stress of around 10 MPa and provides the bearing with a bilinear response (Tyler and Robinson, 1984). The lead must fit tightly in the elastomeric bearing, which is achieved by making the lead plug slightly larger than the hole and forcing it in. Because the effective stiffness and effective damping of the LRB depend on the displacement, it is important to state the displacement when a damping value is specified or reported for an LRB. Lead-plug bearings have been extensively tested in New Zealand (Built, 1982), and there are comprehensive guidelines on their design and modelling (Ministry of Works and Development, 1983; Blakeley, 1982). These bearings have been used to isolate many buildings, and buildings using them performed well during the 1994 Northridge and 1995 Kobe earthquakes.

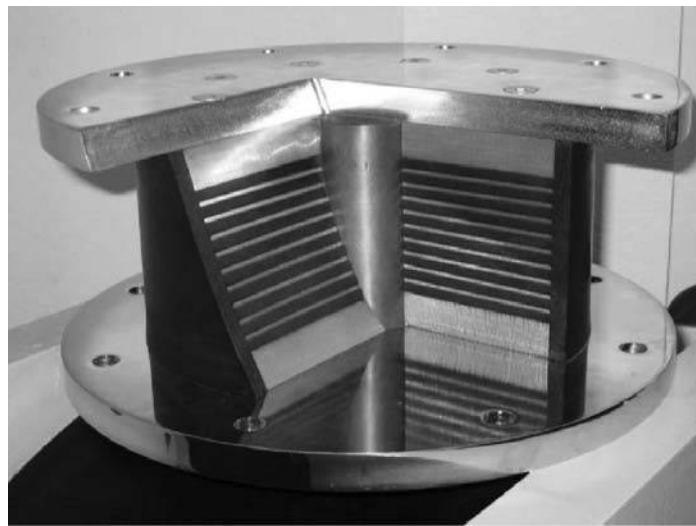


FIGURE 11.8 Cut-away model of a lead-plug isolation bearing (courtesy of DIS, Inc.).

11.3.4 High-Damping Natural Rubber (HDNR) Systems

The development of a natural rubber compound with enough inherent damping to eliminate the need for supplementary damping elements was achieved in 1982 by the Malaysian Rubber Producers' Research Association (MRPRA) of the United Kingdom (Derham et al., 1985). The damping is increased by adding extra-fine carbon black, oils or resins, and other proprietary fillers. The damping is increased to levels between 10 to 20% at 100% shear strains, with the lower levels corresponding to low hardness (50 to 55 durometer) and a shear modulus around 0.4 MPa (60 psi), and the higher levels of high hardness (70 to 75 durometer) and a high shear modulus 1.4 MPa (200 psi). The methods of vulcanization, bonding and construction of the isolators are unchanged.

The material is nonlinear at shear strains less than 20% and is characterized by higher stiffness and damping, which tends to minimize response under wind load and low-level seismic load. Over the range 20 to 120% shear strain, the modulus is low and constant. At large strains the modulus increases due to a strain crystallization process in the rubber, which is accompanied by an increase in the energy dissipation. This increase in stiffness and damping at large strains can be exploited to produce a system that is stiff for small input, fairly linear and flexible at design level input, and which can limit displacements under unanticipated input levels that exceed design levels. An example of a high-damping bearing, in this case one of the bearings for the Hearst Memorial Mining Building retrofit project, is shown in Figure 11.9.

The damping in the isolators is neither viscous, linear in frequency, nor hysteretic, independent of frequency, but somewhat in between. In a purely linear viscous element the energy dissipation is quadratic in the displacement; in a hysteretic system it tends to be linear in displacement. Tests on a large number of different rubber isolators at EERC demonstrated that the energy dissipated per cycle is proportional to the displacement raised to an exponent of 1.5. This characteristic can be exploited to model the bearing response which combines linear viscous and elastic-plastic elements (Clark and Kelly, 1996).

The material characteristics of these high-damping elastomers are somewhat more sensitive to temperature and frequency than low-damping rubber bearings (differences to these sensitivities exist between nominally similar compounds from different manufacturers). The most important characteristic of the high-damping rubber bearings is a dependence on load history (often referred to as the Mullin's effect), although some compounds have little or no manifestation of this effect. For most high-damping com-



FIGURE 11.9 Example of a high-damping rubber bearing: Hearst Memorial Mining Building retrofit project.

pounds the first cycle of several cycles at large shear strain has a higher effective stiffness and damping than in the following cycles. Generally, the characteristics of the material have stabilized by the third cycle.

The advantages to using high-damping laminated bearings are many: these bearings combine the needed flexibility and energy dissipation in a single element; they are easy to design and manufacture; and they are compact, greatly simplifying the installation process. They have been used for 20 years and are installed in a variety of buildings in Japan, the United States and Italy. There is extensive literature on testing and building performance of these bearings.

The first use of high-damping natural rubber bearings to isolate a structure was for the FCLJC in Rancho Cucamonga, California (see Section 11.1). Bearings were manufactured and tested before being installed in November 1983, and in July 1995 two bearings were removed from the building and were retested under the same test regime as before. Comparison of the 1995 test results with the original 1983 test results indicates that the bearing shear stiffness is unchanged 12 years after installation (Clark, 1997).

11.3.5 Other Elastomeric Isolators

The Sumitomo Rubber Company of Kobe, Japan, has developed an isolator that combines a standard low-damping laminated natural rubber bearing with a large internal hole, into which a central plug of a very high-damping synthetic elastomer (such as nitrile rubber) is placed. The shear modulus of the two elastomers is very close. This nitrile rubber has a much higher damping than the surrounding rubber. The diameter of the internal plug is about half that of the surrounding bearing and the effective damping of the combined system is around 18 to 20%.

A similar concept was tested at EERC using a LDRB with a central hole filled with discs of a high-damping acrylic co-polymer alternating with discs of steel. The polymer layers were of the same thickness as the rubber layers, and the steel discs were of the same thickness as the internal shims. It was determined that there was no need to bond the polymer and the steel discs; the discs ensured that the polymer was fully engaged to the rubber and provided a heat sink for the heat generated by the energy dissipated by the polymer. The elastic part of the polymer shear modulus (the storage modulus) was very close to that of the rubber and the loss factor was around 1.5. The combination produced a bearing with high energy dissipation, but with the characteristic that under slow thermal load — for example, of a bridge deck — the polymer can flow under low shear stress, making this a potentially valuable device for isolating highway bridges.

11.3.6 Isolation Systems Based on Sliding

A system using pure sliding was first proposed in 1909 by Johannes Avetian Calantariens, a medical doctor in England. He suggested separating the structure from the foundation by a layer of talc. As is evident in his diagrams, Dr. Calantariens clearly understood that the isolation system reduced accelerations in the isolated building at the expense of large relative displacements between the building and the foundation, for which he designed a set of ingenious utilities connections. In fact, Dr. Calantariens' system incorporated all the elements now considered necessary in a base isolation system: a method of decoupling the building and the foundation, a method whereby utilities lines can withstand large relative displacements, and a wind-restraint system.

Isolation was first considered as a seismic-resistant design strategy by the Italian government after the great Messino-Reggio earthquake of 1908, which killed 160,000 people in unreinforced masonry buildings — the typical building type for the area. Almost all buildings of this type collapsed (Berg, 1983). After the earthquake, a commission was appointed to make recommendations for rebuilding the area with earthquake-resistant structures that were both economical and safe. The commission considered two approaches to earthquake-resistant design: the first approach isolated the building from the ground by either interposing a sand layer in its foundation or using rollers under columns to allow the building to move horizontally; the second approach involved a fixed-based design with height limitations and a lateral force design requirement. The latter approach was recommended and sliding isolation systems were not used (Accademia dei Lincei, 1909).

However, this idea is appealing and proposed time and again. In the severe Indian earthquakes of 1930 and 1934 in Dhubai and Bihar it was observed that small masonry buildings that slid on their foundations survived the earthquake, while similar buildings fixed at the base were destroyed. Based on these observations and because small masonry buildings cannot be isolated cost-effectively using elastomeric isolators, a sliding system was proposed by Arya (1984). Considerable analysis was done on this approach, and an experimental program using a shock-type shake table (the shock produced by rolling a loaded wagon down an incline) (Arya et al., 1978, 1981) was carried out and demonstrated the effectiveness of the approach.

Chinese earthquake engineers observed the same phenomena following the devastating 1976 Tangshan earthquake. A number of multi-story buildings that survived the earthquake had a horizontal crack at the bottom of the walls that allowed a slip of around 6 cm. This was interpreted as having protected the masonry superstructure from damage. After much theoretical analysis, a 1/8 scale shake table test and a blast test on a full-size building were carried out (Li, 1984). A number of small buildings were built using this approach. The largest is a four-story dormitory building for the Earthquake Strong Motion Observatory in Beijing in which the sliding surface is a layer of specially selected sand between terrazzo plates that are located above the foundation and under the walls at the ground floor level.

A considerable amount of theoretical analysis has been done on the dynamics of structures on sliding systems subjected to harmonic input or to earthquake input. For example, as a representation of a base-isolated building, Westermo and Udwadia (1983) studied the periodic response of a linear oscillator on a Coulomb friction sliding interface. Contrary to the general perception that friction will always reduce the response, they found that the response may be larger than that for the same fixed-base model and that the single degree of freedom had subharmonic resonance frequencies generated by the sliding interface. The response of a similar model to earthquake input was studied by Mostaghel et al. (1983a, 1983b).

The assumption of Coulomb friction is generally used in these theoretical analyses, but is unlikely to be an accurate representation of real behavior. The most commonly used materials for sliding bearings are unfilled or filled Polytetrafluoroethylene (PTFE or Teflon) on stainless steel, and the frictional characteristics of this system are dependent on temperature, velocity of interface motion, degree of wear and cleanliness of the surface. Much testing work has been done on these aspects of the mechanical behavior of such sliding components (Tyler, 1977a, 1977b), and an extensive review was done by Campbell and Kong (1987).

11.3.7 Electricité-de-France System

This system was developed in the early 1970s for application to nuclear power plant facilities. The utility developed a standard nuclear power plant with the safety grade equipment qualified for 0.2g acceleration. When a plant was to be located at sites of higher seismicity, it was isolated to keep the equipment acceleration levels below the qualification value. The system combines a laminated neoprene bearing (essentially a standard bridge bearing manufactured to higher quality control standards) with a lead-bronze alloy plate in contact with stainless steel, the sliding surface being mounted on top of the elastomer bearing. The coefficient of friction of the sliding surface is supposed to be 0.2 over the service life of the isolator. The neoprene pad has a very low displacement capacity, probably not more than ± 5.0 cm. When the displacements exceed this, the sliding element provides the needed movement. The system does not include any restoring device and permanent displacements could occur. The system has been implemented only once in a large nuclear power plant at Koeberg, South Africa (Jolivet and Richli, 1977).

11.3.8 EERC Combined System

A combination elastomeric and sliding system was developed and tested on the shake table at EERC. In this system the interior columns of the structure were carried on teflon on stainless steel sliding elements and the exterior columns on the low-damping natural rubber bearings. The elastomeric bearings provided recentering capability and controlled the torsion of the structure while the sliding elements provided damping (Chalhoub and Kelly, 1990). A variant of this system was used to retrofit both the Mackay School of Mines at the University of Nevada, Reno, Nevada, and a new hospital for the County of Los Angeles, the Martin Luther King, Jr.-C. R. Drew Diagnostics Trauma Center in Willowbrook, California. Both of these structures used HDNR bearings; teflon-stainless steel sliding elements were used in the university building while lead-bronze alloy plates on stainless steel were used for the hospital.

11.3.9 The TASS System

The TASS system was developed by the TAISEI Corp. in Japan (Kelly, 1988) where the entire vertical load is carried on teflon-stainless steel elements, with laminated neoprene bearings carrying no load used to provide recentering forces. The pressure on the teflon sliding surface is around 10 MPa, and the coefficient of friction ranges from 0.05 at slow sliding speeds to around 0.15 at higher speeds. The disadvantages of this system are that because the elastomeric bearings carry no vertical load, they experience tension, and the velocity sensitivity of the sliding surface makes modelling of the system quite difficult.



FIGURE 11.10 Example of a friction pendulum bearing (courtesy of Earthquake Protection Systems, Inc.).

11.3.10 Friction Pendulum System

The friction pendulum system (FPS) is a frictional isolation system that combines a sliding action and a restoring force by geometry. The FPS isolator has an articulated slider that moves on a stainless steel spherical surface. The side of the articulated slider in contact with the spherical surface is coated with a low-friction composite material. The other side of the slider is also spherical, coated with stainless steel, and sits in a spherical cavity, also coated with the low-friction composite material. As the slider moves over the spherical surface, it causes the supported mass to rise and provides the restoring force for the system. Friction between the articulated slider and the spherical surface generates damping in the isolators. The effective stiffness of the isolator and the isolation period of the structure is controlled by the radius of curvature of the concave surface. The coefficient of friction depends on pressure and sliding velocity. The coefficient decreases with increasing pressure and becomes independent of velocities above 51 mm/sec, at pressures greater than about 20 ksi. Another aspect of the FPS is that if the displacement is less than a certain factor of the radius, the restoring force can be less than the frictional force and the system will not recenter. An example of an FPS bearing is shown in Figure 11.10. There has been extensive shake table testing of structural and bridge models on the FPS (see Mokha et al., 1990; Al-Hussaini et al., 1994; Constantinou et al., 1993).

11.3.11 Spring-Type Systems

Elastomeric and sliding isolation systems are usually configured to provide only horizontal isolation. When full 3D isolation is required, it is possible, but not common, to use elastomeric bearings. Generally, spring-type systems have been used in these cases.

11.3.12 GERB System

The GERB seismic isolation system was developed originally for the vibration isolation of power plant turbine generating equipment. Using large helical steel springs that are flexible both horizontally and vertically, the vertical frequency is around 3 to 5 times the horizontal frequency. The steel springs are completely without damping and the system is always used in conjunction with the GERB Viscodamper. As in all 3D systems, very strong coupling occurs between horizontal motion and rocking motion because the center of gravity of the isolated structure is above the center of stiffness of the isolation system. This type of system becomes practical in situations where the center of gravity and the center of stiffness are at the same level, for example, in a reactor vessel in a nuclear power plant.

The system has been tested on the shake table at Skopje, Macedonia (Huffman, 1985) and implemented in two steel frame houses in Santa Monica, California. These houses were strongly affected by the 1994 Northridge earthquake. Their response, monitored by strong-motion instruments, demonstrates that the isolation system was not effective in reducing the accelerations in these buildings due to the rocking motion (Makris and Deoskar, 1996).

11.3.13 Sleeved-Pile Isolation System

In situations where it is necessary to use deep piles, for example, for buildings on very soft soil, it can be advantageous to use these piles to provide the horizontal flexibility needed for an isolation system. The piles are made flexible by enclosing them in tubes with a suitable gap for clearance. This system was implemented in one of the earliest base isolation projects, the Union House in Auckland, New Zealand, which was completed in 1983 (Boardman et al., 1983). The building, located in an area of poor soil, required extending piles to the bedrock about 10 m below the surface. These piles are enclosed by steel sleeves with a clearance of 150 mm. The building is 12-stories tall of reinforced concrete construction with exterior bracing. The superstructure is very stiff, and the period of the building on the sleeved-pile system is around 4 sec. Damping is provided by the elastic-plastic deformation of a set of tapered steel plates arranged around the perimeter of the building at ground level. The dampers, located at the top

of the sleeved piles, react against an independently supported basement structure. The steel dampers provide elastic stiffness in addition to damping, reduce the period to around 2 sec, and provide an effective damping of about 12%.

A similar approach was used to isolate the Wellington Central Police Station (Charleson et al., 1987). Completed in 1991, this ten-story reinforced concrete braced frame structure is supported on 15 m long sleeve piles with a clearance of 375 mm. The structural system of the building uses external diagonal bracing. Because the site is very close to an active fault, the seismic requirements were quite severe. Damping is provided by 24 lead-extrusion dampers (Robinson and Greenbank, 1975), with a yield level of 250 kN and a stroke of ± 400 mm.

A variant of this system, referred to as the Damped-Sway Foundation System, was used to isolate a house in Berkeley, California, which uses sleeved piles and hydraulic viscous dampers. A rubber bumper system is also provided. The developer of the system (Langenbach, 1996), who is also the owner of the house, estimates that the system increased the cost of the house by \$15,000, which represents around 5% of the total cost of the house.

11.4 Earthquake Regulations for Seismically Isolated Structures

The first building in the United States to use a seismic isolation system was completed in 1985. Although this building was publicized in national engineering magazines and visited by a great many engineers and architects from the United States and around the world, it was several years before construction of the second base-isolated building was begun. The acceptance of isolation as an antiseismic design approach for some classes of buildings was hampered in the United States by lack of a code covering base-isolated structures. The Structural Engineers Association of Northern California (SEAONC) created a working group to develop design guidelines for isolated buildings. The Seismology Committee of the Structural Engineers Association of California (SEAOC) is responsible for developing provisions for earthquake-resistant design of structures. These provisions, published as Recommended Lateral Design Requirements and Commentary (SEAOC, 1985), generally known as the Blue Book, have served as the basis for various editions of the Uniform Building Code (UBC). Published by the International Conference of Building Officials (ICBO), it is the most widely used code for earthquake design. In 1986 the SEAONC subcommittee produced a document entitled Tentative Seismic Isolation Design Requirements (SEAONC, 1986) — known as the Yellow Book — as a supplement to the fourth edition of the Blue Book.

The approach and layout of the Yellow Book parallels the Blue Book as closely as possible. Equivalent lateral force procedures were emphasized and, as in the Blue Book, the level of seismic input was that required for the design of fixed-base structures — a level of ground motion that has a 10% chance of being exceeded in a 50-year period. Again as in the Blue Book, dynamic methods of analysis are permitted, and for some types of structures required, but the simple statically equivalent formulae provide a minimum level for the design.

The SEAOC Seismology Committee formed a subcommittee in 1988 to produce an isolation design document entitled General Requirements for the Design and Construction of Seismic-Isolated Structures (SEAOC, 1989). In 1990 this was published as an appendix to the fifth edition of the Blue Book and later adopted by ICBO as an appendix to the seismic provisions in the 1991 version of the UBC (ICBO, 1991). This version of the code includes the static method of analysis and retains a minimum level of design based on a factor of the static analysis values, but increases the number of situations where dynamic analysis is mandatory.

Another code document, developed for the design of base-isolated hospitals in California, has been adopted by the Building Safety Board (BSB) of the Office of State Architect. Titled An Acceptable Method for Design and Review of Hospital Buildings Utilizing Base Isolation (OSHPD, 1989), these guidelines were developed in part by SEAONC for the BSB and are similar to both the SEAONC requirements and the UBC code. The version adopted by the BSB in 1989 was revised in January 1992 and includes additional requirements.

The UBC code differs from the SEAONC guidelines in that it explicitly requires that the design be based on two levels of seismic input. A Design Basis Earthquake (DBE) is defined as the level of earthquake ground shaking that has a 10% probability of being exceeded in a 50-year period. The design provisions for this level of input require that the structure above the isolation system remains essentially elastic. The second level of input is defined as the Maximum Capable Earthquake (MCE), which is the maximum level of earthquake ground shaking that may be expected at the site within the known geological framework. This is taken as the earthquake ground motion that has a 10% probability of being exceeded in 100 years. The isolation system should be designed and tested for this level of seismic input and all building separations and utilities that cross the isolation interface should be designed to accommodate the forces and displacements for this level of seismic input.

A number of changes were incorporated into the 1994 version of the UBC (ICBO, 1994) regulations for isolated buildings that made these codes even more conservative in some aspects than the earlier version. The 1994 regulations restricted further the use of static analysis, although the code continued to require static analysis in all cases to provide various minimum levels below which design values obtained by dynamic analysis cannot fall. The design had to be based on two levels of earthquake input: the DBE (used to calculate the total design displacement of the isolation system and the forces in the superstructure) and the MCE (used to calculate the total maximum displacement of the isolation system for which the system must be shown to be safe). The vertical distribution of force was changed from a uniform one to a triangular one generally used for fixed-base structures. The superstructure was to be designed for forces produced by the isolation system at the design displacement reduced by certain reduction factors that were now less than the previous factors (generally one-half of those for fixed-base structures). The result of these two changes for the design forces was that the superstructure will be elastic for the DBE.

The 1994 code specified an extensive, detailed series of prototype tests that must be carried out prior to construction of the isolators. These tests were not for determining quality control in the manufacturing of the isolators, but were intended to establish the design properties of the isolation system. In many cases these tests could not be carried out on full-scale isolators due to the combination of forces, the magnitude of these forces, and the loading rates that would be needed to satisfy the requirements and reduced-scale prototypes that would have to be used. In contrast, no specific tests for production bearings were required, although a quality control test program was mandatory.

Other requirements stipulated that there should be a design review of the isolation system and testing programs for prototypes and production bearings by a peer review panel. This review of the isolation system included the earthquake inputs used for the design, the design itself and the presence of peer review panel at the prototype testing. The peer review panel was also required to review all supporting analysis for the design of the superstructure and review the quality control testing program.

Further changes have been made in the 1997 version of the UBC regulations for isolated structures (ICBO, 1997), resulting in a code that is both more conservative and more complicated. A large number of new terms have been added. For example, there are now six different displacements that have to be computed. The number of soil profile types has been increased to six, of which three are hard rock, rock and soft rock and there are three soil types. There are four seismic coefficients to be calculated, but in zone 4, where most isolated buildings in the United States are located, it is necessary to calculate two factors: N_a and N_v , which depend on seismic source type and seismic source distance, another factor M_M , which depends on ZN_v , and two other factors, C_{AM} and C_{VM} , which depend on M_M , N_a and N_v . The result is that the simple static analysis computation of the earlier versions of the code has been replaced by a sequence of table definition and formulae.

All isolated projects are currently designed using dynamic analysis (based on time histories, as there are many computer programs now available for this purpose), but static analysis is still required to ensure that the design quantities do not fall below certain minimal levels from the static analysis.

In the fixed-base code the reduction factor, R (now called response modification factor), varies widely with structural systems from a high of 8.5 through 7.5, 7.0, 6.5, 6.0, 5.5, 4.5, 4.2, 3.5, 2.8 to a low of 2.2. In the isolation regulations the reduction factor, R_I , is almost everywhere 2.0, with a few systems having

an R_i factor of 1.6. This is intended to ensure elastic behavior in the superstructure at the DBE, but is much too conservative.

The 1997 UBC was replaced in 2000 by the International Building Code (IBC), which has essentially the same provisions for seismically isolated structures, with some changes in notation, but with the same conservatism in calculating design displacements and seismic forces. The irrational use of a triangular distribution of force persists. The reduction factor for seismic-isolated superstructures is specified to be 3/8 that for conventional structures, with the maximum not to exceed 2.

One feature that has persisted through all versions of the UBC isolation regulations is the scaling of the time histories. In essence, the code (IBC 2000, section 1623.3.3.2) requires an increase of 30% in the target spectra to account for bilateral ground motion. Isolation systems are always isotropic, however, the maximum isolator displacement can be in any direction. The basic static formula for maximum displacement is intended to be applied in any direction and why the dynamic analysis should include bilateral displacements is not clear.

The extensive testing requirements for prototype isolators remain from the earlier code versions. New requirements for inspection and replacement have been added, including requirements for periodic monitoring, requirements on repair or retrofit of an isolation system and a requirement for a horizontal displacement monitoring device.

In total, the 1997 version of the UBC regulations for seismic-isolated structures turned the simple, straightforward and rational code developed in the 1986 Yellow Book into a complicated and conservative set of requirements that will seriously undermine the use of isolation technology by the general engineering community. The whole impetus for developing isolation systems, by creating cost-effective, simple strategies to create earthquake-resistant structures, is lost.

It is interesting to compare the design requirements for conventional and isolated buildings from these codes. For example, a steel special moment frame structure with a 2-sec period and 5% damping, at a soil site within 2 km (1.3 miles) of an active fault (such as the San Andreas or Hayward fault), can be designed for an ultimate strength of 7.5% of the structural weight. In contrast, a 2-sec period base-isolated building with 10% damping in the isolation system will have to be designed and tested for displacements of around 0.75 m (30 in.). If it should have a steel moment frame superstructure, the building will have to be designed for 28% of the weight of the structure. The premium for isolation is much too large to encourage use of the technology.

Primarily based on the 1997 UCB, all isolation codes are similar and riddled with the same inconsistencies. In almost all situations, the designer will have to use a dynamic analysis to conform to the codes but will have to use a static analysis first since the static analysis provides a floor level below which the values of design quantities from the dynamic cannot fall. The most important quantity from the static analysis is the DBE displacement at the center of mass. From this are calculated the various displacements for prototype and production testing and the design base shear which is calculated by multiplying this displacement by the effective stiffness of the isolation system. The first inconsistency is that the codes permit the use of high damping in the isolation system to reduce the design displacement but only the elastic force $K_{\max}D_D$ is included in the calculation of the base shear. At 50% damping (permitted in these codes) the damping force is the same as the elastic force. This provides an incentive to use highly damped systems but it is well known that damping, even linearly viscous but especially nonlinear hysteretic damping, generates response in the higher modes of the isolated structure and this in turn produces inter-story drift and floor accelerations which counteract the purpose of isolation.

A further inconsistency is that the method of equivalent linearization used to estimate effective stiffness and damping was shown many years ago (Iwan and Gates, 1979) to be highly inaccurate for systems with high ductility. The isolation system with the highest ductility for the same displacement is the FPS, where the initial yield displacement is almost zero. The effective damping in the FPS is grossly overestimated and the displacements underestimated, but ironically it is not possible to design an FPS project by solely static methods because all codes explicitly deny static design for isolation systems where the force-displacement relationship depends on the carried load — which is uniquely the case for the FPS.

The way in which the forces are distributed over the height of the building is also inconsistent. Although the theory clearly demonstrates that it should be uniform, the codes require it to be triangular, which has a major impact on the computation of the overturning moment. Most isolated buildings have a heavy floor immediately above the isolation level, but because of the triangular distribution the inertial force of this floor is not included; however, since the total inertial force must be the same as the base shear, its resultant is moved to higher levels. The overturning moment can be increased by as much as 50% compared to that from a uniform distribution, causing tensile forces on peripheral isolators, which causes further problems, including that of testing isolators in tension.

There have been further publications that include code requirements for isolated structures, for example, chapter 9 of FEMA-356 (2000) for the seismic rehabilitation of existing buildings and chapter 13 of FEMA-368 (2001) for new construction but these are essentially identical to the 1997 UBC and the 2000 IBC.

Although seismic technology is a mature technology, only a few projects each year are initiated in the United States; these are generally state, county or city projects, with not one multi-family housing project either completed or in the design stage to date. In contrast, Japan and China design and build many isolated projects each year, with a high proportion of these projects being for multi-family housing and commercial buildings.

Seismic isolation is perceived in the United States as expensive, complicated and time-consuming in both design and execution. While these criticisms are valid for many of the recent projects in which isolation has been used, the fault does not lie with the technology itself. The fault lies with the degree of over-regulation associated with the technology. Seismic isolation design is constrained by a series of code documents that are conservative, complicated and burdensome to the designer and the owner.

The benefits of using seismic isolation for earthquake-resistant design are many: isolation leads to a simpler structure with much less complicated seismic analysis as compared with conventional structures; isolated designs are less sensitive to uncertainties in ground motion; and, finally, the components are much more reliable than conventional structural components. The drawbacks to using isolation stem directly from code documents requiring the designer to use significantly larger factors of safety and, despite the availability of extensive test results on full-sized isolators of various types, testing of isolators has to be done for each new project. Because the governing codes are labyrinthian and unnecessarily conservative, professional engineers perceive that isolation design is complicated when in fact it should simplify the design process and lead to more reliable designs.

11.5 Response of Base-Isolated Buildings to Earthquakes

There are now more than 3000 seismically isolated buildings, bridges and other types of structures throughout the world with many of them having experienced earthquakes. Although most of these buildings are instrumented with strong-motion accelerographs the bridges and industrial structures generally are not. In California several instrumented buildings have experienced strong ground motion (albeit at low-level inputs), with the Foothill Communities Law and Justice Center (FCLJC), the Los Angeles County Fire Command and Control Facility (FCCF), the University of Southern California (USC) Hospital and the base-isolated retrofitted Rockwell Seal Beach Facility having experienced more than one earthquake.

The 17 January 1994 Northridge, California, earthquake (M_w 6.7) affected a large number of base-isolated structures, including the four mentioned above, several uninstrumented bridges and two houses (which are instrumented) that are isolated using the GERB system. This earthquake provided structural engineers with a wide range of information on the response of isolated structures.

11.5.1 Response of Buildings to the 1994 Northridge Earthquake

Although seismic isolation is a relatively new technology with a limited number of completed applications in the United States, several seismically isolated structures in Los Angeles area were affected by the 1994 Northridge, California, earthquake. Four steel frame buildings within 40 km of the epicenter were strongly



FIGURE 11.11 University of Southern California Teaching Hospital: base-isolated building affected by the 1994 Northridge, California, earthquake.

shaken, and strong-motion recordings at three of these buildings, which were occupied at the time of the earthquake, indicated peak ground accelerations in excess of $0.20g$. The fourth building was under construction at the time of the earthquake and had not yet been instrumented. While it is apparent that the isolation systems in these structures were activated to some extent, reconnaissance visits made to the buildings immediately after the earthquake, combined with analysis of available strong-motion data, have shown that not all of the buildings responded as intended. At three other isolated buildings 66 km and greater from the epicenter, the intensity of the ground motions was significantly lower, but strong-motion recorders were triggered at two of the sites. The recordings suggest that the isolation systems in these structures were not fully activated, resulting in some amplification of accelerations over the height of the buildings. Table 11.1 summarizes all of the isolated buildings affected by the Northridge earthquake.

The Northridge earthquake has been the most significant test of modern isolated buildings to date, providing a valuable dataset of the response of various types of structures incorporating various types of isolation systems. Summarized below is the response of the three most strongly shaken instrumented buildings, including physical evidence gathered during site reconnaissance visits. The response of the two other, more distant, instrumented buildings is not reviewed. The implications from the observed behavior on the design, construction and maintenance of isolated buildings are discussed here. Complete data and interpretation of the response of these isolated buildings can be found in Clark et al. (1996).

11.5.1.1 University of Southern California Teaching Hospital

The isolated building that best demonstrated the benefits of seismic isolation during the 1994 Northridge earthquake was the USC Teaching Hospital in eastern Los Angeles located approximately 36 km from the epicenter. The hospital, Figure 11.11, is an eight-story concentrically braced steel frame supported on 68 lead-plug rubber isolators and 81 elastomeric isolators. Design and construction details of this building are provided by Asher and Van Volkinburg (1989), Asher et al. (1990) and KPFF Consulting Engineers (1991). The foundation system consists of spread footings and grade beams on rock. The building plan and elevation are highly irregular with numerous setbacks over the height due to functional considerations. Two wings at either side of the building are connected through the “necked-down” portion of the building. The irregular configuration in the original fixed-base design led to both coupling between the

TABLE 11.1 Seismically Isolated Buildings Affected by the 1994 Northridge Earthquake

Name	Epicentral Distance (km)	Isolation System	Lateral System	PGA (g)	Roof Accn. (g)
Private residences	21	GERB	Steel braced frame	0.44	0.63
University of Southern California Teaching Hospital	36	LRB	Steel braced frame	0.37	0.21
LA Emergency Operations Center (under construction)	~38	HDR	Steel braced frame	NA	NA
LA Fire Command and Control Center	38	HDR	Steel braced frame	0.22	0.32
Rockwell Computer Center Seal Beach	66	LRB	Concrete moment frame	0.08	0.15
Foothill Communities Law and Justice Center	90	HDR	Steel braced frame	0.05	0.10
Kaiser Computer Center Corona (not instrumented)	~100	LRB	Steel braced frame	NA	NA

lateral and torsional vibration modes and very large shear force demands in the slender region between the two wings. In the isolated design, steel trusses are required to carry shear through the necked-down region.

The design base shear of the hospital is 0.15g, and the design corner bearing displacement including torsion is 26.0 cm. The effective period of the isolation system at this displacement is approximately 2.3 sec. The lead-plug rubber bearings are distributed on the perimeter of the building under the braced frames to minimize torsional response in the isolated structure. Elastomeric bearings are used in the interior. The base level diaphragm directly above the isolators is a 25-cm reinforced concrete slab with integral deep beams along the frame lines to minimize local vertical uplift. The fixed-base period of the superstructure is approximately 0.7 sec.

The California Strong Motion Instrumentation Program (CSMIP) instrumented the USC Hospital soon after its completion. The instrumentation layout and overall plan and elevation views of the building and digitized acceleration, velocity and displacement recordings from the Northridge earthquake are available (Office of Strong Motion Studies, 1994). The free-field and foundation acceleration time histories recorded at this site and other sites south of the epicenter show two distinct S-wave arrivals. The first P-wave arrived at approximately 5 sec into the record. The first S-wave is seen just over 10 sec into the record, with a second, stronger S-wave arriving at approximately 15.5 sec. These two arrival times are consistent with reports that there were two fault ruptures associated with the Northridge event (Wald and Heaton, 1994; Dreger, 1994).

The strongest motions recorded at the site were in the north-south direction. A peak acceleration of 0.493g and a peak velocity of 31.1 cm/sec were measured in the free field, while at the center of the foundation the peak acceleration was 0.366g and the peak velocity was 25.9 cm/sec. The pseudo-acceleration response spectrum of the north-south foundation motion (Clark et al., 1996) shows significant short-period energy in the range of 0.2 to 0.6 sec, but relatively little energy above a period of approximately 1.3 sec. At periods greater than 2 sec, the corresponding 10% damped spectral displacement is less than 3 cm. In the east-west direction the peak acceleration is only 0.163g and the peak velocity 9.0 cm/sec. The corresponding 10% damped spectral displacement at a period of 4 sec is approximately 7 cm, which is due to a long-period displacement component in the east-west motion that starts about 19 sec into the record; this is absent from the north-south motion. Although this long-period motion is similar to what might be seen in an alluvial basin, the soil underlying the USC Hospital is rock (Asher and Van Volkinburg, 1989). A similar response was seen in the east-west free-field displacement. Although there is a slight reduction in the high-frequency content of the foundation north-south acceleration response spectrum compared to that in the free field, in general there are no significant differences between any components of the free-field and foundation motions.

The relative displacement was calculated by subtracting the absolute displacement of the instrument at the foundation from that of the instrument just above the isolators at the base level. Both components exhibit high-frequency response in the time interval between the arrival of the first S-wave at 10 sec and

that of the stronger, impulsive S-wave at approximately 16 sec. The initial S-wave arrival had a peak ground acceleration of approximately 0.2g in the north-south direction, and even though the frequency of the response appears to be relatively high — roughly 2.0 Hz —this input is effectively filtered out by the isolation system as structural accelerations up to the sixth level are below 0.08g. The two components of the displacement response after 16 sec differ significantly. The peak north-south displacement is 3.5 cm to the south and consists of a single spike at a frequency considerably higher than that of the subsequent cycles. This is likely a result of energy from a higher mode superposed onto the primary response at a period of approximately 1.4 sec. After this spike there is no clear interval of free-vibration decay, as the amplitudes of the five cycles between 19 and 26 sec are approximately constant. The peak reversed displacement (to the north) is 1.8 cm and does not occur within the same cycle as the peak to the south. In contrast, the east-west response from 16 to 22 sec appears more typical of what would be expected of a highly damped system in free-vibration response to an impulsive load. The peak displacements occur within the same cycle, and the vibration period of the system during the decay is approximately 1.5 sec.

The peaks of the north-south pseudoacceleration response spectra at the first floor and at the roof in the spectra at approximately 1.3 sec reflect the fundamental period of the response of the isolation system after 15 sec into the record. Comparatively more energy is contained in the response at the roof than at the first level, indicating that the fundamental mode shape involves some superstructure deformation. Superstructure drift time histories between the roof and the first level also show motion at approximately 1.3 sec, but the maximum drift in the north-south direction was only 2.1 cm, with approximately 30% of this corresponding to drift in the more flexible top two floors. This localized flexibility also contributes to the relatively large peak acceleration recorded at the roof (0.205g), as compared to those in the first through sixth floors of the structure (less than 0.130g). This peak is due to higher mode response as evidenced by the substantial energy in the roof spectra at approximately 0.6 sec. The pseudo-acceleration spectra from the instrument at the sixth floor contain substantially less energy at this period. The peak in the first floor spectra at approximately 0.3 sec likely represents the higher frequency response of the building in the initial portion of the record before the isolation system was fully activated.

The isolation frequency due to the north-south acceleration was approximately 0.7 Hz and the damping ratio approximately 14%. In the east-west direction the isolation frequency was 0.75 Hz and a damping ratio of 13%. These results indicate that the system exhibited good isolation performance and good damping capacity. During the earthquake, the structure was effectively isolated from ground motions strong enough to cause significant damage to other buildings in the medical center. (The estimated total losses at the medical center site due to the Northridge earthquake was \$1 billion with 19 of the 128 buildings at the site to be demolished (Rivera, 1994).)

11.5.1.2 Los Angeles County Fire Command and Control Facility

The Los Angeles County FCCF, a two-story braced steel frame supported on 32 high-damping rubber isolators, serves as the headquarters from which fire equipment is dispatched throughout Los Angeles County. The building is located east of downtown, approximately 39 km from the epicenter of the Northridge earthquake. The bearings on the perimeter of the building have chains installed in the center meant to restrain displacement in the event of a beyond-design level earthquake. The chains (initially slack) are designed to be activated at a displacement of 31.8 cm. Details of the analysis, design and construction of the FCCF are given by Bachman et al. (1990), Anderson (1990) and Anderson et al. (1992).

Analog acceleration time histories of the response of the FCCF were made available by CSMIP within several weeks of the 1994 Northridge earthquake. The recorded response of the FCCF in this event was unusual for a base-isolated structure because several high-frequency spikes were apparent in the east-west acceleration records. Although the peak foundation accelerations in this direction were between 0.19g and 0.22g, the first floor accelerations were between 0.21g and 0.35g and the roof accelerations between 0.24g and 0.32g; therefore, the corresponding amplification ratios were substantially greater than 1.0. In the north-south direction, the building performed as expected, with amplification ratios of

approximately 0.4 and 0.5 at the first floor and the roof, respectively. The peak foundation acceleration in this direction was approximately 0.18g.

Although the FCCF remained fully functional during and after the earthquake, the high-frequency spikes seen in the accelerograms caused concern, and the site was inspected four days after the main shock. Architectural details at an east-facing tile entryway near the north wall of the building may have compromised the isolation gap in the east-west direction. The tiles are not part of the isolated portion of the building and were designed as sacrificial elements that would be dislodged by the steel grillwork that overhangs the isolation gap from the main structure. As originally designed, this joint was damaged under moderate shaking in both the 1991 Sierra Madre, California, earthquake and the 1992 Landers earthquake. The superstructure acceleration time histories recorded during these two events indicated some high-frequency response, perhaps associated with pounding at this joint, but the relatively low levels of shaking in these events make the evidence inconclusive. After the 1992 Landers, California, earthquake, an outside contractor strengthened the tile detail to resist damage in future earthquakes, with the result that the newly installed tiles provided more lateral restraint to the overhanging grill than expected, imparting an impulsive force at the first floor of the structure as the grill pounded on the tiles.

The high-frequency spikes were originally assumed to have been caused by premature activation of the chains in some of the perimeter bearings. A closer examination (Clark et al., 1996) revealed that the mechanism of pounding at the north entryway was consistent with the larger high-frequency acceleration spikes observed at the north side of the building near the entryway than at the south wall; furthermore, the spikes indicated amplified accelerations only toward the west. There was no high-frequency response in the north-south acceleration time histories.

The period of the structure lengthened as the input increased. The foundation acceleration recorded at the FCCF is similar to that recorded at the USC Hospital in that there are two distinct S-wave arrivals, with the second being of greater intensity than the first. The east-west response of the south wall at the second floor has no significant high-frequency components, and well-defined peaks in the response allow the period of vibration to be evaluated directly. If the four cycles of response prior to the arrival of the second S-wave at 16 sec into the record are evaluated, the average response period is approximately 0.9 sec and the peak-to-peak acceleration (double-amplitude) is approximately 0.15g, translating into a displacement of 15 mm. A similar analysis of the two cycles of vibration after 16 sec gives a period of approximately 1.3 sec and a double-amplitude acceleration of about 0.2g, translating into a displacement of about 44 mm.

The total height of rubber in the FCCF bearings is 250 mm, so that the peak shear strain before 16 sec was approximately 6%, while the peak shear strain after this time was approximately 18%. The high-damping elastomer compound used in the FCCF bearings has a similar modulus–shear strain relationship to the 243-62 compound used for the FCLJC (Tarics et al., 1984). This compound has a shear modulus of approximately 4.82 Mpa (700 psi) at 6% strain that drops to approximately 2.41 Mpa (350 psi) at 18% strain. The stiffness ratio is thus 0.5; the squared frequency ratio observed during the two phases of the response of the FCCF is 0.48, showing that a simple analysis of the analog data can lead to a useful confirmation of the observed period shift based on the material characteristics of the rubber compound.

11.5.1.3 Lowe Residences — GERB System

The isolated structures closest to the epicenter of the Northridge earthquake were two identical three-story braced steel frame residences in Santa Monica, California, located 22 km from the epicenter, one of which is instrumented by the United States Geological Survey (USGS). Each building is supported at its corners by GERB helical springs and viscous dashpots (Huffmann, 1991). Additional springs are distributed around the building perimeters. The design frequencies of the isolation system are 2.5 Hz vertically and 1.4 Hz in rocking (both directions). Relatively high-isolation frequencies were chosen with the intention of limiting the structural displacements to 30 mm horizontally and 20 mm vertically. Equivalent viscous damping on the order of 25% to 30% of critical level was anticipated from the dashpots, and the design anticipated that this level of damping would suppress acceleration amplifications due to resonance.

The USGS prepared a digitized version of these records, but it is not included because the vertical component of the records above the isolation system was impossible to follow; furthermore, the high-frequency content in the horizontal records prevented accurate digitization. Makris and Deoskar (1996) used the available digitized records to study the dynamic response of the building by treating the structure as a rigid block and modeling the isolation by a generalized Maxwell model based on fractional derivatives. They showed that the peak acceleration would have exceeded 1.0g if the structure had been fixed base. Although the measured peak acceleration in the building was around 0.6g, implying some reduction from the isolation system., the spectral accelerations for the 145°Component and the 235°Component would indicate that a 2-sec period horizontal isolation system with 15% damping would have accelerations of 0.09g in the 145° direction and 0.196g in the 235° direction and displacements of 89 mm and 198 mm, respectively.

11.5.2 Response of Base-Isolated Buildings in Kobe Earthquake

A large number of approaches to earthquake-resistant design have been developed in Japan where attempts to base isolate structures can be traced back at least 100 years. In the 1980s, the use of laminated rubber bearings became widespread. By the end of the decade, there were approximately 20 isolated buildings built by construction companies and isolator providers for their own use and as demonstrations of the technology developed by these firms. Following this period, base isolation has been applied to office buildings, computer centers and residential buildings. Most of these buildings have been instrumented and, as most have experienced one or more small earthquakes, an impressive history of seismic performance has been recorded. Extensive documentation of the response of the instrumented buildings has been published by the Building Center of Japan (BCJ).

Until the 1995 Kobe, Japan, earthquake, the ground motion levels had been quite low, but two recently completed structures in the northern part of Kobe near the city of Sanda were moderately shaken by the earthquake. One of these is the largest isolated building in Japan, a six-story 47,000 m² composite steel and reinforced concrete computer center. The other, on a site approximately 500 m away, is a three-story 486 m² reinforced concrete laboratory. These structures are supported on relatively stiff soil approximately 35 km northeast of the epicenter of the earthquake. Because of their proximity to one another, it can be assumed that both experienced similar levels of ground motion.

11.5.2.1 The Matsumura-Gumi Technical Research Institute

The smaller of the two structures is part of the Technical Research Institute of the Matsumura-Gumi Construction Company. Completed in March 1994 and used as a laboratory and conference area, the superstructure is a 12.8 m-high reinforced concrete space frame supported on 8 high-damping rubber bearings. The fixed-base period of the superstructure is 0.24 sec, and the target period of the isolation system varies with displacement from 1.2 sec at 1.35 cm to 2.3 sec at 20.3 cm. Adjacent to the isolated structure is a four-story steel moment frame with a rigid foundation; these buildings are connected via sliding joints.

The peak ground accelerations observed at the Matsumura-Gumi site were approximately 0.27g in both the transverse and longitudinal directions of the building, with a duration of strong motion of approximately 7 sec. While there was some attenuation of the horizontal input, it was not as great as anticipated for this level of excitation (Table 11.2). The isolated structure was not damaged, but at the roof of the adjacent fixed-based structure, there were reports of dropped ceiling tiles and a crack in a ventilation duct. The accelerations at the roof of the fixed-based building peaked at 0.98g. The acceleration records indicate that the period of response is approximately 1.45 sec, implying displacements of 10.5 cm in the x-direction and 14.5 cm in the y-direction. Although, the SRSS displacement at the isolation system is 19 cm, suggesting a period of approximately 2 sec, the measured period was closer to 1.5 sec, perhaps because the earthquake struck early in the morning when the temperature in the basement of the building was about 0°C (32°F), leading to a slight stiffening of the rubber isolators.



FIGURE 11.12 West Japan Postal Savings Computer Center: base-isolated building affected by the 1995 Kobe, Japan, earthquake.

TABLE 11.2 Floor Accelerations in the Base-Isolated Matsumura-Gumi Laboratory

		X (N334E) (g)	Y (N64E) (g)	Z (UD) (g)
Office (fixed base)	RF	0.983	0.691	0.376
Laboratory (isolated)	RF	0.200	0.278	0.341
Laboratory	1F	0.150	0.258	0.272
Basement		0.278	0.271	0.236

11.5.2.2 The West Japan Postal Savings Computer Center

The West Japan Postal Savings Computer Center (WJPSCC), Figure 11.12, is owned by the Ministry of Post and Telecommunications and serves as the computer center for all of the financial transactions of this ministry in western Japan. The lateral force-resisting system in the superstructure consists of braced frames with a fixed-base period of 0.68 sec. The target period of the isolation system varies with displacement from 2.8 sec at 120 mm to 3.3 sec at 240 mm. The isolation system for the building has three different types of isolator: 54 1.2-m diameter lead-plug rubber bearings from Oiles Corporation, 46 1.0-m diameter high-damping rubber bearings from Bridgestone Corporation and 20 800-mm diameter plain elastomeric bearings from Showa-Densi Corporation. It has several metallic dampers in the form of lead bars and steel coils. The peak response quantities shown in Table 11.3 demonstrate that the isolation system was very effective.

TABLE 11.3 Floor Accelerations in Base-Isolated West Japan Postal Center

Floor Level	X-Direction (g)	Y-Direction (g)	Vertical (g)
Sixth	0.105	0.076	0.380
First	0.108	0.058	0.197
Foundation	0.306	0.068	0.217

As a result of the response of these two base-isolated buildings in the 1995 Kobe earthquake, base isolation technology in Japan has advanced rapidly with many new projects in the design and construction phase. The number of base-isolated projects approved by the Ministry of Construction committee, which stood at around 75 before the earthquake at the end of 1994, has reached over 700 at the time of this writing. Many of these new projects are multi-family residences.

11.6 Future Challenges for Seismic Isolation

It is clear that the increasing acceptance of base isolation throughout the world will lead to many more applications of this technology. The initial scepticism that was so prevalent when elastomeric systems were initially proposed is no longer evident, and the newer approaches that are under development will benefit from this more receptive climate and lead to a variety of systems based on different mechanisms and materials.

For all systems, the most important area for future research is that of the long-term stability of the mechanical characteristics of the isolator and its constituent materials. The long-term performance of isolators can best be developed from inspection and retesting of examples that have been in service for many years. Elastomeric systems in the form of nonseismic bridge bearings have been used beyond 40 years and a record of satisfactory performance has been established (Stevenson, 1985; Taylor et al., 1992).

Despite recent advances in base isolation research, the widespread application of this technology is still impeded by over-conservative attitudes. For example, in the United States, the number of requirements beyond those for a conventional building that an engineer must satisfy in order to isolate a structure makes it remarkable that anyone does a base-isolated project. Unless bearings become a catalog commodity with certified characteristics and allied to reasonably simple design and analysis procedures that promote the benefits of base isolation, this technology will remain difficult to implement and restricted to a few projects a year. More importantly, while base isolation provisions are now in many codes, the requirements are so conservative that the potential advantages of using base isolation (e.g., reduced design requirements in the superstructure) are lost. This is unfortunate since seismic isolation could play a very important role in performance-based design. In the near future the codes for conventional construction may be modified to incorporate performance-based design to enable the design engineer to give a clearer picture of the anticipated performance of a building. Experience with the design of base-isolated emergency services centers and hospitals which have been required to remain operational after a large earthquake has shown that this performance requirement can be achieved in a cost-effective way.

Many of the completed base-isolated buildings have experienced earthquakes and their performance has been as predicted. With the exception of the USC Medical Center in the 1994 Northridge earthquake (Asher et al., 1995) these earthquakes have been either nearby and small or have been moderate and distant, so that the accelerations experienced by isolated structures have not been large. As more isolated buildings are built in earthquake-prone regions of the world, we can anticipate learning more about the behavior of such structures and it should be possible to reduce the degree of conservatism currently present in the design of these structures. Once there are sufficient data detailing the response of base-isolated buildings to major earthquakes, the next step is an alignment of the codes for fixed-base and isolated structures with a common code based on a specified level of seismic hazard and structural performance, paving the way for cost-effective application of this new technology for those building types for which it is appropriate. Additionally, base isolation can play a major role in the future in projects for the restoration of historic structures in earthquake-prone regions of the world and allow this new engineering technology to play a major role in the preservation of the cultural environment in seismic areas.

Glossary

Isolation system — Collection of individual isolator units that transfers force from foundation to superstructure

HDNR isolator — An isolation unit made from natural rubber specially compounded for enhanced energy dissipation

LP isolator — An elastomeric isolation unit where energy dissipation is provided by a centrally located lead plug

FPS isolator — A metallic isolation unit based on pendulum action and sliding friction

Effective stiffness — Aggregate stiffness of all isolation units in system at a specified displacement

Effective damping — Equivalent viscous damping corresponding to the energy dissipated by the isolation system at a specified cyclic displacement

List of Symbols

C_{AM}	a seismic coefficient
C_{VM}	a seismic coefficient
C_s	design base shear component
c_b	nominal damping constant of the isolation system
c_s	nominal damping constant of the structure above the isolation system
$K_{max}D_D$	elastic force in isolator for design of superstructure
k_b	nominal stiffness of the isolation system
k_s	nominal stiffness of the structure above the isolation system
L_1	participation factor in first mode
L_2	participation factor in second mode
M_1^{eff}	effective modal mass in first mode
M_2^{eff}	effective modal mass in second mode
M_M	coefficient for maximum capable earthquake response
m_b	base mass
m_s	superstructure mass
N_a	near-source factor
N_v	near-source factor
R	reduction factor for fixed-base design
R_I	reduction factor for seismic-isolated design
$S_d(\omega, \beta)$	displacement response spectrum for frequency, ω , and damping factor β
$S_a(\omega, \beta)$	acceleration response spectrum for frequency, ω , and damping factor β
u_s	absolute displacement of superstructure mass
u_g	absolute ground displacement
v_b	base displacement relative to ground
v_s	superstructure displacement relative to base mass
Z	seismic zone factor
β_b	nominal damping factor in the isolation system
β_σ	nominal damping factor in the structural system
β_b^*	damping factor for first mode of combined system
β_s^*	damping factor for second mode of combined system
ϵ	dimensionless ratio of squared frequencies
γ	ratio of structure mass to total mass
ϕ^1	first mode shape
$\overline{\phi^2}$	second mode shape
$\underline{\omega}_b$	nominal isolation frequency
ω_s	nominal fixed-base structure frequency

ω_b^*	shifted isolation frequency in combined system
ω_s^*	shifted structural frequency in combined system
ω_1	first mode frequency of combined system
ω_2	second mode frequency of combined system

References

- Accademia dei Lincei (1909), Relazione della Commissione Reale Incaricata di Designare le Zone piu Adatte per la Reconstruzione degli Abitati Colpiti dal Terremoto del 28 Decembre 1908 o da Altri Precedenti, Roma, Italia.
- Al-Hussaini, T.M., Zayas, V.A. and Constantinou, M.C. (1994). Seismic isolation of multi-story frame structures using spherical sliding isolation systems, National Center for Earthquake Engineering Research, State Univesity of New York at Buffalo, Technical Report NCEER-94-0007.
- Allen, E.W. and Bailey, J. S. (1988). Seismic rehabilitation of the Salt Lake City and County building using base isolation, *Proc. 9th World Conf. Earthquake Eng.*, 633–638.
- Amin, N. and Mokha, A. (1995). U.S. Court of Appeals Building: Seismic Isolation Implementation, *Proc., Joint ASME/JSMR Pressure Vessels and Piping Conf., Seismic, Shock, and Vibration Isolation*, PVP 319:229–240, Honolulu, Hawaii.
- Anderson, T.L. (1989). Seismic isolation for the Los Angeles County Fire Command and Control Facility, *Proc., ASCE Structures Congress*, 1:615–624, San Francisco, CA.
- Anderson, T.L. (1990). Seismic isolation design and construction practice, *Proc., 4th U.S. Nat. Conf. on Earthquake Eng., Earthquake Eng. Res. Inst.*, 3:519–528, Palm Springs, CA.
- Anderson, T.L., Bachman, R.E., and Grant, R.R. (1992). Base isolation response to extreme ground motions, *Proc., 10th World Conf. on Earthquake Eng.*, 4:2491–2498, Madrid, Spain.
- Arya, A.S., Chandra, B., and Qamarruddin, M. (1978). A new building system for improved earthquake performance, *Symp. on Earthquake Eng.*, University of Roorkee, 1:499–504, Roorkee, India.
- Arya, A.S., Chandra, B., and Qamarruddin, M. (1981). A new concept for resistance of masonry buildings in severe earthquake shocks, *J. Inst. of Engrs.*, 61:302–308.
- Arya, A.S. (1984). Sliding concept for mitigation of earthquake disaster to masonry buildings, *Proc., 8th World Conf. on Earthquake Eng.*, Vol. 5, San Francisco, CA.
- Asher, J.W. and Van Volkinburg, D.R. (1989). Seismic isolation of the USC University Hospital, *Proc., ASCE Structures Congress*, 1:605–614, San Francisco, CA.
- Asher, J.W. et al. (1990). Seismic isolation design of the USC University Hospital *Proc., 4th U.S. Nat. Conf. on Earthquake Eng., Earthquake Eng. Res. Inst.*, 3:529–538, Palm Springs, CA.
- Asher J.W. et al. (1995). Seismic performance of the base-isolated USC University Hospital in the 1994 Northridge Earthquake, *Proc., Joint ASME/JSME Pressure Vessels and Piping Conf., Seismic Shock and Vibration Isolation*, PVP-Vol. 319:147–154, Honolulu, Hawaii.
- Bachman, R.E., Gomez, M.J., and Chang, K.C. (1990). Verification analysis of the base-isolated Los Angeles Fire Command and Control Facility, *Proc., 4th U.S. Nat. Conf. on Earthquake Eng.*, 3:539–547, Palm Springs, CA.
- Berg, G.V. (1983). Seismic Design Codes and Procedures, *Earthq. Engrg. Res. Inst.*, Oakland, CA.
- Blakeley, R.W.G. (1982). Code requirements for base isolated structures, *Proc., Inter. Conf. on Natural Rubber for Earthquake Protection of Bldgs. and Vibration Isolation*, pp. 292–311, Kuala Lumpur, Malaysia.
- Boardman, P.R., Wood, B.J., and Carr, A.J. (1983). Union house—A cross braced structure with energy dissipators, *Bull. New Zealand Nat. Soc. Earthquake Eng.*, 16:83–97.
- Built, S.M. (1982). Lead rubber dissipators for the base isolation of bridge structures, 289, School of Engrg., Dept. of Civil Engrg., Univ. of Auckland, New Zealand.
- Campbell, T.I. and Kong, W.L. (1987). TFE sliding surfaces in bridge bearings, *Tech. Rept. MF-87-06*, Ontario Ministry of Transportation and Communications, Toronto, ON.

11-30 Earthquake Engineering: From Engineering Seismology to Performance-Based Engineering

- Chalhoub, M.S. and Kelly, J.M. (1990). Earthquake simulator testing of a combined sliding bearing and rubber bearing isolation system, Report No. UCB/EERC-87/04, Earthquake Eng. Res. Cen., Univ. of Calif., Berkeley, CA.
- Chalhoub, M.S. and Kelly, J.M. (1991). Analysis of infinite-strip-shaped base isolator with elastomer bulk and compression, *J. Eng. Mechanics*, 117:1792–1805.
- Charleson, A.W., Wright, P.D., and Skinner, R.I. (1987). Wellington Central Police Station, base isolation of an essential facility, *Proc., Pacific Conf. on Earthquake Eng., New Zealand Nat. Soc. for Earthquake Eng.*, 2:377–388, Wairekei, New Zealand.
- Clark, P.W., Highashino, M. and Kelly, J.M. (1996). Performance of seismically isolated structures in the January 17, 1994 Northridge Earthquake, *Proc. Sixth U.S.-Japan Workshop on the Improvement of Building Structural Design and Construction Practices in the United States and Japan*. Victoria, B.C., Applied Technology Council and Japan Structural Consultants Association, ATC-15-5.
- Clark, P.W. and Kelly, J.M. (1996). Energy-based modeling of high-damping rubber isolators for dynamic analysis, *Proc., ASCE Structures Congress XIV*, Chicago, IL.
- Clark, P.W. (1997). Evaluation of mechanical property changes for high-damping natural rubber bearings over time, Final Report to Federal Highways Administration.
- Constantinou, M.C., Tsopelas, P., Kim, Y.-S. and Okamoto, S. (1993). NCEER-Taisei Corporation Research Program on sliding isolation systems for bridges: Experimental and analytical study of a friction pendulum system (FPS), National Center for Earthquake Engineering Research, State University of New York. Technical Report NCEER-93-0020.
- Derham, C.J., Learoyd, S.B.B., and Wootton, L.R. (1975). Buildings on springs to resist earthquakes, *Proc., 5th European Conf. on Earthquake Eng.*, Istanbul, Turkey.
- Derham, C.J., Kelly, J.M., and Thomas, A.G. (1985). Nonlinear natural rubber bearings for seismic isolation, *Nuclear Eng. and Design*, 84:417–428.
- Dreger, D.S. (1994). Empirical Green's function study of the January 17, 1994 Northridge, California earthquake, *Geophys. Res. Letters*, 21:2633–2636.
- Federal Emergency Management Agency (FEMA) (2000). NEHRP recommended provisions for seismic regulations for new buildings and other structures. Chapter 9: Seismic isolation and energy dissipation. FEMA 356/November 2000.
- Federal Emergency Management Agency (FEMA) (2001). Prestandard and commentary for the seismic design of new buildings. Chapter 13: Seismic isolation and energy dissipation. FEMA 386/November 2001.
- Huffmann, G.K. (1985). Full base isolation for earthquake protection by helical springs and viscodampers, *Nuclear Eng. Design*, 84:331–341.
- Huffmann, G.K. (1991). Base isolation of two residential buildings in Los Angeles with helical springs and viscodampers, *Proc., 11th Post-SMiRT Conf. Seminar on Seismic Isolation of Nuclear and Non-Nuclear Structures*, Nara, Japan.
- International Conference of Building Officials (ICBO) (1991). Earthquake regulations for seismic-isolated structures, Uniform Building Code, Chapter 23.
- International Conference of Building Officials (ICBO) (1994). Earthquake regulations for seismic-isolated structures, Uniform Building Code, Appendix Chapter 16.
- International Conference of Building Officials (ICBO) (1997). Earthquake regulations for seismic-isolated structures, Uniform Building Code, Appendix Chapter 16.
- International Code Council (ICC) (2000). Section 1623: Seismically isolated structures, International Building Code.
- Iwan, W.D. and Gates N.C. (1979). The effective period and damping of a class of hysteretic structures, *Earthquake Eng. Struct. Dynamics*, 7; 199–211.
- Kelly, J.M. (1982). Aseismic base isolation, *Shock Vibration Dig.*, 14:17–25.
- Kelly, J.M. (1988). Base isolation in Japan, 1988, Report No. UCB/EERC-88/20, Earthquake Engineering Research Center, University of California Berkeley, CA.
- Kelly, J.M. (1990). Base isolation: linear theory and design, *J. Earthquake Spectra*, 6:223–244.

- Kelly, J.M. and Quiroz, E. (1992). Mechanical characteristics of neoprene isolation bearings, *Report No. UCB/EERC-92/11*, Earthquake Engineering Research Center, University of California Berkeley, CA.
- KPFF Consulting Engineers (1991). USC University Hospital, Project Summary, Santa Monica, CA.
- Langenbach, R. (1996). Personal communication to author.
- Li, L. (1984). Base isolation measure for aseismic buildings in China. *Proc., 8th World Conf. on Earthquake Eng.*, Vol. 5, San Francisco.
- Makris, N. and Deoskar, H.S. (1996). Prediction of observed response of base-isolated structure, *J. Struct. Eng.*, 122:485–493.
- Ministry of Works and Development (1983). Design of lead-rubber bearings, Civil Div. Publication CDP 818/A, Wellington, New Zealand.
- Mostaghel, N., Hejazi, M. and Tanbakuchi, J.T. (1983a). Response of sliding structures to harmonic support motion, *Earthquake Eng. Struct. Dynamics*, 11:355–366.
- Mokha, A.S., Constantino, M.C. and Reinhorn, A.M. (1990). Experimental study and analytical prediction of earthquake response of a sliding isolation system with a spherical surface, National Center for Earthquake Engineering Research, State University of New York at Buffalo, Technical Report NCEER-90-0020.
- Mostaghel, N. and Tanbakuchi, J.T. (1983b). Response of sliding structures to earthquake support motion, *Earthquake Eng. Struct. Dynamics*, 11:729–748.
- Office of Statewide Health Planning and Development (1989, Draft revised 1991). An acceptable procedure for the design and review of California Hospital Buildings using base isolation, State of California, Sacramento, CA.
- Office of Strong Motion Studies (1994). Processed data for Los Angeles 7-Story University Hospital from the Northridge Earthquake of 17 January 1994, Report No. OSMS-94-11E, Calif. Div. of Mines and Geology, State of California, Sacramento, CA.
- Rivera, C. (1994). Quake toll for medical center put at \$1 billion, *Los Angeles Times*, p. B6.
- Robinson, W.H. and Greenbank, L.R. (1975). An extrusion energy absorber suitable for the protection of structures during an earthquake, *Bull. New Zealand Nat. Soc. Earthquake Eng.*, 8:187–191.
- Robinson, W.H. and Tucker, A.G. (1977). A lead-rubber shear damper, *Bull. New Zealand Nat. Soc. Earthquake Eng.*, 10:151–153.
- Robinson, W.H. and Tucker, A.G. (1983). Test results for lead-rubber bearings for the William M. Clayton building, Toe Toe bridge, and Waiotukupuna Bridge, *Bull. New Zealand Nat. Soc. Earthquake Eng.*, 14:21–33.
- State of California (1996). Earthquake regulations for seismic-isolated structures, Administrative Code, Title 24, Part 2, Div. III.
- Staudacher, E., Habacher, C., and R. Siegenthaler (1970). Erdbebensicherung in Baum, Neue Zürcher Zeitung, Technikbeilage, Zurich, Switzerland.
- Staudacher, K. (1970). Grundlagen zum Nachweis der Erdbebensicherheit Schwimmend Gelagerter Gebäude, Doctoral Thesis No. 359, Ecole Polytechnique Federale de Lausanne, Switzerland.
- Staudacher, K. (1982). *Integral Earthquake Protection of Structures Iv: Full Base Isolation and Seismic Mass Analogy*, Zurich, Switzerland.
- Stevenson, A. (1985). Longevity of natural rubber in structural bearings, *Plast. Rubber Process. Appl.*, 5:253.
- Structural Engineers Association of California (SEAOC) (1985). Recommended Lateral Design Requirements and Commentary, Blue Book.
- Structural Engineers Association of California (SEAOC) (1989). General Requirements for the Design and Construction of Seismic-Isolated Structures, Ad Hoc Base Isolation Subcommittee of the Seismology Committee, Appendix to Chapter 1 of the SEAOC Blue Book.
- Structural Engineers Association of Northern California (SEAONC) (1986). Tentative Seismic Isolation Design Requirements, Yellow Book.
- Taniwangsa, W. (2002). Design considerations for a base-isolated demonstration building, *Earthquake Spectra*, 18:761–776.

11-32 Earthquake Engineering: From Engineering Seismology to Performance-Based Engineering

- Tarics, A.G., Way, D., and Kelly, J.M. (1984). The implementation of base isolation for the Foothill Communities Law and Justice Center, Technical Report No. RTA-84, San Francisco, CA.
- Taylor, A.W, Lin, A.N., and Martin, J.W. (1992). Performance of elastomers in isolation bearings: A literature review, *J. Earthquake Spectra*, 8:27.
- Tyler, R.G. (1977a). Dynamic tests on PTFE sliding layers under earthquake conditions, *Bull. New Zealand Nat. Soc. Earthquake Eng.*, 10:129–138.
- Tyler, R.G. (1977b). Damping in building structures by means of PTFE sliding joints, *Bull. New Zealand Nat. Soc. Earthquake Eng.*, 10:139–142.
- Tyler, R.G. and Robinson, W.H. (1984). High-strain tests on lead-rubber bearings for earthquake loadings, *Bull. New Zealand Nat. Soc. Earthquake Eng.*, 17:90–105.
- Wald, D.J. and Heaton, T.H. (1994). Spatial and temporal distribution of slip for the 1994 Northridge Earthquake, Open-file Report 94-278, U.S. Geological Survey, Pasadena, CA.
- Way, D. and Howard, J. (1990). Seismic rehabilitation of the Mackay School of mines with base isolation, *J. Earthquake Spectra*, 6:297–308.
- Westermo, B. and Udwadia, F. (1983). Periodic response of a sliding oscillator system to harmonic excitation, *J. Earthquake Eng. Struc. Dyn.*, 11:135–146.
- Zayas, V., Low, S., and Mahin, S. A. (1989). The FPS earthquake resisting system: experimental report, Report No. UCB/EERC-87/01, Earthquake Engineering Research Center, University of California, Berkeley.

12

Seismic Energy Dissipation Systems for Buildings

Andrew Whittaker
Michael Constantinou

12.1	Introduction.....	12-1
12.2	Supplemental Damping Hardware..... General • Hysteretic Dampers • Velocity-Dependent Dampers	12-2
12.3	FEMA 273/274/356 Analysis Procedures for Supplemental Dampers	12-7
	Introduction • Linear Static Procedure: General • Nonlinear Static Procedure: General • Linear Static Procedure: Supplemental Dampers • Nonlinear Static Procedure: Supplemental Dampers	
12.4	NEHRP Analysis and Design Procedures	12-12
12.5	New Configurations for Damping Systems.....	12-15
12.6	Summary and Conclusions	12-18

12.1 Introduction

In conventional construction, earthquake-induced energy is dissipated in components of the gravity- and lateral-load-resisting system. The action of dissipating energy in framing such as beams and joints in a moment-resisting frame produces damage in those components. Repair of such damage after an earthquake is typically expensive and often requires evacuation of the building while repair work on the gravity system is undertaken.

The objective of adding energy dissipation (damping) hardware to new and existing construction is to dissipate much of the earthquake-induced energy in disposable elements not forming part of the gravity framing system. Key to this philosophy is limiting or eliminating damage to the gravity-load-resisting system. Although testing and perhaps replacement of all supplemental damping devices in a building should be anticipated after a severe earthquake, evacuation of the building for repair might not be necessary and the total repair cost will likely be minor compared with the costs associated with repair and business interruption in a conventional building.

This chapter introduces the different types of supplemental passive damping hardware used or proposed for use in the United States at this time (Section 12.2), describes the new analysis procedures for supplemental dampers in FEMA 273; FEMA 1997; FEMA 356; FEMA, 2000 and in the 2000 NEHRP Recommended Provisions (FEMA 2001) that were developed in part by the authors (Sections 12.3 and 12.4) and presents a number of new damper configurations with high efficiency (Section 12.5). No information on semiactive or active supplemental damping systems is provided in this chapter. The reader is referred to the literature (e.g. Soong1990; Soong and Constantinou 1994; ASCE 1997) for information on these systems.

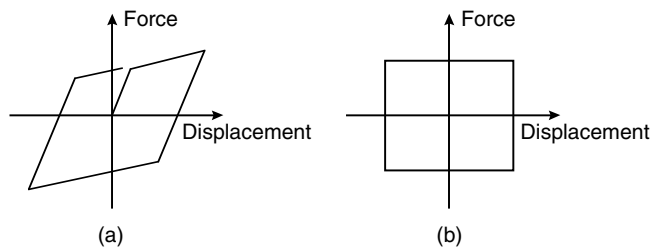


FIGURE 12.1 Force–displacement relations for hysteretic dampers.

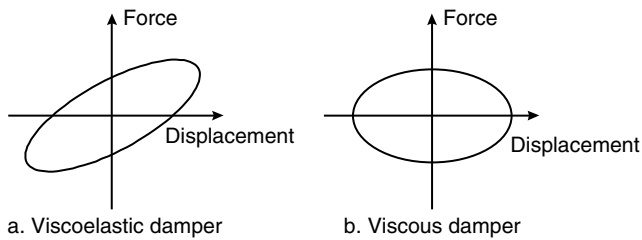


FIGURE 12.2 Force–displacement relations for velocity-dependent dampers.

12.2 Supplemental Damping Hardware

12.2.1 General

Supplemental damping hardware is parsed into three categories: hysteretic, velocity-dependent and others. Examples of hysteretic (displacement-dependent) dampers include devices based on friction and yielding of metal. Figure 12.1 presents sample force–displacement loops of hysteretic dampers. Examples of velocity-dependent systems include dampers consisting of viscoelastic solid materials, dampers operating by deformation of viscoelastic fluids (e.g., viscous shear walls) and dampers operating by forcing fluid through an orifice (e.g., viscous fluid dampers). Figure 12.2 illustrates the behavior of these velocity-dependent systems. Other systems have characteristics that cannot be classified by one of the basic types depicted in Figures 12.1 or 12.2. Examples are dampers made of shape memory alloys, frictional-spring assemblies with recentering capabilities and fluid restoring force/damping dampers. For information on these dampers, the reader is referred to Constantinou *et al.* (1998), EERI (1993), Soong and Constantinou (1994), Soong and Dargush (1997) and Hanson and Soong (2001). Only hysteretic and velocity-dependent dampers are discussed in this chapter.

Some supplemental damping systems can substantially change the force–displacement response of a building by adding strength and stiffness. Such influence is demonstrated in Figure 12.3 for metallic yielding, friction and viscoelastic dampers. Note that these figures are schematic only and that the force–displacement relation for the right-hand figure assumes that the framing supporting the friction dampers is rigid. Viscous damping systems will generally not substantially change the pseudo-static force–displacement response of a building. The analysis procedures described in the following section account for these changes in framing-system response.

12.2.2 Hysteretic Dampers

Hysteretic dampers exhibit bilinear or trilinear hysteretic, elasto-plastic or rigid-plastic (frictional) behavior, which can be easily captured with structural analysis software currently in the marketplace. Two metallic-yielding dampers, ADAS and TADAS, are shown in Figures 12.4a and 12.4b, respectively. Added

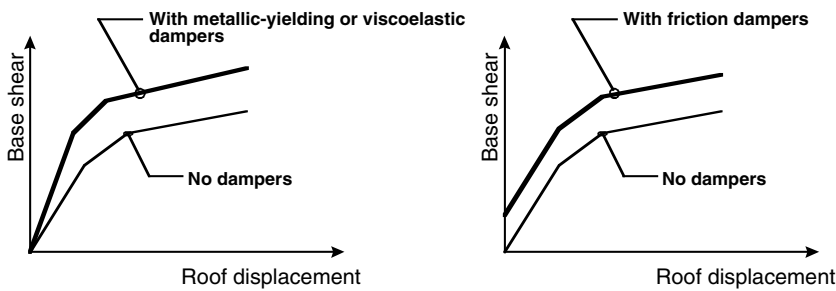


FIGURE 12.3 Influence of dampers on building response.

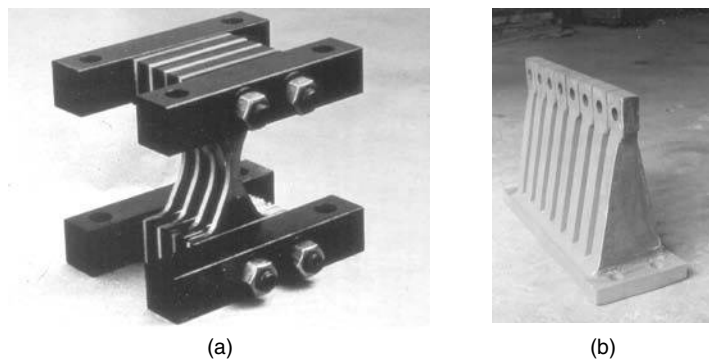


FIGURE 12.4 Examples of metallic yielding dampers. (a) Added damping and stiffness (ADAS) element; (b) triangular ADAS element (TADAS).

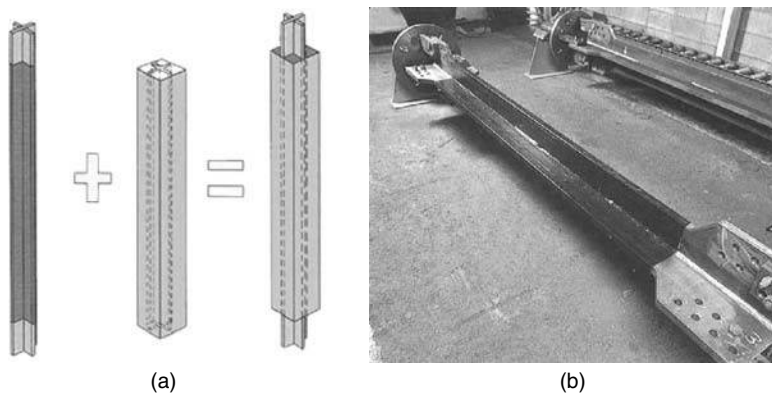


FIGURE 12.5 Unbonded steel brace (courtesy of Nippon Steel). (a) Conceptual details; (b) cruciform configuration of steel.

damping and stiffness (ADAS) elements have been implemented in the United States and Mexico. Triangular added damping and stiffness (TADAS) elements have been implemented in Taiwan.

Stiff support framing is required for the metallic yielding dampers of Figure 12.4 to ensure that the displacement across the height of the damper is maximized and approximately equal to the interstory displacement for that story in which the damper is installed. Such framing is likely more expensive than the damper it supports.



FIGURE 12.6 Unbonded steel brace applications (courtesy of I. Aiken). (a) University of California at Davis; (b) University of California at Berkeley.

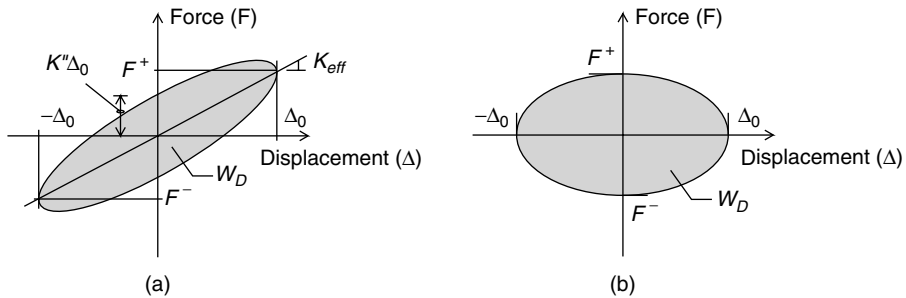


FIGURE 12.7 Parameter definition for velocity-dependent dampers. (a) Viscoelastic damper; (b) viscous damper.

An alternate metallic yielding damper, the unbonded steel brace, is shown in Figure 12.5. This damper was developed in Japan in the mid-1980s (Watanabe et al. 1988) and has been used in a number of projects in California and also found widespread application in Japan. The schematic of Figure 12.5a illustrates the key components of the unbonded steel brace, namely, a cruciform cross section of welded steel plate that is designed to yield in tension and compression, and an exterior steel tube of circular or rectangular cross section that is selected such that the buckling capacity of the tube exceeds the squash load of the cruciform cross section. The space between the cruciform cross section and the steel tube is filled with concrete to delay local buckling of the cruciform cross-section outstands. Materials are used to de-bond the cruciform cross section from the concrete. Figure 12.5b is a photograph of a cruciform cross section. The unbonded brace is designed to have approximately equal strength in tension and compression, and is conceptually superior to the concentrically braced frame because the beam at the intersection point of the chevron braces does not have to be designed for large out-of-balance vertical forces (Bruneau et al. 1998). Sample installations of unbonded braces in California are presented in Figure 12.6.

12.2.3 Velocity-Dependent Dampers

Solid viscoelastic dampers typically consist of constrained layers of viscoelastic polymers. They exhibit viscoelastic solid behavior with mechanical properties dependent on frequency, temperature and amplitude of motion. A force-displacement loop for a viscoelastic solid device, under sinusoidal motion of amplitude Δ_0 and frequency ω , is shown in Figure 12.7a. The force in the damper may be expressed as

$$F = K_{eff} \Delta + C \dot{\Delta} \quad (12.1)$$

where K_{eff} is the effective stiffness (also termed the storage stiffness K') as defined in Figure 12.7a, C is the damping coefficient and Δ and $\dot{\Delta}$ are the relative displacement and relative velocity between the ends of the damper, respectively. The damping constant is calculated as

$$C = \frac{W_D}{\pi \omega \Delta_0^2} \quad (12.2)$$

where W_D is the energy dissipated in one fully reversed cycle of sinusoidal motion at displacement amplitude Δ_0 and angular frequency ω . The damping constant C is also equal to the loss stiffness, K'' , divided by ω . More information on the characteristics of viscoelastic dampers and the derivation of the storage and loss moduli are presented in Soong and Dargush (1997).

The effective stiffness and damping coefficient are dependent on the frequency, temperature and amplitude of motion (Soong and Dargush 1997). The frequency and temperature dependences of viscoelastic polymers generally vary as a function of the composition of the polymer. The standard linear solid model (a spring in series with a Kelvin model), which can be implemented in commercially available structural analysis software, is capable of modeling behavior over a small range of frequencies, which will generally be satisfactory for most projects.

Fluid viscoelastic devices, which operate on the principle of deformation (shearing) of viscoelastic fluids, have behavior that resembles a solid viscoelastic device. However, fluid viscoelastic devices have zero effective stiffness under static loading conditions. Fluid and solid viscoelastic devices are distinguished by the ratio of the loss stiffness to the effective or storage stiffness. This ratio approaches infinity for fluid devices and zero for solid viscoelastic devices as the loading frequency approaches zero. Fluid viscoelastic behavior may be modeled with advanced models of viscoelasticity (Makris et al. 1993). However, for most practical purposes, the Maxwell model (a spring in series with a dashpot) can be used to model fluid viscoelastic devices.

Figure 12.8 presents photographs of two viscoelastic dampers. Figure 12.8a is a solid viscoelastic damper. This damper configuration is similar to that employed to reduce the wind-induced vibrations of buildings. Other configurations employ rectangular tube steel sections with copolymer bonded to all four faces of the tube. Figure 12.8b is a fluid viscoelastic damper that is known by many as a viscous damping wall (VDW). The VDW is composed of a cavity-precast wall that is filled with a viscous fluid and attached at its base to the floor framing. A T-shaped paddle is inserted in the fluid and is attached to the framing above the cavity wall. Interstory drift in the building frame produces relative movement between the paddle and the cavity wall and dissipates energy. Viscoelastic solid devices have found a small number of applications in the United States (Soong and Dargush 1997).

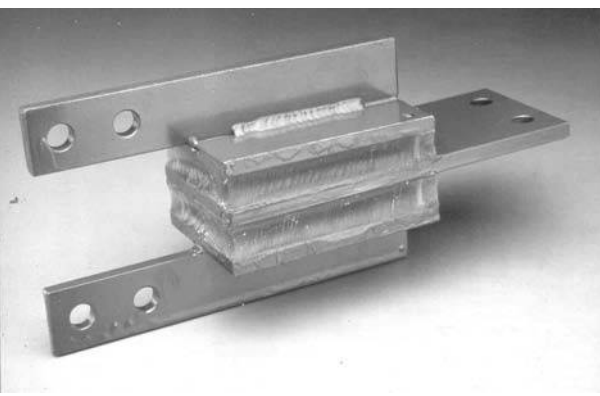
Pure viscous behavior may be produced by forcing fluid through an orifice (Constantinou and Symans 1993; Soong and Constantinou 1994; Soong and Dargush 1997). The force output of a viscous damper has the general form:

$$F = C |\dot{\Delta}|^\alpha \operatorname{sgn}(\dot{\Delta}) \quad (12.3)$$

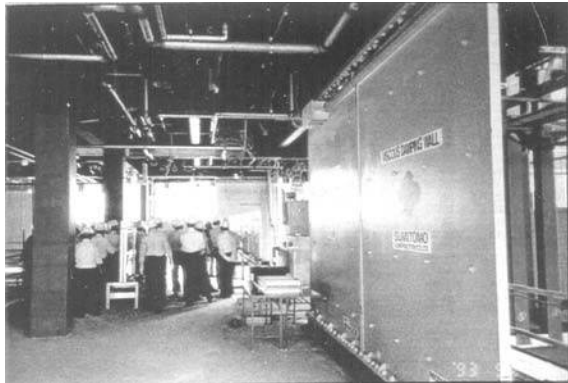
where C is a damping constant, $\dot{\Delta}$ is the velocity, α is an exponent in the range of 0.1 to 2.0 and sgn is the signum function. The simplest form is the linear fluid damper for which the exponent is equal to 1.0. In this chapter, discussion on fluid viscous devices is limited to linear fluid dampers. For a detailed treatment of nonlinear fluid viscous dampers, the reader is referred to Constantinou et al. (1998), EERI (1993), Hanson and Soong (2001) and Soong and Dargush (1997).

Fluid viscous dampers are widely used in the United States at present. Much of the technology used in this type of damper was developed for military, aerospace and energy applications. Figure 12.9 is a

12-6 *Earthquake Engineering: From Engineering Seismology to Performance-Based Engineering*



(a)



(b)

FIGURE 12.8 Solid and fluid viscoelastic dampers. (a) Solid viscoelastic damper; (b) fluid viscoelastic damper.

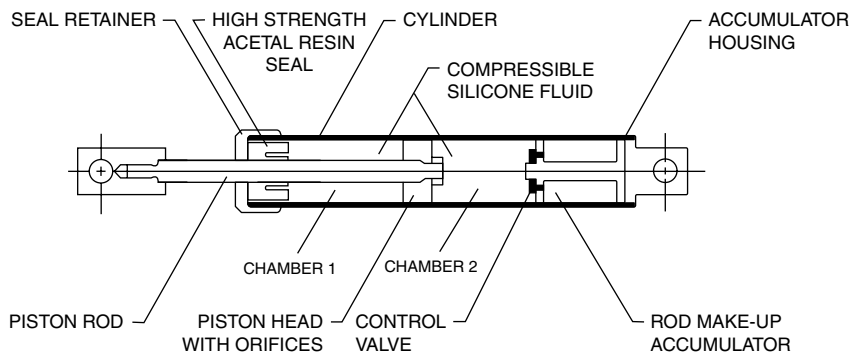


FIGURE 12.9 Schematic section through a fluid viscous damper (courtesy of Taylor Devices).

schematic section through a single-ended fluid viscous damper. Figure 12.10 shows photographs of double acting, nonlinear fluid viscous dampers used in a 14-story building in San Francisco. Such dampers are often compact because the fluid drop across the damper piston head generally ranges between 35 and 70 MPa.

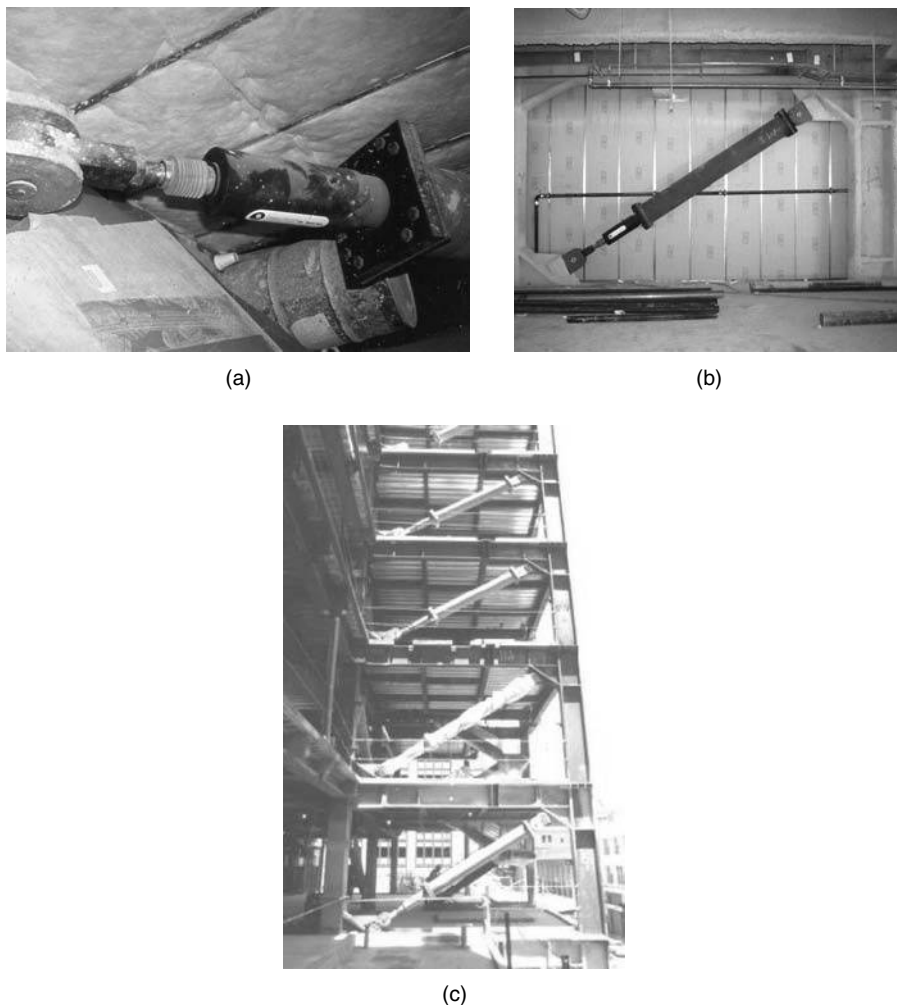


FIGURE 12.10 Fluid viscous dampers. (a) Fluid viscous damper; (b) diagonal damper configuration; (c) installed dampers in the San Francisco Civic Center building frame.

12.3 FEMA 273/274/356 Analysis Procedures for Supplemental Dampers

12.3.1 Introduction

The lack of analysis methods, guidelines and commentary has been the key impediment to the widespread application of supplemental dampers in buildings and bridges. Prior to 1997, seismic design codes and guidelines in the United States focused on designing structures for strength alone, where the design forces were set equal to the elastic forces divided by a response reduction factor (for buildings). Component deformations, which are indicators of damage and performance, were not checked.

FEMA 273 (FEMA 1997), entitled *Guidelines for the Seismic Rehabilitation of Buildings*, was published in 1997 after more than 5 years of development. FEMA 273 represented a paradigm shift in the practice of earthquake engineering in the United States because deformations and not forces were used as the basis for the design of ductile components. Performance and damage were characterized in terms of

component deformation capacity of ductile components. A commentary to FEMA 273 was published as FEMA 274 (FEMA 1997). Recently, FEMA 273 has been updated and republished as FEMA 356 (FEMA 2000), entitled *Prestandard and Commentary for the Seismic Rehabilitation of Buildings*. The discussion below is based primarily on the presentations of FEMA 273 and FEMA 274.

Four methods of seismic analysis were presented in FEMA 273/356: linear static procedure (LSP), linear dynamic procedure (LDP), nonlinear static procedure (NSP) and nonlinear dynamic procedure (NDP). All four procedures can be used to implement supplemental dampers in buildings although the limitations on the use of the linear procedures likely will limit their widespread use. Of the four, only the NDP can explicitly capture nonlinear deformations and strain- and load-history effects. The other three procedures are considered to be less precise than the NDP, although given the additional uncertainties associated with nonlinear analysis, the loss of accuracy might be small. The two nonlinear procedures lend themselves to component checking using deformations and displacements; component deformation limits are given in FEMA 273, but most are based on engineering judgment and evaluation of test data. The two static methods are described below. More information on these procedures and the two dynamic procedures is available in FEMA 273/274/356.

12.3.2 Linear Static Procedure: General

In any linear procedure, there is a direct relation between internal deformations and internal forces. Component checking involves comparing actions with capacities. In building design codes such as the Uniform Building Code (ICBO 1997) and the International Building Code (ICC 2000), component actions due to earthquake effects are calculated using elastic spectral forces divided by a response modification factor. Although inelastic response is implied by the use of values of the factor greater than 1, component deformation capacity is not checked.

The LSP of FEMA 273/356 is substantially different from the static lateral force procedures adopted in modern seismic codes. A pseudo lateral force, V , is applied to a linear elastic model of the building frame such that its maximum displacement is approximately equal to the expected displacement of the yielding building frame. The objective is to estimate displacements in a yielding building using a linear procedure. As such, the pseudo lateral force may be much greater than the yielding strength of the building, and component demands may exceed component capacities by a significant margin. However, the LSP acceptance criteria accommodate this situation by permitting demand-to-capacity ratios (denoted m in FEMA 273/356) greater than 1.0, where the values assigned to m vary as a function of the nonlinear deformation capacity of the component. The FEMA 273/356 equation for the pseudo lateral force is

$$V = C_1 C_2 C_3 S_a W \quad (12.4)$$

where C_1 is a modification factor to relate maximum inelastic displacements to displacements calculated for linear elastic response, C_2 is a modification factor to account for the effects of stiffness and strength degradation on maximum displacement response, C_3 is a modification factor to account for dynamic second-order effects, S_a is the response-spectrum acceleration at the fundamental period and damping ratio of the building frame and W is the total reactive weight. The spectral acceleration and displacement are calculated as shown in Figure 12.11.

In this figure, B is a damping coefficient, which is used to reduce the elastic spectral demands for increases in damping above 5% of critical, and T_o is the period at which the constant acceleration and constant velocity regions of the design spectrum intersect. Table 12.1 presents the values assigned in FEMA 273/356 to the damping coefficients B_s ($T < T_o$) and B_l ($T \geq T_o$). These values are conservative and serve to overestimate lateral forces and displacements (Ramirez et al. 2001). It is evident from analysis of Figure 12.11 and Table 12.1 that displacements (and deformations) can be reduced by adding damping to the framing system and adding stiffness to the framing system. A supplemental damper will add stiffness and damping to a seismic framing system depending upon its mechanical characteristics.

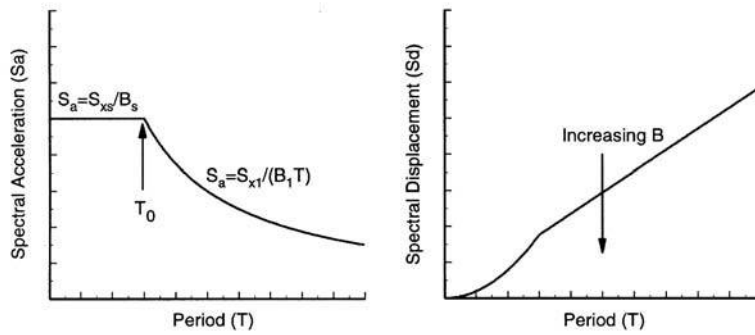


FIGURE 12.11 Spectral accelerations and displacements.

TABLE 12.1 Damping Coefficients as a Function of Effective Damping (FEMA 1997)

Effective damping, β_{eff}	B_s	B_1
<2%	0.8	0.8
5%	1.0	1.0
10%	1.3	1.2
20%	1.8	1.5
30%	2.3	1.7
40%	2.7	1.9
>50%	3.0	2.0

12.3.3 Nonlinear Static Procedure: General

The nonlinear static procedure (NSP) is a displacement-based method of analysis. Structural components are modeled using nonlinear force-deformation relations and the stiffness of the supplemental dampers is included in the model. Lateral loads are applied in a predetermined pattern to the model, which is incrementally pushed to a target displacement thereby establishing a force (base shear) versus displacement (roof) relation for the building. Component deformations are calculated at the target displacement. Component evaluation involves checking maximum deformation versus deformation capacity; force-based checking is not used for deformation-controlled components. Deformation capacities are given in FEMA 273/356 for different components, materials and performance levels. Because higher mode loading patterns are not considered, FEMA 273/356 limits the use of the NSP unless an LDP evaluation is also performed.

The target displacement is established in FEMA 273 by either the coefficient method or a modified version of the capacity-spectrum method. Both methods are equally accurate if the yield strength of the building exceeds 20% of the required elastic strength (Whittaker et al. 1998). Only the coefficient method is described below. For information on the modified capacity-spectrum method, refer to FEMA 274.

Calculation of the target displacement by the coefficient method is based on the assumption that, for periods greater than approximately 0.5 sec (for a rock site), displacements are preserved in a mean sense, that is, mean elastic displacements are approximately equal to mean inelastic displacements. Note that the degree of scatter in the ratio of elastic and inelastic displacements may be substantial, and that this assumption is not conservative for buildings with low strength. The general form of the target displacement, δ_t , equation is

$$\delta_t = C_0 C_1 C_2 C_3 S_a \frac{T_e^2}{4\pi^2} \quad (12.5)$$

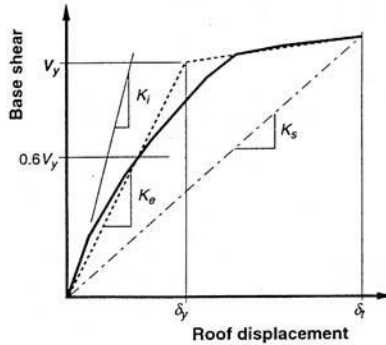


FIGURE 12.12 Calculation of secant stiffness at maximum displacement (FEMA 1997).

where T_e is the effective fundamental period of the building (see Figure 12.12 for the definition of effective stiffness that is used to calculate T_e), C_0 is a modification factor that relates roof displacement to spectral displacement, and all other terms are as defined above.

12.3.4 Linear Static Procedure: Supplemental Dampers

Limits are placed on the use of the linear static procedure (LSP) for implementing dampers in buildings. The LSP can be used only if the framing system exclusive of the dampers remains essentially linearly elastic in the design earthquake after the effects of the added damping are considered. Further, the level of effective damping must not exceed 30% of critical in the fundamental mode. Dampers are modeled using their secant stiffness at the point of maximum displacement. The stiffness of each damper must be included in the mathematical model. Specific requirements for displacement- and velocity-dependent dampers follow.

12.3.4.1 Displacement-Dependent Dampers

Additional restrictions to those noted above are placed on the use of the LSP in FEMA 273/356. Specifically, the maximum resistance in each story must vary uniformly over the height of the building and the maximum resistance (strength) of the supplemental dampers cannot exceed 50% of the lateral resistance of the remainder of the framing so as to provide a significant restoring force.

For use with the LSP, displacement-dependent dampers (see Figure 12.1a) are modeled as viscoelastic dampers (see Figure 12.2a). The effective damping of the frame (see Table 12.1) is calculated as

$$\beta_{eff} = \beta_I + \frac{\sum_j W_j}{4\pi W_k} \quad (12.6)$$

where β_I is the inherent damping in the building frame exclusive of the dampers, W_j is the energy dissipated (work done) by device j in one fully reversed cycle of sinusoidal motion at a displacement corresponding to floor displacements δ_i and the summation extends over all devices. The maximum strain energy in the frame, W_k , can be calculated as

$$W_k = \frac{1}{2} \sum_i F_i \delta_i \quad (12.7)$$

where F_i is the inertial force at floor level i and δ_i is the displacement of floor level i and the summation extends over all floor levels.

The value of β_{eff} is used to calculate a value of B from Table 12.1. The spectral acceleration for use in 12.5 is calculated using the fundamental period of the framing system whose model includes the secant stiffness of the displacement-dependant dampers. Component actions and deformations are checked at the stage of maximum displacement.

12.3.4.2 Velocity-Dependent Dampers

One additional restriction to those noted above is placed on the use of the LSP, namely, that the maximum resistance (strength) of the velocity-dependent supplemental dampers in any story cannot exceed 50% of the resistance of the remainder of the framing in that story. This restriction applies only to viscoelastic dampers.

The effective damping is calculated using equations 12.6 and 12.7. For linear viscous dampers, the work done by damper j can be calculated as

$$W_j = \pi(C_j \dot{\delta}_{rj})\delta_{rj} = \frac{2\pi^2}{T_1} C_j \delta_{rj}^2 \quad (12.8)$$

where C_j is the damper constant for device j , δ_{rj} is the relative displacement between the ends of device j measured *along the axis* of the damper and T is the fundamental period of the framing system whose model includes the stiffness of the dampers. This equation assumes harmonic motion of amplitude δ_{rj} and periodicity T . As such, it may not be applicable if near-field (non-harmonic) ground motions are used for design. FEMA 273 provides an alternative equation for calculating the effective damping provided by linear viscous devices using first mode information:

$$\beta_{eff} = \beta_I + \frac{T_1 \sum_j C_j \cos^2 \theta_j \phi_{rj}^2}{4\pi \sum_i m_i \phi_i^2} \quad (12.9)$$

where ϕ_i is the first mode displacement of floor level i , m_i is the mass of floor level i , θ_j is the angle of device j to the horizontal, ϕ_{rj} is first mode relative horizontal displacement between the ends of device j and all other terms are as described above. Equation 12.9, with minor modification, can be used to calculate modal damping ratios for buildings incorporating nonlinear viscous dampers.

Design actions in components of buildings incorporating velocity-dependent dampers must be checked at three stages: maximum, maximum velocity and maximum acceleration (at the displacement corresponding to the maximum force). Information on the calculation of component actions at the stages of maximum velocity and maximum acceleration can be found in FEMA 273/274/356 and Constantinou *et al.* (1998).

12.3.5 Nonlinear Static Procedure: Supplemental Dampers

Two methods of nonlinear static analysis are provided in FEMA 273/356 for implementing supplemental dampers: Method 1 (known as the coefficient method) and Method 2 (known as the capacity-spectrum method). The two methods are equally precise. The use of the coefficient method to implement dampers is described below. Tsopelas *et al.* (1997) and Section C9.3.5 of FEMA 274 provide information on the use of the capacity-spectrum method with damping devices.

Regardless of which method is used to calculate the target displacement and the associated component deformations, the nonlinear mathematical model of the building frame must include the nonlinear force–velocity–displacement relations for the dampers and the mechanical characteristics of the framing supporting the dampers. If the stiffness of a damper is dependent upon amplitude, frequency or velocity, the stiffness value used for analysis should be consistent with deformations corresponding to the target displacement and frequencies corresponding to the inverse of the effective period T_e .

12.3.5.1 Displacement-Dependent Dampers

The benefit of adding displacement-dependent dampers to a building frame is recognized in FEMA 273 by the increase in building stiffness afforded by the dampers. The increase in stiffness will reduce the effective period T_e in equation 12.5 thereby reducing the maximum displacement. The spectral acceleration in this equation should be calculated using the effective period of the mathematical model that includes the stiffness of the dampers and the value of B assigned to the building frame exclusive of the dampers.

12.3.5.2 Velocity-Dependent Dampers

The benefits of adding velocity-dependent dampers to a building frame are recognized in FEMA 273/356 by (a) the increase in viscous damping and (b) the increase in building stiffness, provided by the dampers. The increase in damping will reduce the spectral acceleration. The increase in stiffness will reduce the effective period and thus generally reduce the spectral displacement.

The effective damping in the building frame at the point of maximum displacement is calculated iteratively using equations 12.6, 12.7, 12.8 and 12.9. In these equations, the floor displacements δ_i are those that correspond to the target displacement, the forces F_i are the lateral forces that correspond to the target displacement, and T_e is replaced by the secant period ($= T_s$) at the point of maximum displacement. Using the force–displacement relation of Figure 12.12, the secant period can be calculated as

$$T_s = T_e \sqrt{\frac{K_e}{K_s}} \quad (12.10)$$

An estimate of target displacement is needed to calculate the effective damping and secant stiffness, which in turn are used to calculate a revised estimate of the target displacement. When the assumed and calculated values of the target displacement are sufficiently close, the solution has converged.

As described above, component actions in a framing system incorporating velocity-dependent dampers must be checked at the stages of maximum drift, maximum velocity and maximum acceleration. Procedures for such checking are presented in FEMA 273/356 and 274. Higher mode damping forces must be considered if velocity-dependent dampers are implemented using the NSP. The magnitude of these forces may be similar to those damping forces calculated using the procedure described above. An example of the calculation of higher mode forces is presented in FEMA 274.

12.4 NEHRP Analysis and Design Procedures

Key aspects of the 2000 NEHRP Recommended Provisions (FEMA, 2001), hereafter termed 2000 NEHRP, analysis and design procedures for new buildings incorporating damping devices are presented below. A detailed description of these procedures, applications and verification studies are presented in Ramirez *et al.* (2001, 2002a, 2002b, 2003) and Whittaker *et al.* (2003). Attention is focused below on the equivalent lateral force (ELF) analysis procedure for which the residual mode is used in lieu of all modes higher than the fundamental mode. The use of the ELF procedure is limited to low-rise regular buildings (five stories or less in height) with rigid floor diaphragms, modest levels of damping ($\beta_1 \leq 0.35$), and at least two damping devices in each story of the building, distributed to resist the effects of torsion. (Because only limited information is presented in this section, the reader should not just use only the steps listed below to design a damping system per 2000 NEHRP.) Although checks are made for maximum earthquake shaking in the 2000 NEHRP, only the key steps in the ELF *design* earthquake analysis are listed below. Further, for the steps listed below it is assumed that (a) $T_1 > T_0$, (b) the importance factor I is equal to 1.0, (c) the target design base shear force for the damped building is greater than or equal to $0.75V$, where V is the minimum design base shear force for a building without the damping system, (d) the target drift in the building is the limiting value of 2000 NEHRP and (e) plastic or pushover analysis is not used to establish the yield strength of the frame.

TABLE 12.2 2000 NEHRP Recommended Provisions Damping Coefficients (FEMA 2001)

Effective damping β_{eff}	Damping coefficient B
2%	0.8
5%	1.0
10%	1.2
20%	1.5
30%	1.8
40%	2.1
50%	2.4
60%	2.7
80%	3.3
100%	4.0

Correct calculation of displacements is key to the use of the 2000 NEHRP provisions for energy dissipation systems. The equal displacements rule is imposed on frames incorporating damping systems by setting the displacement amplification factor, C_d , equal to the response modification factor, R . As such, a number of terms in 2000 NEHRP are multiplied by $[R/C_d]$ to correctly calculate displacements in the building frame.

The main steps in the analysis and design process, subject to the assumptions listed above, are enumerated below:

1. Calculate a minimum seismic base shear, V_{db}^{\min} , for the design of the seismic force resisting system as the greater of

$$V_{db}^{\min} = \frac{V_{cb}}{B_{V+I}}; 0.75V_{cb} \quad (12.11)$$

where V_{cb} is the total design base shear for the framing system exclusive of the damping devices, and B_{V+I} is the damping coefficient for effective damping equal to the sum of the viscous damping in the fundamental mode and the inherent damping in the building frame. The damping coefficients, B , in Table 13.A.3.1 of 2000 NEHRP are listed in Table 12.2 for periods greater than $0.2T_0$ sec.

2. Develop a trial design based on $V_{db} = 0.75V_{cb}$ and a distribution of V_{db} over the height of the building frame similar to that adopted in 2000 NEHRP for conventional buildings.
3. Establish mode shapes, modal participation factors, modal weights and periods for the first and residual modes.
4. Select a target level of supplemental damping in the fundamental mode, β_{v1} , so that the frame of step 2 will meet the drift limits of 2000 NEHRP if the frame was to respond elastically.
5. Assume a trial value for the effective ductility μ_D of the order of 1.5 to 2.0, based on the trial designs of Ramirez *et al.* (2001), and calculate the effective damping and effective period in the fundamental mode

$$\beta_{1D} = \beta_I + \beta_{v1}\sqrt{\mu_D} + q_h(0.64 - \beta_I)(1 - \frac{1}{\mu_D}) \quad (12.12)$$

$$T_{1D} = T_1\sqrt{\mu_D}$$

where q_h is a hysteresis-loop quality factor, less than or equal to 1.0.

6. Calculate B_{1D} , and the seismic coefficient C_{S1} and base shear force V_1 as follows:

$$C_{S1} = \left[\frac{R}{C_d} \right] \frac{S_{D1}}{T_{1D}(\Omega_0 B_{1D})} \quad (12.13)$$

$$V_1 = C_{S1} \bar{W}_1$$

12-14 Earthquake Engineering: From Engineering Seismology to Performance-Based Engineering

7. Check that the base shear force V_1 from step 6 is approximately equal to the value of V_{db} from step 1. If so, proceed to step 8. If not, assume a new value for the effective ductility demand and return to step 5.
8. Calculate displacements D_Y , D_{1D} and the effective ductility demand μ_D

$$\begin{aligned} D_Y &= \left(\frac{g}{4\pi^2}\right) \left(\frac{\Omega_0 C_d}{R}\right) \Gamma_1 C_{sl} T_1^2 \\ D_{1D} &= \left(\frac{g}{4\pi^2}\right) \Gamma_1 \frac{S_{D1} T_{1D}}{B_{1D}} \leq \left(\frac{g}{4\pi^2}\right) \Gamma_1 \frac{S_{DS} T_{1D}^2}{B_{1D}} \\ \mu_D &= \frac{D_{1D}}{D_Y} \end{aligned} \quad (12.14)$$

9. Calculate the *residual* mode contributions to the response and the damping coefficient in the *residual* mode, B_R

$$\begin{aligned} \beta_R &= \beta_I + \beta_{vr} \\ C_{SR} &= \left[\frac{R}{C_d}\right] \frac{S_{DS}}{\Omega_0 B_R} \\ V_R &= C_{SR} \bar{W}_R \\ D_{RD} &= \left(\frac{g}{4\pi^2}\right) \Gamma_R \frac{S_{D1} T_R}{B_R} \leq \left(\frac{g}{4\pi^2}\right) \Gamma_R \frac{S_{DS} T_R^2}{B_R} \end{aligned} \quad (12.15)$$

10. Calculate the seismic base shear, V_{db} , and the design lateral forces at level i ,

$$\begin{aligned} V_{db} &= \sqrt{V_1^2 + V_R^2} \\ F_{i1} &= w_i \phi_{i1} \frac{\Gamma_1}{\bar{W}_1} V_1 \\ F_{iR} &= w_i \phi_{iR} \frac{\Gamma_R}{\bar{W}_R} V_R \end{aligned} \quad (12.16)$$

Refine the design from step 1 as necessary using the first mode and residual mode lateral forces.

11. Calculate the fundamental and residual mode interstory drifts due to the *design* earthquake, Δ_{1D} , and Δ_{RD} , respectively, and the *design* earthquake interstory drift

$$\Delta_D = \sqrt{\Delta_{1D}^2 + \Delta_{RD}^2} \quad (12.17)$$

Check Δ_D versus the 2000 NEHRP drift limits. If the calculated drifts exceed the drift limits, increase the value of V_{db} and return to step 2.

12. If velocity-dependent dampers are considered, the *design* earthquake interstory velocity, ∇_D , is calculated using the velocities in the fundamental and residual modes as follows:

$$\nabla_D = \sqrt{\nabla_{1D}^2 + \nabla_{RD}^2} \quad (12.18)$$

where

$$\begin{aligned}\nabla_{1D} &= 2\pi \frac{\Delta_{1D}}{T_{1D}} \\ \nabla_{1R} &= 2\pi \frac{\Delta_{1R}}{T_R}\end{aligned}\quad (12.19)$$

The values for ∇_D can then be used to size the velocity-dependent dampers by resolving the interstory velocities along the axes of the dampers.

13. Check the components of the frame of steps 2 and 10 for the seismic load combinations of Section 13A.7 of 2000 NEHRP including checks at the stages of maximum displacement (all dampers), maximum velocity (velocity-dependent dampers only) and maximum acceleration (velocity-dependent dampers only).

12.5 New Configurations for Damping Systems

Small interstory drifts and velocities characterize stiff seismic framing systems and all framing systems for wind excitation. Many have assumed that such systems are not candidates for the addition of dampers because significant drifts and velocities are needed to dissipate substantial energy, although the values listed in Table 12.1 indicate that damping is most effective in the short-period (constant acceleration) range of the spectrum. FEMA (1995) writes:

Structural systems best suited for implementation of energy dissipation devices are the moment-resisting frame and the flexible dual system, in either structural steel or reinforced concrete. The interstory response of a stiff lateral load-resisting system, such as a reinforced concrete shear wall system or a steel-braced dual system, is generally characterized by both small relative velocities and small relative displacements. As such it may not be feasible to implement supplemental energy dissipation.

This observation is correct for conventional damper configurations involving diagonal (in-line) or chevron installations. For example, interstory displacements in a stiff code-compliant building will likely not exceed 15 mm in the design earthquake. Large damper forces are then needed to develop moderate levels of supplemental damping. Damper displacements in conventionally configured systems will be less than or equal to the interstory displacements. For a small-stroke fluid viscous damper, special details are required that increase the volume and cost of the damper.

Recent work at the University at Buffalo, State University of New York (Constantinou and Sigaheh 2000; Constantinou et al. 2001; Sigaheh and Constantinou 2003) has sought to expand the utility of fluid viscous damping devices to the short-period range and for wind applications through the use of mechanisms that magnify the damper displacement for a given interstory drift. Such magnification permits the use of dampers with smaller force outputs (smaller damper volume), larger strokes and reduced cost. Two configurations are the toggle-brace and the scissor-jack.

A toggle-brace configuration is shown in Figures 12.13 and 12.14a. The supplemental framing consists of toggles AB and BC that are configured as a shallow truss. The damper is placed perpendicular to toggle AB. The most effective damper site is number 2. Displacement of point C with respect to point A, equal to interstory drift u , causes toggle AB to rotate. The resulting changes in distance between points B and D, and B and E are the damper displacements u_{D1} and u_{D2} , respectively. These displacements are related to the interstory drift, u , through simple equations.

Damping forces in the toggle-brace system are small but are magnified in the shallow truss and delivered to the framing system by axial forces in the braces. The absence of flexure in the toggle-brace assembly facilitates the use of small structural sections and standard connection details. The assembly is compact and can be installed in a square space with a side length equal to the column height

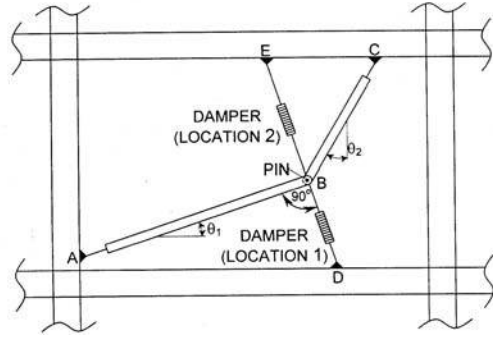


FIGURE 12.13 Toggle-brace assembly.

For small rotations and damper location number 1, the damper displacement is related to the interstory drift, u , as follows:

$$u_D = fu \quad (12.20)$$

For damper location number 2, the relation is

$$u_D = (f + \sin \theta_1)u = f_u u \quad (12.21)$$

where,

$$f = \frac{\sin \theta_2}{\cos(\theta_1 + \theta_2)} \quad (12.22)$$

The displacement magnification factors f and f_u depend only on the inclination of the toggle-braces. High displacement magnifications can be achieved although values are sensitive to small changes in θ_1 and θ_2 . Magnification factors between 2 and 3 can be easily achieved and are insensitive to small variations in changes in θ_1 and θ_2 .

For small rotations, the relation between the damper force, F , and the force exerted by the toggle-brace assembly on the structural frame, F_F , is

$$F_F = f F \quad (12.23)$$

for location number 1 (see Figure 12.13), and

$$F_F = f_u F \quad (12.24)$$

for location number 2. Equations 12.20 through 12.24 have the same form as those equations written for dampers installed in diagonal or in-line braces and dampers atop chevron braces.

The reverse toggle and the scissor-jack assemblies of Figures 12.14b and 12.15 are variants of the toggle-brace assembly. Equations similar to those presented above for the toggle-brace assemblies have been developed for the reverse toggle and the scissor-jack systems. See Figure 12.15 for details.

To illustrate the effectiveness of the toggle-brace and scissor-jack assemblies for short-period framing systems, consider the six damper configurations presented in Figure 12.15. The diagonal (in-line) and chevron brace configurations represent conventional damper assemblies. For the purpose of comparison, assume that (1) the elastic single-bay, single-story frame has a fundamental period of 0.3 sec, (2) the

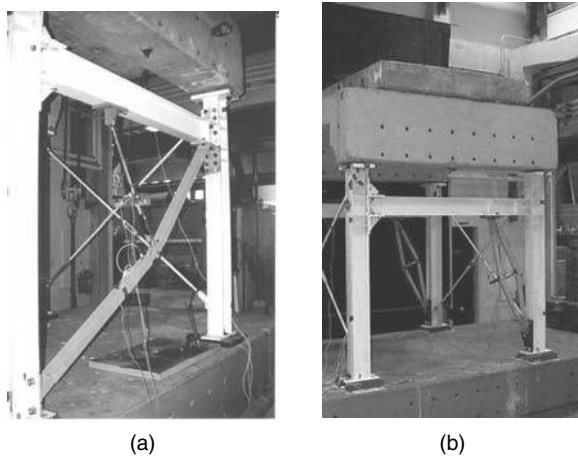


FIGURE 12.14 Toggle-brace and scissor-jack damper assemblies on the Buffalo simulator. (a) Upper toggle brace; (b) scissor jack.

damper is a linear fluid viscous device with a damping constant, C , equal to 160 kNs/m, (3) the weight of the frame is 1370 kN and (4) angles, θ , θ_1 , θ_2 , θ_3 and ψ are as shown in Figure 12.15.

The force output of the damper, F , is given by

$$F = C\dot{u}_D \quad (12.25)$$

where \dot{u}_D is the relative velocity between the ends of the damper along the axis of the damper. The damping force exerted on the frame by the damper assembly, F_F , is given by

$$F_F = C f^2 \dot{u} \quad (12.26)$$

where \dot{u} is the interstory velocity and f is equal to f_u if the damper is placed in location 2 of the toggle-brace in Figure 12.13. The damping ratio of the single-story frame of Figure 12.15, with weight, W_1 , and fundamental period, T_1 , is

$$\beta_{v1} = \frac{C f^2 g T_1}{4\pi W_1} \quad (12.27)$$

Figure 12.15 provides a comparison of various configurations of dampers in a short-period, single-story, single-bay frame. The damping ratios for the conventional diagonal and chevron-brace configurations are less than 5% of critical, and greater than 23% for the toggle-brace and scissor-jack assemblies. The displacement magnification factors for the toggle-brace and scissor-jack assemblies exceed 2.1. These new damper configurations will facilitate the use of dampers in stiff framing systems and for wind applications provided that the cost of the toggle-brace- or scissor-jack-support framing is not substantially greater than the cost of the framing that would be required to support the dampers in conventional configurations.

Three buildings in the U.S. have been built with toggle-brace-damper systems. They are the 37-story Yerba Buena Tower in San Francisco, the 37-story Millennium Place in Boston and the 38-story 111 Huntington Avenue in Boston. The first two utilize reverse toggle systems, whereas the third utilizes a modified lower toggle system. The modification consists in installing the damper at an angle greater than 90° degrees with respect to the lower toggle (see Figure 12.15) so that the two toggles and the damper directly connect to the beam-to-column joints. The magnification factor for this configuration is given

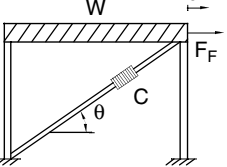
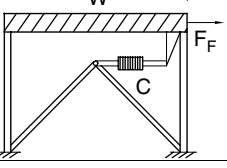
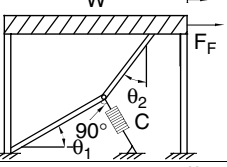
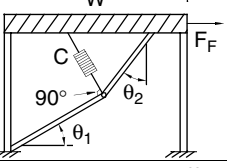
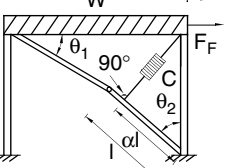
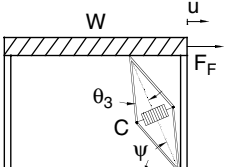
Diagonal		$f = \cos \theta$	$\theta = 37^\circ$ $f = 0.799$ $\beta = 0.032$
Chevron		$f = 1.00$	$f = 1.00$ $\beta = 0.05$
Lower Toggle		$f = \frac{\sin \theta_2}{\cos (\theta_1 + \theta_2)}$	$\theta_1 = 31.9^\circ, \theta_2 = 43.2^\circ$ $f = 2.662$ $\beta = 0.344$
Upper Toggle		$f = \frac{\sin \theta_2}{\cos (\theta_1 + \theta_2)} + \sin \theta_1$	$\theta_1 = 31.9^\circ, \theta_2 = 43.2^\circ$ $f = 3.191$ $\beta = 0.509$
Reverse Toggle		$f = \frac{\sin \theta_2}{\cos (\theta_1 + \theta_2)} - \cos \theta_2$	$\theta_1 = 30^\circ, \theta_2 = 49^\circ, \alpha = 0.7$ $f = 2.521$ $\beta = 0.318$
Scissor-Jack		$f = \frac{\cos \psi}{\tan \theta_3}$	$\theta_3 = 9^\circ, \Psi = 70^\circ$ $f = 2.159$ $\beta = 0.233$

FIGURE 12.15 Effectiveness of damper configurations (Sigaher and Constantinou 2003).

by equation 12.22 after multiplication by $\cos \theta_3$ where θ_3 = angle of damper axis with respect to the 90° line. For the 111 Huntington Avenue building, angle $\theta_3 = 21.5^\circ$ so that the magnification factor is reduced by a small amount (about 7%). However, the installation with connections of the toggles and dampers directly to the beam-to-column joints eliminates additional bending in the beams and provides for easy and reliable calculation of the magnification factor. Figure 12.16 presents a photograph of the Yerba Buena Tower and one of its toggle-brace assemblies.

12.6 Summary and Conclusions

Two types of supplemental damping hardware were described: displacement-dependent and velocity-dependent dampers. Examples of each type of hardware, including metallic yielding ADAS, TADAS and unbonded-brace, solid and fluid viscoelastic, and fluid viscous dampers were presented.

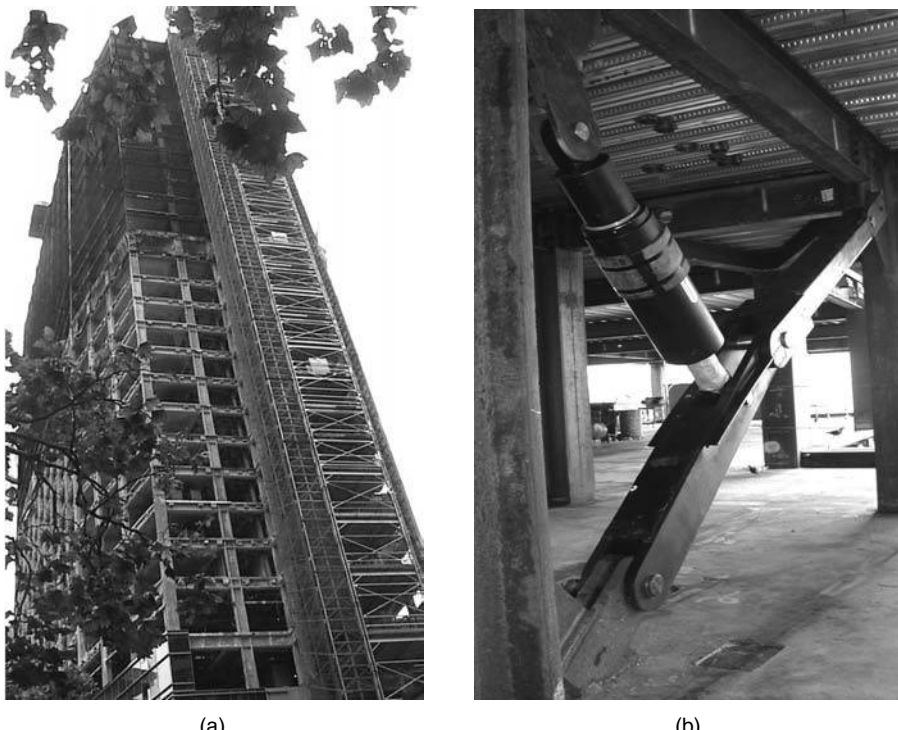


FIGURE 12.16 Toggle-brace assemblies in the Yerba Buena Tower. (a) Elevation of tower; (b) toggle brace assembly.

New procedures for the analysis and design of buildings incorporating displacement- and velocity-dependent dampers were discussed. Linear and nonlinear static methods of analysis were described. These analysis methods are displacement oriented and as such represent a paradigm shift in the analysis of buildings for the effects of earthquakes. For implementing dampers, the linear procedures can be used only if the building is regular, the response of the framing system is essentially elastic in the design earthquake, and the effective damping ratio is 30% of critical or less. Displacement- and velocity-dependent dampers are modeled using their secant stiffness at the maximum displacement and their damping is assumed to be equivalent viscous. The nonlinear analysis procedures of FEMA 273 are displacement based; component checking focuses on deformations rather than on forces. The force-displacement relations for displacement-dependent dampers are modeled explicitly and the key benefit of such dampers is the stiffness they add to the building frame. Velocity-dependent dampers are modeled using their secant stiffness at the stage of maximum displacement and the primary benefit of such dampers is added viscous damping. The ELF method of analysis and design for buildings with damping systems of the 2000 NEHRP has been described. This method is based on the nonlinear static analysis procedures of FEMA 273/274/356 but without the need for pushover analysis.

Until now damping systems have generally been considered appropriate only for flexible framing systems although the greatest benefit of viscous damping, measured as a percentage reduction in displacement, is typically realized for stiff framing systems. Two new damper configurations, toggle-brace and scissor jack, were described. The efficacy of these configurations was demonstrated by application to a stiff framing system with a period of 0.3 sec. Fourfold to tenfold increases in damping ratio with respect to that provided by conventional damper configurations were shown to be possible with the toggle-brace and scissor-jack configurations.

Acknowledgments

The authors thank their colleagues Professors T.T. (Larry) Soong, Andrei Reinhorn, Gary Dargush and Dr. Ani Natali Sigaher-Boyle of the University at Buffalo, Dr. Charles Kircher of Kircher and Associates, California, former graduate students and visiting scholars Professor Oscar Ramirez of the Technological University of Panama, Professor Nicos Makris of the University of Patras, Professor Michael Symans of Rensselaer Polytechnic Institute, NY, Professor Panos Tsopelas of the Catholic University, Washington, DC, and Dr. Christis Chrysostomou of the Higher Technical Institute, Cyprus for their contributions in the development of damping systems and the analysis/design procedures of FEMA 273/274/356 and 2000 NEHRP.

Glossary

Damper — Device added to a building frame to mitigate response due to earthquake shaking

Displacement-dependent damper — Hysteretic damper

Energy dissipation device — Damper

Hysteretic damper — A damper that dissipates energy through yielding of metal or friction where energy dissipation is not a function of the rate of loading

Scissor jack assembly — Assembly that amplifies the motion of a damping device(s)

Toggle-brace assembly — Assembly that amplifies the motion of a damping device(s)

Velocity-dependent damper — A damper that dissipates energy through shearing of solid or fluid viscoelastic materials or by forcing fluid through or past a piston head

List of Symbols

B_S	Damping coefficient in the constant acceleration range of the spectrum
B_{V+I}	Damping coefficient for effective damping equal to the sum of the viscous damping in the fundamental mode and the inherent damping in the building frame
B_1	Damping coefficient in the constant velocity range of the spectrum
B_{1D}	Damping coefficient for effective damping in the fundamental mode per 2000 NEHRP
B_R	Damping coefficient for effective damping in the residual mode per 2000 NEHRP
C	Damping constant
C_d	Displacement amplification factor
C_j	Damping constant for device j
C_{S1}	Seismic coefficient in the fundamental mode per 2000 NEHRP
C_{SR}	Seismic coefficient in the residual mode per 2000 NEHRP
C_0	Factor that relates roof displacement to spectral displacement
C_1	Factor that relates maximum inelastic displacement to maximum elastic displacement
C_2	Factor to account for the effects of stiffness and strength degradation on displacement response
C_3	Factor to account for the effect of dynamic second-order effects on displacement response
D_Y	Yield displacement of the damped frame per 2000 NEHRP
D_{1D}	Fundamental mode displacement of the damped frame per 2000 NEHRP
D_{RD}	Residual mode displacement of the damped frame per 2000 NEHRP
f, f_u	Displacement magnification factors in damper assemblies (see Figure 12.15)
F	Damper force
F_F	Force exerted on the structural frame of Figure 12.15 by the damper assembly
F_i	Inertial force at floor level i
F_{il}	Fundamental mode design lateral force at floor level i per 2000 NEHRP
F_{iR}	Residual mode design lateral force at floor level i per 2000 NEHRP
g	Acceleration due to gravity
I	Importance factor

K_e	Effective initial stiffness of the building frame (see Figure 12.12)
K_{eff}	Effective stiffness of a damping device
K_s	Secant stiffness of the building frame at the maximum displacement (see Figure 12.12)
K'	Storage stiffness
K''	Loss stiffness
m_i	Mass of floor level i
q_h	Building frame hysteresis loop quality factor per 2000 NEHRP
R	Response modification factor
S_a	Spectral acceleration
S_{D1}	Design earthquake spectral ordinate at a period of 1 second
S_{DS}	Design earthquake spectral ordinate at a period of 0.2 second
T_0	Period at the intersection point of the constant acceleration and constant velocity segments of the spectrum
T	Period
T_R	Residual mode period per 2000 NEHRP
T_1	Fundamental period of the building frame inclusive of the damping devices
T_{1D}	Effective fundamental mode period of the building frame inclusive of the damping devices per 2000 NEHRP
T_e	Effective initial period of the frame (see Figure 12.12)
T_s	Secant period of the frame at maximum displacement (see Figure 12.12)
u	Interstory drift in single-story damped frame assembly (see Figure 12.15)
\dot{u}	Interstory velocity in single-story damped frame assembly (see Figure 12.15)
u_{Di}	Relative displacement between the ends of damper at location i (see Figure 12.15)
\dot{u}_D	Relative velocity between the ends of damper at location i (see Figure 12.15)
V	Pseudo lateral force per FEMA 273/356 LSP
V_{cb}	Design base shear for a conventional building per 2000 NEHRP
V_{db}	Design base shear for a damped building per 2000 NEHRP
V_{db}^{\min}	Minimum design base shear for a damped building per 2000 NEHRP
V_1	Base shear force in the fundamental mode per 2000 NEHRP
V_R	Base shear force in the residual mode per 2000 NEHRP
W	Total reactive weight
W_D	Energy dissipated in one fully reversed cycle of sinusoidal motion
W_j	Energy dissipated by damping device j in one fully reversed cycle of sinusoidal motion
W_k	Maximum strain energy in the frame
\overline{W}_1	Reactive weight in the fundamental mode
\overline{W}_R	Reactive weight in the residual mode
α	Velocity exponent on a fluid viscous damper
β_I	Inherent damping in the frame exclusive of the damping devices
β_{eff}	Effective damping in the frame inclusive of the damping devices
β_R	Effective damping in the residual mode per 2000 NEHRP
β_{1D}	Effective damping in the fundamental mode per 2000 NEHRP
β_{vr}	Supplemental damping in the residual mode per 2000 NEHRP
β_{v1}	Supplemental damping in the fundamental mode per 2000 NEHRP
Γ_R	Residual mode participation factor
Γ_1	Fundamental mode participation factor
ϕ_i	Fundamental mode displacement at floor level i
ϕ_{rj}	Fundamental mode relative floor displacement between the ends of device j
ϕ_{il}	Fundamental mode displacement at floor level i per 2000 NEHRP
ϕ_{iR}	Residual mode displacement at floor level i per 2000 NEHRP
θ_j	Angle between the axis of the damper and a horizontal plane
Δ	Relative displacement between the ends of a damper

Δ_D	Design earthquake interstory drift per 2000 NEHRP
Δ_{RD}	Residual mode interstory drift per 2000 NEHRP
Δ_{1D}	Fundamental mode interstory drift per 2000 NEHRP
Δ_0	Displacement amplitude
$\dot{\Delta}$	Relative velocity between the ends of a damper
δ_i	Displacement of floor level i
δ_{rj}	Relative displacement between the ends of device j
$\dot{\delta}_{rj}$	Relative velocity between the ends of device j
δ_t	Target displacement per FEMA 273/356 NSP
μ_D	Effective ductility of the building frame per 2000 NEHRP
Ω_0	Framing system overstrength factor per 2000 NEHRP
ω	Angular frequency of sinusoidal motion
∇_D	Design earthquake interstory velocity per 2000 NEHRP
∇_{RD}	Residual mode interstory velocity per 2000 NEHRP
∇_{1D}	Fundamental mode interstory velocity per 2000 NEHRP

References

- ASCE. (1997). Structural Control: Past, Present, and Future, Special Issue, *J. Engineering Mechanics*, ASCE, Vol. 123, 897–971.
- Bruneau, M., Uang, C. M. and Whittaker, A. S. (1998). *Ductile Design of Steel Structures*, McGraw-Hill, New York.
- Constantinou, M. C., Soong, T. T. and Dargush, G. F. (1998). *Passive Energy Dissipation Systems for Structural Design and Retrofit*, MCEER Monograph No.1, Multidisciplinary Center for Earthquake Engineering Research, Buffalo, New York.
- Constantinou, M. C. and Sigaher, A. N. (2000). Energy dissipation system configurations for improved performance. *Proc., 2000 Structures Congress*, American Society of Civil Engineers, Philadelphia, PA.
- Constantinou, M. C. and Symans, M. D. (1993). Experimental study of seismic response of buildings with supplemental fluid dampers. *Structural Design of Tall Buildings*, 2, 93–132.
- Constantinou, M. C., Tsopelas, P., Hammel, W. and Sigaher, A. N. (2001). Toggle-brace-damper seismic energy dissipation systems. *J. Structural Engineering*, ASCE, 127, 105–112.
- EERI. (1993). Theme Issue: Passive Energy Dissipation, *Earthquake Spectra*, 9, 319–636.
- FEMA. (1995) 1994 NEHRP Recommended Provisions for Seismic Regulations for New Buildings, Report No. FEMA 222A, Federal Emergency Management Agency, Washington, D.C.
- FEMA. (1997). NEHRP Guidelines for the Seismic Rehabilitation of Buildings, Report No. FEMA 273 (Guidelines) and FEMA 274 (Commentary), Federal Emergency Management Agency, Washington, D.C.
- FEMA. (2000). Prestandard and Commentary for the Seismic Rehabilitation of Buildings, Report No. FEMA 356, Federal Emergency Management Agency, Washington, D.C.
- FEMA. (2001). 2001 NEHRP Recommended Provisions for Seismic Regulations for New Buildings and Other Structures, Report No. FEMA 369, Federal Emergency Management Agency, Washington, D.C.
- Hanson, R. D. and Soong, T. T. (2001). *Seismic Design with Supplemental Energy Dissipation Devices*, EERI Monograph MNO-8, Earthquake Engineering Research Institute, Oakland, California, 2001.
- ICBO. (1997). Uniform Building Code, International Conference of Building Officials, Whittier, CA.
- ICC. (2000). International Building Code, International Code Council, Falls Church, VA.
- Makris, N., Constantinou, M. C. and Dargush, G. F. (1993). Analytical model of viscoelastic fluid dampers. *J. Structural Engineering*, ASCE, 119, 3310–3325.
- Ramirez, O. M., Constantinou, M. C., Gomez, J. D., Whittaker, A. S. and Chrysostomou, C. Z. (2002a). Evaluation of simplified methods of analysis of yielding structures with damping systems. *Earthquake Spectra*, 18, 501–530.

- Ramirez, O. M., Constantinou, M. C., Kircher, C. A., Whittaker, A. S., Johnson, M. W., Gomez, J. D. and Chrysostomou, C. Z. (2001). Development and evaluation of simplified procedures for analysis and design of buildings with passive energy dissipation systems. Report No. MCEER-00-0010, Revision 1, Multidisciplinary Center for Earthquake Engineering Research, Buffalo, New York.
- Ramirez, O. M., Constantinou, M. C., Whittaker, A. S., Kircher, C. A. and Chrysostomou, C. Z. (2002b). Elastic and inelastic seismic response of buildings with damping systems. *Earthquake Spectra*, 18, 531–547.
- Ramirez, O. M., Constantinou, M. C., Whittaker, A. S., Kircher, C. A., Johnson, M. W. and C. Z. Chrysostomou. (2003). Validation of the 2000 NEHRP Provisions equivalent lateral force and modal analysis procedures for buildings with damping systems. *Earthquake Spectra*, 19, 981–999.
- Sigaher, A. N. and Constantinou, M. C. (2003). Scissor-jack-damper energy dissipation system. *Earthquake Spectra*, 19, 133–158.
- Soong, T. T. (1990). *Active Structural Control: Theory and Practice*, Longman Scientific and Technical, UK.
- Soong, T. T. and Constantinou, M. C. (1994). *Passive and Active Structural Vibration Control in Civil Engineering*, Springer-Verlag, Wien.
- Soong, T. T. and Dargush, G. F. (1997). *Passive Energy Dissipation Systems in Structural Engineering*, John Wiley & Sons, New York.
- Tsopelas, P., Constantinou, M. C., Kircher, C. A. and Whittaker, A. S. (1997). Evaluation of simplified methods of analysis for yielding structures. Report No. NCEER-97-0012, National Center for Earthquake Engineering Research, State University of New York, Buffalo, New York.
- Watanabe, A., Hitomi, Y., Saeki, E., Wada, A. and Fujimoto, M. (1988). Properties of brace encased in buckling restrained concrete and steel tube. *Proc., Ninth World Conference on Earthquake Engineering*, Tokyo, Japan, 4, 719–723.
- Whittaker, A. S., Constantinou, M. C. and Tsopelas, P. (1998). Displacement estimates for performance-based seismic design. *J. Structural Engineering*, ASCE124 905–912.
- Whittaker, A. S., Constantinou, M. C., Ramirez, O. M., Johnson, M. W. and Chrysostomou, C. Z. (2003). Equivalent lateral force and modal analysis procedures of the 2000 NEHRP Provisions for buildings with damping systems. *Earthquake Spectra*, 19, 959–980.

13

Seismic Behavior of Reinforced Concrete Buildings

13.1	Introduction	13-1
13.2	Estimating Period	13-2
	Approximate Solution for the Period of a Reinforced Concrete Frame • Approximate Solution for the Period of a Building with a Dominant Reinforced Concrete Wall	
13.3	Estimating Base Shear Strength	13-7
	Response of a Section Subjected to Axial Load and Bending Moment • Limit Analysis	
13.4	Estimating Drift	13-16
	Linear and Nonlinear Response • Drift • Drift Determination for a Seven-Story Frame	
13.5	Estimating Drift Capacity	13-21
	An Example of Hysteresis for Reinforced Concrete • Sources Contributing to Capacity for Drift	
13.6	Transverse Reinforcement	13-30
	Axial Load • Combined Bending and Shear	
13.7	Reinforced Concrete Walls	13-33
13.8	Future Challenges	13-34
13.9	Concluding Remarks	13-35

Mete A. Sozen

13.1 Introduction

Reinforced concrete has had a less than perfect record in the earthquake environment. Nevertheless, major earthquakes of the past two decades have not revealed any surprises for reinforced concrete construction. It would appear that the major vulnerabilities have already been identified. We are not in a position to be able to say with confidence that “we have seen everything twice” with respect to behavior of reinforced concrete in earthquakes; however, it is not overly optimistic to believe that our current theory and experience should suffice to avoid the mistakes of the past. We understand the reasons for the vulnerabilities that we have observed in the field and in the laboratory, and we are able to avoid them by design. This chapter summarizes a few basic concepts for understanding the response of reinforced concrete to strong ground motion and the principles behind the rules used for proportioning and detailing.¹

¹“Hands-on” examples in Imperial and SI units are provided in appendices to this chapter, posted on the Web site of this book: http://www.crcpress.com/e_products/downloads/download.asp?cat_no=1439

Because the concern is with design but the focus is on behavior, a note of caution is in order. Current building codes are prescriptive. It is important for the engineer to understand how the structure will respond to strong ground motion, but the engineer's first responsibility is to satisfy the code of practice.

The response of reinforced concrete structures to strong ground motion can be controlled through judicious balancing of three ratios:

1. Ratio of mass to stiffness
2. Ratio of weight to strength
3. Ratio of lateral displacement to height

The stated ratios defy precise definitions. In earthquake-resistant design that is almost universally the case, starting with the definition of the ground motion. Earthquake-resistant design of reinforced concrete is closer to art than to science. One must expect the unexpected. The three ratios cited are simply vehicles for understanding and projecting experience.

In this chapter, we will think of structures as if they were fixed at their bases and as if they existed in only one vertical plane. Neither notion is correct but they do serve to help us understand behavior. Our notional two-dimensional structure sitting on rigid ground is an approximation of the actual structure. No matter how exact our analysis is of the notional structure, the results are, at best, an approximation.

The most convenient definition of the mass-to-stiffness ratio is the translational vibration period of the notional structure corresponding to its lowest natural frequency. That is the quantity we will refer to whenever we invoke "period" unless we specify that it refers to a higher mode. For preliminary proportioning, the period is the most important characteristic of a structure threatened by strong ground motion.

The ratio of weight to strength is usually expressed in terms of the "base shear strength" of the structure, the maximum base shear strength calculated for an arbitrary distribution of lateral forces applied at floor levels. The ratio of tributary weight to strength (usually called the "base shear strength coefficient") is an approximate measure of how strong a structural system is in reference to its tributary load. It is not an important property of the structure as long as it is above a threshold value related to the ground-motion demand.

The third ratio is more properly called "drift capacity" or the "limiting-drift ratio." It can be defined as the capacity for the "mean drift ratio," the roof drift divided by the height to roof above base, or the capacity for the "story drift ratio," the lateral displacement in one story divided by the height of that story. It is a measure of the ability of the structure to distort without losing its integrity.

For a given ground-motion demand, the period and the drift capacity are the two critical considerations for proper proportioning and detailing of a structure. The base shear strength coefficient is not likely to be important unless the engineer has made unreasonable choices (such as assigning an entire parking structure to two lateral-force resisting frames) or unless the peak ground velocity turns out to be high (more than one m/sec).

The earthquake-resistant design of a reinforced concrete structure can be accomplished entirely by use of appropriate software — as it should be. The material in the following sections is not intended for detailed design. Rather, it is intended for preliminary design, which ought to be accomplished without automatic devices, and for ensuring that the final design, obtained with the help of software, is reasonable. The old adage — that an engineer should not accept a result from a computational tool he or she could not have guessed at to within $\pm 20\%$ — is most relevant for proportioning and detailing for earthquake resistance.

13.2 Estimating Period

The period of a notional structure is an important index that identifies vulnerability to excessive drift. Even within its constrained domain defined above (lowest mode of a two-dimensional building based on unyielding ground), it may have different meanings depending on how it has been obtained.

A few of the possible definitions of period for a reinforced concrete building structure may refer to the:

1. Measured or estimated (based on measured data of similar buildings) period of the entire building including the effects of nonstructural elements
2. Calculated period based on gross sections of the structural elements
3. Calculated period based on cracked sections of the structural elements
4. Calculated period based on gross or cracked sections but considering also the effects of the nonstructural elements

One must be discriminating when a period is mentioned in relation to design. In this chapter, we will use the second definition and caution the reader whenever we deviate from it. A reinforced concrete structure does not have a unique period — neither before an earthquake because of time-dependent changes nor during an earthquake because of amplitude-dependent changes in its stiffness. We do not pretend that the period we calculate is an actual attribute of the building. Its importance is due to the fact that an experienced engineer can tell from the calculated period of the structure (for a given/assumed earthquake demand) whether there will be problems with drift. It is simply an index to the mass/stiffness properties of the building structure.

13.2.1 Approximate Solution for the Period of a Reinforced Concrete Frame

A preliminary estimate of the period of a building with reinforced concrete frames acting to resist earthquake demand can be obtained using the time-honored expression

$$T = \frac{N}{10} \quad (13.1)$$

where T is the period in seconds and N is the number of stories.

Equation 13.1 was used in the Uniform Building Code for many years until it was replaced (ICBO, 1997) by

$$T = 0.03h^{\frac{3}{4}} \quad (13.2)$$

where h is the height of the reinforced concrete frame above its base in feet.

Both of the above expressions are based on data from and analyses of buildings in California. They are applicable as long as the dimensions of the frame elements are comparable to those used in California. It is not reasonable to assume that either expression will provide an acceptable approximation to the period of a structure in, say, Paducah, Kentucky.

If it is desired to examine the effect on period of changes in values and distributions of the member stiffnesses and story masses, Equations 13.1 and 13.2 do not provide help. Use of a particular software system is intellectually the least demanding option. However, there are occasions when the software does not produce a value that appears reasonable. At those times, the method to use is the Rayleigh Principle (1877).

The Rayleigh Principle states that the energy of a vibrating system is conserved. In reference to the single-degree-of-freedom (SDOF) oscillator with stiffness k in Figure 13.1, it can be stated that at maximum displacement, X_{\max} , where the mass, M, is momentarily at rest, the potential energy is

$$0.5 k * X_{\max}^2. \quad (13.3)$$

When the mass is at its initial position, the velocity is at maximum and can be expressed as $w * X_{\max}$, for simple harmonic motion. The corresponding kinetic energy is

$$0.5 M * (\omega X_{\max})^2. \quad (13.4)$$

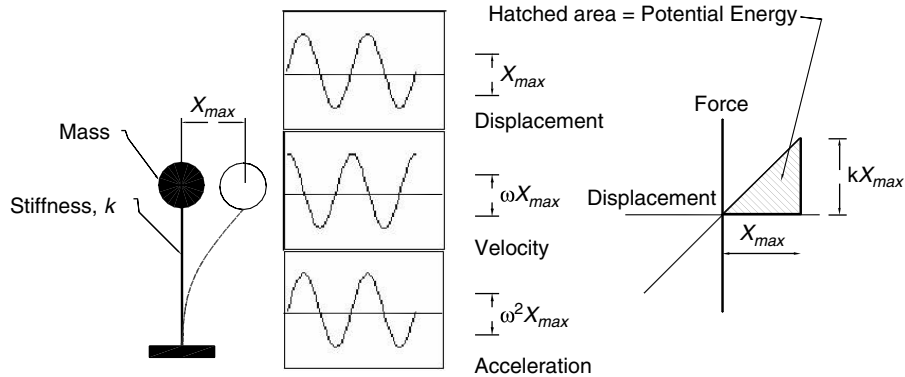


FIGURE 13.1 Response of an SDOF oscillator in harmonic motion.

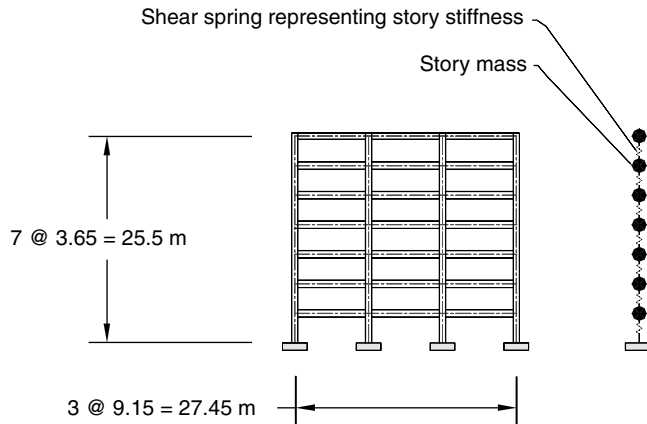


FIGURE 13.2 Seven-story frame and its “shear beam” representation.

Equating the kinetic to the potential energy maxima, the circular frequency is obtained as

$$\omega = \sqrt{\frac{k}{M}} \quad (13.5)$$

in radians per second and the period T in seconds is obtained as $2\pi/\omega$.

Rayleigh suggested that the method would also work for systems with many degrees of freedom as long as the assumed deflected shape was a good approximation of the correct modal shape. To apply the Rayleigh principle to a frame, we will use the numerical procedure by Newmark (1962).

Consider a single two-dimensional frame of a seven-story building (Figure 13.2). The overall dimensions are indicated in the figure. Other relevant properties are:

Young's modulus	25,000 MPa
Column dimensions	
Width	0.60 m
Depth (in plane of frame)	0.60 m
Girder dimensions	
Width	0.45 m
Depth	0.90 m
Tributary mass at each level	145 ton-metric

To simplify the calculations, we will ignore the increase in stiffness at the joints (wire frame).

We approximate the frame by a “shear beam” or a string of concentrated masses connected by shear springs illustrated in Figure 13.2 by concentrating the tributary weight at the floor levels and defining story stiffnesses. Whereas the story stiffness can be determined easily if the girders are assumed to be rigid, in frames with long spans this choice may lead to underestimating the period. To include the effect of girder flexibility, we use an old expression dating from the early design methods for wind (Schultz, 1992).

For intermediate stories, the story stiffness k_{typ} is defined by

$$k_{typ} = 24 \cdot \frac{E_c}{H^2} \cdot \frac{1}{\left(\frac{2}{\sum_{i=1}^{n_c} k_c} + \frac{1}{\sum_{i=1}^{n_{gb}} k_{gb}} + \frac{1}{\sum_{i=1}^{n_{ga}} k_{ga}} \right)} \quad (13.6)$$

k_{typ} = stiffness of a story with flexible girders above and below the story

E_c = Young's modulus for concrete

H = story height

n_c = number of columns

$$k_c = \frac{I_c}{H}$$

I_c = moment of inertia of prismatic column

n_{gb} = number of girders below

$$k_{gb} = \frac{I_{gb}}{L}$$

I_{gb} = moment of inertia of prismatic girder below

L = span length

n_{ga} = number of girders above

I_{ga} = moment of inertia of prismatic girders above

i = number identifying column or girder

To determine the stiffness for the first story, the stiffnesses of the girders below, k_{gb} , are assumed to be infinitely large, with belief in the notion that the footings are inert. Accordingly, the second term in the denominator drops out.

The moments of inertia for the columns and the girders as well as the story stiffnesses are determined in Calculation Sheet A in Appendix A_SI². Axial and shear deformations are neglected. The spreadsheet format (Table A1) offers a very convenient platform for implementing the calculations. The procedure is simple. We assume a deflected shape. The story deflections can be determined arbitrarily but it is helpful if an approximation to the first-mode is selected. In Table A1 the assumed initial story drifts are assumed to vary linearly with height (column D). Mass and stiffness (columns B and C) are entered as coefficients of values listed in cells D17 and D18. The steps in the arithmetic are described in the glossary that is included in Appendix A.

The period from the first iteration is 0.7 sec. (It is usually sufficient to determine a structural period to one tenth of a second.) In iteration 2, we start with the deflected shape resulting from the first iteration. We note that the second iteration does not lead to a change in period, at least not in terms of one tenth of a second. We should note that this is not necessarily always the case. If the masses and the story stiffnesses vary, satisfactory convergence may require a few iterations.

²The material in Appendix A is repeated in Imperial and SI unit systems.

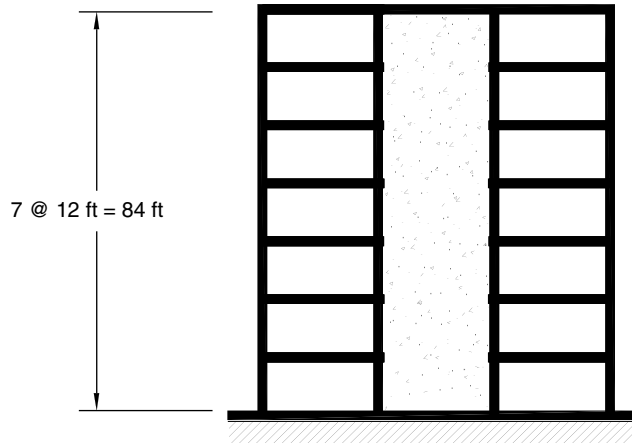


FIGURE 13.3 Frame with dominant wall.

For the frame analyzed, Equations 13.1 and 13.2 lead to periods of 0.7 and 0.8 sec, respectively. For a “regular” frame with members having appropriate sizes and reasonably uniform distribution of typical story heights, the two simple expressions provide satisfactory results and we could have used their results as a frame of reference. The advantage of the calculation we made is that it allows us to get a sense of the effects of changes in stiffnesses and it provides us with a satisfactory deflected shape for the first mode. Both are very useful in preliminary proportioning of reinforced concrete frames.

Tables A2 and A3 illustrate changes in period and modal shape for different stiffness distributions. A reduction in the first-story stiffness, which may be attributed to foundation flexibility and cracking in the column, has a strong effect on the period and the mode shape. Table A3 suggests that increasing girder stiffness is an effective way to reduce the period. The tabular form enables quick investigations of effects of changes in stiffness in any and all members on period.

13.2.2 Approximate Solution for the Period of a Building with a Dominant Reinforced Concrete Wall

In this section, we consider the period of a structure with a wall (Figure 13.3) that dominates the response such that we can neglect the contribution of the frame to its stiffness.

If the wall is prismatic and the story masses are reasonably uniform over the height of the building, a simple and blunt approximation is provided by

$$T_w = \frac{N}{20} \quad (13.7)$$

where T_w is the period of the building and N is the number of stories. Although Equation 13.7 provides a good target for the period, it is likely to underestimate the period unless the wall fills the profile of the building and has a tributary area defined by a width not exceeding approximately 40 ft.

Another simple and direct procedure would be to assume the building to be represented as a uniform cantilever wall with the mass distributed uniformly over its length. For this condition, the period is

$$T_w = \frac{2 \cdot \pi}{3.5 \cdot \sqrt{\frac{E_c \cdot I_w}{m \cdot H^4}}} \quad (13.8)$$

E_c = Young's modulus for concrete

I_w = moment of inertia of wall

m = unit mass assumed to be the total tributary mass divided by height

H = height of wall

Consider a seven-story structure with its lateral stiffness provided by a prismatic wall that is slender enough to permit defining its stiffness based on its bending flexibility. The relevant properties are assumed as follows:

Young's modulus	25,000 MPa
Tributary mass for each level	145 ton-metric
Unit mass	40 ton/m
Moment of inertia	15.5 m ⁴
Total height (uniform story height)	25.55 m

We obtain preliminary estimates, correct to one tenth of a second, from Equation 13.7

$$T_w = 0.4 \text{ sec}$$

and from Equation 13.8

$$T_w = 0.4 \text{ sec}$$

The result from Equation 13.8 suggests that the assumed parameters for the wall are within the experience on which Equation 13.7 is based.

Next, we use the Rayleigh principle as illustrated in Table A4, Appendix A_SI. The arithmetic involved is described in the annotations. The calculated period, to one tenth of a second, is the same as that from the one determined using the simple equations. The only additional information we have is a new approximation to the deflected shape.

The spreadsheet solution provides us with a convenient tool to understand the effects of changes in structural properties. We know that if the wall is cracked uniformly over its full height to have a stiffness of, say, 20% of its initial stiffness, we can estimate its period using Equation 13.5 as a guide for estimating the effect of a reduction in stiffness of 5

$$T_{w\text{cracked}} = T_w * \sqrt{5}$$

or approximately 0.9 sec. But what happens if the stiffness is reduced only at the lowest three levels? Table A5 in Appendix_SI gives us the approximate answer and the understanding that changes in the stiffness of the lower levels, by design or by accident, are critical for the period.

What about such changes in the top three levels? Table A6 provides an answer. The effect on period is negligible.

These exercises prepare us for making quick estimates of the relative drifts of competing framing systems.

13.3 Estimating Base Shear Strength

13.3.1 Response of a Section Subjected to Axial Load and Bending Moment

The assumptions and procedures for determining the moment curvature relationship for reinforced concrete have been presented in many textbooks and notably in Chapter 5 of the book (see Blume et al. 1961). The reader is referred to that document for detailed background information.

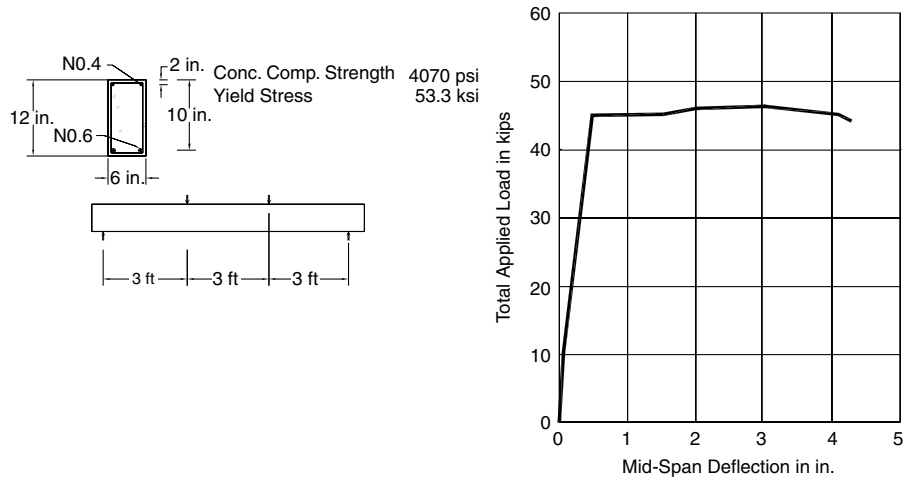


FIGURE 13.4 Measured load-deflection relationship for a reinforced concrete beam loaded at third-points of its span.

For sections with proportions appropriate for earthquake-resistant structures, the flexural strength can be approximated closely using no more than the principles of equilibrium and a rudimentary knowledge of the strengths of the materials involved. Determination of the unit curvature for a specified strain is also easy. However, establishing the limiting unit curvature is difficult because it is sensitive to many parameters. To boot, using this limit to determine rotation is even more difficult. That is why it is preferable to handle the problem of toughness in design by controlling parameters such as the mean unit stress on the section and the amounts of longitudinal and transverse reinforcement. An explicit and accurate calculation of the limiting rotation that is universally applicable under cycling loading is not yet within reach.

Before we start with the details of the computational process, it is instructive to examine the observed flexural response of reinforced concrete members under two different conditions: (1) in a span with no moment gradient and (2) in a span with moment gradient.

The measured moment-deflection response of a reinforced concrete member subjected to bending moment only is shown in Figure 13.4 (Gaston, 1952). Ideally, the moment-deflection curve exhibits three stages identified by different slopes or stiffnesses: (1) Stage 1, before flexural cracking, (2) Stage 2, after flexural cracking and before yielding and (3) Stage 3, after yielding. We must remember that the section considered has specific properties. It is reinforced moderately to develop yielding of tensile reinforcement before the compressed concrete reaches its limiting strain in compression. The reinforcement is concentrated at one layer in the tension and compression flanges. The properties cited are representative of those of members used in earthquake-resistant structures. However, we are considering a case with monotonically increased moment. That is not typical loading for a structure subjected to strong ground motion. The three stages are convenient for describing the general force-displacement properties of a reinforced concrete section but we must not conclude that they would all appear in every cycle of response of a member subjected to moment reversals.

For the case of monotonically increased load, we note that the slope in Stage 3 is close to “flat.” If we ignore Stage 1, which we can do justifiably in all but very lightly reinforced members, we can think of the moment-deflection curve as elasto-plastic. Furthermore, we can notice the reflection of the nearly elasto-plastic stress-strain curve for the reinforcement in the moment-deflection curve.

The measured moment-deflection response of a reinforced concrete member subjected to combined bending and shear is shown in Figure 13.5 (Wight, 1973). For this element the result of one complete cycle of load is shown. The striking feature is that the moment-deflection curve does not have a flat slope in Stage 3 of the first loading to a maximum and the shape of the curve for the reversal does not lend itself well to idealizing it as a straight line.

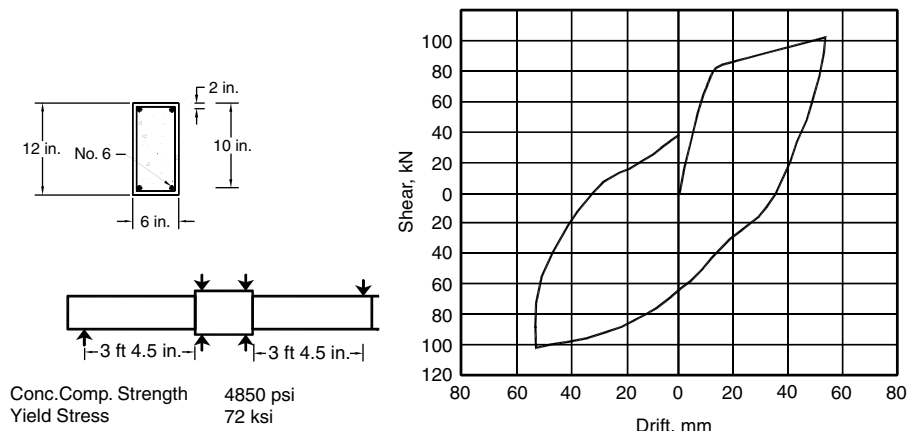


FIGURE 13.5 Load-deflection curve for a reinforced concrete beam with moment constantly changing along its span

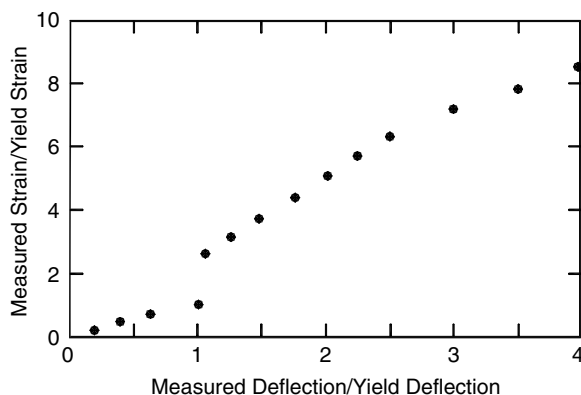


FIGURE 13.6 Measured moment-deflection relationship showing the “jump” phenomenon in reinforcement strain as the applied moment exceeds the yield moment in a span with changing moment.

Why is the “plastic” portion of the load–displacement relationship lost even in the first loading to a maximum? The data in Figure 13.6 reveal the reason. Measured tensile-reinforcement strains, as a coefficient of the yield strain, are plotted against the measured deflection at load point (as a coefficient of the deflection at yield). At the yield deflection, the tensile strain in the reinforcement increases with hardly any increase in deflection. In effect, the reinforcement strain goes abruptly from the yield strain to the value at which strain hardening begins. The flat portion of the stress–strain curve for the reinforcement is thus not perceptible in the load–deflection relationship. Increase in deflection beyond yield requires an increase in moment.

Members resisting earthquake effects are typically subjected to moment gradients. We can and will use the elasto-plastic response to help us simplify certain concepts of analysis, but we should not assume that it is correct. And we should remember that the elasto-plastic response is likely to be less correct for cyclic loading.

In this section we will first consider the moment–curvature relationship as a vehicle for understanding some of the design rules and not as a direct tool for design. For a moderately reinforced section subjected to constant axial load and monotonically increasing moment, a representative moment curvature relationship is shown in Figure 13.7.

Engineering literature contains considerable material on the construction of the moment–curvature diagrams for reinforced concrete sections. It is almost impossible not to think that the topic is at once

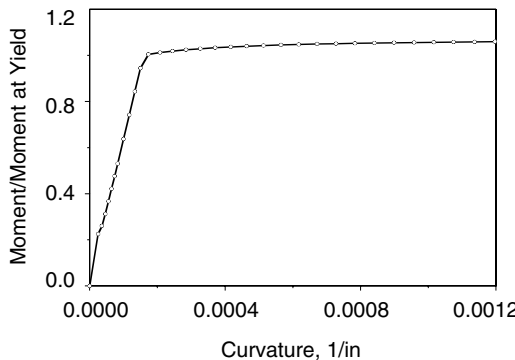


FIGURE 13.7 Calculated relationship between bending moment and unit curvature.

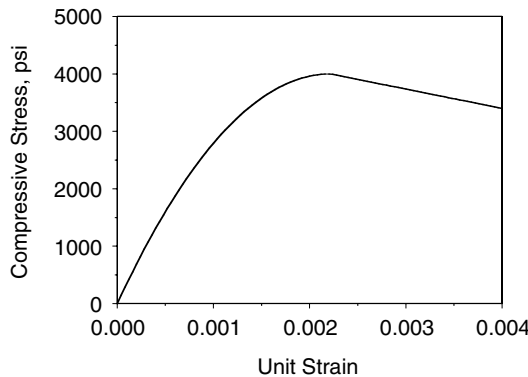


FIGURE 13.8 The Hognestad stress-strain relationship for unconfined concrete in compression.

very well understood and very important. Actually, the relationship between moment and curvature under reversals into the nonlinear range of response is well beyond our ability to determine to the degree of exactness often implied. And fortunately, safe design does not require exact calculation of the relationship between moment and curvature. The critical factor is the detailing of reinforcement. However, understanding the moment–curvature relationship under monotonically increasing moment is helpful to understanding behavior.

We start with the assumption that the reader is familiar with Euclidean geometry and the conditions of equilibrium, two theoretical concepts necessary for relating internal stresses to external forces at a section.

We ignore the effects of the tensile strength of concrete. It is indeed negligible unless the amount of reinforcement is negligible.

The concept for determining the moment–curvature relationship for a reinforced concrete section is simple and direct. For a given section subjected to moment about one axis, two sets of operations are involved. The first set includes those that define the section, the materials and the axes about which moments are traditionally defined. (The moment can be defined about any axis, provided it is consistent with the definition of the external moment.)

1. Assume a relationship between unit stress and unit strain for compressed concrete. An example for unconfined concrete is shown in Figure 13.8 (Hognestad, 1951).
2. Assume a relationship between unit stress and unit strain for the reinforcement. An example is shown in Figure 13.9.
3. Determine the location of the plastic centroid. The plastic centroid is defined as the centroid of the maximum forces in the materials constituting the section. An example is provided in Figure

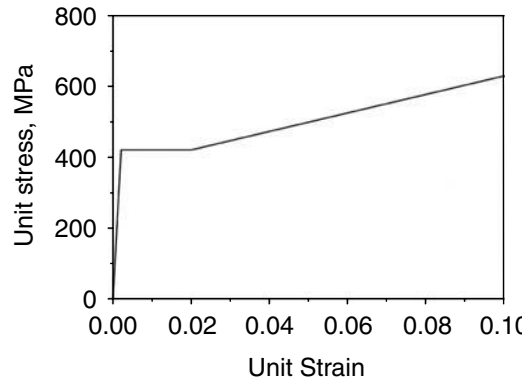
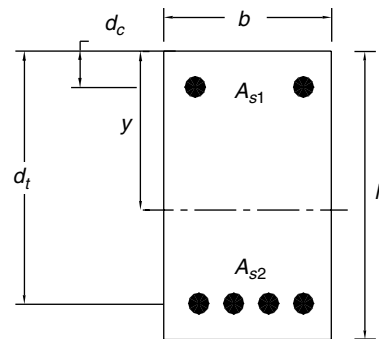


FIGURE 13.9 Representative idealized stress–strain relationship for steel reinforcement.



$$y = \frac{d_c (A_{s1} \cdot f_y) + d_t (A_{s2} \cdot f_y) + \left(b h f'_c \cdot \frac{h}{2} \right)}{(A_{s1} \cdot f_y + A_{s2} \cdot f_y + b h)}$$

f_y : yield stress of reinforcement

f'_c : compressive strength of concrete in the section

The plastic centroid has been determined using “gross section.”

FIGURE 13.10 Definition of plastic centroid for a rectangular reinforced concrete section.

13.10. For a symmetrical section symmetrically reinforced about the bending axis, the plastic centroid coincides with the geometric centroid.

The second set of operations are the ones that are repeated until the correct solution is obtained.

1. Assign a strain $\text{Abs}(\varepsilon_c) \leq \text{Abs}(\varepsilon_{cu})$ to the extreme fiber in compression. The symbol ε_{cu} refers to the limiting strain of the concrete in compression (Figure 13.11).
2. Assume a depth for the neutral axis, κd , where κ is a coefficient and d is the effective depth for the section.
3. Assuming a linear strain distribution, determine the strains in the reinforcement.
4. Using the assumed stress–strain curve for compressed concrete, determine the total force in the concrete and the location of its centroid.

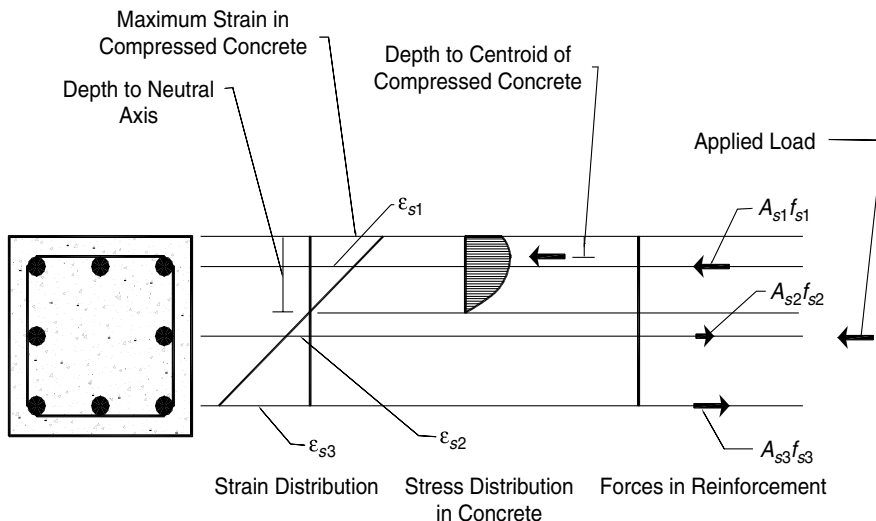


FIGURE 13.11 Assumed strain, stress and force distributions.

5. Using the assumed stress-strain curve for the reinforcement, determine the forces in the reinforcement layers.
6. Sum the axial forces, including the axial load if any, over the section.
7. Compare the deviation of the calculated axial load against an assumed tolerable limit. If the limit is not satisfied, repeat steps 2 through 7. If the limit is satisfied, go to Step 8.
8. Determine the moment generated by the material forces about the plastic centroid, assuming that the external axial load is applied at the location of the plastic centroid. Continue starting in step 1 with a different value of the strain ϵ_c in increments to ϵ_{cu} .

The steps are simple but the work is tedious. Commercial software will provide the answer readily. Unfortunately, using ready-made software tends to provide little insight into the relative effects of the many assumptions made. Appendix B³ contains an open algorithm in MathCad that the reader can use as is or modify easily to suit his/her choices for the stress-strain curves. In addition, two implicit spreadsheet routines for determining moment-curvature and interaction diagrams (interaction of limiting axial load with bending moment) are included in Appendix C⁴.

It is of interest to examine a few cases calculated using the open algorithm in Appendix B simply to obtain perspectives of the effects of some of the parameters.

Consider a 600-mm-square rectangular section with three layers of reinforcement as shown in Figure 13.11. The material properties are assumed to be those in Figures 13.8 and 13.9. We will consider five cases involving different combinations of axial load, concrete compressive strength, and limiting compressive strain in concrete.

First we consider a section reinforced with eight #11 bars ($\rho = 2.2\%$). The concrete strength is taken as 25 MPa. The axial load is zero. We use “Agent Plotter” in Appendix B to develop the moment-curvature relationship. The result is identified as case 1 in Figure 13.12. Sequential yielding in the extreme and middle layers of reinforcement is reflected in the shape of the curve. The limiting curvature is $4.5 \times 10^{-5} \text{ mm}^{-1}$.

For case 2, the compressive strength of the concrete is increased to 50 MPa without modifying the shape of the stress-strain curve. As would be expected, the increase in resisting moment is almost trivial. At the same time, there occurs an increase in calculated limiting curvature. In this case, doubling the concrete strength increases the limiting curvature by approximately one third.

³Appendix B contains versions of the open algorithm in Imperial and SI unit systems.

⁴The spreadsheet routines in Appendix C can be used in SI or Imperial units as long as all input is consistent.

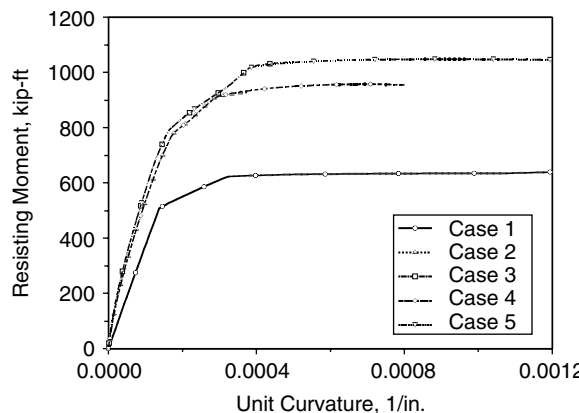


FIGURE 13.12 Calculated moment–curvature relationships.

Case 3 is similar to case 1 except for the addition of a compressive axial load of 2700 kN, corresponding to a unit stress of $0.25f'_c$. There is an increase in the resisting moment accompanied by a strong reduction in the limiting curvature.

The difference between case 3 and case 4 is the concrete strength. For case 4, the concrete strength is assumed to be 50 MPa. It is observed that both the limiting strength and curvature are more sensitive to a change in the concrete strength if the section has an axial compressive load.

The properties used in case 5 differ from those for case 3 in the assumed limiting compressive strain. For Case 5, the compressive strain is assumed to be 0.008. We note that the limiting curvature is doubled with respect to that for case 3.

Admittedly, the results are all notional. But they do emphasize that the most efficient way to improve curvature capacity is to improve the compressive strain limit of concrete. Increase in compressive strain limit can be effected by proper use of transverse reinforcement.

The results also highlight that axial compression reduces curvature capacity. Unless dense spiral reinforcement is used, it is not wise to design columns with axial unit stresses exceeding $0.25f'_c$.

The reader is encouraged to try different cases using the tools provided in Appendix B or C to develop a perspective of the relative effects of the critical parameters affecting curvature capacity.

We note that the moment–curvature relationships calculated all lend themselves to idealization as elasto-plastic despite the caution provided by a comparison of the measured responses in Figures 13.4 and 13.5. We recognize that our calculation of the moment–curvature relationship ignores the moment-gradient. That does not stop us from assuming it to be elasto-plastic in the next exercise.

13.3.2 Limit Analysis

Limit analysis for base shear strength is procedurally identical to limit analysis for gravity loading, but there is an important difference between them.

For gravity loading, the locations and relative magnitudes of vertical loads are known or specified. The result from the analysis is a crisp measure of strength for that loading and it can be more or less than the applied load. It is a valid result if it is concluded that the factor of safety is a certain number or that the applied load exceeds the limiting capacity of the structure.

For lateral loading attributed to earthquake effects, the relative magnitudes of the loads assumed to act at floor levels are very seldom known exactly. Usually, their distribution over the height of the building is assumed arbitrarily. The resulting base shear is not a property independent of the assumed loading pattern.

It is also relevant to note that, if the analysis is made properly, the base shear strength cannot be less than the applied load. In fact, the base shear strength for a given loading pattern defines the magnitudes of the loads. This is a subtle but important characteristic of the behavior of a structure in an earthquake.

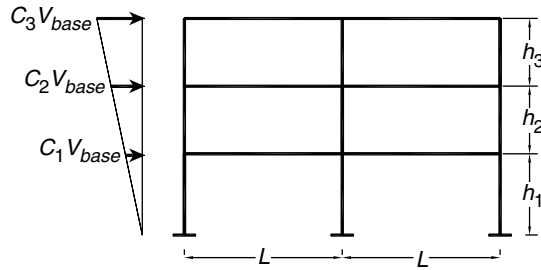


FIGURE 13.13 Story-force distribution assumed for a planar three-story frame.

Subjected to a strong ground motion, the structure generates the maximum forces it can. It is not loaded but loads itself. And the stronger it is, the larger are the lateral loads that may develop during strong ground motion. It is not an exaggeration to claim that the engineer, who proportions the members, and not the earthquake, determines the magnitudes of the lateral forces.

As long as it is understood that the result is simply an index value to the lateral strength of the structure, there is reason to keep the procedure simple and straightforward. It is permissible and safe, with respect to base shear strength, to treat frame members as line elements. All critical joints are assumed to have the requisite rotation capacity, although the shear forces in the members and adequacy of anchorage must be checked after conclusion of the analysis.

The most convenient vehicle for carrying out the necessary computations is provided by the virtual-work method. The process is iterative. It entails successive selections of particular mechanisms until a minimum base shear is found. In each iteration, a base shear force is determined on the principle that the sum of the total external work and the total internal work is zero.

For a given structure analyzed in two dimensions, the main steps are:

1. Assume the relative magnitudes of the lateral loads applied at floor levels.
2. Determine the moment capacities at all critical sections at faces of joints. Moment–rotation response is assumed to be elasto-plastic.
3. Assume a set of plastic hinges at selected joints of the structure to permit lateral movement of the structure without increase in lateral load (a “kinematically admissible” mechanism).
4. Assume a unit virtual displacement at a selected level (usually at the roof level).
5. Determine the virtual work done by the internal forces at the plastic hinges corresponding to the movement of the “mechanism” to accommodate the virtual displacement.
6. Determine the virtual work done by the external loads corresponding to the movement of the selected mechanism to accommodate the virtual displacement.
7. Equate internal to external virtual work to determine the base shear.

Steps 3 to 7 are repeated for several mechanisms to find the one with the minimum base shear force. Strictly, all possible mechanisms need to be investigated. With experience, the engineer can identify the governing mechanism without having to check all.

In the following paragraphs, the procedure associated with the steps listed above is described in reference to the two-dimensional wire-frame shown in Figure 13.13. A numerical implementation is included in Appendix D.

Step 1

We assume for convenience, and not because it represents the truth, that the lateral acceleration that defines the concentrated story forces varies linearly with height.

$$F_i = \frac{w_i h_i}{\sum_{x=1}^n w_x h_x} \cdot V_{\text{base}} \quad (13.9)$$

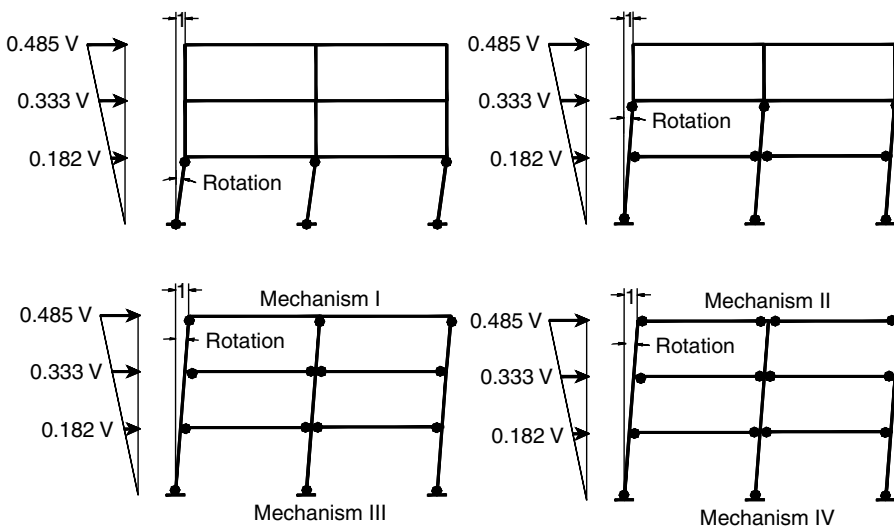


FIGURE 13.14 Mechanisms assumed to determine base shear strength.

F_i = lateral force at level i

h_i = height above base to level i

w_i = concentrated story weight at level i

n = number of levels

w_x = concentrated story weight at level x

h_x = height above base to level x

V_{base} = shear at base

The coefficients C_1 through C_4 in Figure 13.13 are determined as coefficients of the base shear strength or as ratios F_i/V_{base} .

Step 2

The moment capacities of the horizontal and vertical elements of the frame at the joint faces are determined as described in detail in Appendix D. It is plausible to determine the column moments for axial forces related to gravity loads.

Step 3

Four examples of possible mechanisms are shown in Figure 13.14. Mechanism I is called the “first-story mechanism” and Mechanism IV is called the “structural mechanism.” Both are easy to evaluate and, for regular structures, the minimum solution for base shear is likely to be bracketed by their results, the minimum often being closer to the value determined from the structural mechanism. In view of the approximations in the determination of the base shear strength, the lateral-force distribution, it is plausible to do only the first-story and structural mechanism and then estimate the base shear strength if the frame in question has reasonably uniform strength and mass distributions. Strictly, there are more mechanisms than the four shown for the frame. For example, a second- or a third-story mechanism, similar to the first-story mechanism, can also be considered. However, unless the structure has been proportioned completely unreasonably, it is possible to estimate the minimum base shear without having to consider every possible mechanism, as would be required for a rigorous solution.

Step 4

Assumed virtual displacements for the four mechanisms are shown in Figure 13.14. It is important to note that these are virtual (imaginary) and not real displacements. Strictly, the unit displacement has no units. It does not exist. It is simply a ploy to set up the equilibrium equations easily. What is important

is to realize that the displacement is accommodated exclusively by rotation at the assumed plastic-hinge locations. As this nonexistent virtual displacement occurs, there is no bending along the lengths of the members. They remain inert. That, in itself, should show that we are not dealing with structural mechanics as we know it but with a mechanical analog.

We note that for each mechanism of the wire-frame, there is a crisp relationship between virtual displacement and virtual rotation at the plastic hinges. For example, for Mechanism I, with the story height equal to h_1 , the relationship is

$$\text{Virtual Joint Rotation} = \text{Virtual Unit Displacement}/h_1$$

For Mechanism II, the rotation of interest is

$$\text{Virtual Joint Rotation} = \text{Virtual Unit Displacement}/(h_1+h_2)$$

For a wire-frame, the virtual rotation of the column is the same as that for the girder. Instead of virtual displacements, virtual rotations could have been assumed with the same result.

Step 5

The virtual internal work at each hinge is given simply by the relationship:

$$\text{Virtual Internal Work} = \text{Virtual Rotation} * \text{Moment Capacity of Frame Element}$$

The total virtual internal work is the absolute sum of the virtual internal work at each hinge.

Step 6

The virtual external work is determined for each of the lateral loads by

$$\text{Virtual External Work} = \text{Virtual Displacement at Level } i * \text{Lateral Force at Level } i$$

It follows readily that the total external work, determined in terms of the base shear, is the sum of the work at all levels.

Step 7

The virtual internal work determined in Step 6 is equated to the external virtual work determined in Step 7 as a coefficient of the base shear to determine the base shear for that mechanism.

It is proper to ask the questions, "What do we do with the result?" and "Is there a criterion of acceptability?"

Certainly, the calculated base shear force should exceed that specified by the applicable design specifications. If it does not, then it is very likely that something was missed in selecting reinforcement and member sizes.

The base shear force determined from limit analysis has its best use in helping the designer to understand the result of the design process, again vis-à-vis comparable or competing structural systems. It is also useful in checking any static incremental-force analysis that may have been made (the maximum result from the incremental analysis should match that from limit analysis) as well as in providing a frame of reference to base shears obtained in dynamic nonlinear analysis.

Limit analysis for base shear strength is seldom a design requirement, which confirms the relative lack of importance of base shear strength in the design environment despite the fixation on it as the pivotal requirement in traditional design. It would take a rare structure to fail because it did not have adequate base shear strength.

An application is illustrated in detail in Appendix D.

13.4 Estimating Drift

13.4.1 Linear and Nonlinear Response

A reinforced concrete building structure, including its foundation, is a complex entity. So is the typical ground motion. The result of the interaction of a building with a ground motion is even more complex. To try to understand their interaction through the analysis of an SDOF oscillator subjected to a series

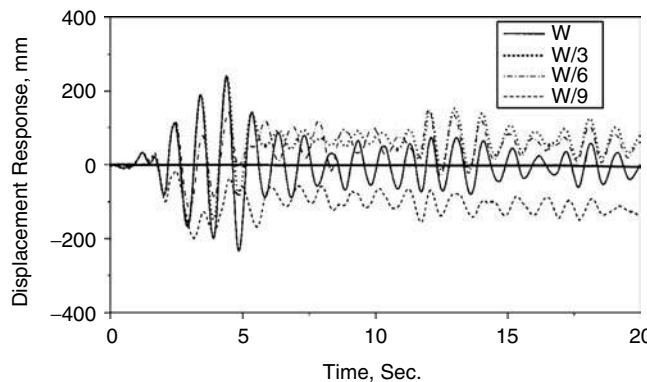


FIGURE 13.15 Calculated displacement responses of oscillators with different strengths to a ground motion with high peak velocity (initial period of oscillator = 1.0 sec.).

of acceleration pulses at its base is not too far away from the parable of the child on the beach trying to pour the ocean into a hole dug in the sand. Nevertheless, study of the response of an SDOF oscillator to a ground-motion component has served well to organize and project experience. In this respect, the SDOF has two supreme advantages. It is easy to implement and it is difficult, though not impossible, to believe that it is an accurate representation of the building.

Because it is such a simple and effective tool for understanding, if not for design, it is important to have hands-on experience with the processing of the SDOF oscillator to determine its response even though it may seem far removed from cement and aggregate. We will take the time to recall in Appendix E1 the simplest numerical solution for the dynamic response of an SDOF oscillator: the central-difference method. We intend to use the method to study and understand the differences between linear and nonlinear response of reinforced concrete systems. More importantly, our direct involvement with the calculation of dynamic response may help us divest ourselves of a considerable amount of misplaced pre-judgment based on our familiarity with static analysis of structures.

Two annotated MathCad routines are included in Appendix E: SDOF-1 and SDOF-2. The reader familiar with the calculation of dynamic response of an SDOF oscillator may skip the text in Appendix E1.

The routine in SDOF-1 describes the response of a linear lightly damped oscillator to one horizontal component of a representative ground motion with a peak acceleration of $g/2$. The period of the oscillator was set to be 1 sec. (It can be reset in SDOF-1 very easily to examine other cases.) The calculated displacement-response history shown by the solid curve in Figure 13.15, developed for linear response, is not surprising. We note that the waveform indicates a periodicity of close to 1 sec and waveform amplitude varies with the variations in the base excitation. The maximum calculated displacement is approximately 0.24 m. The corresponding maximum spring force is equal to the assumed weight of the oscillator mass.

The routine in Appendix SDOF-2 is based on the assumption that the oscillator has an "elasto-plastic" spring. The slope of the force-displacement curve is equal to that for the previous routine, resulting in an initial period of 1 sec., and zero whenever the absolute force reaches a prescribed limit. We use SDOF-2 to calculate displacement responses for the same oscillator for three different levels of base shear strength coefficient: $2/3$, $1/3$, and $1/9$ of its weight as indicated in Figure 13.15. We note that the waveforms are perceptibly different from that for linear response. A permanent set is calculated for each of the three cases, but the maximum displacement is approximately the same as that for linear response. We have no reason to expect this observation to hold for all cases, but the case studied is sufficient to make us question the pre-judgment that comes from static analysis, that if the strength is reduced drastically, all other parameters remaining the same, the displacement response should increase. It is in the interest of the

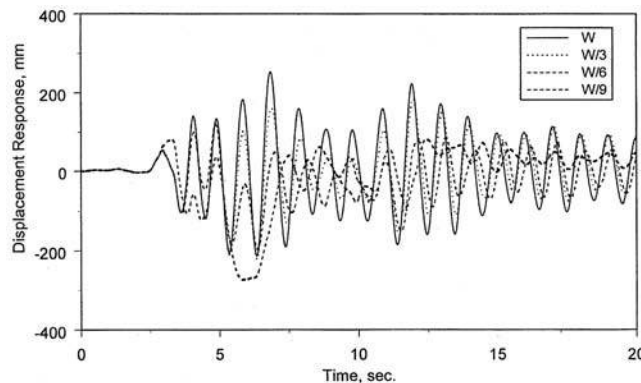


FIGURE 13.16 Calculated displacement responses of oscillators with different strengths to a ground motion with moderate peak velocity (initial period of oscillator = 1.0 sec.).

reader to develop his/her own perspective of the phenomenon by using the routine SDOF-2 for different cases and with different ground motions.

From similar studies made for a wide range of force–displacement relationships and ground motions, Shimazaki (1984) concluded that the nonlinear response displacement for an oscillator with an initial period of T sec would be bounded well by the response displacement calculated for a linear oscillator with the period $\sqrt{2}$ sec, at a damping factor of 2% as long as the initial period was more than approximately 0.6 sec, or the period at which the “nearly constant acceleration” and “nearly-constant velocity” response ranges coincide. LePage (1994) determined that if the response displacement is assumed to increase linearly with period even at low periods, the limitation observed by Shimazaki would be lifted, and stated the bounding displacement for stiff soil to be

$$\text{Displacement} = 500 \cdot \alpha \cdot T \cdot \sqrt{2} \text{ mm} \quad (13.20)$$

where α is the ratio of the effective peak ground acceleration to the acceleration of gravity and T , in sec, is used as a dimensionless coefficient. It is the calculated period based on uncracked section.

The displacement–response plots in Figure 13.16 refer to a different ground motion component having the same maximum acceleration of 0.5g. In this case, we note that nonlinear displacement response for an oscillator with a period of 1 sec does not exceed the linear one as long as the base shear strength coefficient is 1/3 or more. At a base shear strength coefficient of 1/9, the result changes. The nonlinear displacement experienced at approximately 6 sec is comparable in amplitude but has a strongly different shape. This observation drives us to investigate further. Again using SDOF-2, we calculate response histories of 0.5-sec oscillators with base shear strengths of W , $2W/3$, $W/3$, and $W/9$, where W is the weight of the system. The results in Figure 13.17 are quite different. We can consider the response for the oscillator with a base shear strength of $W/3$ tolerable in view of the fact that its maximum displacement is within LePage’s bound, but the response of the oscillator with a base shear strength of $W/9$ indicates that the insensitivity of nonlinear peak displacement response to strength is not universal.

Recognizing that the main utility of Equation 13.20 is to help make judgments about relative flexibility of competing framing schemes rather than predicting drift, we conclude that as long as the base shear strength is not less than $W/3$ we can use it generally to determine the spectral displacement, and if the base shear strength is between $W/10$ and $W/3$ we should limit it to ground motions where we have reason to believe that the ground velocity is not likely to exceed 0.75 m/sec. In fact, if the expected peak ground velocity exceeds 1 m/sec, the spectral drift response should be expected to be intolerable if the base shear strength is less than $W/3$.

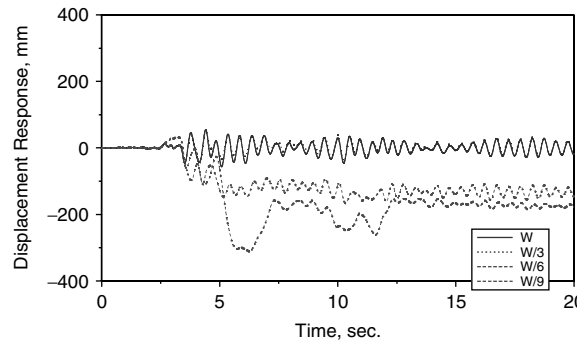


FIGURE 13.17 Calculated displacement responses of oscillators with different strengths to a ground motion with moderate peak velocity (initial period of oscillator = 0.5. sec).

13.4.2 Drift

The primary function of the calculation for drift is not a prediction. The low probability of estimating actual drifts closely should follow readily from the uncertainty associated with the prediction of the ground motion. The primary function of the drift computation is to make the right decision about the ratio of mass to lateral stiffness. Because the mass is usually not an easily modified variable, given the footprint and height of the building, the process for drift control is essentially a process for selection of type and size of framing.

It is true that the pragmatic way to determine drift is to let the software take care of the drudgery. However, as in the case of determining period, it is essential to have access to a transparent procedure to judge the reliability of results from software.

The drift for low- and mid-rise structures with reasonably uniform distribution of masses and stiffness over their heights and around their vertical axes can be estimated closely by considering only the translational mode corresponding to the lowest natural frequency in two dimensions. The relationship between the characteristic response displacement, the spectral displacement related to the first-mode period and the story drifts can be determined by using Equation 13.21:

$$D_i = S_d \cdot \phi_i \cdot \Gamma \quad (13.21)$$

where

D_i = drift at story i

S_d = characteristic (spectral) displacement corresponding to the modal period

Φ_i = modal-shape coefficient for level i

$$\Gamma = \frac{\sum m_i \cdot \phi_i}{\sum n_i \cdot \phi_i^2} \quad (13.22)$$

m_i = mass at level i

n = number of levels above base

It is useful to note that for building structures with uniform mass and stiffness distribution over height, the factor Γ is approximately 5/4 for frames and 3/2 for walls if the modal-shape coefficient at roof is set to unity.

13.4.3 Drift Determination for a Seven-Story Frame

We consider a single interior frame with its tributary mass (Figure 13.2). The period and the modal shape were determined in Appendix A, Table A1.

The period was determined to be 0.7 sec. The modal shape determined is listed below:

$$\phi^T = (1.00 \ 0.95 \ 0.86 \ 0.73 \ 0.56 \ 0.37 \ 0.16)$$

Because the masses are the same at all levels, we can ignore the mass in determining the participation factor:

$$\Gamma = \frac{\sum_{i=1}^7 \phi_i}{\sum_{i=1}^7 (\phi_i)^2}$$

$$\Gamma = 1.27$$

To obtain a plausible estimate of the drift corresponding to nonlinear response for a ground motion indexed by 0.5G on stiff soil, we use Equation 13.20 with period equal to 0.7 sec, and α equal to 0.5.

$$S_d = 500\sqrt{2 \cdot T \cdot \alpha}$$

$$S_d = \sim 250 \text{ mm}$$

Using Equation 13.21, the drifts at the seven levels are estimated to be

$$\text{StoryDrift}^T = (314 \ 299 \ 270 \ 229 \ 176 \ 116 \ 50) \cdot \text{mm}$$

We recognize that reporting drifts to 1 mm is unnecessary even if the quantities were exact but we retain the mm because we are going to take the differences of the calculated drifts in the next step. The interstory drifts or the differences between the calculated drifts at successive levels are

$$\text{InterstoryDrift}^T = (15 \ 29 \ 41 \ 53 \ 61 \ 66 \ 50) \cdot \text{mm}$$

resulting in interstory or story drift ratios, in percent, of

$$\text{InterstoryDriftRatio}^T = (0.4 \ 0.8 \ 1.1 \ 1.5 \ 1.6 \ 1.8 \ 1.4) \cdot \%$$

The values are estimates of the plausible upper-bound drift for an earthquake defined by an effective peak acceleration of 0.5G on stiff soil. They would be considered to be high but not intolerable. However, it is unrealistic to treat them as absolute values. The evaluation is best used in the process of selecting among different types of framing with different sizes of members. In that case, the relative quantities provide a sensible base for decision. By themselves, one must not take them as predictions. Serious prediction would require knowledge of the ground motion, the foundation compliance, and the stiffness changes in structural/nonstructural elements. Under the best of circumstances, the drifts realized could vary $\pm 50\%$ from the estimated values.

We could have anticipated the high drift ratios at the time we calculated the period of 0.7 sec for a seven-story frame. The characteristic displacement corresponding to that period as given by the LePage expression is 0.25 m. Assuming a frame with uniform mass and stiffness properties, the roof drift would be estimated to be

$$(5/4)*0.25 = 0.31 \text{ m}$$

the corresponding mean drift ratio is

$$0.31*100/(7*3.65) = 1.2\%.$$

The result obtained for the mean drift ratio would immediately have suggested to us that a few of the individual story drifts would exceed what is generally considered to be desirable, 1.5%. The expectation is that the maximum story drift in a frame with reasonably uniform distribution of mass and stiffness could be as high as twice the mean drift ratio.

13.5 Estimating Drift Capacity

It is proper to begin the discussion of force–displacement relationship for reinforced concrete members by recognizing that the driving concern is the maximum drift (lateral displacement) that a reinforced concrete structure will sustain without losing its integrity under reversals of displacement into the linear range of response. In the following, we will call that limit “drift capacity.”

To proportion reinforced concrete structures adequately for earthquake resistance, it is not essential to determine the drift capacity. For structures considered to be regular (structural types fitting into the body of experience that has led to the formulation of the applied code), drift capacity is expected to be achieved by following a set of prescriptive rules. To proportion reinforced concrete structures properly in special circumstances does require a basic minimum understanding of the relative effects of the parameters affecting drift capability or limiting drift. However, the object is not the calculation of the limiting drift but the organization of the variables affecting it to be able to weigh the relevant evidence.

The drift capacity, besides being related to the unit curvature capacity of a section, is a complex function of displacement history. The number of cycles beyond yield level and their sequence affect the drift capacity. Many investigators have connected drift capacity directly to shear strength (Wight, 1973, Priestley 1994, Aoyama 1993, Aschheim 2000) independently of the displacement history. Pujol (2002) has observed it to be sensitive to the displacement history and expressed drift capacity as a function of compound stresses using Coulomb (1773) as a paradigm.

We will start the discussion with a particular view of the force–displacement relationship or the hysteretic response of reinforced concrete elements under load reversals. This relationship (hysteresis, a term that is a legacy of the shortfalls observed in wine transported across the Mediterranean in classic times) is often considered in terms of the base shear force vs. the drift ratio at a given height in the structure (ratio of the drift at that height to the height above base). After noting some general characteristics of hysteresis for reinforced concrete, we will focus on the drift capacity followed by a detailed discussion of the relationship between bending moment and unit curvature and its relationship to drift capacity.

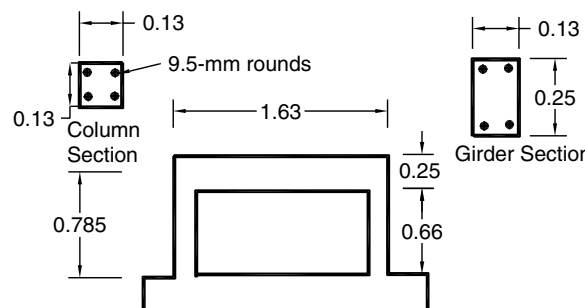


FIGURE 13.18 Test frame.

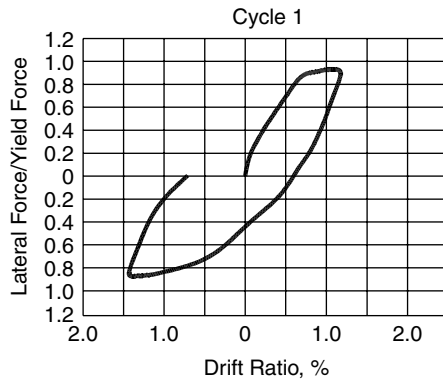


FIGURE 13.19A A force–displacement relationship in a cycle of applied displacement for the test frame in Figure 13.18.

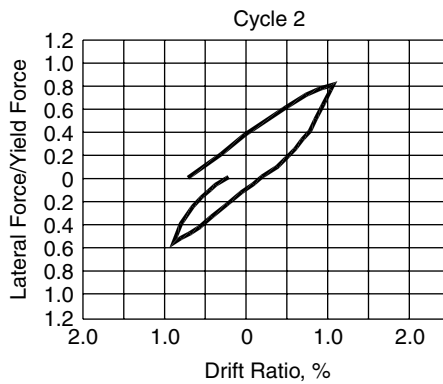


FIGURE 13.19B A force–displacement relationship in a cycle of applied displacement for the test frame in Figure 13.18.

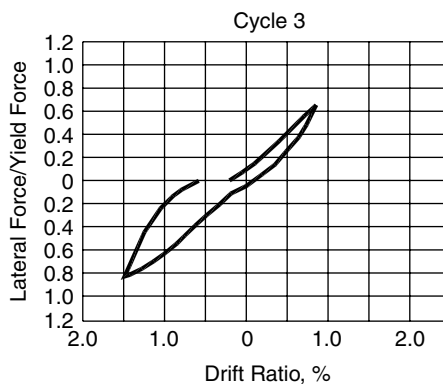


FIGURE 13.19C A force–displacement relationship in a cycle of applied displacement for the test frame in Figure 13.18.

13.5.1 An Example of Hysteresis for Reinforced Concrete

A small-scale reinforced concrete test frame having one story and one bay is shown in Figure 13.18. The top girder of the frame was displaced in its own plane to go through a drift history (drift measured at mid-depth of the “roof” girder) obtained in the earthquake-simulation test of a duplicate test frame. The

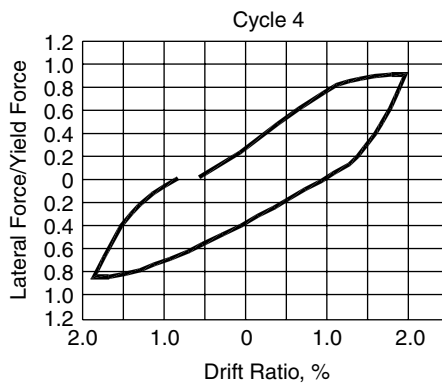


FIGURE 13.19D A force–displacement relationship in a cycle of applied displacement for the test frame in Figure 13.18.

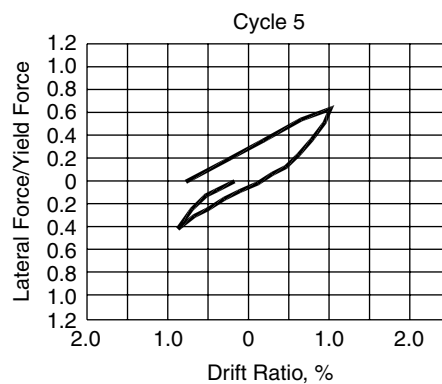


FIGURE 13.19E A force–displacement relationship in a cycle of applied displacement for the test frame in Figure 13.18.

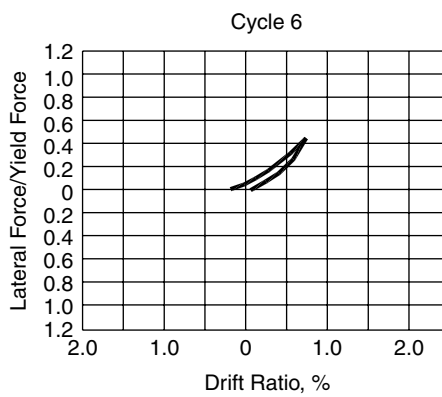


FIGURE 13.19F A force–displacement relationship in a cycle of applied displacement for the test frame in Figure 13.18.

first 12 cycles of response are shown in Figure 13.19 in terms of base shear vs. “roof” drift ratio. (In this case, the roof drift ratio is the drift at the “roof” divided by the clear height of the column.) It is evident from the relative proportions of the columns and the girder that the drift was related primarily to bending in the columns.

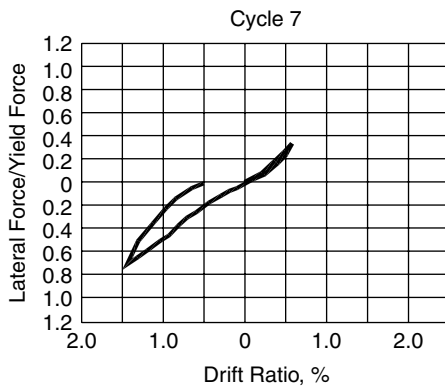


FIGURE 13.19G A force–displacement relationship in a cycle of applied displacement for the test frame in Figure 13.18.

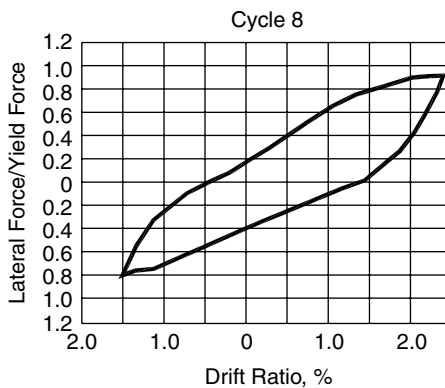


FIGURE 13.19H A force–displacement relationship in a cycle of applied displacement for the test frame in Figure 13.18.

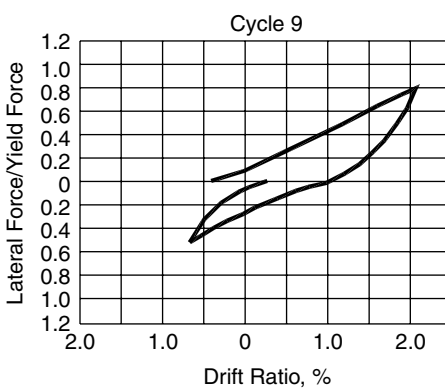


FIGURE 13.19I A force–displacement relationship in a cycle of applied displacement for the test frame in Figure 13.18.

For the particular loading history used, we note that the frame yielded in both directions during the first cycle at a drift ratio of 1% in the positive and 1.4% in the negative direction. We also note that, after yielding, the base shear continued to increase with drift, albeit at a much lower rate. But, there was no “plastic” response that would be implied by a direct projection of a calculated moment–curvature relationship. Another interesting aspect of what we see in the first cycle is that the response of this frame with two identical columns was not anti-symmetrical. The yield occurred at different drift ratios in the two directions.

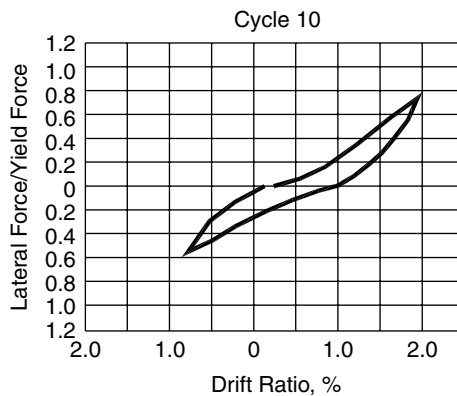


FIGURE 13.19J A force–displacement relationship in a cycle of applied displacement for the test frame in Figure 13.18.

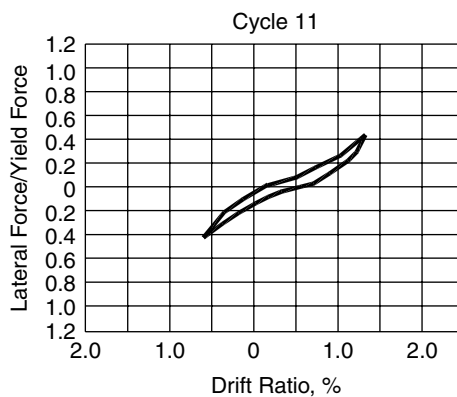


FIGURE 13.19K A force–displacement relationship in a cycle of applied displacement for the test frame in Figure 13.18.

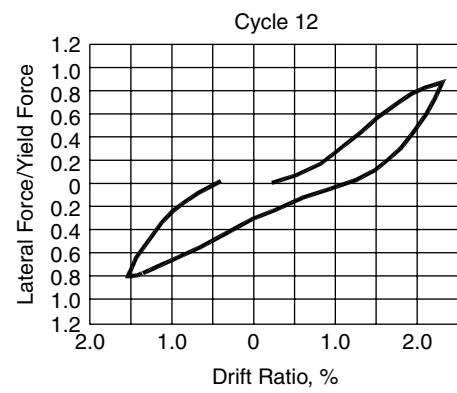


FIGURE 13.19L A force–displacement relationship in a cycle of applied displacement for the test frame in Figure 13.18.

In cycle 2, which ranged in drift ratio from approximately 1% to -0.6% , we do not see strong signs of yielding and see the same phenomenon repeated in cycle 3 that covered drift ratios from approximately 0.6% to -1.5% . In cycle 4, with drift ratios extending from 2% to -1.8% , we observe an indication of yielding in the positive direction. From this limited set of observations, we infer that the force–drift loop is likely to remain anemic as long as the drift remains within the range of the previously attained maxima in each direction. Review of cycles 5 through 12 confirms this impression. We do not expect the hysteresis

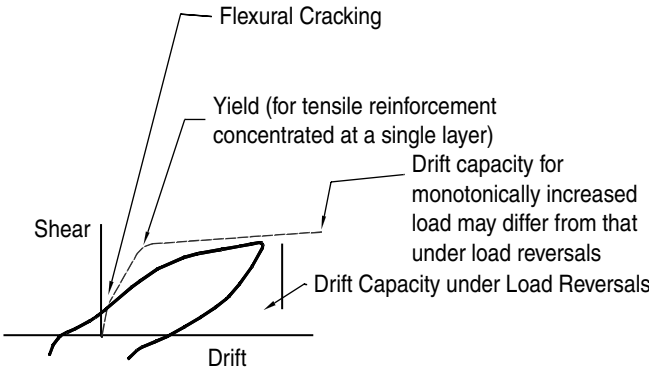


FIGURE 13.20 Drift capacity.

to look as it is pictured under monotonically increased loading in every cycle of response. As opposed to the expectation of the slope for the force-drift curve reducing with drift, we are intrigued by the increase in slope with drift observed faintly in cycle 3 and clearly in later cycles.

We recognize that we have seen but one anecdote of response. The hysteresis loop is likely to be different under different conditions of section properties, axial load, reinforcement anchorage, and earthquake demand. But it is plausible to infer even from the single case we have examined that hysteresis loops will not be anti-symmetrical typically and that unless the previous drift maxima are exceeded, the hysteresis loop will not exhibit yielding or a range of response with a low slope. When we consider the possibility of shifts in “zero-drift” because of large permanent displacements, we decide the best thing we should do is to concentrate on determining the drift capacity and leave alone the characteristics of hysteresis that we can neither control nor predict successfully in each case.

13.5.2 Sources Contributing to Capacity for Drift

The broken curve in Figure 13.20 represents the idealized response of a reinforced concrete member subjected to monotonically increased loading in one direction. It includes the three stages: (1) from beginning of loading to cracking of concrete, (2) from cracking to yielding of tensile reinforcement and (3) from yielding to the drift capacity.

The solid curve in Figure 13.20 represents part of a particular hysteresis cycle that reaches the drift capacity under cyclic loading. We understand that the drift capacity for monotonic loading may not be the same as that for cyclic loading. But we continue to use, if cautiously, the same theoretical constructs used for determining the limiting drift under monotonic loading.

To organize the parameters contributing to the drift capacity, we consider a reinforced concrete member connected to a joint as shown in Figure 13.21 with crack pattern referring to a first loading in one direction. We focus on the drift at the point of contraflexure located at a distance a from the face of the joint. We need to set bounds to the domain within which we will generalize. We assume that the so-called shear-span-to-depth ratio, the ratio a/d , is more than 2 and less than 6. We assume that the section is so reinforced and loaded axially that tensile strength of the concrete has negligible effect and that the section will develop its yield moment. We assume that the response of the member is not affected critically by problems related to bond and shear.

In reference to Figure 13.21 (for monotonically increasing force), the drift at the point of contraflexure may be related to phenomena at the base and along the span a in terms of the following components:

- Component A1. Bending of the member along span a .
- Component A2. Shear distortion of the member along span a .
- Component B1. Rotation of the joint related to flexibility of members restraining the applied moment.
- Component B2. Distortion of the joint in shear related to the applied forces at the joint faces.

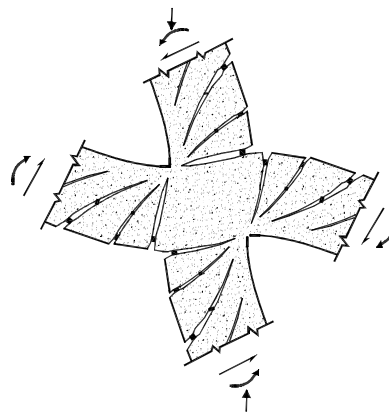


FIGURE 13.21 Deformation of frame joint.

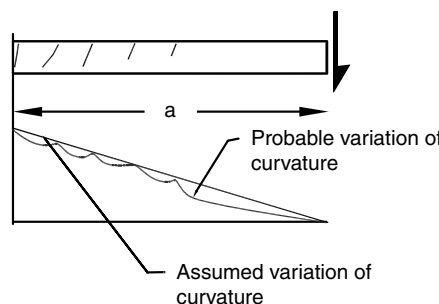


FIGURE 13.22 Distribution of curvature between sections of maximum (at joint face) and zero moment (at inflection point).

- Component B3. Slip of the tensile reinforcement in tension and the “indentation” of the concrete in compression at the face of the joint.

To weigh their relative contributions to drift capacity, we examine them in detail.

Component A1 is best considered in two parts, the part occurring before yielding and that occurring after yielding.

Figure 13.22 shows the moment distribution in span a (ignoring self-weight) and corresponding distributions of unit curvature to yield. Neglecting the variation in curvature caused by cracks along the span (a disturbance that may dominate the result in beams of rectangular section with reinforcement ratios less than 0.3%), the drift ratio related to this component can be stated simply as one third of the product of the curvature and the length a

$$\theta_{A1} = \frac{\epsilon_{sy}}{d(1-\kappa)} * \frac{a}{3} \quad (13.23)$$

θ_{A1} : drift ratio related to bending along span a at yielding of tensile reinforcement, ratio of drift at the point of contraflexure to the distance a

ϵ_{sy} : reinforcement unit strain at yield

d : effective depth

κ : ratio of depth of neutral axis from extreme fiber in compression to effective depth

a : span from face of joint to point of contraflexure

The part of drift that occurs after yielding, the range from yielding to drift capacity, is better stated crudely than analyzed. For background, the reader is referred to Blume et al. (1961). In this section we will state it simply as

$$\theta_{Au} = \frac{\epsilon_{cu} \cdot \alpha_p \cdot d}{\kappa_u \cdot d} = \frac{\epsilon_{cu}}{\kappa_u} \cdot \alpha_p \quad (13.24)$$

θ_{Au} : portion of limiting drift ratio related to curvature beyond yielding

ϵ_{cu} : limiting compressive strain of concrete

κ_u : ratio at limiting drift of depth on neutral axis from extreme fiber in compression to effective depth

$\alpha_p \cdot d$: distance along span a over which the “plastic” curvature is assumed to be distributed uniformly

Blume et al. (1961) and many other texts provide detailed versions of the expression above. If it is considered that the limiting compressive strain may justifiably range from as low as 0.003 to 0.01 for unconfined concrete at the face of the joint, and the coefficient α can be assumed to range from 0.5 to more than 1, it would appear that there is little justification for fine tuning. The simple form given above is appropriate.

Component A2, the shear distortion in a relatively slender member is small. Basing his conclusion on data from a densely instrumented series of tests, Matamoros (2000) concluded that the drift ratio related to shear distortion was considerably more than that based on the standard expression used in text books and varied with the axial compressive stress. From his results, a “reasonable lower-bound expression” can be stated as

$$\theta_{shear} = 75 \cdot \frac{v}{E_c} \left(1 - \frac{\sigma_0}{20 MPa} \right) \text{ but not less than } 25 \cdot \frac{v}{E_c} \quad (13.25)$$

θ_{shear} : drift ratio related to shear distortion along span a

v: unit maximum shear stress

σ_0 : unit axial compression

E_c : Young's modulus for concrete

Component B1, rotation of the joint related to moments applied on it, depends on the flexibility of the members framing into the joint and is independent of the concerns addressed in this section. Component B2, distortion of the joint, depends very much on the cracking within the joint. Considering that the role of drift is a positive one, it is sensible to ignore it.

Component B3, slip of the reinforcement at the face of the joint, can be estimated by the expression

$$\theta_{slip} = \frac{\epsilon_{sy} \cdot \lambda \cdot d_b}{d \cdot (1 - \kappa)} \quad (13.26)$$

θ_{slip} : drift ratio related to slip of reinforcement

ϵ_{sy} : reinforcement unit strain at yield

λ : number of bar diameters over which slip is assumed to occur uniformly

d_b : bar diameter

d: effective depth of member

κ : ratio of depth of neutral axis from extreme fiber in compression to effective depth

The length λd_b may exceed the width of the joint. Considering the approximations involved in determining it, it is appropriate to ignore the effect of indentation at the face of the joint related to the compressive stress.

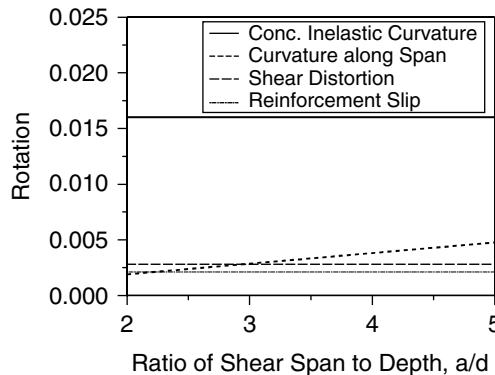


FIGURE 13.23 Relative contributions of rotation components.

We are now ready to compare the relative magnitudes of the drift-capacity sources. We do this within a domain defined by the following:

$$\begin{aligned}
 \text{Section properties} \quad & d = 20 \text{ in.} \quad \kappa_u = \frac{1}{4} \quad d_b = 1 \text{ in.} \quad \kappa = 0.3 \\
 \text{Material properties} \quad & \varepsilon_{sy} = 0.0021 \quad \lambda = 20 \\
 \text{Unit shear stress} \quad & v = 400 \text{ psi}
 \end{aligned}$$

The calculation results summarized in Figure 13.23 refer to a particular case of a girder, a member without axial load. Section properties used are representative for a girder in a frame proportioned for earthquake resistance. The comparison of the contributions of the various sources is instructive even though the case considered is anecdotal. The reader is encouraged to expand the domain of section properties covered using the routine in Appendix F to reach his/her conclusions.

From the data plotted in Figure 13.23 we note that the dominant source is the plastic curvature. From the expression defining the contribution of the plastic curvature

$$\theta_{Au} = \frac{\varepsilon_{cu}}{\kappa_u} \cdot \alpha_p$$

we understand that the contribution is governed by the limiting strain, the coefficient α_p , and the coefficient defining depth of the neutral axis, κ_u . Furthermore, the arrangement is based on the assumption that strain is distributed linearly over the depth of the section. Before we make strong conclusions, we need to refresh our knowledge about these.

The limit to the compressive strain in unconfined concrete is set at 0.003 in the ACI Building Code (ACI, 2002). In many research documents it is set at 0.004. The basis for this assumption varies, but in general the source is strain measured in an axially loaded specimen. It is well known that if there is a strain gradient, the limiting value is higher. Values as high as 0.007 have been confirmed for unconfined concrete (Wight, 1973). At the face of a joint, the compressed concrete is, in effect, confined by strain gradients along and over the depth of the member. It is also restrained by the essentially inert concrete in the joint with which it is in direct contact. There is no reason to think of the magnitude of the limiting strain at the face of the joint being related directly to the measurement obtained in the undisturbed region of a specimen in axial compression. At best, the strain limit obtained from an axially compressed sample may represent a lower bound.

The “spread” of the plastic curvature, explained in detail in Blume et al. (1961), deserves discussion here. We had already noted that in a member with moment gradient along its span, the “flat-top” region of the reinforcement stress-strain relationship appears to have no effect on the force-drift relationship.

As illustrated in Figure 13.5, the force continues to increase after yielding, indicating the immediate initiation of strain hardening. In fact, it has been shown that the spread of plastic curvature requires increase in reinforcement stress above yield. The value of the coefficient α_p depends on a complex interaction of many parameters such as the amount of reinforcement, the ratio a/d , the limiting strain, and the slope of the strain hardening region of the reinforcement. It can indeed be set conservatively at $d/2$ or it can be set at more than d in slender specimens. To calculate it without knowing the answer is moot.

The effect of κ_u is based on the assumption of linear strain distribution over the depth of the section. It is true that the assumption is fairly realistic for monotonically increasing load, but it is difficult to hold a thesis for it under loading reversals.

In summary, the theoretical construct for determining the contribution of plastic curvature on the limiting drift ratio is, at best, a plausible arrangement of the critical parameters but may not be thought of as an expression to be used faithfully in design.

It is seen that the contribution of the curvature at yield to limiting drift ratio can be doubled by the contributions of the slip or shear for the case considered at low ratios of a/d (Figure 13.23).

Undoubtedly, the statement in Figure 13.23 that has the most reliability is that related to the effect of curvature below yield.

It is important to understand the contributions of the critical parameters to the limiting drift ratio but calculating the limiting drift ratio to use in design is effort not efficiently used. It is preferable to follow the prescriptive design rules and increase the amount of transverse reinforcement in any unusual case where the limiting drift may be sensed to be a governing criterion.

13.6 Transverse Reinforcement

The key to integrity of reinforced concrete structures in the earthquake environment is transverse reinforcement. It is good for increasing the strain capacity of the concrete. It is good for reducing the likelihood of brittle failure in shear. It is good for effective anchorage and splices of reinforcement.

What is unfortunate is that there exists no intelligible method for determining exactly how much transverse reinforcement is needed. (Versions of the truss analogy used under different names require leaps in imagination.) The following paragraphs discuss general approaches used in building codes to determine required amounts of transverse reinforcement.

13.6.1 Axial Load

In the 1930s, Richart and fellow researchers (Richart and Brown, 1934) decided that rather than attempt to compute the strength of “spiral columns” (columns with cores confined by helical reinforcement), it would be pragmatic to require a certain amount of spiral reinforcement and use a reduced factor of safety compared with that for columns with ties. The required amount of spiral reinforcement was determined on the premise of making the strength increase of the core effected by spiral reinforcement equal to the strength contribution of the shell concrete. The basic idea was to retain the axial-load strength of the column at relatively large axial displacements after the shell spalled off. The strain limit for the confined core could be ten times that for unconfined concrete. The assured toughness justified the use of a lower factor of safety.

In Blume et al. (1961), this concept was transferred to earthquake-resistant columns. Rather arbitrarily, it was assumed that rectilinear transverse reinforcement would be half as effective as circular transverse reinforcement. On that premise, the amount of transverse reinforcement required was specified to be a function of the relative contributions to axial strength of the confined core and the unconfined shell. To base a design decision having to do with bending on a consideration related to axial load was creative. Even if it was not correct in relation to the physics of the problem, the solution was simple and it appears to have worked. It has been reflected in building codes in the following form.

$$A_{sh} = c_1 \left(sh'' \frac{f'_c}{f''_y} \right) \left(\frac{A_g}{A_{core}} - 1 \right) \quad (13.28)$$

A_{sh}	= total cross-sectional area of transverse reinforcement within spacings
c_1	= a coefficient, 0.3
s	= spacing of transverse reinforcement
h'	= larger dimension of core cross section
f'_c	= compressive strength of concrete
f''_y	= yield stress of transverse reinforcement
A_g	= cross-sectional area of gross section
A_{core}	= cross-sectional area of core

It is not essential to focus on the form or correctness of this expression or maxima/minima associated with it. These will continue to change with experience. Its relation to the desideratum, the capacity for drift, is at best accidental but so far no experience in the field has pointed to an inadequacy resulting from the amount of confining reinforcement so determined.

13.6.2 Combined Bending and Shear

The effect of shear on behavior of reinforced concrete members defies organized description. No matter from what perspective it is viewed, the effect depends on strength of concrete subjected to compound stresses. Repeated loads affect the strength of concrete subjected to combinations of normal and shear stresses more critically than they do its compressive strength. Rather than calculate shear strength, sensitive to number and sequence of repetitions (Pujol, 2002) under load reversals, it is the better strategy to proportion the member so that effects of shear are minimized.

The approach proposed in Blume et al. (1961), which has later been called “capacity design,” is still valid: determine the maximum shear force that is likely to be developed and provide transverse reinforcement to minimize the probability of failure in shear. Establish the demand and provide the resistance. The statement is crisp, but the determination of the demand and the resistance are not as well defined and deserve discussion.

Consider a girder subjected to known bending moments, M_L and M_R , at each end as shown in Figure 13.24. If the tributary load is also known, the shear diagram along the span is determined. How high could M_L and M_R be? We know from our discussion of drift capacity that they are likely to be higher than that corresponding to those calculated with the assumption that the maximum stress in the tensile reinforcement is the yield stress. If there is any nonlinear response, the steel stress will exceed the value at yield and the moment will increase. At the extreme, the increase in stress for the type of reinforcement currently used may exceed 50%. At the same time, we know that there will be some spalling in the unconfined concrete, reducing the effective depth of the girder and compensating for some of the increase in reinforcement stress. The resulting increase in moment is likely to be less than 50%. To determine the moment increase properly, one would need more information than is usually available in the design environment. The approach taken has been to assume the reinforcement stress to be $(5/4)f_y$. The factor is quoted as a fraction to emphasize that its “accuracy” does not merit use of more than one figure. This discussion ignores the probability of the actual yield stress of the reinforcement being more than the design value, a common occurrence. To sum it up, to use a higher yield stress to determine the end moment is the right move but what is normally done does not necessarily result in the maximum moment that can occur (if the anchorages are good).

For a column (Figure 13.25), the question of maximum probable shear demand becomes more interesting. If the axial load on the column does not fluctuate during strong motion, the end moments are properly determined using the specified or known axial load. Unless the axial load is light, it may be plausible not to use an increased yield stress for the reinforcement in determining the end moments. If the axial load fluctuates, it is necessary to determine under what probable axial load the shear will be a maximum.

Once the end moments are known, the expression to determine the demand is simple:

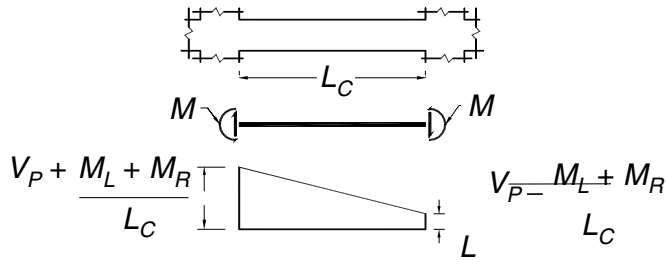


FIGURE 13.24 Shear force in a girder related to development of yield moments at column faces.

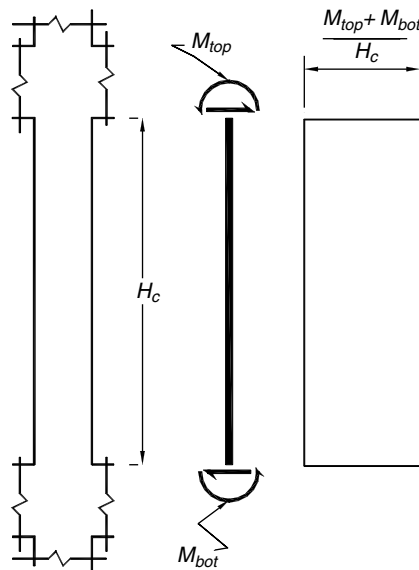


FIGURE 13.25 Shear force in a column related to development of yield moments at joints.

$$V_{\text{demand}} = \frac{M_L + M_R}{L_c} + V_p \quad (13.29)$$

M_L : absolute value of probable moment at one end of member clear span

M_R : absolute value of probable moment at other end of member clear span

L_c : clear span

V_p : reaction related to permanent gravity load

It would be unwise though defensible to reduce the shear by correcting it to its value at a distance d from the face of the joint.

Compared with the unknowns related to the resistance, the unknowns about the demand look crisp. In Blume et al. (1961), the model for determining the amount of reinforcement to be used was the “static” model. It was assumed that the amount of transverse reinforcement could be determined using the time-honored relationship based on an abrogation of the truss-analogy concept:

$$A_w = \frac{(V_{\text{demand}} - V_c)}{f_{wy} \cdot \frac{d}{s}} \quad (13.30)$$

- A_w : cross-sectional area of transverse reinforcement at spacing s
- V_{demand} : shear force determined using the probable moments at each end of the clear span or height and the appropriate shear related to permanent gravity load
- V_c : shear force assigned to concrete. For normal weight aggregate concrete it can be determined as $2\phi \sqrt{f'_c bd}$ where ϕ is the strength reduction factor, f'_c is the compressive strength of the concrete, b is the width of the rectangular section and d is the effective depth
- f_{wy} : yield stress of transverse reinforcement
- d: effective depth
- s: spacing of transverse reinforcement having the total cross-sectional area A_w

Experiments (Wight, 1973; Popov, 1972) and experience subsequent to this proposal suggested that the term V_c should be dropped for frame members without axial load. The contribution of concrete in columns continues in design documents not necessarily because experiments have confirmed it but because it becomes quite onerous to provide transverse reinforcement in a column if V_c is neglected and there exists the belief that, if the frame is proportioned properly, moment reversals well into the range of nonlinear response will not occur in columns.

The golden rule for avoiding a shear failure under cyclic loading is to keep the calculated unit shear stress for members made with normal-weight aggregate concrete below $6\sqrt{f'_c}$.

13.7 Reinforced Concrete Walls

Reinforced concrete walls, whenever building function permits their use, are effective sources of earthquake resistance primarily because they control the drift response efficiently. The behavior of slender walls, those with aspect ratios of more than three, can be understood within the context of the behavior of walls with aspect ratios less than two (ratio of height of wall to its length in its own plane) deserves a few comments on shear strength and stiffness.

The strength of a wall with low aspect ratio may become a limit in design only if the designer makes an unreasonable choice in the selection of the ratio of wall cross-sectional area to tributary floor area (Hassan, 1994). A reasonable lower bound estimate of the unit strength of a low-aspect-ratio wall with normal-weight aggregate concrete is provided by Wood (1990):

$$\nu_{cw} = 6\sqrt{f'_c + \rho_{w\min} \cdot f_{wy}} \quad (13.31a)$$

in the Imperial unit system and

$$\nu_{cw} = \frac{1}{2} \cdot \sqrt{f'_c + \rho_{w\min} \cdot f_{wy}} \quad (13.31b)$$

in the SI unit system.

ν_{cw} = nominal unit strength of wall (low aspect ratio) not to exceed the allowable strength in "shear friction" in psi or MPa.

f'_c = compressive strength of concrete in psi or MPa.

$\rho_{w\min}$ = reinforcement ratio (the smaller of the ratios in the two directions)

f_{wy} = yield stress of wall reinforcement (having a fracture strain of not less than 0.05)

The unit shear-strength demand, calculated assuming yielding at wall base, is best kept below a half of the value indicated by Equation 8.1. Use of code-specified minimum reinforcement is essential.

The stiffness of the wall with a low aspect ratio, related to the three different sources of flexibility (Figure 13.26), has been found to be typically less than that obtained by routine procedures of mechanics (Sozen, 1992). A pragmatic solution to the stiffness of such a wall (defined as the force required at top

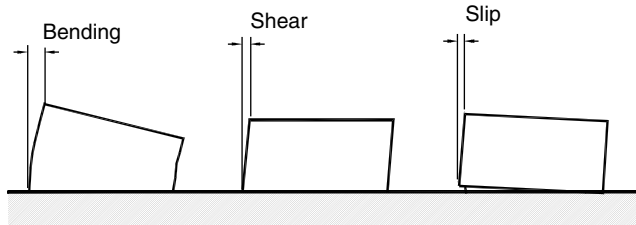


FIGURE 13.26 Idealized sources of deformation for a reinforced concrete wall.

to move the top a unit distance with respect to the base) to be used in period computations (if needed) is provided by Equation 13.32.

$$k_{wall} = 2 \cdot \frac{E_c}{h_w} \cdot \frac{1}{\frac{h_w^2}{I_{wg}} + \frac{10}{A_{wg}}} \quad (13.32)$$

E_c = Young's modulus for concrete

h_w = wall height

I_{wg} = moment of inertia of section of wall (gross)

A_{wg} = area of wall section (gross)

If the aspect ratio is less than one half, it would be appropriate to consider the effect of reinforcement slip on flexibility. A simple approach to estimating the slip component is provided by the following expression:

$$k_s = \frac{M_y}{\epsilon_{sy} \cdot \lambda \cdot d_b} \cdot \frac{L_w}{h_w} \quad (13.33)$$

M_y = moment capacity of wall

ϵ_{sy} = yield strain for reinforcement

λ = coefficient defining half the length in terms of bar diameter to develop bar yield stress (may be assumed to be 25 in normalweight aggregate concrete if data are not available for the particular bar, and its anchorage condition)

d_b = bar diameter

L_w = length of wall

h_w = height of wall

In this case, the stiffness is reduced to k_r

$$k_r = \frac{1}{\frac{1}{k_{wall}} + \frac{1}{k_s}} \quad (13.34)$$

It is very unlikely that Equations 13.33 and 13.34 would impact the proportioning of walls with low aspect ratios. They may be of concern to the designer if there is a question of damage to nonstructural components attached to the wall.

13.8 Future Challenges

At mid-twentieth century, the challenge for reinforced concrete construction was in the dearth of relevant information and design specifications. At the beginning of the twenty-first century, the challenge is in the plethora of information and design specifications.

At the time of the first publication of the "Design of Multi-Story Reinforced Concrete Buildings for Earthquake Motions" (Blume et al., 1961), there was hardly any requirement for reinforcement details related to earthquake effects. Today we have a multiplicity of requirements exemplified in the extreme by an equation that stipulates the exact spacing of transverse reinforcement in the rather modest range from 4 to 6 in. (ACI, 2002, Equation 21-5). With unquestionably good intentions, our code writers have quantified the unquantifiable to produce requirements reminiscent of Edward Lear's Quangle Wangle.⁵

The current challenge is to consolidate the number of competing documents overloaded with ambiguous requirements. There is hope that this will be achieved. There is a trend to focus on drift control rather than strength. It is true that, as in all applications of the new in engineering, the drift paradigm will be overdone. Consider the history of the response modification factor invented to rationalize the relationship of the design base shear, set at approximately 10% of the building weight, to that computed from linear-response analysis, which could be on the order of the weight of the building. First introduced in their format in 1978 (Applied Technology Council, 1978), the proposers were able to restrain themselves to whole numbers, deviating from common sense only in a few cases. With time, the accountants were victorious, as they almost always are, and the factors became decimalized and proliferated into sub-factors. The accountants of drift-based design will probably assign mysterious designations to simple concepts and simple limits will be made complicated. But because drift is a tangible entity, it is possible that the unnecessary sophistication will shake out with use.

It is not pessimistic to end with the recognition that, for earthquake-resistant design, we are not at the end of history.

13.9 Concluding Remarks

Success in structural design hinges on the proper use of an intricate mix of well and poorly understood phenomena. Despite the lengthy analyses required, the product depends on the engineer's knowledge of the exceptions that lie outside the scope of analysis. The pitfall, if any, is not in what the engineer does not know but in what the engineer thinks he or she knows, but is not so.

The object of design is not to predict response but to produce an engineering artifact that is safe, serviceable, and economical. In matters related to earthquake resistance, the criteria can be summarized succinctly in relation to coordinates of the floors before and after the earthquake: (1) The vertical coordinate of the floor should not change and (2) the horizontal coordinate of the floor should change less than 2% and preferably 1% of the height from base to floor level. The first criterion protects lives. The second one protects much of the investment.

The ingredient for satisfying the life-safety requirement is transverse reinforcement. Reinforced concrete structures that have failed catastrophically in earthquakes have failed not because of lack of strength but because of lack of transverse reinforcement necessary to achieve strength. The designer is urged to be sensitive to the amounts, arrangement, and details of transverse reinforcement and always bear in mind that code-writers intend to specify minimum amounts.

The ingredient for satisfying the second criterion is not as simple. Knowledge is needed on two sets of issues: the intensity and nature of the ground motion and the mass/stiffness of the structure. Neither can be estimated exactly before the event.

⁵ On the top of the Crumpty Tree

The Quangle Wangle sat,
But his face you could not see,
On account of his Beaver Hat.

For his hat was a hundred and two feet wide,
With ribbons and bibbons on every side
And bells, and buttons, and loops, and lace,
So that nobody ever could see the face
Of the Quangle Wangle Quee.

Building codes serve to help avoid the exceptions. At the same time, they blur the subtle but critical differences among the methods specified for proportioning. Reading a code, it is difficult to tell the difference between the reproducibility of a shear and a flexural strength. Both appear hard and fast. It is important to remember that there are three classes of methods and the discriminating engineer needs to be aware of their differences.

Class I includes processes — not many — that predict as well as explain. For example, the theory of flexure that defines the relationship between moment and unit curvature not only helps predict response but also enables understanding of the influences on response over a wide domain. It does that even though it relies on observational data for bridging between geometry and statics. And as long as one stops with unit curvature or applies the method within the linear range of response, the theory satisfies both requirements: it is predictive and it explains. Extended to the nonlinear range of response, it has exceptions that can be understood only by experiment and/or experience.

Class II includes processes that serve well to predict response but do not provide an intelligible explanation of why they work. LePage's procedure that was used to estimate bounds to drift response is one such example. Because it is used bundled with the results of the equation of motion, it may appear to follow consistently from first principles. But it does not, and the engineer has the responsibility of making certain it is used within the domain of variables included in its derivation.

Class III has a broad range. It includes the “response modification factors” at the high end as well as the jetsam and flotsam of rules for reinforcing details and cross-sectional minima. Almost none are predictive, nor do they help explain their antecedents.

In implementing building codes, the engineer must be sensitive to the differences among the three classes of requirements. In addition, the engineer must satisfy the code and go one step further, a step that the codes unfortunately do not require. The engineer is wise to estimate the ranges of probable response of the structure after the proportioning exercise has been completed. Simple tools for doing that were provided in this chapter. Explanation of the design procedures follow in the next.

List of Symbols

k_{typ}	stiffness of a story with flexible girders above and below the story
E_c	Young's modulus for concrete
H	story height
n_c	number of columns
k_c	$\frac{I_c}{H}$
I_c	moment of inertia of prismatic column
n_{gb}	number of girders below
k_{gb}	$\frac{I_{gb}}{L}$
I_{gb}	moment of inertia of prismatic girder below
L	span length
n_{ga}	number of girders above
I_{ga}	moment of inertia of prismatic girders above
i	number identifying column or girder
E_c	Young's modulus for concrete
I_w	moment of inertia of wall
M	unit mass assumed to be the total tributary mass divided by height
H	height of wall
F_i	lateral force at level i
h_i	height above base to level i
w_i	concentrated story weight at level i
n	number of levels

w_x	concentrated story weight at level x
h_x	height above base to level x
V_{base}	shear at base
D_i	drift at story i
S_d	characteristic (spectral) displacement corresponding to the modal period
Φ_i	modal-shape coefficient for level i
m_i	mass at level I
n	number of levels above base
θ_{A1}	drift ratio related to bending along span a at yielding of tensile reinforcement, ratio of drift at the point of contraflexure to the distance a
ϵ_{sy}	reinforcement unit strain at yield
d	effective depth
κ	ratio of depth of neutral axis from extreme fiber in compression to effective depth in the range of linear response
a	span from face of joint to point of contraflexure
θ_{Au}	portion of limiting drift related to curvature beyond yielding
ϵ_{cu}	limiting compressive strain of concrete
κ_u	ratio at limiting drift of depth of neutral axis from extreme fiber in compression to effective depth
$\alpha_p \cdot d$	distance along span α over which the "plastic" curvature is assumed to act
a	span from face of joint to point of contraflexure
Θ_{shear}	drift ratio related to shear distortion along span a
ν	nominal unit shear stress
σ_0	unit axial compressive stress
E_c	Young's modulus for concrete
Θ_{slip}	drift ratio related to slip of reinforcement
ϵ_{sy}	reinforcement unit strain at yield
λ	number of bar diameters over which slip is assumed to occur uniformly
d_b	bar diameter
d	effective depth of member
κ	ratio of depth of neutral axis from extreme fiber in compression to effective depth
A_{sh}	total cross-sectional area of transverse reinforcement within spacings
c_1	a coefficient, 0.3
s	spacing of transverse reinforcement
h	larger dimension of core cross section
f'_c	compressive strength of concrete
f''_y	yield stress of transverse reinforcement
A_g	cross-sectional area of gross section
A_{core}	cross-sectional area of core
M_L	absolute value of probable moment at one end of member clear span
M_R	absolute value of probable moment at other end of member clear span
L_c	clear span
V_p	reaction related to permanent gravity load
A_w	cross-sectional area of transverse reinforcement at spacing s
V_{demand}	shear force determined using the probable moments at each end of the clear span or height and the appropriate shear related to permanent gravity load
V_c	shear force assigned to concrete. For normal weight aggregate concrete it can be determined as $2\phi \sqrt{f'_c bd}$ where ϕ is the strength reduction factor, f'_c is the compressive strength of the concrete, b is the width of the rectangular section and d is the effective depth
f_{wy}	yield stress of transverse reinforcement
d	effective depth
s	spacing of transverse reinforcement having the total cross-sectional area A_w

ν_{cw}	nominal unit strength of wall (low aspect ratio) not to exceed the allowable strength in “shear friction” in psi or MPa.
r_{wmin}	reinforcement ratio (the smaller of the ratios in the two directions)
E_c	Young's modulus for concrete
h_w	wall height
I_{wg}	moment of inertia of section of wall (gross)
A_w	area of wall section (gross)
M_y	Moment capacity of wall
e_{sy}	yield strain for reinforcement
λ	coefficient defining half the length in terms of bar diameter to develop bar yield stress (may be assumed to be 25 in normalweight aggregate concrete if data are not available for the particular bar, and its anchorage condition)
d_b	bar diameter
L_w	Length of wall
h_w	height of wall

References

- ACI Committee 318, 1999. Building code requirements for structural concrete and commentary, American Concrete Institute, Farmington Hills, Michigan 48333.
- Anderson, A. W. et al. (1951). Lateral forces of earthquake and wind. *Proceedings, American Society of Civil Engineers*, Vol. 77, April.
- Anderson, J. C. and Bertero, V. V. (1987). Uncertainties in establishing design earthquakes. *J. Structural Engineering, ASCE*, 113 (8).
- Aoyama, H. (1993). Design philosophy for shear in earthquake resistance in Japan. In *Earthquake Resistance of Reinforced Concrete Structures: A Volume Honoring Hiroyuki Aoyama*, Ed. Tsueno Okada, November 25, 140–151.
- Aschheim, M. (2000). Towards improved models of shear strength degradation in reinforced concrete members, *Structural Engineering and Mechanics*, 9, 601–613.
- Bertero, V. V., F. M. Bendimerad and H. C. Shah (1988). Fundamental period of reinforced concrete moment resisting frame structures. The John A. Blume Engineering Center Report No. 87, Stanford University, Stanford, CA.
- Bertero, V. V. Anderson, James C., and Sasani, Mehrdad (1999). Impulse EQGMs: A historical and critical review. *Proc. 1999 Structures Congress Structural Engineering in the 21st Century*.
- Bigaj, A. and Walraven, J. C. (2002). Size effects in plastic hinges of RC members. *Heron*, 47, (1).
- Binder, R. W. and Wheeler, W. T. (1960). Building code provisions for aseismic design *World Congress of Earthquake Engineering*, Tokyo, pp. 1843–1857.
- Blume, J. A., Newmark, N. M. and Corning, L. H. (1961). Design of Multistory Reinforced Concrete Buildings for Earthquake Motions. Portland Cement Association, Skokie, IL.
- Corley, W. G. (1966). Rotational capacity of reinforced concrete beams. *J. the Structural Division, ASCE*, 5.
- Coulomb, C. A. (1773). Essai sur une Application des Règles de Maximis & Minimis à quelques Problèmes de Statique Relatifs à l'Architecture, *Mémoires de Mathématique & de Physique, Présentés à l'Academie Royale des Sciences par divers savans, & lus dans ses assemblées*, Paris, France, Vol. 7, pp. 343–382 (in French).
- Eberhard, M. O. and Sozen, M. A. (1993). Behavior-based method to determine design shear in earthquake-resistant walls. *J. Structural Engineering, ASCE*, 119.
- El-Bahy, A., Kunnath, S. K., Stone, W. C. and Taylor, A. W. (1999). Cumulative seismic damage of circular bridge columns: Benchmark and low-cycle fatigue tests. *ACI Structural Journal*, 96, 633–641.
- Eligehausen, R., Popov, E. and Bertero, V. V. (1983). Local bond stress-slip relationship of deformed bars under generalized excitations. Report No. UCB/EERC/1983/23, University of California, Berkeley.

- FEMA 273 (1997). Guidelines for the Seismic Rehabilitation of Buildings. NEHRP, Federal Emergency Management Agency, Washington DC, October.
- Freeman, S. (1998). Development and use of capacity spectrum method. *6th U.S. NCEE Conference on Earthquake Engineering/EERI*, May 31–June 4, Seattle, WA, Paper #269.
- Gaston, J. R., Siess, C. P. and Newmark, N. M. (1952). An investigation of the load-deformation characteristics of reinforced concrete beams up to the point of failure. Structural Research Series No. 40, University of Illinois, Urbana, IL, December.
- Goel, R. and Chopra, A. (1997). Period formulas for moment-resisting frame buildings. *J. Structural Engineering*.
- Goel, R. and Chopra, A. (1998). Period formulas for concrete shear wall buildings. *J. Structural Engineering*.
- Gulkan, P. and Sozen, M. A. (1974). Inelastic response of reinforced concrete structures to earthquake motions. *J. American Concrete Institute*, 71, 601–609.
- Hassan, A. F. and Sozen, M. A. (1997). Seismic vulnerability assessment of low-rise building in regions with infrequent earthquakes. *ACI Structural Journal*, 94(1).
- Hognestad, E. (1951). A study of combined bending and axial load in reinforced concrete members. *Engineering Experiment Station Bulletin* No. 499, University of Illinois, Urbana, November.
- Housner, G. W. and Brady, A. G. (1963). Natural periods of vibration of buildings. *J. Engineering Mechanics Division*, ASCE.
- Housner, G. W. Behavior of structures during earthquakes. *J. Engineering Mechanics Div.*, ASCE, 85(4), 108–129.
- Ingham, J. M., Liddell, D. and Davidson, B. J. (2001). Influence of loading history on the response of a reinforced concrete beam. *Bulletin of the New Zealand Society for Earthquake Engineering*, 34, 107–124.
- International Conference of Building Officials (1997). Uniform Building Code, Section 1624-1636, Earthquake Design. 5360 Workman Mill Road, Whittier, CA, 90601–2298.
- Iwasaki, T., Kawashima, K., Hasegawa, K., Koyama, T. and Yoshida, T. (1987). Effect of number of loading cycles and loading velocity of reinforced concrete bridge piers. *19th Joint Meeting US-Japan Panel on Wind and Seismic Effects*, UJNR, Tsukuba.
- Jacobsen, Lydik S. (1960). Damping in composite structures. *Proceedings, Second World Conference on Earthquake Engineering*, Tokyo, Japan, Vol. II, 1029–1044.
- Matamoros, A. B. (1999). A study of drift limits for high-strength concrete columns. Ph.D. Thesis, Civil Engineering, University of Illinois, Urbana-Champaign.
- Mattock, A. H. (1965). Rotational capacity of hinging regions in reinforced concrete. *Flexural Mechanics of Reinforced Concrete*, ASCE.
- Moehle, J. P. (1992). Displacement-Based Design of RC Structures Subjected to Earthquakes, *Earthquake Spectra*, 8, 403–428.
- Moehle, J. P., Elwood, K. J. and Sezen, H. (2000). Gravity load collapse of building frames during earthquakes. *M. Uzumeri Symposium*, Special Publication, American Concrete Institute.
- Murakami, M. and Imai H. (1986). A study on influence of different loading histories on failure behavior of R/C column yielding in flexure. *Transactions of the Japan Concrete Institute*, 8, 367–380.
- Newmark, N. M. (1943). Numerical procedure for computing deflections, moments, and buckling loads. *Trans. ASCE*, 108.
- Newmark, N. M. (1962). A method of computation for structural dynamics. *Trans. ASCE*, 127.
- Newmark, N. M., Blume, J. A. and Kapur, K. K. (1973). Seismic design spectra for nuclear power plants. *J. Power Division*, ASCE, November.
- Ohue, M., Morimoto, H., Fujii, S. and Morita, S. (1985). The behavior of R.C. short columns failing in splitting bond shear under dynamic lateral loading. *Transactions of the Japan Concrete Institute*, 7, 293–300.
- Ono, A., Shirai, N., Adachi, H. and Sakamaki, Y. (1989). Elasto-plastic behavior of reinforced concrete column with fluctuating axial force. *Transactions of the Japan Concrete Institute*, 11, 239–246.

- Otani, S. (1995). A brief history of Japanese seismic design requirements. *Concrete International*, ACI.
- Park, R. (1989). Evaluation of Ductility of Structures and Structural Assemblages from Laboratory Testing, *Bulletin of the New Zealand National Society for Earthquake Engineering*, 22(3), 155–166.
- Popov, E. P., Bertero, V. V. and Krawinkler, H. (1972). Cyclic behavior of three R/C flexural members with high shear. Report EERC 72-5, University of California, Berkeley, October.
- Priestley, M. J. N., Verma, R. and Xiao, Y. (1994). Seismic shear strength of reinforced concrete columns. *J. Structural Engineering*, ASCE, 120(8), 2310–2329.
- Pujol, S., Sozen, M. A. and Ramirez, J. A. (2000). Transverse reinforcement for columns of RC frames to resist earthquakes. *J. Structural Engineering*, ASCE, 126(4), 461–466.
- Pujol, S. (2002). Drift Capacity of Reinforced Concrete Columns Subjected to Displacement Reversals, A Thesis submitted to the Faculty of Purdue University for the degree of Doctor of Philosophy, August.
- Rayleigh, J. W. S. (1877). *The Theory of Sound*. Dover Publications (1945), New York, N.Y.
- Richart, F. E. and Brown, R. L. (1934). An investigation of reinforced concrete columns. Engineering Experiment Station Bulletin No. 267, University of Illinois, Urbana, June.
- Saatcioglu, M. and Ozcebe, G. (1989). Response of reinforced concrete columns to simulated seismic loading. *ACI Structural Journal*, 3–12.
- Sakai, K. and Sheikh, S. A. (1989). What do we know about confinement in reinforced concrete columns? *ACI Structural Journal*, 86(2), Mar–Apr.
- Sakai, Y., Hibi, J., Otani, S. and Aoyama, H. (1990). Experimental study on flexural behavior of reinforced concrete columns using high-strength concrete *Transactions of the Japan Concrete Institute*, 12, 323—330.
- Schultz, A. (1992). Approximating lateral stiffness of stories in elastic frames. *J. Structural Engineering*, ASCE, 118(1).
- Shibata, A. and Sozen, M. A. (1976). Substitute-structure method for seismic design in R/C *J. the Structural Division*, ST1.
- Shimazaki, K. and Sozen, M. A. (1984). Seismic drift of reinforced concrete structures. Technical Research Report of Hazama-Gumi, Tokyo, Vol. 5, ISSN 0385-7123.
- Sozen, M. (1974). Hysteresis in structural elements. *Applied Mechanics in Earthquake Engineering*, ASME, AMD, 8.
- Sozen, M. A. (1980). Review of earthquake response of R.C. buildings with a view to drift control. In *State-of-the-Art in Earthquake Engineering, Seventh World Conference on Earthquake Engineering*, Istanbul.
- Sozen, M. A. (1989). Earthquake response of buildings with robust walls. *Proceedings, Fifth Chilean Conference on Earthquake Engineering*, Santiago, Chile, August.
- Sozen, M. A. (1989). A frame of reference. *The Art and Science of Geotechnical Engineering: A Volume Honoring Ralph B. Peck*, Prentice-Hall.
- Sozen, M. A. and J. P. Moehle (1993). Stiffness of reinforced concrete walls resisting in-plane shear, EPRI TR-102731, Tier 1, Project 3094-01, Final Report, August.
- Sozen, M. A. (1997). Drift-driven design for earthquake resistance of reinforced concrete, Proceedings, The EERC-CUREe Symposium in Honor of Vitelmo V. Bertero, Berkeley, CA, January–February.
- Taylor, A. W., Stone, W. C. (1993). A summary of cyclic lateral load tests on spiral reinforced concrete columns, National Institute of Standards and Technology (NIST), Report NISTR 5285, United States Department of Commerce, Technology Administration.
- Taylor, A. W., Kuo, C., Wellenius, K., Chung, D. (1997). A summary of cyclic lateral load tests on rectangular reinforced concrete columns, National Institute of Standards and Technology (NIST), Report NISTR 5984, United States Department of Commerce, Technology Administration.
- Wight, J. K., and Sozen, M. A. (1973). Shear strength decay in reinforced concrete columns subjected to large deflection reversals, *Structural Research Series No. 403*, University of Illinois at Urbana-Champaign, Civil Engineering Studies.

- Wight, J. K. and Sozen, M. A. (1975). Shear strength decay of RC columns under shear reversals, *Proc., ASCE*, 101 (ST5).
- Wood, S. L. (1990). Shear strength of low-rise reinforced concrete walls, *ACI Structural Journal*, V. 87(1).
- Xiao, Y., and Martirosyan A. (1998). Seismic Performance of High Strength Concrete Columns, *J. Structural Engineering*, ASCE-124, 241–251.
- Yamashiro, R., Siess, C. P. (1962) Moment-rotation characteristics of reinforced concrete members subjected to bending, shear, and axial load, Structural Research Series No. 260, University of Illinois at Urbana-Champaign, Civil Engineering Studies.

14

Earthquake- Resistant Design of Reinforced Concrete Buildings

14.1	Introduction.....	14-1
	The Design Process • Stiffness, Strength and Toughness	
14.2	Earthquake-Resistant Requirements for Reinforced Concrete Buildings.....	14-7
	Seismic-Design Categories for Reinforced Concrete Structures • Earthquake Design Ground Motion • Reinforced Concrete Lateral Force-Resisting Structural Systems • Response Modification Coefficient, R, Overstrength Factor, Ω_0 and Deflection Amplification Factor, C_d • Redundancy • Required Base Shear Strength and Seismic Lateral Forces • General Analysis Requirements • Load Combinations, Load Factors and ϕ Factors • Drift Requirements • Materials for Earthquake-Resistant Concrete Structures	
14.3	Predimensioning	14-39
	Coordination with Other Professionals • Structural Layout • Predimensioning for Gravity Loads • Predimensioning for Stiffness • Predimensioning for Strength • Predimensioning for Toughness	
14.4	Analysis.....	14-46
	Cracked Sections • Diaphragm Effect Analysis • Shear Wall Analysis	
14.5	Detailing of Special Moment Frames and Special Shear Walls	14-54
	Girder and Beam Design • Column Design • Wall Design • Floor Diaphragms • Foundations	
14.6	Detailing of Intermediate Moment Frames.....	14-69
	General • Beams • Columns • Slab-Column Systems	
14.7	Economic Implications of Selecting the Structural System.....	14-71
14.8	Future Challenges	14-77

Luis E. Garcia

Mete A. Sozen

14.1 Introduction

Some of the general principles of behavior of reinforced concrete structures subjected to earthquake ground motions were covered in Chapter 13. Chapter 14 is devoted to the proportioning of new cast-in-place

14-2 Earthquake Engineering: From Engineering Seismology to Performance-Based Engineering

reinforced concrete structures in seismic zones. It deals with the design process, including the analysis and detailing of the structure. The presentation is centered on the requirements contained in Chapter 21 of the ACI 318 Code (ACI, 2002) for the reinforced concrete requirements and those of the SEI/ASCE 7-02 document (SEI, 2003) for general seismic-design requirements.

The earthquake-resistant design of reinforced concrete is based on meeting three fundamental requirements for the structure:

1. The structure must have sufficient stiffness to reduce the lateral displacements of the structure to tolerable levels.
2. The structure must have enough strength to resist the inertial forces imposed by the ground motion.
3. The detailing of the structure must be adequate to guarantee an appropriate level of toughness to retain a substantial portion of its strength when responding in the nonlinear range under displacement reversals.

The following presentation is intended to guide the structural designer in the selection of the type of lateral load-resisting system, the definition of the structural layout including member dimensions, the type of analysis procedure and interpretations of the results including story drift to judge the stiffness of the structure, reinforcement amounts that lead to an appropriate strength and the detailing of this reinforcement to guarantee proper toughness.

14.1.1 The Design Process

The lateral load-resisting structural systems for earthquake resistance followed the historical development of reinforced concrete systems for gravity loading. Although there is an emphasis in the literature of treating earthquake-resistant design as a stand-alone problem, the designer should not lose sight of the duality of the role played by the structure in supporting gravity loads while developing an appropriate behavior when subjected to earthquake ground motion. A similar reasoning is used in dealing with wind-induced forces; although they are both mainly lateral loads, there is a radical difference in the design approach because nonlinear response of the structure subjected to the design wind is not taken into account explicitly in the design process although the structure may go into the nonlinear range when subjected to very strong wind.

The structural design process should start with a planned interaction between the architect and other designers of the project. A proper identification of the reasons that lead the architect to develop the proposed architectural layout should guide the structural designer to structural solutions that are agreeable to the architect while meeting the requirements for the proper structural response. For a project to be successful communication channels with the architect must be kept open during the entire design process. Building code requirements are minimum acceptable requirements and although the quest of designing is often confused with just meeting them, the responsibility of the structural designer extends beyond that. The structural designer's obligation is to be sure that no fundamental principle is abrogated and that the proposed solution is within known and accepted principles.

The traditional stages of structural design can be summarized as: (a) predimensioning, (b) analysis, (c) review, (d) detailing, (e) production of the structural drawings and (f) final review. Although this sequence is still valid for earthquake-resistant design, some of the stages must be expanded to address issues not generally encountered in gravity load design. This design process has been influenced by the use of computer, unfortunately to a point that currently the structural engineer can proceed from the analysis stage to structural drawings without having seen, or studied, the results of the intermediate stages. This is what is known as "automatic analysis-design." The main problem brought on by this option is the lack of intermediate stages of review, and a final stage of evaluation of the expected behavior of the structure. When a peer review of the design is performed, these additional stages should be the major concerns of the reviewer.

14.1.2 Stiffness, Strength and Toughness

The three main requirements—stiffness, strength and toughness—that govern the response of a reinforced concrete structure subjected to strong ground motion caused by an earthquake deserve explanation. The listing of stiffness as the first principle is not casual. Structural engineers are trained to deal with strength as the primary issue. The behavioral models used in strength evaluation are deformation dependent, thus for earthquake resistance the primary concern is associated with the stiffness of the structure because a serious stiffness deficiency will affect the effectiveness of the other two principles.

14.1.2.1 Stiffness

Along with mass, stiffness affects the response of the building to the ground motion by defining the dynamic characteristics of the structure as reflected in the fundamental period and the vibration modes. Usually, the structural designer has more freedom in selecting and adjusting stiffness than mass. Beyond the solely vibratory effect in the value of the fundamental period of the structure, the nonlinear response is a function of the stiffness. The individual stiffness of the structural members fixes the relative importance of the member in the overall response of the structure. Global and individual member stiffness affects other aspects of the response including nonparticipating structural elements (elements that are considered by the designer as part of the structure but not of the main earthquake-resistant system) behavior, nonstructural elements (partitions, veneer, architectural elements, mechanical and electrical elements) damage, global stability of the structure and alarm and panic of the occupants.

14.1.2.2 Strength

The structure as a whole, its elements and the cross sections within the elements must have appropriate strength to resist the gravity effects along with the forces associated with the response to the inertial effects caused by the earthquake ground motion. These effects are expressed at the cross-section level as applied axial forces, flexural moments, shear forces and torsional moments. The designer by devising appropriate cross-section dimensions and amounts of reinforcement to account for the expected forces, is indirectly controlling the response of the structure by affecting the sequence of members reaching the nonlinear range of response—for example, girders reaching flexure strength before columns at the same joint—the prevalent mode of response—for example, the element reaching flexure strength before shear strength—and both the amount of energy dissipation contributed by each element and the level of cracking inherent in the nonlinear response of the member. Other issues may indirectly control the strength, and also the response to the ground motion, such as appropriate anchoring of the reinforcement, location and length of splices and the interaction with nonstructural elements.

14.1.2.3 Toughness

The nonlinear response of a reinforced concrete structure is accompanied by a decrease in stiffness and an increase in damping up to a certain level of damage. The term toughness describes the ability of the reinforced concrete structure to sustain excursions in the nonlinear range of response without critical decrease of strength, thus allowing the sought energy dissipation that by increasing damping reduces the effects of the ground motion as compared with those that would occur in a lightly damped structure responding in the linear range. As a consequence of this nonlinear behavior the structure constitutive materials (concrete and steel reinforcement) are subjected to strains greater than those observed in structures under just gravity loading. Proper behavior under these circumstances can only be obtained by the reinforcement meeting special detailing requirements precluding brittle modes of failure and allowing both materials, concrete and steel reinforcement, to reach without failure the large strains expected. An exact, universally accepted, numerical correlation among the earthquake ground motion characteristics, the expected strains in the materials and the amount of reinforcement required to supply an appropriate degree of toughness does not exist at present. This is the reason that current requirements for toughness adopt the form of general detailing rules associated with broad performance or design

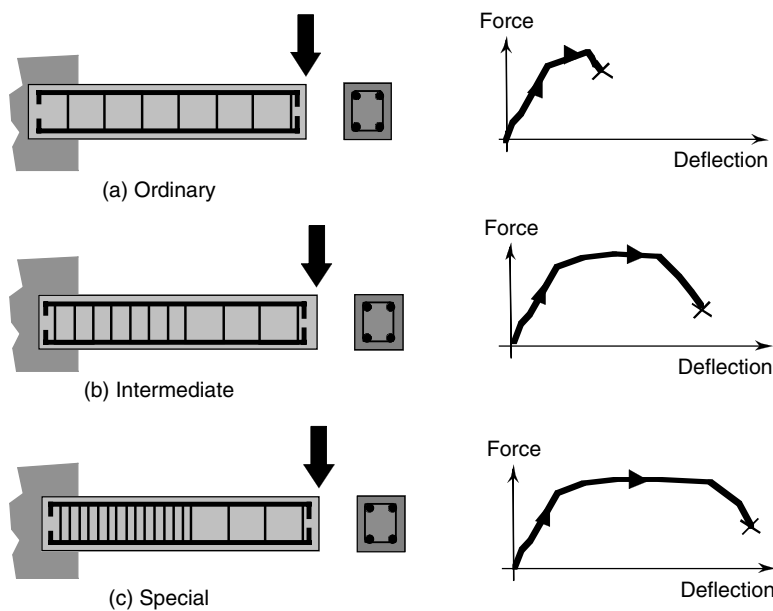


FIGURE 14.1 Force-deflection behavior of a reinforced concrete member having varying degrees of toughness.

categories in turn related to wide-ranging descriptions of the expected ground motion intensity as low, moderate and high.

Just for illustrative purposes, an over-simplification of the meaning of toughness is presented in Figure 14.1 where three variants of the detailing of a reinforced concrete member are presented. In all cases the section-dimension, materials, span and longitudinal reinforcement are the same. The amount—bar diameter and spacing—of transverse reinforcement in all cases is sufficient to resist a shear greater than the one caused by the applied load that would produce yielding of the top longitudinal reinforcement; therefore, all three members will reach moment strength before reaching shear strength. The main difference between the members is the spacing of the transverse reinforcement in the zone close to the support where the moment is greater. In the case labeled (a) ordinary, the spacing of the stirrups is just what is required for shear strength, as described previously. The graph plots the deflection at the tip of the element as the vertical load is increased. The first portion of the deflection reflects the behavior corresponding to the stiffness of an uncracked element. When the cracking moment of the element is reached, the stiffness decreases and this is reflected in a greater deflection increment for a similar load increment before cracking. As the load is increased, the moment at the base of the element increases until the top longitudinal reinforcement reaches the steel yield strength. This corresponds to the element flexural moment strength. As the load is increased beyond that causing yielding of the longitudinal reinforcement, a minor increase in strength caused by strain hardening of the longitudinal reinforcing steel is observed. Failure of the element is reached when the concrete in compression, at the bottom of the section at the support, reaches a level of strain that produces crushing of the material. In the case labeled (b) intermediate, the only difference with the previous case is that the transverse reinforcement spacing has been halved in the region close to the support. The observed behavior in the force-deflection plot is the same except that the deflection when failure of the concrete in compression is reached is larger than in case (a). In the case labeled (c) special, the transverse reinforcement spacing is halved again, being one fourth of the one in (a) and one half of the one in (b) in the region close to the support. The same behavior is observed and the only difference is the maximum deflection reached that is even larger than the one observed in (b).

The effect of closely spaced transverse reinforcement is to allow for greater strains in compression of the concrete enclosed or confined by the transverse reinforcement. It should be noted that this behavior

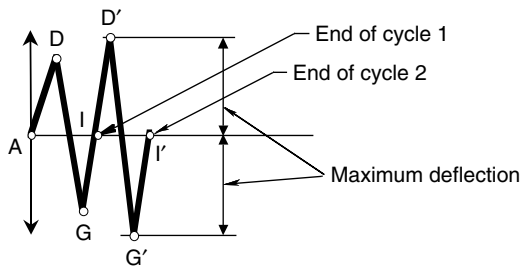


FIGURE 14.2 Vertical deflection program for beam (c) Special in Figure 14.1.

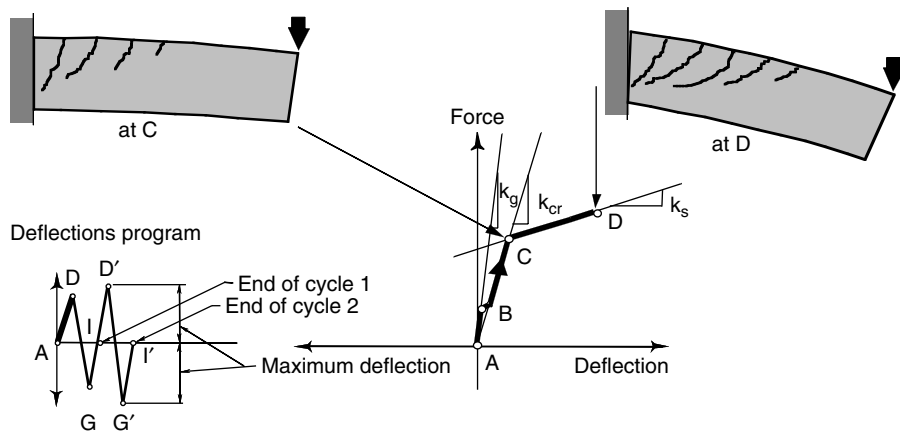


FIGURE 14.3 First quarter-cycle for example beam.

was feasible because other brittle type of failures, such as shear failures, were inhibited. In reinforced concrete structures responding in the nonlinear range this effect of confinement produced by the transverse reinforcement allows for several excursions in the nonlinear range without critical loss of flexural strength.

Now the same reinforced concrete structural element shown in Figure 14.1(c) is subjected to a series of load reversals that impose strains large enough to exceed the elastic limit of the materials (Sozen, 1974). Deflections at the tip of the beam will be imposed as described in the program (protocol) shown in Figure 14.2.

We will be recording the force required to impose the deformation versus the deformation itself in a force-deformation plot as we go from A to I. The response initiates at point A. As load is applied, the observed displacement of the element measured at a selected point directly corresponds to the applied forces in a linear fashion through the uncracked stiffness of the element until cracking presents at point B (see Figure 14.3). A reduction in stiffness commensurable with the amount of cracking governs the response until yielding of the tension reinforcement occurs at point C. As further load is applied, the corresponding displacements increase at a rate governed by the strain-hardening properties of the reinforcing steel until the point of reversal of the direction of forces occur, at D (see Figure 14.3).

When a reversal of the direction of the forces occurs at point D as shown in Figure 14.4, the unloading decreases the displacement, and when the net applied forces become zero, at point E, there is a remnant displacement—distance from A to E—caused by the yielding of the reinforcement. The applied force, now acting in the opposite direction of the initial one, is inducing tension where compression was applied in the initial loading and compression in the former tension regions, closing the tension cracks, at F, caused by the first loading.

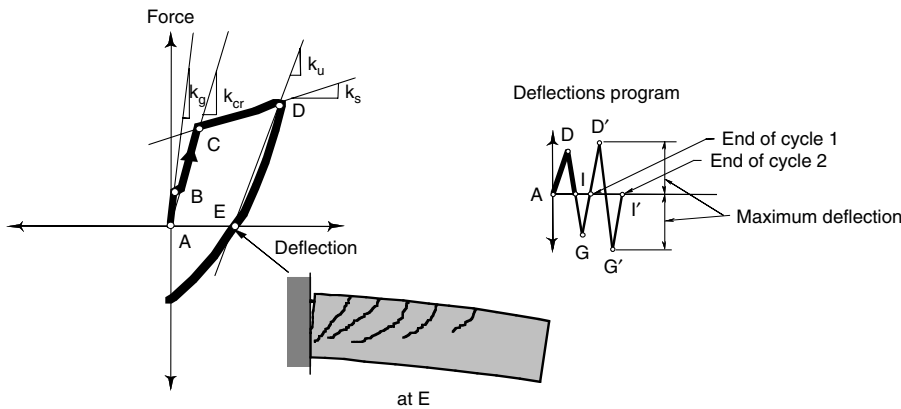


FIGURE 14.4 First one-half cycle for example beam.

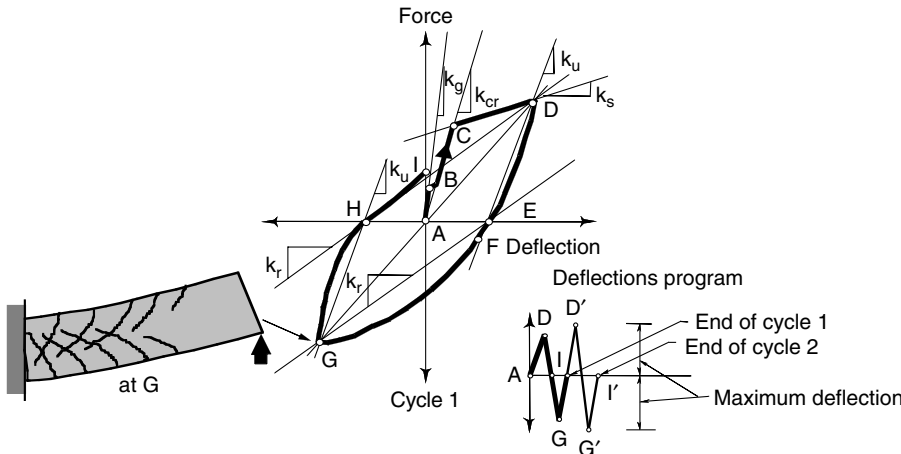


FIGURE 14.5 First cycle for example beam.

Further loading causes tension (see Figure 14.5), even beyond yield, in the reinforcement that was in compression at the beginning of the loading in the opposite direction until the applied load is reversed at G, initiating unloading. When the net applied force is zero, point H, a permanent displacement is observed again—distance A to H—but now in the opposite direction of A to E observed before. This ends the first cycle of loading.

Figure 14.6 shows the second cycle in which the effect of the cracking of the previous cycle affects the shape of the hysteresis cycle by requiring less force to close them. In general, for reinforced concrete elements as new cycles of loading and unloading occur, the displacements become larger than those obtained previously for the same force level. Since stiffness is the ratio between force and displacement, this increase solely of deformation has a corresponding decrease in stiffness known as stiffness degradation. The slope of the line that joins the two extreme points, D and G in this case, shown in Figure 14.6, indicates the general stiffness degradation observed.

The different stiffnesses associated with the hysteretic response shown are in general:

k_g = uncracked stiffness associated with the gross properties of the element section

k_{cr} = cracked stiffness evaluated at first yielding of the tension reinforcement

k_s = slope of the increase of strength caused by strain hardening of the tension reinforcement

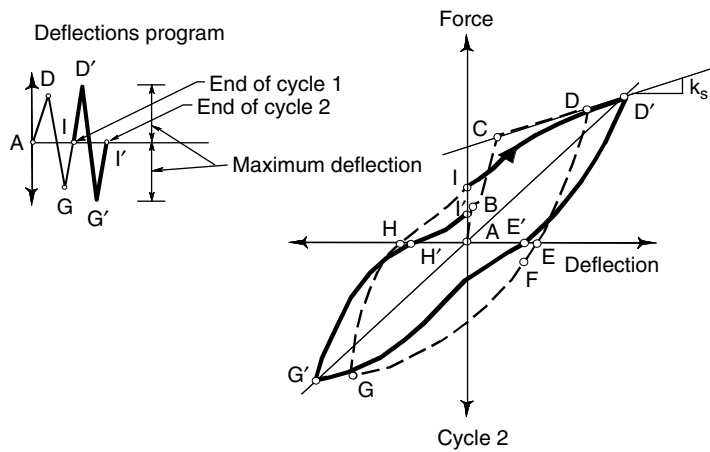


FIGURE 14.6 Second cycle for example beam.

k_u = unloading branch slope, expressed in terms of stiffness

k_r = slope observed when the net applied force changes sign at the end of the unloading. Also known as the reload stiffness

The hysteretic behavior just described corresponds only to that of an element responding in flexure. To observe this type of behavior any kind of fragile response must be avoided at all costs. Among those that should be avoided are shear and bond failures. In addition, the element must be provided with adequate properly anchored transverse reinforcement that confines the core of the element thus permitting large strains in the concrete that could not have been sustained without the beneficial confinement effects of the transverse reinforcement. Lack of appropriate transverse confining reinforcement, introduces degradation of strength, and lack of appropriate anchorage of the longitudinal reinforcement, causes degradation of stiffness and strength. Stiffness degradation is unavoidable and acceptable within certain limits. Strength degradation is not acceptable if proper energy dissipation is sought.

Several factors affect the shape of the hysteresis loops of reinforced concrete members: amount of longitudinal reinforcements and the stress-strain properties of the steel; acting axial load on the section; degree of cracking as a function of the distribution and width of the cracks; effectiveness of the bond between reinforcement and surrounding concrete; distribution of the longitudinal reinforcement in the section, especially in girders with nonsymmetrical reinforcement; shear stresses and the amount of transverse reinforcement; general and local distortions of the joints where members interconnect; shape of the section (a T section behaves differently from a rectangular section) and lateral stability of the longitudinal reinforcing bars.

From the energy point of view in a force-displacement diagram the area under the diagram at any point is a measure of the strain energy stored in the element. For elements responding in the nonlinear range the fact that a remnant displacement exists after a whole unloading has occurred indicates that some energy has been dissipated and only the part of the strain energy corresponding to the linear elastic response is recovered. Therefore, the area enclosed by the hysteresis loop is a measure of the unrecoverable strain energy dissipated.

14.2 Earthquake-Resistant Requirements for Reinforced Concrete Buildings

In the United States, model codes for reinforced concrete buildings have been traditionally divided into two sets of complementary requirements. The first set of requirements, called loosely the "demand," have been the domain of the model codes — ICBO-UBC (ICBO, 1997), BOCA-NBC (BOCA, 1996), SBCCI-SBC

(SBCCI, 1996) and lately ICC-IBC (ICC, 2003) and NFPA-5000 (NFPA, 2003) — engineering societies—SEAOC (SEAOC, 1999), ASCE (SEI, 2003) — and government agencies — NEHRP-FEMA (FEMA, 2001). They contain the description of the design ground motion for the different seismic risk zones including site effects and importance requirements based on occupancy, the permitted seismic load-resisting structural systems with limitations based on configuration of the structure, the analysis and modeling procedures to be used and the limits to lateral displacements. The earthquake design requirements of both the current leading documents: the International Building Code (ICC, 2003) and NFPA-5000 (NFPA, 2003) are based on the SEI/ASCE 7-02 document (SEI, 2003) requirements published in 2003, which in turn are based on the *2000 NEHRP Recommended Provisions for the Development of Seismic Regulations for New Buildings* (FEMA, 2001) prepared by the Building Seismic Safety Council (BSSC) under the sponsorship of the Federal Emergency Management Agency (FEMA).

The second set of requirements for reinforced concrete in all these documents, historically called in a loose manner the “resistance,” are based on the corresponding requirements developed by Committee 318 of the American Concrete Institute, ACI International: “Building Code Requirements for Structural Concrete (ACI 318-02) and Commentary (ACI 318R-02)” (ACI, 2002).

The presentation in this chapter makes reference primarily to: (a) Section 9.0 — earthquake loads, of the SEI/ASCE 7-02 document and those parts relevant for reinforced concrete buildings, and (b) the requirements of ACI 318-02 for reinforced concrete structures.

14.2.1 Seismic-Design Categories for Reinforced Concrete Structures

Seismic-design categories correspond to groups of design and detailing requirements associated with an intended degree of toughness for the structure. The intention of this division is to guarantee that detailing of the structure is compatible with the intensity of the expected seismic ground motion. The minimum acceptable degree of toughness, or seismic design category, required for a reinforced concrete structure in SEI/ASCE 7-02—as for other structural materials—depends on a combination of the intended occupancy of the building and the severity of the expected earthquake ground motion at the site. They are defined as *Seismic Design Categories A to F*, with A being the minimum and F the maximum required toughness. Most modern seismic codes around the world use similar divisions, sometimes denominated as “ductility requirements” or “energy dissipation capacities.”

The specific division of the requirements of ACI 318-02 into Seismic Design Categories A to F is contained in Appendix A.9.9 of SEI/ASCE 7-02. This division includes the addition of terminology related to the seismic load-resisting structural systems permitted by SEI/ASCE 7-02. A general summary of the Seismic Design Categories requirements is presented below. The reader is cautioned that the detailed requirements should be consulted in the SEI/ASCE 7-02 document.

14.2.1.1 Seismic Design Category A

All reinforced concrete structures are designed using Chapters 1 to 22 of ACI 318-02 with the exception of Chapter 21. Special provisions for seismic design are considered as belonging to SDC-A and they are referred to as Ordinary Moment Frames for purposes of classification within the lateral force-resisting systems.

14.2.1.2 Seismic Design Category B

This design corresponds to the same requirements as that of SDC-A and contains some additional requirements (see Section A.9.9.3 of SEI/ASCE 7-02). The resulting lateral force-resisting system is still called an Ordinary Moment Frame. The additional requirements that distinguish SDC-B from SDC-A include for flexural members (beams and girders) belonging to the seismic load-resisting system, at least two continuous longitudinal bars at the top and bottom, and for columns having slenderness ratio of 5 or less that the shear design must be made for a factored shear twice that obtained from analysis, or based on the flexural strength of the member at the ends.

14.2.1.3 Seismic Design Category C

This includes the same requirements as SDC-B plus the additional requirements of Section 21.12—Requirements for intermediate moment frames of ACI 318-02 (see Section A.9.9.4 of SEI/ASCE 7-02). The resulting seismic load-resisting system is referred to as an Intermediate Moment Frame. Shear walls within SDC-C are Ordinary Reinforced Concrete Walls as designed using Chapters 10 and 14 of ACI 318-02. There are other requirements related to columns supporting reactions from discontinuous stiff members, anchor bolts in the top of columns and the use of plain concrete subjected to additional reinforcement than that required by Chapter 22 of ACI 318-02. It is permitted to use in this category the requirements of the whole of Chapter 21 of ACI 318-02 thus supplying an additional degree of toughness.

14.2.1.4 Seismic Design Categories D, E and F

This includes the use of all requirements of Chapter 21 of ACI 318-02 except Section 21.12 (see Section A.9.9.5 of SEI/ASCE 7-02) plus the requirements for SDC-C. Members not assumed to contribute to the lateral force resistance must comply with Section 21.11 devoted to the so-called “nonparticipating elements.” The resulting seismic load-resisting systems are denominated special moment frames and special reinforced concrete shear walls.

14.2.2 Earthquake Design Ground Motion

The earthquake design ground motion must comply with the requirements of the general building code having jurisdiction. The requirements of SEI/ASCE 7-02 will be used here.

14.2.2.1 Maximum Considered Earthquake and Design Ground Motion

The 1997 edition of “NEHRP Recommended Provisions for the Development of Seismic Regulations for New Buildings” (FEMA, 1997) made a total departure from the traditional formulation of the earthquake design ground motion. This modification was kept in NEHRP 2000 (FEMA, 2001) and was incorporated in SEI/ASCE 7-02. Traditionally, seismic codes had defined the probability of seismic hazard exceeding in 50 years at a uniform 10% (return period of 475 years) providing for a uniform likelihood that the design ground motion would not be exceeded. In the new approach, to provide for a uniform margin of failure in structures designed for that ground motion hazard, the earthquake ground motion is defined in terms of a maximum considered earthquake depending on the seismicity of an individual region. The design ground motion is based on a lower bound estimate of the margin against collapse inherent in new structures that was set, arbitrarily, at two thirds of the maximum considered earthquake ground motion.

According to (FEMA, 2001) for most regions, the maximum considered earthquake ground motion is defined with a uniform likelihood of exceedance of 2% in 50 years (approximate return period of 2500 years). In regions of high seismicity, ground shaking calculated at a 2% in 50 years likelihood would be much larger than that which would be expected based on the characteristic magnitudes of earthquakes on known active faults. For these regions, it was considered more appropriate to determine directly maximum considered earthquake ground motion based on the characteristic earthquakes of these defined faults multiplied by 1.5 (inverse of 2/3). See Chapter 5 for more details.

The envisioned maximum considered earthquake ground motion in SEI/ASCE 7-02 is defined as horizontal acceleration spectral ordinates using parameters S_1 and S_S , corresponding to spectral response accelerations in rock at 1-sec and 0.2-sec periods, respectively. The corresponding values of S_1 and S_S for the United States are obtained from a series of maps prepared by the U.S. Geological Survey (these maps can be downloaded from www.usgs.gov). The maximum considered earthquake spectral response accelerations for 5% of critical damping are obtained from:

$$S_{MS} = F_a S_S \quad (14.1)$$

$$S_{M1} = F_v S_1 \quad (14.2)$$

TABLE 14.1 Site Classification

Site Class	\bar{v}_s	\bar{N} or \bar{N}_{ch}	\bar{s}_u
A: Hard rock	> 1500 m/s (>5000 ft/s)	not applicable	not applicable
B: Rock	760 to 1500 m/s (2500 to 5000 ft/s)	not applicable	not applicable
C: Very dense soil or soft rock	370 to 760 m/s (1200 to 2500 ft/s)	> 50	> 100 kPa (> 2000 psf)
D: Stiff soil	180 to 370 m/s (600 to 1200 ft/s)	15 to 50	50 to 100 kPa (1000 to 2000 psf)
E: Soft soil	< 180 m/s <td>< 15</td> <td>< 50 kPa<br (<="" 1000="" psf)<="" td=""/></td>	< 15	< 50 kPa
F: Soils requiring site-specific evaluation	Any profile with more than 3 m (10 ft) of soil having Plasticity Index PI > 20, Moisture content $\omega \geq 40\%$ Undrained shear strength $\bar{s}_u < 25$ kPa Soils vulnerable to potential failure or collapse (liquefiable, quick- or highly sensitive clays, collapsible weakly cemented soils). More than 3 m (10 ft) of peat and/or highly organic clays. More than 7.5 m (25 ft) of very high plasticity clays (PI > 75). More than 37 m (120 ft) of soft to medium clays.		

In Equations 14.1 and 14.2, F_a and F_v are the site coefficients defined in the next section. The design spectral response acceleration parameters are defined as

$$S_{DS} = \frac{2}{3} S_{MS} \quad (14.3)$$

$$S_{D1} = \frac{2}{3} S_{M1} \quad (14.4)$$

The main procedural departure from the previous code-based design earthquake ground motion is that under the current requirements the values of the spectral ordinates are provided, while previous procedures defined peak ground acceleration values that were then amplified to obtain the spectral ordinates. This new procedure lends itself to a more appropriate treatment of site-specific procedures where spectral ordinates do not solely depend on the design earthquake effective peak ground acceleration.

14.2.2.2 Site Classification

For long it has been recognized that the effects of local soil conditions on ground motion characteristics should be considered in building design. The NEHRP 2000 (FEMA, 2001) provisions as incorporated in SEI/ASCE 7-02, consider these effects for several different soil conditions. The soil site must be assigned into one of the six soil profile classes labeled A to F. The definition of the soil profile is based on averaged soil properties for the upper 30 m (100 ft) of soil profile. The properties used for this definition are: average shear wave velocity (\bar{v}_s), average standard penetration resistance (\bar{N}), average standard penetration resistance for the cohesionless soils only (\bar{N}_{ch}) and average undrained shear strength in the case of cohesive soils (\bar{s}_u). These averages are weighted with respect to each layer thickness. Table 14.1 indicates how these parameters are used to define the soil profile.

Figure 14.7 shows the values of the coefficient F_a as a function of the site class and the short period maximum considered earthquake spectral acceleration S_s . Figure 14.8 shows the values of the coefficient F_v as a function of the site class and the 1-sec period maximum considered earthquake spectral acceleration S_1 . For sites class F a site-specific procedure must be used for determining the maximum considered earthquake spectral acceleration.

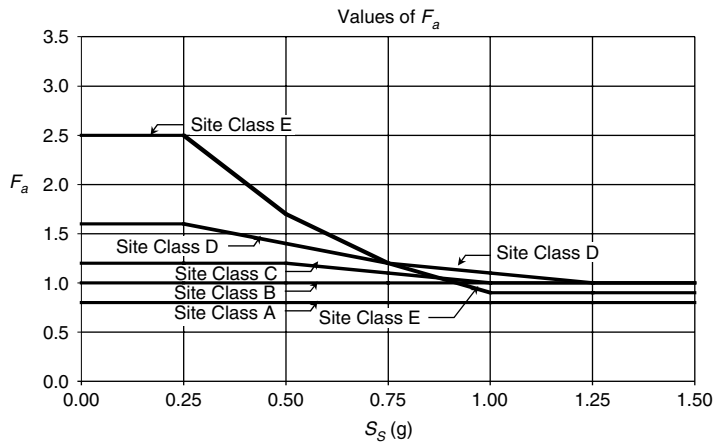


FIGURE 14.7 Values of F_a as a function of site class and S_s .

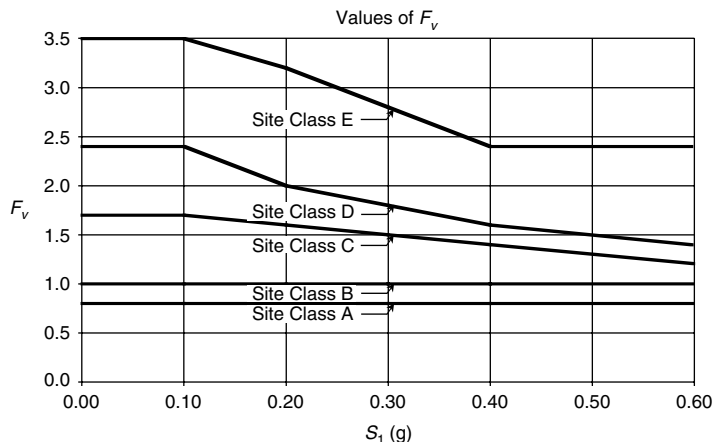


FIGURE 14.8 Values of F_v as a function of site class and S_1 .

14.2.2.3 Design Spectral Response

The design response spectrum provides the basis for determining the design forces and deformation that must be employed in the seismic design of the building. SEI/ASCE 7-02 considers two procedures: one for general usage and one based on site-specific information and analysis.

14.2.2.3.1 General Procedure

The design response spectrum for 5% of critical damping is defined as shown in Figure 14.9.

14.2.2.3.2 Site-Specific Procedure

When a site-specific procedure is used the study must account for regional seismicity and geology, the expected recurrence rates and maximum magnitudes of events occurring on known faults and source zones, the location of the site with respect to these known faults and zones and the characteristics of surface site conditions. The maximum considered earthquake ground motion for the site must be taken as the 5% damping response spectrum (S_{aM}) having a probability of exceedance of 2% in a 50-year period (approximately 2500 year mean return period).

If the acceleration spectral ordinates at 0.2-sec and 1.0-sec periods of S_{aM} exceed limits set at $(1.5gF_a)$ or $(0.6gF_v)$ respectively, the spectral ordinates of the whole spectrum must be adjusted using a check

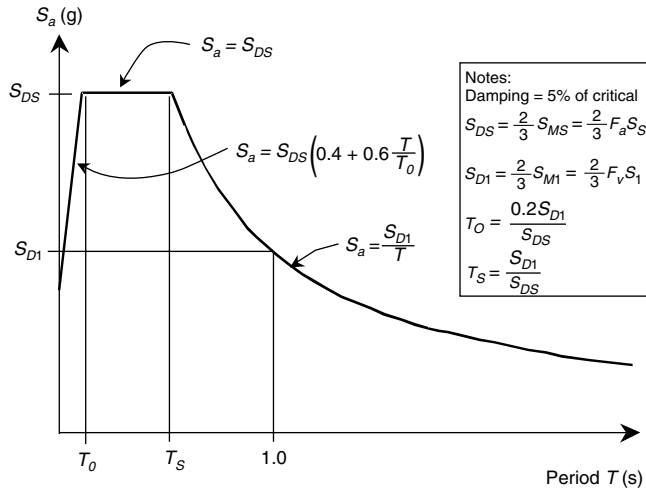


FIGURE 14.9 Design acceleration response spectrum.

based on a deterministic approach. In the deterministic check the maximum considered earthquake ground motion is defined as 3/2 times the median spectral response for all periods resulting from characteristic earthquakes occurring on known active faults in the region. SEI/ASCE 7-02 allows the use of the lesser of the two spectra in all points above lines drawn at $1.5gF_a$ and $0.6gF_v/T$ and no point in the spectra should be below the minimum set by these two limits. The resulting acceleration response spectrum is referred to as S_{aM} .

The site-specific design ground motion is defined as a design response spectrum S_a obtained at any period from:

$$S_a = \frac{2}{3} S_{aM} \quad (14.5)$$

All ordinates of this site-specific response spectrum must be greater or equal to 80% of the spectral value of the response spectra obtained from the mapped values of S_s and S_1 as shown in Figure 14.9. For design purposes the equivalent values of S_{DS} and S_{D1} must be taken as the spectral acceleration S_a from the site-specific design spectrum at a period of 0.2 sec and 1 sec, respectively, but they should not be taken at less than 90% of the peak spectral acceleration response, S_a , at any period. The parameter S_{D1} must be taken as the greater of the spectral acceleration, S_a , at a period of 1 sec or two times the spectral acceleration, S_a , at a period of 2 sec. Parameters S_{MS} and S_{M1} must be taken as 3/2 of S_{DS} and S_{D1} , respectively.

14.2.2.4 Use Groups

SEI/ASCE 7-02 divides all buildings and other structures into four occupancy categories depending on the hazard to human life associated with their use. These categories in turn are used to define three seismic use groups and each one is assigned an importance factor I . These requirements are summarized in Table 14.2.

14.2.2.5 Required Seismic Design Category

The structure to be designed must be assigned to one of the seismic design categories A to F described before. Under SEI/ASCE 7-02 the seismic design category is a function of the seismic use group and the design spectral response acceleration parameters S_{DS} and S_{D1} . The structure must be assigned to the most severe seismic design category obtained from Table 14.3 or Table 14.4, taking into account the exceptions of Table 14.5. Also, buildings of seismic design categories E and F should not be sited at places where

TABLE 14.2 Seismic Use Groups and Importance Factor I

Occupancy Category Table 1-1			Seismic Use Group		
			I	II	III
	I	Low hazard to human life	X		
	II	All buildings not listed in Categories I, III and IV	X		
	II	Substantial hazard to human life. Large groups in same room,			
	I	day care, schools, colleges, jails, etc.		X	
	IV	Essential facilities (hospitals, fire and police stations, emergency shelters, etc.), Hazardous containment.			X
Seismic Occupancy Importance Factor I			1.0	1.25	1.5

TABLE 14.3 Seismic Design Category Based on S_{DS}

Value of S_{DS}	Seismic Use Group		
	I	II	III
$S_{DS} < 0.167g$	A	A	A
$0.167g \leq S_{DS} < 0.33g$	B	B	C
$0.33g \leq S_{DS} < 0.50g$	C	C	D
$0.50g \leq S_{DS}$	D	D	D

TABLE 14.4 Seismic Design Category Based on S_{D1}

Value of S_{D1}	Seismic Use Group		
	I	II	III
$S_{D1} < 0.067g$	A	A	A
$0.067g \leq S_{D1} < 0.133g$	B	B	C
$0.133g \leq S_{D1} < 0.20g$	C	C	D
$0.20g \leq S_{D1}$	D	D	D

TABLE 14.5 Seismic Design Category Based on S_1

Value of S_1	Seismic Use Group		
	I	II	III
$0.75g \leq S_1$	E	E	F

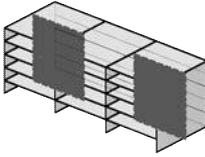
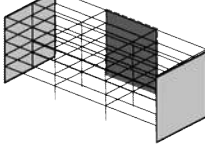
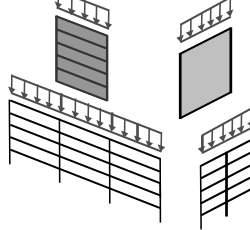
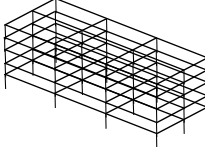
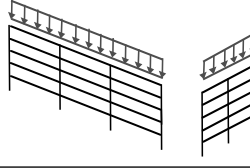
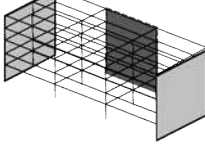
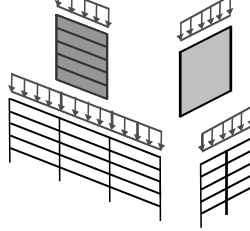
there is a known potential for an active fault to cause rupture of the ground surface at the structure. SEI/ASCE 7-02 has special quality assurance requirements for all seismic design categories except A and B.

14.2.3 Reinforced Concrete Lateral Force-Resisting Structural Systems

The structure must include a complete seismic- and gravity-force-resisting system capable of providing adequate strength, stiffness and energy dissipation capacity to withstand the design ground motion within the prescribed limits of deformation and strength demand. The lateral force-resisting system corresponds to that portion of the structural system that has been considered in design to provide the required resistance to the seismic forces prescribed by the seismic-design requirements.

The general basic lateral force-resisting systems in SEI/ASCE 7-02 follow tradition in their definition as used in North American building codes for several decades. The general systems may be used with any of the structural materials covered by the code (structural steel, structural concrete, composite steel and concrete, structural masonry and wood). The types of vertical element used to resist lateral seismic

TABLE 14.6 Reinforced Concrete Lateral Force-Resisting Systems

Lateral Force-Resisting System	Gravity Loads	Lateral Forces
Bearing walls system		 Note: For gravity loads it includes only load bearing walls
Building frame system		
Moment-resisting frame system		
Dual system		

forces subdivide each system. The structure to be designed must conform to one of the prescribed systems and their subdivision.

The lateral force-resisting systems in SEI/ASCE 7-02 are defined in the following manner (See Table 14.6):

Bearing Wall System — A structural system with bearing walls providing support for all or major portions of the vertical loads. Shear walls or braced frames provide seismic force resistance.

Building Frame System — A structural system with an essentially complete space frame providing support for vertical loads. Seismic force resistance is provided by shear walls or braced frames.

Moment-Resisting Frame System — A structural system with an essentially complete space frame providing support for gravity loads. Moment-resisting frames provide resistance to lateral load primarily by flexural action of members. (This definition comes from UBC-97 (ICBO, 1997) because in SEI/ASCE 7-02 the definition is implicit in that of moment frame.)

Dual System — A structural system with an essentially complete space frame providing support to vertical loads. Seismic force-resistance is provided by moment-resisting frames, and shear walls or braced frames. For a dual system, the moment frame must be capable of resisting at least 25% of the design seismic forces. The total seismic force resistance is to be provided by the combination of the moment frame and the shear walls or braced frames in proportion to their rigidities.

The following definitions from SEI/ASCE 7-02 are relevant for understanding the scope of the lateral force-resisting systems for reinforced concrete structures:

Bearing Wall — Any concrete or masonry wall that supports more than 3 kN/m (200 lbs/linear ft) of vertical load in addition to its own weight.

Braced Frame — An essentially vertical truss, or its equivalent, of the concentric or eccentric type that is provided in a bearing wall, building frame or dual system to resist seismic forces.

Inverted Pendulum-Type Structures — Structures that have a large portion of their mass concentrated near the top and, thus, have essentially one degree of freedom in horizontal translation. The structures are usually T-shaped with a single column supporting the beams or framing at the top.

Note that, in general, in this type of structure the upper portion extends out creating a hammer-like configuration (thus the T-shaped denomination). The lateral displacement of the top is usually accompanied by a swinging up and down of the upper portion. This swinging introduces additional moments to those caused by the lateral displacements at the top of the supporting column. These effects are the reason behind the special requirements for this type of structure.

Moment Frame — A frame in which members and joints are capable of resisting forces by flexure as well as along the axis of the members.

Shear Wall — A wall, bearing or nonbearing, designed to resist lateral seismic forces acting on the plane of the wall (sometimes referred to as a vertical diaphragm).

Space Frame — A structural system composed of interconnected members, other than bearing walls, which is capable of supporting vertical loads and, when designed for such an application, is capable of providing resistance to seismic forces.

It should be noted that space frame covers both moment-resisting and nonmoment-resisting frames. For reinforced concrete applications all frames are moment-resisting because ACI 318-02 requires continuity of the structural elements that compose the main structural framing system, thus limiting the number of systems when compared with other structural materials, such as structural steel, that permit nonmoment-resisting framing systems.

The structural system must be in accordance with the seismic design category and height limitations indicated in Table 14.7. Only reinforced concrete systems are listed there. The corresponding table in SEI/ASCE 7-02 (Table 9.5.2.2) from which this information was extracted, contains information on all the covered structural materials, and also on plain concrete shear wall systems which are permitted, with restrictions, only in seismic design categories A and B, which are not covered here. The special, intermediate and ordinary designation follows the corresponding description in ACI 318-02 as presented in 14.2.1.

Some remarks with respect to reinforced concrete braced frames and slab-column frames are warranted:

- The experience in North America with reinforced concrete braced frames as a lateral force-resisting system is limited. Reinforced concrete concentrically braced frame systems have been used in other parts of the world but no formal interpretation of their behavior in past earthquakes is available. The main concern when using reinforced concrete braced frames is related to the steel congestion in joints where braces frame. Current joint design requirements in Chapter 21 of ACI 318-02 do not cover this type of joint; therefore, they should be used with extreme caution. All experimental research in eccentrically braced frames has been performed on steel structures and practically none in reinforced concrete structures; therefore, they should not be used until relevant research results are available.
- The requirements for slab-column frames in Chapter 13 of ACI 318-02 are mainly intended for gravity effects and only some guidance is given in the Commentary on lateral-load analysis procedures. Slab-column frames have shown poor behavior in past earthquakes associated with extreme lateral flexibility and punching-shear failures. A slab-column system designed following Chapter 13 of ACI 318-02 would classify as an ordinary moment-resisting frame and could only

TABLE 14.7 Structural System Limitation and Building Height Limitation for Basic Reinforced Concrete Lateral Force-Resisting Systems

Basic lateral force-resisting system	Structural system and building height (m) limitation				
	Seismic Design Category				
	A & B	C	D	E	F
Bearing wall systems					
Special reinforced concrete shear walls	NL	NL	50 m	50 m	30 m
Ordinary reinforced concrete shear walls	NL	NL	NP	NP	NP
Building frame systems					
Special reinforced concrete shear walls	NL	NL	50 m	50 m	30 m
Ordinary reinforced concrete shear walls	NL	NL	NP	NP	NP
Moment-resisting frame systems					
Special reinforced concrete moment frames	NL	NL	NL	NL	NL
Intermediate reinforced concrete moment frame	NL	NL	NP	NP	NP
Ordinary reinforced concrete moment frames	NL	NP	NP	NP	NP
Dual with special moment frames capable of resisting 25% of prescribed seismic forces					
Special reinforced concrete shear walls	NL	NL	NL	NL	NL
Ordinary reinforced concrete shear walls	NL	NL	NP	NP	NP
Dual with intermediate moment frames capable of resisting 25% of prescribed seismic forces					
Special reinforced concrete shear walls	NL	NL	50 m	30 m	30 m
Ordinary reinforced concrete shear walls	NL	NL	NP	NP	NP
Inverted pendulum systems and cantilever column systems					
Special reinforced concrete moment frames	NL	NL	NL	NL	NL

Notes: NL = No limit, NP = Not permitted. For 30 m use 100 ft, and for 50 m use 160 ft.

be used in seismic design categories A, and B (see Table 14.7). When the requirements of Section 21.12.6—Two-way slabs without beams (part of Section 21.12—Requirements for intermediate moment frames) are used the slab–column system may be used in seismic design categories A, B and C (see Table 14.7). No corresponding requirements exist for special moment frames and slab–column frames cannot be used as a lateral force-resisting system in seismic design categories D, E and F. Their use in combination with one of the permitted lateral force-resisting system for these seismic design categories as frame members not proportioned to resist forces induced by earthquake motion (see Section 21.11 of ACI 318-02) is still permitted. The designer when using this option must define the maximum lateral displacements that the system can sustain without failure—generally just a fraction of the permitted story drift—and the use of the requirements of section 21.12.6 of ACI 318-02, although not mandatory, gives some additional toughness to the system. See Section 14.6.4 for additional comments.

14.2.4 Response Modification Coefficient, R, Overstrength Factor, Ω_0 and Deflection Amplification Factor, C_d

It is expected, under the SEI/ASCE 7-02 requirements, that the structure when subjected to the design earthquake ground motion would sustain several excursions in the nonlinear range of response without critical decrease of strength. This allows for energy dissipation thus reducing the effects of the ground motion as compared to those that would occur in a lightly damped structure responding in the linear range. The amount of reduction permitted depends on the characteristics of the structural system, the structural material and the degree of toughness provided by the detailing of the structural material.

TABLE 14.8 Design Coefficients and Factors for Basic Reinforced Concrete Lateral Force-Resisting Systems

Basic lateral force-resisting system	Response modification coefficient, R	System over-strength factor, Ω_0	Deflection amplification factor, C_d
Bearing wall systems			
Special reinforced concrete shear walls	5	2.5	5
Ordinary reinforced concrete shear walls	4	2.5	4
Building frame systems			
Special reinforced concrete shear walls	6	2.5	5
Ordinary reinforced concrete shear walls	5	2.5	4.5
Moment-resisting frame systems			
Special reinforced concrete moment frames	8	3	5.5
Intermediate reinforced concrete moment frames	5	3	4.5
Ordinary reinforced concrete moment frames	3	3	2.5
Dual systems with special moment frames capable of resisting 25% of prescribed seismic forces			
Special reinforced concrete shear walls	8	2.5	6.5
Ordinary reinforced concrete shear walls	7	2.5	6
Dual systems with intermediate moment frames capable of resisting 25% of prescribed seismic forces			
Special reinforced concrete shear walls	6	2.5	5
Ordinary reinforced concrete shear walls	5.5	2.5	4.5
Inverted pendulum systems and cantilever column systems			
Special reinforced concrete moment frames	2.5	2	1.25

Note: The tabulated value of the over-strength factor, Ω_0 , may be reduced by subtracting 0.5 for structures with flexible diaphragms, but should not be less than 2 for any structure.

SEI/ASCE 7-02 assigns a response modification coefficient, R , depending on the lateral force-resisting system, the lateral force-resisting structural element type, the structural material and the detailing requirements used in designing the structural elements. This coefficient is used to reduce the inertial forces caused by the design ground motion on the structure, to the reduced expected inertial forces that would be present after the energy dissipation caused by the nonlinear response has occurred.

An overstrength factor, Ω_0 , to be used in the design of selected elements that should remain in the linear range of response because nonlinear response is not feasible, or convenient, is also prescribed by SEI/ASCE 7-02 for each lateral force-resisting system. It is only used during the design process for explicitly indicated elements as an additional safety factor in a special seismic load as explained in Section 14.2.8. In reinforced concrete structures the use of the overstrength factor is required in elements that are part of the load path from point of application of the inertial forces to foundation; in diaphragm collector elements, splices, and their connections to resisting elements; in columns supporting discontinuous elements; in batter piles and their connections; in splices of piles; and in the anchorage of piles to the pile cap.

A deflection amplification factor, C_d , is used to obtain the expected lateral displacement of the structure when subjected to the design ground motion and responding in the nonlinear range. Because the nonlinear response is associated with a decrease in stiffness, the lateral displacements obtained for the R reduced inertial forces and the original stiffness would be substantially less than the expected lateral displacements, thus requiring to be corrected by this deflection amplification factor, C_d .

Table 14.8 presents the values of R , Ω_0 and C_d for the reinforced concrete lateral force-resisting systems presented in Table 14.7. They were extracted from Table 9.5.2.2 of SEI/ASCE 7-02.

SEI/ASCE 7-02 allows for combination of framing systems among those listed in Table 14.8. Different lateral force-resisting systems are permitted with restrictions along the two orthogonal axes of the structure requiring in most cases to use the lower value of R in both directions. For combinations of systems in height the value of R at any level and direction cannot exceed the lowest value in the stories above in the same direction. The last rule also applies for the value of Ω_0 . The detailing requirements corresponding to the highest value of R must be used in the design of structural members common to systems having different values of R .

14.2.5 Redundancy

Redundant is defined by the dictionary as: "having more than enough, overabundant, excess or superfluous." When applied to a structure, it means that its layout is such that it has a number of supports, or elements or both, that is in excess of that required for just equilibrium. Therefore, redundant is synonymous with statically indeterminate. From the point of view of earthquake-resistant design, a redundant structure is one that has multiple paths of resistance. A continuous load path, or paths, with adequate strength and stiffness must be provided to transfer all forces from the point of application to the final point of resistance. For structures that respond in the nonlinear range redundancy provides the possibility of redistributing to other elements the additional inertial forces that an element that has reached the nonlinear range would be called to support. Another way of seeing redundancy would be to be able to depend on a plural number of elements to provide resistance to the inertial forces caused by the earthquake ground motion.

SEI/ASCE 7-02 prescribes a procedure to increase the load factor used in design when lack of redundancy is present in the lateral force-resisting system. The procedure is based on the use of a reliability factor ρ . The value of ρ must be taken as the largest value of ρ_x obtained for any story x of the structure for a given direction of loading. The reliability factor is obtained as follows:

Seismic Design Categories A, B and C — In these categories the value of ρ is 1.0.

Seismic Design Category D — For any story x the value of ρ_x must be computed using Equation 14.6

$$\rho_x = 2 - \frac{6.1}{r_{\max_x} \sqrt{A_x}} \quad (14.6)$$

where

r_{\max_x} is the ratio of the design story shear resisted by the single element carrying the largest shear force in the story to the total story shear, for a given direction of loading

A_x is the floor area in m^2 of the diaphragm level immediately above the story

When the floor area is in square feet, Equation 14.6 is

$$\rho_x = 2 - \frac{20}{r_{\max_x} \sqrt{A_x}}$$

The value of ρ need not exceed 1.5 and cannot be less than 1.0. The value of 1.5 may be used if no computation of ρ is performed.

For reinforced concrete structures, computation of r_{\max_x} must be performed in the following way:

- For moment frames r_{\max_x} must be taken as the maximum of the sum of the shear of two adjacent columns in the plane of a moment frame divided by the story shear. For columns common to two bays with moment-resisting connections on opposite sides at the level under consideration, 70% of the shear of that column may be used in the column shear summation.
- For shear walls, r_{\max_x} must be taken equal to the shear in the most heavily loaded wall or wall pier multiplied by $3.3/\ell_w$ when ℓ_w is in m, and by $10/\ell_w$ when ℓ_w is in ft, where ℓ_w is the horizontal length of the wall or wall pier, divided by the story shear.

- For dual systems, r_{max} must be at the maximum value for the values computed for the moment frame and for the walls as indicated previously. The lateral forces must be distributed to the elements based on the relative rigidities considering the interaction of the dual system. In dual systems the value of ρ may be taken as 80% of the value computed as indicated above.
- When the lateral force-resisting system in any direction is composed only of special moment frames, the system must be configured in such a way that the computed value of ρ does not exceed 1.25.

Numerous designers have pointed out that in some instances the obtained value of the reliability factor ρ unfairly penalizes structures that have adequate redundancy. Chapter 7 discusses issues associated with the reliability associated with the ρ factor.

Seismic Design Categories E and F—In these categories the value of ρ must be computed as required for category D with the following exception:

If the lateral force-resisting system in any direction is composed only of special moment frames, the system must be configured so that ρ does not exceed 1.1.

14.2.6 Required Base Shear Strength and Seismic Lateral Forces

The sum at the base of the structure of the horizontal applied forces is called the base shear. If the design earthquake ground motion is used to obtain the inertial horizontal forces the resulting base shear is referred to as the seismic base shear, V . The SEI/ASCE 7-02 document recognizes several procedures to obtain the required base shear strength with varying degrees of complexity and restrictions in their use depending on the seismic design category and the structure being regular or irregular from the structural configuration point of view. All these procedures are based on the principles of structural dynamics and correspond to the application of Newton's second law. Section 14.3 discusses their use in reinforced concrete structures.

The equivalent lateral force procedure (ELFP) is briefly presented here as a vehicle for introducing later the requirements for analysis for reinforced concrete structures. This procedure is a single-mode approximate dynamic analysis. It uses only the fundamental mode of the structure and the total mass of the structure instead of the fraction corresponding to the effective modal mass of the fundamental mode.

Under the equivalent lateral load procedure the seismic base shear is obtained from:

$$V = C_s W \quad (14.7)$$

where C_s is a seismic response coefficient and W is the total dead load of the structure plus 25% of the live load in storage uses, an allowance for partition load, the total operating weight of all permanent equipment and 20% of the snow load in flat roofs (the detailed requirements for obtaining W in Section 9.5.3 of SEI/ASCE 7-02 must be consulted).

When the fundamental period of the structure is not computed, the seismic response coefficient, C_s , is obtained from the following equation:

$$C_s = \frac{S_{DS}}{R/I} \quad (14.8)$$

S_{DS} is obtained from Equation 14.3 as explained in 14.2.2.1, R is the response modification coefficient from Table 14.8 and I is the seismic occupancy importance factor given in Table 14.2.

If the fundamental period of the structure is computed there is no need for the seismic response coefficient, C_s , to exceed:

$$C_s = \frac{S_{D1}}{T(R/I)} \geq 0.044 S_{DS} I \quad (14.9)$$

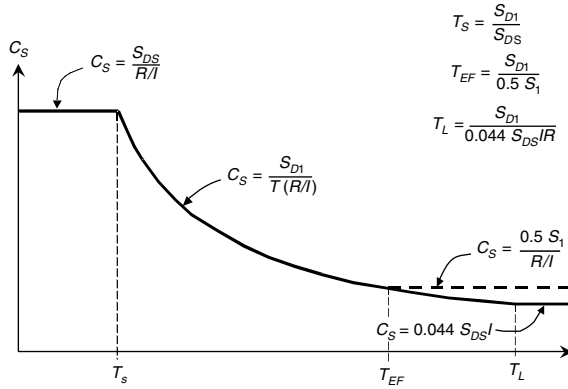


FIGURE 14.10 Seismic response coefficient, C_s , in the equivalent lateral force procedure.

where S_{D1} is obtained from Equation 14.4 as explained in 14.2.2.1, and T is the fundamental period of the structure in seconds. For seismic design categories E and F the value of C_s can not be less than:

$$C_s = \frac{0.5S_1}{R/I} \quad (14.10)$$

where S_1 is the mapped spectral response accelerations in rock at 1 sec described in 14.2.2.1.

Figure 14.10 shows the variation of the seismic response coefficient, C_s , with respect to the fundamental building period, T , of the building. From the figure it is evident that the seismic response coefficient is based on the design response spectrum shown in Figure 14.9 divided by the ratio (R/I). One main difference is that for the short period range, C_s does not decrease as period tends to zero in the same manner as the spectrum and is maintained constant. This is because the reduction in the inertial forces caused by nonlinear response and represented by the response modification coefficient, R , is not appropriate for short period systems where the nonlinear response reduction may not occur. The other difference is that there is a minimum value of C_s for long periods. This is introduced to provide a minimum base-shear strength in design for long period buildings, generally high-rise structures.

Another aspect that should be noted is that because the seismic response coefficient, C_s , is obtained from spectral accelerations S_{Ds} and S_{D1} , both expressed as fractions of the acceleration of gravity, g , and the total weight W used in Equation 14.7 when computing the seismic base shear is the total mass M multiplied by g , then $V = C_s W = C_s g M$. This simple change shows that $C_s g$ is acceleration in units of length over time squared. Therefore, Equation 14.7 is in reality a direct application of Newton's second law that simply states that the inertial forces are the product of the mass times acceleration.

The fundamental building period is needed to obtain the value of the seismic response coefficient. SEI/ASCE 7-02 requires that the fundamental building period in the direction under consideration, T , be obtained using the mechanical properties of the structure in a properly substantiated analysis. It also provides a procedure for obtaining an approximate fundamental period, T_a . The approximate fundamental building period is also used to set a limit for the maximum value of T that can be used to obtain the seismic base shear V . The limit is a function of the design spectral response acceleration at 1 sec, S_{D1} . Table 14.9 lists the maximum permitted building fundamental period. If the fundamental building period, T , is not computed, it is permitted to use the approximate building period T_a .

The upper bound on the value of T calculated using more exact methods, based on T_a , recognizes that the empirical equations for T_a are representative of the type of construction common in North America in high seismicity areas and that buildings located in moderate and low seismicity areas are probably more flexible. Notwithstanding, the designer of buildings in these lower seismicity areas must be aware

TABLE 14.9 Maximum Permitted Values of the Fundamental Building Period T

Value of S_{D1}	Maximum value of T
≥ 0.4	$1.4T_a$
0.3	$1.4T_a$
0.2	$1.5T_a$
0.15	$1.6T_a$
0.1	$1.7T_a$
≤ 0.05	$1.7T_a$

TABLE 14.10 Values of Parameters C_t and x for Obtaining the Approximate Fundamental Building Period T_a

Structure type	C_t (for h_n in m)	C_t (for h_n in ft)	x
Reinforced concrete moment-resisting frames that resist 100% of the required seismic force and are not restricted by more rigid components	0.044	0.016	0.9
Other reinforced concrete structural systems	0.055	0.020	0.75

that observance of the maximum allowable story drift may turn out to be the controlling design parameter when selecting the lateral stiffness of the lateral load-resisting system as opposed to just meeting the base shear strength, especially if stability problems (P-delta) and wind requirements come into play.

The approximate fundamental building period, T_a , in seconds is obtained from:

$$T_a = C_t h_n^x \quad (14.11)$$

where h_n is the building height in m, and coefficients C_t and x are listed in Table 14.10 for reinforced concrete lateral force-resisting systems.

For reinforced-concrete moment-resisting frames not exceeding 12 stories and with story heights of at least 3 m (12 ft) in height, the following equation based only on the number of stories, N , may be used alternatively:

$$T_a = \frac{N}{10} \quad (14.12)$$

For reinforced concrete wall structures the use of the following procedure is permitted to obtain the approximate fundamental building period:

$$T_a = \frac{0.0062}{\sqrt{C_W}} h_n \quad (14.13)$$

for h_n in m. For h_n in feet, the following equation must be used:

$$T_a = \frac{0.0019}{\sqrt{C_W}} h_n$$

C_w is obtained from:

$$T_a = \frac{100}{A_B} \sum_{i=1}^n \left(\frac{h_n}{h_i} \right)^2 \frac{A_i}{1 + 0.83 \left(\frac{h_i}{D_i} \right)^2} \quad (14.14)$$

where:

A_B is the base area of the structure (m^2 or ft^2)

A_i is the area of shear wall i (m^2 or ft^2)

D_i is the length of shear wall i (m or ft)

n is the number of shear walls in the building effective for resisting lateral forces in the direction under consideration

Once the fundamental building period is obtained for each principal direction of the building, the seismic base shear, V , can be computed for each direction using Equation 14.7. The seismic base shear is then distributed in the height of the building using:

$$F_x = C_{vx} V \quad (14.15)$$

and

$$C_{vx} = \frac{w_x h_x^k}{\sum_{i=1}^n w_i h_i^k} \quad (14.16)$$

where:

F_x = lateral seismic force induced at level x

C_{vx} = vertical distribution factor

V = total design lateral force or shear at the base of the structure

w_i, w_x = portion of the total gravity load of the structure (W) located or assigned to levels i or x , respectively

h_i, h_x = height from the base to levels i or x , respectively

k = exponent related to the structure period as follows:

$$k = 1 \quad \text{for } T \leq 0.5 \text{ sec}$$

$$k = 0.75 + 0.5 T \quad \text{for } 0.5 \text{ sec} < T \leq 2.5 \text{ sec}$$

$$k = 2 \quad \text{for } 2.5 \text{ sec} < T$$

The seismic design story shear at any story, V_x is obtained from:

$$V_x = \sum_{i=x}^n F_i \quad (14.17)$$

The seismic design story shear V_x must be distributed to the vertical elements of the lateral force-resisting system in the story under consideration based on the relative lateral stiffness of the vertical lateral resisting elements and the diaphragm.

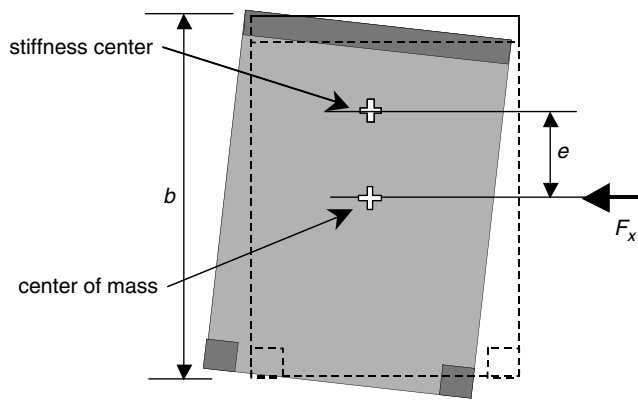


FIGURE 14.11 Torsional moment, M_t , from location of story mass and stiffness.

The overturning moment at any story, M_x (in kN·m or kip·ft) is obtained from:

$$M_x = \sum_{i=x}^n F_i(h_i - h_x) \quad (14.18)$$

At any story, the increment of overturning moment in the story under consideration must be distributed to the vertical elements of the lateral force-resisting system in the same proportion as the distribution of the story shear to these elements. For foundation design, except inverted-pendulum structures, the overturning moment at the foundation-soil interface, M_p can be reduced to 75% of the value obtained using Equation 14.18.

The overturning moment as stated in Equation 14.18 is just an application of the principle of equilibrium for the equivalent lateral forces. The lesser contribution to overturning of dynamic lateral forces caused by vibration modes different from the fundamental forces inspired in previous editions of the model code seismic requirements dates back to the 1960s reductions of the overturning moment which are now not permitted. Currently this reduction can only be used for the structure at the foundation-soil interface based on some uplifting of the foundation edges that are acceptable for the type of building for which the equivalent lateral force procedure is permitted.

When the diaphragm is not flexible, torsional effect of the structure as a whole must be taken into account. This effect results from the inertial forces acting at the center of mass of the diaphragm, while the diaphragm tends to rotate around the center of stiffness. This effect is caused by having the vertical elements of the lateral force-resisting system not symmetrically arranged.

Diaphragms are considered flexible in SEI/ASCE 7-02 when the maximum lateral deformation of the diaphragm is more than two times the average story drift of the story. The loads used for this calculation must be those obtained using the equivalent lateral force procedure. This distinction between flexible and rigid diaphragms has serious implications in design. A flexible diaphragm leads to design forces for the individual lateral force-resisting elements based on tributary mass to the elements, while a rigid diaphragm distributes the whole story shear in proportion to the lateral stiffness of the lateral load-resisting elements independently of the tributary mass. The rule for distinguishing between flexible and rigid diaphragms in reinforced concrete structure seldom comes into play because the intrinsic in-plane stiffness of reinforced concrete diaphragms. Care should be exercised in reinforced concrete structures where the geometry of the diaphragm renders it flexible (see Section 14.2.9).

Figure 14.11 shows a simple rigid diaphragm having a wall in one side and a two-column frame in the opposite side. The torsional moment M_t has a magnitude equal to the applied force, F_x , times eccentricity e . An accidental torsion moment is required for rigid diaphragms in all cases, even when the

centers of mass and stiffness coincide. The accidental torsion moment, M_{ta} , accounts for the distribution of mass in the story not as uniform as assumed. The value of the accidental torsion moment is set as the product of the applied seismic force in the story, F_x , times 5% of the dimension of the structure perpendicular to the direction of the applied force (dimension b in Figure 14.11). When lateral forces are applied concurrently in two orthogonal directions, the accidental torsion should be applied only in the direction producing the greater effect.

It is important to take into account that these torsional effects are critical only if the diaphragm has sufficient stiffness and strength to transport the in-plane forces that arise. There are indications that the 5% accidental eccentricity may be too small in some structures since they may develop torsional dynamic instability (FEMA, 2001). Because of this for structures with torsional irregularities in seismic design categories C, D, E and F, the accidental torsion moment must be amplified by a torsional amplification factor, A_x , obtained from:

$$A_x = \left(\frac{\delta_{\max}}{1.2\delta_{\text{avg}}} \right)^2 \leq 3.0 \quad (14.19)$$

where:

δ_{\max} is the maximum lateral displacement at level x

δ_{avg} is the average of the lateral displacements at extreme points of the structure at level x

This presentation of the requirements for obtaining the design base shear and the seismic lateral forces is a summary of only one—the equivalent lateral force procedure—of the procedures prescribed in SEI/ASCE 7-02 for this purpose. The reader must consult the text of the requirements and be aware there are limitations and additional requirements that were not covered in this limited introduction to the definition of the seismic design forces.

14.2.7 General Analysis Requirements

With respect to analysis, SEI/ASCE 7-02 requires that the adequacy of the structural systems be demonstrated through construction of a mathematical model and evaluation of this model for the effects of the design ground motion. Defining a proper mathematical model for structures under dynamic effects is a challenging problem when compared to static load analysis. The model degree of complexity increases for structures responding dynamically in the nonlinear range. Notwithstanding, for most design applications the use of complex models is not warranted and current Code requirements permit, with limitations, the use of simple linear models for most cases.

The approach used in SEI/ASCE 7-02 for defining the type of mathematical model to be used is based on the configuration of the structure. The degree of irregularity of the configuration of the structure is a subjective matter that is difficult to pose in black and white. SEI/ASCE 7-02 selected a catalog approach in which ten irregularity types — five plan and five vertical irregularities — are described including limits that define when the structure is considered regular or irregular based on the reason stated. The cases listed in this catalog approach are based on poor behavior observed in past earthquakes. It is evident that a list of this nature cannot be exhaustive and this is probably the area of earthquake-resistant design where more engineering judgment and experience are required from the designer. The other aspect that must be taken into account is that the irregularity cases considered are related directly to the North American architectural, structural and construction practice and experience. Other geographical regions of the world have also related different experiences expanding the irregularity cases in many instances. The structural configuration is, in general, a reflection of the architectural layout of the building, and although it is feasible to arrange a regular structural layout for an irregular architectural plan, this is not always possible. This stresses the responsibility of the structural designer in proposing alternate structural layouts that meet the architectural directives while rendering the project as regular as possible from the structural point of view.

TABLE 14.11 Plan Structural Irregularities in SEI/ASCE 7-02

Plan Structural Irregularity Type	Seismic Design Category					
	A	B	C	D	E	F
1a Torsional irregularity			x	x	x	x
1b Extreme torsional irregularity		x	x	x	x	
2 Re-entrant corners				x	x	x
3 Diaphragm discontinuity				x	x	x
4 Out-of-plane offsets	x	x	x	x	x	
5 Nonparallel systems		x	x	x	x	

TABLE 14.12 Vertical Structural Irregularities in SEI/ASCE 7-02

Vertical Structural Irregularity Type	Seismic Design Category					
	A	B	C	D	E	F
1a Stiffness irregularity – Soft story			x	x	x	
1b Stiffness irregularity – Extreme soft story		x	x	x		
2 Weight (mass) irregularity			x	x	x	
3 Vertical geometric irregularity			x	x	x	
4 In-plane discontinuity in vertical elements	x	x	x	x	x	
5 Discontinuity in lateral strength (soft story)	x	x	x	x	x	

Section 9.5.2.3 of SEI/ASCE 7-02 is devoted to structural configuration. The scope of this introductory presentation precludes an in-depth treatment of configuration issues beyond a simple listing of the cases covered and the seismic design categories where they should be considered. Table 14.11 lists plan structural irregularities and Table 14.12 lists vertical structural irregularities indicating by a marker “x” the seismic design categories where they should be considered in design. The reader is encouraged to study the requirements of SEI/ASCE 7-02 in this respect, and associated literature as presented in (Arnold, 2001; Arnold and Reitherman, 1982).

SEI/ASCE 7-02 prescribes six analysis procedures for modeling the effects of earthquake ground motion on the structure. Chapter 6 is devoted to methods of analysis for earthquake-resistant structures and contains an in-depth description. The following are the types of analysis methods, including a brief description of the requirements.

14.2.7.1 Index Force Analysis

For this, analysis procedure of a linear model of the structure fixed at the base is used. Lateral forces consisting of 1% of the total story gravity weight w_x (defined in 14.2.6) of each story are applied simultaneously at each level. The story lateral loads are applied independently in each of the main orthogonal directions.

14.2.7.2 Simplified Analysis

A linear model of the structure fixed at the base is also used in this analysis procedure. The seismic base shear, V , is obtained without having to use the building fundamental period from

$$V = \frac{1.2S_{DS}}{R} W \quad (14.20)$$

all terms have been previously defined. Lateral forces at each level are computed using

$$F_x = \frac{1.2S_{DS}}{R} w_x \quad (14.21)$$

Lateral forces from each story are applied simultaneously at each level. The story lateral loads are applied independently in each of the main orthogonal directions.

14.2.7.3 Equivalent Lateral Force Analysis

This analysis procedure was described in 14.2.6. A linear model of the structure fixed at the base is used. The model must include the stiffness and strength of all elements that are significant to the distribution of forces and deformations in the structure and must represent the spatial distribution of the mass and stiffness of the structure. Stiffness properties for reinforced concrete (and masonry) structures must take into account the effects of cracked sections.

14.2.7.4 Modal Response Spectrum Analysis

A modal response spectrum analysis consists of a dynamic analysis of a linear mathematical model of the structure to determine the maximum accelerations, forces and displacements resulting from the dynamic response to ground shaking represented by the design response spectrum. The structure may be considered fixed at the base or, alternatively, realistic assumptions may be used with regard to the stiffness of foundations. Stiffness properties for reinforced concrete structures must take into account the effects of cracked sections. The analysis must include a sufficient number of modes to obtain a combined modal mass participation of at least 90% of the total mass in two orthogonal directions. The design base shear obtained from the modal response spectrum dynamic analysis in each principal direction, V_p , must be compared to a base shear, V , computed by the equivalent lateral-force procedure using a fundamental period T that does not exceed the approximate fundamental period T_a increased by the factor given in Table 14.9. When the modal base shear, V_p , is less than 85% of V computed as indicated, all response parameters from the modal analysis, including story shear, overturning moment, lateral floor deflection, story drift and internal forces, must be multiplied by the following modification factor:

$$0.85 \frac{V}{V_t} \quad (14.22)$$

For regular structures with independent orthogonal seismic-force-resisting systems, independent two-dimensional models may be used to represent each system. For irregular structures or structures without independent orthogonal systems, a three-dimensional model incorporating a minimum of three dynamic degrees of freedom consisting of translation in two orthogonal plan directions and torsional rotation about the vertical axis must be included at each level of the structure. See Figure 14.12.

Where the diaphragms are not rigid — compared to the vertical elements of the lateral-force-resisting system — the model must include a representation of the flexibility of the diaphragm and as many additional dynamic degrees of freedom as required accounting for the participation of the diaphragm in the dynamic response structure.

The reader is encouraged to study Section 9.5.6 of SEI/ASCE 7-02 for the specific requirements of this analysis method and to consult Chapter 6 — Methods of Analysis for Earthquake-Resistant Structures.

14.2.7.5 Linear Response History Analysis

A linear response history analysis consists of an analysis of a linear mathematical model of the structure to determine its response, through methods of numerical integration, to suites of ground motion acceleration histories compatible with the design response spectrum for the site. For the purposes of analysis, the structure may be considered fixed at the base or, alternatively, it is permitted to use realistic assumptions with regard to the stiffness of foundations. The mathematical model must meet the same requirements of a modal response spectrum analysis. The components corresponding to the translational degrees of freedom used in the mathematical model of at least three appropriate ground motion records must be used meeting detailed specifications to guarantee that they are representative of the design ground motion required for the site. These requirements are presented in Section 9.5.7.2 of SEI/ASCE 7-02. The reader is encouraged to consult this section.

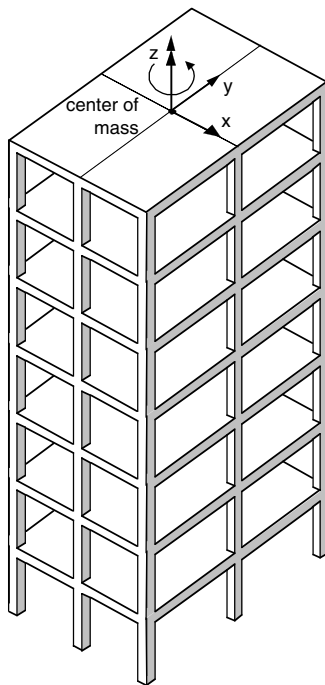


FIGURE 14.12 Three-dimensional model with three degrees of freedom per story.

14.2.7.6 Nonlinear Response History Analysis

A nonlinear response history analysis consists of an analysis of a mathematical model of the structure that directly accounts for the nonlinear hysteretic behavior of the structure components to determine its response, through methods of numerical integration, to suites of ground motion acceleration histories compatible with the design response spectrum for the site. The use of this method of analysis requires a peer review of the design made by an independent team of registered design professionals. Requirement for this type of analysis is presented in Section 9.5.8.1 of SEI/ASCE 7-02, and is beyond the scope of this introductory presentation. The reader is encouraged to study this section and Chapter 6 — Methods of Analysis for Earthquake-Resistant Structures.

The methods of analysis have restrictions in their use depending on the seismic design category, the seismic use group, the number of stories and in some cases the building fundamental period. These general restrictions are presented in Table 14.13.

14.2.8 Load Combinations, Load Factors and ϕ Factors

The load combination equations and load factors required by SEI/ASCE 7-02 in Section 2.3.2 are common for all structural materials. The resulting factored loads are appropriate for use in the strength design method. ACI 318-02 uses the same load combination equations and load factors, and defines the resulting value as required strength, U . The load combinations as defined in Section 2.3.2 of SEI/ASCE 7-02 and Section 9.2.1 of ACI 318-02 are given in Table 14.14.

The load factors given in the load combinations contained in ACI 318-02 are different from and generally lower than those in previous editions of the ACI code. It is important to note that in Table 14.14 the load factor for seismic forces, E , is 1.0 in combinations 5 and 7. This means that the design earthquake ground motion is defined at the strength level and does not require a load factor because it is implicit in the probability of exceedance of the design ground motion. For several decades earthquake requirements contained in the model codes defined the seismic forces at the working stress level, thus requiring a load factor greater than 1 for obtaining factored loads.

TABLE 14.13 Permitted Methods of Analysis in SEI/ASCE 7-02

Seismic design category	Structural characteristics	Index force analysis					
		Simplified analysis	Equivalent lateral force analysis	Modal response spectrum analysis	Linear response history analysis	Nonlinear response history analysis	
A	All structures	P	P	P	P	P	P
B, C	Seismic Use Group I. Light frame construction up to three stories	NP	P	P	P	P	P
	Other Seismic Use Group I buildings up to two stories	NP	P	P	P	P	P
	All other structures	NP	NP	P	P	P	P
D, E, F	Seismic Use Group I. Light frame construction up to three stories	NP	P	P	P	P	NP
	Other Seismic Use Group I buildings up to two stories	NP	P	P	P	P	P
	Regular structures with $T < 3.5T_s$, and all light frame construction	NP	NP	P	P	P	P
	Irregular structures with $T < 3.5T_s$, and having only plan irregularities types 2, 3, 4 or 5, and vertical irregularities types 4 or 5.	NP	NP	P	P	P	P
	All other structures	NP	NP	NP	P	P	P

Notes: $T_s = S_{DI}/S_{DS}$, P = Permitted, NP = Not permitted, NA = Not applicable.

TABLE 14.14 Load Combination Equations in SEI/ASCE 7-02 and ACI 318-02

Combination 1	$U = 1.4(D + F)$
Combination 2	$U = 1.2(D + F + T) + 1.6(L + H) + 0.5(L_r \text{ or } S \text{ or } R)$
Combination 3	$U = 1.2D + 1.6(L_r \text{ or } S \text{ or } R) + (1.0L \text{ or } 0.8W)$
Combination 4	$U = 1.2D + 1.6W + 1.0L + 0.5(L_r \text{ or } S \text{ or } R)$
Combination 5	$U = 1.2D + 1.0E + 1.0L + 0.2S$
Combination 6	$U = 0.9D + 1.6W + 1.6H$
Combination 7	$U = 0.9D + 1.0E + 1.6H$

where:

D = dead load

E = earthquake load

F = load due to fluids with well-defined pressures and maximum heights

H = load due to lateral earth pressure, ground water pressure or pressure of bulk materials

L = live load

L_r = roof live load

R = rain load

S = snow load

T = self-straining force

U = required strength to resist factored loads or related internal moments and forces

W = wind load

The earthquake-induced force effect, E , must include horizontal and vertical effects. For load combination 5 (see Table 14.14) it is obtained from:

$$E = \rho Q_E + 0.2 S_{DS} D \quad (14.23)$$

For load combination 7 (see Table 14.14):

$$E = \rho Q_E - 0.2 S_{DS} D \quad (14.24)$$

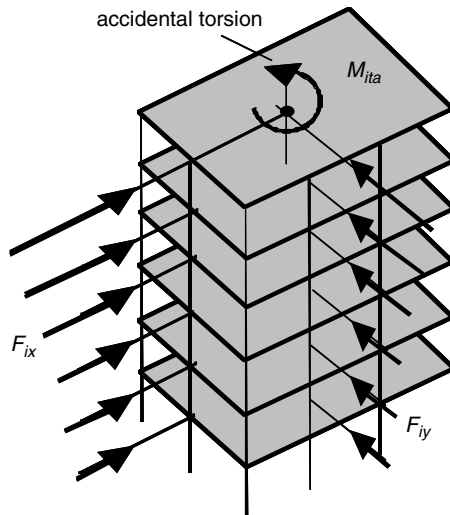


FIGURE 14.13 Six-story building subjected to seismic forces Q_E along the principal axes plus accidental torsion.

In Equations 14.23 and 14.24 ρ is the reliability factor explained in 14.2.5, Q_E is the effect of horizontal seismic (earthquake induced) forces, S_{DS} is the design spectral acceleration at short periods obtained as explained in 14.2.2.3 and D is the effect of dead load. The $0.2S_{DS}D$ factor in both equations represents the vertical acceleration component of the design ground motion as an increase or decrease of the gravity effect on the dead load, represented in D .

The direction of application of Q_E must be that producing the most demanding effects. SEI/ASCE 7-02 varies the requirements depending on the seismic design category. For SDC-A and SDC-B it is permitted to apply Q_E separately in each of the two orthogonal directions and the interaction effect between them (orthogonal interaction effects) may be neglected. For SDC-C the orthogonal interaction effects must be taken into account by applying Q_E independently in any two orthogonal directions and using 100% of the value in one direction plus 30% of the value in the other direction to obtain the most demanding effects. For certain irregular structures, more elaborate procedures are required. For seismic design categories D, E and F, the use of the procedures allowed for SDC-C are permitted, but columns and walls belonging to two or more intersecting seismic-force-resisting systems when the axial load due to seismic forces acting along either principal axis in plan corresponds to 20% or more of the axial design strength of the element must be designed to the most demanding effect from application of the seismic forces Q_E in any direction.

In general, the orthogonal interaction effects are critical for vertical elements such as columns and walls. For horizontal elements such as girders, the critical effect is obtained, in general, when the lateral forces act in a direction parallel to the direction of the element. The application of all load combination requirements leads to a large number of load cases to be studied even in simple structures. Application of torsional effects caused by the location of the structure masses and accidental torsion requirements increases the number of cases to be studied. Requirements for gravity loading contained in other sections of the code, such as pattern loading for live loads, may increase the number of cases even further.

The problem of accounting for all the required cases requires the use of the computer in most situations. To have a glimpse of what is required, let us study a hypothetical six-story building having a moment-resistant space frame composed of columns and girders as the lateral force-resisting system, shown in Figure 14.13. There are three three-bay frames in the x -direction and four two-bay frames in the y -direction.

In Figure 14.13 the seismic forces Q_E are represented by lateral seismic forces F_{ix} and F_{iy} acting at each level i of the structure in the x - and y -directions respectively, plus an accidental torsion effect, M_{ita} , also applied at each level at the center of mass of the story. The floor is a reinforced concrete two-way slab-on-girder

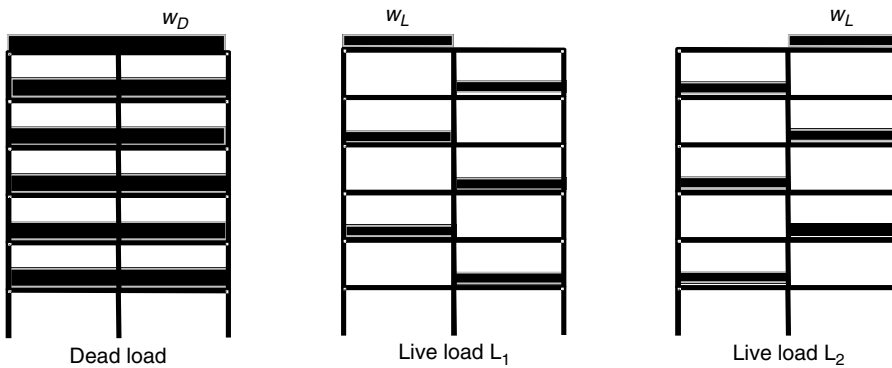


FIGURE 14.14 Distributed gravity (dead and live) loads acting on the girders of the frame.

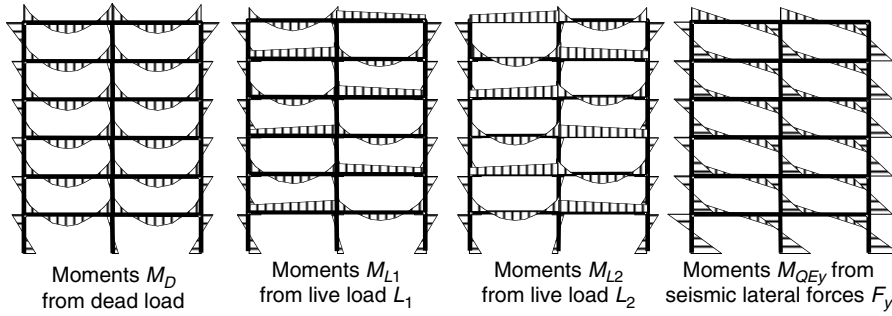


FIGURE 14.15 Moment diagrams obtained from frame analysis due to gravity and lateral loads.

system where all girders are part of the lateral force-resisting system frame. The floor system acts as a rigid in-plane diaphragm that distributes the inertial forces to the vertical elements (columns) of the lateral force-resisting system, therefore for all practical purposes the lateral seismic forces can be modeled as acting at the center of mass of the diaphragm.

Figure 14.14 shows uniformly distributed gravity loads w_D and w_L — nonfactored dead and live loads, respectively — acting on the girders of one of the frames. The dead load includes selfweight of the girders and selfweight and dead load from the tributary slab area. Column selfweight is either applied as a concentrated load at each joint or included as an addition to the dead load of the girders; the last alternative being more practical but not corresponding to the actual load effect. The live load has been divided into an arrangement where alternate bays are loaded with the tributary live load from the floor system. This live load arrangement complies with the requirements for pattern live loading of Chapter 8 of ACI 318-02.

Now let us look at the flexural moment effect on the frame caused by the gravity and earthquake loads. This effect is obtained using a frame analysis procedure that complies with the principles of equilibrium and deformation compatibility. Other effects such as shear forces, axial forces and torsional moments, are obtained from the same analysis at all sections within the structural elements of the frame. Figure 14.15 shows typical moment diagrams (drawn on the side where moment induces tension on the element) caused by the dead loads, live loads and earthquake lateral loads.

To obtain the factored flexural moment at any chosen section within a column or girder all load combination equations with their corresponding load factors (see Table 14.14) must be used. Table 14.15 shows the load combination cases, and the corresponding load combination equation used in each case. Only the effect of dead load, live load and seismic forces is taken into account in this example. Other

loads from those listed in Table 14.14, such as wind lateral earth pressure, rain or snow, require the use of additional load combinations, thus creating additional load cases. The values listed in Table 14.15 correspond to the load factor to be used to multiply each of the basic flexural moments obtained from analysis.

For example, taking load case 5, the required moment strength would be obtained using load combination equation 5 from Table 14.14 as the algebraic sum:

$$M_U = (1.2 + 0.2S_{DS})M_D + 1.0M_{L1} + 1.0M_{L2} + 1.0\rho M_{QEx} + 0.3\rho M_{QEY} + 1.0\rho M_{QET}$$

The load factor that multiplies the unfactored dead load moment, M_D , is composed of the 1.2 factor from load combination 5 (Table 14.14) plus the additional effect caused by the vertical seismic ground motion as required by Equation 14.23. Unfactored live load moments M_{L1} and M_{L2} are both multiplied by a 1.0 load factor. Using both live load moments from the two live-load pattern-loadings means that the total live load is used in all spans of the structure, as required by load combination 5. The load factor for moment M_{QEx} caused by the seismic forces acting only in the x -direction is the reliability factor, ρ , as required by Equation 14.23. To take into account the orthogonal effects, 0.3 times (30%) of the moment M_{QEY} caused by the seismic forces acting alone in the orthogonal direction (y -direction) are added, factored also by the reliability factor, ρ , as required by Equation 14.23. The last term corresponds to the moment caused by the effect of accidental torsion, M_{QET} factored also by the reliability factor, ρ , as required by Equation 14.23.

The seismic effects alternate in sign because they can act in one direction or the opposite. Because of this alternating, the load cases (5 to 20) using combination 5 from Table 14.14 correspond to changing, one at a time, the sign of each of the moments caused by the seismic effects (M_{QEx} , M_{QEY} and M_{QET}). Care must be taken in applying the corresponding 30% orthogonal effect in the correct direction. This produces 16 load cases derived from load combination 5. The same procedure is used to obtain the 16 load cases (21 to 36) derived from load combination 7.

Table 14.15 shows 36 load cases required to meet the gravity — load cases 1 to 4 — and seismic — load cases 5 to 36 — load combinations. Load cases 2 to 4 correspond to the classic load combinations for gravity pattern loading of girders. Load cases 2 and 3 lead to the maximum gravity positive midspan moment whereas load cases 1 and 4 to the minimum gravity negative moments at the supports (largest absolute value for the negative moment). Because of the shape of the gravity and lateral-load girder moment diagrams the load combinations that include lateral load generally produce maximum moments at the supports of the girder. Cases based on load combination 5 — load cases 5 to 20 — lead to the largest absolute-value negative-moment at the supports, whereas those based on load combination 7 — cases 21 to 36 — lead to the smallest absolute-value negative-moment and depending on the relative values between factored gravity moments and lateral load moments would detect the presence of positive moment at the girder supports. The computation of a moment envelope is warranted to obtain the largest positive and negative factored moments that act at any location within the girder span. The same cases must be studied for factored shear forces, axial loads and torsional moments in all elements (girders, column, walls, diaphragm and foundation) that are part of the lateral force-resisting system.

From the earlier discussion it is evident that meeting the load combination requirements without the use of computer-implemented procedures is almost impossible. The main drawback is that the inexperienced engineer may easily lose sight of the important issues that require the greatest attention while being lost in a sea of numbers. Total reliance on the computer without a check performed by an experienced engineer on the order of magnitude of the design controlling parameters would probably lead to unsafe structures or structures with poor expected behavior.

SEI/ASCE 7-02 prescribes also a special seismic load (Section 9.5.2.7.1) that is required in certain cases explicitly indicated. This special seismic load is used for elements and members that must remain in the linear elastic range of response or whose failure could put all the structure at risk. The special seismic load is treated also as an earthquake-induced force effect, E , that must include horizontal and vertical effects. For load combination 5 (see Table 14.14) it is obtained from:

TABLE 14.15 Load Combination Cases for Obtaining Ultimate Moments in a Six-Story Building Example

Load Case	Direction Seismic Forces	Combinatio n Equation Table 14.14	M_D	M_{L1}	M_{L2}	M_{QE_x}	M_{QE_y}	M_{QET}
1		1	1.4					
2		2	1.2	1.6				
3		2	1.2		1.6			
4		2	1.2	1.6	1.6			
5	+x	5	(1.2+0.2S _{DS})	1.0	1.0	1.0p	0.3p	1.0p
6	+x	5	(1.2+0.2S _{DS})	1.0	1.0	1.0p	0.3p	-1.0p
7	+x	5	(1.2+0.2S _{DS})	1.0	1.0	1.0p	-0.3p	1.0p
8	+x	5	(1.2+0.2S _{DS})	1.0	1.0	1.0p	-0.3p	-1.0p
9	-x	5	(1.2+0.2S _{DS})	1.0	1.0	-1.0p	0.3p	1.0p
10	-x	5	(1.2+0.2S _{DS})	1.0	1.0	-1.0p	0.3p	-1.0p
11	-x	5	(1.2+0.2S _{DS})	1.0	1.0	-1.0p	-0.3p	1.0p
12	-x	5	(1.2+0.2S _{DS})	1.0	1.0	-1.0p	-0.3p	-1.0p
13	+y	5	(1.2+0.2S _{DS})	1.0	1.0	0.3p	1.0p	1.0p
14	+y	5	(1.2+0.2S _{DS})	1.0	1.0	0.3p	1.0p	-1.0p
15	+y	5	(1.2+0.2S _{DS})	1.0	1.0	-0.3p	1.0p	1.0p
16	+y	5	(1.2+0.2S _{DS})	1.0	1.0	-0.3p	1.0p	-1.0p
17	-y	5	(1.2+0.2S _{DS})	1.0	1.0	0.3p	-1.0p	1.0p
18	-y	5	(1.2+0.2S _{DS})	1.0	1.0	0.3p	-1.0p	-1.0p
19	-y	5	(1.2+0.2S _{DS})	1.0	1.0	-0.3p	-1.0p	1.0p
20	-y	5	(1.2+0.2S _{DS})	1.0	1.0	-0.3p	-1.0p	-1.0p
21	+x	7	(0.9-0.2S _{DS})			1.0p	0.3p	1.0p
22	+x	7	(0.9-0.2S _{DS})			1.0p	0.3p	-1.0p
23	+x	7	(0.9-0.2S _{DS})			1.0p	-0.3p	1.0p
24	+x	7	(0.9-0.2S _{DS})			1.0p	-0.3p	-1.0p
25	-x	7	(0.9-0.2S _{DS})			-1.0p	0.3p	1.0p
26	-x	7	(0.9-0.2S _{DS})			-1.0p	0.3p	-1.0p
27	-x	7	(0.9-0.2S _{DS})			-1.0p	-0.3p	1.0p
28	-x	7	(0.9-0.2S _{DS})			-1.0p	-0.3p	-1.0p
29	+y	7	(0.9-0.2S _{DS})			0.3p	1.0p	1.0p
30	+y	7	(0.9-0.2S _{DS})			0.3p	1.0p	-1.0p
31	+y	7	(0.9-0.2S _{DS})			-0.3p	1.0p	1.0p
32	+y	7	(0.9-0.2S _{DS})			-0.3p	1.0p	-1.0p
33	-y	7	(0.9-0.2S _{DS})			0.3p	-1.0p	1.0p
34	-y	7	(0.9-0.2S _{DS})			0.3p	-1.0p	-1.0p
35	-y	7	(0.9-0.2S _{DS})			-0.3p	-1.0p	1.0p
36	-y	7	(0.9-0.2S _{DS})			-0.3p	-1.0p	-1.0p

$$E = \Omega_0 Q_E + 0.2 S_{DS} D \quad (14.25)$$

For load combination 7 (see Table 14.14):

$$E = \Omega_0 Q_E - 0.2 S_{DS} D \quad (14.26)$$

In Equations 14.25 and 14.26 Ω_0 is the overstrength factor explained in 14.2.4 and whose values are listed for each lateral force-resisting system in Table 14.8, Q_E is the effect of horizontal seismic (earthquake induced) forces, S_{DS} is the design spectral acceleration at short periods obtained as explained in 14.2.2.3 and D is the effect of dead load. The product $\Omega_0 Q_E$ in Equations 14.25 and 14.26 does not have to be taken greater than the capacity of the elements that transfer force to the component where the special seismic force is used as required. The use of the special seismic force equations to obtain E to be used in the load combination equations is the same as already described for the earthquake-induced force

TABLE 14.16 Strength Reduction Factors in ACI 318-02

Tension-controlled sections		$\phi = 0.90$
Compression-controlled sections	Members with spiral reinforcement Other reinforced members	$\phi = 0.70$ $\phi = 0.65$
Shear and torsion		$\phi = 0.75$
Bearing on concrete		$\phi = 0.65$
For shear in special moment-resisting frames or special reinforced concrete shear walls that resist earthquake effects	In any structural member that resists earthquake effects if its nominal shear strength is less than the shear corresponding to the development of the nominal flexural strength of the member. The ϕ -factor for shear in diaphragms can not exceed the minimum strength reduction factor for shear used for the vertical components of the primary lateral-force-resisting system For shear in joints and diagonally reinforced coupling beams	$\phi = 0.60$ $\phi = 0.85$

effect. Examination of Equations 14.25 and 14.26 indicates that the special seismic load is obtained in a similar manner as the earthquake-induced effect computed using Equations 14.23 and 14.24. The only difference is that in the special seismic load the overstrength factor Ω_0 is used instead of the reliability factor ρ . This leads to larger values of E because the largest possible value for ρ is 1.5, while an examination of the Ω_0 values listed in Table 14.8 for all reinforced concrete lateral force-resisting systems would indicate values always larger than 1.5 with a minimum of 2 and a maximum of 3.

The adoption of the SEI/ASCE 7-02 load combinations and factors brought a change in the strength reduction factors, ϕ , in ACI 318-02. These new ϕ -factors, with the exception of the one for flexure, are lower also than those contained in previous editions of the ACI code. The strength reduction factors, ϕ , for reinforced concrete structures in Section 9.3.2 of ACI 318-02 are summarized in Table 14.16. The ACI code also adopted for the 2002 edition the Unified Design Provisions for reinforced and prestressed flexural and compression members was previously contained in an appendix. Under these provisions the reinforcement limits, ϕ -factors and moment redistribution requirements are defined in terms of the net tensile strain in the extreme tension reinforcement at nominal strength. This new terminology is reflected in the definition of the ϕ -factors in Table 14.16.

The foundation must be designed to resist the forces developed and accommodate the movements imparted to the structure by the design ground motion. The dynamic nature of the forces, the expected ground motion and the design basis for strength and energy dissipation capacity of the structure must be included in the determination of the foundation design criteria. Special care must be taken in meeting the geotechnical study recommendations. The values for the bearing capacity of the foundation soil are given in geotechnical reports at the working stress level. The transformation from forces and stresses at the strength level, as computed for the structure, to working stress level forces and stresses must be performed with great care.

14.2.9 Drift Requirements

The structure being designed must have sufficient stiffness as stated before. The traditional procedure to judge the appropriateness of the general stiffness of the structure has been story drift, Δ_x , defined as the difference of the lateral deflections at the top and bottom of the story x under consideration, δ_x and δ_{x-1} , respectively, as shown in Figure 14.16:

$$\Delta_x = \delta_x - \delta_{x-1} \quad (14.27)$$

The lateral deflection δ_x at the center of mass of level x must be computed from:

$$\delta_x = \frac{C_d \delta_{xe}}{I} \quad (14.28)$$

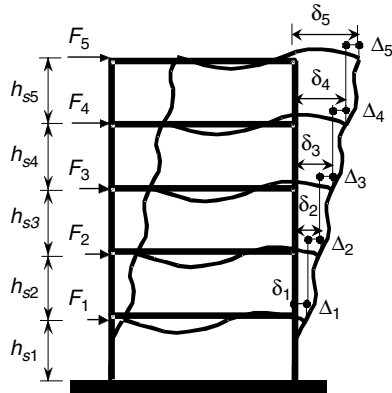


FIGURE 14.16 Story drift computation.

where:

- C_d is the lateral deflection amplification factor given in Table 14.8 for each of the seismic lateral-force resisting systems
- δ_{xe} is the lateral deflection of level x obtained from the elastic analysis made using the prescribed forces already divided by the response modification coefficient R
- I is the seismic occupancy importance factor given in Table 14.2

The analysis is made for a linear elastic mathematical model of the structure subjected to the prescribed design lateral forces. These forces include a reduction obtained by dividing the spectral response by the response modification coefficient, R . See Figure 14.10. The lateral deflections obtained from this analysis are defined as elastic deflections, δ_{xe} . Because the structure is responding in the nonlinear range the stiffness decreases and is less than the one used in the analysis. The deflection amplification factor, C_d , accounts for this difference by amplifying the lateral deflections to those that would have been obtained if the reduced stiffness had been used in analysis. This amplification is performed by Equation 14.28.

SEI/ASCE 7-02 also requires that P- Δ effect must be taken into account. Current analysis procedures are “first-order methods.” This means that during analysis equilibrium is stated on the undeformed structure. In a flexible structure this leads to error, because there is an additional lateral deflection introduced by the overturning effect caused by the gravity loads displacing along with the structure, which is not taken into account by the first-order analysis procedure. Therefore, the additional overturning effect corresponds to the gravity load, P , multiplied by the lateral relative deflection Δ . This is the reason for the name P- Δ . This is an analysis problem caused by the way equilibrium is stated. The usual way to deal with it is to find the magnitude of the error by using a stability coefficient, Θ . If the stability coefficient obtained from Equation 14.29 at any story and direction is equal or greater than 0.10 all forces and displacements obtained from analysis must be adjusted for this effect.

$$\Theta = \frac{P_x \Delta}{V_x h_{sx} C_d} \quad (14.29)$$

where

- P_x is the total vertical design load at and above level x . When computing P_x no individual load factor need exceed 1.0
- Δ is the design story drift occurring simultaneously with V_x
- V_x is the seismic story shear force acting at story x
- h_{sx} is the story height of story x . $h_{sx} = h_x - h_{x-1}$
- C_d is the lateral deflection amplification factor given in Table 14.8 for each of the seismic lateral-force resisting systems

The stability coefficient, Θ , cannot exceed Θ_{max} determined from:

$$\Theta_{max} = \frac{0.5}{\beta C_d} \leq 0.25 \quad (14.30)$$

where β is the ratio of shear demand to shear capacity for story x . This ratio may be taken conservatively as 1.0.

When the stability coefficient is greater than 0.1 and less or equal to Θ_{max} , the structure must be analyzed using a second-order analysis procedure. If the value of the stability coefficient, Θ , is greater than Θ_{max} at any story, SEI/ASCE 7-02 states that the structure is potentially unstable and must be redesigned. The purpose of this requirement is to protect structures from the possibility of stability failures triggered by postearthquake residual deformation. The possibility of such failures may not be eliminated by apparently available overstrength. This is particularly true of structures designed in regions of lower seismicity (FEMA, 2001).

The P- Δ requirements are controversial. One reason for being criticized is that all the effects are evaluated for the elastic component of the lateral deflection — this occurs because the story drift Δ is divided by C_d in Equation 14.29 — and not the expected lateral deflection occurring during the nonlinear response. The other source of discomfort with the requirement is that the reinforced concrete building designer is required to perform the P- Δ check twice with different modeling parameters and limits. ACI 318-02 requires in Section 10.10 slenderness verification for compression members. There the stability coefficient is called Q instead of Θ , and is used to define if a story of the structure classifies as sway or nonsway. The analysis requirements in ACI 318-02 are different from those in SEI/ASCE 7-02, the parameters used for obtaining the value of the stability coefficient are also different — for example the vertical load in ACI 318-02 is the factored load whereas in SEI/ASCE 7-02 corresponds to an unfactored load — and the limits where a second-order analysis is required are also different. This means double work for the designer and what is worse, in some instances the two procedures give conflicting results.

The procedure just explained for obtaining the story drift is applicable in planar analysis. When SEI/ASCE 7-02 requires a three-dimensional analysis (see Section 14.2.7 and Figure 14.12) evaluating the story drift at the center of mass of the story is not appropriate because in many instances that center of mass of the diaphragms of consecutive stories may not be located in the same vertical axis, and the presence of rotation of the diaphragm caused by the story torsional moment introduces an additional story drift at points away from the mass center of the diaphragm. In addition, the orthogonal interaction effects introduce a normal component of displacement, making the maximum story drift not parallel to the principal axis. See Figure 14.17.

When a diaphragm has a lateral deflection at the center of mass with components δx and δy along the principal direction, and a rotation δz (in rad) about a vertical axis that passes through the center of mass of the diaphragm, to determine the coordinates of any point in the diaphragm (see Figure 14.18) after the lateral displacements have taken place the following equations may be used:

$$\begin{aligned}\delta x_{a'} &= \delta x - y_a \delta z \\ \delta y_{a'} &= \delta y + x_a \delta z\end{aligned} \quad (14.31)$$

where x_a and y_a are the coordinates of point a in a coordinate system with the origin at the center of mass.

The evaluation of the torsional amplification factor A_x in Equation 14.19 (see Section 14.2.6) requires the computation of δ_{max} and δ_{avg} . Equation 14.31 may be used to obtain δ_{max} by computing it at selected locations within the diaphragm, usually the outmost corners. δ_{avg} corresponds to the lateral deflection at the center of mass of the diaphragm.

SEI/ASCE 7-02 requires that in seismic design categories C, D, E and F having plan irregularities types 1a and 1b (see Table 14.11) the design story drift Δ must be evaluated as the largest deflection difference along any of the edges of the structure. It is important to note that for this drift evaluation to be

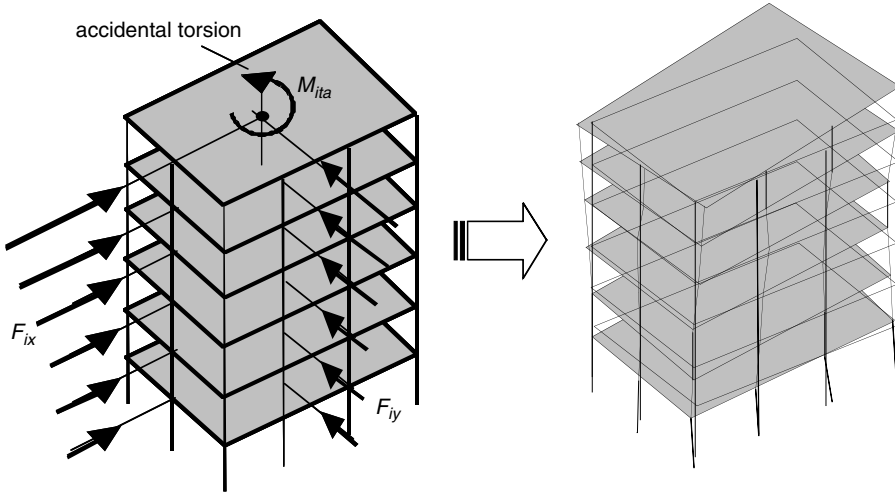


FIGURE 14.17 Lateral deflections of a building due to orthogonal and torsional effects.

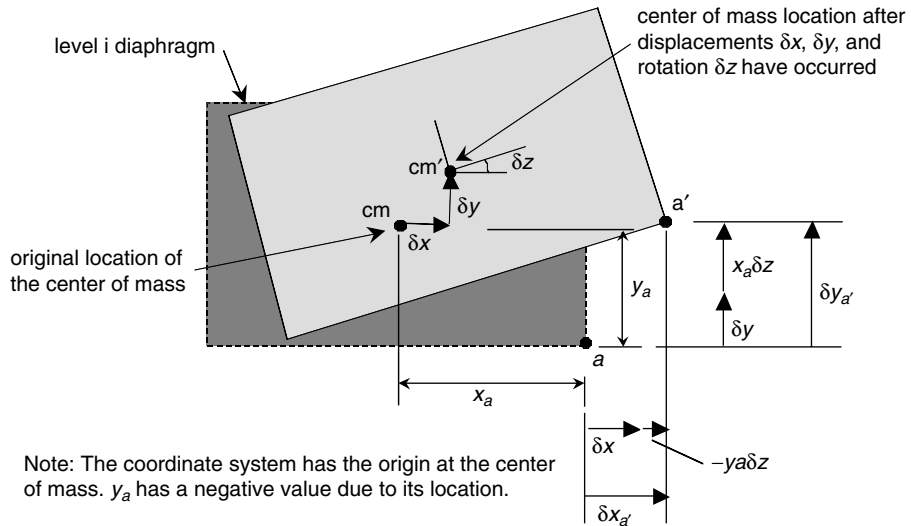


FIGURE 14.18 Location of a point within the diaphragm after lateral deflection have occurred.

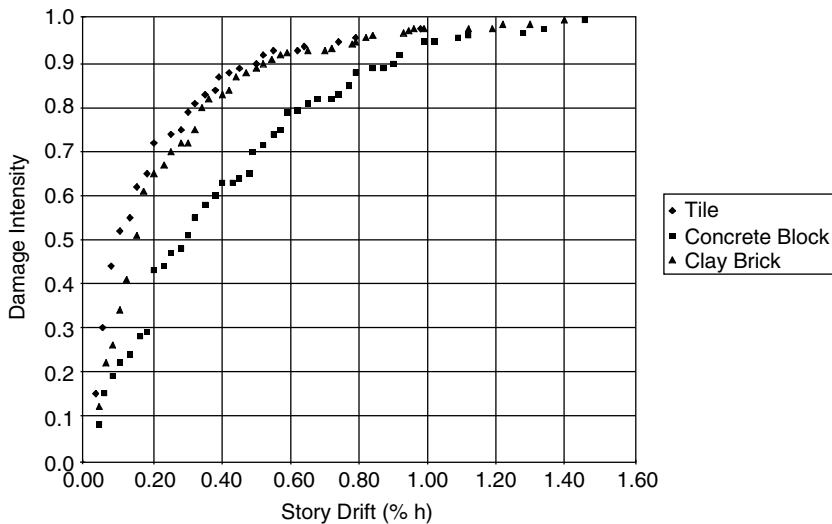
meaningful, it must be performed on points that are in the same vertical axis. One practical way of doing this is to evaluate drift at all columns and wall edges in the story. The procedure would be to obtain the coordinates of the laterally displaced structure at top and bottom of the column or wall edge. This can be made using Equation 14.31 for diaphragm i and $i-1$. Then the story drift, Δ , at the column location at the floor under study can be obtained from:

$$\Delta = \sqrt{(\delta x_i - \delta x_{i-1})^2 + (\delta y_i - \delta y_{i-1})^2} \quad (14.32)$$

The designer must be aware that the drift evaluations made at the center of mass of the diaphragm would underestimate the story drift in most structures, even regular in plan, because the accidental torsion lateral displacement is not taken into account. In irregular in plan structures the underestimation of the

TABLE 14.17 Allowable Story Drift for Reinforced Concrete Structures

Structure	Seismic Use Group		
	I	II	III
Structures four stories or less with interior walls, partitions, ceilings and exterior wall systems that have been designed to accommodate the story drifts	0.025 h_{sx}	0.020 h_{sx}	0.015 h_{sx}
All other structures	0.020 h_{sx}	0.015 h_{sx}	0.010 h_{sx}

**FIGURE 14.19** Damage intensity versus story drift index for masonry partitions.

story drift is even larger. In those cases in which the center of mass in consecutive stories is not located along the same vertical axis, the drift evaluated using the lateral deflection of the consecutive diaphragms does not have any meaning and should not be used.

The story drift limits set by SEI/ASCE 7-02 are given in Table 9.5.2.8 of that document. For reinforced concrete structures only two sets of story drift limits apply and are summarized in Table 14.17 for the seismic use groups defined in Table 14.2.

The maximum allowable story drift is directly associated with the local construction practice of nonstructural elements. The story drift values permitted by SEI/ASCE 7-02 are directly related to the current North American building practice. In many seismic regions around the world construction of partitions and façade elements is made using stiff and brittle unreinforced masonry. Figure 14.19 adapted from (Algan, 1982) shows the damage intensity, defined as the cost of repairing the nonstructural walls divided by the cost of building a new wall, plotted against the story drift index, defined as the story drift divided by the story height in percentage. From the figure it is evident that for story drift indices greater than 0.3% the cost of repairing a nonstructural masonry wall is more than 50% of the cost of building a new wall. This means that in environments where the nonstructural partitions and façades are built using unreinforced masonry the story drift limits as stated in SEI/ASCE 7-02 may be too lax and limits of the order of one half to one quarter of those given in Table 14.17 must be used if the nonstructural elements are to have minimum repairable damage under the design earthquake ground motion.

The other aspect that comes into play when excessively flexible structures are employed in combination with stiff and brittle nonstructural elements is the interaction between the structure and the nonstructural elements that could lead to failure of the structural element, as occurs in the very common captive column effect where a column is partially restrained by a nonstructural wall having a window in its upper part.

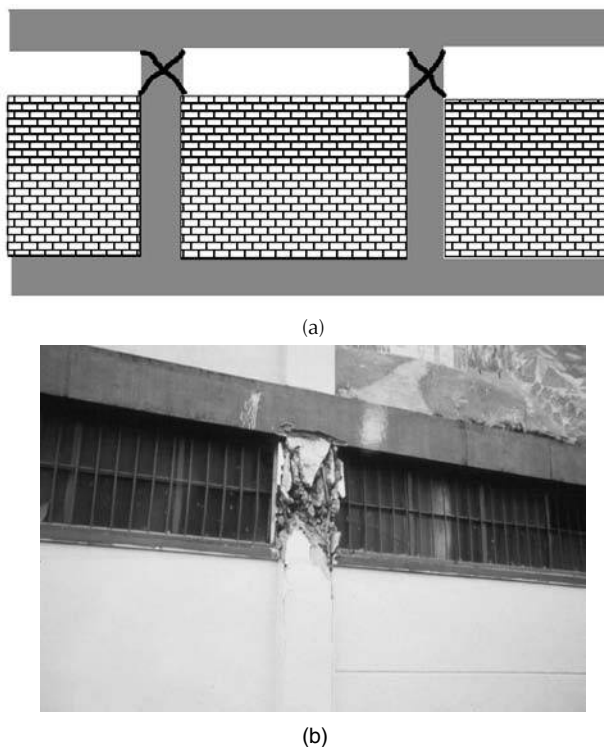


FIGURE 14.20 Captive column effect.

In this case there is a substantial probability of the column failing in shear in the unrestrained height left by the window, as has been observed in many past earthquakes. See Figure 14.20.

14.2.10 Materials for Earthquake-Resistant Concrete Structures

Constituent material for earthquake-resistant reinforced concrete structures must meet special requirements that are not needed in nonseismic regions. Concrete in structures designed and built using Chapter 21 of ACI 318-02 must have a specified compressive strength, f'_c , greater or equal to 20 MPa (3000 psi). The specified compressive strength for lightweight aggregate concrete should not exceed 35 MPa (5000 psi).

Reinforcing steel must comply with standard ASTM A706 "Low-Alloy Steel Deformed and Plain Bars for Concrete Reinforcement." This steel meets, among others, two important mechanical properties:

1. The actual yield strength based on tension tests should not exceed the specified yield strength by more than 120 MPa (17,000 psi).
2. The ratio of the actual ultimate tensile strength to the actual yield strength must be greater or equal to 1.25.

The first requirement is associated with not having excessive yield strength as compared with the nominal value. The reason for this requirement is to avoid elements with greater flexural capacity than intended in design because this could lead to elements that would fail in shear before reaching flexural strength. The second requirement states that it is desirable to have reinforcing steel with definite strain-hardening properties. The strain hardening permits that when the element is responding in the nonlinear range in selected regions of the element by reaching flexural strength by yielding of the tension reinforcement the yield region spreads and is not concentrated in a single section of the member. In an element reinforced with steel without strain-hardening properties the yield region would be short while the strain-hardening properties would extend the yield region giving the element a better inelastic rotation capacity. The length of the yield region is associated with the ratio of ultimate to yield moment strength.

TABLE 14.18 Reinforcing Steel Minimum Elongation Percentage for Grade 420 MPa (60 ksi)

Nominal bar diameter	ASTM A706	ASTM A615
10, 13, 16 and 19 mm (3/8, 1/2, 5/8 and 3/4 in.)	14%	9%
22 and 25 mm (7/8 and 1 in.)	12%	8%
29, 32 and 36 mm (1-1/8, 1-1/4 and 1-3/8 in.)	12%	7%
43 and 57 mm (1-3/4 and 2-1/4 in.)	10%	7%

To have a more ductile steel, Standard ASTM A706 requires larger minimum elongation percentage than other reinforcing steels such as ASTM A615. Table 14.18 shows the minimum elongation percentage measured in a 200 mm (8 in.) length for both these steels. Cold-worked steels should not be used in earthquake-resistant structures because the manufacturing process uses the strain-hardening properties of the steel to obtain apparent larger yield strength at the cost of reducing the ductility of the steel.

In ACI 318-02 full welded and mechanical splices are defined as splices that can develop 125% of the yield strength, f_y , of the bar. Mechanical splices meeting this requirement are denominated type 1 in Chapter 21. The full welded and type 1 mechanical splices cannot be used in regions located within a distance of twice the member depth from the face of the column or beam, or where yielding of the reinforcement is likely to occur as a result of the nonlinear response. Chapter 21 defines also a type 2 mechanical splice that meets the 125% bar yield strength requirement and in addition must develop the specified tensile strength of the spliced bar. Type 2 mechanical splices may be used at any location.

Anchors to concrete resisting earthquake-induced forces in seismic design categories C to F must be designed using *Appendix D — Anchoring to concrete* of ACI 318-02 with only 75% of the value of the appropriate strength reduction factor ϕ .

14.3 Predimensioning

14.3.1 Coordination with Other Professionals

The first stage in a structural design process is predimensioning. It covers several activities and usually follows a first meeting with the project architect and other consultants in which background on the criteria that lead the architect in producing the resulting architectural layout is presented and explained. The importance of the feedback that is expected from the structural designer at this stage has far reaching implications because it affects the architect and all other consultants in finishing their own projects as a coordinated effort. The possibility for the structural designer to later change or modify the results presented is limited and is the main reason why the structural engineer's experience plays such an important role in this stage of the structural design process.

The professionals involved in the design effort expect the following minimum information from the structural designer at this stage:

For the architect — Definition of the floor system including structural material, depth and width of the main structural elements. Description of the lateral force-resisting structural system including location and cross-section dimensions for all columns and structural walls. Limitations on the use of the nonstructural elements proposed by the architect, the means of anchoring them to the structural framing and any affectation to aesthetics for structural reasons. Parameters defined by the structural designer that would be used by the architectural engineer in establishing seismic design forces for architectural components. The expected story drift and its distribution in the height of the building to be used by the architectural engineer in the design of architectural components.

For the geotechnical consultant — Estimation of the building weight and order of magnitude of the expected reactions at the soil–structure interface including the effect of overturning moment caused by lateral forces. Any limitation on allowable maximum total and differential settlement imposed by the building use and structural system proposed. If a site-specific seismic procedure is to be used, the geotechnical consultant may require additional information including estimate of the fundamental period in both principal directions. If the project includes basements, the means for transmitting soil lateral pressures to the structure and the envisioned retaining-structure construction procedure. Any other information that would affect the scope of the geotechnical exploration and the expected recommendations from the geotechnical consultant.

For the mechanical designer — Limitations on the use of the mechanical elements proposed by the designer, the means of anchoring them to the structural framing, and any affection to them for structural reasons. Parameters defined by the structural designer that would be used by the mechanical designer in establishing seismic design forces for mechanical components. Expected story drift and its distribution in the height of the building to be used in the design of mechanical components. Restrictions to perforations in the structural elements, if allowed, including protection procedures for systems that could affect the structure such as steam and coolants. Structural restrictions on location and vibratory characteristics of mechanical equipment. Restrictions on location and volume of water tanks and other liquid containing vessels.

The previous listing indicates that even in the first stage of the design process the information requested from the structural designer needs the structural design to be almost complete. This again stresses the very important role that experience and engineering judgment play. For the structural designer to provide guidance in such diverse areas the structural design process must be approached in a methodical and orderly fashion.

14.3.2 Background Information Required

The structural designer must collect information about the project and draw a list of general structural requirements and related information. A recent ACI publication (ACI IPS-1, 2002) suggests the following general structural requirements as a minimum:

1. Intended use of the building
2. Nominal loads related to the use of the building
3. Special loads defined by the owner
4. Design seismic ground motion
5. Wind forces appropriate for the site
6. Forces from snow, hail or rain
7. Fire rating requirements
8. Type of roof and associated loads when not built of reinforced concrete
9. Site information related to slopes and site drainage
10. Allowable soil-bearing capacity and recommended foundation system derived from the geotechnical investigation and additional restrictions related to expected settlement
11. Environmental requirements derived from local seasonal and daily temperature variations, humidity, presence of deleterious chemicals and salts
12. Availability, type and quality of materials such as reinforcing bars, cement and aggregates
13. Availability of formwork materials and procedures
14. Availability of a testing lab for concrete mixture proportioning and quality control during construction
15. Availability of qualified workmanship.

This information will guide numerous decisions to be made during the design process. Many items in this information are defined and prescribed by the local governing code requirements. Table 14.14 gives a list of the loads that must be taken into account.

14.3.3 Structural Layout

Document (ACI IPS-1, 2002) lists a minimum content for both the architectural and structural layout. The recommendations from this document are divided into general structural layout in plan floor layout and vertical layout, and are presented here with some modifications specially needed for lateral force design.

14.3.3.1 General Structural Plan Layout

The structural designer should define a general structural layout in plan, including all information that is common to all levels of the structure. The general structural layout in plan includes:

1. A dimensioned axis grid, or centerlines, in both principal directions in plan, located at the intersection of the vertical supporting members (columns and reinforced concrete walls)
2. These axes must intersect at the location of the vertical supporting members (columns and reinforced concrete walls)
3. Location in plan of all vertical supporting members, columns and reinforced concrete walls. These vertical-supporting members must be aligned vertically and be continuous all the way to the foundation. Use of walls that separate spaces built of reinforced concrete as structural walls is feasible if they are continuous all the way to the foundation and have no large openings for windows or doors
4. Location of all duct, shafts, elevators and stairways that are continuous from floor to floor
5. Horizontal distance between centerlines, which correspond to the center-to-center span lengths of the floor system
6. The location and distribution of all reinforced concrete walls.

14.3.3.2 Floor Layout

For each typical floor, the structural designer must develop a structural floor layout. This layout should contain:

1. The superposition of the floor perimeter on the general axis grid
2. Girder and beam locations or column and middle strips for slab–column systems
3. Location of vertical supporting elements (columns and reinforced concrete walls)
4. All substantial architectural openings in the floor
5. An approximate load path for gravity loads from all floor areas to the supporting beams and girders, and from these horizontal elements to the vertical supporting members
6. An approximate load path for lateral loads from their point of application in the floor to the lateral load-resisting vertical elements
7. Identification of any plan structural irregularities (see Table 14.11)

14.3.3.3 Vertical Layout

The structural designer should define a general structural layout in elevation. The general structural layout in elevation includes:

1. Number of stories
2. The story height for each floor, defined as the vertical distance from floor finish to floor finish
3. Slope and shape of the roof
4. Architectural clearance from floor finish to ceiling for each floor
5. Space necessary to accommodate power distribution, water supply and drainage, and heating, ventilation and air conditioning
6. Selection of a lateral force-resisting system that can accommodate the architectural layout from the alternatives allowed (see Table 14.6)
7. An approximate lateral-load path from their point of application to the lateral load-resisting vertical elements in all levels to the foundation

8. Identification of any vertical structural irregularities (see Table 14.12)
9. Slope of the terrain and its relationship to the ground floor or basement
10. Supporting soil stratum depth and water-table depth.

14.3.3.4 General Integrity

Any structure must be designed to be able to sustain local damage with the structural system as a whole remaining stable. To achieve general integrity of the structural system, sufficient continuity, redundancy and toughness must be provided. SEI/ASCE 7-02 has several requirements whose intention is to provide integrity and redundancy to structures subjected to earthquake ground motion. Nonredundant systems are penalized by requiring larger load factors through the use of the ρ coefficient. The identification of load paths and the required strength along it is a first step in achieving integrity. On the other hand ACI 318-02 devotes *Section 7.13 — Requirements for structural integrity* to the same issue from a gravity loading perspective. The observance of both sets of requirements should lead to a redundant and sturdy structure.

14.3.4 Predimensioning for Gravity Loads

Structures must be designed to resist all applicable loads and environmental effects. In the role of defining initial dimensions for the structural elements only experience and judgment can indicate the structural designer which is the controlling effect. In the absence of a clear understanding of how to approach the problem the general solution is to initiate the process of proposing dimensions and checking their adequacy by using as initial trial dimensions those controlled by a single loading and proceed by adjusting them later for all the other effects one at a time. This may be time consuming, but has the advantage of being a fail-safe procedure and is the only way to acquire experience in an orderly and methodical way. The following procedure has been used successfully by many designers for establishing a first cut of the required dimensions just from the gravity loading point of view.

Because selfweight for the structure is a direct function of the structural member dimensions, a starting point must be used that would allow for computing it and all the loads and forces that derive from it, especially dead loads and seismic design forces. Many designers around the world initiate the process with an arbitrarily chosen value for the unfactored dead load of the building. Values of 8 to 10 kN/m² (160 to 200 psf) have been popular figures for many years for total unfactored dead load to be used for starting the process in apartment and office buildings.

The main contributor to total dead load is the floor system; therefore, the designer usually spends a great part of the predimensioning effort in optimizing its dimensions. Resulting dimensions may be used for obtaining a better estimate of the unfactored dead load. The depth of the floor system elements is generally controlled by serviceability criteria and the minimum depth requirements of *Section 9.5 — Control of deflections* of ACI 318-02 serve this purpose. For the width of the floor system elements one half of the depth is usually appropriate.

Once a total unfactored dead load per unit area is established, an estimate of the unfactored axial dead load on vertical elements — columns and reinforced concrete walls — can be computed at each floor using the tributary area from all supported floors. For applications where gravity load is the only controlling load effect, the recommendations of documents such as CRSI Handbook (CRSI, 2001) or (ACI IPS-1, 2002) may be used to define the first trial cross-section dimensions. For structures that will be subjected to seismic effects, larger cross-section dimensions are usually employed to provide sufficient stiffness to meet the story drift requirements and the strong-column weak-beam that will be explained later. The approach in this case is to define the cross-sectional area based on a low compression stress on the column and wall concrete from unfactored dead load. Values of the order of $0.15f'_c$ have been used for many years for this purpose.

The resulting first trial structure dimension obtained following the presented procedure will be on the large side of the optimal dimensions, if that concept exists and is true. An experienced structural designer will surely obtain better results for this first trial dimensions without much effort.

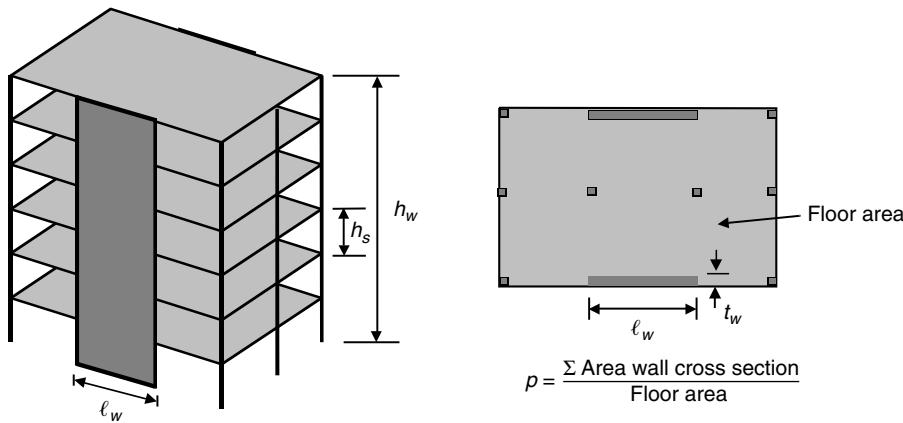


FIGURE 14.21 Definition of the wall index, p , in the direction of the walls.

14.3.5 Predimensioning for Stiffness

It is interesting to notice that the evolution of structural systems started with an intensive use of walls built in masonry and stone, then gravitated to frame systems and is converging at present toward an intensive use of reinforced concrete walls as shear walls. The reason at the beginning was the then available structural materials; the reason now is the repeatedly observed good behavior of structures having shear walls in past and recent earthquakes. There are numerous reasons from the architectural point of view for using frame structures (moment resisting and nonmoment resisting); notwithstanding, when the quest is to provide lateral stiffness; the frame is no match to structural walls.

The predimensioning of frame elements for meeting a set story drift limit requires a mathematical model analysis even in the simplest cases. Chapter 13 has presented some simplified procedures for carrying out an analysis that permits the evaluation of lateral deflections and story drift that are appropriate in a predimensioning exercise.

For structures having walls, the studies carried out after the 1985 Chile earthquake (Sozen, 1989) gave an insight into the relationship among the number of walls, their slenderness and story drift associated with a set intensity of the earthquake design ground motion. The number of walls is defined using a wall index, p , defined as the ratio of the area of all walls acting in the direction of interest to the floor area. See Figure 14.21. This relationship is perfectly suited to be used as a predimensioning procedure for structures with walls.

The expected story drift expressed as a fraction of the story height, Δ/h_s , may be obtained from Equation 14.33. This equation from (Sozen, 1989) has been converted to the nomenclature of SEI/ASCE 7-02

$$\frac{\Delta}{h_s} = 0.2 S_{D1} \left(\frac{h_w}{l_w} \right) \sqrt{\frac{w_d g}{E_c p h_s}} \quad (14.33)$$

where

Δ is the story drift

h_s is the story height

S_{D1} is the spectral design acceleration at 1 sec obtained from Equation 14.4 as explained in 14.2.2.1

h_w is the wall height

l_w is the wall length

w_d is the building weight per unit area

g is the acceleration of gravity

E_c is the wall concrete Young's modulus

p is the wall index (ratio of wall area in the direction of interest to floor area)

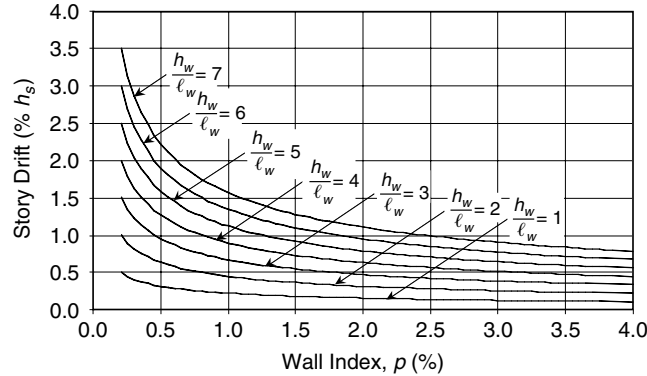


FIGURE 14.22 Relationship between wall index p and story drift index for a spectral acceleration S_{D1} of 100% of g.

This procedure does not take into account the contribution to stiffness of any moment-resisting frame acting along the shear walls; therefore the drift estimation is conservative for dual systems. Figure 14.22 shows the relationship between wall index, p , in percentage and story drift index (Δh_s) also in percentage for different wall slenderness ratios (h_w/ℓ_w) obtained from Equation 14.33 for a spectral acceleration S_{D1} of 100% of g, a weight per unit area of 10 kN/m² (200 psf) and concrete Young's module of 25 GPa (3500 ksi). Similar graphs can be constructed for other values of the parameters of Equation 14.33.

This type of graph may be used for predimensioning by using the story drift index from the seismic regulations, a wall slenderness ratio picked from the building height and a wall length acceptable for the architectural layout. The wall index, p , read from the graph is then used to find appropriate wall cross-section dimensions. A rule of thumb for regions of high seismicity is that walls with a slenderness ratio (h_w/ℓ_w) of the order of 4 and a wall index p of 1% would lead to structures that will meet a 1% story drift index.

14.3.6 Predimensioning for Strength

A strength check must be performed using the cross-section dimensions obtained from the two previous sections. To perform this check the seismic design base shear, V , must be obtained for the structure using the estimated dead load and the design earthquake ground motion at the site. The equivalent lateral force procedure presented in Section 14.2.6 is suitable for this purpose. The design base shear, V , can be obtained from Equation 14.7. The distribution of the seismic base shear in the height of the structure can be obtained using Equation 14.15. Story shear, V_x , and story overturning moment, M_x , can be obtained from Equations 14.17 and 14.18, respectively. Using these forces and moments, two checks must be performed on the vertical lateral force-resisting elements: one for shear strength and the other for flexural strength.

14.3.6.1 Moment-Resisting Frames

A good estimate of the shear carried by each column in the direction of interest at any story can be obtained from:

$$V_{col-ext} = \frac{V_x}{2n_{cin} + n_{cex}} \quad (14.34)$$

and

$$V_{col-int} = 2V_{col-ext} \quad (14.35)$$

where

$V_{col-ext}$ is the fraction of V_x assigned to an exterior column

$V_{col-int}$ is the fraction of V_x assigned to an interior column

V_x is the story shear in the direction of interest

n_{cin} is the number of interior columns in the direction of interest (columns where two girders parallel to direction of interest frame at each joint)

n_{cex} is the number of exterior columns in the direction of interest (columns where only one girder parallel to direction of interest frame at each joint)

A conservative shear strength for a column for predimensioning purposes would be

$$\phi V_n = \frac{\sqrt{f'_c}}{12} A_c \quad (14.36)$$

where ϕV_n is the design shear strength in N, $\sqrt{f'_c}$ is the square root of specified compressive strength of concrete in MPa and A_c is the trial column area in mm². ϕV_n must be compared with the corresponding shear obtained from Equations 14.34 and 14.35, and column trial areas must be adjusted accordingly.

The moment induced by the seismic forces corresponds to the product of the column shear multiplied by one half of the story height h_s . Using the moment obtained this way and factoring the estimated tributary axial load, the appropriateness of the trial column dimensions can be verified. Girder moments are of the order of magnitude of the sum of the exterior column moments of the floors above and below the girder. This moment can be added to the girder gravity negative factored moment at the support to find if the girder trial dimensions are appropriate.

As an example of this procedure we can use the structure shown in Figure 14.13. Suppose we have already obtained the design base shear V . In the x direction there are three three-bay frames. This means that there are two exterior and two interior columns per frame. Applying Equation 14.34 we find that the shear in the exterior columns in the x direction at the base would be $V/(2 \cdot 2 \cdot 3 + 2 \cdot 3) = V/24$ and for the interior columns according to Equation 14.35 twice this value, $V/12$. For the y direction there are four two-bay frames. This means that there are two exterior and one interior column per frame. Applying Equation 14.34 we find that for the y direction the shear in the exterior columns at the base would be $V/(2 \cdot 2 \cdot 4 + 1 \cdot 4) = V/20$ and for the interior columns according to Equation 14.35 twice this value, $V/10$. The moment caused by the seismic forces for any of these columns at the joint with the second story girder would be the corresponding shear in the column multiplied by half the first story height. The girder moment caused by the seismic forces would be of the order of magnitude of the interior column moment.

14.3.6.2 Shear Walls

For buildings with shear walls, for predimensioning purposes, the contribution of any moment-resisting frame can be disregarded. The story shear and overturning moment at any story in the direction of the walls can be distributed to the different walls in proportion to their cross-section moment of inertia.

The appropriateness of the wall cross section for shear can be verified using Equation 14.36 introducing the wall area in A_c . For flexural strength the fraction of the overturning moment can be used to obtain an estimate of the required reinforcement at the wall edge disregarding the wall axial load (obtaining it assuming the wall to be a beam). The obtained vertical reinforcement ratio must be within reasonable wall ratios (from 0.0025 to 0.01), otherwise the wall's sections must be adjusted.

14.3.7 Predimensioning for Toughness

Toughness of the structure is obtained through appropriate detailing that follows the requirements of Chapter 21 of ACI 318-02. For predimensioning purposes some recommendations can be made that

would make the compliance of the detailing requirements easier. These recommendations can be summarized in providing generous cross-section dimensions to avoid reinforcing steel congestion, helping in an appropriate reinforcement placement and casting of the concrete. The following guidelines may help in adjusting the trial dimensions for obtaining good reinforcement details later:

1. Girder width must be substantially less than the transverse column dimension at the joints where they frame. This permits the girder longitudinal reinforcement to pass within the column core without interfering with the column vertical reinforcement.
2. Girder depth must be substantially less than the column cross-section dimension parallel to the direction of the girder. This will help in having a girder flexural strength at the joint lower than the column flexural strength at the same joint; thus making it easier to comply with the weak-beam strong-column requirement.
3. Walls should be provided with beams running parallel to the wall at all floor diaphragms. These beams can either be embedded in the floor system if they are wider than the wall thickness or in the wall if they have width equal to the wall thickness. These beams should be provided with closed transverse reinforcement enclosing the longitudinal reinforcement. If planned from the beginning of the predimensioning stage they will help in designing later all the required collector elements.
4. In all places where girders and beams frame transversely to walls it is good practice to enclose the wall vertical reinforcement with transverse reinforcement, as if an embedded tied column existed at the beam support in the wall. This will help in transferring any beam moment to the wall and helps in avoiding a local failure in the wall.
5. If possible, all edge vertical reinforcement in walls should be enclosed by transverse reinforcement, even if boundary elements are not required. This will provide a much better behavior of the wall edge by providing a defense against concrete spalling at the edge and good anchorage to the horizontal wall reinforcement.

14.4 Analysis

In 1935, Hardy Cross wrote: "The rather awkward methods of analysis current at the beginning of this century undoubtedly delayed the development of continuous structural types. At that time the analysis of some of the more complicated types now proposed was impracticable. The profession has made progress in this field. It may be well now to divert the attention of structural designers from the endless elaboration of analytical technique to the more important matter of interpretation of analyses" (Cross, 1935). These concepts are still valid almost 70 years afterwards, and are especially relevant for earthquake-resistant design.

The ultimate role of analysis is to forecast the behavior of an as yet unbuilt structure, in such a way that it will be able to comply with preestablished performance criteria during its life span. These performance criteria include strength, stiffness to account for unwanted deflections, durability, serviceability and others. Even though it sounds simple, the complexity involved in achieving the objectives contained in the performance criteria could be large even for a simple structure. To make this endeavor feasible, numerous simplifications must be made; both in the definition of what is required of the structure, generally expressed in terms of loads and deflections, and in the description of the behavior of the structure through analysis. This is especially true in the design of reinforced concrete structures for earthquake resistance.

As strength methods for design of reinforced concrete were introduced during the mid-1950s, numerous engineers pointed out that elastic analysis methods were employed to determine stresses that were then used to evaluate strength through inelastic methods. This inconsistency still continues. The great majority of structural designs performed today are still based on elastic analysis and inelastic dimensioning techniques. The solution then devised, and still employed, was the use of cracked sections in the analysis. Unfortunately, in a large number of cases this solution falls short when needed to describe the actual expected behavior of the structure, as is explained later.

When a diversity of loadings on the structure comes into play, it is evident that the description of the behavior under the effect of any of them must be based on different modeling parameters. The main conclusion is that: no single set of modeling parameters in a structural analysis can describe the behavior of the structure under the diversity of effects that should be taken into account in a modern design.

The primary drawback of current automatic analysis-design procedures is that the engineer is generally satisfied with using a single analysis to take all effects into account. This means that the description, through analysis, of the behavior of the structure will be appropriate for some effects and deficient for others. Usually, the different effects are mixed using load combination schemes in the final stages of the analysis to produce forces and stresses that define reinforcement of the structure. Then, structural drawings are made based on these results. If actual structural behavior evaluation is the goal, then the results of the single modeling parameters analysis are just the starting point, and not the final result.

The rest of this section is devoted to issues associated with the analysis of reinforced concrete structures to earthquake ground motion for design under a code-regulated environment.

14.4.1 Cracked Sections

For many years the earthquake-resistant design requirements contained in the model codes did not prescribe special rules for the analysis of reinforced concrete structures. The only requirement was that modeling decisions had to be consistent throughout the analysis and design stages. With the availability of sophisticated computer programs for analysis more requirements were introduced that reflected the capability of analyzing complex structures. This, in turn, brought analysis requirements directly related to reinforced concrete structures. The most important one was the requirement that the analysis of reinforced concrete and masonry structures must take into account the effects of cracked sections. The implications of this recent requirement are far reaching and leave open the door to numerous interpretations.

Even for gravity load effects the possibility of having an uncracked structure is not feasible. By just stripping the forms used to cast the reinforced concrete structure enough cracking is introduced to the elements, especially those part of the floor system. Therefore, a careful evaluation of the cracking state to be used in the earthquake-resistant design situation is warranted. The main associated problem is the determination of the degree and spread of the cracking. This is a challenging problem even for simple structures in a nonseismic environment. The gravity load effects will probably introduce a great part of the cracking, but temperature variation, rheological effects on the concrete, differential settlement and other phenomena also come into play. When the structure is subjected to the earthquake ground motion, a significant amount of cracking will already be present in most reinforced concrete structures. The earthquake motion will introduce additional cracking in some elements and new cracking in others, especially in the vertical elements of the lateral force-resisting elements (columns and walls).

Beyond requiring the use of cracked sections, SEI/ASCE 7-02 does not give any guidance with respect to how to approach the definition of the stiffness to use in analysis. The implication of using different interpretations is important because the estimation of the fundamental building period directly depends on the stiffness assumed which in turn is dependent on the amount of cracking. The actual response during strong and long duration earthquake ground motion is governed by a period longer than the one estimated by using cracked sections, and much longer than a period obtained using uncracked sections. The nonlinear response increases damping, as explained before, to values much larger than the 5% of critical arbitrarily set by the earthquake-resistant design requirements. The fundamental period computed following the requirements (see Section 14.2.6), in principle, refers to the linear elastic response of the structure with cracked sections without taking into account the nonlinear response. This merits an explanation.

From the introductory remarks on nonlinear response of reinforced concrete elements to earthquake-induced ground motion of 14.1.2 it is evident that for a member of the lateral force-resisting system responding in the nonlinear range, as shown in Figure 14.23, the effective stiffness is associated with the displacement demand imposed by the earthquake ground motion, and the uncracked and cracked

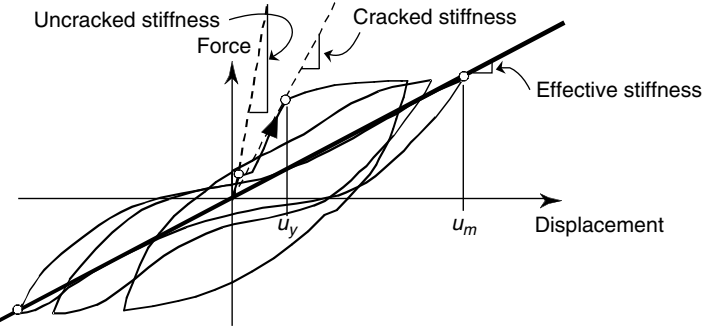


FIGURE 14.23 Stiffness during nonlinear response for a reinforced concrete element.

stiffnesses are lost as descriptive parameters in just the first displacement reversal. The stiffness that will be describing the response will be the effective or secant stiffness that is associated with the actual displacement demand on the structure imposed by the earthquake ground motion.

Referring to Figure 14.23, the initial stiffness of the response, EI_g , corresponds to the uncracked stiffness. The stiffness reduces after cracking, with secant-cracked stiffness, EI_{cr} , being the slope of the line that joins the origin and the yield point. The secant effective-stiffness, EI_{eff} , corresponds to the slope of the line that joins the points of maximum displacement demand. The displacement ductility demand can be defined as $\mu = u_m/u_y$, and the effective stiffness, EI_{eff} , during the inelastic response can be obtained as inversely proportional to the displacement ductility demand μ as:

$$EI_{eff} = \frac{EI_{cr}}{\mu} \quad (14.37)$$

Based on earthquake simulator tests of reinforced concrete SDOF systems, Gulkan and Sozen (1974), found that it is possible to describe the inelastic response of the system using an elastic SDOF system having a reduced stiffness as indicated by Equation 14.37 and increased damping as obtained from:

$$\xi_s = 0.2 \left\{ 1 - \frac{1}{\sqrt{\mu}} \right\} + 0.02 \quad (14.38)$$

For MDOF systems these principles can be implemented as suggested by Shibata and Sozen (1976). From the design point of view the use of these principles leads to fundamental periods of the order of 40% longer than those obtained using cracked sections and effective damping ratios of the order of 10% of critical.

Therefore, from the stiffness point of view there is a divorce between the earthquake-resistant design requirements and the behavior of the structure as understood from experimental research interpretation. It does not mean that the design requirements are not proper. It simply means that they are just a design procedure whose results have been proved to be safe in most situations using the tools available at present, but they are far from being a descriptor of the actual behavior. This stresses the need to comply in design with all requirements and specially the limits included as part of them, otherwise the design procedure would lead to nonappropriate results. Three requirements included in SEI/ASCE 7-02 are relevant with respect to decisions made by the designer in analysis regarding the amount of cracking to be used:

1. The requirements set an upper limit on the fundamental period, T , to be used to obtain the base shear, V . The limit (see Table 14.9) is a function of the approximate period, T_a , and actually sets a boundary to the amount of cracking to be used. If the effective stiffness EI_{eff} is used, this limit

will always control the value of the fundamental period, T , and the value used to obtain the base shear, V , will always be shorter than the period corresponding to the nonlinear response.

2. The base shear, V , obtained by the equivalent lateral force procedure is set as the value of reference to screen the base shear obtained from other analysis procedures. In dynamic spectral analysis the base shear value obtained cannot be less than 85% of that obtained using the equivalent lateral force procedure, and for the linear response history analysis the value is set at 100%. Again, the amount of cracking to be used is limited, because a dynamic analysis made using excessive cracking, in all situations will require increasing the base shear value used in design to that associated with the fundamental period with limited cracking.
3. The seismic coefficient has a minimum that comes into play for long fundamental periods (see Figure 14.10). This minimum introduces an increase in the base shear strength which in turn leads to a reduction of cracking when compared to the amount of cracking that would be observed in buildings designed without taking into account the minimum.

The question would then be if it merits spending time in defining cracking levels for each element? The answer would be certainly yes. The design process for earthquake resistance, as implemented in current requirements, is a tool for proposing dimensions for elements and their reinforcement to obtain a structure with appropriate stiffness, strength and toughness. The amount of reinforcement affects the level of cracking and will define the sequence and relative importance of the element in the nonlinear response of the structure. The level of cracking used must reflect the stiffness present when the element reaches yielding of the longitudinal reinforcement at the initiation of the nonlinear response of the element under the design earthquake ground motion. The internal distribution of forces in the structure — forces that will be used to define the reinforcement — at the onset of the nonlinear response is related to the cracked stiffness of the elements at moment strength. The important issue is that the cracking caused by the lateral inertial forces is the relevant one. Cracking in existence caused by gravity effects affects the initiation of cracking caused by lateral inertial forces or increases it. This is the key to defining an appropriate level of cracking for seismic effects. This is why recommendations such as those presented in Section 10.11.1 of ACI 318-02 for evaluation of slenderness effects have limited use because they are set for different circumstances.

As with many of the current requirements contained in codes and design regulations, the way to proceed is left to the experience and engineering judgment of the designer. Many designers have used the following approach to define the level of cracking to be used in analysis for earthquake-resistant design. It is based on establishing first a set of premises that bound the validity of the procedure and then define a level of cracking consistent with the premises.

The first premise is associated with an interpretation of the intent of the code, or design regulation procedure, and defines the level of cracking and derived stiffness to be used in establishing the seismic lateral forces that should, in turn, be used to obtain the longitudinal reinforcement of the structure at the onset of the nonlinear response to the design earthquake ground motion. Acting on this premise the level of cracking for each element of the structure would be that at moment strength, EI_{cr} , when subjected to the design inertial lateral forces. This is different from the cracked stiffness associated with gravity effects. For example, in a girder part of a moment-resisting frame subjected to lateral load the stiffness for lateral load would be controlled by the moment strength at the face of columns, while for gravity effects, the moment strength at midspan would be as relevant as that at the faces of columns.

The second premise is that during the nonlinear response of the structure not all elements reach moment strength and dissipate energy in the nonlinear range of response. The established design procedure inhibits, or minimizes, nonlinear response in certain elements. The weak-beam strong-column is one of them, requiring greater moment strength for columns than girders at a given joint. Other aspects of design lead to larger moment strength in some elements just by assigning lower ϕ -factors in addition to other design and detailing requirements. This means that some elements will have a lesser degree of cracking just because of these reasons. In girders and beams, and columns with axial loads well below the balanced point, the stiffness after first cracking does not change much up to the longitudinal tension reinforcement yield point. In these elements the use of stiffness based on a reasonable location of the

neutral axis for a fully cracked section will give appropriate results. In heavily loaded columns and wall coupling beams this is not true. In walls the aspect ratio, the preponderant mode of response (shear or flexural), the type and stiffness of the foundation and other related issues will also affect the degree of cracking. Here judgment comes into play. For flexural responding element the construction of moment–curvature relationships would give reasonable results to be used in defining cracking levels. For elements responding in shear, or cracked in shear, more detailed analyses are warranted.

An iterative procedure is required to select appropriate reinforcement, to define response modes, which in turn help identify cracking levels. A by-product of this procedure is the need to perform different analyses for gravity loads and for seismic loads. As mentioned earlier, no set of unique modeling parameters may be reasonably used in a single analysis for all required load effects.

14.4.2 Diaphragm Effect Analysis

One of the modern advances in structural engineering that has had more impact on the design practice is the approach of treating the structure as a whole. A few years ago, both in education and in practice, the emphasis was on studying the elements individually, or in limited groups, subsequently making crude approximations of the response of the full assembly of these elements. This practice is still reflected in many code requirements. Chapter 8 of ACI 318-02 is a good example. In earthquake-resistant design the coupling of the lateral displacements of parallel frames at each story and the possibility of having torsional effects of the whole structure have been a regulated concern for many decades. The 1959 Structural Engineers Association of California — SEAOC, Recommended Lateral Force Requirements included as an Appendix of Blume, Newmark and Corning pioneer 1961 book on design of multistory reinforced concrete buildings for earthquake motions (Blume et. al., 1961), still available in print from the Portland Cement Association, includes as a requirement the need to distribute the story shear, and the associated shear from torsional moments, to the lateral force-resisting elements in proportion to their stiffness through a diaphragm action.

Gradually, mainly due to the use of computer programs such as TABS (Wilson and Dovey, 1972) during the early 1970s, the possibility of making an analysis of the structure as a whole was feasible even with limited memory computers. Nowadays the rule is to analyze the structure as a whole, and from the results obtained proceed to the study of the elements. Some of the advantages of this modern approach for earthquake-resistant design of buildings are: possibility of evaluating in-plane rigid or flexible floor diaphragms, simplification of the analysis for torsion of the structure as a whole, feasibility of taking into account general structural integrity problems, simplification of P-Δ analysis, and capability of studying the response of the structure in general. Recent developments in analysis incorporate the possibility of using finite elements to model for lateral load analysis the main elements that compose the floor diaphragm. The graphical output of many of these applications, when properly used, makes tasks formerly requiring many hours to perform easy.

The responsibility of the designer in supplying appropriate parameters in diaphragm modeling using current available computational tools cannot be taken lightly. The description of a diaphragm as being flexible or rigid is subjective and it is not defined by a single parameter. The relative importance of the geometry of the diaphragm including shape and openings; the floor system being composed of just a slab, a slab on girders, a joist system or a system using precast elements; the strength of connections between diaphragm elements and to the vertical members of the lateral force-resisting system; the relative stiffness of the diaphragm and the vertical structural elements (a diaphragm may be considered rigid if supported on columns, but the same diaphragms would be flexible if shear walls are present); and other considerations come into play. In general, most floor systems currently used in reinforced concrete structures would lead to rigid in-plane diaphragms but this could be misleading if any of the limiting factors mentioned affects behavior.

Some of the analysis procedures are based on an infinitely rigid description of the diaphragm (see Section 14.2.9). This is an analysis subterfuge that reduces the number of lateral degrees of freedom of the structure to just three degrees of freedom per diaphragm. For reinforced concrete structures with

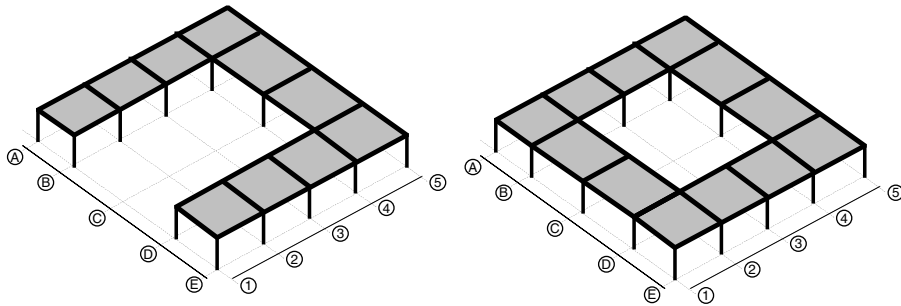


FIGURE 14.24 Examples of diaphragms not appropriate to be modeled as rigid diaphragms.

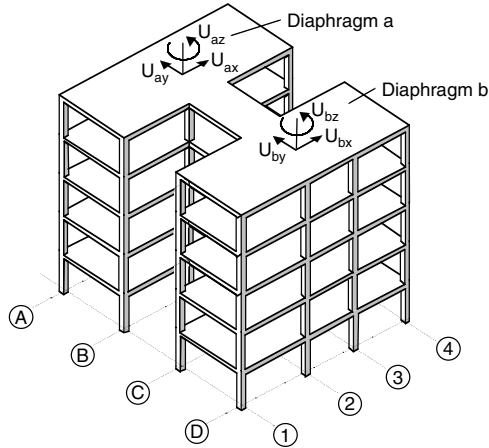


FIGURE 14.25 Independent rigid diaphragms linked by flexible elements.

floor plans approximately square or rectangular up to ratio of long to short side less than 3 and with no large openings, the infinitely rigid approach may be a reasonable descriptor of actual behavior. Notwithstanding, the careless use of this approach can lead to erroneous results especially when the rigid diaphragm approach is used without proper care.

Figure 14.24 gives examples of diaphragm geometry that should not be modeled as rigid diaphragms. When the building has diaphragms that are not connected to all the vertical elements of the lateral force-resisting system, as is the case with mezzanines, the coupling of the lateral displacement degrees of freedom of columns and walls that are not in contact with the diaphragm to the horizontal translation degrees of freedom of the diaphragm is a possible source of error because the free columns would take some of the diaphragm lateral load. A similar case can develop in split level buildings if the columns of one side of the building are coupled to the diaphragm of the other side of the building, i.e., a distortion of the actual shear taken by the columns occurs.

Figure 14.25 shows a common case in apartment buildings in which two independent rigid diaphragms may be used if the floor elements linking the independent diaphragms are appropriately modeled for flexural and axial deformations.

One of the main drawbacks of the infinitely rigid diaphragm analysis scheme is that the designer loses sight of the flow of forces and load paths within the diaphragm. Other effects such as diaphragm in-plane flexure and shear are not evident from the analysis results obscuring the need of collector elements and special reinforcement of the diaphragm elements. The only solution is to study the magnitude and approximate flow direction of the diaphragm internal forces from the difference in shear of the vertical

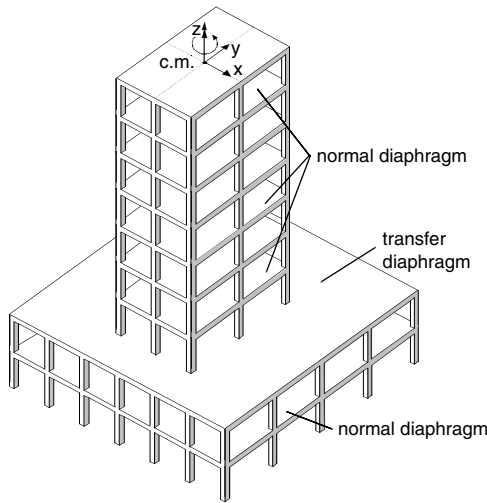


FIGURE 14.26 Example of transfer diaphragm.

elements of the lateral force-resisting system connected above and below to the diaphragm. This is especially important in transfer diaphragms (see Figure 14.26) located at abrupt changes of the geometry and stiffness of the building such as the upper diaphragm in a platform and tower layout or at the upper diaphragm of those connected to basement retaining walls.

In the transfer diaphragm a substantial part of the lateral load shear carried by the individual vertical elements is distributed through the diaphragm to the elements that do not continue upward. This flow of force must be studied with care to devise appropriate collector element reinforced to resist the forces involved. When the infinitely rigid scheme is used, the axial, flexural and shear forces associated with in-plane effects in the diaphragm elements are lost and are not reported in the regular output of the computer programs currently in use, because the modeling scheme is precisely based on inhibiting in-plane diaphragm deformations. This means that any collector element modeled as a beam would report — correctly from the point of view of the mathematical model, and incorrectly from the point of view of the model being a descriptor of actual behavior — zero axial force if its two ends are connected to joints that are in turn connected to or are part of the rigidly modeled diaphragm. The only solution in this case is to obtain the forces flowing through the element from the difference in horizontal shear of the vertical elements connected to the diaphragm.

The alternative to the infinitely rigid diaphragm analysis scheme is to model the in-plane characteristics of the elements that compose the diaphragm using finite elements. This procedure has the advantage that internal forces of the elements are routinely obtained from the analysis results. Notwithstanding, other type of responsibilities are demanded from the designer in selecting appropriate elements from the many available in current analysis computer programs and in defining the descriptive stiffness properties. The designer must be familiar with the characteristic of the particular elements used and the procedure used to interpolate results, both in deformation and stress, between interconnection nodes. As in any finite element analysis the results depend to a great extent on the density of the element grid employed. If a coarse grid is used, the possibility of detecting peak responses is not as good as in a finer grid. The issue of handling tension stresses in cracked sections for defining reinforcement area and spacing common to all finite element applications to reinforced concrete structure analysis for design purposes must be kept in mind by the designer.

14.4.3 Shear Wall Analysis

In parallel with diaphragm analysis, modern analysis procedures have influenced and improved the modeling of shear wall structures specially in aspects related to the interaction of walls and frames, the

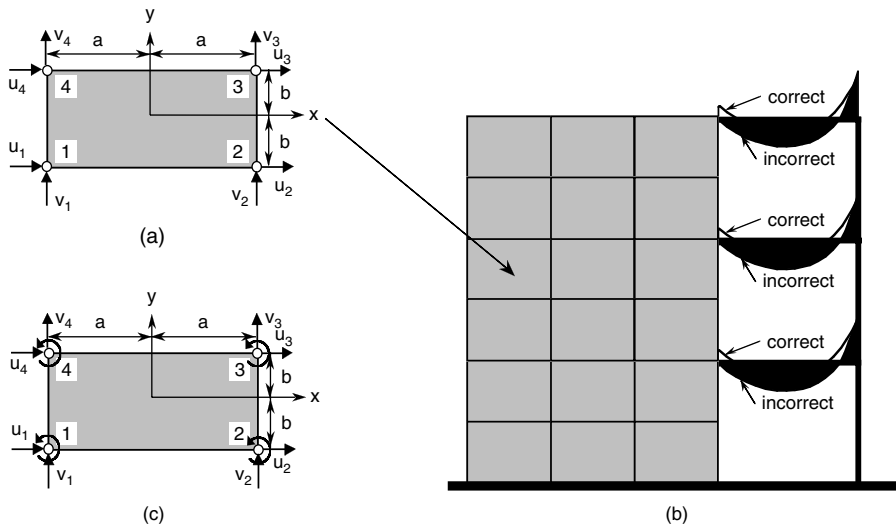


FIGURE 14.27 Use of finite elements in shear wall analysis.

possibility of treating walls with I, L, T and box cross-section shapes as encountered in elevator and stairway cores in high-rise buildings, and the possibility of studying walls coupled by deep beams and with door and window perforations. The use of finite elements has made the evaluation of shear lag in walls with flanges possible although engineering judgment is needed for interpreting the analysis results and translating them into reinforcement during the design process.

The usual procedure is to use finite elements able to describe the in-plane characteristics of the wall segments that jointly would reflect the flexural and shear effects in the whole wall section. Current computer programs use different approaches in defining the characteristics of the finite elements. The alternatives encountered go from very simple elements that can model only the in-plane stresses as in shell-type elements to thick-shell type elements that have in addition even in-plane and out-of-plane flexural characteristics. In all cases the analysis results have to be studied with care and test cases where results are known should be used to study the type of results obtained and their appropriateness. When boundary elements are required, designers sometimes introduce column elements at boundaries that act as part of the wall. These column elements are generally connected in the mathematical model to the shell elements only at the horizontal diaphragm level, meaning that deformations between the two elements are not compatible at intermediate sections. In the last case internal forces in the wall must be recomposed using equilibrium from forces that are presented in different parts of the analysis output.

Figure 14.27 shows a situation that was common, and may still be present, in some of the analysis programs. Figure 14.27(a) shows a rectangular finite element having eight translational degrees of freedom whereas Figure 14.27(b) shows an element having the same translational degrees of freedom plus four additional rotational degrees of freedom. If the former finite element is used to model the wall in Figure 14.27(c), the frame girder shown will behave as simply supported at the wall connection without any moment connectivity to the wall. If the latter element had been used the restraint imposed by the wall would have been modeled.

Present code-accepted wall design procedures require that results from the finite element analysis usually in terms of stress be converted to resultant forces before being used to define reinforcement. ACI 318-02 does not recognize the direct use of stresses in defining reinforcement, especially for flexural effects. This means that using equilibrium the stresses have to be converted into resultants in terms of moment, axial force, shear and torsion, then using principles such as plane sections remaining plane under flexure the proposed reinforcement can be verified. To proceed this way stresses in flanges have to be corrected for effective flange dimensions, so that they can be considered uniform for the same strain as defined from the plane section hypothesis. By performing the design this way the advantage of

a shear-lag evaluation procedure from the results of the finite element analysis is lost and the approximation of effective flange width substitutes the stresses obtained from the analysis in which the stress distribution takes into account the shear-lag effect. The treatment of tension stresses in cracked section, where only the reinforcement is providing for the required strength cannot be directly associated with the stresses evaluated in an anisotropic material as used in the derivation of the finite element. This inconsistency always exists in the application of finite element analysis to reinforced concrete cracked sections.

The other aspect to be taken into account when defining the analysis modeling for shear wall structures is the possibility of rocking the wall foundation. The degree of fixity provided by the foundation is relative even in cases favorable for minimizing rocking. The decrease in overall stiffness of the wall by just a minimum rocking is appreciable. This affects the distribution of story shear between wall and frame in dual systems, the computed fundamental period of vibration, and the story drift evaluated. Moment-resisting frames are less sensitive to column base fixity and in general changes in rocking stiffness of the column base affect only the internal forces and lateral deflection only of first story columns. It is interesting to note that in general better fixity at the base is obtained both for walls and frames in buildings sited in soft soil profiles than in hard or stiff soil. Soft soil shallow foundations are more massive than the corresponding hard soil foundations, and in soft soil conditions in which a deep foundation is used, the degree of fixity is better than that for a corresponding smaller stiff soil solution although being subjected to larger motion because of the amplification of the ground motion caused by the soft soil condition.

In all these cases mentioned the solution is studying alternative models, careful evaluation of the results obtained from each alternative model and design decisions based on engineering judgment and experience.

14.5 Detailing of Special Moment Frames and Special Shear Walls

The required toughness for the element part of the lateral force-resisting system is obtained by following the requirements contained in Chapters 1 to 18 and Chapter 21 of ACI 318-02 (ACI, 2002), with the exception of Section 21.12. The resulting systems are denominated special moment frames and special reinforced concrete shear walls and are appropriate for seismic design categories D, E and F.

The special restrictions on the materials (concrete and reinforcing steel) were presented in 14.2.10. Chapter 21 of ACI 318-02 also contains some general requirements dealing with the scope and correspondence of the requirements with respect to the seismic risk or the seismic design categories. With respect to analysis Chapter 21 indicates that interaction with structural and nonstructural elements that could affect the response of the structure to the earthquake ground motion must be taken into account and the consequences of failure of elements not considered part of the lateral force-resisting system should be considered.

It is important to note that all transverse reinforcement must be hoops. Two conditions are required for a hoop: (a) to be closed or continuously wound around the longitudinal reinforcement and (b) to have at both ends 135° hooks with $6d_b$ (but not less than 75 mm) extensions projecting into the interior of the hoop, where d_b is the bar diameter. These hooks are referred to in ACI 318-02 as seismic hooks. The reason for this requirement is that the likelihood of spalling and loss of shell concrete in some regions of the frame elements is high during the nonlinear response. If the transverse reinforcement loses its ability to confine the core of the member and to provide lateral support to the longitudinal reinforcement, the expected nonlinear energy dissipation will not occur. Both observed behavior under actual earthquakes and experimental research have repeatedly shown that unless the transverse reinforcement is bent around the longitudinal reinforcement and its ends projected into the core of the element, the transverse reinforcement will open at the ends and lose the ability to confine the core concrete.

Crossties are considered part of a hoop if they are made of a continuous bar having a seismic hook in one end and a hook not less than 90° with at least a $6d_b$ extension at the other end. The hooks of the crosstie must engage peripheral longitudinal bars. The 90° hooks of two successive crossties engaging the same longitudinal bars must be alternated end to end.

Only the requirements of ACI 318-02 are presented. The reader is directed to the following references containing detailed numerical examples of the applications of the requirements: (Fanella, 2000; Fanella and Munshi, 1998a; Fanella and Munshi, 1998b; Gupta and Moss, 1993; PCA, 2002).

14.5.1 Girder and Beam Design

Special moment-resisting frame elements primarily proportioned to resist flexure with factored axial load not exceeding $(0.10 f'_c A_g)$ must comply with the requirements of Section 21.3 of ACI 318-02, where A_g corresponds to the gross area of section. These requirements are:

14.5.1.1 Dimensional Requirements

The clear span of the member shall not be less than four times its height, h . The web width-to-height ratio, b_w/h , shall not be less than 0.3. The web width, b_w , shall not be less than 250 mm, nor exceed the corresponding width of the supporting column plus $3/4h$ on each side of the supporting column.

14.5.1.2 Longitudinal Reinforcement

The following requirements must be met:

1. At least two top and bottom longitudinal bars must be provided
2. At any section, the ratio, ρ , of positive and negative moment reinforcement shall be equal to or greater than $0.25\sqrt{f'_c/f_y} \geq 1.4/f_y$
3. At any section, the positive and negative moment reinforcement ratio, ρ , shall not exceed 0.025
4. The area of positive moment reinforcement at the joint face shall not be less than one half the area of negative moment reinforcement at the same joint face
5. The area of positive and negative moment reinforcement at any section shall not be less than one fourth of the maximum area of negative moment reinforcement at the face of either joint
6. Lap splices shall not be used in beam-column joints and for a distance $2h$ from the face of the joint. The full length of the lap splice, where permitted, shall have hoops with spacing not exceeding $d/4$ or 100 mm

14.5.1.3 Transverse Reinforcement

In addition to the requirements of Chapter 11 of ACI 318-02, the following special requirements must be met:

1. Confinement zones must be provided over a distance equal to twice the member depth, h , measured from the face of the supporting member toward midspan, at both ends of the girder. The transverse reinforcement at the confinement zones must be hoops (Figure 14.28)
2. In the confinement zones, hoops must comply with the requirements for column ties of Section 7.10.5 of ACI 318-02 to provide lateral support to the longitudinal reinforcement bars
3. The first hoop shall be located no farther than 50 mm from the face of the supporting member
4. The spacing of hoops shall not exceed $d/4, 8d_b$ of the smallest longitudinal bar, $24d_b$ of hoop nor 300 mm
5. For the central length of the girder span, between confinement zones, the transverse reinforcement shall be closed stirrups with seismic hooks and the maximum stirrup spacing shall not exceed $d/2$.

14.5.1.4 Shear Strength

In addition to the requirements of Chapter 11 of ACI 318-02, the following requirements shall also be met:

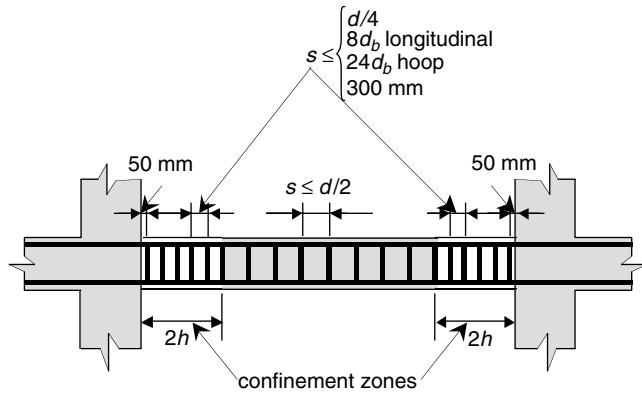
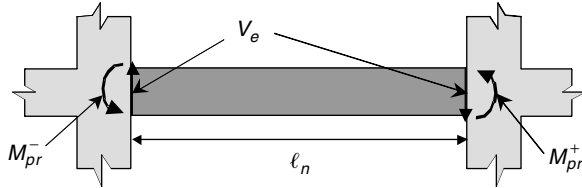


FIGURE 14.28 Hoop spacing in girders.


 FIGURE 14.29 Calculation of V_e .

1. The additional factored shear force, V_e , corresponding to the probable moment strength development of the span at the face of the joint shall be determined as the larger value from Equations 14.39 and 14.40 (Figure 14.29);

$$V_e = \frac{(M_{pr}^+)_{left} + (M_{pr}^-)_{right}}{\ell_n} \quad (14.39)$$

$$V_e = \frac{(M_{pr}^-)_{left} + (M_{pr}^+)_{right}}{\ell_n} \quad (14.40)$$

2. In Equations 14.39 and 14.40 M_{pr} corresponds to the positive and negative moment probable moment strength at the joint faces, determined using the corresponding longitudinal reinforcement area, f_{ypr} instead of f_y ($f_{ypr} = 1.25 f_y$), and a strength reduction factor $\phi = 1$.
3. The largest value of V_e determined from Equation 14.39 or Equation 14.40 shall be added to the factored tributary shear V_u at the face of the support.
4. The required transverse reinforcement for shear shall be determined as prescribed in Chapter 11 of ACI 318-02, except that in the confinement zones where V_e is greater than V_u for tributary gravity loads at the face of the support and the factored axial load including earthquake effects is less than $(0.05 f'_c A_g)$, when computing the shear reinforcement the contribution of concrete to the shear strength shall be taken as $V_c = 0$.
5. The hoops required for confinement may be considered effective as part of the required shear reinforcement.

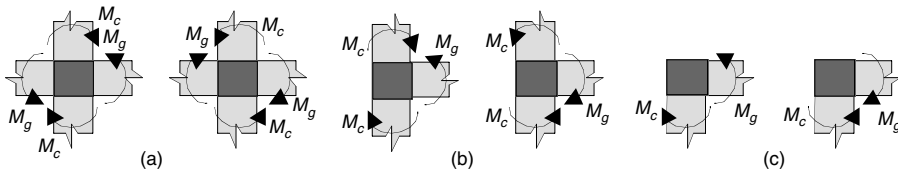


FIGURE 14.30 Minimum flexural strength of columns.

14.5.2 Column Design

Special moment-resisting frame elements having a factored axial load exceeding ($0.10 f'_c A_g$) must comply with the requirements of Section 21.4 of ACI 318-02, where A_g corresponds to the gross area of section. These requirements are:

14.5.2.1 Dimensional Requirements

The least cross-sectional dimension shall not be less than 300 mm and the ratio of the longer to the shorter cross-sectional dimension shall not exceed 2.5.

14.5.2.2 Longitudinal Reinforcement

The longitudinal reinforcement ratio ρ_g shall not be less than 0.01 or greater than 0.06. The location of lap splices is restricted to the center half of the member length and must have special transverse reinforcement.

14.5.2.3 Minimum Moment Strength of Columns

The moment strength of the column shall satisfy Equation 14.41, unless the full length of a column is provided with transverse reinforcement complying with that required for the confinement zones. This requirement leads to the strong-column weak-beam scheme where the flexural nonlinear response is minimized in columns and is emphasized in the girders of the frame

$$\sum M_c \geq \frac{6}{5} \sum M_g \quad (14.41)$$

where ΣM_c is the sum of the nominal moment strengths (M_n) of columns framing into a joint; and ΣM_g is the sum of the nominal moment strengths (M_n) of girders framing into the joint.

The moment strength of a column shall correspond to the minimum nominal moment strength computed for the factored axial load, P_u , consistent with the direction of the lateral forces considered that act on the column. Moment strengths shall be added in such a manner that the column moments oppose the beam moments. Equation 14.41 shall be satisfied for beam moments acting in both directions on the vertical plane of the frame considered (Figure 14.30).

14.5.2.4 Tie Transverse Reinforcement

When ties are used as column transverse reinforcement, the requirements of Section 7.10.5 of ACI 318-02 and the following additional requirements shall be met:

1. The transverse reinforcement shall be hoops (Figure 14.31) over the length of the confinement zone, ℓ_0 , measured from the face of the joint at both ends of the column. The distance ℓ_0 shall not be less than the largest column cross-sectional dimension, one sixth of the clear length of the column or 450 mm.
2. Transverse reinforcement shall be single or overlapping hoops complying with the requirements for column ties of Section 7.10.5 of ACI 318-02.
3. Crossties of the same bar diameter and spacing as the hoops are permitted. Each crosstie shall engage a peripheral longitudinal reinforcing bar. Consecutive crossties shall be alternated end to end along the longitudinal reinforcement.

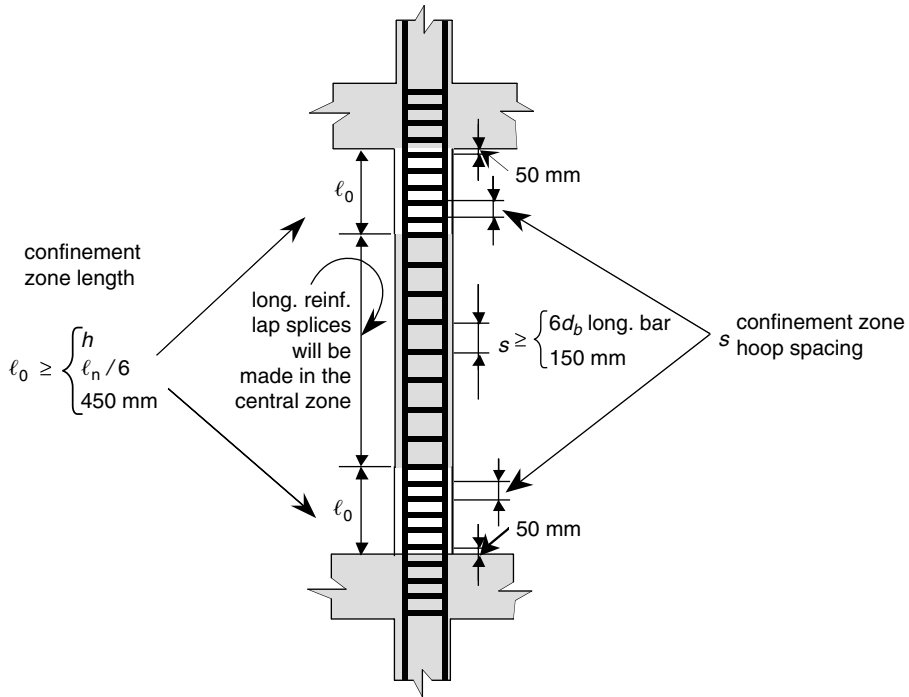


FIGURE 14.31 Confinement hoop spacing in columns.

4. The total cross-sectional area of rectangular hoop reinforcement shall not be less than that required by Equations (14.42) and (14.43).

$$A_{sh} = 0.3 \frac{s h_c f'_c}{f_{yh}} \left(\frac{A_g}{A_{ch}} - 1 \right) \quad (14.42)$$

$$A_{sh} = 0.09 \frac{s h_c f'_c}{f_{yh}} \quad (14.43)$$

5. where A_{sh} is the total cross-sectional area of transverse reinforcement (including crossties) within spacing s and perpendicular to dimension h_c , f_{yh} is the specified yield strength of the transverse reinforcement, h_c is the cross-sectional dimension of column core measured center-to-center of confining reinforcement, A_g is the gross area of section and A_{ch} is the cross-sectional area measured out-to-out of the transverse reinforcement.
6. The horizontal distance, measured center-to-center, between legs of the peripheral hoops and crossties, and between crossties, shall not exceed 350 mm.
7. In the confinement zones, maximum spacing of hoops measured along the axis of the member shall not exceed one quarter of the minimum member dimension, $6d_b$ of the longitudinal reinforcement and s_x defined in Equation 14.44,

$$s_x = 100 + \left(\frac{350 - h_x}{3} \right) \quad (14.44)$$

8. where s_x shall not be greater than 150 mm and does not need to be less than 100 mm, and h_x is the maximum horizontal distance between hoop and crossties legs in all faces of the column.

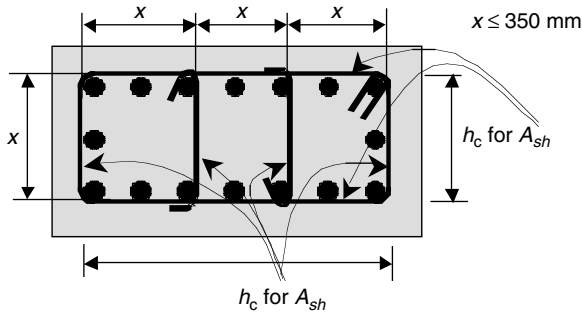


FIGURE 14.32 Separation between legs of hoop and crossties.

9. The first hoop shall be located no farther than 50 mm from the face of the joint.
10. When reinforcement as indicated above is not placed throughout the column clear length, the transverse reinforcement in the central part of the column clear length between confinement zones shall be hoops of the same diameter, yield strength and number of crossties used in the confinement zones, and the maximum center-to-center spacing shall not exceed the smaller of $6d_b$ of the longitudinal column bars or 150 mm (Figure 14.32).

14.5.2.5 Spiral Reinforcement

When spirals are used as the column transverse reinforcement, the requirements of Section 7.10.4 of ACI 318-02 10.4.3.3 and the following additional requirements shall be met:

1. The transverse reinforcement shall be a spiral or circular hoops over the length of the confinement zone, ℓ_0 , measured from the face of the joint at both ends of the column. The distance ℓ_0 shall not be less than the largest column cross-sectional dimension, one sixth of the clear length of the column or 450 mm
2. The volumetric ratio of the spiral shall not be less than indicated by Equation (10-5) of ACI 318-02 and by Equation 14.45

$$\rho_s = \frac{A_b \cdot \pi \cdot (d_c - d_b)}{A_{ch} \cdot s} \geq 0.12 \cdot \frac{f'_c}{f_{yh}} \quad (14.45)$$

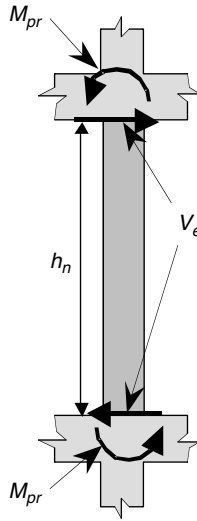
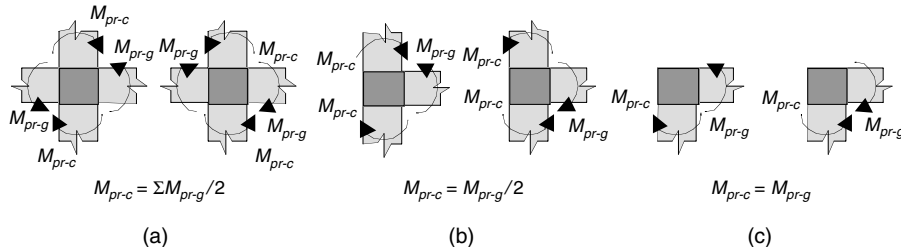
3. where A_b is the spiral bar area, d_c is the out-to-out spiral diameter, d_b the spiral bar diameter, A_{ch} is the cross-sectional area measured out-to-out of the spiral, f_{yh} is the specified yield strength of the spiral and s is the spiral vertical spacing.
4. Outside the confinement zones, the maximum center-to-center spacing of the spiral shall not exceed the smaller of $6d_b$ of the longitudinal column bars or 150 mm.

14.5.2.6 Shear Strength

The following requirements must be met:

1. The factored shear, V_e , corresponding to the probable moment strength of the column at the face of the joints shall be determined using Equation 14.46 for both principal directions in plan. See Figure 14.33;

$$V_e = \frac{(M_{pr})_{top} + (M_{pr})_{bottom}}{h_n} \quad (14.46)$$

FIGURE 14.33 Calculation of V_e for columns.FIGURE 14.34 Maximum M_{pr} for the columns needed to obtain column shear V_e .

2. In Equation 14.46 M_{pr} is the probable moment strength at the joint faces, determined using f_{ypr} instead of f_y ($f_{ypr} = 1.25f_y$) and a strength reduction factor $\phi = 1$. The moment strength of the columns shall correspond to the maximum probable moment strength computed for the range of factored axial loads, P_v , that act on the column. The factored shear for the column, V_e , need not exceed the value determined from the joint shear based on probable moment strength, M_{pr} , of the girders framing into the joint (Figure 14.34)
3. The required transverse reinforcement for shear shall be determined as prescribed in Chapter 11 of ACI 318-02, except that the contribution of concrete to the shear strength shall be taken as ($V_c = 0$) in the confinement zones if V_e is greater than one half of the maximum required shear strength V_u and also the factored axial load including earthquake effects is less than ($0.05 f'_c A_g$)
4. The hoops or spirals required for confinement shall be considered effective as shear reinforcement

14.5.3 Joints on Special Moment Frames

For joints of special moment frames the following requirements apply:

14.5.3.1 Column Dimensions at Joint

Where longitudinal girder reinforcement extends through the column-girder joint, the column dimension parallel to the beam shall not be less than 20 times the diameter, d_b , of the largest longitudinal girder bar.

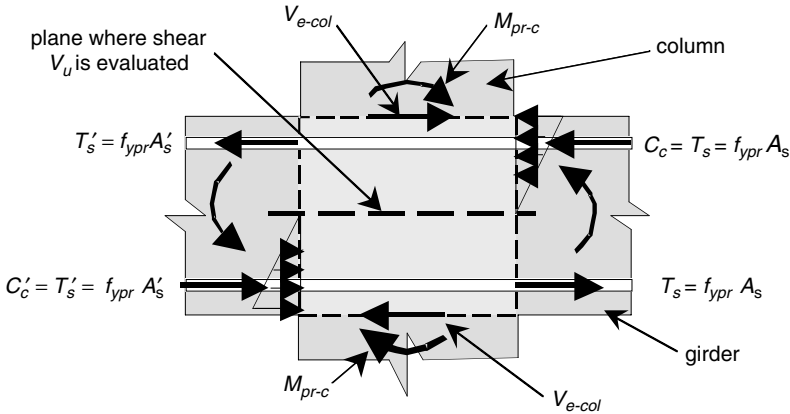


FIGURE 14.35 Joint shear determination.

14.5.3.2 Transverse Reinforcement

Transverse reinforcement conforming to (1) and (2) shall be provided within the column-girder joint:

1. Horizontal transverse hoops with the same area and spacing required for the column shall be provided within the column-girder joint. Where girders, having a width equal to or greater than 3/4 of the column width, frame the joint at all four sides, the hoop spacing can be two times as required for the column, but not exceeding 150 mm
2. Where the longitudinal girder reinforcement is located outside the confined core vertical hoops as required for girders shall be provided to confine it

14.5.3.3 Joint Shear Strength

The horizontal shear strength of the joint shall be equal or exceed the factored shear that develops due to the probable moment strength of columns and girders that frame into the joint (Figure 14.35). The following requirements shall apply:

1. The factored shear at the joint, V_u , shall be determined for both principal directions using Equation 14.47 for joints where girders frame in both sides and using Equation 14.48 where girders frame in one side only.

$$V_u = f_{ypr} (A_s + A'_s)_{\text{girder}} - (V_e)_{\text{column}} \quad (14.47)$$

$$V_u \geq \begin{cases} f_{ypr} (A_s)_{\text{girder}} - (V_e)_{\text{column}} \\ f_{ypr} (A'_s)_{\text{girder}} - (V_e)_{\text{column}} \end{cases} \quad (14.48)$$

In Equations 14.47 and 14.48 the reinforcement area corresponds to the girder longitudinal reinforcement, and $f_{ypr} = 1.25 f_y$. The shear V_e from the development of flexural strength of the column shall be determined as explained before

2. The nominal shear strength at the critical plane in the joint shall be (for A_j see Figure 14.36):

For joints confined on all four faces

$$\phi V_n = \phi 1.70 \sqrt{f'_c} A_j$$

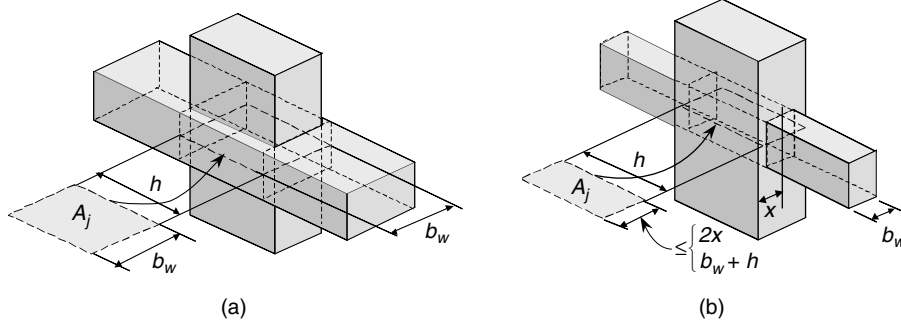


FIGURE 14.36 Definition of A_j for joint shear determination.

$$\text{For joints confined on three faces or on opposite faces } \phi V_n = \phi 1.25 \sqrt{f'_c} A_j$$

$$\text{For other joints } \phi V_n = \phi 1.00 \sqrt{f'_c} A_j ;$$

3. The joint dimensions must be such that $V_u \leq \phi V_n$
4. A member that frames into a face of a joint is considered to provide confinement to the joint if at least the framing member covers 3/4 of the face of the joint
5. A_j corresponds to the effective cross-sectional area within the joint in a plane parallel to the plane of the reinforcement generating the shear and is equal to the product of joint depth by the effective width of the joint. The joint depth corresponds to the dimension of the column parallel to the direction of the girders. The joint effective width is equal to the girder width for girders larger or equal to the column width as shown in Figure 14.36(a). For girders narrower than the column width, the joint effective width is equal to the smaller of the girder width plus the joint depth, or the girder width plus twice the smaller perpendicular distance from the longitudinal axis of the girder to the column side, without exceeding the column width. See Figure 14.36(b).

14.5.3.4 Development Length of Bars in Tension at the Joint

ACI 318-02 contains requirements for defining the development length for bars that end in a standard hook at the joint, and for straight bars within the joint. The requirements are valid only for bars with diameters from 10 mm to 36 mm (3/8 in. to 1-3/8 in.). Because of lack of experimental information, larger diameter bars are not covered.

The development length ℓ_{dh} for a bar with a 90° hook located within the confined core of a column or a boundary element must be the larger of $8d_b$, 150 mm or the length required by Equation (14.49).

$$\ell_{dh} = \frac{f_y d_b}{5.4 \sqrt{f'_c}} \quad (14.49)$$

The development length for straight bars, ℓ_d , are $2.5\ell_{dh}$ just given for bottom bars (less than 300 mm of concrete cast beneath the bar) and $3.5\ell_{dh}$ for top bars (more than 300 mm of concrete cast beneath the bar).

Straight bars terminated at a joint must be located within the confined core of the column or boundary element. Any portion of the straight embedment length of the bar not located within the confined core must be increased by a factor of 1.6.

14.5.4 Wall Design

The designer should note that the requirements of Chapter 21 of ACI 318-02 are additional to the requirements of the rest of the code, therefore the applicable requirements of Chapter 14 for walls must be observed. These last requirements cover issues such as: effective wall length for concentrated loads, limits of thickness and the need to use a minimum of two 16 mm (5/8 in.) diameter bars around all window and door openings, among others. The empirical design method of Section 14.5 of ACI 318-02 must not be used in the design of walls subjected to earthquake ground motion.

One very important requirement is contained in Section 14.3.6 of ACI 318-02 indicating that when the vertical reinforcement ratio exceed 0.01 or the vertical reinforcement may yield in compression, it must be enclosed by lateral ties as in columns. This requirement constitutes within ACI 318-02 the real difference between a wall and a column. Reinforced concrete codes have approached the definition of the dividing line between columns and walls in different ways. ACI chose the behavioral path as opposed to the limiting dimensions path. This requirement implies that the wall will need ties as in a column when a large vertical reinforcement ratio is needed (more than 0.01) or the vertical reinforcement is subjected to compression strains greater than f_c/E_s . There will be, then, no possibility of using a single curtain (or layer) of reinforcement and it will indirectly lead to thicker walls. The issue of seismic (135°) hooks being needed for the ties is not clear in ACI 318-02, but the recommendation would be to use them always.

The transmission of the wall forces at the base to the foundation and then to the underlying soil requires a careful analysis usually not needed for columns. The analysis subterfuge of considering walls clamped at the base requires a corresponding strength and stiffness from the foundation. Any variation of the analysis premises with respect to the layout of the foundation elements would imply a different distribution between the lateral-force shear carried by walls and frames, giving a larger responsibility to the latter. The layout and design of the foundation must be consistent with the premises adopted in analysis and the design forces derived from it.

Finally, the responsibility assigned to structural walls in the general behavior of the structure subjected to earthquake ground motion is larger than for individual columns. Although the requirements of redundancy (see Section 14.2.5) tend to indicate this to the designer, it is important to note that greater care and judgment must be exercised in their design.

In summary, special reinforced concrete walls must comply with the requirements of Chapter 14 of ACI 318-02 plus the following additional requirements.

14.5.4.1 Reinforcement

The reinforcement in walls must comply with the following:

1. The distributed web reinforcement ratios ρ_v and ρ_n , for vertical and horizontal reinforcement respectively, shall not be less than 0.0025
2. If the design shear force does not exceed $(1/12)A_{cv}\sqrt{f'_c}$, where A_{cv} is the gross horizontal area of concrete in mm^2 bounded by web thickness and length of section in the direction of the shear force considered, the minimum reinforcement ratios may be reduced to those prescribed in Section 14.3 of ACI 318-02
3. Reinforcement spacing each way in structural walls shall not exceed 450 mm
4. Reinforcement provided for shear must be continuous and must be distributed across the shear plane
5. If the in-plane factored shear force exceeds $(1/6)A_{cv}\sqrt{f'_c}$ at least two curtains of reinforcement must be used
6. All continuous reinforcement in structural walls must be anchored or spliced following the special requirements for reinforcement in tension at joints (see Section 14.5.3).

14.5.4.2 Design Shear Force

The design shear force, V_u , for structural walls must be obtained from analysis using the appropriate load combinations and load factors. The designer must take into account the possibility of flexural

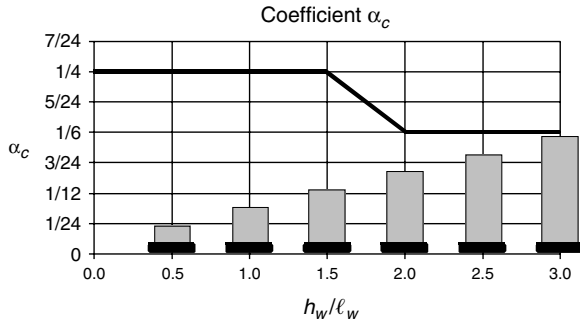


FIGURE 14.37 Coefficient α_c for wall shear design.

yielding of the wall. In that case, the design shear force must be that developed when yielding occurs, in general much larger than the one obtained from analysis. In case the design shear force used is less than the shear corresponding to the development of the nominal flexural strength of the wall, the shear design must be made using a strength reduction factor $\phi = 0.60$ (See Table 14.16).

14.5.4.3 Shear strength

For the shear design of structural walls the requirements presented below must be followed:

1. The nominal shear strength, V_n , of structural walls must be computed using:

$$V_n = A_{cv} \left(\alpha_c \sqrt{f'_c} + \rho_n f_y \right) \leq \frac{2}{3} A_{cv} \sqrt{f'_c} \quad (14.50)$$

where α_c varies with the slenderness ratio (h_w/ℓ_w) of the wall as shown in Figure 14.37 and all the other terms have been previously defined. When the wall has openings the same rule applies for the wall segments, and the larger value of the slenderness ratio for the wall segment or the wall as a whole must be used.

2. The shear reinforcement must be distributed in such a way that it provides resistance in two orthogonal directions in the plane of the wall. For walls with slenderness ratio (h_w/ℓ_w) less and equal to 2.0, the vertical reinforcement ratio, ρ_v , shall not be less than the horizontal reinforcement ratio ρ_h .
3. The sum of the nominal shear V_n of all wall segments shall not exceed the value given by Equation 14.50. The nominal shear strength V_n of any individual wall pier shall not exceed $(5/6)A_{cp} \sqrt{f'_c}$, where A_{cp} is the cross-sectional area of the pier considered.
4. The nominal shear strength V_n of horizontal wall segments and coupling beams shall not exceed $(5/6)A_{cp} \sqrt{f'_c}$, where A_{cp} is the cross-sectional area of the horizontal wall segment or coupling beam.

14.5.4.4 Design for Flexure and Axial Load

Structural walls must be designed for flexure and flexure accompanied by axial load following the requirements of Chapter 10 of ACI 318-02 with two exceptions: (a) the limit on the maximum axial load of ACI 318-02 Section 10.3.6 does not apply, and (b) the nonlinear strain distribution required for deep beams does not apply for structural walls.

Where wall elements intersect to form I, T, C or other cross-sectional shapes, the influence of the flange behavior must be taken into account. The effective flange lengths differ from those given for T-beams in Chapter 8 of ACI 318-02. The limits for walls are set at the lesser of one half of the distance to the adjacent web or 25% of the total wall height. Only concrete and reinforcement contained within the effective flanges can be considered in the flexural strength of the wall. When the wall is analyzed using finite elements, in many cases the mathematical model accounts for the shear lag present in the flanges.

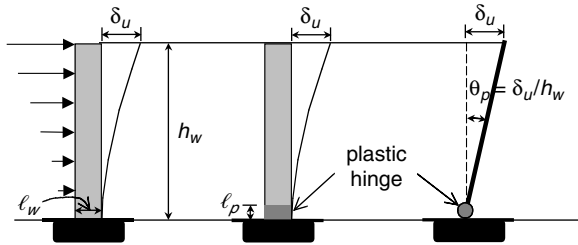


FIGURE 14.38 Wall responding in the nonlinear range.

This usually leads to differences in the stiffness that can be assigned to the wall when analyzed using just the effective flange dimension. Judgment is required from the designer to properly account for these differences.

Rules of design for flexure and flexure accompanied by axial force for structural walls are essentially the same as for columns, including the variations of the strength reduction factors ϕ . In general, an interaction diagram must be computed for the section including only the web and the effective flanges. The procedure for obtaining the interaction diagram must include a careful control of the vertical reinforcement strain both in tension and compression for the range of expected factored axial forces acting on the wall. The reinforcement compression-strain control highlights the need of surrounding the reinforcement with ties as in columns when yielding in compression is detected. The reinforcement tension-strain control is needed to detect strains exceeding the maximum tension elongation that the reinforcement can sustain. This is normally not an issue in columns, but may be present in long walls with little axial load. The maximum elongation in tension must be compatible with the one set by the steel manufacturing standard as listed in Table 14.18.

The designer must keep issues associated with local and global slenderness of the wall in mind. The need to properly anchor the wall to the floor diaphragms is part of the solution for avoiding these problems.

14.5.4.4.1 Boundary elements

Special boundary elements are required in structural walls to confine the concrete when the strain in the extreme compression fiber of the wall exceeds a critical value for walls responding to earthquake-induced ground motion. ACI 318-02 contains two alternative procedures for identifying the need of boundary elements. One procedure is based on indirectly checking the compression strains at the edge of the wall when subjected to the lateral design displacements. The second procedure — that has been in the ACI code for many years — is based on a compressive-stress check at the edge of the wall. Once the need to provide boundary elements is identified by either procedure, the requirements for them are the same.

Boundary element need based on displacement — This procedure for defining the need of boundary elements applies only to walls that act as continuous vertical cantilevers from base of the structure to top of wall and are designed to have a single critical section for flexure and axial load as shown in Figure 14.38. Walls not meeting this requirement need investigation of boundary elements using the stress check method. Special boundary elements must be provided at compression zones when:

$$c \geq \frac{\ell_w}{600 \left(\frac{\delta_u}{h_w} \right)} \quad (14.51)$$

and

$$\frac{\delta_u}{h_w} \geq 0.007 \quad (14.52)$$

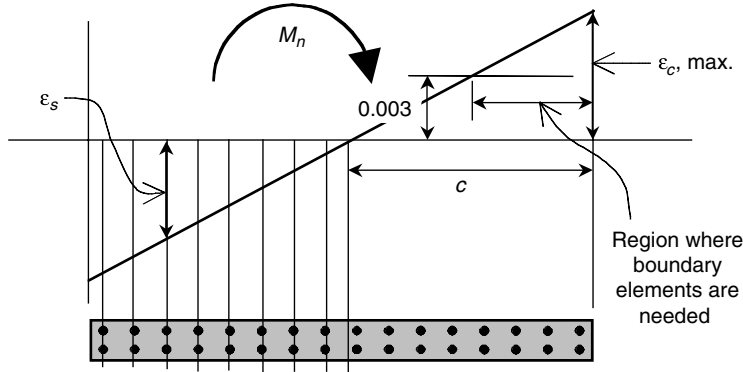


FIGURE 14.39 Strain state at the critical wall section.

where c is the distance from the extreme compression fiber to neutral axis (see Figure 14.39) calculated for the factored axial force and nominal moment strength consistent with the design displacement δ_u at the top of the wall resulting in the largest neutral axis depth, ℓ_w is the length of the entire wall and h_w is the height of the entire wall.

Where special boundary elements are needed according to Equation 14.51 the special boundary element reinforcement must extend vertically from the critical section to a distance not less than the larger of ℓ_w or $M_u/(4V_u)$.

Boundary element need based on stress check — When the displacement-based procedure is not used, boundary element must be provided at boundaries and edges around openings of structural walls where the maximum factored compressive extreme fiber stress corresponding to factored forces, P_u and M_u from the load combinations that include earthquake effects, exceeds $0.2 f'_c$. These boundary elements may be discontinued when the compressive extreme fiber stress is less than $0.15 f'_c$. Stresses must be calculated for the factored forces using a linear elastic model and gross section properties. In walls with flanges the effective flange width for walls must be used. This procedure has been in the ACI 318 code for many years and until the 1999 edition of the code the boundary elements were required to resist all the factored axial and flexural forces from gravity and seismic effects without any contribution from the rest of the wall. In the 1999 edition of ACI 318 this was changed and the whole wall section is permitted to resist the factored forces.

Where the special boundary elements are needed by any of the two alternative procedures just explained, the following requirements must be met:

1. The boundary element must extend horizontally from the extreme compression fiber to a distance greater than the larger of $(c - 0.1\ell_w)$ and $c/2$.
2. In sections with flanges the boundary element must include the flange width in compression and must extend at least 300 mm into the web of the wall.
3. The transverse reinforcement in boundary elements must comply with the requirements for transverse reinforcement in confinement zones of columns with the exception of Equation 14.42. This transverse reinforcement must be used in all the height where boundary elements are needed.
4. The special transverse reinforcement must extend into the support at the wall base at least the development of the largest diameter vertical bar of the boundary element. In mats and footings this distance must be 300 mm.
5. The horizontal wall web reinforcement must be anchored to develop f_y within the confined core of the boundary element.

Where special boundary elements are not required and longitudinal (vertical) reinforcement is concentrated at wall edges, some minimum transverse reinforcement is required to inhibit the buckling of the longitudinal reinforcement. If the longitudinal reinforcement ratio computed for the boundary of the

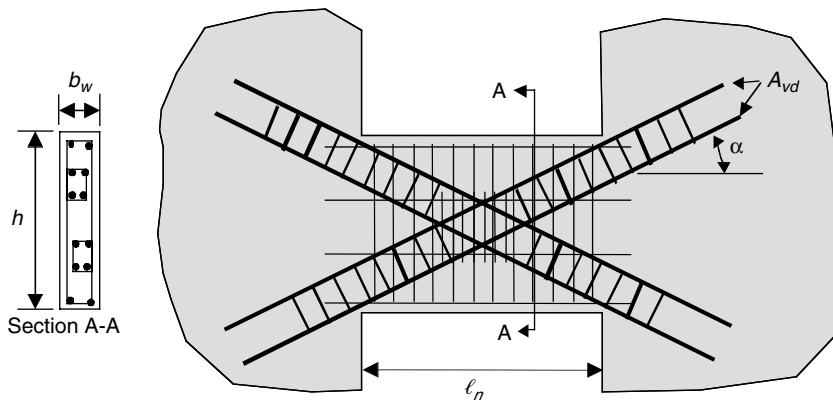


FIGURE 14.40 Wall coupling beam with diagonal reinforcement.

wall exceeds $2.8/f_y$, for a horizontal distance greater than the larger of $(c - 0.1\ell_w)$ and $c/2$, overlapping hoops or hoops and crossties spaced vertically not more than 200 mm must be provided. The horizontal distance between parallel hoop legs and crossties must not exceed 350 mm.

The wall horizontal reinforcement when boundary elements are not needed and the shear force V_u in the plane of the wall exceeds $(1/12)A_{cv}\sqrt{f'_c}$ must end in a standard hook engaging the edge reinforcement, or the edge reinforcement must be enclosed in U-stirrups having the same spacing of the horizontal reinforcement.

14.5.4.4.2 Coupling beams

Coupling beams connecting walls have requirements within ACI 318-02 that depend on the clear span to height ratio ℓ_n/h . For slender coupling beams with ℓ_n/h greater or equal to 4, the requirements for beams can be used, and once it can be demonstrated that the beam has adequate lateral stability, the minimum width and aspect ratio can be waived. For coupling beams with ℓ_n/h ratio less than 4, the code permits the use of groups of intersecting diagonal bars placed symmetrically with respect to midspan (see Figure 14.40), and for a ℓ_n/h ratio less than 2 the diagonal reinforcement is mandatory if the factored shear force V_u exceeds $(1/3)A_{cp}\sqrt{f'_c}$. A waiver is set by the code in the last case if it can be shown that loss of stiffness and strength of the beam does not impair the load carrying capacity of the structure.

When the diagonal reinforcement is used, at least four bars enclosed by transverse reinforcement complying with the requirements of column confinement reinforcement must be used. The dimensions — measured outside of the transverse reinforcement — of the diagonal bar assembly must be at least $b_w/5$ in the plane of the beam and $b_w/2$ in the normal direction, where b_w is the beam width. The nominal shear strength V_n must be computed using:

$$V_n = 2A_{vd}f_y \sin \alpha \leq \frac{5}{6}A_{cp}\sqrt{f'_c} \quad (14.53))$$

where A_{vd} is the total area in mm^2 of reinforcement in each group of diagonal bars, A_{cp} is the area in mm^2 resisting shear in the coupling beam and α is the angle between the diagonal reinforcement and the longitudinal axis of the beam.

14.5.5 Floor Diaphragms

Section 21.9 of ACI 318-02 covers the requirements for floor and roof slabs acting as structural diaphragms that transmit the inertial forces induced by the earthquake ground motion to the lateral force-resisting system vertical-elements. In general the diaphragm includes also all strut, ties, chords, collector elements and trusses serving as part of the lateral force. The requirements cover diaphragms cast in place

and composed of precast elements with a cast in place topping, composite and noncomposite. In all cases the topping and its connections, must have reinforcement adequate to resist the forces transmitted to other elements of the lateral force-resisting system. Concrete slabs and composite topping slabs acting as structural diaphragms must be at least 50 mm thick. Topping slabs cast over precast floor or roof elements acting as diaphragms must be at least 65 mm thick.

The minimum reinforcement corresponds to temperature and shrinkage reinforcement for slabs with a maximum allowable spacing in each direction of 450 mm. If welded wire fabric is used in toppings cast over precast elements, the maximum spacing between wires parallel to the span of the precast elements must be less than 250 mm. Shear reinforcement must be distributed uniformly across the shear plane.

Structural truss elements, struts, ties, diaphragm chords and collector elements must have confinement transverse reinforcement complying with the requirements for columns when the compression stress exceeds $0.2f'_c$ computed for the factored forces using a linear elastic model and the gross-section properties of the elements. The confinement transverse reinforcement may be discontinued when the compressive stress is less than $0.15f'_c$.

The nominal shear strength V_n of diaphragms must not exceed the value computed using Equation 14.54

$$V_n = A_{cv} \left(\frac{\sqrt{f'_c}}{6} + \rho_n f_y \right) \leq \frac{2}{3} A_{cv} \sqrt{f'_c} \quad (14.54)$$

where A_{cv} is the gross cross-sectional area of the diaphragm. For cast-in-place — composite and non-composite — topping on precast elements floor or roof Equation 14.54 may be used with A_{cv} solely based on the topping slab and without taking the term $\sqrt{f'_c}/6$ into account.

Boundary elements of structural diaphragms, when required, must be able to resist the sum of the in-plane factored axial force and the force obtained by dividing the factored moment at the section by the distance between the boundary elements at the section. The splices of the tension reinforcement of chord and collector elements must be able to develop the yield strength of the reinforcement.

14.5.6 Foundations

Section 21.10 of ACI 318-02 contains the requirements that foundation elements must meet. Requirements are given for footing, mat slabs and pile caps, grade beams, slabs on grade, piles, piers and caissons. The reader must consult the text of the requirements.

14.5.7 Nonparticipating Structural Element

Nonparticipating structural elements are frame elements that are assumed not to contribute to the lateral resistance of the structure. Section 21.11 of ACI 318-02 contains the requirements these elements must meet. This section of ACI 318 was completely reviewed after the January 17, 1994, Northridge earthquake that affected the Los Angeles, California, area, where poor behavior of this type of elements was observed in many instances.

Section 21.11 of ACI 318-02 contains two different approaches for detailing these elements; one is based on the forces induced in the element when subjected to the design displacements imposed by the design ground motion and the other can be used when the effects of the design displacement are not explicitly checked. It is important to note that the use of nonseismic detailing is not permitted and additional transverse reinforcement is required in all cases with some instances in which the amount that must be used is practically the same as what must be used in elements that are part of the lateral force-resisting system. The designer must ponder in all cases if it is worth taking the effort to design these structural members as nonparticipating elements.

14.6 Detailing of Intermediate Moment Frames

14.6.1 General

The requirements for intermediate moment frames are contained in Section 21.12 of ACI 318-02. These requirements cover beams and girders, columns and slab-column frames. No requirements for reinforced concrete walls and no special detailing beyond what is required in Chapter 14 of ACI 318-02 are needed.

One important change was introduced in the 2002 edition of the ACI Code related to intermediate moment frames. In previous editions of the code the stirrups and ties for intermediate frames were not required to be hoops having 135° hooks. In the 2002 edition all transverse reinforcement located in confinement zones has to be hoop. This change introduces an additional degree of toughness to intermediate moment frames.

Shear design of beams, columns and two-way slabs resisting earthquake effect can be performed using one of the two options:

1. The design shear corresponds to the sum of the shear associated with the development of nominal moment strengths of the member at each restrained end of the clear span and the shear calculated for factored gravity loads. It should be noted that this option is different from what is required for special moment frames because in this case the strength reduction factor must be taken as unit ($\phi = 1$), but there is no need to increase the value of f_y by 1.25.
2. The design shear corresponds to the maximum shear obtained from design load combinations that include earthquake effect E , with E assumed to be twice that prescribed by the governing code for earthquake-resistant design. In Table 14.14 the load combinations under SEI/ASCE 7-02 were given. For combinations five and seven when applying this requirement for shear design the $1.0E$ must be substituted by $2.0E$. This option is simple to compute and does not require the longitudinal reinforcement to be already defined before designing the shear reinforcement.

14.6.2 Beams

Beams in intermediate moment frames are elements that have a compression axial force less than $(0.1f'_c A_g)$. There are no cross-section dimension restrictions beyond what is required in Chapters 1 to 18 of ACI 318-02.

14.6.2.1 Longitudinal Reinforcement

The longitudinal reinforcement layout must be such that the positive moment strength at the face of the joint is not less than one third of the negative moment strength provided at that face of the joint. Neither the negative nor the positive moment strength at any section along the length of the member can be less than one fifth of the maximum moment strength provided at the face of either joint.

14.6.2.2 Transverse Reinforcement

At both ends of the member, hoops must be provided over lengths equal to twice the member depth measured from the face of the supporting member toward midspan. The first hoop must be located at not more than 2 in. from the face of the supporting member. Maximum hoop spacing shall not exceed the smallest of:

1. $d/4$
2. $8d_b$ of the smallest longitudinal bar enclosed
3. $24d_b$ of the hoop bar
4. 300 mm

Stirrups must be placed at not more than $d/2$ throughout the length of the member.

14.6.3 Columns

Columns in intermediate moment frames are elements that have a compression axial force greater or equal to $(0.1f'_c A_g)$. There are no cross-section dimension restrictions beyond what is required in Chapters 1 to 18 of ACI 318-02. Also there are no additional restrictions on the longitudinal reinforcement.

14.6.3.1 Transverse Reinforcement

All columns must have transverse joint reinforcement as required by Section 11.11.2 of ACI 318-02. If columns are spirally reinforced they must comply with Section 7.10.4 of ACI 318-02. Tied columns must have at both ends of the member hoops at spacing s_o over a length ℓ_o measured from the joint face. Spacing s_o must not exceed the smallest of:

1. $8d_b$ of the smallest longitudinal bar enclosed
2. $24 d_b$ of the hoop bar
3. One half of the smallest cross-sectional dimension of the column
4. 300 mm

Length ℓ_o should not be less than the largest of:

1. One sixth of the clear span of the members
2. The maximum cross-sectional dimension of the member
3. 450 mm

The first hoop must be located at not more than $s_o/2$ from the joint face. Outside the length ℓ_o , spacing of transverse reinforcement must conform to Sections 7.10 and 11.5.4.1 of ACI 318-02.

14.6.4 Slab–Column Systems

Slab–column systems designed using the requirements of Chapters 1 to 18, and specially Chapter 13, of ACI 318-02 are considered ordinary moment frames and are appropriate for seismic design categories A and B. If, in addition, the slab meets the requirements contained in this section, the slab–column frame may be considered as an intermediate moment frame, and it is appropriate for seismic design category C. The additional requirements are related to slab moments, slab reinforcement and punching-shear issues. The excessive lateral load flexibility of slab–column systems is not addressed because it is not the domain of ACI 318. The definition of appropriate story drift limits for slab–column systems is something that the designer should address. The punching-shear strength of slab–column systems subjected to earthquake ground motion is drift dependent (Hueste and Wight, 1999). For seismic design categories D, E and F, slab–column systems are not permitted as lateral force-resisting systems.

Meeting the following requirements would help the slab–column system to be classified as an intermediate moment frame:

14.6.4.1 Slab Moments

The factored slab moment at support related to earthquake effect must be determined for load combinations 5 and 7 given in Table 14.14. All reinforcement provided to resist the portion of slab moment balanced by support moment, must be placed within the column strip of the slab.

14.6.4.2 Slab Reinforcement

Slab reinforcement must comply with the following requirements:

1. An effective width of slab centered with the axis of column centerlines is defined. This effective slab width extends $1.5h$ slab or drop panel thicknesses outside opposite sides of the column for a total effective width of $3h$ plus the column width. For edge and corner columns this width is restricted and the detailed requirements of Section 21.12.6.2 of ACI 318-02 must be consulted.
2. All reinforcement provided to resist earthquake-related effects must be located in the column strip of the slab.

3. The fraction of the unbalanced moment to be transferred by flexure, defined by Equation (13-1) of ACI 318-02, must be resisted by reinforcement placed within the effective slab width defined in (1).
4. At least one half of the reinforcement in the column strip at support shall be placed within the effective width defined in (1).
5. At least one quarter of the top reinforcement at the support in the column strip must be continuous throughout the span.
6. Continuous bottom reinforcement in the column strip must be at least one third of the top reinforcement at the support in the column strip.
7. At least one half of all bottom middle strip reinforcement and all bottom column strip reinforcement at midspan must be continuous and shall develop its yield strength at the face of support.
8. At discontinuous edges of the slab all top and bottom reinforcement at support must be developed at the face of support.

14.6.4.3 Punching-Shear Restriction

Punching shear caused by factored gravity loads shall not exceed 40% of the allowable punching-shear strength of the column-slab joint. This is a restriction based on the poor observed behavior of slab-column systems in numerous earthquakes where punching-shear failures have caused collapses. The intention is to allow for some additional punching-shear strength capacity for the effects caused by the earthquake ground motion.

14.7 Economic Implications of Selecting the Structural System

The structural designer has several alternatives to choose from when defining a structural system that fits the architectural layout. The lateral force-resisting system plays a very important role in this selection. When confronted with the task of deciding on a gravity and lateral force-resisting system, the economic implications of the selection must always be kept in mind. The economics of structural systems is very much dependent on local conditions associated with tradition of usage of certain systems, local costs of material, equipment and workmanship and issues associated with wind and earthquake hazards. Notwithstanding, there are several constants common to different locations that when applied correctly lead to economic structures with good expected behavior.

Currently, there is a worldwide trend toward using more structural walls as opposed to moment-resisting frames in localities where lateral forces play an important role. The reasons behind this trend could probably be associated with a greater awareness of the importance of story drift control and the associated implications of nonstructural element damage. Some countries like Japan and Chile have a long tradition of intensive use of structural walls, whereas other, like the United States have successfully used systems where walls and frames are combined into dual systems. As story drift control is considered more important than just lateral load strength it is possible to forecast a greater use of walls in the future and a corresponding abandonment of pure frames. The structural designer in each particular situation should evaluate the economic implications of this change in the structural system of choice.

These issues have been studied in places where an abrupt change in the generally adopted solution has occurred. The information presented in (Garcia, 1996; Garcia et al., 1996; Garcia and Bonacci, 1995) is an example related to the implications of these changes, where cost related to several variables including the structural system used, building height, story drift requirements and other have been examined.

In one of these studies (Garcia and Bonacci, 1995), buildings with three different plan layouts (see Figure 14.41) and four different heights — 5, 10, 15 and 20 stories — were studied. The buildings had varying amounts of structural walls. Six values of wall area to floor plan area in each direction (wall area index p) — 0.0%, 0.3%, 0.6%, 1.0%, 1.5% and 2.0% — were used. In total, 72 buildings were studied. For each building, an evaluation was performed in which realistic combinations of dimensions of the structural elements were used to obtain a solution that complied with the compromise of least story drift with reasonable material usage, but meeting the code story drift limit in all cases. Expected performance of

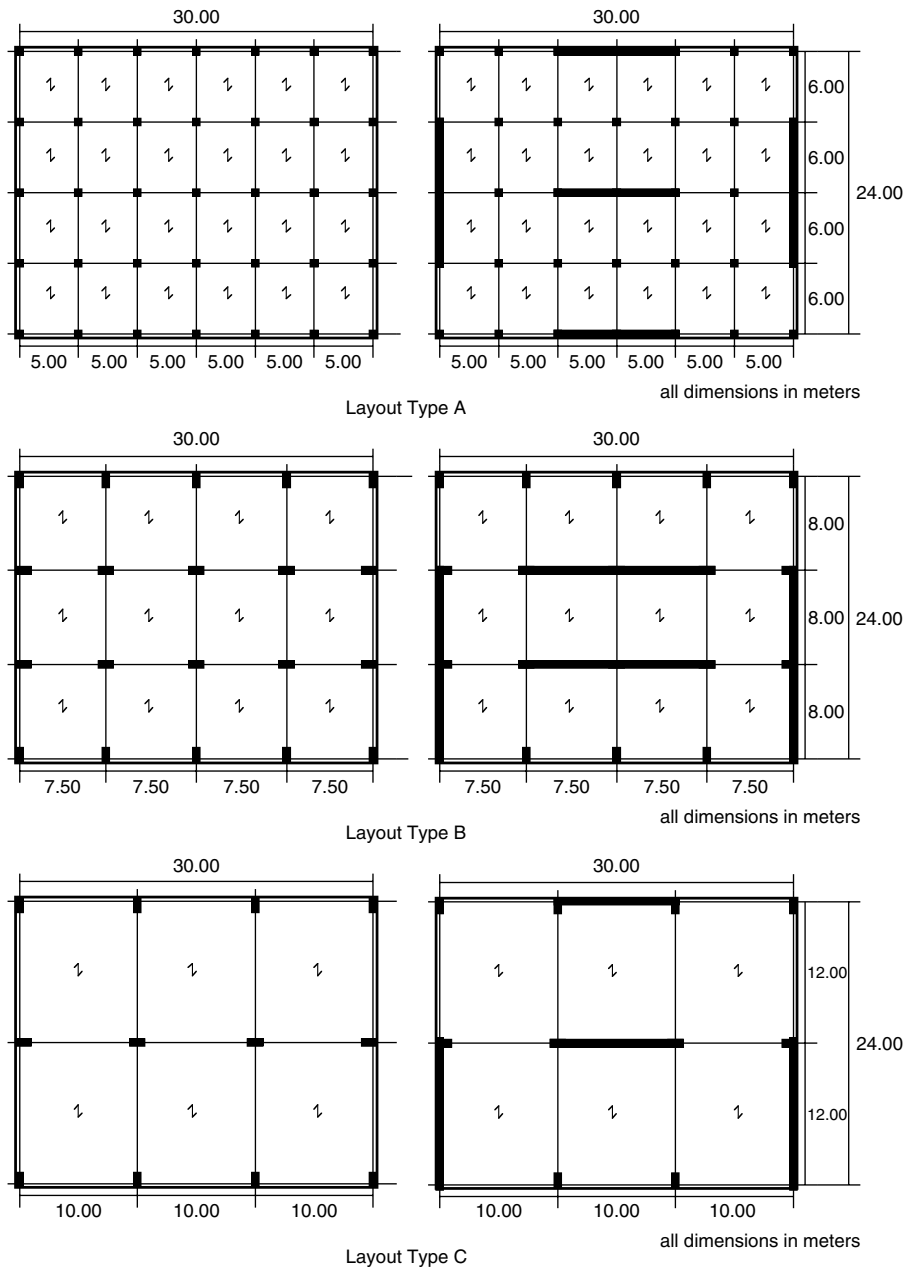


FIGURE 14.41 Plan layout types in buildings studied in (Garcia and Bonacci, 1996).

each of the chosen buildings under code design earthquake ground motion was evaluated using elastic and inelastic procedures. The inelastic procedures in all cases were simplified inelastic methodologies, with some cases being evaluated using explicit time step-by-step inelastic algorithms. Based on the amount of concrete and reinforcing steel required for all the buildings, and prevalent material and labor prices, a cost of the structure per unit area was determined. A cost index was defined as the ratio of the cost of the structure per unit area to the cost of the structure per unit area of the five-story A-type layout building without walls. Figure 14.42 reports the cost index for all the 72 buildings studied. In this graph the continuous line follows the trend of the same type of structural solution, as the number of stories

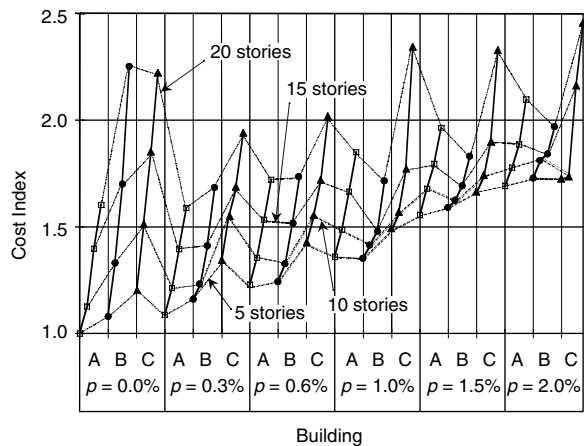


FIGURE 14.42 Cost index (ratio of the cost of the structure for each case to the structure cost for the five-story layout type A building without walls) for the buildings studied in (Garcia and Bonacci, 1996).

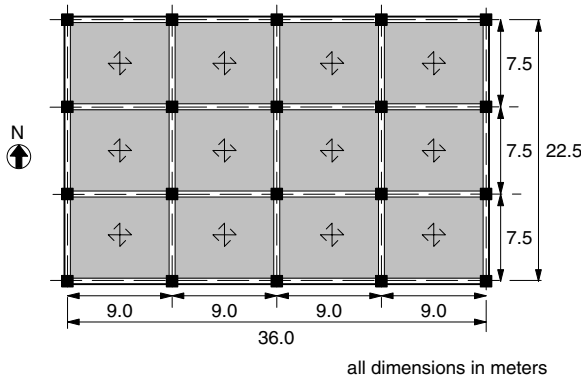


FIGURE 14.43 Plan layout for building studied in (Garcia, 1996).

increases. The broken line corresponds to the same number of stories, for different layouts and wall percentages. Different conclusions can be obtained from this type of graph with respect to structure cost increase as building height increases, effect in cost of changing the structural layout, cost variation of the structure with increasing amount of wall for the same building height and many more. It is evident that the use of walls affects the economics of the structure and in many cases leads to important reductions in cost.

In (Garcia, 1996) the economic impact of meeting different story drift requirements was studied. Figure 14.43 shows the plan layout of the building studied. Square column sections were used for all columns, with the same dimensions used throughout the building. The cases studied had all possible combinations of appropriate square column sections with a set of girder section dimensions. For example, all combinations of 0.4, 0.6, 0.8 and 1.0 m column side dimension and 0.4 m wide and 0.4, 0.5, 0.6, 0.7 and 0.8 m deep girders were employed for the eight-story building located in a moderate seismic risk zone; leading, in this particular case, to the study of a total of 20 different alternatives. Maximum story drift and associated cost of girders and columns were obtained, in all cases. All other structural elements, such as slabs and foundation, remained constant; therefore, their influence on the cost variations was disregarded. The economic evaluation was performed using typical material, equipment and labor costs. The least cost solution was used as a base for comparison, assigning a cost ratio of 1.0 to it. Cost ratio variations were then expressed as a function of this least cost of the building of particular height, and it

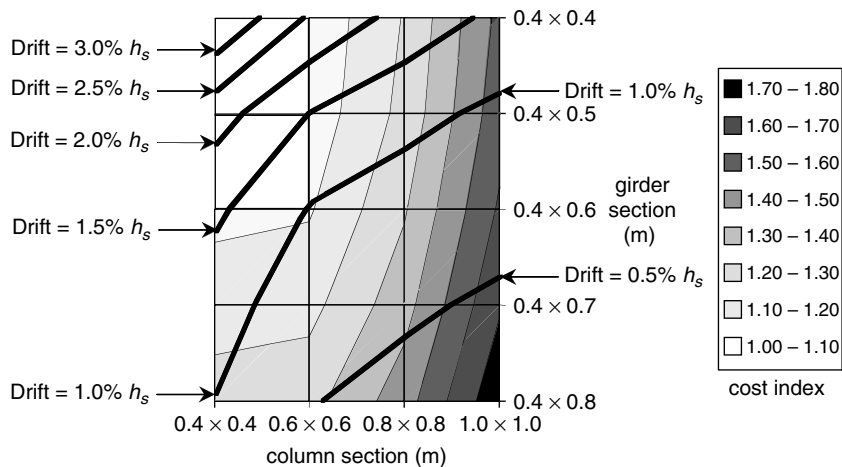


FIGURE 14.44 Maximum story drift and beam and column cost index for an eight-story moment-resistant frame building having the plan layout shown in Figure 14.43 and located in a moderate seismic zone studied in (Garcia, 1996).

reflects only the variation in cost of girder and columns. Figure 14.44 presents the maximum story drift and the cost index obtained for the eight story-building. In the figure vertical reference lines present the four column dimensions (square 0.4, 0.6, 0.8 and 1.0 m columns) and horizontal reference lines present the five girder dimensions (0.4 m wide by 0.4, 0.5, 0.6, 0.7 and 0.8 m deep girders). All intersections of the reference lines represent one building analyzed and designed having the corresponding column and girder dimensions. Story drift and cost index values are reported in the graph. It is interesting to note that drifts as low as 0.3% of the story height can be obtained for the building with larger element sections. For the building with the smaller element sections the reported story drift is 3.5% of the story height. There is a wide range of variation for buildings that in all cases meet the strength requirements of the code. An interesting result arises from this graph: the engineer when confronted with a structure that has to be laterally stiffened usually ponders over the relative merits of increasing the girder depth or enlarging the column sections. Figure 14.44 shows that the right solution is to do both at the same time. This corresponds to traveling in the graph from the upper left corner to lower right, thus decreasing the story drift in the fastest manner. Cost index is costs presented in the same figure where the cost index corresponds to the cost of girders plus columns of each dimensions alternatively divided by the least costly one, in this case the 0.4 m deep girders combined with the 0.4 x 0.4 m columns. The vertical trend of the equal cost lines, suggests that the total cost is much more sensitive to the column dimensions than to the girder dimensions, with the exception of the small section columns, where the impact of the cost of the girders is greater in the total cost. In total, 160 buildings of this type were studied in moderate and high seismic risk zones. Figure 14.45 presents results of the relation between cost index and story drift in moment-resistant frame buildings of different heights in moderate seismic zones.

To study the economic impact of using structural walls, under the same Code and economic constraints used in the study of moment-resistant frames, two wall location schemes were used with the same plan building layout. Figure 14.46 shows a one-bay wall scheme, and Figure 14.47 a two bay wall scheme. Twelve cases of use of walls in the eight-story building were obtained for the two schemes, by using wall thickness of 0.15, 0.30 and 0.45 m, and differentiating between the NS and the EW directions. Frame element dimensions employed were 0.4 x 0.4 m for the girders, 0.6 x 0.6 m for the columns.

Figure 14.48 presents, for moderate seismic risk, the relationship obtained between the wall area index, p and the story drift obtained. The wall area ratios varied from 0.3% to 2.0%. The general trend, for all slenderness ratios, correlates with the theoretical relationship presented in Section 14.3.5, but the values of story drift reported are lower due to the influence of the frame, which further restricts the story drift.

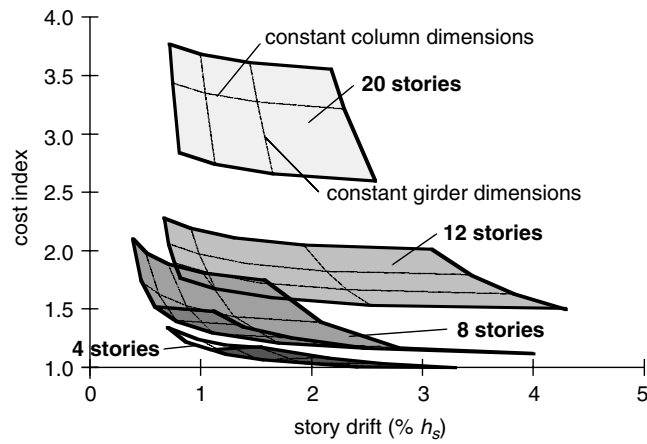


FIGURE 14.45 Relationship of cost of columns and girders against story drift for moment-resisting frame buildings studied in (Garcia, 1996).

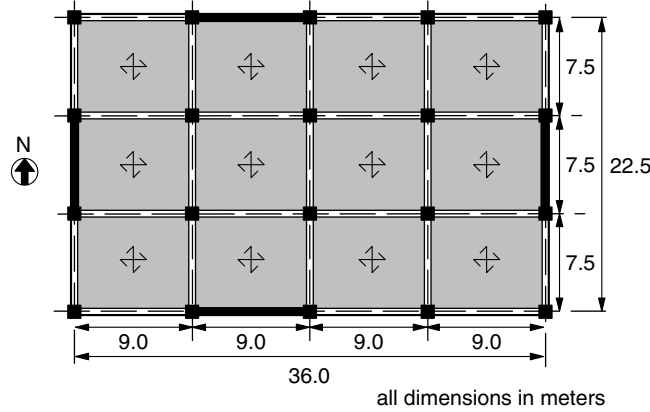


FIGURE 14.46 One-bay wall scheme studied in (Garcia, 1996).

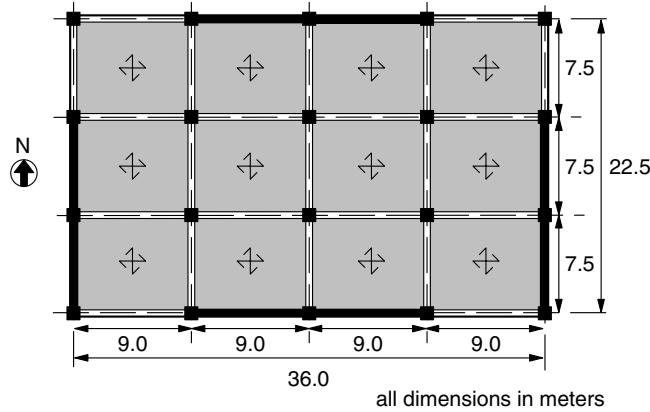


FIGURE 14.47 Two-bay wall scheme studied in (Garcia, 1996).

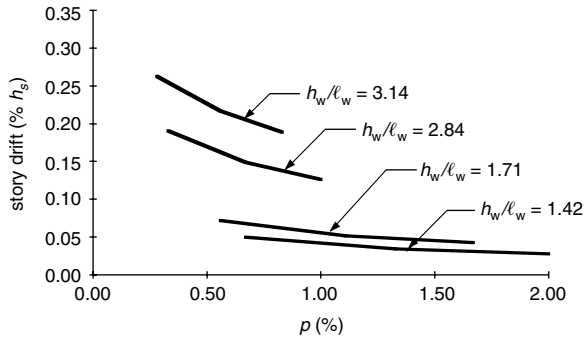


FIGURE 14.48 Story drift as a percentage of story height obtained for different values of the wall area ratio, p , for eight-story building having the plan layouts shown in Figures 14.46 and 14.47 and located in a moderate seismic zone studied in (Garcia, 1996).

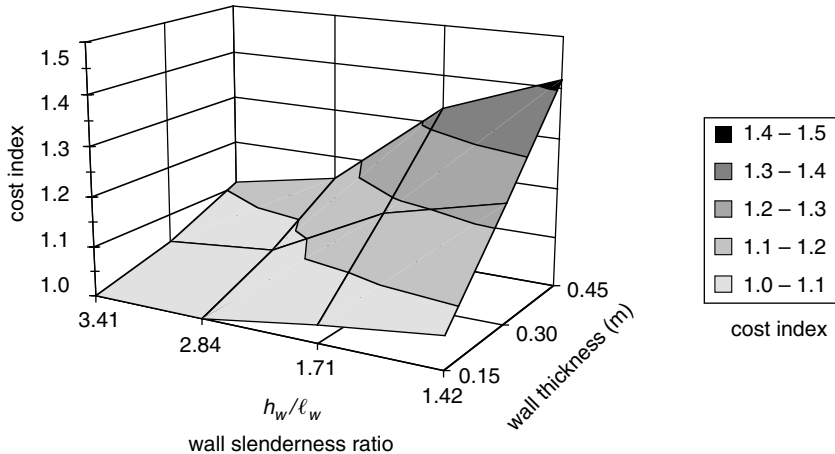


FIGURE 14.49 Wall, beam and column cost index for eight-story building having the plan layouts shown in Figures 14.46 and 14.47 and located in a moderate seismic zone studied in (Garcia, 1996).

It is important to notice that story drift ratios now vary from a minimum of 0.03% to a maximum of 0.26% of the story height, which are of the order of one tenth of those for the frames without walls studied. The cost index, calculated using the frame without walls as a basis, is presented in Figure 14.49. The cost variation is negligible for the case with the more slender 0.15 m thick walls, and reaches a maximum of 1.42 for the stubbier 0.45 m thick walls.

The main conclusions that can be drawn from the information presented are:

- The compliance of a maximum story drift limit of the order of 0.75% of the story height, using a moment-resisting frame, is feasible for buildings in the range of four to twenty stories, within acceptable extra cost, once the appropriate combination of column and girder section dimensions is determined.
- Choosing the right column section dimensions before girder depth is established could help the engineer in finding faster a structure that will meet specific story drift limits, without the risk of incurring unwarranted additional costs.
- For story drift limits below 0.75% of the story height the effectiveness of using structural walls should be investigated by the engineer, as properly chosen wall dimensions can reduce the story drift, when compared with an equivalent moment-resisting frame building, by a factor of the order of 10, without appreciable cost increases.

The selection of an appropriate story drift limit to be employed in the design of a specific building must take into account the type of nonstructural elements that will be employed, and the amount of damage that the client is willing to accept in the event of occurrence of an earthquake of the characteristics of the design earthquake.

14.8 Future Challenges

In earthquake engineering, Nature is the laboratory where the important lessons are learned. Every damaging earthquake that occurs inexorably points out deficiencies in design and construction practices and teaches the profession humility in accepting that although we may have advanced tremendously in our understanding of the effects of earthquakes on the built environment, we still have a long and demanding road to travel.

Earthquake-resistant design of reinforced concrete buildings will be one of the foremost areas of earthquake engineering affected by current and future developments. The impact of the amount of experimental research being conducted worldwide on reinforced concrete elements and structures will be affecting future design procedures and codes. The main challenge is the adequate incorporation of this research effort in helping the design profession produce safe and reliable designs for new buildings while formulating adequate guidelines for improving the earthquake-related safety of the existing inventory of reinforced concrete structures.

The main challenges are associated with the following themes:

Displacement-based versus force based design procedures — The use of displacement-based procedures in current codes and design standards is timid, to say the least. Within ACI 318-02 one of the two alternative procedures for defining the need of using boundary elements in walls is directly based on displacement and the procedures for design of nonparticipating elements include displacement considerations. The future will bring more emphasis on displacement as the governing parameter as opposed to strength. The challenge is to speed up the evolution toward a greater reliance on displacement as the governing behavior indicator. This will require coordination with the drafting bodies of the “demand” portion of current design standards.

Performance-based design — As performance-based design acquires a more direct role in design procedures the challenge beyond just their transcription into design standards and codes and the corresponding acceptance by the design profession relies on bridging and solving the legal issues of a completely different approach to the responsibility of the designer. Designers perceive performance-based design as something full of gray tones that current codes treat in a black and white fashion: “the design met or not the code” as compared with a scenario of being charged with not meeting performance objectives they feel are too general and ideal. Insurance companies have voiced similar concerns. The main challenge for performance-based design requirements is to improve the user’s safety without increasing lawyer’s fees.

Code simplification — A concern voiced consistently and repeatedly by the design profession is the excessive complexity of current codes when applied in the design of small low-rise structures. The challenge in this respect is to provide in codes and design standards for simplified requirements relying on minimum dimensional requirements that are easy to meet and produce safe results. The publication by ACI of the document *Essential Requirements for Reinforced Concrete Buildings (For Buildings of Limited Size and Height Based on ACI 318-02)* (ACI IPS-1, 2002) is a welcome effort in trying to solve the code complexity concern. The challenge is to incorporate this type of documents within the scope of the model codes and extend this approach to other documents dealing with other structural materials such as masonry, structural steel and wood.

Nonlinear analysis-design procedures implications in stiffness and strength — The analysis of reinforced concrete structures specially using finite element procedures requires judgment and experience for introducing the appropriate descriptive parameters to take into account the nonlinear material properties of the constitutive materials, cracking and many issues that are not as relevant

or present in other structural materials. The transit from analysis to design is still an art for reinforced concrete structures and the advances in analysis have not been accompanied with a corresponding development in design techniques. The challenge in this area is the development of fail-safe design procedures compatible with current and future analysis advances that would lend themselves to study the nonlinearity of the materials and element dynamic response, cracked states and the issue that the tension resistance is provided by “discrete” reinforcing bars and is not a smeared property of the material.

Glossary

Base of structure — Level at which earthquake motions are assumed to be imparted to a building. This level does not necessarily coincide with the ground level.

Base shear — Total design lateral force or shear at the base.

Boundary elements — Portions along structural wall and structural diaphragm edges strengthened by longitudinal and transverse reinforcement. Boundary elements do not necessarily require an increase in the thickness of the wall or diaphragm. Boundary members include chords and drag struts at diaphragm and shear wall perimeters, interior openings, discontinuities and re-entrant corners. Edges of openings within walls and diaphragms shall be provided with boundary elements when required.

Collector elements — Elements that serve to transmit the inertial forces within structural diaphragms to members of the lateral-force-resisting systems.

Confined region — That portion of a reinforced concrete or reinforced masonry component in which the concrete or masonry is confined by closely spaced special transverse reinforcement restraining the concrete or masonry in directions perpendicular to the applied stress.

Coupling beam — A beam that is used to connect adjacent concrete wall elements to make them act together as a unit to resist lateral loads.

Crosstie — A continuous reinforcing bar having a seismic hook at one end and a hook not less than 90° with at least a six-diameter extension at the other end. The hooks shall engage peripheral longitudinal bars. The 90° hooks of two successive crossties engaging the same longitudinal bars shall be alternated end for end.

Design displacement — Total lateral displacement expected for the design-basis earthquake, as required by the governing code for earthquake-resistant design.

Design earthquake — The earthquake effects that are two thirds of the corresponding maximum considered earthquake.

Design earthquake ground motion — The earthquake effects that buildings and structures are specifically proportioned to resist.

Diaphragm — Roof, floor or other membrane or bracing system acting to transfer the lateral forces to the vertical resisting elements. Diaphragms are classified as either flexible or rigid according to the requirements of SEI/ASCE 7-02.

Essential facility — A structure required for postearthquake recovery.

Factored loads and forces — Loads and forces multiplied by appropriate load factors.

Frame

Braced frame — An essentially vertical truss, or its equivalent, of the concentric or eccentric type that is provided in a bearing wall, building frame or dual system to resist seismic forces.

Moment frame — Frame in which members and joints resist forces through flexure, shear and axial force. Moment frames shall be categorized as follows:

Intermediate moment frame — A cast-in-place frame complying with the requirements of ACI 318-02 Sections 21.2.2.3 and 21.12 in addition to the requirements for ordinary moment frames.

Ordinary moment frame — A cast-in-place or precast concrete moment frame complying with the requirements of Chapters 1 through 18 of ACI 318-02.

Special moment frame — A cast-in-place moment frame in which members and joints are capable of resisting forces by flexure as well as along the axis of the members. Special moment frames shall conform to the requirements of 21.2 through 21.5 of ACI 318-02. In addition, the requirements for ordinary moment frames shall be satisfied.

Frame system

Building frame system — A structural system with an essentially complete space frame providing support for vertical loads. Seismic force resistance is provided by shear walls or braced frames.

Dual frame system — A structural system with an essentially complete space frame providing support for vertical loads. Seismic force resistance is provided by moment-resisting frames and shear walls or braced frames.

Space frame system — A structural system composed of interconnected members, other than bearing walls, that is capable of supporting vertical loads and, when designed for such an application, is capable of providing resistance to seismic forces.

Hoop — A closed tie or continuously wound tie. A closed tie can be made up of several reinforcement elements each having seismic hooks at both ends. A continuously wound tie shall have a seismic hook at both ends.

Lateral force-resisting system — That portion of the structure composed of members proportioned to resist forces related to earthquake effects.

Plastic hinge region — Length of frame element over which flexural yielding is intended to occur due to design displacements, extending not less than a distance from the critical section where flexural yielding initiates.

Seismic design category — A classification assigned to a structure based on its seismic use group and the severity of the design earthquake ground motion at the site as defined in SEI/ASCE 7-02.

Seismic forces — The assumed forces prescribed by SEI/ASCE 7-02, related to the response of the structure to earthquake motions, to be used in the design of the structure and its components.

Seismic hook — A hook on a stirrup, hoop or crosstie having a bend not less than 135°, except that circular hoops shall have a bend not less than 90°. Hooks shall have a six-diameter (but not less than 75 mm) extension that engages the longitudinal reinforcement and projects into the interior of the stirrup or hoop.

Seismic use group — A classification assigned to a structure based on its use as defined in SEI/ASCE 7-02.

Site class — A classification assigned to a site based on the types of soils present and their engineering properties as defined in SEI/ASCE 7-02.

Site coefficients — The values of F_a and F_v as indicated in Tables 9.4.1.2.4a and 9.4.1.2.4b, respectively.

Special boundary elements — Boundary elements required by Sections 21.7.6.2 or 21.7.6.3 of ACI 318-02.

Special transverse reinforcement — Reinforcement composed of spirals, closed stirrups or hoops and supplementary crossties provided to restrain the concrete and qualify the portion of the component, where used, as a confined region.

Specified lateral forces — Lateral forces corresponding to the appropriate distribution of the design base shear force prescribed by the governing code for earthquake-resistant design.

Story drift — The difference of horizontal deflections at the top and bottom of the story.

Story drift ratio — The story drift divided by the story height.

Story shear — The summation of design lateral seismic forces at levels above the story under consideration.

Toughness — The ability of a material to absorb energy without losing significant strength.

Walls, structural — Walls proportioned to resist combinations of shears, moments and axial forces induced by earthquake motions. A shear wall is a structural wall. Structural walls shall be categorized as follows:

Ordinary reinforced concrete structural wall — A wall complying with the requirements of Chapters 1 through 18 of ACI 318-02.

Special reinforced concrete structural wall — A cast-in-place wall complying with the requirements of 21.2 and 21.7 of ACI 318-02 in addition to the requirements for ordinary reinforced concrete structural walls.

Wall system, bearing — A structural system with bearing walls providing support for all or major portions of the vertical loads. Shear walls or braced frames provide seismic force resistance.

List of Symbols

A_b	area of an individual bar, mm ²
A_B	base area of the structure, (m ² or ft ²)
A_c	trial area of column, mm ²
A_{ch}	cross-sectional area of a structural member measured out-to-out of transverse reinforcement, mm ²
A_{cp}	area of concrete section, resisting shear, of an individual pier or horizontal wall segment, mm ²
A_{cv}	gross area of concrete section bounded by web thickness and length of section in the direction of shear force considered, mm ²
A_g	gross area of section, mm ²
A_i	area of shear wall i (m ² or ft ²)
A_j	effective cross-sectional area within a joint in a plane parallel to plane of reinforcement generating shear in the joint, mm ² . The joint depth shall be the overall depth of the column. Where a beam frames into a support of larger width, the effective width of the joint shall not exceed the smaller of: (a) the beam width plus the joint depth, or (b) twice the smaller perpendicular distance from the longitudinal axis of the beam to the column side.
A_{sh}	total cross-sectional area of transverse reinforcement (including crossties) within spacing s and perpendicular to dimension h_e , mm ²
A_{vd}	total area of reinforcement in each group of diagonal bars in a diagonally reinforced coupling beam, mm ²
A_x	torsional amplification factor
A_x	floor area of the diaphragm level immediately above the story, m ²
b	effective compressive flange width of a structural member, mm
b_w	web width or diameter of circular section, mm
c	distance from the extreme compression fiber to neutral axis calculated for the factored axial force and nominal moment strength consistent with the design displacement δ_u at the top of the wall resulting in the largest neutral axis depth, mm
C_d	lateral deflection amplification factor
C_s	seismic response coefficient
C_t	building period coefficient
C_{vx}	lateral seismic force vertical distribution factor
C_w	coefficient used to obtain the approximate fundamental building period T_a
D	dead loads or related internal moments and forces
D_i	length of shear wall i (m or ft)
d	effective depth of section, mm
d_b	bar diameter, mm
d_c	out-to-out spiral diameter, mm
dx	component along x -axis of the lateral deflection at the center of mass
dy	component along y -axis of the lateral deflection at the center of mass
dz	rotation (in rad) about a vertical axis that passes through the center of mass of the diaphragm
e	eccentricity for computation of accidental torsion
E	load effects of earthquake or related internal moments and forces
E_c	modulus of elasticity of concrete, MPa
EI_{cr}	cracked flexural stiffness (slope of the line that joints the origin and the yield point), N·mm ²

EI_{eff}	effective flexural stiffness (slope of the line that joints the points of maximum displacement demand), N·mm ²
EI_g	uncracked flexural stiffness, N·mm ²
E_s	modulus of elasticity of reinforcement, MPa
F	loads due to weight and pressures of fluids with well-defined densities and controllable maximum heights or related internal moments and forces
F_a	acceleration-based site coefficient (at 0.3-sec period)
F_{ix}, F_{iy}	lateral force acting at level i of the structure in the x and y directions, respectively
F_v	velocity-based site coefficient (at 1.0-sec period)
F_p, F_n, F_i	the portion of the seismic base shear, V , induced at Level i , n or x , respectively
f'_c	specified compressive strength of concrete, MPa
$\sqrt{f'_c}$	square root of specified compressive strength of concrete, MPa
f_y	specified yield strength of reinforcement, MPa
f_{yh}	specified yield strength of the transverse reinforcement, MPa
f_{ypr}	probable yield strength of reinforcement ($f_{ypr} = 1.25 f_y$), MPa
g	acceleration due to gravity
H	loads due to weight and pressure of soil, water in soil or other materials or related internal moments and forces
h	overall thickness of member, mm
h_c	cross-sectional dimension of column core measured center-to-center of confining reinforcement, mm
h_i, h_x	height above the base to levels i or x , respectively
h_n	building height
h_s	story height
h_{sx}	story height below level x . $h_{sx} = h_x - h_{x-1}$
h_w	height of entire wall or of the segment of wall considered, mm
h_x	maximum horizontal spacing of hoop or crosstie legs on all faces of the column, mm
I	seismic occupancy importance factor
k	exponent related to the structure period used for distribution of story lateral forces
k_{cr}	cracked stiffness evaluated at first yielding of the tension reinforcement
k_g	uncracked stiffness associated with the gross properties of the element section
k_r	slope observed when the net applied force changes sign at the end of the unloading, also known as the reload stiffness
k_s	slope of the increase of strength caused by strain hardening of the tension reinforcement
k_u	unloading branch slope, expressed in terms of stiffness
L	live loads or related internal moments and forces
L_r	roof live load or related internal moments and forces
ℓ_d	development length for a straight bar, mm
ℓ_{dh}	development length for a bar with a standard hook, mm
ℓ_n	clear span measured face-to-face of supports, mm
ℓ_w	length of entire wall or of segment of wall considered in direction of shear force, mm
ℓ_o	minimum length, measured from joint face along axis of structural member, over which transverse reinforcement must be provided, mm
M	total mass of the building
M_D	unfactored dead load moment
M_f	overturning moment at foundation-soil interface
M_{L1}	unfactored live load moment caused by pattern loading in half of the bays
M_{L2}	unfactored live load moment caused by pattern loading in the remaining half of the bays
M_{pr}	probable moment strength determined using the properties of members at the joint faces, assuming a tensile strength in the longitudinal bars f_{ypr} instead of f_y ($f_{ypr} = 1.25 f_y$) and a strength reduction factor $\phi = 1.0$, N·mm

M_{QET}	flexural moment caused by the effect of accidental torsion
M_{QEx}	flexural moment caused by the seismic forces acting only in the x -direction
M_{QEy}	flexural moment caused by the seismic forces acting only in the y -direction
M_t	the torsional moment resulting from the location of the building masses
M_{ta}	accidental torsional moment
M_u	factored moment at section, N·mm
M_x	building overturning design moment at level x
N	building number of stories
\bar{N}	average field standard penetration resistance for the top 30 m of soil
\bar{N}_{ch}	average standard penetration resistance for cohesionless soil layers for the top 30 m of soil
n	number of shear walls in the building effective for resisting lateral forces in the direction under consideration
n_{cex}	number of exterior columns in the direction of interest (columns where only one girder parallel to direction of interest frame at each joint)
n_{cin}	number of interior columns in the direction of interest (columns where two girders parallel to direction of interest frame at each joint)
p	wall index (ratio of wall area in direction of interest to floor area)
PI	plasticity index
P_u	factored axial load
P_x	total vertical design load at and above level x
Q	stability index for a story in ACI 318-02 (analogous to Θ in SEI/ASCE 7-02)
Q_E	effect of horizontal seismic (earthquake-induced) forces
R	response modification coefficient
R	rain load or related internal moments and forces
r_{maxx}	ratio of the design story shear resisted by the single element carrying the largest shear force in the story to the total story shear, for a given direction of loading
s	spacing of transverse reinforcement measured along the longitudinal axis of the structural member, mm
\bar{s}_u	average undrained shear strength in top 30 m of soil
s_x	longitudinal spacing of transverse reinforcement within the length ℓ_o , mm
s_o	maximum spacing of transverse reinforcement, mm
S	snow load or related internal moments and forces
S_1	mapped maximum considered earthquake, 5% damped, spectral response acceleration at a period of 1 sec
S_a	design spectral response acceleration
S_{aM}	maximum considered earthquake spectral response acceleration at any period
S_{D1}	spectral design response acceleration at 1-sec period
S_{DS}	design spectral response acceleration at short periods
S_{M1}	maximum considered earthquake, 5% damped, spectral response acceleration at a period of 1 sec, adjusted for site effects
S_{MS}	maximum considered earthquake, 5% damped, spectral response acceleration at short periods adjusted for site effects
S_s	mapped spectral response acceleration at short periods
T	fundamental period of the building in sec
T	cumulative effect of temperature, creep, shrinkage, differential settlement and shrinkage-compensating concrete
T_a	approximate fundamental period of the building in sec
T_o	$0.2 S_{D1}/S_{DS}$
T_s	S_{D1}/S_{DS}
U	required strength to resist factored loads or related internal moments and forces
\bar{v}_s	average shear wave velocity in the top 30 m of soil beneath the foundation at large strain levels, m/s

V	total design lateral force or shear at the base of the structure
V_c	nominal shear strength provided by concrete, N
$V_{col-ext}$	fraction of V_x assigned to an exterior column
$V_{col-int}$	fraction of V_x assigned to an interior column
V_e	design shear force corresponding to the probable moment strength of the column at the face of the joints, N
V_n	nominal shear strength, N
V_t	design base shear obtained from the modal response spectrum dynamic analysis
V_u	factored shear force at section, N
V_x	seismic design story shear force acting at story x
W	effective seismic weight of the structure, including the total dead load and: (1) in areas used for storage, a minimum of 25% of the floor live load (floor live load in public garages and open parking structures need not be included.) (2) where an allowance for partition load is included in the floor load design, the actual partition weight or a minimum weight of 0.48 kN/m ² of floor area, whichever is greater (3) total operating weight of permanent equipment (4) 20% of flat roof snow load where flat roof snow load exceeds 1.44 kN/m ²
W	wind load or related internal moments and forces
w_d	building weight per unit area
w_D	nonfactored dead load
w_i, w_x	portion of the total gravity load of the structure (W) located or assigned to levels i or x , respectively
w_L	nonfactored live load
x	exponent used to obtain the approximate fundamental building period T_a
x_a, y_a	coordinates of point a in a coordinate system with the origin at the center of mass
ΣM_c	sum of the nominal flexural strengths (M_n) of columns framing into a joint moment at the face of the joint, calculated for the factored axial force, consistent with the direction of the lateral forces considered, resulting in the lowest flexural strength, N·mm
ΣM_g	sum of the nominal moment strengths (M_n) of girders at the face of the joint, including slab where in tension, framing into that joint, N·mm
α	angle between the diagonal reinforcement and the longitudinal axis of a diagonally reinforced coupling beam
α_c	coefficient defining the relative contribution of concrete strength to wall strength
b	ratio of shear demand to shear capacity for story x
δ_{avg}	average of the lateral displacements at extreme points of the structure at level x
δ_{max}	maximum lateral displacement at level x
δ_u	design displacement, mm
δ_x	lateral deflection at the center of mass of level x
δ_{x-1}	lateral deflection at the center of mass of level $x-1$
δ_{xe}	lateral deflection of level x at the center of mass obtained from the elastic analysis made using the prescribed forces already divided by the response modification coefficient R
Δ	the design story drift occurring simultaneously with V
Δ_x	story drift obtained as the difference of the lateral deflections at the top and bottom of the story x under consideration, δ_x and δ_{x-1} , respectively
m	displacement ductility
q	stability coefficient for P-delta evaluation
θ_{max}	maximum permitted value for stability coefficient
r	a reliability coefficient based on the extent of structural redundancy present in a building
r	ratio of nonprestressed tension reinforcement, $\rho = A_s/(bd)$
ρ_g	ratio of total longitudinal reinforcement area to cross-sectional area of column
ρ_n	ratio of area of distributed reinforcement parallel to the plane of A_c to gross concrete area perpendicular to that reinforcement

ρ_s	ratio of volume of spiral reinforcement to the core volume confined by the spiral reinforcement (measured out-to-out)
ρ_v	ratio of area of distributed reinforcement perpendicular to the plane of A_{cv} to gross concrete area A_{cv}
ρ_x	reliability coefficient based on redundancy present in direction x
f	strength reduction factor
w	moisture content of soil in percent
Ω_0	overstrength factor

References

- ACI Committee 318 (2002), Building Code Requirements for Structural Concrete (ACI 318-02) and Commentary (ACI 318R-02). American Concrete Institute, Farmington Hills, Michigan, 443 p.
- ACI IPS-1 (2002), Essential Requirements for Reinforced Concrete Buildings (For Buildings of Limited Size and Height Based on ACI 318-02). ACI International Publication Series IPS-1, American Concrete Institute, Farmington Hills, Michigan, 248 pp.
- ACI-ASCE Committee 442 (1991), Earthquake-resistant concrete structures inelastic response and design. Ghosh, S. K., Editor, Special Publication SP-127, American Concrete Institute, Detroit, MI, 558 p.
- Algan, B. B. (1982), Drift and Damage Considerations in Earthquake-Resistant Design of Reinforced Concrete Buildings. University of Illinois at Urbana-Champaign, Urbana, IL, 227 p.
- Arnold, C. (2001), Architectural Considerations. Chapter 6 of The Seismic Design Handbook, 2nd ed., Naeim, F., Ed., Kluwer Academic Publishers, Boston, MA, 2001, 830 p.
- Arnold, C. and Reitherman, R. K., (1982), *Building Configuration and Seismic Design*. John Wiley & Sons, New York, 296 p.
- Blume, J. A., Newmark, N. M. and Corning, L. H. (1961), Design of Multistory Reinforced Concrete Buildings for Earthquake Motions. Portland Cement Association, Skokie, IL, 318 p.
- BOCA (1996), The BOCA National Building Code, 13th Edition. Building Officials and Code Administrators, Inc., Country Club Hills, Illinois, 357 p.
- Cross, H. (1935), The Relation of Analysis to Structural Design. *Proceedings, American Society of Civil Engineers*, Vol. 61, October.
- CRSI (2001), CRSI Handbook. 9th Ed., Concrete Reinforcing Steel Institute, Schaumburg, IL, 960 p.
- Fanella, D. A. (2000), Seismic Detailing of Concrete Buildings. Portland Cement Association, Skokie, IL, 69 p.
- Fanella, D. A. and Munshi, J. A. (1998a), Design of Low-Rise Concrete Buildings for Earthquake Forces. 2nd ed., Portland Cement Association, Skokie, IL, 126 p.
- Fanella, D. A. and Munshi, J. A. (1998b), Design of Concrete Buildings for Earthquake and Wind Forces According to the 1997 Uniform Building Code. Portland Cement Association, Skokie, IL, 135 p.
- FEMA (2001), NEHRP Recommended Provisions for the Development of Seismic Regulations for New Buildings — 2000 Ed., and Commentary. Part 1 — Provisions (FEMA 368) and Part 2 — Commentary (FEMA 369), Building Seismic Safety Council, Federal Emergency Management Agency, Washington D.C., 2 volumes.
- FEMA (1997), NEHRP Recommended Provisions for the Development of Seismic Regulations for New Buildings and Other Structures — 1997 ed., and Commentary. Part 1 — Provisions (FEMA 302) and Part 2 — Commentary (FEMA 303), Building Seismic Safety Council, Federal Emergency Management Agency, Washington D.C., 2 vol.
- Garcia, L. E. (1996), Economic considerations of displacement based seismic design of structural concrete buildings. *Structural Engineering International*, International Association of Bridge and Structural Engineering, IABSE, Zurich, Switzerland, November.

- Garcia, L. E., Perez, A. and Bonacci, J. (1995), Cost Implications of Drift Controlled Design of Reinforced Concrete Buildings. *Proceedings 11th World Conference on Earthquake Engineering*, Acapulco, Mexico.
- Gulkan, P. and Sozen, M. A. (1974), Inelastic Response of Reinforced Concrete Structures to Earthquake Motions, *ACI Journal, Proceedings* V. 71, pp. 604–610.
- Gupta, A. K. and Moss, P. J., Eds. (1993), *Guidelines for Design of Low-Rise Buildings Subjected to Lateral Forces*. Council on Low-Rise Buildings, North Carolina State University, Raleigh, North Carolina, CRC Press, Boca Raton, FL, 286 p.
- Hueste, M. B. and Wight, J. K. (1999), Nonlinear punching shear failure model for interior slab-column connections, *J. Structural Engineering*, ASCE, Vol. 125, pp. 997—1008.
- ICBO (1997), Uniform Building Code — 1997. International Conference of Building Officials ICBO, Whittier, CA, 3 volumes.
- ICC (2003), International Building Code 2003. Published in cooperation by BOCA, ICBO and SBCCI, International Code Council, 632 p.
- NFPA (2003), NFPA 5000 — NFPA Building Construction and Safety Code. National Fire Protection Association, Quincy, MA, 540 p.
- PCA (2002), Notes on ACI 318-02 with Design Applications. Portland Cement Association, Skokie, IL, 1 vol.
- SEAOC — Seismology Committee (1999), Recommended Lateral Force Requirements and Commentary. 7th ed., Structural Engineers Association of California, SEAOC, Sacramento, CA, 440 p.
- SEI/ASCE (2003), Minimum Design Loads for Buildings and Other Structures (SEI/ASCE 7-02). Structural Engineering Institute, American Society of Civil Engineers, Reston, VA, 376 p.
- Shibata, A. and Sozen M.A. (1976), Substitute-structure method for seismic design in R/C. *J. Struct. Div.*, ASCE, Vol. 102, No. ST1, 1–18.
- Sozen, M. A., (1989), The Chilean Formula for Earthquake Resistant Design of Medium-Rise Reinforced Concrete Structures. *Proceedings 5th Chilean Conference on Earthquake Engineering*, Santiago, Chile, August, 24 p.
- Sozen, M. A., (1974), Hysteresis in Structural Elements. Applied Mechanics in Earthquake Engineering, AMD8, American Society of Mechanical Engineers, New York, NY, pp. 63–98.
- Wilson, E. L. and Dovey, H. H. (1972), Three Dimensional Analysis of Building Systems — TABS. Report EERC 72-8, University of California, Berkeley, CA, 78 p.

15

Seismic Design of Steel Moment Frames

James Malley

Qi-Song “Kent” Yu

Kevin Moore

15.1	Introduction	15-1
15.2	The FEMA/SAC Program: Efforts to Reduce Earthquake Hazards in Steel Moment Frame Structures	15-3
	Phase 1 Activities • Phase 2 Activities • Description of Recommended Design Guideline Documents	
15.3	SMF Connection Design Considerations	15-7
	Selection of Connection Type • AISC Seismic Criteria • SMF 350 Connection Details • Design Example—RBS • Full-Size Subassemblage Testing • Connection Details • Fabrication • Nondestructive Evaluation, Testing and Inspection	
15.4	Design of Repair and Upgrade Measures for Existing pre-Northridge SMF Connections	15-23
	General • Moment Connection Research from FEMA/SAC Steel Program Phase 1 • Moment Connection Research from NIST/AISC Program • Connection Modification Options • SMF Upgrade Methodologies — Simplified and Systematic Approaches • Design Example for Connection Seismic Upgrade	
15.5	The 2002 AISC Seismic Provisions	15-33
15.6	Recommendations for Future Work	15-36
15.7	Concluding Remarks	15-36

15.1 Introduction

Welded steel moment frames (WSMF) are commonly used in the United States and elsewhere around the world to construct single-story and multistory buildings. This structural system can be easily configured to accommodate a variety of functional and architectural requirements. Early applications of steel moment frames occurred during the first part of the twentieth century. These frames utilized riveted moment-resisting connections designed to resist nominal wind loads. In most cases, these buildings were clad with unreinforced masonry that provided substantial additional strength and stiffness for the resistance of lateral loads. This class of structure has generally provided life-saving performance following a number of major U.S. earthquakes, including the 1906 San Francisco earthquake (Himmelwright, 1906).

As a result of this commendable early performance record and the modernization of the steel building construction industry, engineers in the United States began to make modifications to the steel moment frame system. In the 1950s, high strength bolting replaced riveted construction. Field welding procedures made the connection of large structural shapes a viable alternative in the late 1960s and early 1970s. At about the same time a movement toward much lighter and more flexible cladding systems for modern

15-2 Earthquake Engineering: From Engineering Seismology to Performance-Based Engineering

buildings meant that the steel frames would no longer benefit from the additional stiffness and strength provided by the masonry cladding used in the older buildings. In many buildings this stiffness was replaced by reinforced concrete walls at the building perimeter or around stair and elevator shafts or all of these. In other buildings, all of the lateral resistance was provided by the steel moment frames.

During this same time frame, engineers continued to search for more economical approaches to steel frame construction. Early applications of steel moment frames (SMF) usually included moment-resisting connections to all columns in both orthogonal directions. For interior columns, this would result in so-called “four way” moment connections. These connections were expensive to construct, and as a result, engineers began to seek ways to limit the number of these connections. The advent of larger rolled structural shapes in the post-World War II era allowed engineers to achieve equivalent lateral stiffness and strength with fewer moment frames, providing some cost savings in the structural steel fabrication and erection. Initially, these less redundant frames incorporated the moment connections at the entire building perimeter with simple connections at the interior columns. As engineers became more comfortable with this approach, they continued to minimize the number of lateral force resisting elements in these moment frames, eventually resulting in many buildings where only one or two bays of moment-resisting connections were provided at the building perimeter. While this approach appeared to provide some economic savings on the total building steel tonnage, the use of a minimal number of frames required the use of very large member sizes (and therefore, very large full penetration field welds) to meet the drift requirements of the building code.

Engineers also attempted to minimize the cost of fabricating the moment-resisting connections. Early moment connections used full penetration welds between the entire beam section (both flanges and the web) and the column. These welds were completed in the field as part of the erection of the steel frame. In the early 1970s, a series of tests on small W18 and W24 beam shapes conducted at the University of California at Berkeley by Professor Egor Popov demonstrated that connections with welded flanges and high strength bolted webs could achieve some inelastic rotation prior to fracturing the flange welds (Popov and Stephen, 1972). Since these connections were more economical to fabricate and erect than the welded beam detail, they quickly became the industry standard and were eventually codified into the 1988 Uniform Building Code.

A number of earthquakes that occurred during the latter half of the 1900s appeared to confirm the good performance of steel moment frame buildings (SMF). In the 1964 Alaska earthquake, a number of SMF with reinforced concrete shear walls performed well, with cracking observed in the concrete walls, but apparently little damage to the steel frames (Berg, 1973). In the 1971 San Fernando earthquake, a number of more modern steel frame buildings appeared to have survived the event intact and were analyzed extensively to evaluate the demands imposed on the system by the ground motion (U.S. Department of Commerce, 1973). The only steel moment frame building shaken by the 1972 Managua, Nicaragua earthquake also appeared to have come through the event unscathed (EERI, 1973). Finally, the lack of damage found in investigations immediately following the 1989 Loma Prieta earthquake appeared to affirm the notion (incorrectly, following the reinvestigation of a number of buildings subsequent to the Northridge earthquake) that SMF provided excellent seismic performance.

By the early 1990s, the performance in previous earthquakes and favorable results from early experimental and analytical investigations led building code developers and structural engineers in the United States to regard the WSMF as one of the best systems available for resisting the damaging effects of earthquakes. As a result, the system was widely used in areas of high seismicity for many major and important buildings.

One of the major signatures of the 1994 Northridge earthquake was the discovery of widespread brittle fractures in the critical beam-to-column connections in a number of WSMF buildings. Damage was observed in a wide variety of WSMF buildings: new as well as old structures; tall buildings as well as short ones; commercial, office and residential buildings as well as hospitals and other major public facilities.

A wide spectrum of brittle connection damage was discovered, ranging from minor cracking to completely severed beams and columns. The most commonly observed damage was located in or near the welded joint connecting a girder bottom flange to the supporting column flange (see Figure 15.1).

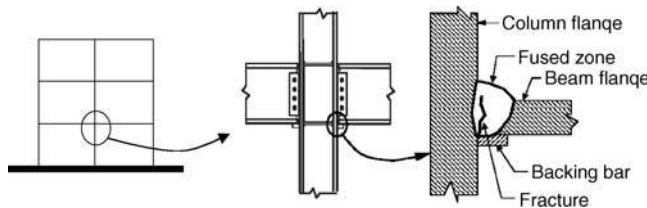


FIGURE 15.1 Common zone of fracture initiation in a typical beam–column connection.

Interestingly, connection fractures were detected in buildings located in regions of relatively modest ground shaking (e.g., below 0.3g peak ground acceleration). In areas with more intense shaking, some buildings were discovered with fractures at all of the moment-resisting connections in one or more floors, resulting in significant permanent lateral displacements. Damage was so severe in a few buildings that they were demolished or evacuated following the earthquake.

Recent investigations have confirmed the presence of similar, though previously undetected, damage in WSMF buildings shaken by the 1989 Loma Prieta, 1992 Landers and 1992 Big Bear earthquakes. Documentation of damage to steel moment frame connections in Northridge and other earthquakes can be found in Bertero et al. (1994). The 1995 Hyogo-ken Nanbu earthquake subjected WSMF steel buildings in Kobe, Japan, to motions more intense than any WSMF steel building has yet experienced in the United States. While Japanese construction practices differ from those used in the United States in several basic ways, WSMF buildings in Kobe suffered even more severe damage than that observed in California; in fact, more than 10% of these structures collapsed. A more detailed discussion of the characteristics and frequency of various types of damage to WSMF structures in the United States, Japan and elsewhere can be found in FEMA-355E (FEMA, 2000j).

No loss of life resulted from damage to WSMF structures in the United States and none of these structures collapsed. Because of the performance observed to date, the basic life safety objective of building codes was deemed to be met. However, little evidence of ductile yielding prior to fracture has been found in damaged buildings in the United States. Such brittle, as opposed to ductile, behavior is contrary to the basic tenets of modern seismic-resistant design and the intent of contemporary building codes. This brittle behavior has raised questions about the safety of WSMF structures in the United States in the event they are subjected to larger earthquakes.

The effect of this brittle damage was a general loss of confidence in the procedures used to design and construct welded connections in SMF. As a result, late in 1994 building code provisions in the United States were quickly changed to require that new WSMF designs be substantiated by testing or test-backed calculations or both. While addressing the safety of individual structures, these provisions did not provide definitive answers identifying the factors that contributed to this unprecedented behavior. Numerous questions remained about the effectiveness of methods to inspect, evaluate and repair WSMF buildings damaged in the Northridge earthquake as well as the safety of existing WSMF structures that might be subjected to future, and possibly stronger, earthquakes.

This chapter will address many of the advances that have been made since the Northridge earthquake to improve the performance of SMF structures. New research results related to both the design of new structures and the rehabilitation of existing structures will be presented. The incorporation of these results into design standards will be discussed. Design examples are provided to explain many of the new concepts and techniques. For issues related to steel braced frames, the reader is referred to Chapter 16.

15.2 The FEMA/SAC Program: Efforts to Reduce Earthquake Hazards in Steel Moment Frame Structures

Answering the questions raised by the Northridge earthquake damage involves consideration of many complex technical, professional and economic issues, including metallurgy, welding, fracture mechanics,

connection behavior, system performance and practices related to design, fabrication, erection and inspection. The state of knowledge in many of these areas was judged inadequate following the Northridge earthquake and the development of rapid reliable and cost-effective solutions was deemed necessary. As a result, the U.S. Federal Emergency Management Agency (FEMA) initiated a comprehensive 6-year program of investigation, guideline development and professional training to develop and evaluate guidelines for the inspection, evaluation, repair, rehabilitation and construction of SMF structures.

FEMA's program to reduce earthquake hazards in steel moment frame structures involved more than 120 engineers, researchers, construction experts and other specialists from throughout the United States. FEMA selected the SAC Joint Venture to manage and administer this complex program. The joint venture consisted of three not-for-profit professional and educational organizations: the Structural Engineers Association of California (SEAOC), Applied Technology Council (ATC) and California Universities for Research in Earthquake Engineering (CUREE). Each organization had experience, capabilities and resources that could uniquely contribute to different aspects of this project.

15.2.1 Phase 1 Activities

The overall program was conducted in two phases. The first phase (Phase 1) focused on the rapid development of interim guidelines for the inspection, evaluation, repair, modification and construction of WSMF structures. This phase was supported by limited amounts of testing and topical investigations. These studies included a survey of damage to steel frame buildings in the Los Angeles area (SAC, 1995e), detailed dynamic analyses of buildings sustaining moderate amounts of damage (SAC, 1995a) and parametric analytical studies of factors that may have contributed to the observed behavior (SAC, 1995d). Experimental efforts in the first phase included ambient vibration tests of damaged buildings, tests of idealized weldments (SAC, 1995b), tests of damaged connections removed from buildings and tests of full-size beam-to-column connections representative of initially undamaged pre-Northridge details, repaired damaged connections and upgraded details intended for use in new construction (SAC, 1995c).

Significantly, all of the full-size specimens tested to evaluate the behavior of well-constructed "pre-Northridge" connections failed in a sudden brittle fashion. Tests of repaired or new connections generally, though not always, exhibited limited amounts of ductile behavior when constructed using high toughness weld metal, careful attention to quality control and connection details that reinforced the weld region at the face of the column by means of heavy cover plates or haunches. Tests and preliminary finite element analyses of these connections indicated that behavior was sensitive to numerous factors and that several common design assumptions regarding the load transfer mechanism and stress distribution in beam to column connections were not valid. As a result, it was not surprising that conventional analyses of buildings subjected to the Northridge earthquake provided only crude indications of the likely location and severity of fractures. Additional details of these initial investigations have been summarized by Mahin et al. (1998).

Based on these early results, a set of *Interim Guidelines: Evaluation, Repair, Modification and Design of Welded Steel Moment Frame Structures* were developed by FEMA in August 1995 (FEMA, 1995). The scope of the *Interim Guidelines* covered welding procedures, quality assurance, postearthquake actions and new construction. Specific chapters cover: (a) welding and metallurgy; (b) quality control and assurance; (c) visual inspection; (d) nondestructive testing; (e) classification and implications of damage; (f) postearthquake evaluation; (g) postearthquake inspection; (h) postearthquake repair and modification and (i) new construction. Recommendations permitted the use of a range of welded beam to column connection styles, including cover plated, haunched and reduced beam section connections, provided satisfactory test results could be found (or conducted) for geometrically and mechanically similar specimens. Two major revisions of these guidelines were released during the second phase of the program (FEMA, 1997b, 1999) as a means of providing as much current information as possible to practicing engineers using the document.

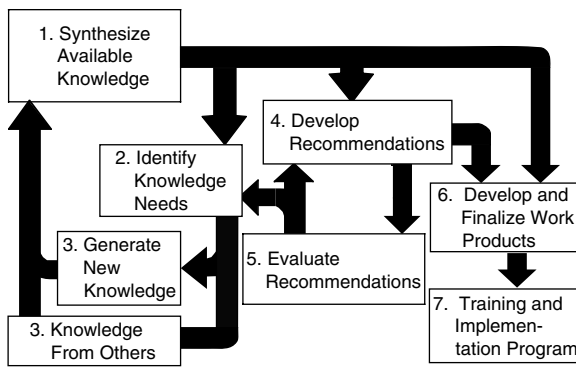


FIGURE 15.2 Technical approach for the Phase 2 steel project.

15.2.2 Phase 2 Activities

The second phase of the program (Phase 2) built upon findings from Phase 1 and other programs and undertook a variety of research and professional activities necessary to more fully achieve the objectives of the program. The specific objective identified for the Phase 2 program was to develop reliable, practical and cost-effective guidelines and standards of practice for SMF buildings related to:

1. The identification, inspection and rehabilitation of existing at-risk buildings prior to a damaging earthquake.
2. The identification, inspection and repair or upgrading of damaged buildings following an earthquake.
3. The design and construction of new buildings.

The Phase 2 program broadened the scope of the project to provide more focus on existing buildings not yet subjected to earthquakes and to include the use of partially and fully restrained bolted connections as an alternative to welded connections in moment frames. To better achieve the goals of project and to understand and quantify the contribution of various factors contributing to the performance of SMF construction, a reliability-based approach to performance-based engineering was incorporated as an integral feature of the Phase 2 effort.

The technical approach for the Phase 2 Steel Project is schematically illustrated by Figure 15.2. It involved seven basic steps:

1. Synthesize current and new knowledge.
2. Evaluate this knowledge to identify specific information needed to develop and verify the new seismic design criteria.
3. Generate the needed knowledge through research, testing and design applications or through acquisition of research results and other information generated by others.
4. Develop recommendations for inspection, evaluation, repair and rehabilitation of existing steel frame buildings and for the design and construction of new ones.
5. Evaluate the technical merit and feasibility of these recommendations, including an assessment of their economic and political impacts, through peer assessments, trial designs, physical testing and other means.
6. Develop, review and finalize the seismic design criteria and other documentation.
7. Implement a knowledge dissemination program.

The intent of this approach was to foster innovation, while simultaneously developing design methodologies and details that would be reliable, feasible and economical. This necessitated balanced consideration of the multidisciplinary technical, professional, economic, social and political issues involved. Care

was exercised to coordinate efforts in the Phase 2 Program with other research and guideline development activities in the United States and abroad.

15.2.3 Description of Recommended Design Guideline Documents

The Phase 2 steel project culminated in the development of design guidelines applicable to SMF buildings located throughout the United States in areas of low, medium and high seismicity. Prior to completion, each of these documents received extensive internal review. Several review workshops and requests for written comments were used to obtain independent external review. The guideline documents were prepared by a team of industry experts and design professionals. The major project recommendations, along with explanatory commentary, are contained in:

- *Recommended Seismic Design Criteria for New Steel Moment Frame Buildings*: This publication provides recommended criteria for the design of new SMF buildings to resist the effects of earthquakes (FEMA, 2000a, <http://www.fema.gov/hazards/earthquakes/fema350.shtm>).
- *Recommended Seismic Evaluation and Upgrade Criteria for Existing Welded Steel Moment Frame Buildings*: This publication provides recommended methods to evaluate the probable performance of existing SMF buildings in future earthquakes and to retrofit these buildings for improved performance (FEMA, 2000b, <http://www.fema.gov/hazards/earthquakes/fema351.shtm>).
- *Recommended Postearthquake Evaluation and Repair Criteria for Welded, Steel Moment Frame Buildings*: This publication provides recommendations for performing postearthquake inspections to detect damage in SMF buildings following an earthquake, evaluating the damaged buildings to determine their safety in the postearthquake environment and repairing damaged buildings (FEMA, 2000c, <http://www.fema.gov/hazards/earthquakes/fema352.shtm>).
- *Recommended Specifications and Quality Assurance Guidelines for Steel Moment Frame Construction for Seismic Applications*: This publication provides recommended supplemental specifications and recommended procedures to ensure that SMF are constructed with sufficient quality to perform as intended when subjected to severe earthquake loading (FEMA, 2000d, <http://www.fema.gov/hazards/earthquakes/fema353.shtm>).

Detailed derivations and explanations of the basis for these design and evaluation recommendations are given in a series of State of the Art Reports. These reports include:

- *State of the Art Report on Base Metals and Fracture*: This report summarizes current knowledge of the properties of structural steels commonly employed in building construction and the production and service factors that affect these properties (FEMA, 2000f).
- *State of the Art Report on Welding and Inspection*: This report summarizes current knowledge of the properties of structural welding commonly employed in building construction, the effect of various welding parameters on these properties and the effectiveness of various inspection methodologies in characterizing the quality of welded construction (FEMA, 2000g).
- *State of the Art Report on Systems Performance*: This report summarizes an extensive series of analytical investigations into the demands induced in SMF buildings designed to various criteria, when subjected to a range of different ground motions. The behavior of frames constructed with fully restrained, partially restrained and fracture-vulnerable connections is explored for a series of ground motions, including motion anticipated at near-fault and soft-soil sites (FEMA, 2000h).
- *State of the Art Report on Connection Performance*: This report summarizes the current state of knowledge of the performance of different types of moment-resisting connections under large inelastic deformation demands. It includes information on fully restrained, partially restrained and partial strength connections, both welded and bolted, based on laboratory and analytical investigations (FEMA, 2000i).
- *State of the Art Report on Past Performance of SMF Buildings in Earthquakes*: This report summarizes investigations of the performance of SMF buildings in past earthquakes, including the 1995 Kobe,

1994 Northridge, 1992 Landers, 1992 Big Bear, 1989 Loma Prieta and 1971 San Fernando events (FEMA, 2000j).

- *State of the Art Report on Performance Prediction and Evaluation:* This report describes the results of investigations into the ability of various analytical techniques, commonly used in design, to predict the performance of SMF buildings subjected to earthquake ground motion. Also presented is the basis for performance-based evaluation procedures contained in the design criteria and guideline documents, FEMA-350 to FEMA-353. (FEMA, 2000k).

In addition to the recommended design criteria and the State of the Art Reports, a companion document was prepared for building owners, local community officials and other nontechnical audiences who need to understand this issue. A *Policy Guide to Steel Moment-Frame Construction* (FEMA, 2000e), addresses the social, economic and political issues related to the earthquake performance of SMF buildings. FEMA 354 also includes discussion of the relative costs and benefits of implementing the recommended criteria.

15.3 SMF Connection Design Considerations

SMF are designed to resist lateral forces associated with moderate to severe earthquakes through the yielding and plastic deformation of frame members without significant strength degradation. The intended and preferred location for plastic deformation is the formation of plastic hinges in the beams near their connections to the columns. These plastic hinges are intended to dissipate energy delivered to the building by the earthquake without detrimental damage to the frame. The plastic hinge is expected to deform through moderate yielding and localized buckling of the steel elements without brittle fractures. Because of the moderate yielding and lack of detrimental damage to the frame, building codes allow the design of these systems for earthquake forces that are much lower than the actual expected earthquake demands (i.e., high R factor).

When designing a new SMF, the engineer must size beams and columns to limit drift of the system to an acceptable level established by the building codes. Once the column bay and floor-to-floor height are established, the engineer iterates through the sizing of beams and columns for the most efficient combination of sections to meet the drift limits. Stiffness of most moment connections is normally large enough that elastic flexibility of the connection does not require special consideration in the global SMF analysis. This process would be very straightforward if there were no limitations placed on the sizes of individual members or allowable combinations of beams and columns. Limitations on individual beam and column sizes are recommended in documents such as FEMA 350 to reflect available test results. The general design process recommended in FEMA 350 is paraphrased below:

- Select a structural system type and frame configuration.
- Select preliminary frame member sizes and perform a structural analysis for earthquake loading and frame adequacy using the applicable R , C_d and Ω_0 values, strength criteria, drift limits and redundancy requirements.
- Select an appropriate connection type. Connections may be prequalified, project qualified or proprietary.
- Perform an analysis considering the effects (if any) of the selected connection type on frame stiffness and behavior, to confirm the adequacy of member sizing to meet the applicable strength, drift and stability limitations.
- Confirm or revise the member sizing based on the connection type selected and results of the analysis completed as part of Step 4; return to Step 4, if required.
- Complete the design of the connections considering panel zone behavior, strong column-weak beam requirements and other connection limitations.

Research completed as part of the FEMA/SAC Phase 2 project has shown that on average less ductility can be expected from large-size beams and welds as compared to smaller beams and welds. This condition

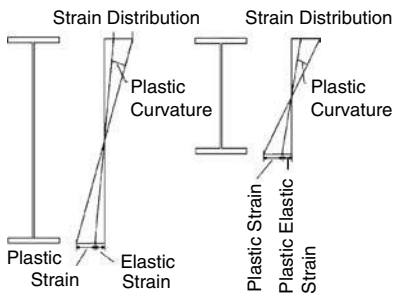


FIGURE 15.3 Elastic and plastic strain distribution (FEMA 355D).

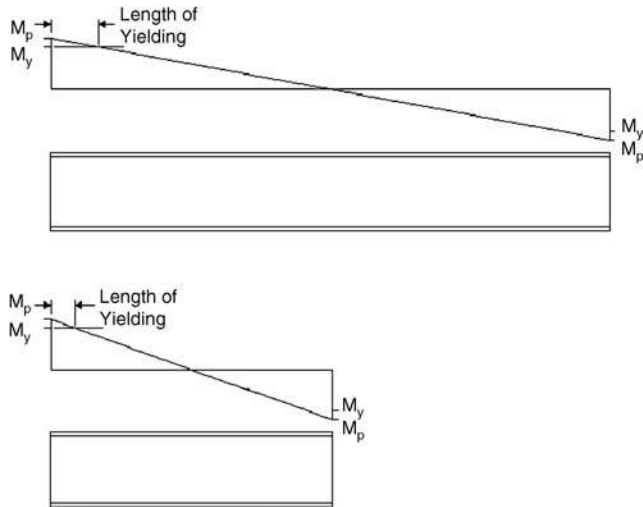


FIGURE 15.4 Span effect on M_p (FEMA 355D).

is applicable for all moment connection types. The reasons for this behavior can be explained using mechanics as illustrated in Figure 15.3. The elastic and plastic strain distribution shown in the two beams are identical except for beam depth. Plastic curvature is defined as the difference between the elastic and plastic strains at the two extreme fibers divided by the beam depth. The plastic strain capacity of a deep beam is also a property of the material and flange geometry. This plastic strain capacity is not increased by increasing beam depth. Therefore, maximum plastic curvature in a deep beam is smaller than that for a shallow beam of the same material and flange geometry. Plastic curvature is integrated over the yield length to obtain plastic rotation. Therefore, smaller plastic rotations are expected for deeper beams if the beam length is essentially constant. In general, the maximum plastic rotation capacity of a beam is inversely proportional to the beam depth. This is discussed further in FEMA 355D.

Short-span beams have less inelastic rotational capacity than longer-span beams. The moment diagram for a moment frame beam under lateral loading (moments applied at the ends of the beams with identical directions) graphically representing the elementary mechanics that provide a basis for understanding this phenomenon is illustrated in Figure 15.4. One type of moment connection, welded-flange-bolted-web, is designed so that plastic hinges form near or at the face of the column. The plastic hinge (and the corresponding plastic rotation) of the beam develops over the short length of the beam, where the applied moment is larger than the yield moment, M_y . This length is limited by the plastic moment, M_p , which considers the strain hardening of the steel and the length of the beam. Regardless of the length or depth of the beam, M_y will occur when yield strain reaches the extreme fiber of the flange and M_p is achieved

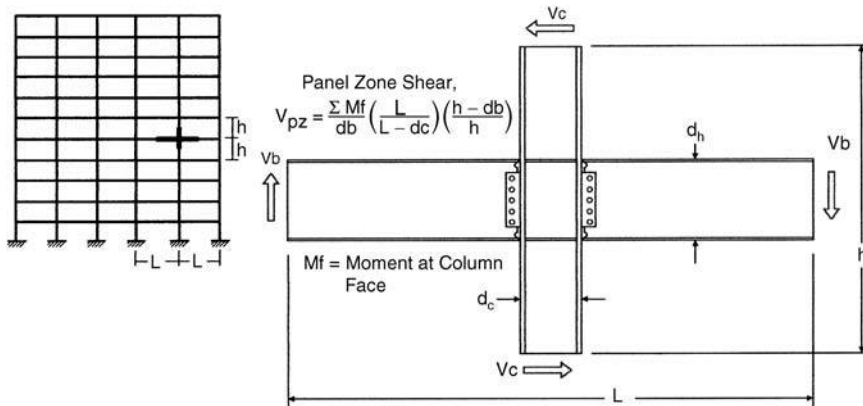


FIGURE 15.5 Calculation of panel zone shear (FEMA 355D).

as the beam continues to resist moment to plastic strains throughout the cross section which are three to six times larger. The length of the beam does not change the maximum strain capacity or the maximum curvature capacity for a particular beam cross section. Plastic curvature is largest at the maximum moment and it decreases to zero at the yield moment. Plastic rotation is the integration of the plastic curvature over the short length of the beam where the applied moment is larger than the yield moment. Therefore, the plastic rotation of the beam depends upon the length of the beam, if the beam depth is constant, because plastic curvature is accumulated over a proportionally shorter length. In general, maximum plastic rotation capacity of a beam is directly proportional to the beam length. Variations in strain hardening and the relationship between the yield strength of steel and the ultimate tensile strength of steel (yield to tensile ratio) cloud this observation. Connections that do not develop their plastic hinge over a length of the beam also do not exhibit this behavior.

The design of SMF must also consider the effect of panel zone yielding on connection performance. Panel zone yielding has been shown (Krawinkler, 1978) to provide considerable ductility in inelastic cyclic deformation. Current codes and recommendations (FEMA 350) recognize the ductility present in the panel zone. However, panel zone behavior and the design equations intended to represent the expected ductility in this region have been evolving over many years with many changes in design equations and experimental research support. (For the definitions of various symbols, refer to the list of symbols provided.)

Experiments clearly show that panel zone yielding occurs when the shear in panel zone, V_{pz} , reaches approximately V_y

$$V_y = 0.55 F_y c d_c t_p \quad (15.1)$$

Figure 15.5 shows the equilibrium conditions for computing V_{pz} for a typical cruciform test subassembly. The equation quantifies shear yielding of the panel zone considering the yield strength of the material, the depth of the column and the thickness of the column web. The value of 0.55 is an empirical value at which shear yielding of a stiffened plate occurs. Common practice has resulted in rounding this equation in the AISC (American Institute of Steel Construction) LRFD provisions (AISC, 1999a) to:

$$V_{yAISC} = 0.6 F_y c d_c t_p \quad (15.2)$$

Krawinkler (1978) derived another equation that estimated the ultimate capacity of the panel zone as it was assumed to have an average shear strain that was four times the yield shear strain at V_p . The equation

15-10 Earthquake Engineering: From Engineering Seismology to Performance-Based Engineering

better considers the plate boundaries and stiffening effects of the column flanges and the interaction between the beams and columns. The initial equation proposed by Krawinkler was

$$V_p = 0.55F_{yc}d_c t_{wc} \left\{ 1 + \frac{3.45b_c t_{cf}^3}{d_b d_c t_p} \right\} \quad (15.3)$$

This equation evolved into the equation shown below after the initial derivation:

$$V_p = 0.55F_{yc}d_c t_{wc} \left\{ 1 + \frac{3b_c t_{cf}^3}{d_b d_c t_p} \right\} \quad (15.4)$$

It should be noted that the present AISC equation for V_{pAISC} is different from that developed in the original derivation, that is

$$V_{pAISC} = 0.6F_{yc}d_c t_{wc} \left\{ 1 + \frac{3b_c t_{cf}^3}{d_b d_c t_p} \right\} \quad (15.5)$$

The equation for V_{pAISC} has been given approximately a 9% increase because of a round off operation as part of the AISC Specification (AISC, 2002).

A few connections tested as part of the research associated with FEMA 350 developed a significant amount of ductility from panel zone yielding. Because of this behavior, FEMA 350 recommends balancing beam flexural yield with panel zone, thereby yielding the greatest potential for connection ductility. For a connection where flexural yielding develops at the face of the column, a balanced condition means that yielding occurs within the panel zone simultaneously with the flexural yielding in the beam near the face of the column. The following equation represents the condition considering the moment developed in the beams at flexural yield, compared to yielding in the panel zone. This equation is derived as follows:

$$V_{pz} = \frac{\sum M_{yield-beam}}{d_b} \left(\frac{L}{L - d_c} \right) \left(\frac{h - d_b}{h} \right) \approx 0.9V_y = (0.9)0.55F_{yc}d_c t_{wc} \quad (15.6)$$

A design that meets this equation further encourages panel zone yielding, because ductile connections have shown the development of significant strain hardening.

SMF are anticipated to develop ductility through yielding of the beam–column assemblies at the connection between the beam flanges and column flanges. Yielding might occur through plastic hinging in the beams (or less desirably, the columns), plastic shear deformation in the panel zones or through a combination of any of these mechanisms.

Flexural yielding of the columns is discouraged and prohibited by the building code (strong column–weak beam) for all connection types described in this chapter. This requirement is established because frame systems built in a manner providing weak column behavior are known to have significantly larger inelastic story drift and local ductility demand than those with strong column behavior (Schneider et al., 1993). Maximum moment resistance provided by the connection must also be considered in estimating the potential for column yielding.

Material properties also play a significant role in the ability to predict behavior of SMF connections through the equations shown earlier. Structural steel material properties have changed significantly over the years. Before 1940, mild steel was specified as ASTM A9 steel with a minimum yield stress of 30 ksi. A9 steel evolved into ASTM A7 between about 1940 and 1960 with a specified minimum yield stress of 33 ksi. After the 1960s until the early 1990s, mild structural steel was sold as A36 steel with a specified minimum yield stress of 36 ksi. ASTM standards used to define A9, A7 and A36 steels differed only in

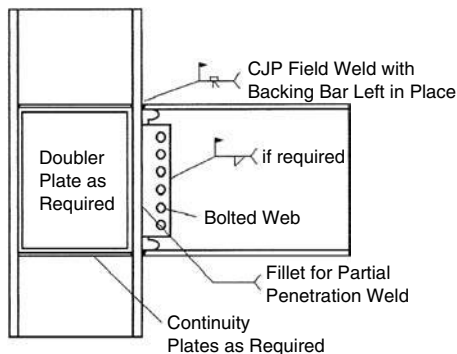


FIGURE 15.6 Pre-Northridge moment connection (FEMA 355D).

minimal increases in specified minimum yield stress and minimal decreases in required elongation. This condition is of concern since the seismic performance of an actual connection or component depends on the actual yield stress of the steel.

Today, wide flange shapes are all produced from recycled steel, using electric furnace technology rather than the integrated mill process of mining, processing and rolling. The yield stress of steel produced using current production methods is significantly higher than steels produced prior to the 1980s. Current design recommendations require the use of expected yield stress in the evaluation of yield mechanisms and failure modes. Therefore, equations included in this chapter are based upon expected or median yield stress rather than specified minimum yield stress values unless otherwise noted.

The design and evaluation of connections in this chapter and current design recommendations (FEMA 350) are all based on the material properties of steels produced today. The structural steel being produced today is specified as ASTM A992. A992 steel has a specified minimum yield stress of 50 ksi and a maximum yield stress to ultimate stress ratio of 0.85. These limits are intended to ensure that adequate ductility is present in the components and connections of structural steel buildings, especially SMF.

As described above, yield mechanisms and failure modes are factors that control lateral force resistance and ductility, providing frequent commonalities between the modes and mechanisms expected for the connections described in this chapter. The connections described in this chapter are all designed to provide increased ductility and reduced potential for brittle fracture.

15.3.1 Selection of Connection Type

After the widespread acceptance of welded steel construction and prior to the 1994 Northridge earthquake, most SMF were designed and constructed utilizing welded-flange-bolted-web connection details. This fully restrained connection was especially common in west coast SMF design for many years. This type of connection utilizes complete joint penetration (CJP) groove welds connecting the beam flanges to the column flanges and a shear tab connecting the beam web to the column flange. The shear tab was typically shop welded to the column with fillet or groove welds and then bolted to the beam web for transfer of shear force as illustrated in Figure 15.6.

Continuity plates were often used to provide continuity of moment capacity across the column depth to resist large forces transmitted by the beam flanges and provide stiffening for the panel zone. This type of connection is still available to the designer and will be discussed later in this section.

Following the 1994 Northridge earthquake and the publication of the FEMA 350 series documents, many issues associated with the “original pre-Northridge” connection were addressed. As a result of the FEMA 350 recommendations, the designer has many options available for the design of an SMF connection. This chapter discusses issues that affect ductility of SMF systems through the behavior of connections. Some of these issues are plastic rotation capacity, reduction of weld strain demand, beam and column web capacity, weld characteristics, weld access holes, web connection details and plastic hinge details. Other detailing issues that will be covered are continuity plate requirements, panel zone

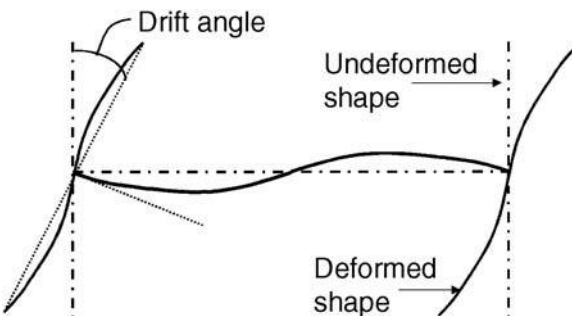


FIGURE 15.7 Interstory drift angle (FEMA 350).

detailling, weak-axis column bending, lateral-torsional and local buckling, deep column behavior, the use of box columns, the effect of composite slabs and the effect of thermal changes on materials. For issues not addressed in this section, the reader is referred to the recommendations and information provided in FEMA 350-353 and FEMA 355A to FEMA 355F.

Connections designed to remain elastic under code design level earthquake ground shaking, should be demonstrated by test and by analysis to be capable of providing the minimum levels of interstory drift angle capacity, as recommended by recommendations in FEMA 350 and as specified in Section 3.9 of the same recommendations. FEMA 350 defines the interstory drift angle as the portion of the interstory drift ratio in a frame resulting from flexural deformation of the frame elements, as opposed to axial deformation of the columns (see Figure 15.7).

When selecting a connection type, the designer should consider local detailing characteristics. The most critical of these characteristics is the connection between the beam flanges and column flanges. If the connection utilizes welded flange details, consideration must be given to the type of weld with a primary focus on reduction of stress concentrations. Part of the consideration for welded connections should be the weld access holes. The weld access hole can have a considerable effect on the total plastic rotation capacity of the connection, especially at high levels of drift. The recommended weld access hole configuration presented in FEMA 350 provides dimensions critical to the size and shape of the access hole that reduces the propensity for stress concentrations at the beam flange–column flange interface. The other important consideration for welded connections is the beam web connection detail. The web connection detail will vary from connection to connection, but the details associated with the web connection are important to consider regardless of what moment connection or web connection is chosen. Another important consideration is to keep the plastic hinge region free of notches and gouges that can present locations where stress might concentrate, resulting in brittle behavior. By specifying that no attachments or connections (bolted or welded) are allowed within the plastic hinge zone, the engineer will comply with requirements set forth in the 2002 AISC Seismic Provisions, as well as the FEMA 350 recommendations.

15.3.2 AISC Seismic Criteria

While this chapter refers to FEMA 350 recommendations, the governing design code for the design of steel construction is the AISC Seismic Provisions (AISC, 2002), as referenced from the next generation of model building codes similar to the Uniform Building Code (ICBO, 1997) and the International Building Code 2000 (International Code Council, 1997). This code indicates requirements for behavior and capacities of SMF and the connections associated with the system. The tie between FEMA 350 recommendations and the AISC Seismic Provisions is Appendix P.

Appendix P is a portion of the AISC Seismic Provisions that enable beam–column connections to be prequalified through a series of analysis and testing as approved by the governing building official through the acceptance of a “connection prequalification panel” (discussed later in this chapter). Certain criteria must be met for a particular beam–column connection to meet these requirements; however, most of

the connections tested as part of the SAC Phase 2 project meet the Appendix P requirements. For other connection types, especially those connections tested as part of a project specific testing program, Appendix S of the Seismic Provisions must be utilized.

Appendix S requires that beam–column moment connections expected to undergo inelastic behavior must meet certain plastic rotation requirements without significant strength degradation. The verification of this requirement must be completed through a series of physical experimental testing with minimal extrapolation allowed by analysis and calculation. The testing that is required must reasonably match expected conditions in the prototype (built structure). The boundary conditions (bracing of the beam to resist lateral–torsional buckling) must also accurately match the expected conditions in the prototype. The testing protocol, specifically the loading history must be clearly established prior to the test and the loadings must subject the connection to rotations commensurate with the expected inelastic rotation demands corresponding to the required building interstory drift.

15.3.3 SMF Connection Details

The FEMA 350 document identifies many different types of connections that have been tested and analyzed to comply with the basic requirements established in FEMA 350. These basic requirements are related to plastic rotation capacity, strength degradation and panel zone demand. The details associated with each of these connection types is beyond the scope of this book, but that detailed information can be found in the FEMA 350 and 355 documents. The following are a few of the connections identified in FEMA 350: Reduced Beam Section (RBS), the Free Flange connection (FF), the Welded Unreinforced Flange with Welded Web (WUF-W), Bolted End Plate (BEP) and the Bolted Unreinforced End Plate (BUEP). Not all of these connections are capable of developing the same level of plastic rotation capacity, nor do they all have the same behavior in terms of panel zone deformations and plastic hinge rotation. However, all of the connections listed above reached a minimum level of plastic rotation (0.03 radians) in accordance with the criteria established within FEMA 350 and indirectly with the inelastic drift capacity required by Appendix S of the 2002 AISC Seismic Provisions.

Other details are in use in SMF designs on the west coast and throughout the country. These connections are used for designs that require different performance and utilize beam and column sizes that provide a more efficient frame. These connections have all been tested for individual projects or as part of a prequalification program. A few of these connections are Haunch, Cover Plated Moment Connection, Ribbed (both RBS and unreduced beam section) and Reinforced RBS. Other connections have been tested and analyzed to provide performance beyond that expected for the “typical connection.” These connections typically provide energy dissipation without excessive local deformations associated with the formation of a plastic hinge. Two of these connection types are the energy dissipating friction connection and the prestressed centering connection. Both of these connections are primarily at the research level and have not yet been used in building practice.

In addition to the details discussed above, some proprietary connections exist for use in SMF building designs. Two of the most widely used proprietary connections are the side plate connection (Uang and Latham, 1995) and the Seismic Structural Design Association (SSDA) slotted connection (Richard et al., 2001). The side plate connection utilizes plate material welded to a beam and column in such a manner as to eliminate the beam flange to column flange weld and interface associated with WUF-W and RBS connections. In addition to the creation of a different beam column connection, the side plate system also adds reinforcing strength and stiffness to the panel zone. One of the features of the side plate system is that the fabricator will often construct the connection in a series of “trees” with beam splices that are erected in the field. This type of fabrication can take advantage of the higher level of welding quality and fabrication quality control that occurs in the fabrication shop than the level typically achieved in the field. The SSDA Slotted connection utilizes a “classic” welded beam–column configuration where beam flanges are CJP welded to the column flange and the beam web is connected to the column flange through a bolted or welded connection. The essence of the connection lies in the slot cut between the beam flange and the beam web. The length, shape and width of the slot are part of the proprietary design and are

intended to significantly reduce the shear resisted by the beam flanges at the face of the connection. This reduction has been analyzed using finite element analysis and has shown that the decrease in shear on the beam flanges reduces triaxial stresses and strain demand on the CJP flange welds. The designer/manufacturer of the connection also claims that the separation of the beam flanges from the beam web eliminates the lateral-torsional buckling response seen in most other connection types at large levels of plastic rotation. The proprietary nature of these connections does not eliminate the need to meet the requirements established in the AISC Seismic Provisions.

15.3.4 Design Example — RBS

Design a typical interior moment frame connection for a perimeter frame: The design will follow the FEMA 350 recommendations for connection design and calculation. There is a process within the FEMA 350 recommendations that follows steps (Step 1 through Step 8). Each step also refers to specific sections within FEMA 350. The pertinent steps and section numbers will be shown throughout the design example:

Description of design example project

- Commercial office building/medical office building
- Located in San Francisco, CA
- Soil type: dune sand with some silt and clay veins
- Distance from nearest earthquake fault: ~9 km (San Andreas)
- High seismicity zone with near fault characteristics

Description of design example frame

- Perimeter moment frames
- Frame centerline dimensions
 - Story height = 13'-0"
 - Bay width = 22'-8"
- Beam: W24 × 117, ASTM A992, $F_{yb} = 50$ ksi
- Column: W14 × 311, ASTM A992, $F_{yc} = 50$ ksi
- Gravity load on beam: 2 kips/ft (0.17 kips/in.)

Gravity loads are due to floor tributary loads as well as exterior wall loads.

15.3.4.1 Member Section Properties

W24 × 117

$$\begin{aligned}d_b &= 24.26 \text{ in. (beam depth)} \\b_f &= 12.80 \text{ in. (beam flange width)} \\t_f &= 0.85 \text{ in. (beam flange thickness)} \\t_w &= 0.55 \text{ in. (beam web thickness)} \\Z_{xb} &= 327 \text{ in.}^3 \text{ (plastic modulus of beam)}\end{aligned}$$

W14 × 311:

$$\begin{aligned}d_c &= 17.12 \text{ in. (column depth)} \\b_c &= 16.23 \text{ in. (column flange width)} \\t_{cf} &= 2.26 \text{ in. (column flange thickness)} \\t_{cw} &= 1.41 \text{ in. (column web thickness)} \\Z_{xc} &= 603 \text{ in.}^3 \text{ (plastic modulus of column)}\end{aligned}$$

Step 1: As per FEMA 350, Section 3.5.5.1, assume dimensions a , b and c . Assume that $a = 7$ in., $b = 19$ in. and $c = 0.20 \times b_f = 2.6$ in. (see Figure 15.8 for dimensioning). Calculate the plastic section modulus at the minimum RBS (Z_{RBS}):

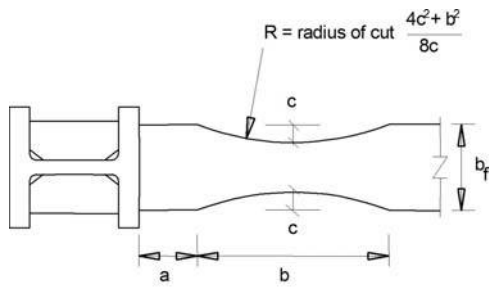


FIGURE 15.8 Reduced beam section dimensions.

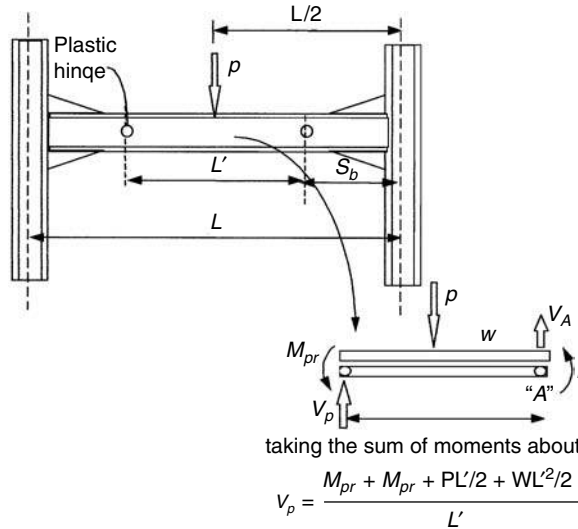


FIGURE 15.9 Sample calculation of shear at plastic hinge (FEMA 350).

$$Z_{RBS} = Z_{be} = Z_{xb} - 2ct_f(d_b - t_f)$$

$$Z_{be} = 327 - 2(2.6)(0.85)(24.26 - 0.85) = 223.5 \text{ in.}^3 \quad (15.7)$$

Step 2: As per FEMA 350, Sections 3.2.4 and 3.2.6, calculate the moment at the face of the column. M_f is calculated considering the plastic moment developed in the beam and the associated shear developed at the plastic hinge location (Figure 15.9). This calculation is used to determine the maximum stress at the face of the column flange. If the maximum stress at the face of the column is larger than the expected plastic capacity of the unreduced beam section, the beam section will need to be further reduced. This check considers the influence of the moment gradient on the RBS and its relationship to the face of the column. (See Figure 15.10)

$$M_f = M_{pr} + V_p x \quad (15.8)$$

$$M_{pr} = C_{pr} R_y Z_{be} F_y$$

$$C_{pr} = 1.15, R_y = 1.1 \quad \text{For ASTM A992, } Z_b = 327 \text{ in.}^3 \quad (15.9)$$

$$M_{pr} = (1.15)(1.1)(223.5 \text{ in.}^3 (50 \text{ ksi}) - 14,136 \text{ in.-kip}$$

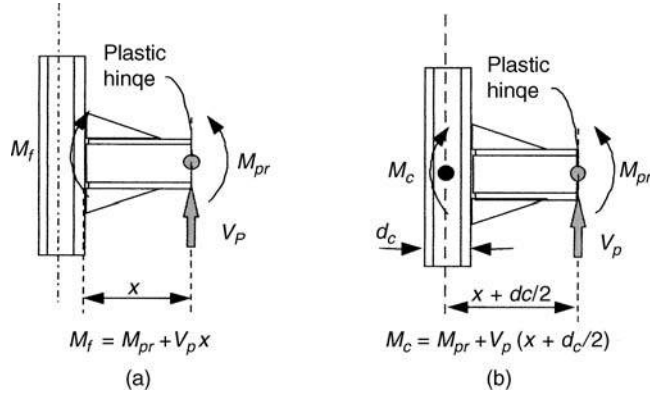


FIGURE 15.10 Calculation of demands at critical sections (FEMA 350). (a) Column face; (b) column centerline.

$$V_p = \frac{M_{pr} + M_{pr} + P(L'/2) + W(L'^2/2)}{L'} \quad (15.10)$$

$$L' = L - x \quad (15.11)$$

$$x = a + b/2 = 16.5 \text{ in.}$$

$$L' = 222 \text{ in.}$$

$$V_p = \frac{2(14,136k - \text{in.}) + 0 + 0.17(222\text{in.}/2)}{222 \text{ in.}} = 127.4 \text{ kips}$$

$$M_f = (14,136k - \text{in.}) + (127.4k)(16.5 \text{ in.}) = 16,238 \text{ in.-kips} \quad (15.12)$$

Check if \$M_f < C_{pr}R_yZ_bF_y\$; if not, increase the value of \$c\$

$$C_{pr}R_yZ_bF_y = (1.15)(1.1)(327 \text{ in.}^3)(50 \text{ ksi}) = 20,683 \text{ in.-kips}$$

$$M_f = 16,238 \text{ in.-kip} < 20,683 \text{ in.-kips}$$

Step 3: Following FEMA 350, Sections 3.2.4 and 3.2.6, calculate the moment in the column. \$M_c\$ is a similar calculation to \$M_f\$ but taken at the center line of the column depth for use in the calculation of panel zone stresses and the determination of the required panel zone thickness. (Equation 15.13 is approximate because the gravity load is distributed along the beam length.)

$$\begin{aligned} M_c &= M_{pr} + V_p(x + d_c/2) \\ M_c &= 14,136 \text{ in.-kip} + 127.4k(16.5 \text{ in.} + \frac{17.12 \text{ in.}}{2}) = 17,329 \text{ in.-kip} \\ M_c &= 17,329 \text{ in.-kip} & M_f &= 16,238 \text{ in.-kip} \end{aligned} \quad (15.13)$$

\$M_{yf}\$ is not required to be calculated, even though FEMA 350 Step 3 indicates to calculate \$M_c\$ and \$M_f\$ as per Section 3.2.7. This omission is acceptable because \$M_{yf}\$ is not a necessary parameter for RBS connection design.

Step 4: Calculate the shear at the face of the column (V_f). V_f is calculated to determine the shear force demand at the beam–column interface at the formation of the plastic hinge. V_f is used to design the shear connection between the beam and column.

$$V_f = 2 \left(\frac{M_f}{L - d_c} \right) + V_g \quad (15.14)$$

$$\begin{aligned} V_g &= \frac{W(a + b/2)}{2} \\ V_g &= \frac{(0.17 \text{ in})(16.5 \text{ in.})}{2} = 1.4 \text{ kips} \\ V_f &= 2 \left(\frac{16,238 \text{ in.-k}}{272 \text{ in.} - 17.12 \text{ in.}} \right) + 1.4k = 128.8 \text{ kips} \end{aligned} \quad (15.15)$$

Step 5: The beam web will be welded with a complete joint groove penetration weld; therefore, no further calculations are required to confirm capacity of beam–column web connection. Since no further calculations are required, Step 5 has been addressed.

Step 6: As per FEMA 350, Section 3.3.3.2, calculate the required thickness of panel zone. The thickness of the panel zone is calculated considering the beneficial effects of having a panel zone that is stiffer and stronger than the adjacent plastic hinge region. C_y is included in the calculation in an effort to provide a panel zone thickness that is conservatively stronger and stiffer than the “conventionally” designed panel zone forcing flexural yielding to occur before or at the same time as shear yielding of the panel zone.

$$F_{yc} = 50 \text{ ksi}, R_{yc} = 1.1, C_{pr} = 1.15, h = 156 \text{ in.}$$

$$\begin{aligned} S_b &= \frac{I_b}{c} \\ I_b &= \left(2 * \left[\frac{(12.8 - 2(2.6))(0.85)^3}{12} + (12.8 - 2(2.6))(0.85) \left(\frac{24.26}{2} - \frac{0.85}{2} \right)^2 \right] \right) \\ &\quad + \left(\frac{(0.55)(24.26 - 2(0.85))^3}{12} \right) = 2297 \text{ in.}^4 \end{aligned} \quad (15.16)$$

$$c = \frac{24.26 \text{ in.}}{2} = 12.13 \text{ in.}$$

$$S_b = \frac{2297}{12.13} = 189.4 \text{ in.}^3$$

$$C_y = \frac{1}{C_{pr} \left(\frac{Z_{be}}{S_b} \right)} \quad (15.17)$$

$$C_y = \frac{1}{(1.15) \left(\frac{223.5 \text{ in.}^3}{189.4 \text{ in.}^3} \right)} = 0.737$$

$$t = \frac{C_y \sum M_c \frac{(h - d_b)}{h}}{(0.9)(0.6)F_{yc}R_{yc}d_c(d_b - t_{fb})}$$

$$t = \frac{0.737(2 * 17,329 \text{ in.-k}) \left(\frac{156 \text{ in.} - 24.26 \text{ in.}}{156 \text{ in.}} \right)}{(0.9)(0.6)(50)(1.1)(17.12 \text{ in.})(24.26 \text{ in.} - 0.85 \text{ in.})} = 1.81 \text{ in.}$$

$t_{cw} = 1.41 \text{ in.} < t \quad \therefore \quad \text{Doubler Plates are Needed--say } 1/2'' \text{ is adequate}$

Use 1/4" Plates on Each Side of Column Web

(15.18)

Step 7: As per FEMA 350, Section 3.3.3.1, calculate whether continuity plates are required. This calculation determines if the column flanges are flexible enough to alter the moment continuity across the column section and between adjacent beams. If the column flanges are stiff enough, no continuity plates are required based on empirical results. (Step 7)

$$t_{cf} < t = 0.4 \sqrt{1.8 b_f t_f \left(\frac{F_{yb} R_{yb}}{F_{yc} R_{yc}} \right)} \quad (15.19)$$

$$t = 0.4 \sqrt{1.8(12.8 \text{ in.})(0.85 \text{ in.})(1.0)} = 1.77 \text{ in.}$$

or

$$t_{cf} < t = \frac{b_f}{6}$$

$$t = \frac{12.8 \text{ in.}}{6} = 2.13 \text{ in.} \quad (15.20)$$

$t_{cf} = 2.26 \text{ in.} > t = 2.13 \text{ in.} > t = 1.77 \text{ in.}$	No Continuity Plate Needed
---	-----------------------------------

Step 8: Detail connection, as per FEMA 350. (See Figure 15.11.)

15.3.5 Full-Size Subassemblage Testing

Full-size subassemblage testing that was completed as part of the SAC Phase 2 program (published as part of the FEMA 350 series documents) answered many questions regarding the behavior of welded steel moment connections. However, some believe that not all aspects of the actual constructed welded steel moment connection in a building can be adequately addressed through subassemblage testing. Some of these concerns are:

- The influence of axial loads on the column.
- The wide range of beam/column sizes used in a real building design.
- The influence of frame geometry on the connection performance.
- The expected performance of deep columns.
- The influence of column moment magnification.
- The influence of the slab on the connection performance.
- The influence of “cross-framing” into the beam/column connection.
- The appropriate level of lateral bracing for beam.

Most of these concerns have been addressed through a combination of testing and analysis completed as part of the work done for the FEMA 350 series documents and the 2002 AISC Seismic Design Provisions. Issues that were not examined as part of the experiments conducted in the SAC Phase 2

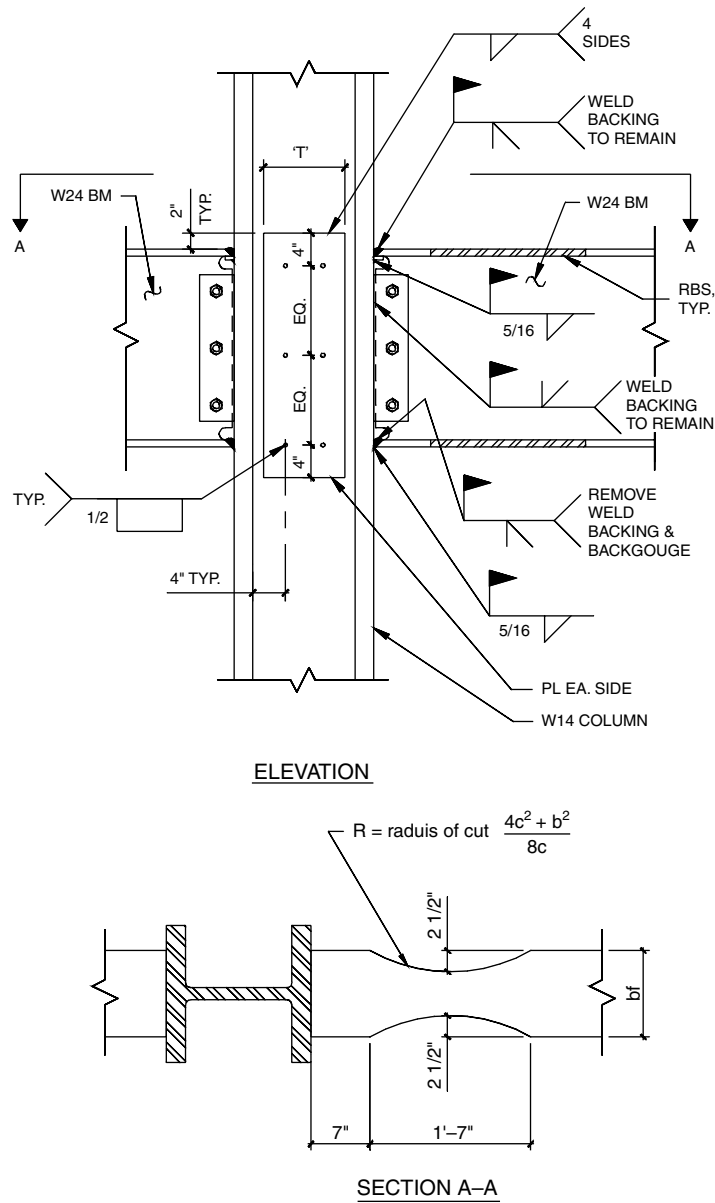


FIGURE 15.11
Example of RBS connection detail.

program were analyzed to determine the effects associated with that issue and its importance in the expected connection performance.

Issues such as axial loads in columns, frame geometry and column moment magnification are believed to be primarily system-level issues that are best analyzed using system-level analyses. The effects of these issues on connection performance have been identified as secondary in reaching expected levels of inelasticity in the connection. The other issues have been tested or analyzed to some degree with a reasonable amount of engineering judgment applied to the design recommendations.

The wide range of beam/column sizes used in buildings is not as random as one may think. Building code requirements and connection performance characteristics (and strength requirements) tend to limit the combinations appropriate for the use in SMF buildings. While recommendations that extrapolate appropriate sizes based on a few tests exist, this extrapolation comes from a detailed evaluation of empirical and analytical data related to SMF connection performance.

The expected performance of deep columns is tied to the level of lateral bracing for column and beam, and current research is being conducted to better understand this issue. A recent paper published by the Structural Steel Education Council (SSEC), *Steel Tips: Use of Deep Columns in Special Steel Moment Frames* (Shen et al., 2002), indicates that further research is required to better understand the expected behavior associated with this special connection condition. In some subassemblage tests (Chi and Uang, 2002), deep columns performed less admirably than their stocky column counterparts. A significant amount of inelasticity was developed in the beam–column connection, but this inelasticity occurred while the column went through a significant amount of torsional deformation.

The presence of the slab significantly influences the behavior of moment connections, particularly the inelastic buckling modes. The slab is effective in providing lateral bracing for the beam top flange and twisting restraint of the column. Laboratory observations show that the beam has to shorten to accommodate lateral–torsional buckling. In an actual building frame, however, the beam is restrained axially at both ends by the columns and the slab. Yu et al. (1999) investigated such axial restraining effects on the RBS moment connection response through finite element analysis and found that the system axial restraining effects to the beams could significantly reduce the web local buckling amplitude, and therefore, dramatically reduce the strength degradation at higher displacement levels. For those connections that have focused areas of inelasticity (i.e. RBS) it is recommended to eliminate any direct shear transfer between the floor system and the top flange of the moment beam. The elimination of direct shear transfer is usually accomplished by omitting the welded steel shear connectors over the expected beam plastic hinge region. Localized elimination of direct shear between beam flange and floor diaphragm will result in the most consistent cyclic behavior.

The influence of beams framing into the beam–column connection perpendicular to the direction of the moment frame have not been tested extensively. The typical connection detail associated with these gravity frame beams framing into the beam–column connection would consist of a single plate shear tab welded to the column web and supplemental plates that are welded to the column flange. Perpendicular framing located at the moment frame connection typically comprises only gravity framing (since bi-directional beam–column connections must be tested in accordance with the AISC Seismic Provision). For most moment connection types, the typical perpendicular framing connection is believed to be significantly more flexible than the beam–column moment connection, including the panel zone flexibility. Therefore, the influence on the performance of the beam–column connection in an earthquake is believed to be minor.

Since the RBS moves the beam plastic hinge away from the column face, some concerns have been raised about the provision of additional lateral bracing near the plastic hinge region. Lateral bracing typically consists of a beam or double angle that braces the bottom flange of a moment beam at a specific point against lateral movement. Lateral bracing can also be provided by using full height vertical web stiffeners connected to a beam or double angle that prevents warping or twisting of the beam cross section. Yu et al. (1999) investigated effects of additional lateral bracing on the cyclic response of two identical full-scale RBS moment connections. The results of these investigations showed that lateral bracing becomes effective at inelastic drift beyond 3%, at which point the connection strength began to degrade and the presence of the lateral bracing reduced the buckling amplitudes and delayed the strength degradation of the connection. The study conducted by Uang and Fan (1999) indicated that the plastic rotation capacity of an RBS connection is not sensitive to lateral–torsional buckling; beam web local buckling was identified as the limiting behavior of the connection rotation. Therefore, for an SMF building where axial restraining effects typically exist, adding lateral bracing near the RBS region appears to be unwarranted. Minimum requirements provided in the 2002 AISC Seismic Provisions ensure a minimum performance level commensurate with building code performance goals. However, for the situation where

the axial restraining effect does not exist or where unusually high story drift demand exists, adding lateral bracing outside of the plastic hinge region can improve the seismic performance of RBS moment connections at high rotations.

15.3.6 Connection Details

Following the Northridge earthquake, many engineers believed that connection details were the most important aspect of the special moment frame. In fact, based on observed damage in Kobe following the 1995 Kobe earthquake, Japanese engineers conducted a significant amount of research and testing to better understand the behavior of connections.

Some aspects considered important for SMF connection details that have been identified (SEAOC, 2002) are:

- Weld metal toughness
- Shear influence on beam flanges
- Through thickness stresses on column flanges
- Local kinking of beam flanges through panel zone behavior
- Strain effects due to beam flange thickness
- Toughness of the base material for beams and columns
- The weld access hole size and geometry
- Low cycle fatigue

Many of these issues have been investigated in depth through the research and analysis completed in support of the FEMA 350 series documents. Not all of these issues have been completely researched and fully understood, but many feel that the design community now has an ample set of data to reliably design steel SMF connections. More information on these issues can be found in the FEMA 350 documents as well as a detailed set of recommendations developed by SEAOC (2002). Items such as through thickness stresses on column flanges, toughness of base material for beams and columns and low cycle fatigue and their effect on SMF connection behavior are now relatively well understood and incorporated into many of the design recommendations provided in FEMA 350.

While issues such as shear influence on beam flanges, local kinking of beam flanges and strain effects due to beam flange thickness are not easily controlled as part of an SMF connection design, some issues such as weld metal toughness and weld access hole size and geometry can be modified as part of the design to help the connection develop more plastic rotation capacity.

15.3.7 Fabrication

Some of the more critical aspects of effective SMF connection seismic performance are related to the fabrication process. Virtually all SMF connections have holes and weld preparation at the ends of the beams. The weld preparation includes the important weld access hole. The weld access hole should be created using a process that will result in the smoothest possible surface to avoid notches presenting conditions that concentrate stresses, which could result in brittle behavior at this important location. The gradual transition of the toe of the weld access hole to the base of the beam flange–column flange weld will help reduce the tendency of this location to develop and propagate cracks when subjected to high strains during cyclic loading (Moore et al., 1999). This type of consideration is also important in the smooth cut of an RBS or other connection types that remove beam material to force the plastic hinge away from the column flange. Accurate fit-up for important welds is also critical for the good behavior of SMF connections. The details associated with the fit-up of beams, columns and plates (preparation, bevel angles, straight cuts, etc.) is one of the most important aspects of good welding.

Good welding practice, materials, specifications and workmanship are some of the most important design aspects for SMF connections. Research and analysis results supporting FEMA 350 indicate that improved weld quality and practice can improve the performance of even pre-Northridge SMF connec-

tions. However, these improved practices involve tough weld metal, removal of backup bars, well-sized and well-fabricated weld access holes and other improvements that differ significantly from the early connections. Improved weld practices consist of adequate preheat, the strict adherence to processes dictated by the American Welding Society (AWS) D1.1 code, multiple pass small-bead techniques for the build up of thick complete joint penetration groove welds, removal of runoff tabs and grinding of weld ends to provide smooth transitions for stress distribution from beam flange to column flange.

Some research has been conducted on understanding the toughness of weld metal. Weld metal is the result of welding two pieces of base metal together with a filler metal. The combination of the three different metals is considered the weld metal. In some cases, final weldments consist of multiple base metals and multiple filler metals. The mixing of filler metals may result in a weld metal that is more brittle than the toughness of the base metals or either filler metal when considered separately. A few papers have been published on the issue (Blodgett et al., 1999; Quintana and Johnson, 1998). These papers, and the supporting research, indicate that engineers need to be aware and diligent in the understanding and application of filler metals for critical welds in SMF connections. One clear lesson associated with welding is that tougher welds are desired and the use of tough filler metals alone will not always result in a tough weld.

For those SMF connections that do not utilize welding, but rather bolting, there are just as many details important to good SMF connection behavior. Bolt holes must be adequately fabricated in accordance with codes and experience. In most cases, this means that bolt holes should be drilled rather than punched to avoid lamellar tearing of the steel material (especially for thick plates, flanges or webs). Also, detailing and fabrication of bolt holes are especially critical for a few of the bolted connection types identified by FEMA 350. Bolts can be ASTM A325 or A490 with threads included or excluded, slip critical or bearing, all dependent on the connection type and the expected connection demands. One of the benefits of a bolted connection is the reduction of special inspection required during construction, which is an expense typically incurred by the building owner. However, the difficulty in calculating an adequate bolted connection for the FEMA 350 recommendations makes some of the bolted connection types less attractive than the welded connections.

15.3.8 Nondestructive Evaluation, Testing and Inspection

Nondestructive evaluation (NDE), testing and inspection are required during the fabrication and erection of structural steel to ensure that the quality of the final constructed structure is consistent with that assumed in the design. All three elements are critical to understanding the base material, fastening material (bolts, filler metals), weld metal and construction quality of the final connection condition. Material characteristics for base material are gathered through coupon testing of representative samples of the project material (yield and ultimate strengths, elongation) and ultrasonic testing of constructed elements (delamination and internal material flaws).

Visual inspection is also important for material verification, connection fit-up and construction quality conditions. Most visual inspection is limited to material identification, erection fit-up, weld procedure verification and fillet weld quality. More detailed testing is required for complete joint penetration groove welds and partial joint penetration groove welds.

There are many types of NDE that can be utilized to establish weld quality. Some testing methods consist of magnetic particle testing, ultrasonic testing and dye penetrant testing. How these methods are appropriately utilized is dependent on the connection type, demands on the connection and importance of the connection. FEMA 353, *Recommended Specifications and Quality Assurance Guidelines for Steel Moment Frame Construction for Seismic Applications*, provides the engineer detailed information on the appropriate type of NDE and application of those methods. FEMA 353 also clearly identifies how certain connections should be categorized for particular levels of testing and inspection. The reader is referred to FEMA 353 for more information with regards to nondestructive testing and quality control/quality assurance.

15.4 Design of Repair and Upgrade Measures for Existing pre-Northridge SMF Connections

15.4.1 General

As was noted earlier, brittle fracture in or around the groove weld between the beam bottom flange and the column flange was observed in more than 100 steel SMF buildings after the January 17, 1994 Northridge earthquake (Youssef et al., 1995). The FEMA/SAC steel program was initiated to investigate the various causes of the failures and develop guidelines and criteria for design, inspection, evaluation, repair and rehabilitation of steel SMFs. A major focus of Phase 1 was the investigation of connection fracture causes and development of interim guidelines for inspection, evaluation and repair of these structures. This section will primarily address the latest recommendations related to the upgradation of existing moment frame buildings that incorporate pre-Northridge moment frame connections.

15.4.2 Moment Connection Research from FEMA/SAC Steel Program Phase 1

In Phase 1 of the FEMA/SAC steel program, tests were performed on a total of 12 exterior pre-Northridge steel moment connections designed and constructed to simulate the design practice prevalent prior to the Northridge earthquake. These laboratory tests confirmed the poor performance of moment connections observed after the Northridge earthquake. Most of the specimens experienced brittle fracture with little ductility. Some specimens failed without the ability to develop any plastic rotation (SAC, 1996).

According to a post-Northridge damage survey (Youssef et al., 1995), about 70 to 80% of the reported damage occurred in the beam bottom flange. A number of contributing factors for the dominance of bottom flange fractures in these connections, which were designed in accordance with the Uniform Building Code (ICBO, 1985, 1988) and constructed prior to the Northridge earthquake have been reported (FEMA, 1997b). After the Northridge earthquake, it was first recognized that the beam flange groove weld made with a low-toughness electrode (e.g., E70T-4) is prone to brittle fracture. While the groove welded joint can be made continuously across the width of the top flange, this is not the case for the bottom flange because of the interference of the beam web. Because the groove weld between the bottom beam flange and the column flange is interrupted at the weld access hole, the quality is difficult to control. Unfortunately, this is also the location where ultrasonic testing is extremely difficult and unreliable. Second, the incomplete fusion zone at the root pass of the weld inevitably creates a notch-like condition when the steel backing is left in place. The location of the notch coincides with the extreme fiber location of the beam bottom flange. This is not the case at the top beam flange. Third, the concrete floor slab may have increased the positive flexural capacity, raising the beam neutral axis, and therefore, creating larger tensile strain demands in the bottom flange. Other contributing factors for the poor performance of the connection might include the use of heavier and deeper beam sizes and column sections than the tested and excessively weak panel zones.

Damaged connections were repaired with different options such as vertical rib plates, cover plates, a triangular haunch, a straight haunch or notch-tough weld metal replacing the "typical" weld metal for the beam flange to column flange welds. For those connections that developed fractures that propagated into the column, portions of the webs and flanges had to be cut away, rewelded and replaced with plates as shown in Figure 15.12. Wherever a haunch was used to strengthen either bottom or top beam flange with a fractured joint, the fractured flange was left disconnected. Experimental tests showed that the bottom-only haunch repair effectively enhanced the performance of damaged connections and that the top and bottom flange haunch repair or cover plate were even more effective. Most of the haunch repairs made use of a triangular haunch consisting of a structural T-shape or modified W-shape welded beneath the beam. Such a repair typically requires a significant amount of overhead welding to make the complete joint penetration groove weld at both ends of the haunch flange. Instead, a rectangular haunch with one free end was proposed to reduce the construction cost. The rectangular haunch repair was capable of a



FIGURE 15.12 Connection failure and connection repair. (a) Bottom flange fracture; (b) connection repair; (c) repaired moment connection. (Yu, Q.-S., Bondad, D. and Uang, C.-M. (1996). Experimental and analytical studies of full-scale pre-Northridge steel moment frame connections under dynamic loading, Report No. SSRP-96/03, Division of Structural Engineering, University of California, San Diego, La Jolla, CA.)

slightly smaller inelastic deformation than the comparable triangular haunch repair (Uang and Bondad, 1996).

15.4.3 Moment Connection Research from NIST/AISC Program

In parallel with the FEMA/SAC steel research program, the National Institute of Standards and Technology (NIST) and the AISC initiated a research project to upgrade existing SMFs and investigate the effectiveness of two seismic rehabilitation schemes (Civjan and Engelhardt, 1998; Yu et al., 1997). Modifications to pre-Northridge moment connections to achieve improved seismic performance in this program focused on reducing or eliminating some of the contributing factors to the brittle fractures mentioned above. Two schemes were adopted to force plastic hinging of the beam away from the column face. The first scheme utilized the RBS concept to weaken a portion of the beam near the column so that plastic hinging would occur at the designated location. The second scheme utilized the addition of a welded haunch to strengthen the steel beam near the welded connection.

Although both methods attempt to achieve the desired performance by reducing the stress in the beam flange groove weld, the quality of the groove weld also needs to be considered. One of the requirements developed following the Northridge earthquake is to make the beam flange groove welds with an electrode having a specified Charpy V-Notch toughness, typically 20 ft·lb at -20°F (FEMA, 1995). However, for economic reasons it is highly desirable to minimize the amount of work required to modify (or replace) the existing low-toughness groove welded joint in existing moment connections. Another economic consideration is related to the concrete slab in existing buildings. Unless the concrete slab around the column is removed, it is difficult to modify the top flange and its welded joint. Fortunately, the majority of reported damage occurred in the bottom beam flange; therefore, modifications focus on the bottom

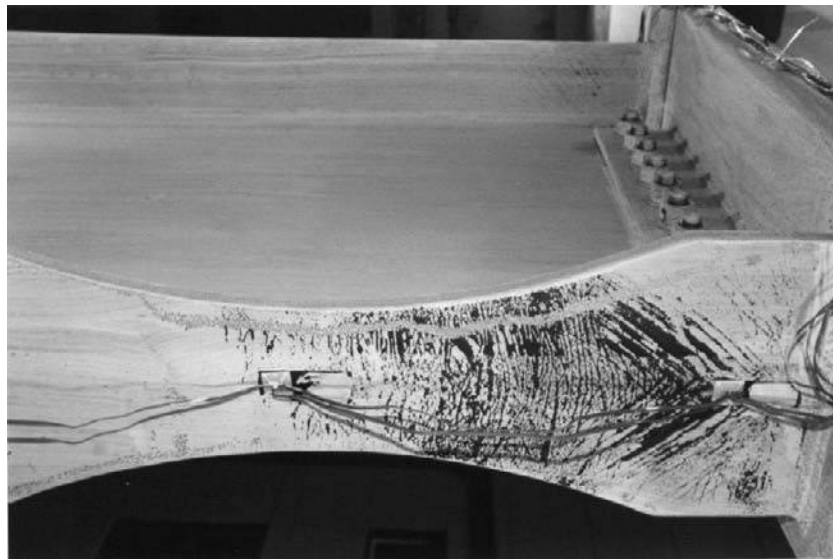


FIGURE 15.13 Moment connection modified with RBS scheme (Yu, Q.-S., Noel, S. and Uang, C.-M. (1997). Experimental studies on seismic rehabilitation of pre-Northridge steel moment connections: RBS and haunch approach, Report No. SSRP-97/08, University of California, San Diego, CA).

flange. No modifications were made at the beam bottom flange in the welded haunch scheme because the force demand at the bottom flange welded joint could be significantly reduced. However, in the RBS scheme, the beam bottom flange welded joint was in a more critical situation. Therefore, the steel backing was removed and a reinforcing fillet weld was placed. A total of 12 pre-Northridge two-sided SMF connection specimens constructed with W30 × 99 and W36 × 150 beams were tested cyclically to study the effectiveness of these two seismic rehabilitation schemes. Six specimens incorporated an 8-ft wide lightweight concrete slab.

15.4.3.1 RBS Scheme

Introducing RBS to the beam bottom flange (see Figure 15.13) and the accompanying removal of the steel backing and weld tabs could not prevent brittle fracture of the low-toughness groove welded joint in the top flange. There was only marginal improvement of the cyclic performance from either removing steel backing of the top flange or incorporating a concrete slab. The plastic rotation capacity was no more than 0.01 radian, at which the story drift ratio was approximately 1.7%, as indicated in Figure 15.14. This rehabilitation scheme was much more effective when the existing low-toughness groove welds (E70T-4) were replaced by new welds made with a notch-tough electrode (E71T-8 in this case). Brittle fracture of welded joints was precluded, but ductile tearing initiating from the beam web weld access hole near the bottom flange and propagating horizontally along the “k” line of the beam. Three of the four beams tested as part of the research program were able to develop a plastic rotation in excess of 0.027 radian, at which the story drift ratio was more than 3.3%.

15.4.3.2 Welded Haunch Scheme

The haunch scheme was implemented by welding a triangular haunch beneath the beam bottom flange. Ideally, the strengthened section of the beam would remain essentially elastic during plastic hinging of the beam, thereby limiting the stress in the welds. Because the beam reaches its full plastic moment away from the column face, this type of reinforced connection is subjected to a higher moment than the RBS connection. Although welded joints of top flanges still suffered brittle fracture for the bare steel specimens, the other specimens with a composite slab did not experience brittle fracture even at 4% story drift ratio (see Figure 15.15). Figure 15.16 shows the force-displacement relationship for a moment connection

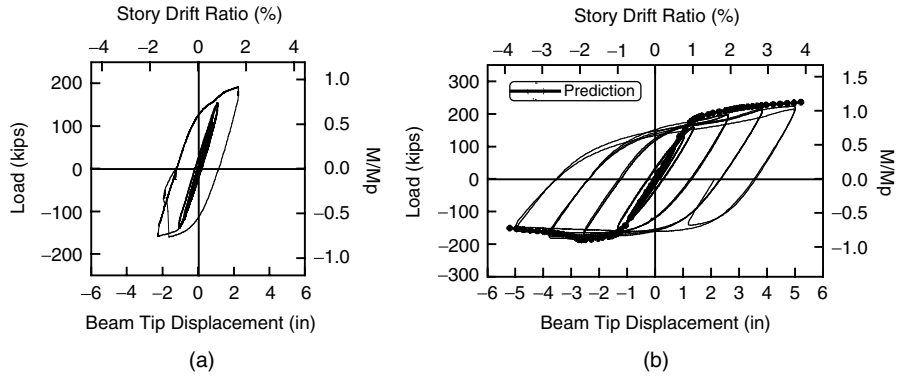


FIGURE 15.14 Load versus beam tip deflection relationships of the composite specimens (Yu, Q.-S., Noel, S. and Uang, C.-M. (1997). Experimental studies on seismic rehabilitation of pre-Northridge steel moment connections: RBS and haunch approach, Report No. SSRP-97/08, University of California, San Diego, CA).



FIGURE 15.15 Buckling and yielding modes of composite welded haunch specimen (Yu, Q.-S., Noel, S. and Uang, C.-M. (1997). Experimental studies on seismic rehabilitation of pre-Northridge steel moment connections: RBS and haunch approach, Report No. SSRP-97/08, University of California, San Diego, CA).

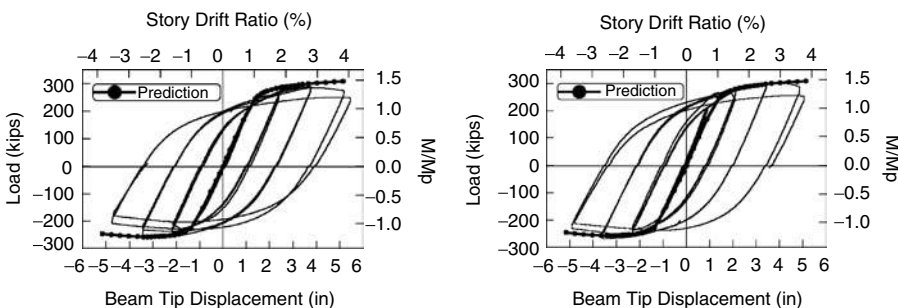


FIGURE 15.16 Load versus beam tip deflection relationships of the composite specimen (Yu, Q.-S., Noel, S. and Uang, C.-M. (1997). Experimental studies on seismic rehabilitation of pre-Northridge steel moment connections: RBS and haunch approach, Report No. SSRP-97/08, University of California, San Diego, CA).

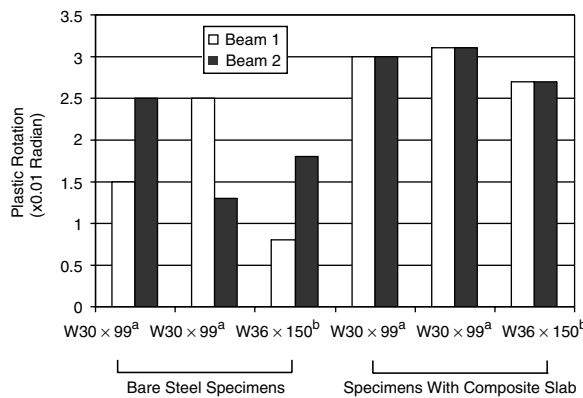


FIGURE 15.17 Plastic rotation capacities of NIST/AISC two-sided beam-to-column subassemblies (a: from Civjan and Engelhardt, 1998; b: from Uang et al., 2000).

specimen consisting of W36 × 150 beams, W14 × 426 column and a triangular haunch cut from a W14 × 143 section.

Figure 15.17 summarizes the test results. Of the three bare steel specimens (two beams per specimen) tested, five beams experienced brittle fracture of the groove weld in the top flange. More than half of the beams, however, were able to develop a plastic rotation of at least 0.024 radians. When the concrete slab was present, none of the six beams experienced weld fracture and the plastic rotation developed in the connection ranged from 0.028 to 0.031 radians, which was considered adequate for rehabilitation purposes (FEMA, 1995). This rehabilitation method not only provides a more redundant moment connection but also eliminates the need to modify the existing groove weld of the top flange, resulting in a significant cost savings.

Yu et al. (2000) found that when the haunch is present, the majority of the beam shear is transferred through the haunch flange acting as a strut to the column. A simplified model and design procedure that considers the interaction of forces and the deformation compatibility between the beam and the haunch was developed (see design example at the end of this Chapter). The proposed procedure was included in an AISC design guide (Gross et al., 1999).

15.4.4 Connection Modification Options

On the basis of the testing results from the two-phased FEMA/SAC steel program, the NIST/AISC rehabilitation program and other research studies, FEMA 351 recommended a series of prequalified connection upgrade details for SMFs. These prequalified connection modifications include (1) welded bottom haunch connection, (2) welded top and bottom haunch connection and (3) welded cover plate flange connection (attaching new cover plates to both the top and bottom flanges of the existing beam). These strengthening schemes are intended to relocate beam plastic hinge away from the column faces thereby reducing the strain demands near the welded joints. FEMA 351 recommends that if the beam flange welds to the column are made with low notch toughness material, the weld shall be gouged out and replaced with notch-tough weld metal. Yu et al. (1997) showed that such a stringent requirement may not be necessary for the bottom flange welded joint when the welded bottom haunch scheme is used. In addition, weld replacement for top flange welded joint is only recommended when there is no concrete floor slab. If the welded top and bottom haunch scheme is used, weld replacement for existing top and bottom welded joints seems unnecessary because the force and deformation demands at existing welded joints are significantly reduced. FEMA 351 also provides a recommended applicable range of member sizes and frame configuration for prequalified connection upgrade details for SMFs. The parameters, such as beam depth, span-depth ratio and beam flange thickness, ensure that the prequalified

upgrade details are applied within the range that has been tested. If the connection upgrade details go beyond the applicable range, project specific connection qualification testing should be performed. Other general design issues such as welding shear studs at the plastic hinge region, base material toughness requirements, avoiding any welding near k-area, removal of weld backing and run-off tabs and through thickness strength are addressed in FEMA 351.

In the Phase 1 of the FEMA/SAC project, a straight haunch repair scheme proposed as an economic alternative for the triangular haunch was shown to be effective in improving the cyclic performance of damaged pre-Northridge moment connections. Clearly, the force transfer mechanism in the straight haunch is different from that of a triangular haunch because a direct strut action does not exist. Recently, Lee and Uang (2001) proposed to treat the web of the straight haunch as a vertical rib plate and the haunch flange as a stiffener to stabilize the rib plate. Based on finite element analysis results, a simplified model considering the force interaction and deformation compatibility between the beam and the haunch was developed. Since the test results (Uang and Bondad, 1996) showed that the stress concentration at the free end of the haunch tended to unzip the weld between the haunch web and beam flange, Lee and Uang (2001) proposed a series of details to alleviate the stress concentration at the haunch tip. These connection modifications will not hinder the ability of the connection to attain significant yielding and local buckling in the beams under the design basis earthquake.

During the past decade, moment frame connections using posttensioning concepts were developed and validated for precast concrete construction (Priestley et al., 1999). A series of self-centering beam–column connections combined with innovative use of energy dissipation devices were proposed. Such posttensioning concepts have been extended to a weld free steel SMF system. Test results (Christopolulos et al., 2002; Ricles et al., 2001) clearly demonstrated (1) the connection stiffness is comparable to that of a welded connection, (2) the connection is self-centering, minimizing the possibility of residual drifts and (3) energy dissipation is confined to some sacrificial elements such as steel angles or energy dissipating bars. Such an approach could provide an alternative scheme to modify existing SMFs. However, more experimental and analytical studies are needed before such a concept is implemented in practice.

15.4.5 SMF Upgrade Methodologies — Simplified and Systematic Approaches

The general methodologies for seismic upgrade of SMF structures are either (1) to reduce the force and deformation demand on the connections or (2) to increase the deformation capacity of the connections. Currently two approaches involving different levels of seismic upgrade efforts are available: simplified and systematic (FEMA 351).

15.4.5.1 Simplified Approach

In the simplified approach, modifications are made to individual fracture-vulnerable moment-resisting connections of the structure to provide capacity for ductile behavior comparable to that presumed to exist at the time of the original design. This upgrade approach does not reduce the deformation demand on the connections. This approach is used when the moment-resisting connections are the only significant vulnerability of the structure and the upgrade goal is to restore the building performance intended at the time of the original design. However, it should be noted that connection modification should not create undesirable seismic features, including weak column-strong beam, weak story, soft story and torsional irregularity. Since the overall performance of SMF structures depends on other features of the building, such as building irregularities, upgrading connections alone will not guarantee improved structural performance.

15.4.5.2 Systematic Approach

In the systematic upgrade approach guided by the philosophy of performance-based earthquake engineering, one or more suitable performance objectives are first selected and then a complete evaluation of the structural performance is conducted to verify the performance capability of the structure. If the structure is not capable of meeting the desired performance objective, structural modifications are

performed at a system level to improve the probable performance. General strategies include, aside from connection improvement, mitigation of system irregularities and discontinuities, global structural strengthening and stiffening and the addition of supplemental energy dissipation devices. Typical global structural strengthening and stiffening approaches include (1) transforming the SMF system into a concentrically braced frame or eccentrically braced frame by adding new bracing, (2) infilling the SMF with steel plates to form a steel plate shear wall system and (3) adding new concrete shear walls. These approaches might require new foundations or foundation strengthening. Furthermore, these approaches could still result in significant damage to the lateral force system and noticeable residual drifts in a major earthquake.

Supplemental energy dissipation devices have been shown effective to reduce deformation demands at the moment connections and minimize building damage. Numerous buildings in North America, Japan and New Zealand have been retrofitted with supplemental damping devices. Commonly used supplemental energy dissipation devices can be categorized into two groups: hysteretic devices and viscoelastic (VE) devices. Hysteretic devices include metallic yielding devices and friction devices, with energy dissipation depending primarily on relative displacements within the devices and not on their relative velocities. Metallic yielding devices such as ADAS (added damping and stiffness) dampers and buckling restrained braces absorb a large portion of the seismic energy through metallic yielding. Friction damper devices include slotted-bolted connections and pall friction devices. VE solid or fluid devices dissipate energy through deformation of VE polymers, deformation of viscous fluids or the passage of fluid through an orifice and their energy dissipation depends on both the relative displacements and relative velocities within the device. These energy dissipation devices are effective to reduce the building deformation response through increasing the structure's effective damping. Furthermore, these devices dissipate the energy that is otherwise dissipated by the structural system, thus reducing potential damage to structural elements. Since the energy dissipation capacity increases as relative displacement in the device increases, energy dissipation devices are expected to perform well with a flexible structural system such as SMF buildings. Finally, they add structural strength and stiffness, which reduces the structural period, and therefore, maximum displacement. Since energy dissipation devices can be integrated into the steel frames as braces or used in series with the braces in the frame, which means that they can be hidden behind partitions or used as exposed elements for architectural enhancement, their effects on building architectural feature are often not detrimental. Therefore, upgrading existing SMF with energy dissipation devices might be a viable option to achieve high level seismic performance.

The selection of the modification approach depends on the seismic performance goals and the total cost associated with the modification including structural and architectural work as well as business interruption. Usually some of these strategies are combined to either reduce the response of the structure to earthquake ground shaking or increase the capacity of the structure to resist earthquake ground shaking with acceptable confidence. The systematic approach provides greater confidence in the ability of the structure to achieve the intended performance than the simplified approach.

15.4.6 Design Example for Connection Seismic Upgrade

The following example follows the design procedure developed by Yu et al. (2000). (For the definitions of various symbols, refer to list of symbols provided.)

15.4.6.1 Description of Existing Frame

Building constructed in early 1980s. Frame Centerline Dimensions: Story height $H_c = 12$ ft; bay width $L = 30$ ft; beam W30 × 99, A36 steel; column W12 × 279, A572 Gr. 50 steel.

15.4.6.2 Pre-Northridge Moment Connection Details

(1) Welded flange-bolted web moment connection; (2) beam flange groove welds: E70T-4 flux-cored arc welding (FCAW) with steel backing and weld tab left in place; (3) beam web connection: seven 1"-diameter A325 high strength bolts, 1/2" × 5" × 21.5") shear plate connected to the column with 5/16"

fillet welds, no supplemental web welds between the shear plate and the beam web; (4) no continuity plates and (5) no doubler plates.

15.4.6.3 Member Section Properties

W30 × 99 beam:

$$d = 29.65 \text{ in.}; b_{bf} = 10.45 \text{ in.}; t_{bf} = 0.67 \text{ in.}; t_{bw} = 0.52 \text{ in.}; A_b = 29.1 \text{ in.}^2; I_x = 3990 \text{ in.}^4; Z_{bx} = 312 \text{ in.}^3; S_{bx} = 269 \text{ in.}^3$$

W12 × 279 column:

$$d_c = 15.85 \text{ in.}; t_{cw} = 1.53 \text{ in.}; t_{cf} = 2.47 \text{ in.}; b_{cf} = 13.14 \text{ in.}; Z_{cx} = 481 \text{ in.}^3$$

15.4.6.4 Connection Modification Design

Consider a uniformly distributed gravity load ($w_g = 0.6 \text{ kip/ft}$) for the beam. Assume a column axial stress (f_a) of 10 ksi.

Step 1: Select preliminary haunch dimensions.

$$a = (0.5 \text{ to } 0.6)d_b \quad \text{Choose } a = 18 \text{ in.}$$

$$\theta = 30^\circ \pm 5^\circ \quad \text{Choose } \theta = 31^\circ$$

$$b = a \tan \theta = 10.8 \text{ in.}$$

Step 2: Determine beam probable plastic moment, M_{pd} , and beam shear, V_{pd} .

$$F_{ye} = 1.3F_y = 1.3(36) = 46.8 \text{ ksi}$$

$$M_{pd} = \alpha Z_{bx} F_{ye} = 1.1 \times 312 \times 46.8 = 16062 \text{ in.-kips}$$

$$L' = 360 - 15.85 - 2 \times 18 = 308.2 \text{ in.}$$

$$V_{pd} = \frac{2M_{pd}}{L'} + \frac{w_g L'}{2} = 112 \text{ kips}$$

Step 3: Check for strong column-weak beam condition.

$$\Sigma M_c = [2M_{pd} + V_{pd}(L - L')] \left(\frac{H_c - d_p}{H_c} \right) = 32161 \text{ in-kips}$$

$$\frac{\Sigma Z_c (F_{yc} - f_a)}{\Sigma M_c} = 1.20 > 1.0$$

Step 4: Determine β_{min} . Compute the required β to limit the top flange groove weld stress to an allowable value, $F_w = 0.8 F_{EXX} = 56 \text{ ksi}$:

$$\beta_{min} = \frac{(M_{pd} + V_{pd}a)/S_x - F_w}{\frac{V_{pd}a}{S_x} + \frac{V_{pd}}{I_b \tan \theta} \left(\frac{d^2}{4} - \frac{I_b}{A_b} \right)} = 0.91$$

Step 5: Size haunch flange. Size haunch flange for strength

$$A_{hf} \geq \frac{P_{hf}}{\phi F_y} = \frac{\beta V_{pd}}{\phi F_y \sin\theta} = 4.40 \text{ in.}^2$$

Select W21 × 93 (A572 Gr. 50 steel), which provides a haunch flange area of 7.83 in.² (= $b_{hf} \times t_{hf} = 8.42" \times 0.93"$). Check the compact section requirement

$$\frac{b_{hf}}{2t_{hf}} = \frac{8.42}{2(0.93)} = 4.5 \leq \frac{52}{\sqrt{F_y}} = 7.35$$

Step 6: Verify the β value for stiffness requirement. Compute the actual β value for the haunch flange stiffness requirement

$$\beta = \frac{b}{a} \left(\frac{3L'd + 3ad + 3bL' + 4ab}{3d^2 + 6bd + 4b^2 + \frac{12I_b}{A_b} + \frac{12I_b}{A_{hf} \cos^3 \theta}} \right) = 1.457 > \beta_{min}$$

The haunch thus sized would ensure that the tensile stress in the top flange groove weld is limited to the allowable stress, $F_w = 56$ ksi. The tensile stress in the top flange groove weld can be computed as follows:

$$f_{wt} = \frac{M_{pd} + V_{pd}(1-\beta)a}{I_b} \left(\frac{d}{2} \right) - \frac{\beta V_{pd} / \tan\theta}{I_b} \left(\frac{d^2}{4} - \frac{I_b}{A_b} \right) = 50.7 \text{ ksi} < 56 \text{ ksi}$$

The haunch flange axial stress is

$$\frac{\beta V_{pd}}{A_{hf} \sin\theta} = \frac{1.457 \times 112}{7.83 \times 0.515} = 40.5 \text{ ksi} < \phi F_y = 45 \text{ ksi},$$

where ϕ is equal to 0.9. Therefore, the selected haunch flange has adequate stiffness and strength. The maximum tensile stress in the groove weld of the beam bottom flange can be computed as follows:

$$f_{wb} = \frac{(V_{pd} L')/2 + V_{pd}(1-\beta)a}{I_b} \left(\frac{d}{2} \right) - \frac{(\beta V_{pd} / \tan\theta) \left(\frac{d^2}{4} + \frac{I_b}{A_b} \right)}{I_b} = 36.4 \text{ ksi} < 56 \text{ ksi}$$

Step 7: Check haunch web and beam web shear capacities. Check the haunch web width-thickness ratio

$$\frac{a \sin\theta}{t_{hw}} = \frac{18 \sin 31^\circ}{0.58} = 16 \leq \frac{260}{\sqrt{F_y}} = 36$$

The average shear stress in the haunch web can be computed

$$\tau_{hw} = \frac{a V_{pd}}{2(1+\nu) I_b} \left(\frac{L'}{2} - \frac{\beta}{\tan\theta} \left(\frac{d}{2} \right) + \frac{(1-\beta)a}{3} \right)$$

$$= 22.4 \text{ ksi} < \phi(0.6 F_y) = 27 \text{ ksi}$$

15-32 Earthquake Engineering: From Engineering Seismology to Performance-Based Engineering

Compute the shear in the beam web

$$V_{bw} = (1 - \beta)V_{pd} = (1 - 1.457) \times 112 = -51.2 \text{ kips}$$

The above computation indicates that the welded haunch is very effective in reducing the beam shear at the column face. Seven existing high strength bolts (1-in. diameter A325 bolts) can provide shear strength of 93.8 kips.

Step 8: Design welds and stiffeners. Complete penetration groove weld (E71T-8 electrode with a specified CVN value of 20 ft-lb at -20° F) at both ends of the haunch flange are specified to transmit the P_{hf} . Design the haunch web fillet weld

$$\nu_{hw} = \tau_{hw} t_{hw} = 22.4 \times 0.58 = 13.0 \text{ kips/in.}$$

The required fillet weld size is

$$a_w \geq \frac{\nu_{hw}}{\phi(0.707)(0.60F_{yw})2} = 0.24 \text{ in.}$$

A 5/16-in. fillet weld size on both sides of the haunch web is sufficient. Without beam web vertical stiffeners, the maximum concentrated compressive strength is governed by local web yielding (AISC, 1993).

$$\phi R_n = 1.0(2.5k + N)F_{yw}t_w = 87.6 \text{ kips} < \beta V_{pd} = 163.2 \text{ kips}$$

Try a pair of $\frac{1}{2}'' \times 5''$ plates (A572 Gr. 50 steel) for the stiffeners. Check the width-thickness ratio

$$\frac{b}{t} = 10 \leq \frac{95}{\sqrt{F_y}} = 13.4$$

Treat the stiffened web as an axially compressed member with an effective length of $0.75h$ ($h = 26.8$ in.), a cross section composed of two stiffeners and a strip of the beam web having a width of $12t_w$ (AISC, 1993).

$$A_{eff} = 2(5.0)(0.5) + 12(0.52)(0.52) = 8.24 \text{ in.}^2$$

$$I_{eff} = 0.5(5.0 \times 2 + 0.52)^3 / 12 = 57.4 \text{ in.}^4$$

$$r = \sqrt{\frac{I_{eff}}{A_{eff}}} = 2.40 \text{ in.}$$

$$\frac{KL}{r} = \frac{0.75h}{r} = 8.4$$

$$\phi F_{cr} = 42.2 \text{ ksi}$$

$$\phi P_n = \phi F_{cr}(A_{eff}) = 42.2(8.24) = 347 \text{ kips} > \beta V_{pd} = 163.2 \text{ kips}$$

Use complete joint penetration groove weld to connect each stiffener to the beam flange. Use two-sided 1/4-in. fillet welds to connect the stiffeners to the beam web. Figure 15.18 shows the welding details.

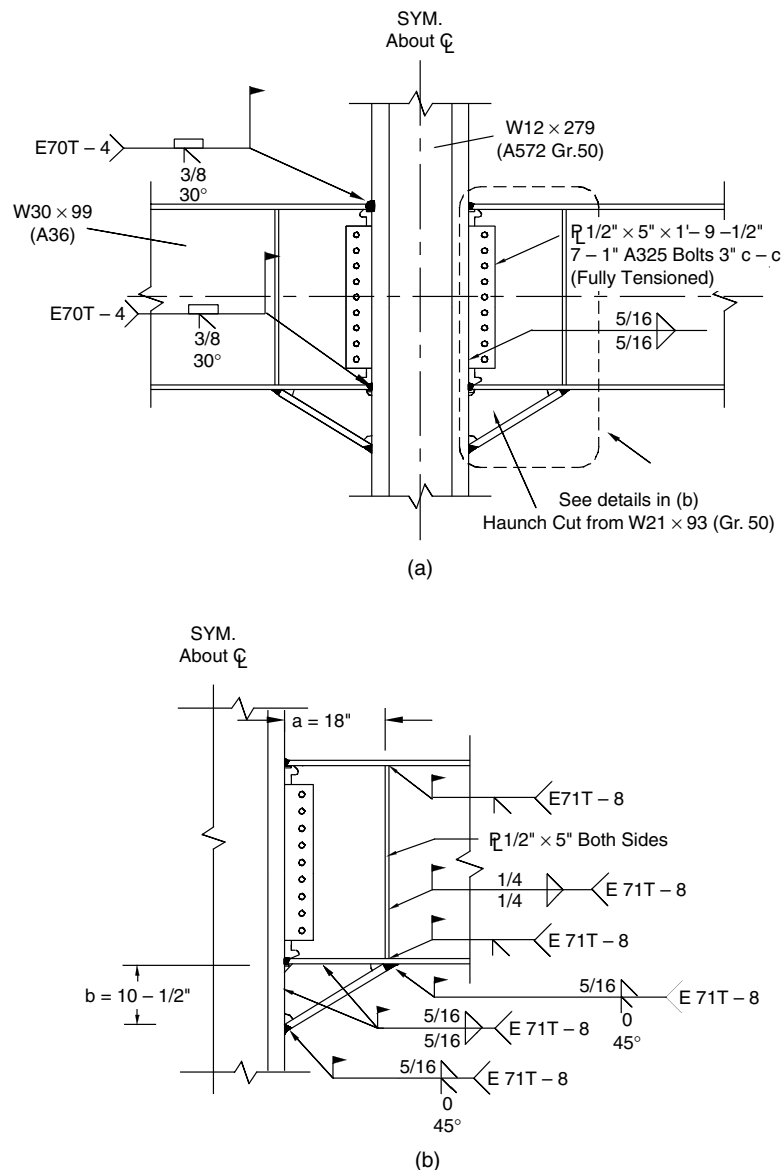


FIGURE 15.18 Haunch retrofit details.

15.5 The 2002 AISC Seismic Provisions

Between the incorporation of seismic design provisions into the Uniform Building Code (UBC) in the early 1950s, and the late 1980s, the SEAOC Seismology Committee was almost completely responsible for the content of these provisions. Spurred on by the federally funded National Earthquake Hazard Reduction Program (NEHRP), in the late 1980s and early 1990s seismic design began to be seen as more of a nationwide issue. During these years, the NEHRP program began to fund the Building Seismic Safety Council (BSSC) to develop model building code provisions for seismic design. The BSSC established a nationally represented committee structure, with technical subcommittees addressing each of the main structural materials, including structural steel. To support this effort, the AISC established a parallel committee and began the development of a set of seismic design provisions for steel buildings. These

provisions, first published in 1992, have scope and content similar to the SEAOC developed UBC provisions, but were developed in the load and resistance factor design (LRFD) format rather than allowable stress design (ASD). Since the entire 1994 NEHRP Provisions (FEMA, 1994) document was based on a strength design basis, the BSSC TS 6 subcommittee on steel structures adopted the 1992 AISC Provisions (AISC, 1992) by reference with minor modifications. With the damage to steel buildings caused by the Northridge earthquake, there was a significant increase in the effort required to update the seismic design provisions. With significant input and coordination with BSSC TS6 and the SEAOC Seismology Committee, the 1997 AISC Seismic Provisions (AISC, 1997) were completed. As a result of this joint effort, these provisions were adopted by reference in the 1997 NEHRP Provisions (FEMA, 1997a), without modification.

The 1997 AISC Seismic Provisions for Structural Steel Buildings (AISC, 1997), published on April 15, 1997, incorporated many of the advances in moment frame design achieved as part of the first phase of the FEMA/SAC program and other investigations. Part I of these provisions, in LRFD format, updates design requirements for materials, welded and bolted joints, columns and column splices as applicable to all structural systems. New system specific requirements were also provided for each different structural system. Two new moment frame systems, intermediate moment frames and special truss moment frames (STMF) were introduced in the 1997 Provisions. A major expansion to the quality assurance requirements for the seismic system (lateral force resisting system) was also included. Finally, an appendix for the testing of steel moment-resisting connections was developed to assist engineers engaged in project specific testing. Part II of the Provisions addresses the design and construction of composite steel and reinforced concrete. Part III of the Provisions mimics Part I, but is written in an ASD format. This part is included in the provisions to ease the transition from working stress to strength seismic design of steel structures. Part I of the 1997 AISC Seismic Provisions was incorporated into the 2000 International Building Code (IBC) (ICC, 2000) by reference. Some specific elements of these provisions that apply to moment frame design and construction included the following:

- ASTM A913 steel as an acceptable material.
- Specified system overstrength factors.
- Recognized variations between nominal yield strength and expected yield strength of different materials. This recognition is important for situations where the provisions require comparison of member strengths to control the location of inelastic deformations.
- Requirements for the design of bolted joints. Specifies that load may not be shared between welds and bolts in the same line of action.
- Requires that all complete penetration welds in the seismic system be made with materials that have a required Charpy V-Notch toughness of 20 ft.-lbs. at -20° F.
- Requires the demonstration of base material Charpy V-Notch toughness for heavy shapes of 20 ft.-lbs. at 70° F.
- Increased design loads for use in the design of column splices.
- Demonstration of moment connection rotation capacity via full scale tests.

Recognizing that rapid and significant changes in the knowledge base were occurring for the seismic design of SMF buildings, the AISC Specifications Committee committed to generating frequent supplements to the Seismic Provisions. The first such supplement was completed and published on February 15, 1999. Supplement No. 1 to the 1997 AISC Seismic Provisions (AISC, 1999b) included the following major items:

- ASTM A992 steel as an acceptable material for rolled shapes.
- All welds in the seismic force resisting system constructed with notch tough filler metals as specified in the 1997 Provisions.
- Identification of potential problems with low toughness materials in the "k" area of rolled shapes.
- Recognition of the moment connection test loading protocol developed for the FEMA/SAC program.

Supplement Number 2 to the 1997 AISC Seismic Provisions (AISC, 2000) was published on November 11, 2000. This supplement attempted to incorporate many of the final recommendations generated by the FEMA/SAC Project. These changes included the following:

- Added requirements to avoid material discontinuities created by fabrication or erection errors, the placement of welded shear studs or the attachment of other construction in the plastic hinging zone. This change was made in recognition that such discontinuities in these critical zones can lead to premature fracture.
- Changed connection test acceptance criteria from inelastic rotation to interstory drift angle. Modified testing appendix to follow a consistent approach.
- Revised requirements for panel zone shear strength in SMFs, such that excessively weak panel zones would be avoided.
- More stringent column width-thickness ratio and lateral bracing requirements for conditions where column inelasticity is a possibility. This criterion recognizes that limited column hinging cannot be precluded from moment frames unless the columns are significantly stronger (on the order of twice as strong) than the beams.
- Intermediate moment frame (IMF) systems are defined to be more consistent with the tested connection system previously defined as part of OMFs. Limitations on usage are defined in the 2000 NEHRP Provisions (FEMA, 2001).
- OMF systems are defined as the untested portion of previous definition, with even more severe application limitations.

The most recent publication of the AISC Seismic Provisions occurred in 2002. Because the scope of changes that have been made to these provisions since 1997 was so large, the provisions were republished in their entirety. The 2002 edition of the AISC Seismic Provisions further incorporated the results of the FEMA/SAC project that were published in 2000. In addition these provisions were modified as necessary to be consistent with the ASCE 7 document, "*Minimum Design Loads for Buildings and Other Structures*." This allowed the document to be incorporated as a reference into latest editions of the IBC and National Fire Protection Agency (NFPA) building codes (ICC, 2003; NFPA, 2002), which use ASCE 7 (ASCE, 2002) as their basis for design loadings.

As with the supplements to the 1997 provisions, a number of specific changes were made to make these provisions as current as possible. Some of the changes included the following:

- Additional requirements for the toughness of filler metals to be used in critical welds of some seismic systems (e.g., complete penetration welds in moment-resisting frames). These additional requirements include a two level toughness similar to that in FEMA 350 and FEMA 353 (FEMA, 2000a, 2000d).
- A revision to clarify member slenderness ratio requirements and better coordinate with the LRFD provisions.
- Increases in the moment frame column splice requirements for consistency with the FEMA/SAC recommendations.
- Clarification of column base design demands for various systems to ensure that these critical connections have adequate capacity and ductility.
- Clarification of lateral bracing requirements of moment frame beams.
- Increase in SMF web connection design requirements for consistency with FEMA 350.
- Incorporation of FEMA 350 recommendations for weld access holes in OMF systems.
- A new appendix that defines procedures to be used in the prequalification of moment connections. This is based on recommendations in the FEMA/SAC program and will be administered by an AISC committee established specifically for this purpose.
- Updates to Parts II and III to be consistent with the changes that were made to Part I.
- A major revision of the commentary.

15.6 Recommendations for Future Work

The efforts following the Northridge earthquake greatly advanced the state of the art in the seismic design of new SMF buildings as well as the evaluation and repair or upgrading of existing buildings. Nevertheless, numerous technical issues have been identified requiring further research, development or implementation. A number of such issues were outlined in FEMA 355D. In addition, the SEAOC Seismology Committee did an extensive review of the various FEMA documents and made a number of suggestions regarding areas needing further research (SEAOC, 2002). Some of the issues requiring further investigation include the following:

- Additional testing on other possible connection methods, such as the Free-Flange connection.
- Additional testing on weld overlay seismic repair and rehabilitation approaches.
- Additional testing and analysis to better define the yield mechanisms and failure modes of bolted moment connections.
- More definitive guidance on the design of moment connection continuity plates.
- Additional testing to better understand the performance of connections configured with columns with sections deeper than W14 shapes.
- Additional testing to better understand the performance of connections configured with box columns.
- Additional testing to better understand the performance of connections to the weak axis of wide flange columns.
- Additional information on the requirements for lateral bracing, both near the plastic hinge locations and along the length of the moment frame beams.

The AISC has recently funded research to fill a number of the gaps identified above. In addition, AISC has also commissioned a “connection prequalification review panel” to develop a national standard regarding the use of pre-qualified moment connections. “Pre-qualified” connections are those connections for which the panel deems sufficient in testing, analysis and design procedure development such that no additional testing is required for use of the connection within a set of preestablished parameters. As their work develops, it is expected that this committee will identify a number of other areas of recommended research that are needed to expand the connection prequalifications.

Another area where extensive additional work is expected in the future is in explicit performance based seismic design. The FEMA/SAC project presented an approach based on reliability theory concepts that set the groundwork for future developments in this area. These principles can be extended to other structural systems where sufficient data exists. More broad-based application of these principles for the design of steel moment framed structures and other forms of construction is expected to occur over the next decade.

15.7 Concluding Remarks

New lessons are learned from every major earthquake. The potential for brittle failures in welded steel connections was one of the major lessons of the 1994 Northridge earthquake. The FEMA-sponsored program and other parallel activities developed considerable new knowledge illuminating the various factors that interact to control the behavior of these connections and developed cost-effective and practical guidelines for the design, analysis and construction of steel frame buildings containing welded, bolted and other types of moment-resisting connections. Much of the information developed has been quickly incorporated into building codes and standards that govern the design and construction of these structures. As engineers become familiar with these procedures and implement them in building designs, new improvements will undoubtedly be made.

Acknowledgments

A portion of the information presented in this chapter summarizes work managed by the SAC Joint Venture under contract to FEMA (Contract EMW-95-K-4672) as part of the Program to Reduce Earthquake Hazards in Steel Moment Frame Structures. The authors are indebted to the outstanding and diligent efforts of numerous individuals and organizations that have supported or contributed to this Program. The authors also acknowledge the efforts of all AISC TC9 members for their contributions to the development of the AISC Seismic Provisions.

Glossary

AISC—American Institute of Steel Construction.

ASTM—American Society of Testing and Materials.

Axial restraining effects—Conditions where the change of length of a structural element is rigidly restrained because of the presence of other structural elements.

Back up bar—A small bar, typically steel, that is used to provide a surface for the placement of a single-bevel CJP weld since the fit up for this weld allows a space between the two connected members.

Base material—Material that composes the beam, column, plate or other shape.

CJP—Complete joint penetration groove weld: a weld that develops the full strength of the welded member element, typically replacing the full thickness base metal of the element with weld metal.

Code design level earthquake ground shaking—A level of seismic ground motion based on a recurrence interval of once every 475 years; design forces based on this level of ground shaking are then typically reduced to account for system ductility based on empirical data.

Deep columns—Columns with a nominal depth greater than 18 in.

Doubler plate—A plate or plates added to a column web to increase the thickness (and stiffness and strength) of the panel zone.

Elastic rotation—The level of measured connection rotation that occurs due to elastic curvature of beams and columns that comprise the moment connection.

Filler metal—Consumable metal welding electrode used in the welding process.

Free-flange connection—A fully rigid moment-resisting connection that holds back the web of the girder from the face of the column.

Lateral-torsional buckling—A phenomenon where a flexural member buckles in a combination of cross-sectional warping (twisting) and out-of-plane buckling of the member about one of the minor axes, typically the weak axis of the member.

Local ductility demand—Ductility demand at a specific location, such as the plastic hinge.

Local kinking of beam flanges through panel zone behavior—Panel zone behavior transforms the rectangular panel zone into a trapezoid shape through shear deformations; this can lead to local kinking at the intersection of beam flange and column flange.

Low cycle fatigue—A phenomenon that results in the formation and propagation of cracking in material because of high-strain demand occurring in relatively few strain reversals.

LRFD—Load and resistance factor design (a specific design methodology that considers limit states opposed to an allowable stress distribution over a given cross section).

Panel zone—The area of a column bounded by the column flanges and the intersecting moment beam flanges, typically comprising the column web or column web and doubler plates.

Plastic curvature—Curvature of a member beyond elastic curvature.

Plastic hinge—Location where focused inelasticity occurs in a structural member.

Plastic rotation—The level of measured connection rotation that occurs due to yielding in the plastic hinge regions, the panel zone or all yielding areas of the moment connection.

Plastic strain capacity—The strain limit of a material between yield and fracture.

Pre-Northridge connections—Welded flange, bolted web moment frame connections that were commonly used prior to the Northridge earthquake.

Shear influence on beam flanges—The condition where shear developed at the end of a moment beam as a result of earthquake forces is carried through the beam flanges, influencing the stresses in the weldments between the beam flange and column flange.

SSDA—Seismic Structural Design Associates, Inc. A company that develops and markets a proprietary steel SMF connection.

Strain effects due to beam flange thickness—Strain is distributed along a cross section based on cross-sectional area; thicker beam flanges will have a nonlinear strain distribution based on the area of the flange.

Subassemblage—A construction of beams and columns that represent a portion of a larger multibay, multistory frame or structure (also defines subassembly).

Through thickness stresses on column flanges—The stresses that flow through the thickness of the column flange (perpendicular to the major axis of the column) due to direct tension application from the moment beam flange.

Toughness of the base material for beams and columns—The ability of the base material to arrest the development and propagation of cracking.

Weld access hole size and geometry—A weld access hole (rat hole) is a hole created in the beam web to allow weld to be placed in a manner resulting in a continuous weld along the beam flange; welds made from the web side of the column flange without the weld access hole will have a discontinuity at the web location, known to be the area of highest stress in moment connections.

Weld metal—The combination of base material and filler metal.

Weld metal toughness—The ability of weld metal to arrest the development and propagation of cracking.

List of Symbols

A_{hf}	area of beam section, in. ²
C_{pr}	haunch flange area, in. ²
F_{EXX}	peak connection strength factor $\left\{ \frac{F_y + F_u}{2F_y} \right\}$, 1.15 for RBS connections
F_y	strength of weld metal, ksi
	specified minimum yield stress of the type of steel to be used, ksi. As used in the LRFD Specification, "yield stress" denotes either the minimum specified yield point (for those steels that have a yield point) or the specified yield strength (for those steels that do not have a yield point)
F_{yb}	F_y of a beam, ksi
F_{yc}	F_y of a column, ksi
F_{ye}	expected yield strength of steel, ksi
F_u	specified minimum tensile strength, ksi
F_w	allowable tensile stress of the groove weld (0.8 F_{EXX})
H	story height, in.
I_b	moment of inertia of beam section, in. ⁴
I_{hb}	moment of inertia of the beam section including haunch, in. ⁴
L	distance between columns (center-to-center) or length of beam between points of inflection, in.
L'	length of beam between plastic hinges (center-to-center), in.
ΣM_c	sum of column moment at the top and bottom of the enlarged panel zone, in.-kips
M_f	moment at column face, in.-kips
M_c	moment at column centerline, in.-kips
$M_{yield-beam}$	moment at column face, in.-kips
M_{pr}	probable moment in beam at plastic hinge, in.-kips
M_p	full plastic moment of beam based on the actual yield strength, in.-kips
M_{pd}	design plastic moment of the beam at the haunch tip, in.-kips

M_{pn}	full plastic moment of beam based on the minimum specified yield strength, in.-kips
P	applied point load, kips
P_{bf}	beam bottom flange force, kips
P_{hf}	haunch flange force, kips
R_y	ratio of the expected yield strength, F_{ye} , to the specified minimum yield strength, F_y
R_{yb}	ratio of the expected yield strength to the minimum specified yield strength F_y for a beam
R_{yc}	ratio of the expected yield strength to the minimum specified yield strength F_y for a column
S_b	elastic section modulus of a beam, in. ³
SDR	story drift ratio
V_{bw}	shear force in the beam web, kips
V_c	shear force in column above and below connection, kips
V_G	beam shear force due to gravity loads, kips
V_{pd}	design beam shear force, kips
V_b	beam shear, kips
V_f	beam shear at the face of the column flange, kips
V_g	beam shear due to gravity loads, kips
V_p	beam shear due to plastic moment in plastic hinge, kips
V_{pz}	panel zone shear, kips
W	applied distributed gravity load, kips/ft
Z_b	plastic section modulus of a beam, in. ³
Z_{be}	expected plastic section modulus of beam, in. ³
Z_{RBS}	plastic section modulus of RBS, in. ³
Z_{xb}	plastic section modulus of beam, in. ³
Z_{xc}	plastic section modulus of column, in. ³
Z_b	plastic section modulus of beam section, in. ³
Z_c	plastic section modulus of column section, in. ³
a	length of welded haunch, in.
a_w	fillet weld size, in.
b	depth of welded haunch, in.
b_{hf}	haunch flange width, in.
d	beam depth, in.
d_c	column depth, in.
d_p	depth of modified beam (i.e., includes haunch), in.
f_a	axial stress in the column above and below, ksi
f_{wt}	tensile stress at the beam top flange groove weld, ksi
f_{wb}	tensile stress at the beam bottom flange groove weld, ksi
b_c	width of column flange, in.
b_f	flange width, in.
d_b	overall beam depth, in.
d_c	overall column depth, in.
h	height of column between points of inflection, in.
l_{hf}	haunch flange length, in.
t_{bf}	beam flange thickness, in.
t_{bw}	beam web thickness, in.
t_{cf}	column flange thickness, in.
t_{cw}	column web thickness, in.
t_{hf}	haunch flange thickness, in.
t_{hw}	haunch web thickness, in.
t_{cf}	thickness of column flange, in.
t_{cw}	thickness of column web, in.
t_f	thickness of beam flange, in.

t_w	thickness of beam web, in.
t_p	thickness of panel zone including doubler plate(s), in.
w_g	uniform beam load, kips/ft
x	distance from beam plastic hinge and face of column flange, in.
a	strain hardening factor of steel
b	ratio of vertical component of haunch flange force to design shear force, V_{pd}
β_{min}	minimum β value to limit beam top flange groove weld stress to F_w
q	acute angle between haunch flange and beam flange
θ_p	connection plastic rotation based on the centerline dimension
ϕ, ϕ_v	resistance factor
τ_{hw}	haunch web shear stress, ksi and
ν	Poisson's ratio of steel (0.3).

References

- American Institute of Steel Construction (1992). *Seismic Provisions for Structural Steel Buildings*, AISC, Chicago, IL.
- American Institute of Steel Construction (1993). *Load and Resistance Factor Design (LRFD) Specification*, 2nd edn., AISC, Chicago, IL.
- American Institute of Steel Construction (1997). *Seismic Provisions for Structural Steel Buildings*, AISC, Chicago, IL.
- American Institute of Steel Construction (1999a). *Load and Resistance Factor Design (RFD) Specification*, 3rd ed., AISC, Chicago, IL.
- American Institute of Steel Construction (1999b). *Seismic Provisions for Structural Steel Buildings* (1997), Supplement No. 1, AISC, Chicago, IL.
- American Institute of Steel Construction (2000) *Seismic Provisions for Structural Steel Buildings* (1997), Supplement No. 2, AISC, Chicago, IL.
- American Institute of Steel Construction (2002). *Seismic Provisions for Structural Steel Buildings*, AISC, Chicago, IL.
- American Society of Civil Engineers (2002). *Minimum Design Loads for Buildings and Other Structures*, ASCE 7-02, ASCE, Reston, VA.
- Berg, G.V. (1973). Response of Buildings in Anchorage, in *The Great Alaska Earthquake of 1964*, National Academy of Science, Washington, D.C.
- Bertero, V.V., Anderson, J.C. and Krawinkler, H. (1994). Performance of steel building structures during the Northridge earthquake, U.C. Berkeley EERC Report 94-09, Berkeley, CA.
- Blodgett, O.W., Funderburk, R.S., Miller, D.K. and Quintana, M. (1999). *Fabricators' and Erectors' Guide to Welded Steel Construction*, James F. Lincoln Arc Welding Foundation, Cleveland, OH.
- Chi, B. and Uang, C.-M. (2002). Cyclic response and design recommendations of reduced beam section moment connection with deep columns, *Journal of Structural Engineering* 128(4), 464–473.
- Christopoulos, C., Filiault, A., Uang, C.-M. and Folz, B. (2002). Post-tensioned energy dissipating connections for moment-resisting steel frames, *Journal of Structural Engineering*, 128(9), 1111–1120.
- Civjan, S. and Engelhardt, M.D. (1998). Experimental investigation of methods to retrofit connections in existing seismic-resistant steel moment frames, Summary Final Report to the National Institute of Standards and Technology, Phil M. Ferguson Structural Engineering Laboratory, University of Texas at Austin, TX.
- Earthquake Engineering Research Institute (1973). *Managua, Nicaragua Earthquake of December 23, 1972*, EERI, Oakland, CA.
- Engelhardt, M.D., Winneberger, T., Zekany, A.J. and Potyraj, T. (1998). Experimental investigation of dogbone moment connections, *Engineering Journal*, 35(4), 128–139.

- Federal Emergency Management Agency (1994). *Recommended Provisions for Seismic Regulations for New Buildings*, National Earthquake Hazards Reduction Program, FEMA, Washington, DC.
- Federal Emergency Management Agency (1995). *Interim Guidelines: Evaluation, Repair, Modification and Design of Welded Steel Moment Frame Structures*, FEMA-267 (SAC 95-02), FEMA, Washington, DC.
- Federal Emergency Management Agency (1997a). *Recommended Provisions for Seismic Regulations for New Buildings*, National Earthquake Hazards Reduction Program, FEMA, Washington, DC.
- Federal Emergency Management Agency (1997b). Supplement No. 1 to the Interim Guidelines, FEMA-267A, FEMA, Washington, DC.
- Federal Emergency Management Agency (1999). Supplement No. 2 to the Interim Guidelines, FEMA-267B, FEMA, Washington, DC.
- Federal Emergency Management Agency (2000a). *Recommended Seismic Design Criteria for New Steel Moment Frame Buildings*, FEMA-350, FEMA, Washington, DC.
- Federal Emergency Management Agency (2000b). *Recommended Seismic Evaluation and Upgrade Criteria for Existing Welded Steel Moment Frame Buildings*, FEMA-351, FEMA, Washington, DC.
- Federal Emergency Management Agency (2000c). *Recommended Post-earthquake Evaluation and Repair Criteria for Welded, Steel Moment Frame Buildings*, FEMA-352, FEMA, Washington, DC.
- Federal Emergency Management Agency (2000d). *Recommended Specifications and Quality Assurance Guidelines for Steel Moment Frame Construction for Seismic Applications*, FEMA-353, FEMA-353, Washington, DC.
- Federal Emergency Management Agency (2000e). *A Policy Guide to Steel Moment-Frame Construction*, FEMA-354, FEMA, Washington DC.
- Federal Emergency Management Agency (2000f). *State of the Art Report on Base Metals and Fracture*, FEMA-355A, K. Frank and J. Barsom (Team Leaders), FEMA, Washington, DC.
- Federal Emergency Management Agency (2000g). *State of the Art Report on Welding and Inspection*, FEMA-355B, M. Johnson (Team Leader), FEMA, Washington, DC.
- Federal Emergency Management Agency (2000h). *State of the Art Report on Systems Performance*, FEMA-355C, H. Krawinkler (Team Leader), FEMA, Washington, DC.
- Federal Emergency Management Agency (2000i). *State of the Art Report on Connection Performance*, FEMA-355D, C. Roeder (Team Leader), FEMA, Washington, DC.
- Federal Emergency Management Agency (2000j). *State of the Art Report on Past Performance of Steel Moment-Frame Buildings in Earthquakes*, FEMA 355E, D. Bonowitz and R. Evans, (Team Leader), FEMA, Washington, DC.
- Federal Emergency Management Agency (2000k). *State of the Art Report on Performance Prediction and Evaluation*, FEMA-355F, D. Foutch (Team Leader), FEMA, Washington, DC.
- Federal Emergency Management Agency (2000l). *Recommended Provisions for Seismic Regulations for New Buildings*, National Earthquake Hazards Reduction Program, FEMA, Washington, DC.
- Gross, J.L., Engelhardt, M.D., Uang, C.M., Kasai, K. and Iwankiw, N.R. (1999). Modification of existing welded steel moment frame connections for seismic resistance, Steel Design Guide Series, No. 12, American Institute of Steel Construction, Chicago, IL.
- Guidelines for Cyclic Seismic Testing of Components of Steel Structures for Buildings. (1992). Report No. ATC-24, Applied Technology Council, Redwood City, CA.
- Hamburger, R.O. and Foutch, D. (2000). Performance basis of guidelines for evaluation, upgrade and design of moment-resisting steel frames, *Proceedings of the Twelfth World Conference on Earthquake Engineering*, Auckland, New Zealand.
- Himmelwright, A.L.A. (1906). *The San Francisco Earthquake and Fire*, The Roebling Construction Company, New York.
- International Code Council (1997). *International Building Code 2000, ICC, Birmingham, AL*.
- International Code Council (2003). *International Building Code 2003, ICC, Birmingham, AL*.
- International Conference of Building Officials (1985). Uniform Building Code, ICBO, Whittier, CA.
- International Conference of Building Officials (1988). Uniform Building Code, ICBO, Whittier, CA.

- International Conference of Building Officials (1997). Uniform Building Code, 1997 edition, ICBO Whittier, CA.
- Krawinkler, H. (1978). Shear design of steel frame joints, *Engineering Journal*, 15(3), 82–91.
- Lee, C.-H. and Uang, C.-M. (2001). Analytical modeling and seismic design of steel moment connection with welded straight haunch, *Journal of Structural Engineering*, 127(9), 1028–1035.
- Mahin, S.A., Hamburger, R.O. and Malley, J.O. (1998). National program to improve seismic performance of steel frame buildings, *Journal of Performance of Constructed Facilities*, 12(4), 172–179.
- Moore, K.S., Engelhardt, M.D. and Malley, J.O. (1999). Design of Reduced Beam Section (RBS) Moment Frame Connections, *Steel Tips*. Structural Steel Educational Council, Moraga, CA.
- National Fire Protection Association (2002). *NFPA 5000, Building Construction and Safety Code*, NFPA, Quincy, MA.
- Plumier, A. (1997). The Dogbone: back to the future, *Engineering Journal*, 34 (2), 61–67.
- Popov, E.P. and Stephen, R.M. (1972). Cyclic loading of full-size steel connections, Bulletin No. 21, American Iron and Steel Institute, Washington, DC.
- Priestley, M.J.N., Sritharan, S., Conley, J.R. and Pampanin, S. (1999). Preliminary results and conclusions from the PRESS five-story precast concrete test building, *PCI Journal*, 44(6), 42–67.
- Quintana, M., Johnson M. (1998). The effects of intermixed weld metal on mechanical properties, Part III, *Proc. International Conference on Welded Constructions in Seismic Areas*, American Welding Society (AWS).
- Richard, R.M., Allen, J. and Partrige, J.E. (2001). Accumulated seismic connection damage based upon full scale low cycle fatigue connection tests, *Proceedings of the Structural Engineers Association of California*. San Diego, CA.
- Ricles, J.M., Sause, R., Garlock, M.M. and Zhao, C. (2001). Post-tensioned seismic-resistant connections for steel frames, *Journal of Structural Engineering*, 217(2), 113–121.
- SAC (1995a). Case studies of steel moment frame building performance in the Northridge earthquake of January 17, 1994, Technical Report SAC 95-07, SAC Joint Venture, Sacramento, CA.
- SAC (1995b). Experimental investigations of materials, weldments and nondestructive examination techniques, Technical Report SAC 95-08, SAC Joint Venture, Sacramento, CA.
- SAC (1995c). Experimental investigations of beam to column connections, Technical Report SAC 96-01, Parts A and B, SAC Joint Venture, Sacramento, CA.
- SAC (1995d). Parametric Analytic Investigations of Ground Motion and Structural Response, Technical Report SAC 95-05, SAC Joint Venture, Sacramento, CA.
- SAC (1995e). Surveys and assessment of damage to buildings affected by the Northridge earthquake of January 17, 1994, Technical Report SAC 95-06, SAC Joint Venture, Sacramento, CA.
- SAC (1996). Experimental investigations of beam-column subassemblies, Technical Report No. SAC-96-01, SAC Joint Venture, Sacramento, CA.
- Schneider, S.P.; Roeder, C.W. and Carpenter, J.E. (1993). Seismic behavior of moment-resting steel frames: experimental study, *Journal of Structural Engineering*, 119(6), 1885–1902.
- Shen, Jie-Hua J., Astaneh-Asl, A. and McCallen, D.B. (2002). Use of steel columns in special steel moment frames, *Steel Tips* Structural Steel Educational Council, Moraga, CA.
- Structural Engineers Association of California (2002). Commentary and recommendations on FEMA 350, prepared by SEAOC Seismology Committee, Sacramento, CA.
- Uang, C.-M. and Bondad, D. (1996). Static cyclic testing of pre-Northridge and haunch repaired steel moment connections, Report No. SSRP-96/02, Division of Structural Engineering, University of California, San Diego, La Jolla, CA.
- Uang, C.-M. and Fan, C.-C. (1999). Cyclic instability of steel moment connections with reduced beam sections, Report No. SSRP-99/21, Department of Structural Engineering, University of California, San Diego, CA.
- Uang, C.-M. and Latham, C.T. (1995). Cyclic testing of full-scale MNH-SMF™ moment connections, Report No. TR-95/01, Structural System Research, University of California at San Diego, La Jolla, CA.

- Uang, C.-M., Yu, Q.-S., Noel, S. and Gross, J. (2000). Cyclic testing of steel moment connections rehabilitated with RBS or Welded haunch, *Journal of Structural Engineering*, 126(1), 57–68.
- U.S. Department of Commerce (1973). *San Fernando, California, Earthquake of February 9, 1971*, Parts A and B, Washington, DC.
- Youssef, N., Bonowitz, D. and Gross, J. (1995). A survey of steel moment-resisting frame buildings affected by the 1994 Northridge earthquake, Report No. NISTIR 5625, NIST, Gaithersburg, MD.
- Yu, Q.-S., Bondad, D. and Uang, C.-M. (1996). Experimental and analytical studies of full-scale pre-Northridge steel moment frame connections under dynamic loading, Report No. SSRP-96/03, Division of Structural Engineering, University of California, San Diego, La Jolla, CA.
- Yu, Q.-S., Noel, S. and Uang, C.-M. (1997). Experimental studies on seismic rehabilitation of pre-Northridge steel moment connections: RBS and haunch approach, Report No. SSRP-97/08, University of California, San Diego, CA.
- Yu, Q.-S., Gilton, C.S. and Uang, C.-M. (1999). Cyclic response of RBS moment connections: loading sequence and lateral bracing effects, Report No. SSRP 99-13, University of California, San Diego, CA.
- Yu, Q.-S., Uang, C.-M. and Gross, J. (2000). Seismic rehabilitation design of steel moment connection with welded haunch, *Journal of Structural Engineering*, 126(1), 69–78.

16

Steel Buckling-Restrained Braced Frames

Chia-Ming Uang

Masayoshi Nakashima

16.1	Introduction.....	16-1
16.2	Types of Braced Frames.....	16-1
16.3	Buckling-Restrained Braced Frames	16-4
	Introduction • Concept of BRB • Components of BRB • Advantages and Disadvantages of BRBFs • Development of BRBs • SEAOC–AISC Qualifying Cyclic Test Requirements • BRBF Subassembly Performance • BRBF System Performance • BRBF Seismic Design Procedure	
16.4	Concluding Remarks	16-34

16.1 Introduction

This chapter presents the seismic analysis and design of a newly developed steel braced frame system called buckling-restrained braced frames (BRBFs). After a brief introduction of the conventional braced frame systems that include the concentrically and eccentrically braced frames, the remainder of the chapter is devoted to the concept of buckling-restrained braces (BRBs), the development of BRBs in several countries, the behavior of BRBs at the component, the subassembly and the system levels. Testing requirements as well as seismic design procedures proposed by SEAOC–AISC are also presented.

16.2 Types of Braced Frames

Braced frames and moment frames are the most widely used framing systems for steel construction in seismic regions. Compared to a moment frame (see Chapter 15), a braced frame offers high-lateral stiffness for drift control. A braced frame can be broadly classified as a concentrically braced frame (CBF) or an eccentrically braced frame (EBF). Figure 16.1 shows examples of concentric bracing configurations. In a CBF, the members (beams, columns and braces) with the centerlines meeting at a joint form a vertical truss system. Members in a CBF are subjected primarily to axial loads in the elastic range. The diagonal bracing members are designed to deform inelastically during a moderate or severe earthquake.

A CBF can be subdivided into two groups. Braces in a conventional CBF are expected to buckle and yield during a significant seismic event. On the basis of a significant amount of research in the past few decades, seismic design provisions have been developed. In the AISC Seismic Provisions (2002), a conventional CBF can be designed as a Special CBF (SCBF) or as an Ordinary CBF (OCBF), depending on the ductility detailing requirements that are implemented into the system. See Bruneau et al. (1997) and Uang et al. (2001) for further information on the development and design of these conventional CBF systems.

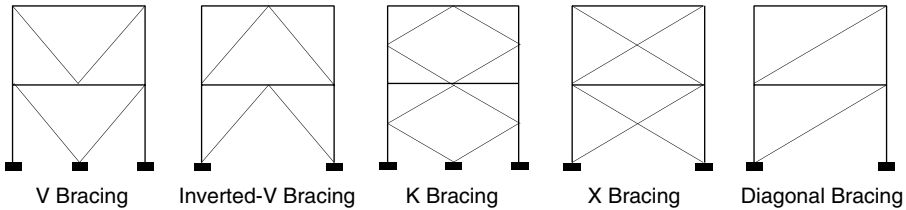


FIGURE 16.1 Examples of concentric bracing configurations (AISC (2002). *Seismic Provisions for Structural Steel Buildings*, American Institute of Steel Construction, Chicago, IL).

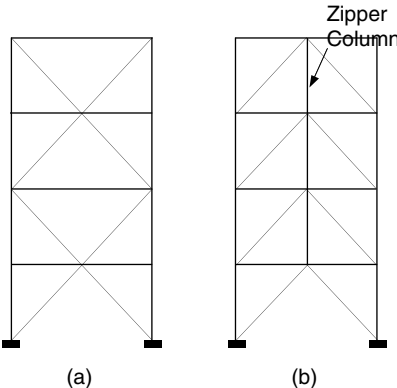


FIGURE 16.2 Configurations that mitigate unbalanced loads in beams (AISC (2002). *Seismic Provisions for Structural Steel Buildings*, American Institute of Steel Construction, Chicago, IL). (a) X configuration; (b) zipper column.

V or inverted-V bracing in Figure 16.1a and Figure 16.1b is a popular configuration in the United States. Because one brace in a story is expected to buckle and lose a significant amount of compressive strength while the other brace is expected to yield during tension, the AISC Seismic Provisions require that for SCBFs the beam be designed for an unbalanced vertical load at midspan. It has been suggested that the adverse effect of this unbalanced load be mitigated by using bracing configurations such as V and inverted-V braces in alternate stories to create an X-configuration over two-story modules (Figure 16.2a and Figure 16.3), or by using a “zipper column” (Figure 16.2b). The effectiveness of these schemes has been demonstrated by Khatib et al. (1988) and Sabelli (2001).

Since buckling of braces is not ideal for energy dissipation, an alternative approach to the conventional CBF system that precludes brace buckling has been developed. The system, called the buckling-restrained braced frame (BRBF), is becoming popular in both Japan and United States. A detailed description of this innovative system is presented in the next section.

Figure 16.4 shows two examples of EBF configurations. At each floor level, the beam segment, which is designated with a length e , is called the link. In an EBF, links are properly designed and detailed such that energy dissipation is concentrated in these elements, while the braces, columns and beams outside the link region are designed to remain elastic during a severe earthquake in accordance with capacity design principles. The expected yielding mechanism is shown in Figure 16.5. Figure 16.6 shows a typical link detail.

On the basis of the extensive research that was conducted in the 1980s, the AISC Seismic Provisions provide guidelines for the design and detailing of EBFs. More detailed description of the development and design of EBFs can be found in Bruneau et al. (1997) and Uang et al. (2001).



(a) Elevation



(b) Gusset Connection Details

FIGURE 16.3 Special concentrically braced frame construction with X configuration.

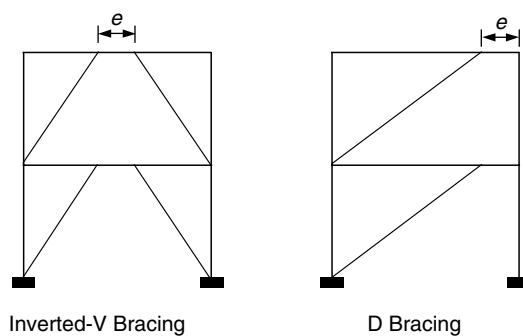


FIGURE 16.4 Examples of eccentric bracing configurations.

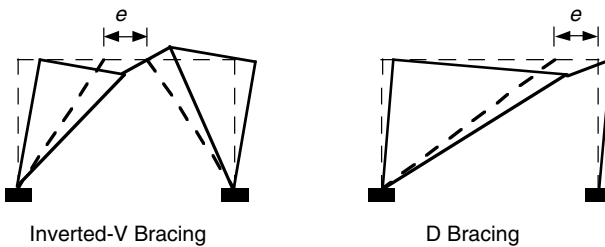


FIGURE 16.5 Yielding mechanism in eccentrically braced frames.



FIGURE 16.6 Typical link detail (courtesy of Structural Engineers, Inc.).

16.3 Buckling-Restrained Braced Frames

16.3.1 Introduction

The disadvantages of the CBF system can be overcome if the brace can yield during both tension and compression without buckling. A braced frame that incorporates this type of brace, i.e., buckling-restrained brace (BRB). Therefore, BRBF is a special class of CBF that precludes brace buckling. Figure 16.7 shows a comparison of the behavior of a BRB and a conventional brace.

A BRB can be viewed as a hysteretic damper. Following the concept of “damage tolerant structures” described in Chapter 10, certain BRBF designs correspond to a “parallel system” in which the main structure remains elastic and only dampers are expected to dissipate energy (Wada et al., 1992); after a major earthquake event the main structure is expected to return to its original shape after the replacement of deformed dampers. BRBFs have been used extensively for seismic applications in Japan after the 1995 Kobe earthquake (Reina and Normile, 1997). This type of framing system also gained its acceptance in the United States a few years after the 1994 Northridge earthquake (Clark et al., 1999). Currently about 250 buildings that use BRBFs have been constructed in Japan, and the construction of about 25 BRBF buildings has been completed or is underway in the United States. Figure 16.8 shows an example application of BRBFs for new construction using a type of BRB called Unbonded Brace. BRBFs have also been applied to seismic rehabilitation of reinforced concrete buildings (see Figure 16.9) (Brown et al., 2001; Tremblay et al., 1999).

16.3.2 Concept of BRB

Most of the BRBs developed to date are proprietary, but the concepts are similar. Figure 16.10 shows the concept of a type of BRB (also see Chapter 10). The brace is composed of a ductile steel core, which is

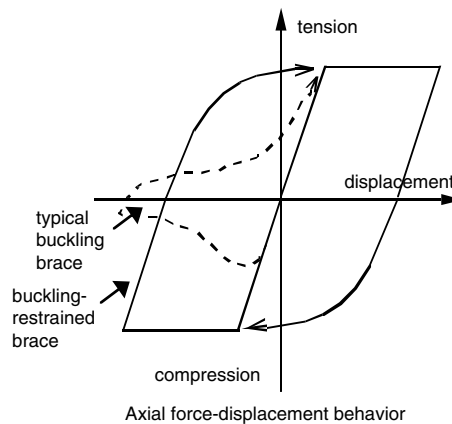


FIGURE 16.7 Behavior of conventional brace versus buckling-restrained brace. (Adapted from Clark, P., et al. (1999). *Proc. 69th Annual SEAOC Convention*, Sacramento, CA. With permission.)

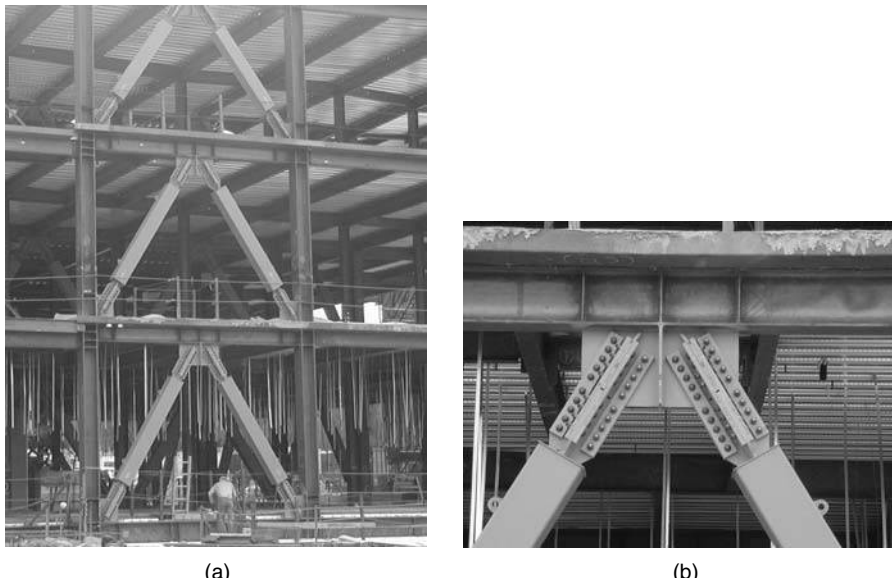


FIGURE 16.8 Buckling-restrained brace frames for new construction. (a) Elevation; (b) connection details (courtesy of SIE, Inc.).

designed to yield during both tension and compression. To preclude global buckling in compression, the steel core is first placed inside a steel casing (usually a hollow structure shape) before the casing is filled with mortar or concrete. Prior to casting mortar, an unbonding material or a very small air gap between the steel core and mortar is provided to minimize, or eliminate if possible, the transfer of axial force from steel core to mortar and the hollow structural section (HSS). The Poisson effect also causes the steel core to expand under compression; this requires that a small gap be provided between the steel core and mortar.

16.3.3 Components of BRB

Figure 16.11 shows an example of a BRB, which is composed of the following five components (also see Chapter 10):



FIGURE 16.9 Buckling-restrained brace frames for seismic rehabilitation of reinforced concrete building. (a) Global view (courtesy of SIE, Inc.); (b) connection details (courtesy of Reaveley Engineers & Associates, Inc.).

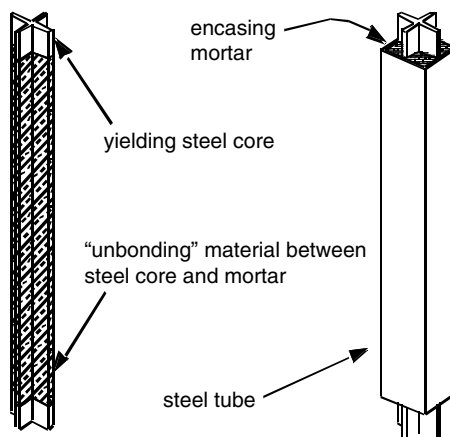


FIGURE 16.10 Concept of a type of buckling-restrained brace (Adapted from Clark, P., et al. (1999). *Proc. 69th Annual SEAOC Convention*, Sacramento, CA. With permission.)

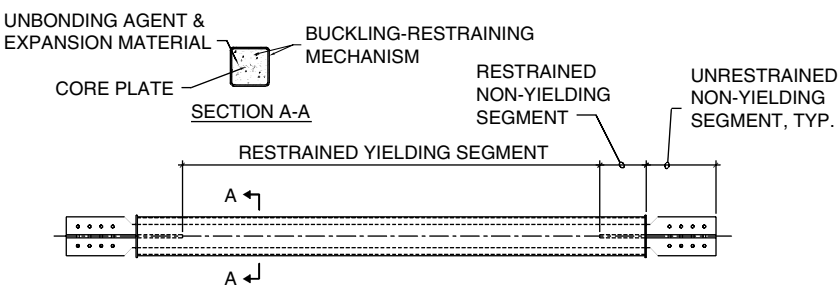


FIGURE 16.11 Components of buckling-restrained brace. (Adapted from Wada et al. (1998) by López 2001.)

1. *Restrained yielding segment:* This steel segment can be rectangular or cruciform in cross section. Although it is common that a steel plate be surrounded in a casing, more than one plate can be used, if desired. Because this segment is designed to yield under cyclic loading, mild steel (e.g., A36 steel or low-strength steel) that exhibits high ductility is desirable. Alternatively, high-strength low-alloy steel (e.g., A572 Gr. 50 steel) has also been used. Also desirable are steel materials with a predictable yield strength with small variations. This latter property is essential for reliable capacity design of BRBFs.

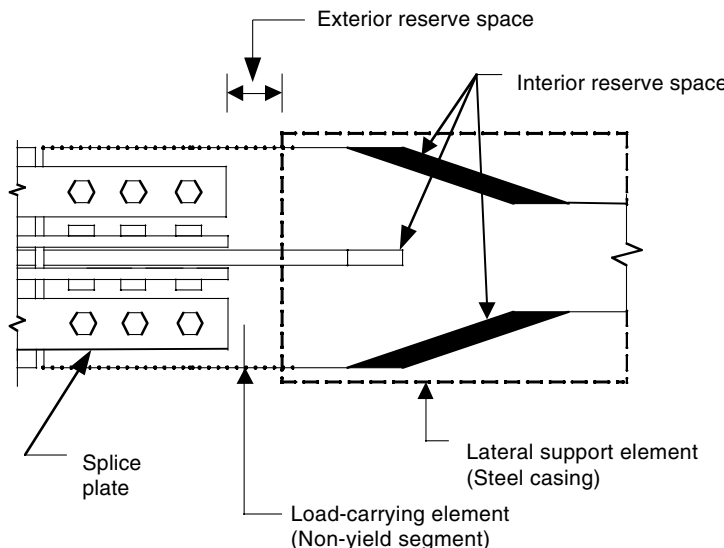


FIGURE 16.12 Gap between mortar and restrained yielding element. (Chen, C.C., Chen, S.Y. and Liaw, J.J. (2001a). Application of low yield strength steel on controlled plastification concentrically braced frames, *Canadian Journal of Civil Engineering*, 28, 823–836.)

2. *Restrained nonyielding segment:* This segment, which is surrounded by the casing and mortar, is usually an extension of the restrained yielding segment but with an enlarged area to ensure elastic response. This can be achieved by widening the restrained yielding segment. (The transition in width needs to be smooth to avoid stress concentration.) It is also common that stiffeners be welded to increase the area in this region.
3. *Unrestrained nonyielding segment:* This segment is usually an extension of the restrained nonyielding segment, except that it projects from the casing and mortar for connection to the frame. This segment is also called the steel core projection. It is common that this segment be designed as a bolted connection for field erection, but other connection designs such as a pin connection or a welded connection are also possible. Design considerations of this segment include (i) construction tolerance for ease of field erection and to facilitate the removal and (ii) local buckling prevention.
4. *Unbonding agent and expansion material:* Inert material that can effectively minimize or eliminate the transfer of shear force between the restrained steel segment and mortar can be used; materials like rubber (Iwata et al., 2000; Staker and Reaveley, 2002), polyethylene (Tremblay et al., 1999), silicon grease (Chen et al., 2001a) or mastic tape (Watanabe et al., 1988) have been reported. The restrained yielding segment is expected to experience small-amplitude buckling in higher modes due to the presence of the restraining mechanism. The gap needs to be sufficiently large to allow for the expansion of the yielding steel core in compression. Otherwise the friction that is created by the bearing action between the expanding yielding steel and mortar would force the buckling-restraining mechanism to carry some axial load. On the other hand, if the gap is too large the buckling amplitude and the associated curvature of the buckled steel-yielding segment can be large, which would reduce the low-cycle fatigue life of the yielding segment. In determining the design gap, the Poisson ratio in the elastic (0.3) and yielding (0.5) range needs to be considered. The design gap is also a function of the maximum design strain.

If a transition in width between the restrained yielding and nonyielding segments is used, a longitudinal gap ("interior reserve space" in Figure 16.12) in front of the widened nonyielding segment also needs to be provided to avoid direct bearing between the steel segment and the mortar. Such bearing action would, unexpectedly, increase the compressive capacity of the brace



FIGURE 16.13 Bulging of steel casing (courtesy of Star Seismic, LLC).

beyond the expected design strength, which is not desirable from the viewpoint of capacity design and also increases the possibility of an unbalanced load in case a chevron bracing configuration is used. Figure 16.12 also shows the exterior reserve space that is needed to avoid contact between the splice plates and the buckling-restraining mechanism.

5. *Buckling-restraining mechanism:* This mechanism is typically composed of mortar and steel casing (e.g., hollow structural shape). But BRBs that do not use mortar have also been proposed; Figure 16.17e to Figure 16.17h and Figure 16.19b to Figure 16.19d show some examples.

Proper mix design and curing is needed to ensure a sufficient compressive strength for the mortar. Otherwise, the mortar cannot effectively restrain the buckling amplitude of the restrained yielding segment. Figure 16.13 shows an example of the bulging of steel casing due to insufficient strength of the mortar.

When properly designed and detailed, steel casing should not resist any significant axial load. To avoid buckling of BRBs, Watanabe et al. (1988) suggested that the steel casing be designed for a sufficient flexural stiffness such that

$$\frac{P_e}{P_y} \geq 1.0 \quad (16.1)$$

where P_y is the yield strength of the restrained yielding segment and P_e is the elastic buckling strength of the steel casing.

$$P_e = \frac{\pi^2 EI_{sc}}{L_{sc}^2} \quad (16.2)$$

In Equation 16.2, E is the Young's modulus, I_{sc} the moment of inertia of steel casing and L_{sc} the work point-to-work point brace length. The effect of mortar, which also contributes to the flexural stiffness of the steel casing (Chen et al., 2001b), is conservatively ignored in Equation 16.2. Note that the effect of cyclic strain hardening is not considered in Equation 16.1. If it is assumed that cyclic strain hardening would increase the compressive strength of the brace by 30% and a resistance factor ϕ of 0.85 is included in the numerator, then (Powell, 2002)

$$\frac{\phi P_e}{1.3 P_y} \geq 1.0 \quad (16.3)$$

or

$$\frac{P_e}{P_y} \geq 1.5 \quad (16.4)$$

The above expression coincides with that proposed by Watanabe et al. (1988); see Section 16.3.5.1.2 for further discussion.

16.3.4 Advantages and Disadvantages of BRBFs

Compared to either moment frames or braced frames, BRBFs offer the following advantages (Shuhaibar et al., 2002):

1. Compared to moment frames, BRBFs exhibit high-elastic lateral stiffness at low-level seismic input motions, making it easy to satisfy code drift requirements.
2. BRBFs eliminate the undesirable buckling of conventional CBFs by yielding under both tension and compression, thereby providing larger and stable energy dissipation at high-level seismic input motions.
3. BRBFs provide economical installation through a bolted or pinned connection to gusset plates, which eliminates costly field welding and inspection.
4. Braces act as a replaceable structural fuse, which minimizes damage to other elements and it is possible to replace damaged braces after major seismic events.
5. BRBFs offer design flexibility because both the strength and stiffness of the braces can be easily tuned. Furthermore, it is easy to model the cyclic behavior of BRBs for inelastic analysis.
6. For seismic rehabilitation, BRBFs can be more advantageous than the conventional bracing system because capacity design provisions for the latter system may require expensive foundation and floor diaphragm strengthening.

BRBFs have some disadvantages:

1. Most BRBs are proprietary.
2. If not properly controlled, steels commonly used to fabricate restrained yielding segment may have a wide range of yield strength.
3. Field erection tolerances are generally lower than those of conventional braced frames.
4. Large permanent deformation might occur under high levels of seismic input because this kind of system, like many others, does not have a recentering mechanism.
5. Testing and peer review are currently required for acceptance by jurisdictions, and projects are currently designed and tested with differing approaches.
6. Criteria for detecting and replacing damaged braces need to be established.

16.3.5 Development of BRBs

A variety of BRBs with various materials and geometries have been proposed and studied in Japan for more than 30 years (see Chapter 10). Variations of BRBs were subsequently developed in several other countries. A brief review of selected studies is presented below.

16.3.5.1 Japan

The concept of BRBs was first developed in two forms in Japan; to avoid buckling, the yielding steel element can be either sandwiched between precast concrete panels or encased in concrete-filled steel sections.

16.3.5.1.1 Steel Core Sandwiched between Concrete Panels

The pioneering work on BRBs was conducted by Wakabayashi et al. (1973), who developed a system in which braces made of steel flat plates were sandwiched between a pair of precast reinforced concrete panels (Figure 16.14). The research included the following: (1) pull-out tests to explore the methods of debonding, (2) compression tests of plates sandwiched between precast panels to examine the required stiffness and strength for the panels, (3) subassemblage tests to examine the effectiveness of end connection details and (4) two-story frame tests for system verification.

In the pull-out tests, epoxy resin, silicon resin, vinyl tapes, etc. were experimented as the debonding material. A total of 11 specimens were tested, and it was concluded that a layer of epoxy resin covered by silicon resin was most effective as the debonding material in terms of debonding effect, constructability and durability. In the compression tests, in which 21 specimens were tested, various reinforcing details

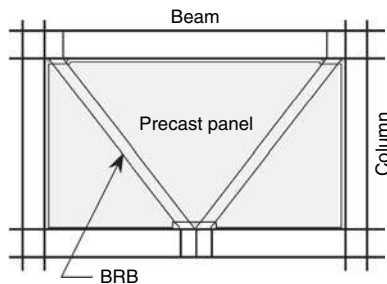


FIGURE 16.14 Buckling restrained braces sandwiched between precast concrete panels.

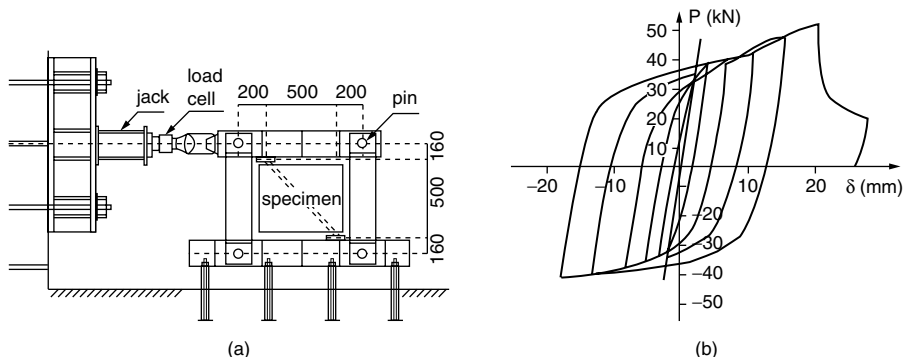


FIGURE 16.15 Subassemblage test of buckling-restrained braces sandwiched between precast concrete panels (a) Test setup; (b) hysteresis behavior. (Wakabayashi, M., Nakamura, T., Kashibara, A., Morizono, T. and Yokoyama, H. (1973). Experimental study of elasto-plastic properties of precast concrete wall panels with built-in insulating braces, *Summaries of Technical Papers of Annual Meeting*, Architectural Institute of Japan, pp. 1041–1044 (in Japanese).)

were adopted for the precast concrete panels, and a special emphasis was placed on the reinforcement along the edges of the panels. Inadequate reinforcement at these locations was found to cause damage earlier in the loading cycles because of the transverse forces that were produced by the out-of-plane deflection of the braces. In the subassemblage test, a pair of flat plates, arranged in either a diagonal or chevron pattern, was connected to a pin-connected steel frame and encased by precast concrete panels; the specimens were about 1/5 in scale (Figure 16.15a). An example of hysteresis behavior is shown in Figure 16.15b. From the strain gage measurements it was confirmed that the embedded flat plates were uniformly strained. At higher deformation levels (see Figure 16.15b) the strength of the brace in compression (i.e., positive δ value) is higher than that in tension. In the system verification tests, 2 two-story and 2 two-bay frames of about a half scale, one with braces arranged diagonally and the other with braces arranged in a chevron pattern, were cyclically tested (Figure 16.16a). Although the compressive strength of an individual brace is higher than the tensile strength at higher deformation levels, Figure 16.16b shows that symmetric response would result when braces are placed in pairs in each story.

Inoue and Sawaishi (1992) extended the work of Wakabayashi. On the basis of both analytical and experimental studies that measured directly the interaction forces between the brace and the panels, the researchers developed both stiffness and strength requirements for the design of precast concrete panels (Inoue et al., 2001).

16.3.5.1.2 Steel Core Encased in Concrete-Filled Steel Shape

Extending the concept of Wakabayashi et al. (1973), various developments on BRBs with a steel core confined by a steel casing were made in Japan in the 1980s to 1990s. Fujimoto et al. (1988) studied the behavior of a type of BRB with a steel core encased in a steel casing filled with mortar (Figure 16.17a);

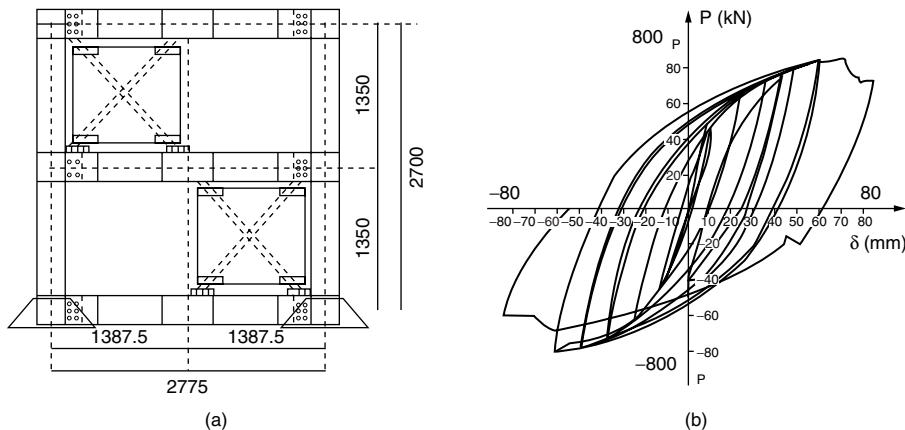


FIGURE 16.16 System test of buckling-restrained braces sandwiched between precast concrete panels. (a) Test setup; (b) hysteresis behavior. (Wakabayashi, M., Nakamura, T., Kashibara, A., Morizono, T. and Yokoyama, H. (1973). Experimental study of elasto-plastic properties of precast concrete wall panels with built-in insulating braces, *Summaries of Technical Papers of Annual Meeting*, Architectural Institute of Japan, pp. 1041–1044 (in Japanese).)

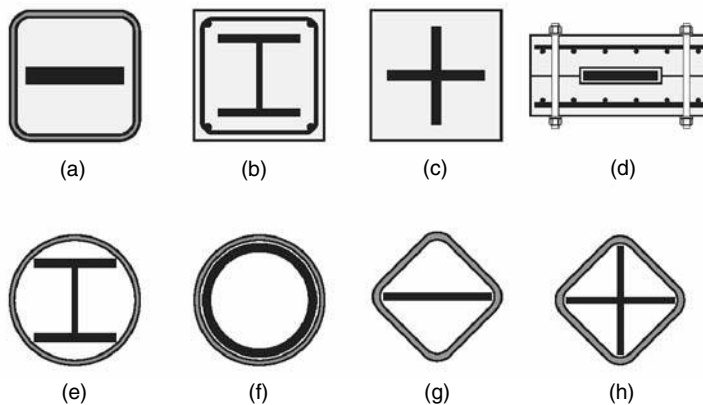


FIGURE 16.17 Cross sections of various buckling-restrained braces developed in Japan.

the end connection is shown in Figure 16.18a. Tests were conducted with different steel casing sizes, and design criteria for both stiffness and strength of the casing were developed.

Nagao and Takahashi (1990) developed a BRB composed of a wide flange section encased in a reinforced concrete member (Figure 16.17b). The end connection detail is shown in Figure 16.18b, in which the wide flange section in the projected portion is stiffened by welded plates. The experimental study by Nagao and Takahashi evaluated the reinforcing, stiffness and strength requirements of the concrete casing.

Figure 16.17c to Figure 16.17h show other BRB types developed by researchers in Japan in the 1990s. Figure 16.17c shows a cruciform steel core encased by concrete reinforced with steel fibers (Horie et al., 1993), and Figure 16.17d shows a steel core plate confined by two precast concrete panels bolted together (Inoue et al., 1993). The steel cores used in Figure 16.17e to Figure 16.17h were confined only by an HSS casing (Kuwahara and Tada, 1993; Manabe et al., 1996; Shimizu et al., 1997; Suzuki et al., 1994).

A study on the global buckling behavior of BRBs, similar to that shown in Figure 16.17a, with either square or rectangular HSS was conducted by Watanabe et al. (1988). A total of five specimens were tested; see Table 16.1 for the P_e/P_y ratios defined in Equation 16.1. The last two specimens were designed to have

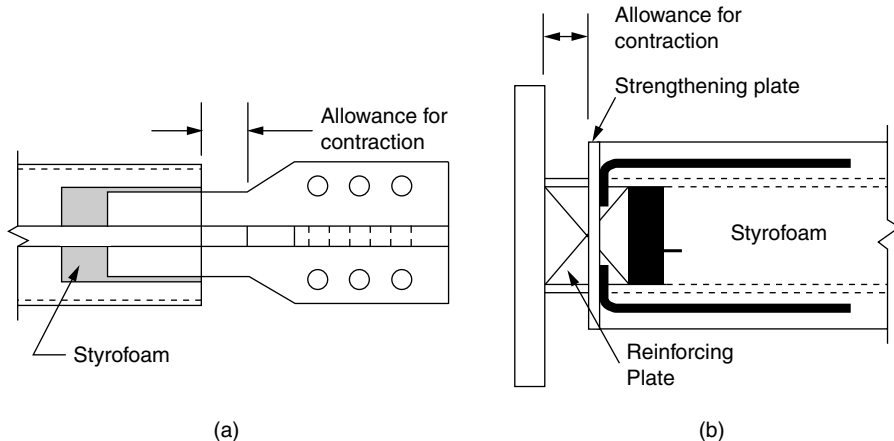


FIGURE 16.18 Buckling-restrained braces end details. (a) Fujimoto, M., Wada, A., Saeki, E., Watanabe, A. and Hitomi, Y. (1988). A study on the unbonded brace encased in buckling-restraining concrete and steel tube, *Journal of Structural Engineering*, 034B, 249–258 (in Japanese); (b) Nagao, N. and Takahashi, S. (1990). A study on the elasto-plastic behavior of unbonded composite bracing (Part 1: experiments on isolated members under cyclic loading), *Journal of Structural Engineering*, 415, 105–115 (in Japanese).

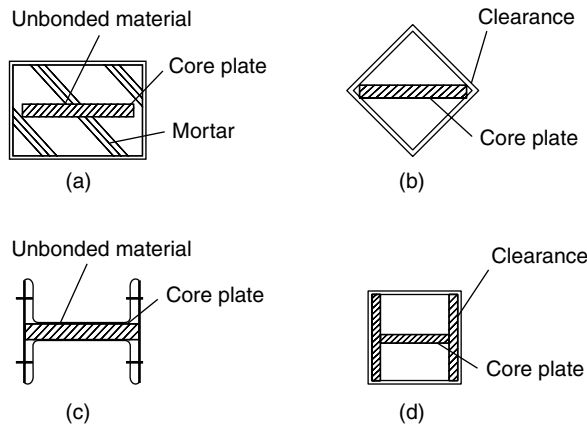


FIGURE 16.19 Section of four test specimens. (a) Type 1; (b) type 2; (c) type 3; (d) type 4. (Iwata, M., Kato, T. and Wada, A. (2000). Buckling-restrained braces as hysteretic dampers, *Proc. STESSA*, Quebec, PQ, pp. 33–38).

TABLE 16.1 P_e/P_y Ratios
(Watanabe et al., 1988)

Specimen No.	P_e/P_y
1	3.53
2	1.39
3	1.03
4	0.72
5	0.55

the ratio of P_e/P_y below 1. Each specimen was loaded cyclically up to 2% story drift. Test results showed that specimen 4 and 5 buckled globally in compression, while the first three specimens exhibited stable and symmetric hysteresis under both tension and compression. This study confirmed that Equation 16.1

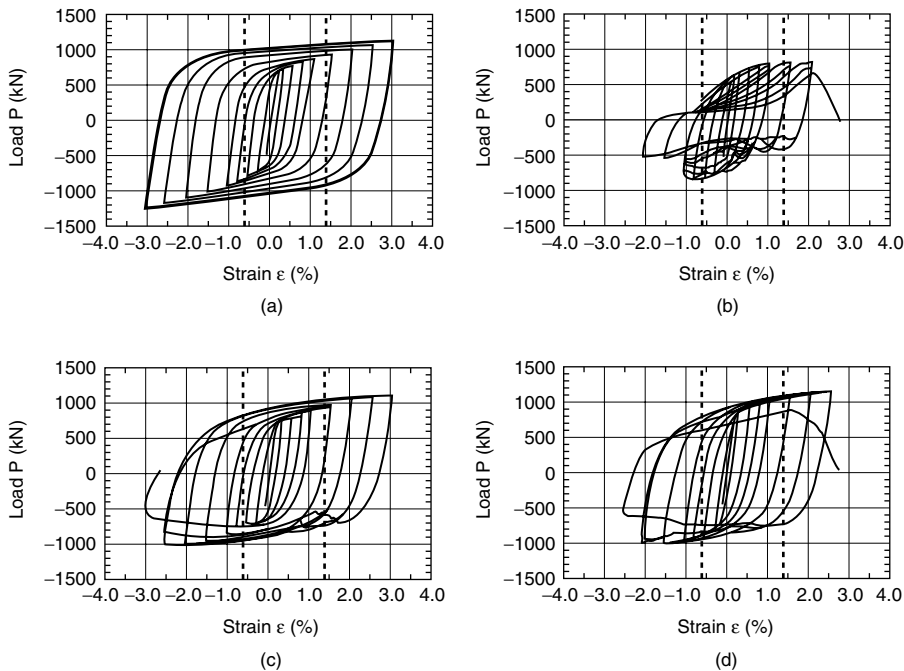


FIGURE 16.20 Cyclic response of four test specimens.(a) Type 1; (b) type 2; (c) type 3; (d) type 4. (Iwata, M., Kato, T. and Wada, A. (2000). Buckling-restrained braces as hysteretic dampers, *Proc. STESSA, Quebec, PQ*, pp. 33–38).

needs to be satisfied to avoid global buckling. Although specimen 3, with a P_e/P_y ratio of 1.03, satisfied Equation 16.1, Watanabe et al. showed from a numerical study that global buckling could still occur if the initial geometric imperfection is large. Watanabe et al. suggested that for practical applications the P_e/P_y ratio be at least equal to 1.5.

Iwata et al. (2000) reviewed the cyclic performance of four commercially available BRBs in Japan. Figure 16.19 shows the cross section of these four products. Note that an unbonding material was not used in either Type 2 or 4 specimen. Specimen 1 was similar to those studied by Watanabe et al. (1988). The buckling-restraining mechanism of specimen 3 was composed of two channels and two plates connected with high-strength bolts. Soft rubber sheets (1-mm thick) were provided between the core plate and the buckling-restraining mechanism for specimens 1 and 3.

Figure 16.20 shows the cyclic responses of all test specimens. Note that specimens 2 and 4 did not perform well, probably because no mortar was used to limit local buckling. The restraining effect of specimen 3 was not as effective as that provided by the mortar and steel tube in specimen 1. As the gap between the core plate and channels grew larger at high-deformation levels, the high-strength bolts in specimen 3 eventually failed in shear. Specimen 1, which sustained 14 cycles at 3% strain, outperformed the other three braces. The failure mode was associated with mortar crushing and local buckling of the core plate.

In Japan, low-yield steels were introduced in the early 1990s and have been used as materials for hysteretic dampers (e.g., Nakashima et al., 1994); the yield strengths of such steels are about 1/3 to 1/2 those of commonly used mild steels. Research and implementation of BRBs made of low-yield steels have also been made (e.g., Shimizu et al., 1997).

16.3.5.2 India

Core-loaded sleeved strut, originally proposed by Sridhara, has been experimentally studied for compression loading capacity (Kalyanaraman et al., 1994; Prasad, 1992; Sridhara, 1990). The idea is to decouple the compression load resistance of the core from the flexural buckling resistance of the sleeve. The behavior of the steel core in a sleeve depends on the relative stiffnesses of the core and the sleeve.

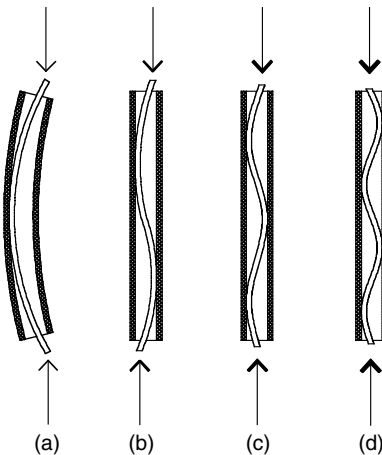


FIGURE 16.21 Concept of sleeved column (Sridhara, B.N. (1990). Sleeved column—as a basic compression member, *Proc. 4th International Conference on Steel Structures & Space Frames*, Singapore, pp. 181–188.).

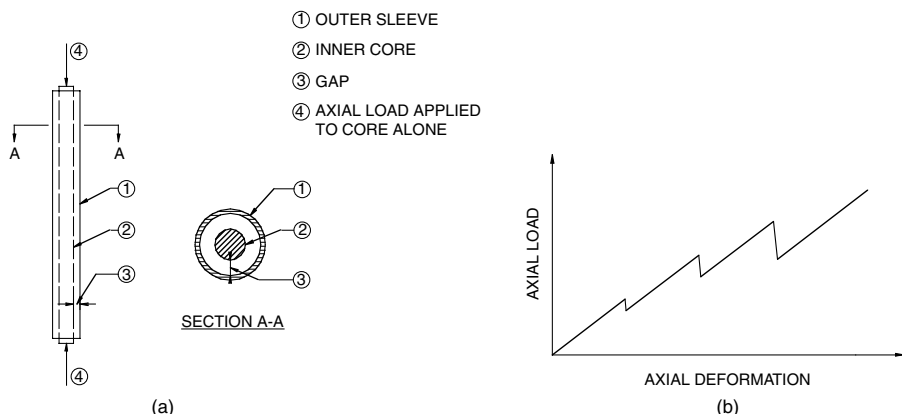


FIGURE 16.22 Concept of sleeved column and typical behavior. (a) Components of sleeved column; (b) typical compression behavior. (Adapted from Prasad, B. (1992). *Proc. 33rd AIAA Structures, Structural Dynamics and Materials Conference*, Dallas, TX. With permission.)

In a sleeve column, the core is loosely placed inside a sleeve and the load is applied only to the core. The core, under the action of the applied load, bends and presses against the inside surface of the sleeve, thus causing primarily bending stress in the sleeve. If the maximum bending stress in the sleeve is kept within the yield strength of the sleeve material, it is possible to stress the core to very high stress levels, much beyond the yield strength of the core material. Figure 16.21 shows the concept of the sleeved column. As the applied load is increased, the core will bear against the sleeve and buckle into higher modes.

Prasad performed compression tests of small-scale models, where a gap existed between the core and the sleeve (Figure 16.22a). By using acrylic materials for both core and sleeve, the buckled shape could be visually observed through the transparent sleeve. Figure 16.22b shows the typical compression behavior of the specimen. The specimen first buckled into the first mode with the core bearing against the sleeve at both ends and near the center. As the load increased, the core would snap into a higher buckling mode; the transition from one mode to the other would cause the load to drop temporarily. Sometimes the specimen would skip a higher mode and deformed into the next higher one (e.g., from the sixth mode to the eighth mode). The compression load capacity increased as the gap between the core and the sleeve

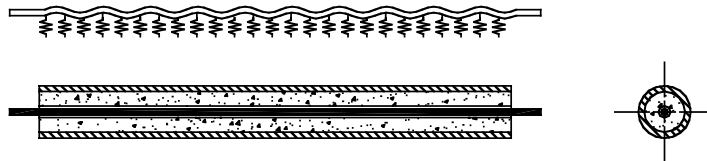


FIGURE 16.23 Core loaded sleeved strut (Kalyanaraman, V., Sridhara, B.N. and Mahadevan, K., (1994). Sleeved column system, *Proc. SSRC Task Group Meetings and Task Force Sessions*, Lehigh University, Bethlehem, PA.).

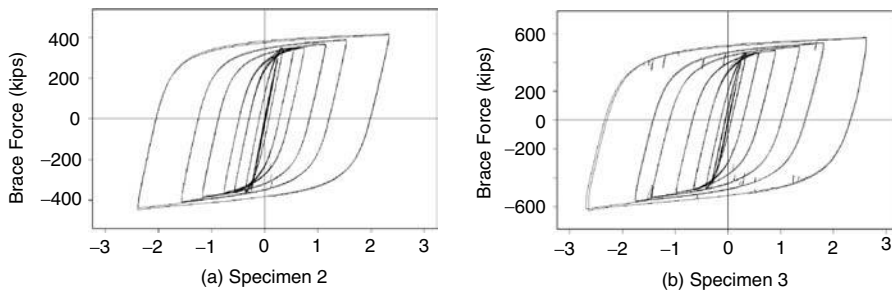


FIGURE 16.24 Cyclic response of Unbonded Braces. (a) Specimen 2; (b) specimen 3. (Clark, P., Aiken, I., Kasai, K., Ko, E. and Kimura, I. (1999). Design procedures for buildings incorporating hysteretic damping devices, *Proc. 69th Annual Convention of SEAOC*, Sacramento, CA.)

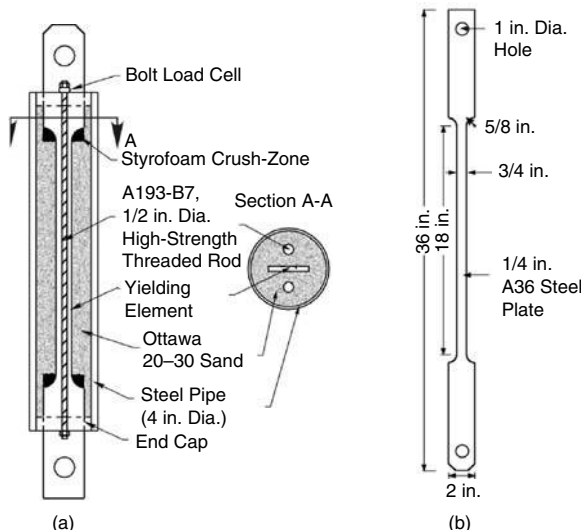


FIGURE 16.25 Composite confined hysteretic damper. (a) Test specimen; (b) steel core. (Higgins, C. and Newell, J. (2002). Development of two new hysteretic dampers, *Proc. 7th U.S. National Conference on Earthquake Engineering*, Engineering Research Institute, Oakland, CA.)

was reduced. Nevertheless, a zero gap would result in a lower capacity because the core cannot buckle into higher modes.

Figure 16.23 shows the core-loaded sleeve strut system with cement grout between the core and the sleeve. The system is equivalent to a compression member laterally supported by continuous springs along its length. Small-scale testing of specimens has shown that the load-carrying capacity is evaluated

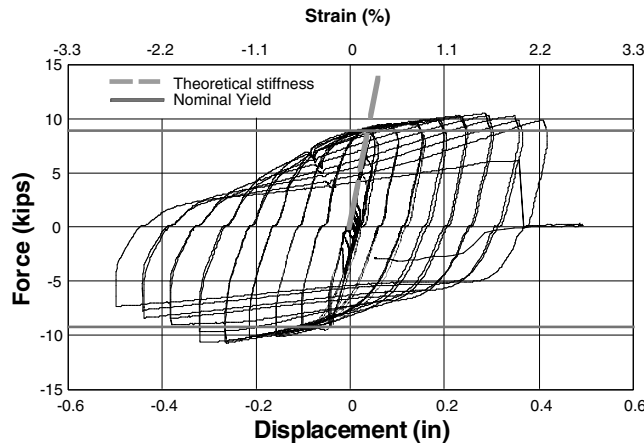


FIGURE 16.26 Hysteresis response of composite confined hysteretic damper (Higgins, C. and Newell, J. (2002). Development of two new hysteretic dampers, *Proc. 7th U.S. National Conference on Earthquake Engineering*, Engineering Research Institute, Oakland, CA).



FIGURE 16.27 Higher-mode buckling of steel core (courtesy of CoreBrace, LLC).

as the smaller of (1) the yield capacity of the core and (2) the elastic buckling load of the sleeve (Kalyanaraman et al., 1994). Cyclic testing of small-scale models has also been conducted by Kalyanaraman et al. (1998).

16.3.5.3 United States

Three large-scale unbonded braces was tested at the University of California, Berkeley, to support the design and construction of the first building that utilized such BRBs in the United States (Clark et al., 1999). The first two specimens had a rectangular yielding cross section and the third specimen had a cruciform cross section. Japanese Industrial Standard Grade SM490A, which is equivalent to A572 Grade 50 steel, was used for the core plate. The measured yield and tensile strengths were 60.7 and 79.2 ksi, respectively. (Most projects that use Unbonded Braces in the United States specify either SN400B or SN490B steel for a better control of the upper limit of the yield strength. Low-yield strength steel has also been used.) In addition to testing the specimens with the SAC loading protocols (Clark et al., 1997) or a simulated earthquake displacement record, constant-amplitude low-cycle fatigue tests were also conducted. The target story drift was 3%; the corresponding brace strain was approximately 2%.

Typical response of the braces is shown in Figure 16.24. Although bolt slip is evident from the sudden drops in the load of specimen 3, all specimens exhibited stable hysteresis. After specimen 2 was tested with the SAC loading history (Figure 16.24a), a low-cycle fatigue test with an axial strain of 2% followed. The specimen was able to sustain 17 cycles before the core plate fractured. Several analyses including stability against global buckling, buckling of the inner core in higher modes and plastic torsional buckling of the inner core were also conducted by Black et al. (2002).

Higgins and Newell (2002) studied a type of BRB that uses a steel pipe filled with noncohesive media as the buckling-restraint mechanism; graded aggregates are used as the noncohesive media. Figure 16.25 shows the assembly of a test specimen. Yielding was confined to the central portion of the A36 steel core. The noncohesive media was ASTM 20-30 Ottawa Sand with 97% being retained between the numbers

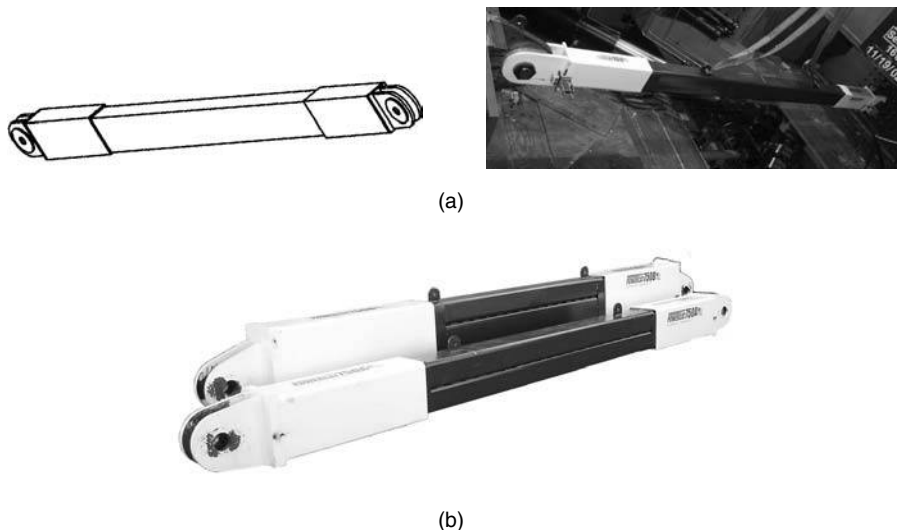


FIGURE 16.28 Star Seismic buckling-restrained brace . (a) Single-tube configuration; (b) multtube configuration. (Courtesy of Star Seismic, LLC.)

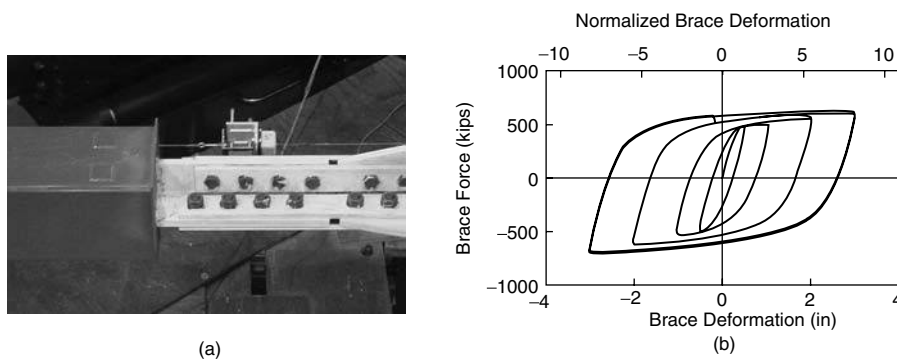


FIGURE 16.29 End details and typical hysteresis response. (a) End details; (b) hysteresis response. (Courtesy of Associated Bracing, Inc.)

20 and 30 sieve seizes. Normal force was applied to the sand with steel end caps and 1/2 in. diameter high-strength threaded rods. The observed hysteretic response under reversed cyclic loading shows stable and reliable energy dissipation to approximately 2% strain (see Figure 16.26). The dampers also exhibit a small amount of friction damping (as seen in the material elastic range) that may be beneficial for wind response mitigation. An examination of the deformed configuration along the length of the steel core after testing indicates the plate buckled primarily in the 18th mode, indicating excellent confinement provided by the noncohesive materials.

At least three proprietary BRBs have been or are being developed in the United States. These BRBs feature a steel core encased in a concrete-filled steel HSS. The first development uses flat or cruciform steel core of A572 Grade 50 and A36 steel with bolted end splice connections. To facilitate erection, holes on the gusset plate and brace are oversized; faying surfaces of the gusset and connection plates were also sandblasted to reduce the number of high-strength bolts, and hence the length of gusset connection. Satisfactory performance has been demonstrated from both uniaxial testing (Staker and Reaveley, 2002) and subassembly testing (Merritt et al., 2003a). See Figure 16.27 for a steel core that experienced higher mode buckling from a uniaxial testing.

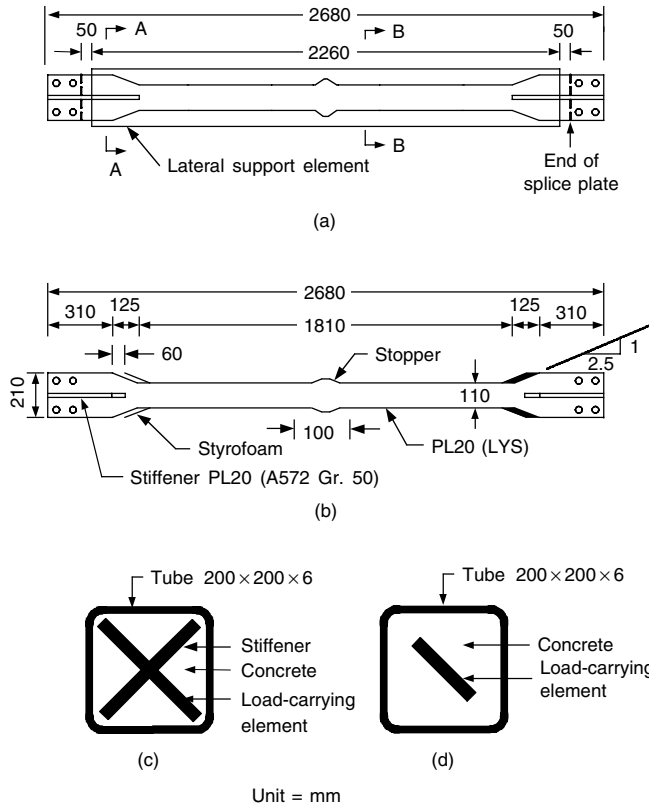


FIGURE 16.30 Details of buckling-inhibiting brace. (a) Overall view; (b) load-carrying element; (c) A-A section; (d) B-B section. (Chen, C.C., Chen, S.Y. and Liaw, J.J. (2001a). Application of low yield strength steel on controlled plasticification ductile concentrically braced frames, *Canadian Journal of Civil Engineering*, 28, 823–836.)

The second development uses a steel core of A36 material and a pin-and-collar assembly at each end of the brace (Figure 16.28a). The use of a pin connection at the gusset plate isolates the brace from any moment or shear that could be transmitted as a result of frame drift. Also by directly connecting the brace to the gusset by using a pin, the overall connection length is reduced, resulting in a long yielding core that reduces the axial strain. The pin also reduces the number of pieces being connected. The collar assembly adds to the overall stability of the brace by preventing out-of-plane buckling of the core section extending beyond the confining shell. If a collar were not in place, the section of the core that extends beyond the confining HSS can buckle and rotate (Figure 16.41c). The use of pin and collar assembly also allows the use of ganging multiple braces together to make large capacity braces (Figure 16.28b).

The third development uses a prismatic steel core along the entire length of the brace; each end is reinforced with welded stiffeners for the bolted splice connection with oversized holes for ease of erection. Figure 16.29a shows the end details of the brace. Uniaxial testing (Merritt et al., 2003c) has also been conducted to verify the cyclic performance (Figure 16.29b).

Section 16.3.7 provides further discussion of the subassemblage performance of the first two developments.

16.5.3.4 Taiwan

Chen et al. (2001a) studied the cyclic behavior of a type of BRB with low-yield strength steel (nominal $F_y = 14.5$ ksi or 100 MPa). The brace, called buckling-inhibiting brace (BIB), used a concrete-filled tube to confine the steel plate (Figure 16.30). A layer of silicon grease was applied to the surface of the steel plate before the concrete was cast to reduce the bonding force. Thus, very little space was provided for

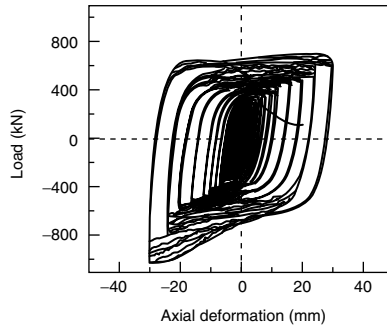


FIGURE 16.31 Typical response of buckling-inhibiting brace (Chen, C.C., Chen, S.Y. and Liaw, J.J. (2001a). Application of low yield strength steel on controlled plastication ductile concentrically braced frames, *Canadian Journal of Civil Engineering*, 28, 823–836.)

the load-carrying steel plate to expand under compression. The low-yield steel did not have a well-defined yield plateau, but the ultimate strain was very high (>50%). Note that low-yield steel would result in a reduced yield deformation, making the brace start yielding at a much smaller drift level. Figure 16.30b also shows a stopper at the center of the load-carrying element that was provided to prevent the buckling-restrained system from slipping down. Figure 16.31 shows the typical response of this type of BRB. Note that the maximum compressive strength was much higher than the maximum tensile strength. As a result, Chen et al. suggested that this type of bracing be used in a diagonal configuration, not V or inverted-V configuration. Chen et al. (2001b) also investigated the steel-only BRBs with built-up steel sections as the buckling-restraining mechanism. Figure 16.32 shows one example with low-yield steel as the load-carrying steel core.

Tsai and Lai (2002) studied the effect of unbonding material on the cyclic response of BRBs. A total of 10 identical braces were tested, the only difference being the unbonding materials used. Figure 16.33 shows the geometry of the test specimens. The A36 steel yielding elements were cruciform in cross section; the measured strength was 50 ksi. Table 16.2 summarizes the unbonding material used for each specimen and the associated test loading history. “Standard” and “Near-Fault” in the table refer to the protocols developed by SAC (Clark et al., 1997).

A typical hysteresis response is shown in Figure 16.34a. Defining the axial load difference as $\Gamma = (C_{\max} - T_{\max})/T_{\max}$, where C_{\max} and T_{\max} are the maximum compressive and tensile brace strengths at a given axial deformation level, the test results of all specimens are shown in Figure 16.34b. The figure shows that silicone rubber sheet produces the least axial load difference.

Note that the hysteresis behavior shown in Figure 16.34a was unsymmetric, with the compressive cycles showing higher force levels. Assuming that the Poisson ratio is equal to 0.5 in the inelastic range, the volume of the yielding steel segment remains constant.

$$A_o L_o = AL \quad (16.5)$$

where A_o and L_o refer to the original area and length, while A and L refer to area and length where the brace is in either tension or compression. It can be shown that the axial strain is

$$\epsilon = 1 - \frac{L_o}{L} = 1 - \frac{A}{A_o} \quad (16.6)$$

Therefore,

$$A = A_o (1 - \epsilon) \quad (16.7)$$

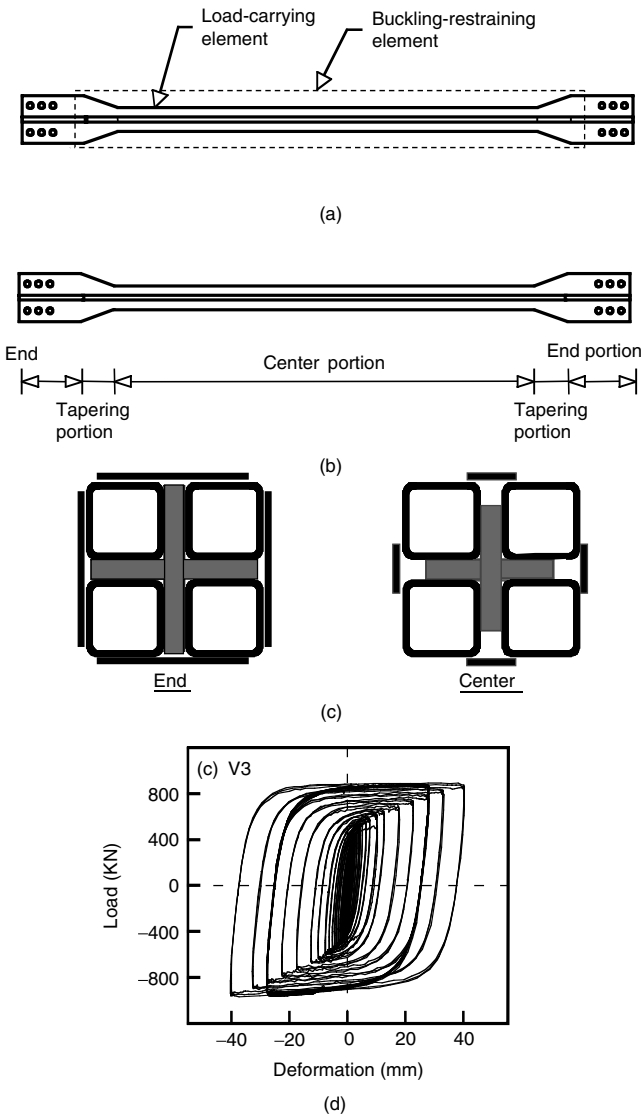


FIGURE 16.32 Steel-only buckling-inhibiting brace. (a) Components; (b) load-carrying core steel; (c) cross sections; (d) hysteresis response. (Chen, C.C., Wang, C.H. and Hwang, T.C. (2001b). Buckling strength of buckling inhibited braces, Proc. 3rd Japan–Korea–Taiwan Joint Seminar on Earthquake Engineering for Building Structures, Taipei, Taiwan, pp. 265–271.)

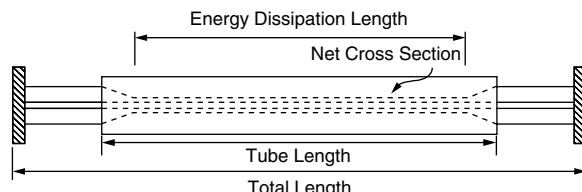


FIGURE 16.33 Geometry of buckling-restrained brace test specimens. (Tsai, K.C. and Lai, J.W. (2002). A study of buckling restrained seismic braced frame, *Structural Engineering*, 17(2), (in Chinese).)

TABLE 16.2 Test Specimens (Tsai and Lai, 2002)

Specimen	Unbonding Material	Thickness (mm)	Loading History
AS-1	Asphalt paint	NA	Standard
VF-1	Vinyl sheet + foaming tape	2	Standard
VK-1	Vinyl sheet + kraft tape	2	Standard
R2-1	Rubber sheet	2	Standard
R5-1	Rubber sheet	5	Standard
SR1-1	Silicone rubber sheet	1	Standard
SR2-1	Silicone rubber sheet	2	Standard
SR2-2	Silicone rubber sheet	2	Low-cycle fatigue
SR2-3	Silicone rubber sheet	2	Near-fault
SR5-1	Silicone rubber sheet	5	Standard

The ratio between the compressive and tensile brace forces for a given (absolute) strain level is (Tsai and Lai, 2002)

$$\Gamma = \frac{C_{\max} - T_{\max}}{T_{\max}} = \frac{A_c - A_T}{A_T} = \frac{A_o(1+\epsilon) - A_o(1-\epsilon)}{A_o(1-\epsilon)} = \frac{2\epsilon}{1-\epsilon} \approx 2\epsilon \quad (16.8)$$

The above equation shows that Γ is about 4% for $\epsilon = 2\%$. But the test results in Figure 16.34b shows much higher Γ values. Other than the Poisson's effect, factors such as the friction between the steel core yielding element and mortar also contribute to the higher brace strength in compression cycles.

The most common applications of BRBs require two sets of bolts and eight splice plates at each brace-to-gusset connection (Figure 16.8b). To reduce the size of the connections and to improve the constructability in the field, double-tube BRBs have been developed and extensively tested by Tsai and Lai (2002). The details of the double-tube BRB are shown in Figure 16.35a. Each brace is composed of two identical parts. Each part comprises a steel core, which is either a plate or a structural tee, encased in a rectangular steel tube. Both ends of the steel core are tee-shaped, thus each part of the brace can be conveniently connected in the field to the gusset in the same manner as the conventional double-T brace is connected to gusset plate connections (Figure 16.35b). After the two parts are installed, tab plates (see Figure 16.35a) are then used to connect the two parts together. In addition to facilitating field installation, a reduced gusset connection length for improved stability in the connection region is another advantage of this type of brace. A typical response of the double-tube BRB is shown in Figure 16.35c and Figure 16.35d.

16.3.6 SEAOC–AISC Qualifying Cyclic Test Requirements

Most of the BRB testing described so far was conducted with different loading sequences, which makes it difficult to compare the performance among different types of BRBs. As BRBFs are becoming increasingly popular in the United States, there is a need for a standard cyclic testing procedure to qualify tests. The proposed *Recommended Provisions for Buckling-Restrained Braced Frames* developed by a joint SEAOC–AISC task group (2001) includes in its appendix requirements for cyclic testing of either brace specimen or subassembly specimen. The loading sequence in the Provisions was developed primarily based on the work of Sabelli (2001), who performed a series of nonlinear dynamic analyses on model buildings to characterize the seismic demand of BRBFs. In accordance with its procedures and acceptance criteria, the Provisions require two successful cyclic tests, at least one being the subassembly test that imposes concurrent axial and flexural demands on the brace end.

The loading sequences require each tested brace to achieve a ductility corresponding to 1.5 times the design story drift. This ductility capacity requirement represents a mean of response values. Furthermore, the Provisions requires the brace to achieve a cumulative inelastic axial deformation of at least 140 times

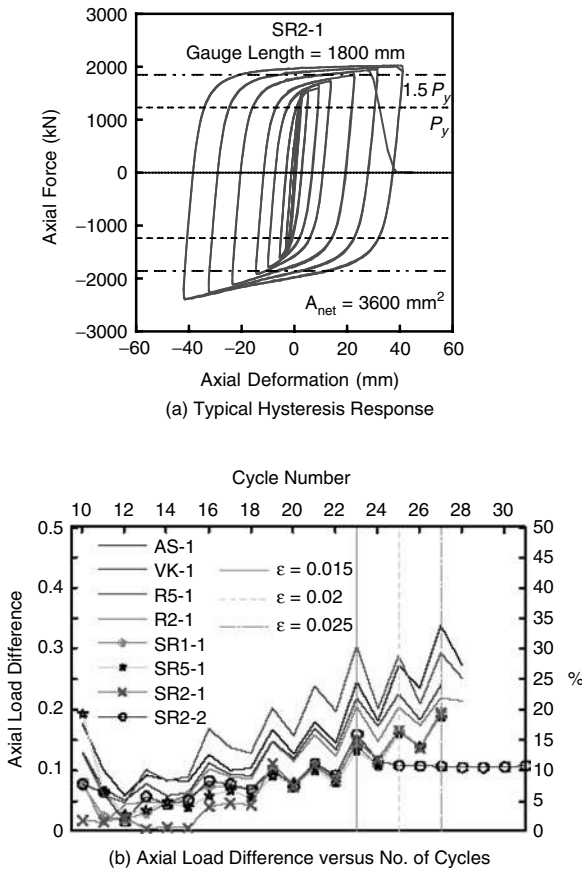


FIGURE 16.34 Buckling-restrained brace effect of unbonding materials on axial load difference. (Tsai, K.C. and Lai, J.W. (2002). A study of buckling restrained seismic braced frame, *Structural Engineering*, 17(2), (in Chinese).)

the yield deformation. This latter requirement, which applies to brace testing but not subassembly testing, represents a mean plus one standard deviation value of response values from the dynamic analyses (Sabelli, 2001).

Defining D_{by} as the value of axial deformation at first significant yield and D_{bm} as the value of deformation corresponding to the design story drift, the SEAOC–AISC loading sequence follows:

1. Six cycles of loading at the deformation corresponding to D_{by} .
2. Four cycles of loading at the deformation corresponding to $0.5D_{bm}$.
3. Four cycles of loading at the deformation corresponding to $1D_{bm}$.
4. Two cycles of loading at the deformation corresponding to $1.5D_{bm}$.
5. Additional complete cycles of loading at the deformation corresponding to $1D_{bm}$ as required for the brace test specimen to achieve a cumulative inelastic axial deformation of at least $140D_{by}$.

The design story drift should not be taken as less than 0.01 times the story height for the purposes of calculating D_{bm} , and D_{bm} need not be taken as greater than $5D_{by}$.

On the basis of a statistical evaluation of seismic response of multistory BRBFs, Tremblay and Bouatay (2002) also developed loading protocols for testing BRBs. Test protocols developed in this study were intended to be used in “pass or fail” type of tests. Four types of earthquake ground motions were considered in the nonlinear time history analysis: crustal events at distance in eastern and western Canada, near-field and subduction earthquakes in western Canada (Figure 16.36).

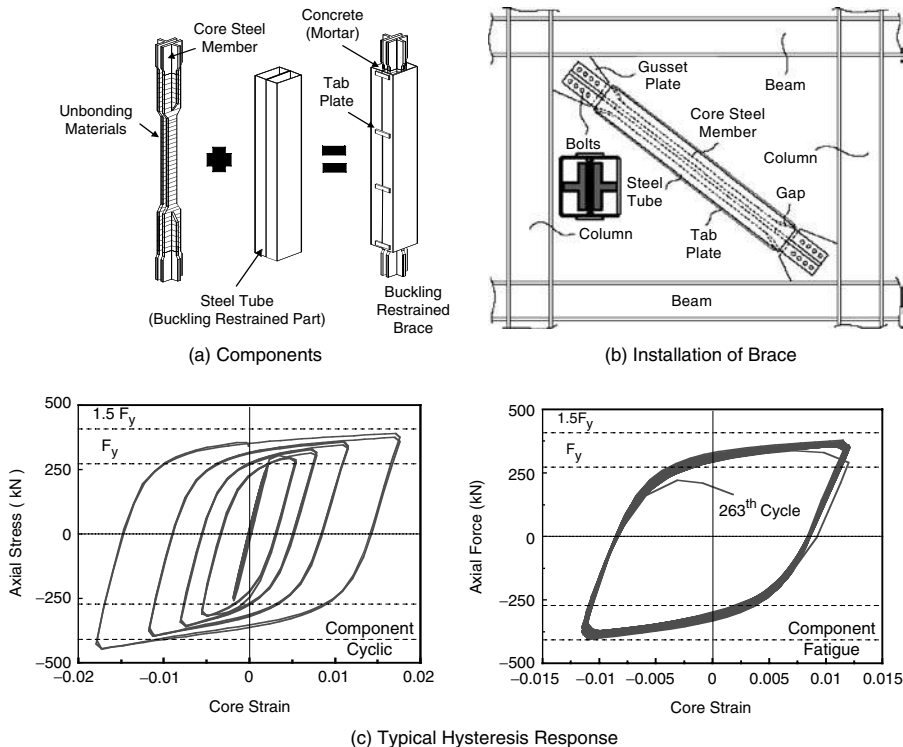


FIGURE 16.35 Double-tube buckling-restrained brace. (Tsai, K.C. and Lai, J.W. (2002). A study of buckling restrained seismic braced frame, *Structural Engineering*, 17(2), (in Chinese).)

16.3.7 BRBF Subassembly Performance

Most testing programs on BRBs conducted to date have focused mainly on uniaxial testing. Design engineers have gradually paid attention to subassembly testing in the past few years. The purpose of subassembly testing is twofold. First, it provides evidence that the brace-connection frame subassembly can satisfactorily accommodate the axial deformation and rotation demands associated with the design. Second, it is intended to demonstrate that the hysteretic behavior of the brace in the subassembly is consistent with those of the brace elements tested individually.

A subassembly test was conducted by Tremblay et al. (1999) to evaluate a type of BRB that was proposed for the seismic retrofit of a four-story steel frame building in Quebec City; un-reinforced masonry walls provided lateral resistance for the original building. BRBFs were considered over the conventional chevron bracing system because the capacity design provisions required expensive retrofit of the foundations and floor diaphragms for the latter system. (The same consideration also drove the seismic rehabilitation of a federal building in the United States (Brown et al., 2001).)

Figure 16.37 shows the test frame, and the details of the BRBs are provided in Figure 16.38. The circular HSS was designed such that its P_e was greater than twice the P_y of the core plates. The core plates, having a measured yield strength of 52 ksi, were wrapped with a membrane made of four plies of polyethylene, 0.2-mm thick each. (The use of four independent plies provided some redundancy to the system in case the outermost layer was damaged during the construction.) The core plates were widened and stiffened at both ends. The widened steel plate was also welded to the top end of the tube only to prevent the buckling-restrained mechanism from slipping down relative to the steel plate. Two No. 3 steel reinforcing bars were used in each brace to prevent cracking of the mortar during the manipulation of the brace members.

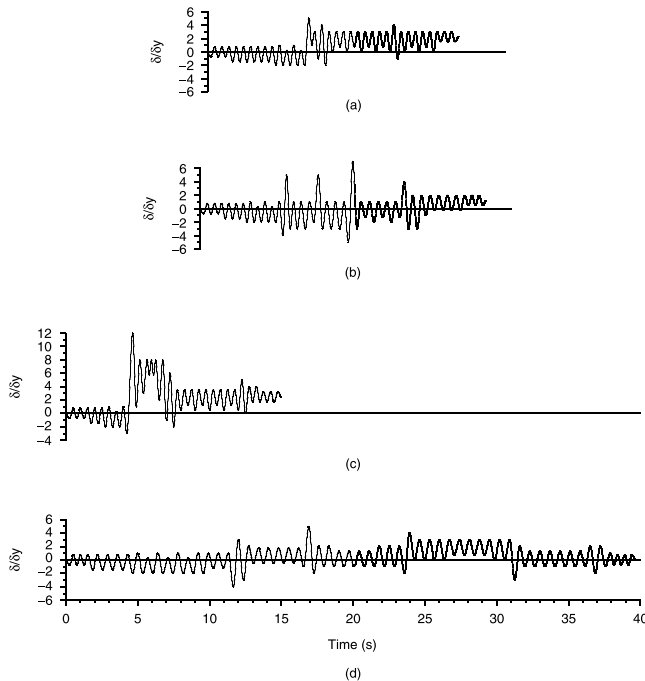


FIGURE 16.36 Loading protocols. (a) East, crustal events at distance; (b) West, crustal events at distance; (c) West, near-field events; (d) West, subduction events. (Tremblay, R. and Bouatay, N. (2002). Loading protocols for the seismic testing of ductile bracing members in concentrically braced steel frames, *Proc. 11th European Conference on Earthquake Engineering*, Cambridge, U.K. (Paper Reference 480).)

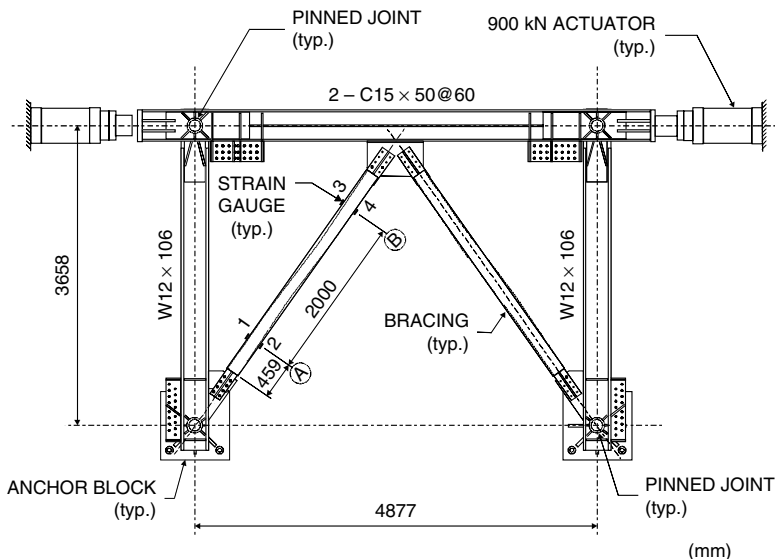


FIGURE 16.37 Buckling-restrained brace test frame. (Tremblay, R., Degrange, G. and Blouin, J. (1999). Seismic rehabilitation of a four-story building with a stiffened bracing system, *Proc. 8th Canadian Conference on Earthquake Engineering*, Vancouver, BC, 549–554.)

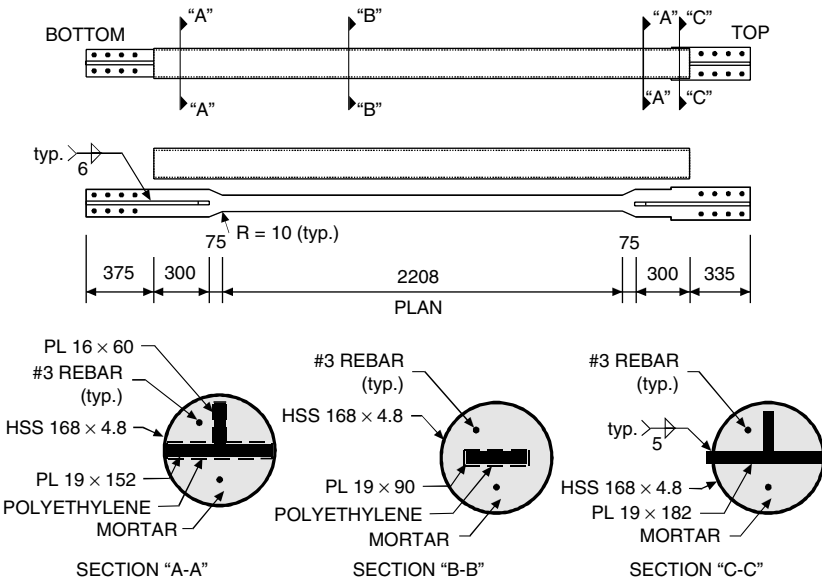


FIGURE 16.38 Details of buckling-restrained brace. (Tremblay, R., Degrange, G. and Blouin, J. (1999). Seismic rehabilitation of a four-story building with a stiffened bracing system, *Proc. 8th Canadian Conference on Earthquake Engineering*, Vancouver, BC, 549–554.)

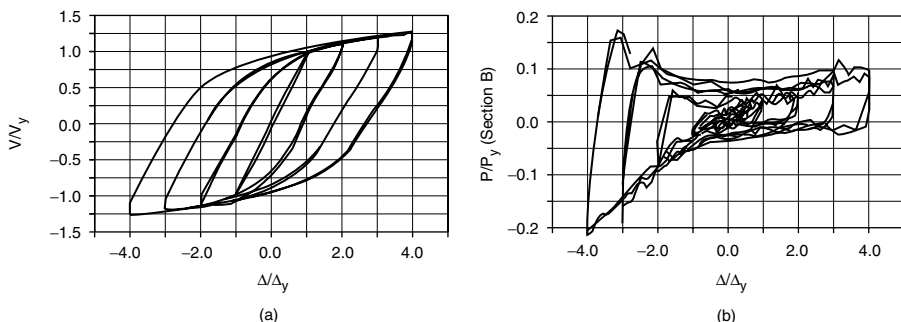


FIGURE 16.39 Measured hysteresis response. (a) Global response; (b) round hollow structural section casing response. (Tremblay, R., Degrange, G. and Blouin, J. (1999). Seismic rehabilitation of a four-story building with a stiffened bracing system, *Proc. 8th Canadian Conference on Earthquake Engineering*, Vancouver, BC, 549–554.)

Figure 16.39(a) shows that the frame subassembly provided stable hysteresis response. (V and Δ represent the lateral load and story drift, respectively, and subscript y refers to yield values.) The postyield stiffness varied between 10 to 15% of the elastic stiffness; Tremblay et al. commented that this large postyield stiffness was highly desirable for distributing inelastic deformation over the building height. On the basis of strain gage readings, the researchers also reported the axial force in the HSS steel casing. Figure 16.39b shows the response of the left brace. The figure shows that large compressive axial load developed in the HSS when the frame was pushed toward the left (i.e., negative Δ). At $\Delta = -3\Delta_y$, the axial load in HSS reached approximately 15% of the P_y of the steel plate. Upon drift reversal, this compressive load rapidly decreased and tension force developed in the tube. This behavior suggested that Poisson's effects in the steel plates were sufficient to increase the friction between the plate and the mortar when the yielding plate was pushed into the tube.

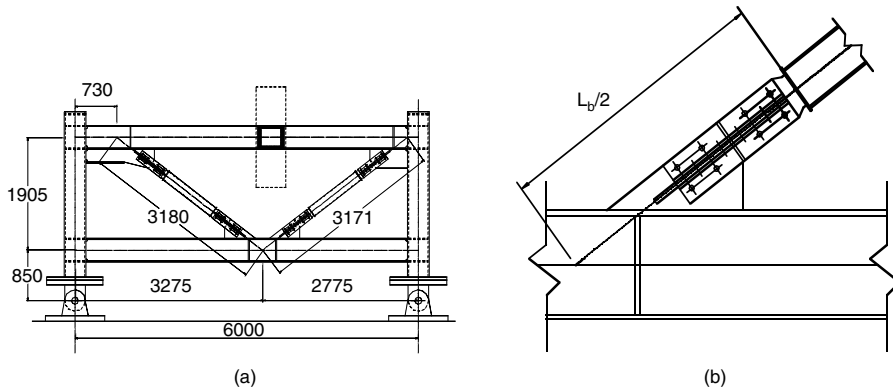


FIGURE 16.40 Geometry of subassembly test. (a) Geometry; (b) connection details. (Tsai, K.C., Hwang, Y.C., Weng, C.S., Shirai, T. and Nakamura, H. (2002), Experimental tests of large scale buckling restrained braces and frames, *Proceedings, Passive Control Symposium*, December 2002, Tokyo Institute of Technology, Tokyo, Japan.)

As part of a proof-testing program for the seismic upgrade of a 33-story office building in Taipei that utilized BRBs, Tsai et al. (2002) conducted cyclic testing of a half-scale subassembly. Figure 16.40 shows the geometry of the subassembly and the typical brace-to-beam-connection details. The subassembly was first subjected to two simulated earthquake motions. Because the braces experienced limited inelastic cycles, it was decided to impose the cyclic loading sequence shown in Figure 16.41a. The measured response in Figure 16.41b shows stable cyclic response up to the first 1% drift cycle. During the second cycle, one brace buckled at the tube end near the brace-to-beam connection. Upon load reversal, the other brace also buckled at the similar location (Figure 16.41c).

The test results clearly show that the gusset connections for BRBs need to be properly designed and stiffened to avoid this type of failure. To prevent gusset buckling like that shown in Figure 16.41c, Nakamura et al. (2000) suggested that the following criterion be satisfied for out-of-plane buckling:

$$P_{e_trans} = \frac{\pi^2 EI_{trans}}{(KL_b)^2} \geq C_{\max} \quad (16.9)$$

where C_{\max} is the maximum compression force of the brace, I_{trans} is the out-of-plane buckling moment of inertia of the unrestrained nonyielding segment of the brace, K , the effective length factor, can be conservatively taken as 1, and L_b is the unbraced connection length defined in Figure 16.40b and Figure 16.42. Note that the denominator on the right-hand side of Equation 16.9 is equivalent to using the gusset connection length as L_b and an effective length factor of 2.

For a given axial deformation, uniaxial tests generally show that the compression force is higher than the tension force. When the V or inverted-V configuration is used, this observation leads to the design requirement of an unbalanced vertical force that the beam must resist. Nevertheless, 3 subassembly tests conducted by Tsai et al. (2004) using the double-tube BRBs revealed that establishing this unbalanced vertical force from uniaxial test results may be conservative. A comparison of the average axial strains of the steel yield plates at different drift levels (see Figure 16.43) indicates that the strain in the tension brace was always larger in magnitude than that in the compression brace. Since the beam is not rigid, Tsai et al. concluded that the peak compression and tension forces in a subassembly have a tendency to self-equilibrate such that the unbalanced vertical force to be resisted by the beam is reduced.

In support of the design and construction of a campus building at the University of California, Berkeley, a series of large-scale subassembly tests were conducted (Aiken et al., 2002; López et al., 2002). The objective of the testing was to investigate the influence of frame distortion, which induces both axial and flexural deformations to the braces. The tests involved a full-story subassembly of beams, columns and braces.

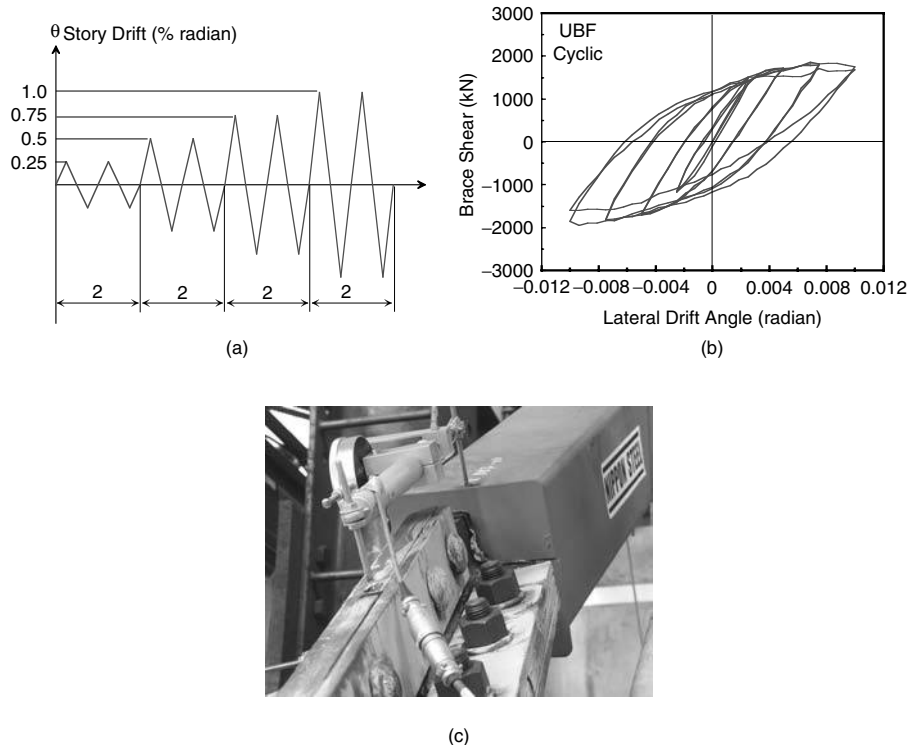


FIGURE 16.41 (a) Loading sequence; (b) measured response; (c) buckling of gusset connection. (Tsai, K.C., Hwang, Y.C., Weng, C.S., Shirai, T. and Nakamura, H. (2002), Experimental tests of large scale buckling restrained braces and frames, *Proc., Passive Control Symposium*, December 2002, Tokyo Institute of Technology, Tokyo, Japan.)

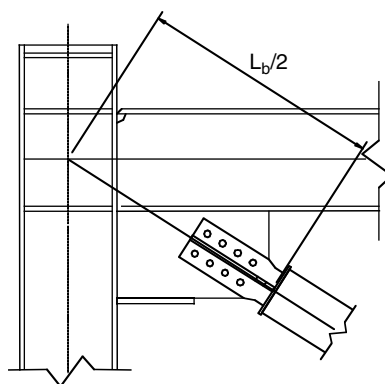


FIGURE 16.42 Unbraced length of gusset connection. (Tsai, K.C., Hwang, Y.C. and Weng, C.S. (2004). Subassembly testing and analysis of buckling restrained brace for seismic resistance, *Structural Engineering*, 18 (in Chinese).)

A total of three tests were conducted. An inverted-V bracing configuration was used for Test 1, while the test frame was reconfigured to diagonal bracing for Tests 2 and 3 (Figure 16.44). Following the SEAOC-AISC loading sequence up to a maximum drift of 2%, the subassembly performed well during Test 1, although yielding was observed at the brace-to-column gusset plates, column bases and beam-to-column moment connections.

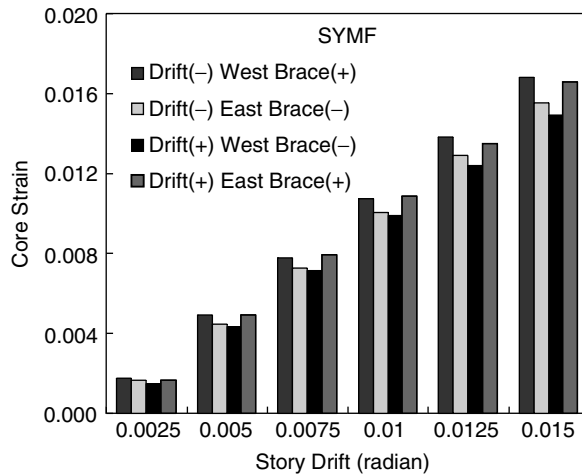


FIGURE 16.43 Axial strains in tension and compression braces (Tsai, K.C., Hwang, Y.C. and Weng, C.S. (2004). Subassembly testing and analysis of buckling restrained brace for seismic resistance, *Structural Engineering*, 18 (in Chinese).)

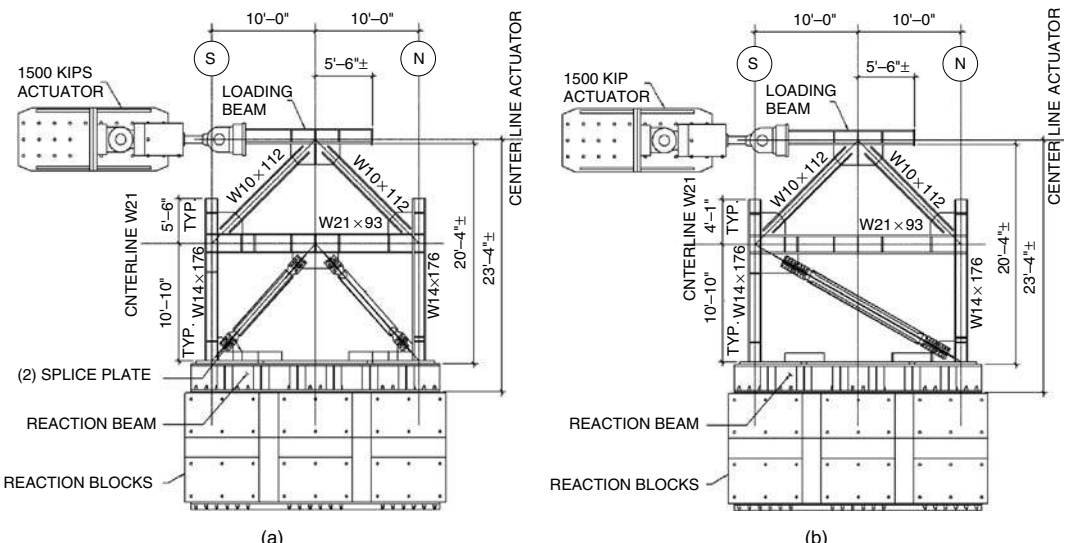


FIGURE 16.44 Subassembly test setup. (a) Test 1; (b) tests 2 and 3. (López, W.A., Gwie, D.S., Saunders, M. and Lauck, T.W. (2002). Lessons learned from large-scale tests of unbonded braced frame subassemblage, *Proc. 71st Annual Convention of SEAOC*, Sacramento, CA, pp. 171–183.)

For Test 2, the gusset plates from Test 1 were removed and new gusset plates connected using single-bevel full-penetration welds were added. Steel backing was not removed from these welds. The complete-penetration groove weld between the gusset and the column at the upper end of the brace initiated a crack at 1.7% drift when the brace was in compression (Figure 16.45a). The crack continued to propagate to a length of 2 in. at 2.6% drift. Also at 2.6% drift, the free edge of the gusset plate buckled when the brace was in tension (Figure 16.45b). The test results showed that the braces performed well and were able to withstand the rotational deformations without negative effects to their axial capacities. However, the unexpected weld cracks and gusset plate buckling due to frame action show the need for a better understanding of the cyclic behavior of BRBFs beyond the component level.



FIGURE 16.45 Damage of gusset plate. (a) Yielding of gusset plate; (b) buckling of gusset plate. (Aiken, I.D., Mahin, S.A. and Uriz, P. (2002). Large-scale testing of buckling-restrained braced frames, *Proceedings, Japan Passive Control Symposium*, Tokyo Institute of Technology, Japan, pp. 35–44.)

Other than testing braces within a frame, an alternative is to impose both the axial and transverse (i.e., rotational) deformations to the brace-gusset subassembly. The latter testing procedure has been applied to braces that were produced in the United States (Merritt et al., 2003a, 2003b). Figure 16.46a shows a shake table facility at the University of California, San Diego, used to perform subassemblage testing of the first two U.S. products presented in Section 16.2.5.3. The figure also shows a brace specimen of the first producer, which was attached at one end to a reaction wall and the other end to a reaction block on the shake table. Figure 16.46b and Figure 16.46c show the input motion to the shake table, which was established from the SEAOC–AISC standard loading protocol with some modifications to include a higher deformation demand to the specimen as well as low-cycle fatigue test. A typical hysteresis response is depicted in Figure 16.46d. Test results in Figure 16.46e show that the brace can dissipate a significant amount of energy, and the cumulative inelastic axial deformation capacity is much higher than that (140) required for uniaxial testing (SEAOC–AISC, 2001). Typical response for the braces of the second development is shown in Figure 16.47 (Merritt et al., 2003b).

16.3.8 BRBF System Performance

Seismic performance of BRBFs at the system level has been studied analytically by Clark et al. (1999), Tremblay et al. (1999), Tsai et al. (2004), Sabelli (2001), Tremblay and Bouatay (2002) and Tsai and Lai (2002) among others.

Clark et al. (1999) compared the seismic performance of a three-story steel special moment-resisting frame (SMRF) and a redesigned BRBF; the design followed the equivalent lateral force procedure for EBF in accordance with the 1994 Uniform Building Code. It was reported that the redesign resulted in about 50% reduction of the total weight of the steel. Static pushover analyses were first conducted on the two framing systems (Figure 16.48). Figure 16.48 shows that the BRBF has a larger lateral stiffness. Since the design of SMRF was governed by drift (i.e., lateral stiffness) rather than strength, a significantly smaller structural overstrength relative to the code-required design strength was observed for the buckling-restrained frame. Figure 16.49 compares the maximum drifts due to three earthquake ground motions: the El Centro record with a scaled peak ground acceleration (PGA) of 0.52g, the Taft record with a scaled PGA of 0.51g, and the JMA Kobe record with a PGA of 0.83g. The maximum roof drift of the buckling-restrained frame is about 50 to 70% that of the moment-resisting frame.

Sabelli et al. (2003) performed a statistical evaluation of the seismic response of BRBFs in addition to conventional braced frames. Both three-story and six-story buildings, assumed to be located in Los Angeles, with an inverted-V configuration were designed using the equivalent lateral force procedure

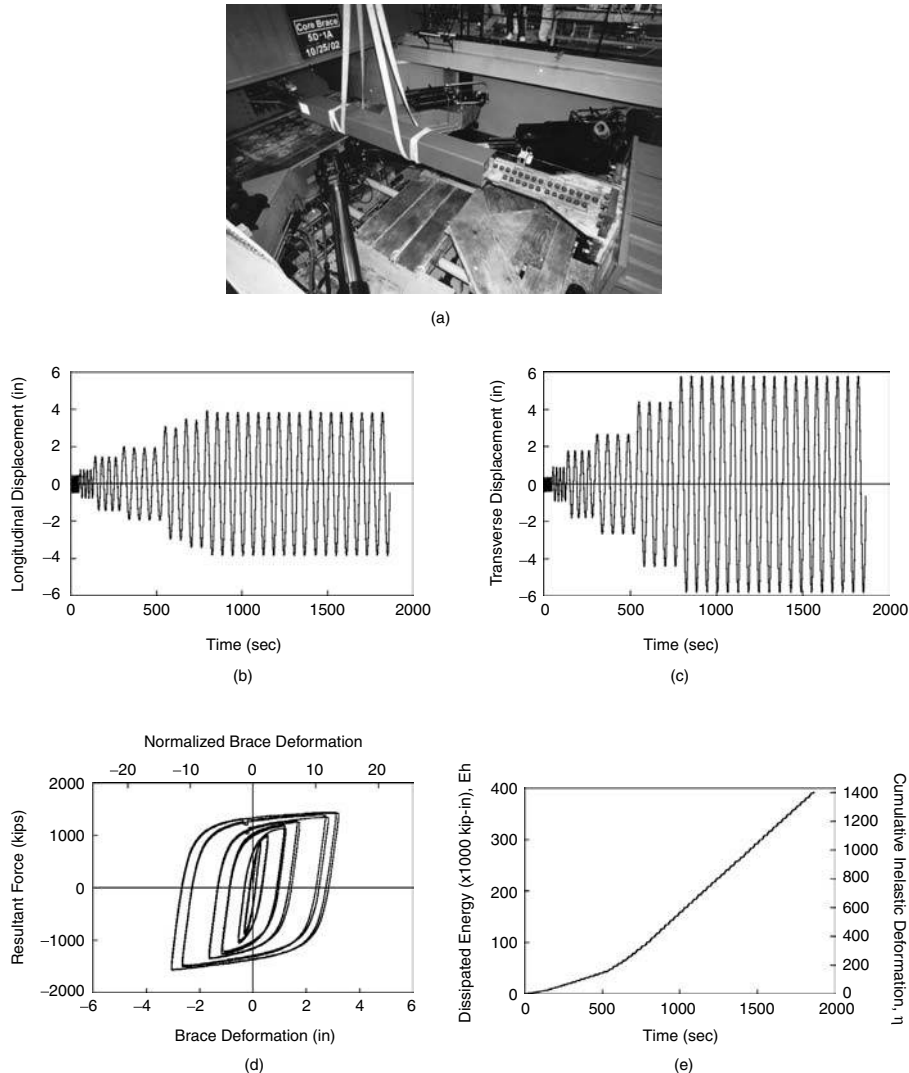


FIGURE 16.46 Subassemblage testing of CoreBrace buckling-restrained braces. (a) Test setup; (b) longitudinal deformation; (c) transverse deformation; (d) hysteresis response; (e) dissipated energy and cumulative inelastic axial deformation capacity. (Merritt, S., Uang, C.M. and Benzoni, G. (2003b), Subassemblage testing of Star Seismic buckling-restrained braces, Report No. TR-2003/04, University of California, San Diego, La Jolla, CA.)

(FEMA, 1997). An R value of either 6 or 8 was assumed, and the system overstrength factor (Ω_o) was taken as 2. To accentuate potential problems with this type of framing system, design assumptions and numerical modeling were intentionally selected to maximize predicted brace demands and the potential for weak-story formation. Brace sizes of A36 steel were chosen to within 2% of their required cross-section area. The brace stiffness was calculated assuming a yielding length of 70% of the brace centerline length and cross-sectional area of the nonyielding zone of 3 to 6 times that of the yielding zone. For modeling purposes, the secondary postyield stiffness was set to zero. Following capacity design procedures, columns were checked using the Ω_o factor. Beams connecting to braces at their midspan were designed for the unbalanced vertical force from the braces; it was assumed that the strength of the compressive brace was 10% higher than that in the tensile brace.

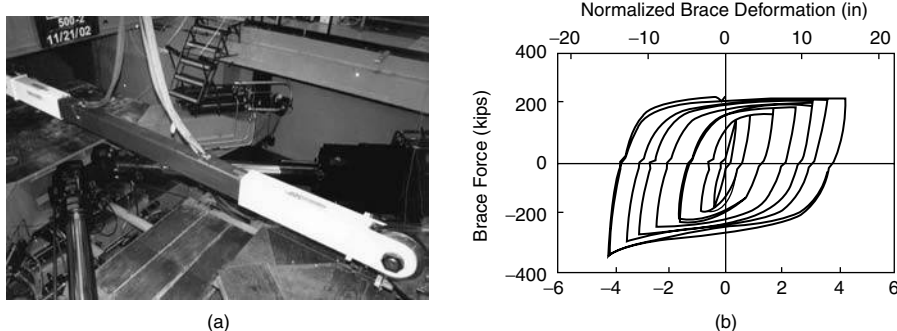


FIGURE 16.47 Test setup and typical response of Star Seismic buckling-restrained braces. (a) Test setup; (b) hysteresis response. (Merritt, S., Uang, C.M. and Benzoni, G. (2003b), Subassemblage testing of Star Seismic buckling-restrained braces, Report No. TR-2003/04, University of California, San Diego, La Jolla, CA.)

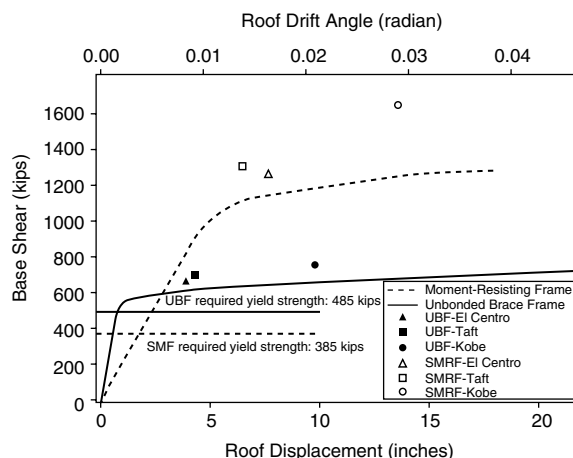


FIGURE 16.48 Comparison of special moment-resisting frame and buckling-restrained brace frame pushover analyses. (Clark, P., Aiken, I., Kasai, K., Ko, E. and Kimura, I. (1999). Design procedures for buildings incorporating hysteretic damping devices, *Proc. 69th Annual Convention of SEAOC*, Sacramento, CA.)

Nonlinear time-history analysis with a set of 20 horizontal ground acceleration records (Somerville, 1997) was performed. Consider the six-story frame that was designed for an R of 8 as an example, the maximum story drifts produced by the earthquake records, which were scaled to correspond to a 10% probability of being exceeded in 50 years, are summarized in Figure 16.50. The median story drift ratio is 1.6% and the median plus one standard deviation value is 2.2%. When these values were compared with those obtained from other framing systems, Sabelli et al. concluded that the behavior of BRBFs is comparable and often better than that associated with conventional concentric braced frames and moment frames.

The study also concludes the following: First, the seismic response is not sensitive to the value of R used (either 6 or 8). Second, the residual displacements are on average about 40 to 60% of the maximum displacement attained (Figure 16.51). Third, brace ductility demands generally vary in the same manner as story drift. Fourth, stiffening the beam to limit upward vertical displacement at midspan has little

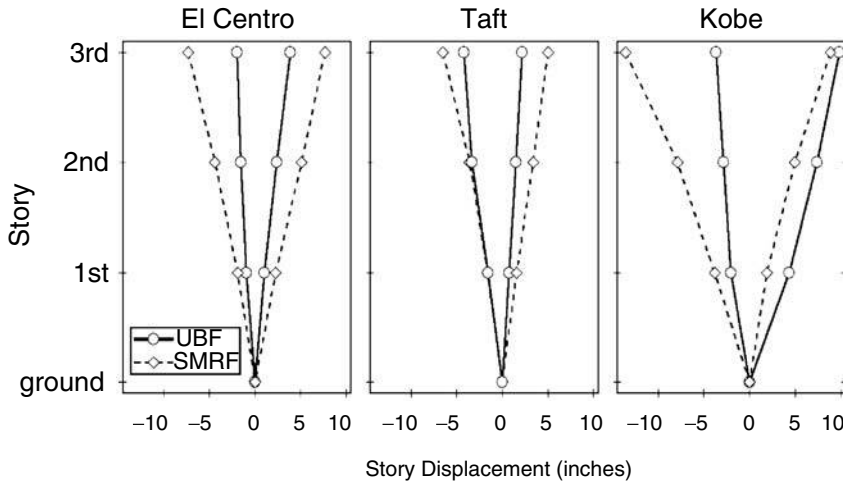


FIGURE 16.49 Comparison of special moment-resisting frame and buckling-restrained brace frame story drift profiles. (Clark, P., Aiken, I., Kasai, K., Ko, E. and Kimura, I. (1999). Design procedures for buildings incorporating hysteretic damping devices, *Proc. 69th Annual Convention of SEAOC*, Sacramento, CA.)

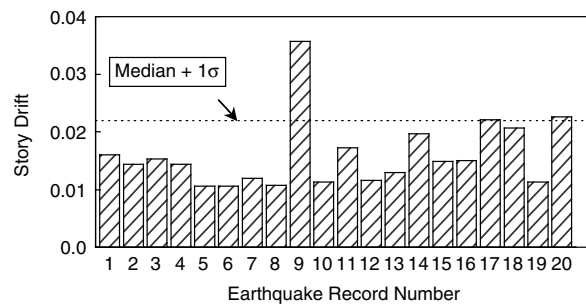


FIGURE 16.50 Maximum story drift distribution of a six-story buckling-restrained brace frame. (Sabelli, R., Mahin, S.A. and Chang, C. (2003). Seismic demands on steel braced-frame buildings with buckling-restrained braces, *Engineering Structures*, 25, 655–666.)

effect on the maximum lateral displacement of the building ((Figure 16.51). However, providing a stiff beam reduces both maximum and cumulative ductility demands by a considerable amount.

16.3.9 BRBF Seismic Design Procedure

Unlike the practice in the United States, proprietary BRBs that have been developed in Japan are treated as hysteretic dampers in design, and no design provisions are available. Since BRBs have been used mainly for major and tall buildings, design of such structures requires peer-review in accordance with the Japanese design codes, in which inelastic time-history analyses are required.

In the United States, the proposed *Recommended Provisions for Buckling-Restrained Braced Frames*, developed by a joint SEAOC–AISC task group (2001) provides basic requirements for the seismic design of BRBFs. The following analysis and design guideline is mainly based on that proposed by López (2001):

1. Establish restrained yielding plate material properties and probable brace force-strain characteristics.
2. Establish system response parameters. Currently published building codes do not include specific criteria for the design of BRBF systems. In the absence of specific requirements from the Applicable Building Code, the following values obtained from recent analytical studies are suggested for

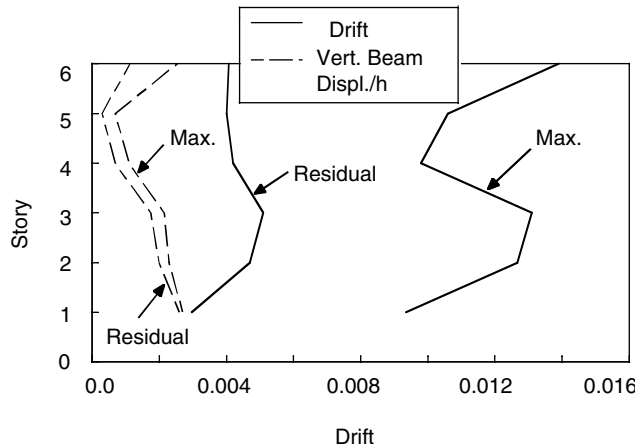


FIGURE 16.51 Envelopes of median peak lateral displacements of a six-story buckling-restrained brace frame. (Sabelli, R., Mahin, S.A. and Chang, C. (2003). Seismic demands on steel braced-frame buildings with buckling-restrained braces, *Engineering Structures*, 25, 655–666.)

consideration by the design engineers: $R = 7$, $\Omega_o = 2$ and $C_d = 5.5$. For period determination, the value of C_t can be taken as 0.03 (Clark et al., 1999).

3. Perform analyses to determine load demands on the braces.
4. Select restrained yielding steel plate areas that meet the requirements of the proposed SEAOC-AISC provisions.
5. Check that the selected restrained yielding plate areas allow for demand-capacity ratios that are balanced over the height of the building. This is suggested as one safeguard against the likelihood of weak-story formation. This is not a requirement of the proposed seismic provisions. Alternatively, instead of balancing demand-capacity ratios, nonlinear analyses may be performed to evaluate the robustness of the design.
6. Determine the size of the casing restraining the steel core from buckling. The state of the practice has involved complying with a minimum moment of inertia as defined by a manufacturer's recommendation. Alternatively, estimate the size of the casing such that the P_e/P_y ratio defined in Equation 16.1 is at least 1.5 (Watanabe et al., 1988). Note that determining casing size is useful in coordination of architectural finishes. Casing size is generally not within the scope of the structural engineer of record since it is the responsibility of the brace manufacturer.
7. Select beam sizes that meet the required strength, detailing and stiffness requirements of the proposed provisions.
8. Select column sizes that meet the required strength and detailing requirements of the proposed provisions.
9. Determine the expected brace strains at the design story drifts.
10. Determine the maximum force, P_{max} , that can be developed in the braces at the expected brace strains. Detail bracing connections to resist the maximum force that can be developed in the braces. Check Equation 16.9 to prevent gusset buckling like that shown in Figure 16.41c.

16.4 Concluding Remarks

BRBFs have emerged as a very promising lateral load-resisting system for seismic applications. A significant number of uniaxial testing of a variety of BRBs have been conducted to date; the majority of these braces are proprietary. Test results usually show very stable hysteresis behavior with an excellent low-cycle fatigue life. With global buckling of the brace eliminated, the compressive strength is typically slightly higher than that in tension for a given axial deformation. Standard loading protocols for quali-

fication testing have also been developed in North America. The loading protocol proposed by SEAOC-AISC requires subassembly testing so that the rotational as well as axial deformations can be properly simulated and imposed on the brace. Limited subassembly testing showed undesirable failure modes in the gusset regions of the frames, which included buckling of gusset plate and weld cracks. Since the cause of failure appears to be common to all types of braced frames (López et al., 2002), further research on the behavior of gusset, including its interaction with the surrounding frame, is needed.

Acknowledgments

The authors acknowledge the following individuals for contributing to this chapter: Dr. I. Aiken (SIE, Inc.), Prof. C.C. Chen (National Taiwan University of Science of Technology), P. Hassett (Associated Bracing, Inc.), Prof. K. Inoue (Kyoto University), W. López (Rutherford & Chekene), S. Powell (Star Seismic, LLC), James Smelser and Andy Hichman (CoreBrace, LLC), R. Sabelli and B. Prasad (DASSE Design, Inc.), Prof. K.C. Tsai (National Taiwan University) and Prof. R. Tremblay (Ecole Polytechnique).

Glossary

Braced Frame — A vertical truss system of concentric or eccentric type that resists lateral forces on the structural system.

Buckling-Restrained Braced Frame (BRBF) — A diagonally braced frame in which all members of the bracing system are subjected primarily to axial forces and the limit state of compression buckling of braces is precluded.

Buckling-Restraining System — A system of restraints that resists buckling of the steel core in BRBF. This system includes the casing on the steel core and structural elements adjoining its connections.

Casing — An element that resists forces transverse to the axis of the brace, thereby restraining buckling of the core; The casing requires a means of delivering this force to the remainder of the buckling-restraining system. The casing resists little or no force in the axis of the brace.

Eccentrically Braced Frame (EBF) — A diagonally braced frame that has at least one end of each bracing member connected to a beam a short distance from another beam-to-brace connection or a beam-to-column connection.

Link — In EBF, the segment of a beam located between the ends of two diagonal braces or between the end of a diagonal brace and a column.

Steel Core — The axial-force-resisting element of braces in BRBF. The steel core contains a yielding segment and connections to transfer its axial force to adjoining elements; it may also contain projections beyond the casing and transition segments between the projections and yielding segment.

V-Braced Frame — A concentrically braced frame in which a pair of diagonal braces located either above or below a beam is connected to a single point within the clear beam span. Where the diagonal braces are below the beam, the system is also referred to as an inverted-V-braced frame.

Zipper Column — A vertical (or nearly vertical) strut connecting the brace-to-beam intersection of an inverted-V-braced frame at one level to the brace-to-beam intersection at another level.

List of Symbols

A	area of steel core
C_d	deflection amplification factor
C_{max}	brace maximum compressive strength
C_t	coefficient for determining empirical fundamental period
D_{bm}	brace deformation corresponding to Design Story Drift
D_{by}	brace deformation at first significant yield

e	length of link
E	Young's modulus
F_y	yield strength of steel
I_{sc}	moment of inertia of steel casing
I_{trans}	moment of inertia of the unrestrained nonyielding segment
K	effective length factor
L	length of steel core
L_b	unbraced length
L_{sc}	length of steel casing
P_e	elastic buckling strength
P_{e_trans}	elastic buckling strength of gusset connection
P_{max}	brace maximum compressive strength
P_y	yield strength
R	response modification factor
T_{max}	brace maximum tensile strength
V	lateral load
ϵ	axial strain
ϕ	resistance factor
Γ	axial load difference [$=(C_{max} - T_{max})/T_{max}$]
Ω_o	system overstrength factor
Δ	story drift

References

- Aiken, I.D., Mahin, S.A. and Uriz, P. (2002). Large-scale testing of buckling-restrained braced frames, *Proceedings, Japan Passive Control Symposium*, Tokyo Institute of Technology, Japan, pp. 35-44.
- AISC (2002). *Seismic Provisions for Structural Steel Buildings*, American Institute of Steel Construction, Chicago, IL.
- Black, C., Makris, N. and Aiken, I. (2002). Component testing, stability analysis and characterization of buckling-restrained braces, Report No. PEER-2002/08, Pacific Earthquake Engineering Research Center, University of California, Berkeley, CA.
- Brown, A.P., Aiken, I.D. and Jafarazadeh, F.J. (2001). Buckling restrained braces provide the key to the seismic retrofit of the Wallace F. Bennett Federal Building, *Modern Steel Construction*, August, 29-37.
- Bruneau, M., Uang, C.M. and Whittaker, A.S. (1997) *Ductile Design of Steel Structures*, McGraw-Hill, New York, 1997.
- Clark, P., Frank, K., Krawinkler, H. and Shaw, R., (1997). Protocol for fabrication, inspection, testing, and documentation of beam-column connection tests and other experimental specimens, Report No. SAC/BD-97/02, SAC Joint Venture, Sacramento, CA.
- Clark, P., Aiken, I., Kasai, K., Ko, E. and Kimura, I. (1999). Design procedures for buildings incorporating hysteretic damping devices, *Proc. 69th Annual Convention of SEAOC*, Sacramento, CA.
- Chen, C.C., Chen, S.Y. and Liaw, J.J. (2001a). Application of low yield strength steel on controlled plastification ductile concentrically braced frames, *Canadian Journal of Civil Engineering*, 28, 823-836.
- Chen, C.C., Wang, C.H. and Hwang, T.C. (2001b). Buckling strength of buckling inhibited braces, *Proc. 3rd Japan-Korea-Taiwan Joint Seminar on Earthquake Engineering for Building Structures*, Taipei, Taiwan, pp. 265-271.
- FEMA (1997). *NEHRP Recommended Provisions for Seismic Regulations of Buildings and Other Structures*, Federal Emergency Management Agency, Washington, DC.
- Fujimoto, M., Wada, A., Saeki, E., Watanabe, A. and Hitomi, Y. (1988). A study on the unbonded brace encased in buckling-restraining concrete and steel tube, *Journal of Structural Engineering*, 034B, 249-258 (in Japanese).

- Higgins, C. and Newell, J. (2002). Development of two new hysteretic dampers, *Proc. 7th U.S. National Conference on Earthquake Engineering*, Engineering Research Institute, Oakland, CA.
- Horie, T., Yabe, Y., Hori, T., Nakamura, S. (1993). Elasto-plastic behavior of steel brace with restraint system for post buckling, *Journal of Steel Structures*, 1, 187–194 (in Japanese).
- Inoue, K. and Sawaizumi, S. (1992). Bracing design criterion of the reinforced concrete panel including unbonded steel diagonal braces, *Journal of Structural and Construction Engineering*, 432, 41–49 (in Japanese).
- Inoue, K., Sawaizumi, S., Higashibata, Y. and Inoue, K. (1993). Stiffening design at the edge of reinforced concrete panel including unbonded steel diagonal braces, *Journal of Structural Engineering*, 443, 137–146 (in Japanese).
- Inoue, K., Sawaizumi, S. and Higashibata, Y. (2001). Stiffening requirements for unbonded braces encased in concrete panels, *Journal of Structural Engineering*, 127(6), 712–719.
- Iwata, M., Kato, T. and Wada, A. (2000). Buckling-restrained braces as hysteretic dampers, *Proc. STESSA*, Quebec, PQ, pp. 33–38.
- Kalyanaraman, V., Sridhara, B.N. and Mahadevan, K., (1994). Sleeved column system, *Proc. SSRC Task Group Meetings and Task Force Sessions*, Lehigh University, Bethlehem, PA.
- Kalyanaraman, V., Mahadevan, K. and Thairani, V. (1998). Core loaded earthquake resistant bracing system, *Journal of Constructional Steel Research*, 46(1–3), 437–439.
- Khatib, I., Mahin, S.A. and Pister, K.S. (1988). Seismic behavior of concentrically braced steel frames, Report No. UCB/EERC 88-01, Earthquake Engineering research Center, Berkeley, CA.
- Kuwahara, S. and Tada, M. (1993). A study on stiffening capacity of double-tube members, *Journal of Structural and Construction Engineering*, 445, 151–158 (in Japanese).
- López, W.A. (2001). Design of unbonded braced frames, *Proc. 70th Annual Convention of SEAOC*, SEAOC, Sacramento, CA, pp. 23–31.
- López, W.A., Gwie, D.S., Saunders, M. and Lauck, T.W. (2002). Lessons learned from large-scale tests of unbonded braced frame subassemblage, *Proc. 71st Annual Convention of SEAOC*, Sacramento, CA, pp. 171–183.
- Manabe, N., Shimokawa, H., Kamitani, M., Morino, S. and Kawaguchi, J. (1996). Elasto-plastic behavior of flat-bar brace stiffened by square steel tube, *Summaries of Technical Papers of Annual Meeting*, Architectural Institute of Japan, pp. 783–784 (in Japanese).
- Merritt, S., Uang, C.M. and Benzoni, G. (2003a). Subassemblage testing of corebrace buckling-restrained braces, Report No. TR-2003/01, University of California, San Diego, La Jolla, CA.
- Merritt, S., Uang, C.M. and Benzoni, G. (2003b). Subassemblage testing of star seismic buckling-restrained braces, Report No. TR-2003/04, University of California, San Diego, La Jolla, CA.
- Merritt, S., Uang, C.M. and Benzoni, G. (2003c). Uniaxial testing of associated bracing buckling-restrained braces, Report No. TR-2003/05, University of California, San Diego, La Jolla, CA.
- Murata, Y., Mochizuki, S., Andou, N. and Takahashi, S. (1980). An experimental study on buckling of unbonded braces under centrally applied loads, *Annual Meeting of Architectural Institute of Japan*, September 1980, pp. 1913–1914 (in Japanese).
- Nagao, N. and Takahashi, S. (1990). A study on the elasto-plastic behavior of unbonded composite bracing (Part 1: experiments on isolated members under cyclic loading), *Journal of Structural Engineering*, 415, 105–115 (in Japanese).
- Nakamura, H., Maeda, Y., Sasaki, T., Wada, A., Takeuchi, T., Nakata, Y. and Iwata, M. (2000). Fatigue properties of practical-scale unbonded braces, *Nippon Steel Technical Report*, 82(July), 51–57.
- Nakashima, M., Iwai, S., Iwata, M., Takeuchi, T., Konomi, S., Akazawa, T. and Saburi, K. (1994). Energy dissipation behavior of shear panels made of low-yield stress steel, *Earthquake Engineering and Structural Dynamics*, 23(12), 1299–1313.
- Powell, S. (2002) Personal communication, Park City, UT.
- Prasad, B. (1992). Experimental investigation of sleeved column, *Proc. 33rd AIAA Structures, Structural Dynamics and Materials Conference*, Dallas, TX. Reina, P. and Normile, D. (1997). Fully braced for seismic survival, *Engineering News Record*, July 21, 34–36.

- Sabelli, R. (2001). Research on improving the design and analysis of earthquake-resistant steel-braced frames, The 2000 NEHRP Professional Fellowship Report, EERI, Oakland, CA.
- Sabelli, R., Mahin, S.A. and Chang, C. (2003). Seismic demands on steel braced-frame buildings with buckling-restrained braces, *Engineering Structures*, 25, 655–666.
- SEAOC-AISC (2001). *Recommended Provisions for Buckling-Restrained Braced Frames* (draft), SEAOC and AISC.
- Shimizu, T., Fujisawa, K., Uemura, K. and Inoue, I. (1997). Design method to prevent buckling of low yield strength steel tube brace and fracturing of joints (Parts 1 and 2), *Summaries of Technical Papers of Annual Meeting*, Architectural Institute of Japan, pp. 781–784 (in Japanese).
- Shuhabar, C., López, W.A. and Sabelli, R. (2002). Buckling-restrained braced frames, *Proceedings, Seminar on Response Modification Technologies for Performance-Based Seismic Design*, ATC-17-2, ATC and MCEER, pp. 321–328.
- Somerville, P. (1997). Development of ground motion time histories for Phase 2 of the FEMA/SAC steel project, Report No. SAC/BD-97/04, SAC Joint Venture, Sacramento, CA.
- Sridhara, B.N. (1990). Sleeved column—as a basic compression member, *Proc. 4th International Conference on Steel Structures & Space Frames*, Singapore, pp. 181–188.
- Staker, R. and Reaveley, L.D. (2002). Selected study on unbonded braces, *Proceedings, Seminar on Response Modification Technologies for Performance-Based Seismic Design*, ATC-17-2, ATC and MCEER, pp. 339–349.
- Suzuki, N., Asano, R., Tohata, Y., Sasaki, T. and Segawa, T. (1994). Experimental study on the H-section steel brace encased in RC or steel tube, *Summaries of Technical Papers of Annual Meeting*, Architectural Institute of Japan, pp. 1621–1622 (in Japanese).
- Takaeda, Y., Kimura, Y., Yoshioka, K., Furuya, N. and Takemoto, Y. (1976). An experimental study on braces encased in steel tube and mortar, *Annual Meeting of the Architectural Institute of Japan*, October 1976, pp. 1041–1042 (in Japanese).
- Tremblay, R., Degrange, G. and Blouin, J. (1999). Seismic rehabilitation of a four-story building with a stiffened bracing system, *Proc. 8th Canadian Conference on Earthquake Engineering*, Vancouver, Canada, pp. 549–554.
- Tremblay, R. and Bouatay, N. (2002). Loading protocols for the seismic testing of ductile bracing members in concentrically braced steel frames, *Proc. 11th European Conference on Earthquake Engineering*, Cambridge, England (Paper Reference 480).
- Tsai, K.C. and Lai, J.W. (2002). A study of buckling restrained seismic braced frame, *Structural Engineering*, 17(2) 3–32, (in Chinese).
- Tsai, K.C., Hwang, Y.C., Weng, C.S., Shirai, T. and Nakamura, H. (2002). Experimental tests of large scale buckling restrained braces and frames, *Proceedings, Passive Control Symposium*, December 2002, Tokyo Institute of Technology, Tokyo, Japan.
- Tsai, K.C., Hwang, Y.C. and Weng, C.S. (2004). Subassembly testing and analysis of buckling restrained brace for seismic resistance, *Structural Engineering*, 19(2), (in Chinese).
- Uang, C.-M., Bruneau, M., Whittaker, A.S. and, K.-C. Tsai (2001). Seismic design of steel structures, *Seismic Design Handbook*, F. Naeim, Ed., Van Nostrand Reinhold, New York, chap 9.
- Wada, A., Connor, J., Kawai, H., Iwata, M. and Watanabe, A. (1992). Damage tolerant structures, *Proc. 5th U.S.–Japan Workshop on the Improvement of Structural Design and Construction Practices*, San Diego, CA, Applied Technology Council, ATC-15-4, pp. 27–39.
- Wada, A., Saeki, E., Takeuchi, T. and Watanabe, A. (1998). Development of unbonded brace, Nippon Steel Corporation Building Construction and Urban Development Division, Tokyo, Japan.
- Wakabayashi, M., Nakamura, T., Kashibara, A., Morizono, T. and Yokoyama, H. (1973). Experimental study of elasto-plastic properties of precast concrete wall panels with built-in insulating braces, *Summaries of Technical Papers of Annual Meeting*, Architectural Institute of Japan, pp. 1041–1044 (in Japanese).
- Watanabe, A., Hitomi, Y., Yaeki, E., Wada, A. and Fujimoto, M. (1988). Properties of brace encased in buckling-restraining concrete and steel tube, *Proc. 9th World Conference on Earthquake Engineering*, Tokyo-Kyoto, Japan, Vol. IV, pp. 719–724.

17

Seismic Behavior and Design of Masonry

17.1	Introduction	17-2
17.2	Masonry in the United States.....	17-2
	Fundamentals of Masonry in the United States • Modern Masonry Construction in the United States • Historical Structural Masonry in the United States	
17.3	Performance of Masonry in U.S. Earthquakes	17-8
	Before the 1933 Long Beach Earthquake • 1933 Long Beach Earthquake • 1971 San Fernando Earthquake • 1989 Loma Prieta Earthquake • 1994 Northridge Earthquake • 2001 Nisqually Earthquake • Concluding Remarks • Relevant Information from non-U.S. Earthquakes	
17.4	Fundamental Basis for Seismic Design of Masonry in the United States	17-15
	Design Approaches for Modern U.S. Masonry	
17.5	Masonry Design Codes Used in the United States.....	17-15
	Introduction • Masonry Design Provisions of Modern Model Codes in the United States • Seismic Design Provisions for Masonry in the 2000 IBC • Future of Design Codes for Masonry in the United States	
17.6	Analysis Approaches for Modern U.S. Masonry	17-24
	Overall Analytical Approach • Elastic vs. Inelastic Behavior • Selection of Earthquake Input • Two-Dimensional vs. Three- Dimensional Analysis of Linear Elastic Structures • Modeling of Gravity Loads • Modeling of Material Properties • Modeling of Structural Elements • Flexural Cracking of Walls • Soil-Foundation Flexibility • In-Plane Floor Diaphragm Flexibility • Explicit Inelastic Design and Analysis of Masonry Structures Subjected to Extreme Lateral Loads • Inelastic Finite Element Analysis of Masonry Structures	
17.7	Seismic Retrofitting of Historical Masonry in the United States	17-29
	Observed Seismic Performance of Historical U.S. Masonry • Laboratory Performance of Historical U.S. Masonry • Basic Principles of Masonry Retrofitting • History of URM Retrofitting in the Los Angeles Area	
17.8	Future Challenges	17-31
	Performance-Based Seismic Design of Masonry Structures • Increased Consistency of Masonry Design Provisions	
17.9	Design Example: One-Story Commercial Building	17-32
	Introduction • Design Steps	

Richard E. Klingner

17.1 Introduction

Masonry is traditionally defined as hand-placed units of natural or manufactured material, laid with mortar. In this chapter, the earthquake behavior and design of masonry structures is discussed, extending the traditional definition somewhat to include thin stone cladding.

Masonry makes up approximately 70% of the existing building inventory in the United States (TMS, 1989). U.S. masonry comprises Indian cliff dwellings, constructed of sandstone at Mesa Verde; the adobe missions constructed by Spanish settlers in Florida, CA, and the southwestern United States; bearing-wall buildings such as the 16-story Monadnock Building, completed in 1891 in Chicago; modern reinforced bearing-wall buildings; and many veneer applications. Clearly, the earthquake behavior and design of each type of masonry is distinct. In this chapter, fundamental applications and nomenclature of U.S. masonry are discussed; major construction categories are reviewed; historical seismic performance of masonry is presented; and principal design and retrofitting approaches are noted. The chapter ends with a comprehensive example problem. Its purpose is to give designers, constructors and building officials a basic foundation for further study of the seismic behavior and design of masonry.

17.2 Masonry in the United States

17.2.1 Fundamentals of Masonry in the United States

Masonry can be classified according to architectural or structural function. Each is discussed later in this chapter. Regardless of how it is classified, U.S. masonry uses basically the same materials: units, mortar, grout and accessory materials. In this section, these materials are discussed, with reference to the national consensus specifications of the American Society for Testing and Materials (ASTM). Additional information is available at the Web sites of associations such as the National Concrete Masonry Association (NCMA), the Brick Industry Association (BIA) and The Masonry Society (TMS).

17.2.1.1 Masonry Units

Of the more than 20 different classifications of masonry units commercially available in the United States, only the most widely used are discussed here.

17.2.1.1.1 Clay or Shale Masonry Units

The most common structural clay or shale masonry units are Building Brick and Facing Brick. The former are specified using ASTM C62 Building Brick (Solid Masonry Units Made from Clay or Shale). The latter, specifically intended for use when appearance is important, are specified using ASTM C216 Facing Brick (Solid Masonry Units Made from Clay or Shale). Units are usually cored rather than being completely solid. The net cross-sectional area of the unit must be at least 75% of the gross area; that is, the cores occupy less than 25% of the area of the unit.

Many different sizes and shapes of clay or shale masonry units are available, varying widely from region to region of the United States. One common size is probably the “modular” unit, which measures 7-5/8 in. (194 mm) long by 2-1/4 in. (57 mm) high by 3-5/8 in. (92 mm) deep. Using mortar joints 3/8 in. (9 mm) thick, this unit produces modules 8 in. (203 mm) wide by 2-2/3 in. (68 mm) high. That is, three courses of such units produce modules 8 in. (203 mm) wide by 8 in. high.

Clay or shale masonry units are sampled and tested using ASTM C67 (Methods of Sampling and Testing Brick and Structural Clay Tile). Specified properties include compressive strength and durability. Facing brick can have more restrictive dimensional tolerances and appearance requirements.

17.2.1.1.2 Concrete Masonry Units

The most common concrete masonry units are hollow load-bearing concrete masonry units, specified in ASTM C90 (Loadbearing Concrete Masonry Units). The units are typically made from low- or zero-slump concrete. In the eastern United States, these units are used for unreinforced inner wythes of cavity walls. In the western United States, these units are used for reinforced, fully grouted shear and bearing

walls. The net area of the units is usually about 55 to 60% of their gross cross-sectional area. These units are commonly 15-5/8 in. (397 mm) long by 7-5/8 in. (194 mm) high by 7-5/8 in. (194 mm) thick. Using mortar joints 3/8 in. (9 mm) thick, this unit produces modules 8 in. (203 mm) wide by 8 in. high. These modules are compatible with those of the “modular” clay brick discussed previously. Concrete masonry units are sampled and tested using ASTM C140 (Methods of Sampling and Testing Concrete Masonry Units). Specified properties include shrinkage, compressive strength and absorption.

17.2.1.2 Mortar

Mortar holds units together, and also compensates for their dimensional tolerances. In the United States, mortar for unit masonry is specified using ASTM C270 (Specification for Mortar for Unit Masonry), which addresses three cementitious systems: portland cement—lime, masonry cement and mortar cement. These cementitious systems are combined with sand and water to produce mortar.

Portland cement-lime mortar consists of portland cement and other hydraulic cements, hydrated mason's lime, sand and water. Masonry-cement mortar consists of masonry cement, sand and water. The contents of masonry cement and mortar cement, specified under ASTM C91 and ASTM C1329 respectively, vary from manufacturer to manufacturer, and are not disclosed. They typically include portland cement and other hydraulic cements, finely ground limestone and air-entraining and water-retention admixtures. Mortar cement has a minimum specified tensile bond strength and a lower maximum air content than does masonry cement. Model codes prohibit the use of masonry cement in seismic design categories C and higher. Portland cement-lime mortars and mortar-cement mortars are not restricted in this respect.

Within each cementitious system, masonry mortar is also classified according to type. Types are designated as M, S, N, O and K (derived from every other letter of the phrase “MaSoN wOrK”). These designations refer to the proportion of portland cement in the mixture. Type M has the most; S less; and so on. Higher proportions of portland cement result in faster strength gain, higher compressive strength and higher tensile bond strength; they also result in lower long-term deformability. Mortar types S and N are typically specified.

Within each cementitious system, mortar can be specified by proportion or by property, with the former being the default. For example, Type S portland cement-lime mortar, specified by proportion, consists of 1 volume portland cement, ½ volume of hydrated mason's lime, about 4-1/2 volumes of mason's sand and sufficient water for good workability. Type S masonry-cement mortar or mortar-cement mortar is made with 1 volume of masonry cement or mortar cement respectively, 3 volumes of mason's sand and sufficient water for good workability.

17.2.1.3 Grout

Masonry grout is essentially fluid concrete, used to fill spaces in masonry, and to surround reinforcement and connectors. It is specified using ASTM C476 (Grout for Masonry). Grout for masonry is composed of portland cement and other hydraulic cements, sand and (in the case of coarse grout) pea gravel. It is permitted to contain a small amount of hydrated mason's lime, but usually does not. It is permitted to be specified by proportion or by property, with the former being the default. A coarse grout specified by proportion would typically contain 1 volume portland cement or other hydraulic cements, about 3 volumes of mason's sand and about 2 volumes of pea gravel.

Masonry grout is placed with a slump of at least 8 in. (203 mm), so that it will flow freely into the cells of the masonry. Because of its high water/cement ratio at time of grouting, masonry grout undergoes considerable plastic shrinkage as the excess water is absorbed by the surrounding units. To prevent the formation of voids due to this process, the grout is consolidated during placement, and reconsolidated after initial plastic shrinkage. Grouting admixtures, which contain plasticizers and water-retention agents, are also useful in the grouting process.

If grout is specified by property (compressive strength), the compressive strength must be verified using permeable molds, duplicating the loss of water and decreased water/cement ratio that the grout would experience in actual use.

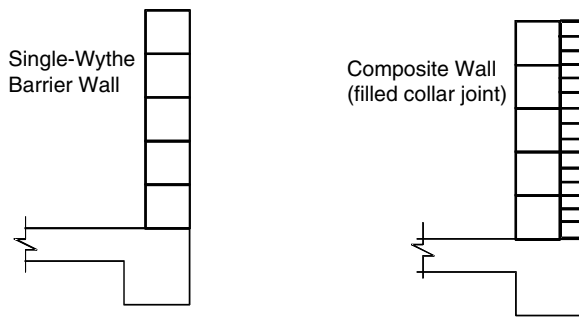


FIGURE 17.1 Examples of barrier walls.

17.2.1.4 Accessory Materials

Accessory materials for masonry consist of reinforcement, connectors, sealants, flashing, coatings and vapor barriers.

Reinforcement consists of deformed reinforcing bars or joint reinforcement. Deformed reinforcing bars are placed vertically in the cells of hollow units, horizontally in courses of bond-beam units or vertically and horizontally between wythes of solid units. Model codes require that these be surrounded by grout. Joint reinforcement is placed in the bed (horizontal) joints of masonry, and is surrounded by mortar.

Connectors are used to connect the wythes of a masonry wall (ties); to connect a masonry wall to a frame (anchors); or to connect something else to a masonry wall (fasteners).

Sealants are used to prevent the passage of water at places where gaps are intentionally left in masonry walls. Three basic kinds of gaps (joints) are used: expansion joints are used in brick masonry to accommodate expansion; control joints are used in concrete masonry to conceal cracking due to shrinkage; and construction joints are placed between different sections of a structure.

Flashing is a flexible waterproof barrier, intended to permit water that has penetrated the outer wythe to re-exit the wall. It is placed at the bottom of each story level (on shelf angles or foundations); over window and door lintels; and under window and door sills. Flashing should be lapped, and ends of flashing should be defined by end dams (flashing turned up at ends). Directly above the level of the flashing, weepholes should be provided at 24-in. spacing. Flashing is made of metal, polyvinyl chloride (PVC) or rubberized plastic (EPDM). Metallic flashing lasts much longer than plastic flashing. Nonmetallic flashings are subject to tearing. Modern EPDM self-adhering flashing is a good compromise between durability and ease of installation.

17.2.1.5 Masonry Nomenclature by Architectural Function

The architectural functions of masonry include acting as a building envelope to resist liquid water. In terms of this function, masonry walls are classified into barrier walls and drainage walls. Barrier walls act by a combination of thickness, coatings and integral water-repellent admixtures. Drainage walls act by the above, plus drainage details. Examples of each are shown in Figure 17.1 and Figure 17.2. In drainage walls, an outer wythe (thickness of masonry) is separated from an inner wythe of masonry or from a backup system by a cavity with drainage details.

17.2.1.6 Masonry Nomenclature by Structural Function

From the viewpoint of structural function, U.S. masonry can be broadly classified as non-load-bearing or load-bearing. The former resists gravity loads from self-weight alone, and possibly out-of-plane wind loads or seismic forces from its own mass only. The latter may resist gravity and lateral loads from overlying floors or roofs. Both classifications of masonry use the same materials.

Non-load-bearing masonry includes panel walls (an outer wythe of masonry connected to an inner wythe of masonry or a backup system), curtain walls (masonry spanning horizontally between columns) and interior partitions.

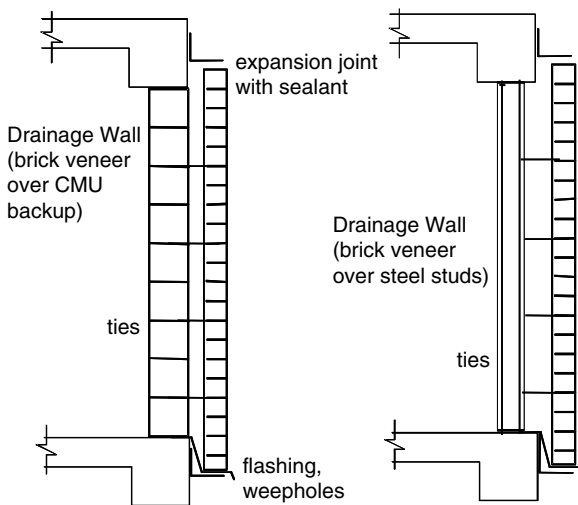


FIGURE 17.2 Examples of drainage walls.

Load-bearing masonry walls resist out-of-plane loads by spanning as horizontal or vertical strips, resist in-plane gravity loads by acting as a shallow beam-column loaded perpendicular to the plane of the wall and resist in-plane shear forces by acting as a deep beam-column loaded in the plane of the wall.

17.2.1.7 Masonry Nomenclature by Design Intent

From the viewpoint of design intent, U.S. masonry can be broadly classified as unreinforced or reinforced. Unreinforced masonry (URM) is designed assuming that flexural tension is resisted by masonry alone, and neglecting stresses in reinforcement. Reinforced masonry is designed assuming that flexural tension is resisted by reinforcement alone, and neglecting the flexural tensile resistance of masonry. Both types of masonry are designed assuming that masonry has some diagonal tensile resistance, because both types permit some shear to be resisted without shear reinforcement.

To decipher design intent may be impossible by examination of the masonry alone, with no knowledge of its design process. Masonry elements, no matter how they are designed, are required to have minimum prescriptive reinforcement whose location and percentage depend on the seismic design category of the structure in which they are located.

Differences in historical tradition have led to potentially confusing differences in nomenclature. For example, in parts of the United States where the Uniform Building Code (UBC) has been dominant (roughly speaking, to the west of Denver), "partially reinforced" masonry referred to reinforced masonry whose reinforcement did not comply with UBC requirements for prescriptive reinforcement in zones of highest seismic risk. East of Denver, however, "partially reinforced" masonry referred to masonry reinforced only with wire-type bed-joint reinforcement, rather than with deformed reinforcement placed in grouted cells or bond beams.

17.2.2 Modern Masonry Construction in the United States

A decade ago, it might have been possible to distinguish between modern masonry in the eastern vs. the western United States, with the latter being characterized by more emphasis on seismic design. As model codes increasingly adopt the philosophy that almost all regions of the United States have some level of seismic risk, such regional distinctions are disappearing.

17.2.2.1 Masonry Veneer

Modern masonry veneer resists vertical loads due to self-weight only, and transfers out-of-plane loads from wind or earthquake to supporting elements such as wooden stud walls, light-gage steel framing or

a backup wythe of masonry. Veneer is most commonly clay masonry units, but concrete masonry units, glass blocks and glazed tiles are also used. Stone cladding can be laid like manufactured masonry units, using masonry mortar. Thin stone can also be attached without mortar to a backup frame, using stainless steel connectors.

17.2.2.2 Masonry Partition Walls

Modern masonry partition walls are interior elements designed to resist vertical loads due to self-weight only, and out-of-plane loads due to inertial forces from their own mass only. They are of clay or concrete masonry units, glass blocks or glazed tiles.

17.2.2.3 Masonry Panel Walls

Modern masonry panel walls are combinations of a veneer wythe and a backup system. They resist vertical loads due to self-weight only. The veneer wythe transfers out-of-plane loads from wind or earthquake to the backup system. The backup system is not intended to resist in-plane shear loads nor vertical loads from overlying roofs or floors. If the space between the masonry veneer and the backup system is separated by a cavity at least 2 in. (50 mm) wide, and is provided with drainage details, the result is a drainage wall.

17.2.2.4 Masonry Curtain Walls

Curtain walls are multi-story masonry walls that resist gravity loads from self-weight only, and out-of-plane loads from wind or earthquake. Their most common application is for walls of industrial buildings, warehouses, gymnasiums or theaters. They are most commonly single-wythe walls. Because they occupy multiple stories, curtain walls are generally designed to span horizontally between columns or pilasters. If a single wythe of masonry is used, horizontal reinforcement is often required for providing resistance to out-of-plane loads. This reinforcement is usually provided in the form of welded wire reinforcement, placed in the horizontal joints of the masonry.

17.2.2.5 Masonry Bearing and Shear Walls

Bearing walls resist gravity loads from self-weight and overlying floors and roofs; out-of-plane loads from wind or earthquake; and in-plane shears. If bearing walls are composed of hollow units, vertical reinforcement consists of deformed bars placed in vertical cells and horizontal reinforcement consists either of deformed bars placed in grouted courses (bond beams), or bed-joint reinforcement. Bearing walls, whether designed as unreinforced or reinforced, must have reinforcement satisfying seismic requirements. If bearing walls are composed of solid units, vertical and horizontal reinforcement generally consists of deformed bars placed in a grouted space between two wythes of masonry.

Although model codes sometimes distinguish between bearing walls and shear walls, in practical terms every bearing wall is also a shear wall, because it is practically impossible for a wall to resist gravity loads from overlying floors or roofs, yet be isolated from in-plane shears transmitted from those same elements.

Reinforced masonry shear walls differ from reinforced concrete shear walls primarily in that their inelastic deformation capacity is lower. They are usually not provided with confined boundary elements, because these are difficult or impossible to place. Their vertical reinforcement is generally distributed uniformly over the plan length of the wall. Sections of masonry shear wall that separate window or door openings are commonly referred to as “piers.”

Using this type of construction, 30-story masonry bearing-wall buildings have been built in Las Vegas, NV, a region of seismic risk in the United States (Suprenant, 1989).

Masonry infills are structural panels placed in a bounding frame of steel or reinforced concrete. This mode of structural action, though common in panel walls, is not addressed directly by design codes. Provisions are under development. Historical masonry infills are addressed later in this chapter.

17.2.2.6 Masonry Beams and Columns

Other modern masonry elements are beams and columns. Masonry beams are most commonly used as lintels over window or door openings, but can also be used as isolated elements. They are reinforced horizontally for

flexure. Although shear reinforcement is theoretically possible, it is difficult to install and is rarely used. Instead, masonry beams are designed deep enough so that shear can be resisted by masonry alone.

Isolated masonry columns are rare. The most common form of masonry beam-column is a masonry bearing wall subjected to a combination of axial load from gravity, and out-of-plane moment from eccentric axial load or out-of-plane wind or seismic loads.

17.2.2.7 Role of Horizontal Diaphragms in Structural Behavior of Modern Masonry

Horizontal floor and roof diaphragms play a critical role in the structural behavior of modern masonry. In addition to resisting gravity loads, they transfer horizontal forces from wind or earthquake to the lateral force-resisting elements of a masonry building, which are usually shear walls. Modern horizontal diaphragms are usually composed of cast-in-place concrete, or of concrete topping overlying hollow core, prestressed concrete planks or corrugated metal deck supported on open-web joists. Distinctions between rigid and flexible diaphragms, and appropriate analytical approaches for each, are addressed later. Performance of horizontal diaphragms in modern masonry is addressed by structural requirements for in-plane flexural and shear resistance, and by detailing requirements for continuous chords and other embedded elements.

17.2.3 Historical Structural Masonry in the United States

17.2.3.1 URM Bearing Walls

URM bearing walls were constructed before 1933 in the western United States, and as late as the 1950s elsewhere in the United States. They commonly consisted of two wythes of masonry, bonded by masonry headers, and sometimes also had an interior wythe of rubble masonry (pieces of masonry units surrounded by mortar).

17.2.3.2 Masonry Infills

Masonry infills are structural panels placed in a bounding frame of steel or reinforced concrete. Before the advent of drywall construction, masonry infills of clay tiles were often used to fill interior or exterior bays of steel or reinforced concrete frames. Although sometimes considered nonstructural, they have high elastic stiffness, and are usually built tight against the bounding frame. As a result, they can significantly alter the seismic response of the frame in which they are placed.

17.2.3.3 Role of Horizontal Diaphragms in Structural Behavior of Historical Masonry

Horizontal diaphragms play a crucial role in the seismic resistance of historical as well as modern masonry construction. In contrast to their role in modern construction, however, the behavior of horizontal diaphragms in historical masonry is usually deficient. Historical diaphragms are usually composed of lumber, supported on wooden joists inserted in pockets in the inner wythe of URM walls. Such diaphragms are not strong enough, and not sufficiently well connected, to transfer horizontal seismic forces to the building's shear walls. Out-of-plane deformations of the bearing walls can cause the joists to slip out of their pockets, often resulting in collapse of the entire building. For this reason, horizontal diaphragms are among the elements addressed in the seismic rehabilitation of historical masonry.

17.3 Performance of Masonry in U.S. Earthquakes

For historical reasons that will be explained in this section, a summary of the historical performance of masonry in the United States can conveniently be divided into two periods: before the 1933 Long Beach earthquake, and after that earthquake. In this section, that history is summarized, with emphasis on design implications.



FIGURE 17.3 Damage to masonry in the Charleston, SC, earthquake of August 31, 1886.

17.3.1 Before the 1933 Long Beach Earthquake

The United States has several regions that have historically been recognized as having relatively high seismic risk. These include Alaska, Hawaii, California, parts of Montana and Idaho, the New Madrid area in southeast Missouri, and the Charleston, SC, area. This judgment is based on historical records of strong earthquakes there, throughout the past several centuries. Those early earthquakes did not cause significant damage to masonry buildings because few or no such buildings existed in seismic regions of the United States until about the middle of the 1700s. California mission records contain references to such earthquakes. The series of earthquakes that occurred between December 1811 and March 1812 in the New Madrid area of southeast Missouri rang church bells in Boston and caused local changes in the bed of the Mississippi River, but caused little structural damage because few structures existed.

The Charleston earthquake of August 31, 1886, with an estimated magnitude of 7.6 on the Richter scale, was felt from Cuba to New York, killed 110 people and damaged 90% of the masonry buildings in Charleston. An example of this damage is shown in Figure 17.3.

The most destructive historical U.S. earthquake was undoubtedly the San Francisco earthquake of April 18, 1906, which had an estimated magnitude of 8.0 on the Richter scale and ruptured more than 400 km of the San Andreas Fault. The earthquake caused extensive damage to masonry buildings throughout the area, and San Francisco was almost completely destroyed by the combination of the earthquake and the subsequent fire (Figure 17.4). Total damage was estimated at \$500 million.

The 1925 Santa Barbara earthquake, while having a magnitude of only 6.3, was notable because it prompted several cities in California to adopt earthquake regulations given in the 1927 UBC, published by the Pacific Coast Building Officials Conference, which later became the International Conference of Building Officials. That document had an optional appendix on seismic design, by which buildings were designed for an equivalent static force applied horizontally at each floor level. The force at each level was obtained by multiplying the dead plus live load at that level by foundation-dependent factor equal to 0.075 for good soil.

17.3.2 1933 Long Beach Earthquake

The earthquake that shook Long Beach, CA, on March 10, 1933, though having a magnitude of only 6.3 on the Richter scale, caused 115 deaths and damaged property worth \$40 million. While reinforced concrete buildings generally behaved well, URM buildings, including many school buildings, collapsed



FIGURE 17.4 Damage from the San Francisco earthquake and subsequent fire.



FIGURE 17.5 Collapse of part of Jefferson Junior High School in Long Beach earthquake (Portland Cement Association).

(see Figure 17.5) (Binder, 1952). The ensuing public outcry led to the passage, less than 1 month later, of the Field Act, which mandated earthquake-resistant design and construction for public schools in California, and prohibited the use of URM for such schools. Public opinion extended this prohibition to most other buildings as well.

When masonry construction was revived in California during the middle 1940s, it was required to comply with the new provisions of the 1943 UBC (UBC, 1943), which were based on the reinforced concrete design practice of the time. The provisions required that minimum seismic lateral forces be considered in the design of masonry buildings, that tensile stresses in masonry be resisted by reinforcement and that all masonry have minimum percentages of horizontal and vertical reinforcement. These provisions led to the development of grouted, reinforced masonry constructed primarily of hollow concrete masonry units, which became the de facto standard for reinforced masonry on the west coast of the United States and remains so up to the present.



FIGURE 17.6 San Fernando Veterans Administration Hospital (U.S. Geological Survey).

17.3.3 1971 San Fernando Earthquake

On February 9, 1971, the San Fernando Valley (in the northwest portion of greater Los Angeles) was shaken by an earthquake that, although having a magnitude of only 6.7, caused extensive damage to modern buildings such as the new Olive View Hospital (Lew et al., 1971). It also caused extensive damage to URM buildings. For example, the San Fernando Veterans Administration Hospital and complex, built in 1926, collapsed, causing 47 of the 58 deaths attributed to the earthquake (Figure 17.6). Failures of URM structures built before 1933 prompted the development of URM retrofitting ordinances, discussed later.

17.3.4 1989 Loma Prieta Earthquake

At 5:04 p.m. on October 17, 1989, the San Francisco Bay area was shaken by an earthquake (magnitude 7.1) whose epicenter was located about 10 mi northeast of Santa Cruz along a segment of the San Andreas Fault (EQE, 1989).

Although damage to modern reinforced masonry buildings was generally low, many unretrofitted URM buildings experienced heavy damage. A large area of URM buildings in the Pacific Garden Mall in Santa Cruz collapsed (Figure 17.7). In the Marina District of San Francisco, a large region of unconsolidated fill was the scene of many collapses of nonengineered houses and apartments with wooden frames and masonry veneer (Figure 17.8).

17.3.5 1994 Northridge Earthquake

The Northridge earthquake, whose epicenter was located in the northwest part of the greater Los Angeles area, occurred at 4:31 a.m. on January 17, 1994. The earthquake had a moment magnitude of 6.7, and strong shaking lasted 15 to 20 sec in the epicentral region. The following description is taken from The Masonry Society's report on the earthquake (TMS Northridge, 1994).

The greater Los Angeles area contains tens of thousands of masonry structures, many of which were strongly shaken. In newer communities such as Northridge and Van Nuys (both in the epicentral region), the most common use of masonry by far was in one-story, reinforced masonry buildings, usually of fully grouted and reinforced hollow concrete blocks. Some multi-story, reinforced masonry bearing-wall structures were also found there, as well as steel or concrete frames with masonry veneer. In residential areas throughout Los Angeles, masonry site walls (landscaping walls)



FIGURE 17.7 Collapsed unreinforced masonry buildings in Santa Cruz after the Loma Prieta earthquake. (Photo by the International Masonry Institute.)



FIGURE 17.8 Collapsed wooden apartments with masonry veneer in the Marina District of San Francisco after the Loma Prieta earthquake. (Photo by the International Masonry Institute.)

and brick chimneys were common. In older communities such as Hollywood, Santa Monica and Pasadena (all 15 mi or more from the epicenter), URM structures, usually two- or three-story storefront buildings, were common. In accordance with the City of Los Angeles' Division 88 ordinance, most such structures had been retrofitted with parapet braces and floor-wall ties.

Throughout Los Angeles were many reinforced masonry schools, post offices, fire stations and police stations. Most of these buildings showed little apparent structural damage, and continued operating after the earthquake.

In the greater Los Angeles area, and particularly in the epicentral region, very little distress was shown by modern one-story reinforced masonry, or by multi-story, reinforced bearing-wall buildings (Figure 17.9).

In some cases, however, masonry veneer was attached using connection details that were inadequate to resist the required inertial forces (Figure 17.10).

Performance of masonry chimneys and site walls was quite variable; many failures were observed (Figure 17.11). Although no freeway noise barriers collapsed, some showed significant damage. URM buildings retrofitted in response to Division 88 requirements generally had parapet and wall damage,



FIGURE 17.9 Seventeen-story high-rise masonry hotel with no visible damage from the Northridge earthquake. (Photo by The Masonry Society.)



FIGURE 17.10 Masonry veneer stripped off wall by Northridge earthquake. (Photo by The Masonry Society.)

but did not collapse. Unretrofitted URM buildings, in contrast, generally had more extensive damage, and some collapses.

In general, masonry structures built since the 1950s, that were engineered, grouted, reinforced and inspected in accordance with then-current building codes, experienced little damage in the January 17,



FIGURE 17.11 Collapsed chimney, Northridge earthquake. (Photo by The Masonry Society.)

1994, earthquake. URM structures that had been retrofitted in accordance with Division 88 requirements experienced less damage than did similar URM structures that had not been retrofitted.

17.3.6 2001 Nisqually Earthquake

At 10:55 a.m. on February 28, 2001, an earthquake with a magnitude of 6.8 struck near Seattle, WA. Although the earthquake was not very strong, local newspapers estimated the damage at nearly \$2 billion.

Observed damage to modern masonry structures was generally light. Older URM structures, however, experienced parapet damage, cracking and evidence of hammering. New as well as older homes with masonry veneer generally appeared to have performed well, although a number of chimneys sustained damage or completely collapsed (Figure 17.12) (TMS Nisqually, 2001).

17.3.7 Concluding Remarks

As noted in the introduction to this section, since the 1940s masonry structures in the western part of the United States have generally been designed and constructed with minimum prescriptive requirements for reinforcement that are similar to those required in higher seismic design categories today. Such buildings have experienced little damage in U.S. earthquakes. URM structures, in contrast, have experienced severe damage or collapse. URM structures with basic seismic retrofitting have experienced much less damage.

17.3.8 Relevant Information from non-U.S. Earthquakes

In recent decades, considerable information has been obtained on the performance of masonry in earthquakes outside the United States. Examples are the Santiago, Chile, and Mexico City earthquakes of 1985; the Quindío, Colombia, earthquake of 1999; and the Izmit, Turkey, earthquake of 1999. Such information is relevant to U.S. practice if the construction is similar to that found in the United States, and if the lessons learned are new. In most cases, both questions are answered in the negative. Most non-U.S. earthquakes show, over and over again, that URM buildings and infilled frame structures in which



FIGURE 17.12 Partial collapse of an unreinforced masonry bearing wall near Pioneer Square in Seattle. (Photo by The Masonry Society.)

the contribution of masonry infills is neglected in design, behave poorly in earthquakes. A large proportion of such buildings collapse or are heavily damaged. Because this information is not relevant to modern U.S. practice, and is not new, it is discussed only briefly here.

17.3.8.1 Santiago, Chile, Earthquake of 1985

On March 3, 1985, an earthquake of magnitude 7.8 occurred off the coast of central Chile. It caused significant damage to Santiago and surrounding areas. Nonengineered masonry structures suffered heavy damage. Many Chilean masonry buildings were designed and constructed in accordance with U.S. practice at that time. As exemplified by Figure 17.13, those U.S.-type masonry buildings suffered only slight damage, in the form of minor flexural and shear cracking (Klingner et al., 1990).

17.3.8.2 1985 Mexico City Earthquake

The Mexico City earthquake (magnitude 8.1) of September 19, 1985, occurred off the west coast of Mexico, causing some damage in the epicentral region, and extensive damage in Mexico City, 400 km inland. At least 8000 people were killed, and 30,000 rendered homeless. Resonant response of the deep, soft clay deposits underlying the central part of the city caused near-sinusoidal, long-period ground motions for more than 60 sec, with maximum accelerations near 20% g (IMI, 1985).

Older, low-rise masonry constructions performed well in some cases, because such structures were stiff enough not to get significantly excited by the long-period ground motions. In many cases, however, URM structures with no formal design collapsed or suffered heavy damage (IMI, 1985).

17.3.8.3 Quindío, Colombia, Earthquake of 1999

On January 25, 1999, an earthquake of magnitude 6.2 occurred near the cities of Armenia and Pereira in Colombia. It caused the collapse of many nonengineered masonry structures, and extensive damage to URM infills (Figure 17.14) (EERI, 1999).

17.3.8.4 Izmit, Turkey, Earthquake of 1999

On August 17, 1999, an earthquake (magnitude 7.4) struck the province of Kocaeli in western Turkey, near the city of Izmit. The unofficial death toll was more than 30,000, most of which were caused by the collapse of multi-story commercial or residential buildings. The most common form of urban construction, reinforced concrete frames with unreinforced clay masonry infills, suffered heavy damage, exemplified by Figure 17.15 (EQE, 1999).



FIGURE 17.13 U.S.-type masonry building after Santiago, Chile, earthquake of 1985. (Photo by R.E. Klingner.)



FIGURE 17.14 Damage to unreinforced masonry infill in Quindio, Colombia, earthquake. (Photo EERI, 1999.)

17.4 Fundamental Basis for Seismic Design of Masonry in the United States

Seismic design of masonry in the United States is based on the premise that reinforced masonry structures can perform well in earthquakes, provided that they meet the following conditions:

1. They must have engineered lateral force-resisting systems, generally consisting of reinforced masonry shear walls distributed throughout their plan area, and acting in both principal plan directions.



FIGURE 17.15 Damage to reinforced concrete frame with unreinforced masonry infill in Kocaeli earthquake. (Photo, EQE International.)

2. Their load-displacement characteristics under cyclic reversed loading must be consistent with the assumptions used to develop their design loadings:
 - If they are intended to respond primarily elastically, they must be provided with sufficient strength to resist elastic forces. Such masonry buildings are typically low-rise, shear-wall structures.
 - If they are intended to respond inelastically, their lateral force-resisting elements must be proportioned and detailed to be capable of resisting the effects of the reversed cyclic deformations consistent with that inelastic response. They must be proportioned, and must have sufficient shear reinforcement, so that their behavior is dominated by flexure (“capacity design”). The most desirable structural system for such response is composed of multiple masonry shear walls, designed to act in flexure, and loosely coupled by floor slabs.

As noted in the previous section dealing with observed seismic response, U.S. masonry has shown good performance under such conditions.

Good load-displacement behavior has also been observed in laboratory conditions. This research is described extensively in U.S. technical literature over the last two decades. A representative sample is given in the Proceedings of North American Masonry Conferences (NAMC, 1985, 1987, 1990, 1993, 1996, 1999).

Of particular relevance is the U.S. Coordinated Program for Masonry Building Research, also known as the TCCMAR Program (Noland, 1990). With the support of the National Science Foundation and the masonry industry, the Technical Coordinating Committee for Masonry Research (TCCMAR) was formed in February 1984 for the purpose of defining and performing both analytical and experimental research and development necessary to improve masonry structural technology, and specifically to lay the technical basis for modern, strength-based design provisions for masonry. Under the coordination of TCCMAR, research was carried out in the following areas:

1. Material properties and tests
2. Reinforced masonry walls
 - In-plane shear and combined in-plane shear and vertical compression
 - Out-of-plane forces combined with vertical compression
3. Floor diaphragms
4. Bond and splicing of reinforcement in masonry
5. Limit state design concepts for reinforced masonry

6. Modeling of masonry components and building systems
7. Large-scale testing of masonry building systems
8. Determination of earthquake-induced forces on masonry buildings

Work began on the initially scheduled research tasks in September 1985, and the program lasted for more than 10 years. Numerous published results include the work of Hamid et al. (1989) and Blondet and Mayes (1991), who studied masonry walls loaded out-of-plane; and He and Priestley (1992), Leiva and Klingner (1994) and Seible et al. (1994a, 1994b), who studied masonry walls loaded in-plane. In all cases, flexural ductility was achieved without the use of confining reinforcement.

Using pseudodynamic testing procedures, Seible et al. (1994a, 1994b) subjected a full-scale, five-story masonry structure to simulated earthquake input. The successful inelastic performance of this structure under global drift ratios exceeding 1% provided additional verification for field observations and previous TCCMAR laboratory testing that with proper proportioning and detailing, reinforced masonry assemblies can exhibit significant ductility.

Limited shaking-table testing has been conducted on reinforced masonry structures built using typical modern U.S. practice:

- Gulkan et al. (1990a, 1990b): A series of single-story, one-third scale masonry houses were constructed and subjected to shaking-table testing. The principal objective of the testing was to verify prescriptive reinforcing details for masonry in zones of moderate seismic risk.
- Abrams and Paulson (1991): Two, three-story, quarter-scale reinforced masonry buildings were tested to evaluate the validity of small-scale testing.
- Cohen (2001): Two low-rise, half-scale reinforced masonry buildings with flexible roof diaphragms were subjected to shaking-table testing. Results were compared with the results of static testing and analytical predictions.

Results of these tests have generally supported field observations of satisfactory behavior of modern reinforced masonry structures in earthquakes.

17.4.1 Design Approaches for Modern U.S. Masonry

Three design approaches are used for modern U.S. masonry: allowable-stress design, strength design and empirical design. Each approach is summarized in this section.

17.4.1.1 Allowable-Stress Design

Allowable-stress design is the traditional approach of building codes for calculated masonry design. Stresses from unfactored loads are compared with allowable stresses, which are failure stresses reduced by a factor of safety, which is usually between 2.5 and 4.

17.4.1.2 Strength Design

Within the past decade, strength-design provisions for masonry have been developed within the 1997UBC; the 1997 and 2000 National Earthquake Hazards Reduction Program (NEHRP) documents; and the 2000 International Building Code (IBC). The 2002 edition of the Masonry Standards Joint Committee (MSJC) Code includes strength-design provisions, and these provisions will be referenced by the 2003 IBC.

Strength-design provisions for masonry are generally similar to those for concrete. Factored design actions are compared with nominal capacities reduced by capacity reduction factors. Strength-design provisions for masonry differ from those for reinforced concrete, however, in three principal areas: URM, confining reinforcement and maximum flexural reinforcement.

- Some masonry can be designed as unreinforced (flexural tension resisted by masonry alone). For this purpose, nominal flexural tensile capacity is computed as the product of the masonry's tensile bond strength (modulus of rupture) and the section modulus of the section under consideration. This nominal strength is then reduced by a capacity reduction factor.



FIGURE 17.16 Monadnock Building, Chicago (1891).

- Because it is impractical to confine the compressive zones of masonry elements, the inelastic strain capacity of such elements is less than that of confined reinforced concrete elements. The available displacement ductility ratio of masonry shear walls is therefore lower than that of reinforced concrete shear walls with confined boundary elements, and corresponding R factors (response modification factors) are lower.
- Maximum flexural reinforcement for masonry elements is prescribed in terms of the amount of steel required to equilibrate the compressive stress block of the element under a critical strain gradient, in which the maximum strain in masonry is the value used in design (0.0025 for concrete masonry and 0.0035 for clay masonry), and the maximum strain in the extreme tensile reinforcement is a multiple of the yield strain. This multiple depends on the ductility expected of the element under reversed cyclic inelastic deformations. In practical terms, if inelastic response is possible, an element cannot be designed to work above its balanced axial load. The intent of these provisions is to ensure, for inelastic elements, that the flexural reinforcement can yield and begin to strain-harden before the compression toe crushes.

17.4.1.3 Empirical Design

At the end of the 19th century, masonry bearing-wall buildings were designed using empirical rules of thumb, such as using walls 12 in. (305 mm) thick at the top of a building, and increasing the wall thickness by 4 in. (102 mm) for every story. The Monadnock Building, built in Chicago in 1891 (Figure 17.16), is 16 stories high, is of URM and has bearing walls 6 ft (1.83 m) thick at the base. It is still in use today.

Today's empirical design is the descendant of those rules, adapted for the characteristics of modern structures. They primarily involve limitations on length-to-thickness ratios of elements, with some rudimentary axial stress checks and limits on the arrangement of lateral force-resisting elements and the plan aspect ratio of floor diaphragms.

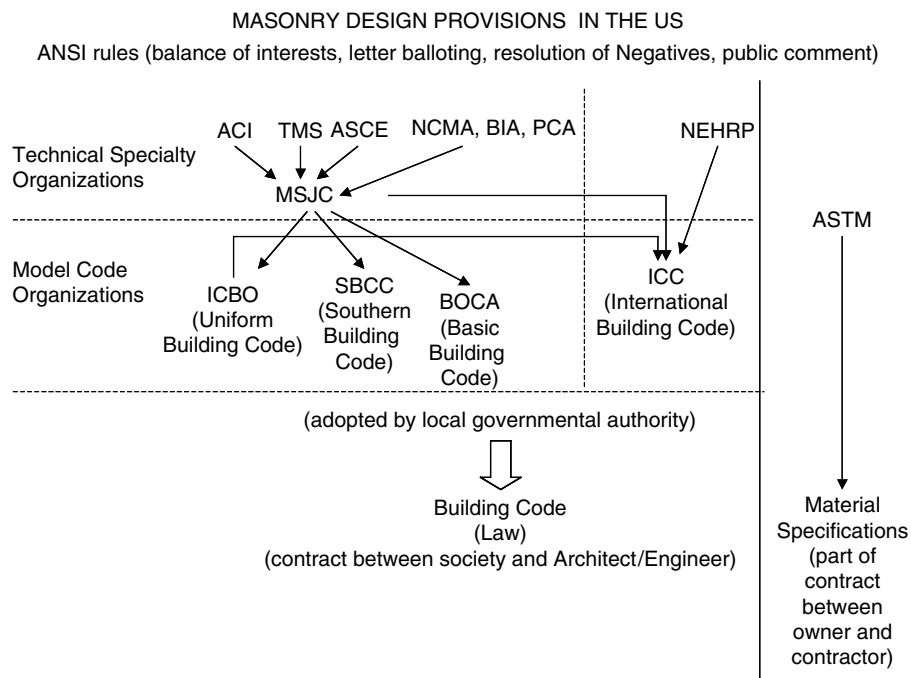


FIGURE 17.17 Schematic of code-development process for masonry in the United States.

17.5 Masonry Design Codes Used in the United States

17.5.1 Introduction

The United States has no national design code, primarily because the U.S. Constitution has been interpreted as delegating building code authority to the states, which in turn delegate it to municipalities and other local governmental agencies. Design codes used in the United States are developed by a complex process involving technical experts, industry representatives, code users and building officials. As it applies to the development of design provisions for masonry, this process is shown in Figure 17.17, and is then described:

1. *Consensus design provisions and specifications for materials or methods of testing* are first drafted in mandatory language by *technical specialty organizations*, operating under consensus rules approved by the American National Standards Institute (ANSI). These consensus rules can vary from organization to organization, but must include requirements for:
 - *Balance of interests (producer, user and general interest)*.
 - *Written balloting of proposed provisions, with prescribed requirements for a successful ballot*.
 - *Resolution of negative votes*. Negative votes must be discussed and found nonpersuasive before a ballot item can pass. A single negative vote, if found persuasive, can prevent an item from being passed.
 - *Public comment*. After being approved within the technical specialty organization, the mandatory-language provisions must be published for public comment. If significant public comments are received (usually more than 50 comments on a single item), the organization must respond to the comments.
2. These consensus design provisions and specifications are adopted, sometimes in modified form, by *model code organizations*, and take the form of *model codes*.
3. These model codes are adopted, sometimes in modified form, by *local governmental agencies* (such as cities or counties). Upon adoption, but not before, they acquire legal standing as *building codes*.

17.5.1.1 Technical Specialty Organizations

Technical specialty organizations are open to designers, contractors, product suppliers, code developers and end users. Their income (except for Federal Emergency Management Agency [FEMA], a U.S. government agency) is derived from member dues and the sale of publications. Technical specialty organizations active in the general area of masonry include the following:

1. *ASTM*: Through its many technical committees, ASTM develops consensus specifications for materials and methods of testing. Although some model code organizations use their own specifications, most refer to ASTM specifications. Many ASTM specifications are also listed by the ISO (International Standards Organization).
2. *American Concrete Institute (ACI)*: Through its many technical committees, this group publishes a variety of design recommendations dealing with different aspects of concrete design. ACI Committee 318 develops design provisions for concrete structures. ACI is also involved with masonry, as one of the three sponsors of the MSJC. This committee was formed in 1982 to combine the masonry design provisions then being developed by ACI, ASCE, TMS and industry organizations. It currently develops and updates the MSJC design provisions and related specifications (MSJC, 2002a, 2002b).
3. *American Society of Civil Engineers (ASCE)*: ASCE is a joint sponsor of many ACI technical committees dealing with concrete or masonry. ASCE is the second of the three sponsoring societies of the MSJC (see above). ASCE publishes ASCE 7-98 (1998), which prescribes design loadings and load factors for all structures, independent of material type.
4. *The Masonry Society (TMS)*: Through its technical committees, this group influences different aspects of masonry design. TMS is the third of the three sponsoring societies of the MSJC (see above). TMS publishes a *Masonry Designers' Guide* to accompany the MSJC design provisions.

17.5.1.2 Industry Organizations

1. *Portland Cement Association (PCA)*: This marketing and technical support organization is composed of cement producers. Its technical staff participates in technical committee work.
2. *National Concrete Masonry Association (NCMA)*: This marketing and technical support organization is composed of producers of concrete masonry units. Its technical staff participates in technical committee work, and also produces technical bulletins, which can influence consensus design provisions.
3. *Brick Industry Association (BIA)*: This marketing, distributing and technical support organization is composed of clay brick and tile producers. Its technical staff participates in technical committee work, and also produces technical bulletins, which can influence consensus design provisions.
4. *National Lime Association (NLA)*: This marketing and technical support organization is composed of hydrated lime producers. Its technical staff participates in technical committee work.
5. *Expanded Clay, Shale and Slate Institute (ECSSI)*: This marketing and technical support organization is composed of producers of expanded clay, shale and slate. Its technical staff participates in technical committee meetings.
6. *International Masonry Institute (IMI)*: This is a labor—management collaborative supported by dues from union masons. Its technical staff participates in technical committee meetings.
7. *Mason Contractors' Association of America (MCAA)*: This organization is composed of nonunion mason contractors. Its technical staff participates in technical committee meetings.

17.5.1.3 Governmental Organizations

FEMA: FEMA has jurisdiction over the NEHRP, and develops and periodically updates the NEHRP provisions (NEHRP, 2000), a set of recommendations for earthquake-resistant design. This document includes provisions for masonry design and is published by the Building Seismic Safety Council (BSSC), which operates under a contract with FEMA. BSSC is not an ANSI consensus organization. Its recommended design provisions are intended for consideration and possible adoption by consensus organizations. The NEHRP *Recommended Provisions* (NEHRP, 2000) is the latest of a series of such documents,

now issued at 3-year intervals, and pioneered by ATC 3-06, which was issued by the Applied Technology Council in 1978 under contract to the National Bureau of Standards. The NEHRP *Recommended Provisions* addresses the broad issue of seismic regulations for buildings. They contain chapters dealing with the determination of seismic loadings on structures, and with the design of masonry structures for those loadings.

17.5.1.4 Model-Code Organizations

Model-code organizations are composed primarily of building officials, although designers, contractors, product suppliers, code developers and end users can also be members. Their income is derived from dues and the sale of publications. The United States has three model-code organizations:

1. *International Conference of Building Officials (ICBO)*: In the past, this group developed and published the *Uniform Building Code* (UBC). The latest and final edition is the 1997 UBC.
2. *Southern Building Code Congress (SBCC)*: In the past, this group developed and published the *Standard Building Code* (SBC). The latest and final edition is the 1999 SBC.
3. *Building Officials/Code Administrators (BOCA)*: In the past, this group developed and published the *Basic Building Code* (BBC). The latest and final edition is the 1999 BBC.

In the past, certain model codes were used more in certain areas of the country. The UBC has been used throughout the western United States, and in the state of Indiana. The SBC has been used in the southern part of the United States. The BBC has been used in the eastern and northeastern United States.

Since 1996, intensive efforts have been underway in the United States to harmonize the three model building codes. The primary harmonized model building code is called the IBC. It has been developed by the International Code Council (ICC), composed primarily of building code officials of the three model-code organizations. The first edition of the IBC (2000) was published in May 2000. In most cases, it references consensus design provisions and specifications. It is intended to take effect when adopted by local jurisdictions. It is intended to replace the three current model building codes. Although not all details have been worked out, it is generally understood that the IBC will continue to be administered by the three model-code agencies. Another harmonized model code is being developed by the National Fire Protection Association, composed primarily of fire-protection officials.

17.5.2 Masonry Design Provisions of Modern Model Codes in the United States

Over the next 3 to 5 years, as the IBC and other harmonized model codes such as that of the National Fire Protection Association are adopted by local jurisdictions, their provisions will become minimum legal design requirements for masonry structures throughout the United States. The 2003 IBC will reference the masonry design provisions of the 2002 MSJC code in essentially direct form.

17.5.2.1 Strength Design Provisions of the 2002 MSJC Code

Strength design provisions of the 2002 MSJC Code deal with unreinforced as well as reinforced masonry.

Strength design provisions for URM address failure in flexural tension, in combined flexural and axial compression and in shear. Nominal capacity in flexural tension is computed as the product of the masonry's flexural tensile strength and its section modulus. Nominal capacity in combined flexural and axial compression is computed using a triangular stress block, with an assumed failure stress of $0.80 f'_m$ (the specified compressive strength of the masonry). Nominal capacity in shear is computed as the least of several values, corresponding to different possible failure modes (diagonal tension, crushing of compression diagonal, sliding on bed joints). Each nominal capacity is multiplied by a capacity reduction factor.

Strength design provisions for reinforced masonry address failure under combinations of flexure and axial loads, and in shear. Nominal capacity under combinations of flexure and axial loads is computed using a moment–axial force interaction diagram, determined assuming elastoplastic behavior of tensile reinforcement and using an equivalent rectangular stress block for the masonry. The diagram also has an upper limit on pure compressive capacity. Shear capacity is computed as the summation of capacity

from masonry plus capacity from shear reinforcement, similarly to reinforced concrete. Nominal capacity of masonry in shear is computed as the least of several values, corresponding to different possible failure modes (diagonal tension, crushing of compression diagonal, sliding on bed joints). Each nominal capacity is multiplied by a capacity reduction factor.

Strength-design provisions of the 2002 MSJC Code impose strict upper limits on reinforcement, which are equivalent to requiring that the element remain below the balanced axial load. Nominal flexural and axial strength are computed neglecting the tensile strength of masonry, using a linear strain variation over the depth of the cross section, a maximum usable strain of 0.0035 for clay masonry and 0.0025 for concrete masonry, and an equivalent rectangular compressive stress block in masonry with a stress of $0.80 f'_m$. These provisions are regarded as too conservative by many elements of the masonry technical community, and are currently undergoing extensive review.

17.5.2.2 Allowable-Stress Design Provisions of the 2002 MSJC Code

The allowable-stress design provisions of the 2002 MSJC Code are based on linear elastic theory.

Allowable-stress design provisions for URM address failure in flexural tension, in combined flexural and axial compression and in shear. Flexural tensile stresses are computed elastically, using an uncracked section, and are compared with allowable flexural tensile stresses, which are observed strengths divided by a factor of safety of about 2.5. Allowable flexural tensile stresses for in-plane bending are 0. Flexural and axial compressive stresses are also computed elastically, and are compared with allowable values using a so-called unity equation. Axial stresses divided by allowable axial stresses, plus flexural compressive stresses divided by allowable flexural compressive stresses, must not exceed unity. Allowable axial stresses are one quarter the specified compressive strength of the masonry, reduced for slenderness effects. Allowable flexural compressive stresses are one third the specified compressive strength of the masonry. Shear stresses are computed elastically, assuming a parabolic distribution of shear stress based on beam theory. Allowable stresses in shear are computed corresponding to different possible failure modes (diagonal tension, crushing of compression diagonal, sliding on bed joints). The factor of safety for each failure mode is at least 3.

Allowable-stress design provisions for reinforced masonry address failure in combined flexural and axial compression, and in shear. Stresses in masonry and reinforcement are computed using a cracked transformed section. Allowable tensile stresses in deformed reinforcement are the specified yield strength divided by a safety factor of 2.5. Allowable flexural compressive stresses are one third the specified compressive strength of the masonry. Allowable capacities of sections under combinations of flexure and axial force can be expressed using an allowable-stress moment–axial force interaction diagram, which also has a maximum allowable axial capacity as governed by compressive axial stress. Shear stresses are computed elastically, assuming a uniform distribution of shear stress. Allowable shear stresses in masonry are computed corresponding to different possible failure modes (diagonal tension, crushing of compression diagonal, sliding on bed joints). If these allowable stresses are exceeded, all shear must be resisted by shear reinforcement, and shear stresses in masonry must not exceed a second, higher set of allowable values. The factor of safety for shear is at least 3.

17.5.3 Seismic Design Provisions for Masonry in the 2000 IBC

In contrast to wind loads, which are applied forces, earthquake loading derives fundamentally from imposed ground displacements. Although inertial forces are applied to a building as a result, these inertial forces depend on the mass, stiffness and strength of the building as well as the characteristics of the ground motion itself. This is true as well for masonry buildings. In this section, the seismic design provisions of the 2000 IBC are summarized as they apply to masonry elements.

Modern model codes in the United States address the design of masonry for earthquake loads by first prescribing seismic design loads in terms of the building's geographic location, its function and its underlying soil characteristics. These three characteristics together determine the building's "seismic

design category." Seismic Design Category A corresponds to a low level of ground shaking, typical use and typical underlying soil. Increasing levels of ground shaking, an essential facility and unknown or undesirable soil types correspond to higher seismic design categories, with Seismic Design Category F being the highest. In addition to being designed for the seismic forces corresponding to their seismic design category, masonry buildings must comply with four types of prescriptive requirements, whose severity increases as the building's seismic design category increases from A to F:

1. Seismic-related restrictions on materials
2. Seismic-related restrictions on design methods
3. Seismic-related requirements for connectors
4. Seismic-related requirements for locations and minimum percentages of reinforcement

The prescriptive requirements are incremental; for example, a building in Seismic Design Category C must also comply with prescriptive requirements for buildings in Seismic Design Categories A and B.

17.5.3.1 Determination of Seismic Design Forces

For structural systems of masonry, as for other materials, seismic design forces are determined based on the structure's location, underlying soil type, degree of structural redundancy and the system's expected inelastic deformation capacity. The last characteristic is described indirectly in terms of shear wall types: "ordinary plain," "ordinary reinforced," "detailed plain," "intermediate reinforced" and "special reinforced." As listed, these types are considered to have increasing inelastic deformation capacity, and a correspondingly increasing response modification coefficient R is applied to the structural systems comprising them. Higher values of R correspond, in turn, to lower seismic design forces.

17.5.3.2 Seismic-Related Restrictions on Materials

In Seismic Design Categories A through C, no additional seismic-related restrictions apply beyond those related to design in general. In Seismic Design Categories D and E, Type N mortar and masonry cement are prohibited because of their relatively low tensile bond strength.

17.5.3.3 Seismic-Related Restrictions on Design Methods

In Seismic Design Category A, masonry structural systems can be designed by strength design, allowable-stress design or empirical design. They are permitted to be designed including the flexural tensile strength of masonry.

In Seismic Design Category B, elements that are part of the lateral force-resisting system can be designed by strength design or allowable-stress design only, but not by empirical design. Elements not part of the lateral force-resisting system, however, can still be designed by empirical design. No additional seismic-related restrictions on design methods apply in Seismic Design Category C.

In Seismic Design Category D, elements that are part of the lateral force-resisting system must be designed as reinforced, by either strength design or allowable-stress design. No additional seismic-related restrictions on design methods apply in Seismic Design Categories E and F.

17.5.3.4 Seismic-Related Requirements for Connectors

In Seismic Design Category A, masonry walls are required to be anchored to the roofs and floors that support them laterally. This provision is not intended to require a mechanical connection. No additional seismic-related restrictions on connection forces apply in Seismic Design Category B.

In Seismic Design Category C, connectors for masonry partition walls must be designed to accommodate story drift. Horizontal elements and masonry shear walls must be connected by connectors capable of resisting the forces between those elements, and minimum connector capacity and maximum spacing are also specified. No additional seismic-related requirements for connectors apply in Seismic Design Categories D and higher.

17.5.3.5 Seismic-Related Requirements for Locations and Minimum Percentages of Reinforcement

In Seismic Design Categories A and B, there are no seismic-related requirements for locations and minimum percentages of reinforcement. In Seismic Design Category C, masonry partition walls must have reinforcement meeting requirements for minimum percentage and maximum spacing. The reinforcement is not required to be placed parallel to the direction in which the element spans. Masonry walls must have reinforcement with an area of at least 0.2 in.² (129 mm²) at corners, close to each side of openings, movement joints and ends of walls, and spaced no farther than 10 ft (3 m) apart. In Seismic Design Category D, masonry walls that are part of the lateral force-resisting system must have uniformly distributed reinforcement in the horizontal and vertical directions, with a minimum percentage of 0.0007 in each direction and a minimum summation of 0.002 (both directions). Maximum spacing in either direction is 48 in. (1.22 m). Closer maximum spacing requirements apply for stack bond masonry. Masonry shear walls have additional requirements for minimum vertical reinforcement and hooking of horizontal shear reinforcement. In Seismic Design Categories E and F, stack-bonded masonry partition walls have minimum horizontal reinforcement requirements. Stack-bonded masonry walls that are part of the lateral force-resisting system have additional requirements for spacing and percentage of horizontal reinforcement. Masonry shear walls must be “special reinforced.”

17.5.4 Future of Design Codes for Masonry in the United States

The next decade is likely to witness increased harmonization of U.S. model codes, and increasing direct reference to the MSJC Code and Specification. In the MSJC design provisions, the Specification is likely to be augmented by a Code chapter dealing with construction requirements.

17.6 Analysis Approaches for Modern U.S. Masonry

Structural analysis techniques for masonry are discussed in this section. To avoid repetition with other chapters, emphasis is placed on analytical considerations that are often different for masonry, than for other common structural systems. General considerations related to the analysis of reinforced concrete and masonry structures are given in other references (ACI SP-127, 1991), and are not repeated here. Similarly, the analysis of masonry structures for gravity loads involves techniques that are routine. In the remainder of this section, analysis of masonry for lateral loads is emphasized.

Analysis of masonry structures for lateral loads, alone or in combination with gravity loads, must address the following issues:

1. Analytical approaches (hand vs. computer)
2. Elastic vs. inelastic behavior
3. Selection of earthquake input
4. Two-dimensional vs. three-dimensional behavior
5. Modeling of gravity loads
6. Modeling of materials
7. Modeling of structural elements
8. Flexural cracking
9. Soil-foundation flexibility
10. Floor diaphragm flexibility

Each of these issues is briefly discussed in this section. Additional details are presented in Klingner et al. (1990) and Jalil et al. (1993). Additional information on analysis of masonry buildings, including diaphragm flexibility, is presented in Tena-Colunga and Abrams (1996).

17.6.1 Overall Analytical Approach

Hand-type as well as computer-type analysis approaches are available. Hand-type approaches usually emphasize the plan distribution of shear forces in wall elements. These can be quite simple (shears in each plan direction can be assigned to wall elements in proportion to their plan lengths, and torsional effects are neglected). They can also be more complex (pier stiffnesses are computed including the effects of shearing and flexural deformations, and torsional effects are included). For buildings with regular plan configurations, even the simplest hand methods are adequate for predicting the distribution of shear among wall elements, and typically show errors of 10% or less. However, hand methods are not sufficiently accurate for computing wall moments; critical design moments can be overestimated by factors as high as 3. This applies to all hand methods, complex as well as simple.

Given the adequacy of the most simple hand methods for estimating wall design shears, and the frequent inadequacy of all hand methods for estimating wall moments, there seems to be little justification, in choosing among hand methods, for selecting any but the simplest. If more precision is required, computer-type analyses approaches should be used. Many microcomputer-based structural analysis programs are available. Some of these are intended for building-type structures only, while others are more general. Different analytical assumptions related to computer-type analyses of masonry structures are discussed in the following subsections.

17.6.2 Elastic vs. Inelastic Behavior

When flexural yielding or shear degradation of significant portions of a masonry structure is anticipated, inelastic analyses should be considered. However, in many cases, masonry structures can be expected to respond in the cracked elastic regime, even under extreme lateral loads.

Many masonry buildings with regular plan configurations, and with plan wall areas (in each principal plan direction) of at least several percentages of their plan area, will probably crack in flexure but not yield, and will probably not experience serious shear cracking. Therefore, the behavior of such buildings can be predicted using elastic analyses, provided that the effects of flexural cracking are accounted for by appropriately reducing the element stiffnesses. Because these stiffnesses do not change further during the analysis, the structure is still linear elastic.

17.6.3 Selection of Earthquake Input

Because structural response is generally expected to be linear elastic (with appropriate consideration for the effects of flexural cracking), linear elastic response spectra are sufficient.

17.6.4 Two-Dimensional vs. Three-Dimensional Analysis of Linear Elastic Structures

In a two-dimensional analysis, a building is modeled as an assemblage of parallel planar frames, free to displace laterally in their own planes only, subject to the requirement of lateral displacements compatibility between all frames at each floor level. Buildings so modeled cannot exhibit torsional response in plan.

In the “pseudo three-dimensional” approach, a building is modeled as an assemblage of planar frames, each of which is free to displace parallel and perpendicular to its own plane. The frames exhibit lateral displacement compatibility at each floor level. In this kind of modeling, however, compatibility of vertical displacements is not required of common columns in intersecting frames.

In a true three-dimensional approach, the building is modeled as a single three-dimensional frame, and appropriate displacement compatibilities are maintained among all frame elements. Because micro-computer-based programs employing a true three-dimensional approach are widely available, there is little justification for using a less sophisticated level of analysis.

17.6.5 Modeling of Gravity Loads

Gravity loads should be based on self-weight, plus an estimate of the probable live load. A uniform distribution of mass should normally be assumed over each floor, except for the masses from the exterior walls, which should normally be included discretely.

17.6.6 Modeling of Material Properties

Material properties should be estimated based on test results. A Poisson's ratio of 0.35 can be used for masonry. This value is greater than that corresponding to compressive tests of masonry prisms. However, it gives a realistic value of the shear modulus, which is very important for the correct estimation of lateral drifts in low-rise masonry wall buildings.

17.6.7 Modeling of Structural Elements

Masonry wall buildings are normally modeled using beams and panels (shell elements), with occasional columns. In-plane modeling of floor diaphragms is discussed later. Modeling of walls, and of the out-of-plane behavior of floor diaphragms, is discussed here.

17.6.7.1 Modeling of Walls

The most crucial point in modeling of walls is to include the walls in the structural model. Masonry buildings are occasionally modeled as frame-type structures composed only of the frame elements, completely neglecting the influence of the masonry. This "frame-only" approach, though often believed to be conservative, is in fact unconservative and erroneous, for the following reasons:

- It greatly increases the building's calculated period of vibration, thereby decreasing (usually) its calculated seismic inertia forces.
- It gives an incorrect estimate of the internal distribution of shears among wall elements, and of the building's plan center of rigidity.
- It gives significant errors in calculating the lateral resistance of the building.

Buildings with essentially unperforated shear walls can usually be modeled adequately considering the walls as solid panels. This approach, however, is inadequate for the design and analysis of masonry buildings having structural walls with large openings. For such buildings, two alternatives are available:

- The walls can be modeled with solid panels having equivalent axial, shear and flexural stiffnesses. These equivalent stiffnesses should be determined by separate finite element modeling of the original panel.
- The building can be modeled using finite elements with appropriately placed openings.

17.6.7.2 Modeling of Beams

The effective widths of cast-in-place reinforced concrete slabs acting as coupling elements between walls have been modeled successfully as 4 times the slab thickness on each side when the slab acted as part of a solid panel, and as 3 times the thickness of the coupled walls for a coupling slab without a supporting beam. As a rule of thumb, the flexural inertia of T and L beams can be approximated as 2.0 and 1.5 times the inertia of the rectangular web respectively. Torsional stiffness can be evaluated as described in Section 13.7.5 of ACI 318-02 (2002). Effective shear areas of beams should be computed using the web area only.

17.6.8 Flexural Cracking of Walls

Whenever analyses of masonry buildings indicate flexural cracking, the analytical model should be modified to take this into account, as explained in the following subsections.

17.6.8.1 Flexural Cracking Criterion

The cracking moment for a wall should be determined by multiplying the modulus of rupture of the wall under in-plane flexure, by the section modulus of the wall. If experimentally determined values of the modulus of rupture are not available, the modulus of rupture can conservatively be taken as the allowable tensile bond stress, normal to the bed joint, for the corresponding combination of masonry materials.

17.6.8.2 Consequences of Flexural Cracking of Walls

Flexural cracking reduces the wall's stiffness from that of the uncracked transformed section to that of the cracked transformed section. For reinforced concrete beams, stiffness reduction factors of 2 to 3 are typical. For walls, however, flexural cracking reduces the stiffness by factors of 5 or more, depending on the cross-sectional shape of the wall and the longitudinal reinforcement ratio.

In some cases, this stiffness reduction changed the distribution of shears and moments in the complete structure. In one building in the cited study (Klingner et al., 1990), consideration of reduced flexural stiffness due to flexural cracking decreased the computed maximum moments by 20%. These computed maxima correlated well with observed damage.

17.6.9 Soil-Foundation Flexibility

When soil and foundation flexibility are included in the analytical model of a low-rise masonry building, two things happen:

- Regardless of how the building's foundation is modeled, the building's periods of vibration significantly increase, and lateral force levels can change significantly.
- If the building's foundation is considered flexible, the resulting increase in support flexibility at the bases of wall elements causes their base moments to decrease substantially.

For low-rise, stiff buildings, these effects can be significant. For example, a four-story masonry wall building showed an increase in fundamental period from about 0.13 sec to about 0.35 sec when soil-foundation flexibilities were included in the model, assuming large soil strains. Moments in the critical wall were reduced by about 30% (Klingner et al., 1990). For more flexible buildings, however (having masonry veneer over a structural frame), these effects were not found to be significant. It is recommended that soil-foundation flexibility be included if a building's calculated fundamental period (assuming a rigid base) is 0.15 sec or less, and if the underlying soil is soft.

Foundation flexibility can be addressed by modeling the foundations as part of the lowest story of panels in each building, and by using equivalent soil springs, placed under the building. Depending on the characteristics of a building's foundation, it may be appropriate to idealize the underlying soil flexibility by a single spring under a stiff mat-type foundation, or by a number of separate springs, each underlying an individual strip footing.

Two procedures can be used to calculate the equivalent spring stiffness:

- Foundations are idealized as circular foundations with equivalent plan areas and inertias.
- Explicit stiffnesses are obtained for strip footings and foundations of arbitrary plan shape.

The second procedure is more sound theoretically. Details of the calculation of soil-foundation stiffness are given in Klingner et al. (1990).

17.6.10 In-Plane Floor Diaphragm Flexibility

Structures in general are often modeled using special-purpose analysis programs that assume that floor diaphragms are rigid in their own planes. This assumption is reasonable for many framed structures, because the in-plane stiffness of their floor diaphragms is much greater than the lateral stiffness of their framing systems. For many masonry wall structures, it is also reasonable (Jalil et al., 1993). However, many masonry wall structures have floor slabs with features that could increase the effects of in-plane

floor flexibility: (1) small openings in critical sections of the floor slab; (2) rectangular floor plans with large aspect ratios in plan; or (3) variations of in-plane rigidity within the slab.

In general, for low-rise masonry buildings considered in the cited study (Klingner et al., 1990), only slight differences were observed between results obtained using otherwise identical analytical models with and without floor diaphragm flexibility. Results did not change by much, because of the following characteristics shared by all the buildings considered in this study:

- Their masses were distributed uniformly in plan.
- Their floor slabs were cast in place, and were stiff in their own planes.
- Their floor slabs consisted mainly of solid areas with small openings.
- The solid areas of their floor slabs were connected so that the lateral rigidities of the overall buildings were distributed symmetrically in plan.

In-plane flexibility of roof diaphragms is very important in the seismic response of warehouse-type buildings. Walls oriented perpendicular to the direction of ground motion are affected most significantly not by the shaking of the ground itself, but rather by the response of the roof diaphragm to which they are connected.

17.6.11 Explicit Inelastic Design and Analysis of Masonry Structures Subjected to Extreme Lateral Loads

In the above discussion of issues related to modeling of masonry structures for lateral loads, it was assumed that response would be essentially elastic (with appropriate consideration of flexural cracking). If inelastic response of a masonry structure is anticipated, a general design and analysis approach involving the following steps is proposed (Leiva and Klingner, 1994):

1. Select a stable collapse mechanism for the wall, with reasonable inelastic deformation demand in hinging regions. Using that collapse mechanism, predict the lateral load capacity of the wall in terms of its flexural capacity in hinging regions.
2. Using general plane-section theory to describe the flexural behavior of reinforced masonry elements, provide sufficient flexural capacity and flexural ductility in hinging regions.
3. Using a capacity design philosophy, provide wall elements with sufficient shear capacity to resist the shears consistent with the development of the intended collapse mechanism. Calculate the shear capacity of masonry elements, and the shear transfer capacity between adjacent elements, using current strength-design provisions.
4. Using reinforcing details from current strength-design provisions, detail the wall reinforcement to develop the necessary strength and inelastic deformation capacity.

This approach was used for the design of multi-story masonry specimens tested under the TCCMAR program (Leiva and Klingner, 1994; Seible et al., 1994a, 1994b). It has been found to lead to masonry walls with predictable strength and stable load-deflection behavior under many cycles of reversed cyclic load, and it is recommended for design of reinforced masonry walls in seismic zones.

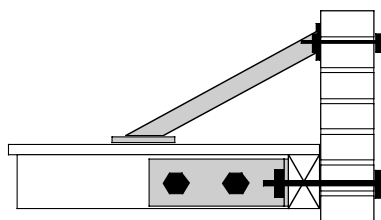


FIGURE 17.18 Schematic of Division 88 masonry retrofitting techniques for unreinforced masonry.

17.6.12 Inelastic Finite Element Analysis of Masonry Structures

A number of finite element models have been developed in recent years to evaluate the inelastic behavior of masonry. Even though such analysis may require considerable computing resources and can be difficult to perform, it is sometimes desirable for a number of reasons. The inelastic behavior of a masonry structure can be very complicated. In the absence of experimental data, finite element analysis is the most viable method to quantify the ductility and post-peak behavior of masonry structures. In addition, the load—deformation relation of a masonry component obtained from a finite element analysis can be used to calibrate structural component models, which can in turn be used for the push-over analysis or dynamic analysis of large structural systems. Furthermore, in the absence of precise material information, finite element analysis can be used to study the inelastic behavior of masonry structures in a qualitative manner to identify possible failure mechanisms and to provide guidance for the repair and retrofit of existing structures.

Inelastic finite element analysis of masonry structures is described in detail in Shing and Klingner (1997). It is not required for design, and is not discussed further here.

17.7 Seismic Retrofitting of Historical Masonry in the United States

The preceding sections of this chapter have dealt primarily with the seismic performance of masonry built under the reinforced masonry provisions that were introduced in the western United States as part of the reaction to the 1933 Long Beach earthquake. Such masonry generally behaves well. URM, in contrast, often collapses or experiences heavy damage. This is true whether the masonry was built in the western United States prior to 1933, or in other places either before or after 1933. As a result of this observed poor behavior, recent decades have witnessed significant interest in the seismic retrofitting of historical masonry in the United States. These retrofitting efforts are briefly reviewed in this section.

17.7.1 Observed Seismic Performance of Historical U.S. Masonry

As noted earlier in this chapter, URM buildings have performed poorly in many U.S. earthquakes. The 1933 Long Beach, CA, earthquake severely damaged many URM buildings, particularly schools. One consequence of this damage was the passage of California's Field Act, which prohibited the use of masonry (as it was then used) in all public buildings in the state. When masonry construction was revived in California during the middle 1940s, it was required to comply with the newly developed UBC provisions. These provisions, based on the reinforced concrete design practice of the time, required that minimum seismic lateral forces be considered in the design of masonry buildings, that tensile stresses in masonry be resisted by reinforcement and that all masonry have at least a minimum percentage of horizontal and vertical reinforcement.

17.7.2 Laboratory Performance of Historical U.S. Masonry

Although laboratory testing of historical U.S. masonry is difficult, some testing has been carried out on masonry specimens cut from existing structures. Much more extensive testing has been carried out on reduced-scale replicas of URM construction. Some is typical of the United States; some is typical of that found in other countries. That testing includes the following:

- Benedetti et al. (1998): Twenty-four, simple, two-story, half-scale, URM buildings were tested to varying degrees of damage, repaired and strengthened, and tested again.
- Tomazevic and Weiss (1994): Two, three-story, reduced-scale, plain and reinforced masonry buildings were tested. The efficacy of reinforcement was confirmed.

- Costley and Abrams (1996): Two reduced-scale brick masonry buildings were subjected to shaking-table testing. Observed and predicted behaviors were compared, and also used to make recommendations for the use of FEMA retrofitting guidelines.

17.7.3 Basic Principles of Masonry Retrofitting

Over the past 15 years, efforts have focused on the seismic response and retrofitting of existing URM buildings. The goals of seismic retrofitting are to correct deficiencies in:

- Overall structural concept
- Behavior of structural elements
- Behavior of nonstructural elements

The most basic elements of seismic retrofitting involve bracing parapets to roofs, and connecting floor diaphragms to walls using through anchors (mechanical, grouted or adhesive).

17.7.4 History of URM Retrofitting in the Los Angeles Area

17.7.4.1 Division 88

In 1949 the city of Los Angeles passed the Parapet Correction Ordinance, which required that URM or concrete parapets above exits, and parapets above public access, be retrofitted to minimize hazards. As a result, such parapets were either laterally braced or removed. Consequently, many URM buildings withstood the 1971 San Fernando earthquake better than previous earthquakes (Lew et al., 1971).

Following the February 1971 San Fernando earthquake, the city of Los Angeles, the Federal Government and the Structural Engineers Association of Southern California joined forces in a 10-year investigation. As a result of this investigation, Los Angeles adopted an ordinance known as Division 68 on February 13, 1981. Division 68 required seismic retrofitting of all URM bearing-wall buildings that were built, under construction or for which a permit had been issued prior to October 6, 1933. The ordinance did not include one- or two-family dwellings nor detached apartment houses comprising fewer than five dwelling units and used solely for residential purposes.

The 1985 edition of the Los Angeles Building Code revised Division 68 into Division 88, and included provisions for the testing and strengthening of mortar joints to meet minimum values for shear strength. Furthermore, Division 88 required that URM be positively anchored to floor and roof diaphragms with anchors spaced not more than 6 ft apart. There were also parapet height limitations, based on wall thickness. Continuous inspection was also required on the retrofitting work. These retrofitting measures are shown schematically in Figure 17.18.

Alternatives to these specific provisions were also possible. Division 88 was renamed Chapter 88 in the 1988 City of Los Angeles Code. In addition to masonry bearing walls, veneer walls constructed before October 6, 1933, were included. This edition also added Section 8811 (“Design Check — Compatibility of Roof Diaphragm Stiffness to Unreinforced Masonry Wall Out-of-Plane Stability”).

At the time of the Northridge earthquake, it is believed that essentially all URM buildings in the city of Los Angeles had their parapets either removed or laterally braced. According to unconfirmed reports about 80% of URM buildings in the city of Los Angeles had been retrofitted to comply with the provisions of Division 88; however, the percentage was reported to be considerably lower in other cities in the Los Angeles area.

17.7.4.2 Other Retrofitting Guidelines

NEHRP, in conjunction with FEMA, has produced a series of documents dealing with the seismic evaluation and retrofitting of structures, including masonry structures:

- FEMA 172 (1992), *Handbook of Techniques for the Seismic Rehabilitation of Existing Buildings*, provides a general list of retrofitting techniques.

- FEMA 178 (1992) presents an overall method for engineers to identify buildings or building components that present unacceptable risks in case of an earthquake.
- FEMA 273 (1997) and FEMA 274 (1997), NEHRP Guidelines and Commentary for the seismic rehabilitation of buildings, provide code-type procedures for the assessment, evaluation, analysis and rehabilitation of existing building structures.
- FEMA 306 (1998), Evaluation of Earthquake-Damaged Concrete and Masonry Wall Buildings: Basic Procedures Manual, provides guidance on evaluation of damage and on performance analysis and includes newly formulated Component Damage Classification Guides, and Test and Investigation Guides. The procedures characterize the observed damage caused by an earthquake in terms of the loss in building performance capability.
- FEMA 307 (1998), Evaluation of Earthquake-Damaged Concrete and Masonry Wall Buildings: Technical Resources, contains supplemental information, including results from a theoretical analysis of the effects of prior damage on single-degree-of-freedom mathematical models, additional background information on the Component Damage Classification Guides and an example of the application of the basic procedures.
- FEMA 308 (1998), Repair of Earthquake-Damaged Concrete and Masonry Wall Buildings, discusses the technical and policy issues pertaining to the repair of earthquake-damaged buildings and includes guidance on the specification of individual repair techniques and newly formulated Repair Guides.
- FEMA 356 (2000), *Prestandard and Commentary for the Seismic Rehabilitation of Buildings*, is an attempt to encourage the use of FEMA 273 and to put the guidelines of that document into mandatory language.

17.8 Future Challenges

This chapter has presented an overview of current issues in the design of masonry for earthquake loads, and of the historical process by which these issues have developed. It would not be complete without at least a brief mention of the challenges facing the masonry technical community in this area.

17.8.1 Performance-Based Seismic Design of Masonry Structures

Across the entire spectrum of construction materials, increased attention has been focused on “performance-based” seismic design, which can be defined as design whose objective is a structure that can satisfy different performance objectives under increasing levels of probable seismic excitation. For example, a structure might be designed to remain operational under a design earthquake with a relatively short recurrence interval; to be capable of immediate occupancy under a design earthquake with a longer recurrence interval; to ensure life safety under a design earthquake with a still longer recurrence interval; and to not collapse under a design earthquake with a long recurrence interval.

This design approach, accepted qualitatively since the 1970s, has been adopted quantitatively in recent documents related to seismic rehabilitation (FEMA 356, 2000), and will probably be incorporated into future seismic design provisions for new structures as well. Because masonry structures are inherently composed of walls rather than frames, they tend to be laterally stiff, which is usually a useful characteristic in meeting performance objectives for seismic response.

17.8.2 Increased Consistency of Masonry Design Provisions

The 2003 IBC will reference the 2002 MSJC Code and Commentary essentially in its entirety. Other model codes will probably do the same. As a result, future development of seismic design provisions for masonry structures will take place almost exclusively within the MSJC, rather than in a number of different technical forums. This is expected to lead to increased rationality of design provisions, increased consistency among designs produced by different design methods (strength vs. allowable-stress design, for example) and

possibly also to simplification of design provisions. As an additional benefit, the emergence of a single set of ANSI-consensus design provisions for masonry is expected to encourage the production of computer-based tools for the analysis and design of masonry structures using these provisions.

17.9 Design Example: One-Story Commercial Building

17.9.1 Introduction

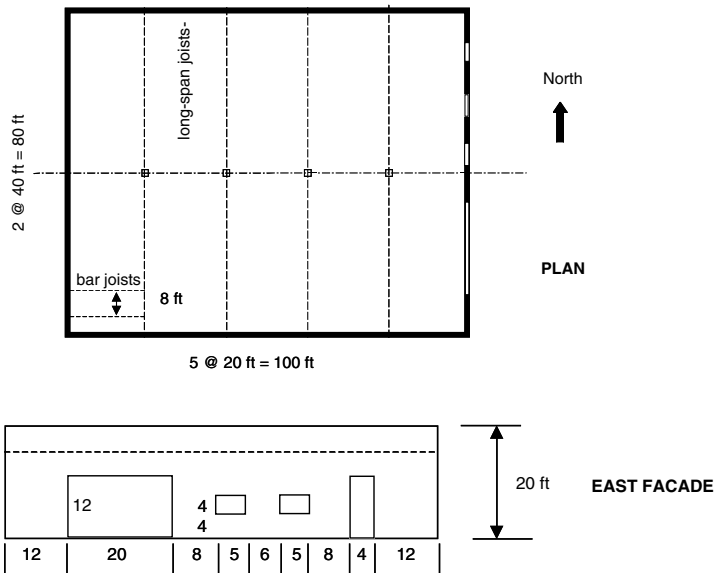
This design example is a one-story commercial building (a warehouse), located in the outskirts of Los Angeles, CA, in a seismic region with a basic wind speed of 90 mi/h. This combined example problem is carried out using the strength-design approach of the 2002 MSJC Code; loads are obtained from the 2000 IBC.

17.9.2 Design Steps

1. Choose design criteria:
 - Propose plan, elevation, materials, $f'm'$
 - Calculate D, L, W, E loads
 - Propose structural systems for gravity and lateral loads
2. Design walls for gravity plus out-of-plane loads
3. Design pilasters and columns
4. Design beams and lintels
5. Conduct lateral force analysis, design floor diaphragms
6. Design piers for combined shear, flexure and axial loads
7. Design and detail connections
8. Design roof framing (not done here — use joist catalog)
9. Design interior columns (not done here — use structural tubes)

17.9.2.1 Choose Design Criteria

The plan and elevation of the building follow.

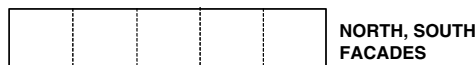


Design for Water-Penetration Resistance

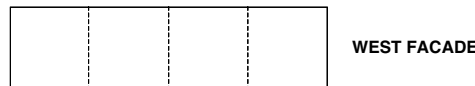
A single-wythe barrier wall will be used. The wall will permit the passage of some water.

Locate Control Joints

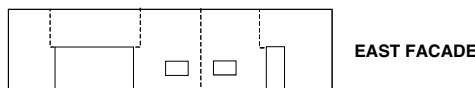
North, South facades — space at 20 ft



West facade — space at 20 ft



East facade — space as shown:



Design for Fire

Use and occupancy: Group F, Division 1 (moderate hazard)

Use Type I or Type II construction (noncombustible material)

No area or height restrictions

2- or 3-h rating required

Must meet separation requirements of Table 602 of the 2000 IBC

Use grouted 8-in. concrete masonry units for bearing walls

Specify Materials

8-in. concrete masonry units (ASTM C90), fully grouted for bearing walls, ungrouted or partially grouted for nonbearing walls

Type S portland cement-lime mortar, specified by proportion (ASTM C270)

$f_m' = 1500 \text{ lb/in.}^2$ This is satisfied using units with a net-area compressive strength of 1900 lb/in.², and

Type S portland cement-lime mortar

Deformed reinforcement meeting ASTM A615, Gr. 60

Roof of long-span joists, supporting bar joists spaced at 8 ft

Corrugated decking with 3-in. lightweight flowable fill

Roof supported by structural steel tube columns at midspan

Calculate Design Roof Load due to Gravity

$$D = 60 \text{ lb/ft}^2$$

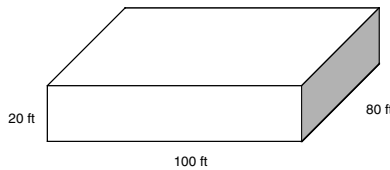
$$L = 20 \text{ lb/ft}^2 \text{ for tributary area up to } 200 \text{ ft}^2$$

$$L = 12 \text{ lb/ft}^2 \text{ for tributary areas greater than } 600 \text{ ft}^2$$

Linear interpolation between these two limits (2000 IBC, Section 1607.11.2)

Calculate Design Wind Load

Calculate Design Base Shear due To Wind



The critical direction for wind will be NS, because the area is greater on the north and south sides, and the area of shear walls is less in the NS direction:

1. Determine the *basic wind speed* V and *wind directionality factor* K_d in accordance with Section 6.5.4 of ASCE 7-98.

The basic wind speed for this area is 90 mi/h (ASCE 7-98, Figure 6-1). K_d is 0.85 (ASCE 7-98, Table 6-6, buildings)

2. Determine the *importance factor* I in accordance with Section 6.5.5 of ASCE 7-98.

Assume that the importance factor is 1.0.

3. Determine the exposure category or exposure categories and velocity pressure exposure coefficient K_z or K_h , as applicable, in accordance with Section 6.5.6 of ASCE 7-98.

Assume Exposure B (urban and suburban areas). The velocity pressure exposure coefficients K_h and K_z are determined from ASCE 7-98, Table 6-5, for Exposure B and Case 2 (all main wind force-resisting systems in other structures).

Height above ground level, z	K_h, K_z
1–15	0.57
20	0.62

4. Determine a *topographic factor* K_{zt} in accordance with Section 6.5.7 of ASCE 7-98.

Because the structure is not located on a hill, ridge or escarpment, $K_{zt} = 1.0$.

5. Determine a *gust effect factor* G or G_p as applicable, in accordance with Section 6.5.8 of ASCE 7-98.

Assume a rigid structure; G is 0.85.

6. Determine an *enclosure classification* in accordance with Section 6.5.9 of ASCE 7-98.

Assume that the building is enclosed.

7. Determine an *internal pressure coefficient* GC_{pi} in accordance with Section 6.5.11.1 of ASCE 7-98.

GC_{pi} is ± 0.18 .

8. Determine the *external pressure coefficients* C_p or GC_{pe} or force coefficients cf , as applicable, in accordance with Section 6.5.11.2 or Section 6.5.11.3, respectively.

The external pressure coefficients GC_p for main wind force-resisting systems are given in Figure 6-3 and Figure 6-8 of ASCE 7-98.

From the plan views in Figure 6-3a, the windward pressure is $q_z GC_p$. The leeward pressure is $q_h GC_p$. The difference between q_z and q_h is that the former varies as a function of the height above ground level, while the latter is uniform over the building height, and is evaluated using the height of the building.

For wind blowing in the NS direction, $L/B = 0.8$. From Figure 6-3b, on the windward side of the building, C_p is 0.8. On the leeward side of the building, it is -0.5.

9. Determine the *velocity pressure* q_z or q_h , as applicable, in accordance with Section 6.5.10.

The velocity pressure is:

$$q_z = 0.00256 K_z K_{zt} K_d V^2 I$$

$$I = 1.0$$

$$K_d = 0.85$$

$$V = 90 \text{ miles/hr}$$

$$K_{zt} = 1.0$$

$$q_z = 17.63 K_z \text{ lb/ft}^2$$

10. Determine the design wind load P or F in accordance with Section 6.5.12 and Section 6.5.13, as applicable.

For main force-resisting systems:

$$P = q G C_p - q_i (G C_{pi})$$

where:

- q = qz for windward walls evaluated at height z above the ground
- = qh for leeward walls, side walls and roofs, evaluated at height h
- q_i = qh for windward walls, side walls, leeward walls and roofs of enclosed buildings and for negative internal pressure evaluation in partially enclosed buildings
- = qz for positive internal pressure evaluation in partially enclosed buildings where height z is defined as the level of the highest opening in the building that could affect the positive internal pressure. For buildings sited in wind-borne debris regions, glazing in the lower 60 ft that is not impact-resistant or protected with an impact-resistant covering, the glazing shall be treated as an opening in accordance with Section 6.5.9.3. For positive internal pressure evaluation, q_i may conservatively be evaluated at height h ($q_i = qh$)

G = gust effect factor from Section 6.5.8

C_p = external pressure coefficient from Figure 6-3 or Table 6-8

C_{pi} = internal pressure coefficient from Table 6-7

Because the building is enclosed, the internal pressures on the windward and leeward sides are of equal magnitude and opposite direction, will produce zero net base shear and therefore need not be considered.

On the windward side of the building:

$$q_z = 0.00256 K_z K_{zt} K_d V^2 I$$

where:

K_d = wind directionality factor defined in Section 6.5.4.4

K_z = velocity pressure exposure coefficient defined in Section 6.5.6.4

K_{zt} = topographic factor defined in Section 6.5.7.2

Building Floor	Height above Ground	Tributary Area	Windward Side						Leeward Side					
			K_z	qz	G	C_p	p	Force	Kh	qh	G	C_p	p	Force
Roof	16.67	1166.5	0.58	10.23	0.85	0.8	6.95	8.11	0.58	10.23	0.85	0.5	4.35	5.07
Ground	0	833.5	0.57	10.05	0.85	0.8	6.83	5.70	0.58	10.23	0.85	0.5	4.35	3.62
Total force								13.81						8.69

The design base shear due to wind load is therefore 13.81 kips plus 8.69 kips, for a total of 22.5 kips.

Calculate Design Pressure on Wall Elements due To Wind

The critical region will be at the parapet, near a corner:

- Determine the *basic wind speed* V and *wind directionality factor* K_d in accordance with Section 6.5.4 of ASCE 7-98.

The basic wind speed for this area is 90 mi/h (ASCE 7-98, Figure 6-1). K_d is 0.85 (ASCE 7-98, Table 6-6, buildings).

- Determine the *importance factor* I in accordance with Section 6.5.5 of ASCE 7-98.

Assume that the importance factor is 1.0.

- Determine the exposure category or exposure categories and velocity pressure exposure coefficient K_z or K_h , as applicable, in accordance with Section 6.5.6 of ASCE 7-98.

Assume Exposure B (urban and suburban areas). The velocity pressure exposure coefficients K_h and K_z are determined from ASCE 7-98, Table 6-5, for Exposure B and Case 2 (all main wind force-resisting systems in other structures).

Height above ground level, z	K_h, K_z
1–15	0.57
20	0.62

- Determine a *topographic factor* K_{zt} in accordance with Section 6.5.7 of ASCE 7-98.

Because the structure is not located on a hill, ridge or escarpment, $K_{zt} = 1.0$.

- Determine a *gust effect factor* G or G_p , as applicable, in accordance with Section 6.5.8 of ASCE 7-98.

Assume a rigid structure; G is 0.85.

- Determine an *enclosure classification* in accordance with Section 6.5.9.

Assume that the building is enclosed.

- Determine an *internal pressure coefficient* GC_{pi} in accordance with Section 6.5.11.1 of ASCE 7-98.

GC_{pi} is ± 0.18 .

- Determine the *external pressure coefficients* C_p or GC_{pb} or *force coefficients* cf , as applicable, in accordance with Section 6.5.11.2 or 6.5.11.3, respectively.

The external pressure coefficients GC_p for components and cladding are given in Figure 6-8 of ASCE 7-98.

Assume a panel with an area of 10 ft². From Figure 6-8, a panel in Zone 5 has a positive pressure coefficient of 0.9, and a negative pressure coefficient of -1.8.

- Determine the *velocity pressure* q_z or q_h , as applicable, in accordance with Section 6.5.10 of ASCE 7-98.

The velocity pressure is:

$$q_z = 0.00256 K_z K_{zt} K_d V^2 I$$

$$I = 1.0$$

$$K_d = 0.85$$

$$V = 90 \text{ miles/hr}$$

$$K_{zt} = 1.0$$

$$q_z = 17.63 K_z lb/ft^2$$

10. Determine the *design wind load P or F* in accordance with Section 6.5.12 and Section 6.5.13 of ASCE 7-98, as applicable.

Since this is a building with $h \leq 60$ ft:

For components and cladding of low-rise buildings and buildings with $h \leq 60$ ft:

$$p = q_h \left[(GC_p) - (GC_{pi}) \right]$$

where:

qh = velocity pressure evaluated at mean roof height h using exposure defined in Section 6.5.6.3.1

GC_p = external pressure coefficients given in Figure 6-5 through Figure 6-7

GC_{pi} = internal pressure coefficients given in Table 6-7

First assume that the wind is blowing so that the element is on the windward wall:

$qh = qz$, evaluated at 16.67 ft

$q_i = qh$, evaluated at 16.67 ft

$GC_p = 0.9$ (Figure 6-8)

$GC_{pi} = \pm 0.18$ (Table 6-7)

The maximum inward pressure on the element will be produced when GC_{pi} acts inward (positive sign):

Maximum Inward Pressure (Windward Wall)							
Building Height, h	Height above Ground, z	Kz	qz	GC_p	$q_i = qh$	GC_{pi}	p design
16.67	16.67	0.58	10.23	0.9	10.23	-0.18	11.04

Next, assume that the wind is blowing so that the element is on the leeward wall:

$q = qh$, evaluated at 16.67 ft

$q_i = qh$, evaluated at 16.67 ft

$GC_p = -1.8$ (Figure 6-8)

$GC_{pi} = \pm 0.18$ (Table 6-7)

The maximum outward pressure on the element will be produced when GC_{pi} acts outward (negative sign):

Maximum Outward Pressure (Leeward Wall)							
Building Height, h	Height above Ground, z	Kz	qh	GC_p	$q_i = qh$	gc_{pi}	p design
16.67	16.67	0.58	10.23	-1.8	10.23	0.18	-20.25

Wall elements must therefore be designed for a pressure of 11.04 lb/ft² acting inward, and 20.25 lb/ft² acting outward.

Calculate Design Earthquake Load

Earthquake loads are calculated according to Section 1614 of the 2000 IBC, essentially the same as ASCE 7-98. Two procedures are prescribed: the general procedure of Section 1615.1, or the site-specific procedure of Section 1615.2. The general procedure is described here, because it is simpler, and is permitted in all but a few situations. The site-specific procedure is required only for cases involving a few unfavorable soil conditions such as liquefiable soils or thick deposits of soft clay.

Summary of Design Procedure

1. Determine the structure's *seismic use group* (related to nature of occupancy), and select the corresponding *seismic importance factor*, i.e., in accordance with Section 1616.2 and Table 1604.5.
2. Determine the *site class* (A through F) in accordance with Section 1615.1.2 and Table 1615.1.1.
3. Determine the ordinates of the maximum considered response acceleration for short periods, S_{MS} , and for a 1-sec period, S_{M1} , depending on the geographical location of the structure (Figure 1615), and adjusted for site-class effects, in accordance with Section 1615.1.2 (Equation 16-16 and Equation 16-17).
4. Determine the key ordinates of the design response spectrum for short periods, S_{DS} , and at 1 sec, S_{DI} , as two thirds the values determined in Step 3 above.
5. Determine the design response spectrum using the key ordinates from Step 4 and Section 1615.1.3 (Equation 16-20 and Equation 16-21).
6. Determine the structure's *seismic design category* (A through D) based on its seismic use group (Step 1), the key ordinate S_{DS} and the key ordinate S_{DI} , using Section 1616.3, Table 1616.3(1) and Table 1616.3(2).
7. Determine the required design approach for each seismic design category in accordance with Section 1616.6, including, for higher seismic design categories, the effects of plan structural irregularities (Table 1616.5.1) and vertical structural irregularities (Table 1616.5.2).
8. Determine the seismic load effect, E and E_m , for use in the load combinations of Section 1605, including the effects of redundancy (ρ) and system overstrength (Ω_0), in accordance with Section 1617.

Now carry out each step in more detail for this hypothetical site near Los Angeles.

Step 1: Determine the structure's *seismic use group* (related to nature of occupancy), and select the corresponding *seismic importance factor*, i.e., in accordance with Section 1616.2 and Table 1604.5.

In accordance with Section 1616.1 of the 2000 IBC:

- Seismic Use Group II structures are those whose failure would result in substantial public hazard, or so designated by the building official.
- Seismic Use Group III structures are those containing essential facilities required for postearthquake recovery, or so designated by the building official.
- Seismic Use Group I structures are those not assigned to Seismic Use Group II or III.

Step 2: Determine the *site class* (A through F) in accordance with Section 1615.1.2 and Table 1615.1.1.

In accordance with Table 1615.1.2 of the 2000 IBC, site classes are assigned as follows:

Table 1615.1.1 Site Class Definitions

Site Class	Soil Profile Name	Average Properties in Top 100 ft
A	Hard rock	Described in terms of soil shear wave velocity, standard penetration resistance and undrained shear strength
B	Rock	
C	Very dense soil and soft rock	
D	Stiff soil profile	
E	Soft soil profile	
E	—	Described in terms of plasticity index, moisture content and undrained shear strength
F	—	Described in terms of vulnerability to liquefaction or collapse, high organic content, very high plasticity or very high flexibility

Step 3: Determine the ordinates of the maximum considered response acceleration for short periods, S_{MS} , and for a 1-sec period, S_{M1} , depending on the geographical location of the structure (Figure 1615), and adjusted for site-class effects, in accordance with Section 1615.1.2 (Equation 16-16 and Equation 16-17).

Determine the maximum considered earthquake acceleration response in % g for short periods (Figure 1615(1)) and for 1-sec periods (Figure 1615(2)) as a function of geographical location. These maps correspond to accelerations with a 2% probability of exceedance within a 50-year period.

For our hypothetical area near Los Angeles, CA, for example, $SS = 1.66 \text{ g}$, and $S1 = 0.47 \text{ g}$.

For illustration, assume Soil Profile D (stiff soil profile). Then the acceleration-dependent site coefficient F_a is 1.0 (Table 1615.1.2(1)), and the velocity-dependent site coefficient F_v is 1.53 (interpolating in Table 1615.1.2(2)).

Then the maximum considered short-period response acceleration is:

$$S_{MS} = F_a \cdot S_S = 1.0 \cdot 1.66g = 1.66g$$

and the maximum considered 1-sec response acceleration is:

$$S_{M1} = F_v \cdot S_1 = 1.53 \cdot 0.47g = 0.72g$$

Step 4: Determine the key ordinates of the design response spectrum for short periods, S_{DS} , and at 1 sec, S_{D1} , as two thirds the values determined in Step 3 above.

The design response acceleration for short periods is:

$$S_{DS} = \frac{2}{3} \cdot S_{MS} = \frac{2}{3} \cdot 1.66g = 1.11g$$

and the design response acceleration for a 1-sec period is:

$$S_{D1} = \frac{2}{3} \cdot S_{M1} = \frac{2}{3} \cdot 0.72g = 0.48g$$

Step 5: Determine the design response spectrum using the key ordinates from Step 4 and Section 1615.1.3 (Equation 16-20 and Equation 16-21).

Define $T_0 \equiv 0.2S_{D1}/S_{DS}$ and $T_S \equiv S_{D1}/S_{DS}$. Then:

- For periods less than or equal to T_0 , the design spectral response acceleration Sa is given by Equation 16-20:

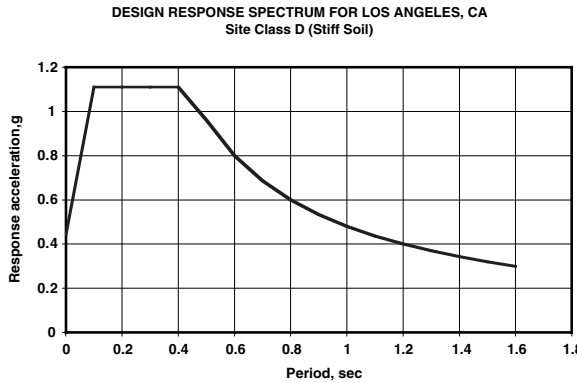
$$S_a = 0.6 \frac{S_{DS}}{T_0} T + 0.4S_{DS} \quad (16-20)$$

- For periods greater than T_0 and less than or equal to T_S , Sa is equal to S_{DS} .
- For periods greater than T_S , Sa is given by Equation 16-21:

$$S = \frac{S_{D1}}{T} \quad (16-21)$$

17-40 Earthquake Engineering: From Engineering Seismology to Performance-Based Engineering

The resulting design acceleration response spectrum is given below:



Step 6: Determine the structure's seismic design category (A through D) based on its seismic use group (Step 1), the key ordinate S_{DS} and the key ordinate S_{DI} , using Section 1616.3, Table 1616.3(1) and Table 1616.3(2).

Table 1616.3(1) Seismic Design Category Based on Short-Period Response Accelerations

Value of S_{DS}	Seismic Use Group		
	I	II	III
$S_{DS} < 0.167 \text{ g}$	A	A	A
$0.167 \text{ g} \leq S_{DS} < 0.33 \text{ g}$	B	B	C
$0.33 \text{ g} \leq S_{DS} < 0.50 \text{ g}$	C	C	D
$0.50 \text{ g} \leq S_{DS}$	D*	D*	D*

According to Table 1616.3(1), a structure in Seismic Use Group I (the default case), and with an S_{DS} of 1.11 g is assigned to Seismic Design Category D. The asterisk refers to footnotes that do not apply in this case.

Table 1616.3(2) Seismic Design Category based on 1-sec period response accelerations

Value of S_{DI}	Seismic Use Group		
	I	II	III
$S_{DS} < 0.167 \text{ g}$	A	A	A
$0.167 \text{ g} \leq S_{DS} < 0.33 \text{ g}$	B	B	C
$0.33 \text{ g} \leq S_{DS} < 0.50 \text{ g}$	C	C	D
$0.50 \text{ g} \leq S_{DS}$	D*	D*	D*

According to Table 1616.3(2), a structure in Seismic Use Group I (the default case), and with a S_{DI} of 0.48 g is assigned to Seismic Design Category D. The asterisk refers to footnotes that do not apply in this case.

The two tables assign the structure to the same Seismic Design Category, D. Had they assigned the structure to different categories, the more severe classification would have governed.

Step 7: Determine the required design approach for each seismic design category in accordance with Section 1616.6, including, for higher seismic design categories, the effects of plan structural irregularities (Table 1616.5.1) and vertical structural irregularities (Table 1616.5.2).

Plan structural irregularities include:

- Plan eccentricities between the center of mass and the center of stiffness
- Re-entrant corners
- Out-of-plane offsets
- Nonparallel systems

These can increase seismic response.

Vertical structural irregularities include:

- Stiffness irregularity
- Mass irregularity
- Vertical geometric irregularity
- In-plane discontinuity in vertical lateral force-resisting elements
- Discontinuity in capacity — weak story

These can also increase seismic response.

While this building has no vertical structural irregularities, it does have some plan irregularity due to the openings in the east wall. In accordance with Table 1615.5.1 of the 2000 IBC, however, the torsional eccentricity does not have to be considered in design, because the roof diaphragm is constructed of lightweight fill over corrugated decking, is not cross-braced and can therefore be assumed to be flexible in its own plane. Consistent with this assumption, design seismic base shear acting in the north-south direction is distributed equally between the west and east walls, even though the east wall is more flexible in-plane than the west wall.

Step 8: Determine the seismic load effect, E and E_m , for use in the load combinations of Section 1605, including the effects of redundancy (ρ) and system overstrength (Ω_0), in accordance with Section 1617.

System overstrength need not be addressed, because the lateral force-resisting system is statically determinate. Seismic base shears are assumed to be resisted equally by the two walls oriented in the direction of the shear. To maintain horizontal equilibrium of the diaphragm, the forces transmitted to the walls by the roof diaphragm cannot exceed these shears.

Redundancy must be addressed.

$$\rho = 2 - \frac{20}{r_{\max} \sqrt{A}} \quad (16-32)$$

For shear walls, r is the maximum value of the product of the shear in the wall or wall pier and $10/\ell_w$, divided by the story shear. Taking the lateral force-resisting system in each direction as two parallel exterior shear walls, the shear per wall is one-half the total base shear, and:

$$r = \left(\frac{1}{2} \right) \cdot \left(\frac{10}{20} \right) = 0.25$$

However, r must not be less than 1.0, and need not exceed 1.5 (2000 IBC, Section 1617.2.1).

So:

$$\rho = 2 - \frac{20}{r_{\max} \sqrt{A}}$$

$$\rho = 2 - \frac{20}{1.0 \sqrt{80 \cdot 100}}$$

$$\rho = 2 - 0.22$$

$$\rho = 1.78$$

Finally, in accordance with Section 1617.1.1 of the 2000 IBC, the design seismic load effect E is:

$$E = \rho Q_E$$

Now compute the seismic base shear. In accordance with Section 1617.4.1 of the 2000 IBC:

$$V = C_s W$$

where C_s is the design seismic coefficient (defined below), and W is the building weight.

In accordance with Section 1617.4.1.1.1 of the 2000 IBC,

$$C_s = \frac{S_{D1}}{\left(\frac{R}{I_E}\right)T} \geq 0.044 S_{DS} I_E \quad (16-36, 16-37)$$

In our case,

$$S_{D1} = 0.48 \text{ g}$$

$R = 5$ (meet detailing provisions for special reinforced masonry shear wall)

$I_E = 1.00$ (2000 IBC, Section 1616.2 and Table 1604.5)

Therefore:

$$C_s = \frac{S_{D1}}{\left(\frac{R}{I_E}\right)T} \geq 0.044 S_{DS} I_E$$

$$C_s = \frac{0.48}{\left(\frac{5}{1.0}\right)T} \geq 0.044 \cdot 1.11$$

$$C_s = \frac{0.096}{T} \geq 0.049$$

Assume a fundamental period less than the corner period, so that the maximum spectral ordinate must be used. Take the fundamental period as 0.4 sec. The seismic coefficient is therefore given by:

$$C_s = \frac{0.096}{0.4} = 0.24$$

This will be multiplied by the redundancy factor of 1.78, giving a product of 0.427. In other words, the building must be designed for about 43% of its weight, applied as a lateral force. In this case, the redundancy factor is almost 2.0, which would be consistent with designing the building to resist the entire seismic design base shear acting on each shear wall alone. This would not address the extreme torsional response resulting from the in-plane failure of one of the two shear walls in each direction. Because the walls have considerably more capacity than required, however, and because the entire building mass is used in computing the base shear, the design is considered sufficient.

$$\text{Roof weight: } 60 \text{ lb/ft}^2 \times 100 \times 80 \text{ ft}^2 = 480 \text{ kips}$$

$$\text{Perimeter wall weight: } 2(100 + 80) \times 20 \text{ ft}^2 \times 80 \text{ lb/ft}^2 = 576 \text{ kips}$$

Total weight of the building is 1056 kips.

The design base shear is conservatively calculated as the design spectral ordinate (% g) multiplied by that total weight. This is conservative because it neglects the fact that one half the inertial force from the perpendicular walls is carried directly to the foundation, and does not have to be resisted by the shear walls.

The total seismic design base shear is $1056 \text{ kips} \times 0.427 = 451 \text{ kips}$.

Out-of-plane loads on wall elements are given by Section 1620.1.7 of the 2000 IBC:

$$F_p = 0.40 I_E S_{DS} w_w$$

In our case, the importance factor is 1.0, and S_{DS} equals 1.11. The out-of-plane design seismic load is equivalent to an out-of-plane pressure equal to $(0.40 \times 1.11 w_w)$, or $0.44 w_w$. For a solid-grouted wall, w_w is 80 lb/ft^2 and the out-of-plane pressure is 35.5 lb/ft^2 . The load factor applied to seismic load is 1.0. The resulting out-of-plane design load of 35.5 lb/ft^2 is more critical than the out-of-plane component load for wind (20 lb/ft^2 , multiplied by a load factor of 1.6). Out-of-plane seismic load therefore controls the design.

Propose Structural Systems for Gravity and Lateral Load

Gravity loads are carried from the corrugated decking to the bar joists, from the bar joists to the long-span joists and from the long-span joists to the north and south walls, and to the interior steel columns.

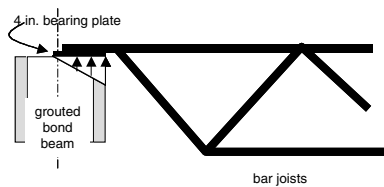
Lateral loads are resisted by perpendicular walls (vertical strips), which transfer their loads to the roof diaphragm and the foundation. Loads transferred to the roof diaphragm are carried to shear walls oriented parallel to the load.

17.9.2.2 Design Walls for Gravity Plus Out-of-Plane Loads

West Wall

The west wall carries gravity load from a portion of the tributary area of the roof, plus seismic loads.

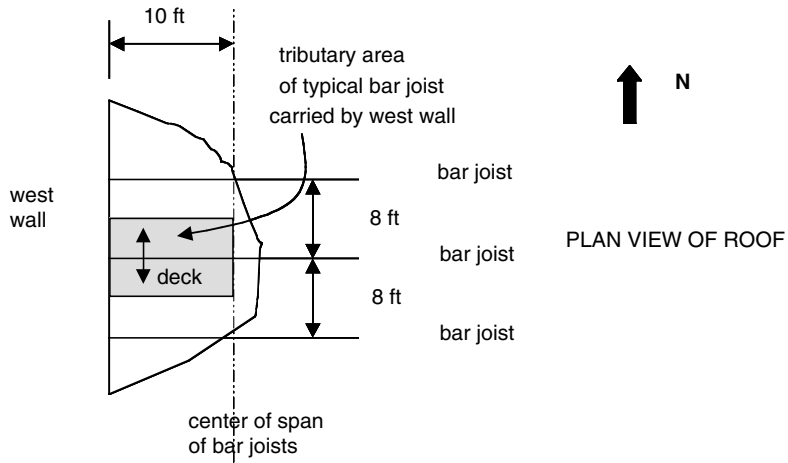
Assume that the load is applied over a 4-in. bearing plate, and that bearing stresses vary linearly over the bearing plate as shown below:



Then the eccentricity of the applied load with respect to the centerline of the wall is

$$e = \frac{t}{2} - \frac{\text{plate}}{3} = \frac{7.63 \text{ in.}}{2} - \frac{4 \text{ in.}}{3} = 2.48 \text{ in.}$$

Compute the load on the west wall from the roof:



The tributary area of an entire bar joist is the product of the span (20 ft) and the distance between bar joists (8 ft). The tributary area of bar joist loading the west wall is one half that, or 80 ft².

The roof dead load is 60 lb/ft². For tributary areas up to 200 ft², the roof live load is 20 lb/ft².

Assume that the critical loading combination is 0.9D + 1.0E. The factored gravity load acting on the wall per foot of length is therefore:

$$w_u = 10\text{ ft} \cdot 0.9(60 \text{ lb}/\text{ft}^2) = 540 \text{ lb}/\text{ft}$$

The west wall will be fully grouted. The minimum percentage of prescriptive reinforcement for a "special reinforced wall" is 0.0007; for a nominal 8-in. wall, this corresponds to a horizontal steel area of 0.06 in.² Use one #5 bar every 48 in. (six courses). This corresponds to a steel percentage of 0.00085. Vertically, use one #6 bar every 48 in. This corresponds to a steel percentage of 0.0012. The sum of the horizontal and vertical steel percentages is 0.00205.

The west wall is idealized as a series of vertically spanning strips, each of which must be designed as a beam-column for combinations of gravity load plus out-of-plane seismic load.

To avoid having to check a large number of loading combinations and potentially critical locations, it is worthwhile to assess them first, and check only the ones that will probably govern.

Because the eccentric axial load places the outer fibers of the wall in tension, the critical lateral load condition is an outward seismic inertial loading of 37.9 lb/ft².

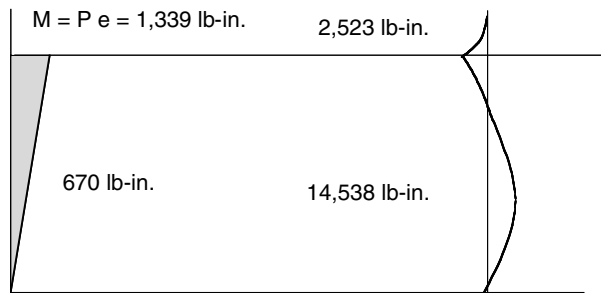
Because of wind only, the unfactored moment at the base of the parapet (roof level) is:

$$M = \frac{qL^2}{2} = \frac{37.9 \text{ lb}/\text{ft} \cdot 3.33^2 \text{ ft}^2}{2} \cdot 12 \text{ in./ft} = 2,523 \text{ lb-in.}$$

The maximum moment is close to that occurring at midheight. The moment from out-of-plane seismic load is the superposition of one-half moment at the upper support due to seismic load on the parapet only, plus the midspan moment in a simply supported beam with that same seismic load:

$$M_{midspan} = \frac{2,523}{2} + \frac{qL^2}{8} = -\frac{2,523}{2} + \frac{37.9 \text{ lb}/\text{ft} \cdot 16.67^2}{8} \cdot 12 \text{ in./ft} = 14,538 \text{ lb-in.}$$

Unfactored moment diagrams due to eccentric dead load and earthquake are as shown below:



Because the out-of-plane seismic moments directly underneath the roof are not very large, they will probably not be critical. The critical location will probably be at midheight; the critical loading condition will probably be $0.9D + 1.0E$.

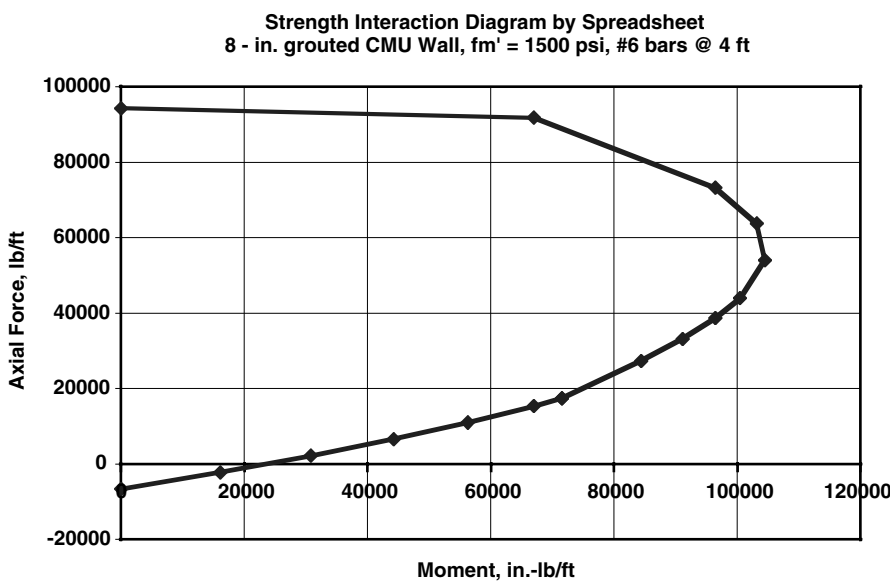
At the midheight of the wall, the axial force due to $0.9D$ is:

$$P_u = 0.9(540 \text{ lb}) + 0.9(3.33 \text{ ft} + 8.33 \text{ ft}) \cdot 48 \text{ lb/ft} = 988 \text{ lb}$$

At the midheight of the wall, the factored design moment per foot of length, M_u , is given by:

$$M_u = P_u \frac{e}{2} + M_{uearthquake} = \left(\frac{1}{2}\right) 0.9 \cdot 540 \text{ lb} \cdot 2.48 \text{ in.} + 1.0 \cdot 14,538 \text{ lb-in.} = 15,141 \text{ lb-in.}$$

The wall's nominal moment—axial force interaction diagram per foot of length is shown below. Clearly, the capacity is more than sufficient.



17-46 Earthquake Engineering: From Engineering Seismology to Performance-Based Engineering

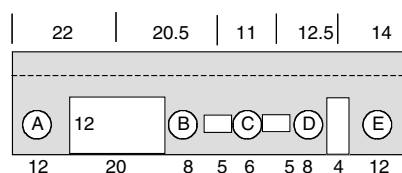
The cells of the spreadsheet are shown below:

Spreadsheet for Calculating Moment–Axial Force Interaction Diagram per Foot of Fully Grouted Wall

Reinforcement at middepth specified thickness	7.625						
Emu	0.0025						
$F'm$	1,500						
F_y	60,000						
E_s	29,000,000						
D	3.8125						
(c/d)balanced	0.54717						
Reinforcement area	0.11						
Effective width	12						
	C/d	c	C	f_s	T	Moment	Axial Force
Points controlled by steel	0	0	0	60,000	6600	0	-6,600
	0.1	0.38125	4,392	60,000	6600	16,075	-2,208
	0.2	0.7625	8,784	60,000	6600	30,810	2,184
	0.3	1.14375	13,176	60,000	6600	44,205	6,576
	0.4	1.525	17,568	60,000	6600	56,262	10,968
	0.5	1.90625	21,960	60,000	6600	66,978	15,360
	0.54717	2.086085	24,032	60,000	6600	71,568	17,432
Points controlled by masonry	0.54717	2.086085	24,032	60,000	6600	71,568	17,432
	0.7	2.66875	30,744	31,071	3418	84,392	27,326
	0.8	3.05	35,136	18,125	1994	91,090	33,142
	0.9	3.43125	39,528	8,056	886	96,448	38,642
	1	3.8125	43,920	0	0	100,467	43,920
	1.2	4.575	52,704	-12,083	-1329	10,4486	54,033
	1.4	5.3375	61,488	-20,714	-2279	10,3146	63,767
	1.6	6.1	70,272	-27,188	-2991	96,448	73,263
	2	7.625	87,840	-36,250	-3988	66,978	91,828
Pure axial load						0	94,334

East Wall

The loads on the east wall are identical to those on the west wall, except for the presence of the openings. Each pier of the east wall must be designed as a beam-column for combinations of gravity load plus out-of-plane earthquake forces. Loads on each pier are increased by the ratio of the tributary width of the pier, to the actual width. By inspection, Pier B, with a ratio of tributary width to actual width of (20.5/8), is most critical.



At the midheight of the west wall, the axial force due to $0.9D$ is:

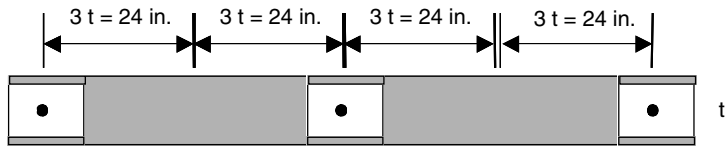
$$P_u = 0.9(600 \text{ lb}) + 0.9(3.33 \text{ ft} + 8.33 \text{ ft}) \cdot 48 \text{ lb/ft} = 1,044 \text{ lb}$$

At the midheight of the west wall, M_u is given by:

$$M_u = P_u \frac{e}{2} + M_{uearthquake} = \left(\frac{1}{2} \right) 0.9 \cdot 600 \text{ lb} \cdot 2.48 \text{ in.} + 1.0 \cdot 14,538 \text{ lb-in.} = 15,208 \text{ lb-in.}$$

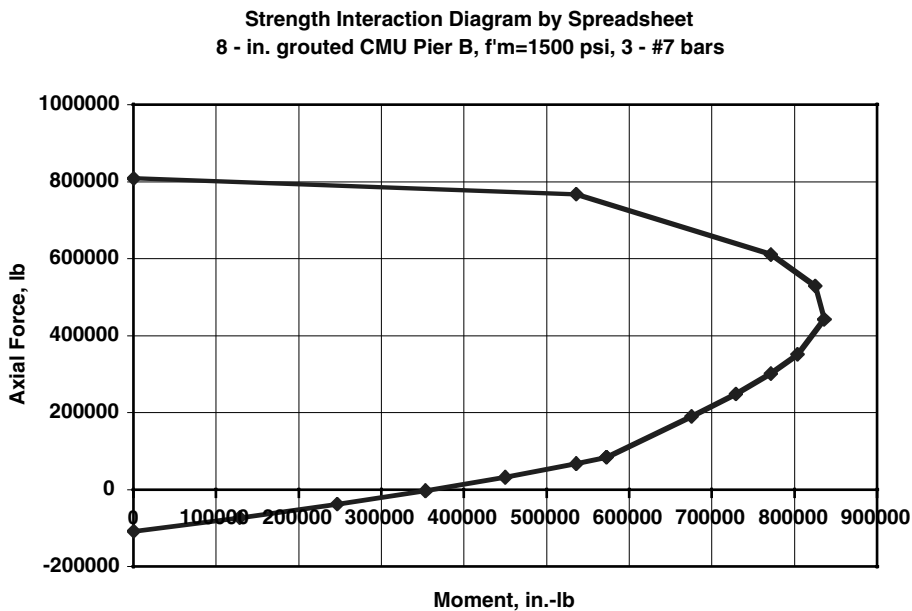
The factored axial force and moment on Pier B of the east wall are obtained by multiplying those values by the tributary width of 20.5 ft, giving 21,402 lb and 311,764 lb-in. The minimum required nominal flexural capacity, corresponding to an axial load of essentially 0, is obtained by dividing this factored design moment by the ϕ -factor of 0.90, for a total required nominal flexural capacity of about 346,000 lb-in.

Our previous design, with #6 bars @ 48 in., had a nominal flexural capacity per foot, at 0 axial load, of about 24,000 in.-lb. An 8-ft pier would therefore have a nominal flexural capacity 8 times this, or 192,000 lb-in., less than that needed. Use a trial design with three #7 bars per pier (steel area equals $3 * 0.60 \text{ in.}^2$, or 1.80 in.^2). For the critical Pier B, the effective width will be $3t$ on each side of each bar.



This is essentially equal to the total pier length of 8 ft. Capacity is insensitive to effective width at low axial loads.

The nominal moment–axial force interaction diagram for the trial design of the critical Pier B is shown below:



17-48 Earthquake Engineering: From Engineering Seismology to Performance-Based Engineering

The cells of the spreadsheet are shown below.

Spreadsheet for Calculating Moment-Axial Force Interaction Diagram for Fully Grouted Concrete Masonry Units Pier B

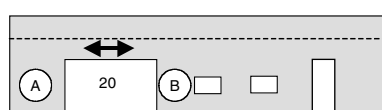
Reinforcement at middepth specified thickness	7.625
Emu	0.0025
$f'm$	1,500
f_y	60,000
E_s	29,000,000
d	3.8125
(c/d)balanced	0.54717
Reinforcement area	1.8
Effective width	96

	C/d	c	C	f_s	T	Moment	Axial Force
Points controlled by steel	0	0	0	60,000	108,000	0	-108,000
	0.1	0.38125	35,136	60,000	108,000	128,598	-72,864
	0.2	0.7625	70,272	60,000	108,000	246,479	-37,728
	0.3	1.14375	105,408	60,000	108,000	353,644	-2,592
	0.4	1.525	140,544	60,000	108,000	450,092	32,544
	0.5	1.90625	175,680	60,000	108,000	535,824	67,680
	0.54717	2.086085	192,254	60,000	108,000	572,544	84,254
Points controlled by masonry	0.54717	2.086085	192,254	60,000	108,000	572,544	84,254
	0.7	2.66875	245,952	31,071	55,929	675,138	190,023
	0.8	3.05	281,088	18,125	32,625	728,721	248,463
	0.9	3.43125	316,224	8,056	14,500	771,587	301,724
	1	3.8125	351,360	0	0	803,736	351,360
	1.2	4.575	421,632	-12,083	-21,750	835,885	443,382
	1.4	5.3375	491,904	-20,714	-37,286	825,169	529,190
	1.6	6.1	562,176	-27,188	-48,938	771,587	611,114
	2	7.625	702,720	-36,250	-65,250	535,824	767,970
Pure axial load						0	808,992

At an axial load of close to 0, the nominal out-of-plane flexural capacity of the critical Pier B is about 400,000 lbin. The design will be satisfactory.

For simplicity, use three #7 bars vertically in every pier of the east wall.

We have completed the design of the piers of the east wall. Now consider the design of the horizontally spanning lintel between Pier A and Pier B, against out-of-plane earthquake forces.



Again, outward loading will be critical. The span of the lintel is the clear span, plus one-half the length of a unit, or 8 in., on each side, for a total span of 21.33 ft. The factored design out-of-plane moment on the lintel is:

$$M_u^{out-of-plane} = (1.0) \frac{qL^2}{8} \frac{(1.0)35.5 \text{ lb}/\text{ft}^2 \cdot (20-12)\text{ft} \cdot 21.33^2 \text{ ft}^2 \cdot 12 \text{ in.}/\text{ft}}{8}$$

$$M_u^{out-of-plane} = 193,817 \text{ lb-in.}$$

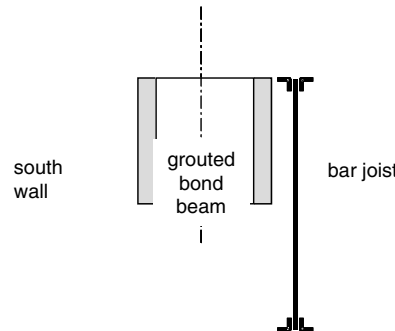
The corresponding required nominal capacity is that value divided by 0.90, or 216,000 lbin.

Conservatively assume an effective depth equal to one-half the wall thickness. Use the preceding design of vertical strips as a guide. At an axial load of essentially 0, the nominal flexural capacity provided by three #7 bars ($A_s = 1.80 \text{ in.}^2$) was about 400,000 lbin. To reach a nominal flexural capacity of 216,000 lbin. therefore requires a steel area of about 1.80 in.^2 multiplied by $(216/400)$, or about 0.97 in.^2 . This can be provided using two #7 bars in a bond beam at the level of the roof, plus two #4 bars at the top of the parapet, plus two #4 bars in the lowest course of the lintel.

North, South Walls

The north and south walls span vertically between the foundation slab and the roof diaphragm. They support gravity loads from self-weight alone, because the long-span joists rest on pilasters separated from the north and south walls by vertically oriented control joints. They also support out-of-plane wind loads.

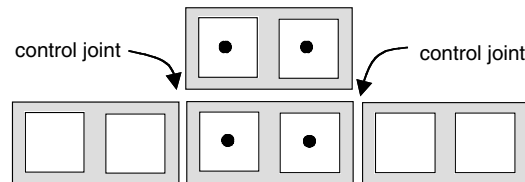
Because the bar joists are oriented parallel to the north and south walls, a bar joist will be placed right next to those walls, and will be connected vertically to the walls only by roof deck, which is quite flexible out-of-plane. The north and south walls will therefore not support any gravity loads except their own weight.



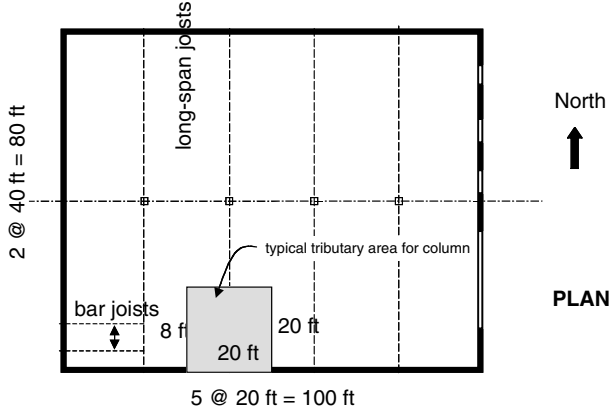
Because the walls are unperforated, the previous design of the west wall will apply. Use the same prescriptive horizontal reinforcement of #5 bars at 4 ft, and prescriptive vertical reinforcement of #6 bars at 4 ft.

17.9.2.3 Design Pilasters (or Columns) in North and South Walls

Because the north and south walls have vertically oriented control joints at each pilaster to accommodate the shrinkage of concrete masonry, the pilasters really behave like columns. Because they are not “isolated,” though, some designers might consider that they do not have to meet the prescriptive reinforcement requirements of the 2002 MSJC Code for columns (including transverse reinforcement). In this problem, such prescriptive reinforcement is used.



The load on the columns comes from eccentric gravity loads from the long-span joists. Their tributary area is shown below:

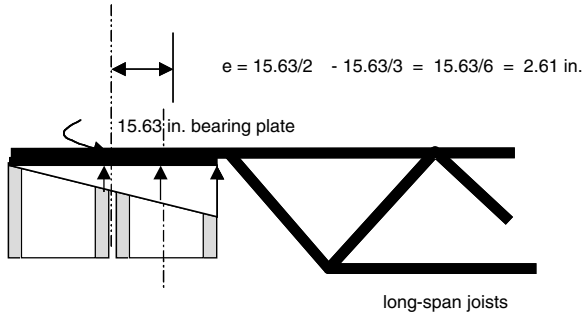


The tributary area is 400 ft^2 , which corresponds to a reduced live load of $20 \text{ lb}/\text{ft}^2 * 0.80 = 16 \text{ lb}/\text{ft}^2$, according to Section 1607.11.2 of the 2000 IBC. This is irrelevant, however, because, as before, axial load significantly increases column capacity below the balance point, and the governing loading combination is $0.9D + 1.0E$. The other possible loading combination, $0.9D + 1.6W$, is almost as critical.

The factored axial load on each column is therefore:

$$P_u = 0.9 \cdot 60 \text{ lb}/\text{ft}^2 \cdot 400 \text{ ft}^2 = 21,600 \text{ lb}$$

The long-span joists rest on the columns through bearing plates that cover the entire specified thickness of the pilaster, or 15.63 in. Assuming a triangular stress distribution under the bearing plates, the eccentricity of gravity load can be calculated:



The corresponding factored moment at the top of the column due to eccentric gravity load is therefore:

$$M_u = P_u e = 21,600 \text{ lb} \cdot 2.61 \text{ in.} = 56,376 \text{ lb-in.}$$

Because of wind only, the factored moment at the base of the parapet (roof level) is:

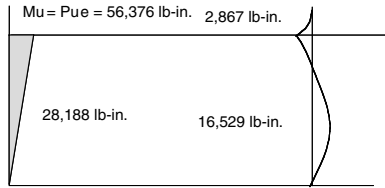
$$M_u = \frac{qL^2}{2} = \frac{1.6 \cdot 20.25 \text{ lb}/\text{ft}^2 \cdot 1.33 \text{ ft} \cdot 3.33^2 \text{ ft}^2}{2} \cdot 12 \text{ in./ft} = 2,867 \text{ lb-in.}$$

The maximum wind-load moment is close to that occurring at midheight. The moment from wind load is the superposition of one-half moment at the upper support due to wind load on the parapet only, plus the midspan moment in a simply supported beam with that same wind load. Because the north and south walls are separated from the columns by control joints, the wind-load moment on the columns is due to their frontal area alone:

$$M_{u \text{ midspan}} = \frac{2,867}{2} + \frac{qL^2}{8}$$

$$M_{u \text{ midspan}} = \frac{2,867}{2} + \frac{1.6 \cdot 20.25 \text{ lb}/\text{ft}^2 \cdot 1.33 \text{ ft} \cdot 16.67^2}{8} \cdot 12 \text{ in./ft} = 16,529 \text{ lb-in.}$$

Factored moment diagrams due to eccentric dead load and wind are as shown below:

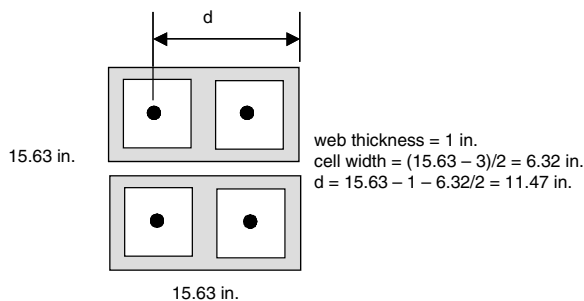


Maximum factored design moment is the summation of that due to eccentric gravity load and that due to wind:

$$M_u = 28,188 + 16,529 = 44,717 \text{ lb-in.}$$

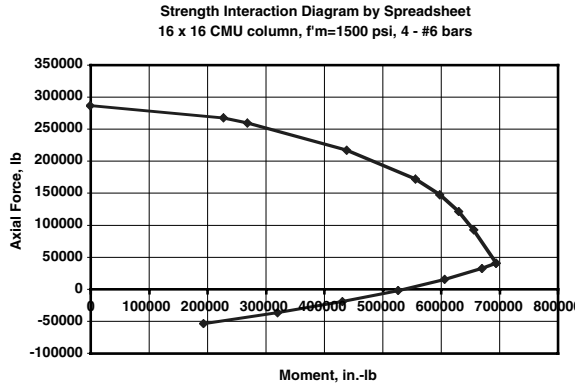
Now design the beam-column to have sufficient capacity:

The effective depth d of the column is computed based on the specified dimensions of nominal 8-in. concrete masonry units:



17-52 Earthquake Engineering: From Engineering Seismology to Performance-Based Engineering

Using a spreadsheet as before, a strength-based, moment–axial force interaction diagram can be generated. For simplicity, the contribution of compressive reinforcement is neglected.



Because the reinforcement is located a good distance from the geometric centroid of the cross section, the shape of the interaction diagram is familiar, with the maximum moment capacity corresponding to the balance point.

The spreadsheet cells are reproduced below:

Spreadsheet for Calculating a Strength-Based Moment–Axial Force Interaction Diagram for 16-in. Concrete Masonry Units Column

Specified thickness	15.625
Emu	0.0025
$f'm$	1,500
f_y	60,000
E_s	29,000,000
D	11.47
(c/d)balanced	0.54717
Reinforcement area	0.88
Width	15.625

	C/d	c	C	f_s	T	Moment	Axial Force
Points controlled by steel	0	0	0	60,000	52,800	193,116	-52,800
	0.1	1.147	17,205	60,000	52,800	319,636	-35,595
	0.2	2.294	34,410	60,000	52,800	430,370	-18,390
	0.3	3.441	51,615	60,000	52,800	525,315	-1,185
	0.4	4.588	68,820	60,000	52,800	604,474	16,020
	0.5	5.735	86,025	60,000	52,800	667,845	33,225
	0.54717	6.276038	94,141	60,000	52,800	692,257	41,341
Points controlled by masonry	0.54717	6.276038	94,141	60,000	52,800	692,257	41,341
	0.7	8.029	120,435	31,071	27,343	654,116	93,092
	0.8	9.176	137,640	18,125	15,950	628,456	121,690
	0.9	10.323	154,845	8,056	7,089	596,268	147,756
	1	11.47	172,050	0	0	554,775	172,050
	1.2	13.764	206,460	-12,083	-10,633	437,391	217,093
	1.4	16.058	240,870	-20,714	-18,229	267,970	259,099
	1.44	16.5168	247,752	-22,153	-19,494	227,433	267,246
Pure axial load						0	286,330

Using four #6 bars, the capacity of the column is much greater than that is required. The 2002 MSJC Code (Section 3.2.4.4.2) requires that transverse reinforcement in columns comply with Section 2.1.6.5. Use #3 ties at 8 in.

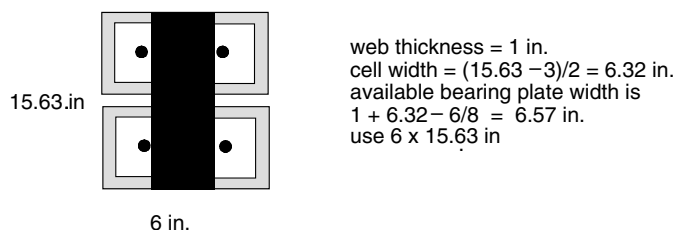
Shear is very small, and will not govern.

Bearing Plate under Long-Span Joists

The 2002 MSJC Code specifies a capacity reduction factor of 0.60 for bearing (Section 3.1.4.6). No formulas are provided for calculated nominal bearing capacity. Based on engineering judgment, use a nominal bearing resistance of $A_n f'_m$, and a ϕ -factor of 0.6:

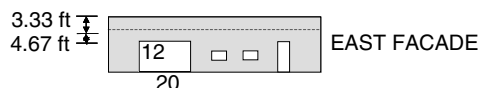
$$\phi P_{n \text{ bearing}} = \phi A_n f'_m = 0.6 \cdot 15.63^2 \cdot 1500 \cdot \text{lb/in.}^2 = 219,867 \text{ lb}$$

This design capacity is far in excess of the factored axial load. The required area of the bearing plate is about 10% of the cross-sectional area of the column. Use a bearing plate measuring about 6 in. x 15 in.



17.9.2.4 Design Lintels

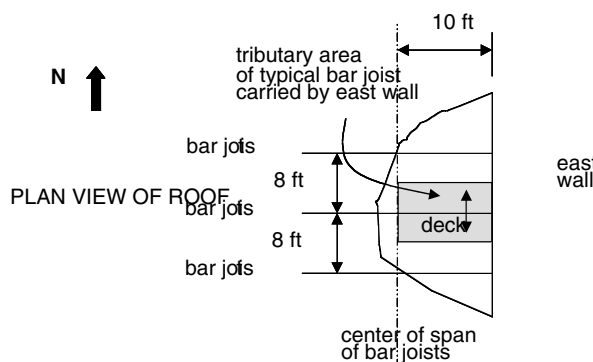
Only the lintel over the 20-ft opening will be critical:



As with the previous design of the area over the lintel for out-of-plane flexure in the horizontal plane, the structural span of the lintel is 20 ft, plus one half unit on each side. The nominal length of a conventional concrete masonry unit is 16 in. (1.33 ft). Adding half that distance on each side of the clear opening gives a span of 21.33 ft. Conservatively, arching action will be neglected. The beam has a depth of at most 8 ft, and a clear span of 20 ft. Deep-beam action is not considered.

Calculate Gravity Load on Lintel

The lintel supports some direct gravity load from the roof decking, based on the tributary area shown below:

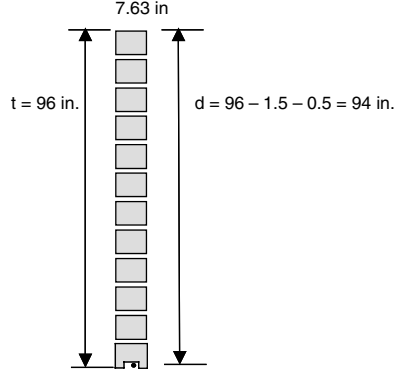


The tributary area supported by the entire lintel is 10 ft (tributary width from the figure above), multiplied by the span of 20 ft, or 200 ft². Because this is exactly equal to the upper limit of the tributary area at which live load reduction starts, no live load reduction is applied.

Factored gravity loads per foot of length on the lintel are itemized in the table below. Since the lintel is uncoupled from the wall system by the control joints at each end, gravity loads alone constitute the critical loading case for it, and the governing loading combination is 1.2D + 1.6L. In calculating the self-weight of the parapet and wall above the opening, the masonry is assumed to be fully grouted, with a unit weight of 76 lb/ft²:

Description	Calculation	Load Factor	Factored Load (lb/ft)
Roof DL	60 lb/ft ² × 10 ft	1.2	720.0
Roof LL	20 lb/ft ² × 10 ft	1.6	320.0
Parapet + wall	8 ft × 76 lb/ft ²	1.2	729.6
Total			1769.6

As in previous examples, the bars in the lintel will probably be placed in the lower part of an inverted bottom course. The effective depth d is calculated using the minimum cover of 1.5 in. (Section 1.12.4.1 of the 2002 MSJC Code), plus one-half the diameter of an assumed #8 bar.



Calculate the factored design moment and shear for the lintel:

$$V_u = \frac{w_u L}{2} = \frac{1770 \text{ lb}/\text{ft} \cdot 21.33 \text{ ft}}{2} = 37,754 \text{ lb}$$

$$M_u = \frac{w_u L^2}{8} = \frac{1770 \text{ lb}/\text{ft} \cdot 21.33^2 \text{ ft}^2 \cdot 12 \text{ in./ft}}{8} = 1,20a8 \text{ kip-in.}$$

Because this is a reinforced element, shearing capacity is calculated using Section 3.2.4.1.2.1 of the 2002 MSJC Code:

$$V_m = \left[4.0 - 1.75 \left(\frac{M}{Vd_v} \right) \right] A_n \sqrt{f'_m} + 0.25P$$

As (M/Vd_v) increases, V_m decreases. Because (M/Vd_v) need not be taken greater than 1.0 (2002 MSJC Code, Section 3.2.4.1.2.1), the most conservative (lowest) value of V_m is obtained with (M/Vd_v) equal to 1.0. Also, axial load P is 0:

$$V_m = [4.0 - 1.75(1.0)] A_n \sqrt{f'_m}$$

$$V_m = 2.25 A_n \sqrt{f'_m}$$

$$V_u = 37,754 \text{ lb} \leq \phi V_n = 0.8 \cdot 2.25 \cdot 7.63 \text{ in.} \cdot 94 \text{ in.} \cdot \sqrt{1500} = 50,000 \text{ lb}$$

and the design is acceptable for shear.

Now check the required flexural reinforcement:

$$M_n \approx A_s f_y 0.9 d$$

In our case:

$$M_n^{\text{required}} = \frac{M_u}{\phi} = \frac{M_u}{0.9} = \frac{1,208,000 \text{ lb-in.}}{0.9} = 1,342,000 \text{ lb-in.}$$

Solve for the required steel area:

$$A_s^{\text{required}} = \frac{M_n^{\text{required}}}{f_y 0.9 d} = \frac{1,342,000 \text{ lb-in.}}{60,000 \text{ psi} \cdot 0.9 \cdot 94 \text{ in.}} = 0.26 \text{ in.}^2$$

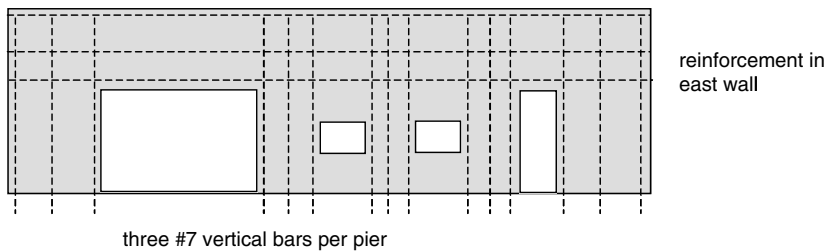
Because of the depth of the beam, this can easily be satisfied with two #4 bars in the lowest course. Also include two #7 bars at the level of the roof (bond beam reinforcement). This will be consistent with the requirements of the design of the lintel for out-of-plane bending in a horizontal plane. Finally, to guard against possible cracking of the lintel near the top, use two more #4 bars at the top course of the parapet.

Summary So Far

Thus far in the design, all walls are fully grouted. The north, west and south walls have #5 bars horizontally at 48 in., and #6 bars vertically at 48 in.

As a result of the design of the piers of the east wall for out-of-plane bending, the lintel of the east wall for out-of-plane bending and the design of the lintel of the east wall as a beam, reinforcement in the east wall is as shown. Each pier has three #7 vertical bars and three sets of horizontal reinforcement are provided, in the form of two #4 bars at the top of the parapet and at the bottom of the lintel, and two #7 bars at the level of the roof. The two sets of #4 bars and the one set of #7 bars will be continued around the perimeter of the entire building.

two #4 horizontal bars at top of parapet and bottom of lintel; two #7 bars at level of roof



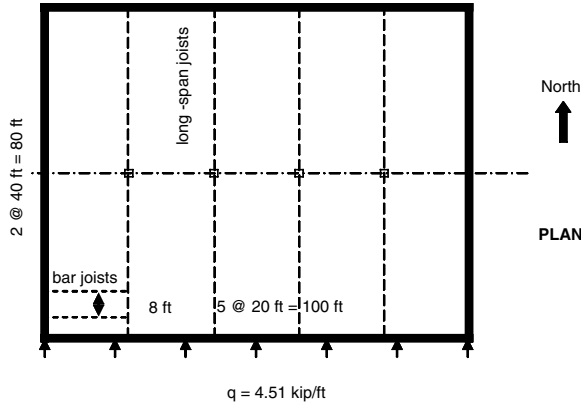
17.9.2.5 Step 5: Conduct Lateral Force Analysis

Lateral force analysis will be critical in the north—south direction, because the area of shear walls is less.

Check Chord Forces in Roof Diaphragm

From the earthquake analysis of Step 2 the design seismic base shear on the building is 451 kips. Conservatively assume that all of this is transmitted to the shear walls. In reality, some of it (that due to the mass of the lower half of the walls oriented perpendicular to the direction of earthquake input) will be transmitted directly to the floor slab.

This load is distributed over the roof length of 100 ft, giving a horizontal load of 4.51 kips/ft on the diaphragm:



Design the roof chords. The load factor for E is 1.0:

$$M_{\text{roof}} = \frac{q_u L^2}{8} = \frac{1.0 \cdot 4.51 \text{ kip}/\text{ft} \cdot 100^2 \text{ ft}^2}{8} = 5,638 \text{ kip-ft}$$

The required chord force is this factored moment, divided by the distance between chords (80 ft), and divided by the ϕ -factor for flexure (0.9). The required steel area is this chord force, divided by the specified yield strength of the reinforcement (60,000 lb/in.²):

$$T_{\text{chord}} = \frac{M_u}{\phi H} = \frac{5,638 \text{ kip-ft}}{0.90 \cdot 80 \text{ ft}} = 78.30 \text{ kip}$$

$$A_s^{\text{required}} = \frac{T_{\text{chord}}}{f_y} = \frac{78.30 \text{ lb}}{60 \text{ kip/in.}^2} = 1.30 \text{ in.}^2$$

We have already specified two #7 bars around the perimeter of the roof, so that will be fine.

Check Shear Capacity of Walls on West and East Sides

Neglect plan torsion. Because a flexible diaphragm is assumed, shear is distributed equally to each of the two walls. The total factored design shear applied to the walls on the west and east sides is 1.0 x (451 kips) divided by 2.0, or 225.5 kips.

Within each wall, assume that shear will be distributed to each pier in proportion to its length.

Distribute the shear to the piers of the east wall in proportion to their plan length:

Pier	Plan Length	Shear
A	12	58.8
B	8	39.2
C	6	29.4
D	8	39.2
E	12	58.8
Total	46	225.4

17.9.2.6 Design Piers

Shear in West Wall

This will be no problem. The factored design shear in the west wall, 225.5 kips, is far less than the shear capacity, reduced by the capacity reduction factor for shear:

Conservatively neglect the beneficial effects of axial load:

$$V_n = \min \begin{cases} 3.8\sqrt{f'_m} A_n = 3.8 \cdot \sqrt{1,500} \text{ lb/in.}^2 \cdot (100 \text{ ft} \cdot 12 \text{ in.}/\text{ft} \cdot 7.63 \text{ in.}) = 1,348 \text{ kips} \\ 300 A_n = 300 \cdot (100 \cdot 12 \cdot 7.63) = 2,747 \text{ kips} \\ 56 A_n + 0.45 N = 56 \cdot (100 \cdot 12 \cdot 7.63) + 0.45 \cdot 0 = 513 \text{ kips} \end{cases}$$

$$V_n = 513 \text{ kips}$$

The corresponding design shear capacity is:

$$\phi V_n = 0.80 \cdot 513 \text{ kips} = 410 \text{ kips}$$

The design shear capacity far exceeds the factored design shear of 225.5 kips, and the west wall is satisfactory for shear.

Shear in East Wall

Because shear has been distributed in proportion to plan length, the nominal shear stress in each pier will be equal. Check any pier, for example, Pier A. The factored design shear in the pier is 58.8 kips. Assuming a point of inflection at midheight, the corresponding moment is $(VH/2)$, or $(58.8 \text{ kips} \times 12 \text{ ft}/2) = 4,230 \text{ kips-in.}$

Capacity of Pier A as Governed by Flexure — Conservatively neglect the effects of axial load, and assume an internal lever arm of 90% of the total depth of the pier. Compute the flexural capacity of the pier with three #7 bars. Neglect the contribution of the compressive reinforcement, and the middle layer of reinforcement:

$$M_n \approx A_s f_y \cdot 0.9t$$

$$M_n \approx 0.60 \text{ in.}^2 \cdot 60,000 \text{ lb/in.}^2 \cdot 0.9 \cdot 144 \text{ in.}$$

$$M_n \approx 4,666 \text{ kip-in.}$$

Using a ϕ -factor of 0.90 for flexure (MSJC Code Section 3.1.4.1), the design flexural capacity is 4200 kips-in., slightly less than the factored design moment. If the middle reinforcement is included, the capacity of the pier will increase by about 50%, and the capacity will certainly be sufficient.

Capacity as Governed by Shear — For a single pier:

$$V_n = V_m = \left[4.0 - 1.75 \left(\frac{M}{Vd_v} \right) \right] A_n \sqrt{f'_m} + 0.25P$$

Conservatively neglect the effects of axial load. Then:

$$\begin{aligned} V_n &= \left[4.0 - 1.75 \left(\frac{VL/2}{Vd_v} \right) \right] \cdot (144.763 \text{ in.}^2) \sqrt{1500} \text{ lb/in.}^2 \\ V_n &= \left[4.0 - 1.75 \left(\frac{12.12 \text{ in.}}{2.144 \cdot 0.9 \text{ in.}} \right) \right] \cdot 1099 \text{ in.}^2 \cdot 38.73 \text{ lb/in.}^2 \\ V_n &= [4.0 - 1.75(0.555)] \cdot 1099 \text{ in.}^2 \cdot 38.73 \text{ lb/in.}^2 \\ V_n &= 3.03 \cdot 1099 \text{ in.}^2 \cdot 38.73 \text{ lb/in.}^2 = 128,875 \text{ lb} \end{aligned}$$

Using a ϕ -factor of 0.80 for shear (3.1.4.3), the design shear capacity clearly exceeds the factored design shear.

17.9.2.7 Design and Detail Connections

Wall–Slab Connections for North and South Walls

No reinforcement needed. Use #6 foundation dowels @ 48 in. if desired. Use #6 foundation dowels connected to longitudinal reinforcement in columns (pilasters).

Wall–Slab connections for West Wall

Use #6 foundation dowels @ 48 in.

Wall–Slab Connections for East Wall

Use #7 foundation dowels connected to pier reinforcement.

Connections between Walls and Roof Diaphragm

Walls will be solid-grouted. Bar joists will be embedded into bond beams at roof level. Long-span joists will rest on bearing plates embedded into column (pilaster) sections. No further shear connection is required.

References¹

- Abrams, D. and Paulson, T. (1991). Modeling earthquake response of concrete masonry building structures, *ACI Struct. J.*, 88(4), 475–485.
- ACI SP-127 (1991). *Earthquake-Resistant Concrete Structures: Inelastic Response and Design*, Ghosh, S.K., Ed., Special Publication SP-127, American Concrete Institute, Farmington Hills, MI, pp. 479–503.
- ACI 318-02 (2002). ACI Committee 318, Building Code Requirements for Reinforced Concrete, ACI 318-99, American Concrete Institute, Farmington Hills, MI.

¹The terminology and symbols used in this chapter are taken from MSJC (2002). Building Code Requirements for Masonry Structures (ACI 530-02/ASCE 5-02/TMS 402-02 of American Concrete Institute, American Society of Civil Engineers, and The Masonry Society). Masonry Standards Joint Committee.

- AISC (1992). *Manual of Steel Construction, Load and Resistance Factor Design*, 2nd ed., American Institute of Steel Construction, Chicago.
- ASCE 7-98. (1998). Minimum Design Loads for Buildings and Other Structures, ASCE 7-98, American Society of Civil Engineers, Reston, VA.
- ATC 3-06 (1978). Tentative Provisions for the Development of Seismic Regulations for Buildings, ATC 3-06, Applied Technology Council, National Bureau of Standards, Redwood City, CA.
- BBC (1999). Basic Building Code, Building Officials/Code Administrators International.
- Benedetti, D., Carydis, P., and Pezzoli, P. (1998). Shaking-table tests on 24 simple masonry buildings, *Earthquake Eng. Struct. Dyn.*, 27(1), 67–90.
- Binder, R.W. (1952). Engineering aspects of the 1933 Long Beach earthquake, in *Proc. Symposium on Earthquake Blast Effects on Structures*, Berkeley, CA, pp. 186–211.
- Blondet, M. and Mayes, R.L. (1991). The Transverse Response of Clay Masonry Walls Subjected to Strong Motion Earthquakes — Vol. 1: General Information, TCCMAR Report 3.2(b)-2, U.S.–Japan Coordinated Program for Masonry Building Research.
- Cohen, G.L. (2001). Seismic Response of Low-Rise Masonry Buildings with Flexible Roof Diaphragms, M.S. thesis, The University of Texas at Austin.
- Costley, A.C. and Abrams, D.P. (1996). Response of building systems with rocking piers and flexible diaphragms, in *Proc. Structures Congress*, American Society of Civil Engineers, Chicago, IL, Apr. 15–18, 1996, pp. 135–140.
- EERI (1999). The Quindío, Colombia Earthquake of January 25, 1999, EERI Special Earthquake Report, Earthquake Engineering Research Institute, Oakland, CA.
- EQE (1989). The October 17, 1989 Loma Prieta Earthquake, EQE International, Houston, TX.
- EQE (1999). Izmit, Turkey Earthquake of August 17, 1999 (M7.4), EQE briefing, EQE International, Houston, TX.
- FEMA 172 (1992). *Handbook of Techniques for the Seismic Rehabilitation of Existing Buildings*, Building Seismic Safety Council, Washington, D.C.
- FEMA 178 (1992). *NEHRP Handbook for the Seismic Evaluation of Existing Buildings*, Building Seismic Safety Council, Washington, D.C.
- FEMA 273 (1997). *NEHRP Guidelines for the Seismic Rehabilitation of Buildings*, Building Seismic Safety Council, Washington, D.C.
- FEMA 274 (1997). *NEHRP Commentary on the Guidelines for the Seismic Rehabilitation of Buildings*, Building Seismic Safety Council, Washington, D.C.
- FEMA 306 (1998). *Evaluation of Earthquake-Damaged Concrete and Masonry Wall Buildings: Basic Procedures Manual*, Federal Emergency Management Agency, Washington, D.C.
- FEMA 307 (1998). *Evaluation of Earthquake-Damaged Concrete and Masonry Wall Buildings: Technical Resources*, Federal Emergency Management Agency, Washington, D.C.
- FEMA 308 (1998). *Repair of Earthquake-Damaged Concrete and Masonry Wall Buildings*, Federal Emergency Management Agency, Washington, D.C.
- FEMA 356 (2000). *Prestandard and Commentary for the Seismic Rehabilitation of Buildings*, Federal Emergency Management Agency, Washington, D.C.
- Gulkan, P., Clough, R.W., Mayes, R.L., and Manos, G. (1990a). Seismic testing of single-story masonry houses, Part I, *J. Struct. Eng.*, 116(1), 235–256.
- Gulkan, P., Clough, R.W., Mayes, R.L., and Manos, G. (1990b). Seismic testing of single-story masonry houses, Part II, *J. Struct. Eng.*, 116(1), 257–274.
- Hamid, A., Abboud, B., Farah, M., Hatem, K., and Harris, H. (1989). Response of Reinforced Block Masonry Walls to Out-of-Plane State Loads, TCCMAR Report 3.2(a)-1, U.S.–Japan Coordinated Program for Masonry Building Research.
- He, L. and Priestley, M.J.N. (1992). Seismic Behavior of Flanged Masonry Shear Walls, TCCMAR Report 4.1-2, U.S.–Japan Coordinated Program for Masonry Building Research.
- IBC (2000). International Building Code, International Code Council, Falls Church, VA.
- IMI (1985). Mexico Earthquake: September, 1985, International Masonry Institute, Annapolis, MD.

- Jalil, I., Kelm, W., and Klingner, R.E. (1993). Performance of masonry and masonry veneer buildings in the 1989 Loma Prieta earthquake, in *Proceedings of the Sixth North American Masonry Conference*, Drexel University, Philadelphia, PA, June 6–9, 1993.
- Klingner, R.E., Villalba, R., Blondet, M., and Mayes, R.L. (1990). Masonry structures in the Chilean earthquake of March 3, 1985: behavior and correlation with analysis, *Masonry Soc. J.*, 9(1), 20–25.
- Leiva, G. and Klingner, R.E. (1994). Behavior and design of multi-story masonry walls under in-plane seismic loading, *Masonry Soc. J.*, 13(1), 15–24.
- Lew, H.S., Leyendecker, E.V., and Dikkens, R.D. (1971). *Engineering Aspects of the 1971 San Fernando Earthquake*, Building Science Series 40, U.S. Department of Commerce, National Bureau of Standards.
- MSJC (2002a). *Building Code Requirements for Masonry Structures (ACI 530-02/ASCE 5-02/TMS 402-02* of American Concrete Institute, American Society of Civil Engineers, and The Masonry Society). Masonry Standards Joint Committee.
- MSJC (2002b). *Specifications for Masonry Structures (ACI 530.1-02/ASCE 6-02/TMS 602-02* of American Concrete Institute, American Society of Civil Engineers, and The Masonry Society). Masonry Standards Joint Committee.
- NAMC (1985). *Proc. Third North American Masonry Conference*, University of Texas, Arlington, TX, June 3–5, 1985, The Masonry Society, Boulder, CO.
- NAMC (1987). *Proc. Fourth North American Masonry Conference*, University of California, Los Angeles, CA, Aug. 16–19, 1987, The Masonry Society, Boulder, CO.
- NAMC (1990). *Proc. Fifth North American Masonry Conference*, University of Illinois at Urbana-Champaign, June 3–6, 1990, The Masonry Society, Boulder, CO.
- NAMC (1993). *Proc. Sixth North American Masonry Conference*, Drexel University, Philadelphia, PA, June 7–9, 1993, The Masonry Society, Boulder, CO.
- NAMC (1996). *Proc. Seventh North American Masonry Conference*, University of Notre Dame, Notre Dame, IN, June 2–5, 1996, The Masonry Society, Boulder, CO.
- NAMC (1999). *Proc. Eighth North American Masonry Conference*, University of Texas at Austin, June 6–9, 1999, The Masonry Society, Boulder, CO.
- NEHRP (1997). *NEHRP Recommended Provisions for the Development of Seismic Regulations for New Buildings*, FEMA 222, National Earthquake Hazards Reduction Program, Building Seismic Safety Council, Washington, D.C.
- NEHRP (2000). *NEHRP Recommended Provisions for the Development of Seismic Regulations for New Buildings*, FEMA 368, National Earthquake Hazards Reduction Program, Building Seismic Safety Council, Washington, D.C.
- Noland, J.L. (1990). 1990 Status report: US coordinated program for masonry building research, in *Proceedings, of the Fifth North American Masonry Conference*, University of Illinois at Urbana-Champaign, June 3–6, 1990.
- SBC (1999). Standard Building Code, Southern Building Code Congress International, Birmingham, AL.
- Seible, F., Hegemier, A., Igarashi, A., and Kingsley, G. (1994a). Simulated seismic-load tests on full-scale five-story masonry building, *J. Struct. Eng.*, 120(3), 903–924.
- Seible, F., Priestley, N., Kingsley, G., and Kurkchubashe, A. (1994b). Seismic response of full-scale five-story reinforced-masonry building, *J. Struct. Eng.*, 120(3), 925–947.
- Shing, P.U.B. and Klingner, R.E. (1997). Analysis of Masonry Structures, in *Monograph on Nonlinear Analysis of Building Structures*, ASCE Committee on Methods of Analysis, American Society of Civil Engineers, chap. 6.
- Supernant, B.A. (1989). A floor a week per tower, *Masonry Const.*, 2(11), 478–482.
- Tena-Colunga, A. and Abrams, D.P. (1996). Seismic behavior of structures with flexible diaphragms, *J. Struct. Eng.*, 122(4), 439–445.
- TMS (1989). *Proc. International Seminar on Evaluating, Strengthening, and Retrofitting Masonry Buildings*, Construction Research Center, The University of Texas at Arlington, Oct. 1989, The Masonry Society, Boulder, CO.

- TMS Nisqually (2001). Performance of Masonry Structures in the Nisqually, Washington Earthquake of February 28, 2001, Hamilton, H.R. III, Ed., Technical Report 301-01, The Masonry Society, Boulder, CO.
- TMS Northridge (1994). Performance of Masonry Structures in the Northridge, California Earthquake of January 17, 1994, Klingner, R.E., Ed., Technical Report 301-94, The Masonry Society.
- Tomazevic, M. and Weiss, P. (1994). Seismic behavior of plain- and reinforced-masonry buildings, *J. Struct. Eng.*, 120(2), 323–338.
- UBC (1943). Uniform Building Code, Coastal Conference of Building Officials.
- UBC (1997). Uniform Building Code, International Conference of Building Officials, Birmingham, AL.

18

Recent Developments in the Seismic Design and Construction of Woodframe Buildings

18.1	Introduction.....	18-1
18.2	Overview of Woodframe Building Behavior	18-1
	Wood as a Construction Material • Introduction to Woodframe Buildings • Seismic Performance	
18.3	Design Practice	18-8
	Engineered Design • Prescriptive Design • Mixed Engineered and Prescriptive Design	
18.4	Recent Research in Seismic Resistance	18-14
	Full Building Testing and Analysis • Shear Wall Research • Other Component and Connection Research • Analysis Tools	
18.5	Directions for Design	18-28
	Short-Term Design Directions • Long-Term Design Directions • Existing Buildings	
18.6	Future Challenges	18-30

Kelly E. Cobeen

18.1 Introduction

Wood is by far the most prevalent building construction material in the United States. This chapter introduces wood as a construction material and reviews the seismic performance of woodframe buildings. Because an understanding of design methods contributes to understanding of seismic performance, this chapter explains design methods, including engineered design, prescriptive methods and combined methods. Recent research efforts that have greatly increased understanding of seismic performance are summarized, including testing and analysis of full buildings, components and interconnections. Finally, the chapter presents implications of research results for design and retrofit, and proposes future challenges for woodframe building research and design.

18.2 Overview of Woodframe Building Behavior

18.2.1 Wood as a Construction Material

The abundance of wood made it an obvious choice for building construction from first settlement of the United States (Perlin, 1989), and it has remained prevalent since. As a result a very large portion of the

existing building stock is of woodframe construction. *Estimating Building Stocks for Earthquake Mitigation and Recovery Planning* (Malik, 1995) states that “the general range of the fraction of wood structures to total structures seems to be between 80 and 90% in all regions of the United States, for example being 89% in Memphis, Tennessee and 87% in Wichita Kansas.” Woodframe construction makes up approximately 99% of residential construction in California, and according to county assessor data, 96% of all construction in Los Angeles County.

From the standpoint of construction, the light weight and small size of individual wood framing pieces accommodates a wide range of construction project sizes and allows easy installation by a single carpenter or construction crew. The ease with which wood framing can be modified on site makes wood readily adaptable to specific framing and detailing conditions. When considering engineering design properties, for many lumber grades, the ratio of tension, compression and flexural strength to unit weight make wood one of the most weight efficient structural materials available. Wood species commonly used for construction have weights in the range of 25 to 35 pounds-per-cubic foot (pcf), while providing flexural allowable stresses in excess of 2000 pound-per-square-inch (psi) for small members. This strength to weight ratio is of particular interest and advantage in areas of high-seismic hazard, since seismic forces are largely proportional to the weight of the supported structure.

The appealing visual appearance of wood makes it popular for use in buildings, including educational buildings, civic buildings, churches and homes, where the wood structure can also serve as a visual element.

Over the twentieth century, wood construction adapted to changes brought on by construction standardization, prefabrication and changes in timber supplies leading to replacement of solid sawn members with engineered wood members, including structural composite lumber, plywood and oriented strand board sheathing and similar products. Among the many text and reference books available addressing wood as a construction material, are The American Institute of Timber Construction's *Timber Construction Manual* (AITC, 1994), *Wood Engineering and Construction Handbook* (Williamson and Faherty, 1999), *APA Engineered Wood Handbook* (Williamson, 2001), *Wood Handbook* (Forest Product Library [FPL], 1999), *Structural Behavior of Timber* (Madsen, 1992), *Behavior of Timber Connections* (Madsen, et al., 2000) and *Design of Wood Structures* (Breyer et al., 1998).

National consensus standards for design of wood structures include the ANSI/AF&PA's *National Design Specification For Woodframe Construction*, addressing allowable stress design (AF&PA, 2001a), and AF&PA/ASCE Standard 16-95, *Standard for Load and Resistance Factor Design (LRFD) for Engineered Wood Construction* (AF&PA, 1996). These national consensus standards for engineered design are adopted and modified by the U.S. model building codes. In addition national consensus documents for prescriptive construction include the AF&PA's *Woodframe Construction Manual* (AF&PA, 2001b).

18.2.2 Introduction to Woodframe Buildings

A close look at most communities will reveal woodframe buildings serving a large number of uses. The size and construction of these buildings can vary greatly; however, three groups stand out as the most common. The first group is wood light-frame construction, using repetitive 2-in.-nominal-width wall studs and floor and roof framing members. Figure 18.1 provides an illustration of typical components of wood light-frame construction. This construction is highly visible in single and multifamily residential buildings. As far back as the mid-1800s, Victorian residences used light-frame construction much like residential construction today. The group also includes smaller commercial buildings, mixed commercial and residential buildings and schools (Figures 18.2 to Figure 18.4).

A second group of buildings often constructed of wood includes halls, gymsnasiums, churches and similar public occupancy buildings (Figure 18.5). These buildings are characterized by large, open interiors and often by the woodframe structure providing the exposed interior finish. Use of interior beam and column systems, combined with light-frame walls, is common in these buildings. In more recent construction, steel columns or beams or both can be found in lieu of wood posts and beams. Also, bracing systems sometimes include masonry or concrete shear walls.

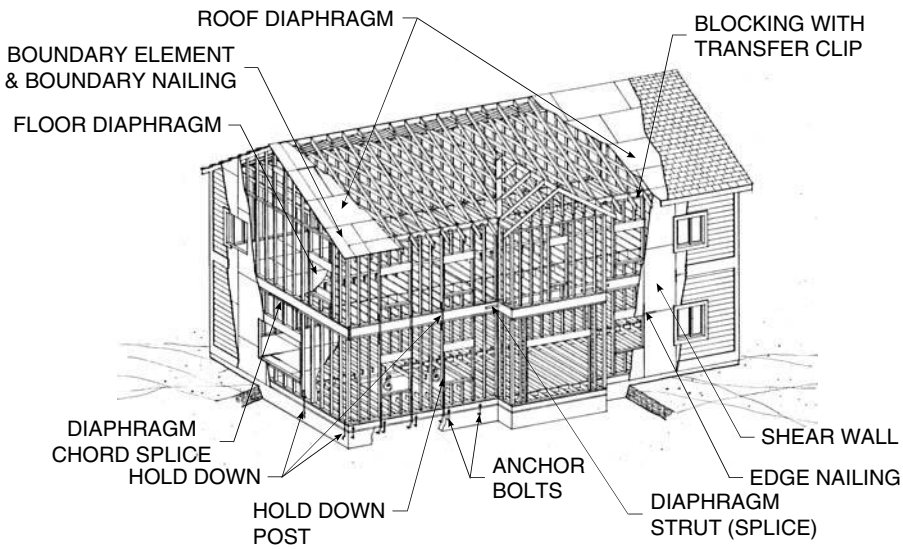


FIGURE 18.1 Typical components of woodframe construction. (From SEAOC, 1997, *Guidelines for Wood Diaphragms and Shear Walls*. With permission.)



FIGURE 18.2 Existing wood frame building and the corner of Ashby and Adeline Streets in Berkeley, CA, residential use.

A third group of buildings includes light industrial and warehouse uses in urban areas and uses ranging from light industrial to barn construction in suburban and rural areas. These buildings commonly have large open interiors with post and beam construction; however, the construction is much more utilitarian than churches and halls. Knee-braces are sometimes provided at the corners of posts and beams to add stiffness to the building frame system. New construction of this building type is no longer common, replaced by more economical prefabricated construction methods and materials. An exception might be the regional use of wood post frame construction.

18-4 *Earthquake Engineering: From Engineering Seismology to Performance-Based Engineering*



FIGURE 18.3 Existing wood frame building at the corner of Ashby and Adeline Streets in Berkeley, CA, mixed commercial and residential use.



FIGURE 18.4 Existing wood frame building at the corner of Ashby and Adeline Streets in Berkeley, CA, mixed commercial and residential use.



FIGURE 18.5 Existing wood frame building at the corner of Ashby and Adeline Streets in Berkeley, CA, public use.

18.2.3 Seismic Performance

For life safety performance of new buildings in areas of high seismic hazard, the philosophy of seismic resistant construction currently incorporated into codes and guidelines (BSSC, 2001; ICBO, 1997; ICC, 2003a) involves the use of systems thought to provide ductile behavior. Ductile behavior can best be characterized as the ability to provide at a defined level of overstrength, a significant inelastic deformation capacity beyond the deformation at yield load (for systems with a defined yield, and at peak load for other systems). According to the Structural Engineers Association of California (SEAOC), *Recommended Lateral Force Requirements and Commentary “Blue Book”* (SEAOC, 1960), the first mention of building system preferences for seismic resistance came from the State of California Office of the State Architect, which in 1933 required increased seismic base shear coefficients for masonry buildings without frames, and in 1937 permitted a lower coefficient for buildings with complete moment-resisting frames. In the earliest SEAOC Blue Book commentary on seismic resistant behavior, the ability of ductile systems to better resist earthquake ground motions was recognized (SEAOC, 1960). In later editions, rules were developed for providing ductile behaviors of materials, starting with concrete frames and concrete shear walls (SEAOC, 1967). Since then, seismic design provisions for areas of high seismic hazard have continued to shift toward a philosophy of providing a ductile failure mechanism.

Irrespective of the guiding philosophy of ductile behavior, a number of well-established systems have until recently been considered categorically acceptable based only on observation of earthquake performance, supplemented by limited component testing. Buildings braced by light-frame shear walls are included in this category. The International Building Code (IBC) permits the use of wood shear walls without a height limit in areas of low to moderate seismic hazard and up to a 65-ft height for areas of high seismic hazard (ICC, 2003a). This is substantially more permissive than for bearing wall systems of other materials and reflects a long history of woodframe design being perceived as providing good seismic performance. Meanwhile, identification of ductile mechanisms and detailing to ensure ductile behavior have not been systematically developed in wood to the extent that they have been in other materials.

In the United States, consideration of earthquake resistance in woodframe buildings can be traced back to the mid-1800s and a series of Northern California earthquakes. *In Building California, Technology and The Landscape* (Corbett, 1998), widespread damage due to urban fires in 1849 and 1850 is cited as creating an 1850s trend toward brick masonry wall construction in San Francisco. In the earthquakes of 1857 to 1868, the brick buildings experienced major damage, while limited damage occurred to other building types, primarily attributed to shoddy construction. This in turn led to a trend toward residential buildings, and particularly mansions, being constructed of wood. Corbin noted, “Balloon-frame buildings generally did not fail in an earthquake because they moved as a unit.” While the residential buildings



FIGURE 18.6 Partial collapse of split-level home in the 1971 San Fernando earthquake. (Source: National Information Service for Earthquake Engineering (NISEE) and University of California Earthquake Engineering Library, Steinbrugge Collection.)

likely did have improved earthquake resistance as compared to unreinforced masonry, they were vulnerable to fire and many San Francisco mansions burned to the ground in the fires following the 1906 San Francisco earthquake. Photographs also indicate that cripple wall failures were experienced in homes in the 1906 San Francisco earthquake (*San Francisco Chronicle*, 1998). The complete collapse of the three-story Hotel Vendome Annex in San Jose and the multistory wood Valencia Street Hotel illustrated the potential for serious damage (Lawson, 1908). From the late 1800s forward, however, woodframe construction appears to have been considered among the more earthquake resistant types of construction.

Although the performance of woodframe construction has generally been very good, earthquakes over the last half-century have repeatedly illustrated some configurations of woodframe buildings to be vulnerable. The 1971 San Fernando earthquake provided evidence that modern woodframe construction could sustain extensive damage and even partial building collapse. As a result of damage experienced by woodframe residences in the 1971 San Fernando earthquake, the Applied Technology Council (ATC) developed a report entitled *A Methodology for Seismic Design and Construction of Woodframe Dwellings* (ATC-4) (ATC, 1976). This report was condensed into *The Homebuilder's Guide for Earthquake Design*, published by the Department of Housing and Urban Development (HUD, 1980) and later updated and published by FEMA (FEMA, 1992, 1998). The Forward to the first printing of the Homebuilder's Guide indicates that 60 million dollars of damage to single-family dwellings occurred due to approximately 12 sec of ground motion in the San Fernando earthquake. The report executive summary notes the conclusion that earthquake monetary losses might be significantly reduced with additional attention to earthquake bracing.

The ATC-4 report provides a summary of observed San Fernando earthquake damage. Primary sources included collapse of cripple walls, separation of split-level homes, absence of effective walls on either side of garage doors (for both one-and two-story houses), inadequate bracing wall lengths leading to shear failure and overturning failure of walls where studs were able to pull off of sill plates. Damage to split-level homes can be seen in Figure 18.6. ATC-4 noted the damaged homes as having been recently constructed using prescriptive requirements, and the report proposes earthquake design methods that could be implemented by nonengineering building designers. Included are simplified methods for calculating building base shears, force distribution by the tributary area method and overturning checks to determine the need



FIGURE 18.7 Damage to multifamily residential building in the 1971 San Fernando earthquake. (Source: National Information Service for Earthquake Engineering (NISEE) and University of California Earthquake Engineering Library, Steinbrugge Collection.)

for tie-down anchors. Not surprisingly, tie-down devices first appeared in manufacturers' brochures in the early 1970s (Simpson Company, 1974). While not specifically recognized in the ATC-4 report, the concept of deformation compatibility between one- and two-story sections, and at split-levels, appears to have played a significant role in the described damage. Not included in the ATC-4 report, but also seen in the San Fernando earthquake was damage to multifamily buildings with open fronts, allowing access to under-building parking at the first story (Figure 18.7).

Sources of information available on woodframe building performance in the 1989 Loma Prieta earthquake include an EERI reconnaissance report (EERI, 1989) and the report of the SEAOC Ad Hoc Earthquake Reconnaissance Committee (SEAOC, 1991). The SEAOC report cites the California Office of Emergency Services as reporting 28,530 residences damaged, 1018 residences destroyed and 7019 persons displaced. Prominent in both reports is the collapse and near collapse of multifamily residential buildings in the Marina District of San Francisco. The worst damage occurred to apartment buildings at the corner of intersecting streets. These buildings were substantially open on two sides at the first story, permitting access to under-building parking, and making the first story weak and highly torsionally irregular (Figure 18.8). Liquefiable soils further exacerbated the building behavior. Similar damage was experienced to a lesser extent in many areas of San Francisco (Figure 18.9). Other observed damage included cripple wall and chimney failures, which were especially common in communities such as Watsonville near the earthquake epicenter. The authors of the SEAOC report clearly differentiated between archaic and modern construction, and concluded that low-rise light-frame residences complying with modern design codes were highly resistant to the moderate seismic shaking generally experienced in this earthquake.

The 1992 Cape Mendocino earthquakes again caused widespread damage to cripple walls as well as to unbraced porches, porch roofs and exit stairs. Performance was aggravated in many cases because post and beam supports for the floor framing were not enclosed (Figure 18.10) or were skirted by spaced sheathing or lattices rather than solid cripple wall sheathing. This support collapse occurred to small and large buildings alike, allowing buildings to fall off of their foundations.



FIGURE 18.8 Typical soft-story apartment building in the Marina District of San Francisco following the 1989 Loma Prieta earthquake (courtesy of Y. Bozorgnia).

Sources of information on performance of woodframe buildings in the 1994 Northridge earthquake include preliminary and final reconnaissance reports by EERI (1994, 1996), reports compiled by city of Los Angeles and SEAOSC committees (LATF 1994a, 1994b, 1994c), case study documents compiled by the California Seismic Safety Commission (Seismic Safety Commission, 1994) and the CUREE-Caltech Woodframe Project (Schierle, 2001). Statistical investigations of damage and repairs are also available from the CUREE-Caltech Woodframe Project (Schierle, 2003).

In Chapter 6 of the EERI Reconnaissance Report (EERI, 1996) Prof. John Hall of Caltech provides an excellent summary of the broad range of damage observed in woodframe buildings, some of the measures suggested as a result of observed damage, and case study buildings. The 1994 Northridge earthquake again illustrated the vulnerability of cripple walls (Figure 18.11) and open front buildings (Figure 18.12), and additionally illustrated that hillside dwellings can pose a collapse hazard (Figure 18.13) causing loss of life. One paper (Hamburger, 1994) estimates that as many as 200 multistory apartment buildings in the San Fernando area with torsional irregularities and soft/weak stories experienced collapse or near collapse. The EERI reconnaissance report notes 157 significantly damaged hillside houses, 15 of which either collapsed or had to be demolished.

In addition to the previously observed vulnerable building configurations, of note in the Northridge earthquake was significant damage to engineered buildings meeting the design requirements of recent building codes. Types of damage included splitting of foundation sill plates, splitting and tension failures of tie-down posts at bolted tie-down devices, some tearing failures of plywood sheathing and widespread separation of stucco from self-furred lath. While these failures generally did not result in a life-safety threat, they did cause temporary or long-term loss of housing units. Further, they resulted in serious questions regarding the adequacy of modern engineered design practice and the levels of construction inspection and observation required by building codes.

18.3 Design Practice

To discuss the seismic performance of woodframe buildings, it is helpful to have an understanding of design methods represented in the existing building stock. Woodframe building design has gone through (and in some cases is still going through) transition between prescriptive and engineered design methods.



FIGURE 18.9 Damage to multifamily residential building in the 1989 Loma Prieta earthquake.



FIGURE 18.10 Racked post and beam supports on house without cripple wall sheathing in the 1992 Cape Mendocino earthquake.

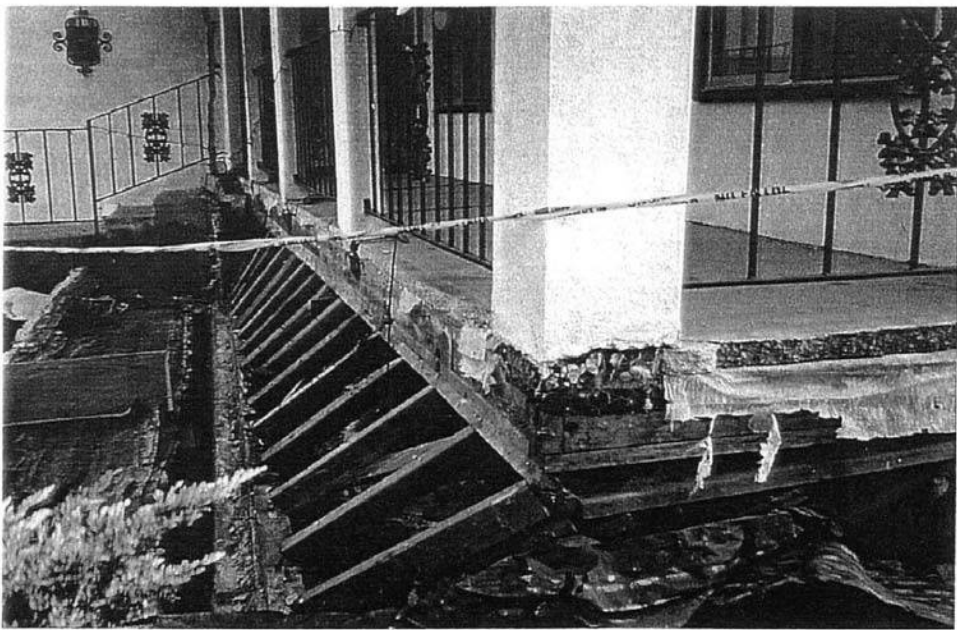


FIGURE 18.11 Single-family residence with collapsed cripple walls in the 1994 Northridge earthquake (courtesy of EERI and City of Los Angeles Department of Building and Safety). (From EERI, *Earthquake Spectra*, January 1996. With permission.)



FIGURE 18.12 Apartment building with collapsed open-front story in the 1994 Northridge earthquake (courtesy of R. Reitherman).



FIGURE 18.13 Aerial view of three collapsed hillside homes in the 1994 Northridge earthquake. (courtesy of EERI and City of Los Angeles Department of Building and Safety). (From EERI, *Earthquake Spectra*, January 1996. With permission.)

Prescriptive methods generally involve selection of members and bracing from tables, and use schedules of minimum fastening. In contrast, engineered methods rely on estimated member stresses due to earthquake, which are compared to allowable member stresses or allowable fastener loads.

Woodframe construction in the United States comes from a tradition of prescriptive construction. Steinbrugge et al. (1996) discuss the evolving standard of care used in design and construction of multifamily woodframe buildings in California from the 1950s through the 1990s. Estimates are provided of when various engineering design issues started being considered. The paper suggests that in multifamily housing, many of the design details associated with providing a complete load path were not being considered until the 1970s, and might not have been consistently considered until the 1990s. In the 1950s and 1960s an engineered seismic design would have included little more than checking of shear wall unit shears, while today it commonly involves detailed checking of shear transfer in and out of each shear wall and diaphragm component, checking of local and global overturning and many additional checks. Design of nonresidential buildings can generally be anticipated to have transitioned over a time period similar to multifamily residential, while the transition of single-family residential lagged behind multifamily residential. Even today many one- and two-family residential buildings are partially or completely constructed from prescriptive provisions.

The Steinbrugge paper cites damage from the 1971 San Fernando earthquake as justification for 1976 and 1979 Uniform Building Code changes giving the building official greater ability to require an engineered design in lieu of prescriptive design. The 1971 San Fernando earthquake and resulting damage to single-family dwellings is further detailed in the ATC-4 report as a reason for encouraging the use of engineering concepts in residential construction.

18.3.1 Engineered Design

Today a woodframe building with an engineered design has a calculated load path provided from every part and portion of the structure to the point where the seismic forces can be transferred to the supporting soils, with consideration given to sliding and overturning of each component. Until recently seismic

design of wood structures has exclusively used allowable stress design methods. An LRFD design specification and supplements became available in 1996 but are still not commonly used. Engineered design mostly uses rational mechanics-based approaches to develop load paths to the foundation. However, there are a few load path details that are not fully rationalized, resulting in variation in some aspects of design practice. Rather than trying to predict the detailed complexity of how the building will resist loads, the engineer's role is seen as providing an engineered load path within the building that is adequately proportioned to carry code-specified loads. In providing this engineered load path, the designer is designating some of the walls to be structural while not considering the contribution to resistance provided by other walls. As a result, the estimation of building behavior based on the "designated structure" does not necessarily provide good prediction of building behavior.

Calculation of seismic design forces for woodframe buildings almost exclusively uses linear equivalent lateral force procedures, although nonlinear static (push-over) methods are starting to be explored for woodframe buildings (Filiatrault and Folz, 2002). When the approximate periods of buildings are calculated in accordance with building code equations, they are most often found to correspond to the acceleration-controlled plateau of the code design spectrum. The vertical distribution of seismic forces follows the triangular distribution generated by building code equations. Horizontal distribution of seismic forces to the various shear wall and other vertical elements most commonly uses a tributary area method. Some building departments, however, are starting to require use of rigid diaphragm distribution or an envelope of worst-case forces from both flexible diaphragm (tributary area) and rigid diaphragm distribution methods. A survey of requirements imposed by Northern California building departments illustrates current practice (Mochizuki and Fennel, 2002).

Shear walls are usually the primary elements acting to resist forces and provide energy dissipation in woodframe shear wall buildings. The fastening of the shear wall sheathing to the wood framing is the primary mechanism for energy dissipation and ductility. Modes of dissipation include fastener bending, wood crushing and tearing the sheathing at the fastener shank and under the fastener head. Connection of shear walls for sliding and overturning is most commonly based on code equivalent static forces. However, the NEHRP Provisions (BSSC, 2001) suggest that the overturning connections be made stronger than the expected strength of the shear wall component to ensure that the shear wall component remains engaged through the ground motion event.

Until recently, engineered design practice for shear walls most commonly modeled each full-story height wall segment as a single-story cantilever from the wall base. This chapter will refer to this wall type as a segmented shear wall. Shear and overturning reactions from the cantilever are accumulated over multiple stories and transferred to the foundation.

An alternative design approach, also used over the last 20 years, considers the full wall including the openings and provides for full continuity around the openings (somewhat like development of coupling beams) (Diekmann, 1986, 1999). In current terminology this would be one of a class called perforated shear walls, and in particular would be considered an engineered, detailed, perforated shear wall. The basis of design is analysis of free-body diagrams, with additional detailing such as strapping, blocking and additional sheathing nailing to resist shear, tension and compression forces in the vicinity of the opening.

A new type of perforated shear wall design approach has been developed and incorporated into building codes recently. Rather than adding detailing to provide continuity around openings, this approach accounts for the somewhat lower effectiveness of providing sheathing above and below openings without special detailing. Even without special detailing for continuity, the sheathing provides added strength and deflection control over that provided by full-height segments alone. The intent of the perforated shear wall provisions is to reduce the level of detailing and connection hardware, while recognizing the level of continuity inherent in light-frame construction. Code provisions exist for engineered design of perforated shear walls (BSSC, 2001). In addition this concept is partially incorporated into prescriptive provisions in the IRC (ICC, 2003b). See Figure 18.14 for illustrations of shear wall types and anchorage.

In spite of the fact that building codes include story drift limits for all seismic bracing systems, until recently, designers of woodframe shear wall buildings seldom calculated shear wall deflections, much less

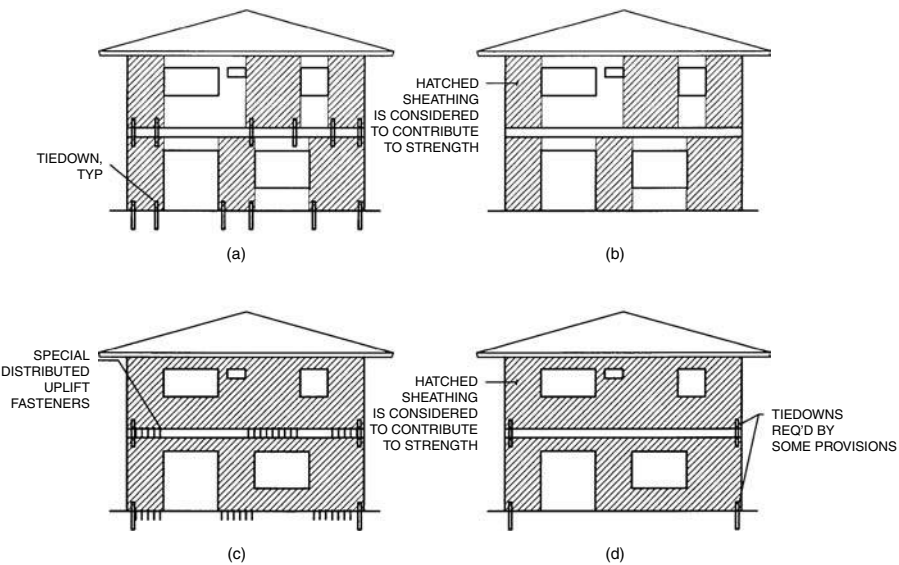


FIGURE 18.14 Diagram of shear wall types. (a) Engineered segmented shear wall; (b) prescriptive braced wall panels; (c) engineered perforated shear wall; (d) prescriptive perforated wall bracing. (From Cobeen et al., 2003, CUREE Publication W-30, CUREE, Richmond, CA. With permission.)

compared to permitted story drifts. Rather, aspect ratio (wall height to wall pier width) limitations were believed to provide adequate drift control. Following observations of damage to slender shear walls in the 1994 Northridge earthquake (EERI, 1996) and testing of slender walls (Shepherd and Allen, 1995), concern developed regarding excessive shear wall deflections. As a result of these recent observations and the increased attention given to rigid and flexible diaphragm classification and horizontal force distribution, engineers are now more frequently calculating shear wall deflections. This has also focused attention on the equations used to calculate shear wall deflection for wood structural panel shear walls. In response, APA — The Engineered Wood Association (formerly the American Plywood Association) has made additional guidance on shear wall deflection calculations available to designers (APA, 2001).

Engineered design of woodframe structures involves design of a number of elements and connections to introduce seismic forces into shear walls at the top and transfer the forces back to the base. Such elements include collector members, accumulating forces from the diaphragms and pulling them into shear walls and shear transfer connections. Starting with the 1997 UBC, two special ductile detailing provisions were imposed on all construction materials, including woodframe, in response to observed earthquake damage. These provisions use a capacity design concept in which member forces are amplified by an overstrength factor to check capacity and ensure the assumed ductile response by eliminating undesirable failure modes. One provision requires a capacity check of collector elements. The other requires a capacity check of beams and columns supporting shear walls and other vertical elements that do not extend down through the lowest story (discontinued elements).

With the exception of the few provisions addressing capacity and desired failure mode, seismic design of woodframe buildings is still largely governed by linear, equivalent static forces and allowable stress design concepts, which over time have yielded generally good performance. Little rational technical explanation beyond historical performance, however, has been produced to provide justification.

18.3.2 Prescriptive Design

Structures meeting the scope limitations of code conventional light-frame construction provisions are allowed to be designed using prescriptive rules rather than engineering design procedures. Included in the prescriptive rules are prescriptive provisions for bracing to resist lateral forces. In Uniform Building

Code editions between 1970 and 1991, and through the most recent CABO One- and Two-Family Code (CABO, 1998) prescriptive seismic bracing involved the installation of wall bracing panels, not less than 4-ft long, in the walls that happened to be included in the building architectural design. Following the 1971 San Fernando earthquake, the codes added language allowing building officials to require engineered design for buildings of unusual size and shape; however, these terms were not defined and the requirement for design was seldom invoked. The Applied Technology Council's *A Methodology for Seismic Design and Construction of Woodframe Dwellings* (ATC-4) (ATC, 1976), *The Homebuilder's Guide for Earthquake Design* (HUD, 1980) and *The Homebuilder's Guide to Seismic Resistant Construction* (FEMA, 1992, 1998) had hoped to introduce basic engineering concepts into prescriptive residential design; however, bracing continues to use fully prescriptive provisions developed for the smaller, more box-like turn of the century bungalow houses and the modest ranch houses of the 1940s and 1950s. In the report of the SEAOC Ad Hoc Earthquake Reconnaissance Committee following the 1989 Loma Prieta earthquake, concern was raised regarding the divergence of prescriptively designed buildings from those with an engineered design (SEAOC, 1991).

In the 1994 UBC, prescriptive seismic provisions were modified to reduce the imbalance between seismic bracing designs resulting from engineered and prescriptive methods (Bossi and Cobeen, 1996). The provisions approached the imbalance from several directions. First, unusual size and shape were given more specific definitions to improve enforceability. Second, it was required that a system of interior and exterior bracing be provided to break the building into a series of boxes, not exceeding 25 ft in plan dimension in areas of high seismic hazard, and 35 ft in areas of lower seismic hazard. The minimum length of required bracing at each of the required walls was not increased. These changes reduced but did not eliminate, the overstress that would be calculated using engineered seismic design provisions. For wind loading, significant levels of overstress generated using engineered wood design provisions were left unaddressed. Prescriptive seismic provisions with an engineered basis were also developed in the NEHRP Provisions (BSSC, 2001).

The development of the International Residential Code (IRC) (ICC, 2000a, 2003a) as the intended single national code for prescriptive one- and two-family residential construction created the need to consolidate the many prescriptive requirements for type and amount of lateral force bracing. Included in the IRC is a compromise between methods with a more rigorous basis and the still widely used CABO methods. When adopted, these provisions will introduce large changes for areas of the country that did not adopt the 1994 and later editions of the UBC. Some of the latest thinking in engineered design has been incorporated into the IRC provisions, including the perforated shear wall concept.

18.3.3 Mixed Engineered and Prescriptive Design

Today the prescriptive design provisions of the UBC, International Building Code (IBC) and IRC allow for the engineering of individual nonconforming portions of residences that otherwise meet the limitations of prescriptive construction provisions. A common location for use of an engineered component is the slender wall at either side of a garage door opening. The use of engineered design on one wall line epitomizes the practice of designing an element without consideration of global building behavior. The NEHRP provisions (BSSC, 2001) attempt to address this issue with language requiring that an engineered element have force and deformation behavior similar to the prescriptive element being replaced.

18.4 Recent Research in Seismic Resistance

Following the 1994 Northridge earthquake, the state of knowledge regarding seismic performance revealed that little effort had been invested in understanding or improving performance of woodframe construction. A number of research efforts have occurred since, providing an improved overall picture of building performance, and detailed information on a wide variety of components and interconnections. A report developed by the CUREE-Caltech Woodframe Project synthesizes a number of research results and recommendations for use by designers and code developers (Cobeen et al., 2003). This section



FIGURE 18.15 UC San Diego two-story house, Phase 9, without finishes. (From Fischer et al., 2001, CUREE Publication W-06, CUREE, Richmond, CA. With permission.)

introduces recent full-building and shear wall studies and describes some striking results, makes note of component and connection research and introduces efforts in the development of analysis tools

18.4.1 Full Building Testing and Analysis

Over the past several years, significant progress has been made in quantifying full-building seismic performance for United States wood light-frame construction, including four testing projects and an analysis project. As part of the CUREE-Caltech Woodframe Project, two full-building shake table tests were conducted: a two-story house at UC San Diego and a three-story apartment building at UC Berkeley. The University of British Columbia (UBC) and Simpson Strong-Tie have tested a two-story house on the UBC shake table, and CSIRO Australia and the National Association of Home Builders tested a one-story house. The results of testing and analysis suggest the need to rethink current seismic design methods.

Testing of the Woodframe Project's two-story single-family residence was conducted at UC San Diego using a uni-axial shake table (Fischer et al., 2001). The house had an engineered design in accordance with the 1994 Uniform Building Code. The objective of testing was quantification of seismic performance and demand for an example of recent construction. In addition to physical observations, nearly 300 digital instruments were provided on the building to record forces, accelerations and displacements over the duration of the tests. To optimize information generated from the shake table testing, the house was tested in a number of different configurations (phases). All of the phases were related to the same overall building size and geometry, but included variations in door and window openings, presence or absence of overturning restraint and other load-path connections and application of finish materials. Phases 9 and 10 had a 3-ft wide pedestrian door centered in the 16-ft long West wall and a 10-ft garage door opening centered in the East wall. Test Phase 9 was conducted without finish materials, while Phase 10 was conducted with a stucco exterior finish and gypsum wallboard interior finish (Figure 18.15 and Figure 18.16). The total building mass was kept constant for all phases.

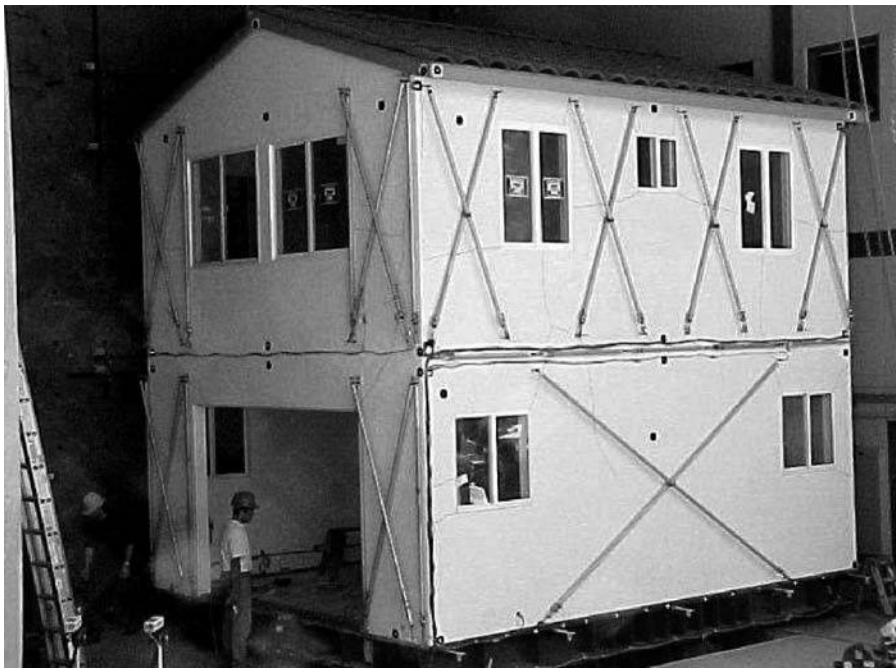


FIGURE 18.16 UC San Diego two-story house, Phase 10, with finishes. (From Fischer et al., 2001, CUREE Publication W-06, CUREE, Richmond, CA. With permission.)

Two different 1994 Northridge ground motion acceleration recordings were used. The Canoga Park record was used to represent ground motions without near-fault characteristics. The Canoga Park ground motion was scaled to four different peak ground acceleration (PGA) levels, designated as Levels 1 through 4. For Level 5, the Rinaldi ground motion record was used to represent ground motions with near fault characteristics. This ground acceleration record was used without any scaling, reflecting the as-recorded 0.89g PGA. The Level 4 ground motion (0.50g PGA) was a representation of the code-anticipated earthquake demand for California nonnear fault conditions. Ground motions for the experimentation were drawn from the CUREE testing protocol developed by Krawinkler et al. (2001).

Testing of a three-story woodframe apartment building was conducted on the tri-axial shaking table at UC Berkeley's Richmond Field Station (Mosalam, 2003). The full-scale three-story apartment building is representative of a “tuck-under parking” apartment building, where some or all of the ground floor area is used for parking instead of living space. The building design replicated 1960’s construction, when many apartments of this type were constructed. The objective of the testing was study of retrofitted building performance. Figure 18.17 shows the test structure with the open front at the first story, where two steel pipe columns support gravity loads.

Phases were again used to describe variations in configuration for the shake table building. For Phase I, the building was tested with framing and structural sheathing in place, but without finish materials or the steel moment-resisting frame retrofit of the open front (Figure 18.17). For Phase II, the building was tested with stucco and gypsum board finish materials in place over the structural framing and plywood sheathing and windows and doors were installed. In addition, a steel moment-resisting frame was provided as a retrofit for the ground floor open front condition (Figure 18.18). For Phase III, the building was tested with stucco and gypsum board finish materials in place over the structural framing and plywood sheathing. The steel moment-resisting frame provided as a retrofit in Phase II was removed for Phase III testing. No repairs were made to the essentially cosmetic stucco cracking that occurred during Phase II testing. Test Levels 1 through 4 used in the UC Berkeley apartment were the same as the UC San Diego house. The Northridge Rinaldi record was used for a near-fault ground motion, with the PGA



FIGURE 18.17 UC Berkeley apartment, Phase I without finishes. (From Mosalam, 2003, CUREE Publication W-19, CUREE, Richmond, CA. With permission.)

scaled to 0.60g instead of 0.89g. While the UC San Diego shake table input motion was one degree of freedom, the UC Berkeley input allowed for six degrees of freedom. As with the UC San Diego house, several qualifications need to be kept in mind when considering test results including building size and high construction quality.

Also of interest is shake table testing of a two-story house conducted by the University of British Columbia and Simpson Strong-Tie (Pryor et al., 2000). The test objective was investigation of full-building behavior with and without inclusion of proprietary slender shear wall components. The building size, construction and testing methods closely paralleled the UC San Diego house testing. Another testing effort, conducted at approximately the same time as Woodframe Project testing, involved full-building testing of a one-story residence by CSIRO, Australia for the National Association of Home Builders (NAHB) Research Center (Paevere, 2002). This testing studied force distribution in the one-story building using quasi-static monotonic and cyclic displacement-based loading. The testing was conducted without finish materials and was for the purpose of calibrating analysis tools.



FIGURE 18.18 UC Berkeley apartment, Phase II with finish materials and steel moment-resisting frame.

Full-building analytical studies were conducted on Woodframe Project Index Buildings using three-dimensional nonlinear time-history analyses. The index buildings are prototype buildings developed by the Woodframe Project to represent four different residential building types. Included are a small one-story single-family house representing construction from around 1950, a larger two-story single-family residence representing recent construction, a townhouse representing recent construction and an apartment building with tuck-under parking representing construction from the 1960s. Design assumptions, descriptions and illustrations of the index buildings and their complete CAD design drawing files are documented in Reitherman and Cobeen (2003). Three different levels of construction quality, described by the loss estimation researchers (Porter et al., 2002), were used to study the effect of quality on building performance.

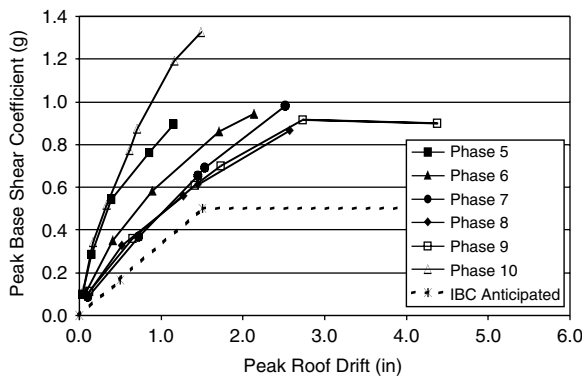


FIGURE 18.19 Load-deflection behavior for UC San Diego house. Phase 9 is final configuration without finish materials. Phase 10 is final configuration with finish materials. No failures were observed. Curves end at stop of testing. (From Cobeen et al., 2003, CUREE Publication W-30, CUREE, Richmond, CA. With permission.)

Analysis used the commercially available program RUAUMOKO (Carr, 1998), in combination with shear wall hysteretic parameters from the Woodframe Project analysis program CASHEW (Folz and Filiatrault, 2001) and available experimental shear wall data. “Pancake” models were developed, in which each horizontal diaphragm was modeled as a semi-rigid plane (pancake), and each wall was modeled as a nonlinear spring, connecting the diaphragm to a diaphragm below. Significant effort went into the description of wall hysteretic parameters to reflect the pinching and degrading behaviors common to wood shear wall components. Recorded ground motion records were used as input for nonlinear time-history analysis. The 1994 Northridge Canoga Park record, scaled to a PGA of 0.5g, was run by the modelers (Isoda et al., 2002), followed by running of a suite of earthquake ground motions for the loss estimation study (Porter et al., 2002).

The primary purpose for development of the index buildings was research of loss estimation methodologies. The loss estimation study used assembly based vulnerability techniques (Porter and Kiremidjian, 2001a; Porter et al., 2001b) that relied on very specific building descriptions. In addition to loss estimation, the analysis data contributed significantly to an understanding of building behavior from a designer’s perspective. Records of force and deformation demands were developed using nonlinear time history analysis with ground motion records as input. The resulting global building demands and distributions of demand generally repeated the patterns seen in shake table testing, as discussed in the following discussion of two significant results.

The most striking outcome from full-building testing and analysis is the impact of finish materials in creating high-force, low-deformation building behavior. Figure 18.19 illustrates load-deflection behavior for Phases 9 and 10 of the UC San Diego house. Plotted on the horizontal axis is the peak roof displacement recorded for each combination of phase and level and on the vertical axis is the peak base shear coefficient recorded for each combination of phase and level. Each data series can be thought of as an approximate pushover curve. For Phase 9 and the top two force levels (Levels 4 and 5), the building could be described as having a ductile (yield) mechanism since there is a significant increase in deformation with a corresponding very slight drop in peak base shear coefficient. Phase 10, in contrast, shows some softening but no sign of yielding and no limitation of base shear coefficient, as might occur if a ductile mechanism had developed (an increase in drift without a resulting increase in base shear coefficient would suggest a ductile mechanism). Figure 18.20 illustrates similar behavior for the UC Berkeley apartment building. In Phase I, without finish materials, the base shear coefficient is eventually limited by a ductile (yield) mechanism, whereas with finish materials in place, a mechanism is not observed even though very high base shear coefficients occur. Again, an increase in drift without a corresponding increase in base shear coefficient would be considered indicative of a mechanism.

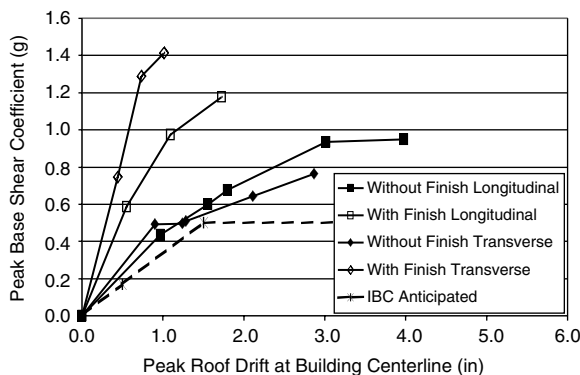


FIGURE 18.20 Load-deflection behavior for UC Berkeley apartment building. Phase I is configuration with no finish materials, Phase III is configuration with finish materials. No failures were observed. Curves end at stop of testing. (From Cobeen et al., 2003, CUREE Publication W-30, CUREE, Richmond, CA. With permission.)

With the finish materials considered, the very high building strength and stiffness can help to explain the generally good performance of woodframe buildings observed in earthquakes to date. The lack of a ductile (yielding) mechanism within the observed range of seismic demand, however, raises concerns in areas of high seismic hazard. The high level of overstrength makes it difficult to pursue the provision of weak links as an approach to providing predictable seismic behavior. The lack of a ductile mechanism observed in the two full building tests at base shear force coefficients in excess of 1.3g does not of itself show brittle behavior. In fact, failure was not observed in either building with finish materials in place and within the range of ground motions run for the Woodframe Project, limited by the shake table capabilities. Brittle failure modes were observed in some component tests that included stucco finishes, suggesting that with additional shake table capacity, brittle failures might have been seen in the shake table buildings. In fact, brittle stud failures were eventually observed in one wall of the UC Berkeley apartment building. Components tests observed to have brittle failures include Gatto and Uang (2002) Tests 17 and 18.

Index building analysis results provide further confirmation of the generally low roof drift ratios when finish materials are considered, with the drifts for the Level 4 ground motion ranging from 0.007 to 0.010 h. Calculated estimates of building deflections have to date primarily only considered the bare wood structure. For the UC San Diego house, the roof drift calculated in accordance with the 2000 IBC (ICC, 2000a) considering the bare wood structure, would be approximately 5.5 in., giving a drift of 0.0264 h for a force level similar to test level four. This is more than twice the observed drift for the bare wood structure and more than 10 times the drift with finishes.

Recently, development of seismic design provisions and systems has been based on achieving a predictable level of overstrength and being able to sustain significant inelastic deformations. In a simplistic sense, the expected deformation capacity can be envisioned as the C_d deflection amplification factors in the NEHRP and IBC R factor tables (BSSC, 2001; ICC, 2000a), which range up to 6.5. This can be seen in the idealized IBC load-deflection curve in Figure 18.19. Figure 18.19 and Figure 18.20 suggest that behavior can be significantly different in woodframe buildings, since higher forces and lower deformations are seen. Without finish materials, the IBC anticipated behavior occurs, but the overstrength is considerably higher than would be anticipated. With finish materials, the behavior is more in line with that of materials the code would assign very low R factors (indicating low anticipated ductility), and that code developers would discourage or seek to prohibit in areas of high seismic hazard.

A second striking outcome of full-building testing and analysis is the repeated observation of a concentration of deformation demand in the first story of woodframe buildings when finish materials are included. The result is a soft story that is often not recognized in story drift calculations based on the bare wood shear wall system. Results from the UC San Diego house testing and Index Building

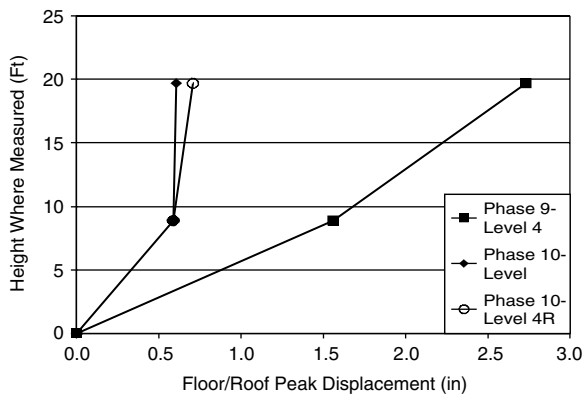


FIGURE 18.21 Vertical distribution of deformation demand in UC San Diego House. (From Cobeen et al., 2003, CUREE Publication W-30, CUREE, Richmond, CA. With permission.)

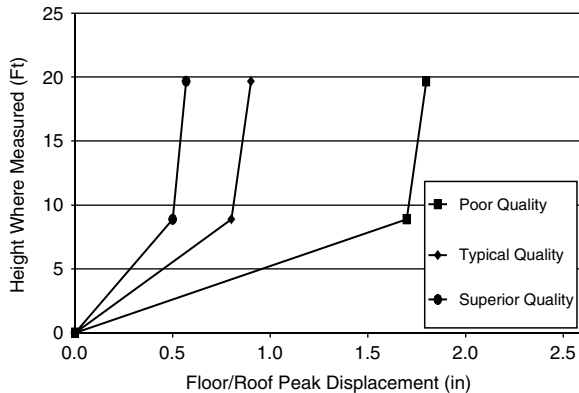


FIGURE 18.22 Vertical distribution of deformation demand in Large House Index Building considering three levels of construction quality. (From Cobeen et al., 2003, CUREE Publication W-30, CUREE, Richmond, CA. With permission.)

analysis provide illustrations of concentration of deformation demand. Figure 18.21 shows the vertical distribution of peak deformation demand for Phases 9 and 10 of the UC San Diego house. Calculations in accordance with the 2000 IBC provisions predict 2.4 in. of drift at the second floor and 5.5 in. at the roof, a fairly uniform distribution of drift. The IBC equations do not come close to predicting the Phase 10 soft first story behavior. Figure 18.22 shows the vertical distribution of peak deformation demand for the South wall of the Large House Index Building (Figure 18.23) based on the Canoga Park ground motion recording, scaled to 0.50g PGA. Analysis results for superior construction (with little or no anticipated flaws), predict the first story drift to be 0.50 in., while the second story drift from analysis is 0.07 in. or one seventh of the first story drift. Vertical distribution results for the other Index Buildings are similar.

Figure 18.21 provides one illustration of the significant contribution of finish materials to creating a concentration of deformation demand and soft story condition. Like many woodframe buildings, the creation of a soft first story is accentuated by the building layout, which places more and larger exterior wall openings and larger rooms in the first story, while including more partition walls in the upper story. In Figure 18.21 it can be seen that the addition of finish materials notably reduced the drift in the first story. The reduction was even greater with addition of finish materials in the second story, however.



FIGURE 18.23 Large House Index Building, South Elevation. (From Isoda et al., 2002, CUREE Publication W-12, CUREE, Richmond, CA. With permission.)

TABLE 18.1 Excerpts from Area Demand Ratio (ADR) Table

ADR Category	Building	Story	ADR Ratio	Test or Analysis Drift (in.)/ Damage Description
Low	Task 1.1.1, Phase 10	2nd	8.2	0.12/cosmetic stucco cracking
	Task 1.5.4, Large house	2nd	11	0.10/cosmetic stucco cracking
Medium	Task 1.1.1, Phase 10	1st	22	0.59/cosmetic stucco cracking
	Task 1.5.4, Large house	1st	28	0.75/cosmetic stucco cracking
High	Task 1.5.4, Apartment	1st	97	4.80/cosmetic stucco cracking
	Element 2 — Northridge Meadows, Building 1	1st	92	4.80/collapse

Figure 18.21 shows almost no drift in the second story with finish materials included. This pattern was also observed in other testing and analysis.

For woodframe construction it should be carefully considered if, and at what point soft stories start posing an elevated hazard level. It should also be considered whether the soft stories are better addressed by trying to eliminate them, which may not be economically feasible, or by requiring detailing appropriate to the high deformation demand. Based on study of concentrations of deformation demand and correlation to the contribution of so called nonstructural finish materials, a characteristic that appears promising as a predictor of soft-story behavior is the relationship of supported building square footage to linear feet of full height wall, called an area demand ratio (Cobeen et al., 2003). An abbreviated set of area demand ratios are shown in Table 18.1.

18.4.2 Shear Wall Research

An understanding of full-building demands and performance must be developed hand in hand with an increased understanding of shear walls as primary components on which performance relies. Recognizing their contribution to performance, past seismic testing for woodframe buildings has almost exclusively focused on shear walls. In recent testing, shear walls have continued to be an important focus. Several very significant shear wall testing efforts were planned or underway at the start of the CUREE-Caltech Woodframe Project. These included an extensive testing program conducted by the City of Los Angeles (CoLA/UCI, 2001); testing of a wide range of wood structural panel shear walls by APA — The Engineered Wood Association; testing involving interior plaster and gypsum wallboard conducted by structural engineer Ben Schmid; and testing conducted at Forintek, Canada and at Virginia Polytechnic Institute

looking at a range of base anchorage configurations. The wealth of information available on wood structural panel shear wall components allowed the Woodframe Project to investigate other shear wall issues and variables, including testing protocols, finish materials and combinations of materials and component relationship to full-building behavior. Woodframe Project results were able to draw from the full range of available testing results.

The City of Los Angeles Department of Building and Safety project tested 36 groups of light-framed shear walls (CoLA/UCI, 2001). The tests were conducted at UC Irvine by Professor Gerard Pardoen, and directed by the CoLA/UCI Light-frame Test Committee of the Structural Engineers Association of Southern California (SEAOSC). The CoLA/UCI testing was conducted on 8 ft by 8 ft shear walls. Only one bracing or finish material was tested at a time, with the exception of one test that combined plywood sheathing and a gypsum wallboard finish. Most of the walls were sheathed on only one face, but a limited number had the same material on both faces.

The CoLA/UCI testing data includes the mean and standard deviation, for both the yield limit state (YLS) and strength limit state (SLS), for a series of wood structural panel test variables. The yield limit state is defined by the SEAOSC/SPD testing protocol (SEAOSC and CoLA, 1997) as occurring when a drop of capacity of more than 5% occurs between the backbone curves represented by the first and last excursions to a given displacement. The authors of the CoLA/UCI report use the results of testing to propose a new method of assigning shear wall allowable unit shears, based on the CoLA/UCI definition of yield limit state. As a result of this methodology, reductions in allowable unit shears have been adopted by the City of Los Angeles, but, to date, not by others.

Woodframe Project results provide ratios for converting values of peak capacity and deflection at peak capacity between the SEAOSC/SPD and the CUREE Ordinary Protocols. The choice of loading protocol has been seen to significantly affect the peak capacity and the deformation at peak capacity. The CoLA/UCI strength limit state data suggests a factor on the order of 2.3 between currently tabulated allowable unit shears and peak capacities for wood structural panel shear walls. Testing by Gatto and Uang suggests an increase in peak capacity of approximately 1.3 for the CUREE Ordinary protocol as opposed to the SEAOSC/SPD protocol. This suggests a factor of safety on the order of 3 with the CUREE Ordinary protocol, which is in line with common expectations.

Regardless of whether strength or yield limit states are of interest, the CoLA/UCI project has provided a wealth of cyclic test information for wood structural panel shear walls. When considering the CoLA/UCI data, the effect of the nonstandard tie-down devices used in testing should be considered.

Ben Schmid, a Los Angeles area structural engineer, conducted wall component tests with gypsum wallboard and interior plaster over gypsum lath to quantify the cyclic behavior of interior plaster over gypsum lath relative to gypsum wallboard finishes (Schmid, 2002). Boundary conditions used for the testing represent an upper bound on the possible level of confinement. At each end of the walls, a 3.5-in.-wide return of the finish material was provided, backed by a 2×12 framing member. Several rows of fasteners were provided between the finish and the framing over the full height of the returns. At the top of the walls, steel plates were placed tight against the finish materials, providing full bearing. In some tests this detail was also used at the wall bottom. Information on results of this testing were provided to the Woodframe Project, and are available in the compiled comments from the September 2001 Woodframe Project Codes and Standards Workshop (CUREE, 2001b). Test results add characteristics of the interior lath and plaster system to available data.

Since the 1994 Northridge earthquake, APA — The Engineered Wood Association has conducted a very substantial number of cyclic loading tests on wood structural panel diaphragms. Discussion of the tests and results are included in a large number of APA publications including APA Report 154, *Structural Panel Shear Walls* (APA, 2000); APA Report 157, *Wood Structural Panel Shear Walls With Gypsum Wallboard and Door/Window Openings* (APA, 1999); APA Report 158, *Performance of Wood Structural Panel Shear Walls Under Cyclic (Reversed) Loading* (Rose, 1998) and *Diaphragms and Shear Walls Design/Construction Guide* (APA, 2001). Technical notes on additional testing topics are anticipated to be available soon.

Several testing efforts have been conducted at Virginia Polytechnic Institute investigating shear wall behavior as a function of wall anchorage. Salenikovich has investigated the relationship between anchored

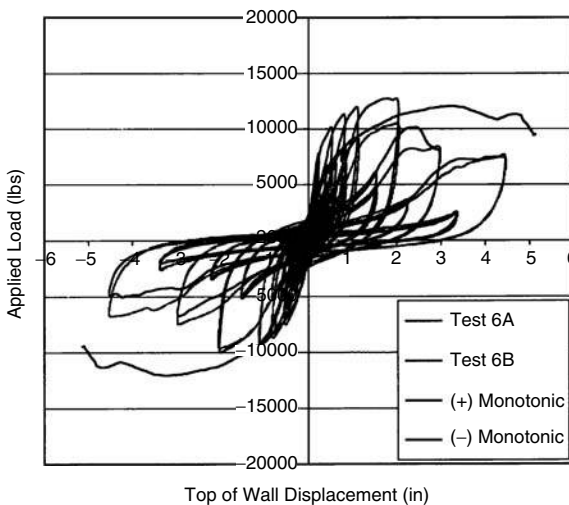


FIGURE 18.24 Variability in identical shear wall component test specimens: Cobeen et al. Tests 6A and 6B. (From Cobeen et al., 2003, CUREE Publication W-30, CUREE, Richmond, CA. With permission.)

and unanchored capacity for walls with lengths varying from 2 to 12 ft (Salenikovich and Dolan, 1999). This testing concluded that without tie-down devices the drop in shear wall capacity varied based on wall length. Further testing at Virginia Polytechnic Institute (Salenikovich and Dolan, 1999) also found that if insufficient shear anchorage is provided when over-turning restraint was absent (as in prescriptive construction), the load capacity of the wall is significantly reduced due to sliding of the wall with respect to the floor framing. In testing an 8-ft by 8-ft shear wall with minimum code sheathing nailing and no tie-down devices, Salenikovich and Dolan found that 128-16d common nails in the bottom plate (an extreme nailing density of 16 nails per linear foot) were required to adequately resist combined sliding and overturning. Based on the current philosophy of forcing the yielding mechanism of shear walls to occur in the sheathing nails, the maximum performance in terms of load capacity, energy dissipation and displacement capacity can only be achieved by ensuring that the bottom of the wall is adequately anchored to resist sliding.

Wood structural panel shear wall testing by Ni and Karacabeyli (2002) explored the influence of both tie-down anchors and vertical dead loads on the capacity of shear wall components. For an 8 ft square shear wall without tie-downs and with no vertical load, the peak capacity was 50 to 60% of the peak capacity with tie-downs. With a vertical dead load of 66% of the horizontal force, the shear wall peak capacity increased to 80% of the capacity with tie downs. With a vertical dead load of 123% of the horizontal load, the peak capacity increased to 85%. This level of vertical load is not typically identified as tributary to a given shear wall in woodframe construction. Testing by Ni and Karacabeyli also examined the effect of shear wall component length on the peak capacity of shear walls without tie-downs. The first anchor bolt was placed at 8 in. from the end of the wall, and then at 16 in. on center. For a 4 ft by 8 ft shear wall the peak capacity without a tie-down was 34% of the capacity with the tie-down. For the 8 ft and 16 ft shear wall lengths the capacities without tie-downs were 59 and 66% respectively. The deflections at peak capacity were reasonably in line with the capacities, not showing the reduced stiffness seen in the Salenikovich testing.

Significant departures from common past testing practice were made in Woodframe Project shear wall component testing. Effects of loading protocol were studied at UC San Diego (Gatto and Uang, 2002). Variables included loading time history, rate of loading and wall materials and combinations of materials. In particular the testing compared the effect of new loading protocols, developed by the Woodframe Project (Krawinkler et al., 2001), to other available loading protocols. The behavior of components can vary tremendously with varying loading histories, rates and materials, including very brittle behavior with a stucco finish. A number of protocol recommendations resulted (Gatto and Uang, 2002).

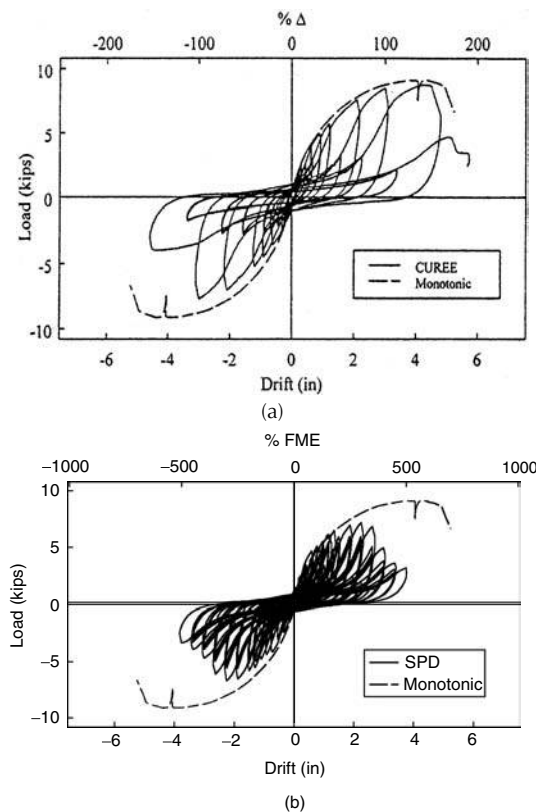


FIGURE 18.25 Variability in shear wall component test results. (a) Gatto and Uang Test 2 using CUREE Ordinary Protocol and (b) Gatto and Uang Test 4 using SEAOSC/SPD Protocol. (From Gatto and Uang, 2002, CUREE Publication W-13, CUREE, Richmond, CA. With permission.)

Shear wall component testing at UC Irvine (Pardoen et al., 2003) also departed from past shear wall testing practice in several respects. First, testing was conducted on a standard 16-ft long wall that replicated one side of the UC San Diego house (Fischer et al., 2001). Within the 16-ft length, configurations included fully sheathed, with a small door opening and with a large door opening. Testing the full wall length made some of the boundary conditions more realistic than they would have been with stand-alone wall piers. Second, a wide variety of structural and finish materials were tested alone and in combination, providing insight into the behavior of a finished building. Finally, some wall components were tested using displacement time histories from the UC San Diego house as the loading input, run at dynamic or “real-time” rates.

The most significant Woodframe Project finding relating to shear wall components is the great variability that can be observed in shear wall component behavior. Figure 18.24 to Figure 18.27 illustrate this variability with component hysteresis curves. This can be as fundamental as variability between two specimens prepared at and tested at the same time, using the same materials, as seen in the variation between Test 6A and 6B in Figure 18.24. Choice of loading protocol also causes significant differences in capacity and deformation at peak capacity, as seen in Figure 18.25, comparing the results of CUREE Ordinary and SEAOSC/SPD protocols. Treatment of confinement at component boundary conditions is another significant source, as seen in Figure 18.26, comparing stucco left free to slide past framing at boundaries with interior plaster and lath confined against moving. Finally, the inclusion of finish materials over the specified structural shear wall can cause variation, as shown in Figure 18.27, comparing results of OSB alone and OSB with stucco applied as a finish. Other sources of variability not shown include the stiffness of the loading beam used to transfer forces to the component. If characterization of shear

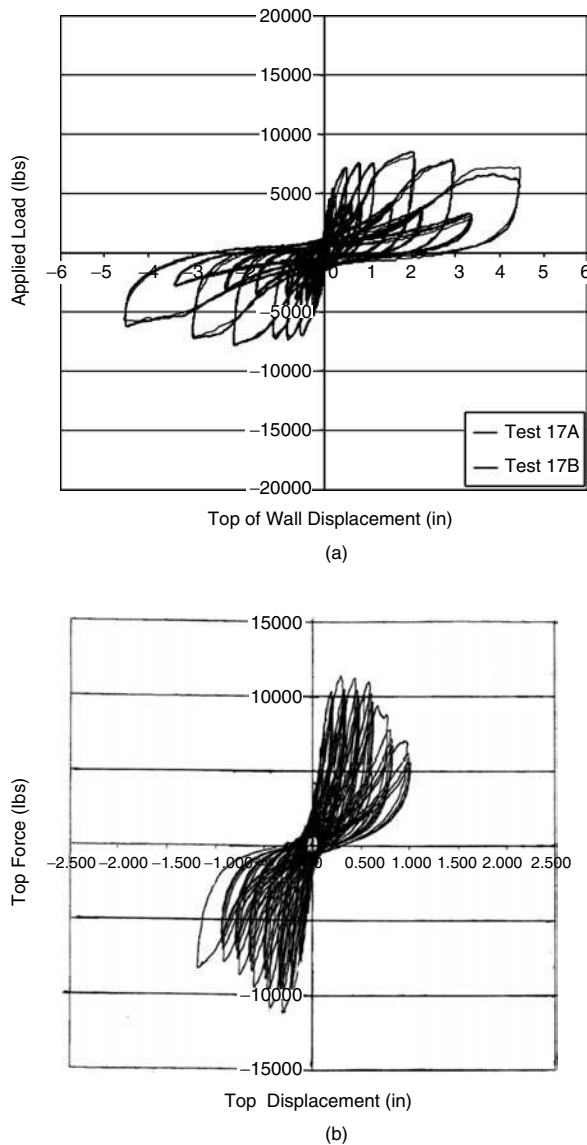


FIGURE 18.26 Variability in shear wall component test results. (a) Pardo et al. Test 17 with stucco free to slide past framing on all edges and (b) Schmid Panel 3 with interior plaster and gypsum lath confined against sliding at edges. (From Cobeen et al., 2003, CUREE Publication W-30, CUREE, Richmond, CA. With permission.)

wall component behavior is going to continue being the primary focus of testing for woodframe shear wall buildings, efforts will need to be made to identify which sources of variability can be systematically removed and to attempt to understand and accommodate the sources of variability that cannot be removed. For designers, this variability in component behavior serves as a reminder that calculated shear wall deflections are approximate at best. Further, the variability dispels any concept that there is a single correct answer for horizontal distribution of design forces; there is in fact a broad range of possible answers.

Issues regarding acceptability of various component-loading protocols remain unanswered within the research and design communities. Also outstanding are issues of whether and how allowable design loads can be assigned based on component testing results. One issue is whether imposing a design procedure

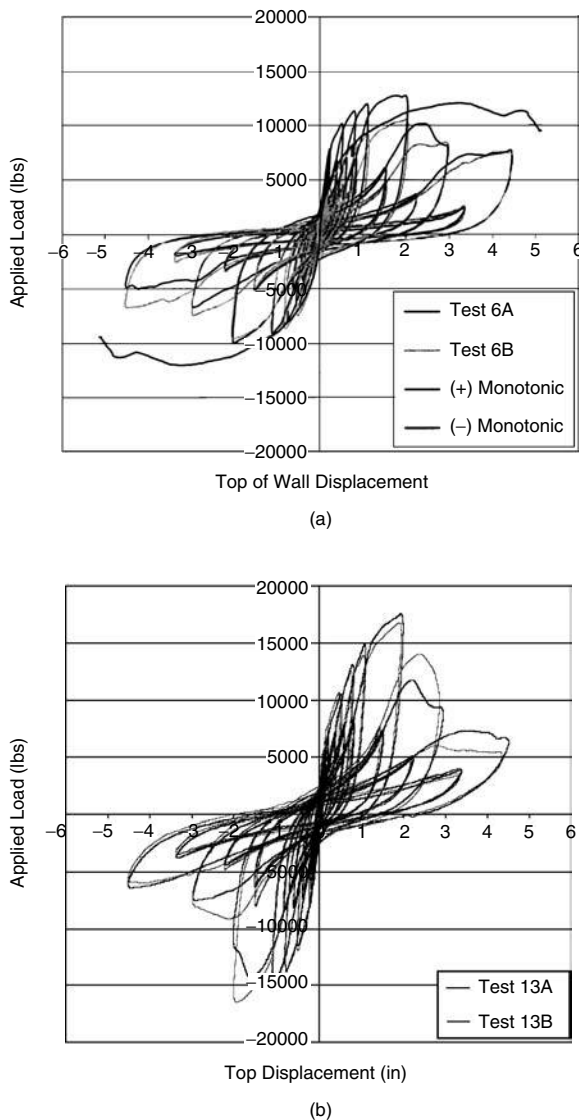


FIGURE 18.27 Variability in shear wall component test results. (a) Cobeen et al. Test 6 with OSB sheathing and (b) Pardoen et al. Test 13 with stucco exterior finish applied over OSB. (From Cobeen et al., 2003, CUREE Publication W-30, CUREE, Richmond, CA. With permission.)

based on the yield limit state on components that do not exhibit yield behavior can lead to a better characterization and understanding of performance than other approaches used to date. Engineers remain divided on this issue.

18.4.3 Other Component and Connection Research

CUREE-Caltech Woodframe Project testing has greatly expanded available data on diaphragm components. Diaphragm component testing was conducted primarily to provide improved methods of calculating diaphragm load deflection behavior. Variables included sheathing gluing and blocking, diaphragm chords and center and edge openings in the diaphragm. Results can be found in CUREE Publication W-27 (Dolan, et al., 2003a).

The CUREE-Caltech Woodframe Project also included three testing investigations addressing shear transfer. Available research reports are *Anchorage of Woodframe Buildings: Laboratory Testing Report* (Mahaney and Kehoe, 2002), *Inter-story Shear Transfer in Woodframe Buildings* (Fridley et al., 2003) and *Cyclic Response of Shear Transfer Connections Between Shear Walls and Diaphragms in Woodframe Construction* (Ficcadenti et al., 2003). The Mahaney and Kehoe testing focused on avoiding brittle splitting failures of foundation sills. The two other projects provide information on force and deformation capacity for a variety of shear transfer details.

18.4.4 Analysis Tools

Development of nonlinear analysis tools was a priority of the CUREE-Caltech Woodframe Project. Two important outcomes include the holding of an international benchmark for blind prediction of full-building behavior and the development of a three-part analysis package for woodframe shear wall buildings. In the international benchmark, teams from six countries competed in predicting the shake table behavior of the UC San Diego house, using the best analysis tools available to them. Five of the teams were from a research background while one was from a consulting engineering firm. Conference proceedings from the June 15, 2001, workshop (Folz and Filiatrault, 2001) detail the variety of analysis programs and models used and suggest that this area of analysis is at the same time very promising and in need of much further development.

The three-part Woodframe Project analysis package starts with a description of hysteretic behavior of an individual fastener used to connect wood structural panel shear wall sheathing to the supporting framing. A database of hysteretic behavior and derived fastener parameters is available with the report *Nail, Woodscrew and Staple Fastener Connections* (Fonseca et al., 2002) and additional fastener parameters are available in *Hysteretic Response of 8d and 10d Nails* (Dolan, 2003b). The hysteretic parameters and a description of sheathing panel layout and fastener lines is then input into a two-dimensional program called *Cyclic Analysis of Woodframe Shear Walls* (CASHEW) (Folz and Filiatrault, 2001). This program can generate a pushover curve, a hysteresis loop for a given displacement history, and cyclic parameters for use in three-dimensional analysis. The hysteretic parameters can then be brought into the third program, *Seismic Analysis of Woodframe Structures* (SAWS) (Folz and Filiatrault, 2002). In SAWS three-dimensional nonlinear time-history analysis is accomplished through a “pancake model,” in which each shear wall is modeled as a zero-height nonlinear spring connection between diaphragms defined as rigid or flexible. Although use of zero-height vertical elements would be a concern in medium or high-rise structures, this simplification appears to be reasonable for low-rise wood frame structures. This analysis package is discussed both in the individual research reports and in the Woodframe Project’s codes and standards report (Cobeen et al., 2003). Although there is only limited calibration of these analysis tools, their use could be a valuable supplement to linear static design methods.

18.5 Directions for Design

Recent research and observed seismic performance of woodframe buildings suggests a number of directions for design. These can be best organized into short-term and long-term directions. In the short-term the current linear static design basis should not be changed, since there is not yet adequate understanding and calibration of analysis tools to exclusively pursue alternate design methods. On the other hand, observed building performance can assist in identifying vulnerable configurations and component-level information can provide insight into detailing requirements that favor ductile component behavior. Finally, tools are available that allow designers to start exploring nonlinear static analysis methods and potentially gain additional insight into building behavior through use of these methods. In the long-term, design needs to recognize anticipated building demands and performance.

18.5.1 Short-Term Design Directions

For the short-term, code (IBC, ASCE 7-02) linear static analysis should continue to be conducted for all buildings, based on the elements that have been designated as structure by the designer. This approach has resulted in generally good performance for the bulk of woodframe buildings and should be used until a high level of confidence is gained using other design approaches. It is suggested that the linear-static analysis be supplemented by a check for soft story concentration of deformation demand, considering the effect of finish materials. This could involve the specific identification of vulnerable building configurations or use of the area demand ratio procedure suggested in Woodframe Project findings (Cobeen et al., 2003). In addition, for higher performance objectives or irregular buildings, it is suggested that nonlinear static or dynamic procedures be used for supplemental analysis to better understand distribution of force and deformation demand. Where a particular story will likely be subjected to high deformation demand, significant attention should be paid to detailing. As an example, selected anchor bolt and tie-down details should be capable of accommodating the anticipated deformation demand.

Building configurations identified as vulnerable are typically the same ones that show up repeatedly in the Section 18.2 discussion of historic seismic performance. Included are open-front buildings such as apartment buildings with tuck-under parking and storefronts with windows at the street face. Recommendations were proposed as part of the update process for the 2003 NEHRP Provisions to provide additional requirements for analysis and design of open front buildings, including combining of horizontal forces on the two orthogonal axes and more restrictive drift requirements to compensate for degradation in shear wall stiffness.

Cripple walls have been observed to be vulnerable in older houses, particularly when constructed using stucco or straight sheathing and not following recent anchorage practices. The lack of interior finishes and partition walls in cripple wall stories (resulting in less bracing material) suggests that a concentration of deformation demand could also occur in newer homes, although specific evidence of vulnerability is not available.

Hillside dwellings are a third building category identified as vulnerable. This is particularly true for houses that extend over a hillside, with either a cripple wall system or stilt system between the house and grade. The flexibility in the tall cripple walls is partially at fault, but a more fundamental issue is primary. There is a lack of deformation compatibility between the flexible cripple walls or other bracing, and the rigid but brittle anchorage of diaphragms to the uphill foundation or foundation wall. This makes it necessary for the connection of the diaphragm at the uphill foundation or foundation wall to fail before the designed load path can act, sometimes also causing the gravity and lateral systems to fail. The solution is to design the anchorage to the uphill foundation or foundation wall as the primary load path. Again, recommendations were proposed as part of the update process for the 2003 NEHRP Provisions, requiring either direct connections to the uphill foundation or accommodation of deformation compatibility by some other method.

In addition to identifying vulnerable buildings, engineering design needs to continue pursuing detailing that supports development of the sheathing nailing as the favored ductile behavior in tested components. The most important contributor to developing ductile behavior of components appears to be the fastening of shear walls to the foundation or supporting structure. The use of wide and suitably thick steel plate washers on anchor bolts near the end of shear wall components has been seen to delay the occurrence of foundation sill plate splitting, allowing other modes of behavior and energy dissipation to develop. Recommendations for plate washer size and location are provided in the test report (Mahaney and Kehoe, 2002) and codes and standards report. Among other Woodframe Project suggestions for ductility are continued use of $3 \times$ framing at abutting sheathing edges, uniform distribution of fasteners around sheathing panel perimeters, placement of structural sheathing above and below wall openings as well as at full height wall piers and increasing the distance between edge of sheathing panel and sheathing fastener centerline.

18.5.2 Long-Term Design Directions

The wider research and engineering community has set performance-based engineering as the long-term direction for seismic design. This direction can provide more rational design approaches, increased confidence in results and also increase efficiency as prescriptive limits are replaced with more reliable performance criteria. While many designers suggest that this direction is not practical for woodframe construction, it is in fact practical and necessary for a number of reasons: first, observations and research have clearly identified that building performance is not being adequately understood through current design methods; second, there are a number of outstanding design issues that cannot be understood within current code descriptions of demand and capacity and finally, there may be considerable design efficiency that could be recognized once building force and deformation demands are better understood. It is important to differentiate that, while advanced analysis tools might be needed for research and code development to move in this direction, the development of simplified tools for design based on performance principles is possible and necessary.

18.5.3 Existing Buildings

The history of woodframe performance described in Section 18.2 can be characterized primarily as a history of lessons relearned. Damage to vulnerable building types establishes a record of repetition that will continue until the vulnerable buildings are gone from the building stock or retrofitted for better performance.

Imposing retrofit requirements is difficult for all building materials, including wood. While the use of improved design requirements for new building construction generally has limited construction-cost impact, retrofit can be both costly and disruptive. Recent research assists in identifying types of vulnerable woodframe buildings and locations of vulnerability within a building. This more specific information on vulnerabilities allows available retrofit resources to be put to best use in achieving improved performance. Significant challenges exist in maintaining a balance between minimum retrofit standards that assure a minimum product level for building owners and standards flexible enough to allow and encourage owners to invest what they are able. The imposition of mandatory retrofit measures has far reaching consequences that must be considered by society at large. Much effort has gone into developing improved seismic evaluation and retrofit methodologies for existing buildings. Recently available from the ASCE are *Seismic Evaluation of Existing Buildings* (ASCE, 2002a) and *Prestandard for Seismic Rehabilitation of Existing Buildings* (ASCE, 2002b).

Communication of vulnerability is a good starting point. Following an earthquake it is not uncommon to hear of building owners that are shocked to find out that their building type was known to be vulnerable. This illustrates the need for better communication. With vigorous communication, some portion of the vulnerable building stock might be improved.

18.6 Future Challenges

As is true for design, both short-term and long-term directions need to be pursued in research. The long-term direction, moving toward design to achieve specific performance objectives will need to reliably quantify the range of global deformation demand seen in woodframe buildings and then develop simplified design approaches. Reliable quantification of global deformation demand will need to involve at least a limited number of additional full-building tests, while relying heavily on full-building analysis tools. Reliability of seismic hazard descriptions for low-deformation structures will require review, or alternately, methods of assuring ductile mechanisms need to be developed.

For the short term, it will remain necessary to address design issues based on the designated structure and component testing. This testing will have to consider sources of variability, some of which are discussed in Section 18.4. Continued component testing will also serve to improve component behavior descriptions for continued development of full-building analysis. At some point in the future it should be possible to analytically predict full-building behavior using any component that has cyclic test data available, and designer selection of components and connections should be possible using deformation demand as a criterion.

Acknowledgments

Thanks to Robert Reitherman and Zeno Martin for their review and valuable input. Much of the research described in Section 18.4 was drawn from work carried out under contract to Consortium of Universities for Research in Earthquake Engineering (CUREE) as part of the CUREE-Caltech Woodframe Project (“Earthquake Hazard Mitigation of Woodframe Construction”) under a grant administered by the California Office of Emergency Services and funded by the Federal Emergency Management Agency. Thanks are extended to these agencies and the many project contributors.

Glossary

- Bungalow** — A house style used extensively in the United States between the 1880s and 1920s, having a strong influence from the Arts and Crafts Movement, and generally characterized by low, sweeping lines and multiple porches (based on Duchscherer and Keister, 1995).
- Cripple wall** — A framed stud wall, less than 8 ft (2400 mm) in height, extending from the top of the foundation to the underside of the lowest floor framing. Cripple walls can occur in both engineered and conventional construction.
- Designated structure** — The portions of a structure designated by and proportioned by the designer to carry code-required seismic forces.
- Diaphragm, flexible** — An assumed diaphragm behavior for purposes of analysis in which the diaphragm is assumed to act as a simple beam spanning between supporting walls.
- Diaphragm, rigid** — An assumed diaphragm behavior for purposes of analysis in which the diaphragm is assumed to be completely rigid and forces are distributed to supporting walls in proportion to their rigidity.
- Foundation sill** — A wood sill plate sitting directly on a foundation, foundation wall or slab on grade.
- Prescriptive construction (conventional construction)** — Construction in which the design is determined using prescriptive rules rather than an engineered basis of demand versus capacity.
- Oriented strand board (OSB) sheathing** — A wood structural panel that is a mat-formed product composed of thin rectangular wood strands or wafers arranged in oriented layers (ICC, 2003a).
- Post frame construction** — A construction system most commonly used for agricultural buildings, but occasionally enclosed for other uses in which the main resistance to lateral forces is commonly provided by wood posts embedded into the ground to provide a fixed base from which the structure cantilevers.
- Ranch house** — A house style developed in the 1940s and 1950s, and still in use today, characterized by “...its simple, informal, one-story structure, its low-pitched eaves, its large expanse of glass which included ‘picture’ windows or ‘window walls’...” (Clark, 1986).
- Structural composite lumber (SCL)** — The term represents a range of engineered wood products, including laminated veneer lumber (LVL) consisting of veneer sheets or strips laminated into panels (Faherty and Williamson, 1999) and parallel strand lumber (PSL) consisting of oriented wood strands, glued under heat and pressure to form column and beam sections.
- Shear wall** — A wall designed to resist lateral forces parallel to the plane of the wall.
- Segmented shear wall** — A fully sheathed segment of shear wall considered to be cantilevered from its base.
- Perforated shear wall** — A shear wall containing openings in which the continuity provided by sheathing above and below openings is considered in accordance with one of the following methods listed below:
- Perforated shear wall—detailed engineered** — A shear wall in which detailing for continuity (i.e., strapping and blocking) is added to boundary members at openings, based on an engineering mechanics method of rationalizing unit sheathing shears and resulting member forces. See

NEHRP Sec. 12.4.2.9 and IBC Sec. 2305.3.7.1. (Sometimes referred to as design “considering force transfer around the openings.”)

Perforated shear wall—engineered — A shear wall in which the capacity is determined using empirical reduction factors. See NEHRP Sec. 12.4.3, IBC Sec. 2305.3.7.2.

Perforated shear wall—prescriptive — A perforated shear wall in which both the sheathing and load path fastening are determined in accordance with prescriptive provisions. See IRC Sec. R602.10.5.

Wood light-frame construction — A type of construction in which the primary structural elements (shear walls and diaphragms) are formed by a system of repetitive wood framing members (ICC, 2003a).

Tie-down (hold-down) — A device used to resist uplift of the chords of shear walls.

Tuck-under parking building — A building in which the first story is used for on-grade parking while upper stories are occupied. This configuration most commonly occurs with multifamily residential buildings.

References

- AF&PA (1996). *Standard for Load and Resistance Factor Design (LRFD) for Engineered Wood Construction*, AF&PA/ASCE 16-95, American Forest and Paper Association, Washington, DC.
- AF&PA (2001a). *National Design Specification (NDS) for Wood Construction*, 2001 ed., American Forest and Paper Association, Washington, DC.
- AF&PA (2001b). *Wood Frame Construction Manual (WFCM) for One- and Two-Family Dwellings*, 2001 ed., American Forest and Paper Association, Washington, DC.
- AITC (1994). *Timber Construction Manual*, 4th ed., Wiley, New York.
- APA (1999). *Wood Structural Panel Shear Walls with Gypsum Wallboard and Door/Window Openings*, APA Report 157, APA — The Engineered Wood Association, Tacoma, WA.
- APA (2000). *Structural Panel Shear Walls*, APA Report 154, APA — The Engineered Wood Association, Tacoma, WA.
- APA (2001). *Diaphragms and Shear Walls, Design/Construction Guide*, Form No. L350G, APA — The Engineered Wood Association, Tacoma, WA.
- ASCE (2000). *Prestandard and Commentary for the Seismic Rehabilitation of Buildings*, FEMA 356, Federal Emergency Management Agency, Washington, DC.
- ASCE (2002a). *Minimum Loads for Buildings and Other Structures*, 2002 ed., ASCE Standard 7-02, American Society of Civil Engineers, Reston, VA.
- ASCE (2002b). *Seismic Evaluation of Existing Buildings*, ASCE Standard 31-02, American Society of Civil Engineers, Reston, VA.
- ATC (1976). *A Methodology for Seismic Design and Construction of Single Family Dwellings*, ATC-4, Applied Technology Council, Redwood City, CA.
- Bossi, R.J. and Cobeen, K.E. (1996). Conventional construction for today’s buildings, *Building Standards Magazine*, September–October 1996.
- Breyer, D.E., Fridley, K.J. and Cobeen, K.E. (1998). *Design of Wood Structures*, 4th ed., McGraw-Hill, New York.
- BSSC (2001). *NEHRP Recommended Provisions for Seismic Regulations for New Buildings and Other Structures and Commentary*, 2000 ed., FEMA 368 and 369, Federal Emergency Management Agency, Washington, DC.
- CABO (1998). CABO One and Two Family Dwelling Code, The Council of American Building Officials, Falls Church, VA.
- Carr, A.J. (1998). *RUAUMOKO Inelastic Dynamic Analysis Program*, Department of Civil Engineering, University of Canterbury, Christchurch, New Zealand.

- Chai, R., Hutchinson, T. and Vukavich, S.M. (2002). *Seismic Behavior of Level and Stepped Cripple Walls*, CUREE Publication W-17, Consortium of Universities Researching Earthquake Engineering, Richmond, CA.
- Clark, C.E., Jr. (1986). *The American Family Home 1800–1960*, University of North Carolina Press, Chapel Hill, NC.
- Cobeen, K.E., Russell, J.E. and Dolan, J.D. (2003). *Recommendations for Earthquake Resistance in the Design and Construction of Woodframe Buildings*, CUREE Publication W-30, Consortium of Universities for Research in Earthquake Engineering, Richmond, CA.
- CoLA/UCI Light Frame Test Committee (2001). Report of a Testing Program of Light-Framed Walls with Wood-Sheathed Shear Panels. Final report to the City of Los-Angeles Department of Building and Safety, Available through G. Pardo, UC Irvine Department of Civil Engineering, Irvine, CA.
- Corbett, M.R. (1998). *Building California, Technology and the Landscape*, William Stout Publishers, San Francisco, CA.
- CUREE (2001a). *CUREE-Caltech Woodframe Project International Benchmark Workshop*, June 15, 2001 (Printed slides from powerpoint presentations), Consortium of Universities for Research in Earthquake Engineering, Richmond, CA.
- CUREE (2001b). Written Comments Compilation Following the CUREE-Caltech Woodframe Project's Codes and Standards Workshop, Coronado, California, September 24 and 25, 2001, Consortium of Universities for Research in Earthquake Engineering, Richmond, CA.
- Diekmann, E.F. (1986). Design of Diaphragms, *Wood Engineering Concepts*, Materials Research Laboratory, Pennsylvania State University, University Park, PA.
- Diekmann, E.F. (1999). Diaphragms and Shearwalls, *Wood Engineering and Construction Handbook*, 3rd ed., McGraw-Hill, New York, Ch. 8.
- Dolan, J.D. (2003a). *Design Methodology for Diaphragms*, CUREE Publication No. W-27, Consortium of Universities for Earthquake Engineering, Richmond, CA.
- Dolan, J.D. (2003b). *Hysteretic Response of 8d and 10d Nails*, Consortium of Universities for Research in Earthquake Engineering, Richmond, CA.
- Duchscherer, P. and Keister, D. (1995). *The Bungalow, America's Arts and Crafts Home*, Penguin Books, New York.
- EERI (1989). *Loma Prieta Earthquake October 17, 1989: Preliminary Reconnaissance Report*, Earthquake Engineering Research Institute, Oakland, CA.
- EERI (1994). *Northridge Earthquake January 17, 1994: Preliminary Reconnaissance Report*, Earthquake Engineering Research Institute, Oakland, CA.
- EERI (1996). Supplement C to Volume 11 Northridge Earthquake of January 17, 1994; Reconnaissance Report Volume 2, *Earthquake Spectra*, January 1996.
- Faherty, K.F. and Williamson, T.G. (1999). *Wood Engineering and Construction Handbook*, 3rd ed., McGraw-Hill, New York.
- FEMA (1992). *Home Builder's Guide to Seismic Resistant Construction*, FEMA 232, Federal Emergency Management Agency, Washington DC.
- FEMA (1998). *Home Builder's Guide to Seismic Resistant Construction*, FEMA 232, Federal Emergency Management Agency, Washington DC.
- Ficcadenti, S., Freund, E., Pardo, G. and Kazanjy, R. (2003). *Cyclic Response of Shear Transfer Connections Between Shear Walls and Diaphragms in Woodframe Construction*, CUREE Publication W-28, Consortium of Universities for Research in Earthquake Engineering, Richmond, CA.
- Filiatrault A. and Folz, B. (2002). Performance-Based Seismic Design of Wood Framed Buildings, *Journal of Structural Engineering*, Vol. 128, No. 1, 39–47.
- Fischer, D. et al. (2001). *Shake Table Test of a Two-Story Woodframe House*, CUREE Publication W-06. Consortium of Universities for Research in Earthquake Engineering, Richmond, CA.
- Folz, B. and Filiatrault, A. (2001). *CASHEW Version 1.0: A Computer Program for the Cyclic Analysis of Shear Walls*, CUREE Publication W-08, Consortium of Universities for Research in Earthquake Engineering, Richmond, CA.

- Folz, B. and Filiatrault, A. (2002). *SAWS Version 1.0, A Computer Program for Seismic Analysis of Wood-frame Structures* CUREE Publication W-21, Consortium of Universities for Research in Earthquake Engineering, Richmond, CA.
- Fonseca, F., Rose, S. and Campbell, S. (2002). *Nail, Wood Screw and Staple Fastener Connections*, CUREE Publication W-16, CUREE Richmond, California.
- Forest Products Laboratory (1999). *Wood Handbook — Wood As An Engineering Material*, United States Department of Agriculture, Forest Service, Forest Products Laboratory, Madison, WI.
- Fridley, K., Ryan, T., Pollock, D. and Itani, R. (2003). *Inter-Story Shear Transfer in Woodframe Buildings*, CUREE Publication W-22, Consortium of Universities for Earthquake Engineering, Richmond, CA.
- Gatto, K. and Uang, C.-M. (2002). *Loading Protocol and Loading Rate Effects on the Cyclic Response of Wood Shear Walls*, CUREE Publication W-13, Consortium of Universities for Research in Earthquake Engineering, Richmond, CA.
- Hamburger, R. (1994). Lessons Learned in the Northridge Earthquake on Wood Frame Buildings, *SEA-ONC Fall Seminar 1994*, Structural Engineers Association of Northern California, San Francisco, CA.
- Heine, C.P. (1997). Effect of Overturning Restraint on the Performance of Fully Sheathed and Perforated Timber Framed Shear Walls, thesis submitted in partial fulfillment of Master of Science Degree in Timber Engineering, Virginia Polytechnic Institute and State University, Blacksburg, VA.
- Heine, C.P. and J.D. Dolan (1998). Effect of Tie-down Restraint on the Performance of Perforated Wood Shear Walls, *Recent Advances in Understanding Full-Scale Behavior of Wood Buildings*, Forest Products Society, Madison, WI.
- HUD (1980). *The Home Builder's Guide for Earthquake Design*, Department of Housing and Urban Development, Washington, DC.
- ICBO (1994). International Conference of Building Officials, Uniform Building Code, 1994 ed., ICBO, Whittier, CA.
- ICBO (1997). International Conference of Building Officials, Uniform Building Code, 1997 ed., ICBO, Whittier, CA.
- ICC (2000a). International Code Council, International Building Code, 2000 ed., ICC, Falls Church, VA.
- ICC (2000b). International Code Council, International Residential Code, 2000 ed., ICC, Falls Church, VA.
- ICC (2003a). International Code Council, International Building Code, 2000 ed., ICC, Falls Church, VA.
- ICC (2003b). International Code Council, International Residential Code, 2000 ed., ICC, Falls Church, VA.
- ISO (1998). *Timber Structures — Joints Made with Mechanical Fasteners — Quasi Static Reversed-Cyclic Test Method*, ISO/TC 165 WD 16670, International Organization for Standardization, Secretariat — Standards Council of Canada, Ottawa, ON.
- Isoda, H., Filiatrault, A. and Folz, B. (2002). *Seismic Modeling of Index Woodframe Buildings*, CUREE Publication W-12, Consortium of Universities for Research in Earthquake Engineering, Richmond, CA.
- Johnson, A.C., 1997. Monotonic and Cyclic Performance of Long Shear Walls With Openings. Thesis submitted in partial fulfillment of the requirements of the Master of Science Degree at Virginia Polytechnic Institute and State University, Blacksburg, VA.
- Krawinkler, H., Parisi, F., Ibarra, L. and Medina, R. (2001). *Development of a Testing Protocol for Wood-frame Structures*, CUREE Publication W-02, CUREE, Richmond, CA.
- LATF (1994a). Task Force on Evaluating Damage From the Northridge Earthquake: Residential Buildings-Cripple Wall Subcommittee Final Report, Attachment A: Recommended Code Changes to the City of Los Angeles Building Code. Attachment C: Provisions with Commentary for the Proposed City of Los Angeles Building Code Chapter 92: Prescriptive Provisions for Seismic Strengthening of Light, Wood-frame Residential Buildings, City of Los Angeles Department of Building and Safety and the Structural Engineers Association of Southern California.

- LATF (1994b). *Task Force on Evaluating Damage From the Northridge Earthquake: Wood Frame Subcommittee Construction Report and Recommendations*, City of Los Angeles Department of Building and Safety and the Structural Engineers Association of Southern California.
- LATF (1994c). *Task Force on Evaluating Damage From the Northridge Earthquake: Hillside Dwelling Subcommittee Report*, City of Los Angeles Department of Building and Safety and the Structural Engineers Association of Southern California.
- Lawson, A. Editor (1908). Report of the State Earthquake Investigation Commission, Carnegie Institute, Washington, D.C.
- Madsen (1992). *Structural Behavior of Timber*, Timber Engineering Limited, North Vancouver, BC.
- Madsen, B. (2000). *Behavior of Timber Connections*, Timber Engineering Limited, North Vancouver, B.C.
- Mahaney, J. and Kehoe, B. (2002). Laboratory Testing Report, Task No. 1.4.1.1 — Anchorage of Wood-frame Buildings CUREE Publication W-14, Consortium of Universities for Research in Earthquake Engineering, Richmond, CA.
- Malik, A.M. (1995). Working Papers: Estimating Building Stocks for Earthquake Mitigation and Recovery Planning, Program in Urban and Regional Studies, Cornell Institute For Social and Economic Research, Ithaca, NY.
- McMullin, K. and Merrick, D. (2002). Seismic Performance of Gypsum Walls — Experimental Test Program, CUREE Publication W-15, Consortium of Universities for Research in Earthquake Engineering, Richmond, CA.
- Mochizuki G. and Fennell W. (2002). Developing a Practical Interpretation and Application of The Building Code to Wood Frame Building Diaphragm Design, *Proc., 2002 SEAOC Convention, Structural Engineers Association of California*, Sacramento, CA.
- Mosalam, K. (2003). *Seismic Evaluation of an Asymmetric Three-Story Woodframe Building*, CUREE Publication W-19, Consortium of Universities for Research in Earthquake Engineering, Richmond, CA.
- Ni, C. and Karacabeyli, E. (2002). Capacity of Shear Wall Segments Without Hold-Downs, *Wood Design Focus*, Vol. 12, No. 2, 10–17.
- Paevere, P. (2002). Full-Scale Testing, Modeling and Analysis of Light-Frame Structures Under Lateral Loading, Doctoral Thesis, University of Melbourne, Melbourne, Australia.
- Pardoens, G., Kazanjy, R., Hamilton, C., Waltman, A. and Freund, E. (2003). *Testing and Analysis of One-Story and Two-Story Shear Walls Under Cyclic Loading*, CUREE Publication W-25, Consortium of Universities for Research in Earthquake Engineering, Richmond, CA.
- Perlin, J. (1989). *A Forest Journey, The Role of Wood in the Development of Civilization*, Norton, New York.
- Porter, K., Beck, J., Seligson, H., Scawthorn, C., Tobin, L.T., Young, R. and Boyd, T. (2002). *Improving Loss Estimation for Woodframe Buildings*, CUREE Publication W-18, Consortium of Universities for Research in Earthquake Engineering, Richmond, CA.
- Porter, K. and Kiremidjian, A. (2001a). *Assembly-Based Vulnerability and Its Use in Seismic Performance Evaluation and Risk-Management Decision-Making*, John A. Blume Earthquake Engineering Center, Stanford University, Palo Alto, CA.
- Porter, K., Kiremidjian, A. and LeGrue, J. (2001b). Assembly-Based Vulnerability of Buildings and Its Use in Performance Evaluation, *Earthquake Spectra*, Vol. 17, No. 2, 291–312.
- Pryor, S., Graham, T. and Carlos Ventura, C. (2000). Seismic Testing and Analysis Program on High Aspect Ratio Wood Shear Walls, *Proceedings, International Timber Engineering Conference*, Whistler, British Columbia, Canada.
- Reitherman R. and Cobeen, K. (2003). *Design Documentation of the Woodframe Project Index Buildings*, CUREE Publication W-29, Consortium of Universities for Research in Earthquake Engineering, Richmond, CA.
- Rose, J. (1998). *Performance of Wood Structural Panel Shear Walls Under Cyclic (Reversed) Loading*, APA Report 158, APA — The Engineered Wood Association, Tacoma, WA.

- Salenikovich, A. and Dolan, J.D. (1999). Effects of Aspect Ration and Overturning Restraint on Performance of Light-Frame Shear Walls Under Monotonic and Cyclic Loading, *Proc. Pacific Timber Engineering Conference*, Vol. 3, Rotorua, New Zealand.
- San Francisco Chronicle (1998). Photo in Home Section, Wednesday February 4, 1998, The Hearst Corporation, San Francisco, CA.
- Schierle, G., Ed. (2001). *Woodframe Project Case Studies*, CUREE Publication W-04, Consortium of Universities for Research in Earthquake Engineering, Richmond, CA.
- Schierle, G. (2003). *Northridge Earthquake Field Investigations: Statistical Analysis of Woodframe Damage*, CUREE Publication W-09, Consortium of Universities for Research in Earthquake Engineering, Richmond, CA.
- Schmid, B. (2002). Results and Ramifications of Cyclic Tests of Typical Sheathing Material Used on One and Two Story Wood Framed Residences, Handout at SEAOC 2002 Convention.
- SEAOC (1960). *Recommended Lateral Force Requirements and Commentary*, 1960 ed., Structural Engineers Association of California, Sacramento, CA.
- SEAOC (1967). *Recommended Lateral Force Requirements and Commentary*, 1967 ed., Structural Engineers Association of California, Sacramento, CA.
- SEAOC (1991). *Reflections On the Loma Prieta Earthquake October 17, 1989*, Structural Engineers Association of California, Sacramento, CA.
- SEAOC (1997). *Guidelines for Wood Diaphragms and Shear Walls*, Structural Engineers Association of California, Sacramento, CA.
- SEAOSC and CoLA (1997). Structural Engineers Association of Southern California ad Hoc Committee Testing Standards for Structural Systems and Components in Conjunction with the City of Los Angeles, Standard Method of Cyclic (Reversed) Load Test for Shear Resistance of Framed Walls for Buildings, September 9.
- Seible, F., Filiatrault, A. and Uang, C.-M., Eds. (1999) *Proc. Invitational Workshop on Seismic Testing, Analysis and Woodframe Construction*, CUREE Publication W-01, Consortium of Universities for Research in Earthquake Engineering, Richmond, CA.
- Seismic Safety Commission, State of California (1994). 1994 Northridge Earthquake Buildings Case Studies Project, Proposition 122: Product 3.2, SSC 94-06, California Seismic Safety Commission, Sacramento, CA.
- Shepherd R. and Allen (1995). Cyclic Testing of Narrow Plywood Shear Walls, ATC-R-1, Applied Technology Council, Redwood City, CA.
- Simpson Company (1974). Strong-Tie Connectors, Catalog No. 74H1, Simpson Strong-Tie Company, San Leandro, CA.
- Steinbrugge, K., Bush, V. and Johnson, J. (1996). Standard of Care in Structural Engineering Wood Frame Multiple Housing, *Proc., 1996 SEAOC Convention*, Structural Engineers Association of California, Sacramento, CA.
- Williamson, T. (2001). *APA Engineered Wood Handbook*, McGraw-Hill, New York.
- Williamson, T and Faherty, K. (1999). *Wood Engineering and Construction Handbook*, 3rd ed., McGraw-Hill, New York.

19

Seismic Analysis and Design of Nonstructural Elements

19.1	Introduction.....	19-1
19.2	Importance of Nonstructural Elements.....	19-2
19.3	General Physical Characteristics	19-4
19.4	General Response Characteristics	19-6
19.5	Modeling of Nonstructural Elements	19-8
19.6	Methods of Analysis	19-8
	Background • Floor Response Spectrum	
	Method • Alternative Methods • Design-Oriented	
	Simplified Method	
19.7	Design Provisions in Building Codes	19-22
	Overview • Uniform Building Code • NEHRP Provisions	
19.8	General Design Considerations.....	19-33
	Architectural Elements • Mechanical and Electrical	
	Equipment	
19.9	Role of Nonstructural Elements in Performance-Based Design	19-39
19.10	Future Challenges	19-42
19.11	Summary	19-42

Roberto Villaverde

19.1 Introduction

Nonstructural elements are those systems and components attached to the floors and walls of a building or industrial facility that are not part of the main or intended load-bearing structural system for the building or industrial facility. Although not part of the main structural system, they may nevertheless also be subjected to large seismic forces and depend on their own structural characteristics to resist these seismic forces. In general, nonstructural elements may be classified into three broad categories: (1) architectural components, (2) mechanical and electrical equipment and (3) building contents. Examples of the first category are elevator penthouses, stairways, partitions, parapets, heliports, cladding systems, signboards, lighting systems and suspended ceilings. Some of the second are storage tanks, pressure vessels, piping systems, ducts, escalators, smokestacks, antennas, cranes, radars and object tracking devices, computer and data acquisition systems, control panels, transformers, switchgears, emergency power systems, fire protection systems, boilers, heat exchangers, chillers, cooling towers and machinery such as pumps, turbines, generators, engines and motors. Among some of those in the third category are bookshelves, file cabinets, storage racks, decorative items and any other piece of furniture commonly

found in office buildings and warehouses. Alternative names by which these elements are also known are “appendages,” “nonstructural components,” “building attachments,” “architectural, mechanical, and electrical elements,” “secondary systems,” “secondary structural elements” and “secondary structures.” The name that best describes their nature is secondary structures, since it reflects the fact that they are not part of the main structure but must possess, nevertheless, structural properties to maintain their own integrity.

This chapter will describe why the survival of nonstructural elements is an important necessity in the event of a strong earthquake and why they are particularly vulnerable to the effect of earthquakes. It will review, in addition, the methods that are available for their seismic analysis and introduce in detail two such methods. In like manner, it will introduce the provisions contained in the Uniform Building Code (UBC) and the NEHRP provisions for the seismic design of nonstructural elements and illustrate the use of these provisions by means of a numerical example. The chapter will also present some general design recommendations and preventive measures that have been proven effective in improving the seismic resistance of some architectural elements and mechanical and electrical equipment. Finally, it will examine the role nonstructural elements play in the performance-based design of buildings, and identify the research needed to advance current efforts to protect nonstructural elements against the effects of earthquakes and to develop methods and techniques to achieve this goal in a practical and economical way.

19.2 Importance of Nonstructural Elements

Despite the fact that they are not part of the main structure, nonstructural elements are far from being secondary in importance. It is nowadays widely recognized that their survival is essential to provide emergency services in the aftermath of an earthquake. Experiences from past earthquakes have shown that the failure of equipment and the debris caused by falling objects and overturned furniture may critically affect the performance of fire and police stations, emergency command centers, communication facilities, power stations, water supply and treatment plants, food treatment and cold storage plants, hospitals and collective transportation systems. For example, during the 1994 Northridge earthquake in Los Angeles, CA, area, several major hospitals had to be evacuated, not because of structural damage, but because of (1) water damage caused by broken water lines and water supply tanks; (2) the failure of emergency power systems and heating, ventilation and air conditioning units; and (3) damage to suspended ceilings and light fixtures and some broken windows (Hall, 1994, 1995). Along the same lines, it is now recognized that damage to nonstructural elements represents a threat to life safety, may seriously impair a building's function and may result in major direct and indirect economic losses. Understandably, the collapse of suspended light fixtures, hung ceilings or partition walls; the fall of cladding components, parapets, signboards, ornaments or pieces of broken glass; the overturning of heavy equipment, bookshelves, storage racks and pieces of furniture; and the rupture of pipes and containers with toxic materials are all capable of causing serious injury or death. Figure 19.1 through Figure 19.8 show a few examples of the failure of nonstructural elements during past earthquakes and vividly illustrate how these failures can cause serious injury and death. A most unfortunate demonstration that the failure of a nonstructural element indeed represents a threat to life safety was the death of a student who was struck by a falling precast panel while walking out of a parking structure during the 1987 Whittier Narrows earthquake in California (Taly, 1988). In like fashion, it is easy to visualize how the normal activities that take place in a building may be critically disrupted when some essential equipment fails, or when debris from failed architectural components gets in the way. Typical examples that illustrate the consequences of such an event are the unwanted solidification of a melted metal in an industrial facility, the inaccessibility of financial records in a timely manner in a banking institution and the failure to fill pending orders in a manufacturing plant. In regard to the economic impact caused by the failure of nonstructural elements, there is nowadays plenty of evidence that shows that because of the loss of the nonstructural components themselves, loss of inventory and loss of business income, the cost of such failures may easily exceed the replacement cost of the building (EERI, 1984). And in today's highly technological environment, this



FIGURE 19.1 Collapse of signboard on street of Kobe, Japan, during the 1995 Great Hanshin earthquake. (Photo courtesy of Chris Arnold/Building Systems Development, Inc.)



FIGURE 19.2 Collapse of pipe originally suspended from below floor system of parking structure during the 1987 Whittier Narrows earthquake. (Photo courtesy of S.S. Rihal/Cal Poly, San Luis Obispo.)



FIGURE 19.3 Failure of hospital penthouse during the 1985 Mexico earthquake.

cost may be even accentuated as a result of the widespread use of electronic and computer equipment and dependence of industry on this type of equipment.

It is thus clear that nonstructural elements should be the subject of a rational and careful seismic design in much the same way as their supporting structures are.

19.3 General Physical Characteristics

Several physical characteristics make nonstructural elements in buildings particularly vulnerable to the effects of earthquakes. Some of these physical characteristics are:

1. Most nonstructural elements are attached to the elevated portions of a building, and thus they are subjected not to the ground motion generated by an earthquake, but to the amplified motions generated by the dynamic response of the building.
2. Their weight is light in comparison with the weight of the structure to which they are connected, and their stiffness is also much smaller than that of the structure as a whole. As a result, it is likely that their natural frequencies are close to the natural frequencies of the structure, and hence their dynamic response to the motion at their supports may be extraordinarily high.



FIGURE 19.4 Failure of window frame in school building during the 1973 Orizaba, Mexico, earthquake.



FIGURE 19.5 Fallen precast element from parking garage, responsible for death of a student during the 1987 Whittier Narrows earthquake in Los Angeles, CA, area. (Photo courtesy of Narendra Taly/California State University, Los Angeles; reproduced with permission of Earthquake Engineering Research Institute.)

3. Their damping ratios may be quite low, much lower than those for the structure, and thus they do not possess the damping characteristics that are necessary for protection against sharp resonant motions.
4. They may be connected to the structure at more than one point and therefore they may be subjected to the distortions induced by the differential motion of their supports.



FIGURE 19.6 Collapse of building's exterior wall during the 1994 Northridge, CA, earthquake. (Photo courtesy of Yousef Bozorgnia.)

5. They are designed to perform a function other than to resist forces. As such, they are built with materials that are far from the ideal materials to resist seismic forces and they may possess parts that are sensitive to even the smallest level of vibration.

19.4 General Response Characteristics

The special physical characteristics described above make nonstructural elements not only susceptible to earthquake damage, but also respond to earthquake ground motions differently from the way building structures do. That is, the response of a nonstructural element exhibits characteristics that are not common in the response of a conventional structure. The following are a few of such characteristics:

1. The response of a nonstructural element depends on the response of the structure to which it is connected, and thus it depends not only on the characteristics of the ground motion that excites the base of the structure, but also on the dynamic characteristics of the structure.
2. The response of a nonstructural element depends on its location within the structure. As a result, identical elements may respond differently to the effects of an earthquake if they are located at different levels of the supporting structure.
3. There may be a significant interaction between a nonstructural element and its supporting structure. That is, the motion of the nonstructural element may modify the motion of its supporting structure, and vice versa. In such cases, therefore, one cannot predict the response of the nonstructural element without knowing in advance the dynamic properties of both the nonstructural element and the supporting structure.



FIGURE 19.7 Dislocation of library bookshelves during the 1987 Whittier Narrows, CA, earthquake. (Photo courtesy of Narendra Taly/California State University, Los Angeles; reproduced with permission of Earthquake Engineering Research Institute.)



FIGURE 19.8 Collapse of 17-ton scoreboard at Anaheim Stadium (black object below stadium's A logo and surrounded by billboards) during the 1994 Northridge, CA, earthquake.

4. When a nonstructural element is connected to the structure at more than one point, the element's supports are excited by motions that are different and out of phase.
5. Since the damping in a nonstructural element is much lower than the damping in the supporting structure, the damping in the system formed by the structure and its nonstructural elements, which is the system that characterizes the response of a nonstructural element, is not uniform. This means that the response of nonstructural elements is governed by the response of a system without classical modes of vibration; that is, the response of a system whose natural frequencies and mode shapes are complex valued.
6. Since, as mentioned earlier, it is likely that some of the natural frequencies of a nonstructural element may be close in value to some of those of the supporting structure, the combined structure–nonstructural system may result in a system with closely spaced natural frequencies. As such, the response of a nonstructural element may be dominated by its response in two or more of its modes of vibration, as opposed to a single mode, which is the case for many low-rise and regular building structures.
7. The response of a nonstructural element is affected by its own yielding as well as the yielding of its supporting structure.

19.5 Modeling of Nonstructural Elements

As may be inferred from the examples given in Section 19.1, and in contrast to building structures, there exists a vast variety of nonstructural elements. Therefore, there are no general rules or accepted standards for the modeling of nonstructural elements. What is more, in many situations, the modeling is left to the manufacturer of the particular element in question, who, in the majority of the cases, is the only one in a position to be able to identify the dynamic properties and significant characteristics that need to be considered in a mathematical model of the element. In general, however, it can be said that as far as their modeling is concerned, nonstructural elements can be considered as belonging to three broad categories: rigid, flexible, and hanging from above. If a nonstructural element is rigid, then its dynamic properties will depend primarily on the flexibility and ductility of its anchors. In this case, the nonstructural element may be modeled as a single-degree-of-freedom system with a mass equal to the total mass of the element and stiffness and ductility equal to the stiffness and ductility of the anchors. Examples of these types of nonstructural elements are engines and motors attached to the floors of a structure by means of steel brackets and bolts. If, on the other hand, a nonstructural element is flexible, then it is necessary to model the element as a multi-degree-of-freedom system with distributed mass, stiffness and ductility, in much the same way as a building structure is normally modeled. In this regard, it should be noted that, unlike a building structure, a nonstructural element may be attached to multiple points of its supporting structure and that it is important to consider these multiple attachments in the modeling of the nonstructural element. Typical examples of flexible nonstructural elements are signboards and pipelines, the latter also being an example of a nonstructural element with multiple points of attachment. Finally, if the nonstructural element hangs from above, then the element behaves and may be modeled as a single-mass pendulum. Ordinarily, however, hanging nonstructural elements are not analyzed since these elements are seldom damaged by earthquakes. The exception is when the nonstructural element may impact its supporting structure or any other nearby object as a result of the large oscillations it may be subjected to during an earthquake. In these cases, an analysis should be performed to investigate the amplitude of such oscillations. Examples of hanging secondary structures are lighting systems, cable trays and some decorative items such as chandeliers.

19.6 Methods of Analysis

19.6.1 Background

A great research effort has been devoted over the last three decades to develop rational methods for the seismic analysis of nonstructural elements. For the most part, this effort has been fueled by the need to

guarantee the survivability of critical equipment such as piping and control systems in nuclear power plants. Therefore, many methods of analysis have been proposed as a result of this research effort, some of them with a strong empirical base, and others based on rigorous principles of structural dynamics. Up to now, however, none of these methods has become the industry standard or the one that is preferred by most analysts.

In the development of methods of analysis for nonstructural elements, it is generally recognized that they are difficult to analyze accurately and efficiently. It is always possible to consider them in conjunction with the analysis of their supporting structures, but a combined structure–nonstructural system generally results in a system with an excessive number of degrees of freedom and large differences in the values of its various masses, stiffnesses and damping constants. As a consequence, the conventional methods of analysis become expensive, inaccurate and inefficient. For example, a modal analysis exhibits difficulties in the computation of natural frequencies and mode shapes, and a step-by-step integration method becomes extraordinarily sensitive to the selected integration time step. Likewise, the analysis of a combined system may be too impractical since during the preliminary design of the nonstructural element, the supporting structure would have to be reanalyzed every time a change is introduced in some of the parameters of the nonstructural element. Considering that normally structures and nonstructural elements are designed by different teams at different times, this approach would also bring serious problems of schedule and efficiency. Thus, most of the methods proposed for the analysis of nonstructural elements have been the result of an effort to avoid the analysis of a combined system and overcome the aforementioned difficulties.

The majority of the methods available for the analysis of nonstructural elements are based on concepts not covered in introductory courses on structural dynamics and, hence, beyond the scope of this discussion. Therefore, only two methods of analysis will be described in this chapter. One is the floor response spectrum method, and the other is a design-oriented approximate method. Although with some limitations, these methods are easy to understand and thus useful to introduce the reader to a difficult problem and illustrate some of the fundamental concepts involved. A brief description of the concepts on which some other methods are based will also be presented.

19.6.2 Floor Response Spectrum Method

One of the first simplified methods used in the analysis of nonstructural elements is the so-called systems-in-cascade, in-structure response spectrum, or floor response spectrum method. In this method, first the excitation at the base of a nonstructural element is defined in terms of a response spectrum in much the same way as in the case of a building structure. Then, the nonstructural element is analyzed, also as in the case of a conventional structure, using such a response spectrum. Since, in general, the response spectrum for the excitation at the base of a nonstructural element is different from the response spectrum of the ground motion that excites its supporting structure, the former is called “floor response spectrum” or “in-structure response spectrum” to distinguish it from the latter. Note also that a floor response spectrum is needed for each of the points or floors of the structure where there is a nonstructural element attached to it. The obvious reason is that the motion may be markedly different at different points or floors of a structure.

Ordinarily, a floor response spectrum is obtained by means of a time-history analysis. That is, given a ground acceleration time history, a step-by-step integration analysis is carried out to determine the acceleration time history of the point or floor to which the nonstructural element under consideration will be attached. Then, this time history is used to generate a response spectrum using any of the conventional methods currently in use. Since the use of a single time history is not acceptable for design purposes, it is necessary to generate floor response spectra for several different ground acceleration time histories and use an average or envelope to all these spectra. As this is a time-consuming process that requires lengthy numerical integrations, an alternative commonly employed in practice is the use of an artificial ground acceleration time history that is fitted to envelop a given ground design spectrum, such as the design spectrum specified by a building code. However, caution should be exercised with this alternative since such an artificial time history is not uniquely defined. That is, different time histories

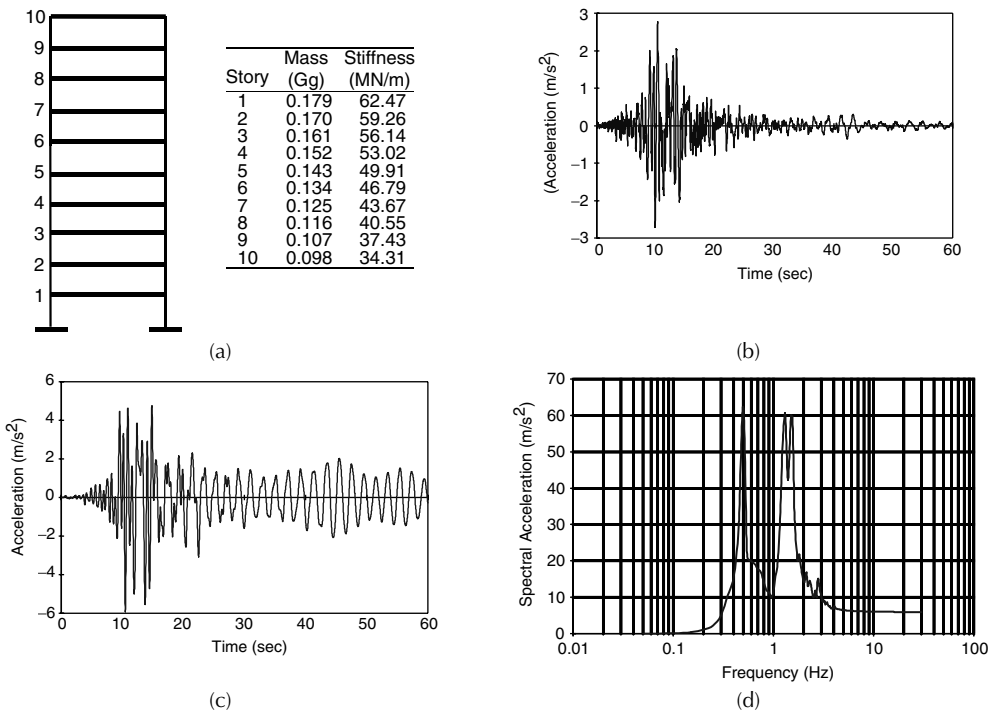


FIGURE 19.9 (a) Ten-story building considered in Example 19.1. (Note: $\bar{G}_g = 68, 525$ slugs; $1 \text{ MN/m} = 737.5$ kips/ft); (b) E-W component of ground acceleration recorded at the Foster City station during the 1989 Loma Prieta, CA, earthquake. (Note $1 \text{ m/s}^2 = 3.28 \text{ ft/s}^2$); (c) Acceleration response for roof level of building considered in Example 19.1 under E-W Foster City accelerogram. (Note $1/\text{ms}^2 = 3.28 \text{ ft/s}^2$); (d) floor response spectrum for roof level of building considered in Example 19.1 under E-W Foster City accelerogram. (Note: $1 \text{ m/s}^2 = 3.28 \text{ ft/s}^2$).

may envelop the target design spectrum but give significantly different results. Another alternative is to use one of the several methods that are now available to generate floor response spectra directly from a specified ground response spectrum or a design spectrum without utilizing a time-history analysis. These methods use as input a specified ground response spectrum and the dynamic properties of the structure. Examples are the methods proposed by Biggs and Roessel (1970), Amin et al. (1971), Kapur and Shao (1973), Peters et al. (1977), Vanmarcke (1977), Atalik (1978) and Singh (1980).

Example 19.1 Analysis of nonstructural element by floor response spectrum method

A piece of equipment is mounted on the roof of the 10-story shear building shown in Figure 19.9a. This piece of equipment can be modeled as a single-degree-of-freedom system with a natural frequency of 2.0 Hz. Determine, using the floor response spectrum method, the maximum acceleration of the piece of equipment when the base of the building is subjected to the East-West component of the ground acceleration recorded at the Foster City station during the 1989 Loma Prieta, CA, earthquake (see Figure 19.9b). Assume that the building's damping matrix is proportional to its stiffness matrix and that the damping ratio in its fundamental mode is 2%. Similarly, assume a damping ratio of 0.5% for the piece of equipment.

Solution: The first step in using the floor response spectrum method for the solution of this problem is the generation of the floor spectrum corresponding to the roof of the building and the given earthquake ground motion. For this purpose, first a time-history analysis of the building is carried out. Then, using the time history corresponding to the acceleration response of the building at its roof level, the desired floor response spectrum is generated.

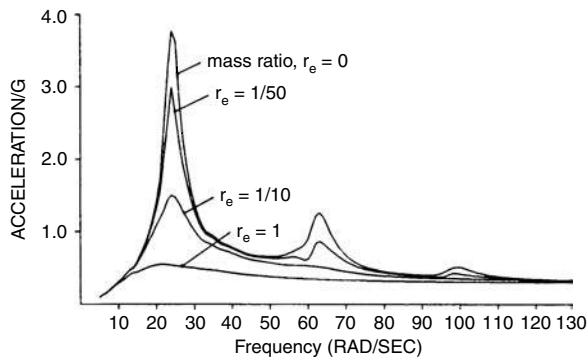


FIGURE 19.10 Floor response spectra for fourth floor of six-story building in Figure 19.11 corresponding to different nonstructural to structural mass ratios. (Adapted from Singh, M.P. and Suárez, L.E., *Earthquake Eng. Struct. Dyn.*, 15, 871–888, 1987. With permission.)

The acceleration time history of the building's roof and the corresponding floor response spectrum obtained are shown in Figure 19.9c and Figure 19.9d, respectively. From this floor response spectrum, it can be seen that the ordinate corresponding to a frequency of 2 Hz is equal to 14.4 m/sec^2 (47.2 ft/sec^2). Therefore, the acceleration of the piece of equipment when the building is subjected to the given excitation is approximately equal to 1.47 g.

Floor response spectrum methods have been proven accurate for nonstructural elements whose masses are much smaller than the masses of their supporting structure and natural frequencies that are not too close to the natural frequencies of the structure. However, these methods may yield overly conservative results for nonstructural elements that do not have these characteristics. (Toro et al., 1989, report that errors may be significant when nonstructural to structural mass ratios are greater than 10^{-3} .) The reason for this overconservatism is that in floor response spectrum methods nonstructural elements are considered separately from their supporting structure, without due consideration to the fact that the response of a nonstructural element may significantly affect the response of its supporting structure and vice versa. That is, floor response spectrum methods neglect the dynamic interaction between a structure and a nonstructural element. An additional reason is that floor response spectrum methods cannot account for the fact that the masses of the structure and the nonstructural element vibrate out of phase, an effect that arises because, in general, the combined system does not possess classical modes of vibration. There is now ample analytical evidence that demonstrates that ignoring these two effects may lead to gross errors in the response calculation of some nonstructural elements (see, for example, Igusa and Der Kiureghian, 1985a, and Chen and Soong, 1988).

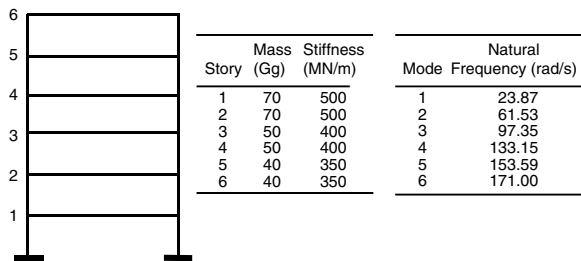


FIGURE 19.11 Properties and natural frequencies of six-story shear building considered in study of interaction and nonclassical damping effects. (Note: 1 Gg = 68,525 slugs; 1 MN/m = 737.5 kips/ft.)

Another problem with floor response spectrum methods is that they cannot be rationally applied for the analysis of nonstructural elements with multiple points of attachment (Wang et al. 1983). This is so because these methods cannot consider that the motions at different attachment points are normally different from one another and out of phase. Attempts have been made to overcome this problem, but for the most part these attempts have been in the form of empirical or ad-hoc procedures. For example, it has been proposed to determine the maximum response of a multiply supported nonstructural element by calculating first the maximum responses that result from using (one at a time) the floor spectra obtained for each of its supports. Then, these maximum responses are combined in an empirical way to estimate the system's true maximum response (Lin and Loceff, 1980; Shaw, 1975; Thaler, 1976). Common among these empirical procedures is the selection of the largest of all the response maxima, or a combination of them on the basis of the square root of the sum of their squares. Other techniques use a spectrum obtained by enveloping the floor spectra for all the non-structural element's supports, or that of including a "pseudo-static" component of the response, determined in terms of the difference between the peak displacements at the various attachment points. It is now recognized, nevertheless, that these techniques are often too crude and in many cases may lead to overly conservative results.

The floor response spectra shown in Figure 19.10 illustrate the accuracy involved in the use of the floor response spectrum method. These floor response spectra have been obtained for the fourth floor of the six-story shear building depicted in Figure 19.11, using as input an ensemble of 75 synthetically generated ground motions and considering a damping ratio of 6% for the fundamental mode of the building. The curve corresponding to a 0 mass ratio is obtained using the traditional procedure that is used to generate floor response spectra; i.e., ignoring the dynamic interaction between the structure and the nonstructural element. The other curves are obtained for different mass ratios but fully considering this interaction. The mass ratio identified in each of these curves is determined by dividing the total mass of the considered nonstructural element by the total mass of the structure.

TABLE 19.1 Absolute Acceleration Response (Expressed as a Fraction of g) of Single-Degree-of-Freedom Nonstructural Element Mounted on Fourth Floor of Structure Depicted in Figure 19.11 When the Nonclassical Damping Nature of the Combined System is and is Not Taken Into Account^a

Nonstructural Element Natural Frequency (rad/sec)	Mass Ratio					
	0.00156			0.000156		
	Classical Damping	Nonclassical Damping	Error (%)	Classical Damping	Nonclassical Damping	Error (%)
24	2.556	3.149	18.8	4.317	3.063	41.0
42	0.446	0.451	1.0	0.449	0.453	1.0
62	0.612	0.312	95.8	0.879	0.313	180.6
97	0.335	0.315	6.4	0.291	0.407	28.6
134	0.281	0.309	8.9	0.386	0.320	20.4
154	0.258	0.257	0.5	0.295	0.258	14.4
162	0.254	0.254	0.0	0.256	0.255	0.3
171	0.252	0.252	0.1	0.252	0.254	0.7

^a Damping ratio in fundamental mode of structure = 6%; damping ratio of nonstructural element = 1%. Source: Singh, M.P. and Suárez, L.E. *Earthquake Eng. Struct. Dyn.*, 15, 871–888, 1987. With permission.

It may be noted from the curves in Figure 19.10 that neglecting the interaction is always conservative, although in some cases it may be grossly conservative. It may also be noted that the interaction effect becomes important when the mass ratio is not too small and the natural frequency of the nonstructural element is close to one of the dominant natural frequencies of its supporting structure.

In like fashion, Table 19.1 and Table 19.2 illustrate the importance of considering nonclassical damping effects in the analysis of nonstructural elements. In these two tables, the absolute acceleration responses

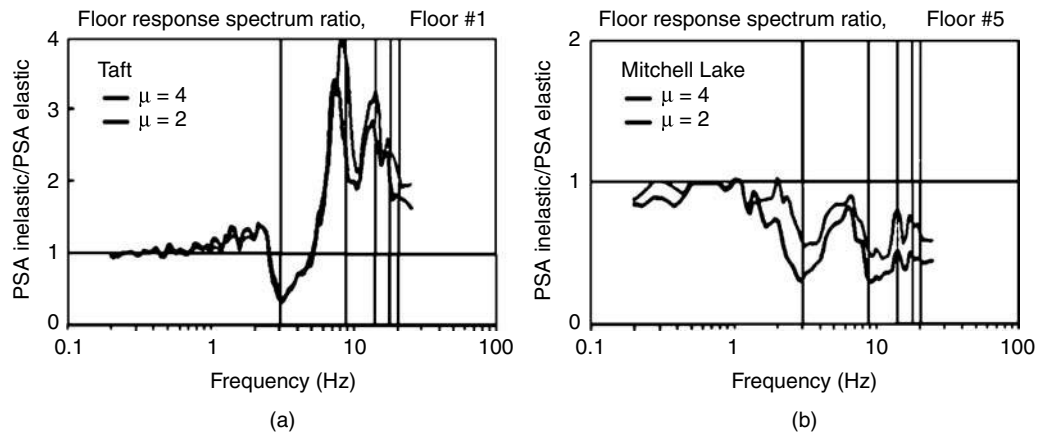


FIGURE 19.12 Floor response spectrum ratios (inelastic structure/elastic structure) corresponding to floor accelerations of five-story shear building with first-floor interstory ductilities of 2 and 4: (a) ratios for first floor when building is subjected to 1952 Taft acceleration record; (b) ratios for fifth floor when building is subjected to 1982 Mitchell Lake acceleration record. Vertical lines identify the natural frequencies of the structure. (Adapted from Sewell, R.T., Damage Effectiveness of Earthquake Ground Motion: Characterizations Based on the Performance of Structures and Equipment, PhD thesis, Stanford University, 1988. With permission.)

TABLE 19.2 Absolute Acceleration Response (Expressed As a Fraction of g) of Single-Degree-of-Freedom Nonstructural Element Mounted on Fourth Floor of Structure Depicted in Figure 19.11 When the Nonclassical Damping Nature of the Combined System Is and Is Not Taken into Account^a

Nonstructural Element Natural Frequency (rad/sec)	Mass Ratio					
	0.00156			0.000156		
	Classical Damping	Non-classical Damping	Error (%)	Classical Damping	Non-classical Damping	Error (%)
24	2.070	2.460	15.9	4.267	2.766	54.3
42	0.451	0.459	1.7	0.455	0.463	1.7
62	0.667	0.299	122.3	1.135	0.301	276.8
97	0.283	0.320	11.7	0.190	0.388	51.2
134	0.252	0.271	6.9	0.359	0.288	24.7
154	0.231	0.231	0.0	0.283	0.234	21.4
162	0.228	0.228	0.1	0.232	0.230	0.9
171	0.225	0.226	0.4	0.225	0.227	0.8

^a Damping ratio in fundamental mode of structure = 8%; damping ratio of nonstructural element = 0.5%.
Source: Singh, M.P. and Suárez, L.E. *Earthquake Eng. Struct. Dyn.*, 15, 871–888, 1987. With permission.

of a single-degree-of-freedom nonstructural element are compared when this element is analyzed considering the nonclassical damping character of the combined system and when it is analyzed assuming that this combined system is classically damped. Table 19.1 summarizes the results for the case when the damping ratios in the fundamental mode of the structure and the nonstructural element are 6 and 1%, respectively, while Table 19.2 summarizes those when these damping ratios are 8 and 0.5%.

It may be noted from these tables that some large errors may be possible if the nonclassical damping effects in question are not accounted for. It is also noted that, in general, such an effect becomes important when the nonstructural to structural mass ratio is small, the natural frequency of the nonstructural element is close to one of the dominant frequencies of the structure and the difference between the damping ratios of the structure and the nonstructural element is large. Furthermore, it is noted that the

discrepancy between the results for the cases with classical and nonclassical damping becomes consistently larger as the nonstructural to structural mass ratio becomes smaller.

Finally, it should also be noted that traditionally floor response spectra are obtained under the assumption that a structure and its nonstructural elements behave as linear systems. As is well known, however, conventional structures are designed to resist strong earthquakes by incurring into their nonlinear range of behavior. Similarly, many nonstructural components have the capability to resist inelastic deformations. Hence, it is likely that a structure and its nonstructural elements will undergo inelastic deformations during a severe earthquake, and that this nonlinear behavior will influence the response of the nonstructural elements significantly.

At present, there is no clear understanding as to how structural nonlinearity may affect a floor response spectrum. In general, response reductions are expected for nonstructural components with natural frequencies equal to or greater than the fundamental natural frequency of the structure. These reductions result from two main factors: (1) an increase in the damping ratio of the structure as a result of its nonlinear behavior (hysteretic damping) and (2) a shift of the fundamental natural frequency of the structure away from the natural frequency of the nonstructural element. A further reduction is attained if the nonstructural element itself is allowed to go nonlinear in much the same way as is observed in a typical nonlinear response spectrum. Some numerical studies have shown, however, that floor response spectrum ordinates for a nonlinear structure may actually increase in comparison to those obtained when the structure is assumed to remain linear at all excitation levels. Moreover, these studies have also shown that this increase is particularly noticeable at high frequencies; that is, at frequencies higher than the structure's fundamental natural frequency.

Figure 19.12 illustrates the contrasting effect of structural nonlinearity in a floor response spectrum. This figure shows floor response spectrum ratios for a nonlinear five-story shear structure, where these ratios are obtained by dividing the floor response spectrum for the nonlinear structure by the corresponding floor response spectrum when the structure is assumed to have a linear behavior. Two values of the ductility factor μ are considered for the structure's first story: $\mu = 2$ and $\mu = 4$. All other stories are assumed to remain in their linear range of behavior. Figure 19.12a shows the aforementioned ratios for the first floor of the structure when the structure is excited by the S69E component of the ground motion recorded at Taft Lincoln School during the 1952 Kern County, CA, earthquake. Figure 19.12b shows those for the fifth floor of the structure when the structure is excited by the N28E component of the ground motion recorded at Mitchell Lake Road during the 1982 New Brunswick, Canada, earthquake. Note that in these figures a ratio of less than 1 represents a reduction in floor response spectrum ordinate due to the structural nonlinearity. Conversely, a ratio of more than 1 represents an increase.

It can be seen from these figures that in one case (Figure 19.12a) there is a considerable amplification in the high frequency range of the spectrum due to the nonlinearity of the structure. In the other case (Figure 19.12b) a reduction is observed over the entire frequency range of the spectrum. Worthwhile to note too is the fact that in both cases the structural nonlinearity produces, as expected, a reduction for frequencies that are near the fundamental natural frequency of the structure.

19.6.3 Alternative Methods

In view of the limitations of the floor response spectrum methods and the impracticality of a direct analysis of the combined structural–nonstructural system, several alternative methods have been developed that take into account not only the aforementioned interaction and nonclassical damping effects, but also overcome the practicality problems associated with such a direct analysis. In general two approaches have been followed. In one of these approaches, in recognition of the convenience and flexibility of the floor response spectrum method and its wide use in the nuclear power industry, corrections are introduced to this method to account for, in an approximate manner, interaction and nonclassical damping effects. Examples of these methods are those proposed by Lee and Penzien (1983), Gupta (1984), Igusa and Der Kiureghian (1985b), Singh and Sharma (1985), Asfura and Der Kiureghian (1986), Gupta and Jaw (1986b), Burdisso and Singh (1987) and Suárez and Singh (1987a, 1989). In the other approach, the response of the nonstructural element is obtained on the basis of an approximate

modal or random vibration analysis of the combined structural–nonstructural system, but using, through a modal synthesis, the dynamic properties of its separate components. This approach eliminates the main source of error inherent in the floor response spectrum method since by considering the two subsystems together as a single unit, the interaction between the two subsystems and the different and out-of-phase support motions are automatically taken into account. This approach is also a practical one. By formulating the analysis in terms of the dynamic properties of independent subsystems, one avoids the numerical difficulties associated with the large differences in the values of the parameters of the structure and the nonstructural element when conventional methods of analysis are used. Furthermore, one avoids solving a large eigenvalue problem, the need to generate intermediary floor response spectra (since the earthquake input is defined at the ground level) and the need to reanalyze the structure every time changes are made to the parameters of the nonstructural element.

Conceptually, the idea of determining the response of a nonstructural element in terms of an analysis of the combined system it forms with its supporting structure, but utilizing only the properties of the individual components, is a simple one. Its implementation, however, is not free of complications and difficulties. For example, if one wants to analyze such a combined system by means of the response spectrum method, one needs to first determine its natural frequencies, mode shapes, damping ratios, and maximum modal responses. Then, one needs to combine these modal responses using a modal combination rule. However, the system that results from combining two subsystems with such a drastic difference in the values of their masses, stiffnesses and damping constants is a system without classical modes of vibration and with closely spaced natural frequencies. This means that the natural frequencies and mode shapes of the system are complex valued and that the combination of its modal responses requires, and highly depends on, an accurate rule to combine the modal responses of a system with nonclassical damping and closely spaced natural frequencies. Notwithstanding such difficulties and complications, several methods that use this technique have been proposed throughout the years — methods that basically differ in the way the dynamic properties of the components are synthesized to obtain the dynamic properties of the combined system, and in the assumptions made to simplify the procedure. In chronological order, some of these methods are those suggested by Newmark (1972), Sackman and Kelly (1979), Newmark and Villaverde (1980), Der Kiureghian et al. (1983), Hernried and Sackman (1984), Gupta (1984), Igusa and Der Kiureghian (1985c), Gupta and Jaw (1986a), Villaverde (1986a, 1986b), Singh and Suarez (1987), Suárez and Singh (1987b), Muscolino (1990), Villaverde (1991), Saudy et al. (1994) and Gupta (1997).

All the methods referred to above have been derived specifically for linear nonstructural elements mounted on linear structures. However, as shown above and as pointed out by Lin and Mahin (1985), Aziz and Ghobarah (1988), Toro et al. (1989), Sewell et al. (1989), Igusa (1990), Singh et al. (1993), Schroeder and Backman (1994) and Adam and Fotiu (2000), the nonlinear behavior of a nonstructural element and that of its supporting structure may significantly affect the behavior of the nonstructural element, either in the form of an increase or a reduction over its linear response. These methods, therefore, may lead to either nonconservative or uneconomical designs.

Recognizing the importance of such nonlinear behavior, a few investigators have made an effort to derive simplified methods that incorporate structural and nonstructural nonlinearity. Given, however, the difficulties in obtaining explicit solutions for such a complex problem, most of the effort has been directed toward the development of reduction and amplification factors by which a linear floor spectrum should be modified to approximately take into account such nonlinearity (Kawakatsu et al., 1979; Lin and Mahin, 1985; Viti et al., 1981). Exceptions are the works of Villaverde (1987) and Igusa (1990). Villaverde (1987) developed a method based on the use of nonlinear ground response spectra for the analysis of linear multi-degree-of-freedom nonstructural elements mounted on an elastoplastic multi-degree-of-freedom building structure. Igusa (1990) derived an analytical solution for the response of a two-degree-of-freedom structural–nonstructural system with small nonlinearities, using random vibration theory and equivalent linearization techniques.

For a description of the difference between the methods of analysis cited above, the reader is referred to the state-of-the-art reviews made by Singh (1990) and Soong (1994), as well as the book by Gupta (1990).

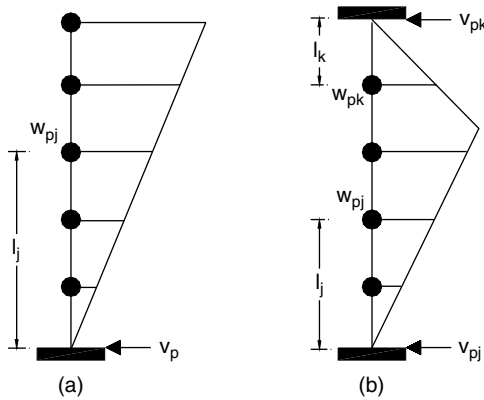


FIGURE 19.13 Assumed mode shapes for nonstructural elements with one and two points of attachment.

19.6.4 Design-Oriented Simplified Method

A procedure to determine in a conservative but simple way equivalent static lateral forces for the seismic design of nonstructural elements attached to buildings is presented next. This procedure is derived on the basis of a modal synthesis and the introduction of simplifying assumptions comparable to those employed in the development of the static method for the seismic design of buildings. It is intended to be valid for the design of nonstructural elements connected to a structure at one or two points, and those that together with their supporting structure form a system with nonclassical damping. It takes into account the dynamic interaction between the two subsystems, the level above the base of the structure of the point or points of the structure to which the nonstructural element is attached, the number of such attachment points and the nonlinear behavior of the structure and nonstructural elements. It uses, in addition, the design spectra specified by building codes for the design of the structure to also define the earthquake input to the nonstructural element. The derivation of the procedure is lengthy and tedious, so it will not be shown here. Interested readers may find this derivation in some of the author's publications (Villaverde 1991, 1997, 2000).

The following are some of the major assumptions made in the derivation of the procedure:

1. The total response of the combined structural–nonstructural system is approximately given by the response in the two modes of the system that correspond to the fundamental natural periods of the two independent subsystems.
2. The fundamental natural period of the nonstructural element coincides with the fundamental natural period of the structure; that is, the fundamental mode of the nonstructural element is in resonance with the fundamental mode of the structure.
3. The fundamental mode shape of the structure varies linearly from 0 at its base to a maximum value at its top.
4. The fundamental mode of the nonstructural element varies linearly along its height. In the case of a single point of attachment, it varies from 0 at its point where it is connected to the structure to a maximum value at its other end. In the case of two points of attachment, it varies from 0 at the two attachment points to a maximum value at the point where it attains its maximum displacement when each of its masses is subjected to a static force equal to its own weight (see Figure 19.13).
5. The generalized masses in the fundamental modes of the structure and the nonstructural element are equal to their respective total masses.
6. The damping ratios in the fundamental modes of the structure and the nonstructural element are equal to 5 and 0%, respectively.

7. Both the structure and nonstructural element exhibit elastoplastic behavior and this behavior is characterized by an initial stiffness and a yield strength.
8. The input response spectrum for the combined structural–nonstructural system is the elastic response spectrum specified for the design of the structure.

The procedure involves the calculation of equivalent static lateral forces whose values are intended to be greater than or equal to the maximum values of the lateral forces that may be generated on the masses of a nonstructural element by a specified design earthquake. These forces are determined according to

$$F_{pj} = \frac{\sum_{j=1}^n w_{pj} l_j}{V_p} V_p \quad (19.1)$$

where

F_{pj} = force acting at the center of the j th mass of the nonstructural element.

w_{pj} = weight of the j th mass of the nonstructural element.

l_j = distance from attachment point to j th mass of nonstructural element in the case of a nonstructural element with a single attachment point (see Figure 19.13a), or distance from the lower or upper attachment point to the j th mass of the nonstructural element in the case of a nonstructural element with two attachment points. The lower attachment point is selected when such j th mass is located below the point at which the element attains its maximum deflection when each mass is subjected to a lateral force equal to its own weight; otherwise, the upper attachment point is selected (see Figure 19.13b).

n = total number of masses in the nonstructural element.

V_p = base shear or sum of the shears at the supports of the nonstructural element (see Figure 19.13), calculated according to

$$V_p = \frac{IC}{\lambda} I_p C_p w_p \quad (19.2)$$

in which, if f is the fundamental natural frequency of the structure,

$$\lambda = \begin{cases} \mu_{eq} & \text{iff } f \leq 2 \text{ Hz} \\ \sqrt{2\mu_{eq}-1} & \text{if } 2 < f < 8 \text{ Hz} \\ 1 + \frac{33-f}{25} (\sqrt{2\mu_{eq}-1} - 1) & \text{if } 8 \leq f \leq 33 \text{ Hz} \end{cases} \quad (19.3)$$

and μ_{eq} is an equivalent ductility factor calculated according to

$$\mu_{eq} = \left[\frac{1}{N+n'} \left(\frac{N}{\mu} + \frac{n'}{\mu_p} \right) \right]^{-1} \quad (19.4)$$

where μ is the ductility factor specified for the structure, μ_p is the ductility factor specified for the nonstructural element, N is the number of floors in the building and n' is the number of resisting elements in the nonstructural system.

In addition,

I = importance factor specified for the structure

C = spectral ordinate, expressed as a fraction of the acceleration of gravity, corresponding to the fundamental natural period of the structure in the response or design spectrum specified for the design of the structure

I_p = importance factor for nonstructural element (specified by local code or arbitrarily selected by designer)

w_p = total weight of nonstructural element

C_p = amplification factor given by

$$C_p = \frac{1}{2\sqrt{\left|\frac{w_p}{W} - \frac{0.0025}{\Phi_0^2}\right|}} \leq 12.5\Phi_0 \quad (19.5)$$

where

W = total building weight and

$$\Phi_0 = \frac{Wh_{av}}{\sum_{i=1}^N W_i h_i} \quad (19.6)$$

in which

h_i = elevation above grade of building's i th floor

h_{av} = average of elevations above grade of points of the building to which the nonstructural element is attached

W_i = weight of building's i th floor

As noted earlier, this procedure is valid only for the case when a nonstructural element is attached to the structure at no more than two points. However, a nonstructural element with more than two attachment points can still be analyzed with this procedure by breaking it up into a series of subsystems with one or two attachment points each, and by considering each of these subsystems separately. For example, a nonstructural element rigidly attached to the 4th, 7th and 10th floors of a supporting building (see Figure 19.14) may be considered as composed of two independent subelements with two attachment points each, one attached to the 4th and 7th floors and the other attached to the 7th and 10th.

As noted earlier, too, the procedure is based on the assumption that the fundamental natural period of the nonstructural element is in resonance with the fundamental natural period of the supporting structure; i.e., that the values of these two periods are equal or are very close to one another. Although this assumption offers the advantage of not having to know the natural periods of the nonstructural element to carry out its seismic design, it may be nonetheless overly conservative for those cases in which two such natural periods are significantly different from one another. As a means to reduce the conservatism involved in the procedure for such cases, the amplification factor C_p may be replaced by a modified amplification factor C_m that varies linearly with the period ratio T_p/T , between the maximum value C_p , when this ratio is close to 1, and the minimum Φ_0 , when such a ratio is substantially different from 1.0. In this period ratio, T_p represents the fundamental natural period of the nonstructural element and T the fundamental natural period of the structure.

The variation of the modified amplification factor C_m is shown in Figure 19.15, together with the limits of the period ratio beyond which the amplification factor for the nonstructural element should be considered equal to Φ_0 , and the limits that define the range for which the structure and the nonstructural element should be considered in resonance with one another. In this figure, b is defined as

$$b = \frac{1}{2} \Phi_0 \sqrt{w_p / W} \quad (19.7)$$

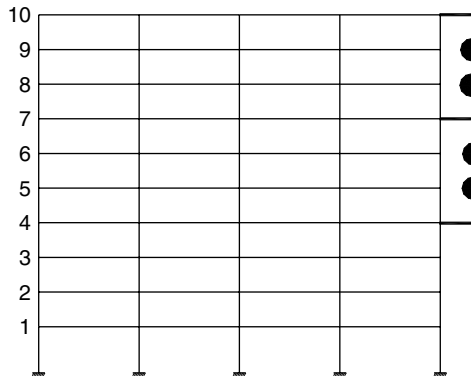


FIGURE 19.14 Example of nonstructural element connected to multiple points of supporting structure.

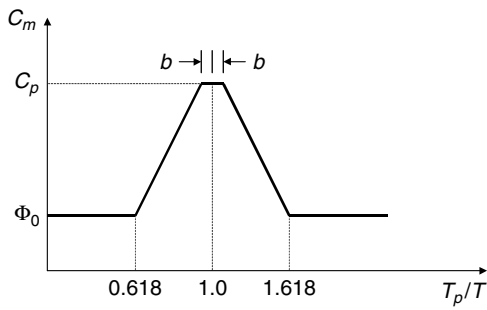


FIGURE 19.15 Variation of modified amplification factor with natural period ratio.

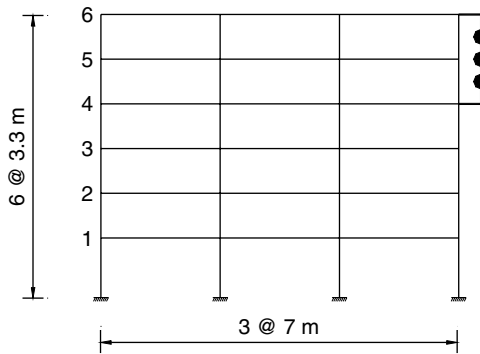


FIGURE 19.16 Building and nonstructural element considered in Example 19.2. (Note 1 m = 3.28 ft.)

Note, thus, that if the fundamental natural period of the nonstructural element is known, the graph in Figure 19.15 may be used to reduce, in terms of the aforementioned natural period ratio, the magnitude of the amplification factor C_p in Equation 19.2 and, as a result, the magnitude of the seismic forces determined with Equation 19.1.

Example 19.2. Lateral forces for design of nonstructural element using simplified procedure

Using the simplified procedure presented above, determine the lateral forces on the masses of the nonstructural element shown in Figure 19.16, when, as indicated in this same figure, the nonstructural element is rigidly connected to the fourth and sixth stories of a six-story office building. The building is located over a deposit of stiff soil in the city of Irvine, CA, and is structured with steel moment-resisting frames. A ductility factor of 6 is specified for the design of these moment-resisting frames. The building's weight per floor is 2200 kN (494.6 kips) and its total weight is thus equal to 13,200 kN (2967.6 kips). The fundamental natural period of the building is 0.6 sec. The nonstructural element, an ordinary architectural fixture for which its importance factor may be considered equal to 1.0, is modeled as a three-degree-of-freedom shear beam with four equal segments, each with a length of 1.65 m (5.41 ft). Each of its three masses weighs 4.4 kN (0.99 kips), and hence its total weight is 13.2 kN (2.97 kips); i.e., 0.1% of the total weight of the building. Its fundamental period is estimated to be 0.5 sec when its two ends are considered fixed. A ductility factor of 2 may be considered in its design. Use the 1997 version of the UBC to define the earthquake input to the building.

Solution: For the case under consideration, the average of the elevations aboveground of the nonstructural element's two attachment points is equal to 16.5 m (54.1 ft). Hence, substitution of this value and the floor weights given above into Equation 19.6 leads to

$$\Phi_0 = \frac{W h_{av}}{\sum_{i=1}^N W_i h_i} = \frac{13200(16.5)}{2200(3.3 + 6.6 + 9.9 + 13.2 + 16.5 + 19.8)} = 1.43$$

Similarly, by substitution of this value of Φ_0 and the given total weights of the structure and the nonstructural element into Equation 19.5, one obtains

$$C_p = \frac{1}{2\sqrt{\left|\frac{w_p}{W} - \frac{0.0025}{\Phi_0^2}\right|}} = \frac{1}{2\sqrt{\left|\frac{13.2}{13200} - \frac{0.0025}{1.43^2}\right|}} = 33.5$$

which exceeds the limit of $12.5\Phi_0 = 12.5(1.43) = 17.87$. Therefore, the amplification factor C_p will be considered equal to

$$C_p = 17.87$$

However, since in this case the fundamental natural frequencies of both the structure and the nonstructural elements are known, it is possible to use a reduced value of this amplification factor using the graph in Figure 19.15. To this end, note that the corresponding period ratio is given by

$$\frac{T_p}{T} = \frac{0.5}{0.6} = 0.833$$

Note, too, that according to Equation 19.7, in the case under consideration the value of the parameter b in such a graph is equal to

$$b = \frac{1}{2} \Phi_0 \sqrt{w_p/W} = \frac{1}{2}(1.43)\sqrt{13.2/13,200} = 0.023$$

Consequently, from Figure 19.15 the reduced amplification factor becomes

$$C_m = 1.43 + \frac{0.833 - 0.618}{0.977 - 0.618} (17.87 - 1.43) = 11.3$$

Now, by substitution of the specified ductility factors of 6 for the structure and 2 for the nonstructural element into Equation 19.4, and by considering that for the building and nonstructural element under analysis $N = 6$ and $n' = 4$, the equivalent ductility factor for the structural–nonstructural system results as

$$\mu_{eq} = \left[\frac{1}{N+n'} \left(\frac{N}{\mu} + \frac{n'}{\mu_p} \right) \right]^{-1} = \left[\frac{1}{6+4} \left(\frac{6}{6} + \frac{4}{2} \right) \right]^{-1} = 3.33$$

In like fashion, for a structural frequency of $1/0.6 = 1.667$ Hz, Equation 19.3 yields

$$\lambda = \mu_{eq} = 3.33$$

Also, according to the 1997 version of the UBC, for the building under consideration one has that

$$C_a = 0.44N_a = 0.44(1.0) = 0.44$$

$$C_v = 0.64N_v = 0.64(1.2) = 0.77$$

$$T_s = \frac{C_v}{2.5C_a} = \frac{0.77}{2.5(0.44)} = 0.7 \text{ sec.}$$

and hence, the spectral acceleration for the design of the building may be considered equal to

$$C = 2.5C_a = 2.5(0.44) = 1.10$$

Finally, note that for an office building the UBC specifies an importance factor I equal to 1.0.

Thus, after substitution of the values found above for λ , C and C_m and the values specified for I and I_p , Equation 19.2 leads to

$$V_p = \frac{IC}{\lambda} I_p C_m w_p = \frac{(1.0)(1.10)}{3.33} (1.0)(11.3) w_p = 3.7 w_p = 3.7(13.2) = 48.8 \text{ kN (11.0 kips)}$$

Now, to distribute this force of 48.8 kN (11.0 kips) among the three masses of the nonstructural element, one needs to first determine its point of maximum deflection under lateral forces equal to the weight of its masses and define the distances l_j that appear in Equation 19.1. It may be noted, however, that in this case the nonstructural element is symmetric in mass and geometry and that consequently such a point of maximum deflection is located at its geometric center. By inspection, therefore, it can be determined that $l_1 = l_3 = 1.65 \text{ m (5.4 ft)}$ and $l_2 = 3.3 \text{ m (10.8 ft)}$, where l_1 , l_2 and l_3 correspond, respectively, to the lower, middle and upper masses. As a result, Equation 19.1 gives

$$F_{p1} = \frac{\frac{w_{p1}}{3} l_1}{\sum_{j=1}^3 w_{pj} l_j} V_p = \frac{4.4(1.65)}{4.4(1.65 + 3.30 + 1.65)} (48.8) = 0.25(48.8) = 12.2 \text{ kN (2.75 kips)}$$

$$F_{p2} = \frac{w_{p2} l_2}{\sum_{j=1}^3 w_{pj} l_j} V_p = \frac{4.4(3.30)}{4.4(1.65+3.30+1.65)} (48.8) = 0.50(48.8) = 24.4 \text{ kN (5.50 kips)}$$

$$F_{p3} = \frac{w_{p3} l_3}{\sum_{j=1}^3 w_{pj} l_j} V_p = \frac{4.4(1.65)}{4.4(1.65+3.30+1.65)} (48.8) = 0.25(48.8) = 12.2 \text{ kN (2.75 kips)}$$

19.7 Design Provisions in Building Codes

19.7.1 Overview

Several building codes and seismic provisions give recommendations for the seismic design of equipment and other nonstructural elements. In the United States, some of these include the UBC (1997), issued by the International Conference of Building Officials; the National Earthquake Hazard Reduction Program (NEHRP) *Recommended Provisions for Seismic Regulations for New Buildings* (2000), issued by the Building Seismic Safety Council; the *Recommended Lateral Force Requirements and Commentary* (1990), issued by the Structural Engineers Association of California; the International Building Code (IBC, 2000); the *Tri-Services Manual* (Departments of the Navy, Army, and Air Force, 1992); and the American Society of Mechanical Engineers (ASME) Boiler and Pressure Vessel Code (ASME, 1993). Only the provisions in the UBC and the NEHRP provisions will be discussed here, as these are the most frequently used for the design of nonstructural elements in ordinary buildings. Although also worth discussing, the provisions in the 2000 IBC will not be described since these provisions are based on and, except for some minor modifications and the values of a few coefficients, are identical to the 2000 NEHRP provisions.

In general, the intention of the provisions contained in the UBC and the NEHRP provisions for nonstructural elements is to ensure that nonstructural elements designed according to these provisions are able to withstand the accelerations and deformations generated by the design earthquake without fracturing, shifting or toppling. In general, too, these provisions are based on concepts and techniques that are similar to those used for the design of building structures. Specifically, they specify an equivalent lateral force, where this force is expressed as a fraction of an element's weight, and is a function of the ground acceleration, location of the component relative to the height of the building, the component's dynamic amplification and the component's ability to absorb inelastic deformations. They also include guidelines for the design of elements that are sensitive to story drifts.

The formulas specified to compute the equivalent lateral forces were developed empirically on the basis of floor acceleration data recorded in buildings during strong earthquakes in California (Kehoe and Freeman, 1998), assuming that the floor accelerations within the structure vary from the ground to the roof according to a trapezoidal distribution. The acceleration at the ground level is intended to be the acceleration used as input for the structure itself. From the examination of the recorded data, assuming a maximum value for the roof acceleration equal to three to four times the ground acceleration was found reasonable. A response modification factor (R_p) is included in the formulas to account for the overstrength and the inelastic deformation capability of the nonstructural element and/or its anchors. The inelastic behavior of the support structure was not included in the erroneous belief that (1) the extent of inelastic behavior is usually minor for structures designed by modern building codes, as their design is in many cases governed by drift limits or other loads; (2) nonstructural components are often designed without knowledge of the structure's composition; and (3) it is a conservative consideration. Altogether, the formulas are intended to account for some of the most important factors that influence the response of nonstructural components but without unduly burdening designers with complicated formulations.

19.7.2 Uniform Building Code

The provisions for nonstructural elements in the 1997 version of the UBC are based on ultimate strength design principles. They specify the use of a lateral force for the seismic design of elements of structures and their attachments, permanent nonstructural components and their attachments and the attachments of permanent equipment supported by a structure. Attachments include anchorages and required braces. Exemptions to these requirements are attachments for floor or roof-mounted equipment weighing less than 400 lb (181 kg) and furniture.

Two alternate formulas are provided to compute the required lateral force. The first one is conservative, but it is simple and easy to apply. This formula has the form

$$F_p = 4.0C_a I_p W_p \quad (19.8)$$

The other formula is more complicated, but it takes more factors into account. It is given by

$$F_p = \frac{a_p C_a I_p}{R_p} (1 + 3 \frac{h_x}{h_r}) W_p \quad (19.9)$$

except that F_p need not be greater than

$$(F_p)_{\max} = 4.0C_a I_p W_p \quad (19.10)$$

and should not be less than

$$(F_p)_{\min} = 0.7C_a I_p W_p \quad (19.11)$$

In the equations above,

F_p = lateral force applied at the component or element's center of mass and distributed in proportion to the component or element's mass distribution

a_p = component amplification factor (i.e., factor that accounts for dynamic response of nonstructural element to building motion) selected from Table 19.3 according to component or element type, varying between 1.0 and 2.5

C_a = seismic coefficient specified for the design of the structure

I_p = component or element importance factor, equal to 1.5 for essential and hazardous facilities and 1.0 for special and standard occupancy structures

R_p = component response modification factor selected from Table 19.3 according to component or element type, varying between 1.5 and 4.0 (considered equal to 1.5 for anchorages with shallow expansion anchor bolts, chemical anchors or cast-in-place anchors and equal to 1.0 for anchorage constructed with nonductile materials or adhesives)

h_x = element or component elevation above grade, always considered to be greater than 0

h_r = elevation above grade of structure's roof

W_p = element or component weight

For the purpose of determining the component amplification factor a_p , the code defines flexible components or elements as those that together with their attachments have a fundamental natural period greater than 0.06 sec.

The code also specifies that components or elements attached to a structure at several points, such as cladding, stairwells, windows, ducts and piping systems, be designed to resist the effects of the relative

TABLE 19.3 Horizontal Force Factors a_p and R_p

Elements of Structures and Nonstructural Components and Equipment ^a	a_p	R_p	Footnote
1. Elements of structures			
A. Walls including the following:	2.5	3.0	
(1) Unbraced (cantilevered) parapets			
(2) Exterior walls at or above the ground floor and parapets braced above their centers of gravity	1.0	3.0	b
(3) All interior-bearing and nonbearing walls	1.0	3.0	b
B. Penthouse (except when framed by an extension of the structural frame)	2.5	4.0	
C. Connections for prefabricated structural elements other than walls. See also UBC Section 1632.2	1.0	3.0	c
2. Nonstructural components			
A. Exterior and interior ornamentations and appendages	2.5	3.0	
B. Chimneys, stacks and trussed towers supported on or projecting above the roof:			
(1) Laterally braced or anchored to the structural frame at a point below their centers of mass	2.5	3.0	
(2) Laterally braced or anchored to the structural frame at or above their centers of mass	1.0	3.0	
C. Signs and billboards	2.5	3.0	
D. Storage racks (include contents) over 6 ft (1829 mm) tall	2.5	4.0	d
E. Permanent floor-supported cabinets and book stacks more than 6 ft (1829 mm) in height (include contents)	1.0	3.0	e
F. Anchorage and lateral bracing for suspended ceilings and light fixtures	1.0	3.0	c, f, g, h
G. Access floor systems	1.0	3.0	d, e, i
H. Masonry or concrete fences over 6 ft (1829 mm) high	1.0	3.0	
I. Partitions	1.0	3.0	
3. Equipment			
A. Tanks and vessels (include contents), including support systems	1.0	3.0	
B. Electrical, mechanical and plumbing equipment and associated conduit and ductwork and piping	1.0	3.0	e, j, k, l, m, n, o, p
C. Any equipment laterally braced or anchored to the structural frame at a point below its center of mass	2.5	3.0	e, j, n, o, p
D. Anchorage of emergency power supply systems and essential communications equipment. Anchorage and support systems for battery racks and fuel tanks necessary for operation of emergency equipment. See also UBC Section 1632.2	1.0	3.0	q, r
E. Temporary containers with flammable or hazardous materials	1.0	3.0	s
4. Other components			
A. Rigid components with ductile material and attachments	1.0	3.0	a
B. Rigid components with nonductile material or attachments	1.0	1.5	a
C. Flexible components with ductile material and attachments	2.5	3.0	a
D. Flexible components with nonductile material or attachments	2.5	1.5	a

^a See UBC Section 1627 for definitions of flexible components and rigid components.

^b See UBC Section 1633.2.4 and Section 1633.2.8 for concrete and masonry walls and UBC Section 1632.2 for connections for panel connectors for panels.

^c Applies to Seismic Zones 2, 3 and 4 only.

^d Ground supported steel storage racks may be designed using the provisions of UBC Section 1634. Chapter 22, Division VI, may be used for design, provided seismic design forces are equal to or greater than those specified in UBC Section 1632.2 or Section 1634.2, as appropriate.

^e Only anchorage or restraints need to be designed.

^f Ceiling weight shall include all light fixtures and other equipment or partitions that are laterally supported by the ceiling. For purposes of determining the seismic force, a ceiling weight of not less than 4 psf (0.19 kN/m^2) shall be used.

^g Ceilings constructed of lath and plaster or gypsum board screw or nail attached to suspended members that support a ceiling at one level extending from wall to wall need not be analyzed, provided the walls are not over 50 ft (15,240 mm) apart.

^h Light fixtures and mechanical services installed in metal suspension systems for acoustical tile and lay-in panel ceilings shall be independently supported from the structure above as specified in UBC Standard 25-2, Part III.

ⁱ W_p for access floor systems shall be the dead load of the access floor system plus 25% of the floor live load plus a 10-psf (0.48 kN/m^2) partition load allowance.

^j Equipment includes, but is not limited to, boilers, chillers, heat exchangers, pumps, air-handling units, cooling towers, control panels, motors, switchgear, transformers and life-safety equipment. It shall include major conduit, ducting and piping, which services such machinery and equipment and fire sprinkler systems. See UBC Section 1632.2 for additional requirements for determining a_p for nonrigid or flexibly mounted equipment.

TABLE 19.3 Horizontal Force Factors a_p and R_p (continued)

^k Seismic restraints may be omitted from piping and duct supports if all the following conditions are satisfied: Lateral motion of the piping or duct will not cause damaging impact with other systems; the piping or duct is made of ductile material with ductile connections; lateral motion of the piping or duct does not cause impact of fragile appurtenances (e.g., sprinkler heads) with any other equipment, piping or structural member; lateral motion of the piping or duct does not cause loss of system vertical support; rod-hung supports of less than 12 in. (305 mm) in length have top connections that cannot develop moments; and support members cantilevered up from the floor are checked for stability.

^l Seismic restraints may be omitted from electrical raceways, such as cable trays, conduit and bus ducts, if all the following conditions are satisfied: Lateral motion of the raceway will not cause damaging impact with other systems; lateral motion of the raceway does not cause loss of system vertical support; rod-hung supports of less than 12 in. (305 mm) in length have top connections that cannot develop moments; and support members cantilevered up from the floor are checked for stability.

^m Piping, ducts and electrical raceways, which must be functional following an earthquake, spanning between different buildings or structural systems shall be sufficiently flexible to withstand relative motion of support points assuming out-of-phase motions.

ⁿ Vibration isolators supporting equipment shall be designed for lateral loads or restrained from displacing laterally by other means. Restraint shall also be provided, which limits vertical displacement, such that lateral restraints do not become disengaged. a_p and R_p for equipment supported on vibration isolators shall be taken as 2.5 and 1.5, respectively, except that if the isolation mounting frame is supported by shallow or expansion anchors, the design forces for the anchors calculated by Equation 8 or 9 shall be additionally multiplied by a factor of 2.0.

^o Equipment anchorage shall not be designed such that lateral loads are resisted by gravity friction (e.g., friction clips).

^p Expansion anchors, which are required to resist seismic loads in tension, shall not be used where operational vibrating loads are present.

^q Movement of components within electrical cabinets, rack- and skid-mounted equipment and portions of skid-mounted electromechanical equipment that may cause damage to other components by displacing, shall be restricted by attachment to anchored equipment or support frames.

^r Batteries on racks shall be restrained against movement in all directions due to earthquake forces.

^s Seismic restraints may include straps, chains, bolts, barriers or other mechanisms that prevent sliding, falling and breach of containment of flammable and toxic materials. Friction forces may not be used to resist lateral loads in these restraints unless positive uplift restraint is provided, which ensures that the friction forces act continuously.

Source: Uniform Building CodeTM, International Conference of Building Officials, Whittier, CA, 1987. With permission. Copyright 1997, International Conference of Building Officials (ICBO). ICBO assumes no responsibility for the accuracy or the completeness of this table.

motion between such attachment points. For this purpose, it is required that the calculation of this relative motion be based on the maximum inelastic displacements of the structure. Lastly, it specifies that the lateral forces determined with the above formulas be used to design the members and connections that transfer these forces to the structure. In the design of these members and connections, it is necessary to make use of the load combinations and factors specified for the design of structures, except that the reliability/redundancy factor used in such load combinations may be taken equal to 1.0.

TABLE 19.4 Component Importance Factors I_p

Component Importance	I_p
Component required to function after an earthquake	1.5
Component containing hazardous contents	1.5
Storage racks in occupancies open to the general public (e.g., warehouse retail stores)	1.5
All components needed for continued operation of the facility, or whose failure could impair the continued operation of the facility (for structures in Seismic Group III)	1.5
All other components	1.0

19.7.3 NEHRP Provisions

As the UBC, the NEHRP provisions are also based on ultimate strength design principles and establish minimum design criteria for architectural, mechanical, electrical and nonstructural systems; components;

and elements permanently attached to structures, including supporting structures and components (henceforth collectively referred to as “components”). These design criteria recognize ground motion and structural amplifications, component toughness and weight, and performance expectations. They are presented in terms of a required minimum equivalent static force and a minimum relative displacement demand when the component is connected to the structure at multiple points.

The required minimum static force is given by

$$F_p = I_p \frac{0.4a_p S_{DS} W_p}{R_p} (1 + 2 \frac{z}{h}) \quad (19.12)$$

except that F_p need not be greater than

$$(F_p)_{\max} = 1.6 S_{DS} I_p W_p \quad (19.13)$$

and must not be less than

$$(F_p)_{\min} = 0.3 S_{DS} I_p W_p \quad (19.14)$$

In the foregoing equations:

F_p = seismic design force applied at the component's center of mass and distributed according to the component's mass distribution

S_{DS} = short-period design spectral acceleration, given by $S_{DS} = (2/3)S_{MS}$, where S_{MS} , in turn, is equal to $S_{MS} = F_a S_s$, in which S_s is the maximum spectral acceleration determined for the site under consideration from the seismic maps in the provisions, and F_a is a coefficient that adjusts S_s for site effects

a_p = component amplification factor selected from Table 19.4 or Table 19.5 according to the type and flexibility of the component, varying between 1.00 and 2.50

I_p = component importance factor equal to either 1.00 or 1.50, selected according to component importance from Table 19.4

R_p = component response modification factor selected from Table 19.5 or Table 19.6 according to the type and deformability of the component, varying between 1.0 and 5.0

z = height above grade of highest point of component attachment (for items at or below structure base, consider z equal to 0)

h = average height of structure's roof relative to grade elevation

W_p = component weight

The seismic force F_p is applied independently longitudinally and transversely in combination with service loads acting on the component. Horizontal and vertical earthquake effects need to be combined according to

$$E = \rho F_p + 0.2 S_{DS} D \quad (19.15)$$

when the vertical and horizontal effects are additive, and

$$E = \rho F_p - 0.2 S_{DS} D \quad (19.16)$$

when the vertical effects counteract the horizontal effects. In these two equations:

TABLE 19.5 Coefficients a_p and R_p for Architectural Components

Architectural Component or Element	a_p ^a	R_p ^b
1. Interior nonstructural walls and partitions (see also NEHRP Section 6.8)		
a. Plain (unreinforced) masonry walls	1.0	1.5
b. All other walls and partitions	1.0	2.5
2. Cantilever elements (unbraced or braced to structural frame below its center of mass)		
a. Parapets and cantilever interior nonstructural walls	2.5	2.5
b. Chimneys and stacks where laterally supported by structures	2.5	2.5
3. Cantilever elements (braced to structural frame above its center of mass)		
a. Parapets	1.0	2.5
b. Chimneys and stacks	1.0	2.5
c. Exterior nonstructural walls	1.0	2.5
4. Exterior nonstructural wall elements and connections (see also NEHRP Section 6.2.4)		
a. Wall element	1.0	2.5
b. Body of wall panel connections	1.0	2.5
c. Fasteners of the connecting system	1.25	1.0
5. Veneer		
a. High deformability elements and attachments	1.0	2.5
b. Low deformability and attachments	1.0	1.5
6. Penthouses (except when framed by an extension of the building frame)	2.5	3.5
7. Ceilings (see also NEHRP Section 6.2.6)		
a. All	1.0	2.5
8. Cabinets		
a. Storage cabinets and laboratory equipment	1.0	2.5
9. Access floors (see also NEHRP Section 6.2.7)		
a. Special access floors (designed in accordance with NEHRP Section 6.2.7.2)	1.0	2.5
b. All other	1.0	1.5
10. Appendages and ornamentations	2.5	2.5
11. Signs and billboards	2.5	2.5
12. Other rigid components		
a. High deformability elements and attachments	1.0	3.5
b. Limited deformability elements and attachments	1.0	2.5
c. Low deformability elements and attachments	1.0	1.5
13. Other flexible components		
a. High deformability elements and attachments	2.5	3.5
b. Limited deformability elements and attachments	2.5	2.5
c. Low deformability elements and attachments	2.5	1.5

^a A lower value for a_p may be justified by detailed dynamic analysis. The value for a_p shall not be less than 1.00. The value of $a_p = 1$ is for equipment generally regarded as rigid and rigidly attached. The value of $a_p = 2.5$ is for flexible components or flexibly attached components. See NEHRP Chapter 2 for definitions of rigid and flexible components including attachments.

^b Where flexible diaphragms provide lateral support for walls and partitions, the design forces for anchorage to the diaphragm shall be as specified in NEHRP Section 5.2.5.

Source: NEHRP Recommended Provisions for the Seismic Regulations for New Buildings, Building Seismic Safety Council, Washington, D.C., 2000.

E = effect of horizontal and vertical earthquake-induced forces

D = dead load

ρ = reliability factor, allowed to be taken as 1.0 for the design of nonstructural elements

When positive and negative wind loads exceed the value of F_p for nonstructural exterior walls, these wind loads will govern the design. Similarly, the code-specified horizontal loads will govern the design for interior partitions when these loads exceed F_p .

TABLE 19.6 Coefficients a_p and R_p for Mechanical and Electrical Components

Mechanical and Electrical Component or Element ^a	a_p ^b	R_p
1. General mechanical		
a. Boilers and furnaces	1.0	2.5
b. Pressure vessels on skirts and free-standing	2.5	2.5
c. Stacks	2.5	2.5
d. Cantilevered chimneys	2.5	2.5
e. Other	1.0	2.5
2. Manufacturing and process machinery		
a. General	1.0	2.5
b. Conveyors (nonpersonnel)	2.5	2.5
3. Piping systems		
a. High deformability elements and attachments	1.0	3.5
b. Limited deformability elements and attachments	1.0	2.5
c. Low deformability elements and attachments	1.0	1.5
4. HVAC system equipment		
a. Vibration isolated	2.5	2.5
b. Nonvibration isolated	1.0	2.5
c. Mounted in-line with ductwork	1.0	2.5
d. Other	1.0	2.5
5. Elevator components	1.0	2.5
6. Escalator components	1.0	2.5
7. Trussed towers (free-standing or guyed)	2.5	2.5
8. General electrical		
a. Distributed systems (bus ducts, conduit, cable tray)	2.5	5.0
b. Equipment	1.0	2.5
9. Lighting fixtures	1.0	1.5

^a Components mounted on vibration isolation systems shall have a bumper restraint or snubber in each horizontal direction. The design force shall be taken as $2F_p$ if the maximum clearance (air gap) between the equipment support frame and restraint is greater than 1/4 in. If the maximum clearance is specified on the construction documents to be not greater than 1/4 in., the design force may be taken as F_p .

^b A lower value for a_p is permitted provided a detailed dynamic analysis is performed, which justifies a lower limit. The value for a_p shall not be less than 1.00. The value of $a_p = 1$ is for equipment generally regarded as rigid or rigidly attached. The value of $a_p = 2.5$ is for flexible components or flexibly attached components. See NEHRP Chapter 2 for definitions of rigid and flexible components including attachments.

Source: NEHRP Recommended Provisions for the Seismic Regulations for New Buildings, Building Seismic Safety Council, Washington, D.C., 2000.

The required minimum relative displacement demand between two of the connection points of a nonstructural component with multiple connection points is determined according to the following equations:

For two connection points on the same structure or same structural system (Structure A), one point at level x and the other at level y , the relative displacement is determined according to

$$D_p = \delta_{xA} - \delta_{yA} \quad (19.17)$$

except that D_p need not be greater than

$$D_p = (X - Y) \frac{\Delta_{aA}}{h_{sx}} \quad (19.18)$$

For two connection points on separate structures or structural systems, Structure A and Structure B, one at level x and the other at level y , D_p is determined according to

$$D_p = |\delta_{xA}| + |\delta_{yB}| \quad (19.19)$$

except that D_p need not be greater than

$$D_p = \frac{X\Delta_{aA}}{h_{sx}} + \frac{Y\Delta_{aB}}{h_{sx}} \quad (19.20)$$

In the foregoing equations:

D_p	= relative seismic displacement a component must be able to resist
$\delta_{xA}, \delta_{yA}, \delta_{yB}$	= deflection at level x of Structure A, deflection at level y of Structure A and deflection at level y of Structure B, respectively, all determined from an elastic analysis and multiplied by the deflection amplification factor C_d
X	= height of upper support attachment at level x as measured from the base of the structure
Y	= height of lower support attachment at level y as measured from the base of the structure
Δ_{aA}, Δ_{aB}	= allowable story drift for Structure A, Structure B
h_{sx}	= story height used in the definition of allowable drift Δ_a

In regard to the relative seismic displacements calculated according to the above equations, the NEHRP provisions require that the effect of these displacements be considered in combination with the displacements induced by other loads, such as those generated by thermal and static loads.

The foregoing equations are introduced in recognition that components with multiple points of connection such as cladding, stairwells, windows and piping systems need to be designed to resist the relative displacement between their attachment points. The first equation involves the computed displacements of the structure. The second, an intended upper bound, is formulated in terms of structural story drift limits in consideration of the fact that the structural displacements are not always available at the time a component is being designed.

For the purpose of the requirements introduced above, components are considered to have the same seismic design category as that of the structure they occupy or to which they are attached. Similarly, flexible components are those that together with their attachments have a fundamental natural period of 0.06 sec or greater. Exempted from such requirements are:

1. All components in Seismic Design Category A.
2. Architectural components in Seismic Design Category B other than parapets supported by bearing walls or shear walls when I_p is equal to 1.0.
3. Mechanical and electrical components in Seismic Design Category B.
4. Mechanical and electrical components in Seismic Design Category C when I_p is equal to 1.0.
5. Mechanical and electrical components in Seismic Design Categories D, E and F that are mounted at 4 ft (1.22 m) or less above a floor level, weigh 400 lb (1780 N) or less, have I_p equal to 1.0 and are provided with flexible connections between the components and associated ductwork, piping and conduit.
6. Mechanical and electrical components in Seismic Design Categories C, D, E and F that weigh 20 lb (95 N) or less (5 lb/ft [7 N/m] or less for distributed systems), have I_p equal to 1.0 and are provided with flexible connections between the components and associated ductwork, piping and conduit.

Example 19.3. Design lateral force for equipment unit

The reciprocating chiller shown in Figure 19.17 is mounted on the roof of a 10-story hospital building. The building is located on the coastal region of Irvine, CA, over a deposit of stiff soil and has a height of 180 ft (54.9 m). The chiller weighs 15.0 kips (66.7 kN) and is mounted on four flexible isolators to damp the vibrations generated during the operation of the unit. Determine the shear and tension demands

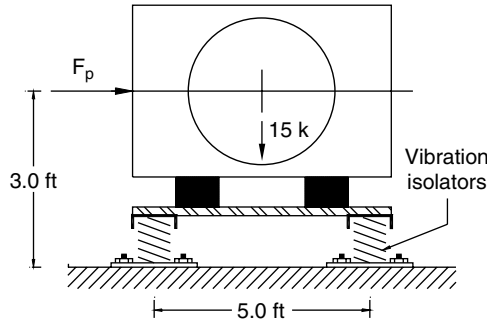


FIGURE 19.17 Equipment considered in Example 19.3. (Note: 1 ft = 0.305 m; 1 kip = 4.45 kN; adapted from Sabol, T.A. (1989). Design of nonstructural systems and components, in *Seismic Design Handbook*, Naeim, F., Ed., Van Nostrand Reinhold, New York, chap. 12. With permission.)

on the vibration isolators under earthquake load using (1) the 1997 edition of the UBC; and (2) the 2000 edition of the NEHRP provisions.

Solution: (1) For the building under consideration, one has that

$$h_x = h_r = 180 \text{ ft (54.9 m)}$$

and for Irvine, CA (Zone 4), Soil Profile S_D (stiff soil profile), and a near-source factor N_a of 1.5 (as known seismic sources around Irvine are at a distance of less than 2 km [1.2 mi]),

$$C_a = 0.44N_a = 0.44(1.5) = 0.66$$

Additionally, according to Footnote of Table 19.3, the horizontal force factors a_p and R_p for equipment supported on vibration isolators need to be considered equal to

$$a_p = 2.5$$

$$R_p = 1.5$$

Moreover, the code specifies that for an essential facility (hospital) $I_p = 1.5$. Therefore, according to Equation 19.9,

$$\begin{aligned} F_p &= \frac{a_p C_a I_p}{R_p} \left(1 + 3 \frac{h_x}{h_r}\right) W_p \\ &= \frac{2.5(0.66)(1.5)}{1.5} \left(1 + 3 \frac{180}{180}\right) W_p = 6.6 W_p \\ &= 6.6(15) = 99.0 \text{ kips (440.4 kN)} \end{aligned}$$

which is greater than

$$(F_p)_{\min} = 0.7 C_a I_p W_p = 0.7(0.66)(1.5)W_p = 0.69(15) = 10.4 \text{ kips (46.3 kN)}$$

but exceeds

$$(F_p)_{\max} = 4.0C_a I_p W_p = 4.0(0.66)(1.5)W_p = 3.96(15) = 59.4 \text{ kips (264.2 kN)}$$

Accordingly, the lateral force for the design of the chiller's support system will be taken equal to

$$F_p = 59.4 \text{ kips (264.2 kN)}$$

Correspondingly, the shear force in each vibration isolator becomes

$$V = F_p / 4 = 59.4 / 4 = 14.8 \text{ kips (66.1 kN)}$$

To compute the uplift force on each isolator, the overturning moment is determined first. For this purpose, note that the moment generated by the lateral force F_p is resisted by the moment generated by the gravity load. Combining, then, the earthquake and gravity loads according to the load combination $0.9D \pm E$, the resultant overturning moment is

$$M_0 = 59.4(3) - 0/9(15)(2.5) = 144.5 \text{ kip-ft (195.9 kN-m)}$$

Hence, the uplift force on each isolator is equal to

$$F_t = \frac{1}{2} \frac{144.5}{5.0} = 14.5 \text{ kips (64.5 kN)}$$

(2) From the seismic maps in the 2000 NEHRP provisions for the coastal region of Irvine, CA, the maximum considered earthquake spectral response acceleration for short periods corresponding to Site Class B is equal to

$$S_s = 2.0$$

and the value of the coefficient F_a to adjust for Site Class D, the site class corresponding to stiff soils, is equal to

$$F_a = 1.0$$

As a result, for the location under consideration, the maximum considered earthquake spectral acceleration for short periods, adjusted for class site, is

$$S_{MS} = F_a S_s = (1.0)(2.0) = 2.0$$

and the corresponding design spectral response acceleration for short periods is

$$S_{DS} = \frac{2}{3} S_{MS} = \frac{2}{3}(2.0) = 1.33$$

In like fashion, from Table 19.6 one has that for vibration-isolated HVAC equipment, a_p and R_p are equal to

$$a_p = 2.5$$

$$R_p = 2.5$$

19-32 Earthquake Engineering: From Engineering Seismology to Performance-Based Engineering

and from Table 19.4, for equipment that is required to function after an earthquake,

$$I_p = 1.5$$

Accordingly, since for the building and equipment location under consideration,

$$z = h = 180 \text{ feet}$$

Equation 19.12 yields

$$\begin{aligned} F_p &= I_p \frac{0.4a_p S_{DS} W_p}{R_p} (1 + 2 \frac{z}{h}) \\ &= (1.5) \frac{0.4(2.5)(1.33)}{2.5} (1 + 2 \frac{180}{180}) W_p = 2.39 W_p \\ &= 2.39(15) = 35.9 \text{ kips (159.7 kN)} \end{aligned}$$

which is greater than

$$(F_p)_{\min} = 0.3 S_{DS} I_p W_p = 0.3(1.33)(1.5)W_p = 0.60W_p = 0.60(15) = 9.0 \text{ kips (40.0 kN)}$$

but less than

$$(F_p)_{\max} = 1.6 S_{DS} I_p W_p = 1.6(1.33)(1.5)W_p = 3.19W_p = 3.19(15) = 47.9 \text{ kips (213.1 kN)}$$

It should be noted, however, that the provisions require that the force F_p be doubled for components mounted on vibration isolators. Therefore, the chiller's support system should be designed for a lateral force equal to

$$F_p = 2(35.9) = 71.8 \text{ kips (319.4 kN)}$$

and, correspondingly, each isolator should be designed for a shear force equal to

$$V = F_p / 4 = 71.8 / 4 = 18.0 \text{ kips (79.9 kN)}$$

In like fashion, if the vertical and horizontal earthquake effects are combined according to Equation 19.15, the overturning moment due to earthquake effects results as

$$M_0 = 71.8(3) + 0.2(1.33)(15)(2.5) = 225.4 \text{ kip - ft (305.6 kN - m)}$$

which, when combined with the gravity load according to the load combination $0.9D \pm E$, leads to

$$(M_0)_{D+E} = 225.4 - 0.9(15)(2.5) = 191.6 \text{ kip - ft (259.8 kN - m)}$$

Consequently, the uplift force on each isolator is equal to

$$F_t = \frac{1}{2} \frac{191.6}{5.0} = 19.2 \text{ kips (85.4 kN)}$$

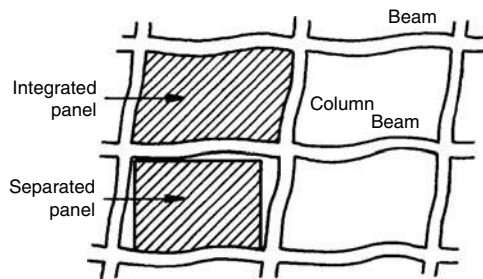


FIGURE 19.18 Separated and integrated infill panels in a framed structure.

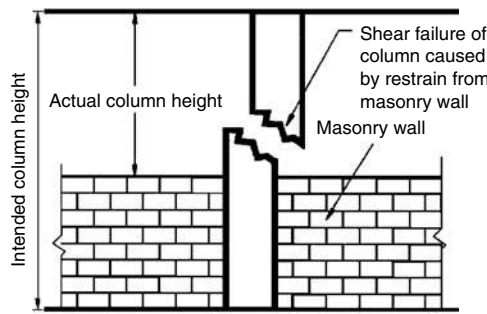


FIGURE 19.19 Schematic illustration of column failure caused by unintended restraint by infill wall. (Adapted from Sabol, T.A. (1989). Design of nonstructural systems and components, in *Seismic Design Handbook*, Naeim, F., Ed., Van Nostrand Reinhold, New York, chap. 12. With permission.)

19.8 General Design Considerations

19.8.1 Architectural Elements

Past earthquakes have provided numerous examples of damage to architectural elements. The most frequently damaged architectural elements have been ceilings, partitions, stairways, facades and parapets. This damage has mainly been due to either inadequate strength or inadequate anchoring. In general, therefore, architectural elements can be made resistant to earthquake motions following one of two strategies: (1) an isolation strategy and (2) a load-bearing strategy. In the isolation strategy the elements are sufficiently separated from the structure so that the deformation of the structure will not produce significant stresses in the architectural elements. In the load-bearing strategy the elements are designed to undergo the required stresses and deformations. An example of the application of these alternative strategies is shown in Figure 19.18. This figure illustrates how an infill panel in a framed building may be either isolated or integrated with the structure. It should be noted, however, that in many instances it is difficult to justify the load-bearing strategy from an economic point of view. The exception would be when the integration of the nonstructural elements with the structure favorably increases the strength and stiffness of the structure. In any case, the designer must recognize that if the architectural elements are not sufficiently separated from the structure, their stiffness and strength may have an unintended effect on the response of the structure itself. A classical example of such an unintended effect is the so-called short-column failures observed during past earthquakes (see Figure 19.19). These failures are induced by the shortening of a column's height by a nonstructural wall and the consequent increase in the magnitude of the shearing forces acting on the column (recall that the shear force in a column is equal to $(M_A + M_B)/H$, where M_A and M_B are the bending moments at the ends of the column and H its height). When the isolation strategy is adopted, the separation required to prevent or limit the damage sustained by

TABLE 19.7 Design Recommendations for Facades and Glazing

-
1. Use heavy rigid facades only on rigid structural systems and not on relatively flexible building frames
 2. Securely attach curtain walls to the building frame. Design and installed flexible gaskets in curtain walls so that they do not come loose when the wall is subjected to repeated racking
 3. Set all glass panels in resilient mounts with sufficient space for in-plane motions and supported by mullions designed to withstand earthquake forces. Use tempered glass in exits or where large glazed areas are near public walks
 4. Avoid brick veneer facades on steel-frame buildings unless the brick veneer is securely tied to a separate wall that is independent of the steel frame
 5. Do not use wire or straight-rod ties to anchor face brick to a wall, especially when a layer of insulation or an air gap separates the two elements
 6. Consider large masonry facades as part of the structural system and not as nonstructural ornaments unless they are properly attached to a structural wall
-

Source: Sabol, T.A. (1989). Design of nonstructural systems and components, in *Seismic Design Handbook*, Naeim, F., Ed., Van Nostrand Reinhold, New York, chap. 12. With permission.

TABLE 19.8 Design Recommendations for Partitions and Infill Panels

-
1. Do not install concrete-masonry-unit filler walls in a manner that would restrain the lateral deflection of the building frame. Leave, instead, a gap with adequately sized resilient filler to separate the structural frame from the nonstructural filler walls (see Figure 19.20 through Figure 19.22 for illustrations of how this separation may be provided while at the same time bracing the wall against out-of-plane motion; Figure 19.20 illustrates one method for heavy partitions, while Figure 19.21 and Figure 19.22 illustrate methods for full and partial light-weight partitions)
 2. Anchor partitions in buildings with flexible structural frames to only one structural element, such as a floor slab, and separate them by a physical gap from all other elements
 3. Do not use unreinforced masonry for partitions or filler walls
 4. Consider reinforced masonry partitions tied to more than one structural element as part of the structural system
 5. Tie conduits and piping in partitions to the structural element to which the partition is anchored
 6. Properly reinforce openings in partitions for pipes, conduits and ducts and make them large enough to preclude direct contact with fixtures
-

Source: Sabol, T.A. (1989). Design of nonstructural systems and components, in *Seismic Design Handbook*, Naeim, F., Ed., Van Nostrand Reinhold, New York, chap. 12. With permission.

architectural elements should be established on the basis of the anticipated structural drifts. In addition, the nonstructural elements themselves must be restrained against the forces acting on them.

A variety of measures to prevent damage to architectural elements have been proven successful during past earthquakes. These measures, adapted here from those reported by Sabol (1989), are summarized in Table 19.7 through Table 19.10. Useful additional guidelines and information may be found in FEMA 74 (Federal Emergency Management Agency, 1994), FEMA 273 (*NEHRP Guidelines for the Seismic Rehabilitation of Buildings*, 1997) and FEMA 274 (*NEHRP Commentary on the Guidelines for the Seismic Rehabilitation of Buildings*, 1997).

19.8.2 Mechanical and Electrical Equipment

Earthquakes have also caused considerable damage to mechanical and electrical equipment, especially to boilers, chillers, generators, tanks, fans, pumps, air handlers, electrical distribution systems, emergency power and lighting systems, elevators, light fixtures, HVAC ducts and piping systems. As opposed to architectural elements, however, most mechanical and electrical equipment units are purchased as manufactured items rather than being fabricated specifically for a project. Therefore, the susceptibility of equipment to seismic damage is controlled mainly by the equipment manufacturer. It is possible, nonetheless, to take preventive measures in the installation of equipment to minimize its susceptibility to damage.

In general, there are two classes of equipment installations that are of interest with respect to seismic design: (1) equipment anchored to the ground or to the building structure or (2) equipment mounted on vibration isolators. Vibrating equipment, such as chillers or emergency generators, has traditionally

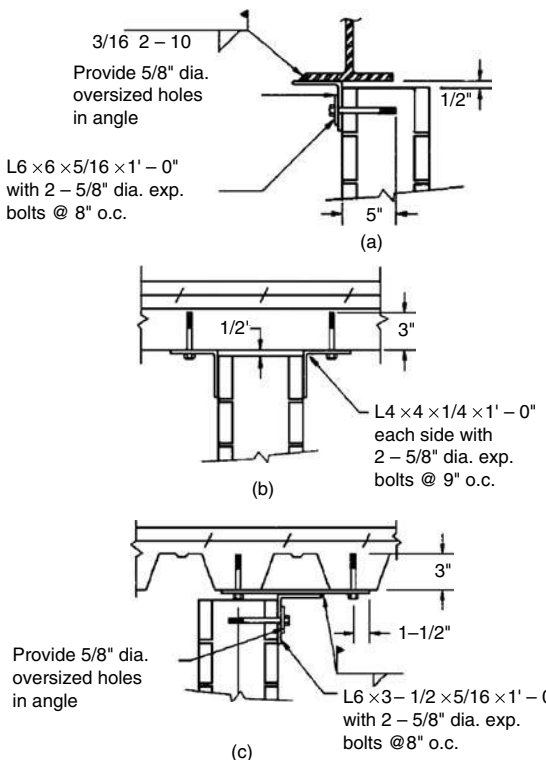


FIGURE 19.20 Details to separate nonbearing masonry wall from structure: (a) under steel beam; (b) perpendicular to steel deck; (c) parallel to steel deck. (Adapted from Sabol, T.A. (1989). Design of nonstructural systems and components, in *Seismic Design Handbook*, Naeim, F., Ed., Van Nostrand Reinhold, New York, chap. 12. With permission.)

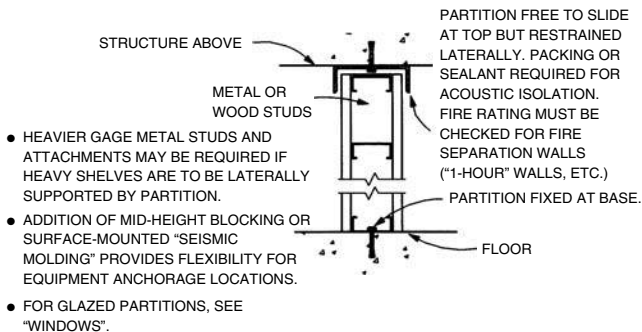


FIGURE 19.21 Seismic bracing of full lightweight partitions. (From Federal Emergency Management Agency, Reducing the Risks of Nonstructural Earthquake Damage, A Practical Guide, FEMA, Washington, D.C., 1994.)

been mounted on resilient mounting systems, particularly when the equipment is on the upper floors of a structure. The resilient mounting devices used may be springs, pneumatic restraining devices or elastic restraining devices. Failure of equipment directly mounted on the ground or building normally reflect insufficient anchor strength or the inability of connecting service piping to reconcile differential settlements. Failure of equipment mounted on vibration isolators occurs because of the isolators' inability

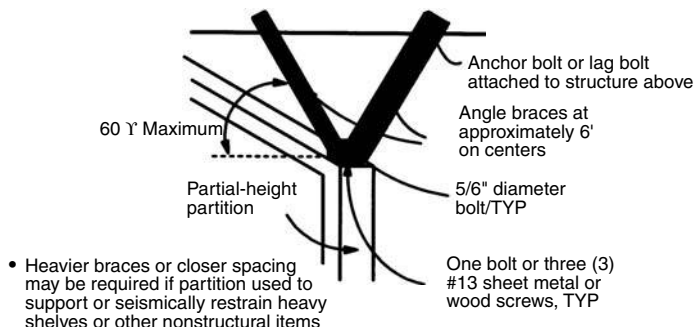


FIGURE 19.22 Seismic bracing of partial lightweight partitions. (From Federal Emergency Management Agency, Reducing the Risks of Nonstructural Earthquake Damage, A Practical Guide, FEMA, Washington, D.C., 1994.)

to undergo the large lateral displacements they are subjected to during an earthquake, displacements that are often significantly greater than those contemplated by the manufacturer. These large lateral displacements are caused by the long period of the resilient mounting devices, which in many cases are in the range of the building period.

TABLE 19.9 Design Recommendations for Ceilings

1. Do not install fluorescent lighting fixtures in or on exposed T-grid or concealed-spline suspended ceilings unless the ceiling suspension system is designed to carry the added weight of the fixtures during an earthquake or the fixtures are independently supported and laterally braced
2. Laterally brace exposed T-grid or concealed-spline suspended ceilings and provide them with a physical separation at the walls, particularly in large rooms with high ceilings and deep attic spaces (see Figure 19.23 and Figure 19.24 for general guidelines to brace suspended ceilings)
3. Do not fasten ceiling system to surrounding walls or partitions. Use soffits to return the ceiling to the supporting slab. Provide an angle wall trim, wide enough to allow for differential movements, where the ceiling must join a wall or partition. Provide hangers for the main and cross runners at the perimeter so that wall trims do not support the ceiling
4. Brace rigid ceiling systems at regular intervals against lateral and vertical movements
5. Reinforce gypsum-board ceilings at nail points by the use of steel nailing strips. Use nails with large heads to install gypsum-board ceilings
6. In gypsum board and lath and plaster ceiling systems, make furring channel joints in irregular-shaped ceilings using rivets, bolts and welds. Brace corners so that they do not pivot
7. In gypsum board and lath and plaster ceiling systems, hold together large ceiling areas separated by rows of linear diffusers or light fixtures with rigid ties and secure the diffusers and light fixtures to the ceiling system

Source: Sabol, T.A. (1989). Design of nonstructural systems and components, in *Seismic Design Handbook*, Naeim, F., Ed., Van Nostrand Reinhold, New York, chap. 12. With permission.

TABLE 19.10 Design Recommendations for Storage Racks and Cabinets

1. Design storage racks to withstand earthquake forces and anchor them to the floor or brace them laterally from the top to the structural elements
2. Design racks with lateral bracing and anchor bolts so that they can withstand anticipated lateral and uplift loads
3. Install rigid ties at the top of rows of racks to brace and stabilize the entire installation
4. Anchor racks placed along walls to the walls to avoid battering between wall and rack
5. Anchor filing cabinets and map or plan drawers to the floor or walls, and fit all drawers with positive-locking safety latches
6. Anchor vital furniture and equipment to the floor or wall
7. Hold in place loose materials stored on high shelves by face bars
8. Keep medical supplies in cabinets that are anchored to the floor or walls and fitted with latched doors

Source: Sabol, T.A. (1989). Design of nonstructural systems and components, in *Seismic Design Handbook*, Naeim, F., Ed., Van Nostrand Reinhold, New York, chap. 12. With permission.

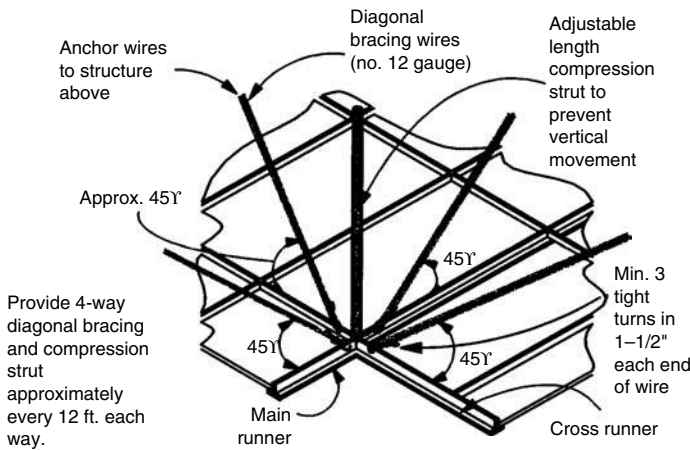


FIGURE 19.23 Seismic bracing system for suspended T-bar ceiling systems. (From Federal Emergency Management Agency, Reducing the Risks of Nonstructural Earthquake Damage, A Practical Guide, FEMA, Washington, D.C., 1994.)

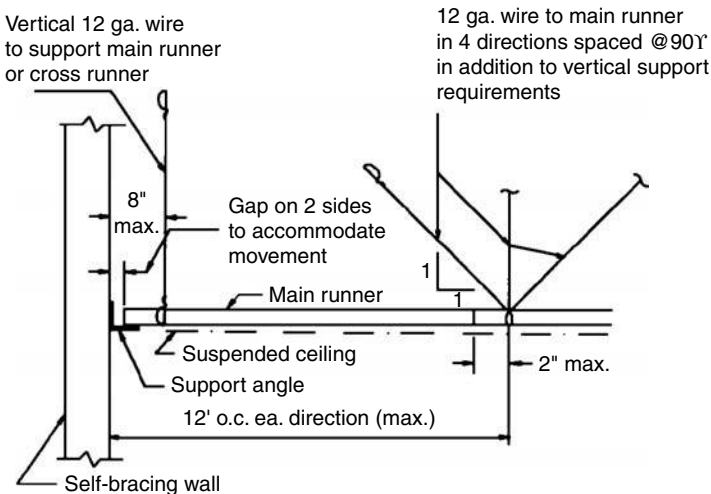


FIGURE 19.24 Bracing detail for suspended ceilings. (Adapted from Sabol, T.A. (1989). Design of nonstructural systems and components, in *Seismic Design Handbook*, Naeim, F., Ed., Van Nostrand Reinhold, New York, chap. 12. With permission.)

A variety of measures may be taken to minimize damage to mechanical and electrical equipment. These measures, also based on those reported by Sabol (1989), are summarized in Tables 19.11 through Table 19.18. FEMA 74 (Federal Emergency Management Agency, 1994), FEMA 273 (*NEHRP Guidelines for the Seismic Rehabilitation of Buildings*, 1997) and FEMA 274 (*NEHRP Commentary on the Guidelines for the Seismic Rehabilitation of Buildings*, 1997) offer useful additional guidelines.

19.9 Role of Nonstructural Elements in Performance-Based Design

It is estimated that approximately 70 to 85% of the cost of a building comes from its nonstructural elements. Given the susceptibility of nonstructural elements to earthquake damage, this means that a major portion of the damage induced in a building during an earthquake will most likely be that inflicted

TABLE 19.11 Design Recommendations for Mechanical Equipment With Vibration Isolation

-
1. Do not mount heavy mechanical equipment on the upper floors of tall buildings unless all vibration-isolation mounts are carefully designed for earthquake resistance
 2. Bolt floor-mounted vibration-isolation devices to the equipment base and to the structural slab
 3. Avoid the use of heavy bases under equipment mounted on vibration isolators to reduce inertial forces
 4. Provide lateral and vertical restraining devices around the base of vibration-isolated, floor-mounted equipment to restrict its displacements
 5. Provide resilient material on the contact surface of the restraining devices to minimize impact loads. Tightly install the vibration-isolation hangers for suspended equipment against the supporting structural member. Provide a structural restraining frame around suspended heavy equipment
 6. Provide cross bracing between hanger rods on all fours sides of suspended lightweight equipment
-

Source: Sabol, T.A. (1989). Design of nonstructural systems and components, in *Seismic Design Handbook*, Naeim, F., Ed., Van Nostrand Reinhold, New York, chap. 12. With permission.

TABLE 19.12 Design Recommendations for Mechanical Equipment without Vibration Isolation

-
1. Design the support for tanks and heavy equipment to withstand earthquake forces and anchor it to the floor or secure it otherwise
 2. Strap suspended tanks and heavy equipment to their hanger system and provide them with lateral bracing
 3. Strap all horizontal tanks to their saddles, weld lugs to the tanks at support points to prevent horizontal movement, and bolt saddles to the structural slab
 4. Provide frames supporting elevated tanks or equipment with adequate bracing and anchor them to the structural slabs and walls
 5. Bolt all floor-mounted equipment to the structural slab
-

Source: Sabol, T.A. (1989). Design of nonstructural systems and components, in *Seismic Design Handbook*, Naeim, F., Ed., Van Nostrand Reinhold, New York, chap. 12. With permission.

TABLE 19.13 Design Recommendations for Piping Systems

-
1. Tie pipelines to only one structural system
 2. Where structural systems change and relative deflections are anticipated, install movable joints in the piping system to allow for such movement (see Figure 19.25 for an illustration of such an arrangement)
 3. Provide suspended piping systems with consistent freedom throughout. For example, do not anchor branch lines to structural elements if the main line is allowed to sway
 4. If the piping system is allowed to sway, install movable joints at equipment connections
 5. Guide pipelines leading to thermal expansion loops or flexible pipe connections to confine the degree of pipe movement
 6. Do not make pipes cross seismic joints. If they must do so, make the crossing at the lowest floor possible, and carefully evaluate all pipe deflections and stresses
 7. Provide pipes with flexible joints where pipes pass through seismic or expansion joints, or where rigidly supported pipes connect to equipment with vibration isolation (see Figure 19.26 for a suggested detail for piping that crosses a seismic joint)
 8. Provide sway bracing in both longitudinal and transverse directions on all pipes with a diameter of 2 1/2 in. or larger to limit the stresses in the pipes (Figure 19.27 illustrates a method to provide this sway bracing)
-

Source: Sabol, T.A. (1989). Design of nonstructural systems and components, in *Seismic Design Handbook*, Naeim, F., Ed., Van Nostrand Reinhold, New York, chap. 12. With permission.

to its nonstructural elements. This also means that a large portion of the potential losses to owners, occupants, insurance companies and other financial institutions will be those associated with nonstructural elements. Evidently, the overall seismic performance of a building greatly depends on the seismic performance of its nonstructural elements.

The need for a satisfactory performance of nonstructural elements and the role of these elements in the overall seismic performance of buildings have been widely recognized in the development of methodologies for the implementation of performance-based designs. As the major goal of a performance-based design is to produce buildings that will endure levels of damage that will not exceed preselected acceptable levels under different ground motion intensities, performance levels have been established for both structural and nonstructural elements. Similar to the performance levels developed for structural systems, the performance-based design concept applied to nonstructural elements also implies the def-

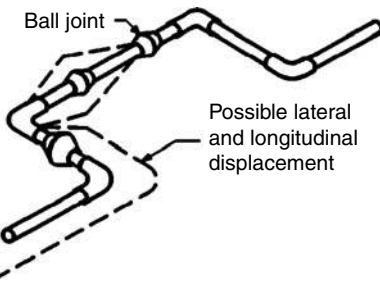


FIGURE 19.25 Possible arrangement to allow for relative deflections in pipes. (Adapted from Sabol, T.A. (1989). Design of nonstructural systems and components, in *Seismic Design Handbook*, Naeim, F., Ed., Van Nostrand Reinhold, New York, chap. 12. With permission.)

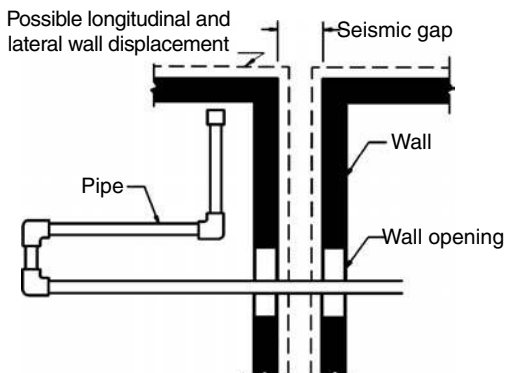


FIGURE 19.26 Detail (plan view) to provide for pipe crossing seismic gap. (Adapted from Sabol, T.A. (1989). Design of nonstructural systems and components, in *Seismic Design Handbook*, Naeim, F., Ed., Van Nostrand Reinhold, New York, chap. 12. With permission.)

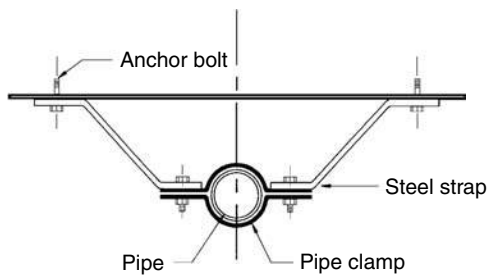


FIGURE 19.27 Pipe clamp and sway bracing. (Adapted from Sabol, T.A., Design of nonstructural systems and components, in *Seismic Design Handbook*, Naeim, F., Ed., Van Nostrand Reinhold, New York, 1989. With permission.)

TABLE 19.14 Design Recommendations for Air Distribution Systems

-
1. Provide long hangers and supports for ductwork with lateral bracing
 2. Install flexible duct connections in a semifolded condition with enough material to allow for the expected differential movement between fans and ductwork
 3. Make pipe sleeves or duct openings through walls or floors large enough to allow for the anticipated movement of the pipes or ducts
 4. Support horizontal ducts as close as possible to the supporting structural member
 5. Secure ceiling diffusers and registers to the ductwork with sheet-metal screws
 6. Tie diffusers connected to flexible ducts with positive ties to the ductwork and/or wall opening
-

Source: Sabol, T.A. (1989). Design of nonstructural systems and components, in *Seismic Design Handbook*, Naeim, F., Ed., Van Nostrand Reinhold, New York, chap. 12. With permission.

TABLE 19.15 Design Recommendations for Elevators

-
1. Bolt vibration isolators under the motor generators to the floor and to the legs of the motor generators. Provide the isolators with sufficient strength to withstand the earthquake forces
 2. Bolt selector and controller panels to the floor and, if possible, provide them with sway braces at the top
 3. Secure all electrical components within the panels to the panel frame, and fit all doors and hinged panels with positive-locking latches
 4. Use counterweight guide rails that are 15 lb/ft or heavier for serving buildings of five or more stories, and design their supports to withstand earthquake forces
 5. Use a safety shoe in the design of the counterweight guide-rail bracket. The type of bracket used should depend on the building height and location in the hoistway
 6. Provide properly designed safety shoes for the roller guides to protect the roller assemblies from being damaged by the counterweights
 7. Strengthen counterweight guide rails by using a section heavier than the typical 8-lb/ft rolled section. Strengthen brackets using gusset plates or ties placed at frequent intervals
 8. Strengthen the car guide rails on long spans by installing spacers between the back-to-back rails at midpoints between the separator beams. This increases the rigidity of both rails
 9. Connect ventilation, communications and lighting systems to emergency power systems and design them to operate when the normal power fails
 10. Provide seismic switches to shut down the elevator during an earthquake and then lower the cars to the nearest floor
 11. Adequately reinforce and brace the elevator hoistway and the surrounding structural system to prevent distortion at the doors and prevent debris from falling into the shaft
 12. Secure hydraulic elevator equipment to floors and walls, and use splash-proof oil tanks
-

Source: Sabol, T.A. (1989). Design of nonstructural systems and components, in *Seismic Design Handbook*, Naeim, F., Ed., Van Nostrand Reinhold, New York, chap. 12. With permission.

TABLE 19.16 Design Recommendations for Light Fixtures

-
1. Provide pendant-hung fluorescent fixtures, especially when mounted end to end in long rows, with flexible lateral bracing at both the ceiling supports and the bottom connections to the fixtures
 2. Locate lighting fixtures supported by flexible hangers so that they will not collide with other building elements
 3. Do not use support systems designed for pendant mounting from a horizontal surface on a sloping surface because some of the freedom of movement is used up in the vertical alignment
 4. Do not locate pendant light fixtures below high ceilings. They should be surface mounted and secured to a supporting grid system that meets the supporting and bracing requirements for suspended ceilings
 5. Preferably, directly attach surface-mounted fixtures to the building structure. However, suspended installations that use positive-locking devices are an acceptable alternative
-

Source: Sabol, T.A. (1989). Design of nonstructural systems and components, in *Seismic Design Handbook*, Naeim, F., Ed., Van Nostrand Reinhold, New York, chap. 12. With permission.

TABLE 19.17 Design Recommendations for Electrical Equipment

-
1. Anchor all electrical equipment such as transformers, switchgears and control panels to the building, etc.
 2. Use flexible braided connections in place of rigid copper bus, whenever relative movement may occur between switchboard components
 3. Provide additional pull boxes with slack conductors in long conduit runs to avoid tension of conductors
 4. Avoid crossing seismic joints with conduits and bus ducts where possible. When seismic joints are crossed, use arrangements that permit the required deflections. Make the crossing at the lowest possible floor
 5. Provide separate ground conductors in all conduit runs that cross seismic joints and elsewhere in the electrical system where grounding systems could be broken
-

Source: Sabol, T.A. (1989). Design of nonstructural systems and components, in *Seismic Design Handbook*, Naeim, F., Ed., Van Nostrand Reinhold, New York, chap. 12. With permission.

inition of multiple target performance levels that are expected to be achieved when the structure is subjected to earthquake ground motions of specified intensities. Some of the proposed performance levels for nonstructural elements are shown in Table 19.19 (Applied Technology Council, 1996). Similar performance levels have also been introduced in the *NEHRP Guidelines for the Seismic Rehabilitation of Buildings* (1997), although those in these guidelines are described separately for different architectural

TABLE 19.18 Design Recommendations for Emergency Power and Lighting Systems

-
1. Mount emergency power generators installed in buildings on adequately designed vibration isolators
 2. Provide vibration isolators and connecting service piping with horizontal restraints
 3. Adequately secure starter battery racks to the structure. Attach each battery to the rack with a positive mounting to restrain movement
 4. Securely tie battery-powered emergency lighting units to the building.
-

Source: Sabol, T.A. (1989). Design of nonstructural systems and components, in *Seismic Design Handbook*, Naeim, F., Ed., Van Nostrand Reinhold, New York, chap. 12. With permission.

TABLE 19.19 Performance Levels for Nonstructural Elements

Performance Objective	Damage State
Operational	Nonstructural elements remain in place and functional with negligible damage; undamaged back-up systems provide protection against failure of external utilities, communications and transportation systems
Immediate occupancy	Nonstructural elements remain in place but may not be functional. No back-up systems for failure of external utilities are provided
Life safety	Nonstructural elements are damaged considerably, but there are no collapses of heavy items, nor secondary hazards such as breaks in high-pressure toxic or fire suppression piping
Reduced hazards	Nonstructural elements are damaged extensively, but there are no collapses of large and heavy items that can cause significant injury to groups of people
Not considered	Performance of nonstructural elements other than those having an effect in structural response is not evaluated

Source: Applied Technology Council, *Seismic Evaluation and Retrofit of Concrete Buildings*, Redwood City, CA, 1996. With permission.

TABLE 19.20 Example of Acceptability Limits for Nonstructural Elements

Performance Objective	Return Period (Years)	Probability of Exceedance (%)	Nonstructural Damage	Contents Damage
			Story Drift Ratio	Floor Acceleration
Fully operational	43	40	0.003	0.6 g
Operational	75	30	0.006	0.9 g
Life safety	475	25	0.015	1.2 g
Near collapse	970	20	0.020	1.5 g

Source: Bertero, R.D. and Bertero, V.V., *Earthquake Eng. Struct. Dyn.*, 31(3), 627–652, 2002. With permission.

elements and mechanical, electrical and plumbing equipment. Acceptability criteria, i.e., the conditions that must be satisfied to ensure that the performance objectives are met, have also been established for nonstructural elements. For the most part, these acceptability criteria have been formulated in terms of key limiting values of measurable structural response parameters such as floor accelerations and story drift ratios. As an example of how these acceptability criteria may be set up, Bertero and Bertero (2002) suggest the format shown in Table 19.20, where the probabilities indicated are those of exceeding the stated performance objectives.

As in the case of structural systems, the selection of the performance levels for nonstructural elements is based on a balance between potential losses and the cost of damage mitigation measures, considering in the potential losses not only the direct cost of earthquake damage, but also indirect losses such as business interruptions. Thus, for example, financial or physical constraints may compel a designer to select the Reduced Hazards objective for the 970-year return period when rehabilitating an existing building. On the other hand, the designer may select the Operational objective for essential facilities such

as hospitals, police and fire stations and emergency command centers since essential facilities are expected to be fully functional during or shortly after an earthquake.

As a final note, it should be mentioned that a performance-based design of nonstructural components is based on the premise that their performance can be predicted and evaluated with sufficient confidence so as to make an intelligent and informed decision on the cost and benefits of earthquake protection. However, as it may be inferred from the material presented in this chapter, such a capability is not quite there yet. It should be realized, therefore, that much research is needed to develop reliable techniques for the assessment of seismic demands and capacities and establish effective damage mitigation measures before the performance-based design of nonstructural elements may be brought into fruition (see also Chapter 9).

19.10 Future Challenges

As seen from the discussion in the preceding sections, much progress has been made toward the understanding of the seismic behavior of nonstructural elements, the development of simplified methods of analysis and the improvement of the code provisions for the seismic design of these elements. Notwithstanding this progress, it is also clear from the same discussion and the damage sustained by nonstructural elements during recent earthquakes that the problem is a complex one and has not been completely solved. Therefore, research is needed to further advance the understanding of the seismic behavior of nonstructural elements, to derive methods of analysis that are rational but also simple enough for their incorporation into building codes and to further improve the code provisions for the design of these elements. One particular area of research that is urgently needed to advance the understanding of the seismic behavior of nonstructural elements and develop effective methods of analysis is that related to the effect on this behavior of the nonlinearity of their supporting structures and the nonstructural elements themselves. As discussed in Section 19.6.2, there is some analytical evidence that indicates that the nonlinearity of a supporting structure may significantly affect the seismic response of a nonstructural element. In some cases it may considerably reduce the response of the nonstructural element, but in some others it may increase it. However, only a limited number of studies have been conducted to clarify and quantify such an effect, and only a few simplified methods of analysis that account for it have been proposed. Another area of research that deserves full consideration is the application of modern isolation and protective systems to nonstructural elements. Given their relatively small size and the high accelerations to which they may be subjected, important benefits may be realized from the use of such systems. An extensive program of experimental tests and field studies is also needed. The experimental tests are needed to verify the findings from analytical studies; to quantify the stiffness, damping, ductility and drift limits of nonstructural elements and their anchorages; to test the adequacy of current and new bracing methods and anchoring systems; and to test the effectiveness of isolation and protective systems. The field studies are needed to study the performance of actual elements on actual buildings under real earthquakes, and to contrast this performance against the results from analytical and experimental studies. Finally, research is needed to develop rational and reliable methodologies for the implementation of performance-based designs (see also Chapter 9).

19.11 Summary

This chapter provided a basic depiction of the behavior of nonstructural elements under the effect of earthquakes, the methods that are presently available to analyze them under such effects and the pertinent design recommendations given in current building codes. It began with a description of what precisely are nonstructural elements, what has been their performance during past earthquakes and why it is so important to make them the subject of a rational seismic design. A description was also given of the characteristics that make nonstructural elements particularly vulnerable to the effects of earthquakes, and what is currently known about their behavior under earthquake excitations. In addition, two methods

to perform the seismic response analysis of nonstructural elements were presented in some detail, and a brief description of some other methods that have been proposed to simplify such an analysis was given. The methods discussed were (1) the floor response spectrum method and (2) a design-oriented simplified method. The floor response spectrum method involves a time-history analysis to obtain the acceleration response of the point of the building to which the nonstructural element is attached and the generation of the response spectrum that corresponds to this acceleration response. The design-oriented simplified method entails the application of a few simple formulas to calculate the magnitude of the lateral seismic forces for which nonstructural elements should be designed. This method incorporates an approximate scheme to take into account the nonlinear behavior of the nonstructural element and the building that supports it. It is pointed out that, in general, nonstructural elements are difficult to analyze accurately and efficiently. The floor response spectrum method, for example, is cumbersome since it requires time-history analyses and the generation of a response spectrum for each building point where there is a nonstructural element attached to it. It ignores, in addition, the dynamic interaction between an element and its supporting structure. As a result, it may sometimes give overly conservative results. Similarly, the design-oriented simplified method, although simple to use, may give results that deviate significantly — usually on the conservative side — from those that one would obtain using a rigorous approach. The chapter proceeded with a review of the recommendations given in the 1997 version of the UBC and the 2000 NEHRP provisions for the seismic design of nonstructural elements. Some general design recommendations and preventive measures that have been proven effective to improve the seismic resistance of some architectural elements and mechanical and electrical equipment were also included. Finally, a brief discussion was given of the important role that nonstructural elements play in the performance-based design of buildings and the research that is needed to further advance the understanding of the seismic behavior of nonstructural elements and improve the methods of analysis and code provisions for the design of these elements.

Glossary

Closely spaced natural frequencies — Natural frequencies with similar numerical values.

Combined system — System that comprises nonstructural element and supporting structure.

Dynamic interaction — Effect that a nonstructural element may have in the dynamic response of its supporting structure and vice versa.

Flexible element — Element having a fundamental natural period greater than 0.06 sec.

Floor acceleration — Acceleration induced by an earthquake ground motion at the level of a building's floor.

Floor response spectrum — Response spectrum of floor motion generated by an earthquake.

In-structure spectrum — A floor response spectrum.

Isolated element — Element separated from the structure in which it is installed to avoid stresses and deformations in it when the structure is deformed.

Load-bearing element — Element designed to resist stresses and deformations.

Modal synthesis technique — Technique by means of which the dynamic properties of a combined system are obtained from the dynamic properties of its separate components.

Multiply connected element — Element connected to its supporting structure at more than one point.

Nonclassical damping effects — Effects that arise when a structure does not possess classical modes of vibration.

Nonstructural element — Element attached to floor or wall of a building but not part of the building's main structural system.

Rigid element — Element having a fundamental natural period equal to or less than 0.06 sec.

List of Symbols

a_p	component amplification factor
b	variable defined by Equation 19.7
C	spectral ordinate
C_m	modified amplification factor
C_p	amplification factor
D	dead load
D_p	component relative displacement
E	effect of horizontal and vertical earthquake forces
f	fundamental natural frequency of structure
F_a	site coefficient for short periods
F_p	design force on nonstructural element
F_{pj}	force at center of j th mass of nonstructural element
h	average height of structure's roof
h_{av}	average of elevations above grade of attachment points
h_i	elevation above grade of i th building floor
h_{sx}	story height used in the definition of allowable drift Δ_a
I	importance factor for structure
l_j	distance from attachment point to j th mass of nonstructural element
I_p	importance factor for nonstructural element
n	number of masses in nonstructural element
n'	number of resisting elements in nonstructural element
N	number of floors in building
R_p	component response modification factor
S_{DS}	design short-period spectral acceleration
S_{MS}	spectral acceleration adjusted for site effects
S_s	maximum spectral acceleration determined from seismic hazard maps
T	fundamental natural period of structure
T_p	fundamental natural period of nonstructural element
V_p	base shear or sum of the shears at the supports of nonstructural element
w_p	total weight of nonstructural element
w_{pj}	weight of j th mass of nonstructural element
W	total building weight
W_i	weight of building's i th floor
W_p	component weight
X	height of upper support attachment
Y	height of lower support attachment
z	height of highest point of component attachment
δ_{xA}	deflection at level x of Structure A
δ_{yA}	deflection at level y of Structure A
δ_{yB}	deflection at level y of Structure B
Δ_{aA}	allowable story drift for Structure A
Δ_{aB}	allowable story drift for Structure B
Φ_0	variable defined by Equation 19.6
λ	variable defined by Equation 19.3
μ	ductility factor of structure
μ_{eq}	equivalent ductility factor
μ_p	ductility factor of nonstructural element
ρ	reliability factor

References

- Adam, C. and Fotiu, P.A. (2000). Dynamic response of earthquake excited inelastic primary–secondary systems, Paper 0310, in *Proceedings of 12th World Conference on Earthquake Engineering*, Auckland, New Zealand, New Zealand Society for Earthquake Engineering, Upper Hutt, New Zealand.
- Amin, M., Hall, W.J., Newmark, N.M. and Kassawara, R.P. (1971). Earthquake response of multiply connected light secondary systems by spectrum methods, in *ASME First National Congress on Pressure Vessels and Piping*, San Francisco, CA, American Society of Civil Engineers, pp. 103–129.
- Applied Technology Council (1996). Seismic Evaluation and Retrofit of Concrete Buildings, Report ATC-40, Vols. 1 and 2, Redwood City, CA.
- Asfura, A. and Der Kiureghian, A. (1986). Floor response spectrum method for seismic analysis of multiply supported secondary systems, *Earthquake Eng. Struct. Dyn.*, 14(2), 245–265.
- ASME (1993). ASME Boiler and Pressure Vessel Code, Section III, Division 1: Rules for Construction of Nuclear Power Plant Components, Appendix N, American Society of Mechanical Engineers, New York.
- Atalik, T.S. (1978). An alternative definition of instructure response spectra, *Earthquake Eng. Struct. Dyn.*, 6(1), 71–78.
- Aziz, T. and Ghobarah, A. (1988). Equipment design: future directions, in *Proceedings of 9th World Conference on Earthquake Engineering*, Tokyo-Kyoto, Japan, Japan Association for Earthquake Disaster Prevention, Tokyo, Vol. 6, pp. 261–266.
- Bertero, R.D. and Bertero, V.V. (2002). Performance-based seismic engineering: the need for a reliable conceptual comprehensive approach, *Earthquake Eng. Struct. Dyn.*, 31(3), 627–652.
- Biggs, J.M. and Roessel, J.M. (1970). Seismic analysis of equipment mounted on a massive structure, in *Seismic Design for Nuclear Power Plants*, Hansen, R.J., Ed., MIT Press, Cambridge, MA, pp. 319–343.
- Burdisso, R.A. and Singh, M.P. (1987). Seismic analysis of multiply supported secondary systems with dynamic interaction effects, *Earthquake Eng. Struct. Dyn.*, 15(8), 1005–1022.
- Chen, Y. and Soong, T.T. (1988). State-of-the-art-review: seismic response of secondary systems, *Eng. Struct.*, 10(4), 218–228.
- Departments of the Army, Navy, and Air Force (1992). *Tri-Services Manual: Seismic Design of Buildings*, Departments of the Army (TM 5-809-10), Navy (NAVFAC 355), and Air Force (AFM 88-3), Washington, D.C.
- Der Kiureghian, A., Sackman, J.L. and Nour-Omid, B. (1983). Dynamic analysis of light equipment in structures: response to stochastic input, *J. Eng. Mech.*, 109(1), 90–110.
- EERI (1984). *Nonstructural Issues of Seismic Design and Construction*, Publication 84-04, Earthquake Engineering Research Institute, Berkeley, CA.
- Federal Emergency Management Agency (1994). Reducing the Risks of Nonstructural Earthquake Damage, A Practical Guide, FEMA Report 74, Washington, D.C.
- Gupta, A.K. (1984). Seismic response of multiply connected MDOF primary and secondary systems, *Nucl. Eng. Design*, 81(3), 385–394.
- Gupta, A.K. (1990). *Response Spectrum Method in Seismic Analysis and Design of Structures*, Blackwell Scientific Publications, Inc., Boston, MA.
- Gupta, A.K. and Jaw, J.W. (1986a). Coupled response spectrum analysis of secondary systems using uncoupled modal properties, *Nucl. Eng. Design*, 92(3), 61–68.
- Gupta, A.K., and Jaw, J.W. (1986b). A new instructure response spectrum (IRS) method for multiply connected secondary systems with coupling effects, *Nucl. Eng. Design*, 96(1), 63–80.
- Gupta, V.K. (1997). Acceleration transfer function of secondary systems, *J. Eng. Mech.*, 123(7), 678–685.
- Hall, J.F., Ed. (1994). Northridge Earthquake, January 17, 1994, Earthquake Engineering Research Institute, Oakland, CA, 453–514.
- Hall, J.F., Ed. (1995). Northridge Earthquake, January 17, 1994: Preliminary Reconnaissance Report, Vol. 1, *Earthquake Spectra*, 11(suppl.).

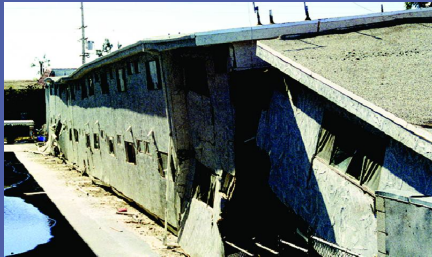
- Hernried, A.G. and Sackman, J.L. (1984). Response of secondary systems in structures subjected to transient excitation, *Earthquake Eng. Struct. Dyn.*, 12(6), 737–748.
- Igusa, T. (1990). Response characteristics of inelastic 2-DOF primary-secondary system, *J. Eng. Mech.*, 116(5), 1160–1174.
- Igusa, T. and Der Kiureghian, A. (1985a). Dynamic characterization of two-degree-of-freedom equipment-structure systems, *J. Eng. Mech.*, 111(1), 1–19.
- Igusa, T. and Der Kiureghian, A. (1985b). Generation of floor response spectra including oscillator-structure interaction, *Earthquake Eng. Struct. Dyn.* 13(5), 661–676.
- Igusa, T. and Der Kiureghian, A. (1985c). Dynamic response of multiply supported secondary systems, *J. Eng. Mech.*, 111(1), 20–41.
- International Building Code (2000). International Code Council, Inc., Falls Church, VA.
- Kapur, K.K. and Shao, L.C. (1973). Generation of seismic floor response spectra for equipment design, in *Proceedings of ASCE Conference on Structural Design of Nuclear Power Plants Facilities*, Chicago, IL, American Society of Civil Engineers, New York, Vol. 2, pp. 29–71.
- Kawakatsu, T., Kitada, K., Takemori, T., Kuwabara, Y., and Okiwara, Y. (1979). Floor response spectra considering elasto-plastic behavior of nuclear facilities, in *Transactions of 5th International Conference on Structural Mechanics in Reactor Technology*, Berlin, Federal Republic of Germany, North-Holland Publishing Co., Amsterdam, K9/4.
- Kehoe, B.E. and Freeman, S.A. (1998). A critique of procedures for calculating seismic design forces for nonstructural elements, in *Proceedings of Seminar on Seismic Design, Retrofit, and Performance of Equipment and Nonstructural Components* (ATC-29-1), Applied Technology Council, Redwood City, CA, pp. 57–70.
- Lee, M.C. and Penzien, J. (1983). Stochastic analysis of structures and piping systems subjected to stationary multiple support excitations, *Earthquake Eng. Struct. Dyn.*, 11(1), 91–110.
- Lin, C.W. and Loceff, F. (1980). A new approach to compute system response with multiple support response spectra input, *Nucl. Eng. Design*, 60, 347–352.
- Lin, J. and Mahin, S.A. (1985). Seismic response of light subsystems on inelastic structures, *J. Struct. Eng.*, 111(2), 400–417.
- Muscolino, G. (1990). Dynamic response of multiply connected primary–secondary systems, *Earthquake Eng. Struct. Dyn.*, 19(2), 205–216.
- NEHRP Commentary on the Guidelines for the Seismic Rehabilitation of Buildings (1997). FEMA Report 274, Federal Emergency Management Agency, Washington, D.C.
- NEHRP Guidelines for the Seismic Rehabilitation of Buildings (1997). FEMA Report 273, Federal Emergency Management Agency, Washington, D.C.
- NEHRP Recommended Provisions for Seismic Regulations for New Buildings (2000)., Building Seismic Safety Council, Washington, D.C.
- Newmark, N.M. (1972). Earthquake response analysis of reactor structures, *Nucl. Eng. Design*, 20(2), 303–322.
- Newmark, N.M. and Villaverde, R. (1980). Computation of seismic response of light attachments to buildings, in *Proceedings of 7th World Conference on Earthquake Engineering*, Istanbul, Turkey, Turkish National Committee on Earthquake Engineering, Ankara, Turkey, Vol. 5, pp. 343–350.
- Peters, K.A., Schmitz, D., and Wagner, U. (1977). Determination of floor response spectra on the basis of the response spectrum method, *Nucl. Eng. Design*, 44(2), 255–262.
- Recommended Lateral Force Requirements and Commentary (1990). Seismology Committee, Structural Engineers Association of California, San Francisco, CA.
- Rihal, S.S. (1990). Performance and behavior of non-structural building components during the Whittier Narrows, California (1987) and Loma Prieta, California (1989) earthquakes: selected case studies, in *Proceedings of ATC-29 Seminar and Workshop on Seismic Design and Performance of Equipment and Nonstructural Components in Buildings and Industrial Structures*, Applied Technology Council, Redwood City, CA, pp. 119–143.
- Sabol, T.A. (1989). Design of nonstructural systems and components, in *Seismic Design Handbook*, Naeim, F., Ed., Van Nostrand Reinhold, New York, chap. 12.

- Sackman, J.L. and Kelly, J.M. (1979). Seismic analysis of internal equipment and components in structures, *Eng. Struct.*, 1(4), 179–190.
- Saudy, A., Aziz, A., and Ghobarah, A. (1994). A new stochastic analysis for multiple supported MDOF secondary systems. I. Dynamic interaction effects, *Nucl. Eng. Design*, 147, 235–249.
- Schroeder, M.E. and Backman, R.E. (1994). Analytical studies in support of the 1994 NEHRP provisions for nonstructural components, in *Proceedings of 5th U.S. National Conference on Earthquake Engineering*, Chicago, IL, Earthquake Engineering Research Institute, Oakland, CA, Vol. 4, pp. 755–764.
- Sewell, R.T. (1988). Damage Effectiveness of Earthquake Ground Motion: Characterizations Based on the Performance of Structures and Equipment, Ph.D. thesis, Stanford University.
- Sewell, R.T., Cornell, C.A., Toro, G.R., and McGuire, R.K. (1986). A Study of Factors Influencing Floor Response Spectra in Nonlinear Multi-Degree-of-Freedom Structures, Report 82, The John A. Blume Earthquake Engineering Center, Stanford University, Stanford, CA.
- Sewell, R.T., Cornell, C.A., Toro, G.R., McGuire, R.K., Kassawara, R.P., Singh, A., and Stepp, J.C. (1989). Factors influencing equipment response in linear and nonlinear structures, in *Transactions of 9th International Conference on Structural Mechanics in Reactor Technology*, Lausanne, Switzerland, A. A. Balkema, Rotterdam, pp. 849–856, K2.
- Shaw, D.E. (1975). Seismic structural response analysis of multiple support excitation, in *Transactions of 3rd International Conference on Structural Mechanics in Reactor Technology*, London, U.K., North-Holland Publishing Co., Amsterdam, Vol. 4, K7/3.
- Singh, M.P. (1980). Seismic design input for secondary systems, *J. Struct. Div.*, 106(2), 505–517.
- Singh, M.P. (1990). An overview of techniques for analysis of non-structural components, in *Proceedings of ATC-29 Seminar and Workshop on Seismic Design and Performance of Equipment and Nonstructural Components in Buildings and Industrial Structures*, Applied Technology Council, Redwood City, CA, pp. 215–224.
- Singh, M.P. and Sharma, A.M. (1985). Seismic floor spectra by mode acceleration approach, *J. Eng. Mech.*, 111(11), 1402–1419.
- Singh, M.P. and Suárez, L.E. (1987). Seismic response analysis of structure-equipment systems with non-classical damping effects, *Earthquake Eng. Struct. Dyn.*, 15, 871–888.
- Singh, M.P., Suárez, L.E., Matheu, E.E., and Maldonado, G.O. (1993). Simplified Procedure for Seismic Design of Nonstructural Components and Assessment of Current Code Provisions, Report NCEER-93-0013, National Center for Earthquake Engineering Research, State University of New York at Buffalo.
- Soong, T. T. (1994). Seismic behavior of nonstructural elements: state-of-the-art report, in *Proceedings of 10th European Conference on Earthquake Engineering*, Vienna, Austria, A.A. Balkema, Rotterdam, Vol. 3, pp. 1599–1606.
- Suárez, L.E. and Singh, M.P. (1987a). Floor response spectra with structure–equipment interaction effects by a mode synthesis approach, *Earthquake Eng. Struct. Dyn.*, 15(2), 141–158.
- Suárez, L.E. and Singh, M.P. (1987b). Seismic response of equipment-structure systems, *J. Eng. Mech.*, 113(1), 16–30.
- Suárez, L.E. and Singh, M.P. (1989). Floor spectra with equipment–structure–equipment interaction effects, *J. Eng. Mech.*, 115(2), 247–264.
- Taly, N. (1988). The Whittier Narrows, California earthquake of October 1, 1987: performance of buildings at California State University, Los Angeles, *Earthquake Spectra*, 4(2), 277–317.
- Thailler, H.J. (1976). Spectral analysis of complex systems supported at several elevations, *Pressure Vessel Technol.*, 98(2), 162–165.
- Toro, G.R., McGuire, R.K., Cornell, C.A., and Sewell, R.T. (1989). Linear and Nonlinear Response of Structures and Equipment to California and Eastern United States Earthquakes, Report NP-5566, Electric Power Research Institute, Palo Alto, CA.
- Uniform Building Code (1997). Structural Engineering Design Provisions (UBC, Vol. 2), International Conference of Building Officials, Whittier, CA.

- Vanmarcke, E.H. (1977). A simple procedure for predicting amplified response spectra and equipment response, in *Proceedings of 6th World Conference on Earthquake Engineering*, New Delhi, India, Sarita Prakashan, Meerut, Vol. III, pp. 3323–3327.
- Villaverde, R. (1986a). Simplified seismic analysis of secondary systems, *J. Struct. Eng.*, 112(3), 588–604.
- Villaverde, R. (1986b). Simplified seismic analysis of piping or equipment mounted on two points of a multistory structure, *Nucl. Eng. Design*, 92(1), 37–50.
- Villaverde, R. (1987). Simplified approach for the seismic analysis of equipment attached to elastoplastic structures, *Nucl. Eng. Design*, 103(3), 267–279.
- Villaverde, R. (1991). Approximate formulas to calculate the seismic response of light attachments to buildings, *Nucl. Eng. Design*, 128(3), 349–368.
- Villaverde, R. (1997). Method to improve seismic provisions for nonstructural components in buildings, *J. Struct. Eng.*, 123(4), 432–439.
- Villaverde, R. (2000). Design-oriented approach for seismic nonlinear analysis of nonstructural components, Paper 1979, in *Proceedings of 12th World Conference on Earthquake Engineering*, Auckland, New Zealand.
- Viti, G., Olivieri, M., and Travi, S. (1981). Development of nonlinear floor response spectra, *Nucl. Eng. Design*, 64(1), 33–38.
- Wang, Y.K., Subudhi, M., and Bezler, P. (1983). Comparison study of time history and response spectrum responses for multiply supported piping systems, in *Transactions of 7th International Conference on Structural Mechanics in Reactor Technology*, Chicago, IL, North-Holland Publishing Co., Amsterdam, k(a), k7/5.

EARTHQUAKE ENGINEERING

From Engineering Seismology to Performance-Based Engineering



Following a brief overview of traditional methods, **Earthquake Engineering: From Engineering Seismology to Performance-Based Engineering** presents the details of these recent advances in a single volume. The book elucidates advances in scientific knowledge, summarizes recent research project findings, covers design guidelines, and discusses the future challenges and directions.

Highlights include:

- Historical development of earthquake engineering and its modern goal
- Geosciences principles needed to define seismic hazards
- Geotechnical hazards and engineering characterizations of ground motion
- Deterministic and probabilistic methods of analysis
- Performance-based earthquake engineering, its applications, and future direction
- Innovative strategies and techniques, including seismic isolation and energy dissipation devices
- Seismic behavior and earthquake-resistant design of building structural systems using different structural materials such as reinforced concrete, steel, masonry, and wood
- Seismic analysis and design of nonstructural elements

The multidisciplinary nature of earthquake engineering is reflected in the diversity of the chapter authors.

Features

- Presents recent advances in engineering seismology, engineering geology, geotechnical engineering, and engineering characterization of ground motions
- Explores methods of computer structural analysis
- Addresses the fundamental and practical issues in performance-based earthquake engineering
- Discusses the need for innovative strategies and techniques and the advantages of those that have been developed
- Includes a discussion of theoretical and practical issues of seismic isolation
- Dedicates a chapter to seismic resistant design through supplemental damping
- Covers the behavior and design procedures for different structural systems using reinforced concrete, steel, masonry, and wood
- Presents analysis and design procedures for various types of nonstructural elements



CRC PRESS

www.crcpress.com

